Recovery and Analysis of Organic Residues from Metal Corrosion

Luciana da Costa Carvalho

Linacre College, Oxford

Submitted according to the requirements for
The Doctor of Philosophy in Archaeological Science

Hillary Term 2021

In memory of

José Roberto Carvalho (1948-2017)

Acknowledgements

First and foremost I would like to thank Dana Goodburn-Brown for introducing me to Prof Mark Pollard and my employer, David Collins, for funding the PhD.

Secondly, I would like to thank my supervisors: Prof Mark Pollard, for supporting me on various academic pursuits and for the inspiring discussions; Dr Colin Johnson for welcoming me at Begbroke Science Park and accepting me as one of his students during particularly difficult personal circumstances; and Prof James McCullagh, my un-official supervisor, who granted me access to the Mass Spectrometry Facility at the Chemistry Research Laboratories and thoroughly assessed my work.

In my research proposal I stated my aim to undertake laboratory experiments and access a variety of analytical techniques, which led me to meet various academics within Oxford and beyond. It was their generosity that enabled this research to flourish.

From Chemistry: Prof Phil Wisemen, who granted access to powder XRD; Prof Richard Compton, who gave his valuable input on the electrochemistry experiments; Dr James Wickens, who introduced me to QTOF-GC-MS; and Elisabete Pires, who carried out the proteomics analyses.

From Materials Science: Chris Salter, who assisted with the initial corrosion experiments, and Dr Phil Holdway for the XPS and XRD analyses of copper-organic complexes.

From the Bodleian Library: David Howell, who let me try his FTIR microscope and Raman on my metal carboxylates and invited me to present the data at a Perkin Elmer's FTIR Workshop. There I met an eclectic cohort of scientists including Dr Chris Dyer (Cranfield University), who I thank for his enthusiasm about my work on metal-organic complexes and for teaching me about Raman spectroscopy.

As I was approaching the end of my research in 2019, David Howell introduced me to Dr Kelly Domoney (Ashmolean Museum). At the time she was looking for a laboratory to analyse a 540BC residue and because of my links with Chemistry, I offered to help. In exchange I was given corrosion samples from Pompeii vessels that had recently arrived at the Museum, which ended up as a substantial part of the thesis you are about to read.

I would like to thank Dr Sergio Henrique Monteiro and Dr Juliano Chaker for sharing their analytical knowhow, Dr John Merkel for reviewing my submissions and Dr Thibaut Deviese, for his input as my supervisor during the early days of this research. Finally, I thank Shirley Jones and Dr Joseph Clayton for proofreading this thesis, and Yann Ticot, my husband, for his unyielding support.

Abstract

This research demonstrates the potential of archaeological copper corrosion for organic residue analysis. In archaeology, analysis of metal corrosion has traditionally been limited to the identification of inorganic compounds, thought to result from the interaction of the metal object with the deposition environment. For the first time a range of analytical techniques are used to analyse archaeological copper corrosion, many from Pompeii vessels, revealing the different types of information they contain and how the identified compounds can be articulated into compelling stories.

The formation of copper-organic complexes is proposed as a pathway for preservation of organic residues in metal objects. This hypothesis is supported by electrochemical experiments to generate copper corrosion impregnated with organic mixtures and to synthetize copper-organic complexes with characterization by a range of analytical techniques. To address the low solubility of copper-organic complexes in organic solvents a gas chromatography with mass spectrometry method using a thermal sample probe is developed and shown to be superior to solvent extraction. This method is incorporated into a new multi-analytical protocol for the analysis of copper corrosion comprised of Fourier-Transform infrared (FTIR) for identification of chemical functions, powder X-ray diffraction (XRD) for identification of mineral phases and identification of organic molecules that also includes IC-MS and proteomics. Validation of the multi-analytical protocol with archaeological copper corrosion enables the recovery of a range of biomarkers including those for substances used in the past, for past environments and associated with changes in the deposition environment.

Table of Contents

Acknowledgments…… iii

Abstract…….. v

Table of Contents…….. vi

List of Figures…… x

List of Tables…….. xiv

List of Appendices…….. xvi

Abbreviations…… xviii

1. INTRODUCTION 20

1.1 Background.....20

1.2 Research Objectives 22

1.3 Thesis Structure 22

2. LITERATURE REVIEW 24

2.1 Organic Residue Analysis in Archaeology 24

2.1.1 Lipids 24

2.1.4 Methods for Analysis of Organic Residues.....30

2.2 Principles of Metallic Corrosion.....31

2.2.1 Corrosion of copper and its alloys 36

2.2.2 Metal-organic complexes.....38

2.3 Information from Archaeological Metal Corrosion.....41

2.3.1 How the object was manufactured.....41

2.3.2 How the object was used.....44

2.3.3 Where the object was deposited 45
2.3.4 Analytical Techniques 46

3. MATERIALS, METHODS AND INSTRUMENTS 57

3.1 Materials 57

3.2 Methods 58
3.2.1 Corrosion experiments 59
3.2.2 Synthesis of copper-organic complexes 60

3.3 Instrumentation 62
3.3.1 Fourier-transform infra-red spectroscopy (FTIR) 62
3.3.2 Raman spectroscopy (Raman) 63
3.3.3 X-ray photoelectron spectroscopy (XPS) 64
3.3.4 Powder X-ray diffraction (XRD) 65
3.3.5 Mass spectrometry techniques 66

4. A NEW PROTOCOL FOR ANALYSIS OF ARCHAEOLOGICAL METAL CORROSION 72

4.1 Corroding Copper in the Laboratory 72
4.4.1 Experiment 1 – Corroding copper in the presence of carbonate and chloride ions 72
4.1.2 Experiment 2 – Corroding copper in the presence of carbonate, chloride and carboxylate ions 75
4.1.3 Experiment 3 - Corroding Copper in the Presence of Organic Mixtures 80

4.2 Electrochemical Synthesis of Copper-organic Complexes 82
4.2.1 Copper-carboxylates 82
4.2.2 Copper-lactose 105
4.2.3 Copper-casein 116
4.2.4 Characterization of Copper-Milk Corrosion 135

4.3 Conclusion 145

5. TESTING THE PROTOCOL ON ARCHAEOLOGICAL COPPER CORROSION 148

5.1 Case Study 1 – The Pewsey Hoard 149
5.1.1 Background 149
5.1.2 Research Question 151
5.1.3 Identification of Chemical Bonds 153
5.1.4 Identification of Mineral Phases 156
5.1.5 Identification of Organic Compounds 159
5.1.6 Discussion 169

5.2 Case Study 2 – Roman Bowl from Wingham 175
5.2.1 Background 175
5.2.2 Research Question 175
5.2.3 Identification of Chemical Bonds 176
5.2.4 Identification of Mineral Phases 178
5.2.5 Identification of Organic Compounds 180
5.2.6 Discussion 185

5.3 Case Study 3 – Pompeii INV10653 188
5.3.1 Background 188
5.3.2 Research Question 189
5.3.3 Identification of Chemical Bonds 189
5.3.4 Identification of Mineral Phases 191
5.3.5 Identification of Elemental Composition 191
5.3.6 Identification of Organic Compounds 194
5.3.7 Discussion 197

5.4 Case Study 4 – Pompeii INV10295 199
5.4.1 Background 199
5.4.2 Research Question 200
5.4.3 Identification of Chemical Bonds 202
5.4.4 Identification of Mineral Phases 203
5.4.5 Identification of Organic Compounds 205
5.4.6 Discussion 212

5.5 Case Study 5 – Pompeii INV10289 215
5.5.1 Background 215
5.5.2 Research Question 216
5.5.3 Identification of Chemical Functions 216
5.5.4 Identification of Mineral Phases 219
5.5.5 Identification of Organic Compounds 220
5.5.6 Discussion 229

5.6 Case Study 6 – The Paestum Residue 231
5.6.1 Background 231
5.6.2 Research Question 233
5.6.3 Identification of Chemical Bonds 236
5.6.4 Identification of Organic Compounds 241
5.6.5 The interaction of the Paestum residue with the Copper Vessel 255
5.6.6 Discussion 257

6. CONCLUSION 259

6.1 A pathway for organic residue preservation in copper corrosion 259

6.2 Proposing a new multi-analytical protocol for characterization of copper corrosion 262

6.3 Evaluating the type of information retrieved from archaeological samples 264

6.5 Evaluating the multi-analytical protocol 269

6.6 Sampling protocols for organic residue analysis in archaeological metal corrosion 270

6.7 Understanding the dynamics of organic residue preservation in copper corrosion 272

6.6. Potential for future work 273

7. BIBLIOGRAPHY 275

8. APPENDICES 324

List of Figures

Figure 1 - Schematic hydrolysis of a triacylglycerol 26
Figure 2 - Examples of Sterols 28
Figure 3 - Examples of terpenoid biomarkers 29
Figure 4 - Metallic corrosion and ionization potential for some common metals 32
Figure 5 - Cu-H_2O Pourbaix Diagram showing the most stable species 34
Figure 6 - Typical electrochemical set up 58
Figure 7 - Pourbaix Diagram based on conditions of Experiment 1 73
Figure 8 - (+) Coupon at the end of Experiment 1 73
Figure 9 - (+) Coupon at the end of Experiment 2 76
Figure 10 - FTIR spectra of Experiment 2 deposit and copper palmitate (RED) 78
Figure 11 - FTIR spectra of Experiment 2 (+) coupon deposits formed at alkaline and at neutral pH 79
Figure 12 - (+) Coupons corroded in milk, red wine and white wine 81
Figure 13 - Coupons used for the synthesis of Cu-carboxylates 82
Figure 14 - FTIR spectra of palmitic acid and Cu-palmitate 83
Figure 15 - FTIR spectra of Cu-carboxylates 84
Figure 16 - FTIR spectra of Cu-carboxylates obtained with a microscope 87
Figure 17 - Raman spectra of palmitic acid and Cu-palmitate 88
Figure 18 - Raman spectra of palmitic acid and Cu-palmitate between 400-130cm^{-1} 89
Figure 19 - Raman spectra of Cu-carboxylates 90
Figure 20 - Raman spectra of oleic acid and Cu-oleate 92
Figure 21 - XPS survey spectrum for Cu-palmitate 93
Figure 22 - Carboxylic acid dimer arrangement 93
Figure 23 - Cu2p spectra of copper, Cu_2O, $CuSO_4$ and Cu-palmitate 95
Figure 24 - Cu2p spectra of Cu-carboxylates 96
Figure 25 - C1s and O1s regions spectra in palmitic acid and Cu-palmitate 97
Figure 26 - Proposed molecular arrangement of Cu-carboxylates 99
Figure 27 - Cu-carboxylates XRD diffractograms 100
Figure 28 - Coupons used for the synthesis of Cu-lactose 105
Figure 29 - Chemical structure of lactose 106
Figure 30 - FTIR spectra of lactose and Cu-lactose 106
Figure 31 - Raman spectra of lactose and Cu-lactose 108

Figure 32 - XPS survey spectrum of Cu-lactose....109
Figure 33 - Cu2p spectrum of Cu-lactose....110
Figure 34 – C1s and O1s regions spectra of lactose and Cu-lactose....111
Figure 35 - XRD diffractogram of Cu-lactose....112
Figure 36 - XRD diffractogram of Cu-lactose showing cuprite as identified mineral phase....113
Figure 37 - EI and CI chromatograms of lactose....114
Figure 38 - EI and CI chromatograms of Cu-lactose....115
Figure 39 - Coupons used for the synthesis of Cu-casein....117
Figure 40 - The general amino acid structure....117
Figure 41 - FTIR spectra of casein and Cu-casein....119
Figure 42 - Raman spectra of casein and Cu-casein....121
Figure 43 - XPS survey spectrum of Cu-casein....123
Figure 44 - Cu2p spectrum of Cu-casein....124
Figure 45 - C1s and O1s regions spectra of casein and Cu-casein....125
Figure 46 - N1s region spectra of casein and Cu-casein....126
Figure 47 - XRD diffractogram of Cu-casein....127
Figure 48 - EI chromograms of casein and Cu-casein....128
Figure 49 - αs1-2 caseins peptide chain with identified peptides in casein (BOLD) and Cu-casein (underlined in RED)....131
Figure 50 - β- and k- caseins peptide chain with identified peptides in casein (BOLD) and Cu-casein (underlined in RED)....132
Figure 51 - FTIR spectra of freeze-dried milk and Cu-milk corrosion....135
Figure 52 - Raman spectra of freeze-dried milk and Cu-milk corrosion....137
Figure 53 - XPS survey spectrum of Cu-milk corrosion....139
Figure 54 - Cu2p spectrum of Cu-milk corrosion....139
Figure 55 – C1s and O1s regions spectra of Cu-milk corrosion....141
Figure 56 – New multi-analytical protocol for analysis of archaeological metal corrosion....147
Figure 57– The Pewsey hoard....149
Figure 58 – Plant remains found inside Vessel B....150
Figure 59– Sampling the Pewsey hoard....152
Figure 60 – FTIR spectra of cauldron samples obtained in ATR mode....153
Figure 61– FTIR spectrum of cauldron rim interior sample....154
Figure 62– FTIR spectra of Vessel A samples....155
Figure 63– FTIR spectra of Vessel B samples....155

Figure 64– Diffractogram of cauldron interior sample 156
Figure 65 – Diffractograms of Vessel A samples 157
Figure 66 – Diffractograms of Vessel B samples 158
Figure 67– EI chromatograms cauldron rim samples 159
Figure 68 – EI chromatograms Vessel A samples 160
Figure 69 – EI chromatograms of Vessel B samples 162
Figure 70 – Top 10 most abundant compounds and their distribution across the samples 165
Figure 71 – "Unique" compounds and their distribution across the samples 166
Figure 72– Pewsey hoard corrosion microclimate 171
Figure 73 – The recent history of the Roman bowl 175
Figure 74 – Sampling the interior of the object 176
Figure 75 – FTIR spectra of green corrosion 176
Figure 76 – FTIR spectra of brown corrosion 178
Figure 77 – Diffractograms of green corrosion 179
Figure 78 - Diffractograms of brown corrosion 180
Figure 79 – EI chromatograms of green corrosion 181
Figure 80 – EI chromatograms of brown corrosion 182
Figure 81 – Most abundant compounds and their distribution across the samples 183
Figure 82 – Most unique compounds and their distribution across the samples 184
Figure 83 – Most common compounds and their distribution across the samples 184
Figure 84 – Pompeii INV10653 and a similar complete specimen 188
Figure 85 – FTIR spectrum of the interior of Pompeii INV10653 190
Figure 86 – Diffractogram of the interior of Pompeii INV10653 191
Figure 87 – XPS survey spectrum and elemental composition of the interior of Pompeii INV10653 192
Figure 88 – C1 and N1 region spectra for urea and the Pompeii INV10653 sample 193
Figure 89 – Cu2p spectrum of the Pompeii INV10653 sample 194
Figure 90 – EI chromatogram of Pompeii INV10653 interior corrosion 195
Figure 91– Pompeii INV10295 199
Figure 92– The different larvae found "mineralized" inside Pompeii INV10295 200
Figure 93 – Sampled areas in Pompeii INV10295 201
Figure 94 – FTIR spectra of samples 6 and 7 of Pompeii INV10295 202
Figure 95 – Pompeii INV10295 (sample 4) diffractogram 204
Figure 96 – Pompeii INV10295 (Sample 6) diffractogram 204
Figure 97– Pompeii INV10295 (Sample 10) diffractogram 205

Figure 98 – Most abundant compounds and their distribution across the samples 208
Figure 99 – Compounds with the highest fold change and their distribution 209
Figure 100 – Most common compounds and their distribution across the samples 209
Figure 101 – Pompeii INV10289 sampled areas 215
Figure 102 – FTIR spectrum of sample 1 216
Figure 103 – FTIR spectrum of sample 2 217
Figure 104 –FTIR spectra of samples 3 and 4 217
Figure 105 – FTIR spectra of samples 5 and 6 218
Figure 106 - Diffractograms of the interior samples 219
Figure 107 – Diffractogram of the exterior samples 220
Figure 108 – Most abundant compounds and their distribution across the samples 224
Figure 109 – Compounds with unusual distribution across the samples 225
Figure 110 – Most common compounds and their distribution across the samples 226
Figure 111– Copper-alloy hydra and the residue 231
Figure 112 – Exterior of the shrine [A], its interior plan [B] and the bronze vessels on display [C] 232
Figure 113– The degradation of honey 233
Figure 114– Sampling the Paestum residue: core [left] and surface [right] 235
Figure 115 – Honeycombs before and after ageing 236
Figure 116 – FTIR spectra of the residue (in RED) and honey 237
Figure 117 – FTIR spectra of the residue (in RED) and beeswax 237
Figure 118 – Partial FTIR spectra of honeycomb from Italy 240
Figure 119 – Partial FTIR spectra of honeycomb from Greece 240
Figure 120 - EI Chromatograms for beeswax, acacia honey and residue core sample 241
Figure 121 – EI chromatograms of the residue's surface samples 242
Figure 122 – Extracted EI chromatograms (mz 60) of residue surface samples 244
Figure 123 – PC1 and PC2 plot for honeycombs and Paestum residue 249
Figure 124 – Hierarchical clustering shown as a dendrogram 250
Figure 125 – Hierarchical clustering shown as a heatmap 251
Figure 126 – Taxa of resin protein matches for the residue 253
Figure 127– XPS survey spectra for the coloured surface of the residue 255
Figure 128 - Cu2p spectra of green and black areas of the Paestum residue 256
Figure 129 – Glucose abundance in the methanol extracts of aged honeycombs and residue 257

List of Tables

Table 1 - Common mineral phases identified in archaeological copper corrosion 53
Table 2 - Compounds used in the copper complexation experiments 61
Table 3 - XRD peak list and phases identified in the deposit on Experiment 1 (+) coupon 74
Table 4 - XRD peak list and phases identified in the deposit on Experiment 2 (+) coupon 77
Table 5 - Characteristic FTIR bands of Cu-carboxylates 86
Table 6 - Carbonyl stretching frequencies and structures of Cu-carboxylates 87
Table 7 - Characteristic Raman bands (cm^{-1}) and assignments for Cu-carboxylates 91
Table 8 - Elemental composition of palmitic acid and Cu-carboxylates 94
Table 9 - Theoretical and experimental C, O and Cu proportions in palmitic acid and Cu-carboxylates 94
Table 10 - C1s and O1s peaks binding energies (BE) for Cu-carboxylates 98
Table 11 – XRD peak list for Cu-palmitate 100
Table 12 - XRD peak list for Cu-stearate 101
Table 13 - XRD peak list for Cu-oleate 101
Table 14 - Cu-carboxylates relative solubilities in acetonitrile, chloroform and methanol 103
Table 15 – Retention times of carboxylate ligands 103
Table 16 - Characteristic FTIR bands in lactose and Cu-lactose 107
Table 17 - Elemental composition of lactose and Cu-lactose 110
Table 18 - Some of the properties of caseins 118
Table 19 - Characteristic FTIR bands of casein and Cu-casein 120
Table 20 - Characteristic Raman bands of casein and Cu-casein 122
Table 21 - Elemental composition of casein and Cu-casein 123
Table 22 - Proteins matches for casein (CSN) and Cu-casein (Cu-CSN) 130
Table 23 - Characteristic FTIR bands of freeze-dried milk and Cu-milk corrosion 136
Table 24 - Characteristic Raman bands of freeze-dried milk and Cu-milk corrosion 138
Table 25 – C1s and O1s binding energies in organic compounds and respective copper complexes 140
Table 26– Identified compounds in freeze-dried milk and Cu-milk corrosion cross-referenced with Cu-organic complexes by QTOF-GC-MS with TSP 142
Table 27 - Identified compounds in the BSTFA-derivatized extracts of freeze-dried milk and Cu-milk corrosion 143

Table 28 – Most intense proteins identified in freeze-dried milk (MILK) and Cu-milk corrosion (Cu-MILK).....144
Table 29 – Description of Pewsey hoard samples.....152
Table 30– Infrared frequencies (cm-1) and band assignments for cauldron interior sample 154
Table 31– Compounds identified in the evaporated chloroform/MeOH extracts of the samples from the interior of Vessel A and Vessel B.....163
Table 32 – Proteins matches for Vessel A and Vessel B samples.....168
Table 33 – Summary of the multi-analytical characterization of the Pewsey hoard corrosion 170
Table 34 – Infrared frequencies (cm^{-1}) and band assignments for green corrosion.....177
Table 35 – Summary of the Multi-analytical characterization of the Roman bowl corrosion 186
Table 36– Infrared frequencies (cm-1) and band assignments for Pompeii INV10653 interior sample 190
Table 37 – Conservator's description of the Pompeii INV10295 samples.....201
Table 38– Infrared frequencies (cm^{-1}) and band assignments for samples 6 and 7 of Pompeii INV10295.....203
Table 39– Compounds identified in Pompeii INV10295 by QTOF-GC-MS with TSP 207
Table 40 – Selected proteins identified in the mineralized larva and in samples 4 and 8 211
Table 41– Summary of the multi-analytical characterization of INV10265 corrosion.....213
Table 42 – Conservator's description of the samples.....215
Table 43 – Infrared frequencies (cm^{-1}) and band assignments for samples 2-4.....218
Table 44– Compounds identified in Pompeii INV10289 samples by QTOF-GC-MS with TSP 222
Table 45– Diagnostic protein matches for Pompeii INV10289 228
Table 46 – Summary of the multi-analytical characterization of Pompeii INV10289 corrosion 230
Table 47– Infrared frequencies (cm-1) for beeswax, residue and honey.....238
Table 48 – Compounds identified in the residue's surface samples monosaccharide furan derivatives highlighted.....243
Table 49– Identified compounds in the diluted water extracts and their relative abundance 246
Table 50 – Unique compounds identified in the water extract of the residue 248
Table 51– Protein identifications in the Paestum residue and honeycombs.....254

List of Appendices

Appendix 1	XRD measurements for copper palmitate recrystallized with chloroform
Appendix 2	FTIR datasets for Cu-carboxylates
Appendix 3	Raman datasets for Cu-carboxylates
Appendix 4	XPS dataset for Cu-carboxylates
Appendix 5	QTOF-GC-MS with TSP datasets for Cu-carboxylates
Appendix 6	GC-MS datasets for the BSTFA-derivatized extracts of Cu-palmitate and Cu-stearate
Appendix 7	XPS datasets for lactose and Cu-lactose
Appendix 8a	QTOF-GC-MS with TSP datasets for lactose
Appendix 8b	QTOF-GC-MS with TSP datasets for Cu-lactose
Appendix 9	XPS dataset for casein and Cu-casein
Appendix 10a	QTOF-GC-MS with TSP datasets for casein
Appendix 10b	QTOF-GC-MS with TSP datasets for Cu-casein
Appendix 11a	Peptides recovered from casein
Appendix 11b	Peptides recovered from Cu-casein
Appendix 12a	QTOF-GC-MS with TSP datasets for freeze-dried milk
Appendix 12b	QTOF-GC-MS with TSP datasets for Cu-milk corrosion
Appendix 13a	GC-MS datasets for the BSTFA-derivatized extracts of freeze-dried milk
Appendix 13b	GC-MS datasets for the BSTFA-derivatized extracts of Cu-milk corrosion
Appendix 14a	Peptides recovered from milk
Appendix 14b	Peptides recovered from Cu-milk corrosion
Appendix 15	Pewsey Hoard: XRD peak lists
Appendix 16a	Pewsey Hoard: QTOF-GC-MS with TSP datasets for cauldron rim samples
Appendix 16b	Pewsey Hoard: QTOF-GC-MS with TSP datasets for Vessel A samples
Appendix 16c	Pewsey Hoard: QTOF-GC-MS with TSP datasets for Vessel B samples
Appendix 17a	Pewsey Hoard: QTOF-GC-MS with TSP datasets for evaporated extracts of Vessel A samples
Appendix 17b	Pewsey Hoard: QTOF-GC-MS with TSP datasets for evaporated extracts of Vessel B Base
Appendix 18	Pewsey Hoard: IC-MS results
Appendix 19	Pewsey Hoard: proteomics results

Appendix 20 Roman Bowl: XRD peak lists
Appendix 21a Roman Bowl: QTOF-GC-MS with TSP datasets for green corrosion
Appendix 21b Roman Bowl: QTOF-GC-MS with TSP datasets for brown corrosion
Appendix 22 Roman Bowl: IC-MS results
Appendix 23 Pompeii INV10653: XRD peak list
Appendix 24 Pompeii INV10653: QTOF-GC-MS with TSP datasets
Appendix 25 Pompeii INV10653: IC-MS results
Appendix 26 Pompeii INV10295: XRD peak lists
Appendix 27 Pompeii INV10295: QTOF-GC-MS with TSP datasets
Appendix 28 Pompeii INV10295: IC-MS results
Appendix 29 Pompeii INV10289: XRD peak lists
Appendix 30 Pompeii INV10289: QTOF-GC-MS with TSP datasets
Appendix 31 Pompeii INV10289: IC-MS results
Appendix 32 Pompeii INV10289: Proteomics results
Appendix 33 Paestum Residue: QTOF-GC-MS with TSP datasets
Appendix 34 Paestum Residue: QTOF-GC-MS with TSP datasets for carboxylic acids
Appendix 35 Paestum Residue: IC-MS results for diluted water extracts
Appendix 36 Paestum Residue: IC-MS results for stock water extracts
Appendix 37 Paestum Residue: IC-MS results for methanol extracts
Appendix 38 Paestum Residue: Proteomics Results

Abbreviations

ATR	Attenuated Total Reflectance
BE	Binding Energy
BSTFA	N,O-Bis(trimethylsilyl)trifluoroacetamide
COD	Crystallography Open Database
ECS	Electrochemical Series
EDS	Energy Dispersive X-ray Spectroscopy
EI	Electron Ionization
EPMA	Electron Microprobe
EPR	Electron Paramagnetic Resonance
FDR	False Discovery Rate
FIA	Flow Injection Analysis
FTIR	Fourier Transform Infra-Red Spectroscopy
GC-MS	Gas Chromatography coupled with Mass Spectrometry
HCA	Hierarchical Clustering Analysis
IC-MS	Ion-Chromatography coupled with Mass Spectrometry
LAB	Lactic Acid Bacteria
LDF	Linear Discriminative Function
LIBS	Laser-Induced Breakdown Spectroscopy
NAA	Neutron Activation Analysis
NMR	Nuclear Magnetic Resonance
PCA	Principal Component Analysis
PGAA	Prompt Gamma Activation Analysis
PSM	Peptide Spectrum Match

PXRF	Portable X-Ray Fluorescence
QTOF-GC-MS	Quadrupole Time-of-Flight Gas Chromatography coupled with Mass Spectrometry
SEM	Scanning Electron Microscopy
TAGs/TGs	Triacylglycerols (also called triglycerides)
TSP	TSP: Thermal Separation Probe
VIMP	Voltammetry of Immobilized Particles
WDS	Wavelength Dispersive Spectroscopy
XPS	X-ray Photoelectron Spectroscopy
XRD	X-ray Diffraction
XRF	X-ray Fluorescence

1. INTRODUCTION

1.1 Background

Organic residue analysis is an established field in archaeological science. The identification of substances used in the past enhances our understanding of cultural practices and everyday life in the past. Although the earliest archaeological residue analyses were undertaken in the early 20th Century,[1] it was the coupling of chromatography with mass spectrometry fifty years later that enabled the chemical profiling of complex organic residues.[2]

The identification of archaeological organic residues is complicated by chemical changes due to the processing of substances (e.g. mixing or cooking) in the past, their degradation during deposition and modern contamination.[3] Notwithstanding these complexities, an increasing number of biomarkers for specific substances[4] are being reported in the literature. Currently these biomarkers are mostly extracted from porous ceramic sherds – their porosity believed to confer some protection against degradation and contamination. Although conservators routinely find fibres, insects and plant remains "mineralized" amidst corrosion covering archaeological copper objects (particularly those recovered from graves),[5] metal corrosion has seldom been considered a locus for organic residue preservation.

[1] Lucas 1911.
[2] Pollard et al. 2007; Colombini and Modugno 2009.
[3] Evershed 2008a.
[4] Condamin et al. 1976; Passi et al. 1981; Morgan et al. 1984; Robinson et al. 1987; Gülaçar et al. 1989; Hurst et al. 1989; Oudemans and Boon 1991; Evershed et al. 1990, 1991, 1994, 1995a,b, 1997, 2002, 2004, 2008a; Connan et al. 1992; Proefke et al. 1992; Charters et al. 1993, 1995; Bethell et al. 1994; Heron et al. 1994; Boëda et al. 1996; McGovern et al. 1999; Simpson et al. 1999; Stern et al. 2003; Guasch-Jané et al. 2004; Colombini et al. 2005; Modugno et al 2006; Ribechini et al. 2008, 2009, 2013; Łucejko et al. 2012; Salque et al. 2013; Saliu et al. 2014; Carrer et al. 2016; Manzano et al. 2016; Brettell et al. 2017; Shoda et al. 2017; Fulcher et al. 2020.
[5] Peška et al. 2006.

The mineralization of organic remains by metal corrosion includes the replacement of the organic matrix with inorganic salts.[6] In the case of copper alloys, preservation of organic residues may include encapsulation of residues by corrosion products, with preservation aided by copper's biocidal properties.[7]

Historically, archaeological metal corrosion has always been considered as the formation of inorganic substances that result from the metal surface's interaction with the deposition environment (i.e. soil, air and/or water). Consequently, studies of archaeological metal corrosion have seldom included analytical techniques targeting organic molecules. In a pilot study of bronze corrosion, Merriman[8] recovered pine resin and oil biomarkers from a *patera* a pan-like object found in ritual contexts throughout the Roman empire. The innovation of Merriman's study was that it targeted corrosion products themselves, as opposed to clearly distinguishable residues found amidst corrosion products of metal vessels.[9]

Because standard methods for organic residue analysis were used, Merriman suggested that these methods would not have recovered organic residues that may be trapped within corrosion as metal-organic or organometallic complexes.[10] Although the study of these compounds,[11] particularly metal carboxylates,[12] is becoming increasingly popular amongst

[6] Gillard et al. 1994.
[7] Pollard *pers. comm.* 27th January 2015.
[8] Merriman et al. 2017.
[9] E.g. Curt et al. 1994; McGovern et al. 1999; Solazzo et al. 2014; Steele 2017; Oras et al. 2017.
[10] Merriman 2014.
[11] Kühn 1970; Scott et al. 2003.
[12] van der Berg et al. 1999; Gunn et al. 2002; Robinet and Corbeil et al. 2003; Verhoeven et al. 2006 and Keune 2005 in Boon et al. 2007; Otero et al. 2014; Cotte et al. 2017.

heritage professionals and painting conservators,[13] their identification in archaeological contexts has seldom been reported.[14]

1.2 Research Objectives

Building on Merriman's preliminary work, this research demonstrates copper corrosion's potential for preserving organic molecules. Through laboratory experiments and using a range of analytical techniques for the characterization of archaeological copper corrosion, this research:

- Proposes a pathway for organic residue preservation in copper corrosion
- Suggests a new multi-analytical protocol for the characterization of metal corrosion
- Evaluates the type of information retrieved from archaeological copper corrosion
- Suggests sampling protocols for organic residue analysis in archaeological metal corrosion

1.3 Thesis Structure

The literature review (chapter 2) consists of three parts. The first part contains a brief account of organic residue analysis in archaeology with examples of targeted molecules and typical analytical techniques used for their recovery and identification. The second part describes the corrosion of copper and its alloys, and the formation of metal-organic complexes. The third part explores the different types of information that may be retrieved

[13] See Casadio et al. 2019 for an overview of the current research on metal soaps.
[14] McGovern et al. 1999; Daniels 2007; Werner et al. 2012; Merriman et al. 2017; Liang and Scott 2014.

from metal corrosion with examples of analytical techniques. The chapter concludes by proposing a new multi-analytical protocol that can identify organic and inorganic substances within archaeological copper corrosion.

To evaluate the new multi-analytical protocol, copper corrosion samples impregnated with organics were produced in the laboratory. A small library of copper-organic complexes was also created to facilitate the interpretation of results. The materials and methods used to produce these samples are described in Chapter 3 alongside the analytical techniques and instruments used in their characterization.

The characterization of the corrosion samples produced in the laboratory and an evaluation of the multi-analytical protocol are presented in Chapter 4. Chapter 5 comprises a series of case studies where the multi-analytical protocol is applied to archaeological samples. A summary of the findings and the conclusion of the research are included in Chapter 6 alongside a proposed sampling protocol and suggested areas for future research.

2. LITERATURE REVIEW

2.1 Organic Residue Analysis in Archaeology

The matching of an organic residue to its origin relies on the "archaeological biomarker concept".[15] Its principle rests on identifying within organic residues a particular compound or distribution of compounds that can act as markers for biological materials known to have been used in the past.

Archaeologists are used to encountering organic remains in the form of visual deposits on the exterior and interior of artefacts. Whilst these deposits may be linked to an artefact's manufacture and/or use (for instance cooking soot, surface finishes and repair), characterization is challenging given degradation of residues during deposition and contamination during and post-excavation. Due to these difficulties, organic residue analysis has evolved from the analysis of surface deposits[16] to targeting organic molecules trapped in porous matrices such as ceramics. This focuses on the recovery of large molecules such as lipids, which are most likely to survive degradation partly because of their hydrophobicity.

2.1.1 Lipids

Lipids are long-chained, hydrophobic molecules[17] commonly found in an archaeological context such as food residues, in rituals (e.g. burials), in cosmetics, medicinal preparations and as fuel (e.g. oil lamps). Some lipids are only produced by a single or small number of

[15] Evershed 2008a.
[16] Evershed et al. 1990.
[17] Evershed 1993.

species of plants or animals, making them biomarkers for these commodities and ideal targets for organic residue analysis.

Although the survival of organic residues is dependent on an artefact's physical and chemical properties and its history and the deposition environment, the general rule is that substances that are more polar are more reactive and thus more susceptible to decay.[18] The polarity of a compound is determined by the difference in electronegativity between its atoms and their spatial arrangement. Due to their low polarity, some of the lipids commonly found in archaeological residues are triacylglycerols, fatty acids, sterols and terpenoids.[19]

2.1.1.1 Triacylglycerols, diacylglycerols and fatty acids

Triacylglycerols, also called triglycerides (TAGs/TGs) are composed of a glycerol backbone and three long-chain carboxylic acids (or fatty acids) represented as R1, R2 and R3 in Figure 1. TAGs/TGs are the main constituents of fats and act as energy stores in animals and plants. They are highly diagnostic but rarely survive intact in archaeological contexts. Their degradation is often due to chemical and enzymatic hydrolysis[20] and oxidative processes[21] generating diacylglycerols or monoacylglycerols. Diacylglycerols contain two fatty acids connected to a glycerol backbone and monoacylglycerols are composed by a glycerol connected to a fatty acid.

[18] Evershed 2008a.
[19] Evershed et al. 2001; Brown and Brown 2011.
[20] Evershed et al. 1991.
[21] McGovern and Hall 2016.

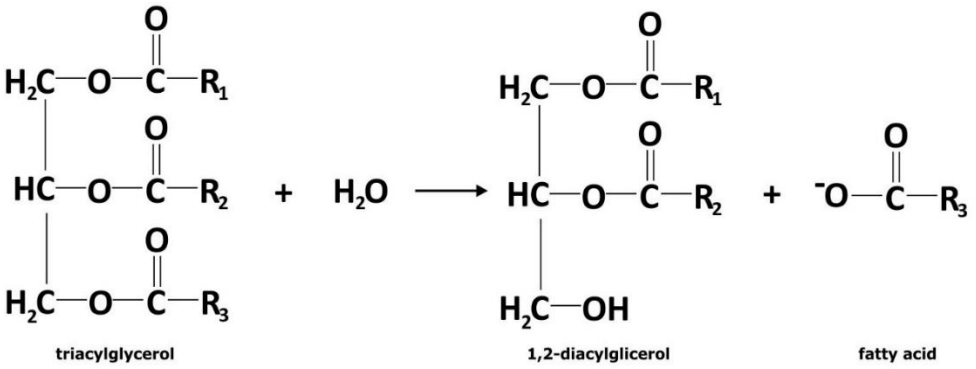


Figure 1 - Schematic hydrolysis of a triacylglycerol

where R1, R2 and R3 are different fatty acids

A fatty acid is called *unsaturated* if its carbon chain contains one or more double bonds. The presence of unsaturated fatty acids in a triacylglycerol molecule lowers their melting point as the double bonds keep the fatty acid chains from aligning uniformly. This explains why plant oils, which contain primarily unsaturated fatty acids, are liquids at room temperature.

The most common fatty acids in triacylglycerols are:

- n-hexadecanoic acid ($C_{16:0}$) a saturated fatty acid with a 16-carbon chain, commonly referred to as palmitic acid
- n-Octadecanoic acid ($C_{18:0}$) a saturated fatty acid with an 18-carbon chain, commonly referred to as stearic acid
- cis-9-Octadecenoic acid, ($C_{18:1}$)[22] an unsaturated fatty acid with an 18-carbon chain containing one double bond, commonly referred to as oleic acid
- cis-9, cis-12-Octadecadienoic acid ($C_{18:2}$) a polyunsaturated fatty acid with an 18-carbon chain containing two double bonds, commonly referred to as linoleic acid

[22] Lipids are named according to the number of carbon atoms in the fatty acid and the number of double bonds in the fatty acid. Palmitic acid $C_{16:0}$ has 16 carbon atoms and 0 double bonds while oleic acid $C_{18:1}$ has 18 carbon and one double bond.

Patterns of fatty acids and mono- and/or diacylglycerols in organic residues can be used to differentiate between fats from animal and plant origins. A high concentration of stearic acid in relation to palmitic acid is sometimes interpreted as an indication of an animal source, their ratios in the R2 position of triacylglycerols being used to differentiate between ruminant and non-ruminant fats.[23] This analogy is now considered problematic, not least because residues can be mixtures including fats from different origins already subject to degradation.[24] However, a distinction is still possible between fats deriving from an animal's carcass and dairy fats by investigating the carbon isotope composition of ruminant fats.[25]

Milk and adipose fats have high proportions of short-chain saturated fatty acids in the C_8-C_{14} carbon number range. They are more susceptible to decay via hydrolysis where they join with a glycerol in a triacylglycerol molecule due to their small size compared to their long-chain counterparts.[26] Laboratory experiments of milk degradation have shown that released short chain fatty acids are more soluble and volatile, perhaps explaining why they are rarely detected in archaeological residues. Identification of dairy is done via stable carbon isotope ($\delta^{13}C$) ratios of the main fatty acids (palmitic and stearic)[27] and other compound markers.[28]

2.1.2 Sterols

Sterols are complex ring derivatives of terpenes, characterized by tetracyclic hydrocarbon structures (see Figure 2) linked to an open chain of carbon atoms. They are important

[23] Evershed et al. 2002.
[24] Evershed 2008b; Nigra et al. 2015.
[25] Mukherjee et al. 2005 in Evershed 2008.
[26] Gurr and Harwood 1991 in Merriman 2014.
[27] Dudd et al. 1999; Copley et al. 2003; Craig et al. 2005; Evershed et al. 2008a; Dunne et al. 2012, 2013, 2019; Salque et al. 2013; Kherbouche et al. 2016; Grillo et al. 2020.
[28] Craig et al. 2000.

biomarkers as their diagnostic value remains unchanged after degradation. Cholesterol is the most common animal sterol while stigmasterol is the most common sterol found in plants.[29]

Some sterols have side chains that terminate in a carboxylate group such as bile acids. Bile acids are synthetized by the liver and help breakdown fats in the intestine. They are excreted in faeces and are therefore biomarkers for the use of manure in archaeological land management contexts.[30] Sterols are only a minor constituent of fats and oils so they may be undetectable within archaeological residues.[31]

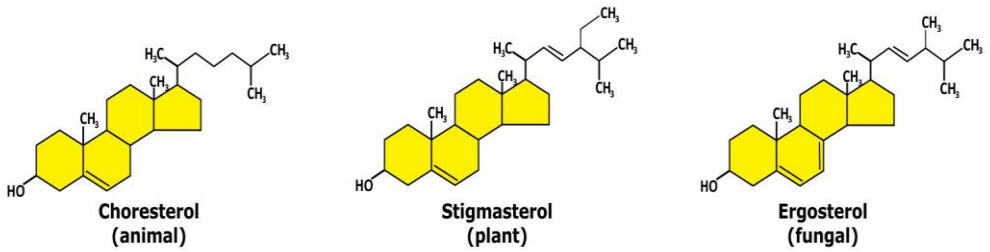


Figure 2 - Examples of Sterols

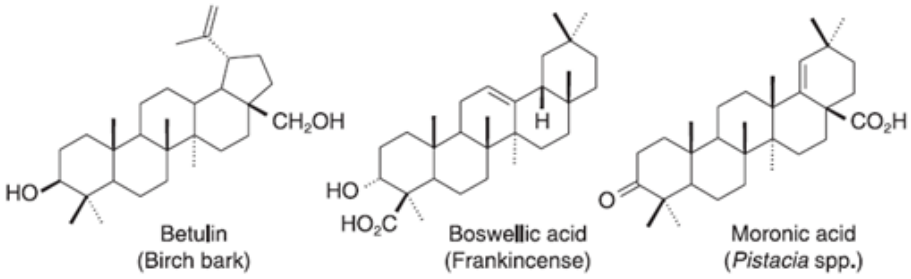
tetracyclic hydrocarbon structures in YELLOW

2.1.3 Terpenes and Terpenoids

Terpenoids are derivatives of terpenes. They are the main constituents of natural resins and gums with a chemical structure based on *isoprene* units, used in their classification.[32] When heated terpenes produce tars and pitches,[33] which were widely used by past societies as

[29] Evershed 1993.
[30] Brown and Brown 2011.
[31] Evershed 1993.
[32] Mills and White 1994.
[33] Mills and White 1977.

sealants and adhesives,[34] for embalming,[35] as paint binders,[36] in rituals[37] (e.g. incense) and in medical treatments.[38] Terpenoids (Figure 3) are excellent biomarkers because they are readily extractable with organic solvents and easy to identify by their characteristic molecular fragmentation when using mass spectrometry techniques.



Source: Evershed 1993

Figure 3 - Examples of terpenoid biomarkers

Monoterpenoids and sesquiterpenoids are based on 10 and 15 carbons and are the main constituents of essential oils. Due to their volatility they are not normally found in an archaeological context unless the sample being analysed has been removed from the centre of a block of resin. Diterpenoids containing 20 carbon atoms are mainly found in coniferous and leguminous resins[39] such as pine and copals.[40] Abietic acid is a major diterpenoid compound and its oxidation products (dehydroabietic acid and 7-oxodehydroabietic acid) in archaeological samples indicate the presence of pine resin.[41] Triterpenoid skeletons have 30 carbon atoms and have tetracyclic or pentacyclic structures. They are the main constituents

[34] E.g. Boëda et al. 1996; Stacey et al. 1998; Serpico and White 2000; Regert and Roland 2002; Colombini et al. 2003; Connan and Nissenbaum, 2003; Regert et al. 2003; Helwig et al. 2008.
[35] E.g. Buckley et al. 1999; Buckley and Evershed 2001; Koller et al. 2003.
[36] E.g. van der Berg et al. 2000; White and Kirby 2001; Scaralone et al. 2003.
[37] E.g. Stern et al 2003; Baeten et al. 2014; Bruni and Guglielmi 2014.
[38] E.g. Stacey 2011; Steigenberger and Herm 2011; Giachi et a. 2013.
[39] van der Berg et al. 2000.
[40] Mills and White 1994.
[41] Evershed 1993; Mills and White 1977.

of gum resins (e.g. frankincense and myrrh) and are never found in the presence of diterpenoids.[42]

2.1.4 Methods for Analysis of Organic Residues

The focus of organic residue analysis in archaeology has been the recovery of lipids from ceramic sherds which are used because of their porosity and the fact that they are the most common artefact recovered in archaeological excavations.[43] Absolute and relative recovery yields of lipids depend on many factors including the various molecules' affinity to the ceramic matrix, their chemical stability and the efficiency of extraction and detection techniques.[44] The most common method for the recovery of lipids is based on solvent extraction followed by separation and identification using gas chromatography coupled with mass spectrometry (GC-MS).[45] GC-MS is normally limited to soluble and thermally-stable molecules that can be made volatile by derivatization.[46] Notwithstanding these limitations GC-MS remains the most popular technique in archaeology as the data it generates, electron ionization (EI) fragmentation patterns of compounds in the sample, can be compared against mass spectral reference libraries for identification.[47]

In archaeological contexts, organic residues may be found as the actual contents of vessels, as visible surface deposits or absorbed into porous matrices.[48] The extraction yields of absorbed residues is dependent upon their distribution within the vessel[49] and the contact

[42] Evershed 1993.
[43] Evershed 2008a; Nigra et al. 2015.
[44] Barnard et al. 2007.
[45] Mills and White 1987.
[46] Colombini et al. 2009; Degano et al. 2018.
[47] Nigra et al. 2015.
[48] Evershed 2008.
[49] Charters et al. 1993, 1997; Stern et al. 2000.

between solvent and ceramic matrix.[50] Treating ceramics with an alkali or acid increases recovery of organic residues thus indicating that certain types of lipids may be chemically bound to the ceramic matrix.[51] Goldenberg et al.[52] demonstrated that archaeological and modern ceramic matrices rich in calcium minerals (particularly calcite - $CaCO_3$) have an affinity for unsaturated organic compounds. This effect is explained by the ability of the polar fraction of organic molecules (i.e. carboxylate groups in fatty acids) to ionise, thus having a similar chemical behaviour as carbonate groups.[53]

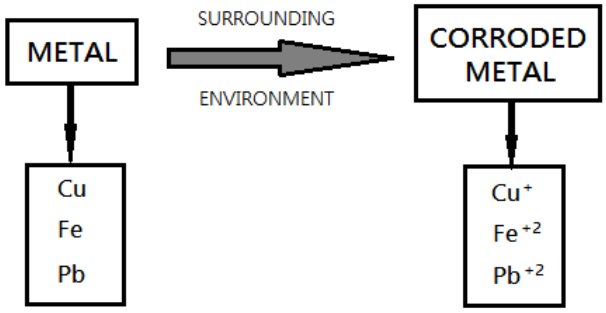
Metal surfaces would not normally be expected to have absorbent properties. Therefore an understanding of metal corrosion processes is the starting point for an evaluation of its potential for preserving organic residues.

2.2 Principles of Metallic Corrosion

Some metal elements are found in nature in a metallic state and are mostly stable. Others are found as mineral deposits. The energy required to extract these metals is the same energy that is released as they interact with the surrounding environment to form more thermodynamically stable compounds. Corrosion can be defined as the release of energy as the solid metal oxidizes, transforming into positive ions by losing electrons (Figure 4).

[50] Evershed et al. 1990, 2002.
[51] Regert et al. 1998; Stern et al. 2003; Correa-Ascencio and Evershed 2014.
[52] Goldenberg et al. 2014.
[53] Carter 1978 in Goldenberg et al. 2014.

The reactivity of a metal is often expressed by its electrode potential (E°), measured in relation to a reference electrode (e.g. hydrogen electrode) when immersed in an electrolyte (e.g. water) at 25°C and 1 atmospheric pressure and reported in Electrochemical Series (ECS). E° values for the ionization reaction of some common metals are included in Figure 4 - the more positive the E° value the less reactive the metal. The reactivity of some metals (e.g. aluminium) can sometimes contribute to their stability because of the creation of a protective oxide layer. In addition to ECS, there are Galvanic Series, which are used to predict the relative tendency of metals and alloys to corrode in a given environment (e.g. sea water).



Name	Reaction	E° (V)*
Aluminium	$Al \rightarrow Al^{+3}$	-1.66
Zinc	$Zn \rightarrow Zn^{2+}$	-0.76
Iron	$Fe \rightarrow Fe^{2+}$	-0.45
	$Fe \rightarrow Fe^{3+}$	-0.04
Tin	$Sn \rightarrow Sn^{2+}$	-0.14
Lead	$Pb \rightarrow Pb^{2+}$	-0.13
Copper	$Cu \rightarrow Cu^{2+}$	+0.34
	$Cu \rightarrow Cu^{+}$	+0.52
Silver	$Ag \rightarrow Ag^{+}$	+0.80
Mercury	$Hg \rightarrow Hg^{2+}$	+0.85
Gold	$Au \rightarrow Au^{3+}$	+1.50

*Source Vanýsek 2010

Figure 4 - Metallic corrosion and ionization potential for some common metals

Corrosion can be described as a chemical or electrochemical process. Chemical corrosion involves the local transfer of electrons between materials. Electrochemical corrosion involves the transfer of electrons from one location (or surface) to another with the help of a conductor (or electrolyte). The electrochemical corrosion process consists of two main

reactions: the oxidation of a metal (*anode*) and the reduction of an oxidizing agent (*cathode*) in the presence of an ionic connection (*electrolyte*). The most common electrolyte is water in the form of air humidity, rain or seawater. The corrosion of copper in water can be expressed by the following reaction:

$$Cu^{+} \tfrac{1}{2}O_2 + H_2O \rightarrow Cu^{2+} + 2OH^{-}$$

This can be broken down into the following half reactions:

ANODE $Cu \rightarrow Cu^{2+} + 2e^{-}$

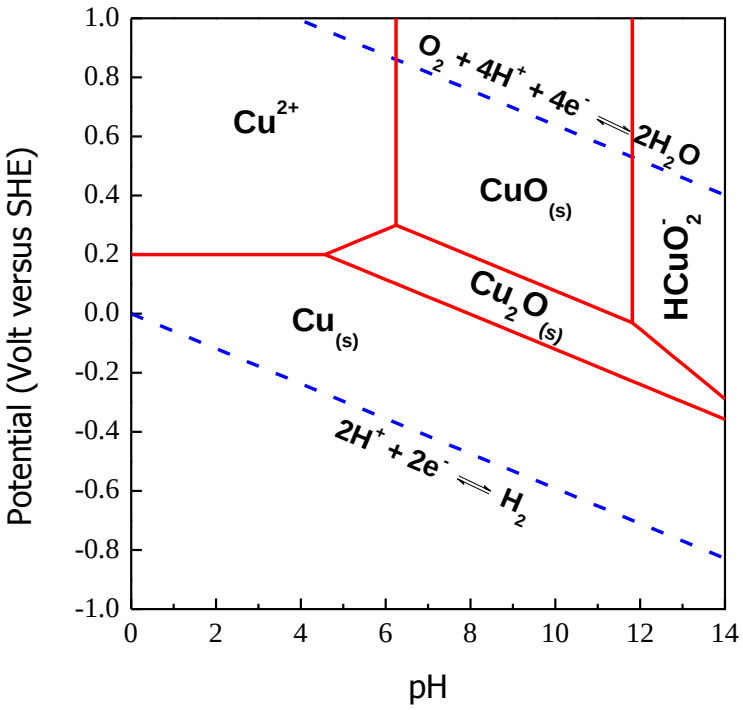
CATHODE $\tfrac{1}{2}O_2 + H_2O + 2e^{-} \rightarrow 2OH^{-}$

The increase in pH (given the production of OH^{-} ions) allows the precipitation of slightly soluble salts, copper oxides or hydroxides, which can form a uniform passive layer over the object.

The intensity of the corrosive process is a function of endogenous and exogenous factors. Examples of endogenous factors include alloy composition, process of manufacture, size and shape of the object. Amongst exogenous factors are the presence of oxidising agents, microorganisms, acidity or alkalinity (pH), oxygen levels, humidity and temperature of the environment to which the metal object is exposed.

Corrosion studies use thermodynamics concepts to predict corrosion phenomena. A common tool is a Pourbaix Diagram, which plots the redox potential of a system (E_h) against its pH at a fixed concentration of ions in an aqueous medium temperature and pressure. These diagrams are based on various assumptions which are discussed in detail in corrosion

textbooks.[54] Many software packages exist to help generate them. Figure 5 shows a simple Pourbaix Diagram for a copper-water system. Regions where active corrosion takes place are those containing ions (Cu^{2+}, $HCuO_2^-$ and CuO_2^-), which are more stable species than metallic copper. The other regions are those where metallic copper would not corrode or corrode slowly through the formation of passive layers.



Prepared by Dr M F de Souza Teixeira

Figure 5 - Cu-H_2O Pourbaix Diagram showing the most stable species

1 x 10^{-6} M Copper, 298K and 1 atmospheric pressure

A range of conditions can be found in the natural environment. Normally pH levels range from acidic (e.g. pH 4 in peat bogs) to alkaline (e.g. pH 9 in water flowing over limestone). The potential (E_H) scale is usually correlated with the presence of free oxygen, the more aerated environment corresponding to the highest potential values. The corrosion potential

[54] Pourbaix 1973; Davis 2000; Stansbury and Buchanan 2000.

of a metal (E_c) and the pH of the aqueous phase are then plotted onto a suitable Pourbaix Diagram to help predict the condition on the surface of the metal. In practice, many micro-environmental conditions can exist at the metal surface, thus limiting the utility of these diagrams.

Thermodynamics can predict the formation of corrosion products but not corrosion kinetics. The formation of insoluble green copper carbonate hydroxide (malachite) can be predicted on a copper-alloy object buried in a soil containing carbonate ions. If conditions are such that a uniform layer of malachite is formed over the whole surface of the object, corrosion rates would be low as the metal underneath is protected from further corrosion. However numerous factors influence the corrosion of metal objects in the soil. One factor influences many others with all factors feeding back into the corrosion environment. If conditions are such that a corrosion product does not precipitate on the metal surface, or if the corrosion product is soluble or unstable or lacks uniformity, corrosion rates would be faster.

Most archaeological metal objects are found in a corroded state. Corrosion products are often mixtures of compounds which may include intentional or unintentional surface finishes (commonly referred to as “patinas”) that result from the object’s manufacture, use and its interaction with the deposition environment. Corrosion may cover the whole object or only part of it, protect the metallic surface or disfigure it with craters or growths. The most common metals found in archaeological sites are copper, iron, lead, silver and gold, sometimes mixed amongst themselves and/or including other chemical elements to form alloys or as multi-metallic objects (e.g. gold inlay on iron).

2.2.1 Corrosion of copper and its alloys

Copper's main oxidation states are +1 and +2. Archaeological copper-based objects are normally found covered by layers of corrosion of variable thicknesses and consistencies. The outer layers are sometimes composed of blue-green Cu(II) corrosion products such carbonates, sulphates and chlorides.[55] Sometimes under this layer is a primary powdery red or dark compact layer of Cu(I) oxide close to the surface of the object, preserving its original shape.

The most common Cu(II) mineral compounds found on copper objects recovered from soils are copper carbonates: malachite and azurite. Malachite [$Cu_2CO_3(OH)_2$] is formed when an object comes into contact with ground water rich in carbon dioxide with azurite [$Cu_3(CO_3)_2(OH)_2$] being formed in drier conditions. If chloride ions are present, the inner corrosion layer may contain nantokite [CuCl] deposited in pits on the surface of the object. With a grey waxy consistency (sometimes stained green) nantokite converts to hydrochloric acid and cuprous chloride in the presence of moisture and oxygen. The acid then attacks any remaining metal to form more cuprous chloride and hydrochloric acid until no metal is left, a problem known as "bronze disease".[56]

Copper is found commonly alloyed with tin, zinc and lead. Tin compounds can be detected within the outer and/or inner corrosion layers of copper-tin alloys,[57] the latter promoting copper diffusion through its pores.[58] Tin oxides are more stable and less soluble than copper

[55] Meyer-Roudet 1999; Scott 2002.
[56] Scott 1990.
[57] Robbiola et al. 1998.
[58] Robbiola and Fiaud 1992 in Piccardo et al. 2013.

carbonates and are thus present at higher concentrations in the outer corrosion layers of copper-tin objects than the inner layers.

White zinc corrosion products are sometimes found amidst the corrosion layers covering copper-zinc alloys. Given their high solubility, they leave behind a surface rich in copper. Copper-zinc alloys containing less than 15% zinc tend to be less prone to dezincification. Copper-lead alloys might display spots of white lead carbonates when lead was originally present in high concentration and is now found separated in the form of small aggregates on the surface of the metal.[59]

In marine environments, the toxic Cu(I) oxide layer inhibits the colonization of the surface of objects by marine creatures.[60] However, if this protective film is broken and/or converted into Cu(II) products, colonization will occur.[61] Copper sulfides will precipitate over the surface of the object under anaerobic conditions but marine growth over this layer will be supported if there is an increase in oxygen levels. If less noble metals (such as iron) are close to copper objects, an electrochemical cell will form. Consequently, the local pH will increase, facilitating the formation of a concretion due to the precipitation of calcium carbonate over the inert copper object substrate.[62]

Sulfate-reducing bacteria, which are common in waterlogged soils and underwater, produce high levels of hydrogen sulfide or elemental sulphur. Copper sulfides (the most common

[59] Selwyn 2004.
[60] see Borkow and Gabbay 2005 for more details.
[61] Efird 1976 in MacLeod 1982.
[62] MacLeod 1982.

being chalcocite) have been identified on copper alloy objects recovered from these environments. Microbial activity has also been linked to the formation of "tentacle like" corrosion morphology (when the metal surface is viewed in cross-section) in all types of deposition environments.[63]

Iron-containing copper sulfides have also been identified on copper alloy objects recovered from anaerobic soils. Chalcopyrite often has a golden yellow colour, resembling gilding when precipitated on the surface of an object. It is therefore sometimes difficult to decide whether the sulphides were deliberately applied as a surface finish at the point of the object's manufacture or the result of a microbiological attack during deposition.

Studies of archaeological corrosion have mainly focused on the identification and characterization of inorganic compounds using X-ray diffraction and occasionally in conjunction with Fourier Transform Infrared and Raman - the exception being microbial corrosion, which can also result in organic metabolites.[64]

2.2.2 Metal-organic complexes

Metals can combine with carboxylic acids, amino acids, proteins and saccharides to form metal-organic complexes, compounds that lack a direct metal-carbon interaction. The coordination of a metal ion with a long-chain aliphatic carboxylic acid (i.e. fatty acid) results

[63] Ghiara et al. 2019.
[64] ibid.

in a ‘metal soap’. Metal soaps have wide applications such as anticaking, wetting, waterproofing and as an antimicrobial/fungicidal and siccative agent.[65]

The identification of metal soaps is a popular topic in the conservation of paintings and metal/organic composite objects. In paint systems, metal soaps are formed spontaneously as metal ions from pigments and metallic substrates react with fatty acids from the paint media. Within 50-100 years, lipids in oil paint undergo autoxidation[66] and hydrolysis forming glycerol, fatty acids, diacids and other cross-linked compounds. Environmental factors contribute to these reactions which are catalysed by certain metal ions.[67] In spite of the degradation of the paint media it is perhaps the rapid[68] coordination of metal ions with newly-formed acid groups that ensures the painting’s survival.[69] This stabilizing effect of metal soaps is often contrasted with efflorescence, darkening and delamination of old paintings – all attributed to their precipitation.[70]

The most common techniques for the identification of metal soaps in paintings are Raman and FTIR microscopy.[71] Lead[72] and zinc[73] soaps are the most common metal soaps found in oil paintings, with copper soaps present in green glazes[74] and pigments[75] such as verdigris and *beeswax green*.[76] Verdigris can react with proteinaceous paint media such as egg

[65] Cotte et al. 2017.
[66] Porter 1986.
[67] van den Berg 1999.
[68] Schrenk 1991 in Schrenk 1994.
[69] van den Berg et al. 1999; Schilling et al. 2007; Verhoeven et al. 2006 and Keune 2005 in Boon et al. 2007.
[70] O’Neill and Brett 1969 in Robinet and Corbeil 2003; Brühl 2014; Cotte et al. 2017.
[71] Meilunas et al. 1990; Otero et al. 2014; Sotiropoulou et al. 2016.
[72] Keune et al. 2019.
[73] Osmond 2019.
[74] Cotte et al. 2017.
[75] Gunn et al. 2002; Poli et al. 2017.
[76] Daniels 2007.

tempera, causing its degradation.[77] Metal ions in pigments can also react with terpenoid acids derived from resins forming metal-carboxylate complexes.[78]

Driving the study of metal-organic complexes in art is the conservators' preoccupation with their negative impact on the aesthetic quality of paintings. However, these compounds also present an opportunity to curators and archaeologists (in the case of archaeological material) as they preserve a portion of the original organic substance with which they have come into contact in the past. Copper soaps have been found in composite archaeological metal objects where copper alloy fittings are in contact with leather[79]and animal fat,[80] sculptures coated with oils[81] and waxes,[82] and on painted copper surfaces.[83] Metal soaps have also been found on museum objects corroded by acids generated by degraded storage materials such as polyurethane foam.[84] It is therefore possible that these compounds may be found mixed with inorganic metal corrosion products.

Copper-organic complexes have been found in mineralized textile fibres preserved in archaeological copper objects.[85] Laboratory experiments and data from archaeological samples demonstrated that cellulose fibres (such as cotton and linen) appear to bind to copper ions through hydroxyl groups, while protein fibres (for instance silk and wool) form complexes via carboxyl and amide groups.[86] Wool fibres are most susceptible to copper

[77] Khandekar and Phoenix 1999 in Scott 2002.
[78] Gunn et al. 2002; Doménech-Carbó et al. 2006; Poli et al. 2017.
[79] Werner et.al. 2012.
[80] Tilbrooke 1980.
[81] Schrenk 1994.
[82] Burmester and Koller 1987.
[83] Pavlopoulou and Watkinson 2006.
[84] Korenberg 2006.
[85] Gillard et al. 1994.
[86] Gillard and Hardman 1996.

uptake with the oxidation of its sulfide bonds catalysed by Cu(II) ions forming copper(II) carboxyl complexes. Although mineralized fibres are normally identified by their morphology, even fibres that appear completely mineralized appear to retain enough organic material to permit fibre identification via FTIR.

2.3 Information from Archaeological Metal Corrosion

The presence of corrosion is sometimes perceived as an obstacle to the study of archaeological metal objects because it obscures the metallic surface of objects. Nevertheless, corrosion layers themselves contain information about the object's manufacture, use and deposition.

2.3.1 How the object was manufactured

Information about the shape, raw materials and techniques used to make a metal object can sometimes be found preserved within inner corrosion layers. Inner corrosion layers are usually denser than outer layers and seldom incorporate external inclusions such as soil grains and dirt. The inner corrosion layer of copper objects can sometimes conform to their original shape, thus conferring some protection to the metal core. Iron corrosion is often a more disruptive process. Iron's inner corrosion layers are not easily distinguishable from the outer corrosion layers; often little or no metal is left preserved underneath it.

Corrosion products can also replicate macro details of an object's fabrication. Rehren et al.[87] used neutron radiography to document a set of completely corroded 5,000-year-old Egyptian iron beads with no visible holes for stringing. Radiographs taken in different orientations revealed that the beads were originally tubular in shape, made from rolled-up thin metal sheets overlapping at the seams.

Some idea of the original alloy composition can be gained from characterization of corrosion layers via cross-section analysis, with ion migration and preferential corrosion processes evaluated across all layers. Groups can be established based on major and minor elements, in a similar way to the analysis of metals. The elemental composition of the Egyptian iron beads mentioned above was found to be very similar to corroded meteoric iron.[88] Given the natural brittleness of meteoric iron, its transformation into thin metal sheets would have required many cycles of hammering and heating testifying to the high skill of the metalsmiths who made the beads. [89]

An important question to consider when studying archaeological metal artefacts is their original appearance. Ancient and historical records document metallurgical and chemical processes used to change the colour and texture of metallic surfaces.[90] Of particular relevance to the study of corrosion are those processes applied in antiquity to modify the surface of the alloy (often via oxidation) to create a particular colour, commonly referred to as "intentional patinas".[91] There is much debate amongst scientists over intentional patinas

[87] Rehren et al. 2013.
[88] ibid.
[89] Rehren et al. 2013
[90] La Niece and Craddock 1993.
[91] For more information on patinas see Craddock and Giumla-Mair 1993a.

as often their characterization is based on the identification of mineral phases that contain the same inorganic compounds that can result from the interaction between a metal object and the deposition environment.[92] Some researchers argue that specific characteristics of the mineral phase may support its identification as an intentional patina. An example is "black bronze" or "black copper", a dark patina identified on archaeological copper alloy objects containing small amounts of gold, and sometimes silver from Egypt,[93] the Roman Empire, China (known as *wu-tong*) and Japan (*shakudo).* [94]

Characterization studies have shown that this black patina is often composed of cuprite with gold and/or silver particles.[95] Experiments demonstrated that the presence of metallic gold and silver affects the optical properties of cuprite, which is naturally red,[96] and promotes homogenous formation and better adhesion of the patina to the metal substrate.[97] Dark patinas with different compositions and without any gold or silver have also been identified within the same culture, thus representing different socioeconomic traditions for the adoption of one recipe over the other.[98]

Evidence of other types of decorative techniques are also preserved in corrosion products. Pattern-welding, where pieces of metal of different compositions are hammered together to create a decorative motif, is an example of such a technique.[99] Other aspects of manufacture that may be found amidst corrosion products are traces of casting material, inlays and

[92] E.g. Born 1993; Franke and Mircea 2005; Berger 2015.
[93] La Niece et al. 2002; Mohamed and Darweesh 2012.
[94] Craddok and Giumla-Mair 1993b; Aucouturier and Darque-Ceretti 2007; Benzonelli et al. 2017.
[95] Mathis et al. 2007.
[96] Aucouturier et al. 2010.
[97] Benzonelli et al. 2017.
[98] Mohamed and Darweesh 2012.
[99] See Gilmour 2017 for more information on the technique and the archaeological evidence.

gilding. Organic remains are also found in composite objects such as shields, boxes, belts and swords.

The best preservation of organic material is found in copper corrosion due to its biocidal properties.[100] Organic remains are found in corrosion products as "negative" or "positive" impressions. If the organic material decays, it leaves behind a hollow case and a negative impression on the encapsulating corrosion matrix. Whereas in positive impressions, the mechanisms are thought to include the formation of metal organic complexes prior to mineral deposition.[101]

2.3.2 How the object was used

Corrosion products can preserve macro and micro-organic remains that are related to how the object was used in the past. An example of macro remains are textile fibres found on the back of metal brooches. At the micro scale there are remains of organic substances that were in contact with the object, such as protective coatings. Historical accounts such as Pliny the Elder's (Roman author - AD 23/24–79), describe the application of oil, bitumen and pitch to copper alloy objects to create protective patinas against fire damage and corrosion,[102] and this can be detectable in the interface between the metallic surface and inner corrosion layer.[103]

[100] Sibley and Jakes 1982; Janaway 1985; Edwards 1989; Gillard et al. 1994; Chen et al. 1998; Angiorama et al. 2020; Scott 2002.
[101] Gillard and Hardman 1996.
[102] Craddock and Giumlia-Mair 1993.
[103] Paparazzo 2003.

2.3.3 Where the object was deposited

The bulk of corrosion products found on archaeological metal objects are formed as a result of the object's interaction with the deposition environment, thus preserving physical and chemical information about that environment with any variations therein (e.g. change in water levels) being "recorded" in the corrosion layers.

Some corrosion products may be formed during the first few years of deposition. Corrosion products that can be associated to past human activity are particularly relevant to archaeology. Identification of copper phosphates in the corrosion layers of copper alloy objects is often used as evidence of human activity.[104]

The least common copper phosphate is libethenite, often associated with cremation sites. Fan and Freestone[105] identified libethenite and pyromorphite in corroded swords recovered from tombs dating from 475–221 BC in Chongping, China. The researchers attributed the formation of these compounds to the practice of attaching swords to the waist of the deceased, the decomposing body being the source of phosphate ions. Scott and Maish's[106] examination of a Lydian metal bed dating from 505BC revealed unusual corrosion products formed at different periods due to fluctuating ground water levels. A particularly interesting discovery was the occurrence of sampleite as a result of the contact between a decomposing body (the source of calcium and phosphorus) to the bed's copper lattice. A decomposing

[104] Figueiredo et al. 2015.
[105] Fan and Freestone 2017.
[106] Scott and Maish 2010.

body was also likely to be responsible for the higher-than-expected levels of phosphorus found in the corroded ancient Egyptian iron beads studied by Rehren.[107]

Another type of depositional evidence can be found in natural residues preserved within corrosion products. These include random vegetation remains, pupa cases of insects from eggs laid on bodies prior to burial and vegetation deliberately placed in graves. Tardigrades (micro invertebrates) have been found preserved within the corrosion of Anglo-Saxon grave goods,[108] their presence often used as a proxy for the deliberate addition of moss to the grave. Seeds and pollen are also found within corrosion.[109] They are very diagnostic and, when the deposition environment is not conducive to organic preservation, are the only surviving archaeobotanical evidence about the archaeological context in which the object was found.

2.3.4 Analytical Techniques

The ideal analytical protocol for analysis of archaeological corrosion products would include a variety of techniques, their choice dictated by research questions and curatorial constraints. Is the focus of the research a single object or a group of objects? If sampling is permitted, are they representative of the whole object? For organic residue analysis, samples may be required from the exterior and interior of the object with strategies designed to avoid the contamination of the samples during excavation, storage and transport for analysis. For large or multiple objects, it may be possible to remove samples that include the metal core so that the whole stratigraphy of the corrosion layers may be examined. Another consideration is

[107] Rehren et al. 2013.
[108] Goodburn-Brown *pers. comm.* 2019
[109] ibid.

sample preparation. If the aim of the research is to study the distribution of elements or compounds within corrosion layers, the sample must be mounted in resin to preserve its structure for cross-section examination. Otherwise, the sample may be ground to a powder and analysed in bulk. There is an ever-increasing number of techniques from material sciences, physics and organic chemistry being used to study archaeological material. However, their restricted availability and high operating cost mean that their use is not yet widespread.

Analytical techniques can be classified under three categories:

- Imaging techniques
- Techniques that provide elemental composition
- Those that provide structural composition

Below are some of the techniques available under each category.

2.3.5 Imaging Techniques

Preliminary information on the distribution of corrosion products according to their different hues is done using an optical microscope with photographs taken to document the stratigraphy of corrosion layers and the presence of macro-organic remains.

Radiography is often the first step taken in the documentation of an archaeological metal object, particularly those made of iron and its alloys whose surfaces are obscured by thick corrosion deposits. The advantage of radiography is that it is not intrusive, with images

taken in various orientations providing information about the shape of the object and guiding sampling and conservation interventions. X-ray is the most widely available radiography technique. It shows any remaining metal core as white or, in the case of completely corroded objects, as void areas surrounded by the haloed contour of inner corrosion layers. A less common radiography technique uses a neutron beam which penetrates heavy elements whilst showing light elements in high contrast. As a result, neutron images reveal details invisible to X-rays such as manufacturing information preserved by the morphology of corrosion products.[110]

Scanning electron microscopy (SEM) is commonly used for producing higher magnification images. The technique measures the interaction of the sample with an electron beam, with images being generated by secondary and backscattered electrons. Analysis requires samples to be removed from the object, although some bench models have experimental chambers big enough to accommodate small brooches. SEM is particularly useful for documenting the stratigraphy of corrosion layers when samples are mounted in cross-section. In backscattered mode, heavier atoms appear lighter, making gilding layers easily distinguishable. Images obtained with secondary electrons are ideal for documenting morphological characteristics of organic remains. Depending on the image resolution of the equipment, they can be used for identification of corrosion products via their characteristic crystalline morphology. For example, "curly" structures in copper corrosion are normally associated with malachite,[111] while needle-shaped crystals in iron corrosion are characteristic of hydrohematite.

[110] Deschler-erb et al. 2004.
[111] Nienhuis et al. 2016.

2.3.6 Elemental composition

Elemental composition of a sample is expressed by the chemical elements and their relative ratios in the sample.

A powerful technique for the elemental characterization of corrosion products is the combination of scanning electron microscopy with energy dispersive X-ray spectroscopy (SEM-EDS), which enables qualitative and semi-quantitative elemental composition analysis of the area of interest. Although SEM-EDS is a surface technique, it enables the study of ion migration through the stratigraphy of corrosion layers via distribution maps of major and minor constituent elements. Koleini[112] used SEM-EDS to analyse corroded iron artefacts dating from 825–1220 BC. Remnant structures of two phases of bloomery[113] inclusions were visualized in cross-section with the identification of grains of silica and changes in oxygen and iron ratios between the layers being indicative of different corrosion products. Given the uneven nature of the iron corrosion, these features were the only indication of the limit between the "original" surface of the object and the deposition environment.

A similar instrument to SEM-EDS is the electron microprobe (EPMA), which permits the elemental characterization of areas as little as 1-2 microns required for the identification of patinas. By using wavelength dispersive spectroscopy (WDS) the probe can provide absolute quantification of elements, although the sample must be flat and finely polished to remove any possibility of interference with the electron signal.

[112] Koleini et al. 2013.
[113] a type of furnace capable of smelting iron from its oxides.

Another popular technique is X-ray fluorescence (XRF). It measures the interaction of the sample with an X-ray beam. Its classical set up requires the sample to be ground to a powder but the availability of portable XRF (pXRF) and its relative low cost make the technique particularly popular amongst field archaeologists and curators. Despite its limitations,[114] pXRF enables different areas of the object to be analysed with minimal effort with results used for grouping objects according to major element constituents. Given the limited depth of penetration of the technique, the information obtained is limited to the surface of the corrosion layer.

The bulk elemental composition of corrosion layers can be determined non-destructively by neutron activation analysis (NAA). The technique measures the gamma-rays emitted by a sample irradiated with a neutron beam. Measures of the irradiated sample are taken at different time intervals to enable the identification of short-lived and long-lived chemical species. A variation of this technique is prompt gamma activation analysis (PGAA) which measures the prompt gamma rays emitted by the sample as it is irradiated. As the neutron beam can penetrate several centimetres into the sample, it is possible to obtain its bulk elemental composition which covers a wide range of elements with high sensitivity and accuracy. NAA had been the standard analytical technique in archaeology since its invention,[115] with the first studies of metal objects (whole coins) published in 1958.[116] However, a decrease in neutron irradiation facilities alongside new research agendas later facilitated its replacement by other analytical techniques.[117]

[114] Nørgaard 2017.
[115] Pollard et al.2007.
[116] Emeleus 1958; Kraay 1958.
[117] Pollard et al. 2007.

Stratigraphic elemental characterization of corrosion layers with minimal sample requirements can be obtained by laser-induced breakdown spectroscopy (LIBS). The technique measures emissions from the sample as it is ionised into the plasma state by a pulsating incident laser beam. Successive pulses on the same spot can provide depth-profiling elemental composition information thus helping map metal ions migration between layers whilst causing minimal damage.[118] LIBS analysis is performed by placing the object inside an experimental chamber or directly onto the object using optical fibre cables to deliver the laser beam and collect data. This analytical set up enables analyses to be carried out even under water.[119]

A useful technique for the study of corrosion is X-ray photoelectron spectroscopy (XPS). The technique measures the energy of the photoelectrons (50–2000eV) emitted when the surface of a sample is bombarded with X-rays. XPS provides elemental characterization and their chemical state within the sample. The technique is useful for identification of patinas when archaeological samples are analysed in cross-section.

2.3.7 Structural composition

The structural composition of a sample is expressed by the type and ratio of compounds in the sample. The identification of a specific compound in the corrosion layer is sometimes the most interesting piece of information. For example, it is the presence of red hematite in the corrosion of an iron object that indicates that the object was burnt, not the fact that the corrosion is composed of iron and oxygen.

[118] Pérez-Serradilla et al. 2007; Alberghina et al. 2011.
[119] Guirado et al. 2012.

Traditionally, analysis of metal corrosion has focused on the identification of inorganic compounds as crystalline phases using X-ray diffraction (XRD). Its usual set up requires a few milligrams of sample to be removed from the object, ground to a powder and then placed on a glass or silica sample holder for analysis. The advantage of this technique is the ease of sample preparation and the ability to reuse the sample for other analyses. A sample containing more than one crystalline phase can be easily characterized and quantified using specific software and databases. Analysis without sample removal is also possible by placing the whole object in a model equipped with mirrors to control the incident beam.[120] Table 1 contains some common inorganic crystalline compounds found in archaeological metal corrosion. Amorphous and poorly crystallized compounds are difficult to detect by XRD and they yield poorly resolved diffractograms.

A complementary technique to XRD is Raman spectroscopy, a technique that measures the scattering of light caused by molecular bonds of the compounds present in the sample. Raman can provide information on less crystallised samples, with the possibility of creating distribution maps. With handheld devices, it is possible to analyse large objects without sample removal. However, Raman spectra can sometimes be obscured by fluorescence of the sample, and its interpretation can be problematic given the absence of a certified database other than for mineralogical compounds. Notwithstanding these issues, and depending on the laser, the technique can pick up signals given by the bond of a metal ion coordinating with oxygen in a metal soap and other copper-organic complexes.

[120] Scott 2017.

Chemical Name*	Mineral Name	Chemical Formula	Colour**
copper(I) oxide	cuprite[121]	Cu_2O	red
copper(II) oxide	tenorite[122]	CuO	black
copper(II) hydroxide	spertiniite[123]	$Cu(OH)_2$	blue
copper(II) carbonate hydroxide	malachite[124]	$Cu_2CO_3(OH)_2$	green
copper(II) carbonate hydroxide	azurite[125]	$Cu_3(CO_3)_2(OH)_2$	blue
copper(II) sodium carbonate trihydrate	chalconatronite[126]	$CuNa_2(CO_3)_2 \cdot 3H_2O$	blue
copper(I) chloride	nantokite[127]	$CuCl$	pale grey
copper(II) chloride hydroxide	atacamite	$Cu_2Cl(OH)_3$	dark green
copper(II) chloride hydroxide	paratacamite[128]	$Cu_2Cl(OH)_3$	pale green
copper(I) sulfide	chalcocite[129]	Cu_2S	black
copper iron(II) sulfide	chalcopyrite[130]	$CuFeS_2$	yellow
copper(II) hydroxide sulphate	brochantite[131]	$Cu_4(OH)_6SO_4$	green
copper(II) hydroxide phosphate	libethenite[132]	$Cu_2(OH)(PO_4)$	green

* Numbers between brackets represent the state of oxidation.

**These are the colours of pure compounds. They are likely to change due to the presence of impurities so must not be relied upon for identification.

Table 1 - Common mineral phases identified in archaeological copper corrosion

The presence of carboxylate ions in a metal soap can be visualized using Fourier transform infra-red spectroscopy (FTIR), a technique that measures the absorption of light by molecular vibrations within compounds. Samples for Raman and FTIR can be prepared in cross-section and analysed in mapping mode to create distribution maps. In the case of complex samples, dedicated software and mathematical manipulation of the data may be necessary to uncover the signal of trace compounds.

[121] Craddock and Giumlia-Mair 1993; Schrenk 1994.
[122] MacLeod 1991; Berger 2015.
[123] Stoffyn-Egli et al. 1998; Paterakis 2003; Dowsett et al. 2020.
[124] Schweizer 1994; Casaletto et al. 2010; Ingo et al. 2010.
[125] Casaletto et al. 2010; Ingo et al. 2010.
[126] Pollard et al. 1990; Thickett and Odlyha 2000; Trentelman et al. 2002.
[127] E.g. Gettens 1951; Scott 2000.
[128] Scott 2002; Scott 2017.
[129] E.g. MacLeod 1991; Ghoneim 2014.
[130] E.g. Duncan and Ganiaris 1987; Tweddle 1992; Schweizer 1994; Ingo et al. 2006.
[131] E.g. Nord et al. 2005; Muros and Scott 2018.
[132] E.g. Geilmann and Meisel 1942 in Scott 2002; Scott and Maish 2010; Fan and Freestone 2017; Wei et al. 2019.

Despite its low cost, FTIR is rarely considered as a technique for the study of corrosion. The technique can be used to screen samples for the presence of organic compounds in corrosion as these molecules give out characteristic signals. The drawback is that for the best results the sample may have to be analysed using the KBr disc method where the sample is mixed with potassium bromide and turned into a disc with applied pressure. This hinders further analysis of the samples by other techniques.

An increasing number of techniques based on solid-state electrochemistry are being developed. These techniques measure the response of a solid in an electrolyte. Voltammetry of immobilized particles (VIMP) is an example of such a technique. Particles of the sample are transferred to a base electrode (typically a paraffin-impregnated graphite electrode) and its voltametric signal in an electrolyte (e.g. 1.0M HCl) measured using a reference electrode (normally AgCl/Ag). The voltametric response is then compared to a reference library. Although individual corrosion products may be identified within a mixture, the application of VIMP is seriously limited if one compound largely prevails as its signal will obscure that of minority components. Despite other limiting factors[133] VIMP is an attractive technique due to its simplicity, low cost and non-destructive nature. These qualities are driving an increasing number of articles, demonstrating its application to archaeological questions such as dating of artefacts[134] and identification of corrosion products.[135] VIMP is a suitable technique for archaeological studies where extensive characterization of corrosion layers is

[133] Doménech-Carbó 2013; Scholz et al. 2014.
[134] Doménech-Carbó et al. 2018; Doménech-Carbó and Scholz 2019.
[135] Šatović et al. 2010; Di Turo et al. 2017.

not required, such as grouping objects for establishing provenance and workshops[136] and where sample removal is not permitted.

2.3.8 A new multi-analytical protocol for the analysis of archaeological metal corrosion

The scientific potential of archaeological metal corrosion can only be revealed if its characterization includes analytical techniques able to identify inorganic and organic phases. Although there is an increasing number of analytical techniques available to archaeological scientists, selection criteria are based on availability, cost of the analysis and sample requirements.

The multi-analytical protocol used in this research was initially composed of XRD and FTIR as screening techniques and GC-MS for the separation and identification of organic compounds. Although GC-MS is the most popular technique for archaeological organic residue analysis, there is no standard method for lipid extraction. In fact, there are many articles in the literature dedicated to method development with known samples being applied to archaeological samples. In this research, two GC-MS methods were evaluated: a simple chloroform/methanol solvent extraction followed by derivatization with N,O-Bis(trimethylsilyl)trifluoroacetamide (BSTFA) and a low temperature pyrolysis method using thermal separation probe (TSP) that does not require wet-chemistry pre-treatment of samples.

[136] Redondo-Marugán et al. 2017.

To evaluate the performance of the multi-analytical protocol described above, a supply of copper corrosion samples containing organic molecules and copper-organic complexes were produced in the laboratory using an electrochemical cell. The multi-analytical protocol was then used for the characterization of archaeological copper corrosion samples.

3. MATERIALS, METHODS AND INSTRUMENTS

3.1 Materials

The copper coupons used for the corrosion experiments were cut from an Alfa Aesar™ copper foil, 0.127mm (0.005in.) thick, annealed, 99.9% (metals basis) purchased from Fisher Scientific UK Ltd.

Organic substances that contain organic molecules that could form complexes with copper and that may have been used by past civilizations were selected for the corrosion experiments. These were:

- Bovine milk: Pensworth's full-fat pasteurized milk purchased from McColls, UK
- Olive oil: Extra Virgem Azeite de Oliva Classico Gallo, purchased from Delicias de Portugal, UK
- Red wine: Vina Ulmo Chilean Cabernet Sauvignon purchased from Marks & Spencer, UK
- White wine: Vina Ulmo Chilean Sauvignon Blanc purchased from Marks & Spencer, UK

All reagents were analytical or chromatography grade and purchased from Sigma-Aldrich or Fisher Scientific UK Ltd. Deionized water was obtained from a Milli Q reverse osmosis system (typically 18.2Ω resistivity and <4ppb carbon).

3.2 Methods

Given the relative difficulty in corroding copper in soil or via immersion, an electrochemical method was developed, initially in order to produce typical inorganic copper corrosion and later to include organic substances.

In these experiments, a Thurlby Thandar TSX1820 Precision DC Power supply was connected to two copper coupons as shown in Figure 6. The surface of the anode coupon was abraded on both sides with a fiberglass pen. Both coupons were washed with deionized water and degreased with acetone prior to immersion in an electrolyte. The voltage was adjusted to guarantee a minimum anodic current of 0.01A through the system, thus ensuring the slow release of Cu ions into the solution and the electrolyte not being agitated in order to facilitate solids deposition onto the cathode coupon.

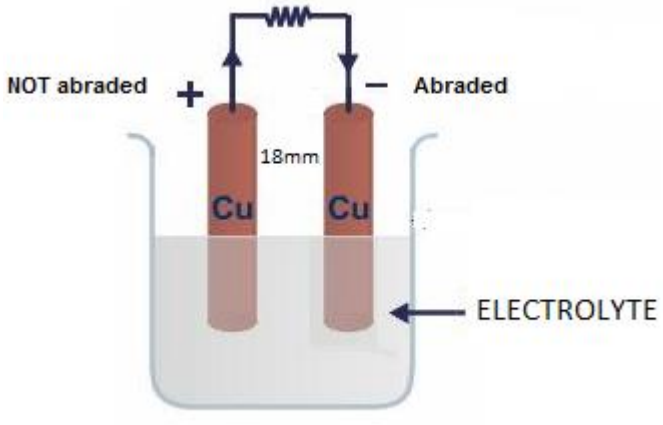


Figure 6 - Typical electrochemical set up

Given the impossibility of obtaining copper-organic complex standards, the apparatus in Figure 6 was also used to synthetize copper-organic compounds. In these experiments the

anodic current was set to 0.02A to promote the fast release of copper ions and the electrolyte agitated to facilitate reaction with the organic ligand.

The electrochemical synthesis method was validated with a copper palmitate synthetized via a two-step precipitation method[137] as described in section 3.2.2.1. All experiments were repeated three times to verify reproducibility.

3.2.1 Corrosion experiments

3.2.1.1 Corroding copper in an electrolyte containing carbonate and chloride ions

The electrolyte used to produce inorganic corrosion was 0.02M Na_2CO_3 and 0.01M NaCl in deionized water. The starting voltage was 2.04V and increased to 2.40V after 90 minutes in order to maintain a minimum current of 0.01A. After 48 hours the experiment was stopped, the coupons carefully removed and washed with deionized water and allowed to dry in a fume cupboard for seven days prior to characterization. The pH of the electrolyte at the start of the experiment was 10.5 and remained unchanged until the end of the experiment.

3.2.1.2 Corroding copper in an electrolyte containing carbonate, chloride and carboxylate ions

The composition of the electrolyte was modified to include palmitic acid – a ubiquitous substance commonly extracted from archaeological ceramics and known to spontaneously react with copper ions to form copper palmitate.[138] Given its low solubility in water, palmitic acid was dissolved in warm methanol prior to being incorporated into the

[137] Corbeil and Robinet 2002.
[138] Schrenk 1991 in Schrenk 1994.

electrolyte. The final composition of the electrolyte was 0.02M Palmitic acid, 0.01M Na_2CO_3 and 0.01M NaCl in 50:50 v/v methanol/deionized water and the pH adjusted to 10.5 with 1M NaOH. The power supply was set to maintain 0.01A minimum current and the experiment was run for a period of two days. The coupons were carefully removed, washed with deionized water, and allowed to dry in a fume cupboard for seven days prior to analysis. The pH of the electrolyte was unchanged at the end of the experiment.

3.2.1.3 Corroding copper in olive oil, wine and bovine milk

Separate experiments using an electrolyte 50:50 v/v olive oil/deionized water, white wine, red wine and bovine milk were performed. In all experiments the power supply was set to maintain 0.01A minimum current over a period of two days. At the end of the experiment the coupons were carefully removed, washed in deionized water and allowed to dry in a fume cupboard for seven days prior to characterization. Samples of the organic mixtures were also subjected to freeze-drying cycles to yield a solid residue to be used as controls.

3.2.2 Synthesis of copper-organic complexes

The electrochemical synthesis of copper-organic complexes was attempted by immersing abraded and degreased copper coupons in a solution containing the organic compound of interest and ammonium acetate to aid conductivity. The list of organic compounds used in the electrochemical synthesis experiments is included in Table 2.

In all experiments the organic compound was pre-dissolved in an organic solvent (methanol or acetone) heated in a *bain-marie* to aid dissolution. This solution was then combined with an electrolyte (ammonium acetate or sodium chloride dissolved in deionized water). The concentration of the final solution was 0.01M organic compound, 0.01M electrolyte in 50:50 v/v co-solvent/deionized water. The pH of the solution was adjusted to 10-11 with 1M NaOH, the copper coupons (abraded and degreased with acetone) inserted and the voltage set to 5.0V – which provided a 0.02A current in the system. After one hour, the coupons were removed and washed in methanol (or acetone). The electrolyte was vacuum filtered using fibre glass paper and washed with methanol (or acetone in the case of unsaturated carboxylic acids). The coupons and paper filter were left to dry in a fume cupboard for seven days prior to characterization.

Type	Compound	Co-Solvent	Electrolyte
Aromatic	Phenol	Methanol	Ammonium acetate
Carbohydrate	Lactose	Methanol	Ammonium acetate
Carboxylic Acid (saturated)	Palmitic and Stearic acids	Methanol	Sodium chloride
Carboxylic Acid (unsaturated)	Linoleic and Oleic acids	Acetone	Ammonium acetate
Diacyglycerol	Glyceryl 1,3-dipalmitate	Methanol	Ammonium acetate
Ester	Ethyl Palmitate	Methanol	Ammonium acetate
Phenolic acid	Gallic Acid	Methanol	Ammonium acetate
Phosphoprotein	Bovine casein	Methanol	Ammonium acetate
Polyol	Glycerol	Methanol	Ammonium acetate
Polyphenol	Resveratrol	Methanol	Ammonium acetate
Triacylglycerol	1,3-dipalmitol 2-oleyglycerol	Methanol	Ammonium acetate

Table 2 - Compounds used in the copper complexation experiments

3.2.2.1 Synthesis of copper palmitate[139]

1g of palmitic acid was dissolved in 50mL of ethanol and mixed with 50mL of saturated solution of copper sulphate in deionized water and the pH adjusted to 9 with a saturated solution of sodium hydroxide in deionized water. The mixture was heated at 70^{o}C for 20 minutes. The resulting blue precipitate was filtered, washed with warm ethanol (to remove the excess acid), followed by water (to remove the excess copper sulphate) and allowed to dry at 100^{o}C for two hours prior to characterization.

3.3 Instrumentation

This section details the various analytical techniques used in this research. The author performed most of the analyses except where otherwise indicated.

3.3.1 Fourier-transform infra-red spectroscopy (FTIR)[140]

Samples were analysed in reflection or in transmission mode.

In reflection mode, the technique used was Attenuated Total Reflectance (ATR) where around 1mg of sample was pressed against the reflective crystal of the equipment or analysed using a microscope fitted with a micro-ATR objective which is pressed against the surface containing the sample (in this case the copper coupons). ATR measurements were obtained with a Perkin Elmer Spotlight 200i FTIR Microscope System at the Heritage Science Laboratory at the Bodleian Library, University of Oxford.

[139] Corbeil and Robinet 2002.
[140] For an introduction to the technique see Cross and Alan Jones 1969.

In transmission mode, the technique used was the KBr pellet method. The sample was mixed with KBr (kept warm and desiccated before use) in an agata mortar with a pestle in a 2mg/200mg ratio. The mixture was transferred to a pellet die and pressure applied with a hydraulic pump to form a disc of around 1mm thickness which was immediately transferred to the equipment for analysis. Transmittance measurements were taken with an Excalibur Series Varian UMA600 at Begbroke Science Park, University of Oxford.

Measurements were a combination of 64 scans between the 4000-400cm^{-1} range and included background subtraction. Data was processed using Perkin Elmer Spectrum Software v.10.5.4 or Digilab Resolutions Pro 4.0 software and figures created with Spectragryph v.1.2.12. Band assignments were based on FTIR tables published by Cross and Jones 1969 and Socrates 2001 and, where applicable, articles in the literature.

3.3.2 Raman spectroscopy (Raman)[141]

Spectra were obtained using a Horiba™ Jobin Yvon spectrometer at Cranfield University operated by Dr Chris Dyer. Samples were scraped off the copper coupon onto a glass slide. Each sample was run on a low laser power and short exposure to judge the level of Raman scattering and fluorescence, and to check for visible sample damage.

Selected laser power and exposure time were those that maximised the Raman signal without causing damage to the sample. Typical values were 6 seconds under maximum power at 5-10 mW with excitation at 532 nm from a continuous-wave solid-state laser. The

[141] For an introduction to the technique see Gardiner 1989.

microscope system was based around a BX-41 microscope operating in epi-illumination mode (reflection), collecting Raman data on back scattered geometry. A x50 metallurgical (dry) objective was used throughout except when a x10 gave a longer distance between end of lens and sample surface, at the expense of signal collection efficiency.

The spectrograph used to disperse the light was fitted with a cooled charge coupled device (CCD) to record the resulting signal. For practical purposes, there is an inverse relationship between reduction in laser power and increase in exposure time when using a CCD-based system: if the power is dropped ten-fold to avoid thermally affecting the sample, then the acquisition time is increased ten-fold to achieve a comparable S/N ratio. For fragile samples, 10% power with 120 seconds exposure was used.

Data was processed and figures created with Spectragryph v.1.2.12. Band assignments were based on Raman tables published by Nakamoto 1997 and Socrates 2001 and, where applicable, articles in the literature.

3.3.3 X-ray photoelectron spectroscopy (XPS)[142]

Spectra were obtained with Thermo Scientific™ K-Alpha™ X-ray photoelectron spectrometer at the Begbroke Science Park, University of Oxford. The system was calibrated for a carbon peak at 284.80eV. A flood gun was used to stop the sample charging. The spot size was 400µm. For a survey scan, a step size of 1eV and dwell time of 10ms

[142] For an introduction to the technique see van der Heide 2011.

were used and, for a detailed scan, a step size of 0.1eV and dwell time of 50ms. Two spots were measured for each sample, with peak fittings undertaken using Casa© software with assignments based on XPS reference spectra published by reference libraries and, where applicable, articles in the literature. Dr Phillip Holdway operated the equipment and performed curve fitting in consultation with the author.

3.3.4 Powder X-ray diffraction (XRD)[143]

The archaeological samples were pulverized and set on a silicon plate and spectra obtained using a PANalytical X'Pert PRO Cu alpha instrument at the Crystallography Laboratory in the Department of Chemistry, University of Oxford. The equipment was set to operate in continuous mode at 40kV/40mA with a scanned area set between 1^{o}-70^{o} 2θ, 0.02 step size and 3^{o} per minute.

The copper organic complexes were analysed in a Bruker d* ADVANCE Eco X-ray Powder Diffractometer operating with a Cu tube at 40Kv 20µA with a Lynxeye XE solid state detector at Begbroke Science Park, University of Oxford by Dr Phil Holdway. The scanned area was set between 5^{o}-40^{o} 2θ, 0.02 step size and 1^{o} per minute.

Data was processed using QualX© software with phase identification using the Crystallography Open Database (COD).

[143] For an introduction to the technique see Pecharsky and Zavalij 2009.

3.3.5 Mass spectrometry techniques[144]

All analyses were performed at the Mass Spectrometry Facility at the Department of Chemistry, University of Oxford except 3.3.5.5, which was performed at the Research Laboratory for Archaeology and History of Art at the School of Archaeology, University of Oxford.

3.3.5.2 Ion chromatography coupled with mass spectrometry (IC-MS)

About 1mg of sample was extracted with 1000µL of deionized water (or methanol) under one-hour sonication. After centrifugation, the supernatant was transferred to a vial for analysis. Analysis was performed using a Thermo Scientific ICS-5000+ ion chromatography system coupled with a Q-Exactive HF Hybrid Quadrupole-Orbitrap mass spectrometer with a HESI II electrospray ionisation source. The system incorporated an electrolytic anion generator (KOH) programmed to produce an OH^- gradient from 5-100mM over 37 minutes. An inline electrolytic suppressor removed the OH^- ions and cations from the post-column eluent prior to its delivery to the electrospray ion of a Thermo Scientific Dionex AERS 500 MS system. A 10µL partial loop injection was used for all analyses and the chromatographic separation was performed using a Thermo Scientific Dionex IonPac AS11-HC 2 × 250mm, 4µm particle size column with a Dionex Ionpac AG11-HC 4µm 2x50mm guard column inline. The IC flow rate was 0.250mL/min and the column temperature kept at 30°C throughout the experiment. Analysis was performed in negative ion mode, the scan range was m/z 80-900amu and resolution set to 70,000. The tune file source parameters were Sheath gas flow 60; Aux gas flow 20; Spray voltage 3.6; Capillary temperature 320°C; S-lens RF value 70; Heater temperature 450oC. AGC target was set to 1e6 and the Max IT

[144] For the principles and application of mass spectrometry see Hoffmann and Stroobant 2007.

value was 250ms. Full scan data was acquired in continuum mode across the mass range m/z 60-900amu. Sample replicates were not produced due to the limited amount of sample available. Samples were run only once due to high cost of analysis.

Data was analysed using the Progenesis software. Searches were undertaken for compounds as M-H adducts in >5ppm mass accuracy against an in-house database of metabolites. Only compounds with an isotope accuracy of >90% were shortlisted for manual selection according to the highest fragmentation score and lowest retention time deviation.

3.3.5.3 Quadrupole time-of-flight gas chromatography coupled with mass spectrometry with a thermal sample probe (QTOF-GC-MS with TSP)

A glass microvial containing 1mg of pulverized sample was placed inside TSP attached to an Agilent 7890B gas chromatograph equipped with a Restek Rxi-5ms column (30 m x 320 μm x 0.25 μm). The mass spectrometer was an Agilent 7250 GC/Q‑TOF equipped with a low-energy-capable EI source (70 eV) and an interchangeable CI source.

Different settings were used to optimize conditions so that analyses were relatively fast and reproducible. Heat-assisted derivatization with BSTFA was also attempted without any detectable change in the results. The best results were achieved with the TSP set at 300^{o}C and the oven temperature set at 40^{o}C for one minute, increasing by 20^{o}C/minute until it reached 320^{o}C where it was held for five minutes. Helium was used as a carrier gas, at 1.4338 mL/min flow rate and 8.7045 psi pressure. The equilibration time was set at 0.5

minutes and the sample injection was splitless. The mass range was 50 to 650 *m/z*. All samples were run in triplicate.

Data was analysed with Agilent Mass Hunter Qualitative Analysis 10.0 with compound assignments using NIST Library 17.

3.3.5.4 Proteomics

The proteomics method used was bottom-up proteomics, where the identification of proteins is made via their peptides using specialist software and protein databases.

Around 2mg of sample was partially dissolved in 2:1 v/v chloroform/methanol under sonication. After centrifugation, the supernatant was transferred to a clean tube and ice-cold acetone added prior to overnight incubation at -20^{o}C to precipitate the proteins. The following day, after centrifugation, the supernatant was discarded, and the precipitate extracted with RIPA Buffer (prepared in the laboratory). The protein extract was digested using LysC and trypsin followed by desalting and sample concentration using C18 ZipTip.[145]

The tryptic digest was re-suspended in 40µL milli-Q water with 2% acetonitrile and 0.1% formic acid. 2µL was analysed by nanoLC-MS/MS using a Waters NanoAcquity-UPLC system interfaced with a Thermo LTQ Velos Orbitrap Elite mass spectrometer possessing an

[145] Pires et al. 2021

EASY-Spray ion source. Initial peptide trapping on a packed guard column (75µm i.d. x 20mm, Acclaim Pep-map100 C18, 3µm, 120Å) was carried out with solvent A (0.1% Formic Acid in water) at 140bar. Peptides were separated on an EASY-spray Acclaim Pep-Map® analytical column (75µm i.d. × 15mm, RSLC C18, 3µm, 100Å) using a 120min linear gradient ranging from 3 to 97% of solvent B (0.1% formic acid in acetonitrile), with 300nL/min flow rate and 40ºC column temperature. The nanoESI source operated at 1600V needle voltage with the temperature of the ion transfer tube set to 275°C.

The separated peptides were ionized via electrospray directly into the mass spectrometer operating in a data-dependent acquisition mode using a CID-based method. Full scan MS spectra (scan range 350-1500m/z, resolution 120000, AGC target 1e6, maximum injection time 250ms) and subsequent CID MS/MS spectra (AGC target 5e4, maximum injection time 100ms) of the 10 most intense peaks were acquired in the Ion Trap. CID fragmentation was performed at 35% of normalized collision energy and the signal intensity threshold kept at 500 counts. Brand new guard and separation columns were used to avoid contamination from previous samples analysed in the laboratory. Bovine Serum Albumin standard was also digested and analysed in parallel using the same conditions. Samples were run only once and with no duplicates.

Data analysis was performed using PEAKS 8.5v (Bioinformatics Solutions Inc., Waterloo, ON, Canada). Raw MS data was searched against the general Uniprot database and identifications confirmed with Uniprot taxonomy databases with LysCTryp selected as the protease. Carbamidomethylation (Cysteine) was set as a fixed modification and Oxidation (Methionine), Deamination (Asparagine, Gluta-mine) and +12Da on N-terminal proline set

as variable modifications. Precursor mass tolerance was set as 15 ppm and fragment mass tolerances for CID set to 0.8 Da.

PEAKS DB measures the quality of the Peptide Spectrum Match (PSM) internally with a Linear Discriminative Function (LDF) score. To identify the protein, LDF considers the matching of fragment ions and spectrum peaks and the similarity between the de novo sequencing peptide and the universal database peptide amongst other factors. The LDF score is converted to -10lgP to facilitate assessment. Only peptides with a -10lgP >20 (p-value of 1%) were selected for PSM validation with a Target Decoy PSM Validator node based on q-values at a 5% false discovery rate (FDR). Only validated peptides were used in Uniprot protein database searches. Analyses and data processing were performed by Elisabete Pires in consultation with the author.

3.3.5.5 Solvent extraction with BSTFA derivatization followed by GC-MS

Around 2mg sample was extracted with 2:1 v/v chloroform/methanol mixture under sonication for 30 minutes. The extract was derivatised prior to GC-MS analyses by adding 20µL of BSTFA with 5µL tridecanoic solution (100µg/µL in hexane) and kept for one hour at 70°C for the reaction to be completed. The solution was then transferred to micro-inserts and 10µL hexadecane solution (50µg/g in iso-octane) added as an internal standard.

Analysis was performed using an Agilent 7820A gas chromatograph equipped with a Restek Rxi-5ms column (30 m x 0.25 mm i.d., 0.25 µm). The mass spectrometer was an Agilent 5975 quadrupole mass spectrometer, operated in EI mode (70eV), and the scan range was

m/z 50−650 amu. The inlet temperature 300°C, flow rate 1.2 mL/min, transfer line temperature 280°C. Helium was used as the carrier gas. The temperature program for the GC oven started with two minutes at 50°C, followed by a ramp from 50°C to 300°C at 10°C/min and finishing by 10 minutes isothermally held at 300°C. Injections were made by an Agilent 7693A autosampler and sample injection volume was 1μL in split mode.

Compounds were identified using the University of Pisa database of compounds.

4. A NEW PROTOCOL FOR ANALYSIS OF ARCHAEOLOGICAL METAL CORROSION

This chapter is divided into three parts. The first part contains the results of the electrochemical corrosion of copper coupons in the presence of inorganic ions (experiment 1) and with the addition of organic ions (experiment 2). The second part contains the results of the electrochemical synthesis of copper-organic complexes with the results of the electrochemical corrosion of copper coupons in the presence of organic mixtures and its characterization by the multi-analytical protocol presented in part three.

4.1 Corroding Copper in the Laboratory

4.4.1 Experiment 1 – Corroding copper in the presence of carbonate and chloride ions

The purpose of this experiment was to verify if typical archaeological copper corrosion products could be produced in the laboratory. Figure 7 shows the Pourbaix Diagram based on the concentration of the ionic species in the electrolyte used in the experiment. Given the high experimental voltages, the voltage axis of the diagram is irrelevant.

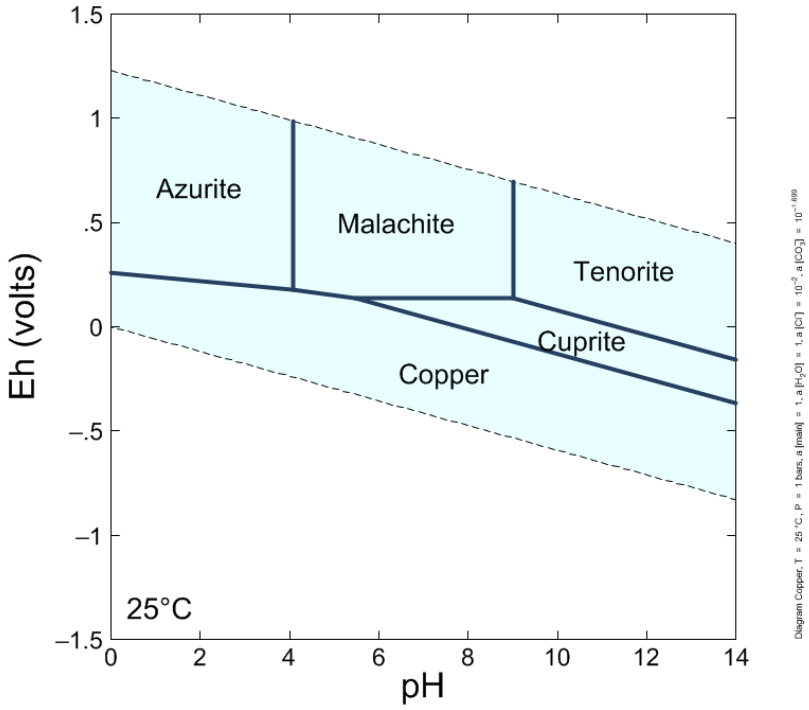


Figure 7 - Pourbaix Diagram based on conditions of Experiment 1

at 25ºC and 1 bar pressure

At the start of the experiment, both coupons were "fizzing", with blue deposits forming along the edges of (+) coupon. Figure 8 shows the (+) coupon at the end of the experiment.



Figure 8 - (+) Coupon at the end of Experiment 1

The dark deposits were removed from the (+) coupon and analysed by XRD. The peak list and phase identification is shown in Table 3.

2θ (°)	d-spacings (nm)	I/I_0 (%)	Mineral Phase
14.8483	5.9676	12.76	Malachite
16.2469	5.4558	11.55	
17.6243	5.0324	32.47	Malachite
24.0653	3.6981	42.59	Malachite
31.2190	2.8651	62.34	Malachite
32.2690	2.7742	42.74	Malachite
35.6540	2.5182	67.62	Tenorite
36.3704	2.4702	100.00	Cuprite
38.5509	2.3354	47.57	Tenorite
42.3216	2.1356	40.23	Cuprite
43.3031	2.0895	88.54	Copper
50.4232	1.8099	43.32	Copper
54.8286	1.6744	18.18	
58.0789	1.5882	19.50	
61.4149	1.5097	30.59	Cuprite
66.0172	1.4152	16.28	
67.8739	1.3809	12.53	
73.4421	1.2894	16.90	Cuprite
74.1092	1.2783	23.23	Copper

Table 3 - XRD peak list and phases identified in the deposit on Experiment 1 (+) coupon

Although some of the peaks have remained unassigned, the deposit was identified as a mixture containing malachite [$Cu(CO_3)\cdot Cu(OH)_2$], cuprite (Cu_2O) and tenorite (CuO). Malachite and tenorite are typical corrosion products of copper in seawater, with the formation of cuprite (as opposed to cupric chloride) due to the alkaline pH of the electrolyte.[146] However, according to the Pourbaix Diagram in Figure 7, the corrosion products of the experiment should only be composed of tenorite. The difference between the theoretical and experimental corrosion products may be explained by the formation of

[146] Bianchi and Longui 1973; Alfantazi et al. 2009.

microclimates with different pH and ions concentration at the coupons' surface when compared to the bulk of the electrolyte. The experiment was repeated three times and the same mineral phases identified, thereby demonstrating that the electrochemical method used is a simple, fast and reliable one. Given the mineral phases identified, the alkaline pH (10.5) and the observations during the experiment, these are some of the possible reactions:

Anode (+) $2Cu + 2OH^- \rightleftharpoons \mathbf{Cu_2O} + H_2O + 2e^-$

$Cu + H_2O \rightleftharpoons \mathbf{CuO} + H_2(gas)$

$2Cu^{2+} + 2OH^- + CO_3^{2-} \rightleftharpoons \mathbf{Cu(CO_3)\cdot Cu(OH)_2}$

$Cu \rightleftharpoons Cu^{2+} + e^-$

$Cu \rightleftharpoons Cu^{+} + e^-$

$2Cl^- \rightleftharpoons Cl_2(gas) + 2e^-$

Cathode (-) $\mathbf{2H_2O + 2e^- \rightleftharpoons H_2(gas) + 2OH^-}$

$Na^+ + e^- \rightleftharpoons Na$

4.1.2 Experiment 2 – Corroding copper in the presence of carbonate, chloride and carboxylate ions

The purpose of this experiment was to see whether copper ions would react with carboxylate ions and inorganic ions in the same electrolyte. A Pourbaix Diagram could not be generated for the Experiment 2 electrolyte because there is no thermodynamics data for copper in the presence of carboxylate ions in the GWB Essentials software.

Upon adding the palmitic acid (dissolved in methanol) to the electrolyte, a white flocculent formed, rising to the top half of the beaker. This white solid was probably sodium palmitate, the first of a two-step method for the synthesis of divalent metal soaps.[147] Figure 9 shows the (+) coupon at the end of the experiment. The coupon was carefully washed with ethanol to remove excess acid and white solids. Once dried, a sample was scraped off, homogenized and analysed by XRD. The peak list and phase assignments is shown in Table 4.



Figure 9 - (+) Coupon at the end of Experiment 2

The corrosion products were identified as atacamite [$Cu_2Cl(OH)_3$], cuprite [Cu_2O] and copper palmitate – synthetized according to Corbeil and Robinet[148] and analysed with the same equipment following recrystallization in chloroform. Its peak list and d-spacings are included in Appendix 1.

[147] Koenig 1914.
[148] Corbeil and Robinet 2002.

2θ (°)	d-spacings (nm)	I/I_o (%)	Crystalline Phase
6.1505	1.4370	9.52	Copper Palmitate
8.2511	1.0716	0.66	Copper Palmitate
10.2987	0.8589	3.93	Copper Palmitate
15.4371	0.5740	17.68	
16.1899	0.5475	29.96	Atacamite
21.1714	0.4167	23.07	
22.4314	0.3963	24.72	
29.4484	0.3033	26.90	
32.1716	0.2782	39.42	
36.3971	0.2468	100.00	Cuprite
39.6965	0.2271	31.77	Atacamite
42.2995	0.2137	40.18	Cuprite
43.3024	0.2090	36.70	Copper
50.5016	0.1807	19.94	Copper
61.3207	0.1512	25.29	Cuprite
67.7420	0.1383	7.89	
73.5524	0.2877	11.14	Cuprite
74.12.09	0.1278	10.20	Copper

Table 4 - XRD peak list and phases identified in the deposit on Experiment 2 (+) coupon

The Experiment 2 deposits and the reference copper palmitate were also analysed by FTIR.

The resulting spectra are shown in Figure 10.

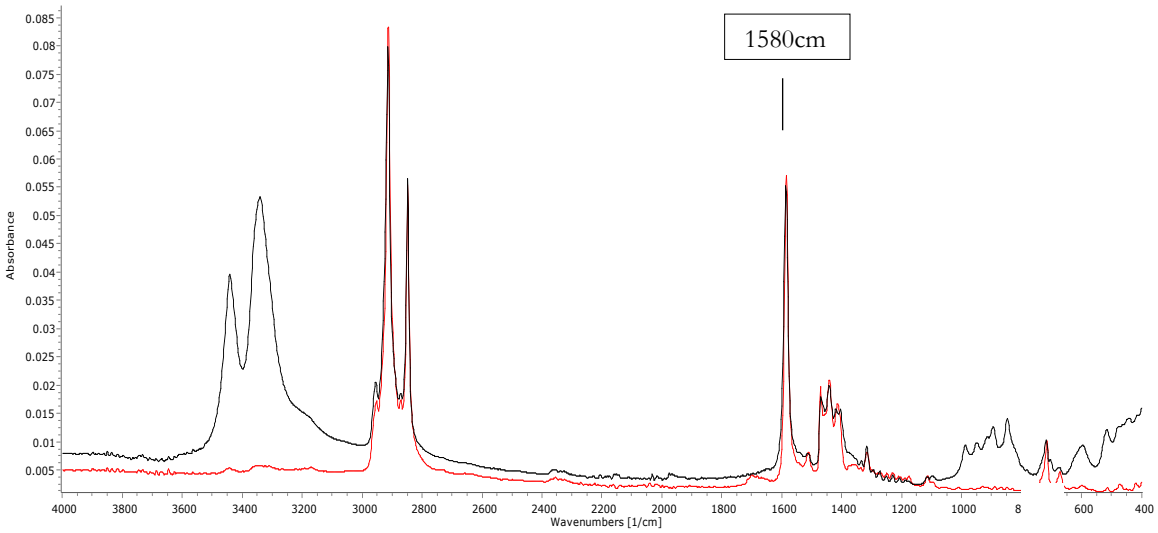


Figure 10 - FTIR spectra of Experiment 2 deposit and copper palmitate (RED)

All peaks in the reference copper palmitate spectrum also appear in the spectrum of the Experiment 2 deposit. Of interest is the strong peak at 1580cm^{-1} being the COO^- asymmetric stretch characteristic of all metal soaps[149] and additional peaks from atacamite[150] in the 3,500-3100cm^{-1} and 1,000-800cm^{-1} regions formed due to the presence of chloride ions in the electrolyte. Given the compounds identified in the corrosion products, the possible reactions are:

Anode (+)

$2Cu + H_2O \rightleftharpoons \mathbf{Cu_2O} + 2H^+ + 2e^-$

$2Cu + 3H_2O + Cl^- \rightleftharpoons \mathbf{Cu_2(OH)_3Cl} + 3H^+ + 2e^-$

$Cu^{n+} + nRCOONa \rightleftharpoons \mathbf{(RCOO)_nCu} + nNa^+$

$Cu^{n+} + nRCOO^- \rightleftharpoons \mathbf{(RCOO)_nCu}$

$Cu \rightleftharpoons Cu^{2+} + e^-$

$Cu \rightleftharpoons Cu^+ + e^-$

[149] Robinet and Corbeil 2003, 28.
[150] https://rruff.info/Atacamite.

Cathode (-) $\mathbf{2e^- + 2H_2O \rightarrow H_2(gas) + 2OH^-}$

$e^- + Na^+ \rightarrow Na$

$Cu^{2+} + 2e^- \rightarrow Cu$

To test the effect of the pH in the composition of the deposits, Experiment 2 was repeated at neutral pH. The resulting deposit was analysed by FTIR and is shown alongside the deposit produced in alkaline in Figure 11. The carboxylate ion peak at 1580cm^{-1} is present in both spectra, indicating that copper can react with palmitic acid in both neutral and alkaline environments.

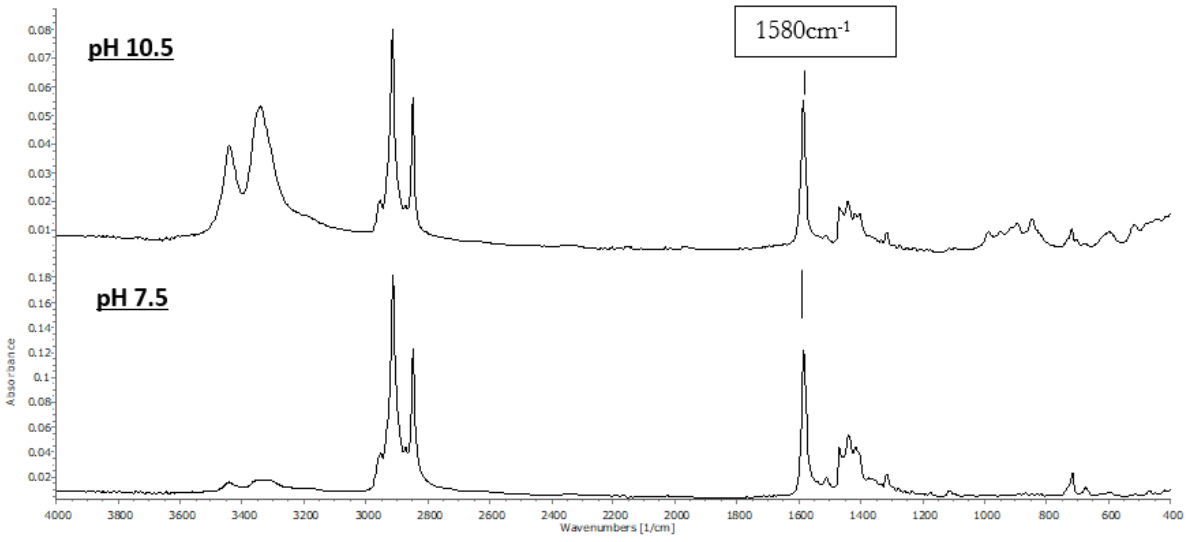


Figure 11 - FTIR spectra of Experiment 2 (+) coupon deposits formed at alkaline and at neutral pH

These simple experiments were intended to test whether copper could react with organic and inorganic compounds in the same environment. By applying a high voltage to the electrochemical cell, it was possible to accelerate the rate of corrosion of copper and

generate corrosion deposits containing organic and inorganic compounds identifiable by XRD and FTIR. With access to a more complex apparatus, the electrochemical cell could be modified to enable full characterization of the electrolyte (bulk composition vs metal surface) at different conditions (at varying potential ranges, temperature and pH) so that the thermodynamics of copper palmitate formation could be better understood. Because of the complexity and timescale involved in such an approach, the current experimental arrangement was simply modified to include complex organic mixtures and used to synthesize copper-organic complexes to aid the characterization of the resulting deposits.

4.1.3 Experiment 3 - Corroding Copper in the Presence of Organic Mixtures

The (+) coupon for milk, red wine and white wine at the end of the experiments are shown in Figure 12. From now on, the dried deposits will be referred to as *copper-milk corrosion*, *copper-red wine corrosion* and *copper-white wine corrosion*.

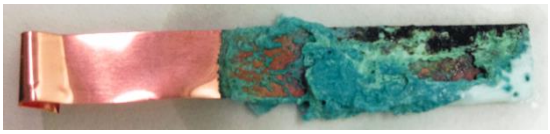
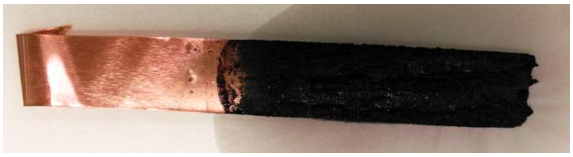
ELECTROLYTE	CONDITIONS At the start	At the end
 **Full-Fat Bovine Milk**	pH 7 E = 1.83V	pH 10.5 E = 10V
 **Red Wine**	pH 3.5 E = 1.60V	pH 5.0 E = 2.21V
 **White Wine**	pH 3.5 E = 1.60V	unchanged

Figure 12 - (+) Coupons corroded in milk, red wine and white wine

The (+) coupon used for the olive oil/water experiment did not contain any deposits on the top half, which was exposed to the oil whilst the bottom half was completely corroded.

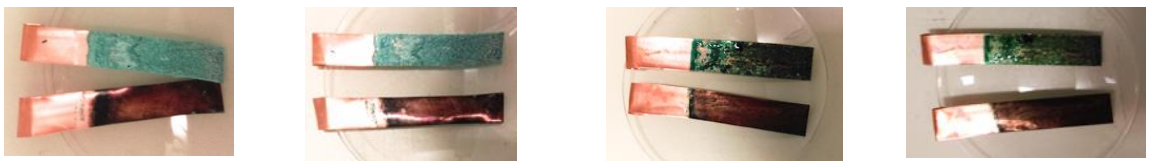
To create reference samples for the milk, red wine and white wine, aliquots of these liquids were subjected to freeze drying but a solid residue could only be obtained from milk. Attempts were made to concentrate the wine samples prior to freeze drying but these concentrated samples also did not yield a solid residue in sufficient quantity for characterization by the multi-analytical protocol. Therefore, only the pair with freeze-dried milk/copper-milk corrosion were characterized by the multi-analytical protocol in section 4.3.

4.2 Electrochemical Synthesis of Copper-organic Complexes

The experiments with electrolytes containing phenol, glyceryl 1,3-dipalmitate, ethyl palmitate, gallic acid, glycerol, resveratrol and 1,3-dipalmitol-2-oleyglycerol did not generate a deposit over the (+) coupon nor a solid precipitate. Deposits were obtained for the carboxylate acids, lactose and casein, their characterization by FTIR, XRD, Raman, XPS and mass spectrometry techniques are described in the following sections.

4.2.1 Copper-carboxylates

The (+) coupons from the electrolyte containing palmitic and stearic acids were covered by a light greenish/blue powdery substance whilst those containing oleic and linoleic acids were covered by a dark green, reflective sticky film. See Figure 13.



Palmitic Acid **Stearic Acid** **Oleic Acid** **Linoleic Acid**

Figure 13 - Coupons used for the synthesis of Cu-carboxylates

For ease of reference, the coupon deposits will be referred to as Cu-palmitate, Cu-stearate, Cu-oleate and Cu-linoleate.

4.2.1.1 Characterization by FTIR

The full set of FTIR spectra and peak tables are included in Appendix 2. Figure 14 contains the spectra of palmitic acid and its copper complex.

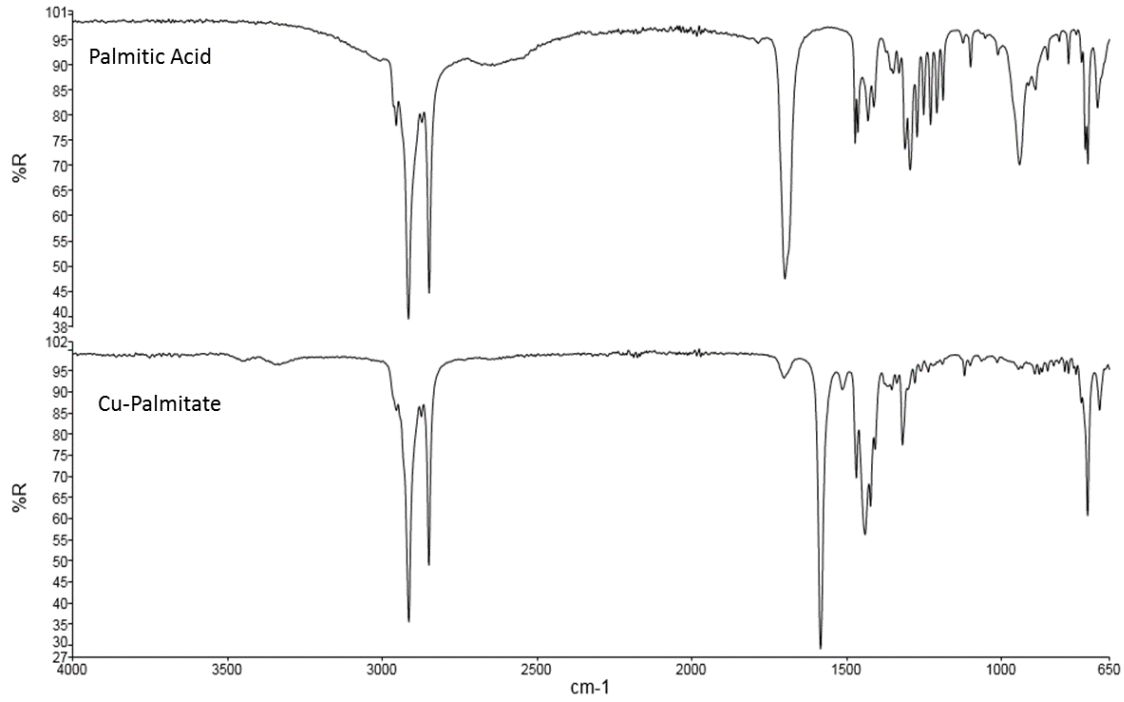


Figure 14 - FTIR spectra of palmitic acid and Cu-palmitate

obtained in ATR mode

Carboxylic acids normally exist as dimers due to strong intermolecular hydrogen bonding[151] and are characterized by hydroxyl (OH) and carbonyl (C=O) vibrations. Their most recognizable OH vibrations are a broad band in the 3300-2500cm^{-1} region and a variable intensity band around 955-890cm^{-1} whilst the C=O vibration appears as a strong band within 1715-1680cm^{-1}region. When ionization occurs forming the COO^- carboxylate ion, resonance

[151] Socrates 2001.

is possible between the two C-O bonds.[152] The C=O band is replaced by two vibrations: a characteristic strong band between 1610-1550cm^{-1} (COO^- asymmetric stretching) and a medium band between 1420-1300cm^{-1}(COO^-symmetric stretching).

The COO^- bands in copper palmitate appear as a strong band around 1583cm^{-1} and a medium band around 1422cm^{-1}. Analogous bands were also found in the spectra of the remaining copper-carboxylate complexes (see Figure 15 and Table 5).

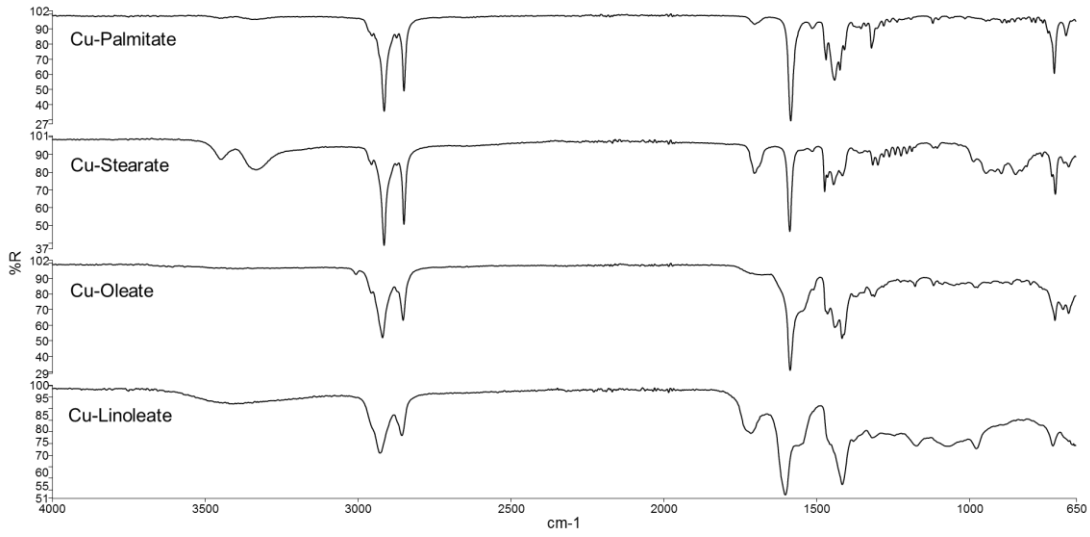


Figure 15 - FTIR spectra of Cu-carboxylates

obtained in ATR mode

[152] Satake and Matuura 1960.

The small peaks at around 1700cm^{-1} and at 950cm^{-1} are from acid residues - unreacted acid or resulting from the carboxylate ions in aqueous medium[153] according to the following reactions:

$$\mathbf{2H_2O \rightleftharpoons H_3O^+ + OH^-}$$

$$\mathbf{RCOO^- + H_3O^+ \rightleftharpoons RCOOH + H_2O}$$

Studies have demonstrated that the mode of coordination between a metal ion and a carboxylate ion can be predicted by comparing the Δ value of the carboxylate ion stretchings [ν_a COO$^-$ - ν_s COO$^-$] in the complex with those for its sodium salt.[154]

When the Δ νCOO$^-$ value of the carboxylate ion is *much higher* than that of the ionic complex, the mode of complexation with the metal is unidentate. If Δ νCOO$^-$ value is *significantly less* than that of the ionic complex, the mode of coordination with the metal is mono (unidentate) or bidentate. When Δ νCOO$^-$ values are *greater than chelating complexes but closer to* that of ionic complexes, the mode of coordination with the metal is bridging. In the literature, copper(II) carboxylates have been described as mono or binuclear structures with two or four carboxylate ligands respectively.[155]

The Δ νCOO$^-$ values for the sodium salt of each carboxylate acid used in the research alongside the Δ νCOO$^-$ values for the copper carboxylate complex are listed in Table 5. Given their similar order of magnitude, it is suggested that the copper ions formed an ionic

[153] Gunn et al. 2002.
[154] Itoh and Bernstein in Nakamoto 1997; Nakamoto 1997.
[155] Pavlopoulou and Watkinson 2006.

bond with the carboxylate ions in the copper-carboxylate complexes synthetized for this research.

Cu-Palmitate	Cu - Stearate	Cu-Oleate	Cu-Linoleate	Band Assignment
2914 vs	2912 vs	2916 vs	2924 vs	C-H stretching vibrations
2849 vs	2846 vs	2849 s	2853 s	C-H stretching vibrations
1583 vs	1585 vs	1583 vs	1601 vs	COO^- asymmetric stretching vibration
1422 m	1419 m	1414 m	1413 m	COO^- symmetric stretching vibration
721 m	716 m	718 w		COO^- scissor vibration
682 m	673 w			COO^- wagging vibration

broad (br), very strong (vs), s (strong), m (medium), w (weak), vw (very weak)

Table 5 - Characteristic FTIR bands of Cu-carboxylates

The (+) coupons containing the copper-carboxylate complexes were also analysed by microscope FTIR (Figure 16). The main advantage of microscope FTIR is that it enables spatial-resolved analysis without sample removal, which makes it ideal for the study of paintings and manuscripts. The asymmetric carbonyl stretching vibration characteristic of metal soaps - well-defined for the palmitic and stearic complexes (top two in Figure 16) - are less prominent for the unsaturated acids complexes, perhaps explaining why unsaturated copper soaps are not reported in the literature.[156]

[156] Prati et al. 2016; La Nasa et al. 2018; Salvadó et al. 2019.

Compound	ν_a (COO^-)[a]	ν_s (COO^-)[a]	Δ	Structure
$HCOO^-$ (formate ion)	1567	1366	201	Ionic[157]
CH_3COO^- (acetate ion)	1578	1414	164	Ionic[5]
Na-Palmitate	1580	1420	160	Ionic[158]
Cu-Palmitate	1583	1422	161	ionic
Na-Stearate	1580	1425	155	Ionic[6]
Cu-Stearate	1585	1419	166	ionic
Na-Oleate	1585	1425	160	Ionic[6]
Cu-Oleate	1583	1414	169	ionic
Na-Linoleate	1560	1410	150	Ionic[6]
Cu-Linoleate	1601	1413	188	ionic

[a] These correspond to the ν(C=O) free and ν(C-O) coordinated of the unidentate carboxylates, respectively.

Table 6 - Carbonyl stretching frequencies and structures of Cu-carboxylates

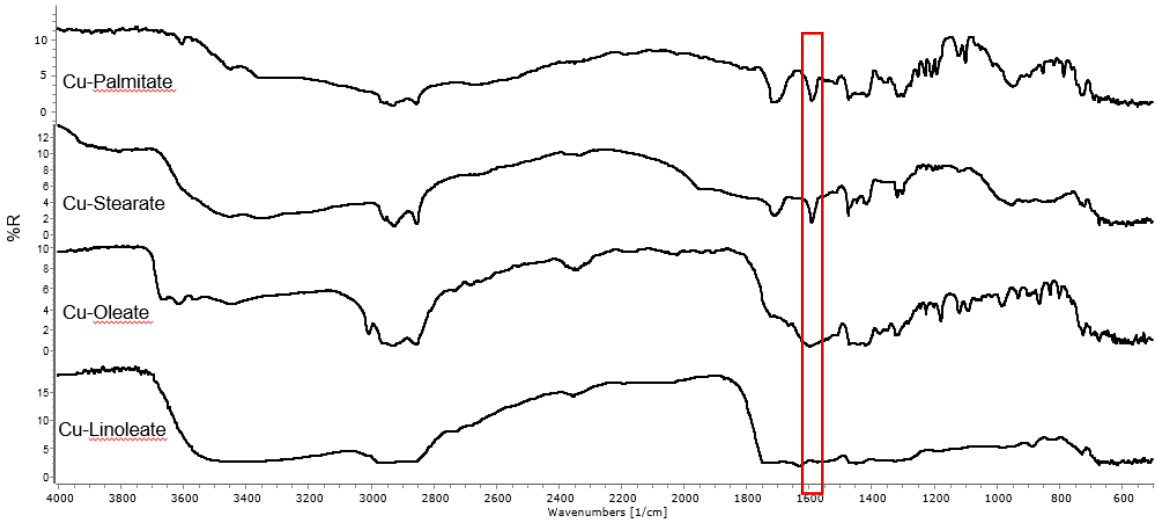


Figure 16 - FTIR spectra of Cu-carboxylates obtained with a microscope

[157] Itoh and Bernstein in Nakamoto 1997.
[158] FTIR reference spectra for sodium salts from spectrabase.com.

4.2.1.2 Characterization by Raman

The full set of Raman spectra for the metal carboxylate complexes is included in Appendix 3. Figure 17 shows the Raman spectra of palmitic acid and copper palmitate.

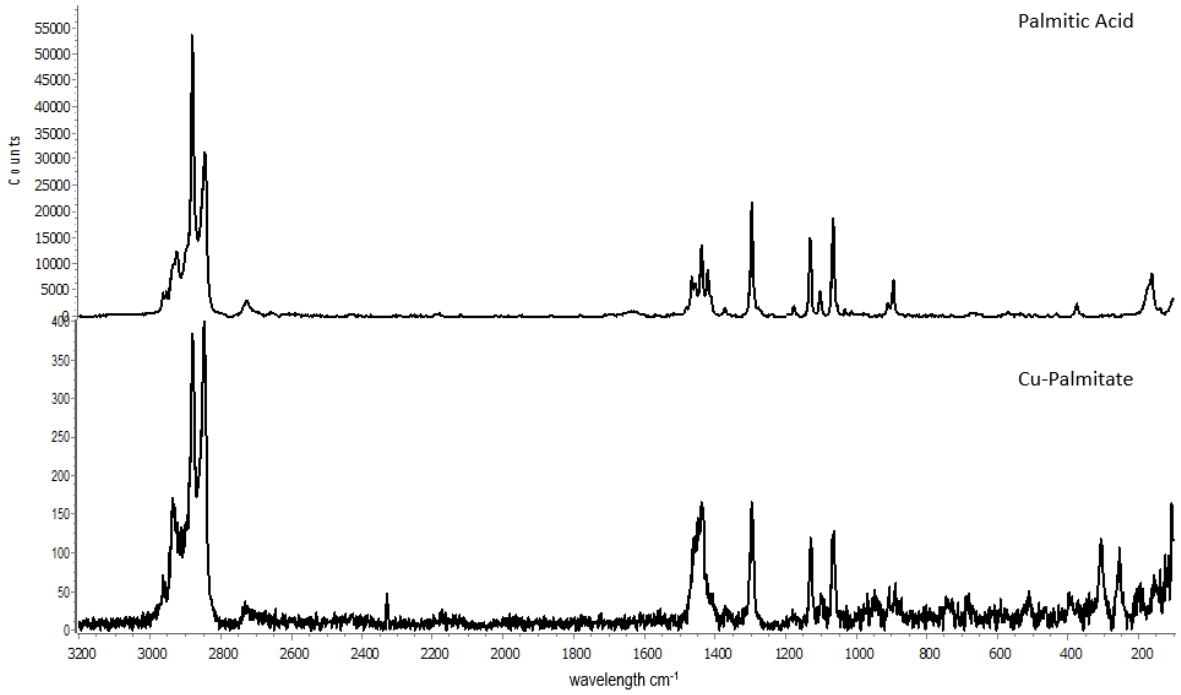


Figure 17 - Raman spectra of palmitic acid and Cu-palmitate

baseline corrected

Theoretical and experimental studies have assigned bands below 590cm^{-1} in the infrared and Raman spectra of metal-organic complexes to metal-nitrogen (M-N) and metal-oxygen (M-O) vibrations.[159] Cu-O vibrations have been specifically assigned to bands in the 350-180cm^{-1} region for copper(II) acetate,[160] copper(II) hexanoate,[161] copper palmitate and

[159] Nakamoto 1997; Socrates 2001.
[160] Mathey et al. 1981; Conti et al. 2013.
[161] Doyle et al. 2000.

copper stearate.[162] Therefore, the 307cm^{-1} and 255cm^{-1} bands in the copper palmitate complex (Figure 18) may be attributed to Cu-O vibration, thus providing evidence of metal-organic complexation.

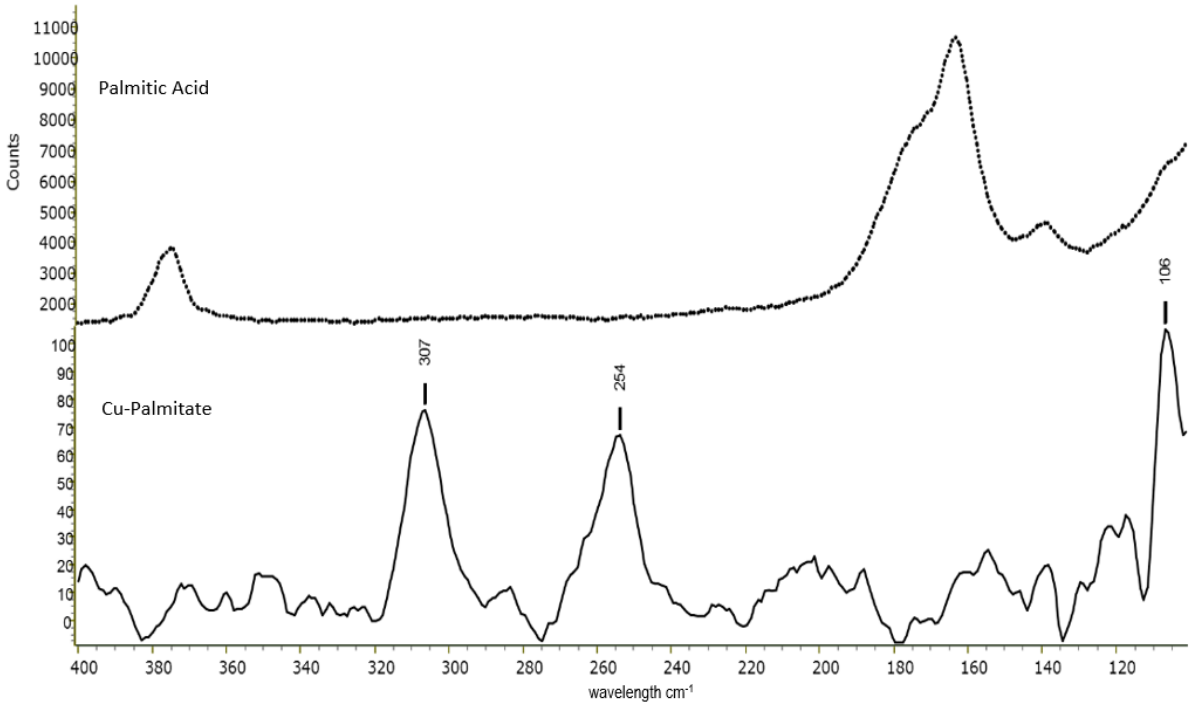


Figure 18 - Raman spectra of palmitic acid and Cu-palmitate between 400-130cm^{-1}
baseline corrected

The Raman spectra from all copper carboxylates are shown in Figure 19 and characteristic bands in Table 7. The Raman shifts assigned to Cu-O vibrations have been detected in all complexes except for copper linoleate, due to fluorescence.

[162] Robinet and Corbeil 2003.

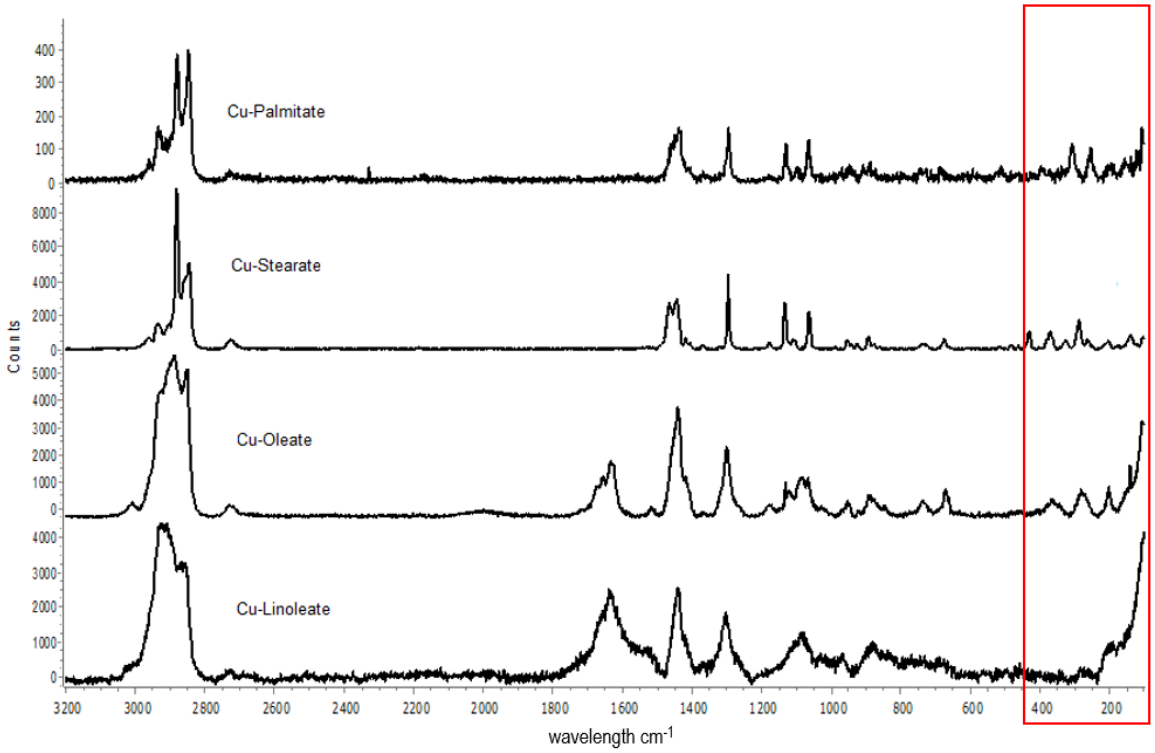


Figure 19 - Raman spectra of Cu-carboxylates

shifts due to metal chelation within RED square, **baseline corrected**

The main difference in the copper carboxylates' spectra is the broad peak at around 1630cm^{-1} in copper oleate and copper linoleate corresponding to the carbon double bond(s), which are very weak in FTIR.

Cu-Palmitate	Cu-Stearate	Cu-Oleate	Cu-Linoleate	Band Assignment
2934 m	2931 m	3007 m	2920 s	C-H stretching vibrations
2880 vs	2880 vs	2867 s	2867 s	C-H stretching vibrations
2847 vs	2847 vs			C-H stretching vibrations
		1633 s	1638 s	C=C stretching vibrations
1556 vw	1523 vw	1517 w		COO^- asymmetric stretching vibration
1437 s	1442 s	1440 s	1440 s	CH_2 scissors aliphatic
1296 s	1297 s	1301 s	1302 s	CH_2 torsion
1130 s	1132 s	1132 s		C-C vibrations
1066 s	1063 s	1070 s	1085 s	C-C vibrations
950 w	953 w	952 vw	967 vw	COO^- deformation
			880 m	
	431 m			Cu-O vibration
	371 m	364 m		Cu-O vibration
307 m				Cu-O vibration
	287 m	282 m		Cu-O vibration
255 m				Cu-O vibration

Table 7 - Characteristic Raman bands (cm^{-1}) and assignments for Cu-carboxylates

Figure 20 shows the spectra for oleic acid and its copper complex. Although there is a change in the position of the Raman shift assigned to the carbon double bond from 1657cm^{-1} in the acid to 1633cm^{-1} in the copper complex, it does not characterize an organometallic coordination. If metal-ethylene coordination had occurred, the band would have changed to 1580-1500cm^{-1} or near to 1220cm^{-1}.[163]

[163] Socrates 2001.

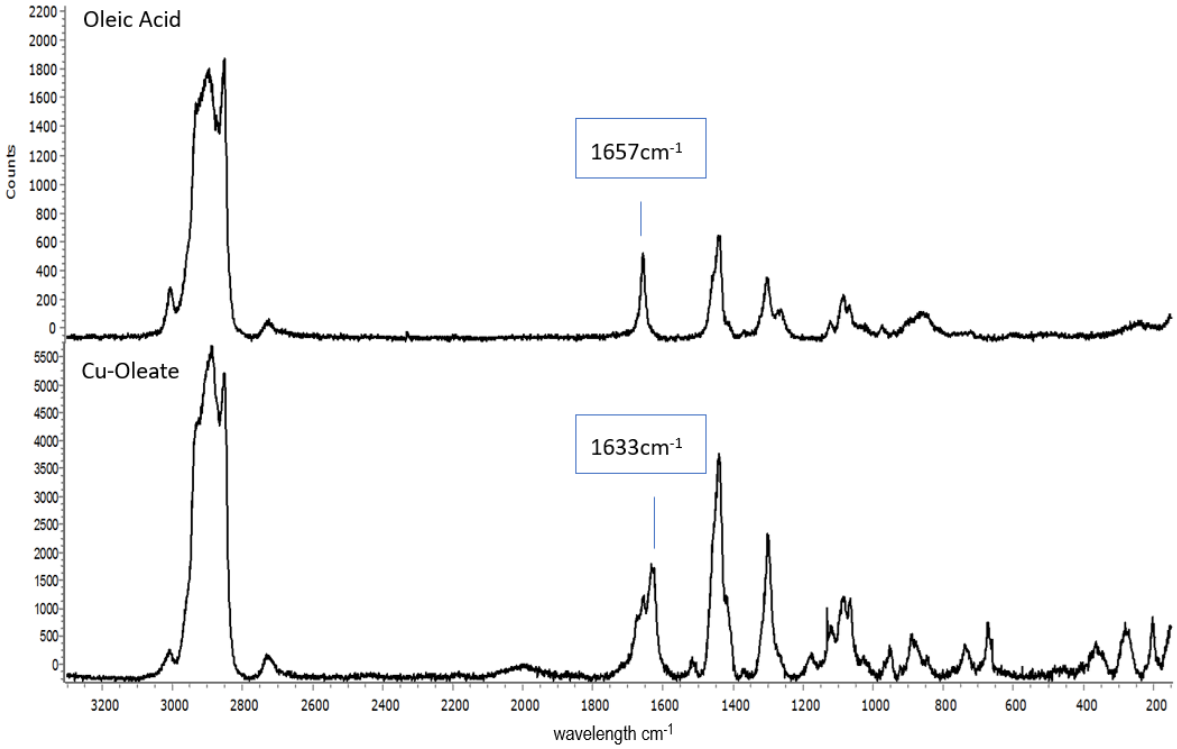


Figure 20 - Raman spectra of oleic acid and Cu-oleate

4.2.1.3 Characterization by XPS

The full set of XPS spectra is included in Appendix 4.

The XPS survey spectrum for copper palmitate is shown in Figure 21. In addition to oxygen and carbon, it shows the presence of copper and chloride ions, the latter a trace contaminant from the electrolyte.

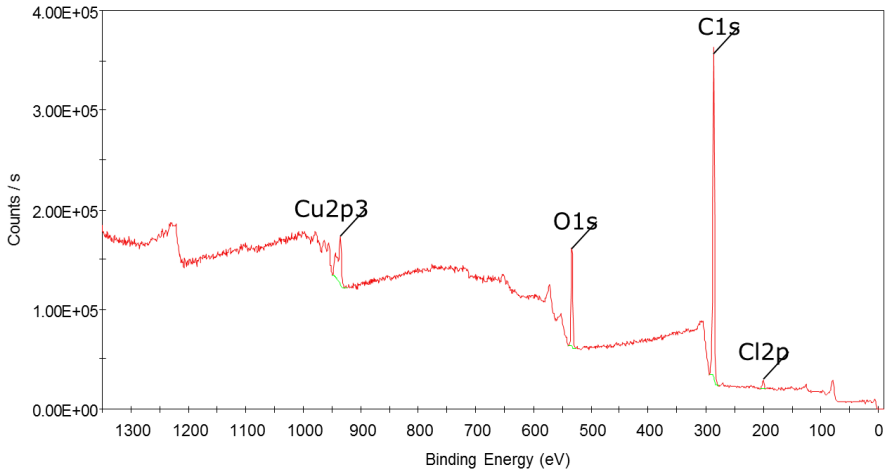


Figure 21 - XPS survey spectrum for Cu-palmitate

Table 8 shows the atomic percentages for palmitic acid and copper carboxylate complexes. As discussed in section 3.2.1.1, the frequency of C=O vibration measured with FTIR for palmitic acid indicated a dimer structure. The generic dimer structure for carboxylic acids is shown in Figure 22.

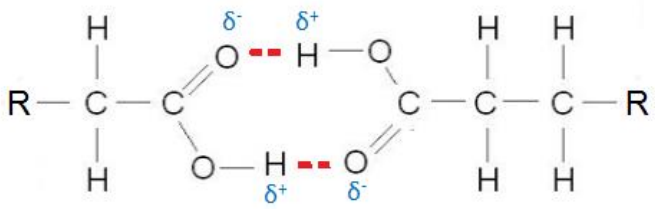


Figure 22 - Carboxylic acid dimer arrangement

due to hydrogen bonding of the acidic hydrogen and the carbonyl oxygen marked by RED dashed line

	Relative Atomic Percentages		
	Cu (%)	C (%)	O (%)
Palmitic Acid	-	89.32	10.62
Cu-Palmitate	2.81	85.53	10.72
Cu-Stearate	2.93	84.62	10.62
Cu-Oleate	2.25	87.97	9.81
Cu- Linoleate	3.00	68.93	24.23

Table 8 - Elemental composition of palmitic acid and Cu-carboxylates

Using the experimental XPS atomic percentages in Table 8 and assuming four oxygen atoms as the base for calculations, the carbon, oxygen and copper proportions for the palmitic acid and copper carboxylates were calculated and are presented alongside the experimental values in Table 9. There is agreement between theoretical and experimental values for the copper palmitate and copper oleate, but there are deviations for copper stearate of 11% and of 61% for copper linoleate – indicating the decomposition of the organic ligand prior to or during analysis.

	Chemical Formula of Organic ligand	C:O:Cu (theoretical)	C:O:Cu (experimental)*
Palmitic Acid	$C_{16}H_{32}O_2$	32:4:0	34:4:0
Cu-Palmitate	$C_{16}H_{32}O_2$	32:4:1	32:4:1
Cu- Stearate	$C_{18}H_{36}O_2$	36:4:1	32:4:1
Cu-Oleate	$C_{18}H_{34}O_2$	36:4:1	36:4:1
Cu-Linoleate	$C_{18}H_{32}O_2$	36:4:1	11:4:1

* rounded to closest integer

Table 9 - Theoretical and experimental C, O and Cu proportions in palmitic acid and Cu-carboxylates

In XPS, Cu(II) atoms can be differentiated from Cu(I) atoms by the presence of shake-up (or satellite) peaks in its Cu 2p spectrum, independent of the ligand.[164] For comparison purposes, the Cu 2p spectra for metallic copper, cuprous oxide and cupric sulphide were collected and shown alongside that of Cu-palmitate in Figure 23.

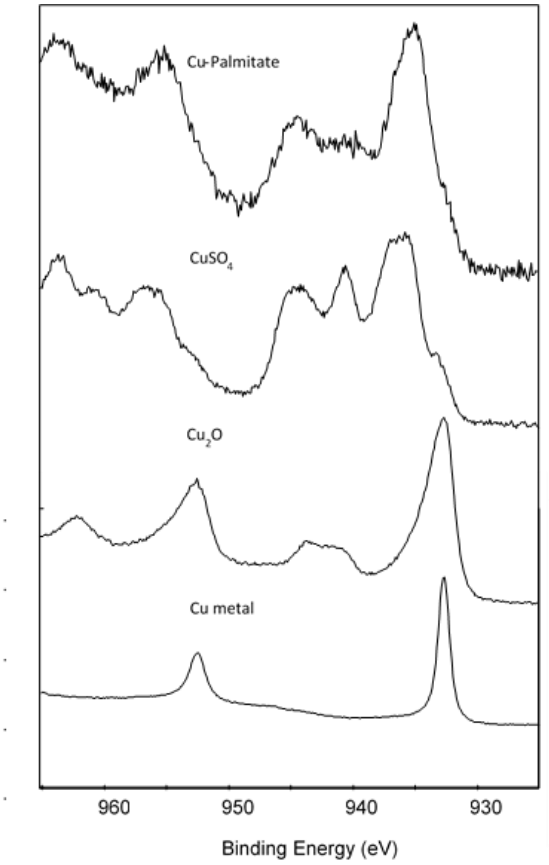


Figure 23 - Cu2p spectra of copper, Cu_2O, $CuSO_4$ and Cu-palmitate

Although the Cu metal surface had been cleaned prior to the analysis, its Cu2p spectra shows two peaks of Cu(I) ions, deriving from an invisible copper oxide film. As expected, Cu(I) peaks appear in cuprous oxide, but although weak, extra satellite peaks appear in the regions below 960eV and between 945-940eV. These extra peaks show the oxidation of

[164] Frost et al. 1972; Larson 1974; Biesinger et al. 2010.

Cu(I) to Cu(II) because the cuprous oxide container had been opened for some years prior to analysis. These satellite peaks characteristic of Cu(II) are better defined in the Cu2p spectra of cupric sulphide. The Cu2p spectra of copper palmitate and the remaining metal carboxylates (Figure 24) all contain satellite peaks, thus confirming the presence of Cu(II) ions.

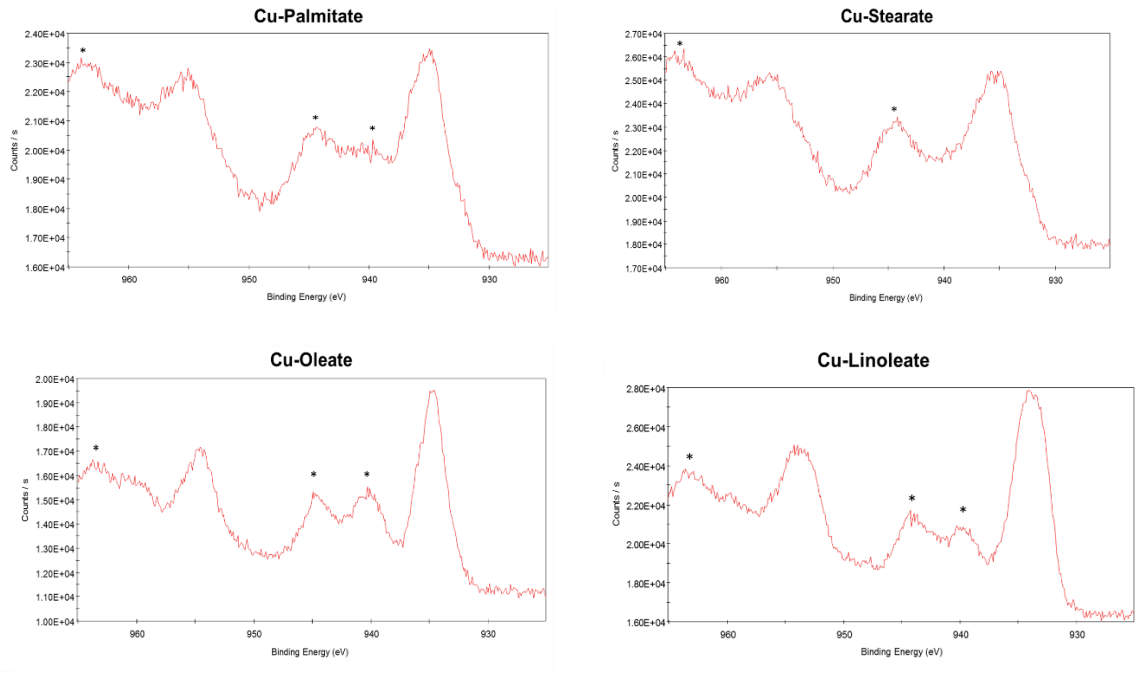
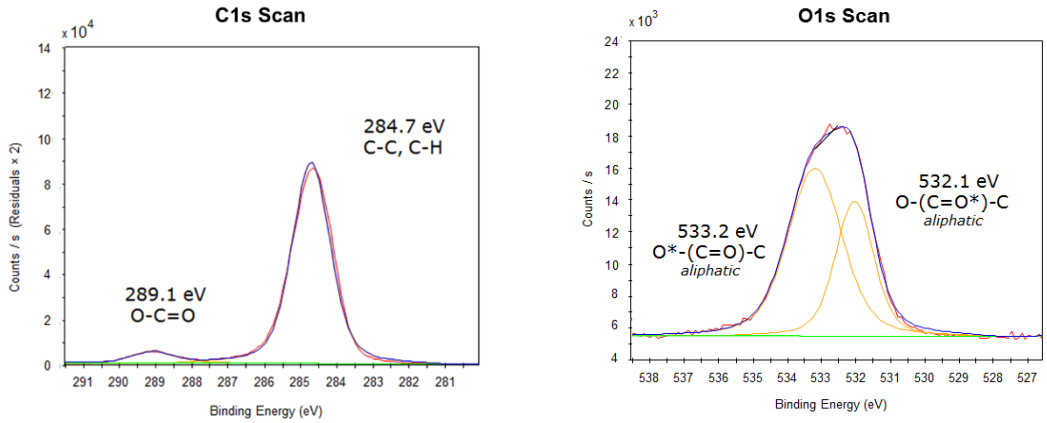


Figure 24 - Cu2p spectra of Cu-carboxylates [*] denoting Cu(II) satellite peaks

Further evidence of metal complexation can be obtained by comparing the high-resolution spectra of C1s and O1s regions of carboxylic acid and copper palmitate (Figure 25).

PALMITIC ACID



Cu-PALMITATE

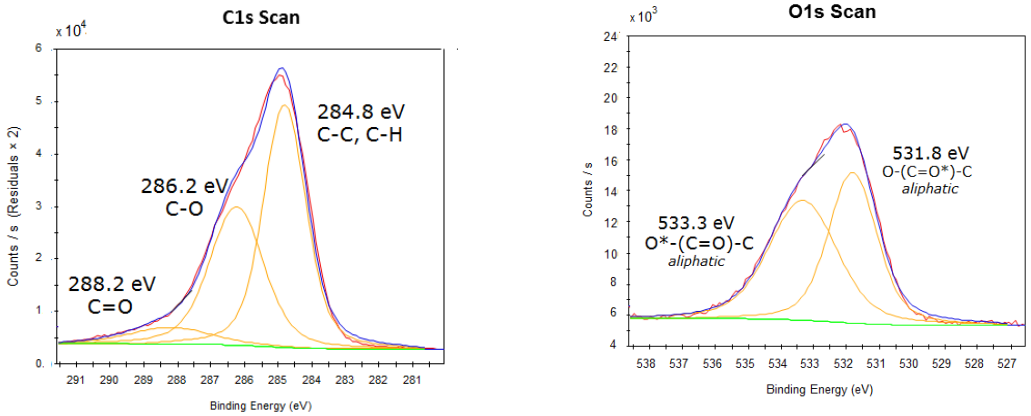


Figure 25 - C1s and O1s regions spectra in palmitic acid and Cu-palmitate

ORANGE curves denoting peak fittings

Palmitic acid's C1s spectrum contains peaks at 284.7 and 289.1eV binding energy (BE) corresponding to C-C/C-H bonds in a carbon chain and a carbon coordinated to oxygen atoms of a carboxylic acid, respectively. On the other hand, the C1s spectrum for the copper palmitate can be decomposed into three peaks: the C-C/C-H peak at a slightly higher BE at 284.8eV and two peaks for the carboxylate carbon, one at 286.2eV and another at 288.2eV

assigned to C-C=O[165] and C-O[166] bonding respectively. There are also slight changes in the O1s spectra: a decrease in the energy of the O=C from 532.1 to 531.8eV and an increase in the O-C from 533.2 to 533.3eV with copper complexation. Similar values are observed in the XPS spectra of the remaining copper carboxylates, as summarized in Table 10.

Element	Chemical Bonds	Cu- Palmitate	Cu-Stearate	Cu-Oleate	Cu-Linoleate
C1s	**C-C, C-H, C=C**	284.8	284.6	284.6	284.4
BE (eV)	**C-O**	286.2	285.8	285.9	285.9
	C=O, C-O-Cu	288.2	287.8	288.7	288.2
O1s	**O-(C=O*)-C**	531.8	531.7	531.7	531.6
BE (eV)	**O*-(C=O)-C**	533.3	533.1	533.0	532.8

Table 10 - C1s and O1s peaks binding energies (BE) for Cu-carboxylates

As the position of an XPS peak for an atom is affected by the initial binding energy of the electron in its orbital, any changes in the atom's vicinity are likely to shift peak positions. However, copper carboxylates exist as coordination complexes where the bond between the metal ion and the organic component is often delocalized without having a distinct covalent or ionic character. Hence, the chemical shifts imposed by the metal ion on the carboxylic function cannot be easily measured by XPS.

[165] Cano et al. 2001.
[166] Ávila-Torres et al. 2013.

Considering the XPS atomic proportions and C1s, O1s and Cu2p spectra, the general chemical structure of the copper carboxylates may be represented as a dimer structure as shown in Figure 26.

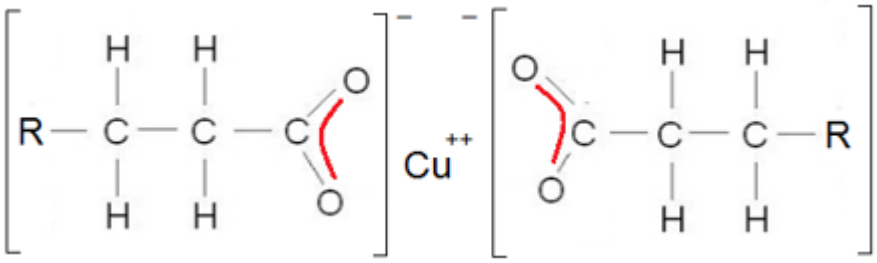


Figure 26 - Proposed molecular arrangement of Cu-carboxylates

the uniform distribution of the negative charge between the two oxygen atoms in each carboxylate ion denoted by RED line

4.2.1.4 Characterization by XRD

Diffraction patterns for the copper carboxylates were obtained between 5-40^{o} 2θ and shown in Figure 27 and in Tables 11-13. Below 25^{o} 2θ, the intensity and position of the peaks appear to correlate with the length of the carbon chain and its level of unsaturation. An increase in the carbon chain (from C16 in the copper palmitate to C18 in the copper stearate) resulted in a shift in peak positions to lower angles, analogous to the acid forms as reported in the literature.[167]

[167] Corbeil and Robinet 2002.

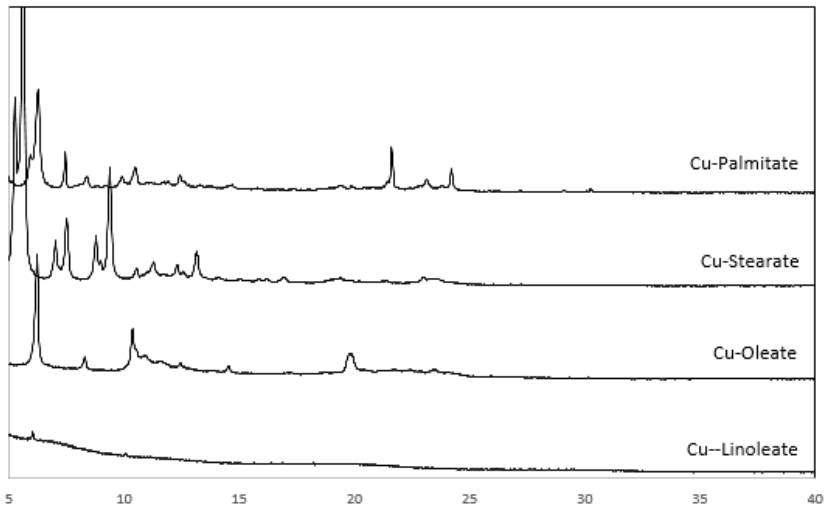


Figure 27 - Cu-carboxylates XRD diffractograms

2θ (°)	d-spacings (nm)	I/I₀ (%)	2θ (°)	d-spacings (nm)	I/I₀ (%)
5.991	**1.4739**	**28.3**	18.522	0.4787	1.3
6.246	**1.4139**	**100.0**	18.989	0.4670	1.5
7.435	**1.1880**	**34.7**	19.385	0.4575	3.5
8.353	1.0576	10.8	19.893	0.4460	3.4
8.812	1.0027	0.8	20.443	0.4341	1.9
9.196	0.9607	1.7	20.813	0.4265	2.1
9.901	0.8927	10.4	**21.612**	**0.4109**	**43.1**
10.462	0.8449	18.6	22.463	0.3955	1.5
11.129	0.7944	4.2	22.866	0.3886	3.7
11.739	0.7533	5.2	23.135	0.3842	10.8
11.878	0.7445	5.7	23.803	0.3735	4.4
12.402	0.7131	12.0	24.207	0.3674	22.4
13.315	0.6644	1.9	27.212	0.3276	1.0
13.755	0.6433	1.9	27.625	0.3227	0.6
14.548	0.6084	2.5	29.083	0.3068	1.0
15.799	0.6047	1.1	30.26	0.2951	3.0
17.367	0.5102	1.1			

Table 11 – XRD peak list for Cu-palmitate

most intense peaks highlighted

2θ (°)	d-spacings (nm)	I/I$_o$ (%)	2θ (°)	d-spacings (nm)	I/I$_o$ (%)
5.272	**1.6749**	**39.8**	13.145	0.6730	6.5
5.611	**1.5739**	**100.0**	14.071	0.6289	0.6
7.012	1.2596	9.0	15.047	0.5883	0.5
7.499	1.1779	14.5	15.846	0.5588	0.7
8.772	1.0073	10.2	16.188	0.5471	0.6
8.959	0.9862	3.9	16.94	0.5230	1.1
9.375	**0.9426**	**26.9**	19.385	0.4575	1.0
10.528	0.8396	2.2	19.752	0.4491	0.5
10.851	0.8147	0.8	20.196	0.4394	0.3
11.108	0.7959	1.6	21.378	0.4153	0.4
11.261	0.7852	3.6	23.01	0.3862	1.4
12.299	0.7191	3.3	23.565	0.3772	1.2
12.56	0.7042	1.4			

Table 12 - XRD peak list for Cu-stearate

most intense peaks highlighted

2θ (°)	d-spacings (nm)	I/I$_o$ (%)	2θ (°)	d-spacings (nm)	I/I$_o$ (%)
6.194	**1.4257**	**100.0**	**19.823**	**0.4475**	**19.1**
8.265	1.0689	10.1	20.382	0.4354	3.1
10.388	**0.8509**	**37.0**	21.741	0.4085	3.8
10.87	0.8133	14.5	22.404	0.3965	3.9
11.532	0.7666	9.3	22.816	0.3895	3.1
12.438	0.7111	7.6	23.446	0.3791	5.1
14.525	0.6093	6.9	24.091	0.3691	3.0
18.752	0.4728	1.6	25.953	0.3430	0.8

Table 13 - XRD peak list for Cu-oleate

most intense peaks highlighted

The effect of carbon chain unsaturation on the diffraction patterns can be observed by comparing the patterns for copper stearate with those obtained for copper oleate. The latter has highest intensity peak at similar d-spacing (1.4257nm) in the same order as that of copper palmitate (1.4139nm) as reported in the literature.[168]

The diffraction patterns obtained for the copper carboxylates conform to the general structural arrangement of a metal soap where metal atoms form a mono cationic layer sandwiched by the carboxylate carbon chains.[169] The effect of this arrangement results in high intensity long d-spacings at low angles, as the x-ray strikes the length of the metal soap dimer molecule, with the short d-spacings at higher angles corresponding to the chain packing arrangement.[170] No diffraction pattern could be obtained for copper linoleate.

4.2.1.5 Characterization by mass spectrometry techniques

4.2.1.5.1 Direct mass measurement by Flow Injection Analysis (FIA)

Only the mass of the carboxylate ions (i.e. without the copper ion) could be found, but at extremely low counts and varying with the solvent (Table 14).

The low abundance of carboxylate ions may be a consequence of the strength of the bond between copper and carboxylate ligand. The low ion count for the carboxylate ions obtained in acetonitrile was expected as this solvent can chelate Cu(II) ions producing copper(I)-

[168] Satake and Matuura 1960; Norazzizi et al 2014; Corbeil and Robinet 2002.
[169] Corkery 1997.
[170] Lomer and Perera 1974 in Corkery 1997.

acetonitrile complexes.[171] Interestingly, copper(I)-acetonitrile complexes were only identified in the copper stearate (main ion peak) and copper oleate samples.

	Ion Mass	Acetonitrile	Chloroform	Methanol
Cu-Palmitate	255.2327	*	***	**
Cu-Stearate	283.2636	*	*	**
Cu-Oleate	281.2486	**	***	**
Cu-Linoleate	279.2327	*	*	**

KEY: * trace ** low ***medium in logarithmic scale

Table 14 - Cu-carboxylates relative solubilities in acetonitrile, chloroform and methanol

4.2.1.5.2 QTOF-GC-MS with TSP

The retention times obtained for the carboxylate ions are listed in Table 15 with the full data set included in Appendix 5.

	Organic ligand	Retention Time (min)
Cu- Palmitate	Hexadecanoic acid	12.4
Cu- Stearate	Octadecanoic acid	13.5
Cu-Oleate	Oleic Acid	13.4
Cu- linoleate	Linoleic acid	13.3

Table 15 – Retention times of carboxylate ligands

[171] Kolthoff and Coetzee 1957.

Despite the presence of minor impurities and/or thermal decomposition products, the chromatograms of Cu-palmitate, Cu-stearate and Cu-oleate all contained a large chromatographic peak of the corresponding carboxylic acid. For copper linoleate, the largest peak corresponds to azelaic acid ($C_9H_{16}O_4$) from the oxidative cleavage of linoleic acid.[172]

4.2.1.5.3 Solvent extraction with BSTFA derivatization followed by GC-MS

Only the palmitic and stearic ligands (as methyl esters) were identified at 19.44 and 21.95 minutes respectively. The dataset is included in Appendix 6.

4.2.1.6 Discussion

The FTIR, Raman and XRD results for the synthetized copper carboxylates largely agree with those published in the literature, except that their mode of coordination in this study is ionic as opposed to bridging bidentate as reported in the literature.[173] Confirmation that copper is coordinating with oxygen ions was obtained by the strong peak at around 1580cm^{-1} in the FTIR spectra and the peaks under 450cm^{-1} in the Raman spectra, which also showed that the C=C bonds in the copper oleate and copper linoleate remained practically unchanged when compared to the spectra of the precursor acids.

The blue/green colour of the compounds indicated the presence of Cu(II) ions, which was confirmed by XPS. The XPS survey data also indicates that each Cu(II) ion coordinates with two carboxylate ions in a dimer arrangement, leading to the long d-spacings in the XRD

[172] Morrison and Boyd 1992; Asomaning et al. 2014; Sembiring et al. 2020.
[173] Nelson and Taylor 2014.

data. This stoichiometry could not be confirmed for copper linoleate, possibly because the sample was damaged/degraded during data acquisition.[174] The results obtained from the mass spectrometry analyses demonstrate that the thermal separation probe method for extraction of the organic ligand is much more efficient than solvent extraction because it overcomes the low solubility of copper carboxylates in organic solvents.

4.2.2 Copper-lactose

Figure 28 shows the copper coupons at the end of the experiment after drying; the (+) coupon covered by a blue/greenish waxy deposit, from this point onwards referred to as Cu-lactose.



Figure 28 - Coupons used for the synthesis of Cu-lactose

4.2.2.1 Characterization by FTIR

Saccharides usually bind to a metal ligand via deprotonation of one or more hydroxyl groups.[175] Lactose is a disaccharide consisting of one galactose unit linked to a glucose unit

[174] Baer et al. 2003.
[175] Gottschaldt et al. 2004; Geibelmann et al. 2005 in Cerchiaro et al. 2005.

by an O-glycosidic bond (see Figure 29). Given its many hydroxyl groups, many modes of coordination between lactose and metal ions are possible. Figure 30 shows the spectra for pure lactose and Cu-lactose, with characteristic bands listed in Table 16.

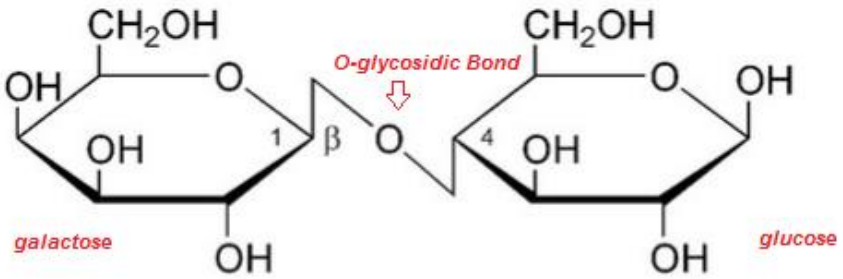


Figure 29 - Chemical structure of lactose

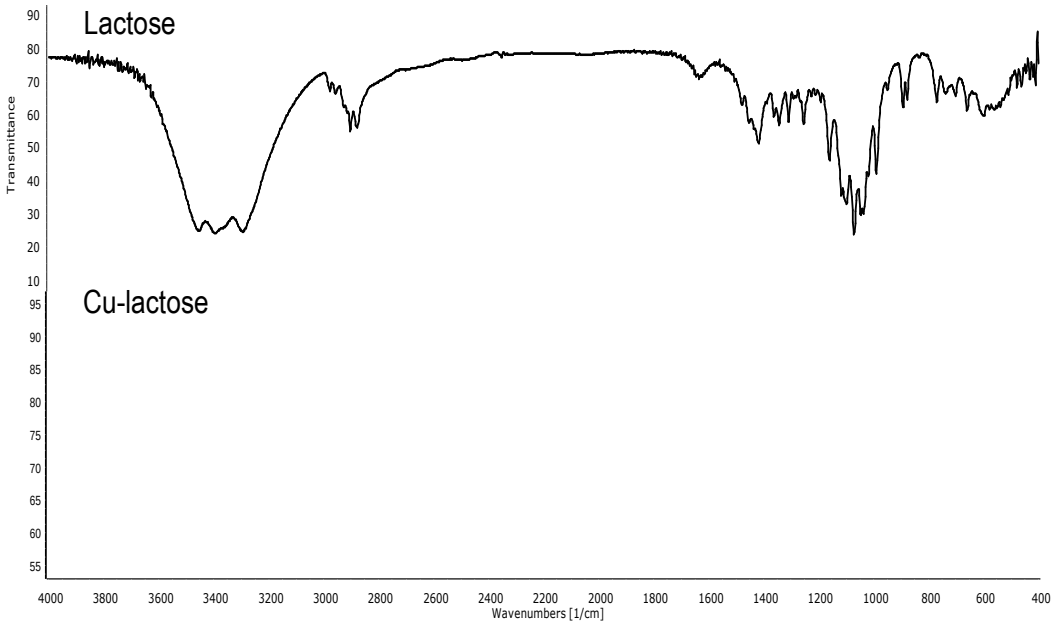


Figure 30 - FTIR spectra of lactose and Cu-lactose

KBr method

Lactose		Cu-Lactose		Band Assignments*
3744-3000	br	3694-3003	br	OH stretching vibration
2978	w			CH stretching vibrations
2957	w			CH stretching vibrations
2925	sh	2925	w	CH stretching vibrations
2903	m			CH symmetric vibration of CH_2OH group
2878	m	2853	w	CH asymmetric vibration of CH_2OH group
1634	w	1636	w	Bound water molecules
1454	w			H-CH group scissoring vibrations
1417	m			CH_2 wagging (galactose)
		1400-1300	br	
1361	m			OCH deformation
1343	m			CCH deformation
1253	m			C-H rocking, OH rocking (glc)
1192	w			OH in-plane bending, CH_2 rocking
1160	s	1160-890	br	C-O-C stretching vibration (glc)
1097	m			C-O-C stretching vibrations (gal)
1070	s			C-C stretching vibrations (gal)
990	m			C-H out-of-phase ring stretching and twisting
892	m			C-H out-of-phase ring stretching and twisting
659	m	660-460	br	
597	m			OCO in-plane bending (gal)
461	m			C-C-O in-plane bending (glc)

Table 16 - Characteristic FTIR bands in lactose and Cu-lactose

The spectra of lactose and copper-lactose are very similar, with the most characteristic peak being the hydroxylated broad band centred around 3400cm^{-1}. For lactose, this band contains small peaks at 3453, 3392 and 3294cm^{-1} corresponding to its level of crystallinity.[176] Instead

[176] Norris and Greenstreet 1958; Listiohadi et al. 2009.

of these small peaks, the copper-lactose complex has a shoulder peak at 3250cm^{-1} that can be assigned to intermolecular hydrogen-bonded species and OH stretching vibrations of water molecules[177] trapped within the complex during synthesis. The three sharp bands at 1480-1300cm^{-1}, 1160-890cm^{-1} and 660-460cm^{-1} in the pure lactose appear in the copper-lactose complex around 1400cm^{-1}, 1080cm^{-1} (including shoulders at 1100cm^{-1} and 1040 cm^{-1}) and 500cm^{-1} and indicate metal-disaccharide interaction.[178]

4.2.2.2 Characterization by Raman

The spectra for pure lactose and copper-lactose are shown in Figure 31.

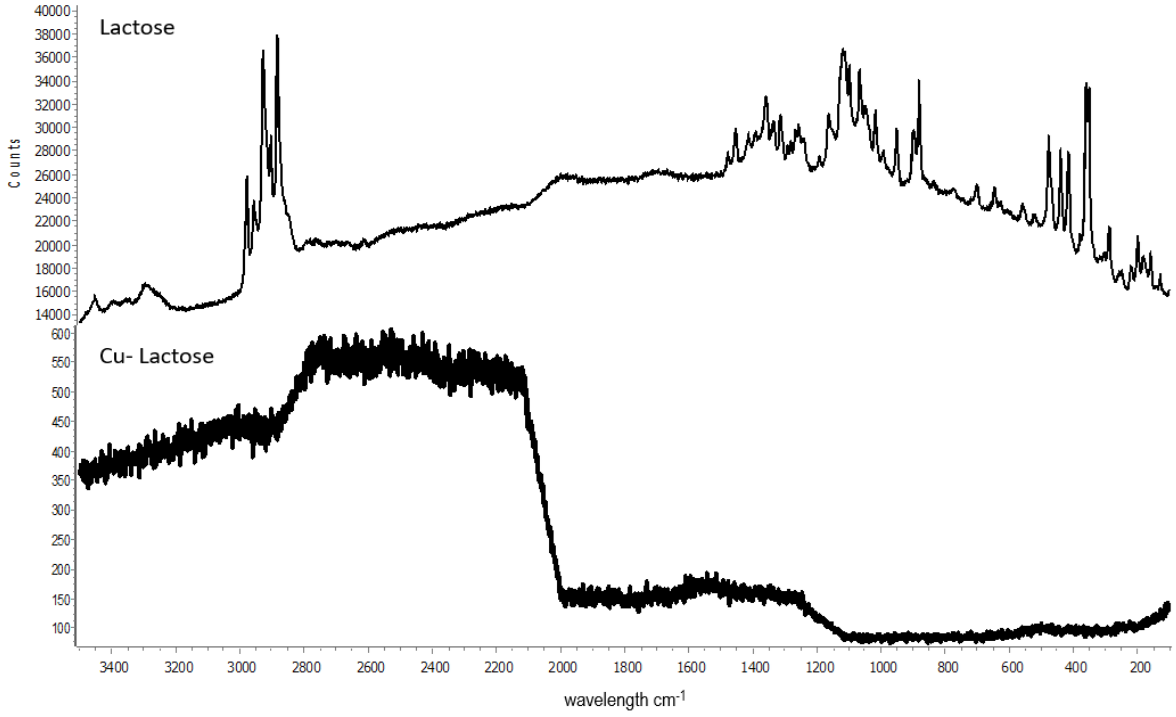


Figure 31 - Raman spectra of lactose and Cu-lactose

[177] Bandwar et al. 1995.
[178] Bandwar et al. 1995; Cerchiara et al. 2005.

The shape of the spectrum of copper-lactose indicates fluorescence from the complex itself or impurities within it. Fluorescence results from the emission of energy absorbed by the molecule as they return to a lower state of energy. If the laser excitation energy is close to the electronic transition energy of the molecule, fluorescence may obscure Raman scattering.[179] The most common method for dealing with fluorescence is to use a laser with lower wavelengths,[180] but none were available. Attempts were made to reduce the fluorescence by photobleaching the sample and by analysing Cu-lactose directly off the copper coupon (as opposed to removing it to a glass slide) – both without success.

4.2.2.3 Characterization by XPS

The XPS survey spectrum and atomic percentages for copper-lactose are shown in Figure 32 and the full dataset is included in Appendix 7.

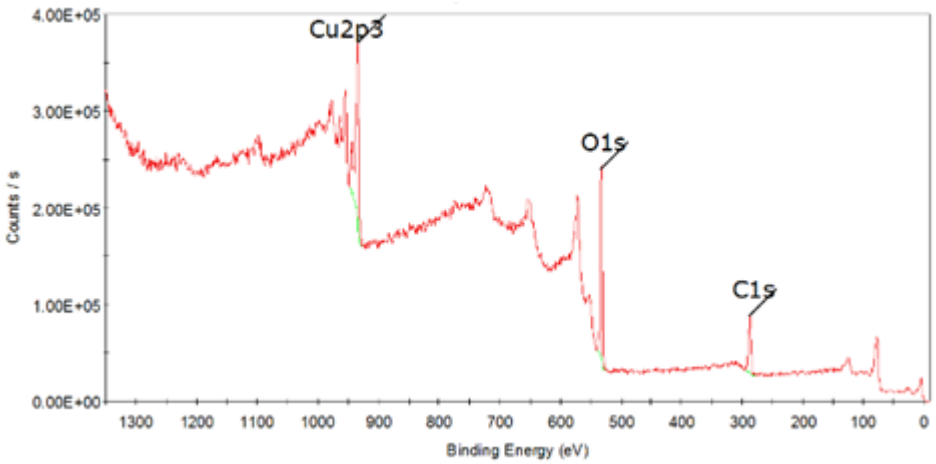


Figure 32 - XPS survey spectrum of Cu-lactose

[179] Cebeci-Maltas et al. 2017.
[180] Kagan and McCreery 1994; Cebeci-Maltas et al. 2017.

The atomic percentages obtained for lactose and the Cu-lactose complex are included in Table 17.

Sample	Relative atomic percentages (%)			
	C	O	Si	Cu
Lactose	52.4	43.5	4.1	
Cu-Lactose	43.3	41.0		15.7

Table 17 - Elemental composition of lactose and Cu-lactose

Despite the silicon contamination, the carbon and oxygen relative atomic percentages in lactose are close to those reported for anhydrous α/β lactose in the literature.[181] Interestingly, silicon was not detected in the Cu-lactose complex. The Cu2p spectrum of the copper-lactose (Figure 33) contains the characteristic satellite peaks indicating the presence of Cu(II) ions.

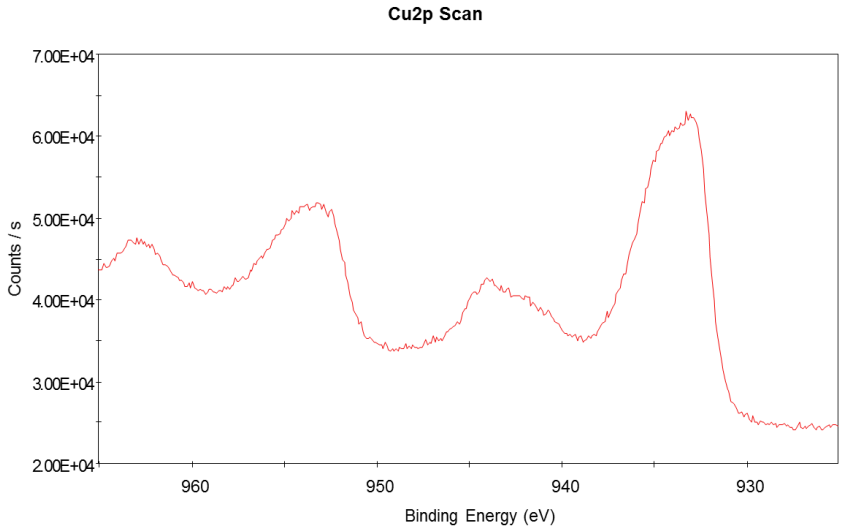
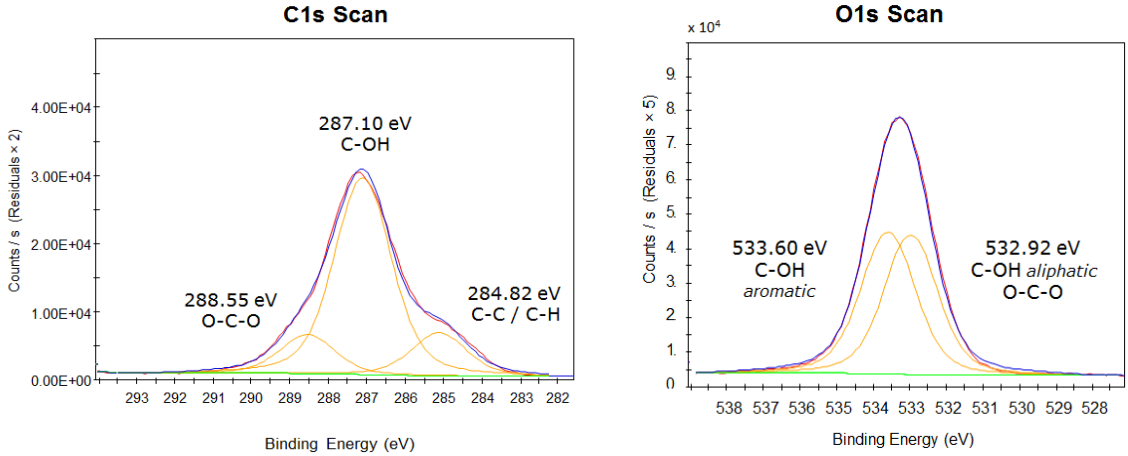


Figure 33 - Cu2p spectrum of Cu-lactose

[181] Stevens and Schroeder 2009.

The C1s and O1s spectra for lactose and copper-lactose are shown in Figure 34. Copper-lactose complex yielded broad peaks due to charging during data collection, which affected mostly the carbon species. This effect made peak fitting challenging. The main difference between the carbon spectra of lactose and copper-lactose is that the latter clearly decomposes in more than three peaks (bottom left in Figure 34), with the extra peak centred at 285.84eV.

Lactose



Cu-lactose

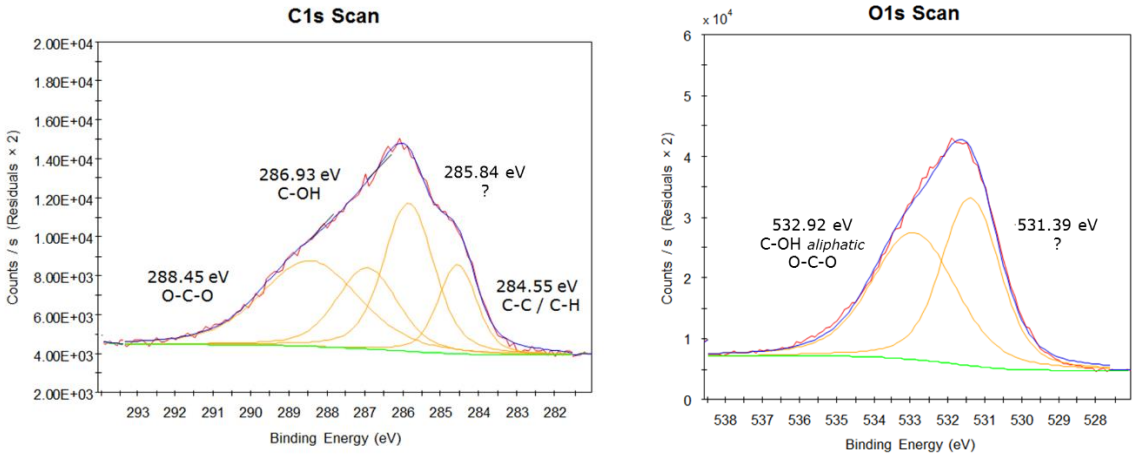


Figure 34 – C1s and O1s regions spectra of lactose and Cu-lactose

ORANGE curves denote peak fittings

The oxygen peaks for lactose and Cu-lactose also differ. Complexation with copper resulted in the disappearance of the C-OH aromatic peak at 533.60eV and the appearance of a new peak centred at 531.39eV. Although according to the literature, dehydroxylation of saccharides can occur during XPS analysis[182] there was no sign of degradation of the copper-lactose sample during or after analysis. Therefore, the peak at 531.39eV in the Cu-lactose could be attributed to Cu-O bonds, which in inorganic compounds appear between 530.99-531.25eV.[183]

4.2.2.4 Characterization by XRD

Figure 35 shows the XRD diffraction patterns obtained for Cu-lactose.

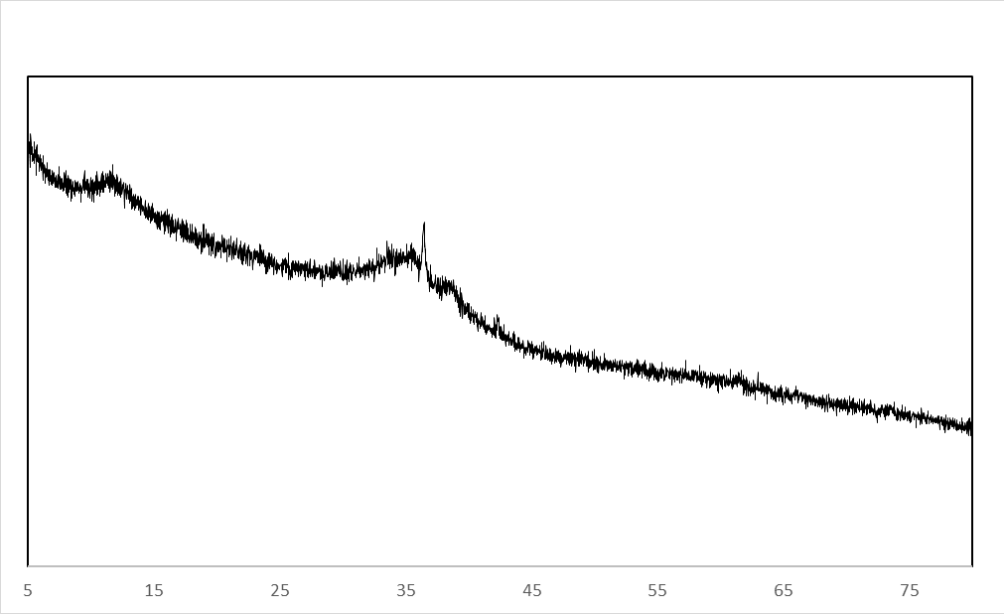


Figure 35 - XRD diffractogram of Cu-lactose

After some data manipulation it was possible to identify a cuprite phase within the largely amorphous deposit (Figure 36) despite the lack of data above 80º 2θ.

[182] Stevens and Schroeder 2009.
[183] Biesinger et al. 2010.

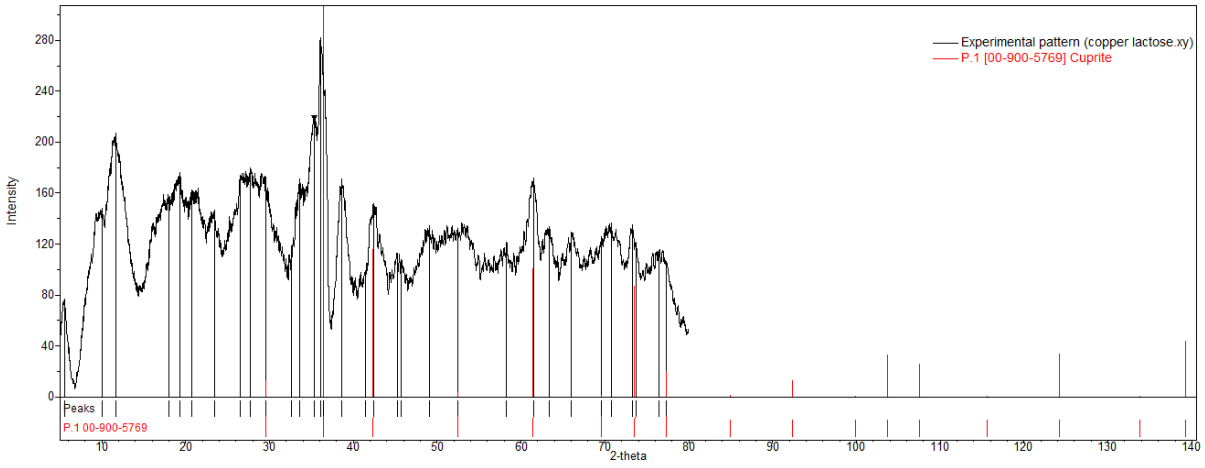


Figure 36 - XRD diffractogram of Cu-lactose showing cuprite as identified mineral phase

4.3.3.5 Characterization by Mass Spectrometry Techniques

4.3.3.5.1 Direct Mass Measurement by FIA

No ions with mass corresponding to copper lactose were found in any of the solvents. Lactose was detected in all solvents, albeit at low ion counts. The highest relative count achieved in acetonitrile.

4.3.3.5.2 QTOF-GC-MS with TSP

The CI and EI chromatograms for lactose and copper-lactose complex are shown in Figures 37 and 38 respectively. The spectral data is included in Appendix 8. Poor peak resolution only permitted the identification of a low number of compounds.

Lactose converts into its monosaccharide units after long exposure to temperatures above 180ºC,[184] yielding characteristic anhydro sugars and furan derivatives at 650ºC.[185] The high number of chromatographic peaks – each representing at least one compound – obtained for lactose and copper-lactose complex were therefore expected as the thermal sample probe (set at 320ºC) acted as a low temperature pyrolysis chamber. The identification of levoglucosenone is therefore significant, as the compound is a derivative of levoglucosan and a pyrolysis product of glucose[186] and lactose.[187]

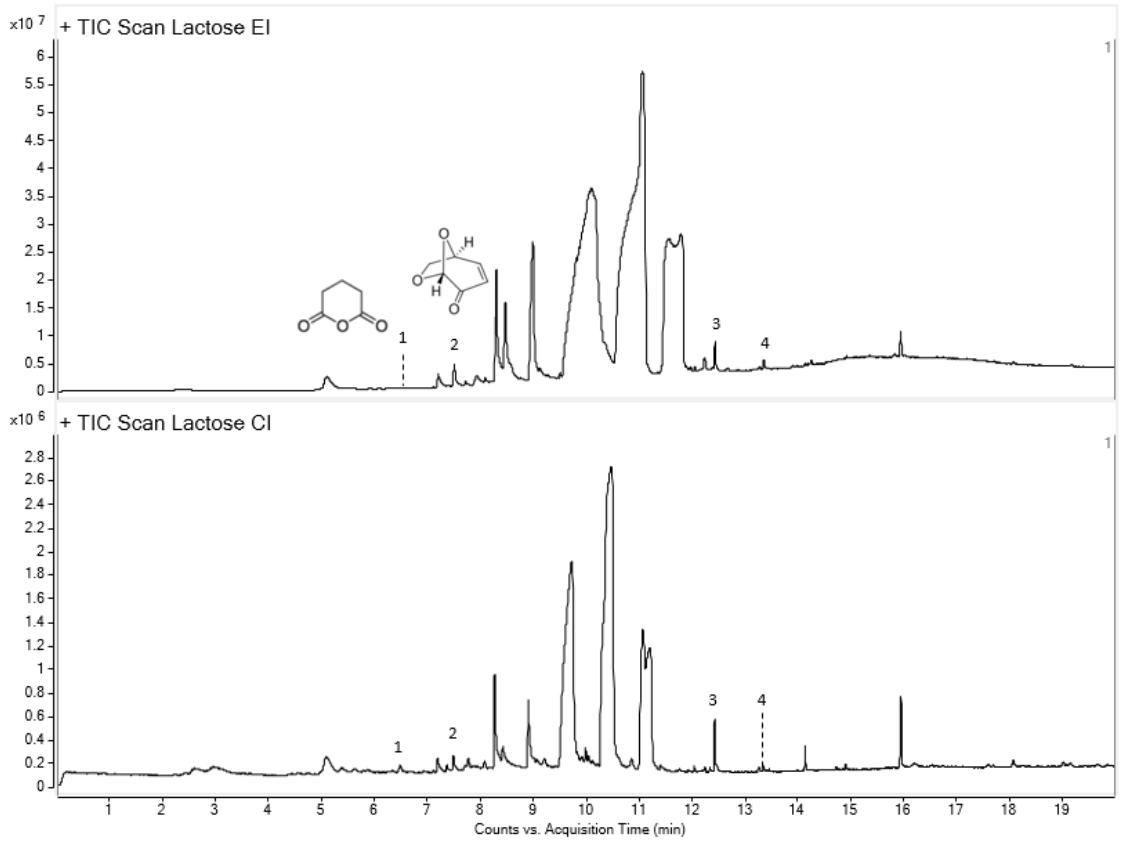


Figure 37 - EI and CI chromatograms of lactose

[1] 2H-Pyran-2,6(3H)-dione; [2] levoglucosenone; [3] n-hexadecanoic acid; [4] octanoic acid

[184] Paez and Martinez-Castro 1987.
[185] Budgel et al. 1987; Delidovich et al. 2014 and da Silva et al. 2016.
[186] Pilath et al. 2010.
[187] Pushkaraj et al. 2009; Torri et al. 2009.

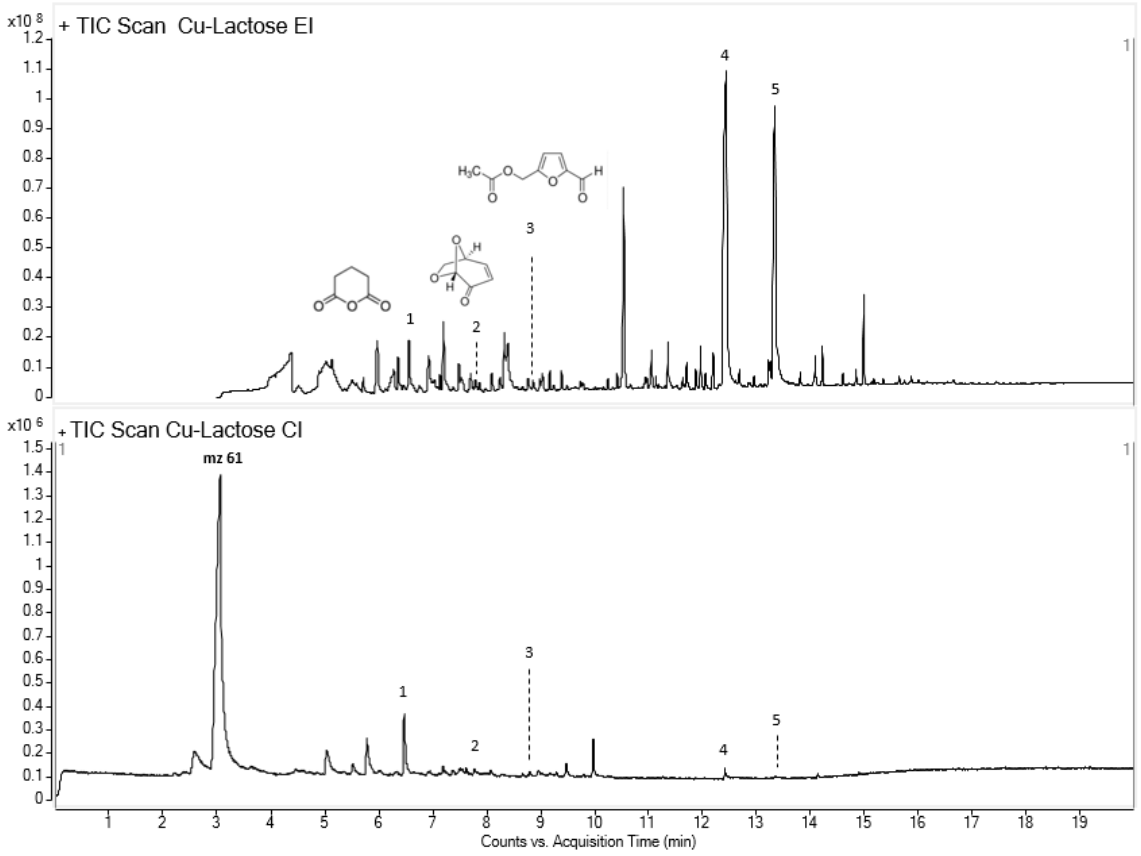


Figure 38 - EI and CI chromatograms of Cu-lactose

[1] 2H-Pyran-2,6(3H)-dione; [2] levoglucosenone; [3] 5-acetoxymethyl-2-furaldehyde; [4] n-hexadecanoic acid and [5] octadecanoic acid

The four compounds identified in lactose were also present in copper-lactose. The stronger fatty acid signals in copper-lactose perhaps indicate copper's preference for forming complexes with carboxylic acids or contamination. Copper-lactose contains additional peaks for 5-acetoxymethyl-2-furaldehyde and a strong mz 61 peak (in CI mode only). The presence of these compounds may be explained by the presence of Cu(II) ions which can reduce the decomposition temperature of cellulose, leading to higher yields of acetic acid, furans and gases.[188]

[188] Terakado et al. 2009.

4.2.2.5.3 Solvent extraction with BSTFA derivatization followed by GC-MS

No results were obtained because BSTFA is not suitable for identification of carbohydrates.

4.2.2.5 Discussion

The characterization of the copper-lactose complex by FTIR/Raman was complicated by poor peak definition and fluorescence. The XPS data confirmed the presence of Cu^{2+} ions within the compound suggesting coordination via the deprotonation of hydroxyl groups of the saccharide molecule. The identification of a cuprite phase by XRD in Cu-lactose is not surprising given that the glucose moiety in lactose is a reducing agent via its free aldehyde function that easily oxidises to acid.[189]

The mass spectrometry characterization of the copper-lactose complex was only possible using the thermal sample probe method, via identification of carbohydrate thermal decomposition products. This was despite the copper ions' catalyst effect.

4.2.3 Copper-casein

The (+) copper coupon (see Figure 39) was covered by a hardened translucent blue/greenish film, which peeled off from the coupon upon drying. From this point onwards it will be referred to as Cu-casein.

[189] Morrison and Boyd 1983.



Figure 39 - Coupons used for the synthesis of Cu-casein

Casein is a protein. Proteins are three-dimensional macro molecules composed of amino acids and peptides. All 20 amino acids found in proteins have a central carbon atom (α-carbon) connected to a carboxylic group, an amino group, a hydrogen atom and a unique R group (or side chain), as shown in Figure 40.

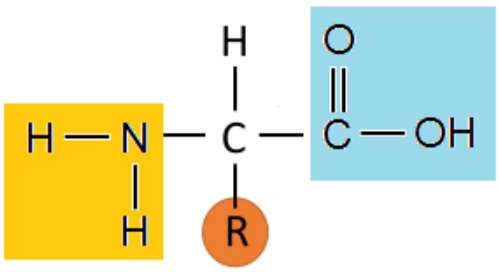


Figure 40 - The general amino acid structure

A central α-carbon bonded to a carboxylic group (BLUE), an amino group (YELLOW), a hydrogen atom and a R group (ORANGE) unique for every amino acid.

Individual amino acids are joined via the amino group of one amino acid and the carboxylic group of another to form a peptide (if they contain fewer than 50 amino acids) or polypeptides.

The structure of a protein is organized in four different levels. Its primary structure is determined by the amino acid composition of the main polypeptide chain and is dominated by covalent bonds between atoms. The folding of the polypeptide chain results in different types of interaction which are responsible for their secondary, tertiary and quaternary structures.

Bovine casein is a mixture of αs1-, αs2-, β-, κ-casein and other proteinaceous impurities, some of whose properties are listed in Table 18. Despite having many hydrophobic amino acids, caseins have an open hydrated structure with areas of high negative charge enabling them to form colloidal aggregates.[190]

	αs1-casein	αs2-casein	β-casein	κ-casein
Mass	24529	26019	25107	21269
Theoretical Isoelectric Point	4.91	8.34	5.13	5.93
# negative R / # positive R	32 / 20	28 / 30	23 / 15	16 / 14
Instability Index	57.99	46.27	96.62	57.46
Aliphatic index	75.43	68.70	88.47	73.31
% aromatic AA (% tryptophan)	14 (5)	9.7 (2)	6.7 (0.5)	8.3 (0.6)
# sulphur atoms	5	6	6	4
hydrophobicity		Least	Most	

Source: Uniprot

Table 18 - Some of the properties of caseins

Complexation between metal ions and proteins requires coordination with a donor atom, possibly via the deprotonation of a nitrogen from an amino group, the oxygen from a carboxylic acid group, and/or by interactions with the π-electrons from aromatic rings in the

[190] Alaimo et al. 1999.

side chain of amino acids. In milk, αs- and β-caseins bind Ca^{2+} ions at phosphorylated serine residues[191] providing stability to micelle structures.[192]

4.2.3.1 Characterization by FTIR

The spectra for casein and the copper-casein are shown in Figure 41. The characteristic bands are listed in Table 19.

.

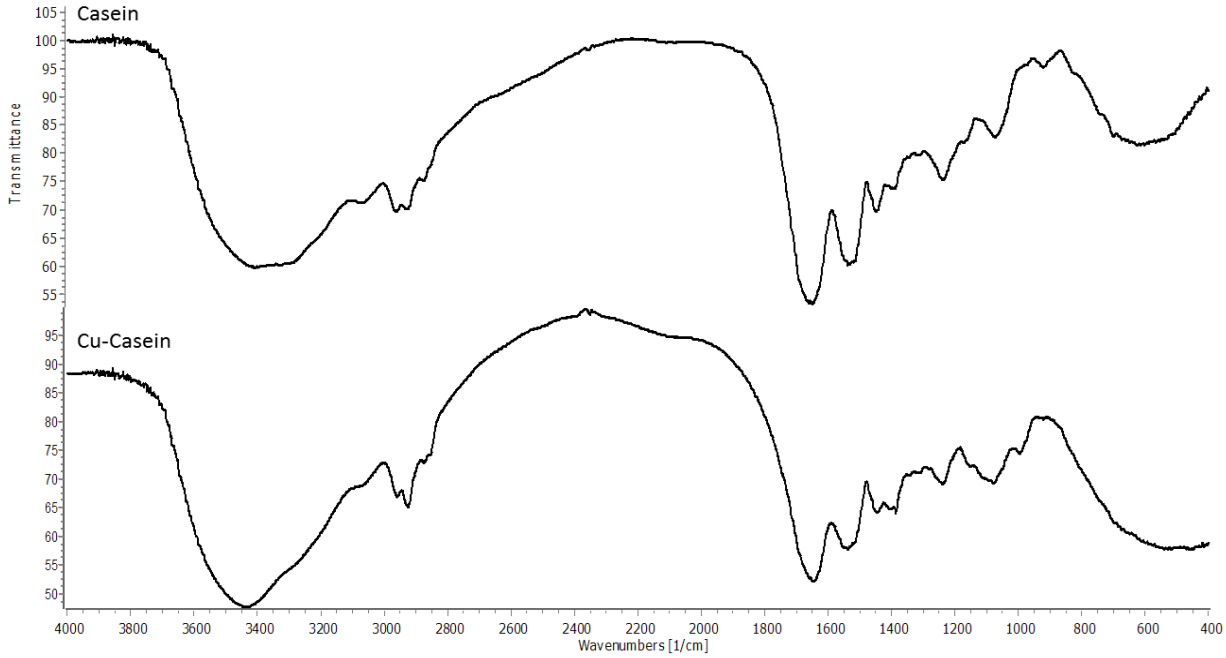


Figure 41 - FTIR spectra of casein and Cu-casein

KBr method, baseline corrected

[191] Dalgleish and Parker 1980.
[192] For a review of casein micelles structures see Dalgleish 2011.

Casein		Cu-Casein		Band Assignments
3700-3300	br	3700-3300	br	N-H and O-H stretching vibrations
3072	sh	3071	sh	Overtone of amide II band
2961	m	2961	m	
2924	m	2924	m	NH_3+ and CH stretching vibrations
2870	vw	2877	w	CH stretching vibrations
1651	vs	1647	vs	Amide I band α helix (80% C=O stretching or COO^- asymmetric stretching vibrations; 10% C-N stretching vibrations and 10% N-H vibrations)
1536	s	1540	s	Amide II band and C=O stretching or COO^- asymmetric stretching vibrations
1335	vw	1335	vw	
1314	vw	1314	vw	C-H deformation vibrations
1238	m	1238	m	Amide III α helix
1073	m	1070	m	C-C stretching vibrations
900-400	br	900-400	br	

Table 19 - Characteristic FTIR bands of casein and Cu-casein

The minor differences between the FTIR spectra of casein and copper-casein are the sharpening of the 3700-3300cm^{-1} broad band, a decrease in the amide I band from 1651 to 1647cm^{-1} and an increase in the amide II band from 1536 to 1540cm^{-1}.

4.2.3.2 Characterization by Raman

The Raman spectra of casein and copper-casein are shown in Figure 42 with characteristic Raman shifts listed in Table 20.

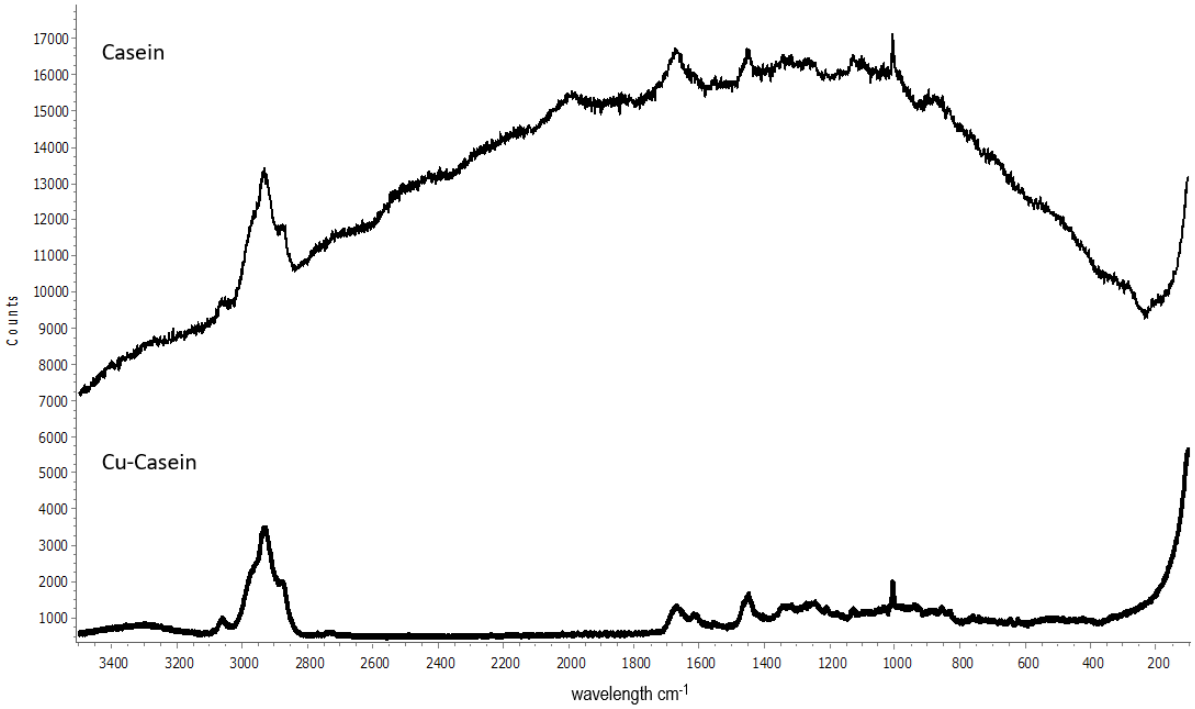


Figure 42 - Raman spectra of casein and Cu-casein

The spectrum of casein is arched due to fluorescence. Fluorescence in proteins result from the movement of electrons in conjugated systems such as those present in double bonds of aromatic rings.[193] Changes to these systems, such as metal complexation, lead to fluorescence suppression.

[193] Represented in chemical formulas by alternating single and multiple bonds e.g. aromatic ring.

Casein		Cu-Casein		Band Assignments
3061	w	3061	w	Overtone of amide II band
2934	vs	2934	m	Asymmetric CH_2 stretching
2879	sh	2879	sh	Symmetric CH_2 stretching
1673	s	1670	s	Amide I band (random chain) and COO^- asymmetric stretching vibration
1616	sh	1616	m	
1555	w	1555	w	Amide II band
1323	vw			Amide III band (incl. CN stretching, NH bending, C-O stretching, O=C-N bending etc)
1262	vw	1251	vw	
1211	w	1211	w	C-O vibrations
1073	m	1070	m	C-C stretching vibrations

Table 20 - Characteristic Raman bands of casein and Cu-casein

The results obtained for both FTIR and Raman are not surprising given how challenging metalloproteins are to analyse, often requiring deconvolution and specific excitation to enhance the vibration of certain bonds. In the case of blue proteins – those that contain copper(II) ions - it is possible to observe shifts due to Cu-N, Cu-S or Cu-O bonds using a 600nm laser.[194] The data presented in Table 20 was obtained with a 514nm laser.

[194] Nakamoto 2009.

4.2.3.3 Characterization by XPS

The XPS survey spectrum is shown in Figure 43 and the full dataset is included in Appendix 9.

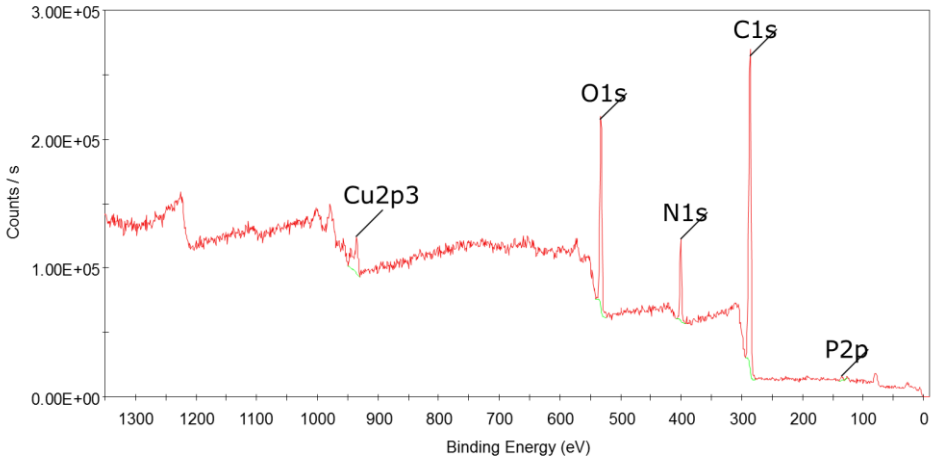


Figure 43 - XPS survey spectrum of Cu-casein

As the casein used in this study does not have a defined chemical formula, theoretical stoichiometric values for pure casein cannot be easily calculated. Table 21 shows the atomic percentages of the constituent atoms measured for casein and copper-casein.

Sample	Relative atomic percentage (%)				
	C	O	N	P	Cu
Casein	75.0	16.96	8.03	-	-
Cu-Casein	72.2	16.34	9.36	0.6	1.5

Table 21 - Elemental composition of casein and Cu-casein

The atomic percentages of the carbon and oxygen atoms of copper-casein are of similar magnitude to casein. In terms of the oxidation state of the copper in the complex, the

satellite peaks in the Cu2p spectrum (Figure 44) indicate the presence of Cu(II) species, which is not surprising, given its blue colour.

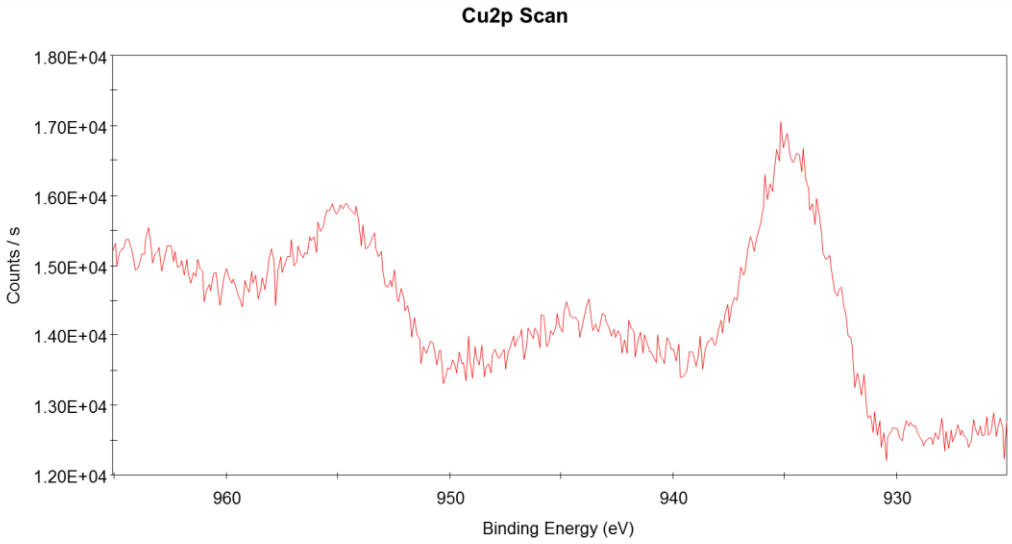
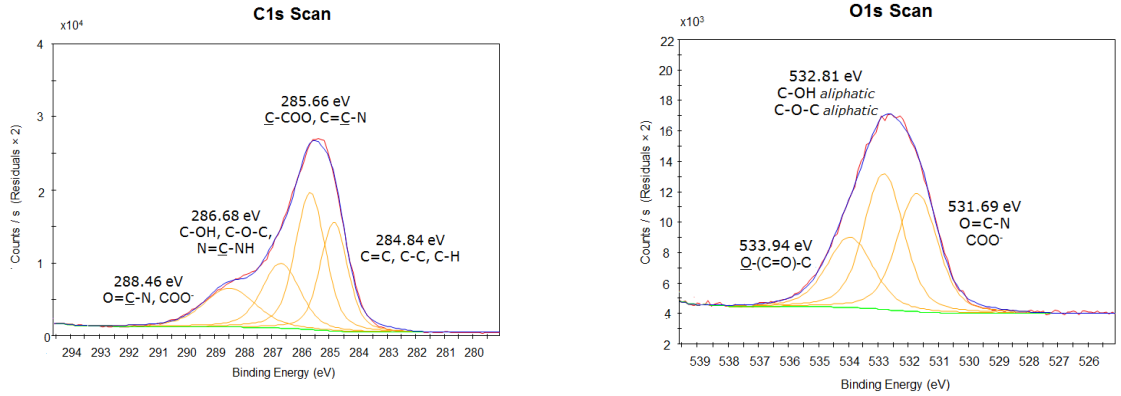


Figure 44 - Cu2p spectrum of Cu-casein

The decomposed peaks for C1s and O1s and for N1s in casein and Cu-casein are shown in Figure 45 and 46. Peak decomposition and peak assignment is complicated by the broad shape of the peaks obtained due to sample charging and the complexity of casein, which contains a variety of chemical environments. Notwithstanding these difficulties, there are clear differences between the casein and the copper complex. The peaks of the C1s and O1s regions in the copper-casein complex are narrower than casein's, with the opposite effect observed in the N1s region.

CASEIN



Cu-CASEIN

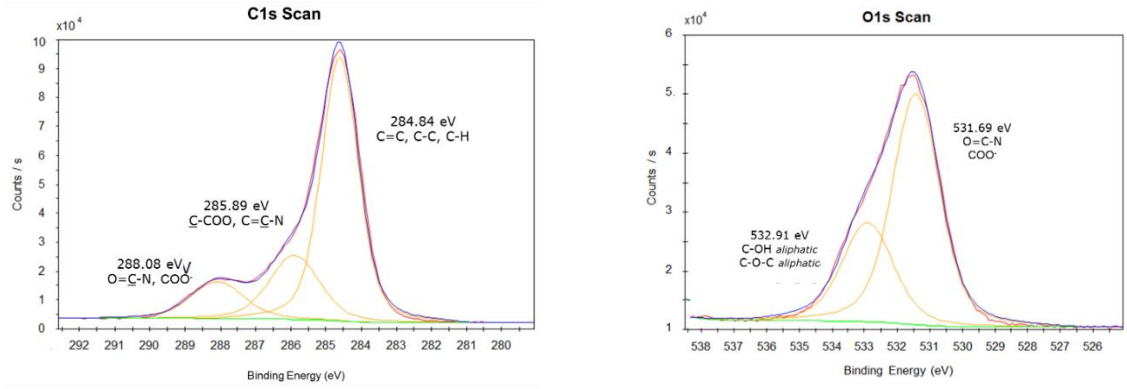


Figure 45 - C1s and O1s regions spectra of casein and Cu-casein[195]

It is tempting to interpret an increased Oxygen carboxylate peak at 531.69eV and, due to Brønsted donation,[196] an increase in the Nitrogen protonated amide peak at 401.61eV as evidence of Cu(II) coordination with the second carboxylic acid groups of aspartic and glutamic acids in the peptide chain. These findings would contrast with values observed in biological systems where copper coordination is predominantly with nitrogen and sulfur

[195] Suggested peak fitting, assignments and positions based on XPS reference; Rouxhet and Genet 2011; Stevens et al. 2013.
[196] Eggleston and Feldman 1990.

donor atoms in the side chains of histidine, cysteine and methionine[197] and, at high pH values (above 10), with the amine of lysine.[198]

CASEIN **Cu-CASEIN**

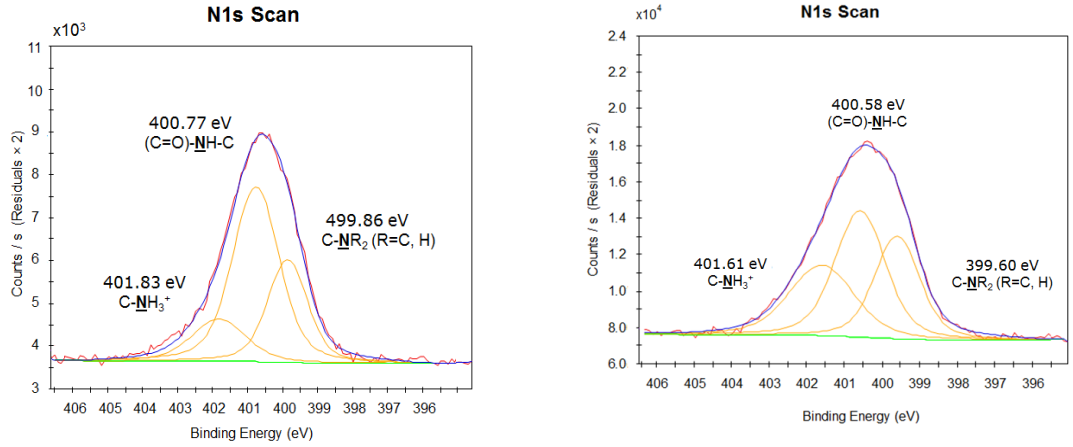


Figure 46 - N1s region spectra of casein and Cu-casein[199]

The sensitivity of XPS compounded by the structural complexity of proteins means that such deductions would have to be confirmed by supplementary analysis such as magnetic nuclear resonance (NMR) or electron paramagnetic resonance (EPR).[200]

[197] See for example this review by Rubino and Franz 2012.
[198] Gomes and Wittung-Stafshede 2011 in Jeżowska-Bojczuk and Stokowa-Sołtys 2018.
[199] Suggested peak fitting, assignments and positions based on XPS reference, Stevens et al. 2013 and Rouxhet and Genet 2011
[200] Stevenson et al. 2020.

4.2.3.4 Characterization by XRD

The XRD diffraction patterns obtained for Cu-casein (Figure 47) are characteristic of an amorphous substance, except for a peak above 35º2θ which coincide with that present in Cu-lactose (section 4.2.2.4) identified as copper oxide phase.

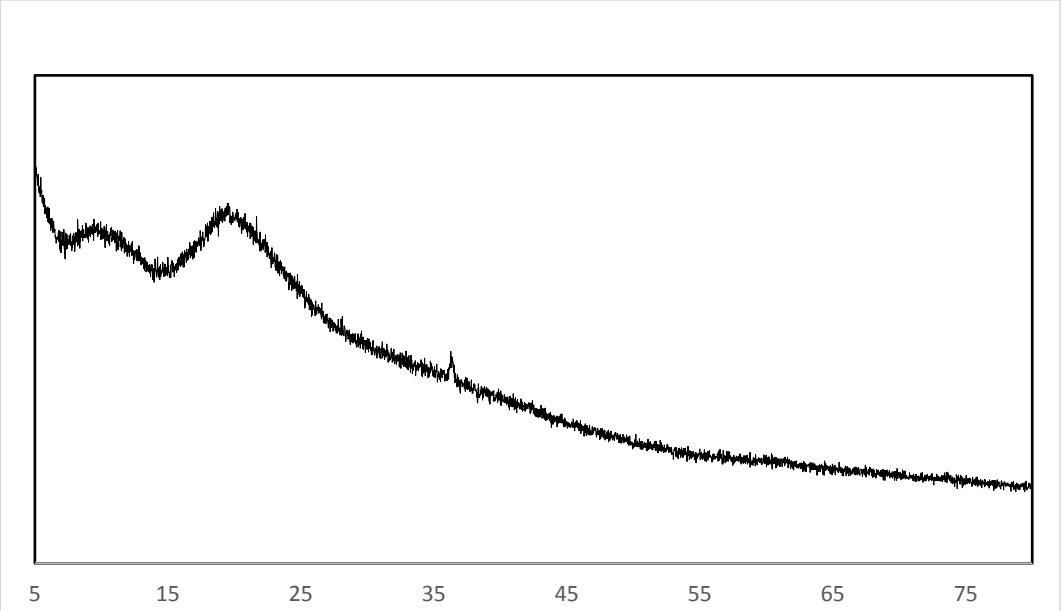


Figure 47 - XRD diffractogram of Cu-casein

4.2.3.5 Characterization by Mass Spectrometry Techniques

4.2.3.5.1 Direct Mass Measurement by FIA

No high mass ions could be detected in any of the solvents.

4.2.3.5.1 QTOF-GC-MS with TSP

The chromatograms for casein and copper-casein in EI mode are shown in Figure 48. Most of the chromatographic peaks relate to nitrogen-containing aromatic compounds, which are products of the cyclisation of amino acids in the polypeptide chain subjected to pyrolysis.[201]

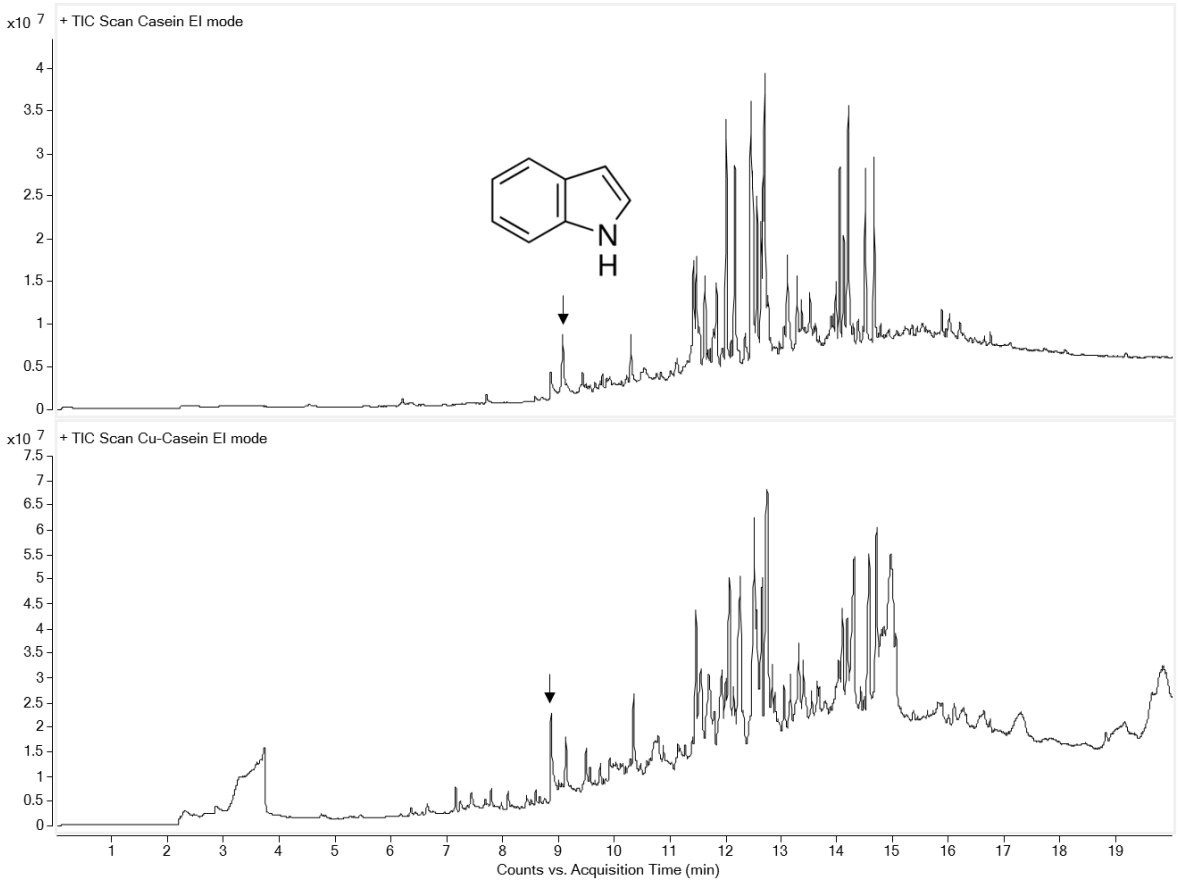


Figure 48 - EI chromograms of casein and Cu-casein

Indole (8.9 min) was the only compound identified also in CI mode (dataset is in Appendix 10). This compound is one of the main products of the thermal degradation of bovine β-

[201] Moldoveanu 1998.

casein.[202] There are clear differences between the chromatograms of pure casein and copper-casein, the latter appearing to contain more peaks. This perhaps represents specific thermal decomposition products associated with the presence of copper ions.

4.2.3.5.2 Solvent extraction with BSTFA derivatization followed by GC-MS

No results were obtained as the method is not appropriate for extraction/identification of proteins.

4.2.3.5.3 Proteomics

Table 22 shows the-10lgP values and number of peptides used for the assignments of the four caseins in pure casein and copper-casein. A complete list of proteins and corresponding peptides is included in Appendix 11. The -10lgP values for the identified caseins are well above the minimal threshold for both pure casein and copper-casein, thus validating the extraction and digestion method. The lower number of peptides identified in Cu-casein may reflect metal complexation. Although metal chelation by proteins is extremely complex[203] and dependent on many factors,[204] some tentative observations may be made by comparing the peptide coverage of casein and the copper-casein.

[202] Orsini et al. 2017.
[203] Koslowski et al. 2013.
[204] Dudev and Lim 2014.

Protein	Average Mass (Da)	Coverage (%)		-10lgP*		# Peptides/Unique Peptides	
		CSN	Cu-CSN	CSN	Cu-CSN	CSN	Cu-CSN
αs1-casein	24529	75	59	259.41	191.20	70/68	19/19
αs2-casein	26019	64	39	217.78	130.88	47/47	12/12
β-casein	25107	91	73	208.26	190.11	49/49	28/28
κ-casein	21269	71	43	247.12	194.55	64/63	18/18

***** The -10lgP value is a statistical indicator used to validate protein assignments – 20 being the threshold for publication.

Table 22 - Proteins matches for casein (CSN) and Cu-casein (Cu-CSN)

Figure 49 shows the peptide coverage obtained for αs1- and αs2-caseins for casein and copper-casein. For αs1-casein, half of the unidentified peptide residues in copper-casein contain tryptophan (W). Part of a group of amino acids that includes phenylalanine (F), tyrosine (Y) and histidine (H), tryptophan is known to form non-covalent bonds with Cu(II) ions via the π-electrons from its aromatic ring.[205]

The other half of the unidentified peptide fragments contain histidine, an essential metal chelating site,[206] either via the imidazole ring supported by the amino group[207] or via a deprotonated amide nitrogen supported by a carboxylate oxygen.[208] As for αs2-casein, the unidentified peptide residues in copper-casein imply an interaction between histidine and glutamic acid (E) which could interact with Cu(II) ions via its deprotonated carboxylic groups. Metal complexation with the peptide chain of αs2-casein may also have been facilitated by its low hydrophobicity in relation to the other caseins.

[205] Remko et al. 2011; Kadej et al. 2016.
[206] Rulíšek and Vondrášek 1998.
[207] Altun and Köseoğlu 2005.
[208] Dunbar et al. 2018.



Figure 49 - αs1-2 caseins peptide chain with identified peptides in casein (BOLD) and Cu-casein (underlined in RED)

short sequencies containing tryptophan (W) within a BLUE square

The peptide coverage obtained for β- and k-caseins for pure casein and copper-casein are shown in Figure 50.

β-CASEIN

MKVLILACLV ALALA**RELEE LNVPGEIVES LSSSEESITR** INKKIE**KFQS EEQQQTEDEL**

QDKIHPFAQT QSLVYPFPGP IPNSLPQNIP PLTQTPVVVP PFLQPEVMGV SKVKEAMAPK

HKEMPFPKYP VEPFTESQSL TLTDVENLHL PLPLLQSWMH QPHQPLPPTV MFPPQSVLSL

SQSKVLPVPQ KAVPYPQRDM PIQAFLLYQE PVLGPVRGPF PIIV

K-CASEIN

MMKSFFLVVT ILALTLPFLG **AQEQNQEQP**I RCEKDER**FFS DK**IAK**YIPIQ YVLSRYPSYG**

LNYYQQKPVA LINNQFLPYP YYAKPAAVRS PAQILQWQVL SNTVPAKSCQ AQPTTMARHP

HPHLSFMAIP PKKNQDK**TEI PTINTIASGE PTSTPTTEAV ESTVATLED**S PEVIESPPEI

NTVQVTSTAV

Figure 50 - β- and k- caseins peptide chain with identified peptides in casein (BOLD) and Cu-casein (underlined in RED)

short peptide sequences containing tryptophan (W) within a BLUE square

For β-casein, the unidentified peptide residues in the copper complex appear to indicate an interaction with glutamic acid (E) alongside serine (S), with tryptophan (W) and with proline (P). Proline is the only amino acid that contains a second amide so Cu-N coordination is not possible.[209] Consequently, coordination with copper only happens when proline is in the N-terminal position of the peptide chain. In other positions, proline residues force the peptide chain to bend,[210] thus facilitating the formation of macro-chelating sites.[211]

An important caveat of the peptide coverage discussion is that the data is based on the most intense peptide fragments, which were selected based on their intensities. Only further experiments and characterization with techniques such as NMR could elucidate metal-peptide chelation sites.

4.2.3.6 Discussion

Evidence of copper complexation with casein has been obtained with spectroscopic and mass spectrometry techniques. Notwithstanding the similarities between the FTIR spectra of pure casein and copper-casein, the slight changes on bands of the latter indicate an interaction between copper and nitrogen/oxygen atoms. In Raman, the most obvious effect of copper complexation was the quenching of fluorescence, which indicates coordination with amino acids containing aromatic rings.

[209] Siemion et al. 1985.
[210] Krieger et al. 2005.
[211] Pettit et al. 1985.

Fluorescence in proteins usually arises from the amino acid residues phenylalanine (Phe), tyrosine (Tyr) and tryptophan (Trp), the latter being a popular marker for studying proteins' interaction with cofactors.[212] These amino acids are present in casein[213] and known to coordinate with Cu(II) ions.[214]

The presence of Cu(II) ions in copper-casein, although anticipated by its blue colour, was confirmed by XPS. Its presence appears to affect the thermal degradation of casein given that the chromatogram of the copper-casein complex obtained by GC-MS with TSP analysis contained more peaks than that of pure casein. Nonetheless, indole, one of the main pyrolysis products of casein – was identified in casein and copper-casein.

The peptide fragments obtained from copper-casein matched all four types of caseins but at a lower coverage and intensity than those from pure casein. The difference in peptide coverage appears to correlate with sites of coordination when interpreted alongside the FTIR and Raman spectra. The data indicates different centres of interactions between the Cu(II) ions and deprotonated nitrogen, oxygen and amino acids containing aromatic rings as reported in the literature[215] and as observed in blue copper proteins.[216]

[212] E.g. Lai et al. 2016; Li et al. 2015; Tayeh et al. 2009; Vivian and Callis 2001; Chen and Barkley 1998; Bent and Hayon 1975.
[213] Gordon et al. 1949.
[214] E.g. Hussein et al. 2018; Reddy and Manjula 2007; Davies et al. 1999.
[215] For reviews of metal ion complexes with proteins see for example Sovago et al. 2016; Bal et al. 2013 and the seminal work by Sigel and Martin 1982.
[216] Pérez-Henarejos et al. 2015, Rubino and Franz 2012, Nakamura and Go 2005.

4.2.4 Characterization of Copper-Milk Corrosion

4.2.4.1 Characterization by FTIR

Figure 51 shows the spectra for freeze-dried milk and the copper-milk corrosion, with band assignments included in Table 23.

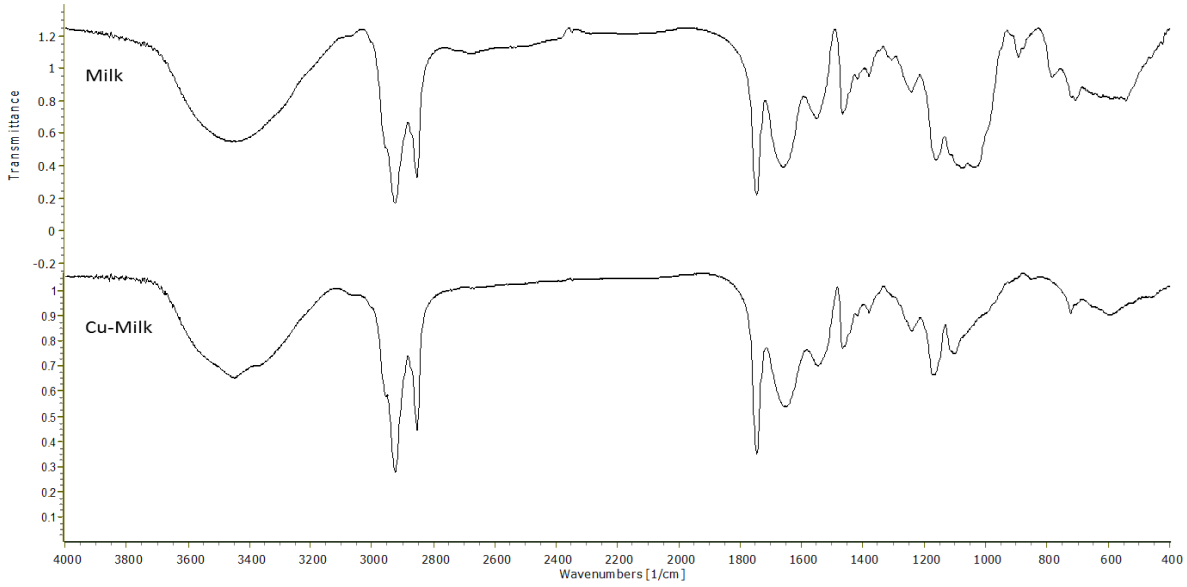


Figure 51 - FTIR spectra of freeze-dried milk and Cu-milk corrosion

KBr method, baseline corrected

Freeze- dried Milk		Cu-Milk Corrosion		Band Assignments[217]
3700-3300	br	3700-3300	br	N-H stretching vibrations
2924	s	2924	s	C-H asymmetric stretching
2856	s	2856	s	CH_2 symmetric stretching vibrations
1747	s	1747	s	(C=O) ester stretching vibrations
1718-1587	br	1715-1587	br	(C=O) carboxylic acids and Amide I band
1550	m	1550	m	Amide II band and CO_2^- stretching (for Cu-milk corrosion)
1465	m	1465	m	CH_2 symmetric bending
1379	w	1379	w	CH_2 asymmetric bending
1311	vw	1311	vw	Amide III band, CH deformation
1243	w	1243	w	C-O vibrations
1165	m	1165	m	$[CH_2(C=O)OCH_2]$ asymmetric stretching + CH_2 symmetric bending (out of plane)
1132-928	br			C-C stretching (-C-O stretching; CH_2 bending)
		1100	m	CH_2 asymmetric bending (out of plane)
893	w			C-H out of plane ring stretching twisting (lactose)
		721	w	CO_2^- scissors vibrations (carboxylates)
		689-456	br	C-O out-of-plane deformation (carboxylates) at 688 cm^{-1} and O-C-O in-plane bending (galactose) at 587 cm^{-1}

Table 23 - Characteristic FTIR bands of freeze-dried milk and Cu-milk corrosion

The only differences between the spectra of freeze-dried milk and copper-milk corrosion appear below 1200cm^{-1}, where some of the bands may be assigned to lactose and carboxylate complexes. The absence of characteristic and well–resolved peaks in the spectra overshadows any peak shifts that could unequivocally indicate metal complexation.

4.2.4.2 Characterization by Raman

[217] Mendes et al. 2016.

The Raman spectra for freeze-dried milk and copper-milk corrosion are shown in Figure 52. The characteristic Raman shift frequencies are listed in Table 28.

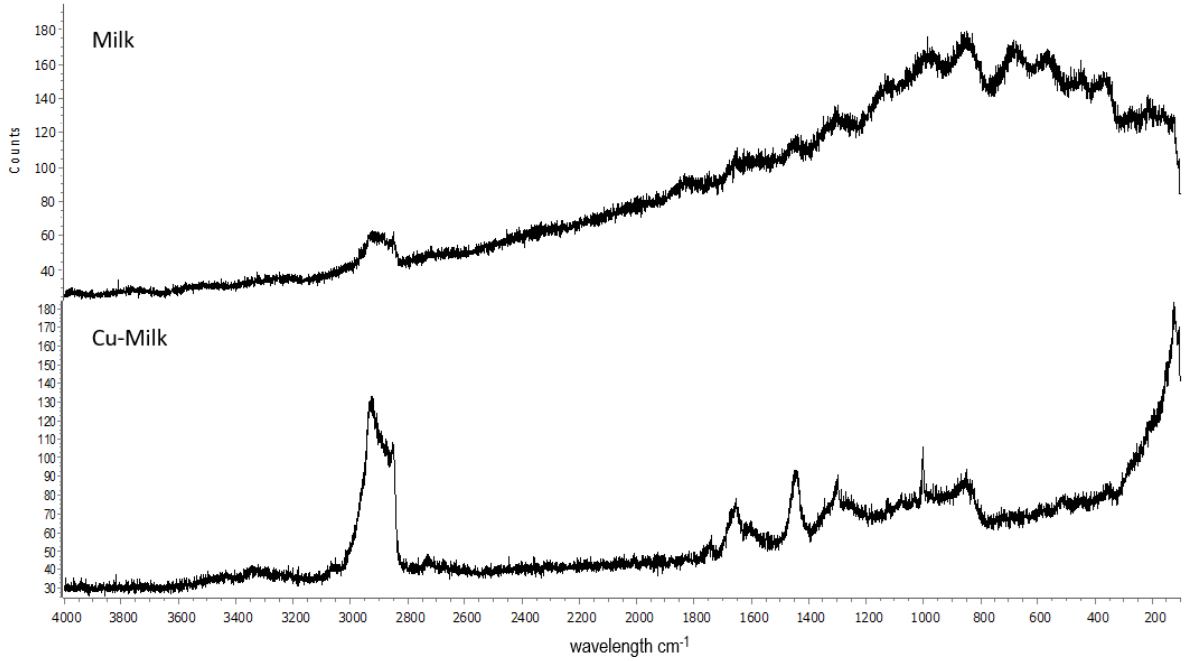


Figure 52 - Raman spectra of freeze-dried milk and Cu-milk corrosion

The Raman spectrum of freeze-dried milk contains poorly defined bands and more fluorescence than that of copper-milk corrosion. The fluorescence is possibly due to a high percentage of casein (see section 3.2.3) in the sample with poor band definition resulting from the variety of particle sizes which can adversely affect Raman scattering.[218] Notwithstanding these differences, both spectra contain characteristic bands belonging to milk proteins at 1611 and 1005cm^{-1} and milk fat at 1743cm^{-1}, with copper-milk corrosion showing an increased fluorescence under 400cm^{-1}, and a very strong band at around 123cm^{-1} that could be tentatively assigned to Cu-O.

[218] McGoverin et al. 2010.

Freeze- dried Milk		Cu-Milk Corrosion		Band Assignments[219]
		3400-3200	br	N-H and OH stretching vibrations
		3060	w	N-H stretching vibrations
2997-2830	br			H-CH_2 asymmetric stretching
		2932	vs	CH_2 asymmetric and symmetric stretching vibrations
		2854	vs	
1746	vw	1743	w	C=O stretching vibrations
		1611	w	C=O amide I and C=C stretching vibrations
1444	w	1454	m	CH_2 deformation
1304	w	1304	w	CH_2 torsion
1126	w	1126	w	(C-O) + (C-C) stretching and C-O-H deformation
		1078	w	
		1005	m	Ring-breathing (phenylalanine)
854	m	854	w	C-C-H + C-O-C deformation (amino acids mode)
687	m			C-C-O
457	w	457	w	C-C-C deformation and C-O torsion
360	w	360	w	
		123	vs	Cu-O

Table 24 - Characteristic Raman bands of freeze-dried milk and Cu-milk corrosion

4.2.4.3 Characterization by XPS

The XPS survey spectrum of copper-milk corrosion is shown in Figure 53. As this is a surface technique, the absence of nitrogen from the results may indicate that compounds containing nitrogen are located below 10nm into the sample.

[219] McGoverin et al 2010, Mendes et al 2016.

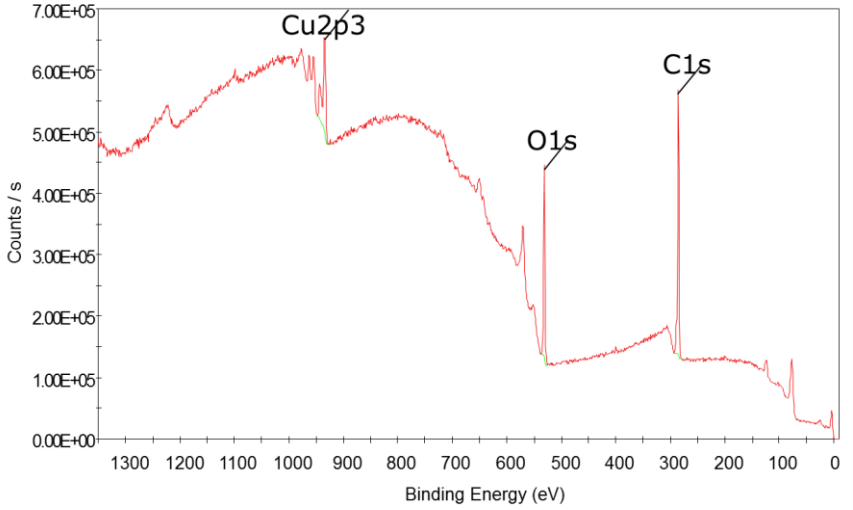


Figure 53 - XPS survey spectrum of Cu-milk corrosion

Analogously to all the copper-organic complexes synthetized in this research, the high resolution spectrum of Cu2p for the copper-milk corrosion (Figure 54) contains satellite peaks that confirm the presence of Cu(II) ions.

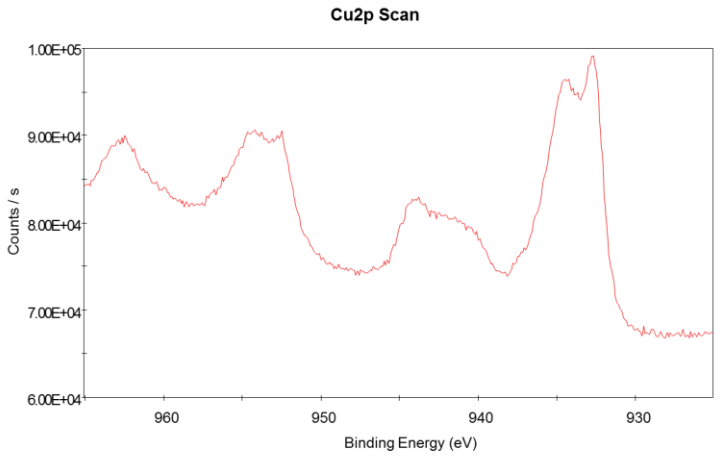


Figure 54 - Cu2p spectrum of Cu-milk corrosion

Some information can also be obtained from the C1 and O1 scans (Figure 55). For comparison purposes, the XPS data obtained from the copper-organic complexes is summarized in Table 25.

Element	Chemical Bonds	Palmitic Acid	Cu-Palmitate	Lactose	Cu-Lactose	Casein	Cu-Casein
C1s BE (eV)	C-C, C-H, C=C	284.7	284.8	284.8	284.6	284.8	284.8
	C-O		286.2		285.8	285.7	285.9
	C-OH			287.1	286.9	286.7	
	O-C-N/ COO^-		288.2	288.6	288.5	288.5	288.1
	C=O	289.1					
O1s BE (eV)					531.4		
	O-(C=O*)-C	532.1	531.8			531.7	531.7
	$C\text{-}OH_{aliph}$/ O*-(C=O)-C	533.2	533.3	532.9	532.9	532.8	532.9
	$C\text{-}OH_{aromatic}$			533.6		533.9	

Table 25 – C1s and O1s binding energies in organic compounds and respective copper complexes

The carbon peak in copper-milk corrosion can be decomposed as three peaks. The first peak at 284.99eV corresponds to the carbon chain. The peak at 286.69eV for C-O species is within the energy range of C-OH species in lactose, copper-lactose and casein, whereas the peak for O-C=O at 289.11eV species matches that of palmitic acid. For oxygen types, the peak at 533.70eV for O*-(C=O)-C has similar energy values to the C-OH aromatics in lactose and casein.

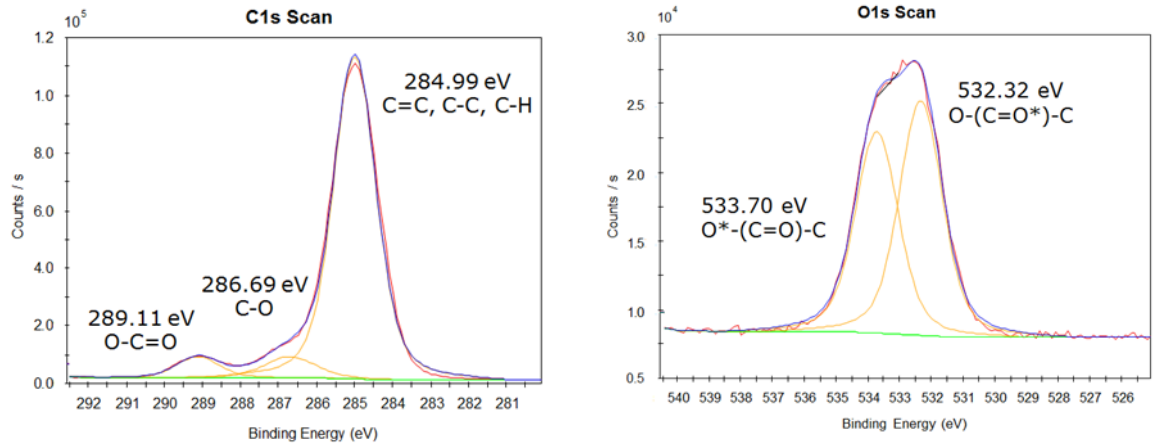


Figure 55 – C1s and O1s regions spectra of Cu-milk corrosion

ORANGE curves denote peak fitting

4.2.4.3 Characterization by XRD

The waxy consistency of copper-milk corrosion was not suitable for analysis by powder diffraction.

4.2.4.4 Characterization by Mass Spectrometry

4.2.4.5.1 QTOF-GC-MS with TSP

The identified compounds in the freeze-dried milk and copper-milk corrosion (cross-referenced with the copper organic complexes) are listed in Table 26 with the mass spectra dataset included in Appendix 12.

Most identified compounds were present in both matrices, with differences restricted to carbohydrate derivatives. The presence of copper ions would have favoured the oxidation of

alcohols (e.g. furanmethanol) into aldehydes (e.g. 2-Furancarboxaldehyde, 5-methyl) and favoured the formation of levoglucosenone.

RT (min)	Compound	Milk	Cu-Milk	Cu-complex
3.15-3.34	Formic acid	X	X	
3.72-3.75	Acetic acid	X		
4.86-4.96	3-Furanmethanol	X		
4.98-5.01	3-Furaldehyde	X	X	
5.36-5.41	2-Furanmethanol	X		
6.19-6.23	2-Furancarboxaldehyde, 5-methyl		X	
6.51-6.58	**2H-Pyran-2,6(3H)-dione**	X	X	Cu-Lactose
7.08-7.13	Furaneol	X		
7.46-7.52	**Levoglucosenone**		X	Cu-Lactose
8.85-8.92	**Indole**	X	X	Cu-Casein
9.08-9.16	n-Decanoic acid (C10:0)	X	X	
10.31-10.36	Dodecanoic acid (C12:0)	X	X	
11.42-11.49	Tetradecanoic acid (C14:0)	X	X	
12.43-12.54	**n-Hexadecanoic acid (C16:0)**	X	X	Cu-Palmitate
13.36-13.42	**Octadecanoic acid (C18:0)**	X	X	Cu-Stearate
14.50-14.64	Pyrrolo[1,2a]pyrazine-1,4-dione,hexahydro-3-(phenylmethyl)-	X	X	
18.05-18.21	Cholesterol	X	X	

[x] = present

Table 26– Identified compounds in freeze-dried milk and Cu-milk corrosion cross-referenced with Cu-organic complexes by QTOF-GC-MS with TSP

4.2.4.5.2 Solvent extract derivatized with BSTFA followed by GC-MS

The compounds identified in freeze-dried milk and copper-milk corrosion are listed in Table 27 with the mass spectrometry dataset included in Appendix 13.

RT (min)	Compound	Milk	Cu-Milk	Cu- complex
12.39	Nonanoic acid (C9:0)		X	
14.49	Dodecanoic acid (C12:0)	X		
16.87	Tetradecanoic acid (C14:0)	X		
18.01	n-pentadecanoic acid (C15:0)		X	
20.14	**n-Hexadecanoic acid (C16:0)**		X	Cu-Palmitate
21.92	**Octadecanoic acid (C18:0)**		X	Cu-Stearate
29.04	Cholesterol		X	

[x] = present

Table 27 - Identified compounds in the BSTFA-derivatized extracts of freeze-dried milk and Cu-milk corrosion

Only one compound – dodecanoic acid – was identified in freeze-dried milk compared to five in the copper-milk corrosion extract. The difference in composition between the extracts was probably due to protein contamination, as a few days after analysis, when the vials were removed from the equipment for disposal, the milk extract was opaque, whilst the copper-milk vials were still translucent.

4.2.4.5.3 Proteomics

The most intense proteins identified in freeze-dried milk and copper-milk corrosion are listed in Table 28. The full dataset is included in Appendix 14.

The most intense proteins identified in freeze-dried milk were also identified in Cu-milk corrosion, but the number of peptides recovered were lower than those obtained for casein/Cu-casein (reported in Table 22).

	Coverage (%)		-10lgP*		# Peptides/Unique Peptides	
Protein	MILK	Cu-MILK	MILK	Cu-MILK	MILK	Cu-MILK
αs1-casein	70	73	289.42	246.02	63/62	59/59
αs2-casein	61	57	223.61	167.00	40/38	27/26
β-casein	76	82	256.79	225.55	64/64	49/49
κ-casein	57	65	266.95	237.50	64/63	33/32
β-lactoglobulim	78	72	225.50	217.11	30/29	40/39

Table 28 – Most intense proteins identified in freeze-dried milk (MILK) and Cu-milk corrosion (Cu-MILK)

In milk, the caseins are mostly arranged as micelles, in which k-casein concentrates on the surface, β-casein in the middle and the αs caseins distributed throughout (and stabilized by Ca^{2+} ions).[220] As changes in pH, temperature, mineral and water content can affect the structure of casein micelles,[221] the results obtained for freeze-dried milk may not be directly comparable to those of copper-milk corrosion which was produced by direct immersion of copper in milk. Furthermore, although complexation between Cu^{2+} and the peptide chain may not be favoured at a neutral pH (the copper corrosion in milk experiment was conducted at pH 7) the metal ions could still have disrupted the casein micelles,[222] affected trypsin's enzymatic activity[223] and/or lead to mis-cleavage of the peptide chain during digestion.[224] Therefore, the identification of characteristic proteins in the presence or absence of copper ions, with a method that did not include a dedicated metal chelation step[225] is an excellent result.

[220] For a review of micellar arrangement of caseins in milk see for instance Dalgleish and Corredig 2012.
[221] For an exhaustive review on the chemistry of casein micelles see Horne 2014.
[222] For a review of metal coordination with proteins see for instance Hellinga 1998 and Sigel and Bruce 1982.
[223] Higaki et al. 1990.
[224] Tesařová et al. 2015.
[225] Janecki and Reilly 2015.

4.2.4.6 Discussion

The results obtained confirmed that the electrochemical experiment succeeded in creating a deposit which mimicked the main chemical characteristics of milk.

Real insights into copper-milk corrosion were obtained from the mass spectrometry techniques, while the best results were obtained from the QTOF-GC-MS with TSP over the solvent extraction and derivatization method. It was possible to correlate the results with those obtained for Cu-carboxylates, Cu-lactose and Cu-casein complexes, but validation of NIST assignments by analysis in chemical ionization mode still left most chromatographic peaks unassigned.

4.3 Conclusion

Corrosion processes are extremely complex. To explain in more detail the various chemical processes that led to the corrosion products and copper-organic complexes produced in these electrochemical experiments would require additional experiments and complementary analytical techniques. But it is perhaps the limited knowledge of these processes that brings the analysis of these substances closer to the challenge faced by scientists working on the characterization of archaeological metal corrosion.

The electrochemical experiments were intended to create copper corrosion containing organics so that the performance of different analytical techniques could be evaluated.

The first observation is that Cu(II) corrosion containing organics have the same characteristic blue/greenish colour as Cu(II) inorganic corrosion products but a different consistency. The ability to analyse copper-organic complexes by powder XRD decreased with an increase in unsaturation/chemical complexity of the organic ligand. Although some copper-organic complexes can exist as crystalline phases, their identification will always be limited by the availability of reference data in open-source libraries. However the results obtained for recrystalized copper palmitate support the idea of creating bespoke libraries for copper-organic complexes with diffractograms obtained by techniques other than powder XRD.

The ability to interpret an FTIR spectrum decreases with the complexity of the organic molecule and when the sample contains a mixture of substances including inorganic compounds. However, organic chemical functions can still be identified and contrasted with reference spectra of minerals readily available on the internet. The analysis by Raman was particularly informative in corroborating the coordination between copper and carboxylic acids but for the remaining complexes and the Cu-milk corrosion the analyses were affected by fluorescence that could not be easily circumvented.

The main role of XPS in the study was to confirm the state of oxidation of copper in the copper-organic complexes and the Cu-milk corrosion. Although some tentative observations could be made from the data obtained for the remaining elements, these would require validation by other analytical techniques. XPS is ideal for characterizing the chemical environment of constituent atoms of homogenous inorganic samples, but its limitations were

evident in the characterization of casein/Cu-casein and Cu-milk corrosion, which yielded broad peaks.

With regards to mass spectrometry techniques, there were clear advantages of using a thermal sample probe:

- Analysis of small solid samples with little sample manipulation
- A variety of organic compounds identifiable in the same sample run
- Overcoming the low solubility of copper-organic complexes in organic solvents

The most disappointing results obtained by QTOF-GC-MS with TSP were in respect of proteins. But if the protein profile of the sample is required, the proteomics method used in this research has proved effective in recovering proteins despite the interference of copper ions. Figure 56 summarizes the analytical protocol that will be used to analyse the archaeological corrosion samples, which are presented as case studies, in the next chapter.

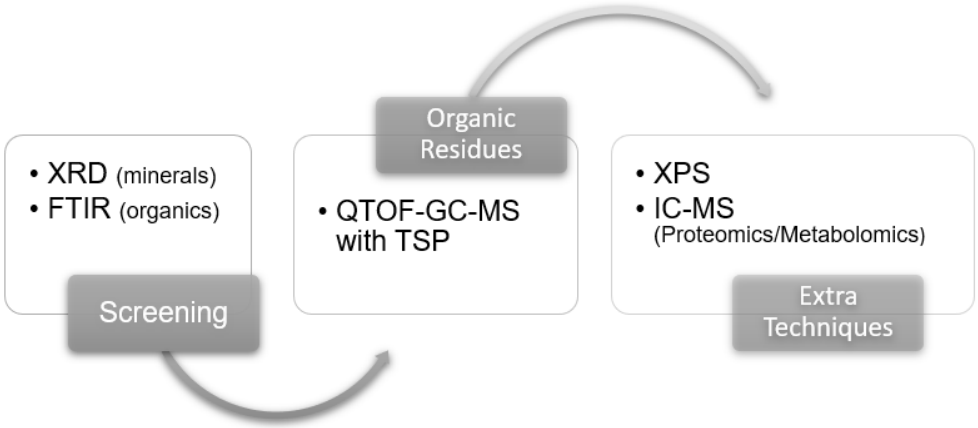


Figure 56 – New multi-analytical protocol for analysis of archaeological metal corrosion

5. TESTING THE PROTOCOL ON ARCHAEOLOGICAL COPPER CORROSION

This chapter presents five case studies where archaeological corrosion samples were analysed by the multi-analytical protocol generally comprising:

1. Fourier-Transform Infrared (FTIR) for chemical functions characterization of the sample
2. X-ray Powder Diffraction (XRD) for identification of mineral phases in the sample
3. Mass spectrometry techniques for identification of organic compounds

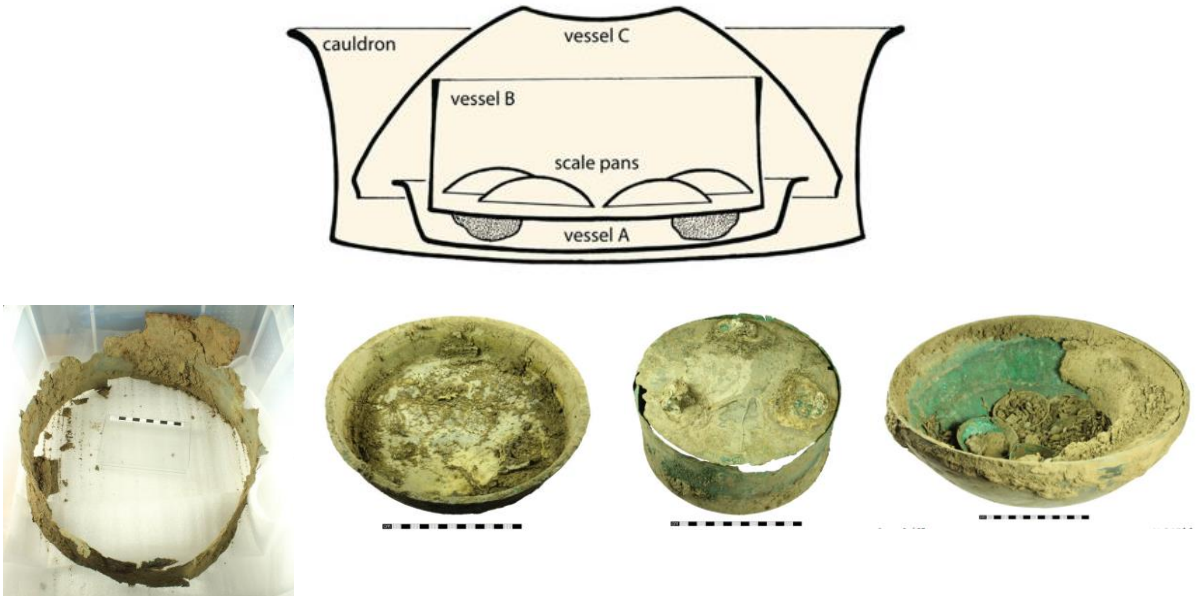
The case studies have varying archaeological contexts and research questions, with the multi-analytical protocol adapted to include extra analytical techniques where required.

The chapter concludes with a sixth case study – a residue from a copper vessel. Although the sample for this case study was not metal corrosion, the investigation was centred on a specific research question that involved targeted analysis and accelerated ageing experiments.

5.1 Case Study 1 – The Pewsey Hoard

5.1.1 Background

The Pewsey Hoard is a group of Roman copper-alloy vessels found at a depth of c. 300–400mm below the surface of the topsoil[226] in a field in the Vale of Pewsey, Wiltshire (UK) by metal detectorists in October 2014. The hoard (Figure 57) was excavated by the metal detectorists themselves and consists of a large, iron-rimmed cauldron containing two bowls (Vessels A and C) and another vessel (Vessel B) within which there were four scale pans carefully packed with plants. Subsequent excavation of the area by Historic England surrounding the findspot concluded that the hoard was deposited in a pit, dug in an actively used landscape with no structures or ditches in its immediate vicinity.[227]



Cauldron
Ø 310mm

Vessel A
Ø 246 mm

Vessel B
Ø 246 mm
(shown upside down)

Vessel C
Ø 296mm

Figure 57– The Pewsey hoard

[226] Henry et al. 2017.
[227] ibid.

The results of macrofossil and pollen analyses of the contents of the vessels were published in 2019.[228] The desiccated flowers and bracts (a type of leaf associated with the reproductive part of a flower) recovered from within Vessel B represents various grassy woodland plants including *Centaurea* sp, *Pteridium aquilinum* and *Centaurea nigra* (Figure 58).[229] Vessel B also contained a distinctive pollen composition dominated by *Succisa pratensis*, a plant used for the treatment of various ailments including scabies and swellings at least since medieval times.[230] As its pollen was not found anywhere else in the hoard, *Succisa pratensis* is the only plant that is definitely associated with the packing material as opposed to post-burial contamination.[231] The plant remains and pollen distribution within the hoard indicate a late summer deposition.



Centaurea sp (knapweed) | *Pteridium aquilinum* (bracken) | *Succisa pratensis* (devil's bit scabious)

Source: Henry et al. 2019 and rhs.org.uk

Figure 58 – Plant remains found inside Vessel B

[228] Henry et al. 2019.
[229] Ibid.
[230] Culpeper 1649, 54.
[231] Henry et al. 2019.

The specific microclimate within Vessel B was conducive to mineralization of plant remains, with some containing lead and copper (their signals measured by portable X-ray fluorescence).[232] Radiocarbon dating of some of the plant remains showed a calibrated date range for deposition at 345-405 AD.

Although several late Roman vessel hoards containing cauldrons and bowls have been found in Britain, the Pewsey Hoard is unusual because of the inclusion of scale pans and plant packing material. On one hand, the combination of objects of different functions points to the broad economic value of metal artefacts. On the other hand, the inclusion of the scale pans (possibly pairs given the similar dimensions and weights), uncommon in a rural setting, suggests a symbolic intention.[233]

5.1.2 Research Question

The vessels' alloy compositions were published,[234] but because the analyses were made using a surface technique (i.e. pXRF), they are unreliable. The colour of the corrosion products differs between vessels and within the same vessel. As these differences may result from the interaction between the metal and different types of organic matter (prior and/or during deposition) the following research questions are proposed:

1. **Can organic residues be retrieved from the vessels' corrosion products?**
2. **If yes, can these residues be related to how the vessel was used in the past?**

[232] Henry et al. 2019.
[233] Ibid.
[234] Ibid.

Seven samples were collected by the author, their positions marked in Figure 59 with a brief description in Table 29.

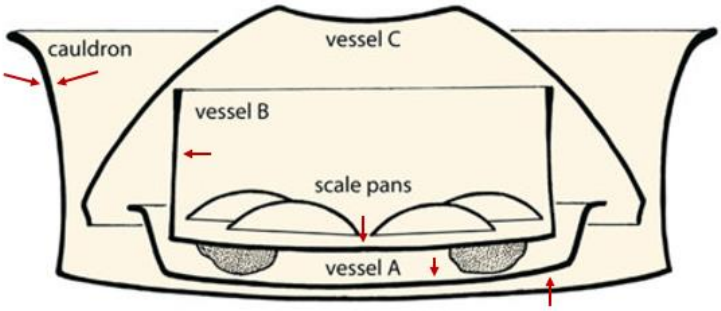


Figure 59– Sampling the Pewsey hoard

arrows marking the areas sampled

Sample	Description
Cauldron Rim interior	Blue/greenish hard corrosion
Cauldron Rim exterior	Blue/greenish hard corrosion
Vessel A interior	Green/brownish powdery corrosion
Vessel A exterior	Dark hard corrosion
Vessel B interior body	Green/brownish powdery corrosion
Vessel B interior base	Green/bluish hard corrosion
Soil under Vessel B	Brownish powdery with crystals

Table 29 – Description of Pewsey hoard samples

Samples were scrapped (or flicked) off metal surfaces with a scalpel and placed inside glass vials with hard plastic caps. Sample sizes varied between 5-15mg. Vessel C and the scale pans were not sampled because their corrosion layer was too thin and adhering too strongly to the metal substrate.

5.1.3 Identification of Chemical Bonds

Analysis in attenuated total reflectance (ATR) mode yielded poorly defined bands and baseline with spectra as those included in Figure 60 for the cauldron samples.

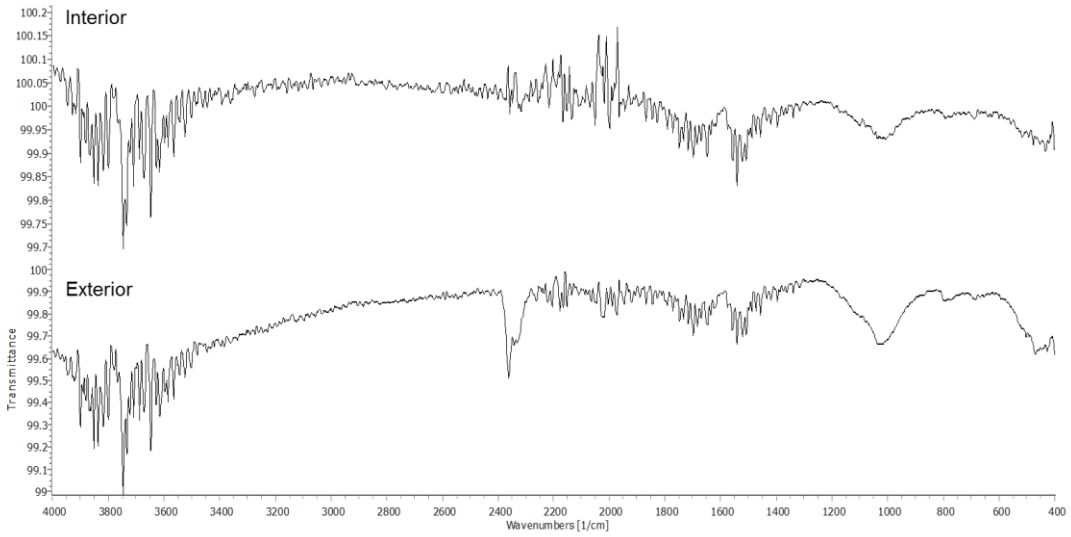


Figure 60 – FTIR spectra of cauldron samples obtained in ATR mode

The larger samples were re-analysed using the KBr method which, albeit destructive, yielded better spectra than the ATR method. Figure 61 shows the spectrum of the cauldron rim interior corrosion with peaks and tentative band assignments listed in Table 30. There was not enough sample from the exterior to perform the analysis.

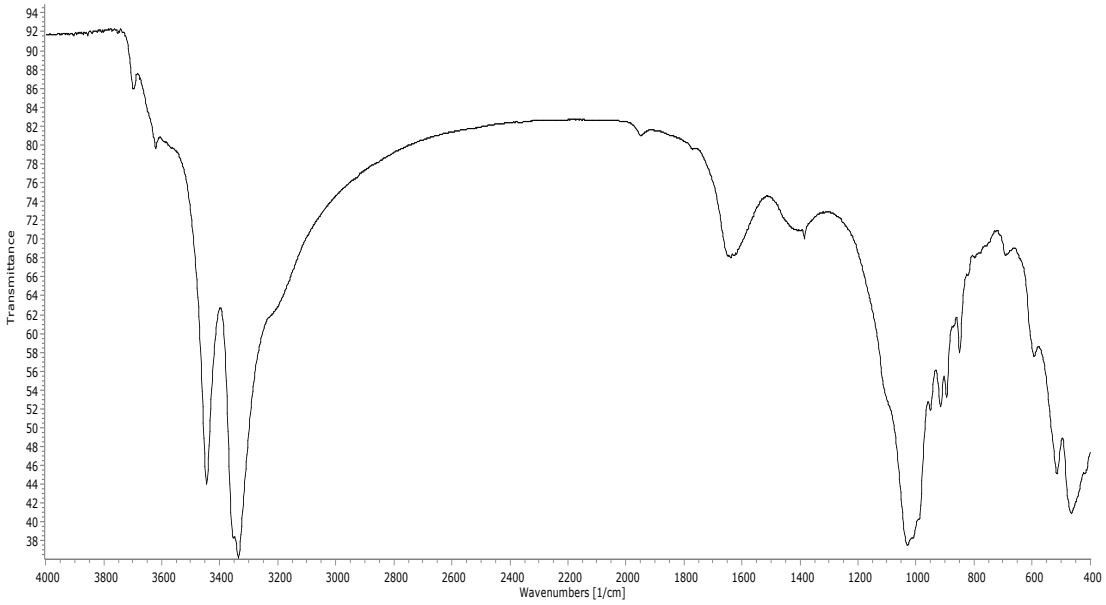


Figure 61– FTIR spectrum of cauldron rim interior sample

KBr method

Cauldron Interior		Attribution
3447	vs	NH asymmetric and OH stretching vibrations
3336	vs	NH symmetric and OH stretching vibrations
1640	m	NH amide deformation
1032	vs	silicates
915	m	silicates
893	m	silicates
850	m	organic nitrates
513	m	N-C=O primary saturated aliphatic amides and/or N-C=O secondary and tertiary amides deformation
463	m	C-H out-of-plane, monosubstituted benzenes and/or C-N-C secondary amines deformations

Table 30– Infrared frequencies (cm^{-1}) and band assignments for cauldron interior sample

Figure 62 shows the spectra of the Vessel A samples and Figure 63 shows those of the Vessel B samples. Band attribution was not possible because the peaks are too broad.

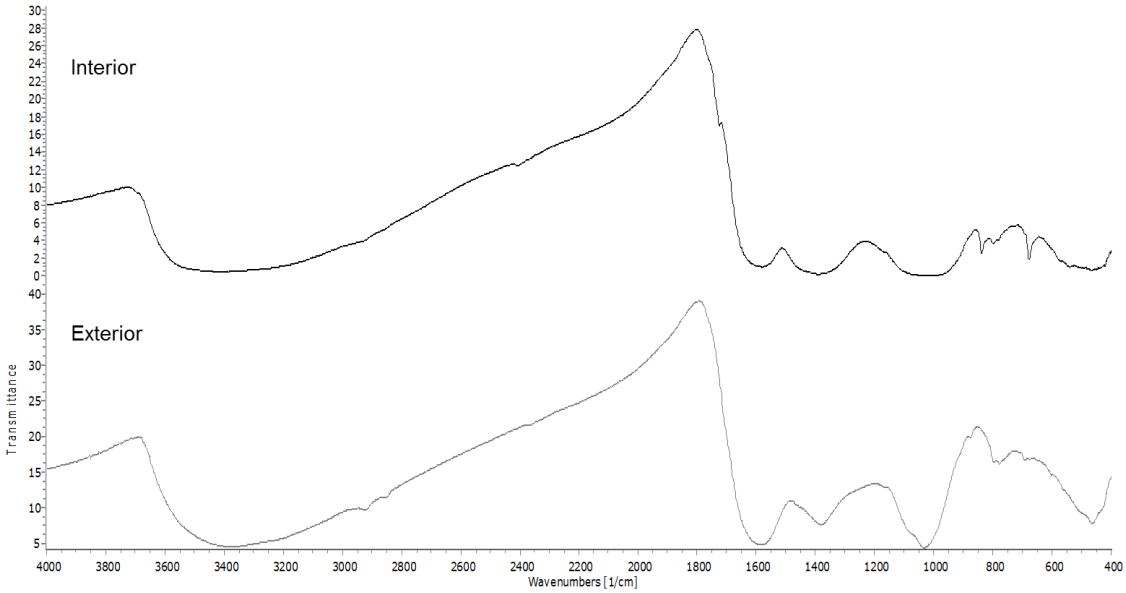


Figure 62– FTIR spectra of Vessel A samples

KBr method

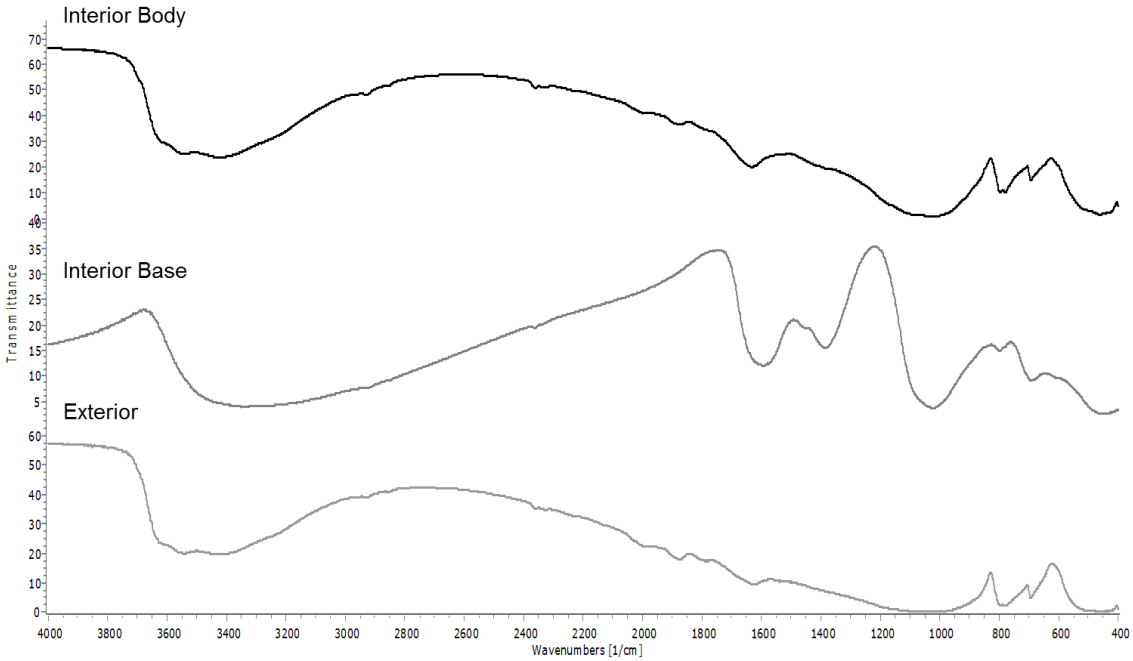


Figure 63– FTIR spectra of Vessel B samples

KBr method

5.1.4 Identification of Mineral Phases

The peak lists of all samples analysed are included in Appendix 15. Figure 64 shows the powder diffractogram with phase identification of the cauldron's interior corrosion. The only mineral phase identified was silicon dioxide (quartz). A powder diffractogram could not be obtained of the cauldron exterior corrosion sample because it was too small.

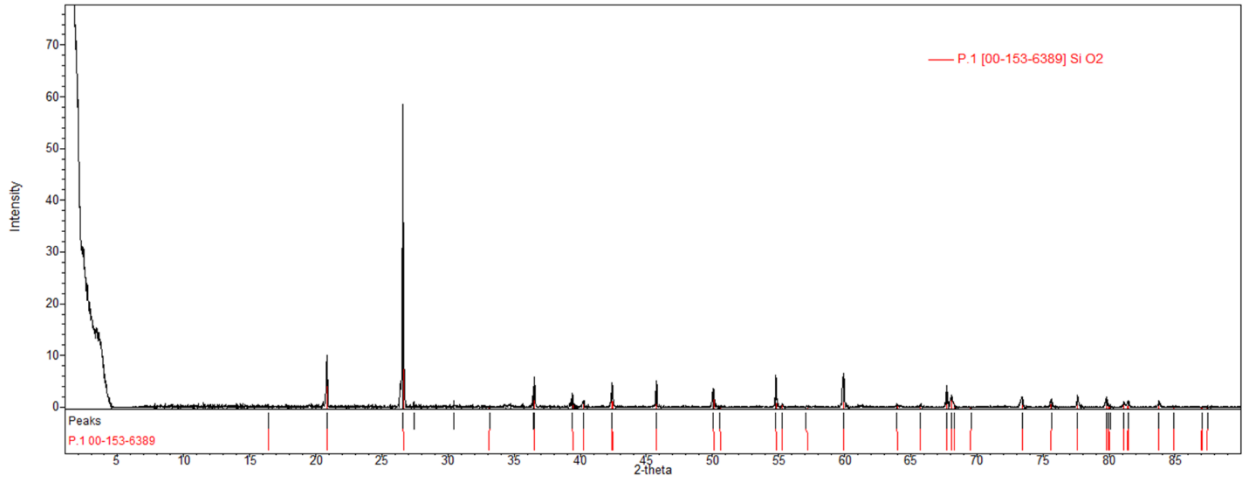


Figure 64– Diffractogram of cauldron interior sample

quartz identified as mineral phase

The powder diffractograms with phase identification of the Vessel A samples are shown in Figure 65. The interior corrosion is composed of 75% $Pb_3(CO_3)_2(OH)_2$ (hydrocerussite) and 25% $Pb_{10}(CO_3)_6O(OH)_6$ (plumbonacrite). The exterior corrosion sample of Vessel A is composed of 86% SiO_2 (quartz) and 14% copper sulfide Cu_2S (chalcocite).

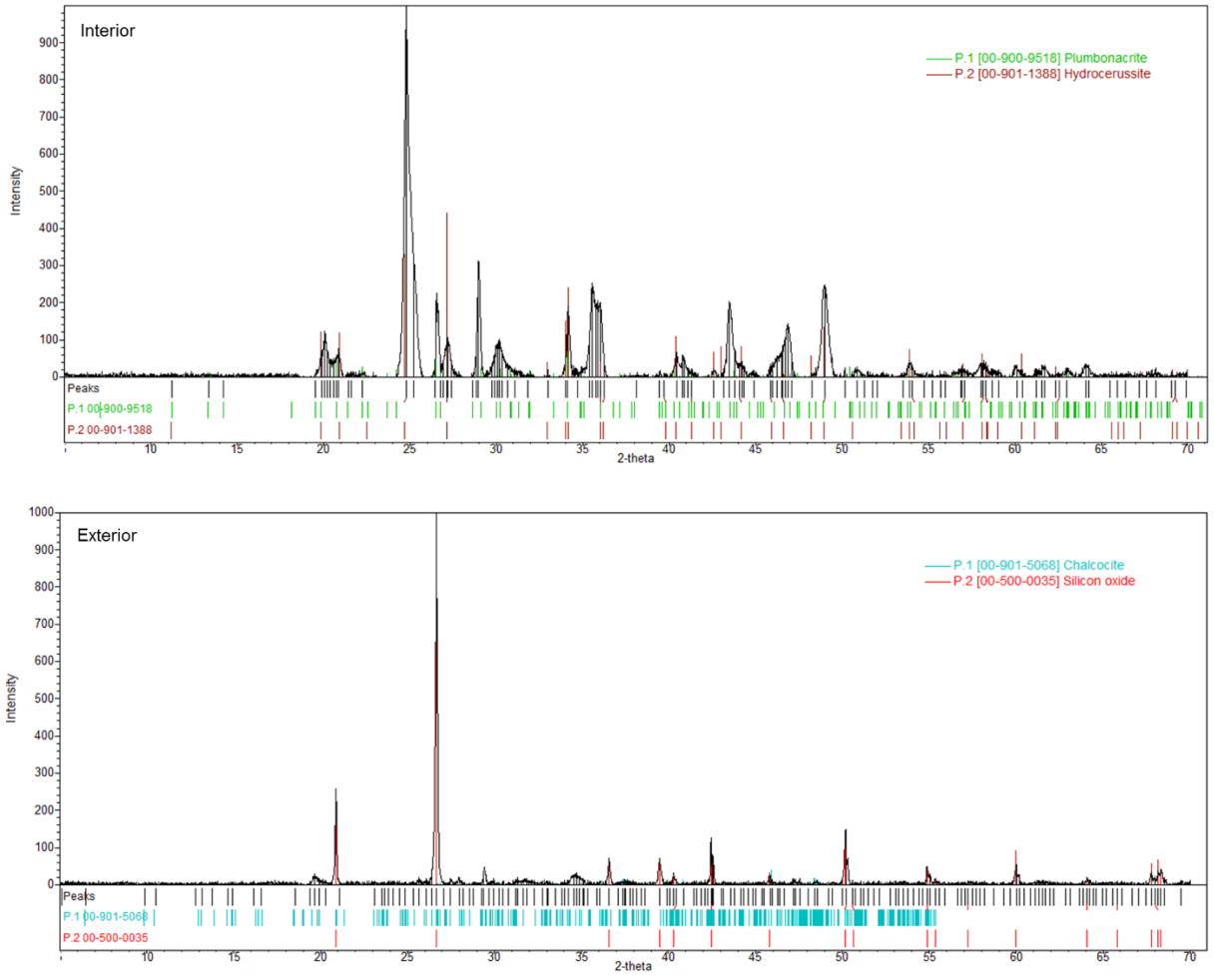


Figure 65 – Diffractograms of Vessel A samples

plumbonacrite and hydrocerussite identified as mineral phases in the interior sample and chalcocite and quartz identified in the exterior sample

The powder diffractograms and phase identifications for the Vessel B samples are included in Figure 66. They contain mostly SiO_2 (quartz), although many peaks remained unassigned, particularly for the Base sample.

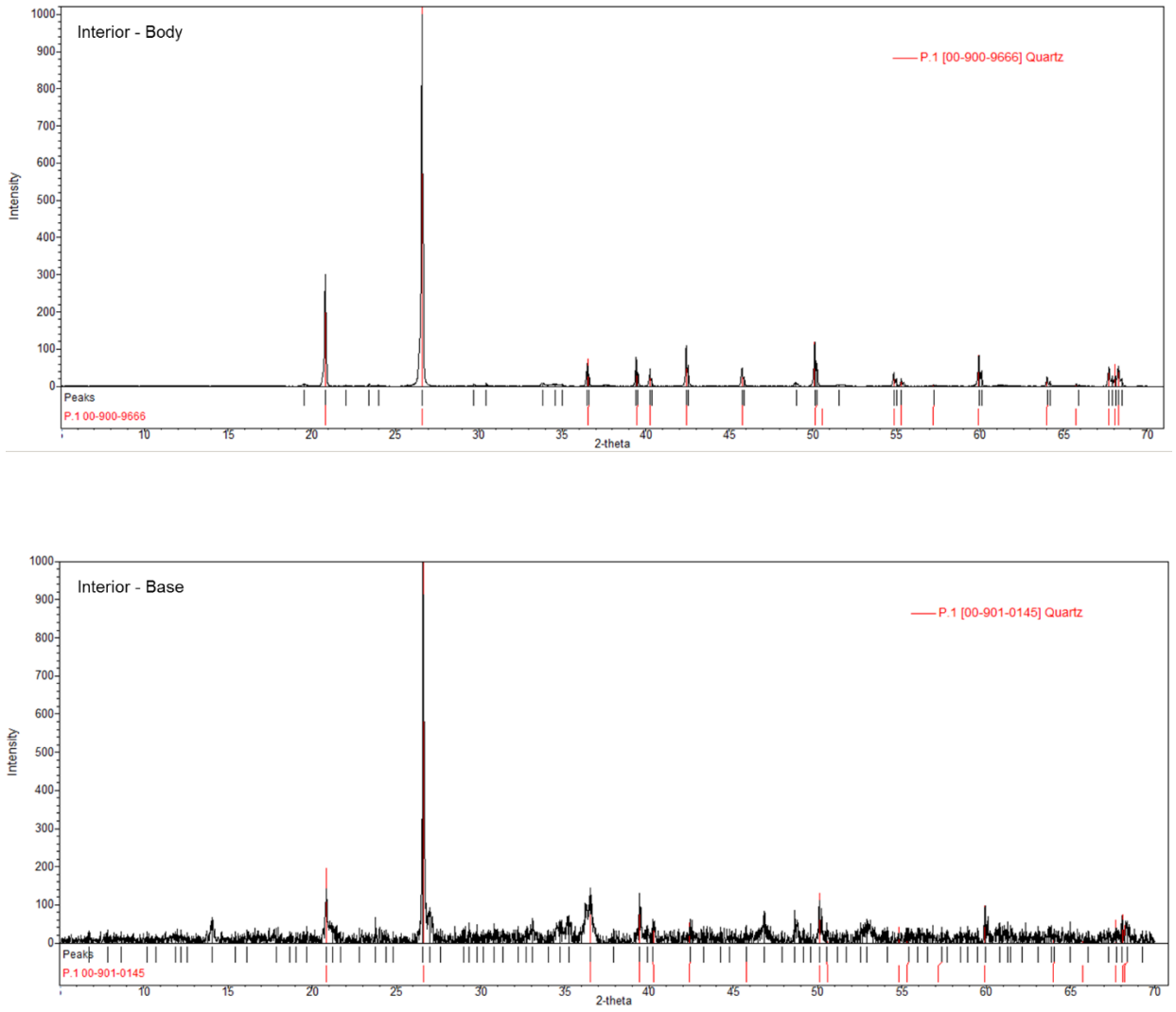


Figure 66 – Diffractograms of Vessel B samples

quartz identified in the body and base samples

5.1.5 Identification of Organic Compounds

5.1.5.1 QTOF-GC-MS with TSP

The EI chromatograms and identified compounds of the cauldron samples are shown in Figure 67 with spectrometry datasets included in Appendix 16a.

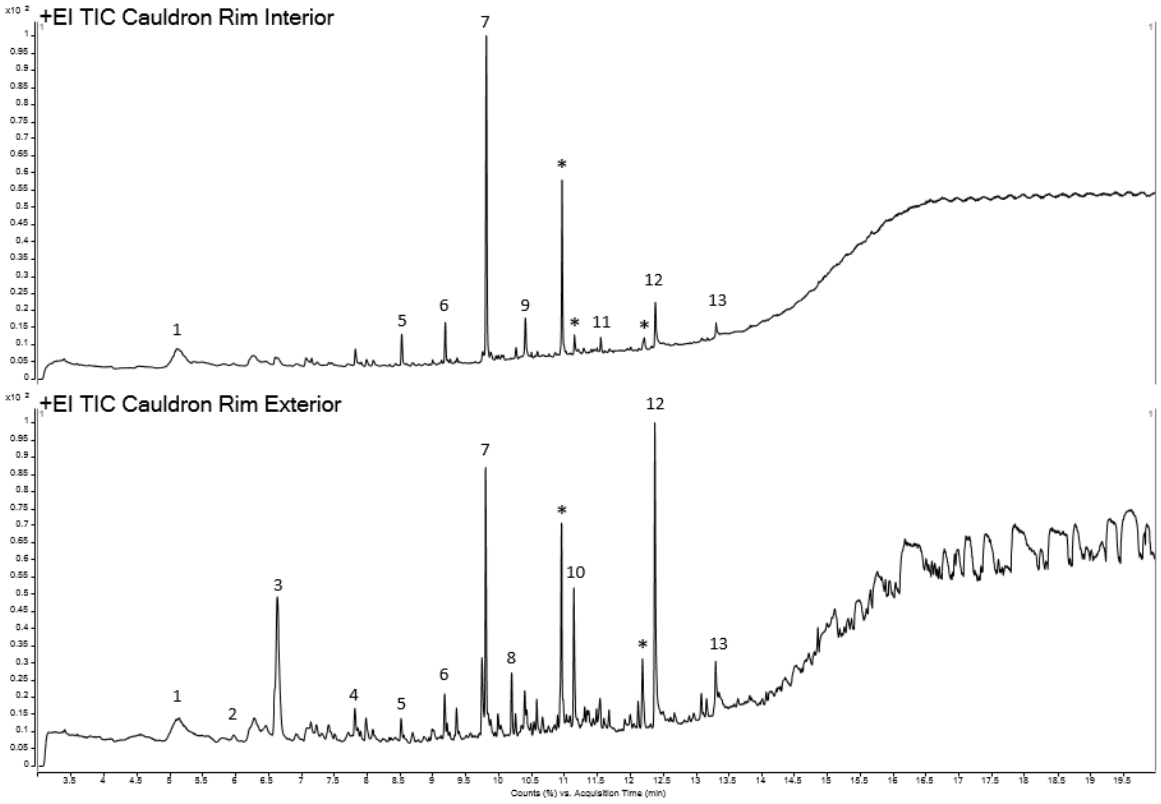


Figure 67– EI chromatograms cauldron rim samples

[1] Furfural; [2] Benzaldehyde; [3] Cymene; [4] 4-Dodecene; [5] 1-Tridecene; [6] 1-Tetradecene; [7] 1-Pentadecene; [8] 1,1,4,5,6-Pentamethyl-2, 3-dihydro=1H-indene; [9] Benzene, nonyl; [10] Pentadecanal; [11] Benzene, undecyl; [12] n-Hexadecanoic acid; [13] Octadecanoic acid and [*] long carbon chain aliphatic compounds

The chromatograms of the cauldron rim samples have similar compositions: a sugar derivative compound [1], a series of medium chain n-alkenes compounds [4, 5, 6 and 7], two ubiquitous long-chain carboxylic acids [12 and 13] together with a few unidentified long-

chain aliphatic compounds. The greatest number of compounds were identified in the exterior corrosion, including a large peak for a naturally occurring aromatic organic compound [3],[235] unique to this sample. Alkylbenzenes compounds [9 and 10], were only present in the chromatogram of the interior corrosion, which also contained a markedly smaller peak for palmitic acid [12] than that found in the exterior sample.

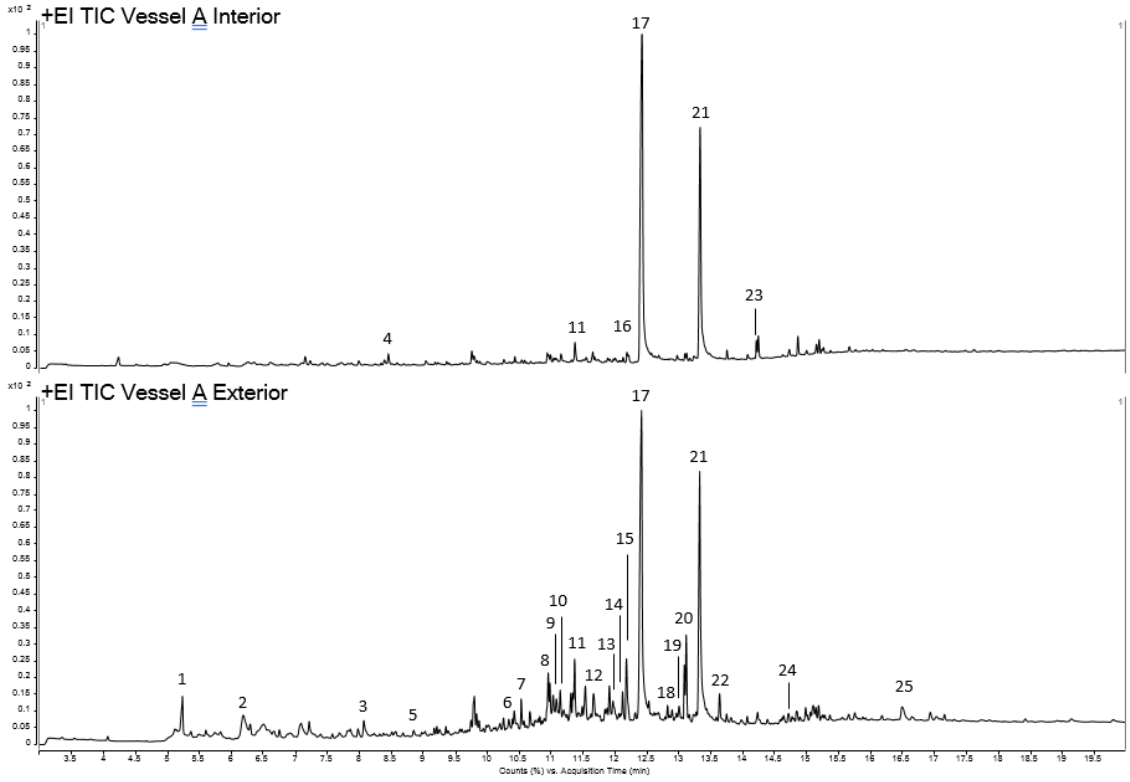


Figure 68 – EI chromatograms Vessel A samples

[1] Acetic Acid; [2] 5-methyl Furfural; [3] Naphthalene; [4] Methenamine; [5] 1-methyl Naphthalene; [6] Hexadecane; [7] Diethyl Phthalate; [8] 2,6-Diisopropylnaphthalene; [9] 1,4-di-iso-propylnaphthalene [10] Pentadecanal; [11] Tetradecanoic acid; [12] 9H-Fluoren-9-one; [13] Phenanthrene; [14] Hexadecanenitrile; [15] 1,9-Dihydropyrene; [16] Hexadecanoid acid methyl ester; [17] n-Hexadecanoic acid; [18] 2-phenyl Naphthalene; [19] 9-Octadecenitrile; [20] Octadecanenitrile; [21] Octadecanoic acid; [22] Pyrene; [23] Octadecanoic acid, butyl ester; [24] (Z)-docos-9-enenitrile and [25] Benzo[b]fluoranthene

[235] https://www.ebi.ac.uk/chebi/searchId.do?chebiId=CHEBI:28768.

Figure 68 shows the EI chromatograms of the Vessel A samples and identified compounds, with spectrometric datasets included in Appendix 16b. The chromatograms of the interior and exterior corrosion of Vessel A are both dominated by the large palmitic [17] and stearic acid [21] peaks. A significant difference between the chromatograms is the unique chemical profile of the external corrosion, dominated by polycyclic aromatic hydrocarbons (PAHs) [3, 5, 7-9, 12, 13, 15, 18, 22 and 25], and long-chain aliphatic nitriles [14, 19, 20 and 24]. Long-chain aliphatic nitriles are not commonly found in nature[236] other than as a bacterial metabolite so far identified in *Pseudomonas veronii* and *Micromonospora echinospora* feeding on fatty acids.

Figure 69 contains the EI chromatograms and compounds for Vessel B corrosion samples, with spectrographic datasets for all compounds included in Appendix 16c. The chromatograms for Vessel B samples are practically identical. The most dominant species are esters [3, 14, 15, 17, 21, 23 and 24], fatty acids [5, 6, 7, 11 and 12], a triterpene [18], sterols, [22] and its oxidation products [19 and 20], and compounds typically associated with plasticizers [14 and 17].[237] Cholesterol is a marker for animal fat. Squalene [18] is an intermediate of sterol biosynthesis in animals and plants. Isolated from shark liver oil,[238] squalene is abundant in human skin,[239] present in vegetable oils[240] (averaging 7g/L in olive oil)[241], plant cells and produced, in smaller quantities, by microbes including bacteria.[242]

[236] Fleming 1999.
[237] Evershed 1993.
[238] Allaby 2020.
[239] Downing et al.1981.
[240] Yannai 2013.
[241] Boskou 20008; Newmark 1999.
[242] Spanova and Daum 2011.

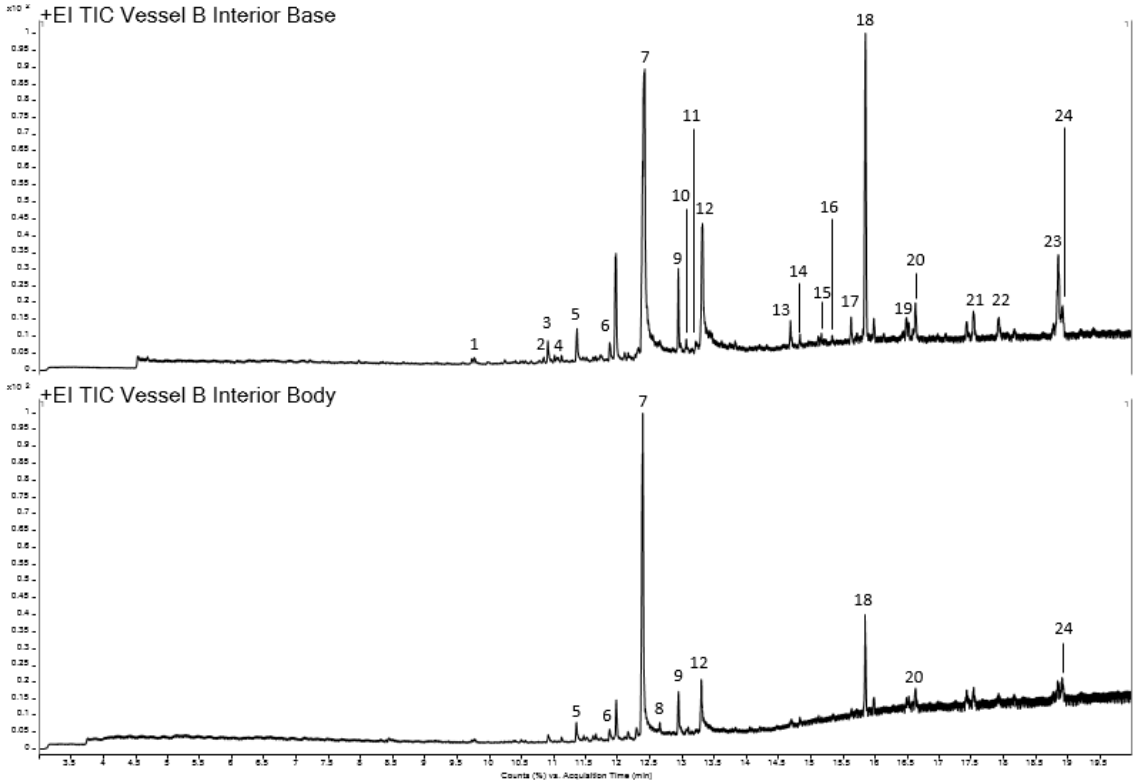


Figure 69 – EI chromatograms of Vessel B samples

[1] 2,5-Cyclohexadiene-1,4-dione, 2,6-bis (1,1-dimethylethyl)-; [2] Cyclopentaneacetic acid, 3-oxo-2-pentyl-, methyl ester; [3] 3-Buten-2-one, 4-(2,5,6,6-tetramethyl-1-cyclohexen-1-yl); [4] Tetradecanal; [5] Tetradecanoic acid; [6] Pentadecanoic acid; [7] n-Hexadecanoic acid; [8] Ethanol, 2-(9-octadecenyloxy)-, (Z); [9] Cyclohexadecane [10] Octadecanenitrile; [11] 6-Octadecenoic acid [12] Octadecanoic acid; [13] (Z)-docos-9-enenitrile; [14] Phthalic acid, di(2-propylpentyl)ester; [15] 1,4-Diphenyl-1,3-butadiene; [16] Hexacosane; [17] 1,4-Benzenedicarboxylic acid, bis(2-ethylhexyl) ester; [18] Squalene; [19] Cholesta-5,7-dien-3-ol, acetate, (3β)-; [20] Cholesta-3,5-diene; [21] Hexadecanoic acid, tetradecyl ester; [22] Cholesterol; [23] Tetradecanoic acid, eicosyl ester; [24] Hexadecanoic acid, hexadecyl ester

To try to gain further insights into the chemical profile of Vessel B Base sample, its evaporated chloroform/methanol extract was analysed and its composition compared with that of Vessel A's interior corrosion. The identified compounds are listed in Table 31 and the datasets included in Appendix 17. The most notable compounds identified in Vessel B

Base are α-terpineol (associated with pine oil)[243] and methyl dehydroabietate, a decomposition product of abietic acid.[244] Abietic acid is found in coniferous resins (particularly from the *Pinus* family)[245] and biosynthetically produced by aquatic (cyano)bacteria.[246] Because abietic acid decomposes upon heating,[247] it is possible that the methyl dehydroabietate identified in the sample was originally abietic acid which decomposed during analysis.

RT(min)	Name	MW	Vessel A	Vessel B Base
73.32-7.34	Benzoic acid, methyl ester	136	X	
8.00-8.05	α-Terpineol	154		X
8.05-8.09	Nonanoic acid, methyl ester	172	X	
9.11-9.14	Phenol, 2-(1,1-dimethylethyl)-4-methyl-	164		X
9.21-9.23	Tetradecane	198		X
10.04-10.08	1,4-Benzenedicarboxylic acid, dimethyl ester	194	X	
10.15-10.18	Benzoic acid, 4-ethoxy-, ethyl ester	194		X
10.41-10.42	Hexadecane	226		X
10.52-10.55	Diethyl Phthalate	222		X
10.97-11.01	3-Dodecene, (Z)	168	X	
11.15-11.17	Tridecanoic acid, 12-methyl-, methyl ester	242	X	
11.50-11.54	Octadecane	254		X
11.66-11.67	Pentadecanoic acid, methyl ester	256	X	
11.67-11.70	Tetradecanoic acid, 12-methyl-, methyl ester	256		X
12.16-12.19	Hexadecanoic acid, methyl ester	270	X	X
12.37-12.41	n-Hexadecanoic acid	256	X	X
12.89-12.93	Methyl dehydroabietate	314		X
13.10-13.13	Methyl stearate	298	X	X
13.19-13.21	6-Octadecenoic acid	282		X
13.29-13.35	Octadecanoic acid	284	X	
13.38-13.41	Docosane	310		X

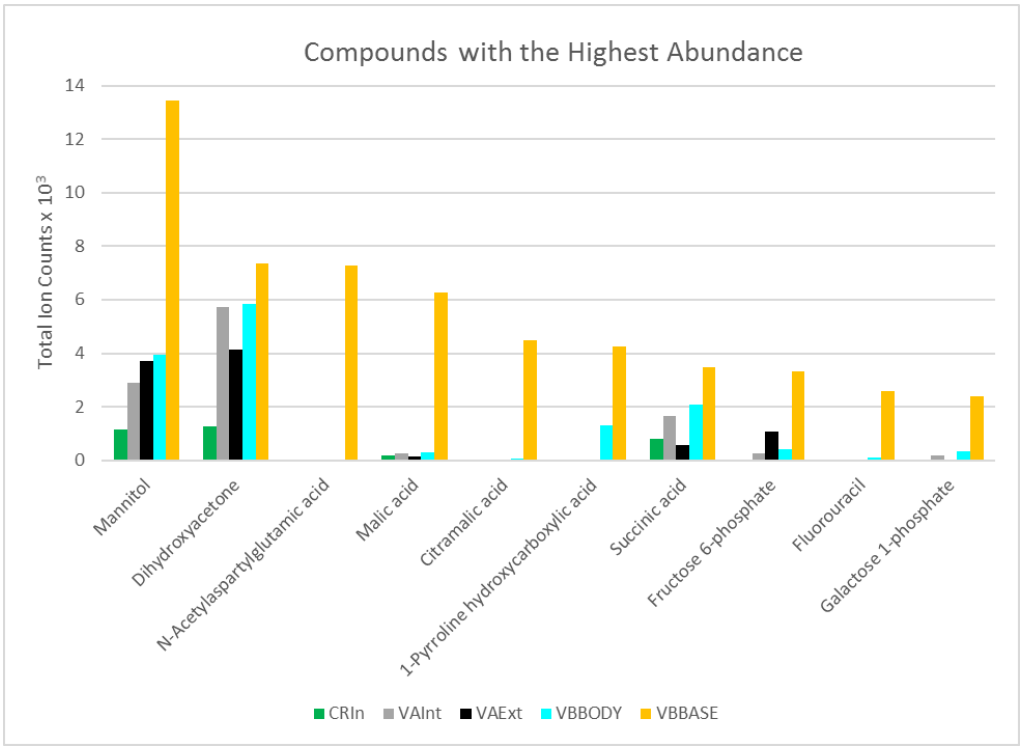
[X] = present, biomarkers highlighted

Table 31– Compounds identified in the evaporated chloroform/MeOH extracts of the samples from the interior of Vessel A and Vessel B

[243] Brown and Brown 2011.
[244] Mills and White 1994.
[245] ibid.
[246] Costa et al. 2016.
[247] Evershed 1993; Colombini et al. 2005.

5.1.5.2 IC-MS

A total of 44 compounds were identified in the Pewsey hoard samples; their measurements included in Appendix 18. To facilitate the analysis, the identified compounds were divided into two groups. The first group is composed of the top 10 compounds with the highest overall abundance (measured as ion counts) and their distribution across the samples shown in Figure 70. The second group is composed of the compounds with “infinity” fold change (Figure 71). The fold change of a compound expresses its variation between two experimental conditions as a ratio. For instance, if the abundance of a compound in sample A is 50 and in sample B it is 100, the fold change for this compound for this sample pair is 100/50 = 2. In all case studies reported in this research, each sample is treated as an experimental condition and the reported fold change for a compound is the highest value found in a sample pairing. Compounds with “infinity” fold change may be practically unique to an experimental condition.



[CRIn] = Cauldrom Rim Interior; [VAIn] = Vessel A Interior; [VAExt] = Vessel A Exterior; [VBBase] = Vessel B Base Interior and [VBBody] = Vessel B Body Interior Corrosion

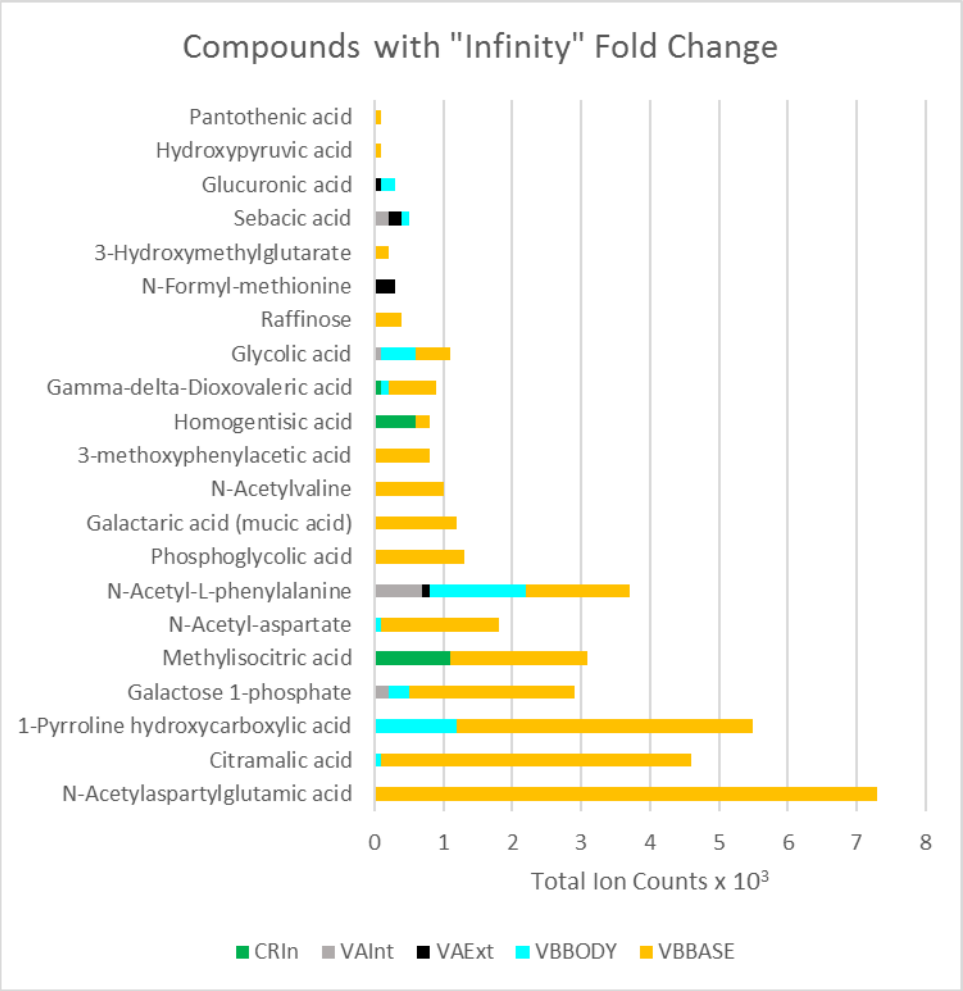
Figure 70 – Top 10 most abundant compounds and their distribution across the samples

Mannitol, a common microbial metabolite,[248] is present in all samples but its highest abundancy is in Vessel B base. Microbial activity across all samples is further validated by the dihydroxyacetone, which is often derived from the fermentation of glycerin in plant sugars.[249]

Looking at the distribution of "unique" compounds, the majority is present in Vessel B base with only a few also present in Vessel B body sample. N-acetylaspartylglutamic acid (a dipeptide metabolite), citramalic acid (a metabolite of Saccharomyces yeast and

[248] https://hmdb.ca/metabolites/HMDB0000765.
[249] https://hmdb.ca/metabolites/HMDB0001882.

Propionibacterium acnes species), 1-Pyrroline hydroxycarboxylic acid (an alpha amino acid derivative) and N-acetyl-aspartate (is a derivative of aspartic acid, found in sugar cane/beet molasses and proteins/peptides) indicate a specific set of conditions in this area of the hoard.



[CRIn] = Cauldrom Rim Interior; [VAIn] = Vessel A Interior; [VAExt] = Vessel A Exterior; [VBBase] = Vessel B Base Interior and [VBBody] = Vessel B Body Interior Corrosion

Figure 71 – "Unique" compounds and their distribution across the samples

In terms of the remaining samples, it is worth noting the cauldron rim interior and the Vessel A cauldron rim contain homogentisic and methylisocitric acids, both metabolites of *Yarrowia (Candida) lipolytica,*[250] a yeast that can degrade lipids and proteins and found in

[250] https://hmdb.ca/metabolites/HMDB0000130.

soils and dairy products.[251] Vessel A exterior sample stands out for being the only sample where N-Formyl-methionine was detected. This compound is a methionine derivative detected in cow's milk, initiates protein synthesis[252] and belongs to the sulfur-metabolism pathway[253] in bacteria. N-Formyl-methionine can be biosynthesised by *Escherichia coli*[254] and *Corynebacterium glutamicum* grown in a carbon and sulfur-rich medium.[255]

5.1.5.3 Proteomics

To try to characterize the microbial environment and confirm the presence of resins the Vessel A and Vessel B base samples were submitted to proteomics analysis. Table 32 is a summary of the protein matches found against Uniprot Resin and Uniprot Bacteria databases. The complete lists of proteins identified are include in Appendix 19.

Although pinus resin proteins were identified in all samples the highest scoring proteins were found in the Vessel B: M4HXU7 from *Pinus banksiana* (8% coverage from 5 peptides all unique to this protein) and B9U4U6 from *Pinus densiflora* (15% coverage from 9 peptides 5 of which unique). M4HXU7 was also identified in the Vessel A Exterior but at a lower coverage (3% from 3 peptides all unique). The resin proteins identified in Vessel A Interior belong to a different *pinus* taxa.

[251] Heard and Fleet 1999.
[252] https://hmdb.ca/metabolites/HMDB0001015.
[253] Thomas and Surdin-Kerjan 1997; Vermeij and Kertesz 1999; Lee and Gladyshev 2011.
[254] Ferla and Patrick 2014.
[255] Krömer et al. 2006.

	Taxa	Vessel A Interior	Vessel A Exterior	Vessel B Interior Base
Resin	Pinus banksiana		1 (43.52)	1 (59.67)
	Pinus densiflora			1 (52.12)
	Cannabis sativa			3
	Pinus contorta	2 (51.09)	2 (43.52)	
	Picea abies	1		
	Picea sitchensis	1		
	Pseudomonas abietaniphila		2	
Bacteria	Pseudomonas aeruginosa	1(236.58)	1 (192.98)	2 (177.15)
	Desulfobacterium autotrophicum		1 (31.52)	1 (37.03)
	Clostridium botulinum			1
	Salmonella schwarzengrund			1
	Blochmannia pennsylvanicus			1
	Streptococcus agalactiae	1 (39.66)	3 (31.8)	
	Corynebacterium kroppenstedtii	1		
	Oligotropha carboxidovorans	1		
	Neisseria meningitidis	1 (29.22)	1 (23.05)	
	Escherichia coli	1 (25.82)	1 (26.84)	
	Campylobacter jejuni	1		
	Oenococcus oeni	2		
	Mesoplasma florum	1		
	Shigella flexneri		1	
	Streptococcus suis		1	
	Streptococcus pneumoniae		4	
	Bordetella pertussis		1	
	Pseudothermotoga lettingae		1	
	Rhizobium meliloti		1	
	Nostoc sp.		2	
	Trichormus variabilis		1	
	Sinorhizobium medicae		1	
	Blochmannia pennsylvanicus		1	
	Rhodopirellula baltica		1	
	Chromobacterium violaceum		1	
	Mycolicibacterium gilvum		1	
	Wolbachia		3	
	Rhodobacter sphaeroides		1	

Table 32 – Proteins matches for Vessel A and Vessel B samples

expressed as number of proteins (highest --10lgP value)

The identification of *Desulfobacterium autotrophicum* in Vessel A exterior and Vessel B (where *Clostridium botulinum* was also identified) indicates that an anaerobic environment existed in these areas. Despite the similarities between the bacterial profiles of Vessel A interior and exterior areas, the latter appears to be more diverse.

Searches were also conducted with *Uniprot Flower* and *Uniprot Pinus* databases with similar results obtained across all samples.

5.1.6 Discussion

The results of the characterization of the samples from the Pewsey hoard are summarized in Table 33. The cauldron was the outermost vessel of the hoard. FTIR analysis of the cauldron interior corrosion indicated the presence of amides, nitrates and silicates: the latter confirmed by the identification of quartz as the only mineral phase. Most compounds identified in the exterior sample of the cauldron rim were also present in the interior. The identification of microbial metabolites in the interior corrosion point to a microbial source of palmitic and stearic acids as opposed to historical fat remains. Long chain saturated fatty acids are produced via elongation of short chain acids by specific enzymes in bacteria.[256]

[256] Heath et al. 2001; Parsons and Rock 2013; Zhao et al. 2018.

	Location	Colour	Consistency	FTIR	XRD	TSP-GC-MS	IC-MS	PROTEIN
CAULDRON	Interior (rim)	Blue/green	Hard	N-H, silicates, Organic nitrates, amides, benzenes	quartz	Furfural n-alkenes: C15 (main peak) n-alkanes FA: C16 and C18	Mannitol, dihydroxyacetone Homogentistic and methylisocitric acids	-
	Exterior (rim)	Blue/green	Hard	N/A	N/A	As above + benzaldehyde cymene FA: C16 (main peak) and C18	N/A	-
VESSEL A	Interior (base)	Green/brown	Powdery	-	Hydrocerussite Plumbonacrite	Methenamine FA: C16 and 18 (main peaks)	Mannitol, dihydroxyacetone Sebacic acid	Pinus contorta Streptococcus agalactiae, Neisseria meningitidis, Escherichia coli + 5 other types
	Exterior (base	Black	Hard	-	Chalcocite quartz	5-methyl furfural PAHs Long-chain nitriles FA: C16 and 18 (main peaks)	Mannitol, dihydroxyacetone Sebacic acid N-Formyl-methionine	Pinus banksiana + P. contorta Streptococcus agalactiae, Neisseria meningitidis, Escherichia coli Desulfobacterium autotrophicum + 15 other f bacteria
VESSEL B	Interior (body)	Green/blue	Hard	-	Quartz ?	Esters FA: C15,16, 18 and 18:1 Squalene Cholesterol derivatives	Mannitol, dihydroxyacetone	
	Interior (base)	Green/brown	Powdery	-	Quartz ?	As above + α-Terpineol methyl dehydroabietate	Mannitol, dihydroxyacetone	Pinus banksiana + P. densiflora Clostridium botulinum Desulfobacterium autotrophicum

Table 33 – Summary of the multi-analytical characterization of the Pewsey hoard corrosion

The Vessel A samples yielded similar FTIR spectra but different crystalline phases, within which metal corrosion was identified. Copper sulfide found in the exterior sample is a sulfate-reducing bacteria metabolite characteristic of anaerobic waterlogged environments.[257] Such an environment could have existed in the Pewsey hoard given the way the vessels were arranged. Rainwater percolating through the soil would reach Vessel A through the gap between the rim of Vessel C and the cauldron, as shown in Figure 72. Corrosion at the water surface level would have been promoted by the extra oxygen eventually leading to the detachment of the bottom of Vessel B and the corrosion of its feet.

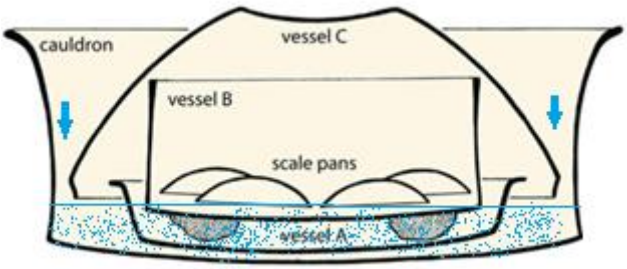


Figure 72– Pewsey hoard corrosion microclimate

arrows indicating water ingress with area affected by waterlogging etched blue.

The black deposits (now identified as copper sulfide) were originally thought to be soot deposits from a wood fire with the identification of PAHs initially supporting this hypothesis. Although burning of wood is a common source of PAHs[258] this would require retene[259] to be amongst the identified compounds. An alternative source of PAHs

[257] Duncan and Ganiaris 1987.
[258] Zou et al. 2010.
[259] Ramdhal 1983.

is the combustion of fossil fuels,[260] in this case bitumen, which could have been applied to copper vessels to protect them from the effects of fire when it was in use. However, the abundance of naphthalene-based compounds[261] indicates a biological source. The identification of other bacterial metabolites supports the idea of a carbon-rich, water-logged and anaerobic environment in this area of the hoard, where bacterial colonies may include certain species of sulfate-reducing bacteria supported by PAHs.[262] Indeed the hypothesis of a varied bacterial community in the Vessel A Exterior corrosion is supported by proteomics data.

The samples removed from the interior of Vessel B yielded the most interesting results. The FTIR spectrum of the Base sample was similar to Vessel A samples' spectra, reflecting the contributions from a bioactive microenvironment. However, the chromatogram of the Base and Body samples were practically identical both containing peaks for cholesterol (and its oxidation products) and squalene.

Cholesterol is rarely found in organic residues extracted for archaeological ceramics,[263] possibly due to its degradation resulting from interactions with the fired clay and fatty acids, conditions created by cooking in clay pots.[264] Therefore when cholesterol appears in archaeological residues its source is considered modern contamination from fingerprints,[265] particularly when it appears alongside squalene.

[260] Baek et al. 1991; Peters et al. 2005.
[261] Sporstol et al. 1983; Thiele and Brümmer 2002.
[262] Annweiler et. al. 2000; Davidova et al. 2007; Kümmel et al. 2015.
[263] Whelton et al. 2021.
[264] Hammann et al. 2018
[265] Smith and Thiboutot 2008.

However, cholesterol and some of its oxidation products found in Vessel B samples have been identified in carbonised residues found in copper cauldrons.[266] There was no suggestion of contamination because the vessels were block-lifted by archaeologists, sampled during micro-excavation in a controlled environment. Although the sampled residues were clearly distinguishable from soil and copper corrosion, the latter is suggested to have contributed to their preservation.[267]

The vessels of the Pewsey hoard were excavated and transported to a museum by the finders, who probably did not wear gloves. Although the author took precautions against contamination (wearing disposable gloves, using disposable metal scalpels and sterilised glass vials) sampling the vessels within a few days from their arrival at the museum, it is possible that the sampled surfaces had already been contaminated by human fingerprints. Notwithstanding the risk of contamination, it significant that cholesterol, its oxidation products and squalene were only found in the Vessel B samples, when analysed as solids. Analysis of the evaporated solvent extract of the Vessel B base sample yielded different compounds, including a terpenoid associated with coniferous resin.

Vessel B samples also contained a disproportionally high abundance of bacterial metabolites, the peptides recovered matched to four types of bacteria in this sample (two of which anaerobic). Their presence perhaps supports a reassignment of the origin of

[266] Steele 2017.
[267] Ibid.

phthalates[268] to a microbial source. As this area of the hoard was shielded from the soil, some of the bacterial/microbe colonies may be of historical value.

[268] Keire et al. 2001; Babu and Wu 2010; Tian et al. 2016.

5.2 Case Study 2 – Roman Bowl from Wingham

5.2.1 Background

The Roman bowl in Figure 73c was also found by metal detectorist [redacted] in November 2016, along a grassy track in a pear orchard [redacted] near the village of Wingham (Kent, UK). Upon finding the object, Mr [redacted] contacted a local archaeologist, who advised that the object should be left in situ and protected until it could be excavated by archaeologists. The bowl was block-lifted in its surrounding soil and after stabilization, put on display at Sandwich Museum.

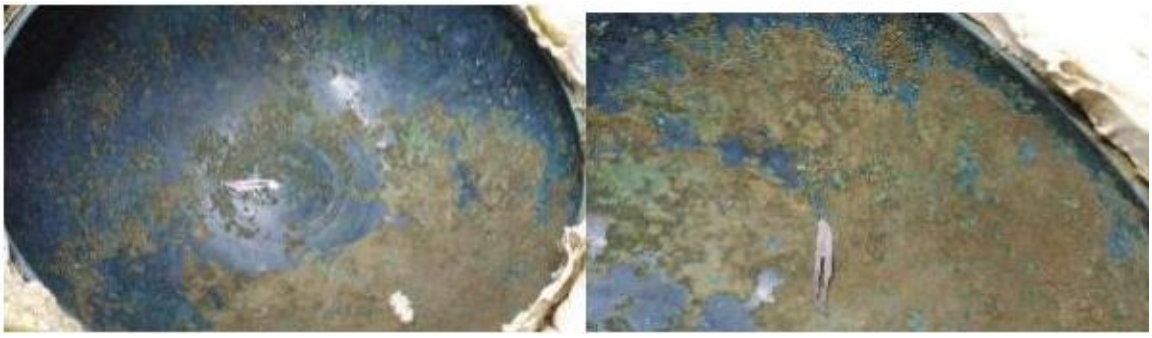


Figure 73 – The recent history of the Roman bowl

[redacted] and his find (A), the bowl's excavation (B), and the bowl on display at Sandwich Museum (C)

5.2.2 Research Question

The conservation/stabilization of the bowl was undertaken by Dana Goodburn-Brown, who prior to any intervention on the object, removed corrosion samples from the interior (Figure 74) and exterior of the object. The samples were removed with a metal scalpel from the metal surface, placed in glass vials with metal caps and submitted for analysis. Each sample weighted between 15-20 mg and submitted for analysis to see whether any contained biomarkers of substances used in the past.



Supplied by Dana Goodburn-Brown

Figure 74 – Sampling the interior of the object

5.2.3 Identification of Chemical Bonds

The spectra for green corrosion are included in Figure 75 with peak and band assignments listed in Table 34.

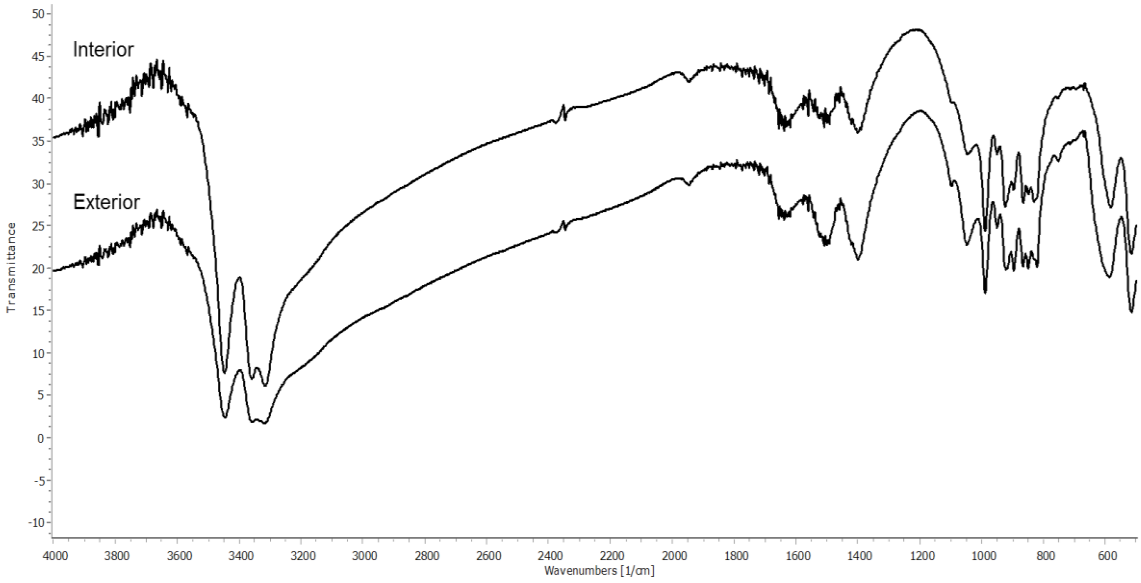


Figure 75 – FTIR spectra of green corrosion

KBr method

Interior		Exterior		Attribution
3447	s	3446	s	OH intramolecular bonded stretching vibrations
3357	w	3356	vw	N-H stretching vibrations (?)
3319	w	3317	vw	
1638	m	1638	m	C=O carboxylic acid, amides I and II stretching vibrations
1509	m	1509	m	aromatic ring stretching vibrations
1399	m	1398	m	CH_2 deformation
987	s	987	s	$R_1CH=CHR_2$
921	m	921	m	aromatic ring stretching vibrations
864	m	865	w	
847	vw	848	w	
828	w			C-Cl stretching vibrations
		819	w	
582	s	584	s	substituted aromatics stretching vibrations
514	s	514	s	

Table 34 – Infrared frequencies (cm^{-1}) and band assignments for green corrosion

The spectra of the green corrosion samples are identical. Both spectra contain characteristic bands for OH intramolecular bonded species, carboxylic acid and/or amides and aromatic compounds. Of interest are the C-Cl vibrations between 847 and 819cm^{-1} and the strong bands at 584-582 and 514cm^{-1} for substituted aromatics.

The spectra for brown corrosion are shown in Figure 76. Band assignment was not possible for these samples as the peaks are too broad.



Figure 76 – FTIR spectra of brown corrosion

KBr method

5.2.4 Identification of Mineral Phases

Figure 77 shows the diffractograms and phase identifications for green corrosion (the peak lists are included in Appendix 20). Despite their low intensity two mineral phases were identified in the interior green corrosion: basic copper chloride atacamite ($Cu_2Cl(OH)_3$: 75%) and quartz (25%). The main mineral phase identified in the exterior green corrosion is also basic copper chloride, a mixture of atacamite (68%), paratacamite ($Cu_3(OH)_6Cl_2$: 5%) and copper oxide cuprite (32%). Atacamite and paratacamite interconvert,[269] their presence in the corrosion samples points to high chloride ions concentration in the burial environment.

[269] Pollard et al. 1989.

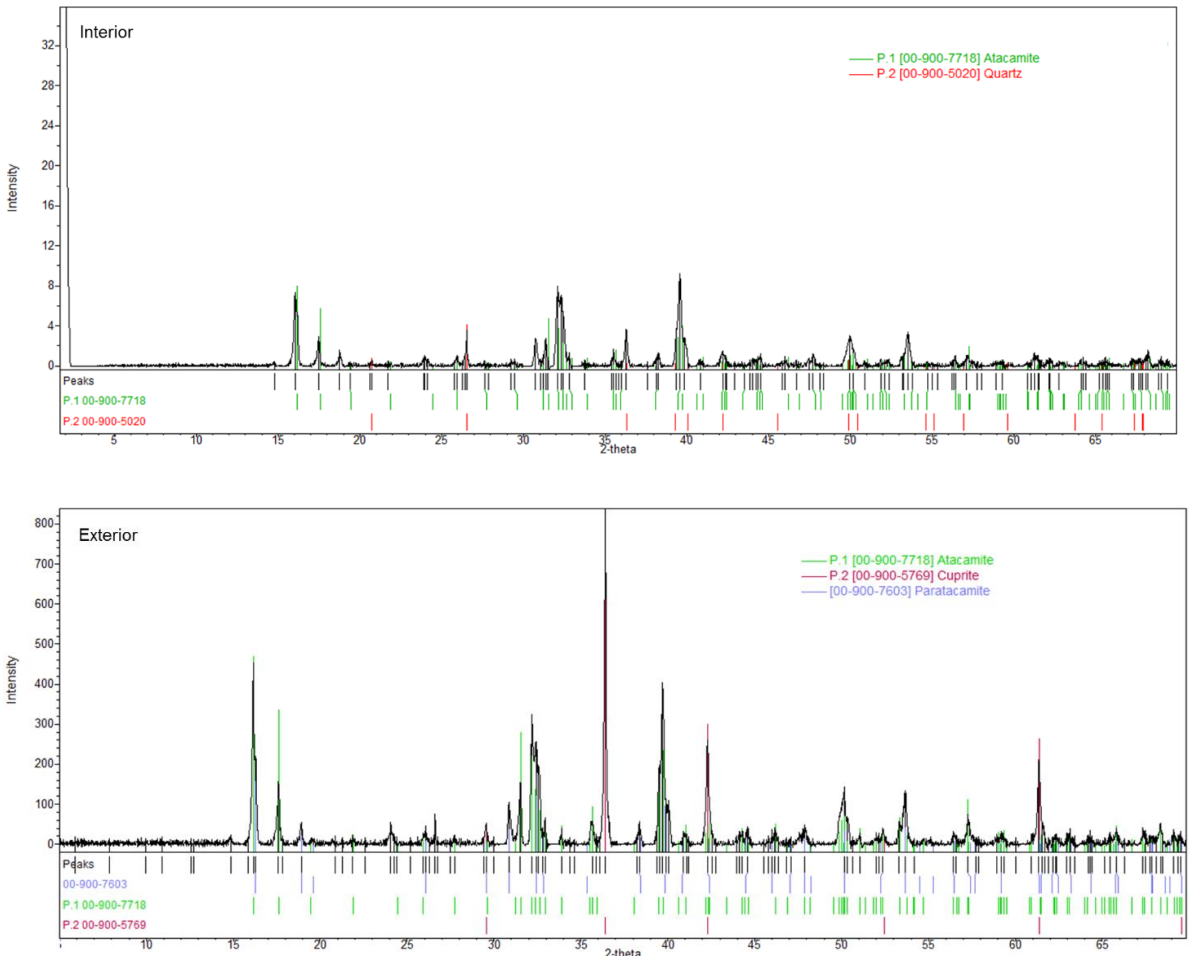


Figure 77 – Diffractograms of green corrosion

atacamite and quartz identified in the interior sample and atacamite, cuprite and paratacamite identified in the exterior sample

The patterns and phase identification for the brown corrosion samples are shown in Figure 78 (with peak lists included in Appendix 16b). The samples are practically identical – the only mineral phase identified is quartz.

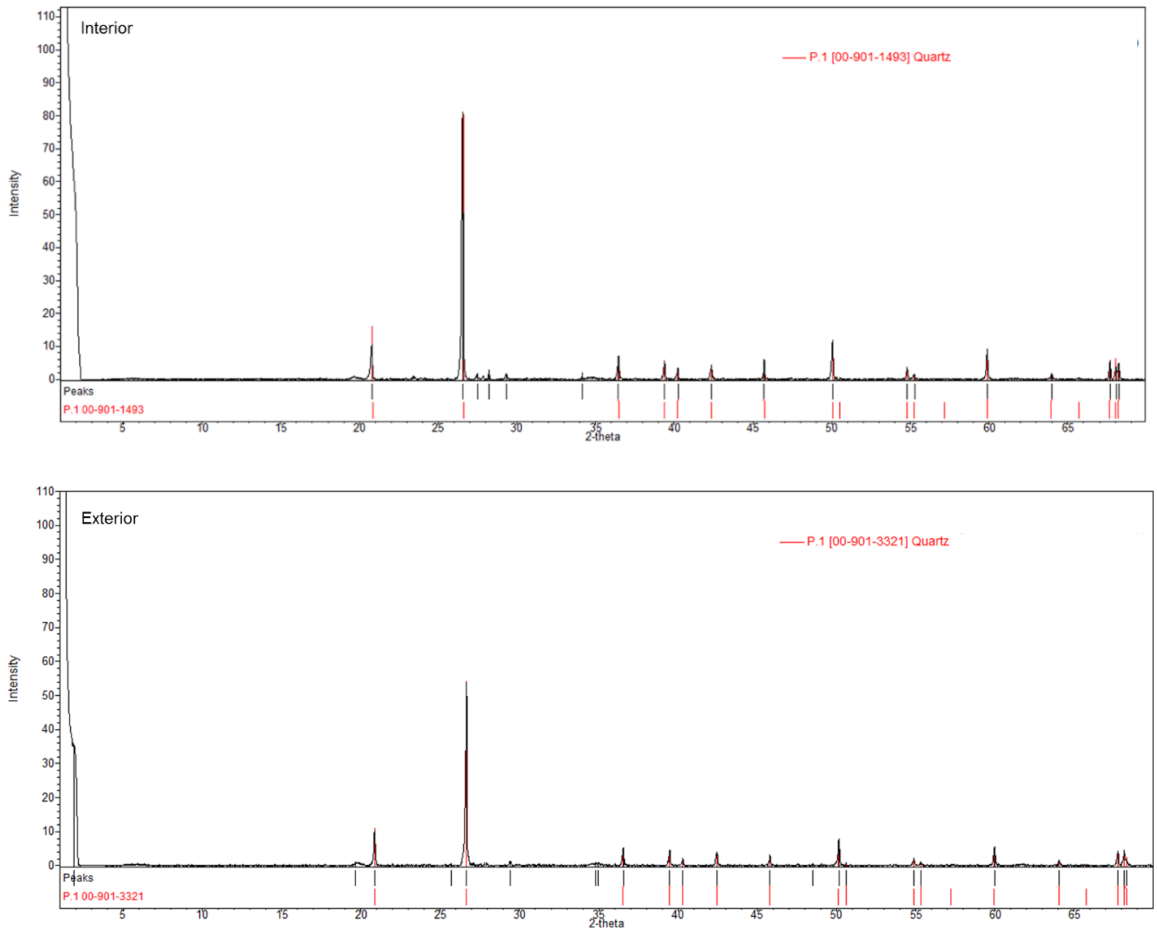


Figure 78 - Diffractograms of brown corrosion

quartz identified in the interior and exterior samples

5.2.5 Identification of Organic Compounds

5.2.5.1 QTOF-GC-MS with TSP

The EI chromatograms and identified compounds of the green corrosion are shown in Figure 79 with spectrometric datasets included in Appendix 21. Both chromatograms are dominated by palmitic acid [8] and chlorobenzenes [1, 2, 4 and 5]. Chlorobenzenes are

common soil contaminants from pesticides.[270] The interior green corrosion also contains a very strong peak for stearic acid [10], also present in the exterior sample but at much lower intensity. C15 fatty acid [6] and methyl esters [7 and 9] were only identified in the interior sample, with unassigned plant material present in both samples.

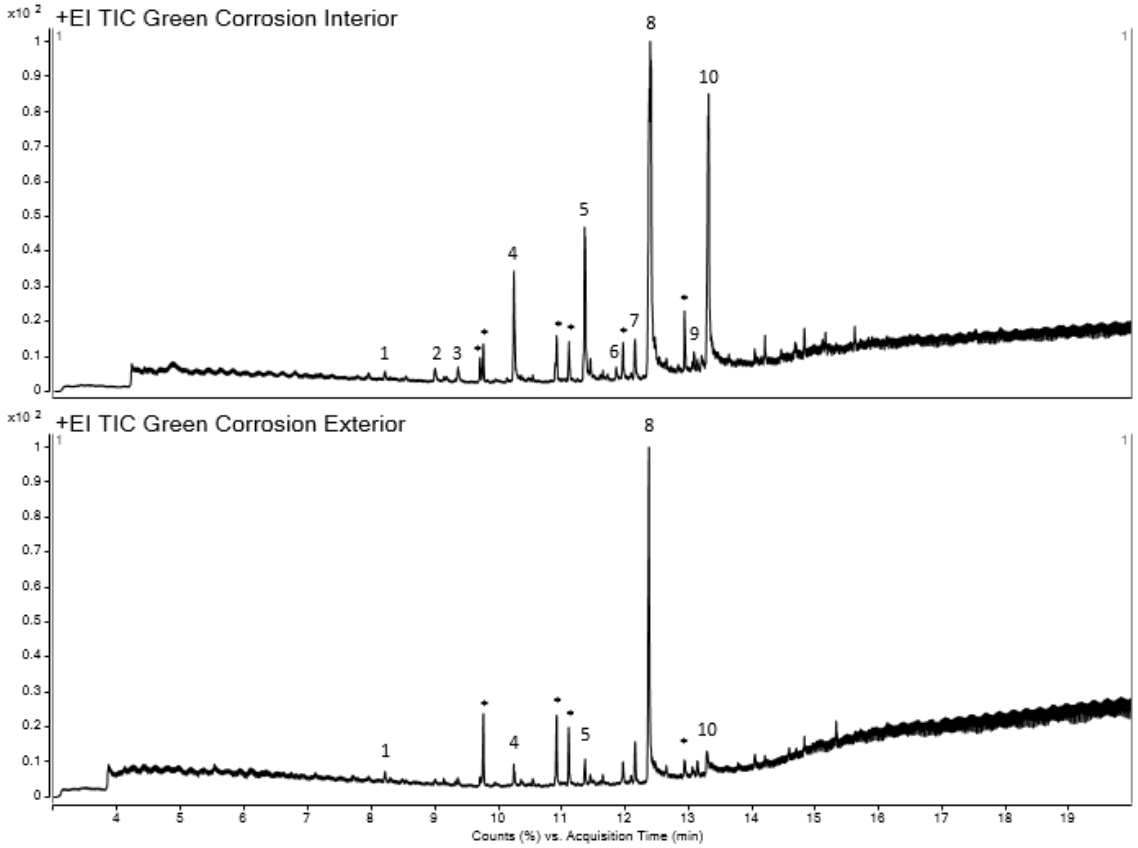


Figure 79 – EI chromatograms of green corrosion

[1] Benzene, 1,2,3-trichloro; [2] Benzene, 1,2,4,5-tetrachloro; [3] Benzene, 1,2,3,5-tetrachloro; [4] Benzene, pentachloro-; [5] Benzene, hexachloro-; [6] Pentadecanoic acid; [7] Hexadecanoic acid, methyl ester; [8] n-hexadecanoic acid; [9] Methyl stearate; [10] n-octadecanoic acid; [*] plant material

The EI chromatograms and identified compounds in brown corrosion are shown in Figure 80 with spectrometric datasets included in Appendix 17b. Palmitic acid [8] and

[270] Brahushi et al. 2017.

Diethyltoluamide [4] (a common ingredient of insect repellents)[271] are the most prominent peaks in the interior sample. Both compounds are also present in the exterior sample, although its second most prominent compound is stearic acid [9] – unique to this sample. Amongst the unidentified compounds are plant materials (long-chain alkanes, alkenes, alkanols) and polycyclic substances, which could not be assigned to a specific compound with any degree of certainty.

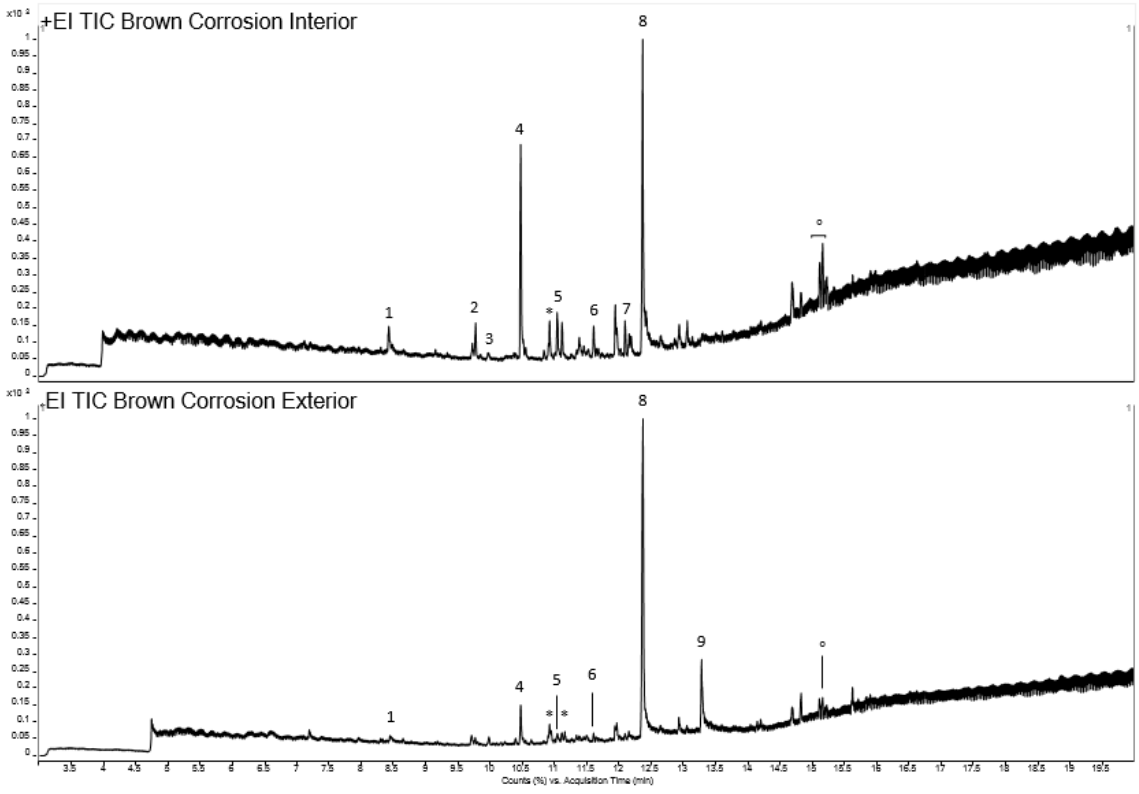


Figure 80 – EI chromatograms of brown corrosion

[1] Methenamine; [2] 1-Hexadecene; [3] 2,4-Di-tert-butylphenol; [4] Diethyltoluamide; [5] Benzenesulfonamide, N-ethyl-2-methyl-; [6] 2-Propanol, 1-chloro-,phosphate (3:1); [7] Hexadecanenitrile; [8] n-hexadecanoic acid; [9] octadecanoic acid; [*] plant material; [°] polycyclic compounds

[271] https://pubchem.ncbi.nlm.nih.gov/compound/Diethyltoluamide.

5.2.5.2. IC-MS

A total of 46 compounds were identified in the Roman bowl samples, the full measurement details are included in Appendix 22. To facilitate the analysis of the data, the identified compounds were divided into three groups. The first group is made of the top 10 compounds with the highest ion count (Figure 81), the second group the top 10 compounds with the highest fold change (Figure 82) and the third group the top 10 most common compounds (Figure 83) and their distribution across the samples.

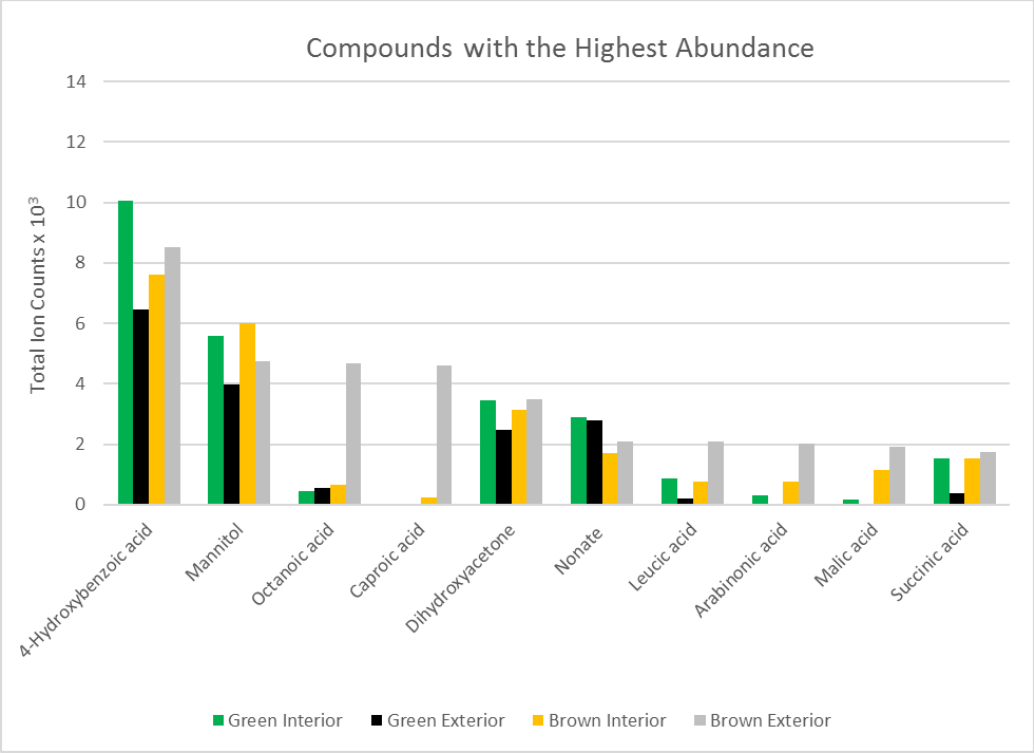


Figure 81 – Most abundant compounds and their distribution across the samples

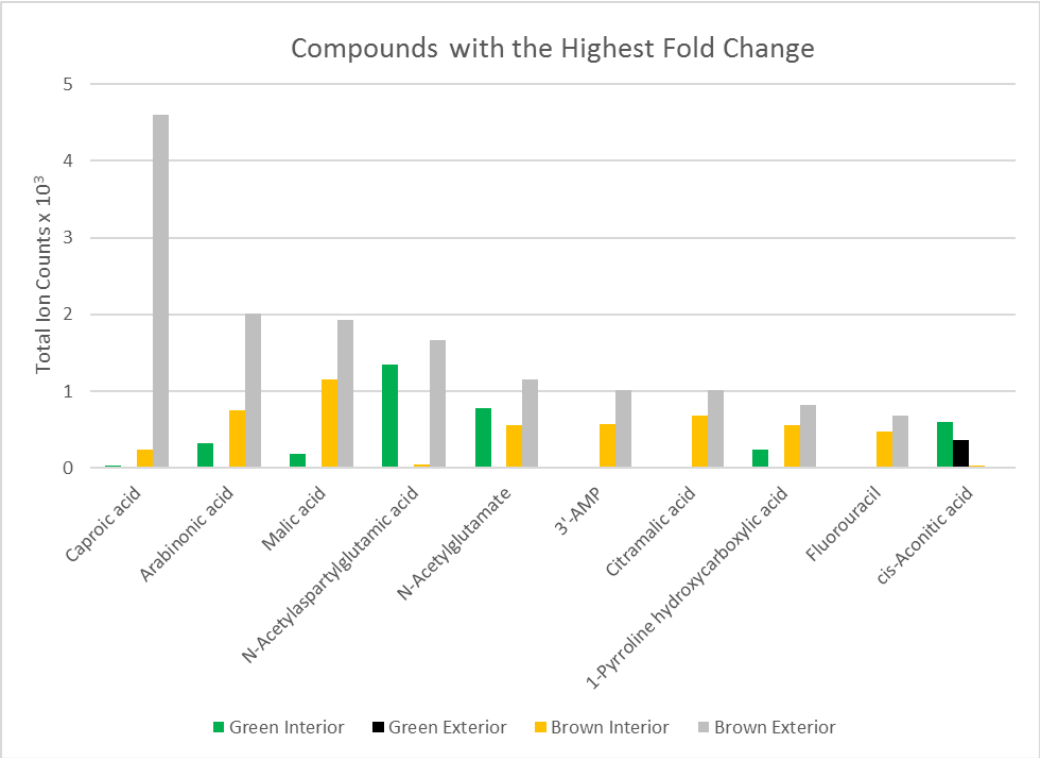


Figure 82 – Most unique compounds and their distribution across the samples

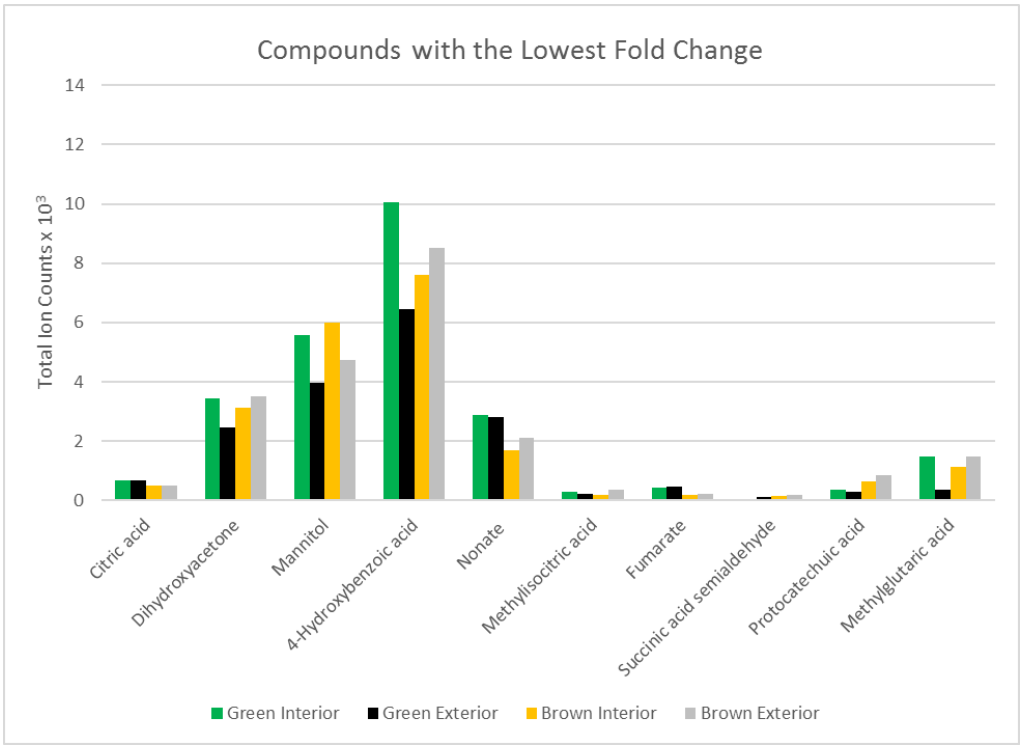


Figure 83 – Most common compounds and their distribution across the samples

The most distinctive compound profile is that of the brown exterior corrosion. This sample is dominated by short-chain acids including caproic acid that features almost uniquely in this sample. Caproic acid is present in apples, grapes, animal fats, dairy products and essential oils and fermentation product of butyric acid.[272] However, the likely source of caproic acid in the sample is ruminant bacteria[273] from animal faeces (perhaps at some point used as fertilizer?) or decaying plant material, carried into the soil via rainwater. Information about the composition of the soil surrounding the object would be included in the excavation report, which was not disclosed by the archaeological unit.

Regarding the green corrosion samples, their only characteristic feature is cis-aconitic acid, a tricarboxylic acid that has been identified in a variety of vegetable and fruits,[274] its (Z) form present in apple and passion fruit juice.[275] Because aconitic acid is a fungi[276] and yeast[277] metabolite, a bacterial source for cis-aconitic acid in the corrosion samples – as opposed to decaying fruits from the orchard at ground level – cannot be disregarded.

5.2.6 Discussion

The results of the characterization of the samples from the Roman bowl are summarized in Table 35. The organic compounds identified in the corrosion samples of the Roman bowl relate to pesticides, plant materials and microbial metabolites. Although no

[272] Yannai 2013.
[273] Kenealy et al. 1995; Weimer and Kohn 2016; Carvajal Arroyo et al. 2019.
[274] https://hmdb.ca/metabolites/HMDB0000072.
[275] Yannai 2013.
[276] Calam et al. 1939.
[277] Tabuchi et al. 1981.

biomarkers for substances used in the past were identified in the corrosion samples, chlorobenzenes were identified in the green corrosion samples which also contain copper chloride mineral phases. The copper chlorides have contributed to the strong bands at 3,600-3,200cm^{-1} in the FTIR spectra of the green corrosion products.

	Location	Consistency	FTIR	XRD	TSP-GC-MS	IC-MS
GREEN CORROSION	Interior	Hard	O-H, N-H, amides, C-Cl substituted aromatics	Atacamite quartz	FA: C15, C16 (main peak) and C18 Chlorobenzenes Plant material	Cis-Aconitic acid
	Exterior	Hard		Atacamite, paratacamite cuprite	FA: C16 (main peak) and C18 Chlorobenzenes	Cis-Aconitic acid
BROWN CORROSION	Interior	Hard	-	Quartz	FA: C16 (main peak) and 18 Diethyltoluamide Polycyclic aromatics Plant material	Caproic acid
	Exterior	Hard	-	Quartz	FA: C16 (main peak) and 18 Diethyltoluamide Polycyclic aromatics Plant material	Caproic acid

Table 35 – Summary of the Multi-analytical characterization of the Roman bowl corrosion

In 2004, a group of scientists led by Prof. Mark Pollard attempted to gather empirical evidence that agrochemicals would accelerate the corrosion of archaeological metal objects that may be buried in the soil.[278] Laboratory and field experiments attempted to measure the effect of different fertilizers with geochemical modelling predicting the

[278] Pollard et al. 2004.

following order of corrosivity: KCl > N > P,[279] KCl commonly known as muriate of potash.

The bond disassociation energy between K-Cl is 427kJ/mol and for C-Cl 397(28) kJ/mol,[280] thus less energy is required for a chlorine to disassociate from a bond with carbon than with potassium. The C-Cl bond disassociation energies (calculated and experimentally measured) for 13 different chlorobenzenes vary from 375 to 399 kJ/mol[281] supporting the hypothesis that these compounds supplied the chloride ions responsible for the copper chlorides identified as mineral phases in the green corrosion samples. Given that the site where the object was found is/was an orchard, the green corrosion samples from the Roman bowl are evidence of how agrochemicals dictate the form of corrosion found on archaeological metal objects.

[279] Wilson et al. 2006.
[280] Lange 2005.
[281] Zhang et al. 2009.

5.3 Case Study 3 – Pompeii INV10653

5.3.1 Background

Pompeii INV10653 is a shallow bowl that originally contained a pair of long handles (one is missing), shown in Figure 84.



Figure 84 – Pompeii INV10653 and a similar complete specimen

This vessel was amongst a group of copper alloy vessels loaned to the Ashmolean Museum in 2019 for the *Last Supper in Pompeii* exhibition, which ran between 25 July 2019 – 12 January 2020. All vessels were excavated from a simple taverna in the archaeological remains of Pompeii, Italy, and kept in storage on site ever since. The loan agreement stipulated that the vessels would be conserved at the Ashmolean Museum

prior to the exhibition with the conservation treatment aimed at revealing as much of the metal surface as possible.[282]

5.3.2 Research Question

Paul Roberts, the Sackler Keeper of the Department of Antiquities at the Ashmolean Museum, has for some time considered that "bread basket" is not the correct function/description for Pompeii INV10653 and similar objects. He believes that their long handles indicate that their content was something that should not touch the holder's hands. Mr Roberts's theory is that this object was a chamber pot used by guests at the dinner table.[283] Samples (c. 10-20 mg each) from the interior corrosion were submitted for analysis in an Eppendorf (polypropylene) tube and in gelatine capsules together with the picture shown in Figure 84.

5.3.3 Identification of Chemical Bonds

The spectrum for the sample is shown in Figure 85 with peak and band assignments listed in Table 36.

[282] Kelly Domoney *pers. comms*. 13th August 2019
[283] Paul Roberts *pers. comms.* 24th June 2021



Figure 85 – FTIR spectrum of the interior of Pompeii INV10653

KBr method

interior		Attribution
3426	m	OH intramolecular bonded / N-H? stretching vibrations
2926	w	C-H aliphatic stretching vibrations
2855	w	
1495	s	aromatic ring stretching vibrations
1466	sh	
1415	s	CH_2 / CO_3^{3-} deformation
1046	s	silicates
955	m	
833	m	aromatic ring stretching vibrations
818	m	
749	w	
572	w	substituted aromatic stretching vibrations
491	w	
455	w	

Table 36– Infrared frequencies (cm^{-1}) and band assignments for Pompeii INV10653 interior sample

The spectrum of the sample indicates the presence of a variety of OH intramolecular bonded/N-H species, traces of aliphatic compounds (2926 and 2855cm^{-1}) and a higher

proportion of aromatic species (1495, 833 and 818cm^{-1}). Strong peaks at 1415 and 1046cm^{-1} are due to the presence of inorganic carbonates and silicates, respectively.

5.3.4 Identification of Mineral Phases

Figure 86 shows the XRD patterns obtained for the sample, most corresponding to the mineral azurite, $Cu_3(CO_3)_2(OH)_2$. The complete peak list is included in Appendix 22.

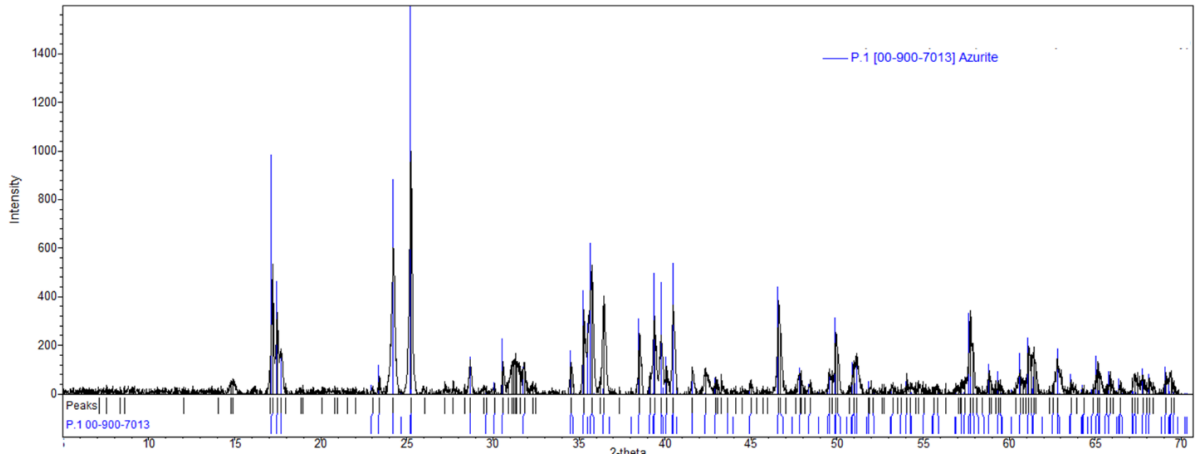


Figure 86 – Diffractogram of the interior of Pompeii INV10653

azurite as identified mineral phase

5.3.5 Identification of Elemental Composition

The survey spectrum of the sample is shown in Figure 87. The elemental composition of the sample is dominated by carbon and oxygen. The other remaining elements in the sample are copper, silica and nitrogen, with traces of calcium and zinc.

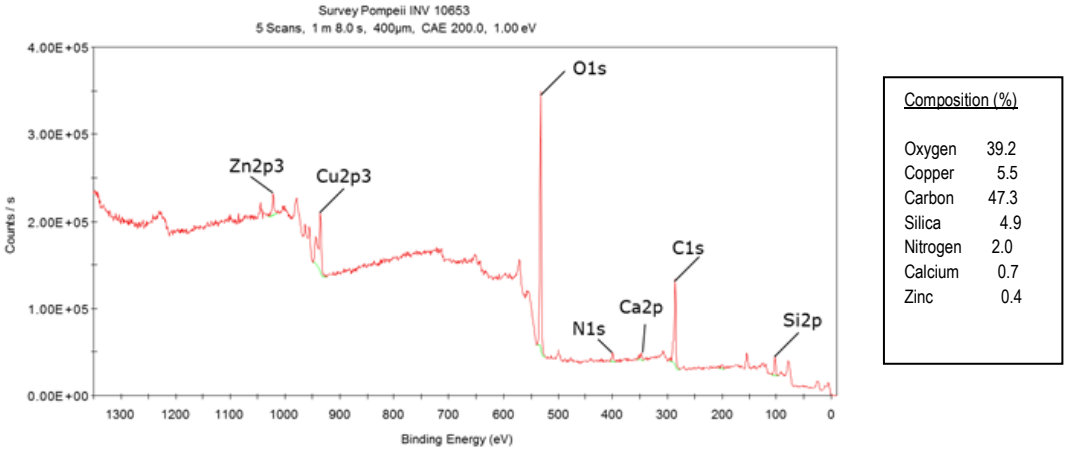


Figure 87 – XPS survey spectrum and elemental composition of the interior of Pompeii INV10653

Urea is the most common compound in excreted in urine and the source of more than 80% of its total nitrogen content.[284] Figure 88 shows the carbon and nitrogen scans for a urea reference and the Pompeii INV10653 sample. The binding energy for nitrogen is the same as that measured for the urea reference at 399.5eV, the latter matching the value published by NIST library for this compound.[285]

An unambiguous assignment of the source of the nitrogen in the sample to urea is not possible because of the large proportion of carbonates.[286] The binding energies of metal carbonates vary between 288-290eV, overlapping with esters and amides $(NH_2)_2C=O$. In the sample, these three species are represented by the first deconvoluted peak (bottom left of Figure 88) followed by at least three more peaks representing the variety of chemical environments where carbon is present.

[284] Folin 1905.
[285] https://srdata.nist.gov/xps/query_chem_name_detail.aspx?ID_NO=2165&CName=urea.
[286] Alison Crosby *pers. comm* 2019.

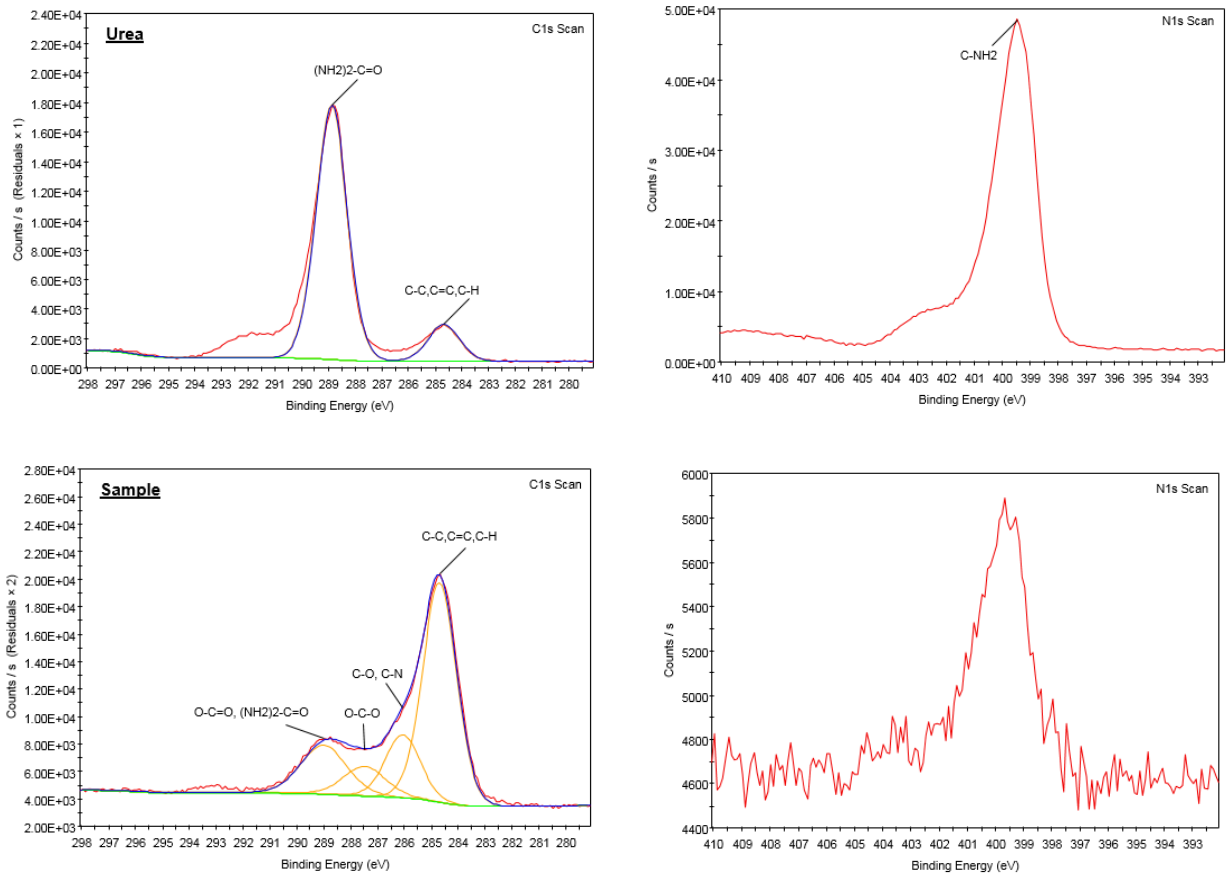


Figure 88 – C1 and N1 region spectra for urea and the Pompeii INV10653 sample

ORANGE curves denoting peak fittings

In terms of the copper ions in the sample, these are mostly Cu(II) as shown by the Cu2p scan included in Figure 89.

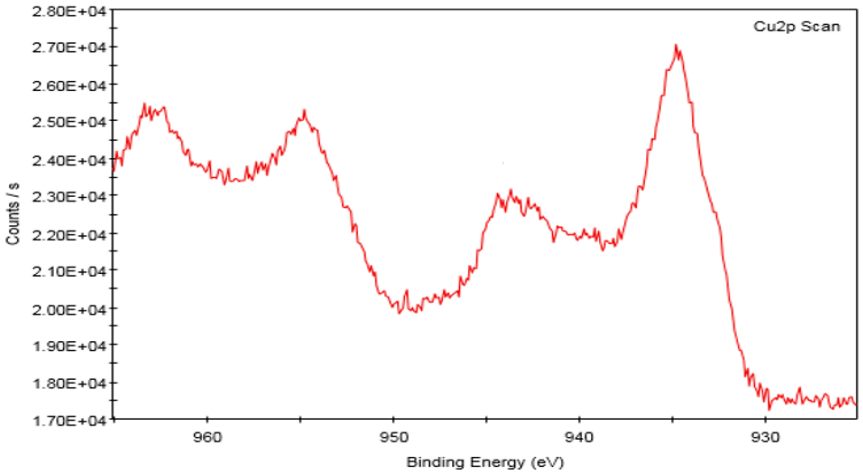


Figure 89 – Cu2p spectrum of the Pompeii INV10653 sample

5.3.6 Identification of Organic Compounds

5.3.6.1. QTOF-GC-MS with TSP

The EI chromatogram and identified compounds for the Pompeii INV10653 sample are shown in Figure 90 with spectrometric datasets for identified compounds included in Appendix 23. The chromatogram is dominated by a plasticiser [17] and convoluted peaks at around 9.40 minutes and between 14.55-14.90 minutes. Amongst the identified compounds were sulphur-containing compounds [1, 2 and 5], nitrogen-containing compounds [6, 7, 10 and 16], long-chain carboxylic acids [12 and 15] acids, and long-chain aliphatic compounds including [11 and 13].

Relevant to the research question are:

- Benzaldehyde [3] – a volatile compound occasionally found in human urine[287]
- Benzyl alcohol [4] – found in human faeces and saliva[288]
- n-Propyl benzoate [9] – an ester derivative of benzoic acid[289]

Benzoic acid is present in all human body fluids, including urine.[290]

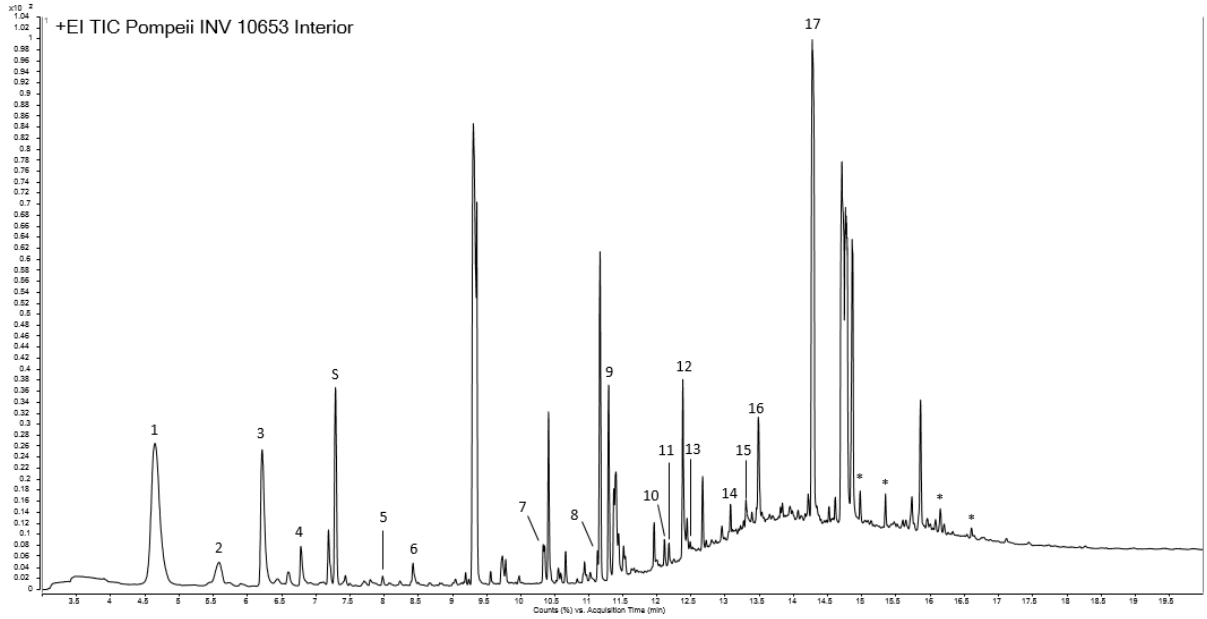


Figure 90 – EI chromatogram of Pompeii INV10653 interior corrosion

[1] 1,3-Oxathiolane; [2] 1,4-Oxathiolane; [3] Benzaldehyde; [4] Benzyl alcohol [5] 1,4,5 Oxadithiepane; [6] Methenamine; [7] Benzamide, N-propyl-; [8] Pentadecanal-; [9] n-Propyl benzoate; [10] Hexadecanenitrile; [11] 1-Heptadecyne; [12] n-Hexadecanoic acid; [13] Eicosane; [14] Octadecanenitrile; [15] Octadecanoic acid; [16] Hexadecanamide; [17] Benzyl butyl phthalate; [S] thiol compound and [*] long carbon chain aliphatic compound

[287] https://hmdb.ca/metabolites/HMDB0006115.
[288] https://hmdb.ca/metabolites/HMDB0003119.
[289] https://hmdb.ca/metabolites/HMDB0031761.
[290] https://hmdb.ca/metabolites/HMDB0001870.

The identification of compounds [1,2 and 5] in the sample is puzzling as no references listing them amongst human or bacterial metabolites could be found. The alkyl amides and nitriles can be interpreted as biomarkers for bacterial activity.[291] The identification of alkyl nitriles in the sample is also intriguing. These compounds are formed during biomass burning[292] as fatty esters[293] and acids[294] react with ammonia from protein residues.

5.3.6.2. IC-MS

The Pompeii INV10653 sample was analysed alongside sooty material from other objects from Pompeii. Amongst the 38 compounds identified, 12 were present in the INV10653 sample with fold change > 2 (their measurements are included in Appendix 24). The compounds with the highest fold change are: malondialdehyde (fold change 35.9) and 3-methoxyphenylacetic acid (7.68), both human metabolites excreted in urine.[295] Malondialdehyde is an oxidation product of polyunsaturated fatty acids.[296] In humans, malondialdehyde is a marker for oxidative stress[297] and alcohol ingestion.[298] In food chemistry, the compound is not only associated with rancidity, but also with food processing (e.g. cooking).[299] 3-methoxyphenylacetic acid has a similar chemical composition to a metabolite of *Rhizoctonia solani*,[300] a soya bean fungus.

[291] Buckley et al. 1999; Wang et al. 2017.
[292] Schauer et al. 1999.
[293] Mckee and Hatcher 2010.
[294] Simoneit et al. 2003.
[295] https://hmdb.ca/metabolites/HMDB0006112; https://hmdb.ca/metabolites/HMDB0059969.
[296] Ayala et al. 2014.
[297] Del Rio et al. 2005.
[298] Clot et al. 1994; Worrall and Thiele 2005.
[299] Newburg and Concon 1980.
[300] Orellana and Mandava 1983.

5.3.7 Discussion

The Pompeii INV10653 interior corrosion sample is difficult to assess because of the lack of a control sample (e.g. from the exterior of the object, which unfortunately wasn't sampled) and the fact that urine residues are water soluble. Amongst these compounds is urea, which cannot be identified by QTOF-GC-MS with any degree of certainty because its main fragment ion is below the detection limit of the equipment.

Notwithstanding the above, the characterization of the sample indicates the presence of nitrogen-containing compounds (amine and amides), difficult to detect by FTIR and XPS because of the copper carbonate interference. Some of the compounds identified by QTOF-GC-MS are also found in urine, but others are notable for their uncertain source. Amongst these is methenamide, a bacterial metabolite but also a medicine for treating urinary infections under the trade name Hiprex[301] and other medical conditions.[302] The compound is produced by the reaction of ammonia and formaldehyde in a aqueous phase under reduced pressure at ca. 40 - 90 °C.[303] If Pompeii INV10653 contained urine, ammonia (from the hydrolysis of urea)[304] and formaldehyde (excreted in urine)[305] could have combined to form methenamide, making it a biomarker for urine.

An interdisciplinary study[306] of Pompeii's victims indicate that thermal impact (as opposed to asphyxia or impact force) was the cause of death of victims found indoors at a

[301] Concise Medical Dictionary 2010.
[302] Altinoz et al. 2019.
[303] ECB 2008.
[304] Zhou et al. 2015.
[305] Wang et al. 2012; Yi et al. 2018.
[306] Mastrolorenzo et al. 2010.

shelter at the edge of the town. It was demonstrated that these individuals would have to have experienced temperatures of at least 250^{o}C, well above the 90^{o}C maximum temperature required for the synthesis of methenamide. The findspot of Pompeii INV10653 within the taverna and the presence of charred wood in its vicinity would support the hypothesis that the object was also subjected to high temperatures. A request for the object's excavation report or any other relevant notes has been lodged with the Ashmolean Museum but so far nothing has been made available for consultation.

Human metabolites commonly excreted in urine were also identified in the sample by IC-MS. Although an alternative source to these compounds cannot be disregarded, the data presented here could support the hypothesis that Pompeii INV10653 could have been used as a chamber pot, subject to the information contained in the excavation report.

5.4 Case Study 4 – Pompeii INV10295

5.4.1 Background

Pompeii INV10295 is a *bacile* (Figure 91), a copper alloy bowl (originally with handles as the Roman Bowl in Case Study 2) usually found in rich households where it was offered to diners to wash their hands in before a meal. According to the archaeological records, this *bacile* was found outdoors in the garden of the taverna. As both handles are missing and given its poor state of preservation, curators/conservators think that the object had been repurposed at the time of deposition.



Figure 91– Pompeii INV10295

Conservator Miriam Orsini worked on five vessels from Pompeii. She said that compared to the other vessels,

> *"the corrosion inside the bacile immediately looked special. It was incredibly easy to remove, and I think this was what alarmed me and brought me to investigate the surface more closely. Scanning under the microscope, to me it looked obvious that the bacile had contained something at the time of deposition, which had become englobed in the corrosion, even before I spotted the larvae. The softness of some of the patches of corrosion was just unusual. And here and there I could see raised 'structures', which were visible to the naked eye."*

Ms Orsini uncovered four larvae-like specimens (shown in Figure 92), each about 1.5-2 mm long, and other insects including a beetle, preserved amongst the interior corrosion, each looking quite different from one another.

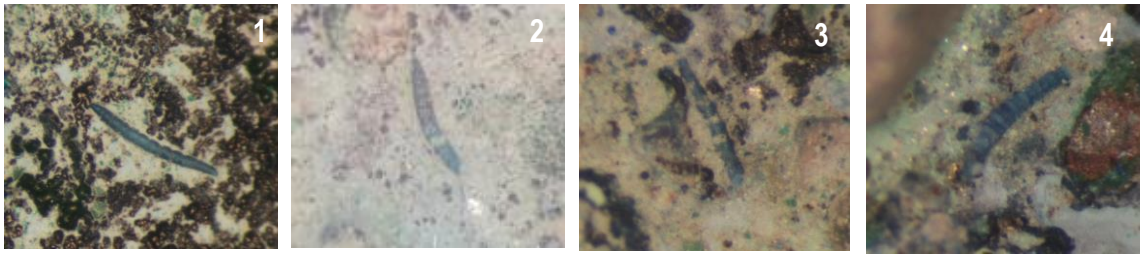


Figure 92– The different larvae found "mineralized" inside Pompeii INV10295

The mineralized remains were assessed by an entomologist who confirmed the presence of various insects at different stages of development. The remains which contained the best morphological preservation were identified as an *Anotylus* (a type of rove beetle which feeds on organic matter), *Sphaerocidae* (a type of fly), and *Chironomidae* (non-biting midges) that live in dirty water.

5.4.2 Research Question

Ms Orsini submitted 10 samples (ranging from 1-5mg each in gelatine capsules) from Pompeii INV10295 for analysis, their location marked in Figure 93 with descriptions included in Table 36. The aim of the analysis was to see whether the organic composition of the samples differed and whether they contained any food biomarkers. A larva with poor morphological preservation was removed from the objects and submitted for

analysis to test if despite mineralization, any proteins could be recovered to enable identification of the parent insect.

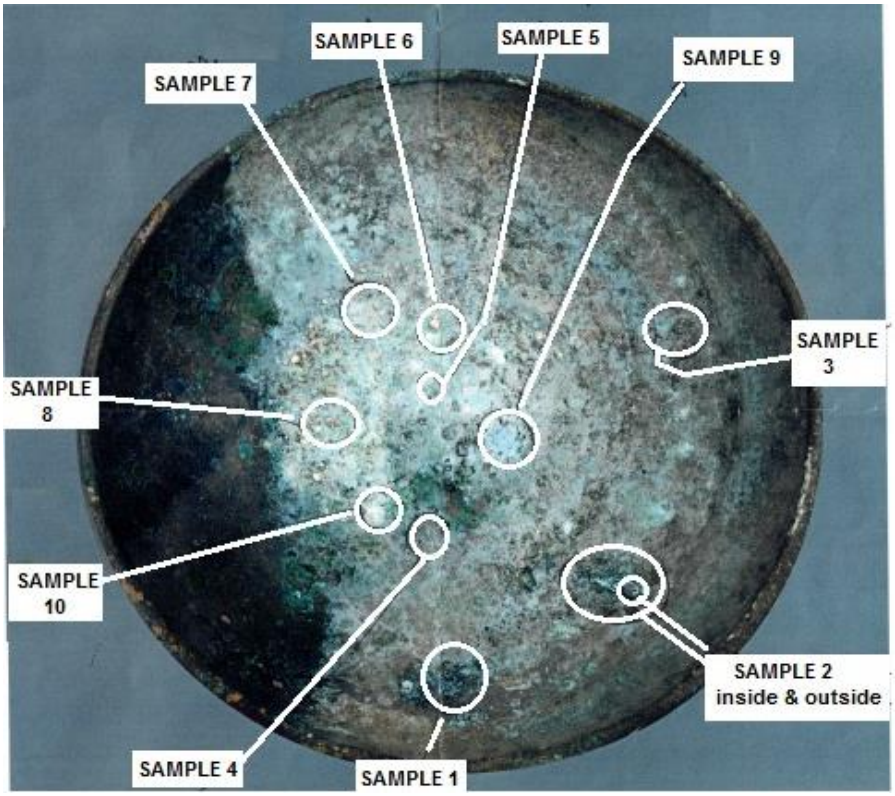


Figure 93 – Sampled areas in Pompeii INV10295

Sample	Description
1	Tiny agglomerated light blue spheres, like cous-cous
2	Raised lump of soft corrosion shaped like a small fish. Inside sample is white-ish, outside is black-ish.
3	Dark green/black soft “blob” corrosion, which looked like a residue.
4	Scraped from around a larvae. Under magnification it appears to have a white-ish under-layer (ash?), with loads of grains-like black corrosion on top and hard emerald-green corrosion.
5	Collected from around another larvae. White/light blue corrosion, soft as ash.
6 – 7	Soft, ash-like corrosion, ranging in colours from white to light blue.
8	Taken from around another larvae. The area contained a lot of powdery light green/blue copper corrosion crystals mixed with pumice.
9	A spot of bright light blue corrosion about 1 cm in diameter, extremely soft.
10	Ash-like light blue/green corrosion surrounding the rove beetle imprint.

Table 37 – Conservator’s description of the Pompeii INV10295 samples

Because of sample size limitations, it was not possible to characterize every sample with more than one technique.

5.4.3 Identification of Chemical Bonds

Because the KBr method is destructive, only samples 6 and 7 were analysed by FTIR. Their spectra are shown in Figure 94 with the peaks and band assignments listed in Table 38. The samples are practically identical. The most diagnostic bands are 3407 and 3318cm^{-1} for OH/NH species, 1499cm^{-1} for aromatics, 1397cm^{-1} for carbonates, 1098 and 1050cm^{-1} for silicates, a strong band for organic nitrates at 880cm^{-1} and various bands between 818-502 denoting C-Cl and/or substituted aromatics.

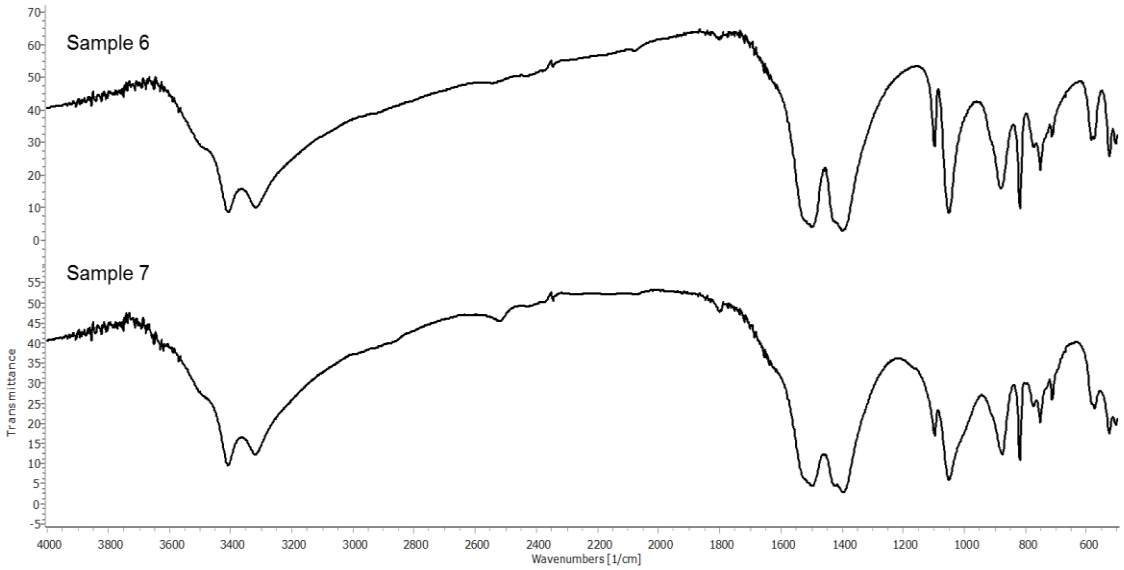


Figure 94 – FTIR spectra of samples 6 and 7 of Pompeii INV10295

KBr method

Sample 6		Sample 7		Attribution*
3407	m	3408	m	OH intramolecular bonded / N-H stretching vibrations
3318	m	3319	m	
1800	vw	1800	w	C=O carboxylic acids stretching vibrations
1499	s	1499	s	aromatic ring stretching vibrations
1397	s	1396	s	CH_2 / CO_3^{2-} deformations
1098	m	1098	m	silicates
1050	s	1050	s	
880	s	880	s	Organic nitrates
818	s	818	s	
751	m	752	m	
585	m	574	m	
526	m	526	m	C-Cl / substituted aromatic stretching vibrations
502	w	502	w	

Table 38– Infrared frequencies (cm^{-1}) and band assignments for samples 6 and 7 of Pompeii INV10295

5.4.4 Identification of Mineral Phases

Only samples 4, 6 and 10 where large enough to yield diffractograms (Figures 95, 96 and 97 respectively). The complete peak list is included in Appendix 25. Only copper carbonates were identified as mineral phases in the samples. Azurite and malachite were identified in samples 4 (70% and 30%) and 10 (30% and 70%) – the latter containing unassigned peaks of moderate intensity under 30^o 2θ. The only mineral phase identified in sample 6 was malachite.

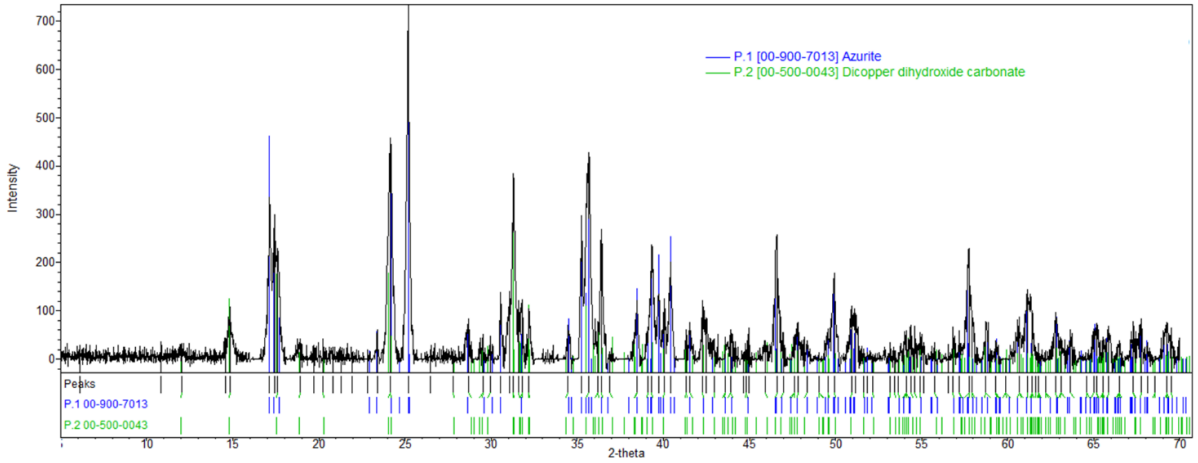


Figure 95 – Pompeii INV10295 (sample 4) diffractogram

showing azurite and malachite as identified mineral phases

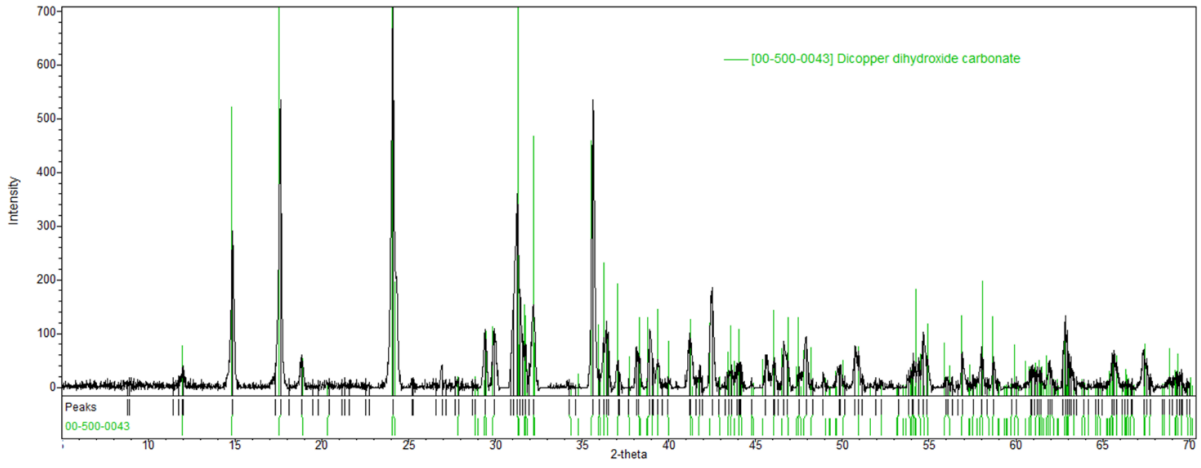


Figure 96 – Pompeii INV10295 (Sample 6) diffractogram

showing malachite as identified mineral phase

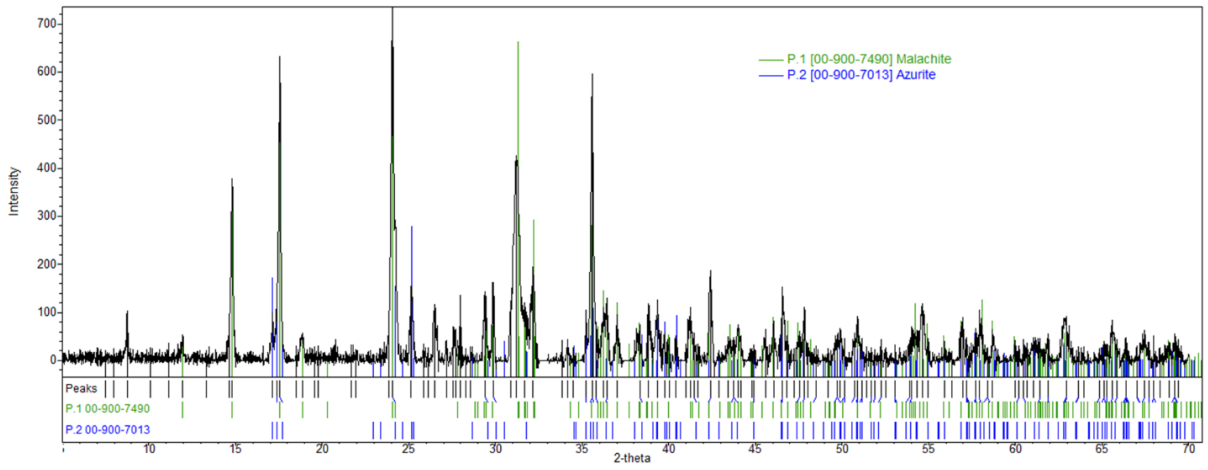


Figure 97– Pompeii INV10295 (Sample 10) diffractogram

showing malachite and azurite as identified mineral phases

5.4.5 Identification of Organic Compounds

5.4.5.1 QTOF-GC-MS with TSP

Only samples 4, 6, 9 and 10 were analysed by this technique. The identified compounds are listed in Table 39 with the spectrometric datasets included in Appendix 26.

Common to all samples are the carboxylic acids [4, 8, 9 and 11]. Sample 10 stands out for possessing the greatest variety of carboxylic acids (ranging 14 to 18 carbons), long chain alkyl nitriles [10 and 19], amides [13 and 17] and a palmitic acid glycidyl ester [14]. Glycidyl esters are thermal degradation products mainly of diacylglycerols, resulting in the liberation of a fatty acid.[307] These compounds are found in edible oils,[308] fats[309] and cooked meat[310] exposed to temperatures above 200°C. As the temperature of

[307] Destaillats et al. 2012.
[308] Cheng et al. 2017.
[309] Weißhaar and Perz 2010.
[310] Inagaki et al. 2016.

the thermal probe was set at 320ºC it is possible that the glycidyl palmitate is an analytical artefact alongside the fatty acids identified, both resulting from the degradation of the sample's diacylglycerols content. However, glycidyl esters were not produced during analysis of milk and copper-milk corrosion samples by the same method (reported in Chapter 4).

Cholesterol [27] and its derivatives [24, 25 and 28] – biomarkers for animal fats – were only found in sample 6. Usually, the presence of cholesterol is interpreted as modern contamination but given this, perhaps because it was not identified in the remaining samples, it may have a historical origin. The alkyl amides and nitriles can be interpreted as biomarkers.[311] These compounds are formed during biomass burning[312] and from thermal-assisted reactions of fatty esters[313] and acids[314] with ammonia from protein residues. Alkyl nitriles were present in all samples, thus indicating that the archaeological residue may have contained proteinaceous material.

[311] Buckley et al. 1999; Wang et al. 2017.
[312] Schauer et al. 1999.
[313] Mckee and Hatcher 2010.
[314] Simoneit et al. 2003.

#	RT (min)	Name	Formula	MW	SAMPLES 4	6	9	10
1	10.82	Tridecanoic acid	$C_{13}H_{26}O_2$	214				X
2	10.94	1-Heptadecene	$C_{17}H_{34}$	238		X		
3	11.12	Pentadecanal	$C_{15}H_{30}O$	226				X
4	11.35	Tetradecanoic acid	$C_{14}H_{28}O_2$	228	X	X	X	X
5	11.62	Isopropyl myristate	$C_{17}H_{34}O_2$	270		X		
6	11.87	Pentadecanoic acid	$C_{15}H_{30}O_2$	242		X	X	X
7	12.11	Hexadecanenitrile	$C_{16}H_{31}N$	237		X	X	
8	12.39	n-Hexadecanoic acid	$C_{16}H_{32}O_2$	256	X	X	X	X
9	12.84	Heptadecanoic acid	$C_{17}H_{34}O_2$	270				X
10	13.07	Octadecanenitrile	$C_{18}H_{35}N$	265		X	X	X
11	13.21	9-Octadecenoic acid	$C_{18}H_{34}O_2$	282	X	X		X
12	13.30	Octadecanoic acid	$C_{18}H_{36}O_2$	284	X	X	X	X
13	13.46	Hexadecanamide	$C_{16}H_{33}NO$	255				X
14	13.88	Glycidyl palmitate	$C_{19}H_{36}O_3$	312				X
15	14.15	Eicosanoic acid	$C_{20}H_{40}O_2$	312				X
16	14.21	Mono-2-ethylhexyl adipate	$C_{14}H_{26}O_4$	258	X	X		X
17	14.32	Octodecanamide	$C_{18}H_{37}NO$	283				X
18	14.59	Pentacosane	$C_{25}H_{52}$	352		X		
19	14.68	(Z)-Docos-9-enenitrile	$C_{22}H_{41}N$	319	X			X
20	14.83	Phthalic acid, di(2-propylpentyl) ester	$C_{24}H_{38}O_4$	390	X			X
21	14.98	Hexacosane	$C_{26}H_{54}$	366		X		
22	15.34	Heptacosane	$C_{27}H_{56}$	380	X	X		
23	15.88	Squalene	$C_{30}H_{50}$	410	X	X		X
24	16.53	Cholesta-4,6-dien-3-ol, (3β)-	$C_{27}H_{44}O$	384		X		
25	16.64	Cholesta-3,5-diene	$C_{27}H_{44}$	368		X		
26	17.55	Octadecenoic acid, dodecyl ester	$C_{30}H_{60}O_2$	452		X		
27	17.95	Cholesterol	$C_{27}H_{46}O$	386		X		
28	19.23	Cholesta-4, 6-dien-3-one	$C_{27}H_{42}O$	382		X		

Table 39– Compounds identified in Pompeii INV10295 by QTOF-GC-MS with TSP biomarkers highlighted

5.4.5.2 IC-MS

Only samples 1, 2 (outer and inner), 4, 5, 6 and 10 were analysed by this technique, resulting in 26 compound identifications, grouped according to their overall abundancy (Figure 98), singularity (Figure 99) and prevalence (Figure 100) across the samples. The compound measurements are included in Appendix 27. Nonate (a derivative of succinic

acid, a microbial metabolite)[315] is the most abundant compound in all samples but Sample 10. In Sample 10 the most abundant compound is dihydroxyacetone, a simple sugar found in many vegetables,[316] also present in Sample 2 (inner) but with a much higher ion count than all other samples. Sample 2 contains the highest amount of lactose, followed by Sample 10.

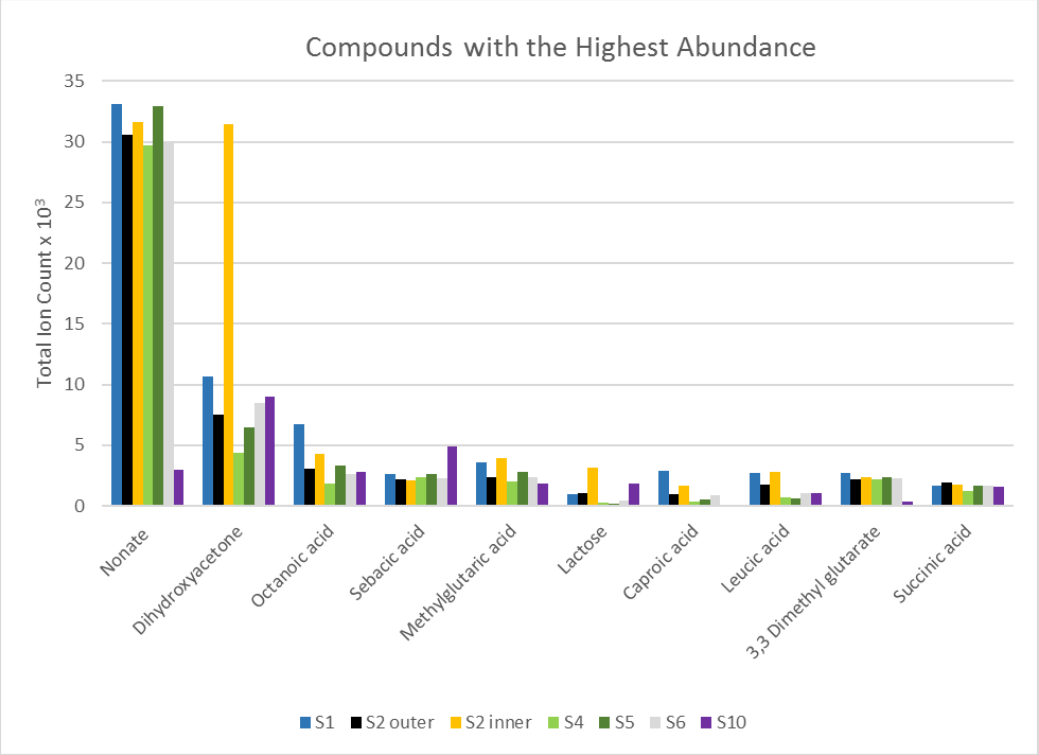


Figure 98 – Most abundant compounds and their distribution across the samples

[315] https://hmdb.ca/metabolites/HMDB0000254.
[316] https://hmdb.ca/metabolites/HMDB0001882.

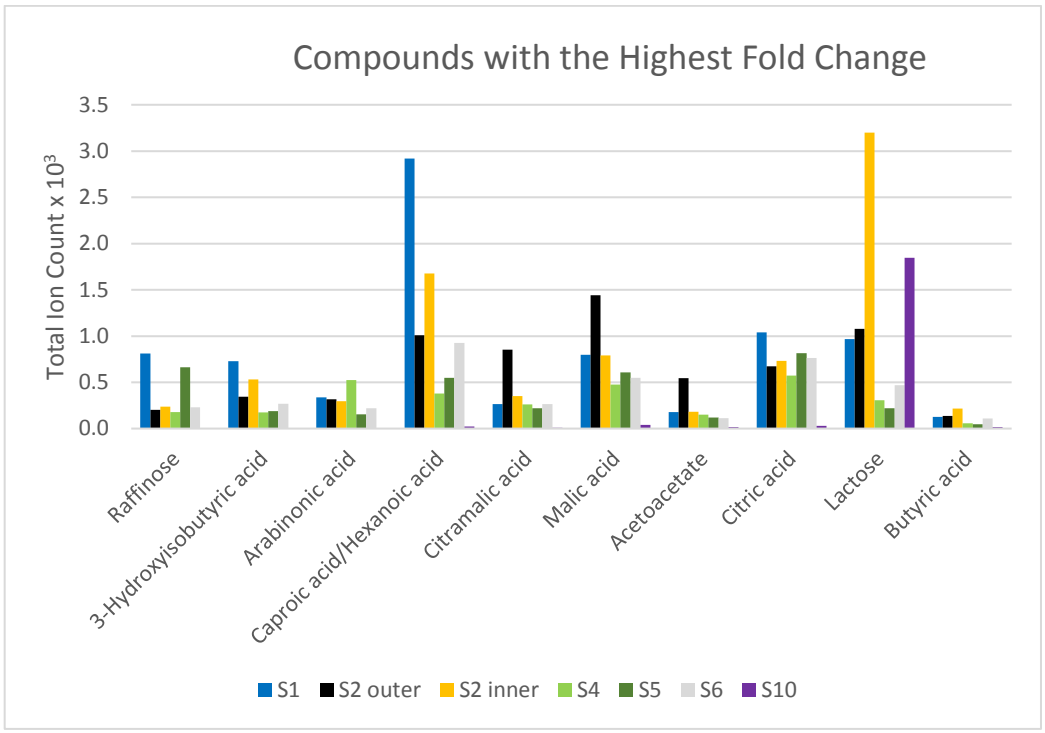


Figure 99 – Compounds with the highest fold change and their distribution

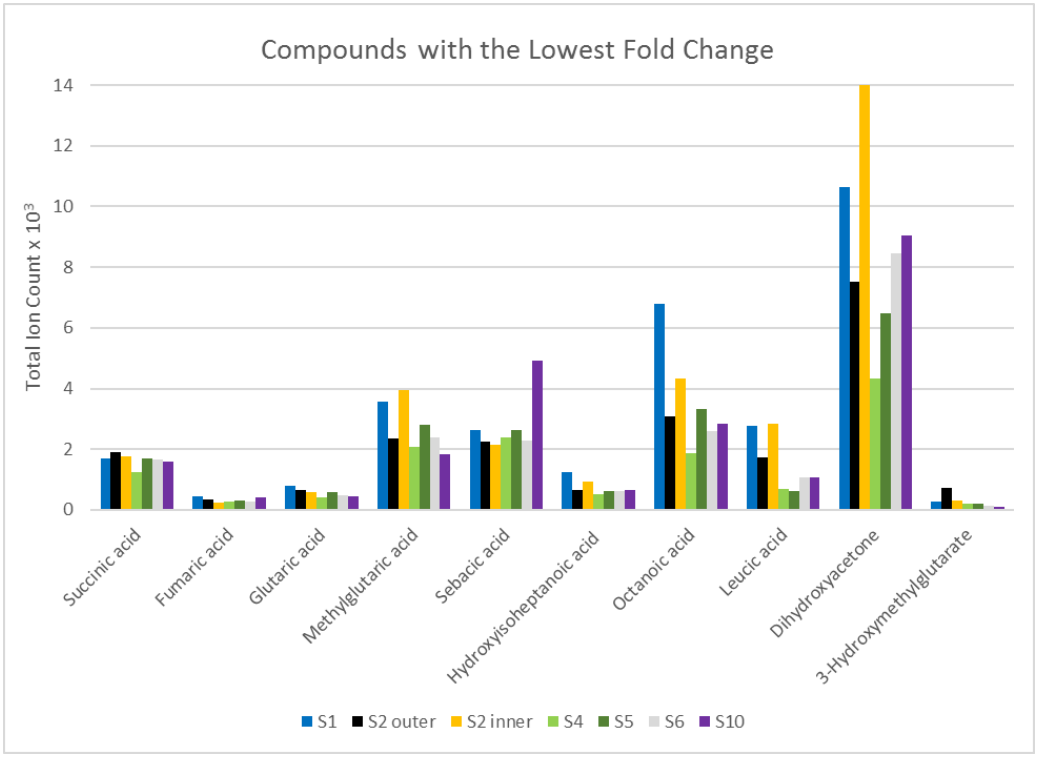


Figure 100 – Most common compounds and their distribution across the samples

The identification of raffinose (a trisaccharide widely distributed in plants) may be significant given its highest abundancy in samples 1 and 5.

5.4.5.3 Proteomics

Only the larvae and samples 4 and 8 were analysed. The diagnostic proteins with the highest intensity are listed in Table 40.

The proteins identified in the larva were all from *Ignatzschineria ureiclastica* and *Ignatzschineria indica*, common bacterium isolates from the larvae of *Wohlfahrtia magnifica* (a fly that feeds on carrion)[317] and other types of flies.[318]

Samples 4 and 8 were practically identical: both contained proteins from various fish species, including *Larimichthys crocea* (large yellow croaker), *Pagrus major* (seabream), *Oreochromis mossambicus* (tilapia), *Thunnus orientalis* (bluefin tuna) and *Epinephelus coioides* (orange-spotted grouper), and from human saliva.

[317] Gupta et al. 2011.
[318] Barker et al. 2014.

	Accession Number	-10lgP	Coverage (%)	Intensity	#Peptides (unique)	Avg. Mass	Protein Name
LARVA	A0A2U2AC97	102.18	26	2.39E+06	45(44)	230491	Uncharacterized protein (Fragment) *Ignatzschineria ureiclastica*
	A0A2U2ACH6	47.28	2	7.80E+04	4(4)	337379	Uncharacterized protein (Fragment) *Ignatzschineria ureiclastica*
	A0A2U2AG96	42.83	9	1.60E+06	1(1)	22155	Uncharacterized protein *Ignatzschineria ureiclastica*
	A0A2U2AID7	42.29	4	2.63E+04	5(4)	220107	Uncharacterized protein *Ignatzschineria indica*
SAMPLES 4 AND 8	W8G4Y5	121.56	40	2.27E+06	12(5)	13110	Trypsin (Fragment) *Larimichthys crocea*
	G5EMQ8	115.8	16	7.06E+04	10(1)	26151	Trypsinogen *Pagrus major*
	Q5J327	115.72	26	1.46E+05	10(7)	12240	Trypsinogen (Fragment) *Oreochromis mossambicus*
	A0A4P2UYG7	112.8	19	8.81E+04	7(1)	22664	Trypsinogen 1e (Fragment) *Acipenser persicus*
	G5EMQ3	112.57	27	2.61E+06	8(2)	26223	Trypsinogen 1 *Thunnus orientalis*
	V5W7H8	110.69	25	4.22E+05	8(1)	13151	Trypsin (Fragment) *Larimichthys crocea*
	Q7ZZU3	108.07	26	1.13E+07	6(6)	16502	Keratin 8 (Fragment) *Oreochromis mossambicus*
	F2WR16	106.79	20	3.18E+05	7(1)	26551	Trypsinogen 1a *Epinephelus coioides*
	A0A4P2V9R6	104.14	16	7.74E+03	7(1)	26319	Trypsinogen 1d *Acipenser persicus*
	O93594	103.02	30	2.15E+05	7(1)	19352	Trypsin (Fragment) *Dicentrarchus labrax*
	A7MBP7	98.92	11	1.53E+07	11 (10)	61021	Wu:fb15e04 protein (Fragment) *Danio rerio*
	Q04118	207.47	69	1.05E+06	29 (25)	30980	Basic salivary proline-rich protein 3 *Homo sapiens*
	Q02413	200.94	36	1.42E+07	42 (40)	113748	Desmoglein-1 *Homo sapiens*
	P02788	198.39	28	1.20E+06	20 (20)	78182	Lactotransferrin *Homo sapiens*
	P12273	176.97	50	3.31E+05	9 (9)	16572	Prolactin-inducible protein *Homo sapiens*

Flesh fly Fish human saliva

Table 40 – Selected proteins identified in the mineralized larva and in samples 4 and 8

5.4.6 Discussion

The results of the characterization of the samples are summarized in Table 41.

The colour differences between sample 2 (inner) and sample 2 (outer) appear to be reflected by their IC-MS characterization, with the identified compounds having an inversed relationship between them.

Sample 4 (extracted from around a larva) contained copper carbonates as mineral phases and an organic composition dominated by long chain carboxylic acids, perhaps explaining its “soft and hard” consistency.

Sample 6 was the only sample characterized by all techniques. Its FTIR spectra indicated the presence of carbonates (corroborated by the identification of malachite) and organic acids and aromatic compounds. Organic compounds containing these chemical functions were identified by TSP-QTOF-GC-MS, including biomarkers for animal fat.

The same mineral phases identified in sample 4 were also identified in sample 10, albeit the remaining unassigned peaks, indicating the presence of at least one additional crystalline phase. Sample 10 contained the most extensive range of long-chain carboxylic acids and the only sample where amides were identified. Given the presence of lactose (identified by IC-MS) and its fatty acid distribution (C13-15 and C17) the sample may have contained a dairy fat.

Sample	Colour	Consistency	FTIR	XRD	TSP-GC-MS	IC-MS	Proteomics
1	Light blue	soft	-	-	-	Raffinose, caproic acid	-
2 - inner	Whitish	Soft	-	-	-	Lactose, caproic acid	-
2 - outer	Blackish	Soft	-	-	-	Citramalic and malic acids	-
3	Dark green/black	n/a	-	-	-	-	-
4*	Whitish with black spots and emerald green crystals	Soft with hard crystals	-	Azurite Malachite	Fatty Acids: C16, 18, 18:1 Nitriles: C22	Arabinonic acid	Fish and Human saliva
5*	Light blue	Soft	-	-		Raffinose	
6	White/light blue	Soft	N-H, C=O (acids), carbonates, C-Cl, aromatics	Malachite	Fatty acids: C14-16, 18:1 and 18 Nitriles: C16 and 18 Sterols: cholesterol and derivatives		
7	White/light blue	Soft	N-H, C=O (acids), carbonates, C-Cl, aromatics		-	-	-
8*	Light green/blue	Powdery crystals	-	-	-		Fish and Human saliva
9	Light blue	Soft	-	-	FA: C14-16 and 18 Nitriles: C16 and 18	-	-
10**	Light blue/green	n/a	-	Azurite Malachite	FA: C13-18 and 18:1 Nitriles: C18 and 22 Amides: C16 and 18	Lactose	-

[*]from around larvae [**] from around beetle

Table 41– Summary of the multi-analytical characterization of INV10265 corrosion

The proteomics analysis of the mineralized larva alongside samples 4 and 8 provides further clues to the original organic residue in the object. Proteins linked to a carrion flesh-eating fly were only identified in the mineralized larva, as expected. However, the proteins found in samples 4 and 8 (from areas surrounding other larvae) matched those of fish and human saliva. The difference in protein profile between these samples supports the idea that the object could have contained scraps of fish. This hypothesis could potentially be supported by the presence of cholesterol (and its derivatives), main sterol in raw and cooked fish.[319] But, it is important to note that cholesterol is normally considered a contaminant and none of the compounds typically associated with the cooking of aquatic resources in ceramic pots[320] has been detected in the sample.

With regards to the human saliva, a further marker for its presence in sample 4 is the relatively large quantities of arabinonic acid (a sugar acid excreted in human saliva),[321] also identified in the remaining samples. Human saliva is likely to be modern contamination during conservation, as the micro-excavation of the mineralized insects remains would have required the conservator to work close to the surface of the object.

The results of the characterization of INV10265 samples support the hypothesis that this object contained diverse food residues in various states of degradation at the time of the eruption.

[319] Ozyurt et al. 2013; Ozogul et al. 2015.
[320] Hansel et al. 2004; Craig et al. 2007; Evershed et al. 2008b; Hansel and Evershed 2009; Craig et al. 2013
[321] https://hmdb.ca/metabolites/HMDB0000539.

5.5 Case Study 5 – Pompeii INV10289

5.5.1 Background

Pompeii INV10289 is *caccabus*, a wide-mouthed copper alloy bowl used for cooking casseroles and stews. Six samples were submitted to analysis in Eppendorf tubes from the interior and exterior of the object, their location on the object is shown in Figure 101 with brief descriptions as provided by the conservator listed in Table 42.



Figure 101 – Pompeii INV10289 sampled areas

Sample	Description
1	Interior dust
2	Hard black corrosion from interior base
3	Soft green corrosion from interior base
4	Powdery green corrosion from interior amidst lapilli
5	Dark brown residue from exterior body
6	Dark brown residue from exterior below rim

Table 42 – Conservator's description of the samples

5.5.2 Research Question

The availability of samples from the interior and the exterior of the object presented an opportunity to focus on the differences between these two areas. The aim of the analysis was to see whether any organic residues linked to food processing could be identified in the corrosion products.

5.5.3 Identification of Chemical Functions

The spectrum for the interior dust is shown in Figure 102. No bands could be assigned because the peaks are too broad.



Figure 102 – FTIR spectrum of sample 1

KBr method

The spectra for the remaining samples from the interior of the vessel are included in Figure 103 (sample 2) and Figure 104 (samples 3 and 4) with band assignments included in Table 43. The spectra of these samples are very similar: all dominated by aromatic

ring stretching vibration around 1500cm^{-1} and aliphatic C-H deformation around 1400cm^{-1}.

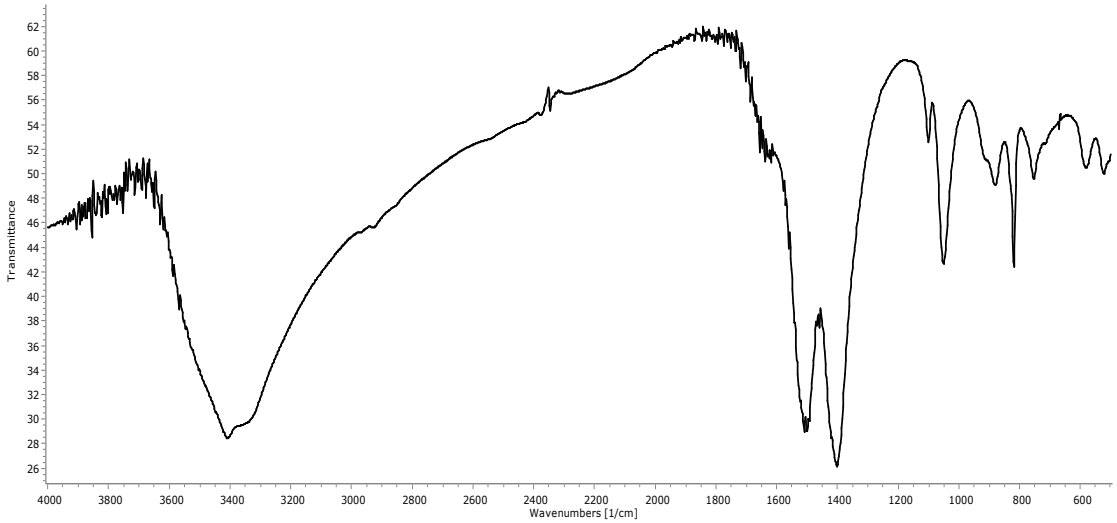


Figure 103 – FTIR spectrum of sample 2

KBr method

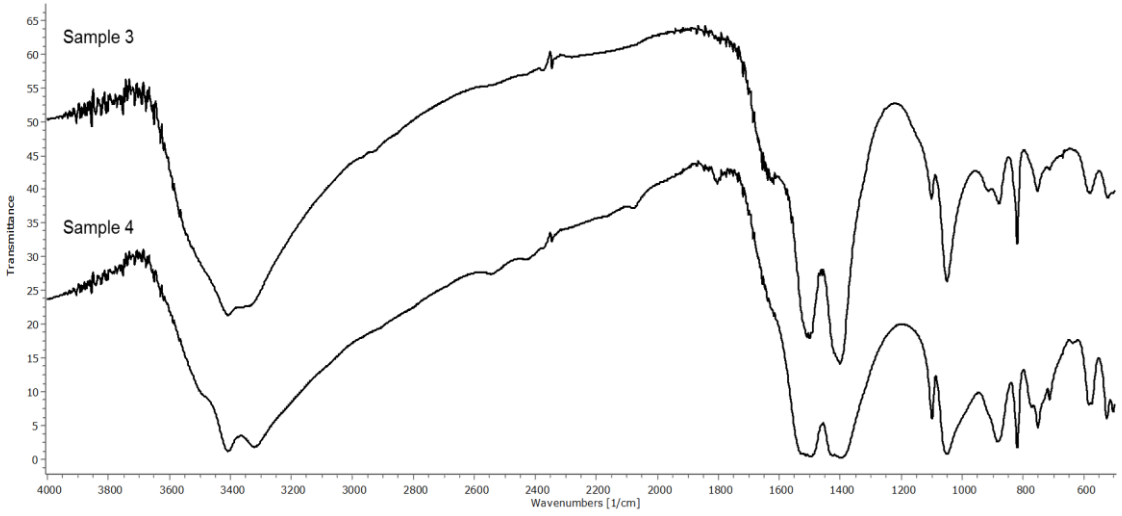


Figure 104 –FTIR spectra of samples 3 and 4

KBr method

Sample 2		Sample 3		Sample 4		Attribution
3408	w	3408	w	3408	w	
				3321	w	OH intramolecular bonded / N-H stretching vibrations
2927	vw					C-H aliphatic stretching vibrations
				1803	w	C=O carboxylic acids stretching vibrations
1509	vs	1500	vs	1500	br	aromatic ring stretching vibrations
1401	vs	1400	vs	1399	vs	CH_2 / CO_3^{2-} deformation
1100	m	1100	m	1100	m	silicates
1050	s	1050	s	1050	s	
		915	sh			
880	m	878	m	882	m	Organic nitrates
818	s	819	s	818	s	
753	m	753	m	751	m	C-Cl / substituted aromatic stretching vibrations
		581	m	544	m	

Table 43 – Infrared frequencies (cm^{-1}) and band assignments for samples 2-4

The spectra for the exterior samples (5 and 6) are included in Figure 105. The peaks obtained are too broad so they could not be assigned to a specific band.

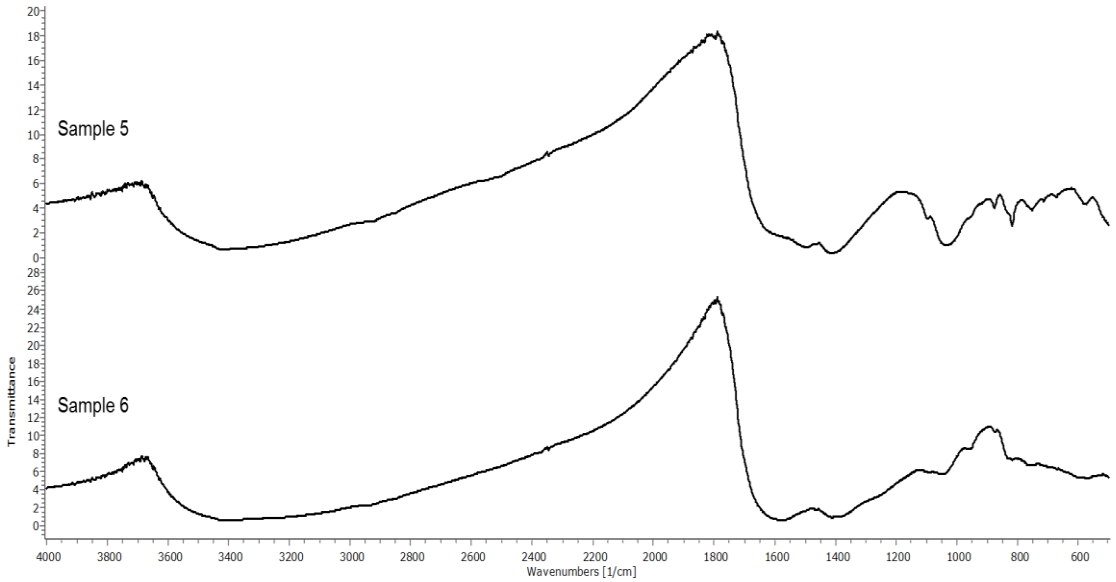


Figure 105 – FTIR spectra of samples 5 and 6

KBr method

5.5.4 Identification of Mineral Phases

The diffractograms with phase identifications for the interior samples (samples 3 and 4) are shown in Figure 106, and those for the exterior samples (samples 5 and 6) are included in Figure 107. The peak lists are included in Appendix 28. The mineral phases identified in the samples were all copper carbonates. Azurite and malachite were identified in samples 3 and 5. Malachite was the only mineral phase identified in sample 4, whilst azurite was identified in sample 6.

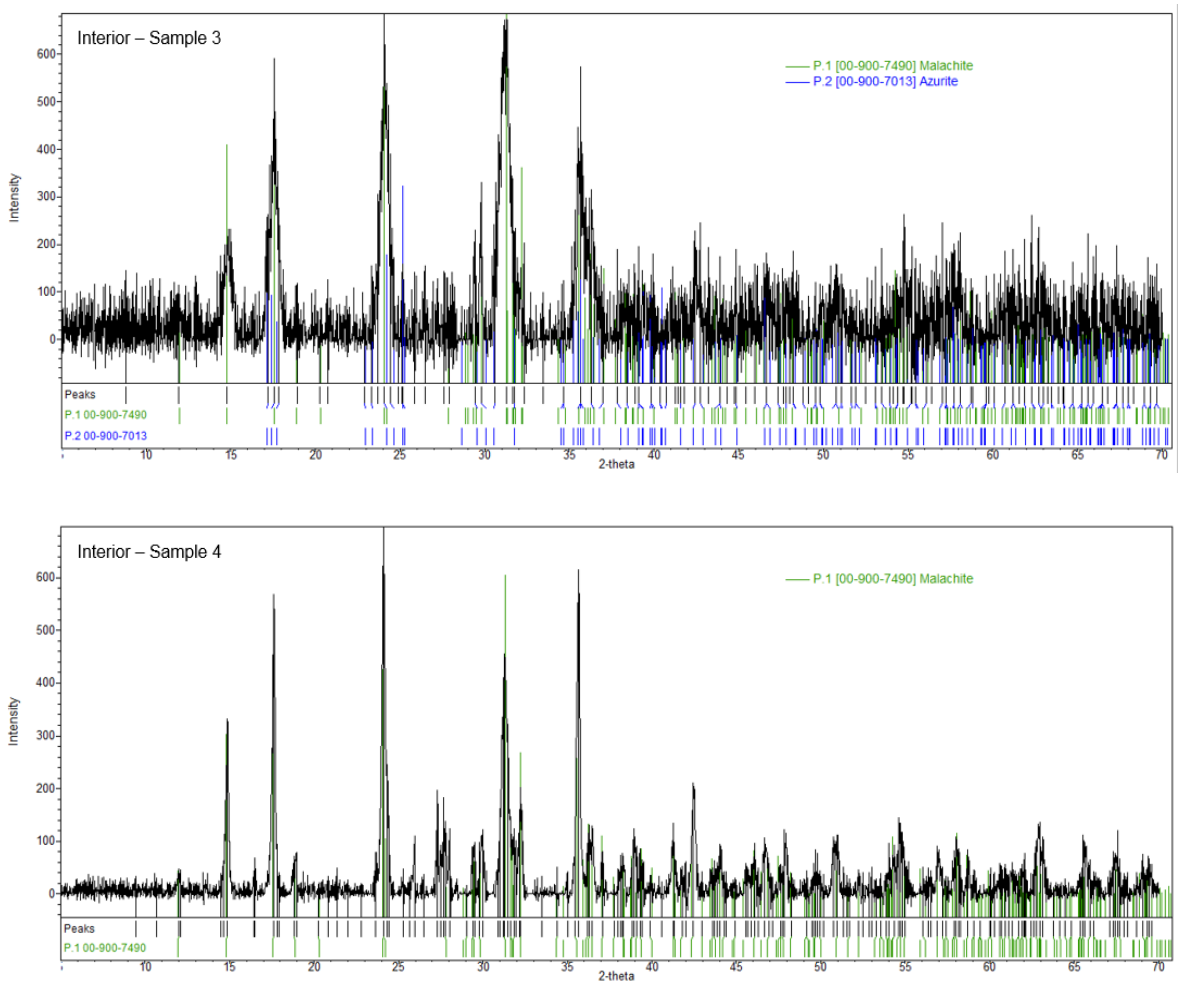


Figure 106 - Diffractograms of the interior samples

showing as identified phases malachite and azurite in sample 3 and malachite in sample 4

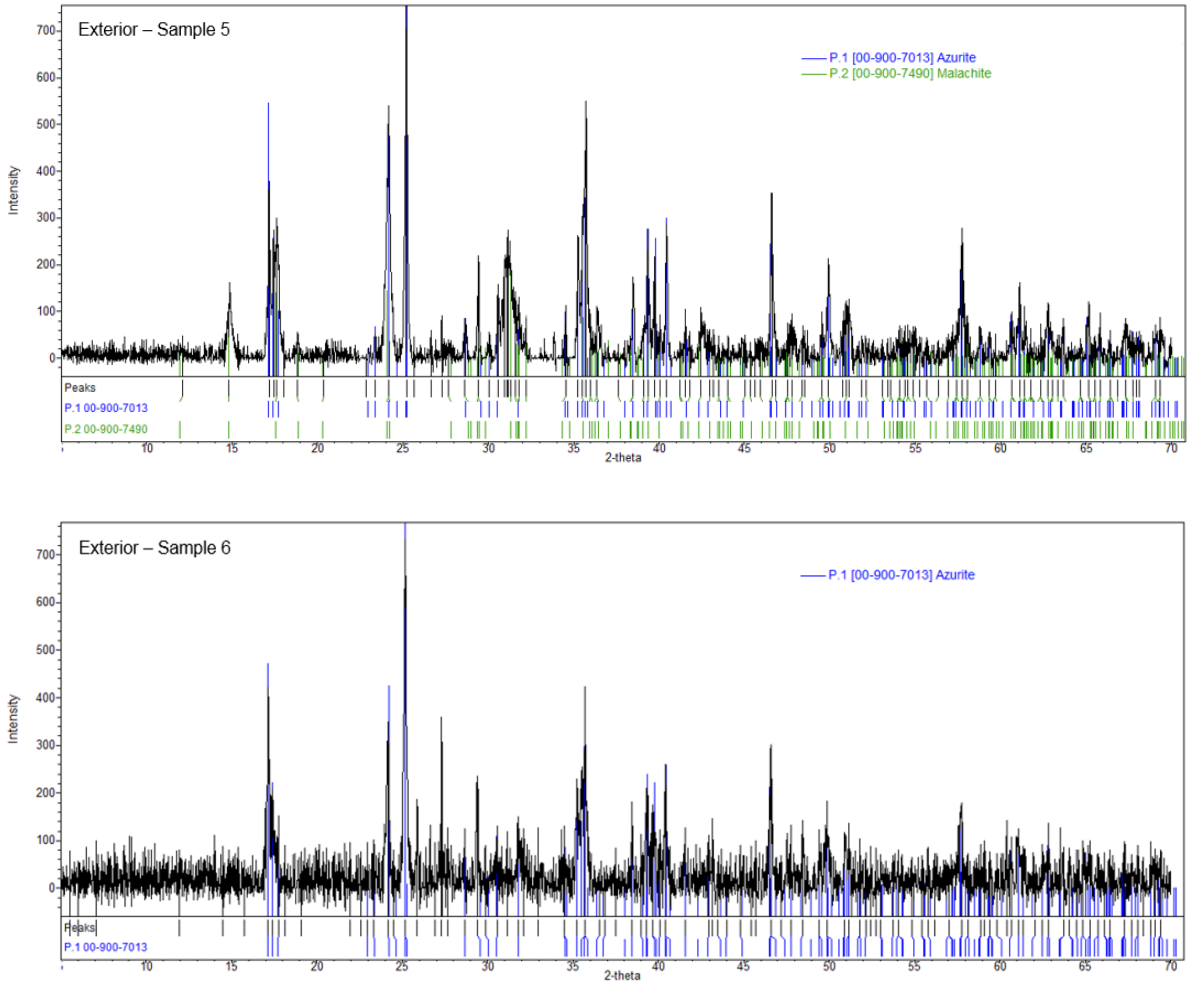


Figure 107 – Diffractogram of the exterior samples

showing azurite and malachite identified in sample 5 and azurite in sample 6

Sample 2 was not large enough to yield a powder diffractogram.

5.5.5 Identification of Organic Compounds

5.5.5.1. QTOF-GC-MS with TSP

The compounds identified in the samples by this technique are listed in Table 44 with spectrographic datasets included in Appendix 29.

The long-chain fatty acids [13, 14, 18, 20 and 21] are common to most samples. Sample 4 from the interior of the vessel and sample 5 from its exterior stand out from the remaining samples. A short chain fatty acid [1], a series of medium-chain carboxylic acids from C7 to C10 [2-5] and a long-chain methyl ester [16] were only identified in sample 4. Short and medium-chain fatty acids are biomarkers for certain plant oils[322] and fresh dairy fats,[323] but can also be formed by thermo-oxidation of unsaturated carboxylic acids in oils used for frying.[324] Medium-chain carboxylic acids are rarely detected in archaeological residues although C14 has been detected in residues characterized as dairy fat based on carbon isotope levels of its C16 and C18 content.[325] Sample 5 is dominated by C14-17 and C20 alkanes [6, 8, 9, 10 and 11] and three alkyl nitriles [15, 19 and 22], the latter also identified in sample 6.

The identification of a polycyclic aromatic compound [15] in samples 2-3 and 6 is perhaps significant because the compound one of the pyrolytic products of ergosterol[326] when heated at temperatures above 650ºC. [327] Such high temperatures could not have been produced by the QTOF-GC-MS with TSP method nor the pyroclastic density currents resulting from the eruption of Vesuvius,[328] but could result from cooking on fires.[329] Ergosterol is a sterol mostly associated with fungi[330] and yeast,[331] and used as

[322] Kałużna-Czaplińska et al. 2016.
[323] Evershed et al. 2002; Fontecha et al. 2005.
[324] Márquez-Ruiz and Dobarganes 1996; Brühl 2014.
[325] Dunne et al. 2013; 2019.
[326] Cai et al. 2008.
[327] Parsi and Gorecki 2006.
[328] Cioni et al. 2004; Gurioli et al. 2005.
[329] Braadbaart and Poole 2008; Bentsen 2012; Braadbaart et al. 2012.
[330] Weete 1973.
[331] E.g. Parks and Casey 1995; Alvarez-Vasquez et al. 2011; Henderson et al. 2011.

indicator for microbial biomass in soils,[332] mould growth in foodstuffs[333] and in an archaeological context as a potential biomarker for beer.[334]

#	RT (min)	Name	Formula	MW	Interior 2	3	4	exterior 5	6
1	6.2	Hexanoic acid	$C_6H_{12}O_2$	116			X		
2	6.9	Heptanoic acid	$C_7H_{14}O_2$	130			X		
3	7.7	Octanoic acid	$C_8H_{16}O_2$	144			X		
4	8.4	Nonanoic acid	$C_9H_{18}O_2$	158			X		
5	9.0	n-Decanoic acid	$C_{10}H_{20}O_2$	172			X		
6	9.2	Tetradecane	$C_{14}H_{30}$	198				X	
7	9.8	Cyclopentadecane	$C_{15}H_{30}$	210		X			
8	9.8	Pentadecane	$C_{15}H_{32}$	212				X	X
9	10.4	Hexadecane	$C_{16}H_{34}$	226				X	
10	10.6	Heptadecane	$C_{17}H_{36}$	240				X	
11	10.9	Eicosane	$C_{20}H_{42}$	282				X	
12	11.2	Pentadecanal	$C_{15}H_{30}O$	226	X	X			
13	11.4	Tetradecanoic acid	$C_{14}H_{28}O_2$	228	X	X		X	X
14	11.9	Pentadecanoic acid	$C_{15}H_{30}O_2$	242	X	X			X
15	12.1	Hexadecanenitrile	$C_{16}H_{31}N$	237				X	
16	12.2	Hexadecanoic acid methyl ester	$C_{17}H_{34}O_2$	270			X		
17	12.2	1H-Indene, 1-(phenylmethylene)-	$C_{16}H_{12}$	204	X	X			X
18	12.4	n-Hexadecanoic acid	$C_{16}H_{32}O_2$	256	X	X	X	X	X
19	13.1	Octadecanenitrile	$C_{18}H_{35}N$	265				X	
20	13.2	9-Octadecenoic acid	$C_{18}H_{34}O_2$	282	X	X			X
21	13.3	Octadecanoic acid	$C_{18}H_{36}O_2$	284	X	X		X	X
22	14.7	(Z)-Docos-9-enenitrile	$C_{22}H_{41}N$	319				X	X

where [X] = present

Table 44– Compounds identified in Pompeii INV10289 samples by QTOF-GC-MS with TSP

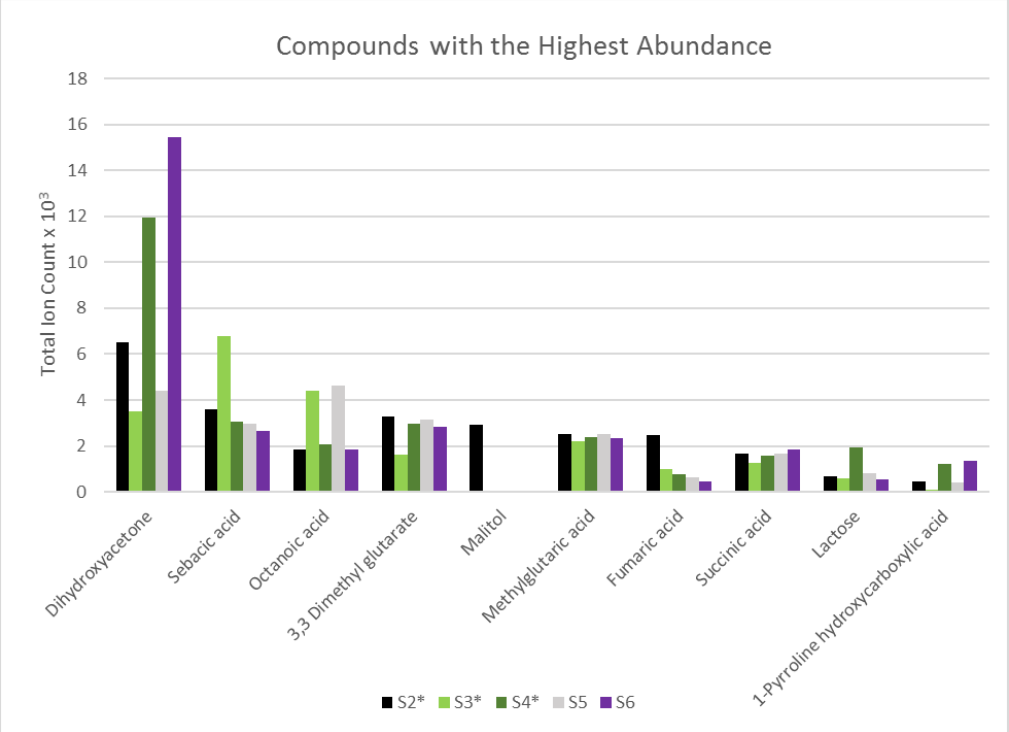
[332] E.g. Grant and West 1986; Stahl and Parkin 1996.
[333] E.g. Marín et al. 2008; Boarelli et al. 2020.
[334] Isaksson et al. 2010.

5.5.5.2. IC-MS

Some 23 compounds were identified in the Pompeii INV10286 samples, their measurements are included in Appendix 30. The compounds have been grouped according to their overall abundance (Figure 108), uniqueness (Figure 109) and prevalence (Figure 110) across the samples.

Dihydroxyacetate (a simple sugar found in sugar cane and sugar beets and as a fermentation product of glycerine)[335] is the compound with the highest abundancy in samples 6, 4 and 2. Dicarboxylic acids were identified in varying abundances across all samples. Succinic acid's abundancy was higher in the exterior than the interior samples, whilst sebacic and fumaric acids were more abundant in the interior samples. Malic acid was also found across all samples. It is a sour-tasting dicarboxylic acid found in fruits and wine, and is also a metabolite of yeasts[336] (including *Saccharomyces cerevisiae*)[337]and fungi when grown on fermentable substrates.[338]

[335] https://hmdb.ca/metabolites/HMDB0001882.
[336] Kapsopoulou et al. 2005; Taing and Taing 2007.
[337] Wang et al. 1998; Nakayama et al. 2012; Yéramian et al. 2007.
[338] Peleg et al. 1988; Battat et al. 1991; Goldberg et. al. 2006.



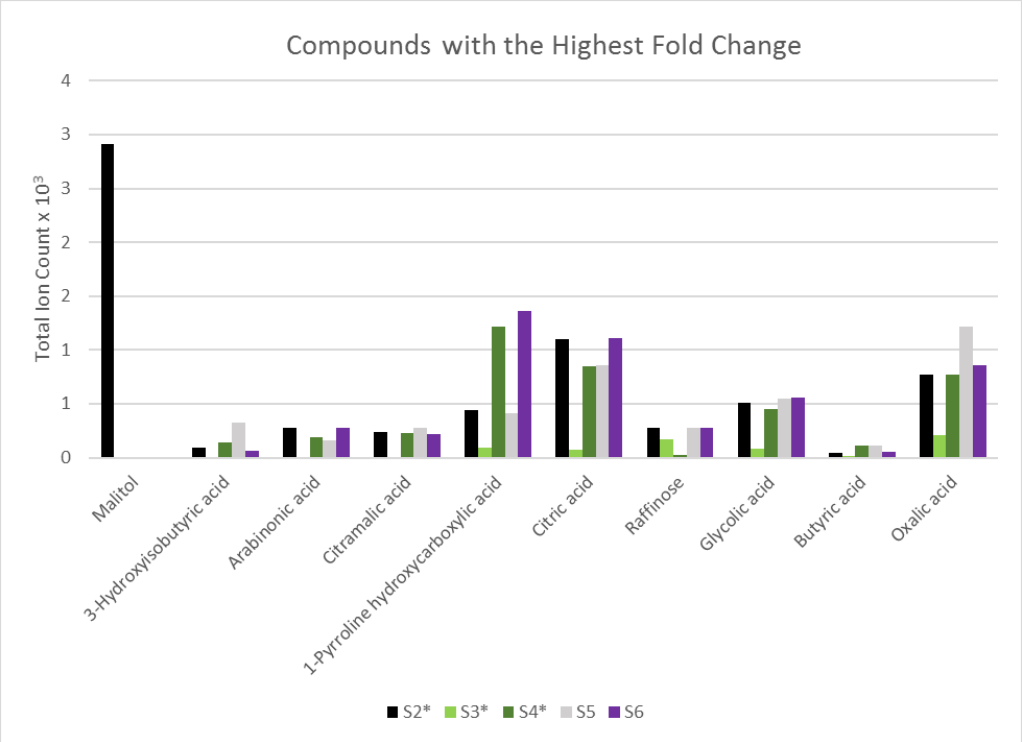
[*] interior of the vessel

Figure 108 – Most abundant compounds and their distribution across the samples

Sample 2 stands out for being the only sample where maltitol, a polyol, was identified. Polyols are a subgroup of sugar alcohols formed via dehydrogenation of carbohydrates. Maltitol is a disaccharide polyol made up of sorbitol and glucose. It is used in processed foods and beverages as an alternative sweeter to sucrose.[339] Most commercially available polyols (e.g. xylitol) are produced using bacteria,[340] but maltitol is produced via dehydrogenation of maltose.[341] Maltose occurs naturally in some plants as a starch hydrolytic degradation product[342] of α and β-amylases during malting and fermentation

[339] Lenhart and Chey 2017.
[340] For a review see Paulino et al. 2021.
[341] Kearsley and Boghani 2012; Bender 2014.
[342] Yannai 2013.

of wort.[343] Sample 2 also contains higher amounts of fumaric acid (an isomer of maleic acid) and glucose than the other samples.



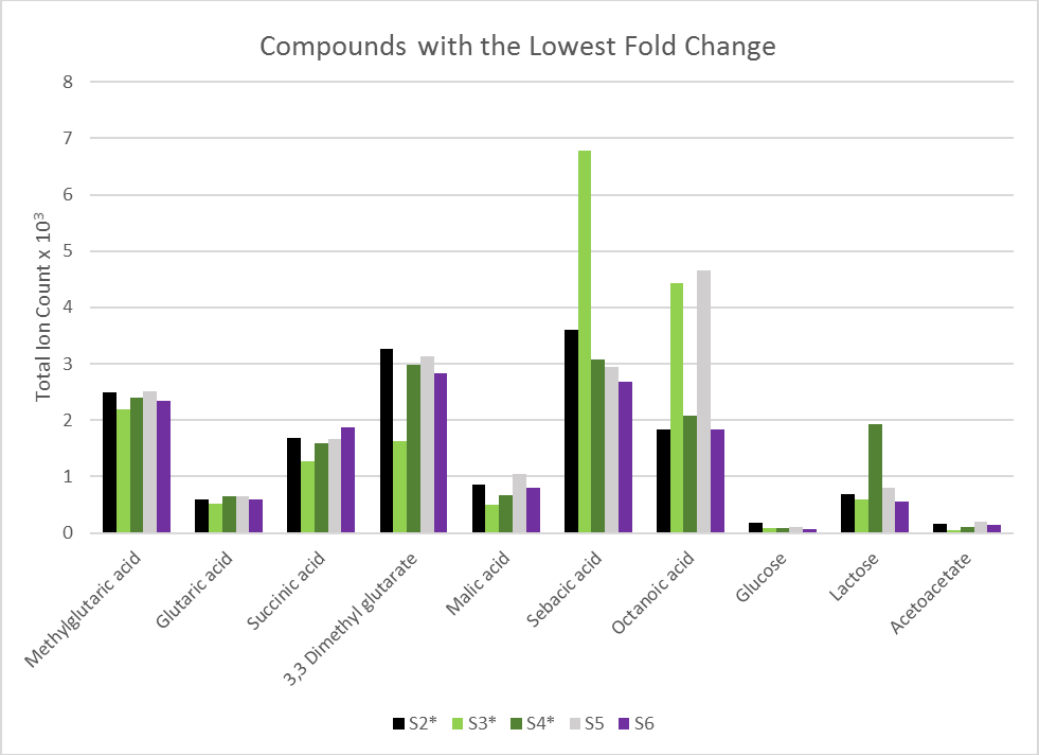
[*] interior of the vessel

Figure 109 – Compounds with unusual distribution across the samples

Sample 3 is characterized by a high abundance of sebacic acid (and has twice the amount of octanoic acid out of the remaining interior samples) and by having no citramalic acid, which is present in similar abundancy across all remaining samples. Citramalic acid is a metabolite of *Saccharomyces* yeast species and *Propionibacterium acnes*.[344] Various herbs[345] have antibacterial properties against *Propionibacterium acnes*, including hops extract,[346]an ingredient of modern beer. Sample 4 contains twice the amount of lactose as the remaining samples and has the highest abundance of 1-Pyrroline hydroxycarboxylic

[343]von Rymon Lipinski 2006.
[344] https://hmdb.ca/metabolites/HMDB0000426.
[345] Tsai et al. 2010.
[346] Weber et al. 2019.

acid (an amino acid derivative present in all living organisms and a metabolite of *Saccharomyces cerevisiae*)[347] out of all interior samples. Moreover, this sample has practically no raffinose (a trisaccharide composed of galactose, fructose and glucose) that occurs in a variety of plants.[348]



[*] interior of the vessel

Figure 110 – Most common compounds and their distribution across the samples

Regarding the exterior of the vessel, sample 5 is characterized by higher abundancy of 3-Hydroxyisobutyric acid (which can be produced by *Cupriavidus necator* fed with fructose[349] and *Pseudomonas* feeding on glucose).[350] Sample 5 is also characterized by a higher abundancy of oxalic acid, a dicarboxylic acid found in many plants and

[347] http://www.ymdb.ca/compounds/YMDB00718.
[348] Yannai 2013.
[349] Hoefel et al. 2010; Przybylski et al. 2013.
[350] Lang et al. 2015.

vegetables,[351] and which is a marker for yeast[352] overgrowth from *Aspergillus*,[353] *Penicillum* and/or *Candida*.[354] Sample 6 contains the highest amount of dihydroxyacetone, 1-Pyrroline hydroxycarboxylic acid and succinic acid of all samples.

5.5.5.3 Proteomics

Sample 3 from the interior and samples 5 and 6 from the exterior of the object were analysed by proteomics, with data searches performed against Uniprot Meat, Milk, Cereal and Yeast databases. The complete results of these searches are included in Appendix 31. The most diagnostic protein matches are listed in Table 45.

The highest scoring meat protein in the interior is Desmin (a protein linked to muscle activity in beef) also found in the exterior samples but with a much lower score than Glycinin G1 (a protein from soya beans). The identification of β and α-casein from goat (as opposed to cow) with a 65% protein coverage is the most significant result. Because the amino acid sequence of caseins varies only slightly between mammals[355] the taxa would require confirmation with a goat milk control. Caseins from cow and goat were also found in the exterior samples but at lower score and coverage than in the interior. Another interesting result was the identification of *Saccharomyces cerevisiae* and *Yarrowia lipolytica* only in the interior sample.

[351] Yannai 2013.
[352] https://hmdb.ca/metabolites/HMDB0002329.
[353] Hilt et al. 2016.
[354] https://hmdb.ca/metabolites/HMDB0002329.
[355] Holt 2016

	Accession Number	-10lgP	Coverage (%)	Intensity	#Peptides (unique)	Avg. Mass	Protein Name
INTERIOR (SAMPLE 3)	O62654	87.16	6	2.83E+04	4(4)	53532	Desmin Bos taurus
	P13135	55.51	28	3.00E+05	8(8)	27931	Calpain small subunit 1 Bos taurus
	B9DKW3	38.48	3	8.53E+03	2(2)	53847	Cysteine--tRNA ligase Staphylococcus carnosus (strain TM300)
	Q38W81	31.58	4	5.48E+04	2(2)	103215	Translation initiation factor IF-2 =Lactobacillus sakei subsp. sakei (strain 23K)
	Q6B411	145.85	48	3.68E+05	5(5)	16783	Lysozyme C milk isozyme Bos taurus
	Q95L76	66.89	65	5.24E+05	6(4)	24992	Beta-casein Capra hircus
	I6WY32	48.84	28	2.49E+04	4(3)	24177	Alpha-S1-casein Capra hircus
	P85295	46.51	20	3.35E+04	2(2)	10078	Serum albumin (Fragments) Capra hircus
	Q8MIH3	25.61	17	1.13E+03	2(1)	12999	Alpha s1 casein Capra hircus
	A0A2S4VGG4	28.53	1	2.00E+06	1(1)	118765	Suf domain-containing protein Puccinia striiformis
	K3VT46	26.16	1	8.86E+04	1(1)	73085	Uncharacterized protein Fusarium pseudograminearum (strain CS3096)
	B3LNV9	28.22	3	1.44E+04	1(1)	26976	MICOS complex subunit MIC27 Saccharomyces cerevisiae (strain RM11-1a)
	B5RSM1	28.22	7	1.44E+04	1(1)	10282	Transcription and mRNA export factor SUS1 Yarrowia lipolytica (strain CLIB 122 / E 150)
EXTERIOR (SAMPLES 5 AND 6)	P04776	121.2	5	1.26E+04	2(2)	55706	Glycinin G1 Glycine max
	O62654	64.99	6	4.56E+04	3(3)	53532	Desmin Bos taurus
	Q712N8	48.03	15	1.20E+06	3(2)	24865	Beta-casein Capra hircus
	A0A452DHW7	37.46	16	7.95E+03	4(3)	29221	Beta-casein Bos taurus
	Q95115	45.57	5	6.57E+03	4(4)	90700	Signal transducer and activator of transcription 5A OS=Bos taurus
	Q865B7	42.11	4	4.57E+04	3(3)	90309	Peroxisome proliferator-activated receptor gamma coactivator 1-alpha OS=Bos taurus
	K3W1C1	61.3	3	1.73E+03	1(1)	41608	Uncharacterized protein Fusarium pseudograminearum (strain CS3096)
	M4GR03	61.3	3	1.73E+03	1(1)	39219	Actin 2 Heterodera avenae
	A0A1B2JEH8	41.43	2	7.73E+03	2(2)	69361	BA75_02906T0 Komagataella pastoris
	A0A1B2J5M9	33.31	1	5.08E+03	2(2)	59865	Amidophosphoribosyltransferase Komagataella pastoris

Meat Milk Cereal Yeast

Table 45– Diagnostic protein matches for Pompeii INV10289

5.5.6 Discussion

The results of the characterization of the samples from INV10289 are summarized in Table 46.

The most distinctive feature is the identification of lactose alongside caseins which are both biomarkers for milk. The presence of malitol in the interior of the vessel indicate fermentation of sugars, corroborated by the identification of *Saccharomyces cerevisiae.* The identification of *Fusarium pseudograminearum* (a fungal pathogen of wheat) in both interior and exterior samples validates the identification of the pyrolate of ergosterol by QTOF-GC-MS with TSP.

Sample	Location	Colour	Consistency	FTIR	XRD	TSP-GC-MS	IC-MS	PROTEOMICS
2	Interior (base)	Black	Hard	C-H aromatics Silicates, C-Cl	-	Fatty aldehyde: C15 Cyclic alkane: C15 FA: C14-16, C18 and 18:1 Pyrolate of Ergosterol (?)	Malitol High in Citric acid	-
3	Interior (base)	Green	Soft	C-H aromatic CO_3^{2-}, silicates, organic nitrates, C-Cl	Malachite azurite		High in Sebacic and Octanoic acids	Desmin (beef) β and α1Caseins (goat/cow) wheat fungus Saccharomyces cerevisiae (cereal yeast)
4	Interior (amidst lapilli)	Green	Powdery		Malachite other (?)	Medium-chain acids: C6-10 FA methyl ester: C17 FA: C16	High in Lactose High in 1-Pyrroline hydroxycarboxylic acid	-
5	Exterior (body)	Dark brown	-	-	Malachite azurite	Alkanes: C15-17 and 20 FA: C14, 16 and C18 Nitriles: C16, 18 and 22	High in 3-Hydroxyisobutyric and Oxalic acids	Glycinin G1 (soya beans) + Desmin (beef) β and α1Caseins (goat/cow) wheat fungus
6	Exterior (under rim)	Dark brown	-	-	Azurite	Pyrolate of Ergosterol (?) Alkanes: C15 FA: C14-16, C18 and 18:1	High in dihydroxyacetone, 1-Pyrroline hydroxycarboxylic acid and succinic acid	wheat fungus

Table 46 – Summary of the Multi-analytical characterization of Pompeii INV10289 corrosion

5.6 Case Study 6 – The Paestum Residue

5.6.1 Background

Included amongst the loaned objects for the *Last Supper in Pompeii* exhibition at the Ashmolean Museum was a waxy substance found in a copper vessel (Figure 111) excavated in 1954 from a shrine in the 530-510 BC Roman settlement of Paestum, Italy.

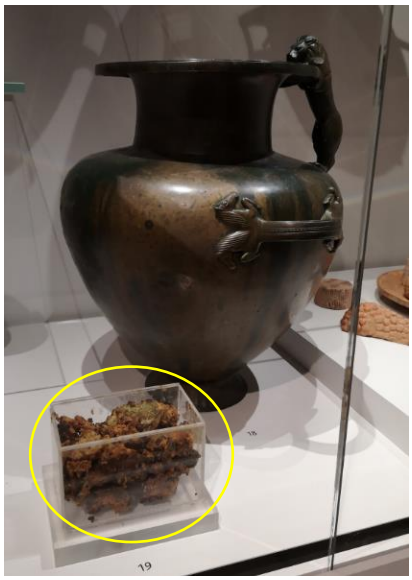
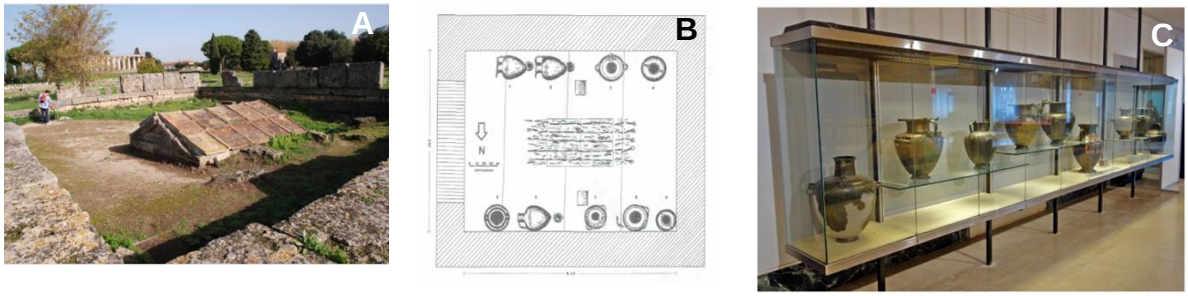


Figure 111– Copper-alloy hydra and the residue

The excavation report describes that the shrine contained eight bronze vessels (six hydrae and two amphorae) surrounding an empty iron bed (Figures 112a-c). These vessels contained a yellow-brown paste-like substance smelling of wax. The residue was reported to have been a liquid or viscous liquid. Traces of it were found on the exterior of the vessels, which were originally sealed with cork discs – one of which survived intact.[356]

[356] Sestieri 1956.



Source: [A and C] Paestum.org.uk [B] Sestieri 1956

Figure 112 – Exterior of the shrine [A], its interior plan [B] and the bronze vessels on display [C]

The report emphasises the sacredness of the shrine: the empty bed in the absence of an image and the inaccessibility of the shrine, signifying that the deity was actually there, the bronze vases containing honey, a symbol of immortality. Different laboratories analysed the residue over the years but all excluded honey from its composition. The residue was not soluble in water, thus it did not contain carbohydrates. The most recent analysis of the residue was carried out in 1983. It states that the residue was soluble in ethyl ether and its sterol composition (with a 99% saponification index) indicated the presence of animal and vegetable fats.[357] The following fatty acids identified by GC-MS:[358]

Residue Composition	%
Palmitic acid	77.4
Heptadecanoic acid	1.0
Stearic acid	5.2
Oleic acid	6.1
Linoleic acid	0.4
Linoleic + arachidic acid	1.0
Non-identified	6.5

[357] Sestieri 1985.
[358] No experimental details provided.

5.6.2 Research Question

Fresh honey is composed of 79% carbohydrates (of which fructose is the most abundant at 39%), 18% water and:

- Minerals 0.4%
- Proteins 1.1%
- Vitamins, enzymes and flavonoids 0.1%
- Phenolic compounds <0.1%
- Acids (formic, citric and gluconic being the most abundant) varying between 0.17–1.17%[359]

Over time, honey undergoes degradation and change its chemical composition, as illustrated in Figure 113.

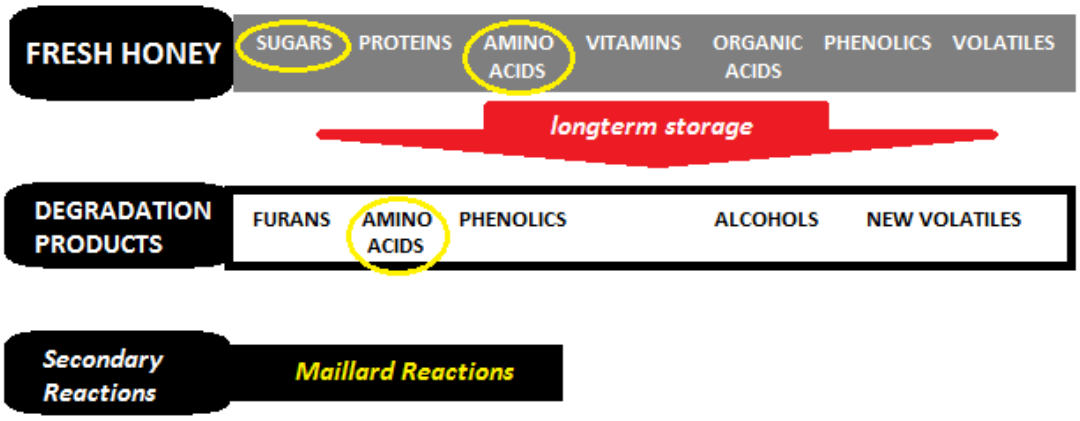


Figure 113– The degradation of honey[360]

[359] Santos-Buelga and González-Paramás 2017.
[360] Silva et al. 2019.

Maillard reactions are chemical reactions between reducing sugars and amino acids in food subject to heat and/or storage. Their products are responsible for the change of colour and taste of food, such as the development of a brown crust in baked bread. During long-term storage (particularly at temperatures above 20^{o}C) honey acquires a darker hue, sugars degrade into furans and its acid content increases.[361]

Evidence of honey in archaeological and historical contexts is routinely associated with the identification of beeswax in lipids extracts of unglazed pottery vessels. It is assumed that beeswax would have been absorbed into the ceramic matrix from honey used for cooking or during the processing of wax combs.[362] As the Paestum residue has a strong waxy smell, it may contain beeswax. Although also produced by honeybees, beeswax has a very different composition to honey. Fresh beeswax is composed of 64% esters (35% are C_{40}-C_{52} monoesters, predominantly alkyl palmitates), 14% odd medium chain n-alkanes ($C_{27}H_{56}$ being the most abundant), 12% free acids and:

- 1% C_{16}-C_{20} acid monoesters
- 2% acid polyesters
- 1% free alcohols
- 6% of unidentified material[363]

Beeswax is considered highly stable as most of its alkanes and esters are saturated.

The main research question posed by Kelly Domoney from the Ashmolean Museum regarding the Paestum residue is whether it originally contained honey. A second

[361] da Silva et al. 2016.
[362] Heron et al. 1994; Decavallas 2007 in Roffet-Salque et al. 2015.
[363] Tulloch et al. 1972 and Tulloch 1980 in Bonaduce and Colombini 2004; Roffet-Salque et al. 2015.

research question is in respect of the surface of the residue, specifically the origin of its different colours. Samples from the core of the residue and the surface were provided (Figure 114), the latter collected according to colour (i.e. black, green and brown).

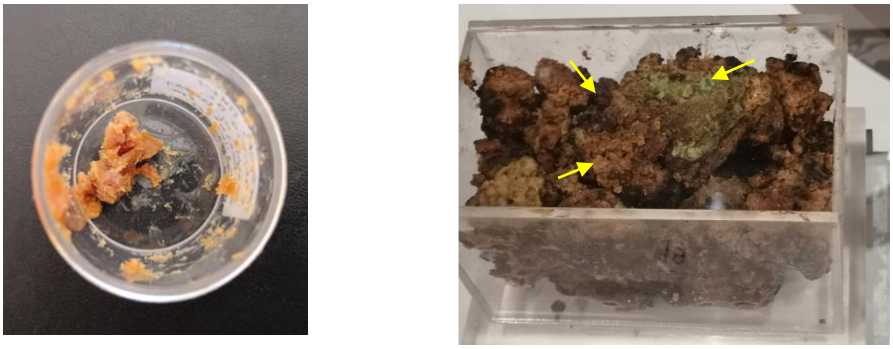


Figure 114– Sampling the Paestum residue: core [left] and surface [right]

arrows marking examples of sampled colours

The following substances were also analysed:

- Fresh Acacia honey (purchased from Abel & Cole)
- Fresh white beeswax (supplied by the Bodleian Library)
- Fresh honeycombs from Italy and Greece (purchased online and supplied by the Ashmolean Museum)

Accelerated aged honeycomb samples were prepared by heating the honeycombs (in separate glass vials) at 70°C[364] over a month, with and without copper coupon (Figure 115).

[364] Based on Sramek et al. 2016 and Arrhenius equation that predict the temperature dependence of chemical reactions.

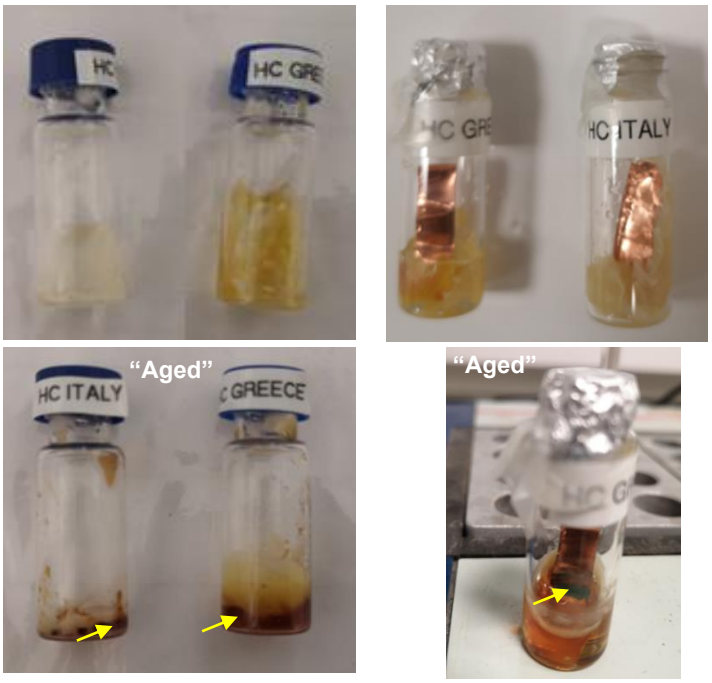


Figure 115 – Honeycombs before and after ageing

arrows marking sampled areas

5.6.3 Identification of Chemical Bonds

The spectrum of the Paestum residue (core sample) is shown superimposed over the spectrum of honey (Figure 116) and beeswax (Figure 117), with main peaks and band assignments listed in Table 47. The only similarity between the spectra of the Paestum residue and honey is the long-chain alkane bands at 2916 and 2849cm^{-1}. In honey, these bands are less intense as its spectrum is dominated by water and carbohydrate bands. In the case of beeswax however, these bands are much more intense as long-chain alkanes are one of its main constituents.

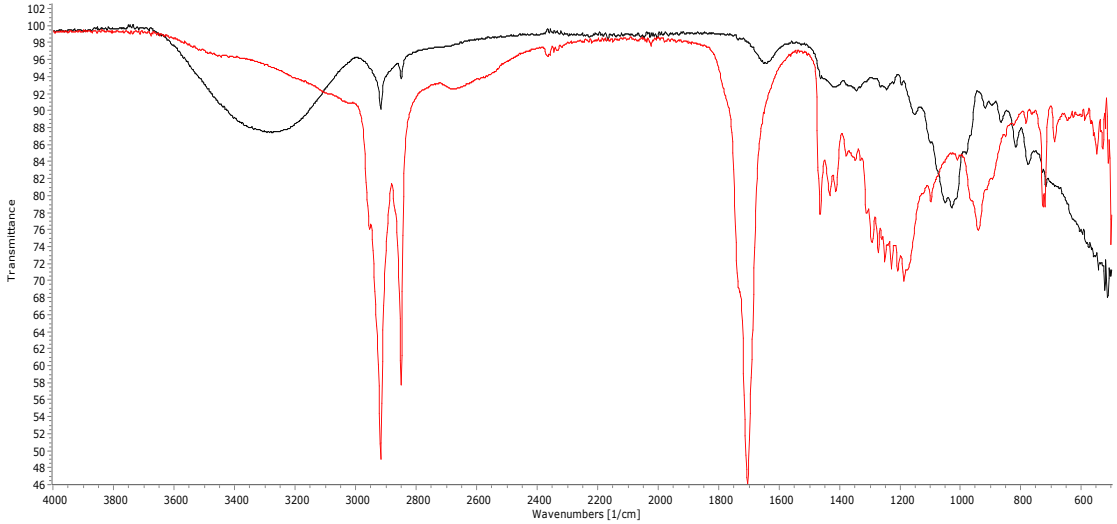


Figure 116 – FTIR spectra of the residue (in RED) and honey

ATR mode

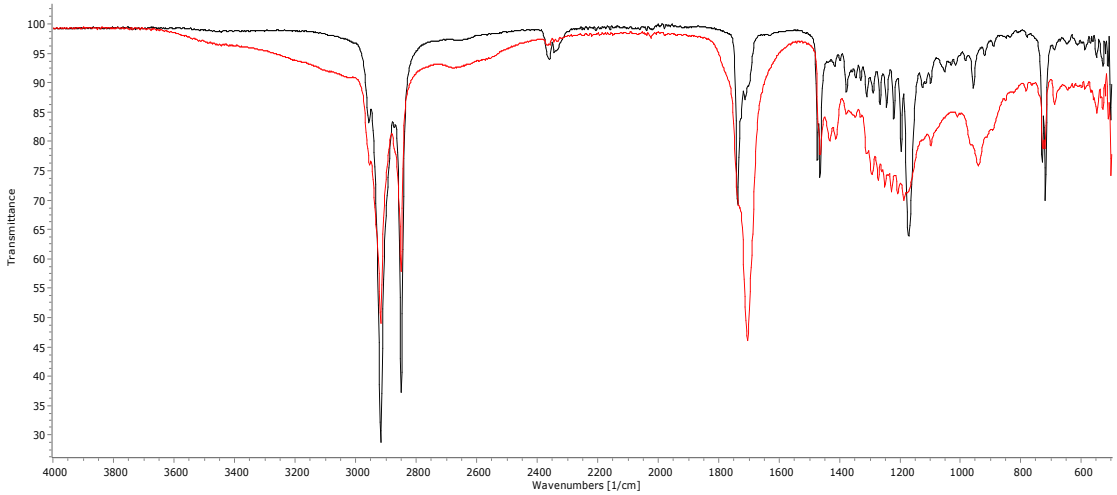


Figure 117 – FTIR spectra of the residue (in RED) and beeswax

ATR mode

BEESWAX		RESIDUE		ACACIA HONEY		ATTRIBUTION[365]
				3400	br	OH in H_2O and intermolecular hydrogen bonding stretching vibrations
2955	sh	2954	sh			CH_3 (aliphatic) alkanes stretching vibrations
2916	vs	2916	vs	2916	m	CH_2 (acyclic) alkanes and carbohydrates stretching vibrations
2848	vs	2849	vs	2849	m	CH_2 alkanes stretching vibrations
1736	s	1735	sh			C=O esters stretching vibrations
1712	sh					C=O saturated carboxylic acids stretching vibrations
		1703	vs	1700	br	
1472						
1463	s doublet	1463	s			$C-(CH_3)_3$ alkanes deformations
		1431	m			CH_2 deformations
1414	vw	1411	m	1413	br	CH_2 alkanes and δ OH carbohydrates deformations
1376	m	1377	vw			CH_2 stretching vibrations
1345	w	1347	vw	1343	br	CH_2 and OH in C-OH group deformations
1329	w					CH_2 deformations
1309	w	1310	vw			
		1291	w			
1288	w					
		1271	w			
1265	w					
1243	w			1244	br	CH_2 and C-O-C carbohydrates stretching vibrations
		1228	w			
1220	m					
		1207	w			C-O-C esters and $C(CH_3)_3$ (skeletal) alkanes stretching vibrations
1195	m			1195	vw	
1171	s					C-O esters and v $C(CH_3)_2$ (skeletal) alkanes stretching vibrations
				1150	w	C-H and C-O carbohydrates stretching vibrations
1051	w			1050		
1030	w			1028	m doublet	C-O in C-OH group or C-C carbohydrate stretching vibrations
956	w					C-H alkanes deformations
		941	m			
919	w			917	w	
		893	vw	896	vw	
889	w					
				865	w	C-H carbohydrates deformations
				816	m	
				776	vw	
729		727	s			
716	s doublet			717	w	$(CH_2)_3$ skeletal stretching vibrations

Table 47– Infrared frequencies (cm-1) for beeswax, residue and honey

[365] Regert et al. 2001; Kędzierska-Matysek et al. 2018; Cuní et al. 2012; Socrates 2001.

The spectra of beeswax and the Paestum residue are very similar, except for a strong carbonyl group peak at 1703cm^{-1}, which in beeswax appears at 1736cm^{-1}. Normally, when the FTIR spectra of a complex material shows a strong peak at 1735-1740cm^{-1} it would be assigned to "fats and waxes" category, as both are rich in ester. At 1690-1705cm^{-1}, the material would fall under "tree resins and oils", which are rich in fatty acids.[366]

Although beeswax is considered highly stable, the literature contains FTIR spectra showing a strong peak at around 1705cm^{-1} for beeswax, which have undergone accelerated ageing tests using heat,[367] and for historical beeswax artefacts exposed to UV radiation.[368] Moreover, a reduction of the ester carbonyl stretch has been observed in the FTIR spectrum of archaeological beeswax, probably as a result of hydrolysis of esters into fatty acids.[369]

Further insights on the carbonyl stretch can be obtained from the FTIR spectra of the honeycombs, presented in Figure 118 and 119. Both sets of spectra are practically identical. Carbonyl stretch bands appear only in the FTIR spectra of the aged green residues: one at 1737cm^{-1} corresponding to esters (as seen in the fresh beeswax) and another at 1587cm^{-1} corresponding to COO^- asymmetric stretch. As seen in the experiments described in Chapter 4, this peak indicates the complexation of carboxylic

[366] Derrick et al. 1999.
[367] Regert et al. 2001.
[368] Čížová et al. 2019.
[369] Heron et al. 1994.

acids and copper ions. The spectra of the aged honeycombs without copper remaining are practically identical to the fresh honeycombs and similar to fresh honey.

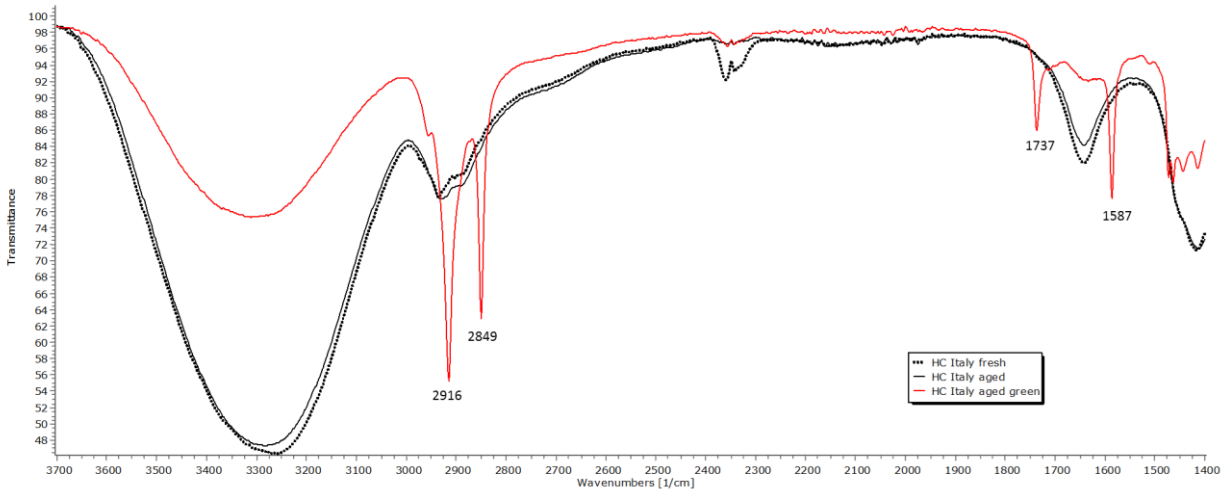


Figure 118 – Partial FTIR spectra of honeycomb from Italy

ATR mode

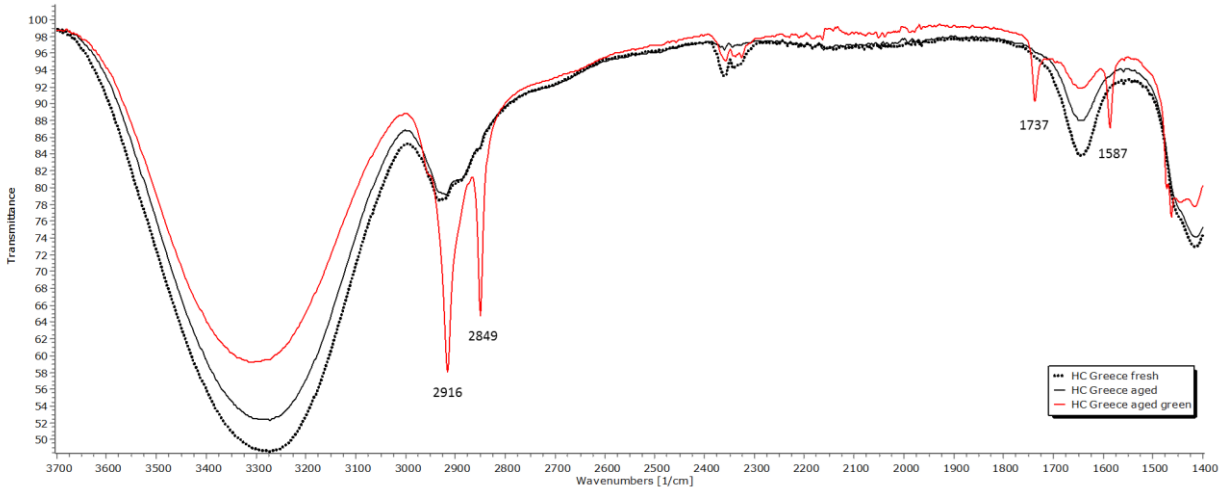


Figure 119 – Partial FTIR spectra of honeycomb from Greece

ATR mode

5.6.4 Identification of Organic Compounds

5.6.4.1. QTOF-GC-MS with TSP

The chromatograms obtained from the solid samples of beeswax, honey and the Paestum sample were very different from one another. are shown in Figure 120.

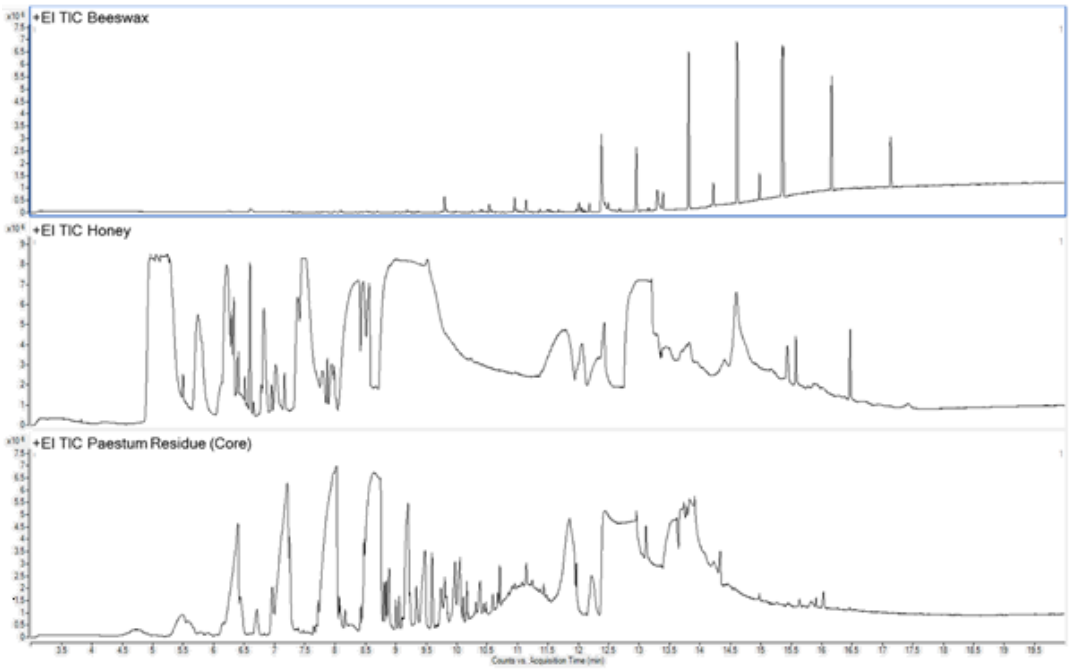


Figure 120 - EI Chromatograms for beeswax, acacia honey and residue core sample

The chromatogram of beeswax contains the characteristic well-resolved peaks of substances of increasing carbon chain, while that of honey and the Paestum sample are mostly convoluted peaks with many compounds in high concentration. After analysis, the microvial that contained beeswax was completely “clean” whilst the microvials used for honey and the Paestum sample had a dark brown residue that had a burnt sugar smell.

Three further samples from the surface of the Paestum residue were analysed: orange, black and green "crystals", their chromatograms are included in Figure 121. Given the poor peak definition, the chromatograms were processed using Agilent's Mass Profiler Professional Software prior to identification using ID Browser. Table 48 lists the accepted identifications for the compounds with datasets included in Appendix 32.

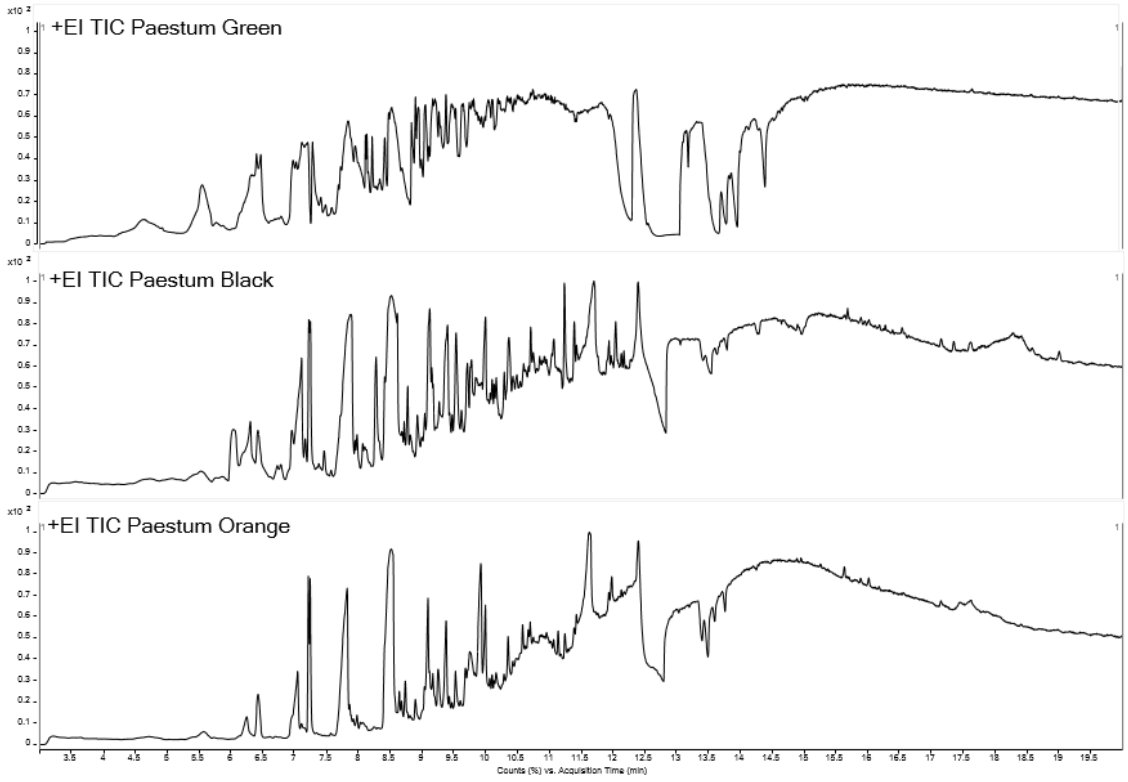


Figure 121 – EI chromatograms of the residue's surface samples

Under acidic conditions, such as those found in honey, Maillard reactions can yield furan derivatives out of monosaccharides.[370] Two examples of this type of compounds are 5-methyl furfural[371] and levoglucosenone (a derivative of levoglucosan)[372] identified in the Paestum black residue (highlighted in Table 48). Levoglucosenone could have also been an analytical artefact acting as a marker for carbohydrate in the presence of copper (as reported for copper-lactose complex and copper-milk corrosion in Chapter 4).

				PAESTUM RESIDUE		
RT(min)	Compound	Formula	mz (Da)	Orange	Black	Green
5.88	Bicyclo[2.2.2]oct-5-en-2-one	$C_8H_{10}O$	80.0588		X	X
6.18	5-methyl furfural	$C_6H_6O_2$	110.107		X	
6.49	2-butyl-Pyridine	$C_9H_{13}N$	93.0701			X
6.72	2-methyl-2H-Tetrazole	$C_2H_4N_4$	56.0615		X	
7.02	3-propyl-Pyridine	$C_8H_{11}N$	92.061			X
7.46	Levoglucosenone	$C_6H_6O_3$	68.0611		X	
7.83	Octanoic acid, 3-hexenyl ester, (Z)-	$C_{14}H_{26}O_2$	57.0699		X	
7.98	Hex-4-yn-3-one	$C_7H_6O_2$	67.0479			X
8.13	Benzoic acid	$C_6H_{10}O$	105.072			X
8.41	2-Cyclohexen-1-ol	$C_6H_{10}O$	70.0767	X	X	
8.45	1-phenyl-1-Butanone	$C_{10}H_{12}O$	105.072			X
8.76	2-Nonenoic acid	$C_9H_{16}O_2$	69.07	X	X	
8.84	m-Aminophenylacetylene	C_8H_7N	117.066		X	
9.11	n-Decanoic acid	$C_{10}H_{20}O_2$	73.0296	X	X	
10.29	Dodecanoic acid	$C_{12}H_{24}O_2$	73.0296	X	X	
11.29	Octahydro-1,3-Methanopentalene	C_9H_{14}	79.0514			X
11.39	Tetradecanoic acid	$C_{14}H_{28}O_2$	73.0296	X	X	X
11.70	Bicyclo(3.3.1)nonane-2,6-dione	$C_9H_{12}O_2$	152.084		X	
16.18	2-ethyl-2-methyl-Tridecanol	$C_{16}H_{34}O$	71.085		X	

Table 48 – Compounds identified in the residue's surface samples
monosaccharide furan derivatives highlighted

[370] Pilath et al. 2010.
[371] da Silva et al. 2016.
[372] Silva et al. 2019.

Other significant changes in the composition of honey under long-term storage include an increase in its acid content.[373] Figure 122 shows extracted chromatograms for the Paestum residue with identified carboxylic acids (the datasets are included in Appendix 33).

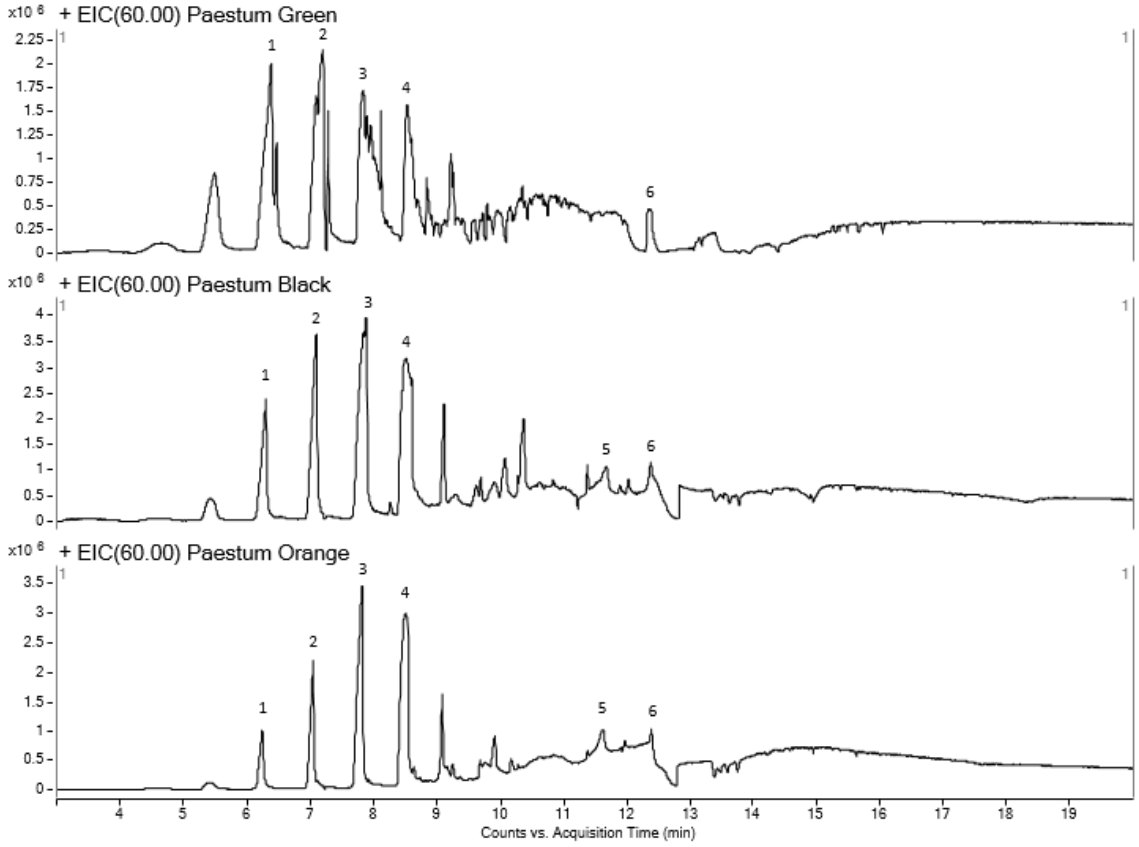


Figure 122 – Extracted EI chromatograms (mz 60) of residue surface samples

[1] hexanoic acid; [2] heptanoic acid; [3] octanoic acid; [4] nonanoic acid;
[5] tetradecanoic acid and [6] n-hexadecanoic acid

[373] Castro-Vázquez et al. 2008.

The concentration of 5-methyl furfural, benzoic acid, decanoic acid and the organic acids [2, 3, 4 and 5] are reported to progressively increase as a function of storage time and temperature.[374] Free fatty acids in honey are amongst the compounds produced by lactic acid bacterial (LAB) strains. LABs from the honey stomach of honeybees (also found in fresh honey) are responsible for honey's antimicrobial action. In a metabolomical study of 13 LAB symbionts from honeybees, the genus *Lactobacillus apinorum* was the only strain that produced decanoic, dodecanoic, tetradecanoic and hexadecanoic acids.[375] The same study also looked at the presence of LABs and free fatty acids in nine fresh and stored honeys. Although none were found to contain all four fatty acids monitored in the study, C10, C12 and C16 were found in stored Linden Honey, which also contained protein metabolites from *Bifidobacterium asteroids* and *Lactobacillus rossiae*.[376]

5.6.4.2. IC-MS

5.6.4.2.1 Water Extracts

To target carbohydrates, water extracts were obtained from the Paestum residue (core sample), honey and beeswax. Table 49 lists the identified compounds in the diluted water extract of the samples and their relative abundance adopting a logarithmic scale. The analyses results are included in Appendix 34

[374] Castro-Vásquez et al. 2008.
[375] Olofsson et al. 2014b.
[376] ibid

RT	COMPOUND	FORMULA	mz (Da)	HONEY	BEESWAX	PAESTUM
2.89	Fructose	$C_6H_{12}O_6$	180.0559	***	*	**
4.34	Arabinonic acid	$C_5H_{10}O_6$	166.0405	**	**	**
4.46	Taurine	$C_2H_7NO_3S$	125.0072	**	*	***
10.50	Succinic acid	$C_4H_6O_4$	119.0190	*****	***	***
10.82	3,3-Dimethylglutaric acid	$C_7H_{12}O_4$	160.0661	***	***	***
11.27	Dimethyl fumarate	$C_6H_8O_4$	144.0348	**.	**	**
16.13	Citric acid	$C_6H_8O_7$	192.0196	***	**	***
29.37	p-Coumaric acid	$C_9H_8O_3$	163.0400		*	*

[*] based on logarithmic scale

Table 49– Identified compounds in the diluted water extracts and their relative abundance

There was only one peak assigned to a carbohydrate, with nine monosaccharides matches with the same chemical formula. As the IC-MS method is not able to differentiate isomers, fructose was selected as it is in general the most dominant carbohydrate in honey. The Paestum residue showed a higher concentration of fructose than beeswax, but lower than honey. In terms of the minor constituents, taurine – the second most abundant amino acid in honeybee[377] – its highest abundancy identified the Paestum residue. An interesting result was the detection of p-coumaric acid, a compound only slightly soluble in water. P-Coumaric acid belongs to the cinammic derivatives group within phenolic compounds most abundant in chestnut and heather honeys, followed by sunflower, lime, eucalyptus and rapeseed.[378] Thus, its absence from the honey sample (i.e. Acacia honey) is not surprising.

[377] Schäfer et al. 1988.
[378] Dimitrova et al. 2007.

The (undiluted) stock water extracts of honey, beeswax and Paestum residue were also analysed. The most abundant compounds only present in the Paestum residue are listed in Table 50 (the analyses results included in Appendix 35). Amongst these were:

- At least three different carbohydrate derivatives
- Sebacic and pimelic acids, honeybee gut microbiota metabolites[379] also found in honey and beeswax but at a much lower abundancy
- 10-Hydroxydecanoic acid, one of the main fatty acid constituents of royal jelly[380]
- 2-o-ethyl ascorbic acid – a derivative of ascorbic acid, the main vitamin in honey[381]
- Butyrin – a triglyceride of butyric acid, which is found in trace quantities in lavender and rapeseed honeys[382]

[379] Kešnerová et al. 2017.
[380] Xue et al. 2017.
[381] Santos-Buelga and González-Paramás 2017.
[382] Daniele et al 2012.

RT	COMPOUND	FORMULA	mz (Da)	OCCURRENCE
9.39	4,6-O-Ethylidenehexopyranose	$C_8H_{14}O_6$	206.0718	A glucose derivative
9.85	Triacetin	$C_9H_{14}O_6$	218.0716	Plant metabolite
9.95	Methyl 2,3-O-isopropylidenepentofuranoside*	$C_9H_{16}O_5$	204.0926	A carbohydrate derivative
10.53	1,2-O-Isopropylidenehexofuranose	$C_9H_{16}O_6$	220.0874	A carbohydrate derivative
10.97	**Pimelic acid**	**$C_7H_{12}O_4$**	**160.0662**	**Metabolic found in the gut of honeybee[383]**
11.00	(2E)-2-Hexenal	$C_6H_{10}O$	98.0656	Plant metabolite
11.14	Methyl 2,3-O-isopropylidenepentofuranoside*	$C_9H_{16}O_5$	204.0925	A carbohydrate derivative
12.36	Suberic acid	$C_8H_{14}O_4$	174.0818	A metabolic breakdown product derived from oleic acid
12.61	Methyl 2,3-O-isopropylidenepentofuranoside*	$C_9H_{16}O_5$	204.0926	A carbohydrate derivative
13.57	p-coumaroylagmatine	$C_{14}H_{20}N_4O_2$	276.1503	Plant metabolite
13.99	Diethyl 2-(2-oxopropyl)succinate	$C_{11}H_{18}O_5$	230.1080	
14.28	**Azelaic acid**	**$C_9H_{16}O_4$**	**188.0975**	**Found in cereals and animal products. Derivative of sebacic acid**
15.58	2-o-ethyl ascorbic acid	$C_8H_{12}O_6$	204.0563	Derivative of ascorbic acid
17.64	**Sebacic acid**	**$C_{10}H_{18}O_4$**	**202.1133**	**Metabolic found in the gut of honeybee[384]**
18.96	6-(2,2-Dimethyl-1,3-dioxolan-4-yl)-2,2-dimethyltetrahydrofuro[3,4-d][1,3]dioxol-4-ol	$C_{12}H_{20}O_6$	260.1188	A carbohydrate derivative
24.35	10-Hydroxydecanoic acid	$C_{10}H_{20}O_3$	188.1339	Acid present in royal jelly[385]
24.74	Camphoric acid monomethyl ester	$C_{11}H_{18}O_4$	214.1132	
25.91	Butyrin	$C_{15}H_{26}O_6$	302.1655	Plant and animal metabolite.

*or similar

Table 50 – Unique compounds identified in the water extract of the residue

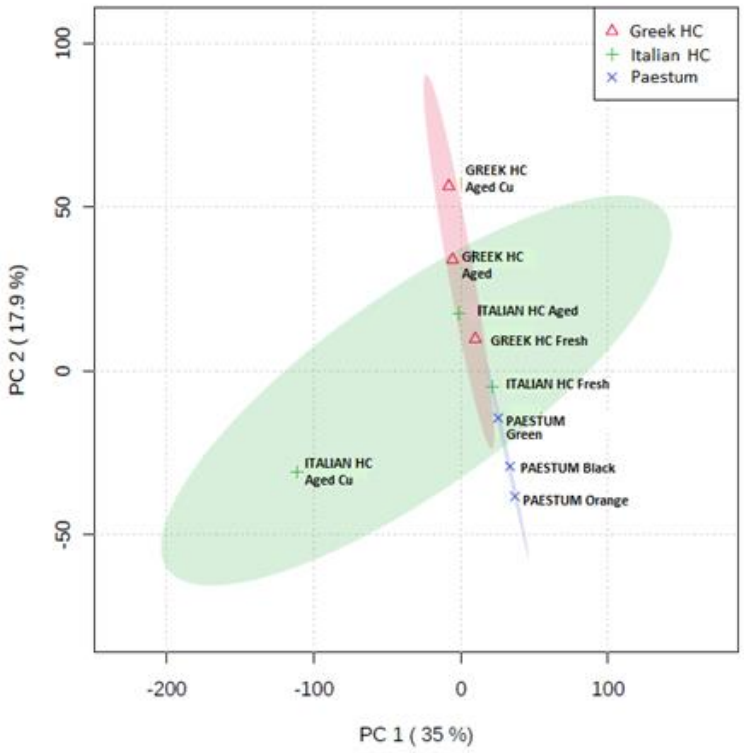
highlighted compounds also present in honey and beeswax but at a lower abundancy

5.6.4.2.2 Methanol Extracts

Methanol extracts of the Paestum residue (surface samples: green, black and orange) were analysed alongside the methanol extracts of the honeycombs (fresh, aged and aged with copper). The MS Data for the top 26 most abundant identified compounds is included in Appendix 36. As there were three samples for each subject (e.g. Paestum, Italian honeycomb and Greek honeycomb) the dataset including unidentified compounds

[383] Kešnerová et al 2017.
[384] Ibid.
[385] Xue et al. 2017.

were submitted to Metaboanalyst. The relationship between the samples can be expressed as a PCA score plot. Figure 123 shows the score plot for PC1 and PC2 obtained for the full dataset, which together explain 52.9% of the variance between the samples. There seems to be an order in the position of the samples in each group although the "Italian HC Aged Cu" sample is a clear outlier. Replicates of all samples would be required to confirm these relationships.



varPC1	35.0%
varPC2	17.9%
varPC3	13.7%
varPC4	9.4%
varPC5	7.4%

Figure 123 – PC1 and PC2 plot for honeycombs and Paestum residue showing the Italian honeycomb aged with copper as an outlier because its PC1 is completely different from the other samples

To investigate the relationship between the samples, the statistical analysis was restricted to the identified compounds for hierarchical cluster analysis, expressed as a dendrogram in Figure 124 and as a heatmap of identified compounds in Figure 125.

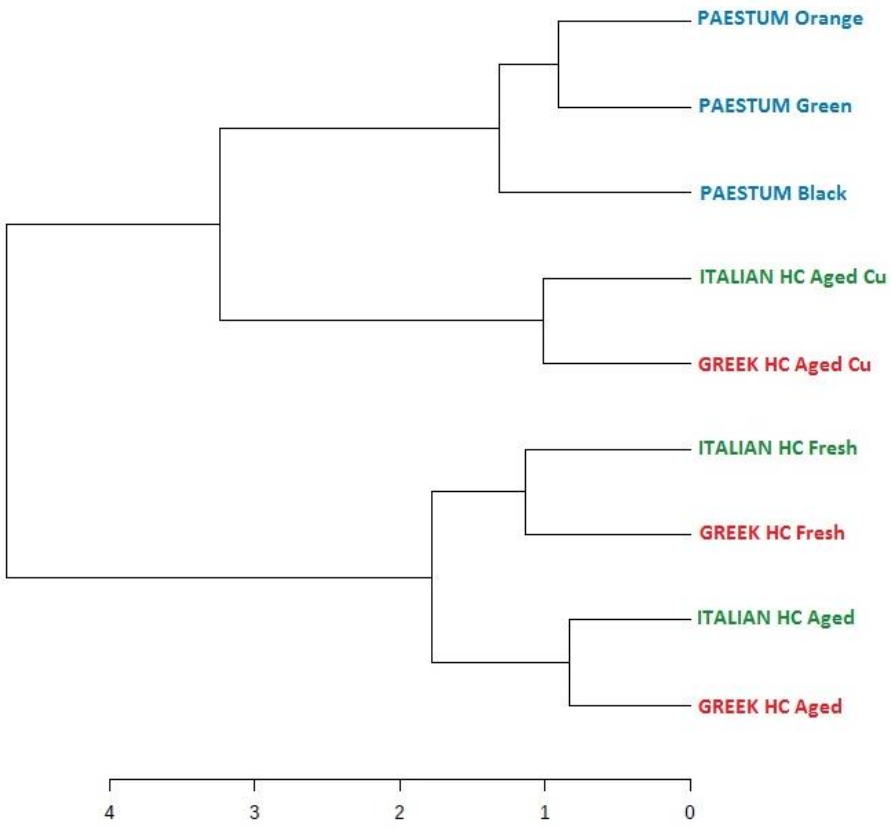


Figure 124 – Hierarchical clustering shown as a dendrogram

distance measured using Pearson's correlation and clustering algorithm using ward.D

The hierarchical clustering divides the samples into two groups. The first group includes all Paestum samples plus the honeycombs aged with copper, their composition dominated by acids (top right-hand corner in Figure 125). The remaining honeycomb samples belong to a second group, their composition dominated by carbohydrates (bottom left-hand corner in Figure 125).

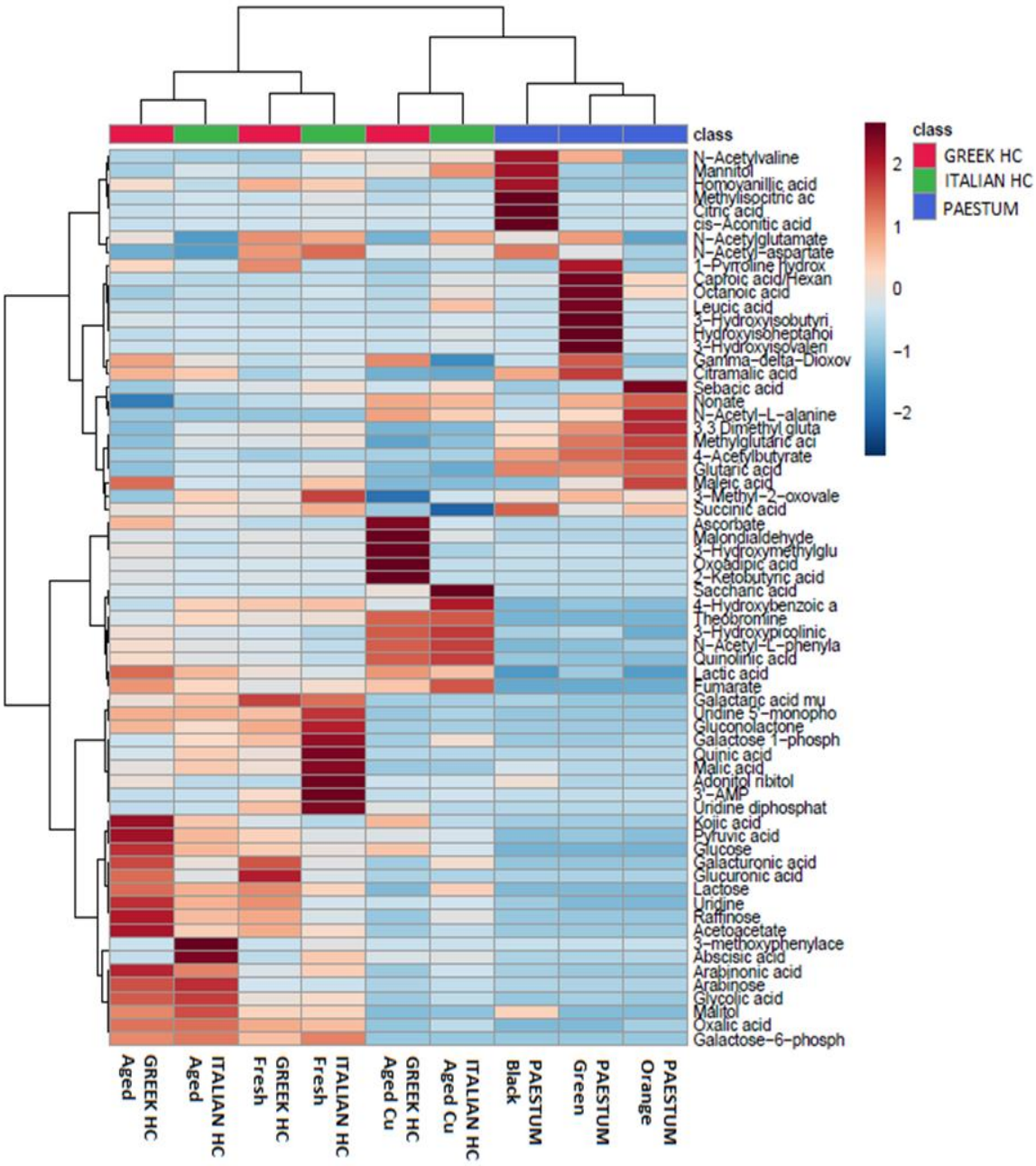


Figure 125 – Hierarchical clustering shown as a heatmap

distance measured using Pearson's correlation and clustering algorithm using ward.D

5.6.4.3 Proteomics

The purpose of the proteomics analysis was to verify the presence of *Lactobacillus* bacteria and/or resin proteins in the Paestum residue, which could have been responsible for its high acidity. The Paestum residue (core sample) and the honeycomb samples (fresh and aged) were also analysed by proteomics.

The peptides recovered from the Paestum residue were screened against the general *Uniprot All* database. Amongst the keratin/trypsin proteins (considered contamination) there were three main royal jelly proteins of *Apis Mellifera* and a protein from *Pseudomonas aeruginosa* (a common bacteria). The Paestum residue peptides were then run against *Uniprot Honey* and *Uniprot Resin* databases with results compared to those obtained from fresh and aged honeycombs as summarized in Table 51. The complete list of protein identifications for each database search are included in Appendix 37.

The Paestum residue can be characterized as honey because of the identification of three major royal jelly proteins: from *Apis Mellifera*, *Apis Cerana* and *Tropilaelaps mercedesae*,[386] (a common honeybee parasite) all also identified in the honeycombs. Furthermore, *Lactobacillus kimbladii*[387] and *Lactobacillus Bombi*[388] protein matches were also identified in the Paestum residue. Despite *Lactobacillus* being the largest lactic acid bacteria group in honeybee gut microbiota[389] no matches for their proteins were identified in the honeycombs. Honeybee gut microbiota is a function of bees' foraging

[386] Khongphinitbunjong et al. 2016; Dong et al. 2017; Phokasem et al. 2019.
[387] Olofsson et al. 2014a.
[388] Killer et al. 2014; Praet et al. 2018.
[389] Olofsson et al. 2014a.

activities,[390] seasonal changes[391] and social contact amongst bees from different colonies[392] amongst other variables. The final species identified in the residue was *Armillaria Gallica*, a tree fungus,[393] also present in fresh honeycomb from Greece.

The search conducted against *Uniprot Resin* revealed proteins from three species of coniferous trees (Figure 126).



Picea Abie (Norway spruce) *Picea Glauca* (White spruce) *Picea Sitchensis* (Sitka spruce)

Figure 126 – Taxa of resin protein matches for the residue

As these resin proteins were also identified in the honeycomb controls, their presence in the Paestum residue may be interpreted as a marker for the honeybees' food source or environmental contamination, as opposed to coniferous resins being an original component of the residue. The final search conducted with the residue peptides was against *Uniprot Bacteria* database, with full results include at the end of Appendix 38.

[390] Baffoni et al. 2016; Jones et al. 2017.
[391] Kešnerová et al. 2020.
[392] Billiet et al. 2017.
[393] Gunn 2005.

The three most prominent bacteria are: *Pseudomonas aeruginosa*, *Escherichia coli* and *Mycobacterium tuberculosis*, all found in honey.[394]

Identifications against Uniprot Honey	Paestum Residue	Honeycomb Greece		Honeycomb Italy	
		Fresh	Aged	Fresh	Aged
Honeybees					
O18330 - Major Royal Jelly Protein *Apis Mellifera*	X	X	X	X	X
O77061 - Major Royal Jelly Protein *Apis Mellifera*	X	X	X	X	
Q17060 - Major Royal Jelly Protein *Apis Mellifera*	X	X	X	X	
Proteins from *Apis Cerana*	X	X	X	X	X
Honeybee Parasite					
Tropilaelaps mercedesae	X	X	X	X	X
Honeybee Gut Microbiota					
Lactobacillus	X				
Bifidobacterium			X		X
Apibacter		X			
Fungus					
Armillaria Gallica	X	X			
		Fresh	Aged	Fresh	Aged
Plants					
Picea Abie	X	X	X	X	X
Picea Glauca	X		X		
Picea Sitchensis	X		X	X	X
Pinus Bankiana		X	X	X	X
Pinus Contorta		X	X	X	X
Pinus Desiflora		X	X	X	X
Cannabis Sativa		X	X		
Panax Ginseng			X	X	X
Ginko Biloba		X			X

Table 51– Protein identifications in the Paestum residue and honeycombs

[394] Snowdon and Cliver 1996.

5.6.5 The interaction of the Paestum residue with the Copper Vessel

A sample of the surface of the Paestum residue which contained three different colours (orange, green and black) was analysed by XPS. The survey scans obtained for each area are included in Figure 127 alongside the elemental percentages. Copper was identified only in the black and green areas of the sample.

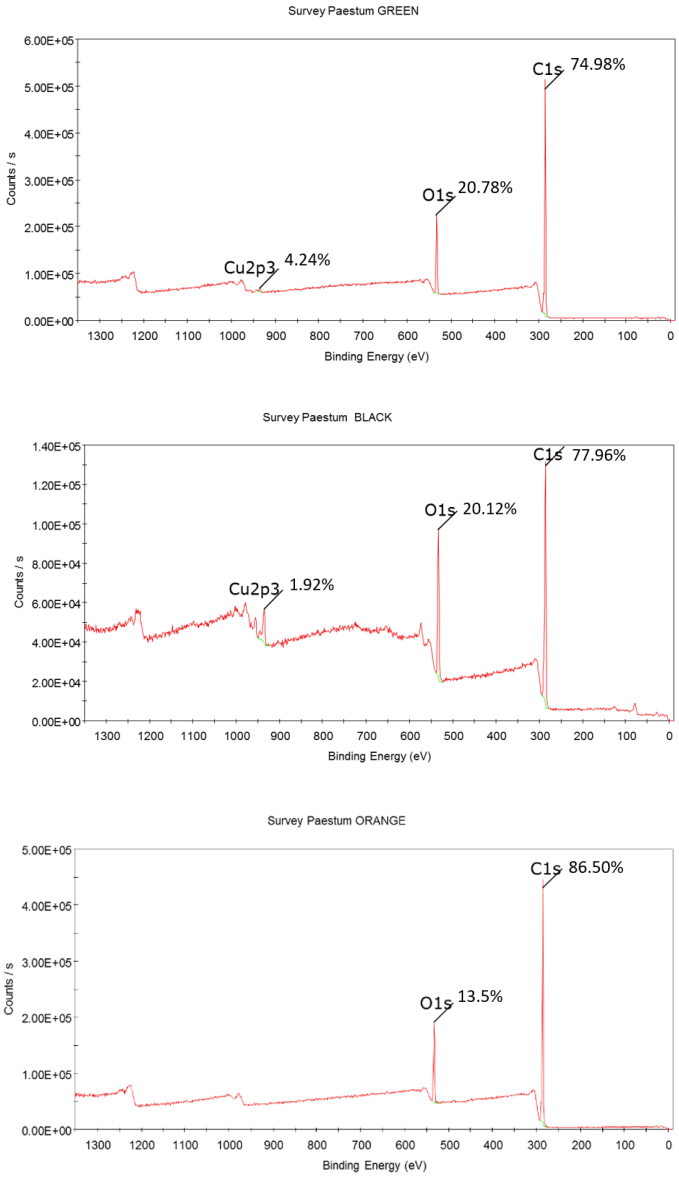


Figure 127– XPS survey spectra for the coloured surface of the residue

As discussed in Chapter 4, XPS analysis can reveal the state of oxidation of copper by the presence or absence of satellite peaks in the Cu2p scan. Satellite peaks are present in the Cu2p scan of the green area of the Paestum residue indicating a 2+ state of oxidation for copper in this area. The Cu2p scan of the black area of the Paestum residue does not contain satellite peaks thus indicating that copper is present at +1 state of oxidation (Figure 128).

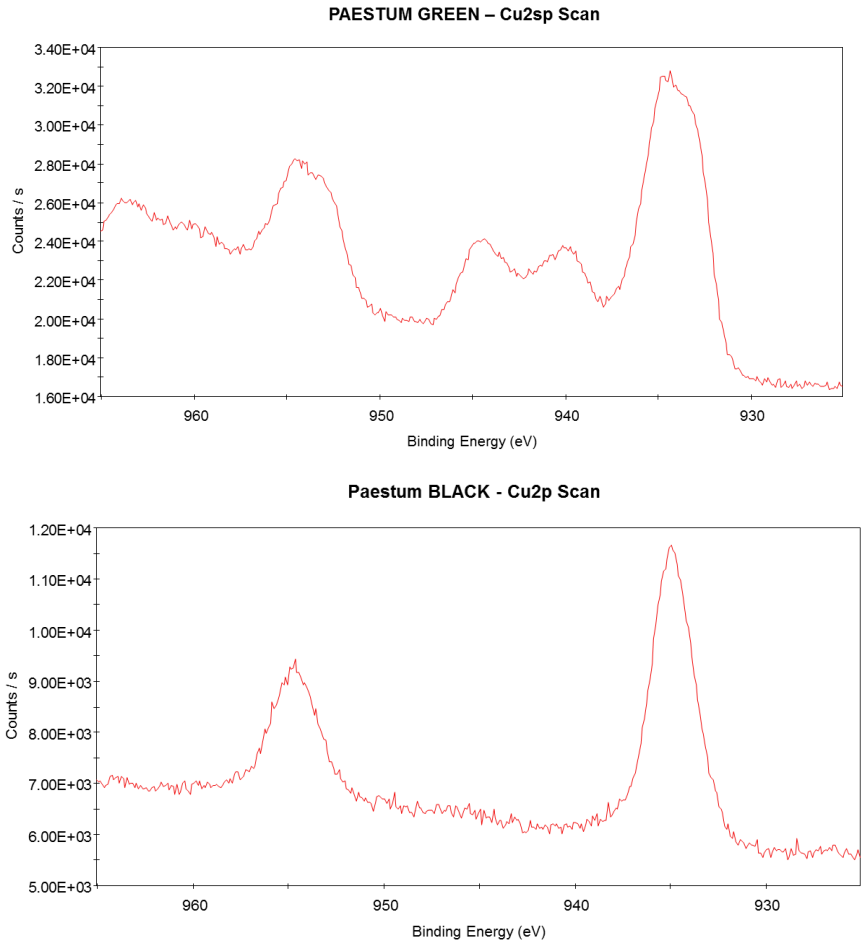


Figure 128 - Cu2p spectra of green and black areas of the Paestum residue

The state of oxidation of copper ions can act as a proxy for the presence or absence of reducing monosaccharides (e.g. glucose and fructose). Figure 129 shows the relative abundance of glucose in the aged honeycombs and Paestum residue samples obtained by IC-MS. There is a marked difference between the aged honeycombs and the aged honeycombs with copper, not surprising given the green colour of the latter, which indicates the presence of Cu(II) ions as seen in the XPS of the Paestum residue. The glucose abundance in the Paestum residue, albeit much reduced in comparison to the honeycomb samples, also differs. The highest abundance is seen in the Paestum black sample which is also richer in sugar derivatives compounds.

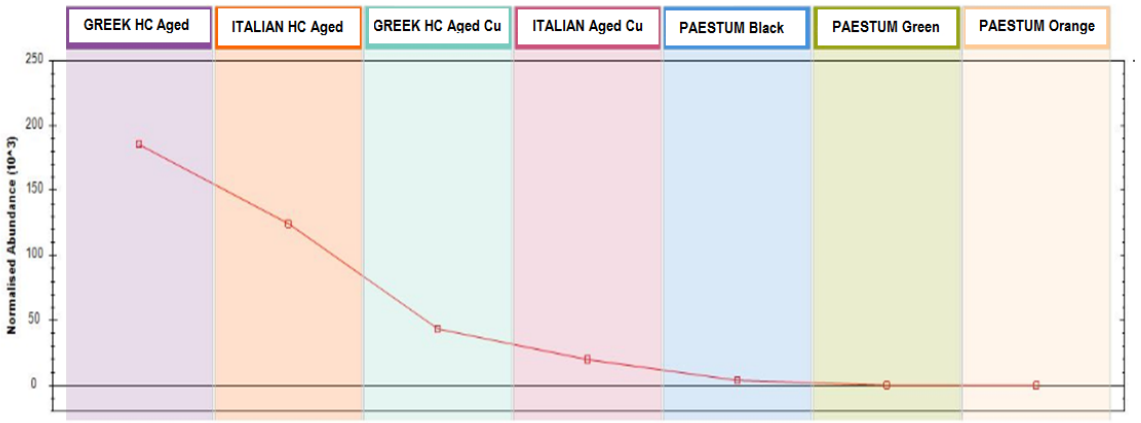


Figure 129 – Glucose abundance in the methanol extracts of aged honeycombs and residue

5.6.6 Discussion

The aim of this investigation was to see if honey was present in the Paestum residue. A range of techniques were used to characterize the residue initially targeting carbohydrates and its derivatives. It has been demonstrated that the Paestum residue contained carbohydrates, evidenced by the presence of glucose/fructose and its derivatives

alongside recognized honeybee metabolites. There is a correlation between the state of oxidation of copper ions on the surface of the residue and carbohydrates which would require further investigation.

Experiments with honeycomb failed to mimic the acid profile of the Paestum residue. One possibility is that the Paestum residue was composed of honey mixed with other substances rich in fatty acids such as resins. Another possibility is that the acid content in the residue has a bacterial origin. The source of some acids including free carboxylic acids in fresh and stored honey are due to the activity of lactic acid bacteria. The proteomics results presented here support the presence of honey in the Paestum residue.

Further investigation of the residue's microbiota is planned to further characterize the various strains and their metabolites as the *Lactobacillus* strains found in the residue are not amongst those associated with long-chain carboxylic acid production studied by Olofsson et al. 2014b. It can be hypothesized that the sugars in honey would have supported the various bacterial colonies, but the residue's increased acidity (resulting from the bacterial metabolites) favours certain types of bacterial colonies over others. Once sugar is no longer available, bacterial colonies would have to rely on beeswax as a source of carbon, which in turn would support bacterial strains containing specific enzymes able to catabolize wax esters into fatty acids.[395] Further bacterial characterization of the Paestum residue is planned to characterize its bacterial colonies.

[395] Downs et al. 2002; Kalscheuer and Steinbuchel 2003; Sakr et al. 2013; Barcus et al. 2017; Miller et al. 2020.

6. Conclusion

The aim of this research has been to demonstrate copper corrosion's potential for preserving residues of substances used in the past. Traditionally, metal corrosion has been considered a mixture of inorganic compounds, resulting from the oxidation of the metal surface by substances in the depositional environment. Although conservators routinely find macro-organic remains (e.g. textiles and wood) of historical importance amidst corrosion products covering archaeological copper objects, this medium is seldom considered a locus for preservation of micro-organic residues of historical importance. In this thesis, the preservation of organic molecules in copper corrosion via metal complexation has been investigated and a new multi-analytical protocol has been developed and tested on archaeological copper corrosion to illustrate the different types of information retrievable from copper corrosion. It has also been demonstrated that microbes may play a bigger role than originally anticipated in shaping the composition of organic molecules preserved in copper corrosion and the importance of excavation and conservation records for the interpretation of the laboratory results.

6.1 A pathway for organic residue preservation in copper corrosion

In order to test copper complexation with organic molecules, a series of electrochemical experiments were performed where an anodic current was applied on copper coupons immersed in electrolytes of varying compositions. Firstly, copper coupons were exposed to chloride and carbonate ions in deionized water, which yielded a deposit on the (+)

coupon identified as cuprite, tenorite and malachite. In the second experiment, palmitic acid (previously dissolved in methanol) was added to the electrolyte and the resulting corrosion deposit identified as cuprite, atacamite and copper palmitate. These results indicate that copper ions could readily react with organic or inorganic ligands in the same medium, thus suggesting that a mechanism for preservation of organic residues within copper corrosion would include metal organic complexation.

The third set of experiments comprised the corrosion of copper in the presence of bovine milk, red wine and white wine. To aid characterization of the resulting corrosion products an electrochemical setup was used to create a library of copper organic complexes standards. This was done by corroding copper in the presence of organic compounds containing potential sites for copper chelation. Deposits on (+) coupons were obtained from fatty acids (palmitic, stearic, oleic and linoleic acids), carbohydrate (lactose) and protein (casein) which were characterized by a range of analytical techniques.

Cu(II) ions were identified in all copper-organic complexes but the site of complexation between the metal and organic ligand could only be ascertained for copper-carboxylates. Most copper-organic complexes resulted in amorphous substances and thus did not yield a powder XRD diffractogram. This is an important result as unless copper-organic complexes are crystalline they cannot be identified in archaeological metal corrosion by the most popular technique used for their characterization.

During mass spectrometry characterization, it was identified that the copper-organic complexes had a limited solubility in chloroform and methanol, common solvents used for organic residue analysis. This is an important result as the low solubility of copper-organic complexes in these solvents perhaps explains the low yields obtained by traditional extraction protocols compared to those containing solvent modifiers (e.g. acid or supercritical extraction) or metal chelating agents.

A QTOF-GC-MS with TSP method was developed to confirm the presence of the organic ligand in the copper-organic complexes as an alternative to solvent extraction. All carboxylate ligands were recovered intact except for linoleate, which also yielded azelaic acid due to oxidative cleavage. The chromatograms of copper-lactose and copper-casein were expectedly more complex than those of lactose and casein as copper ions catalysed the decomposition of the organic ligands. Notwithstanding this drawback three characteristic thermal decomposition compounds of carbohydrates were identified in lactose/Cu-lactose chromatograms. For casein/Cu-casein, the only common compound identified was indole which is characteristic of the thermal decomposition of proteins.

The copper-casein complex was also characterized via proteomics, using casein as a control. More peptides were recovered from casein than from copper-casein which was anticipated as the extraction method did not contain a chelating agent. However, the peptides recovered from copper-casein were present in sufficiently high intensity to enable a positive protein matches to caseins in bovine milk using Uniprot database.

The electrochemical experiments were intended to test the viability of copper-organic complexation as an alternative pathway for organic residue preservation by metals to encapsulation by inorganic corrosion products. The results presented indicate that copper ions would coordinate with carboxylic acids present in a mixed medium. Further experiments should be conducted to establish the various reaction parameters, in the same way as those that exist for inorganic ligands.

The results of the characterization of copper-organic complexes presented also complement the existing research in the field of cultural heritage which has so far focused on copper soaps.

6.2 Proposing a new multi-analytical protocol for characterization of copper corrosion

A new multi-analytical protocol for characterization of copper corrosion using powder X-ray Diffraction, FTIR and QTOF-GC-MS with TSP was developed. The protocol enables the identification of inorganic compounds and small and large organic molecules. XRD and FTIR are low-cost techniques available in large museum laboratories. QTOF-GC-MS with TSP has the advantage of low sample requirements (1-3mg), untargeted analyses with identification of compounds via EI fragmentation using the NIST library, and recovery of organics bound to copper ions.

The new multi-analytical protocol was developed through the characterization of copper-milk corrosion using freeze-dried milk as a control and validated with archaeological samples. The range of techniques evaluated originally included Raman, XPS and chloroform/methanol followed by BSTFA derivatization with GC-MS. There were only minor differences between the FTIR spectra of freeze-dried milk and copper-milk corrosion, the characteristic COO^- stretch of copper-carboxylates possibly masked by the broad C=O amide band. The Raman spectrum of copper-milk corrosion contains an extra band and lower fluorescence than freeze-dried milk, perhaps indicating Cu-O complexation. Analysis by XPS confirmed the presence of Cu(II) ions in copper-milk corrosion and carbon and oxygen binding energies similar to those found in palmitic acid, lactose, copper-lactose and casein. It was not possible to obtain a powder diffractogram from the copper-milk corrosion because of its waxy consistency.

The characterization of copper-milk corrosion by QTOF-GC-MS with TSP presented advantages over solvent extraction. Firstly, the new method was able to recover a wider range of carboxylic acids, all of which matched those obtained from freeze-dried milk. Secondly, carbohydrates and protein could be identified via thermal decomposition products as those obtained for copper-lactose and copper-casein. Further characterization of copper-milk corrosion and freeze-dried milk by proteomics yielded similar results.

After excluding Raman and chloroform-methanol with BSTFA derivatization, the multi-analytical protocol was tested on archaeological copper corrosion. During these analyses,

an opportunity arose to include analyses by IC-MS following a protocol used in metabolomics research.

6.3 Evaluating the type of information retrieved from archaeological samples

Beyond lipids, the range of organic compounds recoverable by QTOF-GC-MS with TSP includes polycyclic aromatics, carbohydrates (and derivatives), alkyl nitriles and amides, plasticizers, and others. Small organic molecules were recovered by IC-MS and proteins (via peptides) recovered by protein analysis.

In Case Study 1 – Pewsey Hoard, the information retrieved from the corrosion products included biomarkers from substances used in the past and reflected different microclimates within the deposition environment. Intense microbial activity was identified in an area protected from soil contamination, which could support the hypothesis that compounds routinely considered modern contaminants (cholesterol from handling and plasticizers from packaging) may have a bacterial origin. Complex bacterial colonies were characterized by proteomics, inorganic and organic metabolites and a terpenoid resin marker identified in one of the vessels, validated by resin protein matches for peptides recovered from the same sample.

In Case Study 2 – Roman Bowl, the different techniques in the multi-analytical protocol yielded well-correlated results. The range of molecules identifiable by the QTOF-GC-MS

with TSP method included chlorobenzenes, a modern substance found in pesticides. Although initially surprising the presence of these compounds in the samples is explained by the fact that the object was found in an orchard. The idea that corrosion products are biographical records of the deposition environment (and any changes thereto) is not new, but the evidence has hitherto been recorded via the identification of inorganic compounds. The identification of chlorobenzenes is archaeological corrosion is evidence of how changes in land use and modern developments in agriculture may affect material culture still underground.

Case studies 3-5 are copper vessels recovered from a small tavern in Pompeii. The objects were sampled by conservators at the Ashmolean Museum during their preparation for an exhibition. Most of the corrosion covering the objects was going to be removed and disposed as the aim of the conservation treatment was to reveal as much of the metal substrate as possible.

Case Study 3 - Pompeii INV10653, was the only vessel with a very specific research question: was it used as a chamber pot? Thus, it was possible to tailor the analytical protocol and interpret results within the framework of the types of compounds that could be present given the proposed use and its unique deposition context. Organic compounds that could support the use of the object as a chamber pot were obtained by QTOF-GC-MS with TSP and IC-MS. Of note is the identification of methenamide, a bacterial metabolite that could have been formed by ammonia and formaldehyde (from urine) at

temperatures that could have been achieved during Vesuvius's eruption. Access to the object's excavation report is being sought to further validate the results.

In Case Study 4 - Pompeii INV10295, is a bowl normally used for handwashing that appeared to have been repurposed and which was found in the garden of the taverna. Amongst the samples submitted for analysis was an insect larvae and surrounding corrosion. Protein analysis enabled the identification of the larvae as that of a flesh-eating fly whilst the peptides from the surrounding corrosion matched fish proteins. Biomarkers for animal fat and dairy were also identified supporting the idea that this object had contained mixed food remains sometime before its abandonment, perhaps to feed a pet? The recovery of proteins from this object is an interesting result because it demonstrates that proteins can survive high temperatures and a long period of deposition and used to validate morphological identifications.

Next, it was Case Study 5 – Pompeii INV10289, a type of cauldron used to make stews/casseroles. Milk was identified via lactose and α1 and β-casein proteins and cereal fermentation via yeast proteins and metabolites (only present in the interior samples). Most of the casein matches were from goat as opposed to cow. Although pending validation with controls, these results exemplify the potential of using proteomics to investigate organic residues.

In Case Study 6 – the Paestum Residue, proteomics, metabolomics and lipidomics were combined with spectroscopic techniques to investigate the presence of honey in a 540BC

waxy residue found in a copper alloy vessel. Samples of the residue had previously been characterized as fat, wax or resin given the apparent absence of carbohydrates.

Four grades of biomarkers were identified using honeycombs as controls. The first grade of biomarkers were carbohydrates (and their derivatives) and royal jelly/honeybee proteins. The second grade were honeybee gut microbes and some of their metabolites. The third grade of biomarker was the identification of a honeybee parasite. The final fourth grade of biomarkers were proteins associated with coniferous trees from the natural environment where the honey was produced.

It was also demonstrated that the residue interacted with the container. This interaction manifested itself as coloured stains on the surface of the residue: copper(I) ions and a higher abundancy of carbohydrates (and its derivatives) were detected in a black area whilst copper(II) ions and high acid content were detected in a green area. These findings support the hypothesis that copper(II) ions have a preference for coordinating with acids over other compounds. Because these colours appear to be stratigraphically arranged (with black over green) it can be argued that copper (II) ions were reduced to copper(I) by the carbohydrates in the residue. Although chemical reactions that take place over more than 1,000 years are impossible to replicate, the heating of honeycombs with copper coupons illustrated that food residues will cause the oxidation of copper in the presence of oxygen to form copper carboxylates in a short period of time.

The conditions under which the Paestum residue has been kept since its excavation is not known thus making it susceptible to many sources of contaminants, in particular microbial activity. An attempt to mitigate this was to request a sample from the core area of the residue. Given the specific hypothesis investigated it was possible to combine the characterization of the surface and core of the residue into a narrative underpinned by the honey proteins identified by bottom-up proteomics.

Contamination is a major factor that complicates organic residue analysis in archaeology. In the case of corrosion samples, potential sources of contaminants include the deposition environment (e.g. soil, water), handling of the object during and post-excavation, contact with packaging, conservation treatments applied to the object in the field and contamination introduced during processing of samples in the laboratory.

Many samples analysed in this thesis come from objects with complex stories. It is tempting to disregard the findings presented because of potential contamination and the absence of controls. As an archaeological conservator with a background in analytical chemistry, the author has witnessed many situations where protocols aimed at preserving the scientific potential of finds for organic residue analysis did not exist or were not implemented by field archaeologists or conservators. It is hoped that the diffusion of the contents of this thesis will raise awareness of the potential of metal corrosion products for organic residue analysis. At present, this material is either discarded or its composition changed by the application of corrosion inhibitors or protective coatings thus hindering its study.

6.5 Evaluating the multi-analytical protocol

The initial assumption was that FTIR and XRD could be used as screening techniques. For FTIR, even after suspension in KBr, some samples yielded poorly defined spectra, absence of diagnostic bands for organic compound which were later identified by mass spectrometry or interference from inorganic phases. Based on the results presented the presence or absence of organics in the sample cannot be judged simply based on FTIR spectra. Although FTIR does not work as a screening technique it still gives an overview of the general fingerprint of the most abundant compounds in the sample. In the case of XRD, many samples were not big enough to yield a diffractogram or did not contain crystalline phases that could be identified beyond quartz using the Crystallography Open Database. Despite these shortcomings, FTIR and XRD are relatively cheap analyses and are available in most laboratories.

GC-MS with TSP is often used as screening technique prior to the selection of the best protocol (based on solvents and derivatization agents) in laboratories that conduct organic residue analysis. In this research the advantage of QTOF-GC-MS with TSP over a solvent protocol was its ability to release molecules that may be tightly bound to inorganic matrices and without the need of derivatization. This was demonstrated with the analysis of copper-milk corrosion and in the Case Study 1 where different compounds were identified in the chromatogram of Vessel B sample analysed as a solid and as an evaporated chloroform/methanol extract, which are simpler to analyse. The cost of analysis is also relatively low as there is little sample preparation and compounds can be identified using the NIST library of compounds (via molecular fragmentation and molecular ion). Compound identification can either be confirmed with standards or by

reanalysing the sample in chemical ionization mode. Even though the NIST library contains a range of compounds, assignments are dependent on compounds being present in the library.

This research also demonstrated that XPS (despite interference from inorganic phases), IC-MS and Proteomics are useful techniques that complement the data obtained by QTOF-GC-MS with TSP. Proteomics, despite the laborious sample preparation and peptide validation, allows for a variety of hypothesis to be tested with the same dataset.

Most studies of organic residues in archaeology only characterize samples with mass spectrometry techniques, often GC-MS and stable isotopes. The combination of different analytical techniques allows for the triangulation of different datasets, a more holistic approach to sample characterization.

6.6 Sampling protocols for organic residue analysis in archaeological metal corrosion

The initial sampling strategy was to compare the organic profile of interior versus exterior corrosion, with compounds identified only in the interior likely to be of historical importance. Although a valid approach, it does not account for the different types of corrosion (with different organic profiles) that may exist within the same area of a vessel. Even corrosion products of the same colour have shown to have different organic profiles. Another consideration is sample consistency: often samples described as “soft”

by conservators yielded a greater variety of organic compounds. Perhaps the organics in these samples were present as copper complexes given that most of the copper-organic complexes synthetised as part of this research could also be described as soft. This is an important consideration particularly when sampling objects subject to curatorial constraints.

Regarding contamination of samples, potential sources include deposition, excavation, storage, sampling and analysis. For objects found in soil, it would be tempting to also analyse soil samples to act as potential controls. However, many of the compounds identified in this study are polar and thus mobile in water. Amongst these compounds are bacterial metabolites and proteins which can migrate into and out of the corrosion. Soils also contain a range of microbial colonies which may not necessarily be distinguishable from the microbial colonies found within food residues.

Notwithstanding these considerations, the following sampling protocol is suggested:

- Sample the object and surrounding soil in a dust free environment. Wear gloves, long-sleeved shirts and a mask;
- Remove samples with a degreased metal scalpel
- Submit samples in labelled single use Eppendorf tubes (one sample per tube)
- Place tubes inside a labelled plastic bag together with an annotated picture of the object marking the areas sampled, a short description of the samples (e.g. colour, consistency), reason for sampling and a hypothesis for the identity of the residue

Additional information about the object should also be provided including a summary of excavation and conservation reports and curatorial considerations. Even after disclosure of this information, archaeologists, curators and conservators should be available for consultation during the investigation of the data. To date, only Case Studies 2, 4 and 6 have benefitted from such discussions.

6.7 Understanding the dynamics of organic residue preservation in copper corrosion

The data presented indicates that preservation of organic residues in copper corrosion involves more than encapsulation by inorganic corrosion products. Several types of compounds identified in archaeological copper corrosion appear to be associated with microbial activities, which was unexpected given the toxicity of copper ions. Although the bacterial origin of certain mineral phases identified in archaeological metal corrosion has long been recognized, studies published to date only consider the deposition environment as the source of microbes. As some microbes are habitat-specific, their identification in organic residues (alongside their metabolites) may be used as proxies for materials, plants, animals and environments.

Microbes have started to attract the attention of archaeological scientists. Recent studies of archaeological dental plaque, coprolites (faeces) and soils have been published where microbial populations and their metabolites are used as markers for health and diet, the study of pathogens and parasites, and for the reconstruction of ancient microbial

genomes. Targeting microbes and their metabolites as proxy for substances in the past, alongside the identification of more traditional biomarkers, would be a novel approach to archaeological residue analysis. Copper corrosion may be the ideal locus for such studies by establishing proteomics and metabolomics techniques as part of metal corrosion characterization.

6.6. Potential for future work

There is no doubt that copper corrosion products contain organic molecules, potentially opening a new avenue for organic residue analysis in archaeology. What is required to take this research forward is to:

- analyse freshly-excavated copper alloy objects to limit the effect of post-excavation contamination;
- apply the multi-analytical protocol to different corrosion products (e.g. iron, lead, tin);
- apply the multi-analytical protocol to corrosion products from different burial environments;
- test different proteomics methods and gain a better understanding of how proteomics databases work in terms of the attribution of taxa.

A complementary line of investigations could focus on the recovery of bacterial biofilms from archaeological copper objects. Biofilms can acquire additional physical and

chemical characteristics over and above those inherent to the bacterial colonies including resistance to toxic metal ions via strategies that include chelation. This type of research would require background experiments perhaps using copper coupons exposed to different bacterial colonies to measure how these colonies are affected by changes humidity.

Organic residue analysis in archaeological metal corrosion will probably take a different route to that of porous ceramics for which there are standard protocols. Because of the complexity of corrosion processes, organic residue analysis in archaeological metal corrosion may have to be question oriented, each question demanding a specific set of analytical approaches.

7. Bibliography

Alaimo, M. H., Farrell Jr, H. M. and Germann, M. W. (1999). Protein Structure and Molecular Enzymology. *Biochimica et Biophysica Acta*, 1431(2), 410-420. DOI:10.1016/S0167-4838(99)00061-8

Alberghina, M. F., Barraco, R., Brai, M., Schillaci, T. and Tranchina, L. (2011) Integrated analytical methodologies for the study of corrosion processes in archaeological bronzes. *Spectrochimica Acta Part B Atomic Spectroscopy*. 66:129-37. DOI: 10.1016/j.sab.2010.12.010

Alfantazi, A. M., Ahmed, T. M. and Tromans, D. (2009). Corrosion behaviour of copper alloys in chloride media. *Materials in Engineering*, 30(7), 2425-2430. DOI:10.1016/j.matdes.2008.10.015

Allaby, M. (2020). *A Dictionary of Zoology*. 5th ed. Oxford University Press

Altinoz, M. A., Ozpinar, A., Ozpinar, A., Perez, J. L. and Elmaci, İ. (2019). Methenamine's journey of 160 years: Repurposal of an old urinary antiseptic for treatment and hypoxic radiosensitization of cancers and glioblastoma. *Clinical and experimental pharmacology & physiology*, 46(5), 407-412. DOI:10.1111/1440-1681.13070

Altun, Y. and Köseoğlu, F. (2005). Stability of Copper(II), Nickel(II) and Zinc(II) Binary and Ternary Complexes of Histidine, Histamine and Glycine in Aqueous Solution. *Journal of Solution Chemistry*, 34, 213-231. DOI:10.1007/s10953-005-2763-7

Alvarez-Vasquez, F., Riezman, H., Hannun, Y. A. and Voit, E. O. (2011). Mathematical Modeling and Validation of the Ergosterol Pathway in Saccharomyces cerevisiae (Ergosterol Pathway Mathematical Modeling in Yeast). *PLoS ONE*, 6(12). DOI:10.1371/journal.pone.0028344

Angiorama, C. I., Campeny, S. M. L. L. and Taboada, C. (2020). Exceptional cases of textile mineralization in archaeological metallic objects from Santiago del Estero's lowlands (Argentina). *Journal of Archaeological Science: Reports*, 33. DOI:10.1016/j.jasrep.2020.102478

Annweiler, E., Materna, A., Safinowski, M., Kappler, A., Richnow, H. H., Michaelis, W. and Meckenstock, R. U. (2000). Anaerobic degradation of 2-methylnaphthalene by a sulfate-reducing enrichment culture. *Applied and environmental microbiology*, 66(12), 5329-5333. DOI:10.1128/AEM.66.12.5329-5333.2000

Asomaning, J., Mussone, P. and Bressler, D. C. (2014). Pyrolysis of polyunsaturated fatty acids. *Fuel Processing Technology*, 120, 89-95. DOI:10.1016/j.fuproc.2013.12.007

Aucouturier, M. and Darque-Ceretti, E. (2007). The surface of cultural heritage artefacts: physicochemical investigations for their knowledge and their conservation. *Chemical Society Reviews*, 36(10), 1605-1621. DOI:10.1039/b605304c

Aucouturier, M., Mathis, F., Robcis, D., Castaing, J., Salomon, J., Pichon, L., . . . Descamp, S. (2010). Intentional patina of metal archaeological artefacts: non-destructive investigation of Egyptian and Roman museum treasures. In: Dillmann, P. (ed.), *Corrosion Engineering, Science and Technology*. 45, 314-321

Ayala, A., Muñoz, M. F. and Argüelles, S. (2014). Lipid Peroxidation: Production, Metabolism, and Signalling Mechanisms of Malondialdehyde and 4-Hydroxy-2-Nonena. *Oxidative Medicine and Cellular Longevity*,360438. DOI:10.1155/2014/360438

Babu, B. and Wu, J. (2010). Production of phthalate esters by nuisance freshwater algae and cyanobacteria. *The Science of the total environment*, 408(21), 4969-4975. DOI:10.1016/j.scitotenv.2010.07.032

Baek, S., Field, R., Goldstone, M., Kirk, P., Lester, J. and Perry, R. (1991). A review of atmospheric polycyclic aromatic hydrocarbons: Sources, fate and behavior. Water, Air, and Soil Pollution, 60(3), 279-300. DOI:10.1007/BF00282628

Baer, D. R., Engelhard, M. H. and Lea, A. S. (2003). Introduction to Surface Science Spectra data on electron and x-ray damage: Sample degradation during XPS and AES measurements. *Surface Science Spectra*, 10(1), 47-56. DOI:10.1116/11.20040199

Baeten, J., Deforce, K., Challe, S., De Vos, D. and Degryse, P. (2014). Holy Smoke in Medieval Funerary Rites: Chemical Fingerprints of Frankincense in Southern Belgian Incense Burners. *PLoS ONE*, 9(11). DOI:10.1371/journal.pone.0113142

Baffoni, L., Gaggìa, F., Alberoni, D., Cabbri, R., Nanetti, A., Biavati, B. and Di Gioia, D. (2016). Effect of dietary supplementation of *Bifidobacterium* and *Lactobacillus* strains in *Apis*. *Beneficial Microbes*, 7, 45–51. DOI:10.3920/BM2015.0085

Bal, W., Sokołowska, M., Kurowska, E. and Faller, P. (2013). Binding of transition metal ions to albumin: Sites, affinities and rates. *Biochimica et Biophysica Acta*, 1830, 5444-5455. DOI:10.1016/j.bbagen.2013.06.018

Barcus, M., Mizrachi, D. and Lei, X. G. (2017). Identification and kinetics characterization of a wax ester hydrolase from a feather-degrading actinomycete. *bioRxiv*. DOI:10.1101/178673

Barnard, H., Ambrose, S. H., Beehr, D. E., Forster, M. D., Lanehart, R. E., Malainey, M.E., Parr, R.E., Rider, M., Solazzo, C. and Yohe, R. M. (2007). Mixed results of seven methods for organic residue analysis applied to one vessel with the residue of a known foodstuff. *Journal of Archaeological Science*. 34(1):28-37. DOI: 10.1016/j.jas.2006.03.010

Barker, H. S., Snyder, J. W., Hicks, A. B., Yanoviak, S. P., Southern, P., Dhakal, B. K., . . . Couturier, M. R. (2014). First case reports of Ignatzschineria (Schineria) indica associated with myiasis. *Journal of Clinical Microbiology*, 52(12), 4432-4434. DOI:10.1128/JCM.02183-14

Battat, E., Peleg, Y., Bercovitz, A., Rokem, J. S. and Goldberg, I. (1991). Optimization of L-malic acid production by Aspergillus flavus in a stirred fermentor. *Biotechnology and bioengineering*, 37(11), 1108-1116.

Bender, D. A. (2014). Maltitol. In *A Dictionary of Food and Nutrition* (4th ed.): Oxford University Press.

Bent, D. V. and Hayon, E. (1975). Excited state chemistry of aromatic amino acids and related peptides. III. Tryptophan. *Journal of the American Chemical Society*, 97(10), 2612-2619. DOI:10.1021/ja00843a004

Bentsen, S. E. (2012). Size matters: Preliminary results from an experimental approach to interpret Middle Stone Age hearths. *Quaternary International*, 270, 95-102. DOI:10.1016/j.quaint.2011.09.002.

Benzonelli, A., Freestone, I. C. and Martinón-Torres, M. (2017). A Better Shade of Black: Effects of Manufacturing Parameters on the Development of Ancient Black Bronzes. *Archaeometry*, 59(6), 1034-1049. DOI:10.1111/arcm.12299

Berger, D. (2015). Artificial patination in Early Iron Age Europe: an analytical case study of a unique bronze artefact. *Journal of Archaeological Science*, 57, 130-141. DOI:10.1016/j.jas.2015.01.025

Bethell, P. H., Ottaway, J., Campbell, G., Goad, L. J. and Evershed, R. P. (1994). The study of molecular markers of human activity: the use of coprostanol in the soil as an indicator of human faecal material. *Journal of Archaeological Science*, 21, 619-632. DOI:10.1006/jasc.1994.1061

Bianchi, G. and Longhi, P. (1973). Copper in seawater, potential-ph diagrams. *Corrosion Science*, 13(11), 853-864. DOI:10.1016/S0010-938X(73)80067-8

Biersm, W. R. and McGovern, P. E. (1990). Organic Contents of Ancient Vessels: Materials Analysis and Archaeological Investigation. *MASCA Research Papers in Science and Archaeology*, 7.

Billiet, A., Meeus, I., Van Nieuwerburgh, F., Deforce, D., Wäckers, F. and Smagghe, G. (2017). Colony contact contributes to the diversity of gut bacteria in bumblebees (*Bombus terrestris*). *Insect Science*, 24(2), 270-277. DOI:10.1111/1744-7917.12284

Boarelli, M. C., Biedermann, M., Peier, M., Fiorini, D. and Grob, K. (2020). Ergosterol as a marker for the use of degraded olives in the production of olive oil. *Food Control*, 112. DOI:10.1016/j.foodcont.2020.107136

Boëda, E., Connan, J., Dessort, D., Muhesen, S., Mercier, N., Valladas, H. and Tisnerart, N. (1996). Bitumen as a hafting material on Middle Palaeolithic artifacts. *Nature*, 380, 336-338. DOI:10.1038/380336a0

Bonaduce, I. and Colombini, M. P. (2004). Characterisation of beeswax in works of art by gas chromatography-mass spectrometry and pyrolysis-gas chromatography-mass spectrometry procedures. *Journal of Chromatography A*, 1028, 297-306. DOI:10.1016/j.chroma.2003.11.086

Boon, J. J., Hoogland, F. and Keune, K. (2007). Chemical processes in aged oil paints affecting metal soap migration and aggregation. In Parkin, M. (ed.) *AIC Paintings Specialty Group Postprints, Providence, Rhode Island, 16-19 June 2006*, 16-23. Rhode Island: AIC

Borkow, G. and Gabbay, J. (2005). Copper as a Biocidal Tool. *Current Medicinal Chemistry*, 12(18), 2163-2175. DOI:10.2174/0929867054637617

Born, H. (1993). 2 - Multi-coloured antique bronze statues. In La Niece, S. and Craddock, P. T. (eds) *Metal Plating and Patination: Cultural, Technical and Historical Developments*, 19-29, Oxford: Butterworth-Heinemann

Bostock, J. (Translator) (1855). Book XXXIV - The History of Metals (J. Bostock, Trans.). In *Pliny the Elder - The Natural History*. London: Taylor and Francis.

Braadbaart, F. and Poole, I. (2008). Morphological, chemical and physical changes during charcoalification of wood and its relevance to archaeological contexts. *Journal of Archaeological Science*, 35(9), 2434-2445. DOI:10.1016/j.jas.2008.03.016

Braadbaart, F., Poole, I., Huisman, H. D. J. and van Os, B. (2012). Fuel, Fire and Heat: an experimental approach to highlight the potential of studying ash and char remains from archaeological contexts. *Journal of Archaeological Science*, 39(4), 836-847. DOI:10.1016/j.jas.2011.10.009.

Brahushi, F., O., K. F., Song, Y., Jiang, X., Munch, J. C. and Wang, F. (2017). Fate Processes of Chlorobenzenes in Soil and Potential Remediation Strategies: A Review. *Pedosphere*, 27(3), 407-420. DOI:10.1016/S1002-0160(17)60338-2

Brettell, R., Martin, W., Atherton-Woolham, S., Stern, B. and McKnight, L. (2017). Organic residue analysis of Egyptian votive mummies and their research potential. *Studies in Conservation*, 62(2), 68-82. DOI:10.1179/2047058415Y.0000000027

Brown, K. and Brown, T. A. (2011). *Biomolecular Archaeology: An Introduction*. Singapore: Wiley-Blackwell.

Brühl, L. (2014). Fatty acid alterations in oils and fats during heating and frying. European *Journal of Lipid Science and Technology*, 116(6), 707-715. DOI:10.1002/ejlt.v116.6/issuetoc

Bruni, S. and Guglielmi, V. (2014). Identification of archaeological triterpenic resins by the non-separative techniques FTIR and 13C NMR: The case of Pistacia resin (mastic) in comparison with frankincense. *Spectrochimica Acta Part A: Molecular and Biomolecular Spectroscopy*, 121, 613-622. DOI:10.1016/j.saa.2013.10.098

Buckley, S. A. and Evershed, R. P. (2001). Organic chemistry of embalming agents in Pharaonic and Graeco-Roman mummies. *Nature*, 413, 837-841. DOI:10.1038/35101588

Buckley, S. A., Stott, A. W. and Evershed, R. P. (1999). Studies of organic residues from ancient Egyptian mummies using high temperature-gas chromatography-mass spectrometry and sequential thermal desorption-gas chromatography-mass spectrometry and pyrolysis-gas chromatography-mass spectrometry. *Analyst*, 124(4), 443-452. DOI:10.1039/A809022J

Burmester, A. and Koller, J. (1987). Known and new corrosion products on bronzes: their identification and assessment, particularly in relation to organic protective coatings. In: Black, J. (ed.). *Recent advances in the conservation and analysis of artifacts : jubilee conservation conference papers.* University of London. Institute of Archaeology: London: Summer Schools Press; 1987. 97-104.

Cagan, A., Theunert, C., Laayouni, H., Santpere, G., Pybus, M., Casals, F., . . . Andrés, A. M. (2016). Natural Selection in the Great Apes. *Molecular Biology and Evolution*, 33(12), 3268-3283. DOI:10.1093/molbev/msw215 %

Cai, J., Wang, S. and Su, Q. (2008). Analysis of Polycyclic Aromatic Hydrocarbons Formed During Off-Line Pyrolysis of Ergosterol by GC–MS–SIM. *Chromatographia*, 68(5), 357-363. DOI:10.1365/s10337-008-0720-5

Calam, C. T., Oxford, A. E. and Raistrick, H. (1939). Studies in the biochemistry of micro-organisms: Itaconic acid, a metabolic product of a strain of *Aspergillus terreus Thom*. *The Biochemical Journal*, 33(9), 1488-1495.

Carrer, F., Colonese, A. C., Lucquin, A., Petersen Guedes, E., Thompson, A., Walsh, K., . . . Craig, O. E. (2016). Chemical Analysis of Pottery Demonstrates Prehistoric Origin for High-Altitude Alpine Dairying. *PLoS ONE*, 11(4), e0151442 -e0151442. DOI:10.1371/journal.pone.0151442

Carvajal Arroyo, J. M., Candry, P., Andersen, S. J., Props, R., Seviour, T., Ganigué, R. and Rabaey, K. (2019). Granular fermentation enables high rate caproic acid production from solid-free thin stillage. *Green Chemistry*. DOIi:10.10.9/c8gc03648a

Casadio, F., Keune, K., Noble, P., Loon, A. v., Hendriks, E., Centeno, S. A. and Osmond, G. (2019). *Metal soaps in art : conservation and research*, Cham, Switzerland: Springer.

Casaletto, M. P., Ingo, G. M., Albini, M., Lapenna, A., Pierige, I., Riccucci, C. and Faraldi, F. (2010). An integrated analytical characterization of corrosion products on ornamental objects from the necropolis of Colle Badetta-Tortoreto (Teramo, Italy). *Applied Physics A: Materials Science & Processing*, 100(3), 801-808. DOI:10.1007/s00339-010-5675-3

Castro-Vázquez, L., Diaz-Maroto, M. C., González-Vinas, M. A., De la Fuente, E. and Pérez-Coello, M. S. (2008). Influence of Storage Conditions on Chemical Composition and Sensory Properties of Citrus Honey. *Journal of Agricultural and Food Chemistry*, 56, 1999-2006. DOI:10.1021/jf072227k

Charters, S., Evershed, R. P., Goad, L. J., Blinkhorn, P. W. and Denham, V. (1993). Quantification and distribution of lipid in archaeological ceramics: implications for sampling potsherds for organic residue analysis. *Archaeometry*, 35, 211-223. DOI:10.1111/j.1475-4754.1993.tb01036.x

Charters, S., Evershed, R. P., Blinkhorn, P. W. and Denham, V. (1995). Evidence for the mixing of fat and wax in archaeological ceramics. *Archaeometry*, 37, 113-127. DOI:10.1111/j.1475-4754.1995.tb00730.x

Charters, S., Evershed, R. P., Quye, A., Blinkhorn, P. W. and Reeves, V. (1997). Simulation experiments for determining the use of ancient pottery vessels: the behavior of epicuticular leaf wax during boiling of a leafy vegetable. *Journal of Archaeological Science*, 24, 1-7. DOI:10.1006/jasc.1995.0091

Chen, H. L., Jakes, K. A. and Foreman, D. W. (1998). Preservation of Archaeological Textiles Through Fibre Mineralization. *Journal of Archaeological Science*, 25, 1015–1021. DOI:10.1006/jasc.1997.0286

Chen, Y. and Barkley, M. D. (1998). Toward Understanding Tryptophan Fluorescence in Proteins. *Biochemistry*, 37(28), 9976–9982. DOI:10.1021/bi980274n

Cheng, W., Liu, G., Wang, L. and Liu, Z. (2017). Glycidyl Fatty Acid Esters in Refined Edible Oils: A Review on Formation, Occurrence, Analysis, and Elimination Methods. Comprehensive *Reviews in Food Science and Food Safety*, 16(2), 263-281. DOI:10.1111/1541-4337.12251

Cioni, R., Gurioli, L., Lanza, R. and Zanella, E. (2004). Temperatures of the A.D. 79 pyroclastic density current deposits (Vesuvius, Italy). *Journal of Geophysical Research: Solid Earth*, 109(B2). DOI:10.1029/2002JB002251

Cížová, K., Vizárová, K., Ház, A., Vykydalová, A., Cibulkováb, Z. and Šimon, P. (2019). Study of the degradation of beeswax taken from a real artefact. *Journal of Cultural Heritage*, 37, 103-112. DOI:10.1016/j.culher.2018.04.020

Clot, P., Tabone, M., Aricò, S. and Albano, E. (1994). Monitoring oxidative damage in patients with liver cirrhosis and different daily alcohol intake. *Gut*, 35(11), 1637 - 1643. DOI:10.1136/gut.35.11.1637

Colombini, M. P., Giachi, G., Modugno, F., Pallecchi, P. and Ribechini, E. (2003). The characterization of paints and waterproofing materials from the shipwrecks found at the archaeological site of the Etruscan and Roman harbour of Pisa (Italy). *Archaeometry*, 45(4), 659-674. DOI:10.1046/j.1475-4754.2003.00135.x

Colombini, M. P., Giachi, G., Modugno, F. and Ribechini, E. (2005). Characterisation of organic residues in pottery vessels of the Roman age from Antinoe (Egypt). *Microchemical Journal*, 79(1), 83-90. DOI:10.1016/j.microc.2004.05.004

Colombini, M. P. and Modugno, F. (2009). *Organic mass spectrometry in art and archaeology*. Oxford: Wiley-Blackwell.

Colombini, M. P., Modugno, F. and Ribechini, E. (2005). Direct exposure electron ionization mass spectrometry and gas chromatography/mass spectrometry techniques to study organic coatings on archaeological amphorae. *Journal of Mass Spectrometry*, 40(5), 675-687. DOI:10.1002/jms.841

Colombini, M. P., Modugno, F., Silvano, F. and Onor, M. (2000). Characterization of the balm of an Egyptian mummy from the seventh century B.C. *Studies in Conservation*, 45, 19-29. DOI:10.1179/sic.2000.45.1.19

Condamin, J., Formenti, F., Metais, M. O., Michel, M. and Blond, P. (1976). The application of gas chromatography to the tracing of oil in ancient amphorae. *Archaeometry*, 18(2), 195-201. DOI:10.1111/j.1475-4754.1976.tb00160.x

Connan, J. and Nissenbaum, A. (2003). Conifer tar on the keel and hull planking of the Ma'agan Mikhael Ship (Israel, 5th century BC): identification and comparison with natural products and artefacts employed in boat construction. *Journal of Archaeological Science*, 30, 709-719. DOI:10.1016/S0305-4403(02)00243-1

Connan, J., Nissenbaum, A. and Dessort, D. (1992). Molecular archaeology: export of Dead Sea asphalts to Canaan and Egypt in the Chalcolithic—Early Bronze Age (4th–3rd millennium BC). *Geochimica et Cosmochimica Acta*, 56, 2743-2759. DOI:10.1016/0016-7037(92)90357-O

Copley, M. S., Berstan, R., Dudd, S. N., Docherty, G., Mukherjee, A. J., Straker, V., . . . Evershed, R. P. (2003). Direct chemical evidence for widespread dairying in prehistoric Britain. *Proceedings of the National Academy of Sciences*, 100, 1524-1529. DOI:10.1073/pnas.0335955100

Corbeil, M. C. and Robinet, L. (2002). X-ray powder diffraction data for selected metal soaps. *Powder Diffraction*, 17(1), 52-60. DOI:10.1154/1.1431950

Correa-ascencio, M. and Evershed, R. P. (2014). High throughput screening of organic residues in archaeological potsherds using direct acidified methanol extraction. *Analytical Methods*, 6(5):1330-40. DOI: 10.1039/c3ay41678j

Costa, M., Rego, A., Ramos, V. Afonso, T. B., Freitas, S., Preto, M., Lopes, V., Vasconcelos, V., Magalhães, C. and Leão, P. N. (2016). The conifer biomarkers dehydroabietic and abietic acids are widespread in Cyanobacteria. *Scientific Reports*, 6: 23436. DOI: 10.1038/srep23436

Cotte, M., Checroun, E., De Nold, W., Taniguchi, Y., De Viguerie, L., Burghammer, M., . . . Susini, J. (2017). Lead soaps in paintings: Friends or foes? *Studies in Conservation*, 62(1), 2-23. DOI:10.1080/00393630.2016.1232529

Craddock, P. and Giumlia-Mair, A. (1993a). Chapter 3 - Beauty is skin deep: evidence for the original appearance of classical statuary. In La Niece, S. and Craddock, P. T. (eds) *Metal Plating and Patination: Cultural, Technical and Historical Developments*, 30-38, Oxford: Butterworth-Heinemann

Craddock, P. and Giumlia-Mair, A. (1993b). Chapter 9 - śmn-Km, Corinthian bronze, shakudo: black-patinated bronze in the ancient world. In La Niece, S. and Craddock, P. T. (eds.), *Metal Plating and Patination*: *Cultural, Technical and Historical Developments,* 101-127, Oxford: Butterworth-Heinemann.

Craig, O. E., Mulville, J., Pearson, M. P., Sokol, R., Gelsthorpe, K., Stacey, R. and Collins, M. (2000). Detecting milk proteins in ancient pots. *Nature*, 408, 312. DOI:10.1038/35042684

Craig, O. E., Chapman, J., Heron, C., Willis, L. H., Bartosiewicz, L., Taylor, G., . . . Collins, M. (2005). Did the first farmers of central and eastern Europe produce dairy foods? *Antiquity*, 79(306), 882-894. DOI:10.1017/S0003598X00115017

Craig, O. E., Forster, M., Andersen, S.H., Koch, E., Crombe, P., Milner, N. J., Stern, B., Bailey, G. N. and Heron, C. P. (2007). Molecular and isotopic demonstration of the processing of aquatic products in northern European prehistoric pottery. *Archaeometry*, 49 (1), 135-52. DOI: 10.1111/j.1475-4754.2007.00292.x.

Craig, O. E., Saul, H., Lucquin, A., Nishida, Y., Taché, L., Clarke, L., Thompson, A., et al. (2013). Earliest evidence for the use of pottery. *Nature*, 496(7445), 351-54. DOI: 10.1038/nature12109

Cross, A. D. and Alan Jones, R. (1969). *An Introduction to Practical Infra-Red Spectroscopy*. 3rd ed. London: Butterworth & Co.

Culpeper, N. (1649). *A physicall directory, or, A translation of the London dispensatory*. London : Printed for Peter Cole and are to be sold at his shop at the sign of the Printing-presse near to the Royall Exchange

Cuní, J., Cuní, P., Eisen, B., Savizky, R. and Bové, J. (2012). Characterization of the binding medium used in Roman encaustic paintings on wall and wood. *Analytical Methods*, 4(3), 659-669. DOI:10.1039/C2AY05635F

Curt, W. B., Hostetter, E. and Stewart, D. R. (1993). A bronze situla from tomb 128, Valle Trebba: chemical evidence of resinated wine at Spina. *Studi Etruschi*, 59, 211-25.

da Silva, P. M., Gauche, C., Gonzaga, L. V., Costa, A. C. O. and Fett, R. (2016). Honey: Chemical composition, stability and authenticity. *Food Chemistry*, 196, 309-323. DOI:10.1016/j.foodchem.2015.09.051

Dalgleish, D. G. (2011). On the structural models of bovine casein micelles—review and possible improvements. *Soft Matter*, 7, 2265-2272. DOI:10.1039/C0SM00806K

Dalgleish, D. and Law, A. (1988). PH-Induced dissociation of bovine casein micelles. I. Analysis of liberated caseins. *Journal of Dairy Research*, 55(4), 529-538. DOI:10.1017/S0022029900033306

Dalgleish, D. G. and Corredig, M. (2012). The Structure of the Casein Micelle of Milk and Its Changes During Processing. *Annual Review of Food Science and Technology*, 3, 449-467. DOI:10.1146/annurev-food-022811-101214

Dalgleish, D. G. and Parker, T. G. (1980). Binding of calcium ions to bovine αsl-casein and precipitability of the protein–calcium ion complexes. *Journal of Dairy Research*, 47(1), 113-122. DOI:10.1017/S002202990002094X

Daniele, G., Maitre, D. and Casabianca, H. (2012). Identification, quantification and carbon stable isotopes determinations of organic acids in monofloral honeys. A powerful tool for botanical and authenticity control. *Rapid Communications in Mass Spectrometry*, 26(17), 1993-1998. DOI:10.1002/rcm.6310

Daniels, V. (2007). Analysis of Copper- and Beeswax-containing Green Paint on Egyptian Antiquities. *Studies in Conservation*, 52, 13-18. DOI:10.1179/sic.2007.52.1.13

Davidova, I. A., Gieg, L. M., Duncan, K. E. and Suflita, J. M. (2007). Anaerobic phenanthrene mineralization by a carboxylating sulfate-reducing bacterial enrichment. *The ISME Journal*, 1(5), 436-442. DOI:10.1038/ismej.2007.48

Davies, R. R., Kuang, H., Qi, D., Mazhary, A., Mayaan, E. and Distefano, M. D. (1999). Artificial metalloenzymes based on protein cavities: Exploring the effect of altering the metal ligand attachment position by site directed mutagenesis. *Bioorganic & Medicinal Chemistry Letters*, 9(1), 79-84. DOI:10.1016/S0960-894X(98)00684-2

Davis, J. R. (2000). *Corrosion: understanding the basics*. Materials Park, Ohio:ASM International

Degano, I., Modugno, F., Bonaduce, I., Ribechini, E. and Colombini, M. P. (2018). Recent Advances in Analytical Pyrolysis to Investigate Organic Materials in Heritage Science. *Angewandte Chemie International Edition*, 57(25), 7313-7323. DOI:10.1002/anie.201713404

Del Rio, D., Stewart, A. J. and Pellegrini, N. (2005). A review of recent studies on malondialdehyde as toxic molecule and biological marker of oxidative stress. *Nutrition, metabolism, and cardiovascular diseases*, 15(4), 316-328. DOI:10.1016/j.numecd.2005.05.003

Derrick, M. R., Stulik, D. and Landry, J. M. (1999). *Infrared Spectroscopy in Conservation Science – Scientific Tools for Conservation*: The Getty Conservation Institute.

Deschler-erb, E., Lehmann, E. H., Pernet, L., Vontobel, P. and Hartmann, S. (2004). The Complementary Use of Neutrons and X-Rays for the Non-Destructive Investigation of Archaeological Objects from Swiss Collections. *Archaeometry*, 46(4), 647-661. DOI:10.1111/j.1475-4754.2004.00180.x

Destaillats, F., Craft, B. D., Dubois, M. and Nagy, K. (2012). Glycidyl esters in refined palm (Elaeis guineensis) oil and related fractions. Part I: Formation mechanism. *Food Chemistry*, 131(4), 1391-1398. DOI:10.1016/j.foodchem.2011.10.006

Devantier, A. E., Murcha, S. J. and McNeil, W. S. (2011). Exploration and characterisation of novel bronze patinas derived from simple coordination complexes. *Dalton Transactions*, 3, DOI:10.1039/C0DT00793E

Dimitrova, B., Gevrenova, R. and Anklam, E. (2007). Analysis of Phenolic Acids in Honeys of Different Floral Origin by Solid-phase Extraction and High-performance Liquid Chromatography. *Phytochemical Analysis*, 18(1), 24–32. DOI:10.1002/pca.948

Doménech-Carbó, M. T., Kuckova, S., de La Cruz-Cañizares, J. and Osete-Cortina, L. (2006). Study of the influencing effect of pigments on the photoageing of terpenoid resins used as pictorial media. *Journal of Chromatography A*, 1121(2), 248-258. DOI:10.1016/j.chroma.2006.04.005

Doménech-Carbó, A. (2013). Electrochemical analysis of metallic heritage artefacts: voltammetry of microparticles (VMP). In: Dillmann, P., Watkinson, D., Angelini, E., and Adriaens, A. (eds) *Corrosion and Conservation of Cultural Heritage Metallic Artefacts*, 165-189, Cambridge: Woodhead Publishing

Dong, X., Armstrong, S. D., Xia, D., Makepeace, B. L., Darby, A. C. and Kadowaki, T. (2017). Draft genome of the honeybee ectoparasitic mite, Tropilaelaps mercedesae, is shaped by the parasitic life history. *GigaScience*, 6(3). DOI:10.1093/gigascience/gix008

Downing, D. T., Stewart, M. E. and Strauss, J. S. (1981). Estimation of sebum production rates in man by measurement of the squalene content of skin biopsies. *Journal of Investigative Dermatology*, 77(4), 358-60. DOI: 10.1111/1523-1747.ep12493260.

Downs, C. T., van Dyk, R. J. and Iji, P. (2002). Wax digestion by the lesser honeyguide Indicator minor. Comparative biochemistry and physiology. *Part A, Molecular & integrative physiology*, 133(1), 125-134. DOI:10.1016/S1095-6433(02)00130-7

Dowsett, M. G., Sabbe, P.-J., Jorge, A. A., Schofield, E. J., Walker, D., Thomas, P., York, S. Browns, S. Wermeille, D. and Adriaens, M. (2020). Synchrotron X-ray diffraction investigation of the surface condition of artefacts from King Henry VIII's warship the Mary Rose. *Journal Of Synchrotron Radiation*, 27, 653-663. DOI:10.1107/S1600577520001812

Duce, C., Orsini, S., Spepi, A., Colombini, M. P., Tiné, M. R., and Ribechini, E. (2015). Thermal degradation chemistry of archaeological pine pitch containing beeswax as an additive. *Journal of Analytical and Applied Pyrolysis*, 111, 254-264. DOI:10.1016/j.jaap.2014.10.020

Dudd, S. N., Evershed, R. P., and Gibson, A. M. (1999). Evidence for varying patterns of exploitation of animal products in different prehistoric pottery traditions based on lipids preserved in surface and absorbed residues. *Journal of Archaeological Science*, 26(12), 1473-1482. DOI:10.1006/jasc.1998.0434

Dudev, T., and Lim, C. (2014). Competition among Metal Ions for Protein Binding Sites: Determinants of Metal Ion Selectivity in Proteins. *Chemical Reviews*, 114(1), 538-556. DOI:10.1021/cr4004665

Dumas, G., Malesys, S., and Bourgeron, T. (2021). Systematic detection of brain protein-coding genes under positive selection during primate evolution and their roles in cognition. *bioRxiv*, 658658. DOI:10.1101/658658

Dunbar, R. C., Martens, J., Berden, G. and Oomens, J. (2018). Binding of Divalent Metal Ions with Deprotonated Peptides: Do GasPhase Anions Parallel the Condensed Phase? *The Journal of Physical Chemistry A*, 122(25), 5589-5596. DOI:10.1021/acs.jpca.8b02926

Duncan, S. J. and Ganiaris, H. (1987). Some sulfide corrosion products on copper alloys and lead alloys from London waterfront sites. *Paper presented at the Recent advances in the conservation and analysis of artifacts: jubilee conservation conference papers*, University of London, Institute of Archaeology

Dunne, J., Evershed, R. P., Salque, M., Cramp, L., Bruni, S., Ryan, K., . . . di Lernia, S. (2012). First dairying in green Saharan Africa in the fifth millennium BC. *Nature*, 486, 390-394. DOI:10.1038/nature11186

Dunne, J., Evershed, R. P., Cramp, L. J. E., Bruni, S., Biagetti, S., and di Lernia, S. (2013). The beginnings of dairying as practised by pastoralists in 'Green' Saharan Africa in the 5th millennium BC. *Documenta Praehistorica*, 40, 118-130. DOI:10.4312/dp.40.10

Dunne, J., Rebay-Salisbury, K., Salisbury, R. B., Frisch, A., Walton-Doyle, C. and Evershed, R. P. (2019). Milk of ruminants in ceramic baby bottles from prehistoric child graves. *Nature*, 574, 246–248. DOI:10.1038/s41586-019-1572-x

Eakin, C. M., Knight, J. D., Morgan, C. J., Gelfand, M. A. and Miranker, A. D. (2002). Formation of a Copper Specific Binding Site in Non-Native States of β-2-Microglobulin. *Biochemistry*, 41(34), 10646–10656. DOI:10.1021/bi025944a

Edwards, G. (1989). Guidelines for dealing with material from sites where organic remains have been preserved by metal corrosion products. In Janaway, R. C. and Scott, B. (eds.), *Evidence Preserved in Corrosion Products: New Fields in Artifact Studies* (Vol. 8): The United Kingdom Institute for Conservation.

Eggleston, D. S. and Feldman, S. H. (1990). Structure of the fibrinogen binding sequence: arginylglycylaspartic acid (RGD). *International Journal of Peptide and Protein Research*, 36(2), 161-166.

EINECS. (2008). *Methenamine - Summary Risk Assessment Report*. (202-905-8). Dortmund (Germany): European Communities

Emeleus, V. M. (1958). The technique of neutron activation analysis as applied to trace element determination in pottery and coins. *Archaeometry*, 1, 6-15. DOI:10.1111/j.1475-4754.1958.tb00203.x

Evershed, R. P. (1993). Biomolecular Archaeology and Lipids. *World Archaeology*, 25(1):74-93. DOI: 10.1080/00438243.1993.9980229

Evershed, R. P. (2008a). Organic Residue Analysis in Archaeology: The Biomarker Revolution. *Archaeometry*, 50(6), 895-924. DOI:10.1111/j.1475-4754.2008.00446.x

Evershed, R. P. (2008b). Experimental approaches to the interpretation of absorbed organic residues in archaeological ceramics. *World Archaeology*, 40(1), 26-47. DOI:10.1080/00438240801889373

Evershed, R. P., Heron, C., and Goad, L. J. (1990). Analysis of organic residues of archaeological origin by high-temperature gas chromatography and gas chromatography-mass spectrometry. *Analyst*, 115, 1339-1342. DOI: 10.1039/AN9901501339

Evershed, R. P., Heron, C. and Goad, L. J. (1991). Epicuticular wax components preserved in potsherds as chemical indicators of leafy vegetables in ancient diets. *Antiquity*, 65(248), 540-544. DOI:10.1017/S0003598X00080145

Evershed, R. P., Arnot, K. I., Collister, J., Eglinton, G. and Charters, S. (1994). Application of isotope ratio monitoring gas chromatography/mass spectrometry to the analysis of organic residues of archaeological interest. *Analyst*, 199(5), 909-914. DOI:10.1039/AN9941900909

Evershed, R. P., Stott, A. W., Raven, A., Dudd, S. N., Charters, S. and Leyden, A. (1995). Formation of long-chain ketones in ancient pottery vessels by pyrolysis of acyl lipids. *Tetrahedron Letters*, 36, 8875–8878. DOI: 10.1016/0040-4039(95)01844-8

Evershed, R. P., Turner-Walker, G., Hedges, R. E. M., Tuross, N. and Leyden, A. (1995b). Preliminary results for the analysis of lipids in ancient bone. Journal of Archaeological Science, 22, 277-290. DOI: 10.1006/jasc.1995.0030

Evershed, R. P., Bland, H. A., van Bergen, P. F., Carter, J. F., Horton, M. C. and Rowley-Conwy, P. A. (1997). Volatile compounds in archaeological plant remains and the Maillard reaction during decay of organic matter. *Science*, 278(5337), 432-433. DOI:10.1126/science.278.5337.432

Evershed, R. P., Dudd, S. N., Lockheart, M. J. and Jim, S. (2001). Lipids in Archaeology. In: Brothwell, D. R. and Pollard, A. M. (eds.), *Handbook of Archaeological Science*. Chichester: John Wiley & Sons.

Evershed, R. P., Dudd, S. N., Copley, M. S., Berstan, R., Stott, A. W., Mottram, H., Buckley, S. A. and Crossman, Z. (2002). Chemistry of Archaeological Animal Fats. *Accounts of Chemical Research*, 35(8), 660-668. DOI:10.1021/ar000200f

Evershed, R. P., Berstan, R., Grew, F., Copley, M. S., Charmant, A. J. H., Barham, E., Mottram, H. R. and Brown, G. (2004). Formulation of a Roman cosmetic. *Nature*, 432, 35-36. DOI:10.1038/432035a

Evershed, R. P., Payne, S., Sherratt, A. G., Copley, M. S., Coolidge, J., Urem-Kotsu, D., . . . and Burton, M. M. (2008). Earliest date for milk use in the Near East and Southeastern Europe linked to cattle herding. *Nature*, 445, 528–531. DOI: 10.1038/nature07180

Evershed, R. P., Copley, M. S., Dickson, L. and Hansel, F. A. (2008b). Experimental evidence for the processing of marine animal products and Other Commodities Containing Polyunsaturated Fatty Acids in Pottery Vessels. *Archaeometry*, 50(1), 101-13. DOI: 10.1111/j.1475-4754.2007.00368.x.

Fan, X. and Freestone, I. C. (2017). Occurrence of phosphatic corrosion products on bronze swords of the Warring States period buried at Lijiaba site in Chongqing, China. *Heritage Science*, 5(1), 1-9. DOI:10.1186/s40494-017-0161-2

Fell, V. (2004). Cremated: Analysis of the metalwork from an Iron Age grave. In: Ashton, J. and Hallan, D. (eds.), *Metal 04 : proceedings of the International Conference on Metals Conservation : Canberra, Australia, 4-8 October 2004*. Canberra: National Museum of Australia.

Ferla, M. P. and Patrick, W. M. (2014). Bacterial methionine biosynthesis. *Microbiology (Reading)*, 160, 1571-1584. DOI:10.1099/mic.0.077826-0

Figueiredo, J. C. D., Oliveira, J. A. S., Souza, G. S. M., Froner, Y., Souza, L. A. C. and Zarankin, A. (2015). Characterization of corrosion products on metals excavated from seal hunters' occupation in Antarctica in the eighteenth and nineteenth centuries. *Studies in Conservation*, 60(3), 211-216. DOI:10.1179/2047058414Y.0000000138

Fleming, F. F. (1999). Nitrile-containing natural products. *Natural Product Reports*, 16(5), 597-606. DOI:10.1039/a804370a

Folin, O. (1905). Laws Governing the Chemical Composition of Urine. *American Journal of Physiology-Legacy Content*, 13(1), 66-115. DOI:10.1152/ajplegacy.1905.13.1.66

Fontecha, J., Goudjil, H., Ríos, J. J., Fraga, M. J. and Juárez, M. (2005). Identity of the major triacylglycerols in ovine milk fat. *International Dairy Journal*, 15(12), 1217-1224. DOI:10.1016/j.idairyj.2004.11.013

Franke, W. A. and Mircea, M. (2005). Plutarch's Report on the Blue Patina of Bronze Statues at Delphi: A Scientific Explanation. *Journal of the American Institute for Conservation*, 44(2), 103-116. DOI:10.1179/019713605806082356

Fulcher, K., Stacey, R. and Spencer, N. (2020). Bitumen from the Dead Sea in Early Iron Age Nubia. *Scientific Reports*, 10(8309). DOI:10.1038/s41598-020-64209-8

Gardiner, D. J. (1989). Introduction to Raman Scattering. In: Gardiner, D. J. and Graves, P. R. (eds) *Practical Raman Spectroscopy*, 1-11. Heidelberg: Springer-Verlag

Gettens, R. J. (1951). The corrosion products of an ancient Chinese bronze. *Journal of Chemical Education*, 28(2), 67-71. DOI:10.1021/ed028p67

Ghiara, G., Repetto, L. and Piccardo, P. (2019). The Effect of Pseudomonas fluorescens on the Corrosion Morphology of Archaeological Tin Bronze Analogues. *The Journal of The Minerals, Metals & Materials Society*, 71, 779-783. DOI:10.1007/s11837-018-3138-z

Ghoneim, M. (2014). An Egyptian Partially Gilded Bronze Group Statue: Examination and Analysis. *Archaeometry*, 57(S1), 130-146. DOI:10.1111/arcm.12103

Giachi, G., Pallecchi, P., Romualdi, A., Ribechini, E., Lucejko, J. J., Colombini, M. P. and Lippi, M. M. (2013). Ingredients of a 2,000-y-old medicine revealed by chemical, mineralogical, and botanical investigations. Paper presented at the *Proceedings of the National Academy of Sciences, 22 January 2013, Mexico*.

Gillard, R. D., Hardman, S. M., Thomas, R. G. and Watkinson, D. E. (1994). The mineralization of fibres in burial environment. *Studies in Conservation*, 39(2), 132-140. DOI:10.1179/sic.1994.39.2.132

Gillard, R. D. and Hardman, S. M. (1996). Investigation of Fiber Mineralization Using Fourier Transform Infrared Microscopy. *Archaeological Chemistry*.623. DOI:10.1021/bk-1996-0625.ch014

Gilmour, B. (2017). The metallurgy, development, and purpose of pattern welding. Historical Metallurgy – *Journal of the Historical Metallurgy Society*, 51(2), 57-70.

Goldberg, I., Rokem, J. S. and Pines, O. (2006). Organic acids: old metabolites, new themes. *Journal of Chemical Technology & Biotechnology*, 81(10), 1601-1611. DOI:10.1002/jctb.1590

Goldenberg, L., Neumann, R. and Weinera, S. (2014). Microscale distribution and concentration of preserved organic molecules with carbon–carbon double bonds in archaeological ceramics: relevance to the field of residue analysis. *Journal of Archaeological Science*, 42, 509-518. DOI:10.1016/j.jas.2013.11.025

Gordon, W. G., Semmett, W. F., Cable, R. S. and Morris, M. (1949). Amino Acid Composition of α-Casein and β-Casein. *Journal of the American Chemical Society*, 71(10), 3293–3297. DOI:10.1021/ja01178a006

Graham, K. and Williams, J. (2008). *Fiskerton Conservation Management: Analysis of Modern Copper Samples Buried for 6, 12, 18 and 30 Months.* Research Department Report Series Volume 39. English Heritage. Available at https://research.historicengland.org.uk/PrintReport.aspx?i=14670&ru=%2FResults.aspx%3Fn%3D10%26p%3D250 Accessed on 10th January 2021

Grant, W. D. and West, A. W. (1986). Measurement of ergosterol, diaminopimelic acid and glucosamine in soil: evaluation as indicators of microbial biomass. *Journal of Microbiological Methods*, 6(1), 47-53. DOI:10.1016/0167-7012(86)90031-X

Grillo, K. M., Dunne, J., Marshall, F., Prendergast, M. E., Casanova, E., Gidna, A. O., . . . and Evershed, R. P. (2020). Molecular and isotopic evidence for milk, meat, and plants in prehistoric eastern African herder food systems. Paper presented at the *Proceedings of the National Academy of Sciences of the United States of America, 05 May 2020, United States of America*

Guasch-Jané, M. R., Ibern-Gómez, M., Andrés-Lacueva, C., Jáuregui, O. and Lamuela-Raventós, R. M. (2004). Liquid chromatography with mass spectrometry in tandem mode applied for the identification of wine markers in residues from ancient Egyptian vessels. *Analytical Chemistry*, 76(6), 1672-1677. DOI:10.1021/ac035082z

Guirado, S., Fortes, F. J., Lazic, V. and Laserna, J. J. (2012). Chemical analysis of archaeological materials in submarine environments using laser-induced breakdown spectroscopy. On-site trials in the Mediterranean Sea. *Spectrochimica Acta Part B: Atomic Spectroscopy*,74-75:137-43. DOI: 10.1016/j.sab.2012.06.032

Gülaçar, F. O., Buchs, A. and Susini, A. (1989). Capillary gas-chromatography mass-spectrometry and identification of substituted carboxylic acids extracted from a 400-year-old Nubian burial. *Journal of Chromatography A*, 479, 61-72. DOI:10.1016/s0021-9673(01)83317-3

Gunn, S. (2005). Honey Fungus. *Horticulture Week*. 30-31.

Gunn, M., Chottard, G., Rivière, E., Girerd, J. and Chottard, J. (2002). Chemical Reactions between Copper Pigments and Oleoresinous media. *Studies in Conservation*, 47(1), 12-23. DOI:10.1179/sic.2002.47.1.12

Gupta, A. K., Dharne, M. S., Rangrez, A. Y., Verma, P., Ghate, H. V., Rohde, M., . . . and Shouche, Y. S. (2011). *Ignatzschineria indica sp. nov*. and *Ignatzschineria ureiclastica sp. nov*., isolated from adult flesh flies (*Diptera: Sarcophagidae*). *International Journal of Systematic and Evolutionary Microbiology*, 61(6), 1360-1369. DOI:10.1099/ijs.0.018622-0

Gurioli, L., Pareschi, M. T., Zanella, E., Lanza, R., Deluca, E. and Bisson, M. (2005). Interaction of pyroclastic density currents with human settlements: evidence from ancient Pompeii. *Geology*, 33(6), 441-444.

Hamilton, W. A. (1985). Sulphate-reducing bacteria and anaerobic corrosion. *Annual review of microbiology*, 39, 195-217. DOI:10.1146/annurev.mi.39.100185.001211

Hansel, F. A., Copley, M.S., Madureira, L. A. S. and Evershed, R. P. (2004). Thermally produced □-(*o*-alkylphenyl) alkanoic acids provide evidence for the processing of marine products in archaeological pottery vessels. *Tetrahedron Letters*, 45(14), 2999-3002. DOI: 10.1016/j.tetlet.2004.01.111.

Hansel, F. A and Evershed, R. P. (2009). Formation of dihydroxy acids from Z-monounsaturated alkenoic acids and their use as biomarkers for the processing of marine commodities in archaeological pottery vessels. *Tetrahedron Letters*, 50(40), 5562-64. DOI: 10.1016/j.tetlet.2009.06.114.

Heard, G. M. and Fleet, G. H. (1999). CANDIDA | Yarrowia (Candida) lipolytica. In: Robinson, R. K., Batt, C. and Patel, P. (eds.) *Encyclopedia of Food Microbiology*, 360-365, London England: Elsevier.

Heath, R. J., White, S. W. and Rock, R. O. (2001). Lipid biosynthesis as a target for antibacterial agents. *Progress in Lipid Research*, 40(6), 467-497.

Hellinga, H. W. (1998). The construction of metal centers in proteins by rational design. *Folding and Design*, 3(1), R1-R8. DOI:10.1016/S1359-0278(98)00001-7

Helwig, K., Monahan, V. and Poulin, J. (2008). The Identification of Hafting Adhesive on a Slotted Antler Point from a Southwest Yukon Ice Patch. *American Antiquity*, 73(2), 279-288. DOI:10.2307/25470478

Henderson, C. M., Lozada-Contreras, M., Naravane, Y., Longo, M. L. and Block, D. E. (2011). Analysis of major phospholipid species and ergosterol in fermenting industrial yeast strains using atmospheric pressure ionization ion-trap mass spectrometry. *Journal of Agricultural and Food Chemistry*, 59(4), 12761-12770. DOI:10.1021/jf203203h

Henry, R., Grant, M. J., Pelling, R. and Roberts, D. (2017). The Pewsey vessel hoard, an initial assessment. The Wiltshire Archaeological and Natural History Magazine, January, 230-233.

Henry, R., Roberts, D., Grant, M. J., Pelling, R. and Marshall, P. (2019). A Contextual Analysis of the Late Roman Pewsey and Wilcot Vessel Hoards, Wiltshire. *Britannia*, 50, 149-184. DOI:10.1017/S0068113X19000266

Heron, C., Nemcek, N., Bonfield, K. M., Dixon, D. and Ottaway, B. S. (1994). The chemistry of Neolithic beeswax. *Naturwissenschaften*, 81, 266-269. DOI:10.1007/BF01131579

Heron, C., Nilsen, G., Stern, B., Craig, O. and Nordby. C. (2010). Application of lipid biomarker analysis to evaluate the function of 'slab-lined pits' in Arctic Norway. *Journal Of Archaeological Science,* 37(9), 2188-97. DOI: 10.1016/j.jas.2010.03.016.

Higaki, J. N., Haymore, B. L., Chen, S., Fletterick, R. J. and Craik, C. S. (1990). Regulation of serine protease activity by an engineered metal switch. *Biochemistry*, 29(37), 8582-8586. DOI:10.1021/bi00489a012

Hilt, K. M., Harrison, J. H. and Bowers, K. (2016). 1207 Oxalic acid production by Aspergillus niger when using whey permeate lactose as a carbon source. *Journal of Animal Science*, 94, 580-580. DOI:10.2527/jam2016-1207

Hjulström, B., Isaksson, S. and Hennius, A. (2006). Organic Geochemical Evidence for Pine Tar Production in Middle Eastern Sweden During the Roman Iron Age. *Journal of Archaeological Science*, 33(2), 283-294. DOI:10.1016/j.jas.2005.06.017

Hoefel, T., Wittmann, E., Reinecke, L. and Weuster-Botz, D. (2010). Reaction engineering studies for the production of 2-hydroxyisobutyric acid with recombinant Cupriavidus necator H 16. *Applied Microbiology and Biotechnology*, 88, 477-484. DOI:10.1007/s00253-010-2739-4

Hoffmann, E. de and Stroobant, V. (2007). *Mass Spectrometry: Principles and Applications*

3rd ed. Chichester: Wiley.

Holt, C. (2016). Casein and casein micelle structures, functions and diversity in 20 species. *International Dairy Journal*, 60:2-13. DOI:10.1016/j.idairyj.2016.01.004.

Horne, D. S. (2014). Casein Micelle Structure and Stability. In: Singh, H., Boland, M. and Thompson, A. (eds.), *Milk Proteins: from expression to food* (2nd ed.). London England: Academic Press.

Hurst, W. J., Martin, R. A., Tarka, S. M. and Hall, G. D. (1989). Authentication of cocoa in Maya vessels using high performance liquid chromatographic techniques. *Journal of Chromatography*, 466, 279-290. DOI:10.1016/S0021-9673(01)84623-9

Husain, A., Kumar, G., Sood, T., Walia, S., Justino, L. L. G., Fausto, R. and Kumar, R. (2018). Synthesis, structural characterization and DFT analysis of an unusual tryptophan copper(II) complex bound via carboxylate monodentate coordination: Tetraaquabis(l-tryptophan) copper(II) picrate. *Inorganica Chimica Acta*, 482, 324-332. DOI:10.1016/j.ica.2018.06.021

Inagaki, R., Hirai, C., Shimamura, Y. and Masuda, S. (2016). Formation of glycidol fatty acid esters in meat samples cooked by various methods. *Journal of Food Processing & Technology*, 7(2). DOI:10.4172/2157-7110.1000557

Ingo, G. M., Cilingiroglu, A., Faraldi, F., Riccucci, C., Casaletto, M. P., Erdem, A., and Batmaz, A. (2010). The bronze shields found at the Ayanis fortress (Van region, Turkey): manufacturing techniques and corrosion phenomena. *Applied Physics A: Materials Science & Processing*, 100(3), 793-798. DOI:10.1007/s00339-010-5656-6

Ingo, G. M., de Caro, T., Riccucci, C., and Khosroff, S. (2006). Uncommon corrosion phenomena of archaeological bronze alloys. *Applied Physics A: Materials Science & Processing*, 83(4), 581-588. DOI:10.1007/s00339-006-3534-z

Isaksson, S., Karlsson, C. and Eriksson, T. (2010). Ergosterol (5, 7, 22-ergostatrien-3β-ol) as a potential biomarker for alcohol fermentation in lipid residues from prehistoric pottery. *Journal of Archaeological Science*, 37(12), 3263-3268. DOI:10.1016/j.jas.2010.07.027

Janaway, R. C. (1985). Dust to Dust: The Preservation of Textile Materials in Metal Artefact Corrosion Products with Reference to Inhumation Graves. *Science and Archaeology*, 27, 29-34.

Janaway, R. C. (1989). Corrosion preserved textile evidence: mechanism, bias and interpretation. In: Janaway, R. C. and Scott, B. (eds.), *Evidence Preserved in Corrosion Products: New Fields in Artefact Studies. Proceedings of a joint conference between UKIC*

Archaeology Section and the Council for British Archaeology Science Committee, Leeds 1983, 21-29. London: United Kingdom Institute for Conservation of Historic and Artistic Works.

Janecki, D. J. and Reilly, J. P. (2005). Denaturation of metalloproteins with EDTA to facilitate enzymatic digestion and mass fingerprinting. Rapid communications in mass spectrometry : *RCM*, 19(10), 1268-1272. DOI:10.1002/rcm.1924

Jenkins, R. and Snyder, R. L. (1996). *Introduction to X-ray powder diffractometry*. Chichester: Wiley.

Jeżowska-Bojczuk, M. and Stokowa-Sołtys, K. (2018). Peptides having antimicrobial activity and their complexes with transition metal ions. *European Journal of Medicinal Chemistry*, 143, 997-1009. DOI:10.1016/j.ejmech.2017.11.086

Jones, J. C., Fruciano, C., Hildebrand, F., Al Toufalilia, H., Balfour, N. J., Bork, P., . . . and Hughes, W. O. (2017). Gut microbiota composition is associated with environmental landscape in honeybees. *Ecology and Evolution*, 8, 441–451. DOI:10.1002/ece3.3597

Kadej, A., Kuczer, M., Czarniewska, E., Urbański, A., Rosiński, G. and Kowalik-Jankowskaa, T. (2016). High stability and biological activity of the copper(II) complexes of alloferon 1 analogues containing tryptophan. *Journal of Inorganic Biochemistry*, 163, 147-161. DOI:10.1016/j.jinorgbio.2016.07.006

Kalscheuer, R. and Steinbuchel, A. (2003). A novel bifunctional wax ester synthase/acyl-CoA: diacylglycerol acyltransferase mediates wax ester and triacylglycerol biosynthesis in Acinetobacter calcoaceticus ADP1. *Journal of Biological Chemistry*, 278(10), 8075-8082. DOI:10.1047/jbc.M210533200

Kałużna-Czaplińska, J., Rosiak, A., Kwapińska, M, and Kwapiński, W. (2016). Different Analytical Procedures for the Study of Organic Residues in Archaeological Ceramic Samples with the Use of Gas Chromatography-mass Spectrometry. *Critical reviews in analytical chemistry*, 46(1), 67-81. DOI:10.1080/10408347.2015.1008130

Kapsopoulou, K., Kapaklis, A. and Spyropoulos, H. (2005). Growth and fermentation characteristics of a strain of the wine yeast Kluyveromyces thermotolerans isolated in Greece. *World Journal of Microbiology and Biotechnology*, 21, 1599–1602. DOI:10.1007/s11274-005-8220-3

Kearsley, M. W. and Boghani, N. (2012). Maltitol. In O'Brien-Nabors, L. (ed.), *Alternative Sweetners* (4th ed., pp. 299-313). Boca Ratton, FL: CRC.

Kędzierska-Matysek, M., Matwijczuk, A., Florek, M., Barlowska, J., Wolanciuk, A., Matwijczuk, A., . . . and Gladyszewska, B. (2018). Application of FTIR spectroscopy for analysis of the quality of honey. *BIO web of conferences*, 10. DOI:10.1051/bioconf/20181002008

Keepax, C. A. (1989). Corrosion 'preserved wood': advances since 1975. In: Janaway, R. C. and Scott, B. (eds.), *Evidence Preserved in Corrosion Products: New Fields in Artefact Studies : Proceedings of a joint conference between UKIC Archaeology Section and the Council for British Archaeology Science Committee, Leeds 1983*, 15-20. London: United Kingdom Institute for Conservation of Historic and Artistic Works.

Keire, D. A., Anton, P., Faull, K. F., Ruth, E., Walsh, J. H., Chew, P., . . . and Reeve, J. R. (2001). Diethyl phthalate, a chemotactic factor secreted by Helicobacter pylori. *The Journal of Biological Chemistry*, 276(52), 48847-48853. DOI:10.1074/jbc.M109811200

Kenealy, W., Cao, Y. and Weimer, P. (1995). Production of caproic acid by cocultures of ruminal cellulolytic bacteria and Clostridium kluyveri grown on cellulose and ethanol. *Applied Microbiology and Biotechnology*, 44(3), 507-513. DOI:10.1007/BF00169952

Kešnerová, L., R. A. T. Mars, K. M. Ellegaard, M. Troilo, U. Sauer, and P. Engel. (2017). Disentangling Metabolic Functions of Bacteria in the Honey Bee Gut.*PLoS Biology 15*, 12, p.e2003467. DOI:10.1371/journal.pbio.2003467.

Kešnerová, L., Emery, O., Troilo, M., Liberti, J., Erkosar, B. and Enge, P. (2020). Gut microbiota structure differs between honeybees in winter and summer. *The ISME Journal*, 14, 801-814. DOI:10.1038/s41396-019-0568-8

Keune, K., Kramer, R. P., Stangier, S. and Hommer, M. H. v. E. (2019). Chapter 6 - Impact of Lead Soaps on the Formation of Age Craquelure. In Casadio, F., Keune, K., Noble, P., v. Loon, A., Hendriks, E., Centeno, S. A. and Osmond, G. (eds.), *Metal soaps in art : conservation and research*, 107-121. Cham, Switzerland: Springer.

Kherbouche, F., Dunne, J., Merzoug, S., Hachi, S. and Evershed, R. P. (2016). Middle Holocene hunting and herding at Gueldaman Cave, Algeria: An integrated study of the vertebrate fauna and pottery lipid residues. *Quaternary International*, 410, 50-60. DOI:10.1016/j.quaint.2016.01.005

Khongphinitbunjong, L., Neumann, P., Chantawannakul, P. and Williams, G. R. (2016). The ectoparasitic mite *Tropilaelaps mercedesae* reduces western honeybee, *Apis mellifera*, longevity and emergence weight, and promotes Deformed wing virus infections. *Journal of Invertebrate Pathology*, 137, 38-42. DOI:10.1016/j.jip.2016.04.006

Killer, J., Votavova, A., Valterova, I., Vlkova, E., Rada, V. and Hroncova, Z. (2014). *Lactobacillus bombi sp. nov.,* from the digestive tract of laboratory-reared bumblebee queens (*Bombus terrestris*). *International Journal of Systematic and Evolutionary Microbiology*, 64, 2611–2617. DOI:10.1099/ijs.0.063602-0

Koenig, A. E. (1914). On the Stearates and Palmitates of the Heavy Metals with Remarks Concerning Instantaneous Precipitations in Insulating Solutions. *Journal of the American Chemical Society*, 36, 951–961. DOI:10.1021/ja02182a018

Koleini, F., Prinsloo, L. C., Schoeman, M. H. A., Pikirayi, I. and Chirikure, S. (2013). Characterization of the corrosion layer on iron archaeological artefacts from K2 (825-1220 AD), an archaeological site in South Africa. *Studies in Conservation*. 58(3):274-282. DOI: 10.1179/2047058412Y.0000000044

Koller, J., Baumer, U., Kaup, Y., Schmid, M. and Weser, U. (2003). Ancient materials: analysis of a pharaonic embalming tar. *Nature*, 425, 784. DOI:10.1038/425784a

Kolthoff, I. M. and Coetzee, J. F. (1957). Polarography in Acetonitrile. II. Metal Ions Which Have Significantly Different Polarographic Properties in Acetonitrile and in Water. Anodic Waves. Voltammetry at Rotated Platinum Electrode. *Journal of the American Chemical Society*, 79(8): 1852–1858. DOI:10.1021/ja01565a023

Korenberg, C. (2006). Corrosion on Metallic Tokens Stored in Polyurethane Foam. *Studies in conservation*. 51(1):1-10. DOI: 10.1179/sic.2006.51.1.1

Kozlowski, H., Potocki, S., Remelli, M., Rowinska-Zyreka, M. and Valensin, D. (2013). Specific metal ion binding sites in unstructured regions of proteins. *Coordination Chemistry Reviews*, 257(19-20), 2625-2638. DOI: 10.1016/j.ccr.2013.01.024

Kraay, C. M. (1958). Gold and copper traces in early Greek silver. *Archaeometry*, 1, 1-5. DOI:10.1111/j.1475-4754.1958.tb00203.x

Krieger, F., Möglich, A. and Kiefhaber, T. (2005). Effect of Proline and Glycine Residues on Dynamics and Barriers of Loop Formation in Polypeptide Chains. *Journal of the American Chemical Society*, 127(10), 3346–3352. DOI:10.1021/ja042798i

Krömer, J. O., Wittmann, C., Schröder, H. and Heinzle, E. (2006). Metabolic pathway analysis for rational design of L-methionine production by Escherichia coli and Corynebacterium glutamicum. *Metabolic engineering*, 8(4), 353-369. DOI:10.1016/j.ymben.2006.02.001

Kümmel, S., Herbst, F., Bahr, A., Duarte, M., Pieper, D. H., Jehmlich, N., . . . and Lueders, T. (2015). Anaerobic naphthalene degradation by sulfate-reducing Desulfobacteraceae from various anoxic aquifers. *FEMS Microbiology Ecology*, 91(3), 1-13. DOI: 10.1093/femsec/fiv006

Kühn, H. (1970). Verdigris and Copper Resinate. *Studies in Conservation*, 15(1), 12-36. DOI:10.2307/1505549

La Nasa, J., Lluveras-Tenorio, A., Modugno, F. and Bonaduce, I. (2018). Two-step analytical procedure for the characterization and quantification of metal soaps and resinates in paint samples. *Heritage Science*, 6(1), 1-10. DOI:10.1186/s40494-018-0222-1

La Nasa, J., Modugno, F., Aloisi, M., Lluveras-Tenorio, A. and Bonaduce, I. (2018). Development of a GC/MS method for the qualitative and quantitative analysis of mixtures of free fatty acids and metal soaps in paint samples. *Analytica Chimica Acta*, 1001, 51-58. DOI:10.1016/j.aca.2017.11.017

La Niece, S., Shearman, F., Taylor, J. and Simps, A. (2002). Polychromy and Egyptian Bronze: New Evidence for Artificial Coloration. *Studies in Conservation*, 47(2), 95-108. DOI:10.1179/sic.2002.47.2.95

Lai, C. W., Schwab, M., Hill, S. C., Santarpia, J. and Pan, Y.-L. (2016). Raman scattering and red fluorescence in the photochemical transformation of dry tryptophan particles. *Optics Express*, 24(11), 11654-11667. DOI:10.1364/OE.24.011654

Lang, K., Buehler, K. and Schmid, A. (2015). Multistep Synthesis of (S)-3-Hydroxyisobutyric Acid from Glucose using Pseudomonas taiwanensis VLB120 B83 T7 Catalytic Biofilms. *Advanced Synthesis and Catalysis*, 357(8), 1919-1927. DOI:10.1002/adsc.201500205

Lange, N. A. (2005). *Lange's handbook of chemistry* (16th ed.). New York; London: McGraw-Hill.

Lee, B. C. and Gladyshev, V. N. (2011). The biological significance of methionine sulfoxide stereochemistry. *Free radical biology & medicine*, 50(2), 221-227. DOI:10.1016/j.freeradbiomed.2010.11.008

Lenhart, A. and Chey, W. D. (2017). A Systematic Review of the Effects of Polyols on Gastrointestinal Health and Irritable Bowel Syndrome. *Advances in Nutrition*, 8(4), 587-596. DOI: 10.3945/an.117.015560

Li, Y. H., Wang, W. J., Xu, X. J., Meng, Y. C., Zhang, L. W., Chen, J. and Qiu, R. (2015). Changes in fluorescence intensity induced by soybean soluble polysaccharide–milk protein interactions during acidification. *Journal of Dairy Science*, 98(12), 8577-8580. DOI:10.3168/jds.2015-9971

Liang, J. and Scott, D. A. (2014). Green-copper containing waxy paint on two Egyptian polychrome artifacts: A technical study. *Studies in Conservation*, 59(6), 391-403. DOI:10.1179/2047058413Y.0000000106

Lucas, A. (1911). *Preservative materials used by the ancient Egyptians in embalming*. Egypt: National Printing Department.

Lucas, A. (1931). "Cedar"-Three Products Employed in Mummification. *The Journal of Egyptian Archaeology*, 17(1), 13-21. DOI: 10.1177/030751333101700103

Łucejko, J. J., Lluveras-Tenorio, A., Modugno, F., Ribechini, E. and Colombini, M. P. (2012). An analytical approach based on X-ray diffraction, Fourier transform infrared spectroscopy and gas chromatography/mass spectrometry to characterize Egyptian embalming materials. *Microchemical Journal*, 103, 110-118. DOI: 10.1016/j.microc.2012.01.014

MacLeod, I. D. (1982). Formation of marine concretions on copper and its alloys. The *International Journal of Nautical Archaeology*, 11(4), 261-275. DOI:1 0.1111/j.1095-9270.1982.tb00091.x

MacLeod, I. D. (1991). Identification of corrosion products on non-ferrous metal artifacts recovered from shipwrecks. *Studies in Conservation*, 36(4), 222-234. DOI: 10.2307/1506320

MacLeod, I. D. and Pennec, S. (2004). Characterisation of corrosion products on artefacts recovered from the RMS Titanic (1912). In MacLeod, I. D., Theile, J. M. and Degrigny, C. (eds) *Metal 01: Proceedings of the International Conference on Metals Conservation, Santiago, Chile. 2-6 April 2001*, 270-78, Perth : Western Australian Museum

Manzano, E., Cantarero, S., García, A., Adroher, A. and Vílchez, J. L. (2016). A multi-analytical approach applied to the archaeological residues in Iberian glasses. Earliest evidences on the consumption of fermented beverages in votive rituals. *Microchemical Journal*, 129, 286-292. DOI: 10.1016/j.microc.2016.07.006

Marín, S., Cuevas, D., Ramos, A. J. and Sanchis, V. (2008). Fitting of colony diameter and ergosterol as indicators of food borne mould growth to known growth models in solid medium. *International Journal of Food Microbiology*, 121(2), 139-149. DOI: 10.1016/j.ijfoodmicro.2007.08.030

Márquez-Ruiz, G. and Dobarganes, C. (1996). Short-Chain Fatty Acid Formation during Thermoxidation and Frying. *Journal of the Science of Food and Agriculture*, 70(1), 120-126. DOI: 10.1002/(SICI)1097-0010(199601)70:1<120::AID-JSFA473>3.0.CO2-M

Mastrolorenzo, G., Petrone, P., Pappalardo, L. and Guarino, F. (2010). Lethal Thermal Impact at Periphery of Pyroclastic Surges: Evidences at Pompeii (Thermal Impact at Pompeii). *PLoS ONE*, 5(6). DOI: 10.1371/journal.pone.0011127

Mathis, F., Salomon, J., Pagès-Camagna, S., Dubus, M., Robcis, D., Aucouturier, M., Descamps, S. and Delange, E. (2007). 13 - Corrosion patina or intentional patina: contribution of non-destructive analyses to surface study of copper-based archaeological objects. In P. Dillmann, G. Béranger, P. Piccardo, and H. Matthiesen (eds.) *Corrosion of Metallic Heritage Artefacts: Investigation, Conservation and Prediction of Long Term Behaviour*, 219-238, Cambridge, UK: Woodhead Publishing.

Mcgoverin, C. M., Clark, A. S. S., Holroyd, S. E., and Gordon, K. C. (2010). Raman spectroscopic quantification of milk powder constituents. *Analytica Chimica Acta*, 673(1), 26-32. DOI: 10.1016/j.aca.2010.05.014

McGovern, P. E., Glusker, D., Moreau, R. A., Nunez, A., Simpson, E., Butrym, E. D., Exner, L. J. and Stout, E. C. (1999). A funerary feast fit for King Midas. *Nature*, 402, 863-864. DOI: 10.1038/47217

McGovern, P. E. and Hall, G. R. (2016). Charting a Future Course for Organic Residue Analysis in Archaeology. *Journal of Archaeological Method and Theory*, 23, 592-622. DOI: 10.1007/s10816-015-9253-z

McGovern, P. E., Luley, B. P., Rovira, N., Mirzoian, A., Callahan, M. P., Smith, K. E., . . . and Henkin, J. M. (2013). Beginning of viniculture in France. *Proceedings of the National Academy of Sciences of the United States of America*, 110(25), 10147-10152. DOI: 10.1073/pnas.1216126110

Mckee, G. A. and Hatcher, P. G. (2010). Alkyl amides in two organic-rich anoxic sediments: A possible new abiotic route for N sequestration. *Geochimica et Cosmochimica Acta*, 74(22), 6436-6450. DOI: 10.1016/j.gca.2010.08.004

McNeil, M. B., Jones, J. and Little, B. J. (1991). Mineralogical fingerprints for corrosion processes induced by sulfate-reducing bacteria. *National Association of Corrosion Engineers International Corrosion 91*, 1 – 18, Houston, Texas: NACE

Meilunas, R. J., Bentsen, J. G., and Steinberg, A. (1990). Analysis of aged paint binders by FTIR spectroscopy. *Studies in Conservation*, 35, 33-51. DOI: 10.1179/sic.1990.35.1.33

Merriman, K. R. (2014). *The Context of Organic Residues in Archaeological Vessels of Ceramic and Bronze*. (PhD), University of Oxford, unpublished.

Merriman, K. R., Ditchfield, P., Goodburn-Brown, D. and Pollard, A. M. (2017). Where bio- and geochemistry meet: Organic Residues in Copper-corrosion Products? In: S. Kluiving, L. Kootket, and R. Hermans (eds.), *Interdisciplinarity between Humanities and Science: A fetschrift in honour of Prof. Df. Henk Kars*, 177-183, Leiden: Sidestone Press.

Meyer-Roudet, H. (1999). *A la recherché du metal perdu: Nouvelles technologies dans la restauration des métaux archéologiques* Paris: Éditions Errance.

Milardi, D., Grasso, D. M., Verbeet, M. P., Canters, G. W. and La Rosa, C. (2003). Thermodynamic analysis of the contributions of the copper ion and the disulfide bridge to azurin stability: synergism among multiple depletions. *Archives of Biochemistry and Biophysics*, 414, 121–127.

Miller, C. A., Holm, H. C., Horstmann, L., George, J. C., Fredricks, H. F., Van Mooy, B. A. S. and Apprill, A. (2020). Coordinated transformation of the gut microbiome and lipidome of bowhead whales provides novel insights into digestion. *The ISME Journal*, 14(3), 688-701. DOI:10.1038/s41396-019-0549-y

Mills, J. S. and White, R. (1977). Natural resins of art and archaeology, their sources, chemistry and identification. *Studies in Conservation*, 22, 12-31. DOI: 10.1179/sic.1977.003

Mills, J. S. and White, R. (1994). *The Organic Chemistry of Museum Objects* (2nd ed.). London: Butterworths.

Mocz, G. and Ross, J. A. (2013). Fluorescence Techniques in Analysis of Protein–Ligand Interactions. In Williams, M. A. and Daviter, T. (eds.), *Protein-ligand interactions : methods and applications* (2nd ed.), 169-210, New York : Humana Press

Modugno, F., Ribechini, E. and Colombini, M. P. (2006). Aromatic resin characterisation by gas chromatography–mass spectrometry: Raw and archaeological materials. *Journal of Chromatography A*, 1134(1-2), 298-304. DOI:10.1016/j.chroma.2006.09.010

Mohamed, W. and Darweesh, S. (2012). Ancient Egyptian black-patinated copper alloys. *Archaeometry*, 54(1), 175-192. DOI:10.1111/j.1475-4754.2011.00602.x

Montañés, F., Olano, A., Ibáñez, E. and Fornari, T. (2007). Modeling solubilities of sugars in alcohols based on original experimental data. *AIChE Journal*, 53(9), 2411-2418. DOI:10.1002/aic.11258

Montes Vidal, D., Von Rymon-Lipinski, A., Ravella, S., Groenhagen, U., Herrmann, J., Zaburannyi, N., Zarbin, P. H. G., Varadarajan, A. R., Ahrens, C. H., Weisskopf, L., Müller, R. and Schulz, S. (2017). Long-Chain Alkyl Cyanides: Unprecedented Volatile Compounds Released by Pseudomonas and Micromonospora Bacteria. *Angewandte Chemie International Edition*, 56(15), 4342-4346. DOI: 10.1002/anie.201611940

Morgan, E. D., Titus, L., Small, R. J. and Edwards, C. (1984). Gas-chromatographic analysis of fatty material from a Thule midden. *Archaeometry*, 26(1), 43-48. DOI: 10.1111/j.1475-4754.1984.tb00316.x

Morrison, R. T. and Boyd, R. N. (1992). *Organic Chemistry* (6th ed.). London: Prentice-Hall International.

Muros, V. and Scott, D. A. (2018). The occurrence of brochantite on archaeological bronzes: a case study from Lofkënd, Albania. *Studies in Conservation*, 63(2), 113-125. DOI: 10.1080/00393630.2016.1264179

Nakamura, K. and Go, N. (2005). Function and molecular evolution of multicopper blue proteins. *Cellular and Molecular Life Sciences CMLS*, 62(18), 2050-2066. DOI: 10.1007/s00018-004-5076-x

Nakayama, S., Tabata, K., Oba, T., Kusumoto, K., Mitsuiki, S., Kadokura, T. and Nakazato, A. (2012). Characteristics of the high malic acid production mechanism in Saccharomyces cerevisiae sake yeast strain No. 28. *Journal of bioscience and bioengineering*, 114(3), 281-285. DOI:10.1016/j.jbiosc.2012.04.003

Nelson, P. N. and Taylor, R. A. (2014). Theories and experimental investigations of the structural and thermotropic mesomorphic phase behaviors of metal carboxylates. *Applied Petrochemical Research*, 4(3), 253-285. DOI:10.1007/s13203-014-0044-3

Newburg, D. S. and Concon, J. M. (1980). Malonaldehyde Concentrations in Food are Affected by Cooking Conditions. *Journal of Food Science*, 45(6), 1681-1683. DOI:10.1111/j.1365-2621.1980.tb07588.x

Nienhuis, J., Robbiola, L., Giuliani, R., Joosten, I., Huisman, H., van Os, B. and Sietsma, J. (2016). Curly malachite on archaeological bronze: A systematic study of the shape and phenomenological approach of its formation mechanism. *e-Preservation Science*, 13, 23-32.

Nigra, B. T., Faull, K. F. and Barnard, H. (2015). Analytical Chemistry in Archaeological Research. *Analytical Chemistry*, 87, 3-18. DOI:10.1021/ac5029616

Nord, A., Mattsson, E. and Tronner, K. (2005). Factors Influencing the Long-term Corrosion of Bronze Artefacts in Soil. *Protection of Metals*, 41(4), 309-316. DOI:10.1007/s11124-005-0045-9

Nørgaard, H. W. (2017). Portable XRF on prehistoric bronze artefacts: Limitations and use for the detection of Bronze Age metal workshops. *Open Archaeology*. 3:101-22. DOI: 10.1515/opar-2017-0026

Olofsson, T. C., Alsterfjord, M., Nilson, B., Butler, È. and Vásquez, A. (2014a). *Lactobacillus apinorum sp. nov., Lactobacillus mellifer sp. nov., Lactobacillus mellis sp. nov., Lactobacillus melliventris sp. nov., Lactobacillus kimbladii sp. nov., Lactobacillus helsingborgensis sp. nov. and Lactobacillus kullabergensis sp. nov.*, isolated from the honey stomach of the honeybee *Apis mellifera*. *International Journal of Systematic and Evolutionary Microbiology*, 64(9), 3109–3119. DOI:10.1099/ijs.0.059600-0

Olofsson, T. C., Butler, Ė., Markowicz, P., Lindholm, C., Larsson, L. and Vásquez, A. (2014b). Lactic acid bacterial symbionts in honeybees – an unknown key to honey's antimicrobial and therapeutic activities. *International Wound Journal*, 13(5), 668-679. DOI:10.1111/iwj.12345

Oras, E., Higham, T. F.G., Cramp, L. J. E. and Bull, I. D. (2017). Archaeological science and object biography: a roman bronze lamp from Kavastu bog (Estonia). *Antiquity*, 91(335), 124-38. DOI: 10.15184/aqy.2016.247.

Orellana, R. G. and Mandava, N. B. (1983). m-Hydroxyphenylacetic and m-Methoxyphenylacetic Acids of Rhizoctonia solani : Their Effect on Specific Root-Nodule Activity and Histopathology in Soybean. *Journal of Phytopathology*, 107(2), 159-167. DOI:10.1111/j.1439-0434.1983.tb00063.x

Osmond, G. (2019). Zinc Soaps: An Overview of Zinc Oxide Reactivity and Consequences of Soap Formation in Oil-Based Paintings. In F. Casadio, K. Keune, P. Noble, A. v. Loon, E. Hendriks, S. A. Centeno, and G. Osmond (Eds.), *Metal soaps in art : conservation and research*, 25-45. Cham, Switzerland: Springer.

Otero, V., Sanches, D., Montagner, C., Vilarigues, M., Carlyle, L., Lopes, J. A. and Melo, M. J. (2014). Characterisation of metal carboxylates by Raman and infrared spectroscopy in works of art. *Journal of Raman Spectroscopy*, 45, 1197-1206. DOI:10.1002/jrs.4520

Otto, A. and Simoneit, B. R. T. (2001). Chemosystematics and diagenesis of terpenoids in fossil conifer species and sediment from the Eocene Zeitz formation, Saxony, Germany. *Geochimica et Cosmochimica Acta*, 65(20), 3505-3527. DOI:10.1016/S0016-7037(01)00693-7

Oudemans, T. F. M. and Boon, J. J. (1991). Molecular archaeology: analysis of charred (food) remains from prehistoric pottery by pyrolysis–gas chromatography/mass spectrometry. *Journal of Analytical and Applied Pyrolysis*, 20, 197-227. DOI:10.1016/0165-2370(91)80073-H

Ozogul, F., Kuley, E. and Ozogul, Y. (2015). Sterol Content of Fish, Crustacea and Mollusc: Effects of Cooking Methods. *International Journal of Food Properties*, 18(9), 2026-2041. DOI:10.1080/10942912.2014.958770

Ozyurt, G., Kuley, E., Etyemez, M. and Ozoğul, F. (2013). Comparative seasonal sterol profiles in edible parts of Mediterranean fish and shellfish species. *International Journal of Food Science Nutrition*, 64(4), 476-483. DOI:10.3109/09637486.2012.749836

Paparazzo, E. (2003). Organic substances at metal surfaces: Archaeological evidence and The Elder Pliny's account. *Archaeometry*, 45(4), 615-624. DOI:10.1046/j.1475-4754.2003.00132.x

Parks, L. W. and Casey, W. M. (1995). Physiological Implications of Sterol Biosynthesis in Yeast. *Annual Reviews in Microbiology*, 491(1), 95-116. DOI:10.1146/annurev.mi.49.100195.000523

Parsi, Z. and Gorecki, T. (2006). Determination of ergosterol as an indicator of fungal biomass in various samples using non-discriminating flash pyrolysis. *Journal of Chromatography A*, 1130(1), 145-150. DOI:10.1016/j.chroma.2006.07.045

Parsons, J. B. and Rock, C. O. (2013). Bacterial lipids: Metabolism and membrane homeostasis. *Progress in Lipid Research*, 52(3), 249-276. DOI:10.1016/j.plipres.2013.02.002

Passi, S., Rothschild-Boros, M. C., Fasella, P., Nazzaro-Porro, M. and Whitehouse, D. (1981). An application of high performance liquid chromatography to analysis of lipids in archaeological samples. *Journal of Lipid Research*, 22(5), 778-784.

Paterakis, A. B. (2003). The influence of Conservation Treatments and Environmental Storage Factors on Corrosion of Copper Alloys in the Ancient Athenian Agora. *Journal of the American Institute for Conservation*, 42(2), 313-336. DOI:10.2307/3180074

Paulino, B. N., Molina, G., Pastore, G. M. and Bicas, J. L. (2021). Current perspectives in the biotechnological production of sweetening syrups and polyols. *Current opinion in food science*, 41, 36-43. DOI:10.1016/j.cofs.2021.02.004

Pavlopoulou, L. and Watkinson, D. E. (2006). The degradation of oil painted copper surfaces. *Studies in Conservation*, 51:55-65. DOI: 10.1179/sic.2006.51.Supplement-1.55

Pecharsky, V. and Zavalij. P. (2009). *Fundamentals of Powder Diffraction and Structural Characterization of Materials.* 2nd edition. Springer. DOI::10.1007/978-0-387-09579-0.

Peleg, Y., Stieglitz, B. and Goldberg, I. (1988). Malic acid accumulation by Aspergillus flavus *Applied Microbiology and Biotechnology*, 28, 69–75. DOI:10.1007/BF00250501

Pérez-Henarejos, S. A., Alcaraz, L. A. and Donaire, A. (2015). Blue Copper Proteins: A rigid machine for efficient electron transfer, a flexible device for metal uptake. *Archives of Biochemistry and Biophysics*, 584, 134-148. DOI:10.1016/j.abb.2015.08.020

Pérez-Serradilla, J. A, Jurado-López, A. and Luque de Castro, M. D. (2017). Complementarity of XRFS and LIBS for corrosion studies. *Talanta*. 71(1):97-102. DOI: 10.1016/j.talanta.2006.03.034

Peška, J., Králík, M. and Selucká, A. (2006). Organic Matter Residuals and Imprints in Products of Copper and Copper Alloy Corrosion: A Preliminary Study: Early Bronze Age Industry. *Památky Archeologické*, 97, 5-46.

Peters, K. E., Walters, C. C. and Moldowan, J. M. (2005). *The Biomarker Guide. Volume 1: Biomarkers and Isotopes in the Environment and Human History* (2nd ed.). Cambridge, UK: Cambridge University Press.

Pettit, L. D., Steel, I., Formicka-Kozlowska, G., Tatarowski, T. and Bataille, M. (1985). The L-proline residue as a 'break-point' in metal–peptide systems. Journal of the Chemical Society, *Dalton Transactions*, 3, 535-539. DOI:10.1039/DT9850000535

Phokasem, P., de Guzman, L. I., Khongphinitbunjong, K., Frake, A. M. and Chantawannakul, P. (2019). Feeding by *Tropilaelaps mercedesae* on pre- and post-capped brood increases damage to *Apis mellifera* colonies. *Scientific Reports*, 9. DOI:10.1038/s41598-019-49662-4

Piccardo, P., Mődlinger, M., Ghiara, G., Campodonico, S. and Bongiorno, V. (2013). Investigation on a "tentacle-like" corrosion feature on Bronze Age tin-bronze objects. *Applied Physics A: Materials Science & Processing*, 113, 1039-1047. DOI:10.1007/s00339-013-7732-1

Pilath, H. M., Nimlos, M. R.; Mittal, A., Himmel, M. E. and Johnson, D. K. (2010). Glucose Reversion Reaction Kinetics. *Journal of agricultural and food chemistry*, 58:10, 6131-6140. DOI: 10.1021/jf903598w.

Pires, E., da Costa Carvalho, L., Shimada, I. and McCullagh, J. (2021). Human Blood and bird egg proteins identified in red paint covering a 1,000-year-old gold mask from Peru. *Journal of Proteome Research* in press

Poli, T., Piccirillo, A., Nervo, M. and Chiantore, A. (2017). Interactions of natural resins and pigments in works of art. *Journal of Colloid and Interface Science*, 503(1), 1-9. DOI:10.1016/j.jcis.2017.04.094

Pollard, A. M., Thomas, R. G. and Williams, P. A. (1989). Synthesis and stabilities of the basic copper(II) chlorides atacamite, paratacamite and botallackite. *Mineralogical Magazine*, 53(373), 557-563. DOI:10.1180/minmag.1989.053.373.06

Pollard, A. M., Thomas, R. G. and Williams, P. A. (1990). Mineralogical changes arising from the use of aqueous sodium carbonate solutions for the treatment of archaeological copper objects. *Studies in Conservation*, 35, 148-153. DOI:10.1179/sic.1990.35.3.148

Pollard, A. M., Wilson, L., Wilson, A. S., Hall, A. J. and Shiel, R. (2004). Assessing the influence of agrochemicals on the rate of copper corrosion in the vadose zone of arable land Part 1: field experiments. *Conservation and Management of Archaeological Sites*, 6(3-4), 363-376. DOI:10.1179/135050304793137784

Pollard, A. M., Batt, C., Stern, B. and Young, S. M. M. (2007). *Analytical Chemistry in Archaeology*: Cambridge University Press.

Pollard, A. M., Bray, P., Gosden, C., Wilson, A. and Hamerow, H. (2015). Characterising copper-based metals in Britain in the first millennium AD: a preliminary quantification of metal flow and recycling. *Antiquity*, 89(345), 697-717. DOI:10.15184/aqy.2015.20

Porter, N. A. (1986). Mechanisms for the Autoxidation of Polyunsaturated Lipids. *Accounts of Chemical Research*, 19(9), 262-268. DOI:10.1021/ar00129a001

Pourbaix, M. (1973). *Lectures on electrochemical corrosion* (J. A. S. Green, Trans.). New York: Plenum Press.

Pozdnyakova, I., Guidry, J. and Wittung-Stafshede, P. (2001). Copper stabilizes azurin by decreasing the unfolding rate. *Archives of Biochemistry and Biophysics*, 390(1), 146-148. DOI: 10.1006/abbi.2000.2369

Praet, J., Parmentier, A., Schmid-Hempel, R., Meeus, I., Smagghe, G. and Vandamme, P. (2018). Large-scale cultivation of the bumblebee gut microbiota reveals an underestimated bacterial species diversity capable of pathogen inhibition. *Environmental Microbiology*, 20(1), 214-227. DOI: 10.1111/1462-2920.13973

Prati, S., Bonacini, I., Sciutto, G., Genty-Vincent, A., Cotte, M., Eveno, M., Menu, M. and Mazzeo, R. (2016). ATR-FTIR microscopy in mapping mode for the study of verdigris and its secondary products. *Applied Physics A*, 122(1), 1-16. DOI:10.1007/s00339-015-9519-z

Proefke, M. L., Rinehart, K. L., Raheel, M., Ambrose, S. H. and Wisseman, S. U. (1992). Probing the mysteries of ancient Egypt—chemical analysis of a Roman period Egyptian mummy. *Analytical Chemistry*, 64, 105-111. DOI:10.1021/ac00026a002

Przybylski, D., Rohwerder, T., Harms, H., Yaneva, N. and Müller, R. H. (2013). Synthesis of the building block 2-hydroxyisobutyrate from fructose and butyrate by *Cupriavidus necator* H16. *Applied Microbiology and Biotechnology*, 97, 8875–8885 DOI:10.1007/s00253-013-5064-x

Ramdahl, T. (1983). Retene—a molecular marker of wood combustion in ambient air. *Nature*, 306(5943), 580-582. DOI:10.1038/306580a0

Reddy, P. R. and Manjula, P. (2007). Mixed-ligand copper(II)-phenanthroline-dipeptide complexes: Synthesis, characterization, and DNA-cleavage properties. *Chemistry and Biodiversity*, 4(3), 468-480.

Regert, M., Bland, H. A., Dudd, S. N., Bergen, P. F. V. and Evershed, R. P. (1998). Free and bound fatty acid oxidation products in archaeological ceramic vessels. *Proceedings of the Royal Society B: Biological Sciences*, 265(1409), 2027-2032. DOI:10.1098/rspb.1998.0536

Regert, M., Colinart, S., Degrand, L. and Decavallas, O. (2001). Chemical Alteration and Use of Beeswax Through Time: Accelerated Ageing Tests and Analysis of Archaeological Samples from Various Environmental Contexts. *Archaeometry*, 43(4), 549-569. DOI:10.1111/1475-4754.00036

Regert, M. and Rolando, C. (2002). Identification of archaeological adhesives using direct inlet electron ionization mass spectrometry. *Analytical Chemistry*, 74(5), 965-975. DOI:10.1021/ac0155862

Regert, M., Vacher, S., Moulherat, C. and Decavallas, O. (2003). Adhesive production and pottery function during the Iron Age at the site of Grand Aunay (Sarthe, France). *Archaeometry*, 45(1), 101-120. DOI:10.1111/1475-4754.00098

Rehren, T., Belgya, T., Jambon, A., Káli, G., Kasztovszky, Z., Kis, Z., Kovács, I., Maróti, B., Martinón-Torres, M., Miniaci, G., Pigott, V. C., Radivojević, M., Rosta, L., Szentmiklósi, L. and Szőkefalvi-Nagy, Z. (2013). 5,000 years old Egyptian iron beads made from hammered meteoritic iron. *Journal of Archaeological Science*, 40(12), 4785-4792. DOI:10.1016/j.jas.2013.06.002

Remko, M., Fitz, D., Broer, R. and Rode, B. M. (2011). Effect of metal Ions (Ni2+, Cu2+ and Zn2+) and water coordination on the structure of L-phenylalanine, L-tyrosine, L-tryptophan and their zwitterionic forms. *Journal of Molecular Modelling*, 17, 3117–3128. DOI:10.1007/s00894-011-1000-0

Ribechini, E., Modugnoa, F., Colombinia, M. P. and Evershed, R. P. (2008). Gas chromatographic and mass spectrometric investigations of organic residues from Roman glass unguentaria. *Journal of Chromatography A.* 1183(1-2), 158-169. DOI:10.1016/j.chroma.2007.12.090

Ribechini, E., Orsini, S., Silvano, F. and Colombini, M. P. (2009). Py-GC/MS, GC/MS and FTIR investigations on LATE Roman-Egyptian adhesives from opus sectile: New insights into ancient recipes and technologies. *Analytica Chimica Acta*, 638(1), 79-87. DOI:10.1016/j.aca.2009.02.004

Ribechini, E., Pérez-Arantegui, J. and Colombini, M. P. (2013). Positive and negative-mode laser desorption/ionization-mass spectrometry (LDI-MS) for the detection of indigoids in archaeological purple. *Journal of Mass Spectrometry*, 48(3), 384-391. DOI:10.1002/jms.3169

Robbiola, L., Blengino, J. M. and Fiaud, C. (1998). Morphology and mechanisms of formation of natural patinas on archaeological Cu-Sn alloys. *Corrosion Science*, 40(12), 2083-2111 DOI:10.1016/S0010-938X(98)00096-1

Robinet, L. and Corbeil, M.-C. (2003). The Characterization of Metal Soaps. *Studies in Conservation*, 48(1), 23-40. DOI:10.1179/sic.2003.48.1.23

Robinson, N., Evershed, R. P., Higgs, W. H., Jerman, K. and Eglinton, G. (1987). Proof of a pine wood origin for pitch from Tudor (Mary Rose) and Etruscan shipwrecks: application of analytical organic chemistry in archaeology. *Analyst*, 112, 367–644. DOI:10.1039/AN9871200637

Rodriguez, J. A., Valentine, J. S., Eggers, D. K., Roe, J. A., Tiwari, A., Brown Jr., R. H. and Hayward, L. J. (2002). Familial Amyotrophic Lateral Sclerosis-associated Mutations Decrease the Thermal Stability of Distinctly Metallated Species of Human Copper/Zinc Superoxide Dismutase. *Journal of Biological Chemistry*, 277(18), 15932–15937. DOI:10.1074/jbc.M112088200

Roffet-Salque, M., Regert, M., Evershed, R. P., Outram, A. K., Cramp, L. J. E., Decavallas, O., . . . and Zoughlami, J. (2015). Widespread exploitation of the honeybee by early Neolithic farmers. *Nature*, 527 226–230. DOI:10.1038/nature15757

Roffet-Salque, M., Dunne, J., Altoft, D. T., Casanova, E., Cramp, L. J. E., Smyth, J., Whelton, H. L. and Evershed, R. P. (2017). From the inside out: Upscaling organic residue analyses of archaeological ceramics. *Journal of Archaeological Science: Reports*, 16, 627-640. DOI:10.1016/j.jasrep.2016.04.005

Rouxhet, P. G. and Genet, M. J. (2011). XPS analysis of bio-organic systems. *Surface and Interface Analysis*, 43(12), 1453-1470. DOI:10.1002/sia.3831

Rubino, T., and Franz, K. J. (2012). Coordination chemistry of copper proteins: How nature handles a toxic cargo for essential function. *Journal of Inorganic Biochemistry*, 107(1), 129-143. DOI:10.1016/j.jinorgbio.2011.11.024

Rulíšek, L., and Vondrášek, J. (1998). Coordination geometries of selected transition metal ions (Co2+, Ni2+, Cu2+, Zn2+, Cd2+, and Hg2+) in metalloproteins. *Journal of Inorganic Biochemistry*, 71(3-4), 115-127. DOI:10.1016/S0162-0134(98)10042-9

Sakr, A. A., Ghaly, M., Ali, M. and Abdel-Haliem, M. (2013). Biodeterioration of binding media in tempera paintings by Streptomyces isolated from some ancient Egyptian paintings. *African Journal of Biotechnology*, 12(14). DOI:10.5897/AJB12.2393

Saliu, F., Degano, I. and Colombini, M. P. (2014). Identification of triacylglycerols in archaelogical organic residues by core–shell reversed phase liquid chromatography coupled to electrospray ionization-quadrupole-time of flight mass spectrometry. *Journal of Chromatography A*, 1346, 78-87. DOI:10.1016/j.chroma.2014.04.049

Salque, M., Bogucki, P., Pyzel, J., Sobkowiak-Tabaka, I., Grygiel, R., Szmyt, M. and Evershed, R. P. (2013). Earliest evidence for cheese making in the sixth millennium BC in northern Europe. *Nature*, 493, 522–525. DOI:10.1038/nature11698

Salvadó, N., Buti, S., Pradell, T., Beltran, V., Cinque, G. and Juanhuix, J. (2019). Identification and Distribution of Metal Soaps and Oxalates in Oil and Tempera Paint Layers in Fifteenth-Century Altarpieces Using Synchrotron Radiation Techniques. In: Casadio, F., Keune, K., Noble, P., v. Loon, A., Hendriks, E., Centeno, S. A. and Osmond, G. (eds.), *Metal Soaps in Art - Conservation and Research*, 195-210. Cham, Switzerland: Springer.

Sandberg, A., Leckner, J., Shi, Y., Schwarz, F. P. and Karlsson. B. G. (2002). Effects of Metal Ligation and Oxygen on the Reversibility of the Thermal Denaturation of Pseudomonas aeruginosa Azurin. *Biochemistry*, 41(3), 1060–1069. DOI:10.1021/bi0157621

Santos-Buelga, C. and González-Paramás, A. M. (2017). The Chemical Composition of Honey. In Alvarez-Suarez, J. M. (ed.), *Bee Products - Chemical and Biological Properties*. Cham, Switzerland: Springer.

Scalarone, D., Kazaari, M. and Chiantore, O. (2003). Aging behaviour and pyrolytic characterisation of diterpenic resins used as art materials: Manila copal and sandarac. *Journal of Analytical Applied Pyrolysis*, 68(69), 115–136. DOI:10.1016/S0165-2370(03)00005-6

Schäfer, S., Bicker, G., Ottersen, O. P. and Storm-Mathisen, J. (1988). Taurine-like immunoreactivity in the brain of the honeybee. *Journal of Comparative Neurology*, 268(1), 60-70.

Schauer, J. J., Kleeman, M. J., Cass, G. R., and Simoneit, B. R. T. (1999). Measurement of emissions from air pollution sources. 1. C1 through C29 organic compounds from meat charbroiling.(what barbeques do to the environment). *Environmental Science & Technology*, 33(10), 1566-1572. DOI:10.1021/es980076j

Scholz, F., Schrőder, U., Gulabosk,i R. and Doménech-Carbó, A. (2014). *Electrochemistry of Immobilized Particles and Droplets*. 2nd ed. Berlin-Heidelberg: Springer

Schrenk, J. L. (1994). The Royal Art of Benin: Surfaces, Past and Present. In Scott, D. A., Podany, J. and Considine, B. B. (eds.), *Ancient Art and Historic Metals: conservation and scientific research : proceedings of a symposium organized by the J. Paul Getty Museum and the Getty Conservation Institute, November 1991*, 51-62. Marina del Rey, CA: Getty Conservation Institute.

Schweizer, F. (1994). Bronze objects from lake sites : from Patina to "biography" In Scott, D. A., Podany, J. and Considine, B. B. (eds.), *Ancient Art and Historic Metals: conservation and scientific research : proceedings of a symposium organized by the J. Paul Getty Museum and the Getty Conservation Institute, November 1991*, 33-50. Marina del Rey, CA: Getty Conservation Institute.

Scott, D. A. (1990). Bronze Disease: A Review of Some Chemical Problems and the Role of Relative Humidity. *Journal of the American Institute for Conservation*, 29, 193-206. DOI:10.1179/019713690806046064

Scott, D. A. (2000). A Review of Copper Chlorides and Related Salts in Bronze Corrosion and as Painting Pigment. *Studies in Conservation*, 45(1), 39-53. DOI:10.1179/sic.2000.45.1.39

Scott, D. A. (2002). *Copper and Bronze in Art: corrosion, colorants, conservation*. Los Angeles, California: Getty Conservation Institute.

Scott, D. A. (2017). New insights on the corrosion of ancient bronzes using X-ray powder diffraction: The importance of paratacamite, sampleite, and connellite. *Studies in Conservation*, 62(7), 410-418. DOI:10.1080/00393630.2016.1219466

Scott, D. A., Dennis, M., Khandekar, N., Keeney, J., Carson, D. and Dodd, L. S. (2003). An Egyptian Cartonnage of the Graeco-Roman Period: Examination and Discoveries. *Studies in Conservation*, 48(1), 41-56. DOI:10.1179/sic.2003.48.1.41

Scott, D. A., Dodd, L. S., Furihata, J., Tanimoto, S., Keeney, J., Schilling, M. R. and Cowan, E. (2004). An Ancient Egyptian Cartonnage Broad Collar - Technical Examination of Pigments and Binding Media. *Studies in Conservation*, 49(3), 177-192. DOI:10.1179/sic.2004.49.3.177

Scott, D. A. and Maish, J. P. (2010). A Lydian Bed of Iron, Bronze and Copper - Technical Examination of a Metallurgical Masterpiece. *Studies in Conservation*, 55(1), 3-19. DOI:10.1179/sic.2010.55.1.3

Sedlák, E., Žoldák, G., and Wittung-Stafshede, P. (2008). Role of Copper in Thermal Stability of Human Ceruloplasmin. *Biophysical Journal*, 94(4), 1384–1391. DOI:10.1529/biophysj.107.113696

Selwyn, L. (2004). *Metals and corrosion: a handbook for the conservation professional*. Ottawa: Canadian Conservation Institute.

Sembiring, K. C., Minami, E., Kawamoto, H. and Saka, S. (2020). Oxidative Cleavage of Linoleic and Linolenic Acids followed by Decarboxylation for Hydrocarbon Production. *Journal of the Japan Institute of Energy*, 99, 1-7. DOI:10.3775/jie.99.1

Serpico, M. and White, R. (2000). Adhesives and binders. In Nicholson, P. and Shaw, I. (eds.), *Ancient Egyptian Materials and Technology*, 475-494. Cambridge: Cambridge University Press.

Sestieri, M. B. (1985). Nuove ricerche sull'ipogeo di Paestum. Mélandes de l'Ecole française de Rome. *Antiquité*, 97, 647-691.

Sestieri, P. C. (1956). An underground shrine at Paestum. *Archaeology*, 9(1), 22-33.

Shillings, M. R., Mazurek, J. and Learner, T. S. (2007). Studies of Modern Oil-Based Artists' Paint Media by Gas Chromatography/Mass Spectrometry. In Learner, T. S., Smithen, P., Krueger, J. and Schilling, M. (eds) Modern Paints Uncovered - Proceedings from the Symposium in London, 129-139, Los Angeles, Calif. : Getty Conservation Institute

Shoda, S., Lucquina, A., Ahn, J., Hwang, C. and Craiga, O. E. (2017). Pottery use by early Holocene hunter-gatherers of the Korean peninsula closely linked with the exploitation of marine resources. *Quaternary Science Reviews*, 170, 164-173. DOI:10.1016/j.quascirev.2017.06.032

Sibley, L. R. and Jakes, J. A. (1982). Textile Fabric Pseudomorphs, A Fossilized Form of Textile Evidence. *Clothing and Textile Research*, 1, 24–30. DOI:10.1177/0887302X8200100105

Siemion, I. Z., Kubik, A., Jezowska-Bojczuk, M. and Kozłowski, H. (1984). The absolute configuration on the chiral nitrogen atom of proline residue in the metal complexes of oligopeptides. *Journal of Inorganic Biochemistry*, 22(2), 137-141. DOI:10.1016/0162-0134(84)80022-7

Silva, P. S., Moreira, A. S. P., Domingues, M. R. M., Evtuguin, D. V., Coelho, E. and Coimbra, M. A. (2019). Contribution of non-enzymatic transglycosylation reactions to the honey oligosaccharides origin and diversity. *Pure and Applied Chemistry*, 91(7), 1231-1242. DOI:10.1515/pac-2019-0209

Simoneit, B., Rushdi, A., Bin Abas, M. and Didyk, B. (2003). Alkyl amides and nitriles as novel tracers for biomass burning. *Environmental Science & Technology*, 37(1), 16-21. DOI:10.1021/es020811y

Simpson, I. A., Bol, R., Bull, I. D., Evershed, R. P., Petzke, K.-J. and Dockrill, S. J. (1999). Interpreting early land management through compound specific stable isotope analysis of archaeological soils. *Rapid Communications in Mass Spectrometry*, 13, 1315-1319. DOI:10.1002/(SICI)1097-0231(19990715)13:13<1315::AID-RCM629>3.0.CO;2-0

Šlechtová, T., Gilar, M., Kalíková, K. and Tesařová, E. (2015). Insight into Trypsin Miscleavage: Comparison of Kinetic Constants of Problematic Peptide Sequences. *Analytical Chemistry*, 87(15), 7636–7643. DOI:10.1021/acs.analchem.5b00866

Smith, K. R. and Thiboutot, D. M. (2008). Thematic review series: skin lipids. Sebaceous gland lipids: friend or foe? *Journal of Lipid Research*, 49(2), 271-81. DOI: 10.1194/jlr.R700015-JLR200

Snowdon, J. A. and Cliver, D. O. (1996). Microorganisms in honey. *International Journal of Food Microbiology*, 31(1), 1-26. DOI:10.1016/0168-1605(96)00970-1

Socrates, G. (2001). *Infrared and Raman Characteristic Group Frequencies: Tables and Charts*. 3rd edition. Chichester: John Wiley & Sons

Solazzo, C., Rogers, P. W., Weber, L., Beaubien, H. F., Wilson, J., and Collins, M. (2014). Species identification by peptide mass fingerprinting (PMF) in fibre products preserved by association with copper-alloy artefacts. *Journal of Archaeological Science*, 49, 524-534. DOI:10.1016/j.jas.2014.06.009

Sotiropoulou, S., Papliaka, Z. E. and Vaccari, L. (2016). Micro FTIR imaging for the investigation of deteriorated organic binders in wall painting stratigraphies of different techniques and periods. *Microchemical Journal*, 124, 559-567. DOI:10.1016/j.microc.2015.10.002

Sovago, I., Varnagy, K., Lihi, N. and Grenacs, A. (2016). Coordinating properties of peptides containing histidyl residues. *Coordination Chemistry Reviews*, 327–328, 43-54. DOI:10.1016/j.ccr.2016.04.015

Spanova, M. and Daum, G. (2011). Squalene – biochemistry, molecular biology, process biotechnology, and applications. *European Journal of Lipid Science and Technology*, 113(11), 1299-1320

Sporstol, S., Gjos, N., Lichtenthaler, R. G., Gustavsen, K. O., Urdal, K., Oreld, F. and Skei, J. (1983). Source identification of aromatic hydrocarbons in sediments using GC/MS. *Environmental Science & Technology*, 17(5), 282-286. DOI:10.1021/es00111a008

Sramek, M., Woerz, B., Horn, H., Weiss, J. and Kohlus, R. (2016). Inactivation kinetics of invertase in honey and honey-glucose syrup formulations: effects of temperature and water activity. *Science of Food and Agriculture*, 97(4), 1178-1184. DOI: 10.1002/jsfa.7846

Stacey, R. (2011). The composition of some Roman medicines: evidence for Pliny's Punic wax? *Analytical and Bioanalytical Chemistry*, 401(6), 1749-1759. DOI:10.1007/s00216-011-5160-7

Stacey, R. J., Heron, C. and Sutton, M. K. (1998). The Chemistry, Archaeology and Ethnography of a Native American Insect Resin. *Journal of California and Great Basin Anthropology*, 20(1), 53-71.

Stahl, P. D. and Parkin, T. B. (1996). Relationship of soil ergosterol concentration and fungal biomass. *Soil Biology & Biochemistry*, 28(7), 847-855. DOI:10.1016/0038-0717(96)00061-2

Stansbury, E. E. and Buchanan, R. A. (2000). *Fundamentals of Electrochemical Corrosion*. Materials Park, OH: ASM International.

Steele, V. J. (2017). Analysis of partially carbonised residues from the chiseldon cauldrons by gas chromatography-mass spectrometry and gas chromatography-combustion-isotope ratio mass spectrometry. In Baldwin, A., Joy, J. and Armstrongs, A. (eds) *A Celtic Feast: The Iron Age Cauldrons from Chiseldon, Wiltshire*, 78-86. London: The British Museum.

Steigenberger, G. and Herm, C. (2011). Natural resins and balsams from an eighteenth-century pharmaceutical collection analysed by gas chromatography/mass spectrometry. *Analytical and Bioanalytical Chemistry*, 401(6), 1771-1785. DOI:10.1007/00216-011-5169-y

Stern, B., Heron, C., Corr, L., Serpico, M. and Bourriau, J. (2003). Compositional variation in aged and heat treated Pistacia resin found in Late Bronze Age Canaanite amphorae and bowls from Amarna, Egypt. *Archaeometry*, 45(3), 457-469. DOI:10.1111/1475-4754.00121

Stevens, J. S., Luca, A. C., Pelendritis, M., Terenghi, G., Downes, S. and Schroeder, S. L. M. (2013). Quantitative analysis of complex amino acids and RGD peptides by X-ray photoelectron spectroscopy (XPS). *Surface and Interface Analysis*, 45(8), 1238-1246. DOI:10.1002/sia.5261

Stevenson, M. J., Janisse, S. E., Tao, L., Neil, R. L., Pham, Q. D., Britt, R. D. and Heffern, M. C. (2020). Elucidation of a Copper Binding Site in Proinsulin C-peptide and Its Implications for Metal-Modulated Activity. *Inorganic Chemistry*, 59(13), 9339-9349. DOI:10.1021/acs.inorgchem.0c01212

Stoffyn-Egli, P., Buckley, D. E. and Clyburne, J. A. (1998). Corrosion of Brass in a Marine Environment: Mineral Products and their Relationship to Variable Oxidation and Reduction Conditions. *Applied Geochemistry*, 13(5), 643-650. DOI:10.1016/S0883-2927(97)00108-X

Tabuchi, T., Sugisawa, T., Ishidori, T., Nakahara, T. and Sugiyama, J. (1981). Itaconic Acid Fermentation by a Yeast Belonging to the Genus Candida. *Agricultural and Biological Chemistry*, 45(2), 475-479. DOI:10.1080/00021369.1981.10864534

Taing, O. and Taing, K. (2007). Production of malic and succinic acids by sugar-tolerant yeast Zygosaccharomyces rouxii. *European Food Research and Technology*, 224(3), 343-347. DOI:10.1007/s00217-006-0323-z

Tayeh, N., Rungassamy, T. and Albani, H. R. (2009). Fluorescence spectral resolution of tryptophan residues in bovine and human serum albumins. *Journal of Pharmaceutical and Biomedical Analysis*, 50(2), 107-116. DOI:10.1016/j.jpba.2009.03.015

Thickett, D. and Odlyha, M. (2000). Note on the Identification of an Unusual Pale Blue Corrosion Product from Egyptian Copper Alloy Artifacts. *Studies in Conservation*, 45(1), 63-67. DOI:10.2307/1506684

Thiele, S. and Brümmer, G. W. (2002). Bioformation of polycyclic aromatic hydrocarbons in soil under oxygen deficient conditions. *Soil Biology & Biochemistry*, 34(12), 733-735. DOI:10.1016/S0038-0717(01)00204-8

Thomas, D. and Surdin-Kerjan, Y. (1997). Metabolism of sulfur amino acids in *Saccharomyces cerevisiae*. *Microbiology and Molecular Biology Reviews*, 61(4), 503

Tian, C., Ni, J., Chang, F., Liu, S., Xu, N., Sun, W., . . . and Wang, Y. (2016). Bio-Source of di-n-butyl phthalate production by filamentous fungi. *Scientific Reports*, 6, 19791. DOI:10.1038/srep19791

Tilbrooke, D. (1980). The fatty acid corrosion of copper alloys and its treatment. ICCM Bulletin. 6(3-4):46-52.

Trentelman, K., Stodulski, L., Scott, D. A., Back, M., Stock, S., Strahan, D., . . . and Garrett, S. J. (2002). The Characterization of a New Pale Blue Corrosion Product Found on Copper Alloy Artifacts. *Studies in Conservation*, 47(4), 217-227. DOI:10.2307/1506782

Tsai, T., Tsai, T., Wu, W., Tseng, J. T. and Tsai, P. (2010). In vitro antimicrobial and anti-inflammatory effects of herbs against *Propionibacterium acnes*. *Food Chemistry*, 119(3), 964-968. DOI:10.1016/j.foodchem.2009.07.062

Tweddle, D. (1992). *Anglian helmet from Coppergate*. London: Council for British Archaeology.

van den Berg, J., van den Berg, K. and Boon, J. J. (1999). Chemical changes in curing and ageing oil paints. In. Bridgland, J. (ed.) *ICOM-CC ICOM Committee for Conservation 12th Triennial Meeting Lyon 29 August - 3 September 1999*, 248-253, Lyon: James

van den Berg, K. J., Boon, J. J., Pastorova, I. and Spetter, L. F. M. (2000). Mass Spectrometric Methodology for the Analysis of Highly Oxidized Diterpenoid Acids in Old Master Paint. *Journal of Mass Spectrometry*, 35(4), 512-533. DOI:10.1002/(SICI)1096-9888(200004)35:4<512::AID-JMS963>3.0.CO;2-3

van der Heide, P. (2011). *X-Ray Photoelectron Spectroscopy: An Introduction to Principles and Practices*. Hoboken, N.J: John Willey & Sons. DOI:10.1002/9781118162897.

Vermeij, P. and Kertesz, M. A. (1999). Pathways of assimilative sulfur metabolism in Pseudomonas putida. *Journal of Bacteriology*, 181(18), 5833-5837. DOI:10.1128/JB.181.18.5833-5837.1999

Vivian, J. T. and Callis, P. R. (2001). Mechanisms of Tryptophan Fluorescence Shifts in Proteins. *Biophysical Journal*, 80(5), 2093-2109. DOI:10.1016/S0006-3495(01)76183-8

von Rymon Lipinski, G. W. (2006). 10 - Reduced-calorie sweeteners and caloric alternatives. In Spillane, W. J. (ed.), *Optimising Sweet Taste in Foods*, 252-280. Cambridge: Published by Woodhead Publishing Limited.

Wang, J., Su, T., Liu, Y., Yue, Y. and He, R. (2012). Postoperative Cognitive Dysfunction is Correlated with Urine Formaldehyde in Elderly Noncardiac Surgical Patients. *Neurochemical Research*, 37(10), 2125-2134. DOI:10.1007/s11064-012-0834-x

Wang, J., Simoneit, B., Sheng, G., Chen, L., Xu, L., Wang, X., . . . and Sun, L. (2017). The Potential of Alkyl Amides as Novel Biomarkers and Their Application to Paleocultural Deposits in China. *Scientific Reports*, 7(1), 14667-14667. DOI:10.1038/s41598-017-15371-z

Wang, Q., Huang, H. and Shearman, F. (2009). Bronzes from the Sacred Animal Necropolis at Saqqara, Egypt: a study of the metals and corrosion. In *The British Museum – Technical Research Bulletin*, 3, 73-82

Wang, X., Gong , C. S. and Tsao , G. T. (1998). Production of L-malic acid via biocatalysis employing wild-type and respiratory-deficient yeasts. Applied biochemistry and biotechnology, 70, 845-852. DOI:10.1007/BF02920194

Wang, Y., Nan, X., Zhao, Y., Jiang, L., Wang, M., Wang, H., . . . and Xiong, B. (2021). Rumen microbiome structure and metabolites activity in dairy cows with clinical and subclinical mastitis. *Journal of Animal Science and Biotechnology*, 12(1). DOI:10.1186/s40104-020-00543-1

Weber, N., Biehler, K., Schwabe, K., Haarhaus, B., Quirin, K., Frank, U., . . . and Wölfle, U. (2019). Hop Extract Acts as an Antioxidant with Antimicrobial Effects against *Propionibacterium Acnes* and *Staphylococcus Aureus*. *Molecules*, 24(2), 223. DOI:10.3390/molecules24020223

Weete, J. D. (1973). Sterols of the fungi: Distribution and biosynthesis. *Phytochemistry*, 12(8), 1843-1864. DOI:10.1016/S0031-9422(00)91502-4

Wei, H., Kockelmann, W., Godfrey, E. and Scott, D. A. (2019). The metallography and corrosion of an ancient Chinese bimetallic bronze sword. *Journal of Cultural Heritage*, 37, 259-265. DOI:10.1016/j.culher.2018.10.004

Weimer, P. J. and Kohn, R. A. (2016). Impacts of ruminal microorganisms on the production of fuels: how can we intercede from the outside? *Applied Microbiology and Biotechnology*, 100, 3389-3398. DOI:10.1007/s00253-016-7358-2

Weißhaar, R. and Perz, R. (2012). Fatty acid esters of glycidol in refined fats and oils. European *Journal of Lipid Science and Technology*, 11(2), 158-165. DOI:10.1002/ejlt.200900137

Werner, U., Selwyn, L. S., Stone, T., McKinnon, W. R., MacKay, A. and Grant, T. (2012). The removal of metal soaps from brass beads on a leather belt. *Studies in Conservation*, 57(1), 20-23. DOI:10.1179/2047058411Y.0000000004

Weser, U., Kaup, Y., Etspuler, H., Koller, J. and Baumer, U. (1998). Embalming in the Old Kingdom of Pharaonic Egypt. *Analytical Chemistry*, 1, 511A-516A.

Whelton, H. L., Hammann, S., Cramp, L. J. E., Dunne, J., Roffet-Salque, M. and Evershed, R. P. (2021). A call for caution in the analysis of lipids and other small biomolecules from archaeological contexts. *Journal of Archaeological Science*, 132: 105397. DOI: 10.1016/j.jas.2021.105397.

White, R. and Kirby, J. (2001). *A Survey of Nineteenth- and Early Twentieth-Century Varnish Compositions found on a Selection of Paintings in the National Gallery Collection*. Available at https://www.nationalgallery.org.uk/research/research-resources/technical-bulletin/a-survey-of-nineteenth-and-early-twentieth-century-varnish-compositions-found-on-a-selection-of-paintings-in-the-national-gallery-collection. Accessed on 20th December 2020

Wilson, L., Pollard, A. M., Hall, A. J. and Wilson, A. S. (2006). Assessing the influence of agrochemicals on the nature of copper corrosion in the vadose zone of arable land Part 3: Geochemical modelling. *Conservation and Management of Archaeological Sites*, 7(4), 241-260. DOI:10.1179/135050306793137331

Witkowska-Banaszczak, E. and Długaszewska, J. (2017). Essential oils and hydrophilic extracts from the leaves and flowers of Succisa pratensis Moench. and their biological activity. *Journal of Pharmacy and Pharmacology*, 69(11), 1531-1539. DOI:10.1111/jphp.12784

Worrall, S. and Thiele, G. M. (2005). 92 - Modification of Proteins by Reactive Ethanol Metabolites: Adduct Structure, Functional and Pathological Consequences. In Preedy, V. R. and Watson, R. R. (eds.), *Comprehensive Handbook of Alcohol Related Pathology*, 1209-1222. San Diego, Calif. : Elsevier Academic

Xue, X., Wu, L. and Wang, K. (2017). Chemical Composition of Royal Jell. In Alvarez-Suarez, J. M. (ed.) *Bee Products - Chemical and Biological Properties* Cham, Switzerland: Springer.

Yannai, S. (2013). *Dictionary of Food Compounds with CD-ROM* (2nd ed.). Boca Raton, Florida: CRC Press, Taylor & Francis Group

Yéramian, N., Chaya, C. and Suárez Lepe, J. A. (2007). L-(-)-malic acid production by Saccharomyces spp. during the alcoholic fermentation of wine (1). *Journal of Agricultural and Food Chemistry*, 55(3), 912-919.

Yi, F., Liu, L., Zhang, M., Wang, T., Ye, J., Chu, Q. and Huang, D. (2018). Electrophoretic Determination of Formaldehyde in Human Urine: Application to Alzheimer's Disease. *Analytical Letters*, 51(9), 1358-1372. DOI:10.1080/00032719.2017.1378661

Zhang, R., Li, X. and Zhang, X. (2009). Theoretical Study of the C-Cl Bond Dissociation Enthalpy and Electronic Structure of Substituted Chlorobenzene Compounds. *Chinese Journal of Chemical Physics*, 22(3), 235-240. DOI:10.1088/1674-0068/22/03/235-240

Zhao, L., Huang, Y., Lu, L., Yang, W., Huang, T., Lin, Z., . . . and Bian, Z. (2018). Saturated long-chain fatty acid-producing bacteria contribute to enhanced colonic motility in rats. *Microbiome*, 6(1). DOI:10.1186/s40168-018-0492-6

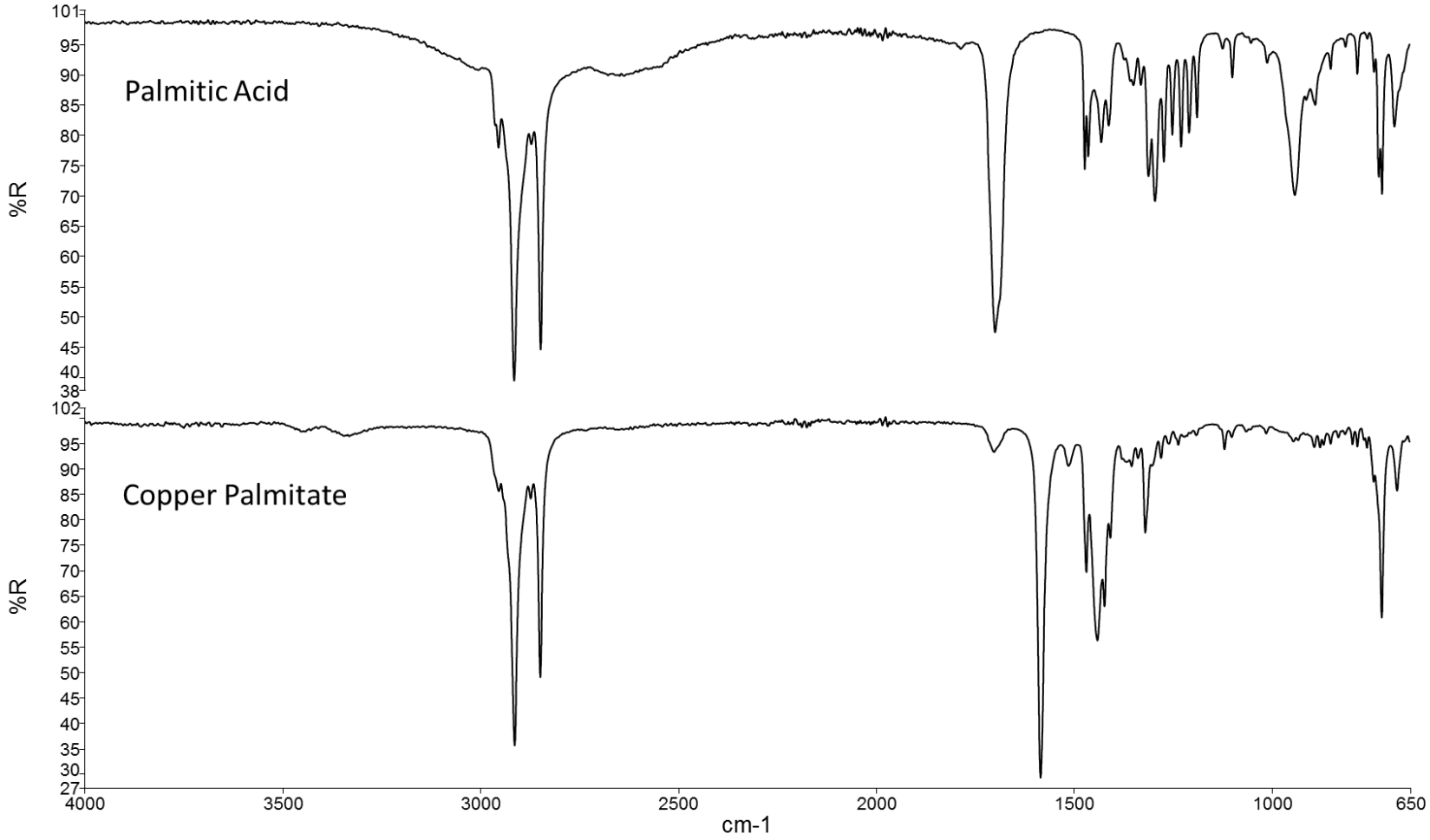
Zhou, X., Qu, Y., Kim, B. H., Du, Y., Wang, H., Li, H., . . . Feng, Y. (2015). Simultaneous current generation and ammonia recovery from real urine using nitrogen-purged bioelectrochemical systems. *RSC Advances*, 5(86), 70371-70378. DOI:10.1039/c5ra11556f

Zou, S., Li, R., Xie, S., Zhu, J., Wang, X. and Huang, J. (2010). Paleofire indicated by polycyclic aromatic hydrocarbons in soil of Jinluojia archaeological site, Hubei, China. *Journal of Earth Science*, 21(3), 247-256. DOI:10.1007/s12583-010-0089-x

8. Appendices

XRD peak list for Reference Copper Palmitate recrystallized in Chloroform

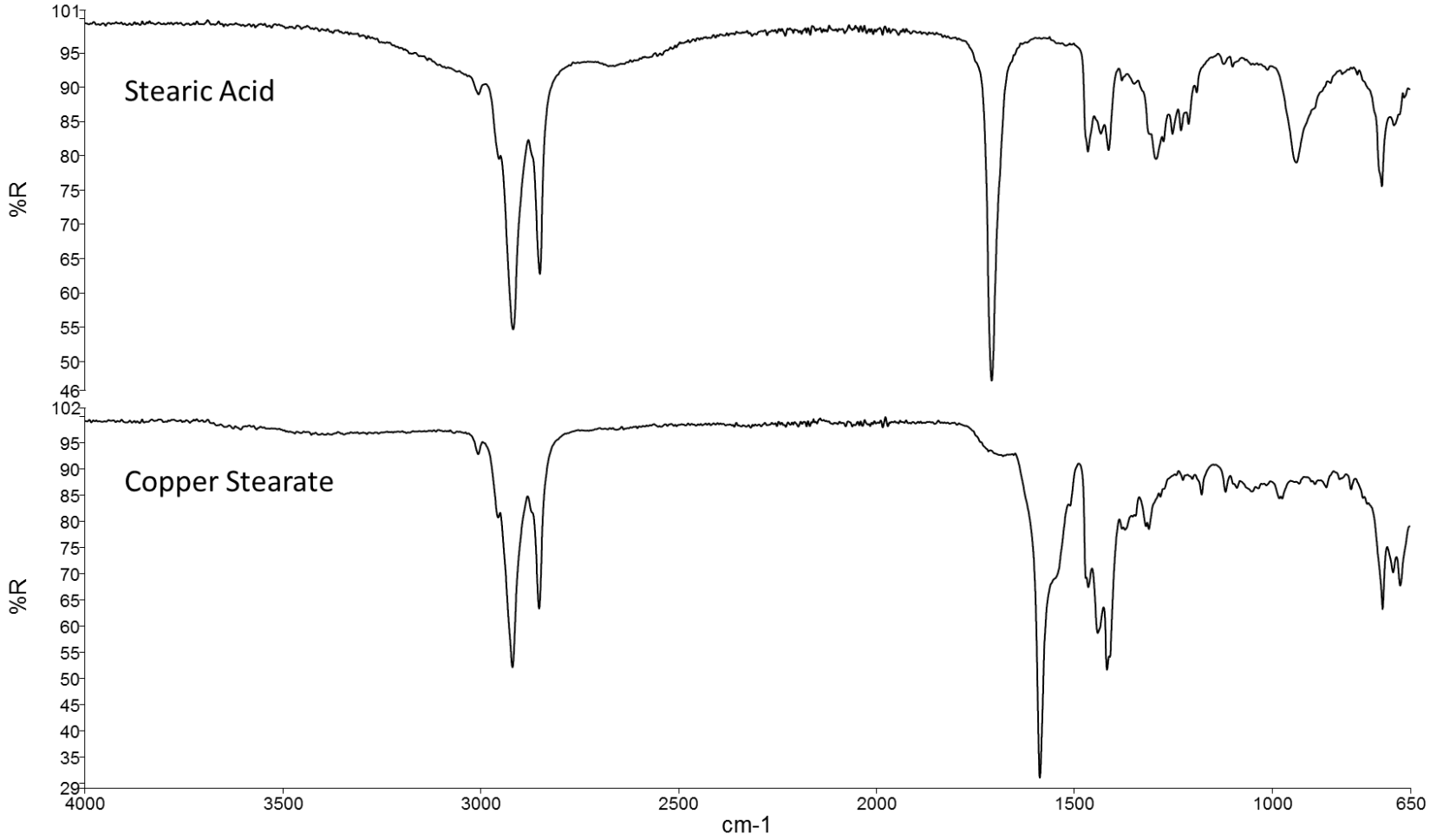
°2Theta	FWHM[°2Th.]	d-spacing[Å]	Rel.Int.[%]
2.04	0.1337	4.3278	100.00
4.11	0.1337	2.1481	28.98
6.18	0.1674	1.4296	55.80
8.29	0.2005	1.0706	11.09
10.35	0.2005	0.8547	20.62
21.33	0.2674	0.4166	12.92
22.84	0.2005	0.3894	10.49



FT-IR Spectra of Palmitic Acid and Copper Palmitate in ATR mode

Infrared frequencies (cm^{-1}) for Palmitic Acid and Cu-palmitate

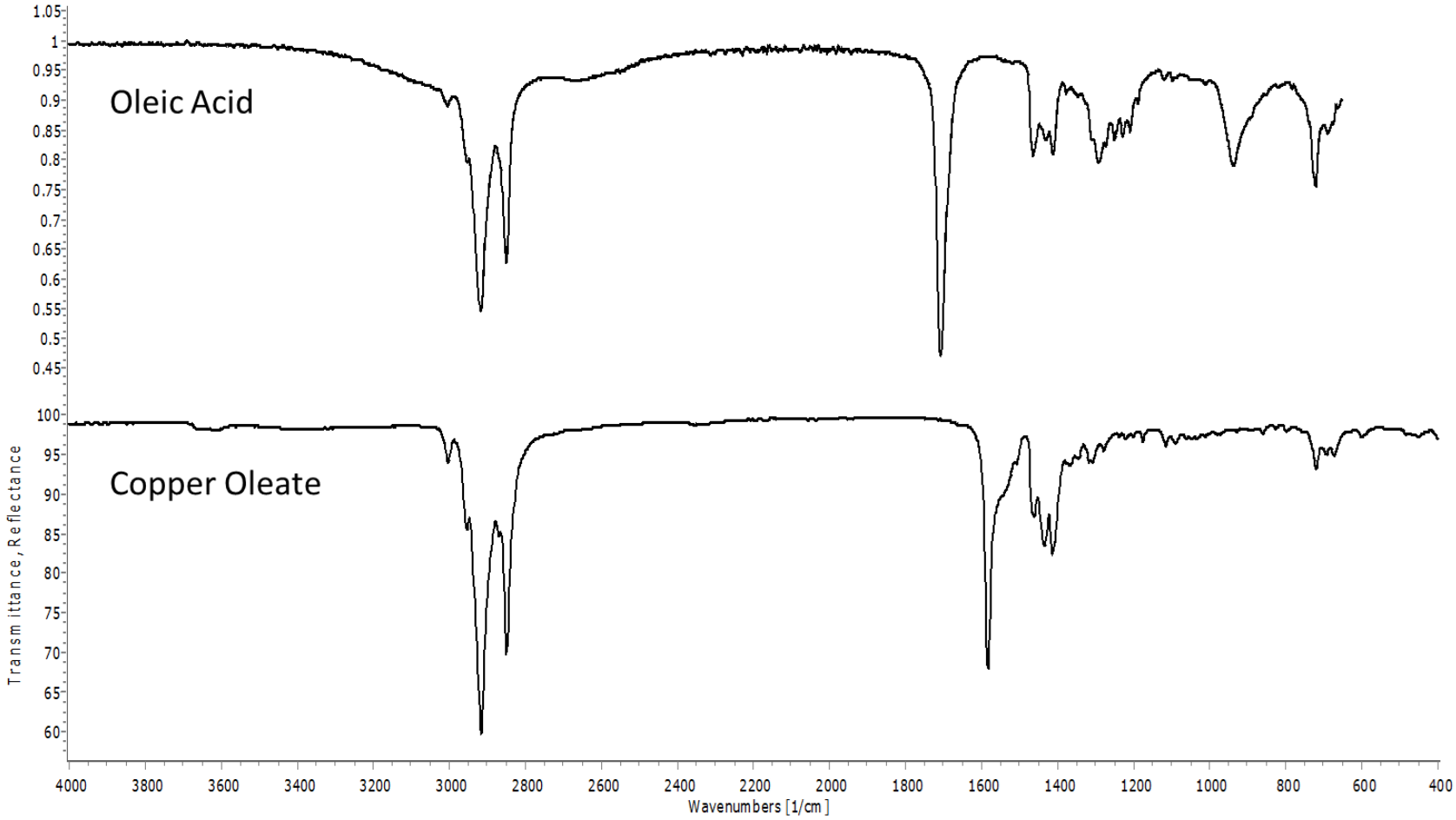
Palmitic Acid		Cu-Palmitate		Band Assignment
3300-2500	br			OH (bonded) stretching
2954	m	2957	s	CH_3 asymmetric stretching
2915	vs	2914	vs	CH_2 asymmetric stretching
2878	m	2873	s	CH_3 symmetric stretching
2848	vs	2849	vs	CH_2 symmetric stretching
2662	m,br			OH stretching
1695	vs	1701	w	C=O (dimer) stretching
		1583	vs	COO^- asymmetric stretching
1472	m	1468	m	C-CH_3 deformation
1463	m			CH_2 scissors deformation
		1440	m	CH_2 scissors deformation
1430	m			
		1422	m	COO^- symmetric stretching
1411	m			CH_2 deformation
1350	w	1351	w	CH_2 stretching
1330	w	1338	w	
		1318		
1310	m			
1294	m			
1272	m	1279	w	
1250	m	1258	vw	
1228	m	1234	vw	
1208	m			
1189	m	1187	vw	CH_2 stretching
1121	w	1117	W	
1099	w	1098	w	
1012	w	1013	vw	
940	m	946	vw	OH deformation
		931	vw	
889	w	892	w	
		875	w	
		866	w	
850	w	850	w	
		793	w	
728	m			
720	m	721	m	
688	m			
		682		



FT-IR Spectra of Stearic Acid and Copper Stearate in ATR mode

Infrared frequencies (cm^{-1}) for Stearic Acid and Cu-stearate

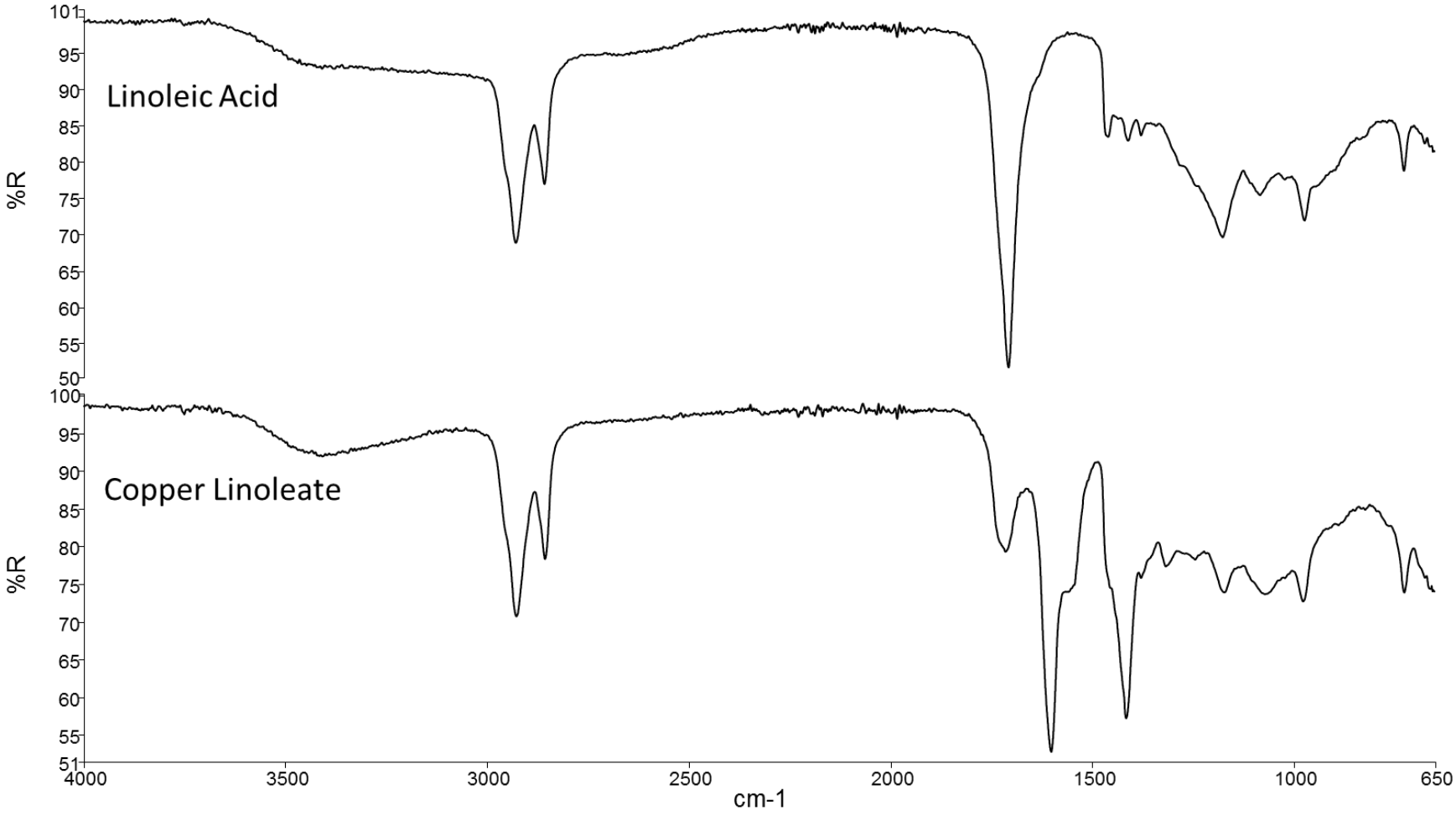
Stearic Acid		Cu-Stearate		Band Assignments
3300-2500	br			OH stretching
2954	m			CH_3 asymmetric stretching
915	vs	2912	vs	CH_2 asymmetric stretching
2878	m		vw	CH_3 symmetric stretching
2848	vs	2846	vs	CH_2 symmetric stretching
2643	m, br			OH symmetric stretching
1695	vs		w	C=O stretching
		1585	vs	COO^- asymmetric stretching
		1516	w	
1472	m	1469	m	C-CH_3 deformation
1463	m	1462	vw	CH_2 deformation
		1440	m	
1430	m			CH_2 deformation
		1419	w	COO^- symmetric stretching
1411	m	1413	w	CH_2 deformation
		1362	w	
		1340	vw	
1348	w	1351	w	CH_2 stretching
1328	w	1328	vw	
1310	m	1315	m	
1294	m	1296	sh	
1272	m			
1250	m	1261	w	
1228	m			
		1224	w	
1208	m			
1188	m			CH_2 stretching
1122	w	1114	w	
1099	w			
1009	w			
941	m			OH deformation
889	w			
850	w			
782	w			
728	m			
720	m			
		716	m	
688	m	687	vw	
		673	w	



FT-IR Spectra of Oleic Acid and Copper Oleate in ATR mode

Infrared frequencies (cm^{-1}) for Oleic Acid and Cu-oleate

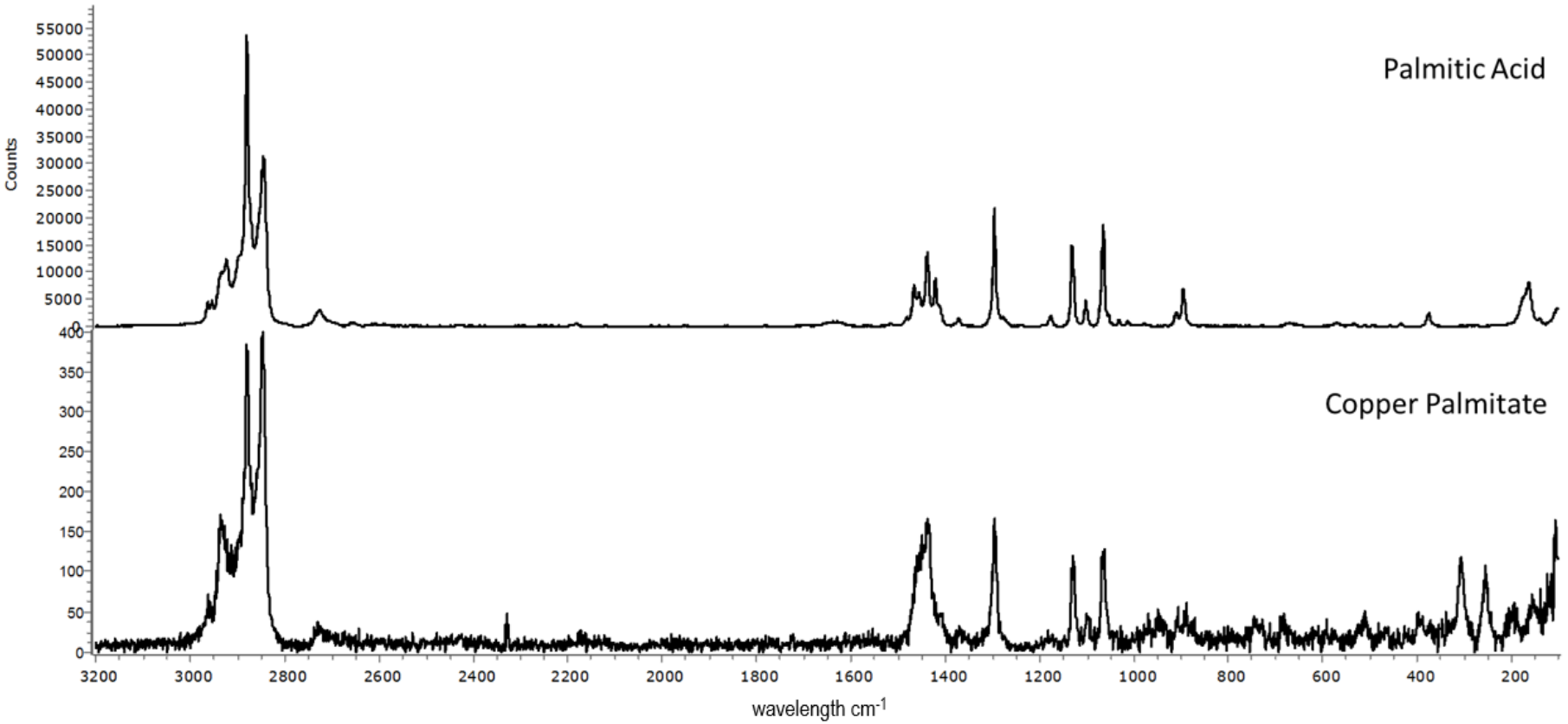
Oleic Acid		Cu-Oleate		Band Assignments
3300-2500	br			OH stretching
3004	w	3004	m	CH stretching
		2954	vw	CH_2 asymmetric stretching
2921	vs	2916	vs	CH_2 asymmetric stretching
2852	s	2849	s	CH_2 symmetric stretching
2664	vw			OH symmetric stretching
1707	vs			C=O stretching
1655	sh	1655	vw	C=C stretching
		1583	s	COO^- asymmetric stretching
		1551	sh	
		1462	m	$C\text{-}CH_3$ deformation
		1435	m	CH_2 deformation
		1414	m	COO^- symmetric stretching
1460	m			
1412	m			
		1368	sh	
		1344	sh	
		1308	w	
1284	m			
		1279	w	
1246	w			
		1175	vw	
		1114	vw	
1090	vw	1088	vw	
935	m			OH deformation
723	m			
		718	w	



FT-IR Spectra of Linoleic Acid and Copper Linoleate in ATR mode

Infrared frequencies (cm^{-1}) for Linoleic Acid and Cu-linoleate

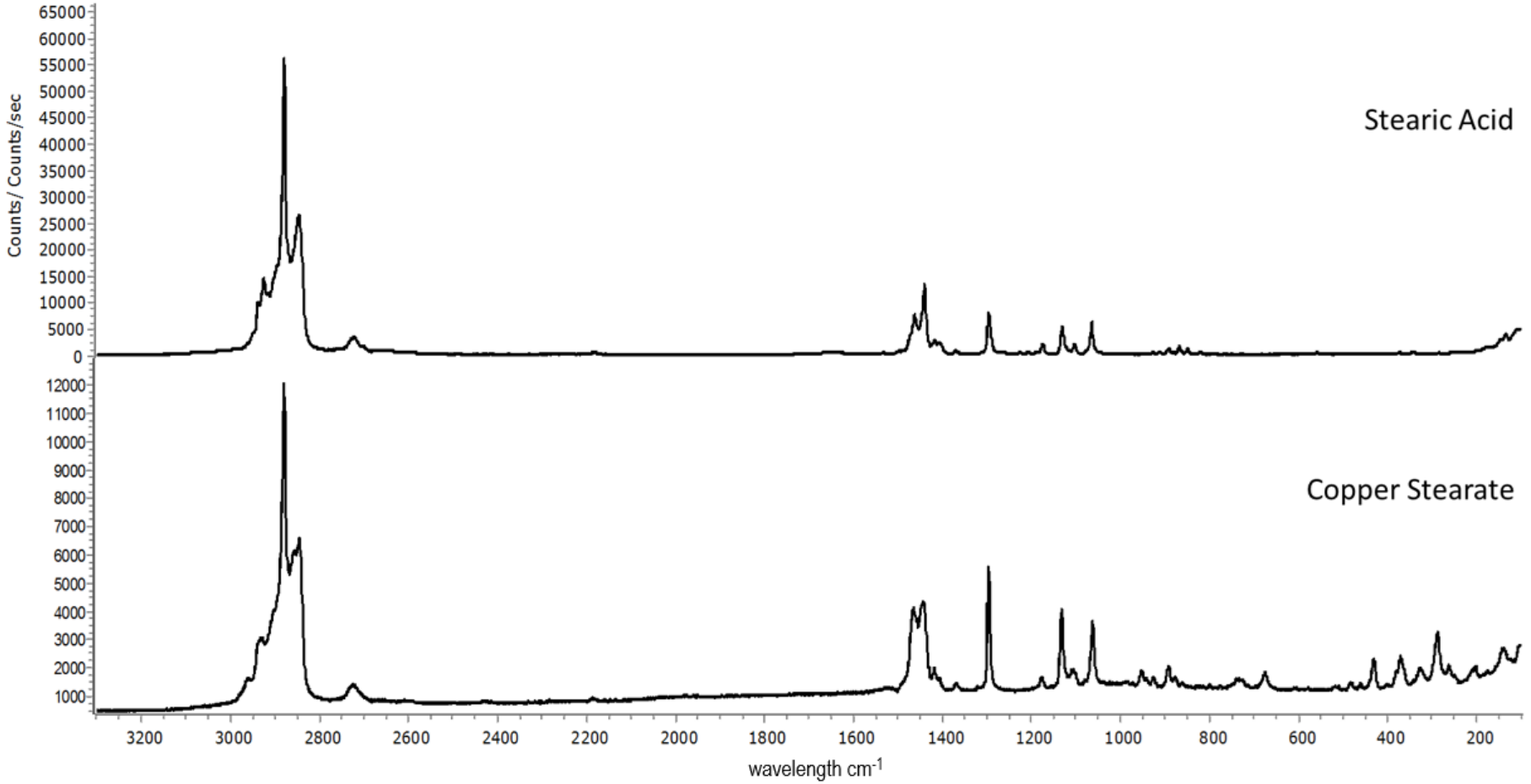
Linoleic Acid		Cu-Linoleate		Band Assignments
3400-2500	br	3600-3100	br	OH stretching
3008	m	3007	m	CH stretching
2955	sh	2955	sh	CH_3 asymmetric stretching
2924	vs	2924	vs	CH_2 asymmetric stretching
2854	s	2853	s	CH_2 asymmetric stretching
		2359	w	CH_2 symmetric stretching
2674	vw			OH stretching
		1729	m	
1705	vs			C=O stretching
		1591	vs	COO^- asymmetric stretching
1459	m			CH_2 deformation
		1452	sh	
1434	sh			
		1413	m	COO^- symmetric stretching
1411	m			
		1375	w	
1282	m			
		1243	m	
		1172	m	
1089	vw	1090	w	
		1016	vw	
		969	w	
947	m			OH deformation
		876	w	
724	m	724	m	
604	vw			



Raman Spectra Palmitic Acid and Copper Palmitate (baseline corrected)

Raman frequencies (cm^{-1}) for Palmitic acid and Cu-Palmitate

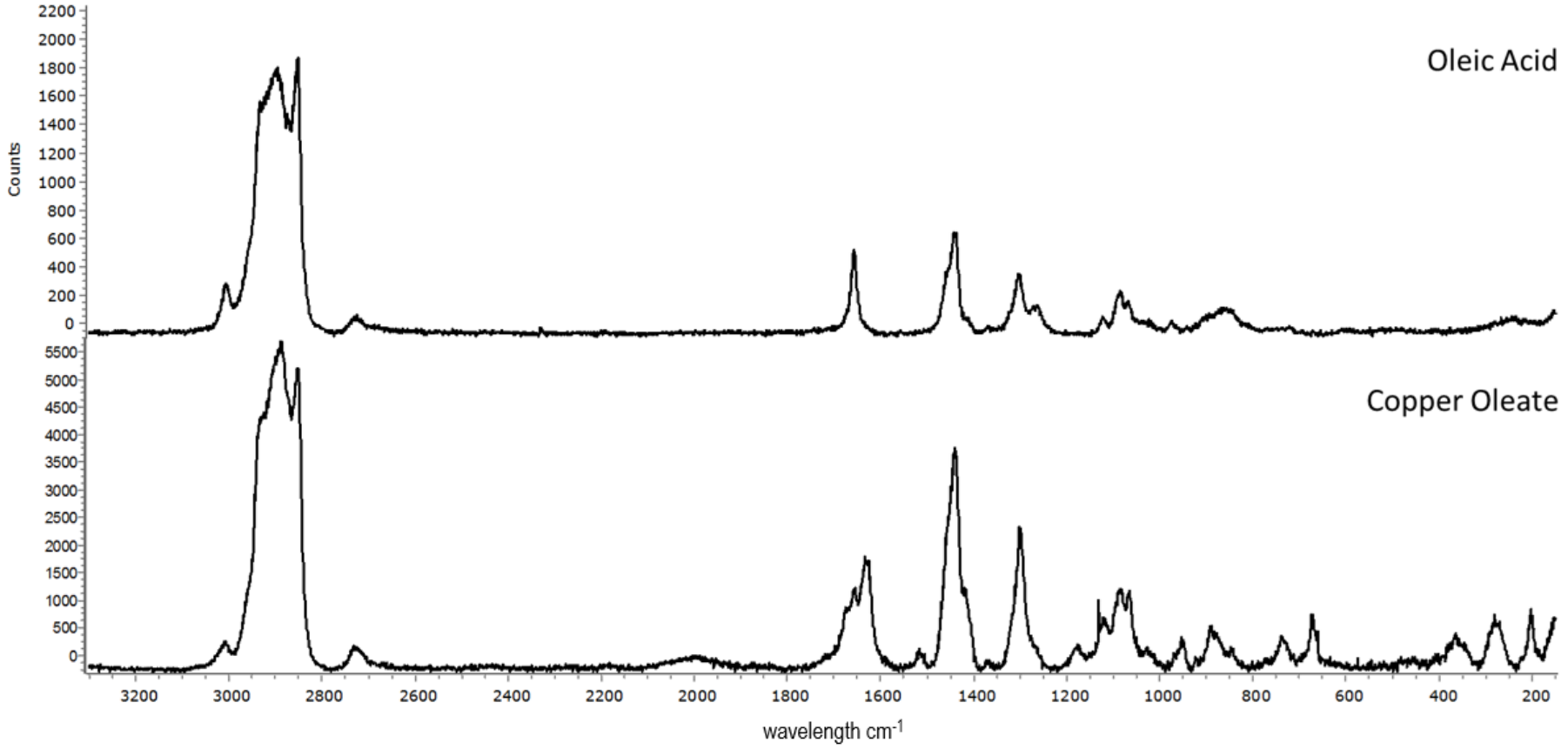
Palmitic Acid		Cu-Palmitate		Band Assignments
2957	sh	2957	sh	CH_3 asymmetric stretching
		2934	m	CH stretching
2925	m			CH_3 symmetric stretching
2880	vs	2880	vs	CH_2 asymmetric stretching
2845	vs	2847	vs	CH_2 symmetric stretching
		2329	w	
1643	w			C=O (dimer) stretching
		1556	vw	COO^- asymmetric stretching
1466	m			CH_2, CH_3 bending
1456	s	1458	s	
1438	s	1437	s	CH_2, CH_3 bending
				C-O + β OH (dimer) stretching
1296	s	1296	s	CH_2 twisting
1131	m	1130	m	C-C stretching
1102	w	1098	w	C-C stretching + C-C bending
1066	m	1066	m	C-C stretching
971	vw			O-H···H (dimer) out-of-plane stretching
		949	w	M-OCO
				CH_2 in plane stretching
908	w			C-C (carboxyl) stretching
895	m	892	w	CH_3 deformation + C-C stretching
		685	w	COO^- deformation
		464	w	COO^- stretching
		308	m	M-O stretching
		255	m	M-O stretching
163	m			
		154	m	



Raman Spectra Stearic Acid and Copper Stearate

Raman frequencies (cm^{-1}) for Stearic Acid and Cu-Stearate

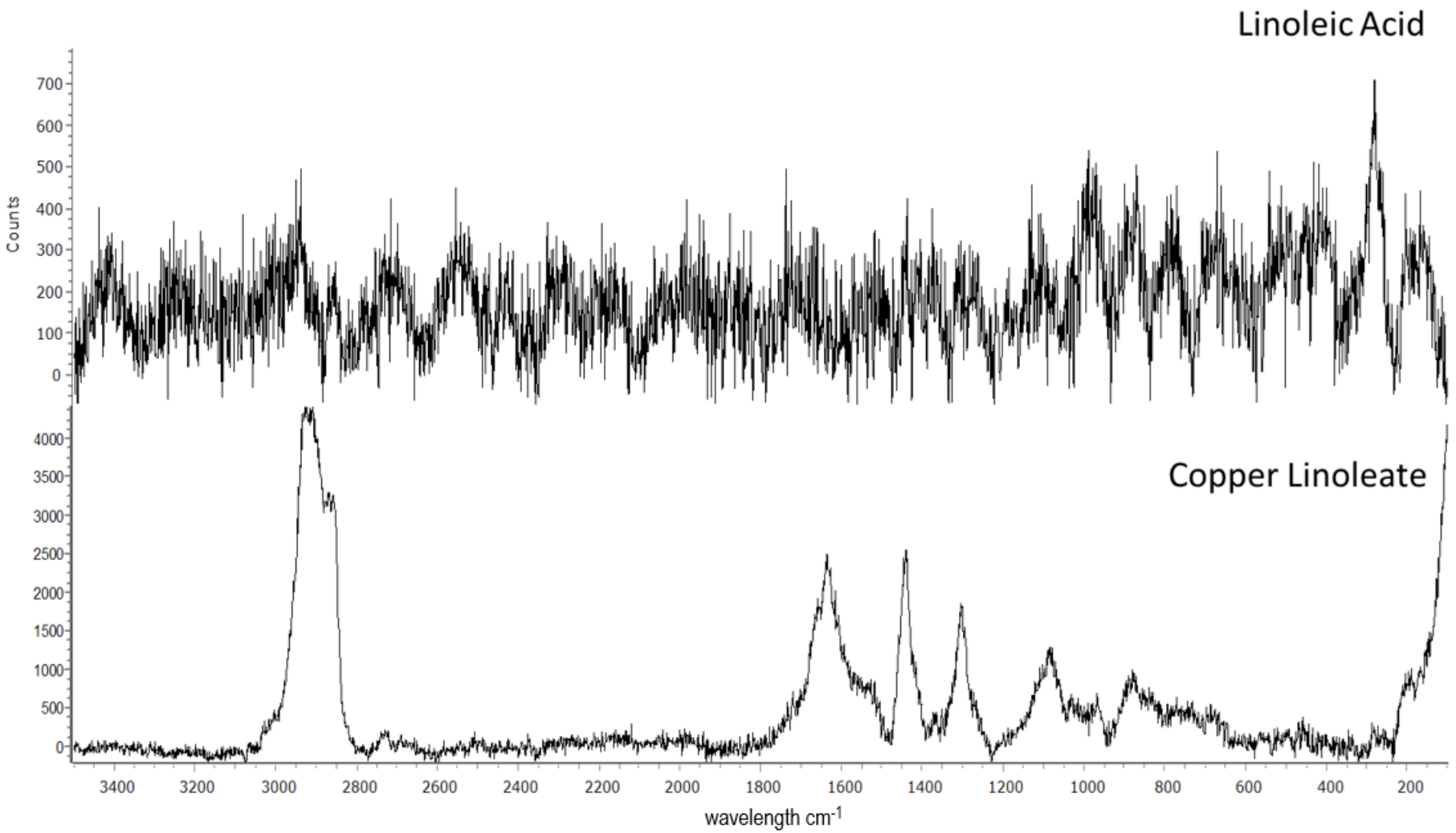
Stearic Acid		Cu-Stearate		Band Assignments
		2960	sh	CH_3 asymmetric stretching
2931	sh	2931	m	CH_2 asymmetric stretching
2926	m			CH_3 symmetric stretching
		2902	sh	
2879	vs	2880	vs	CH_2 asymmetric stretching
2847	s	2847	vs	CH_2 symmetric stretching
2723	w	2723	w	
1644	w			C=O stretching
		1526	vw	COO^- stretching
1463	s	1463	s	CH_2 bending
	s		s	CH_2 bending
1441		1443		
				C=O + β OH (dimer) stretching
1417	w	1417	w	
1408	sh	1408	sh	CH_2 bending
1372	vw	1369	w	CH_3 deformation
1297	s	1297	s	CH_2 bending
1178	w	1177	w	
1133	m	1132	s	C-C stretching
1107	w	1107	w	C-C stretching + C-C bending
1065	m	1063	s	C-C stretching
		953	w	M-OCO
				CH_2 stretching
893	vw	892	w	CH_3 deformation + C-C stretching
		740	w	
		675	w	COO^- deformation
		483	w	
		460	w	
		431	m	M-O stretching
		371	m	
		327	w	
		287	m	M-O stretching
		260	w	M-O stretching
140	w	138	w	
109	w	104	w	



Raman Spectra Oleic Acid and Copper Oleate (baseline corrected)

Raman frequencies (cm^{-1}) for Oleic Acid and Cu-Oleate

Oleic Acid		Cu-Oleate		Band Assignments
3007	m	3007	m	CH asymmetric stretching
2896	vs	2888	vs	CH_3 symmetric stretching
2853	vs	2853	vs	CH_2 symmetric stretching
2726	w	2730	w	
1657	s			C=C and C=O stretchings
		1633	s	C=C stretching
		1517	w	COO^- asymmetric stretching
1443	s	1440	s	CH_2, CH_3 bending, C-O stretching + OH (dimer) deformation
1417	w	1417	w	CH_2 deformation
		1374	vw	CH_3 deformation
1304	s	1301	s	CH_2 twisting
1269	w			CH bending
		1178	w	
		1132	s	C-C stretching + C-C-C deformation
1122	w			C-C stretching + C-C-C deformation
1086	m	1082	s	
1070	s	1070	s	C-C deformation C-C stretching
		1029	w	
974	vw			CH out-of-plane deformation + δ CH_2 deformation
		952	w	M-OCO stretching
		927	vw	COO^-
		893	w	
862	w			CH_3 deformation + C-C stretching
		845	w	
		738	w	
		672	m	COO^- deformation
667	vw			COO^- in plane deformation
		364	m	
		282	m	M-O stretching
		202	m	



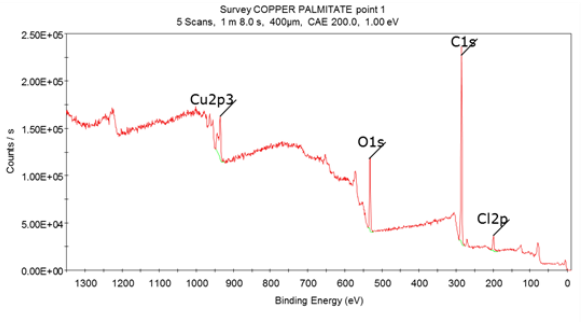
Raman Spectra Linoleic Acid and Copper Linoleate (baseline corrected)

Raman frequencies (cm^{-1}) for Linoleic Acid and Cu-Linoleate

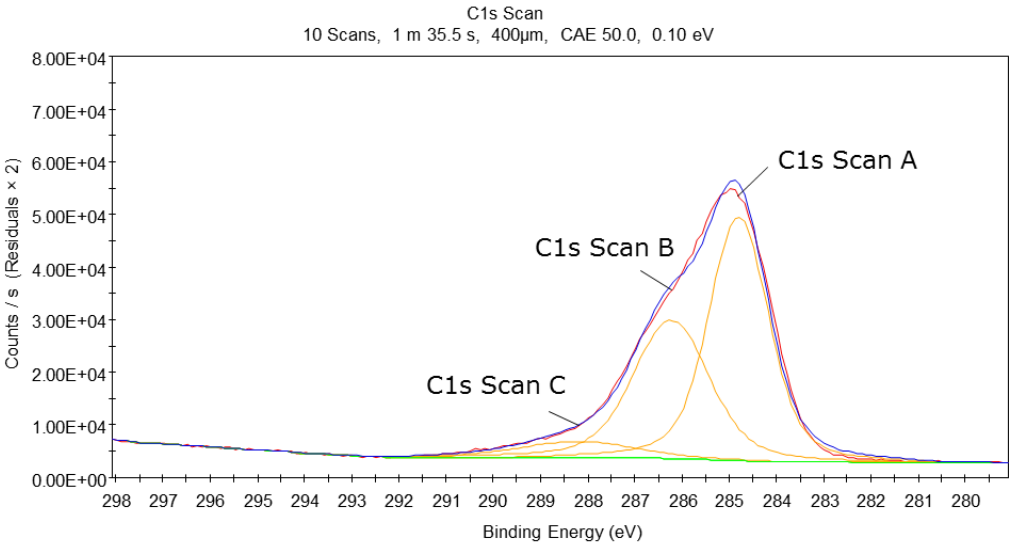
Linoleic Acid		Cu-Linoleate		Band Assignments
3016	m			CH symmetric stretching
		2920	vs	CH_2 asymmetric stretching
2869	vs			CH_2 stretching
		2730	w	
1661	s	1661	0073	C=C stretching
1640	s	1638	s	C=C stretching
		1538	sh	
1445	s	1440	s	CH_2, CH_3 bending
1306	m	1303	m	CH_2 bending
1296	s			(CH_2) aliphatic twisting
1269	s			C-C stretching + C-C deformation
1112	w			
1096	m			C-C stretching
		1086	m	C-C stretching + C-C deformation
1062	m			C-C stretching
1041	w			
		1037	w	
974	m			C=C deformation + C-C stretching
926	m			
912	m			C-C deformation
887	w	881	m	
		775	W	
732	w			
716	w			
		687	W	
671	w			
589	w			
574	w	281	W	
		196	m	

Cu-Palmitate – POINT 1

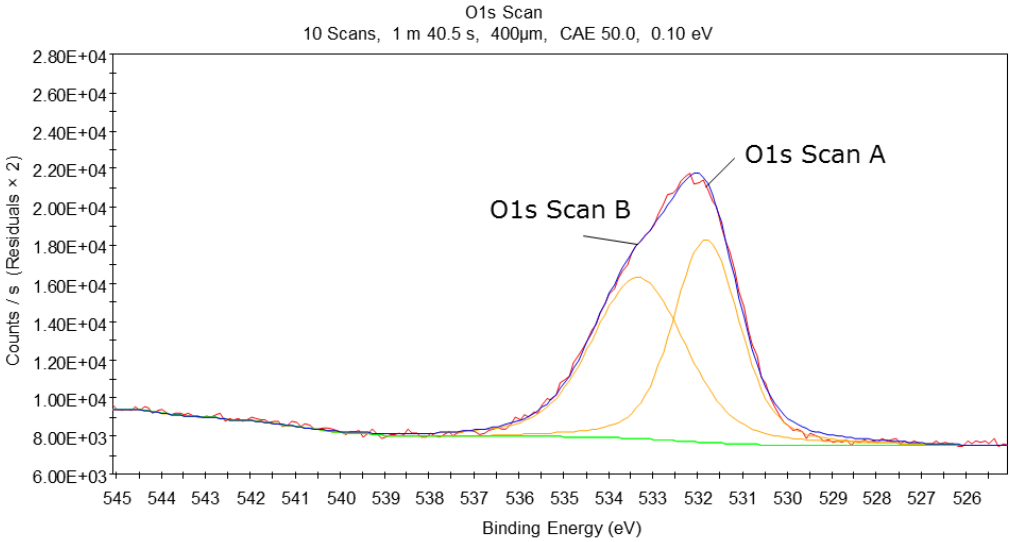




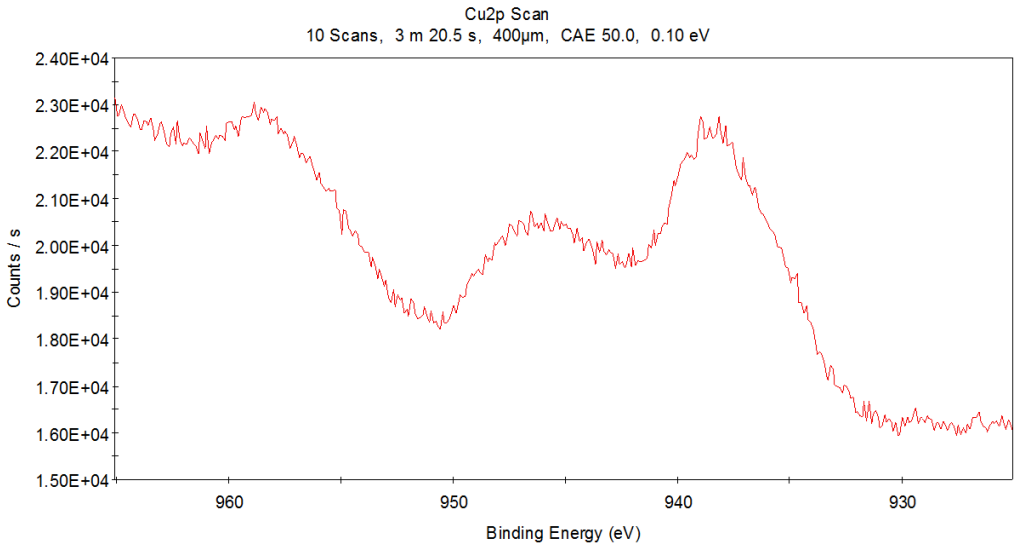
Element	Start BE	Peak BE	End BE	FWHM eV	Area (P) CPS.eV	Atomic %
C1s	292.08	285.36	277.08	3.03	666535.67	79.63
O1s	537.58	532.5	523.58	3.36	269951.01	13.34
Cu2p3	948.58	935.92	923.08	4.44	328052.2	3.85
Cl2p	207.08	199.86	188.08	3.95	76888.56	3.18



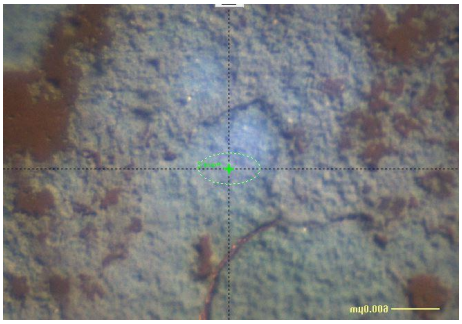
Name	Peak BE	FWHM eV	Area (P) CPS.eV	Atomic %
C1s Scan A	284.80	1.49	80999.94	54.00
C1s Scan B	286.23	1.90	58626.33	39.12
C1s Scan C	288.19	2.89	10299.34	6.88

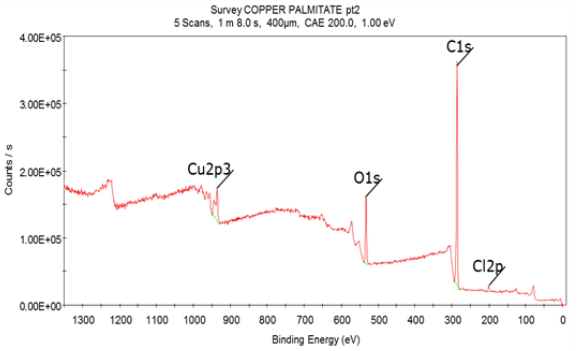


Name	Peak BE	FWHM eV	Area (P) CPS.eV	Atomic %
O1s Scan A	531.81	1.75	21777.08	47.14
O1s Scan B	533.33	2.46	24386.69	52.86

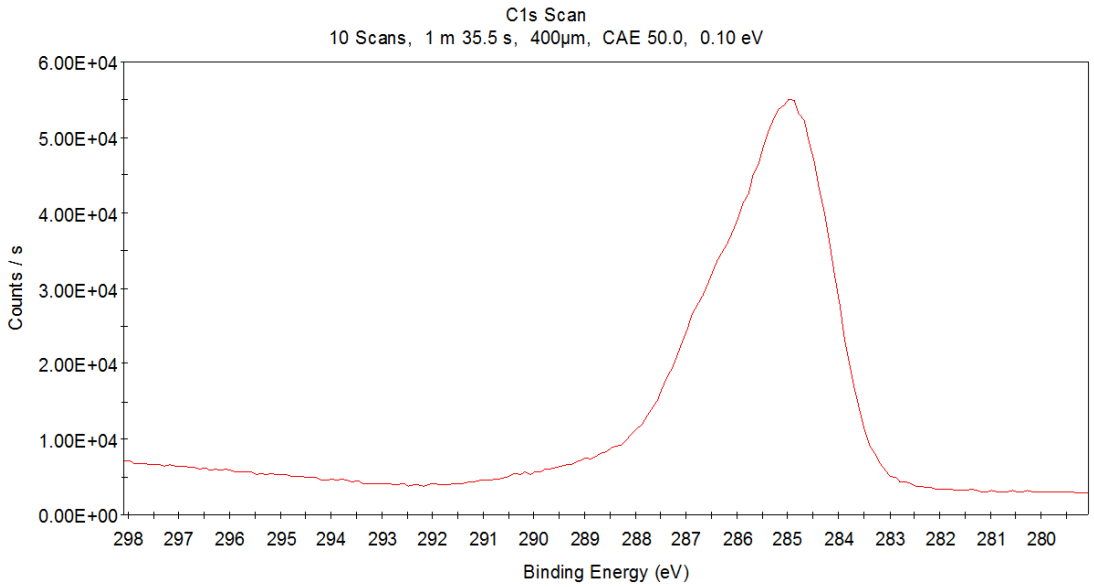


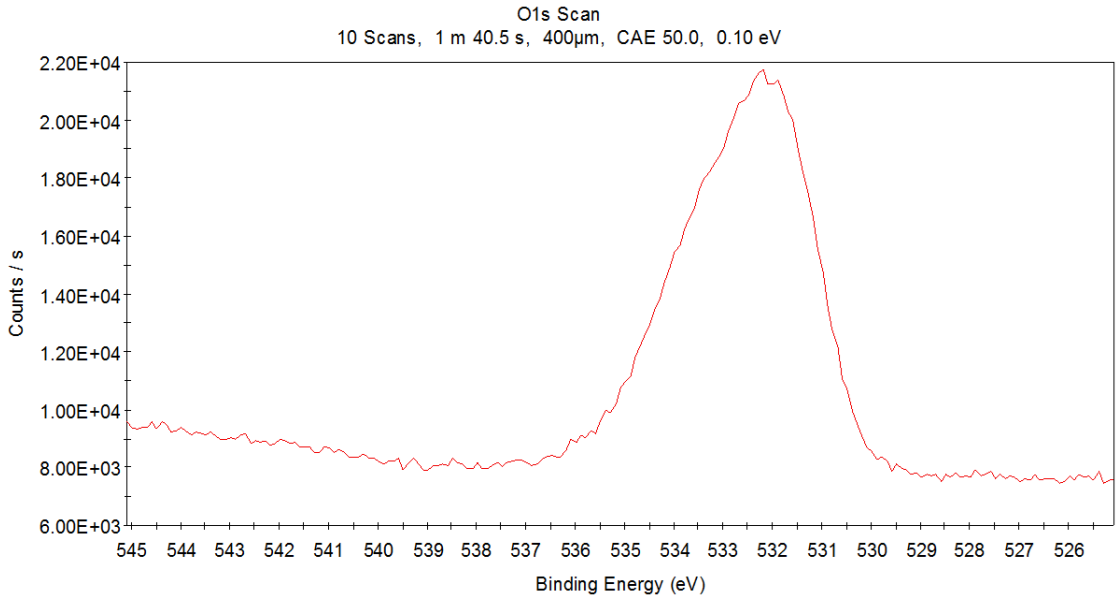
Cu-Palmitate – POINT 2

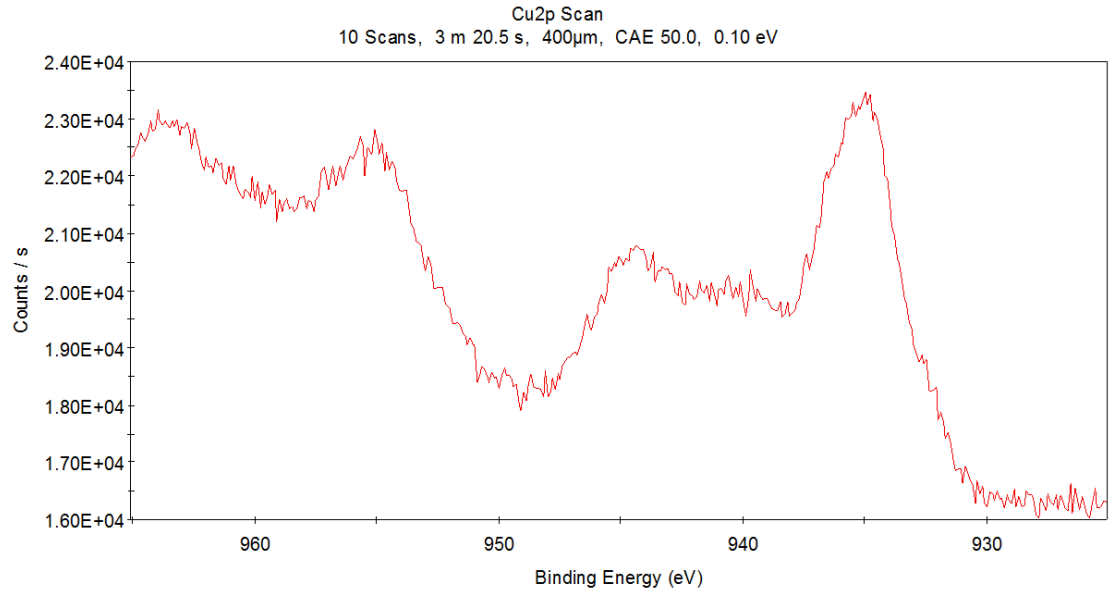




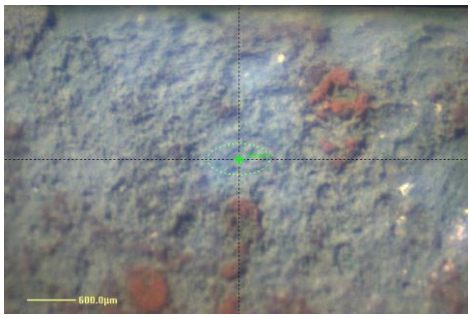
Element	Start BE	Peak BE	End BE	FWHM eV	Area (P) CPS.eV	Atomic %
C1s	293.08	285.52	277.08	1.99	1171455	85.53
O1s	539.08	532.82	525.58	3.38	354716.9	10.72
Cu2p3	949.08	935.56	923.08	2.78	391526.8	2.81
Cl2p	206.58	200.15	195.34	3.95	37358.78	0.94

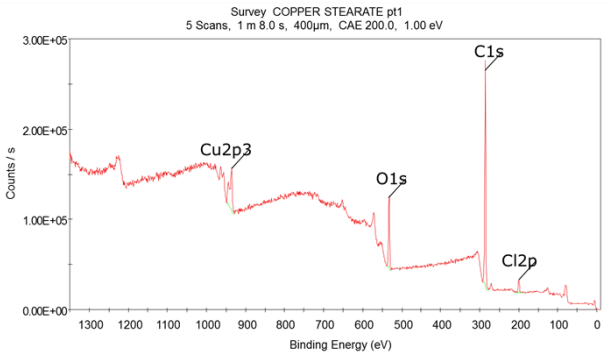



O1s Scan
10 Scans, 1 m 40.5 s, 400µm, CAE 50.0, 0.10 eV
Counts / s
2.20E+04
2.00E+04
1.80E+04
1.60E+04
1.40E+04
1.20E+04
1.00E+04
8.00E+03
6.00E+03
545 544 543 542 541 540 539 538 537 536 535 534 533 532 531 530 529 528 527 526
Binding Energy (eV)

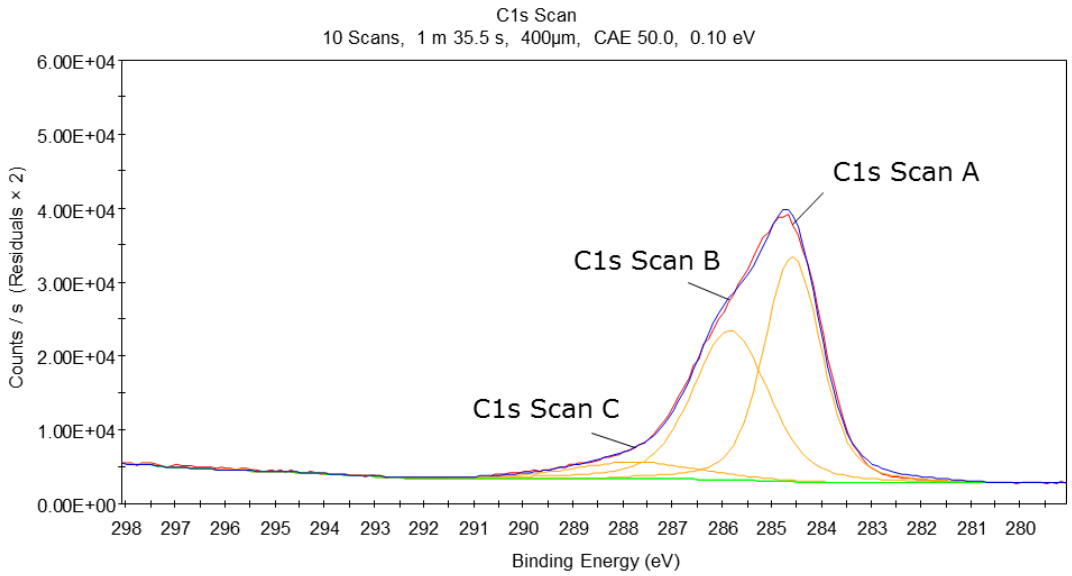

Cu2p Scan
10 Scans, 3 m 20.5 s, 400µm, CAE 50.0, 0.10 eV
Counts / s
2.40E+04
2.30E+04
2.20E+04
2.10E+04
2.00E+04
1.90E+04
1.80E+04
1.70E+04
1.60E+04
960 950 940 930
Binding Energy (eV)

Cu-Stearate – POINT 1

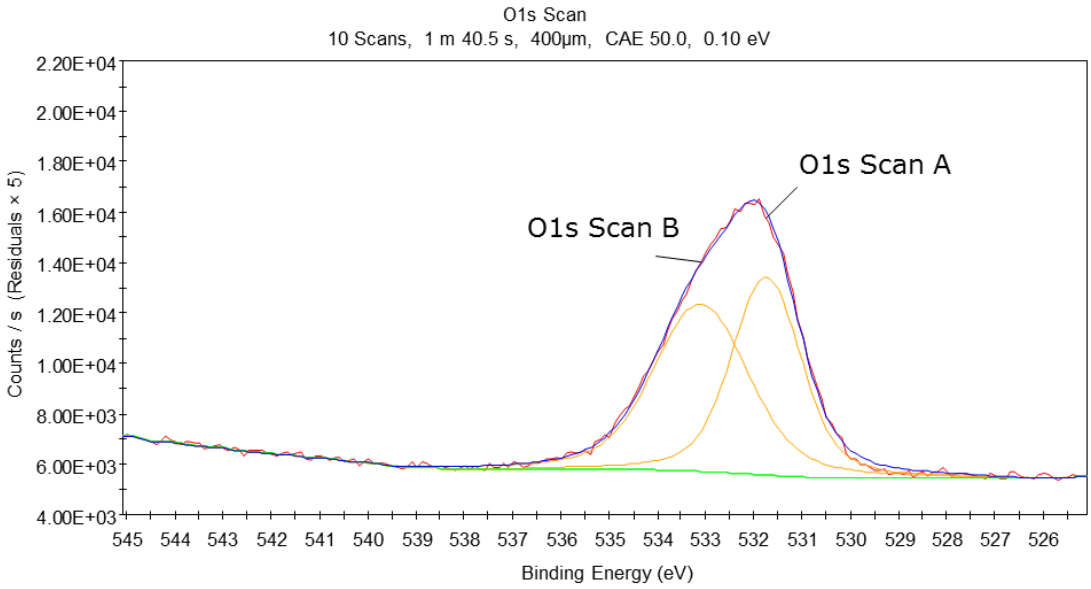




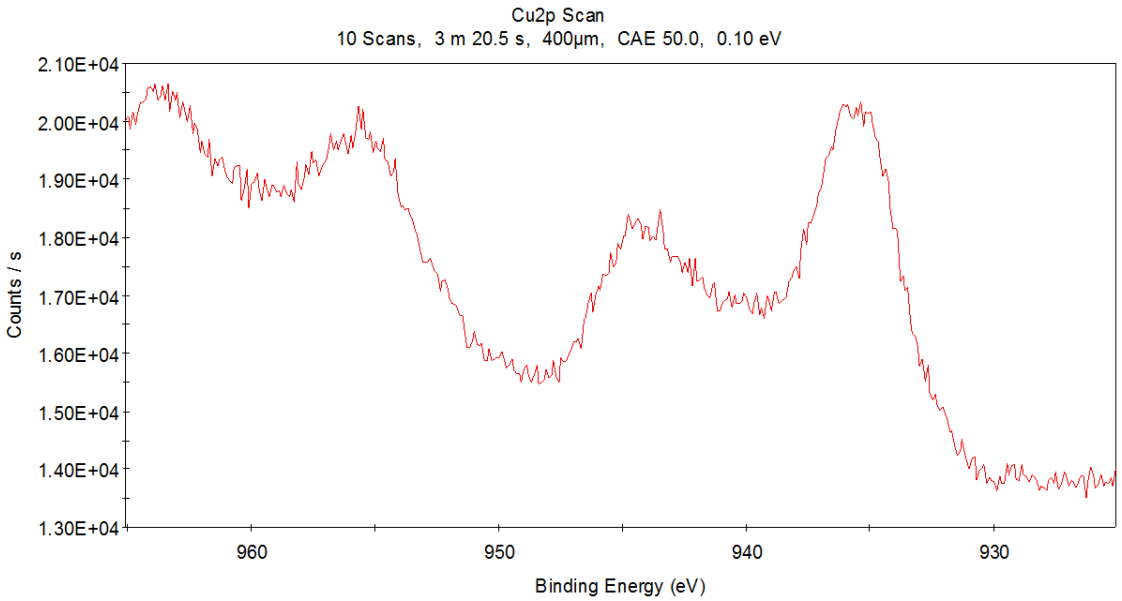
Element	Start BE	Peak BE	End BE	FWHM eV	Area (P) CPS.eV	Atomic %
C1s	291.58	285.29	277.08	3.04	783653.18	82.27
O1s	537.58	532.33	527.08	3.12	263663.39	11.45
Cu2p3	948.58	935.58	927.58	4.28	378935.52	3.91
Cl2p	210.08	200.05	188.08	3.86	65347.72	2.37



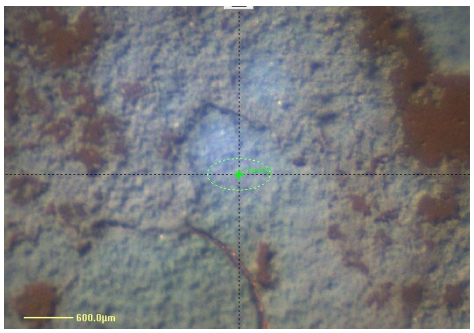
Name	Peak BE	FWHM eV	Area (P) CPS.eV	Atomic %	Q
C1s Scan A	284.59	1.35	47889.44	49.08	1
C1s Scan B	285.84	1.79	42124.65	43.21	1
C1s Scan C	287.75	3.00	7509.49	7.71	1

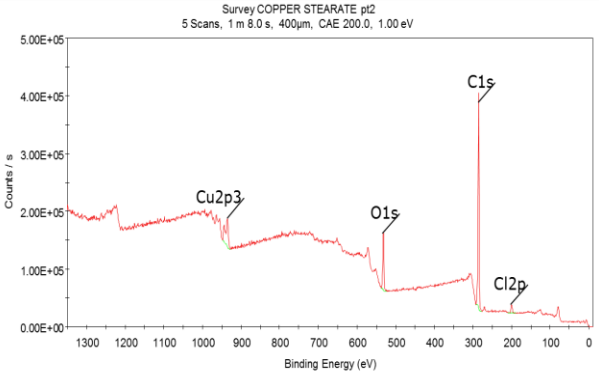


Name	Peak BE	FWHM eV	Area (P) CPS.eV	Atomic %
O1s Scan A	531.74	1.70	15635.54	46.40
O1s Scan B	533.09	2.32	18044.75	53.60

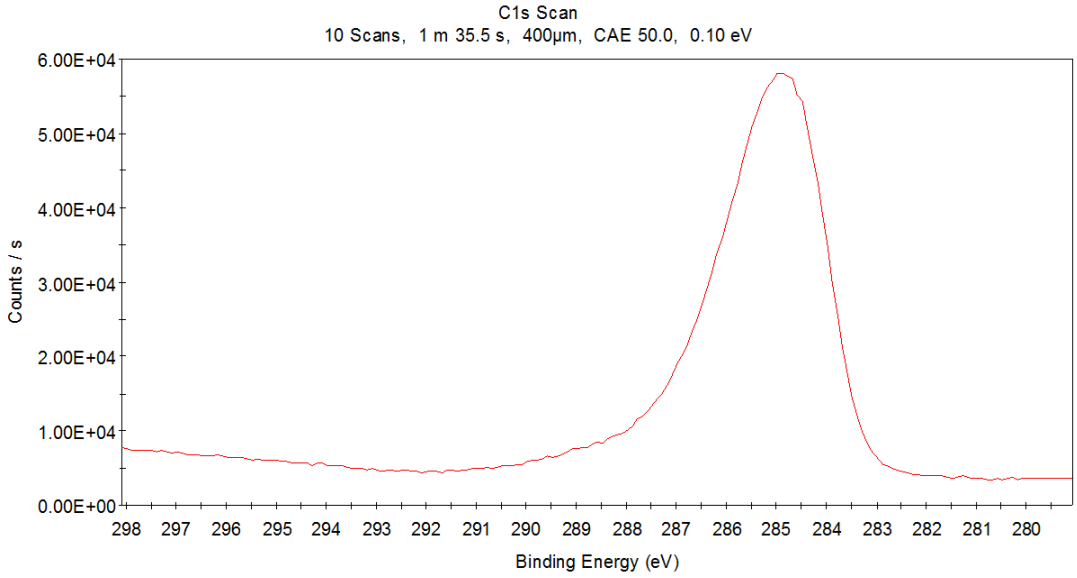


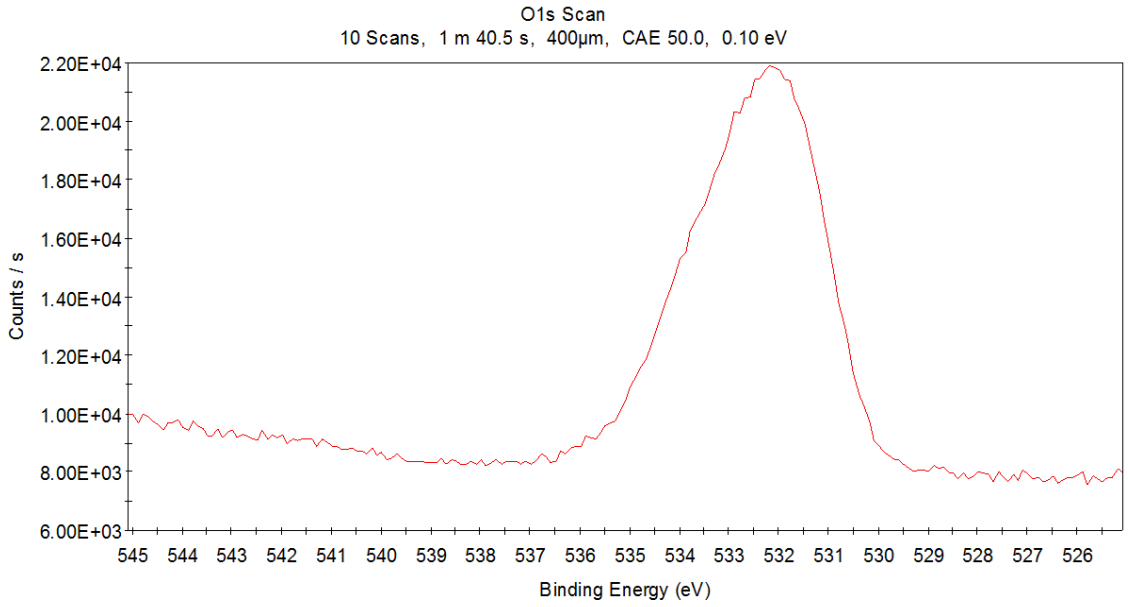
Cu-Stearate – POINT 2

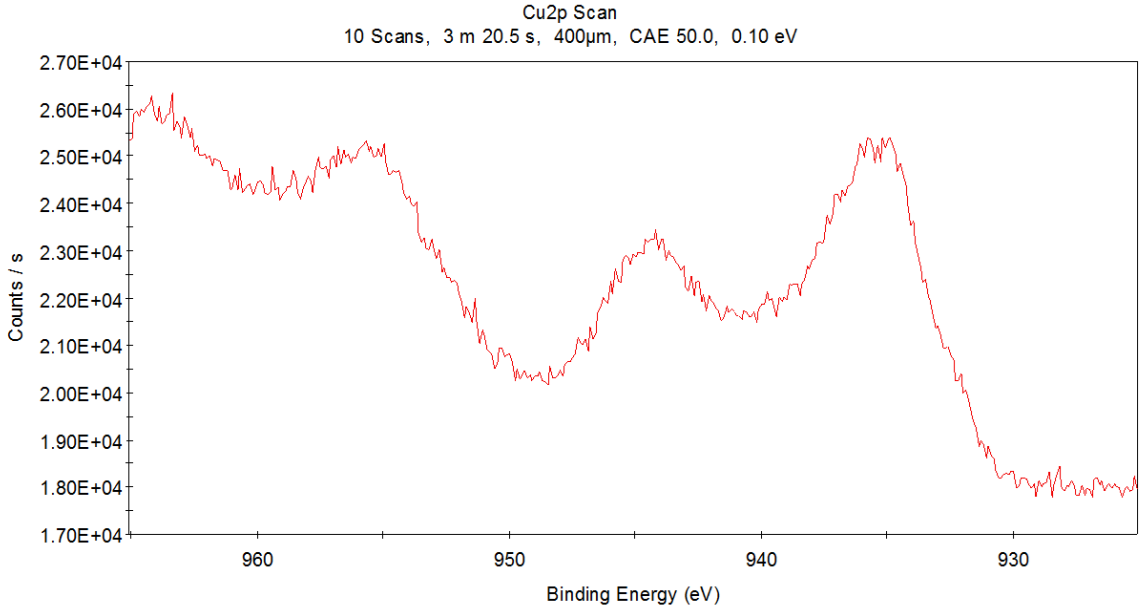




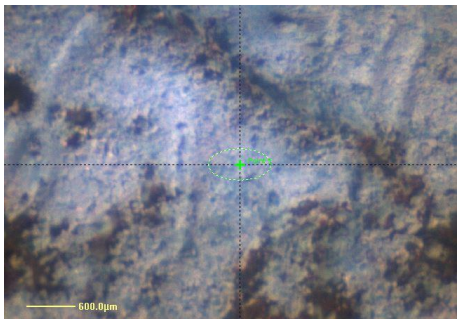
Element	Start BE	Peak BE	End BE	FWHM eV	Area (P) CPS.eV	Atomic %
C1s	292.08	285.34	277.08	3	1183733.75	84.62
O1s	538.08	532.48	523.08	3.31	359091.27	10.62
Cu2p3	948.58	935.82	927.58	5.1	417062.85	2.93
Cl2p	209.08	200.33	189.58	4.24	73683.97	1.82

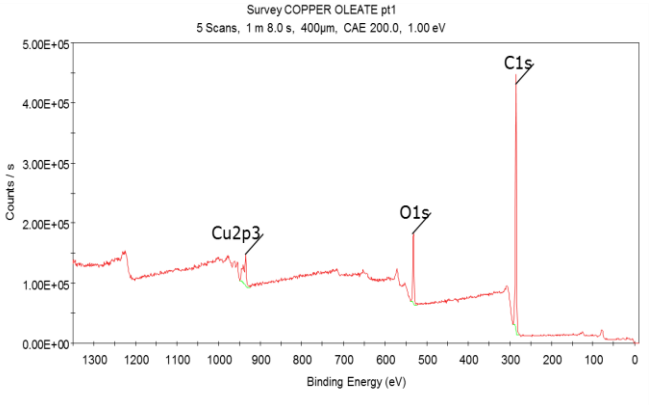



O1s Scan
10 Scans, 1 m 40.5 s, 400µm, CAE 50.0, 0.10 eV
Counts / s
2.20E+04
2.00E+04
1.80E+04
1.60E+04
1.40E+04
1.20E+04
1.00E+04
8.00E+03
6.00E+03
545 544 543 542 541 540 539 538 537 536 535 534 533 532 531 530 529 528 527 526
Binding Energy (eV)


Cu2p Scan
10 Scans, 3 m 20.5 s, 400µm, CAE 50.0, 0.10 eV
Counts / s
2.70E+04
2.60E+04
2.50E+04
2.40E+04
2.30E+04
2.20E+04
2.10E+04
2.00E+04
1.90E+04
1.80E+04
1.70E+04
960 950 940 930
Binding Energy (eV)

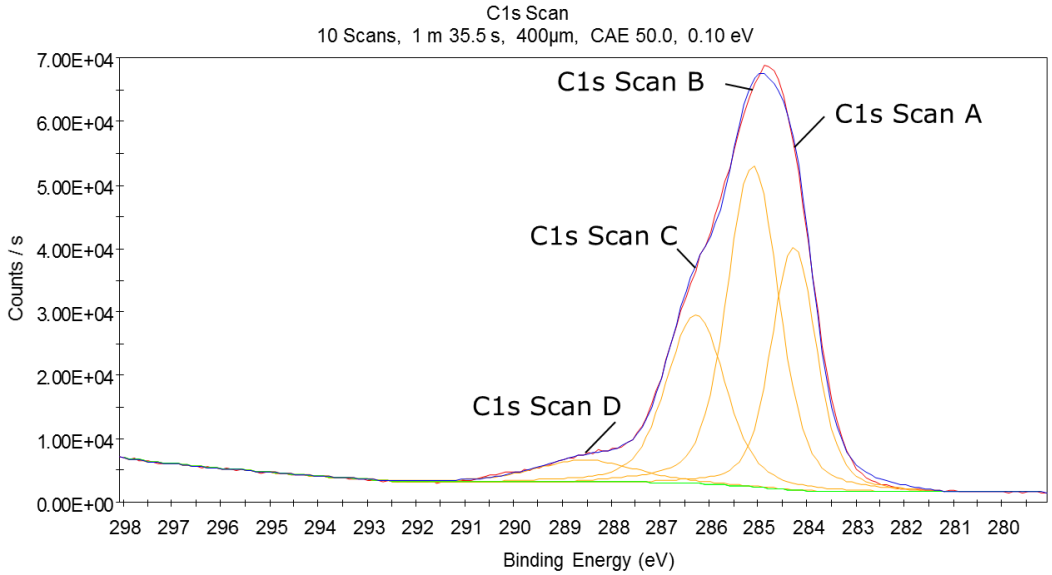
Cu-Oleate – POINT 1



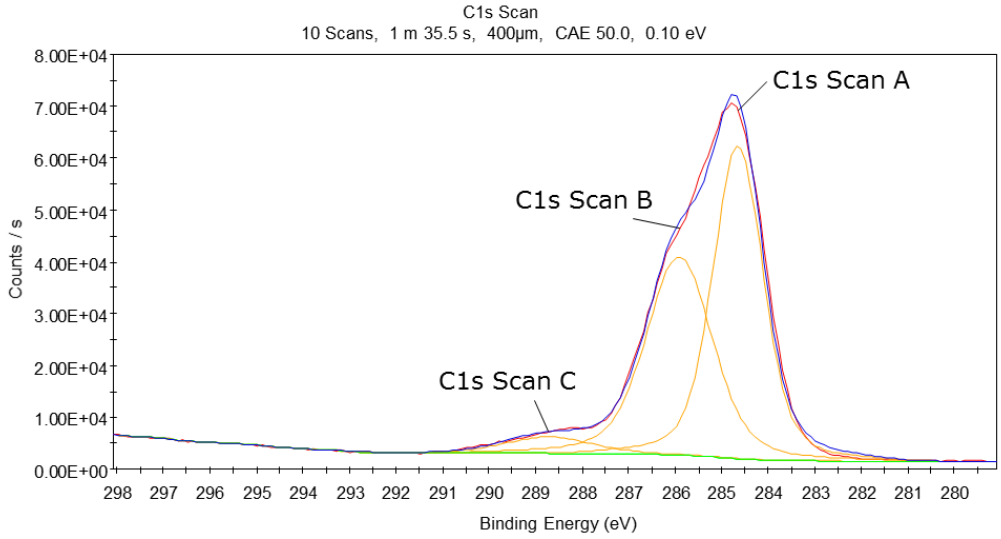


Element	Start BE	Peak BE	End BE	FWHM eV	Area (P) CPS.eV	Atomic %
C1s*	292.58	285.38	277.08	3.14	1411054.19	87.1
O1s	539.08	532.46	523.08	3.2	412614.25	10.54
Cu2p3	949.08	935.26	924.08	3.71	389296.46	2.36

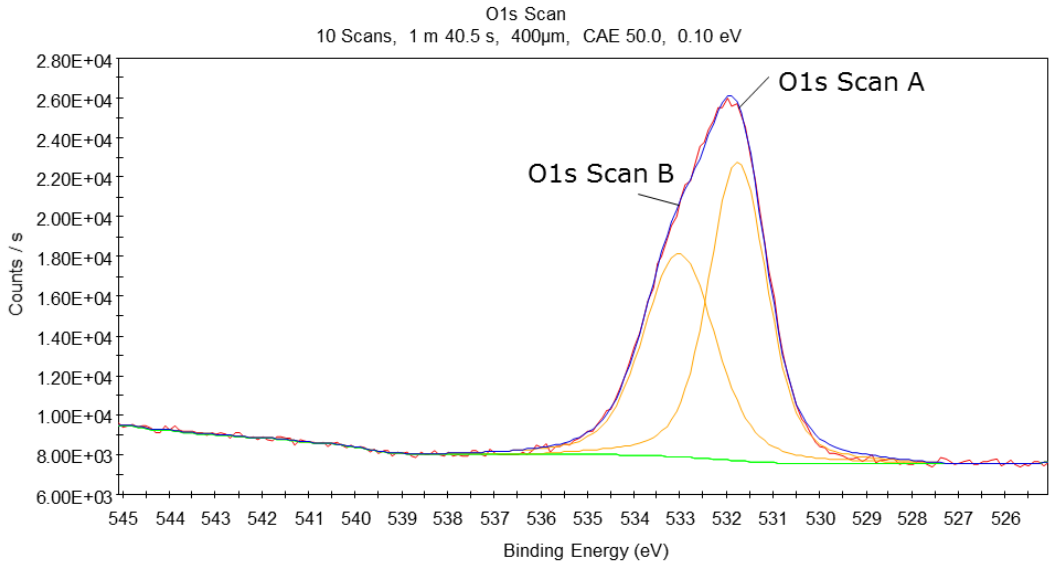
* C1s peak deconvoluted as 4 or 3 peaks



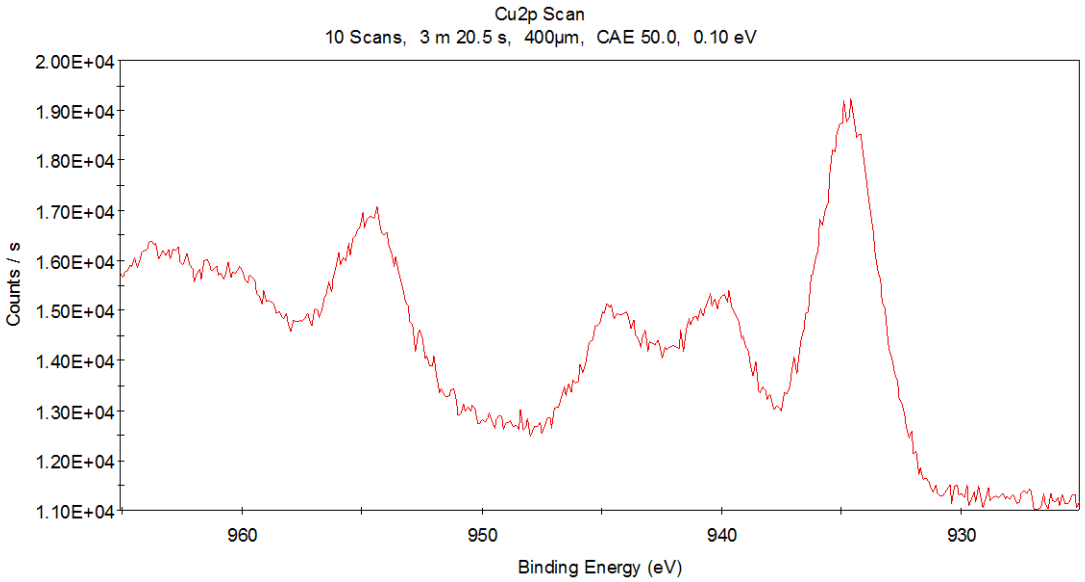
Name	Peak BE	FWH eV	Area (P) CPS.eV	Atomic %
C1s Scan A	284.26	1.09	48599.56	27.51
C1s Scan B	285.10	1.26	74266.59	42.06
C1s Scan C	286.27	1.42	44227.45	25.06
C1s Scan D	288.53	2.41	9470.80	5.37



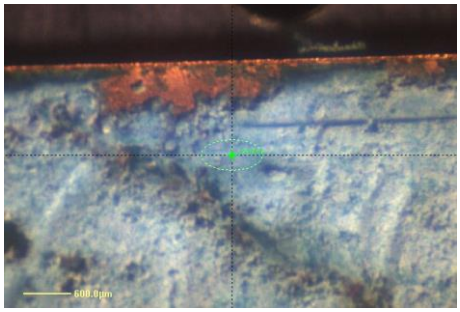
Name	Peak BE	FWHM eV	Area (P) CPS.eV	Atomic %
C1s Scan A	284.64	1.27	89674.04	51.95
C1s Scan B	285.91	1.67	74957.92	43.46
C1s Scan C	288.73	2.16	7913.78	4.60

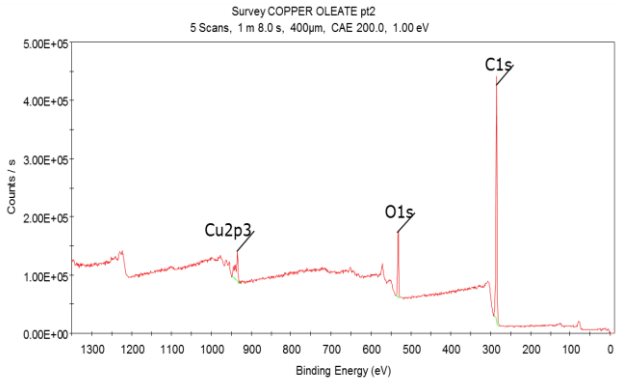


Name	Peak BE	FWHM eV	Area (P) CPS.eV	Atomic %
O1s Scan A	531.75	1.48	26291.85	54.46
O1s Scan B	533.01	1.83	21965.10	45.54

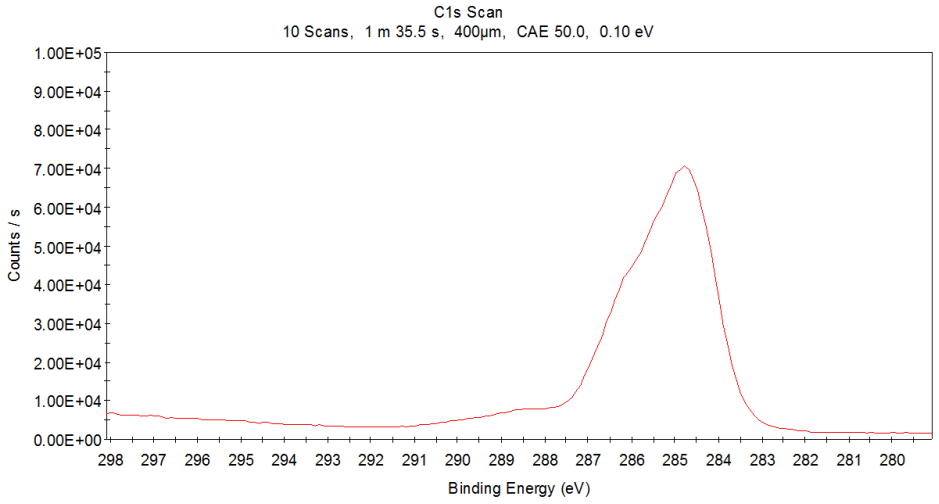

Cu2p Scan
10 Scans, 3 m 20.5 s, 400µm, CAE 50.0, 0.10 eV
2.00E+04
1.90E+04
1.80E+04
1.70E+04
1.60E+04
1.50E+04
1.40E+04
1.30E+04
1.20E+04
1.10E+04
Counts / s
960
950
940
930
Binding Energy (eV)

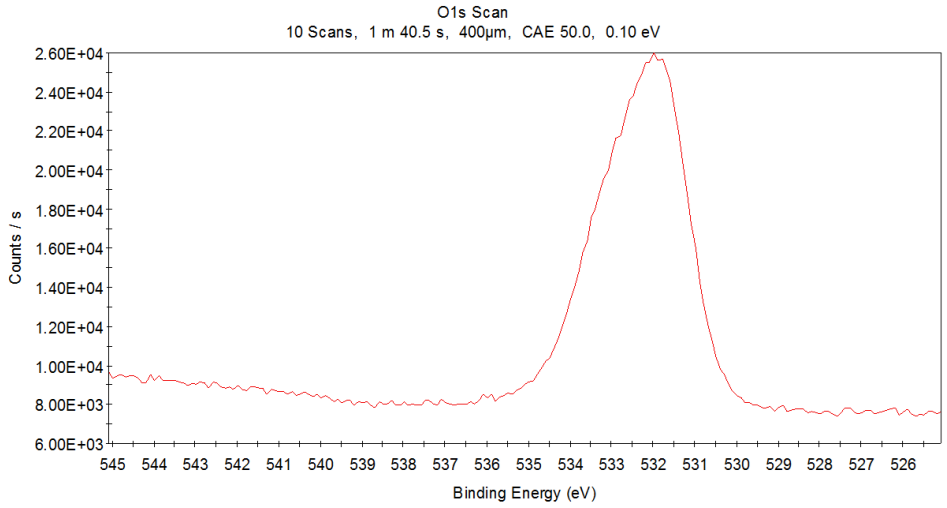
Cu-Oleate – POINT 2

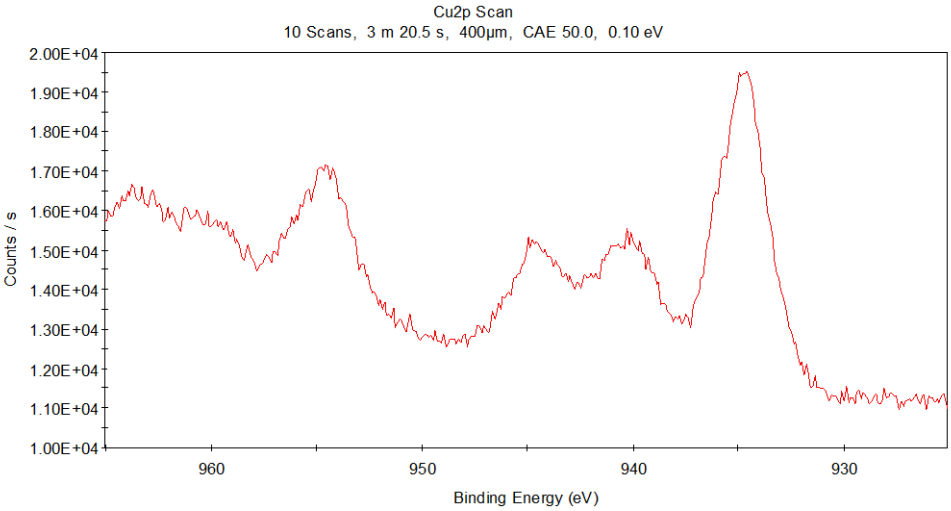




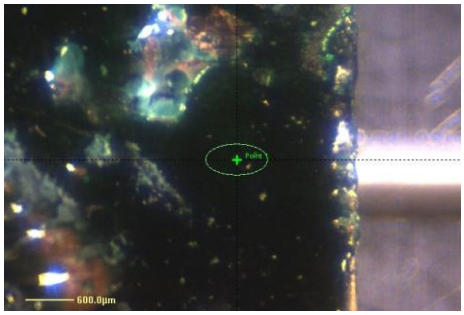
Element	Start BE	Peak BE	End BE	FWHM eV	Area (P) CPS.eV	Atomic %
C1s	292.58	285.36	277.08	3	1354547.5	87.94
O1s	538.08	532.48	523.58	3.18	365037.35	9.81
Cu2p3	949.08	935.16	926.08	3.44	353410.45	2.25

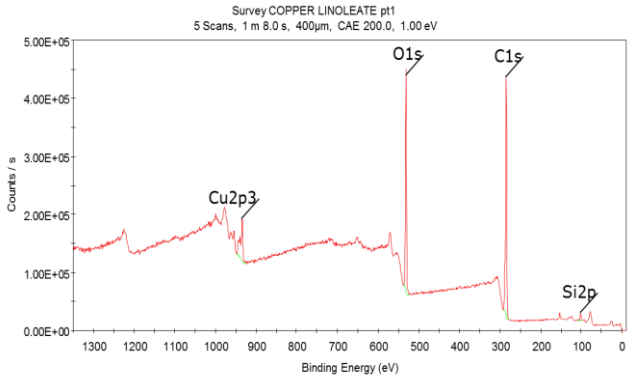



O1s Scan
10 Scans, 1 m 40.5 s, 400µm, CAE 50.0, 0.10 eV
Counts / s
2.60E+04
2.40E+04
2.20E+04
2.00E+04
1.80E+04
1.60E+04
1.40E+04
1.20E+04
1.00E+04
8.00E+03
6.00E+03
545 544 543 542 541 540 539 538 537 536 535 534 533 532 531 530 529 528 527 526
Binding Energy (eV)


Cu2p Scan
10 Scans, 3 m 20.5 s, 400µm, CAE 50.0, 0.10 eV
Counts / s
2.00E+04
1.90E+04
1.80E+04
1.70E+04
1.60E+04
1.50E+04
1.40E+04
1.30E+04
1.20E+04
1.10E+04
1.00E+04
960
950
940
930
Binding Energy (eV)

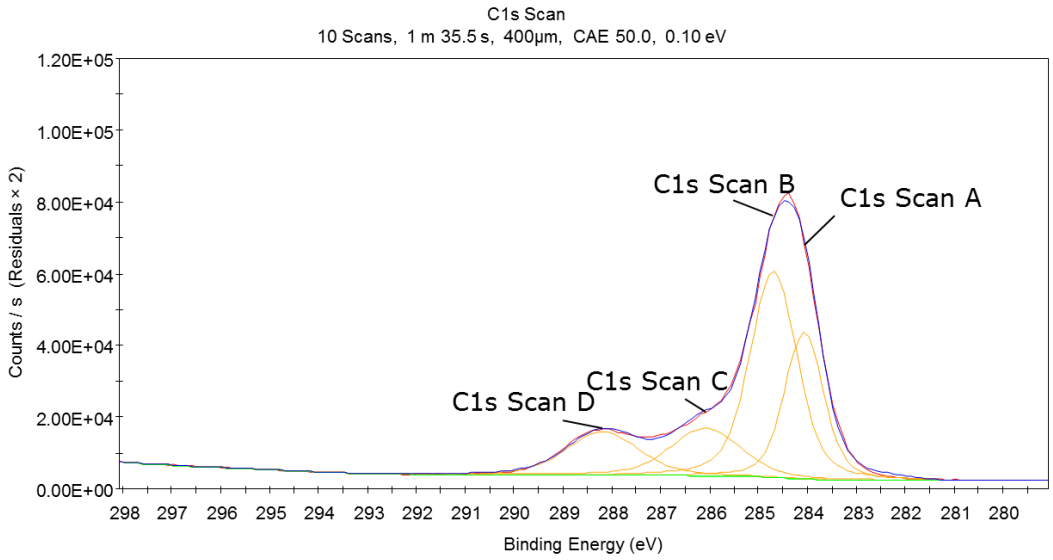
Cu-Linoleate – POINT 1



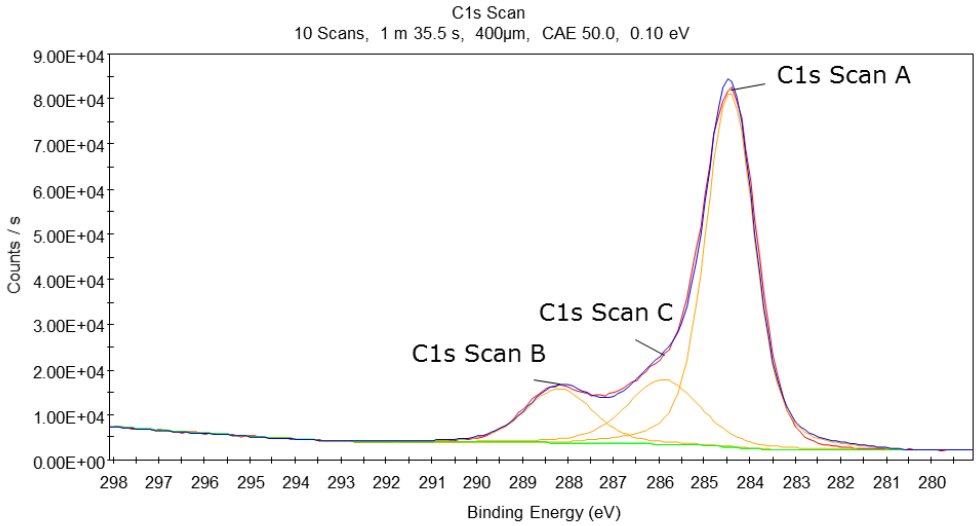


Element	Start BE	Peak BE	End BE	FWHM eV	Area (P) CPS.eV	Atomic %
O1s	537.58	532.17	524.08	2.96	1122315.8	24.34
C1s*	292.08	285.05	278.08	2.9	1349883.71	70.77
Cu2p3	948.08	934.78	924.08	3.73	510960.55	2.63
Si2p	110.08	102.1	97.08	2.84	43261.32	2.26

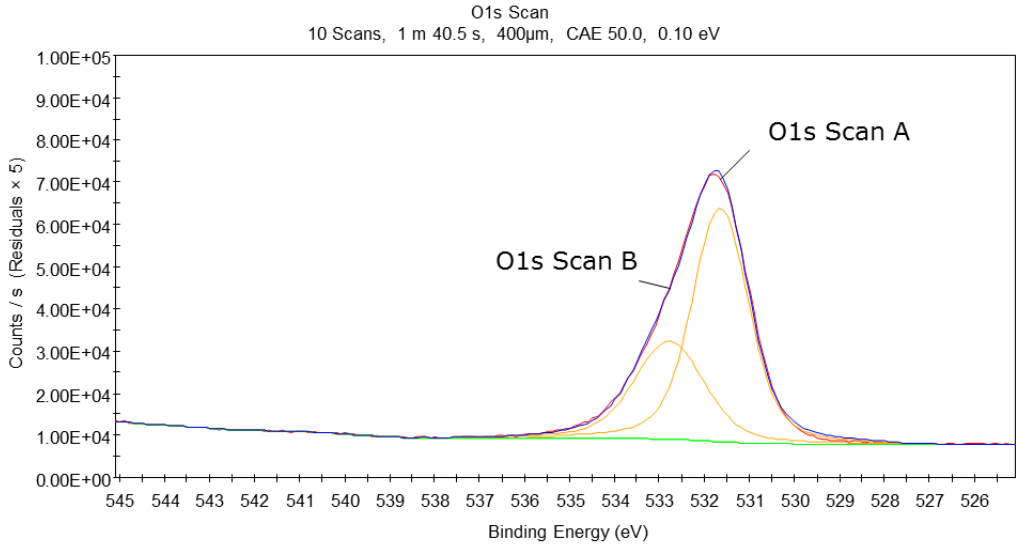
* C1s peak deconvoluted as 4 or 3 peaks



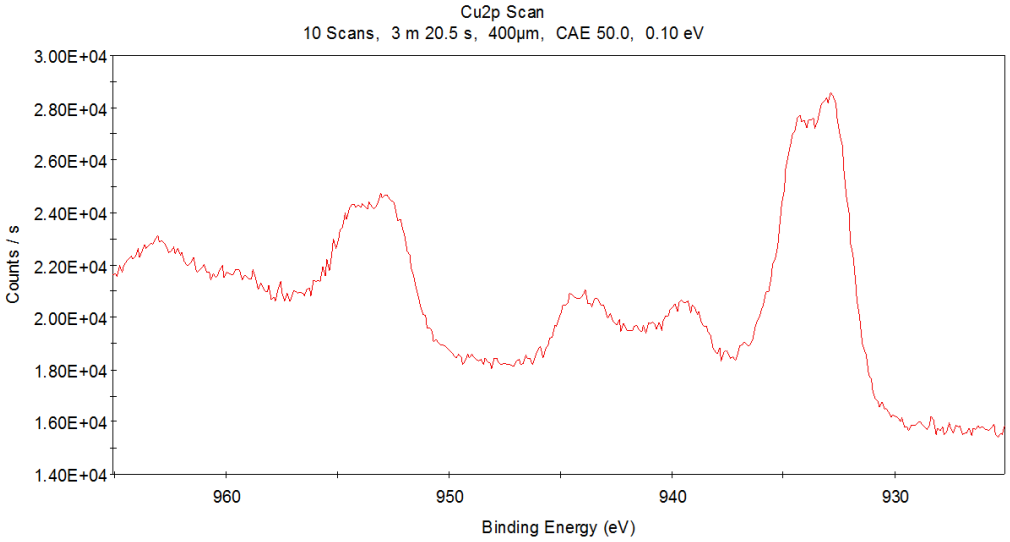
Name	Peak BE	FWHM eV	Area (P) CPS.eV	Atomic %
C1s Scan A	284.07	0.94	44907.74	26.06
C1s Scan B	284.69	1.13	76247.65	44.26
C1s Scan C	286.08	1.68	26354.25	15.31
C1s Scan D	288.18	1.74	24711.54	14.38



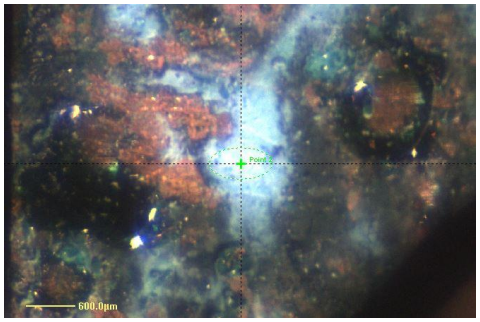
Name	Peak BE	FWHM eV	Area (P) CPS.eV	Atomic %
C1s Scan A	284.43	1.27	116989.61	67.77
C1s Scan B	288.19	1.73	24162.45	14.03
C1s Scan C	285.90	1.89	31396.69	18.20

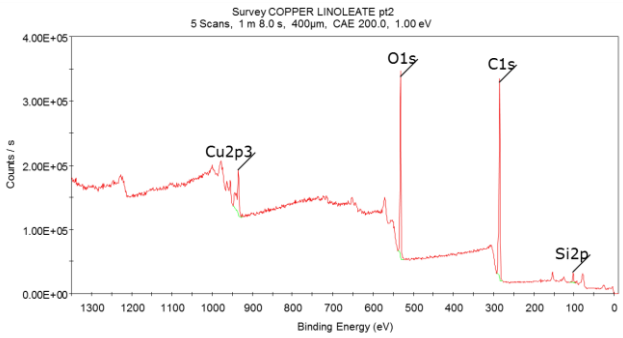


Name	Peak BE	FWHM eV	Area (P) CPS.eV	Atomic %	Q
O1s Scan A	531.64	1.48	95754.18	65.84	1
O1s Scan B	532.78	1.82	49634.02	34.16	1

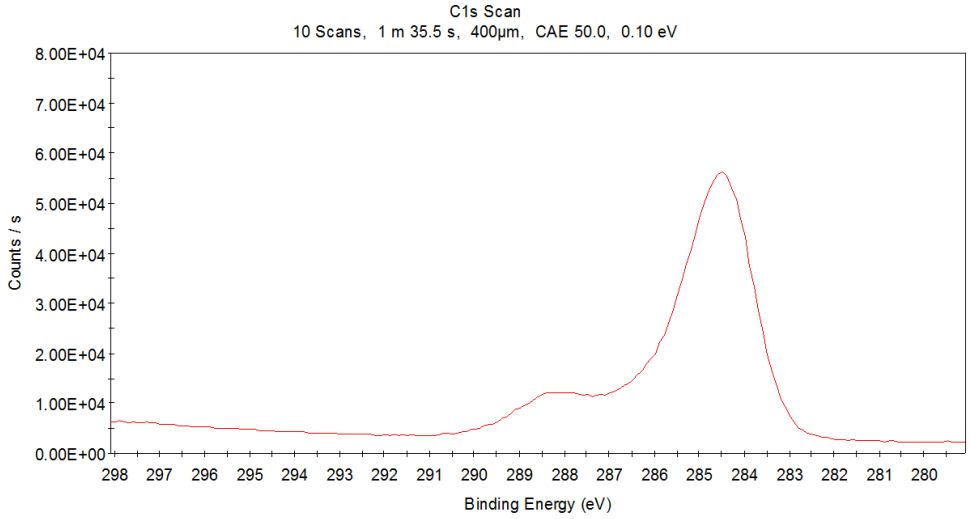

Cu2p Scan
10 Scans, 3 m 20.5 s, 400µm, CAE 50.0, 0.10 eV
3.00E+04
2.80E+04
2.60E+04
2.40E+04
2.20E+04
2.00E+04
1.80E+04
1.60E+04
1.40E+04
Counts / s
960
950
940
930
Binding Energy (eV)

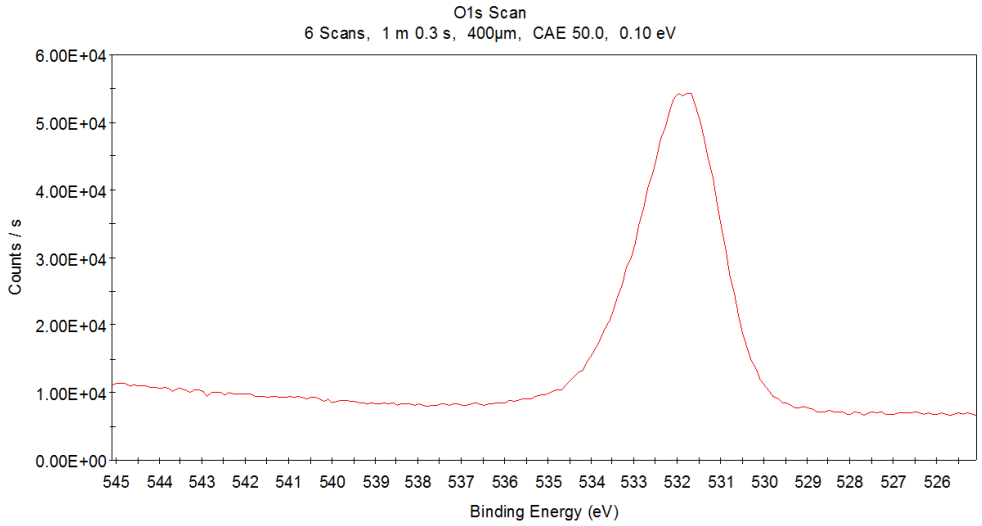
Cu-Linoleate– POINT 2

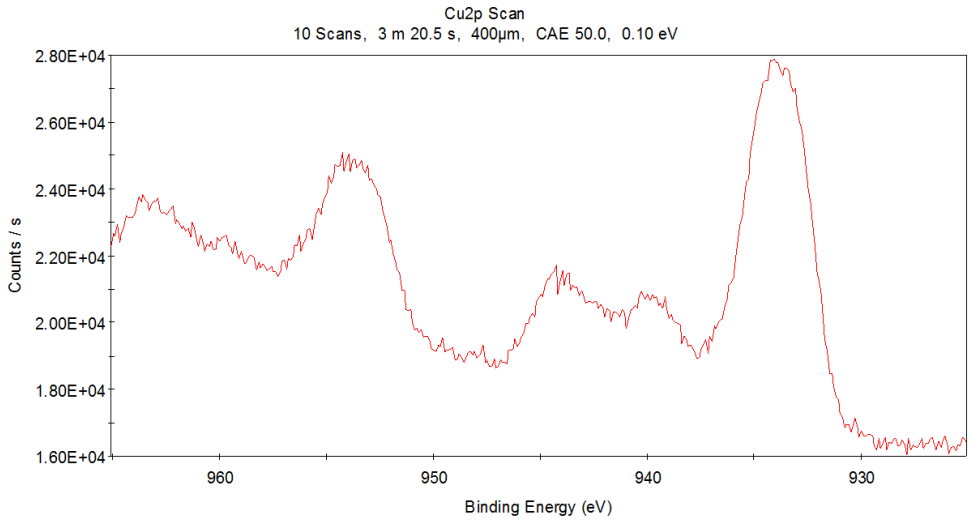


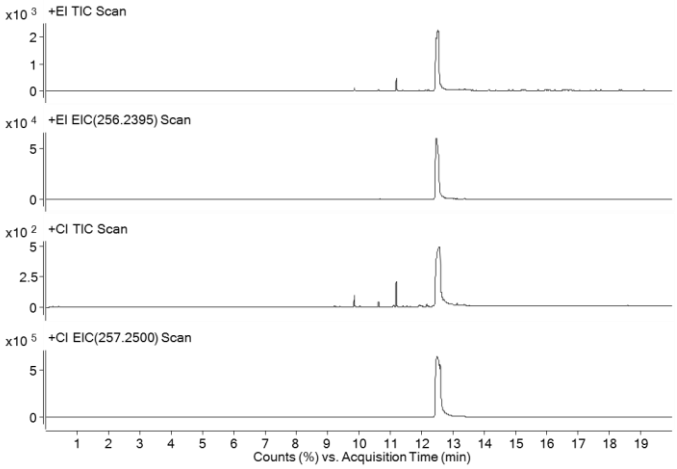


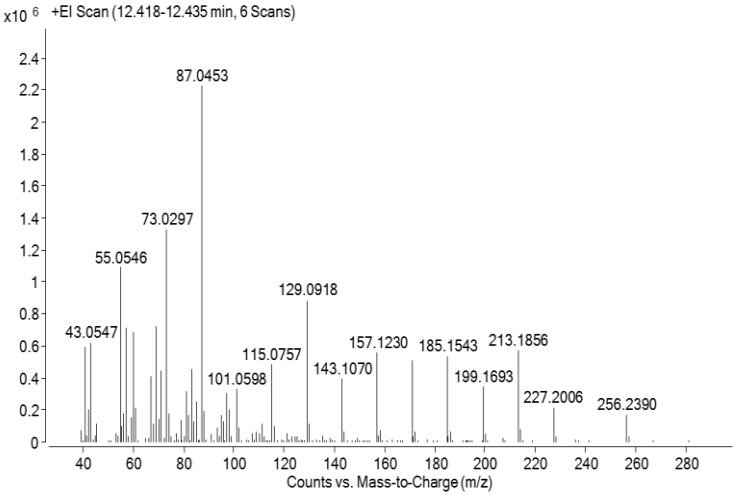
Element	Start BE	Peak BE	End BE	FWHM eV	Area (P) CPS.eV	Atomic %
O1s	538.58	532.24	523.08	3.02	871523.32	24.23
C1s	292.08	285.14	278.58	3.07	1025968.74	68.93
Cu2p3	948.08	934.98	923.08	3.73	455185.38	3
Si2p	110.08	102.13	96.08	3.07	57384.81	3.84

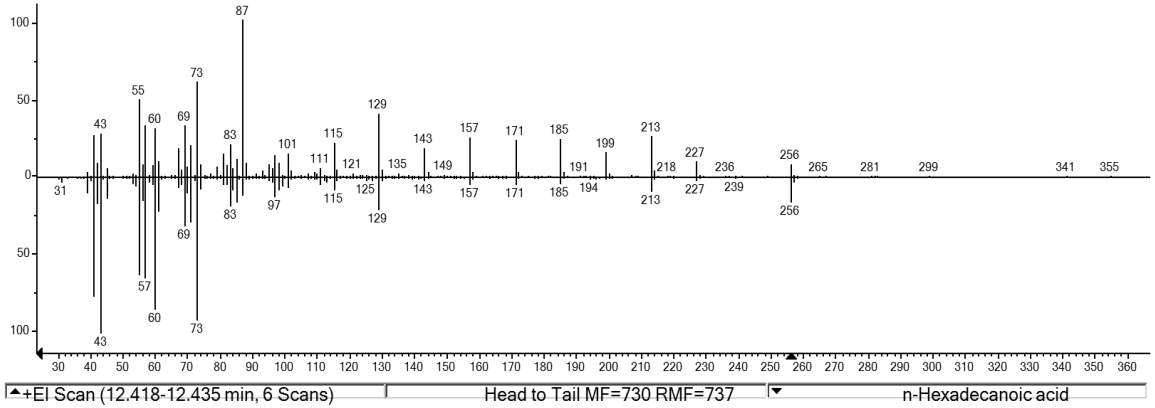


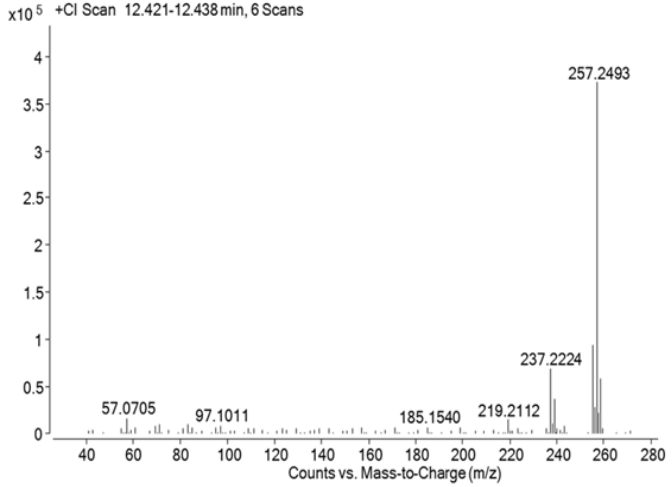

O1s Scan
6 Scans, 1 m 0.3 s, 400µm, CAE 50.0, 0.10 eV
6.00E+04
5.00E+04
4.00E+04
3.00E+04
2.00E+04
1.00E+04
0.00E+00
Counts / s
545 544 543 542 541 540 539 538 537 536 535 534 533 532 531 530 529 528 527 526
Binding Energy (eV)


Cu2p Scan
10 Scans, 3 m 20.5 s, 400µm, CAE 50.0, 0.10 eV
2.80E+04
2.60E+04
2.40E+04
2.20E+04
2.00E+04
1.80E+04
1.60E+04
Counts / s
960 950 940 930
Binding Energy (eV)

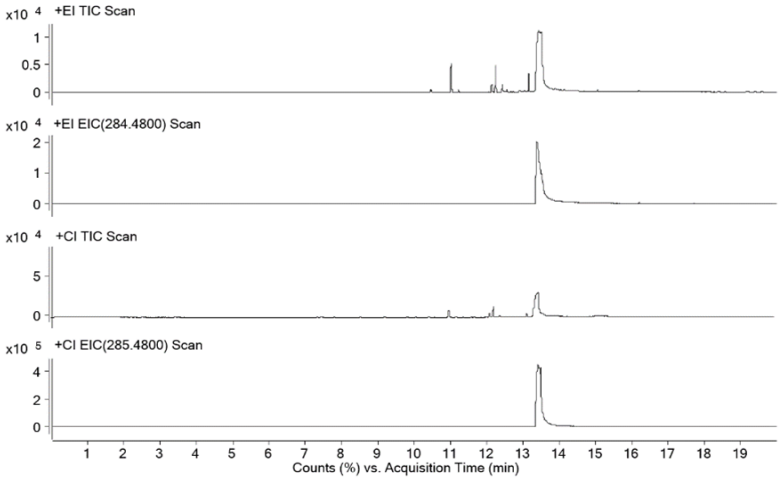


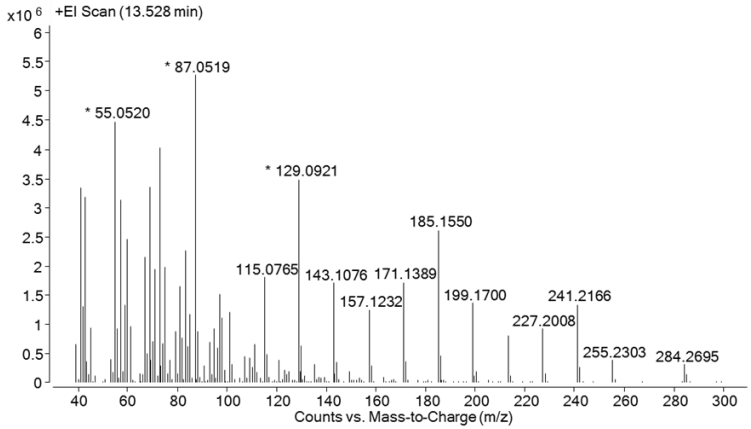


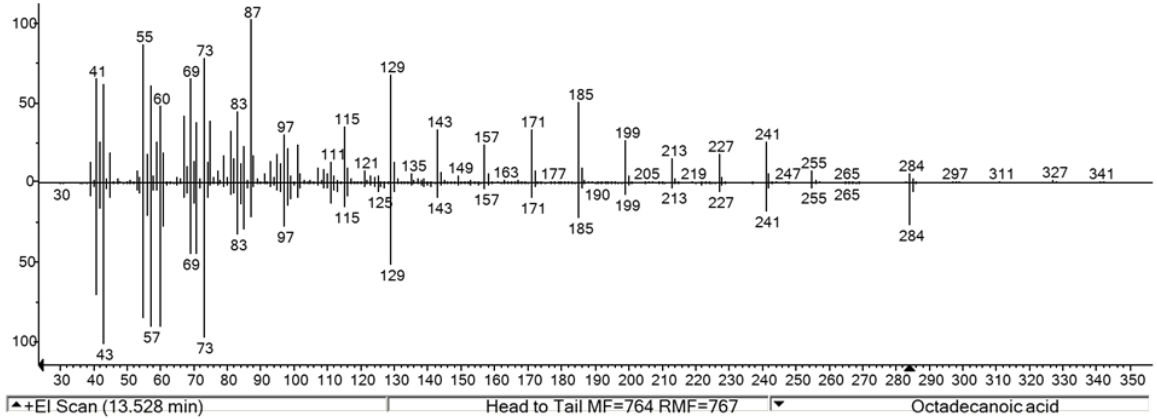


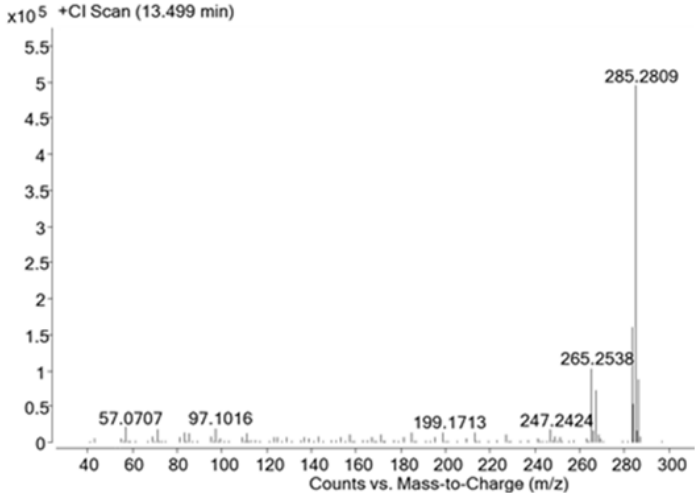


EI and CI Chromatograms and Mass Spectra with NIST library match for Cu-Palmitate

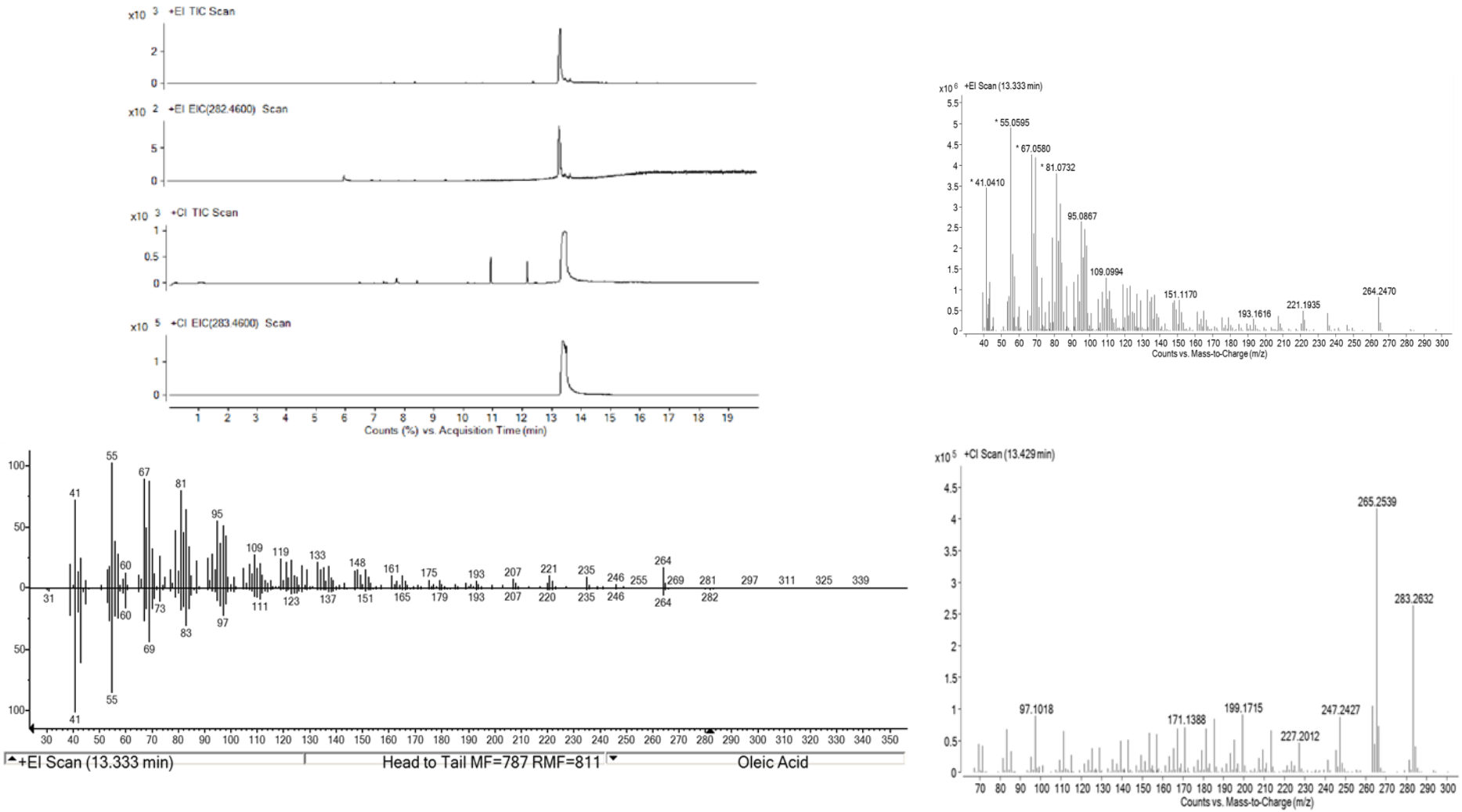




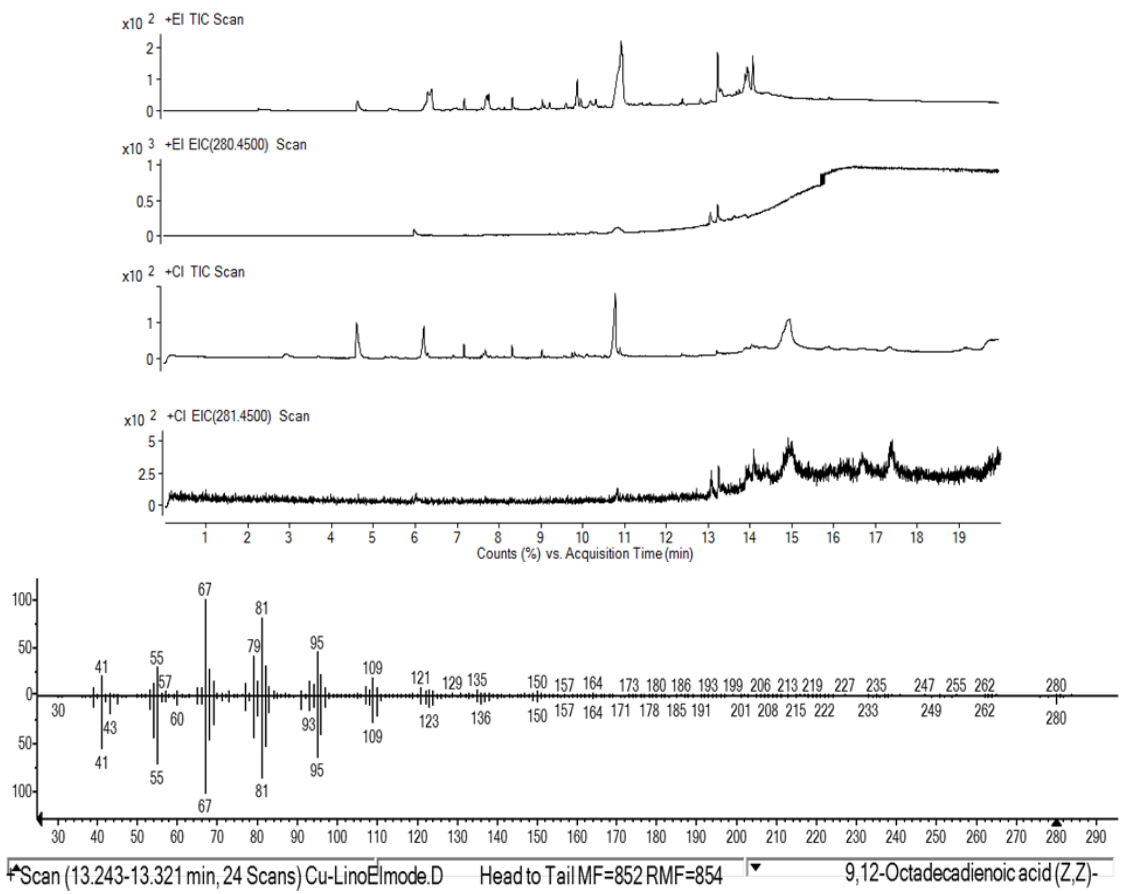


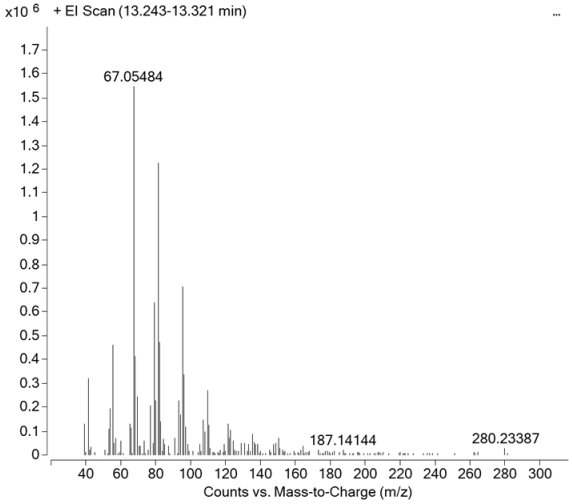


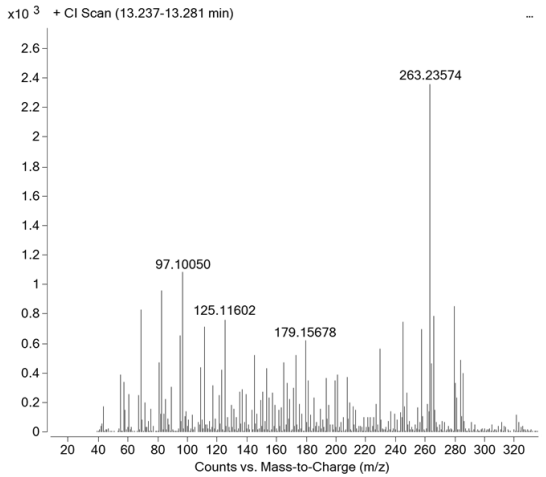
EI and CI Chromatograms and Mass Spectra with NIST library match for Cu-Stearate



EI and CI Chromatograms and Mass Spectra with NIST library match for Cu-Oleate

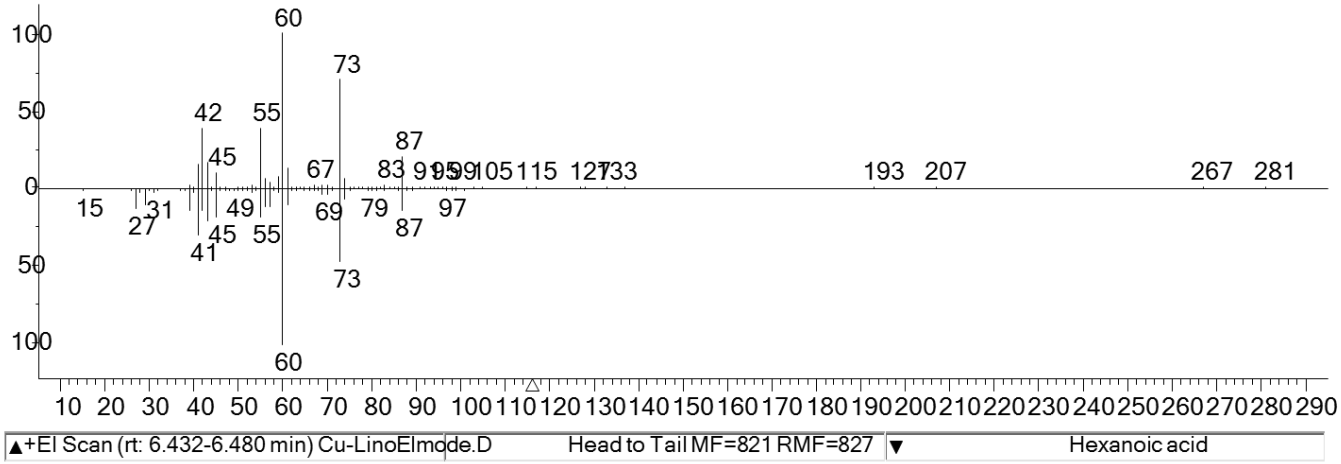






EI and CI Chromatograms and Mass Spectra with NIST library match for Cu-Linoleate

1. Hexanoic acid $C_6H_{12}O$ · Mass: 116.1583

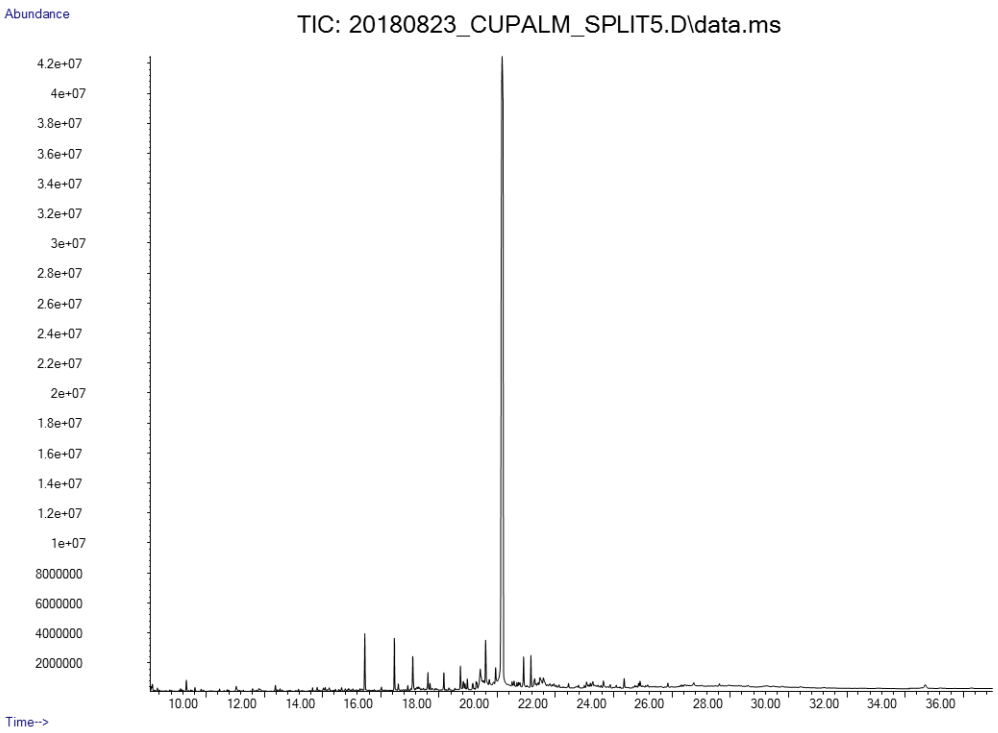


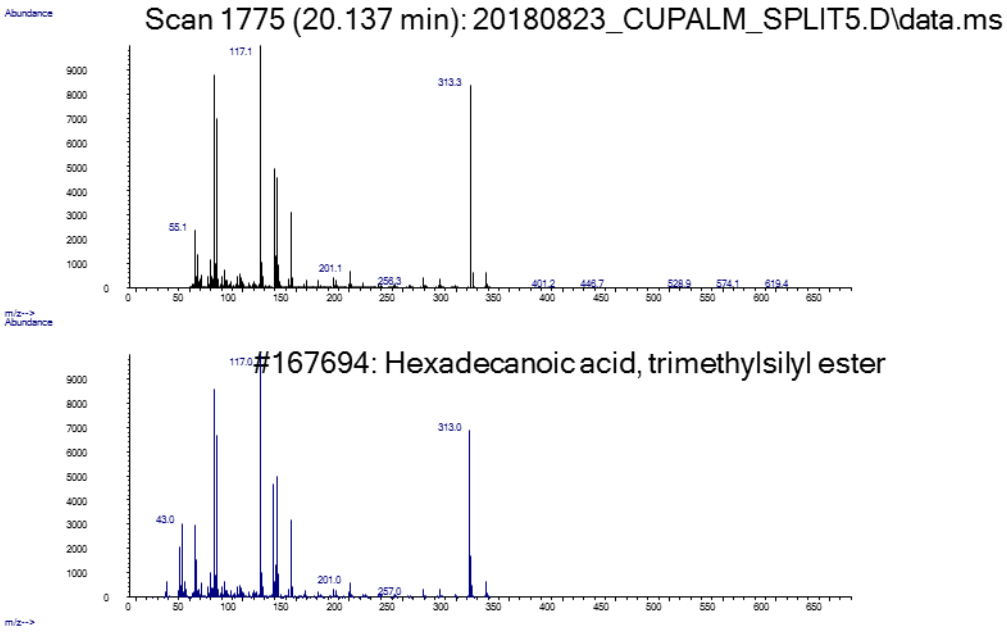
2. Azelaic acid $C_9H_{16}O_4$ · Mass: 188.2209



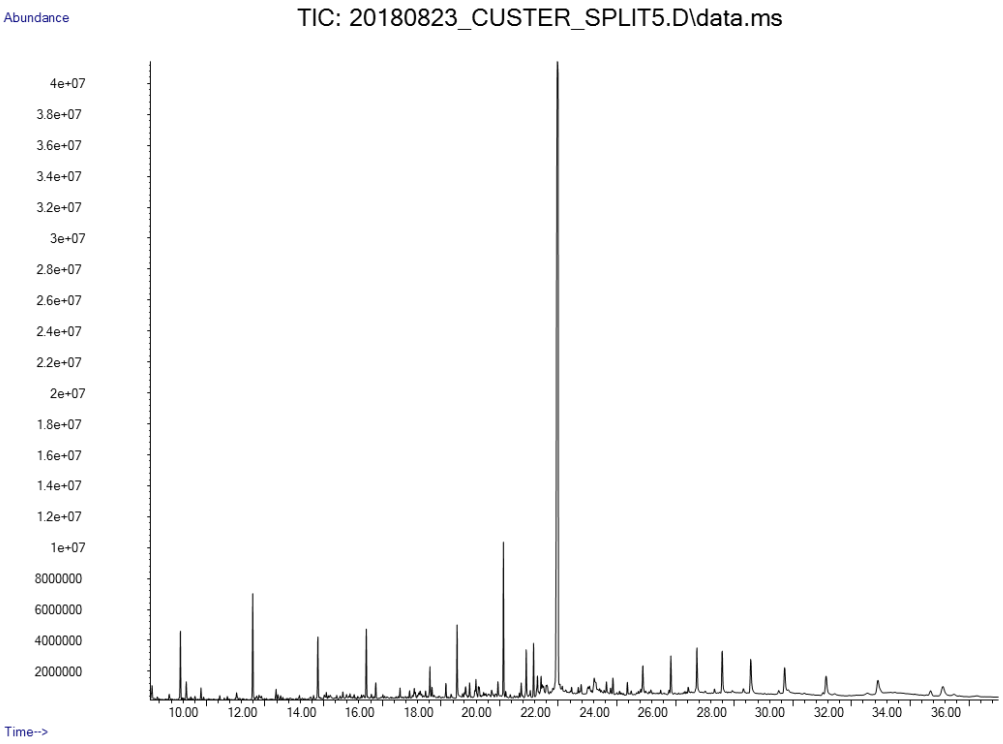
Degradation Compounds of Cu-Linoleate

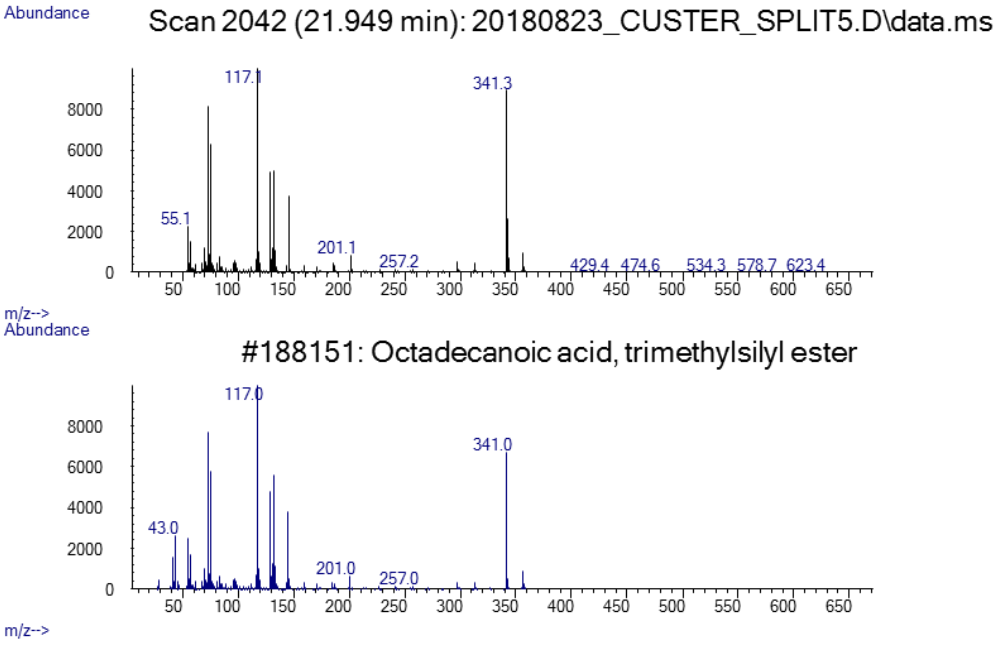
Cu-Palmitate



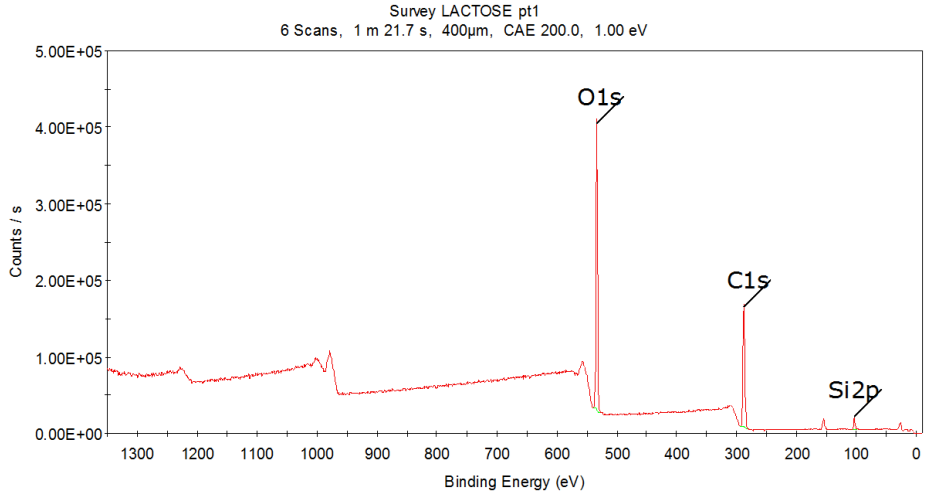


Cu-Stearate

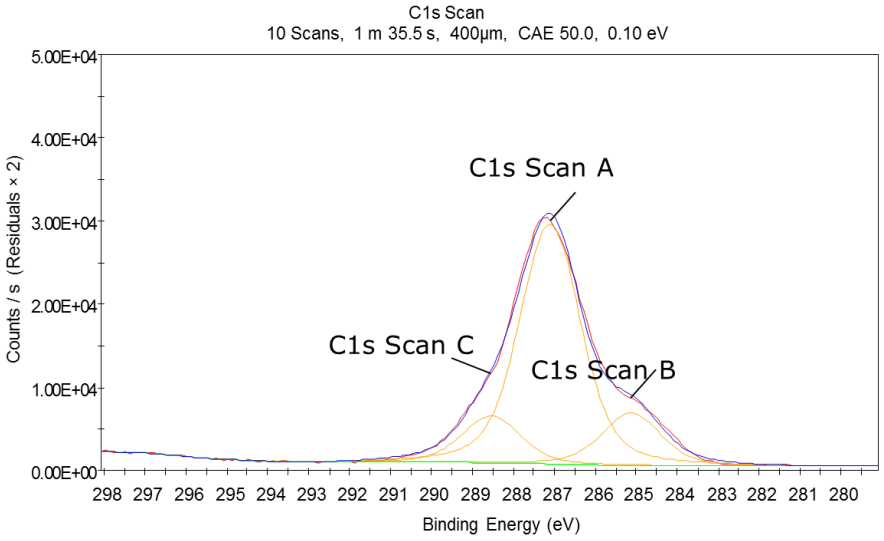

TIC: 20180823_CUSTER_SPLIT5.D\data.ms
Abundance
4e+07
3.8e+07
3.6e+07
3.4e+07
3.2e+07
3e+07
2.8e+07
2.6e+07
2.4e+07
2.2e+07
2e+07
1.8e+07
1.6e+07
1.4e+07
1.2e+07
1e+07
8000000
6000000
4000000
2000000
Time-->
10.00
12.00
14.00
16.00
18.00
20.00
22.00
24.00
26.00
28.00
30.00
32.00
34.00
36.00


Abundance
Scan 2042 (21.949 min): 20180823_CUSTER_SPLIT5.D\data.ms
117.1
341.3
55.1
201.1
257.2
429.4
474.6
534.3
578.7
623.4
8000
6000
4000
2000
0
50
100
150
200
250
300
350
400
450
500
550
600
650
m/z-->
Abundance
#188151: Octadecanoic acid, trimethylsilyl ester
117.0
341.0
43.0
201.0
257.0
m/z-->

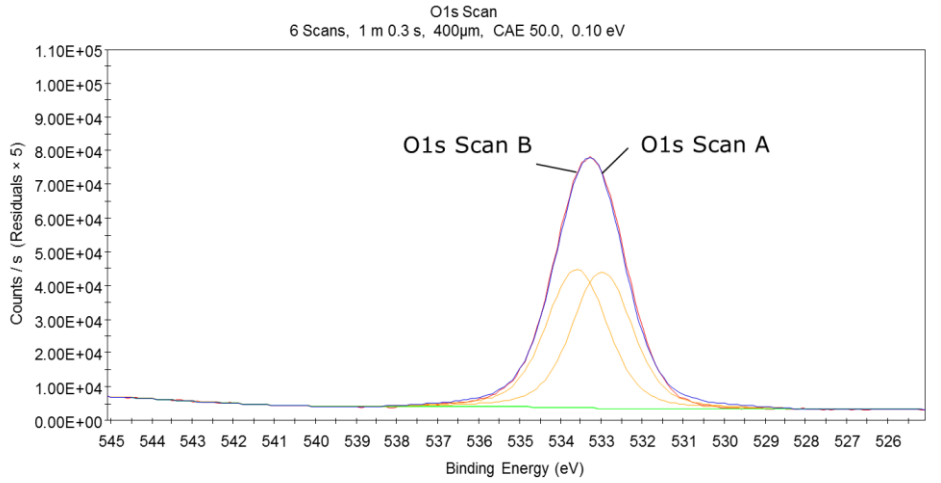
Lactose – POINT 1



Element	Start BE	Peak BE	End BE	FWHM eV	Area (P) CPS.eV	Atomic %
O1s	539.58	533.81	526.96	2.91	1186442.71	43.51
C1s	293.58	287.72	281.73	3.43	591108.16	52.42
Si2p	106.35	103.16	99	2.65	46093.41	4.07

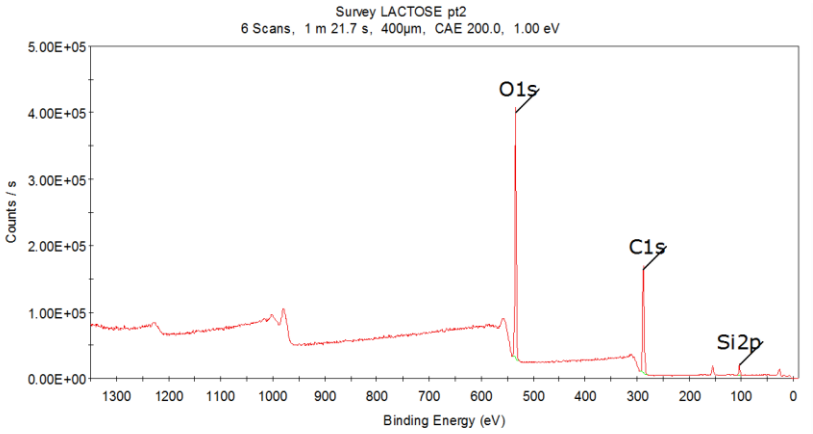


Name	Peak BE	FWHM eV	Area (P) CPS.eV	Atomic %
C1s Scan A	287.10	1.75	59035.02	71.46
C1s Scan B	285.12	1.71	12502.96	15.12
C1s Scan C	288.55	1.68	11080.27	13.42

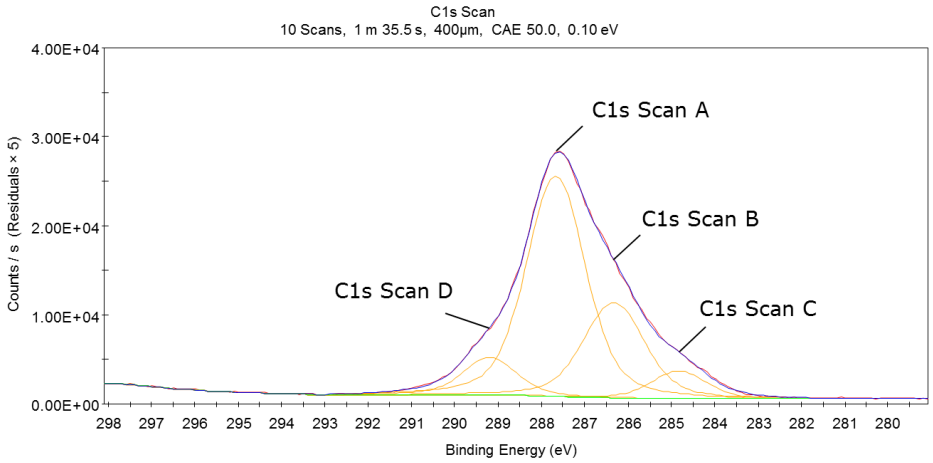


Name	Peak BE	FWHM eV	Area (P) CPS.eV	Atomic %
O1s Scan A	532.98	1.73	82478.52	49.26
O1s Scan B	533.60	1.76	84929.92	50.74

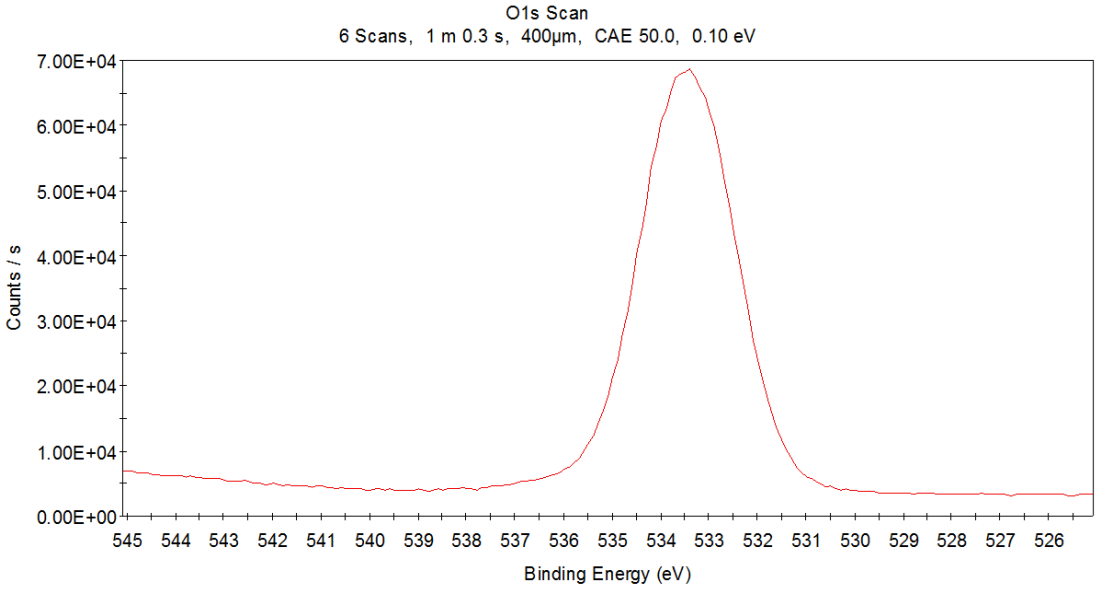
Lactose – POINT 2



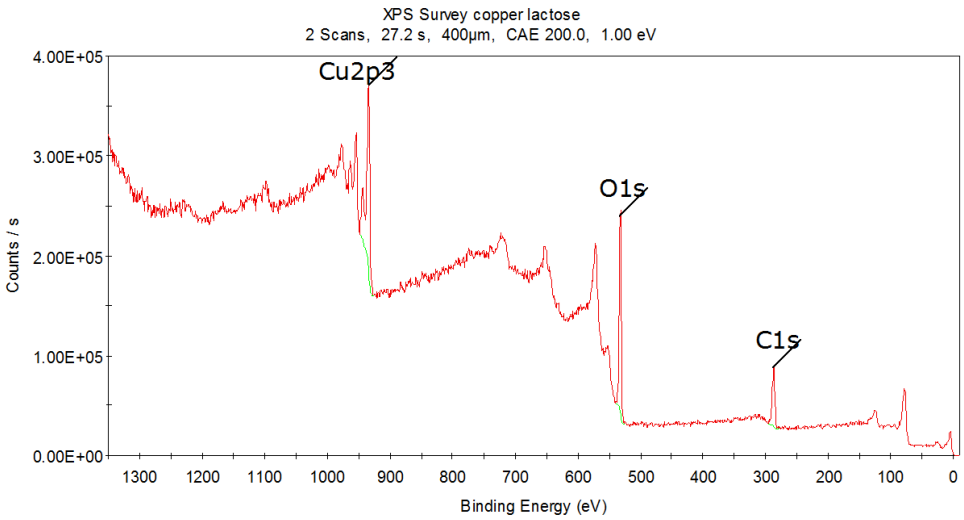
Element	Start BE	Peak BE	End BE	FWHM eV	Area (P) CPS.eV	Atomic %
O1s	539.59	533.99	527.31	3.09	1171323.88	43.53
C1s	293.08	287.89	280.02	3.47	583987.99	52.47
Si2p	107.47	103.22	99.88	2.49	44757.86	4



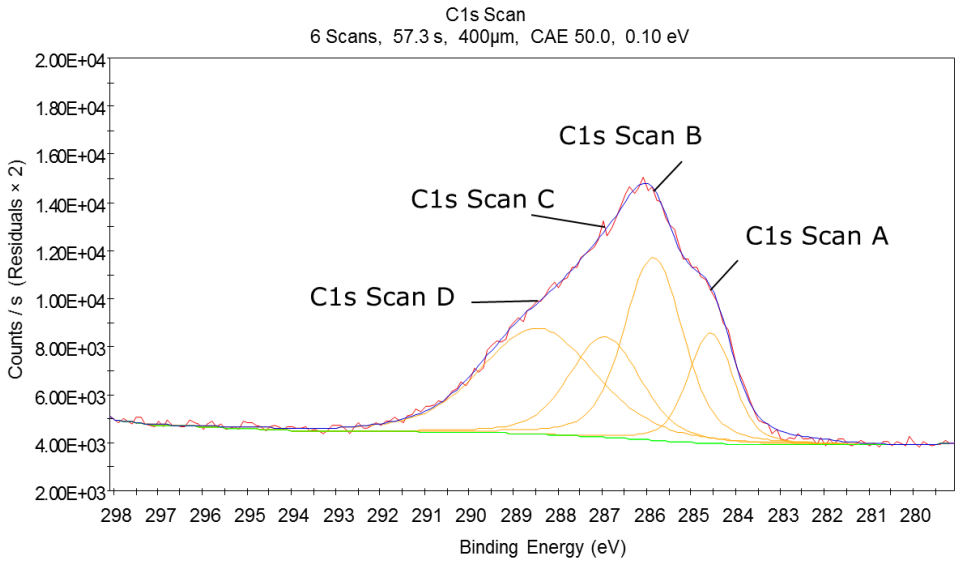
Name	Peak BE	FWHM eV	Area (P) CPS.eV	Atomic %
C1s Scan A	287.66	1.60	46533.07	58.29
C1s Scan B	286.32	1.66	20793.78	26.03
C1s Scan C	284.82	1.48	5374.14	6.72
C1s Scan D	289.20	1.45	7144.53	8.96



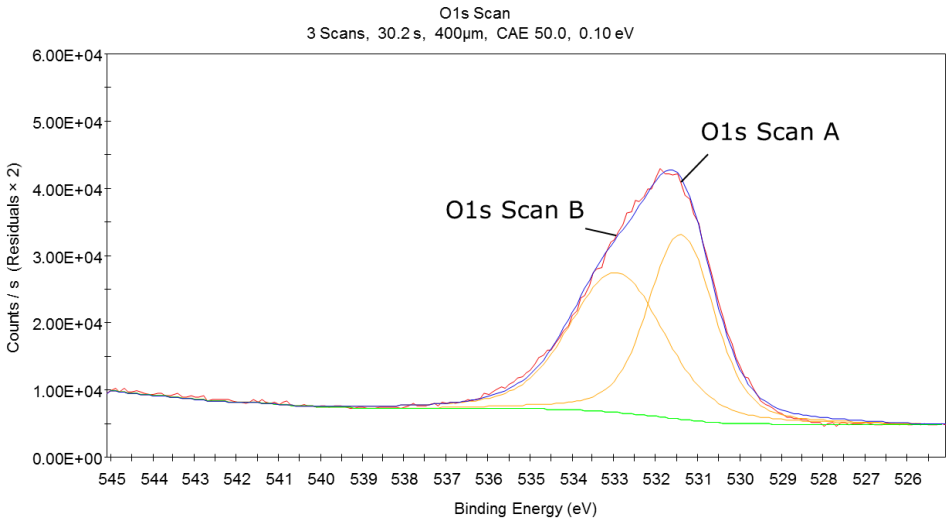
Cu-Lactose



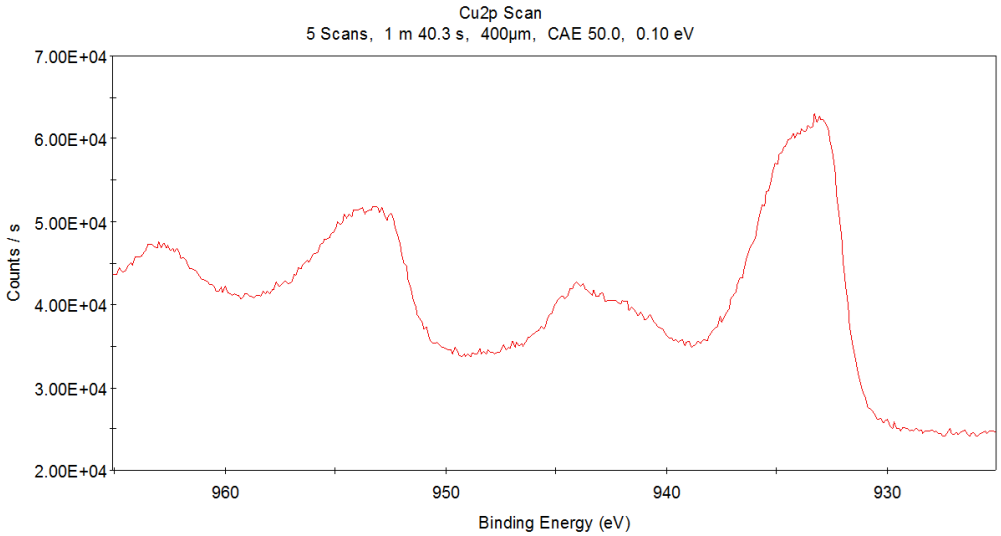
Element	Start BE	Peak BE	End BE	FWHM eV	Area (P) CPS.eV	Atomic %
Cu2p3	948.58	934.16	926.58	4.5	1242987.92	15.73
O1s	540.58	532.37	526.08	3.81	810583.95	43.27
C1s	295.58	286.85	278.58	4.92	317407.11	41



Name	Peak BE	FWHM eV	Area (P) CPS.eV	Atomic %
C1s Scan A	284.55	1.20	6462.19	14.23
C1s Scan B	285.84	1.57	13945.84	30.73
C1s Scan C	286.93	1.90	9291.15	20.49
C1s Scan D	288.45	3.03	15659.62	34.56

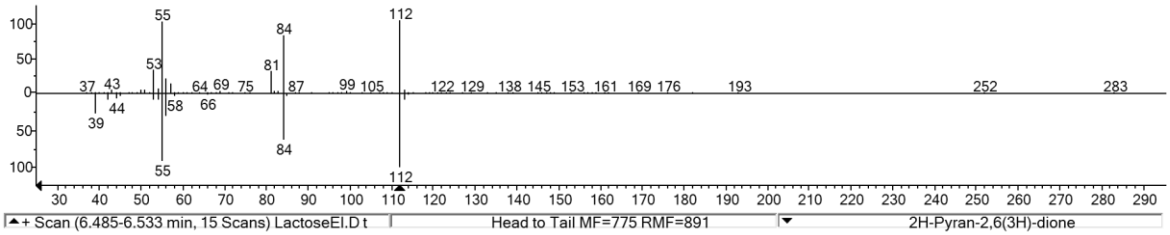


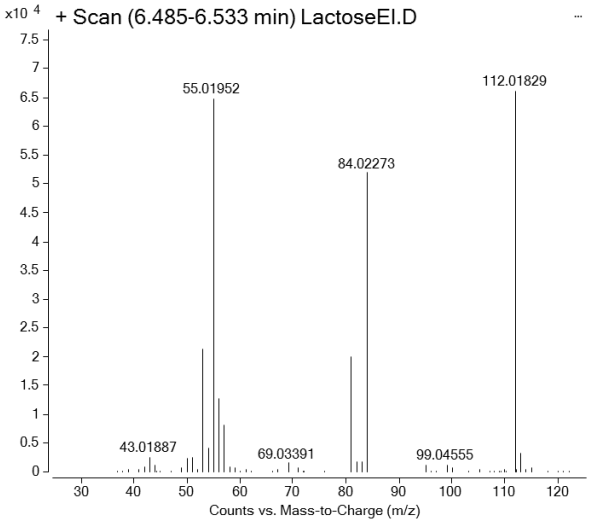
Name	Peak BE	FWHM eV	Area (P) CPS.eV	Atomic %
O1s Scan A	531.39	1.86	60084.48	47.73
O1s Scan B	532.92	2.67	65712.41	52.27

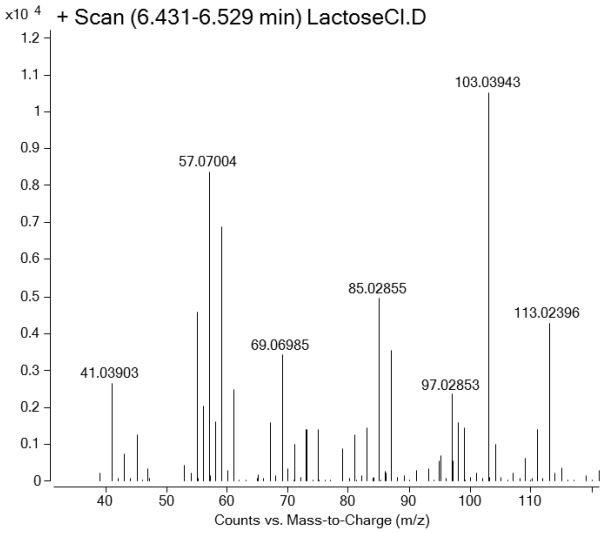


2H-Pyran-2,6(3H)-dione

Mass: 112.016044

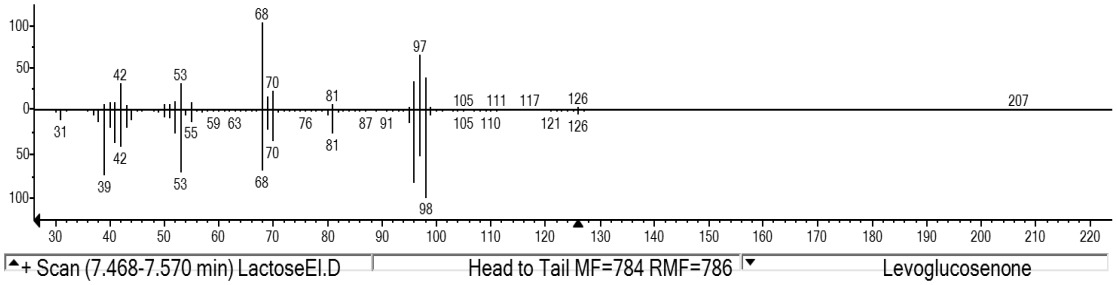


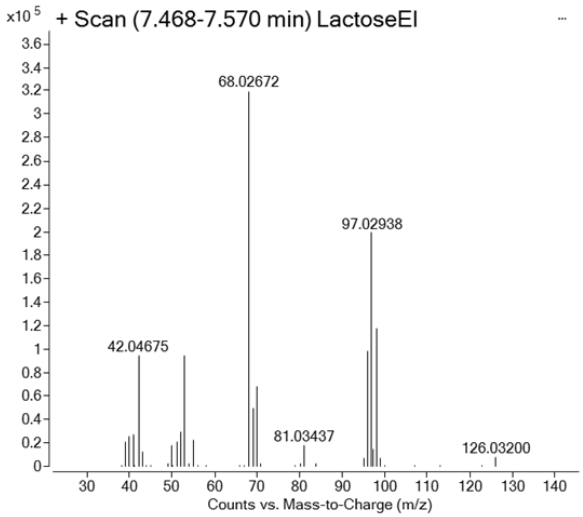


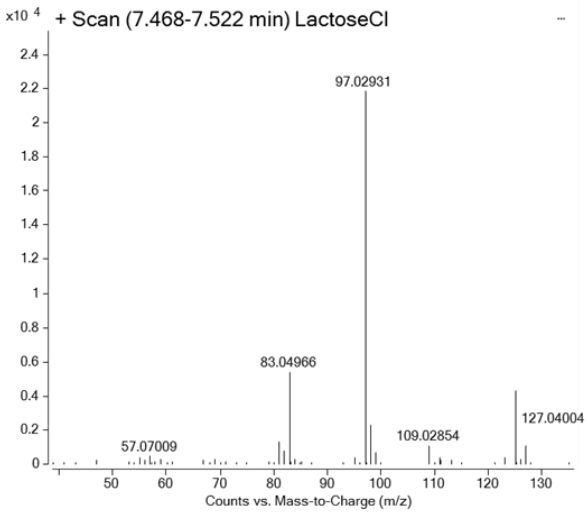


Levoglucosenone

Mass: 126.031694

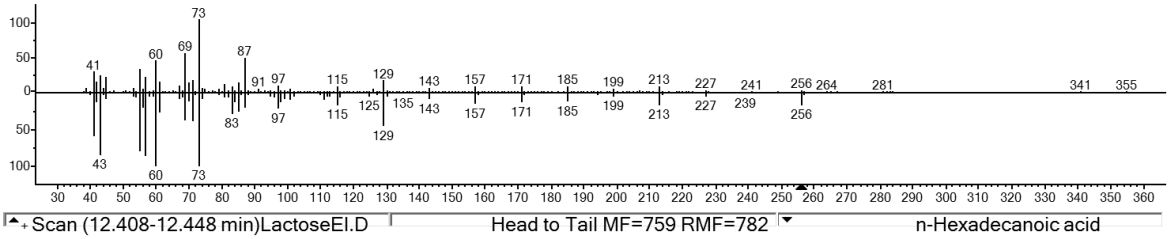


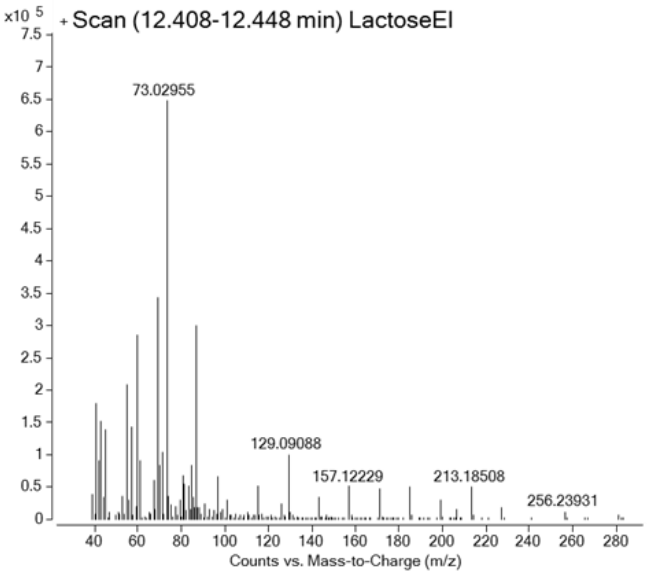


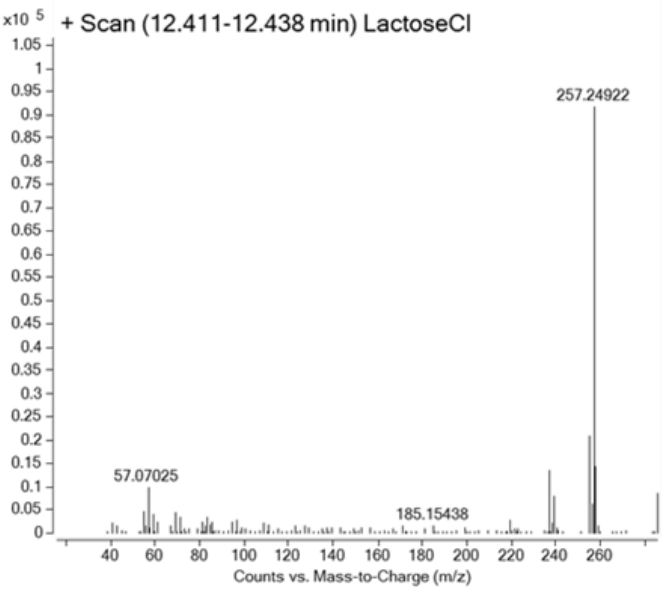


n-Hexadecanoic acid

Mass: 256.24023

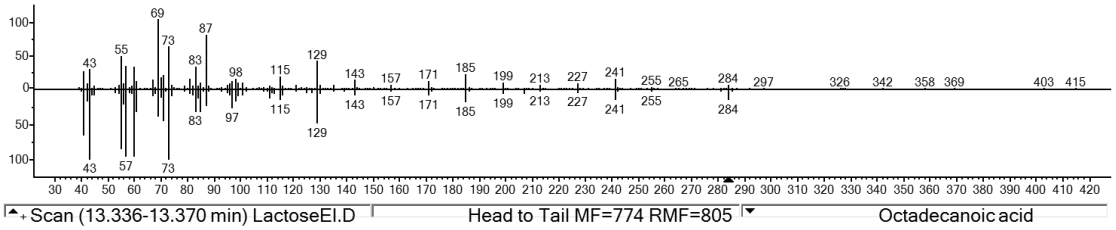


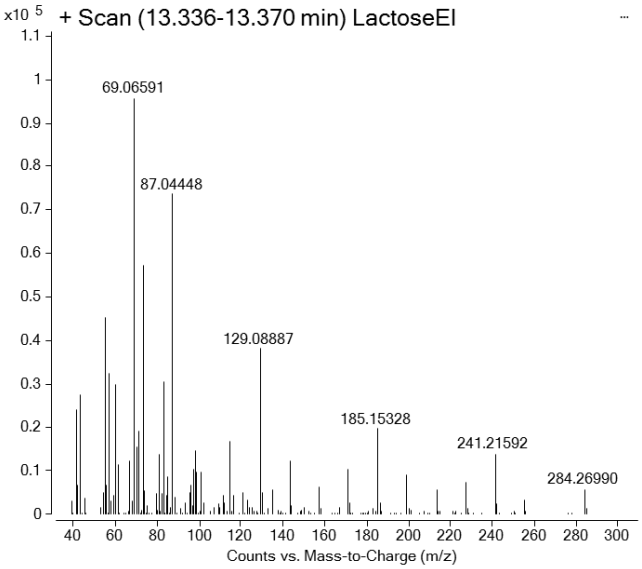


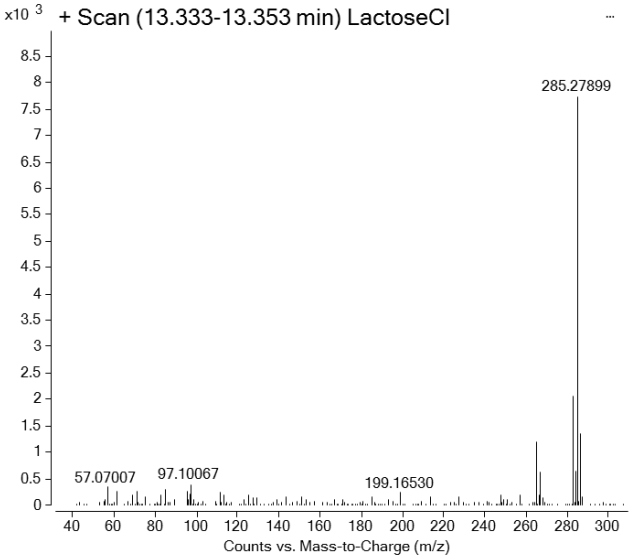


Octadecanoic acid

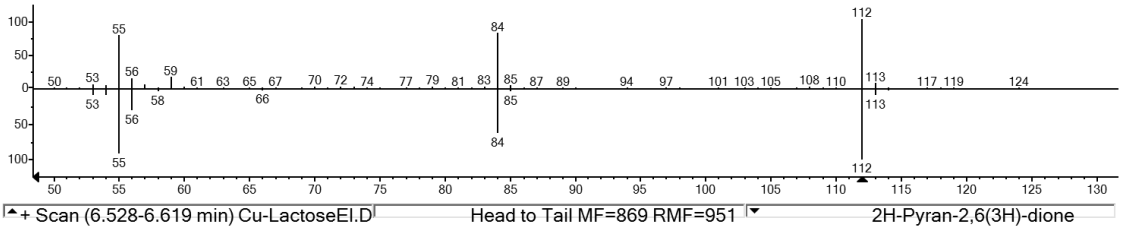
Mass: 284.27153

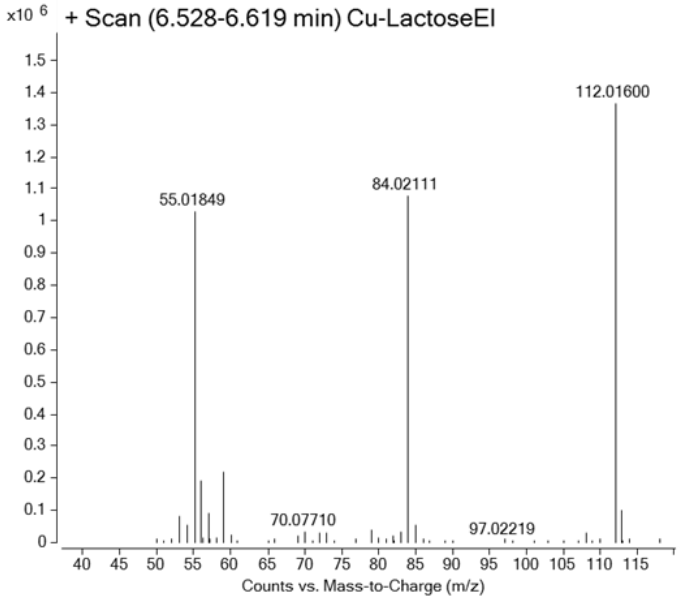


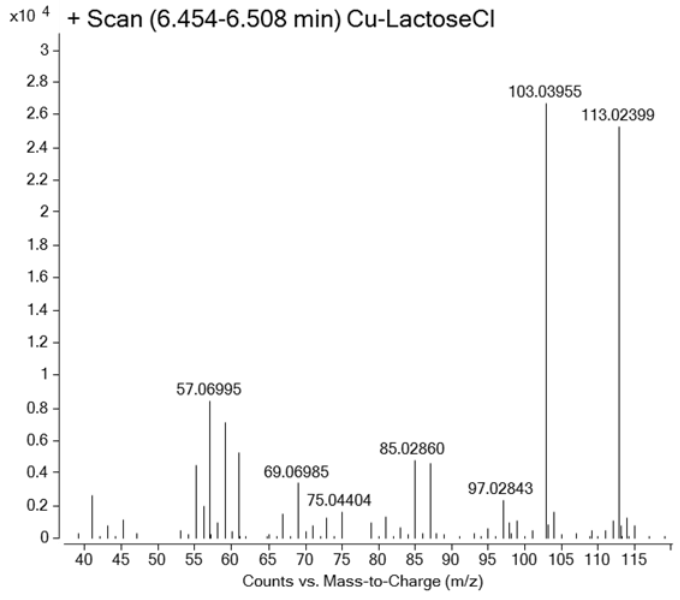




2H-Pyran-2,6(3H)-dione

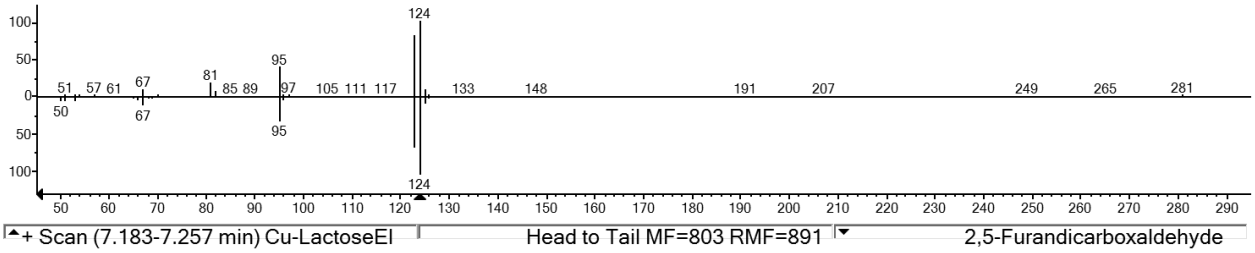


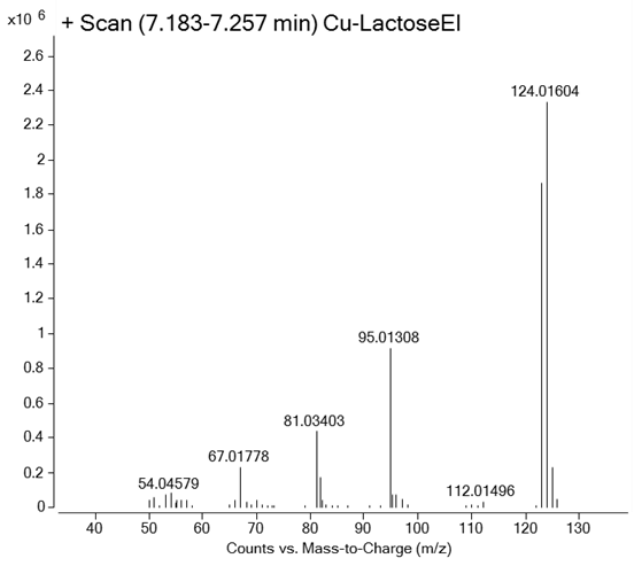


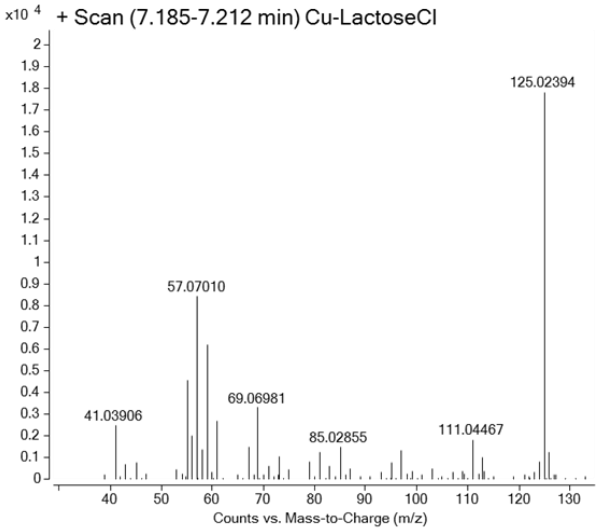


2,5-Furandicarboxaldehyde

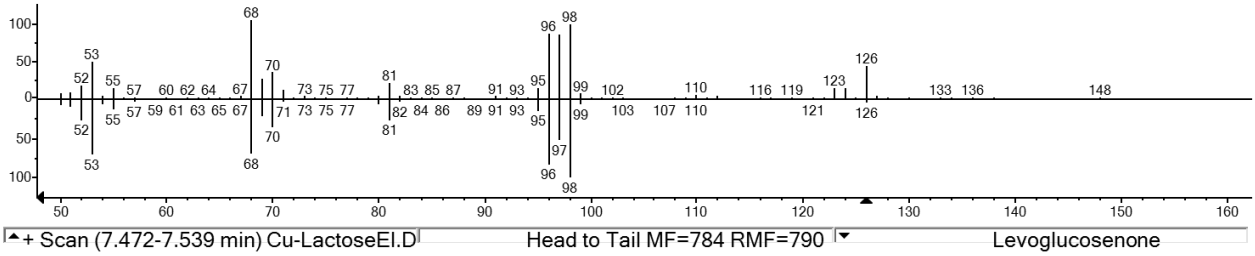
Mass: 124.016044

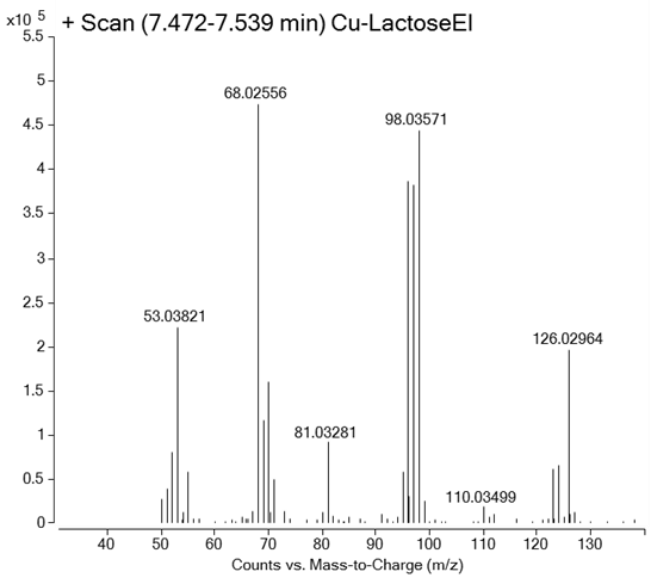


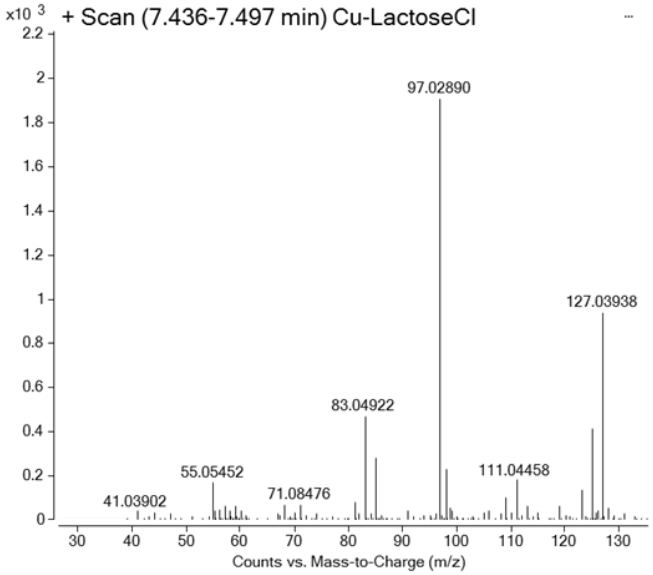




Levoglucosenone

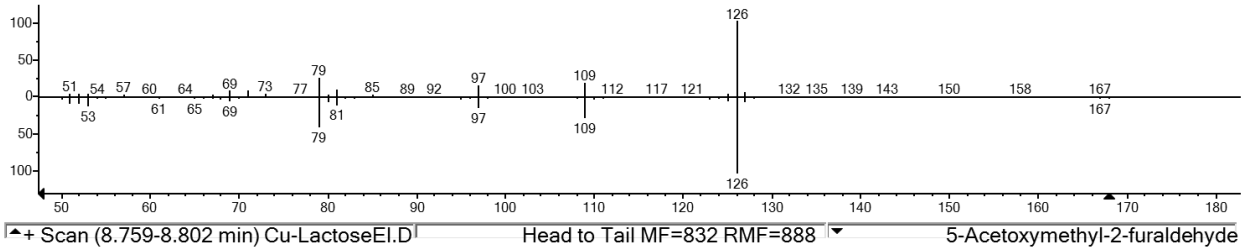


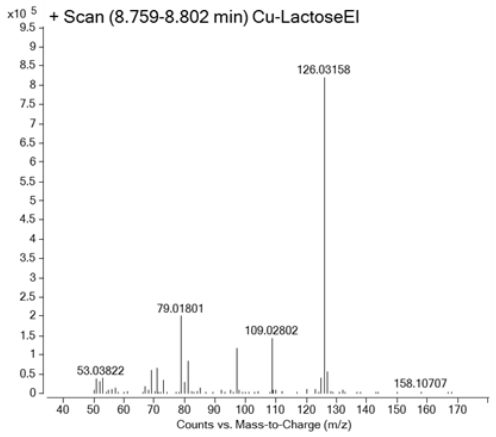


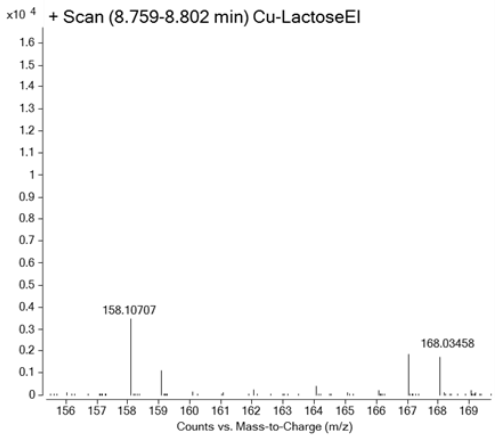


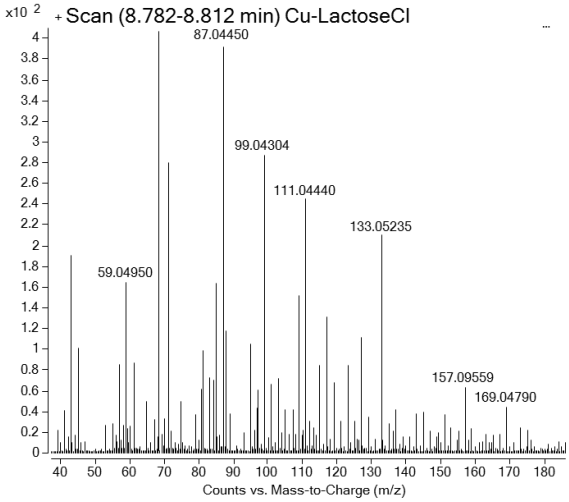
5-Acetoxymethyl-2-furaldehyde

Mass: 168.042258

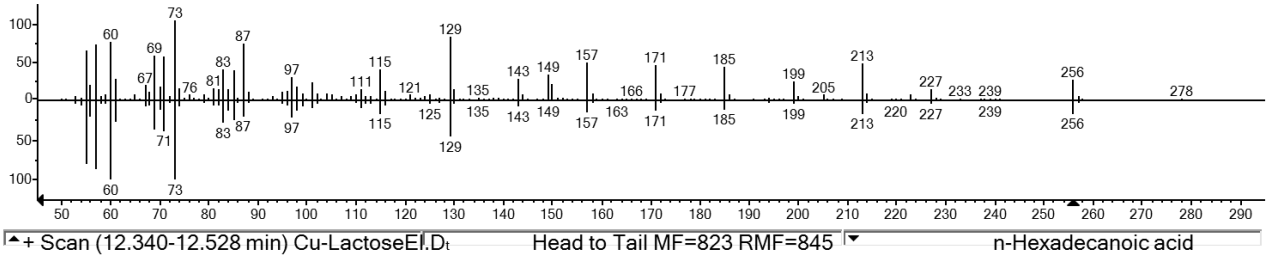


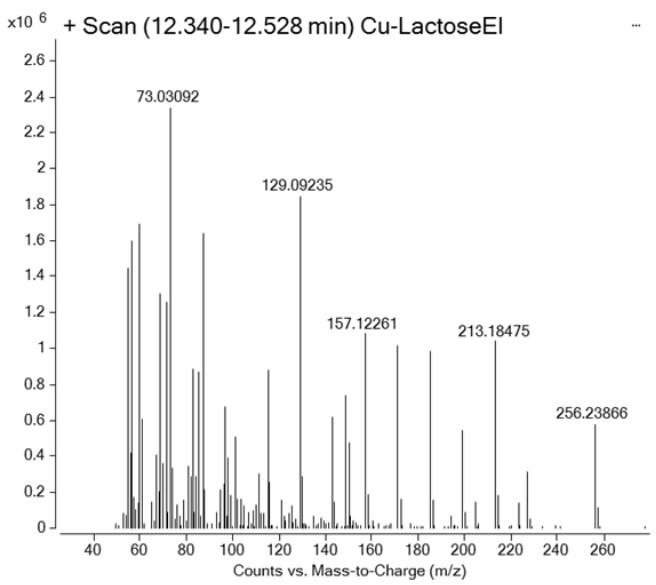


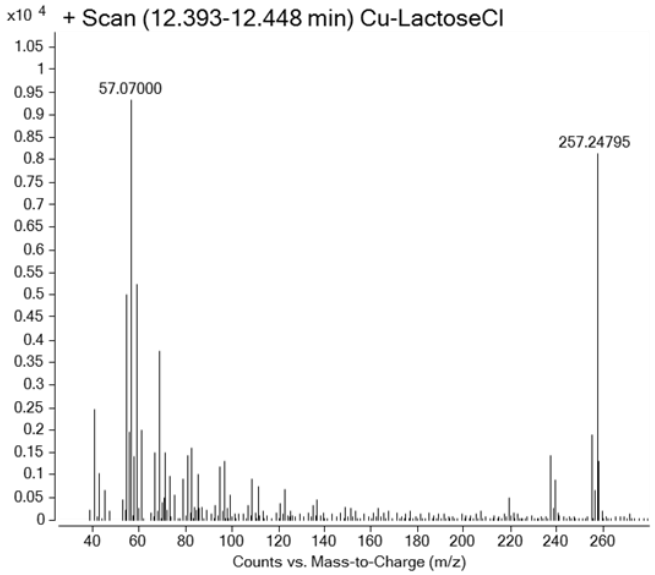




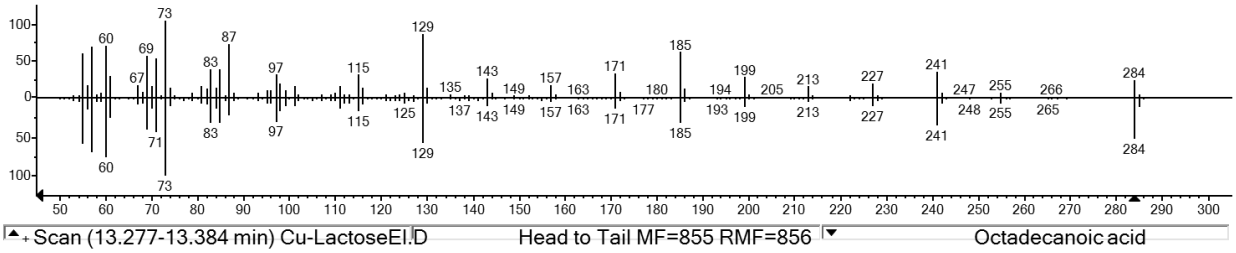
n-Hexadecanoic acid

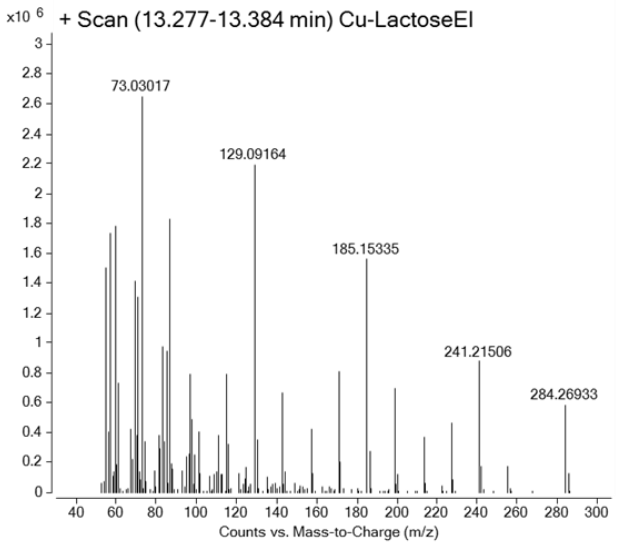


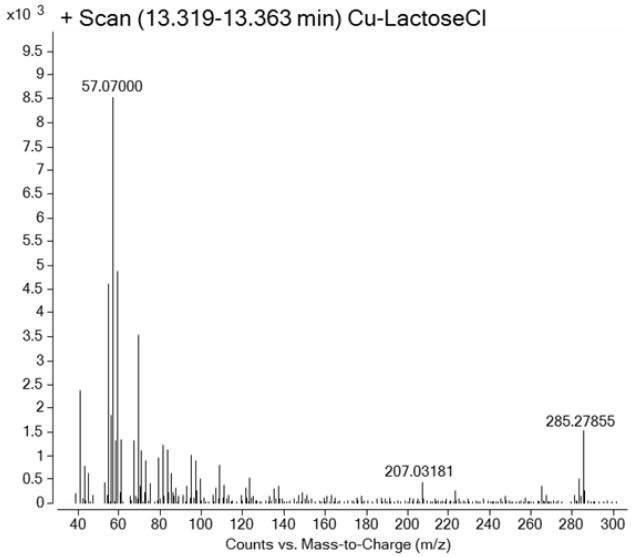




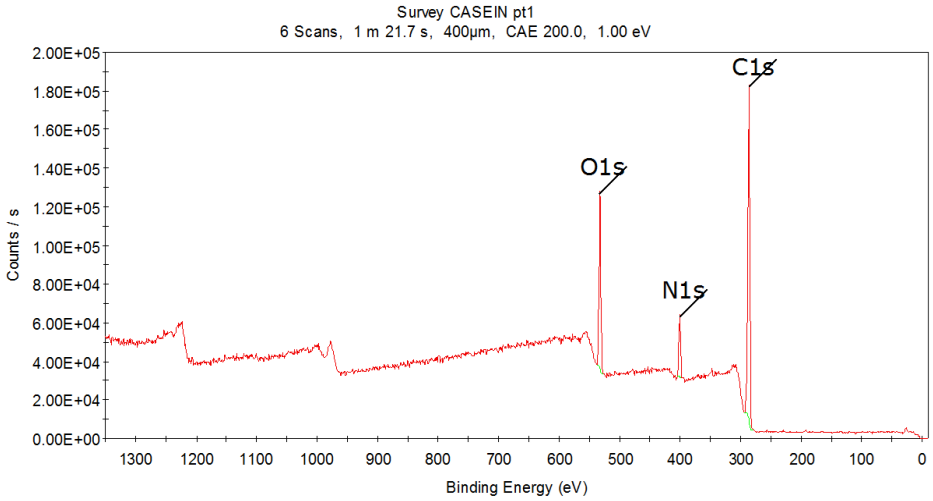
Octadecanoic acid



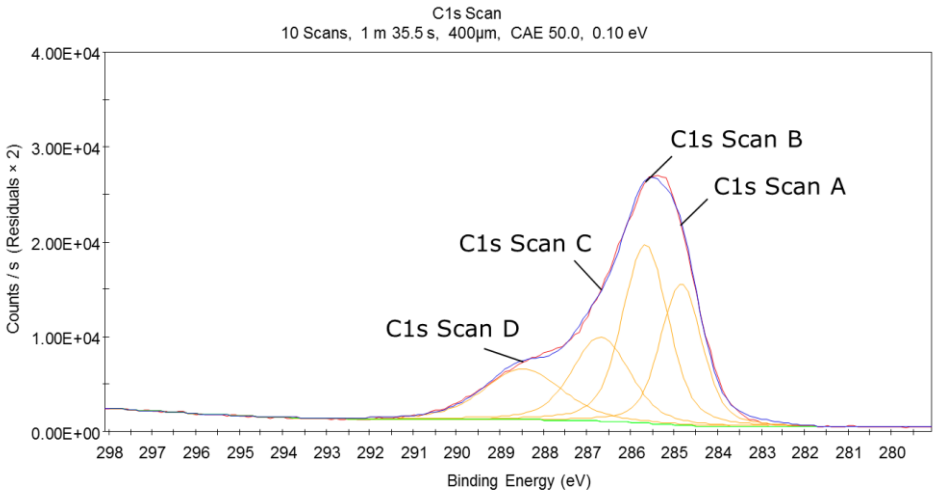




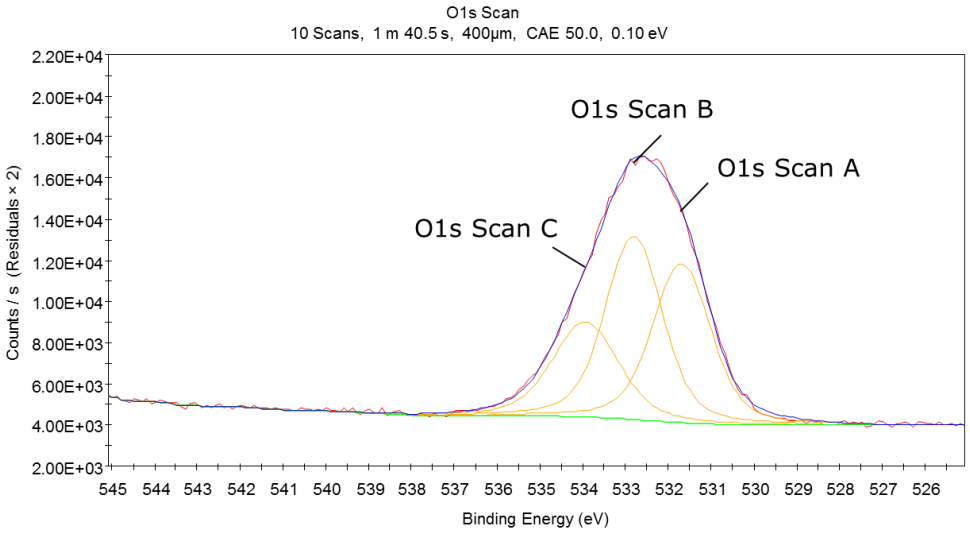
Casein – POINT 1



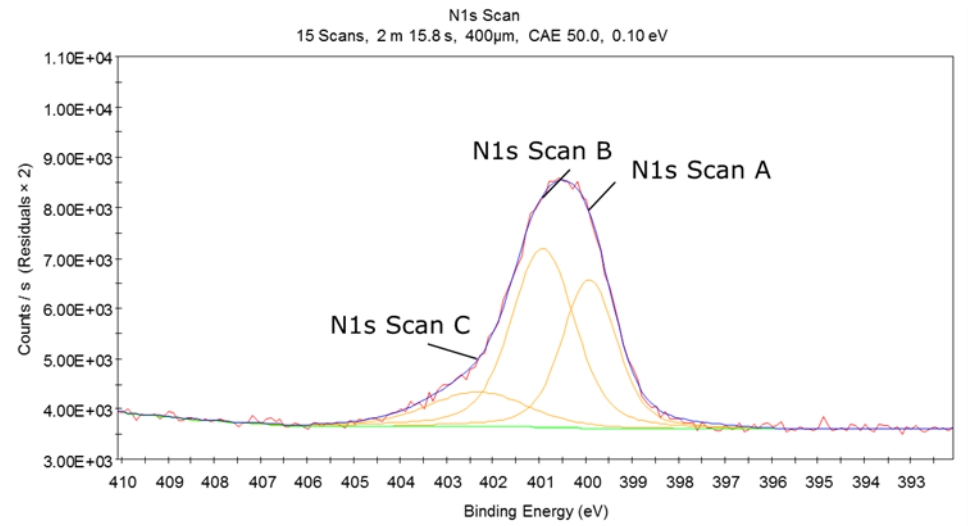
Element	Start BE	Peak BE	End BE	FWHM eV	Area (P) CPS.eV	Atomic %
N1s	405.95	400.92	397.66	2.93	101388.18	8.07
C1s	292.62	286.06	279.77	3.23	608307.15	75.11
O1s	538.08	532.86	527.11	3.31	329426.4	16.83



Name	Peak BE	FWHM eV	Area (P) CPS.eV	Atomic %
C1s Scan A	284.84	1.12	19662.53	25.72
C1s Scan B	285.66	1.24	27202.28	35.60
C1s Scan C	286.68	1.57	16254.02	21.29
C1s Scan D	288.46	2.12	13267.26	17.39

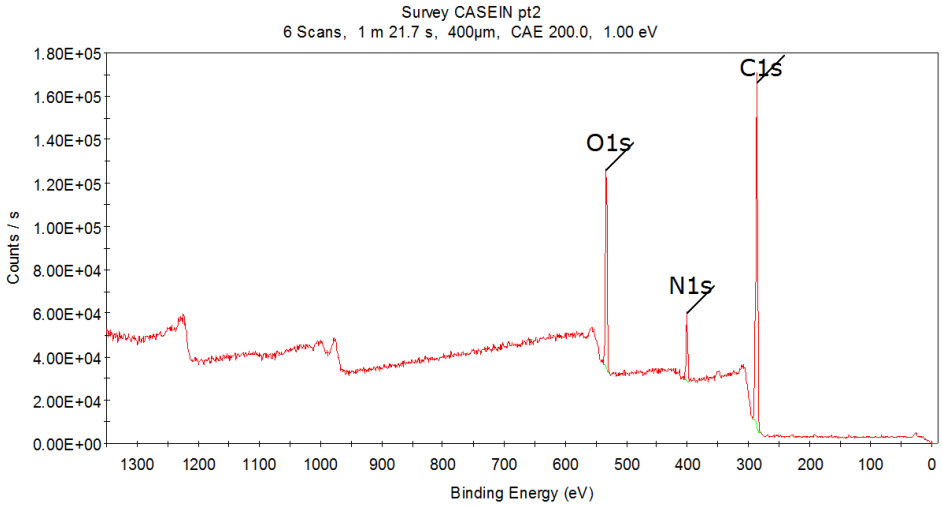


Name	Peak BE	FWHM eV	Area (P) CPS.eV	Atomic %
O1s Scan A	531.69	1.60	14581.63	35.73
O1s Scan B	532.81	1.57	16341.81	40.07
O1s Scan C	533.94	1.83	9859.96	24.20

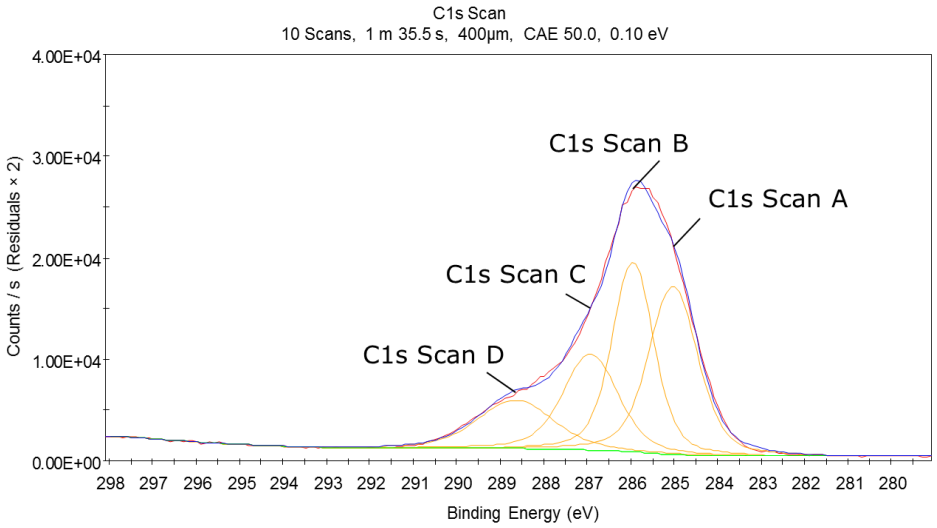


Name	Peak BE	FWHM eV	Area (P) CPS.eV	Atomic %
N1s Scan A	399.93	1.39	4801.54	35.46
N1s Scan B	400.92	1.60	6698.74	49.50
N1s Scan C	402.32	2.52	2032.55	15.04

Casein – POINT 2

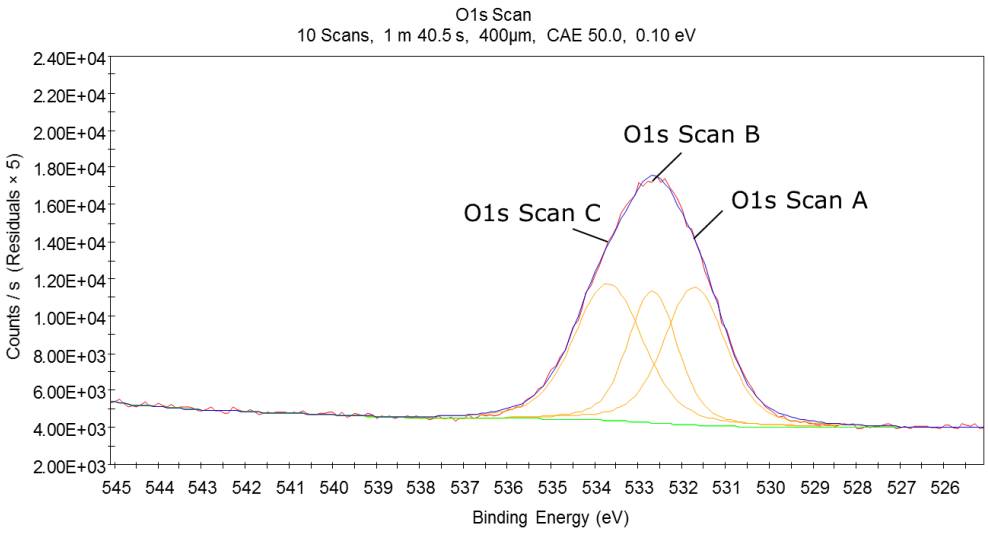


Element	Start BE	Peak BE	End BE	FWHM eV	Area (P) CPS.eV	Atomic %
C1s	293.08	286.19	280.11	3.37	583103.78	75.02
O1s	538.08	533.05	527.73	3.38	318628.31	16.96
N1s	405.16	400.97	396.85	3.05	96813.43	8.03

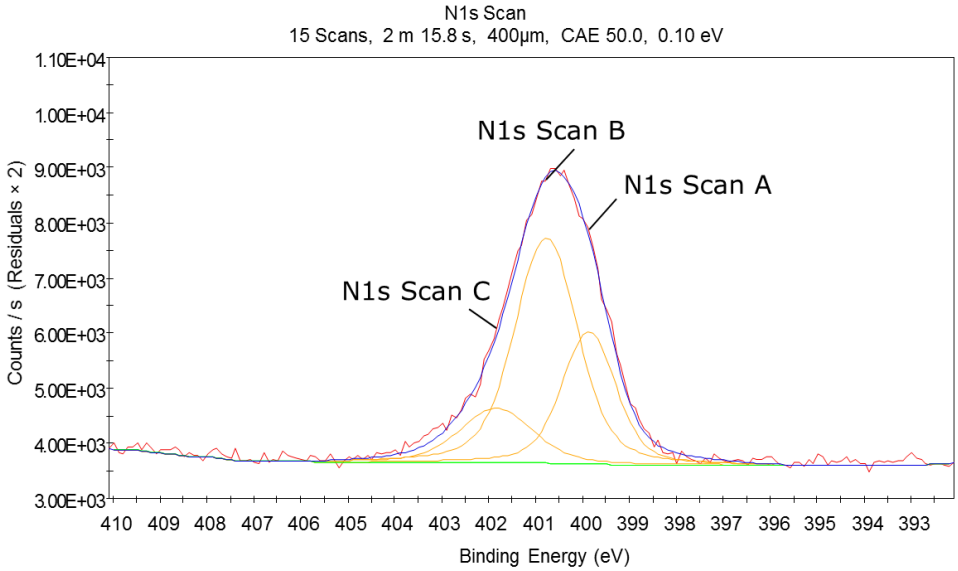


Name	Peak BE	FWHM eV	Area (P) CPS.eV	Atomic %
C1s Scan A	285.02	1.33	25812.15	32.89
C1s Scan B	285.95	1.13	24676.15	31.46
C1s Scan C	286.92	1.49	16453.06	20.99

Name	Peak BE	FWHM eV	Area (P) CPS.eV	Atomic %
C1s Scan D	288.64	2.05	11470.56	14.65



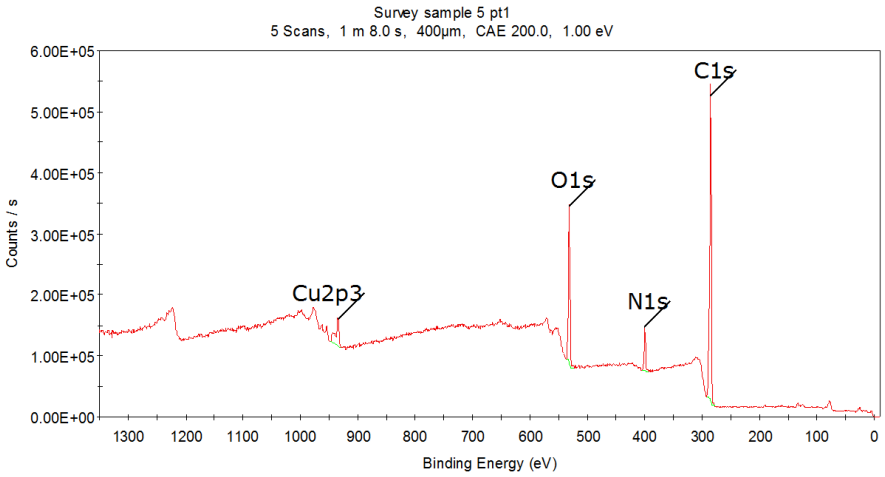
Name	Peak BE	FWHM eV	Area (P) CPS.eV	Atomic %
O1s Scan A	531.70	1.67	14583.51	34.80
O1s Scan B	532.66	1.35	11204.41	26.75
O1s Scan C	533.68	1.86	16088.25	38.45



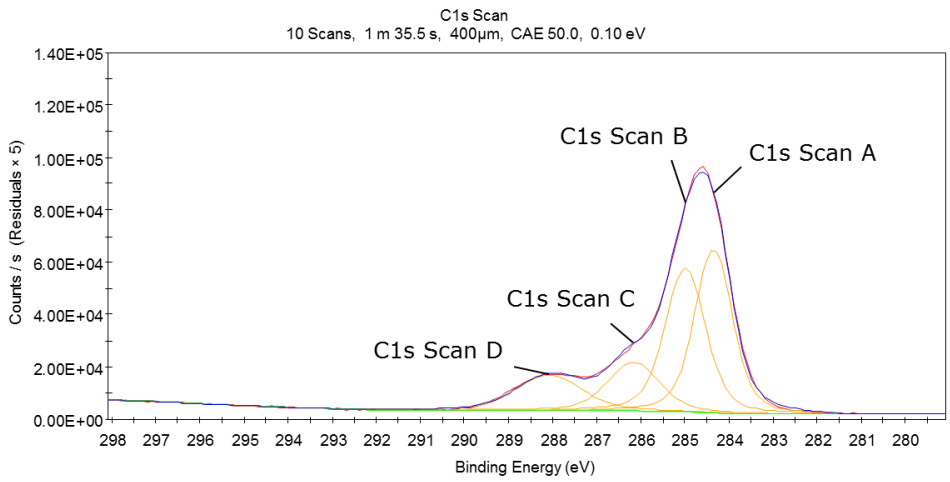
Name	Peak BE	FWHM eV	Area (P) CPS.eV	Atomic %
N1s Scan A	399.86	1.35	3815.64	28.48

Name	Peak BE	FWHM eV	Area (P) CPS.eV	Atomic %
N1s Scan B	400.77	1.57	7501.27	56.02
N1s Scan C	401.83	1.82	2074.33	15.50

Cu-Casein – POINT 1

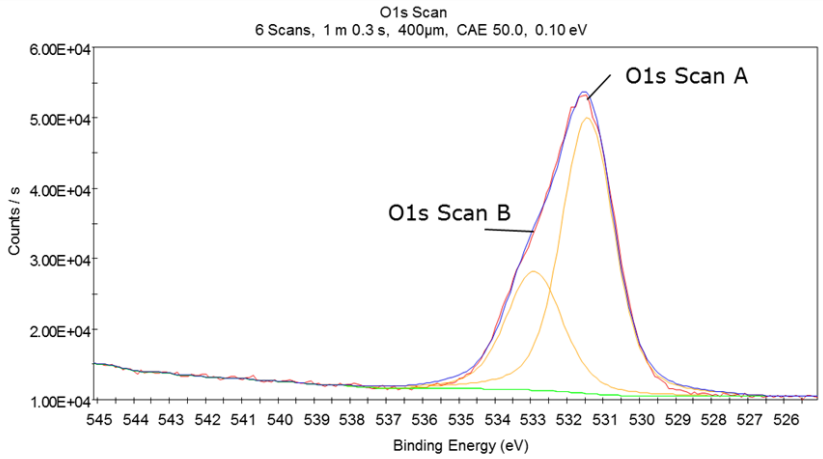


Element	Start BE	Peak BE	End BE	FWHM eV	Area (P) CPS.eV	Atomic %
C1s	292.08	285.17	277.08	2.89	1570014.45	75.62
O1s	536.58	532.06	523.08	3.19	850794.4	16.95
N1s	405.58	400.07	392.58	2.67	192940.76	5.99
Cu2p3	947.08	934.34	929.08	4.08	303475.12	1.43

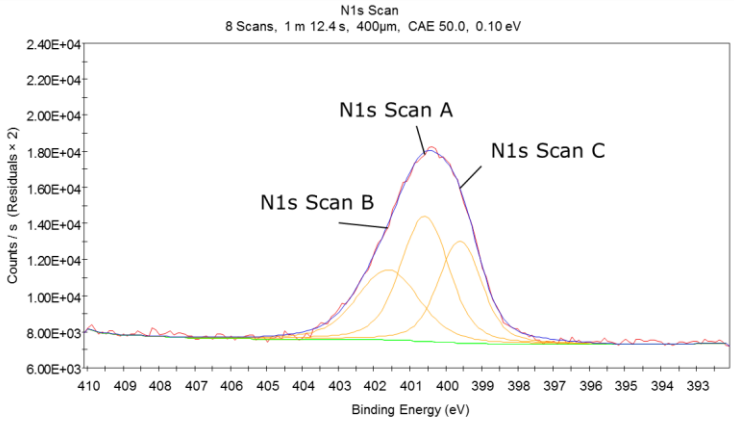


Name	Peak BE	FWHM eV	Area (P) CPS.eV	Atomic %

Name	Peak BE	FWHM eV	Area (P) CPS.eV	Atomic %
C1s Scan A	284.35	1.02	73825.98	36.71
C1s Scan B	284.98	1.09	69709.59	34.68
C1s Scan C	286.16	1.38	30227.43	15.05
C1s Scan D	288.07	1.75	27217.45	13.57

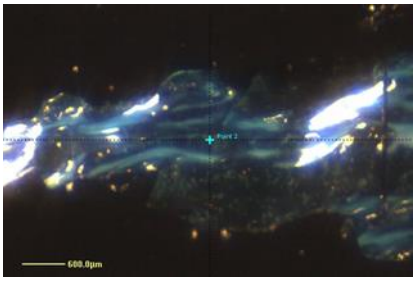


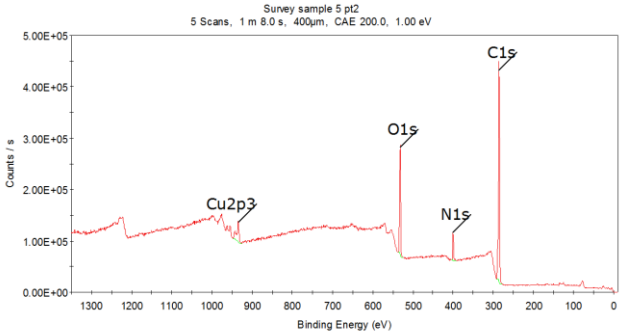
Name	Peak BE	FWHM eV	Area (P) CPS.eV	Atomic %
O1s Scan A	531.43	1.71	78815.68	68.40
O1s Scan B	532.91	1.85	36374.14	31.60



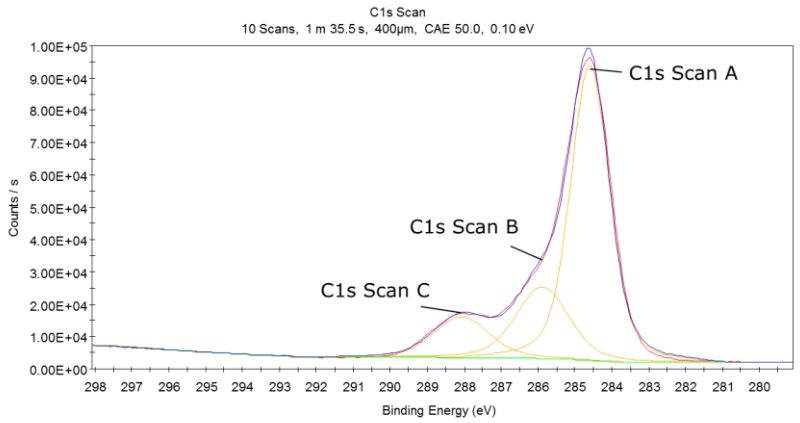
Name	Peak BE	FWHM eV	Area (P) CPS.eV	Atomic %
N1s Scan A	400.58	1.59	12903.28	40.74
N1s Scan B	401.61	2.05	9277.96	29.31
N1s Scan C	399.60	1.43	9493.65	29.95

Cu-Casein – POINT 2

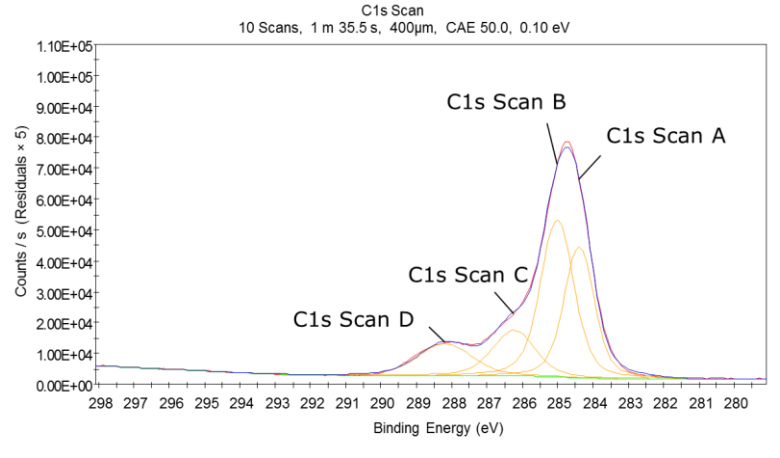




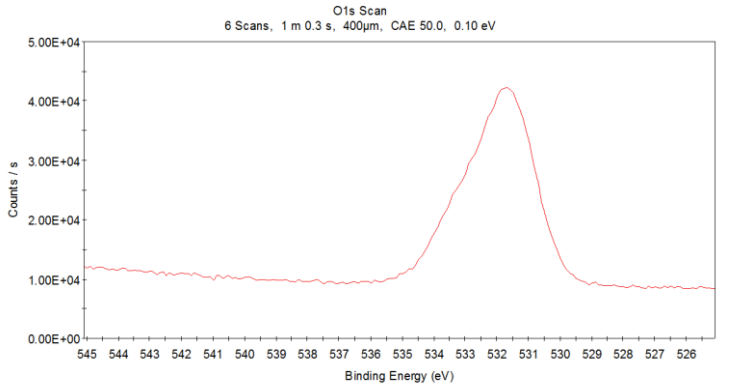
Element	Start BE	Peak BE	End BE	FWHM eV	Area (P) CPS.eV	Atomic %
C1s	292.08	285.19	278.08	2.85	1277305.56	76.06
O1s	537.58	532.13	524.58	3.22	682546.98	16.81
Cu2p3	947.08	934.39	925.58	3.82	277138.18	1.62
N1s	405.58	400.07	393.08	2.71	143373.26	5.5

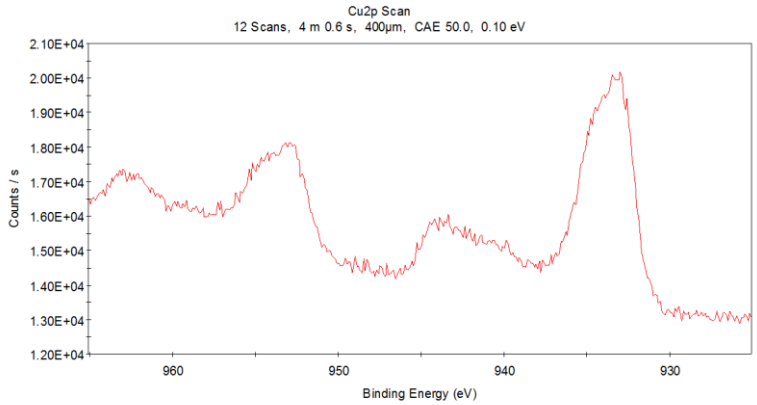


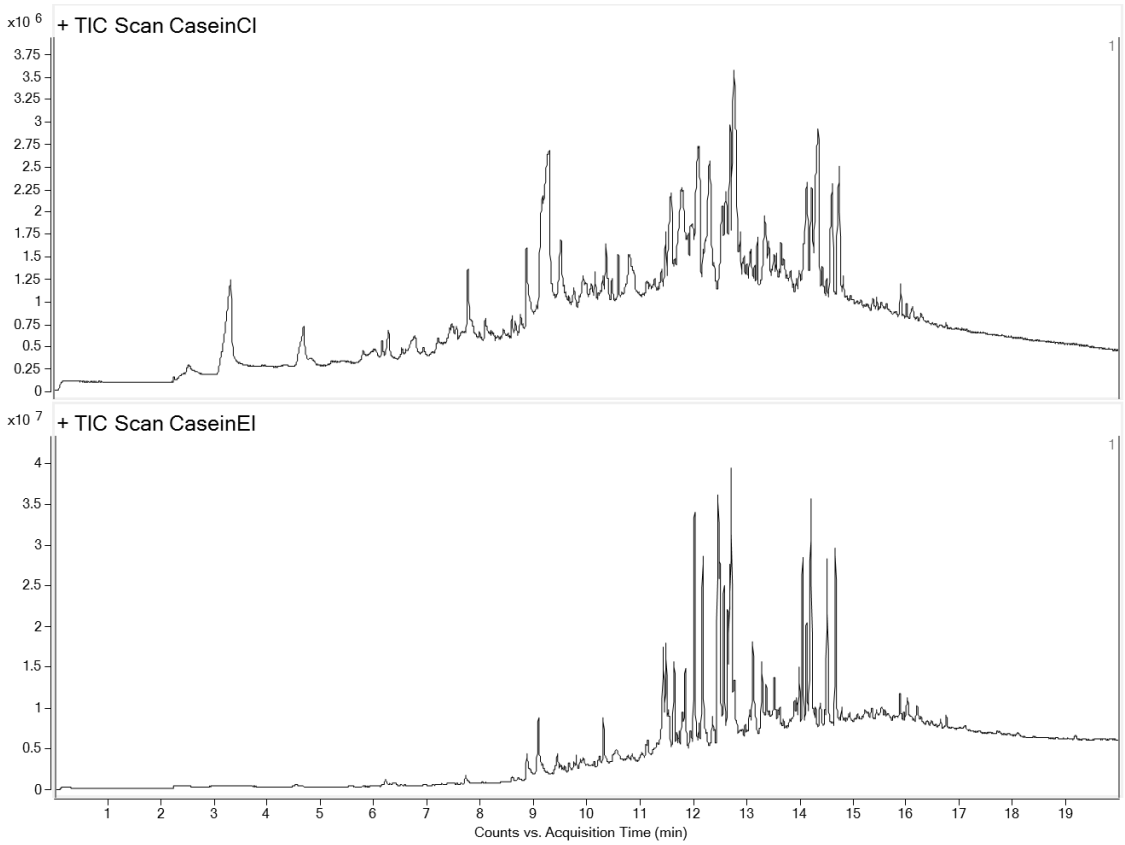
Name	Peak BE	FWHM eV	Area (P) CPS.eV	Atomic %
C1s Scan A	284.60	1.23	131781.39	65.43
C1s Scan B	285.89	1.68	43387.10	21.56
C1s Scan C	288.08	1.76	26150.17	13.01



Name	Peak BE	FWHM eV	Area (P) CPS.eV	Atomic %
C1s Scan A	284.39	1.01	50253.84	30.81
C1s Scan B	285.01	1.11	66360.73	40.70
C1s Scan C	286.24	1.42	24712.85	15.17
C1s Scan D	288.18	1.81	21664.34	13.32



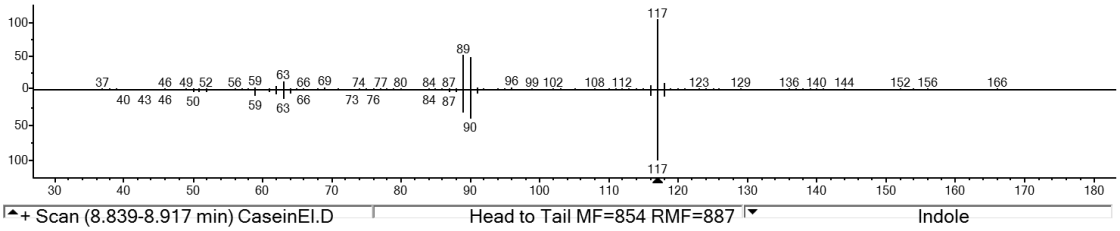


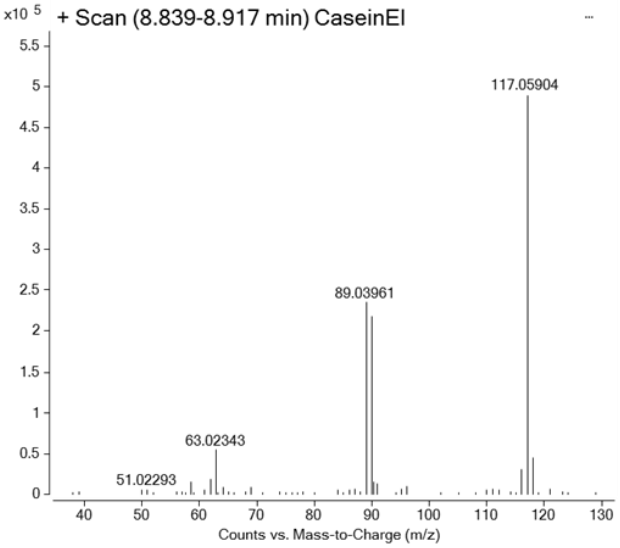


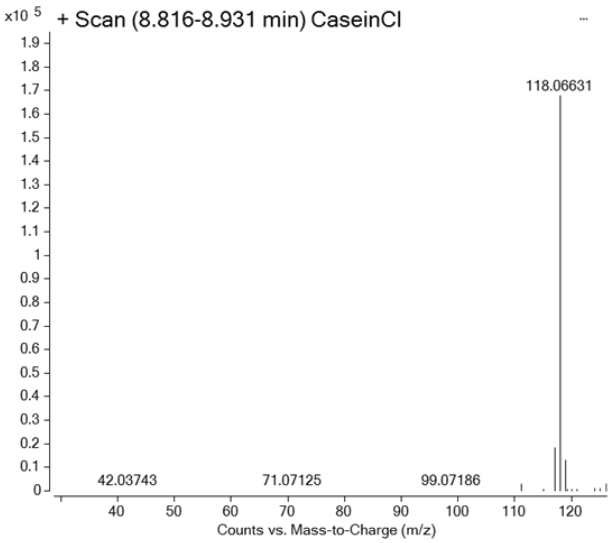
CI and EI Chromatograms

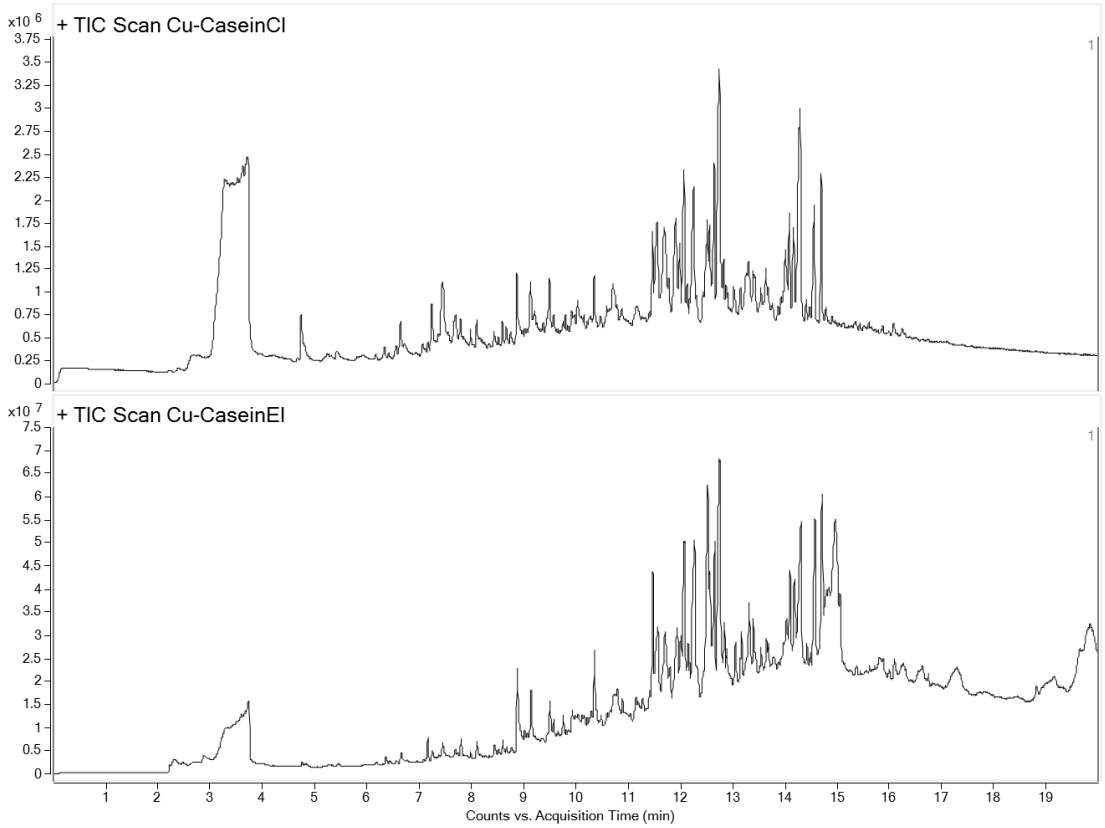
Indole

Mass: 117.0578494



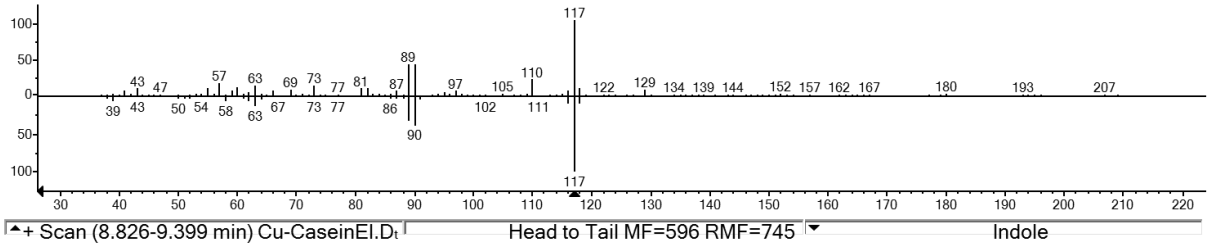


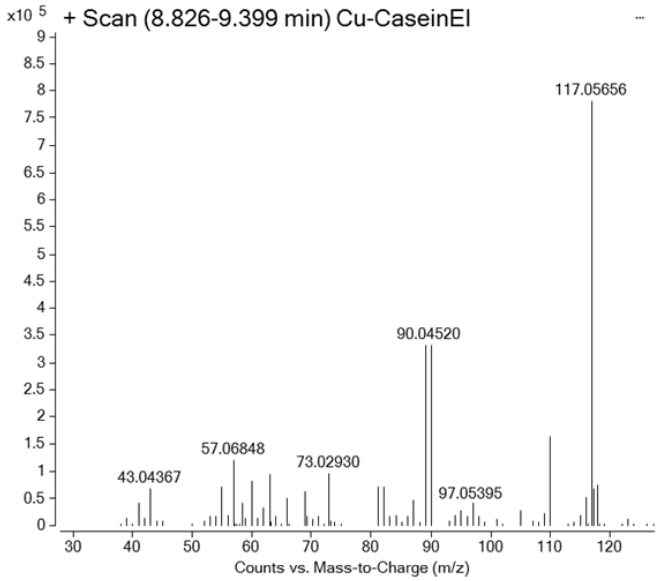


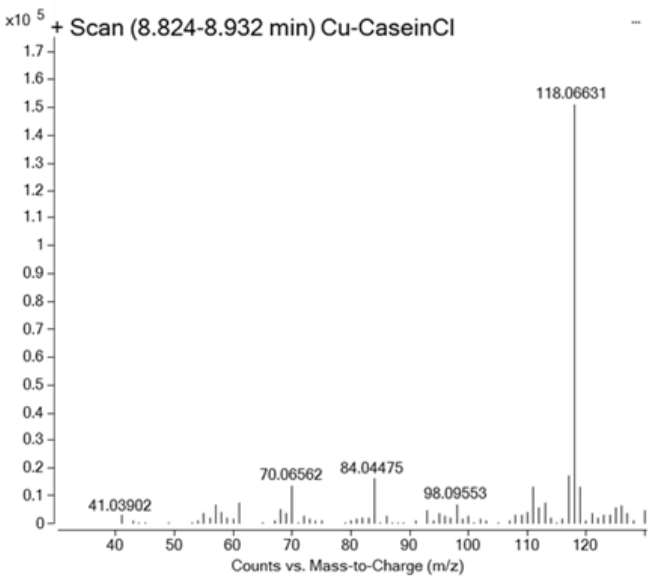


CI and EI Chromatograms

Indole


+ Scan (8.826-9.399 min) Cu-CaseinEI.Dt
Head to Tail MF=596 RMF=745
Indole


x10 5
+ Scan (8.826-9.399 min) Cu-CaseinEI
117.05656
90.04520
57.06848
73.02930
43.04367
97.05395
Counts vs. Mass-to-Charge (m/z)


x10 5
+ Scan (8.824-8.932 min) Cu-CaseinCI
118.06631
70.06562
84.04475
98.09553
41.03902
Counts vs. Mass-to-Charge (m/z)

P02662 Peptides	-10lgP	m/z	Peptide intensity	PTM/Score
Q.YTDAPSFSDIPNPIGSENSEK.T	67.1	1134.5187	6.63E+06	
T.QYTDAPSFSDIPNPIGSENSEK.T	66.58	1198.5471	8.28E+04	
L.GTQYTDAPSFSDIPNPIGSENSEK.T	62.47	1277.5846	2.46E+06	
K.HQGLPQEVLNENLLR.F	62.23	880.4761	1.08E+09	
Y.TDAPSFSDIPNPIGSENSEK.T	61.41	1052.9873	9.90E+05	
K.HQ(+.98)GLPQEVLNENLLR.F	61.23	880.9679	2.40E+07	Q2:Deamidation (NQ):109.97
K.EPMIGVNQELAYFYPELFR.Q	59.75	1158.5717	1.26E+07	
Y.YVPLGTQYTDAPSFSDIPNPIGSENSEK.T	54.66	1513.7178	2.45E+07	
T.DAPSFSDIPNPIGSENSEK.T	54.38	1002.4648	1.39E+05	
D.APSFSDIPNPIGSENSEK.T	54.07	944.9488	7.94E+06	
K.YKVPQLEIVPNSAEER.L	52.88	936.4967	1.18E+07	
K.EPM(+15.99)IGVNQELAYFYPELFR.Q	52.15	1166.569	2.60E+07	M3:Oxidation (M):1000.00
D.IPNPIGSENSEK.T	51.13	642.8252	2.72E+06	
F.SDIPNPIGSENSEK.T	50.31	743.8546	7.69E+05	
W.YYVPLGTQYTDAPSFSDIPNPIGSEN(+.98)SEK.T	49.87	1595.7421	5.45E+05	N26:Deamidation (NQ):53.33
A.WYYVPLGTQYTDAPSFSDIPNPIGSENSEK.T	49.72	1125.8616	1.55E+05	
K.VPQLEIVPNSAEER.L	48.89	790.9175	3.41E+07	
S.GAWYYVPLGTQYTDAPSFSDIPNPIGSENSEK.T	48.71	1168.5479	1.41E+06	
S.FSDIPNPIGSENSEK.T	47.86	817.3885	2.14E+05	
H.QGLPQEVLNENLLR.F	47.84	811.9464	7.62E+05	
W.YYVPLGTQYTDAPSFSDIPNPIGSENSEK.T	46.88	1063.8354	1.16E+08	
K.HQ(+.98)GLPQEVLN(+.98)ENLLR.F	46.7	881.459	1.08E+06	Q2:Deamidation (NQ):67.76;N10:Deamidation (NQ):41.60
M.IGVNQELAYFYPELFR.Q	46.6	980.0042	7.46E+07	
R.QFYQLDAYPSGAWYYVPLGTQYTDAPSFSDIPNPIGSENSEK.T	46.1	1179.7986	9.75E+07	
G.AWYYVPLGTQYTDAPSFSDIPNPIGSENSEK.T	45.82	1149.5388	3.70E+05	
V.NQELAYFYPELFR.Q	45.76	845.4168	1.74E+05	
K.VPQLEIVPN(+.98)SAEER.L	45.45	791.4065	2.10E+05	N9:Deamidation (NQ):95.17
K.HIQ(+.98)KEDVPSER.Y	45.43	669.836	3.45E+06	Q3:Deamidation (NQ):1000.00
W.YYVPLGTQYTDAPSFSDIPN(+.98)PIGSENSEK.T	44.28	1064.1637	6.04E+07	N20:Deamidation (NQ):18.01
D.AYPSGAWYYVPLGTQYTDAPSFSDIPNPIGSENSEK.T	42.94	1961.4075	1.60E+06	
K.HQGLPQEVLNEN.L	42.11	689.3409	9.63E+05	
R.FFVAPFPEVFGK.E	41.84	692.8688	1.02E+09	
G.LPQEVLNENLLR.F	41.33	719.4062	2.80E+05	
L.DAYPSGAWYYVPLGTQYTDAPSFSDIPNPIGSENSEK.T	41.16	1009.9666	2.85E+06	
F.FVAPFPEVFGK.E	40.55	619.3337	8.03E+06	
K.HIQKEDVPSER.Y	40.35	669.344	5.91E+06	
R.YLGYLEQLLR.L	39.46	634.356	8.32E+08	
K.HQGLPQEVLNENLL.R	38.45	802.4255	4.74E+05	
K.YKVPQLEIVPN.S	37.81	650.3689	6.18E+05	
K.EGIHAQQK.E	37.49	455.7407	1.17E+08	
K.HQGLPQEVLNEN(+.98)LLR.F	37.21	587.6473	5.55E+06	N12:Deamidation (NQ):30.36
Y.VPLGTQYTDAPSFSDIPNPIGSENSEK.T	37.13	955.1259	2.95E+05	
Y.QLDAYPSGAWYYVPLGTQYTDAPSFSDIPNPIGSENSEK.T	36.41	1426.666	2.10E+06	
M.KEGIHAQQK.E	35.65	519.788	1.22E+05	
Y.LGYLEQLLR.L	35.21	552.8243	9.47E+05	
K.EKVNELSK.D	34.82	473.764	1.40E+07	
K.EGIHAQQ(+.98)K.E	34.42	456.2326	2.64E+06	Q7:Deamidation (NQ):15.10
L.AYFYPELFR.Q	34.04	603.303	3.59E+06	
N.PIGSENSEK.T	33.76	480.7351	3.10E+05	
R.QFYQLDAYPSGAW.Y	33.51	773.3541	5.40E+06	
K.EKVN(+.98)ELSK.D	32.89	474.2559	6.10E+05	N4:Deamidation (NQ):1000.00
R.YLGYLEQ(+.98)LLR.L	32.88	634.8478	2.24E+06	Q7:Deamidation (NQ):1000.00
F.VAPFPEVFGK.E	32.39	545.8002	3.06E+06	
M.IGVN(+.98)QELAYFYPELFR.Q	32.2	980.4973	2.20E+05	N4:Deamidation (NQ):40.00

P02662 Peptides	-10lgP	m/z	Peptide intensity	PTM/Score
K.HPIKHQGLPQEVLNENLLR.F	32.11	745.7507	1.30E+05	
K.HQGLPQEVLNE.N	31.89	632.3201	7.26E+04	
Y.YVPLGTQ(+.98)YTDAPSFSDIPNPIGSENSEK.T	30.92	1514.2068	2.04E+05	Q7:Deamidation (NQ):0.00
K.VNELSK.D	29.53	345.1951	1.65E+08	
K.TTMPLW	28.72	374.6883	1.56E+05	
K.EGIHAQQKEPM(+15.99).I	28.64	642.3063	1.68E+04	M11:Oxidation (M):1000.00
K.VN(+.98)ELSK.D	27.37	345.6872	1.11E+06	N2:Deamidation (NQ):1000.00
A.YFYPELFR.Q	27.22	567.7847	9.82E+05	
R.QFYQLDAYPSGAWY.Y	26.81	854.8842	5.85E+05	
Y.YVPLGTQYTDAPSFSDIPNPIGSEN(+.98)SEK.T	26.36	1514.2123	2.04E+05	N25:Deamidation (NQ):36.87
L.GYLEQLLR.L	26.31	496.2822	3.75E+05	
K.HQGLPQEVLNENL.L	24.96	745.884	1.48E+05	
K.EGIHAQQKEPM(+15.99)IGVN(+.98)QELAYFYPELFR.Q	24.63	806.8959	2.60E+05	M11:Oxidation (M):1000.00;N15:Deamidation (NQ):0.00
F.YQLDAYPSGAW.Y	23.62	635.7906	1.00E+05	
K.EDVPSER.Y	22.28	416.1956	2.79E+08	
E.GIHAQQK.E	22.1	391.2192	1.20E+07	
A.RPKHPIK.H	21.53	438.2821	1.37E+05	
E.KVNELSK.D	21.17	409.2423	4.69E+05	
Q.KEDVPSER.Y	19.85	480.2433	6.64E+04	
K.EGIHAQQ.K	19.79	391.6928	2.44E+05	
R.LHSMK.E	19.68	308.1676	8.86E+05	
Y.FYPELFR.Q	19.62	486.2527	2.18E+06	
P.KHPIK.H	17.96	208.1394	4.04E+05	
I.HAQQK.E	16.54	306.1665	6.81E+06	
L.EQLLR.L	15.75	329.6978	3.41E+04	

P02663 Peptide	-10lgP	m/z	Peptide intensity	PTM/Score
L.QYLYQGPIVLNPWDQVK.R	63.07	1031.0428	8.27E+05	
K.FPQYLQYLYQGPIVLNPWDQVK.R	62.85	1355.2061	7.81E+07	
Q.YLYQGPIVLNPWDQVK.R	58.87	967.014	6.52E+05	
Y.LYQGPIVLNPWDQVK.R	54.16	885.4824	2.16E+07	
K.ALNEINQFYQK.F	52.87	684.3517	3.98E+08	
L.YQGPIVLNPWDQVK.R	51.28	828.9402	1.41E+07	
K.ALNEIN(+.98)QFYQK.F	48.98	684.8428	1.51E+06	N6:Deamidation (NQ):14.02
K.ITVDDKHYQK.A	46.65	623.8251	4.47E+06	
K.ITVDDKHYQ(+.98)K.A	45.33	624.3168	1.79E+06	Q9:Deamidation (NQ):1000.00
K.RNAVPITPTLN(+.98)R.E	45.29	676.8854	3.21E+06	N11:Deamidation (NQ):116.37
K.FPQYLQ(+.98)YLYQGPIVLNPWDQVK.R	44.19	904.1351	1.01E+06	Q6:Deamidation (NQ):6.57
K.ALN(+.98)EINQFYQK.F	44.08	684.8431	1.46E+07	N3:Deamidation (NQ):60.70
Y.QGPIVLNPWDQVK.R	43.88	747.4091	3.79E+05	
L.YQGPIVLNPWDQ(+.98)VK.R	42.75	829.433	1.72E+05	Q12:Deamidation (NQ):0.00
K.NM(+15.99)AINPSKENLC(+57.02)STFC(+57.02)K.E	41.79	677.3096	1.59E+05	M2:Oxidation (M):1000.00;C12:Carbamidomethylation:1000.00;C16:Carbamidomethylation:1000.00
K.TVYQHQK.A	40.57	452.2375	4.53E+07	
K.EN(+.98)LC(+57.02)STFC(+57.02)K.E	39.95	580.2416	6.55E+05	N2:Deamidation (NQ):1000.00;C4:Carbamidomethylation:1000.00;C8:Carbamidomethylation:1000.00
K.AMKPWIQPK.T	39.71	549.8099	3.31E+06	

P02663 Peptide	-10lgP	m/z	Peptide intensity	PTM/Score
K.ENLC(+57.02)STFC(+57.02)K.E	39.64	579.7499	1.27E+08	C4:Carbamidomethylation:1000.00;C8:Carbamidomethylation:1000.00
K.AM(+15.99)KPWIQPK.T	38.16	557.8075	6.04E+06	M2:Oxidation (M):1000.00
R.EQLSTSEENSK.K	36.52	626.2885	1.21E+06	
K.FALPQYLK.T	35.95	490.2841	2.02E+08	
K.NMAINPSK.E	35.27	437.7263	1.03E+06	
K.NM(+15.99)AINPSK.E	34.89	445.7234	9.45E+06	M2:Oxidation (M):1000.00
K.KTVDM(+15.99)ESTEVFTK.K	33.36	510.9167	2.23E+04	M5:Oxidation (M):1000.00
K.TVYQ(+.98)HQK.A	31.92	452.7303	2.38E+06	Q4:Deamidation (NQ):39.76
K.ITVDDK.H	30.91	345.6873	9.83E+07	
K.FALPQ(+.98)YLK.T	30.31	490.7758	2.51E+06	Q5:Deamidation (NQ):1000.00
R.EQLSTSEEN(+.98)SK.K	30.28	626.7808	2.01E+04	N9:Deamidation (NQ):50.34
K.LTEEEKNR.L	30.13	509.7615	2.27E+07	
M.KPWIQPK.T	29.68	448.7715	3.99E+05	
K.LTEEEK.N	28.23	374.6895	4.68E+07	
K.NRLN(+.98)FLKK.I	27.92	345.2101	1.43E+05	N4:Deamidation (NQ):16.66
R.N(+.98)AVPITPTLNR.E	26.64	598.8353	5.49E+06	N1:Deamidation (NQ):123.34
K.PWIQPK.T	26.6	384.724	6.24E+06	
K.RNAVPITPT.L	26.47	484.7798	1.73E+06	
T.KLTEEEK.N	26.46	438.7373	2.72E+05	
K.RNAVPITPTL.N	25.96	541.322	1.45E+05	
K.LTEEEKN(+.98)R.L	25.28	510.2534	3.81E+05	N7:Deamidation (NQ):1000.00
V.KITVDDK.H	23.95	409.7343	1.18E+05	
N.AVPITPTLNR.E	23.89	541.3214	9.89E+05	
V.YQHQK.A	23.72	352.1795	8.78E+06	
K.LTEEEKNRLNFLK.K	22.85	545.3016	1.21E+05	
N.LC(+57.02)STFC(+57.02)K.E	21.91	458.2065	7.67E+04	C2:Carbamidomethylation:1000.00;C6:Carbamidomethylation:1000.00
V.PITPTLNR.E	21.75	456.269	1.68E+06	
K.FPQYLQYL.Y	21.69	536.2791	2.04E+05	
K.RN(+.98)AVPITPTLNR.E	21.16	451.5929	3.88E+06	N2:Deamidation (NQ):54.99
L.C(+57.02)STFC(+57.02)K.E	20.7	401.6649	5.56E+04	C1:Carbamidomethylation:1000.00;C5:Carbamidomethylation:1000.00
K.LTEEEKN(+.98)RLNFLK.K	20.25	545.6298	2.29E+05	N7:Deamidation (NQ):0.00
K.FPQYLQY.L	20.1	479.737	3.04E+05	
K.AMKPW.I	19.97	316.6649	1.32E+05	
R.NAVPITPTLNR.E	19.71	598.3434	1.54E+08	
F.ALPQYLK.T	18.79	416.7501	3.29E+05	
N.PWDQVK.R	17.84	386.7029	3.32E+04	
I.TVDDKHYQK.A	15.31	378.5244	8.55E+05	

P02666 Peptide	-10lgP	m/z	Peptide intensity	PTM/Score
R.DMPIQAFLLYQEPVLGPVR.G	60.18	991.4352	1.59E+07	
K.IHPFAQTQSLVYPFPGPIPNSLPQNIPPLTQTPVVVPPFLQPEVMGVSK.V	55.92	1101.5841	4.03E+07	M2:Oxidation (M):1000.00
K.IHPFAQTQSLVYPFPGPIPN.S	53.23	1093.5869	7.32E+07	
M.PIQAFLLYQEPVLGPVR.G	52.72	1772.9523	4.02E+05	
M.PIQ(+.98)AFLLYQEPVLGPVR.G	51.74	1112.0844	1.15E+08	
K.IHPFAQTQ(+.98)SLVYPFPGPIPN.S	50.84	970.5536	8.22E+07	
A.FLLYQEPVLGPVR.G	49.16	971.0465	3.15E+05	Q3:Deamidation (NQ):145.19
K.YPVEPFTESQSLTLTDVENLHLPLPLLQSW.M	48.71	1112.5754	2.71E+06	Q8:Deamidation (NQ):13.13
M.FPPQSVLSLSQSK.V	47.85	765.9371	2.82E+06	
R.DM(+15.99)PIQAFLLYQEPVLGPVRG.P	47.74	1733.8907	1.86E+05	
N.SLPQNIPPLTQTPVVVPPFLQPEVMGVSK.V	46.97	709.3881	4.99E+06	
F.LLYQEPVLGPVR.G	44.83	1130.0947	2.27E+06	M2:Oxidation (M):1000.00
F.LLYQ(+.98)EPVLGPVR.G	44.42	1556.8601	4.25E+07	
W.MHQPHQPLPPTVMFPPQSVLSLSQSK.V	43.44	692.4034	1.48E+08	
E.EQQQTEDELQDK.I	42.49	692.8949	1.19E+06	Q4:Deamidation (NQ):1000.00
N.SLPQNIPPLTQTPVVVPPFLQPEVM(+15.99)GVSK.V	42.47	971.1719	1.21E+06	
K.YPVEPFTESQSL.T	41.83	745.8339	1.22E+05	
K.HKEM(+15.99)PFPK.Y	41.72	1564.8538	4.35E+06	M25:Oxidation (M):1000.00
L.LYQEPVLGPVR.G	40.33	698.835	5.11E+06	
R.DMPIQAFLLYQEPVLGPVRG.P	40.06	515.2626	5.21E+06	M4:Oxidation (M):1000.00
L.YQEPVLGPVR.G	39.4	635.8611	5.78E+07	
L.VYPFPGPIPN.S	37.84	1122.098	3.71E+06	
M.PIQAFLLYQEPVLGPVRG.P	35.28	579.3195	4.82E+07	
K.YPVEPFTESQSLTLTDVENLHLPLPLLQSWMHQPHQPLPPTVMFPPQSVLSLSQSK.V	35.27	550.7924	1.58E+05	
K.HKEMPFPK.Y	35.1	999.0647	1.98E+06	
M.PIQAFLLYQ(+.98)EPVLGPVR.G	34.34	1272.6584	3.56E+07	
K.VKEAMAPK.H	34.31	338.5129	3.30E+05	
A.RELEELNVPGEIVE.S	34.14	647.6996	1.91E+05	Q9:Deamidation (NQ):0.00
K.YPVEPFTESQSLTLTDVENLHLPLPLLQSWMHQPHQPLPPTVM(+15.99)FPPQSVLSLSQSK.V	33.73	437.2462	6.07E+04	
K.IHPFAQTQSLVYPFPGPIPN(+.98).S	33.49	813.4208	8.28E+05	
A.RELEELNVPGEIVESLSSSEESITR.I	32.97	1275.8564	1.23E+07	M43:Oxidation (M):0.00
K.YPVEPFTESQSLTLTDVENLHLPLPLLQSWM(+15.99)HQ(+.98)PHQPLPPTVM(+15.99)FPPQSVLSLSQSK.V	32.75	1112.5837	2.71E+06	N20:Deamidation (NQ):161.93
F.AQTQSLVYPFPGPIPN.S	32.38	934.806	6.21E+05	
K.VKEAM(+15.99)APK.H	31.17	1279.255	2.99E+06	M31:Oxidation (M):1000.00;Q33:Deamidation (NQ):0.00;M43:Oxidation (M):1000.00
K.YPVEPFTESQSLTLTDVENLHLPLPLLQSWM(+15.99)HQPHQPLPPTVMFPPQSVLSLSQSK.V	30.52	864.9509	4.52E+06	
K.IHPFAQTQS.L	29.97	297.1653	7.66E+04	M5:Oxidation (M):1000.00
K.IHPFAQTQ.S	29.61	1275.8547	1.23E+07	M31:Oxidation (M):3.99
S.VLSLSQSK.V	29.45	514.7614	9.78E+05	
K.IHPFAQTQSL.V	28.91	471.2455	1.22E+07	
K.YPVEPFTESQSLTLTDVEN(+.98)LHLPLPLLQSW.M	28.31	431.2556	1.72E+05	
K.YPVEPFTESQSLTLTDVENLHLPLPLLQSWMHQPHQPLPPTVMFPPQSVL.S	27.47	571.303	1.54E+06	
K.YPVEPFTESQ(+.98)SLTLTDVENLHLPLPLLQSWMHQPHQ(+.98)PLPPTVMFPPQSVLSLSQSK.V	27.28	1156.5975	2.95E+05	N19:Deamidation (NQ):28.25
L.LYQ(+.98)EPVLGPVR.G	26.96	1432.9852	6.13E+05	
K.VLPVPQK.A	26.47	1273.0571	1.78E+07	Q10:Deamidation (NQ):4.25;Q36:Deamidation (NQ):0.00
K.IHPFAQ.T	24.56	636.3531	3.05E+05	Q3:Deamidation (NQ):1000.00
K.EM(+15.99)PFPK.Y	23.21	390.7524	1.50E+08	
Q.KAVPYPQR.D	22.9	356.6923	1.22E+06	
A.FLLYQEPVLGPVRG.P	22.41	382.6859	5.45E+06	M2:Oxidation (M):1000.00

P02666 Peptide	-10lgP	m/z	Peptide intensity	PTM/Score
K.AVPYPQR.D	22.27	479.7774	2.85E+05	
Y.QEPVLGPVR.G	21.71	794.4481	2.25E+05	
S.KVLPVPQK.A	21.29	415.7295	2.84E+08	
R.GPFPIIV	20.6	497.7879	1.27E+06	
R.DMPIQAF.L	20.53	454.7998	1.71E+05	
Q.AFLLYQEPVLGPVR.G	19.87	371.7285	2.82E+06	
V.KEAMAPK.H	19.78	411.1966	7.42E+04	
E.KFQSEEQQQTEDELQDK.I	19.61	801.4565	2.03E+05	
F.LLYQEPVLGPVRG.P	17.21	387.7123	1.02E+04	
K.AVPYPQ(+.98)R.D	16.84	703.9895	6.87E+04	

P02668 Peptide	-10lgP	m/z	Peptide intensity	PTM/Score
K.PVALINNQFLPYPYYAK.P	64.51	1006.0379	2.75E+07	
R.SPAQILQWQVLSNTVPAK.S	62.23	990.5471	4.62E+08	
R.SPAQILQWQVLSN(+.98)TVPAK.S	59.84	991.0416	1.09E+07	N13:Deamidation (NQ):116.06
K.PVALINN(+.98)QFLPYPYYAK.P	59.04	1006.53	1.22E+06	N7:Deamidation (NQ):30.46
N.YYQQKPVALINNQFLPYPYYAK.P	58.17	1361.2069	1.11E+07	
A.QILQWQVLSNTVPAK.S	56.89	862.9882	4.33E+05	
Y.YQQKPVALINNQFLPYPYYAK.P	55.48	1279.6755	3.19E+07	
R.YPSYGLNYYQQKPVALIN(+.98)NQFLPYPYYAK.P	55.24	1172.9216	1.52E+08	N18:Deamidation (NQ):0.00
P.SYGLNYYQQKPVALINNQFLPYPYYAK.P	54.77	1085.8882	2.37E+06	
R.YPSYGLNYYQQKPVALINNQFLPYPYYAK.P	54.76	1172.5945	1.84E+08	
V.ALINNQFLPYPYYAK.P	54.09	907.9774	6.34E+04	
P.AQILQWQVLSNTVPAK.S	53.69	898.5071	3.07E+06	
R.YPSYGLNYYQQK.P	52.79	762.3616	4.01E+07	
K.PAAVRSPAQILQWQVLSNTVPAK.S	51.59	825.4669	4.25E+05	
R.YPSYGLNYYQQKPVALIN.N	50.98	1066.0459	1.84E+05	
S.YGLNYYQQKPVALINNQFLPYPYYAK.P	50.69	1056.8785	1.46E+06	
Q.ILQWQVLSNTVPAK.S	50.57	798.9584	2.04E+05	
R.YPSYGLNYYQQKPVAL.I	49.3	952.4825	9.38E+06	
Y.QQKPVALINNQFLPYPYYAK.P	47.79	1198.1434	5.67E+06	
R.HPHPHLSFM(+15.99)AIPPK.K	46.89	542.2851	6.17E+06	M9:Oxidation (M):1000.00
R.YPSYGLNYYQQKPV.A	46.43	860.4225	1.06E+06	
K.SC(+57.02)QAQPTTMAR.H	45.82	625.7844	6.27E+06	C2:Carbamidomethylation:1000.00
Y.GLNYYQQKPVALINNQFLPYPYYAK.P	45.68	1002.5206	2.38E+06	
K.PVALINNQFLPYPYYAKPAAVR.S	45.58	835.7926	3.59E+05	
R.YPSYGLNYYQQ(+.98)K.P	45.21	762.8535	1.64E+05	Q11:Deamidation (NQ):27.96
L.INNQFLPYPYYAK.P	44.85	815.9171	1.34E+07	
R.HPHPHLSFMAIPPK.K	44.69	536.9538	1.58E+07	
L.NYYQQKPVALINNQFLPYPYYAK.P	44.43	945.8212	1.52E+05	
K.TEIPTINTIASGEPTSTPTTEAVESTVATLED.S	43.74	1092.5342	9.63E+05	
K.YIPIQYVLSR.Y	43.54	626.3581	1.92E+08	
K.SC(+57.02)QAQPTTM(+15.99)AR.H	42.77	633.7819	2.42E+07	C2:Carbamidomethylation:1000.00;M 9:Oxidation (M):1000.00
S.YGLNYYQQK.P	42.14	588.7874	1.34E+05	
K.SC(+57.02)Q(+.98)AQPTTM(+15.99)AR.H	41.18	634.2738	5.50E+05	C2:Carbamidomethylation:1000.00;Q 3:Deamidation (NQ):55.92;M9:Oxidation (M):1000.00
R.YPSYGLNYYQQKPVALINNQFLPYPY.Y	37.74	1051.8624	4.88E+06	
K.YIPIQ(+.98)YVLSR.Y	37.6	626.8502	2.11E+06	Q5:Deamidation (NQ):1000.00
Y.YQQKPVALINNQ(+.98)FLPYPYYAK.P	37.19	853.782	1.53E+06	Q12:Deamidation (NQ):0.00
R.YPSYGLNYYQQKPVA.L	36.48	895.9406	3.95E+05	
Q.KPVALINNQFLPYPYYAK.P	36.14	713.7261	1.90E+05	
Y.YQQKPVALINNQFLPYPY.Y	36.12	1098.5776	6.41E+05	
Q.VLSNTVPAK.S	35.28	464.7763	1.02E+05	
K.TEIPTINTIASGEPT.S	34.91	772.3962	2.92E+04	

P02668 Peptide	-10lgP	m/z	Peptide intensity	PTM/Score
Y.QQKPVALIN(+.98)NQFLPYPYYAK.P	34.54	799.4252	6.29E+05	N9:Deamidation (NQ):24.44
K.YIPIQYVL.S	32.6	504.7917	1.76E+05	
W.QVLSNTVPAK.S	32.43	528.8062	6.02E+06	
R.YPSYGLNYYQQKPVALINN(+.98)QFLPYPYYAK.P	31.26	1758.8854	8.07E+06	N19:Deamidation (NQ):17.01
S.YGLNYYQQKPVALINN(+.98)QFLPYPYYAK.P	31.15	1057.2108	7.30E+05	N16:Deamidation (NQ):12.28
F.MAIPPK.K	31	328.6938	4.01E+05	
R.YPSYGLNYY.Q	30.72	570.2556	5.20E+05	
L.QWQVLSNTVPAK.S	30.04	685.8751	5.99E+05	
R.HPHPHLSF.M	29.97	486.2459	8.26E+06	
L.SNTVPAK.S	29.85	358.7003	7.97E+05	
N.YYQQKPVAL.I	29.03	555.3031	6.18E+04	
H.LSFM(+15.99)AIPPK.K	28.6	510.2839	2.53E+05	M4:Oxidation (M):1000.00
I.PIQYVLSR.Y	27.16	488.2845	1.13E+07	
Q.WQVLSNTVPAK.S	26.94	621.8455	3.09E+05	
Y.YQQKPVALIN(+.98)NQFLPYPYYAK.P	25.92	853.7813	1.53E+06	N10:Deamidation (NQ):0.00
Y.YQQKPVALINNQFLPYPYYAKPAAVR.S	25.9	763.9163	8.69E+04	
L.INN(+.98)QFLPYPYYAK.P	25.38	816.4092	2.17E+05	N3:Deamidation (NQ):8.14
R.YPSYGLNY.Y	25.23	488.7239	3.18E+05	
A.QEQNQEQPIR.C	25.2	635.3127	3.26E+05	
A.Q(+.98)EQNQEQPIR.C	24.77	635.8048	1.37E+05	Q1:Deamidation (NQ):0.00
K.YIPIQY.V	23.51	398.7151	2.20E+06	
Q.NQEQPIR.C	23.25	442.7329	3.60E+05	
K.SC(+57.02)Q(+.98)AQPTTMAR.H	23.04	626.2759	1.07E+05	C2:Carbamidomethylation:1000.00;Q 3:Deamidation (NQ):51.51
N.NQFLPYPYYAK.P	22.25	702.3525	1.10E+05	
K.PVALINNQFLPYPY.Y	21.42	824.94	2.21E+06	
I.PIQ(+.98)YVLSR.Y	21.15	488.7767	1.19E+05	Q3:Deamidation (NQ):1000.00
R.FFSDK.I	20.47	322.158	3.26E+07	
Y.YAKPAAVR.S	20.19	438.2583	3.83E+05	
P.HPHLSF.M	19.46	369.1899	2.32E+05	
R.HPHPHLS.F	18.82	412.7111	2.56E+05	
R.SPAQILQW.Q	18.67	471.7553	9.63E+05	
R.HPHPHL.S	17.31	369.1957	4.40E+04	
L.INNQFLPYPY.Y	15.86	634.8191	6.80E+04	

P02662 Peptides	-10lgP	m/z	Peptide intensity	PTM/Score
E.GIHAQQK.E	16.19	391.2192	9.28E+03	
T.DAPSFSDIPNPIGSENSEK.T	66.07	1002.4623	2.59E+04	
K.YKVPQLEIVPNSAEER.L	41.8	624.6675	2.74E+04	
K.VPQLEIVPNSAEER.L	42.82	790.9175	3.23E+04	
H.QGLPQEVLNENLLR.F	52.16	811.9474	3.48E+04	
F.FVAPFPEVFGK.E	36.97	619.3346	3.80E+04	
K.EKVNELSK.D	32.19	473.7638	5.32E+04	
Y.YVPLGTQYTDAPSFSDIPNPIGSENSEK.T	51.74	1009.481	1.01E+05	
Q.GLPQEVLNENLLR.F	45.03	747.918	1.14E+05	
K.HQGLPQEVLNENLL.R	40.11	802.4261	1.33E+05	
K.HIQKEDVPSER.Y	43.02	446.5652	1.44E+05	
K.EGIHAQQK.E	40.23	455.7404	2.09E+05	
K.EPM(+15.99)IGVNQELAYFYPELFR.Q	16.12	1166.5695	2.24E+05	M3:Oxidation (M):1000.00
K.HQGLPQEVLNEN.L	49.73	689.3415	2.73E+05	
K.VNELSK.D	34.5	345.195	2.92E+05	
R.YLGYLEQLLR.L	42.68	634.3561	4.57E+05	
K.EDVPSER.Y	18.79	416.1959	5.42E+05	
R.FFVAPFPEVFGK.E	39.16	692.8677	2.10E+06	
K.HQGLPQEVLNENLLR.F	70.14	880.4763	3.72E+06	

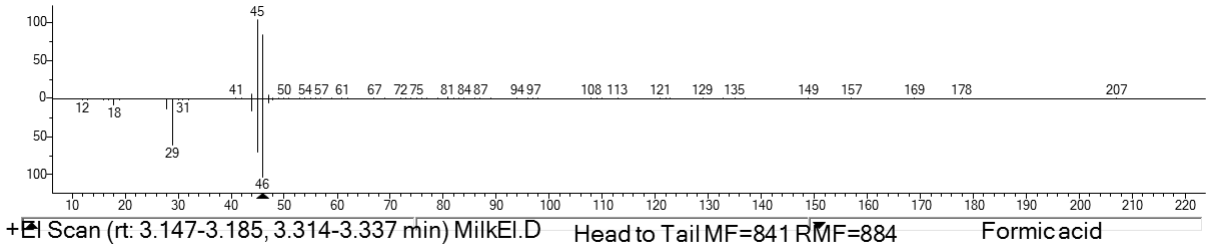
P02663 Peptides	-10lgP	m/z	Peptide intensity	PTM/Score
K.ENLC(+57.02)STFC(+57.02)K.E	35.08	579.7497	1.86E+04	C4:Carbamidomethylation:1000.00; C8:Carbamidomethylation:1000.00
K.NM(+15.99)AINPSK.E	36.44	445.7237	3.07E+04	M2:Oxidation (M):1000.00
R.LNFLK.K	19.33	317.6998	4.59E+04	
K.ITVDDKHYQK.A	47.01	623.8254	6.06E+04	
K.ALNEINQFYQ(+.98)K.F	52.01	684.8428	1.31E+05	Q10:Deamidation (NQ):91.37
K.ITVDDK.H	33.61	345.6871	1.44E+05	
K.TVYQHQK.A	19.97	301.8275	1.48E+05	
R.NAVPITPTLNR.E	19.29	598.3436	3.86E+05	
K.FALPQYLK.T	40.24	490.2844	5.28E+05	
K.LTEEEK.N	32.34	374.6898	5.96E+05	
K.ALNEINQFYQK.F	57.7	684.3516	1.54E+06	C4:Carbamidomethylation:1000.00; C8:Carbamidomethylation:1000.00

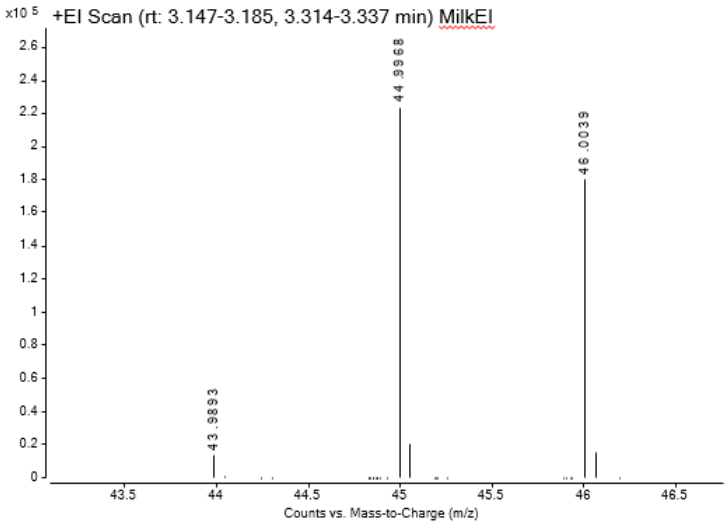
P02666 Peptides	-10lgP	m/z	Peptide intensity	PTM/Score
R.GPFPIIV	16.33	371.7286	4.69E+03	
K.YPVEPFTESQSLTLTDVENL.H	39.13	1141.558	5.10E+03	
L.YQEPVLGPVRGPFPIIV	53.51	941.0372	1.10E+04	
L.LYQEPVLGPVR.G	37.95	635.8616	1.24E+04	
K.IHPFAQ(+.98)TQSLVYPFPGPIPN.S	26.16	1112.5759	1.46E+04	Q6:Deamidation (NQ):12.19
L.YQEPVLGPVR.G	40.53	579.3193	2.29E+04	
F.AQTQSLVYPFPGPIPN.S	15.46	864.9522	2.40E+04	
K.FQSEEQQQTEDELQDK.I	41.74	661.2926	2.48E+04	
A.RELEELNVPGEIVE.S	17.14	813.4216	2.50E+04	
K.VKEAM(+15.99)APK.H	30.82	297.1653	3.21E+04	M5:Oxidation (M):1000.00
S.VLSLSQSK.V	29.08	431.2554	3.37E+04	
R.DM(+15.99)PIQAFLLYQEPVLGPVRG.P	55.17	1130.0955	5.13E+04	M2:Oxidation (M):1000.00
K.YPVEPFTESQ.S	40.88	598.7773	5.42E+04	
M.PIQAFLLYQEPVLGPVR.G	56.6	970.5527	5.87E+04	
K.IHPFAQTQSL.V	33.39	571.3036	6.98E+04	
K.HKEM(+15.99)PFPK.Y	24.34	343.8443	9.47E+04	M4:Oxidation (M):1000.00
K.EM(+15.99)PFPK.Y	25.5	382.6859	1.04E+05	M2:Oxidation (M):1000.00
K.VLPVPQK.A	22.26	390.7524	1.32E+05	
K.AVPYPQR.D	17.34	415.7295	2.24E+05	
K.IHPFAQTQ.S	32.77	471.2453	2.44E+05	
F.LLYQEPVLGPVR.G	48.96	692.4039	8.81E+05	
N.SLPQNIPPLTQTPVVVPPFLQ(+.98)PEVM(+15.99)GVSK.V	19.22	1043.9008	1.11E+06	Q21:Deamidation (NQ):0.00;M25:Oxidation (M):1000.00
R.DM(+15.99)PIQAFLLYQEPVLGPVR.G	55.66	1101.5844	1.34E+06	M2:Oxidation (M):1000.00
N.SLPQNIPPLTQTPVVVPPFLQPEVM(+15.99)GVSK.V	31.58	1564.8522	1.38E+06	M25:Oxidation (M):1000.00
K.IHPFAQTQSLVYPFPGPIPN.S	60.28	1112.0823	1.80E+06	

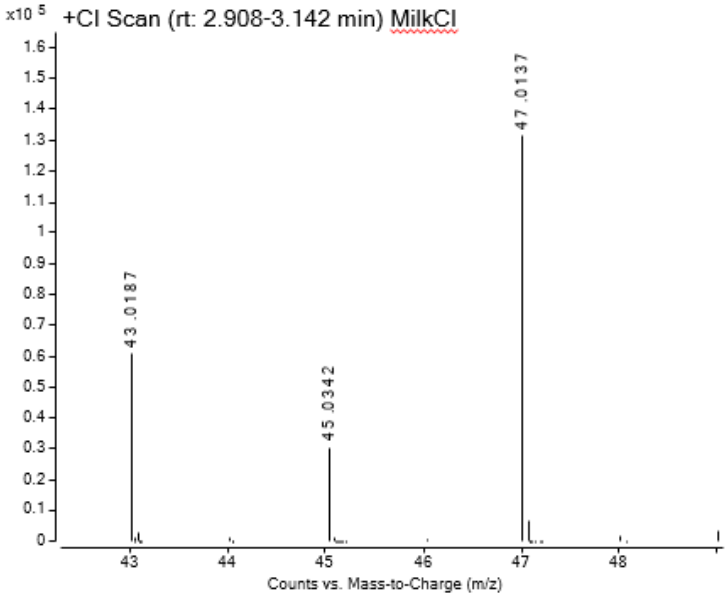
P02668 Peptides	-10lgP	m/z	Peptide intensity	PTM/Score
K.PVALINNQFLPYPY.Y	21.93	824.9406	1.84E+04	
I.PIQYVLSR.Y	16.93	488.2851	2.05E+04	
K.SC(+57.02)QAQPTTM(+15.99)AR.H	45.8	633.7825	2.19E+04	C2:Carbamidomethylation:1000.00;M9:Oxidation (M):1000.00
R.YPSYGLNYYQQKPV.A	48.89	860.4225	2.35E+04	
R.YPSYGLNYYQQKPVAL.I	51.11	952.4845	2.99E+04	
V.ALINNQFLPYPYYAK.P	59.43	907.9788	3.13E+04	
K.DERFFSDK.I	39.99	522.2432	3.49E+04	
K.PAAVR.S	15.01	257.1611	4.91E+04	
Y.QQKPVALINNQFLPYPYYAK.P	39.03	799.0991	5.65E+04	
Y.YQQKPVALINNQFLPYPYYAK.P	50.82	853.4535	7.68E+04	
R.FFSDK.I	17.34	322.1579	1.28E+05	
L.INNQFLPYPYYAK.P	45.64	815.9174	1.47E+05	
R.SPAQILQWQVLSN.T	22.25	742.3986	1.90E+05	
K.PVALINNQFLPYPYYAK.P	68.15	1006.0393	2.59E+05	
R.YPSYGLNYYQQK.P	64.83	762.3619	2.77E+05	
K.YIPIQYVLSR.Y	33.68	626.3589	5.83E+05	
R.SPAQILQWQVLSNTVPAK.S	68.87	990.5509	7.33E+05	

Formic acid

Mass: 46.0054793

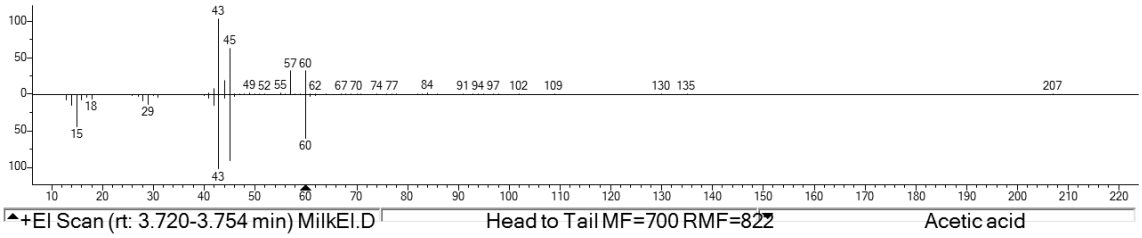


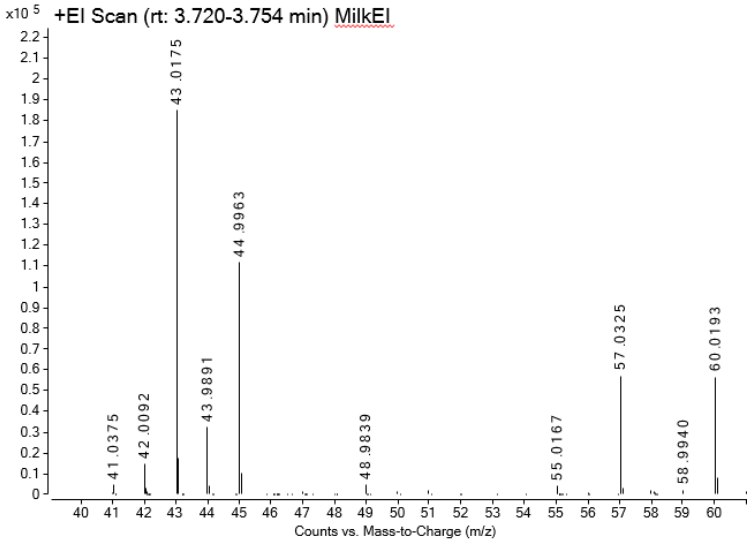


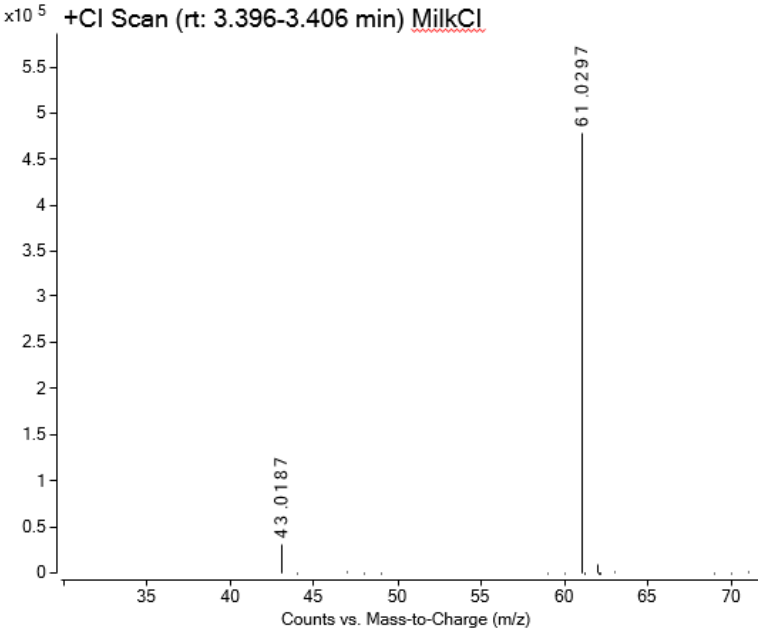


Acetic acid

Mass: 60.0211294

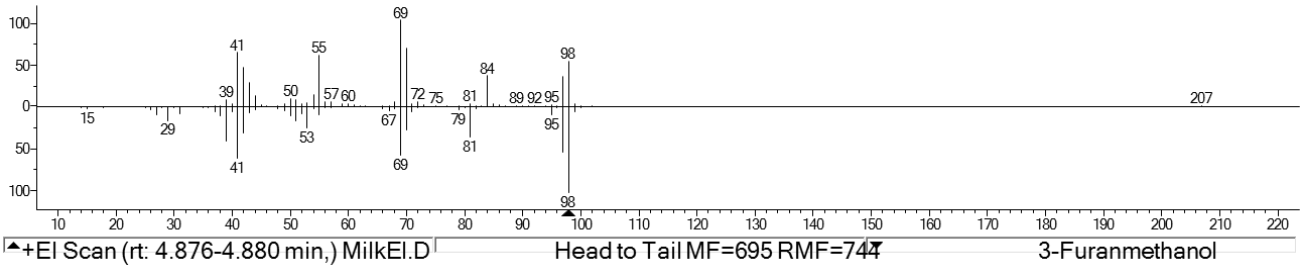


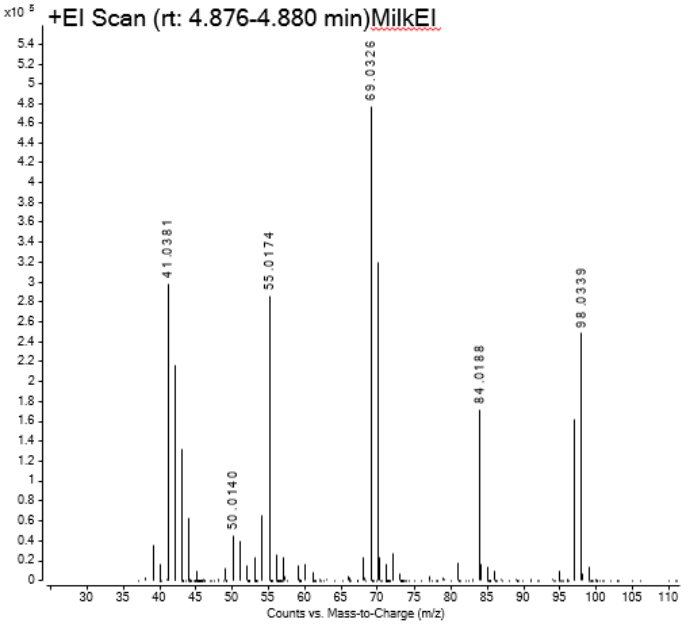


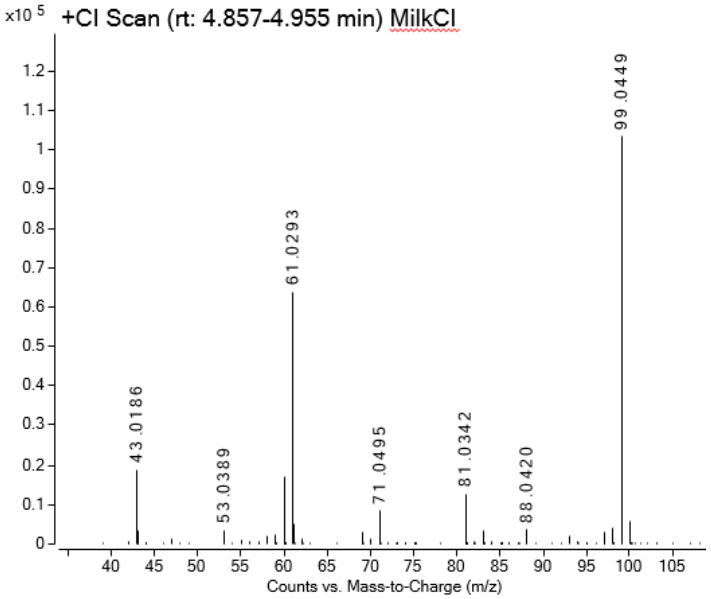


3-Furanmethanol

Mass: 98.0367794

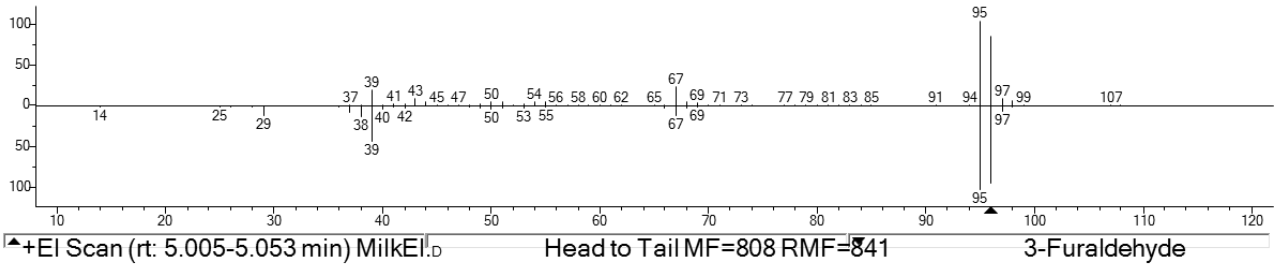


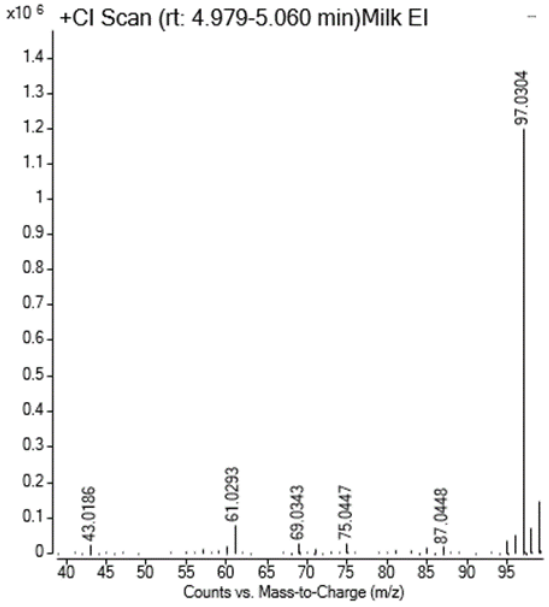


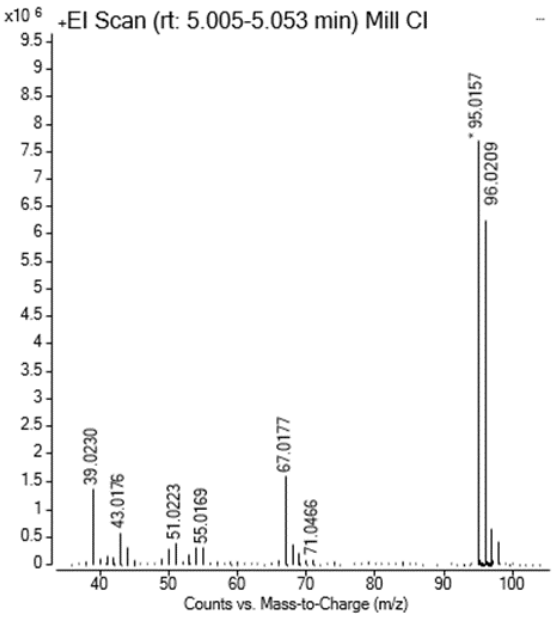


3-Furaldehyde

Mass: 96.021129

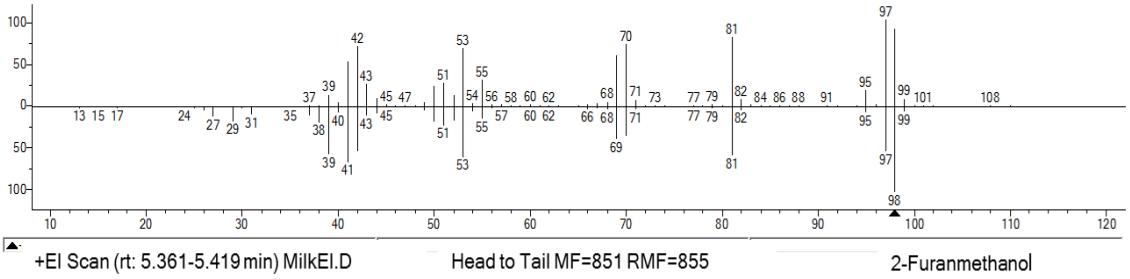


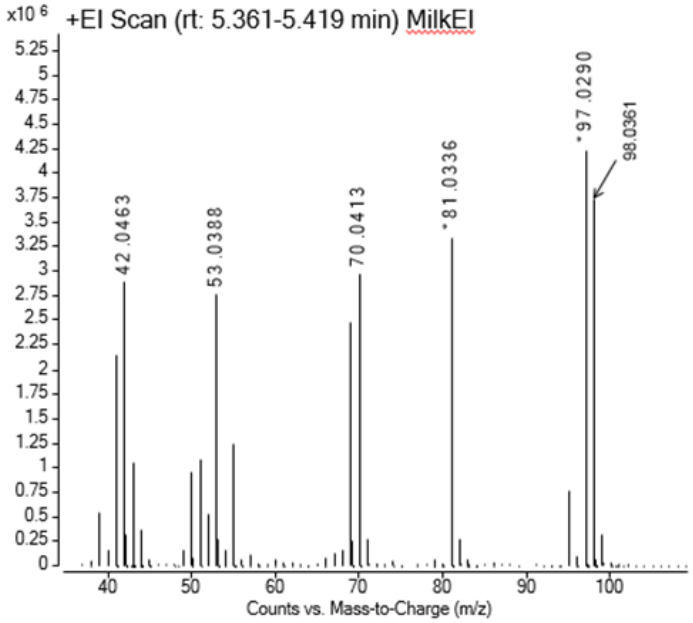


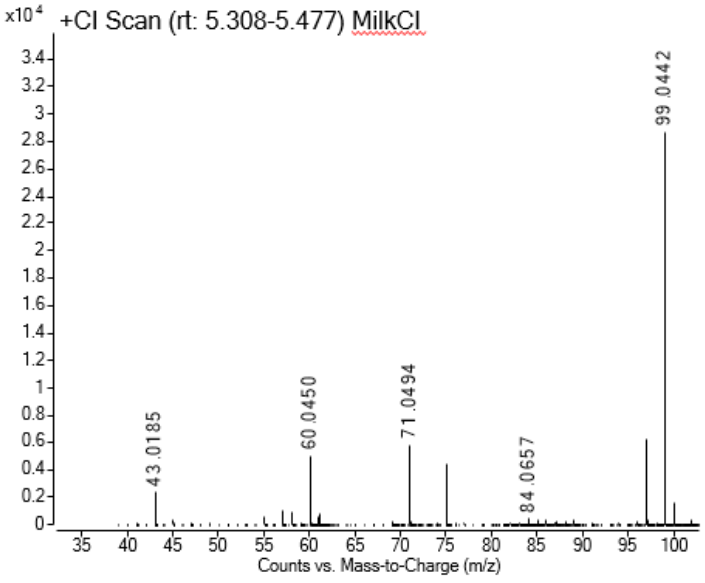


2-Furanmethanol

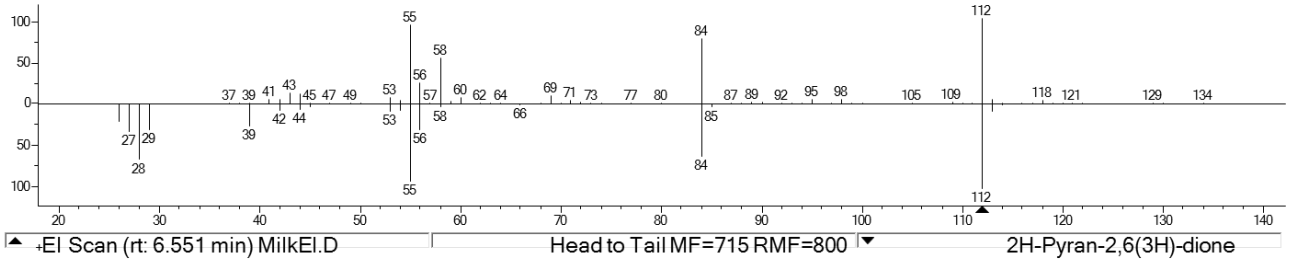
Mass: 98.0367794

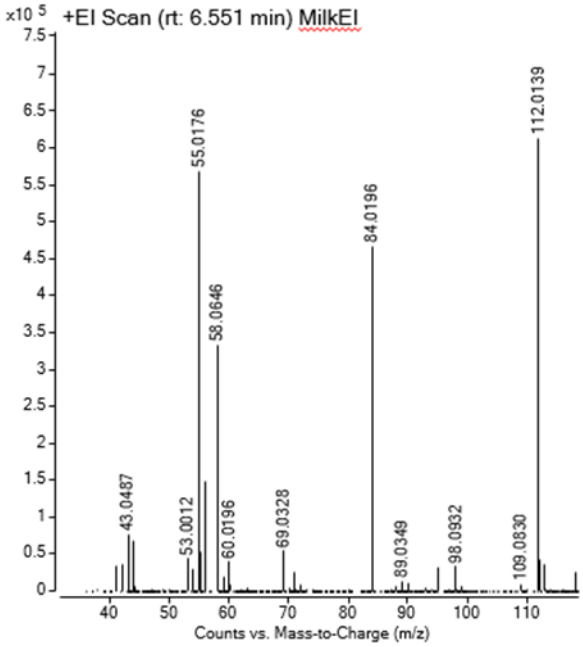


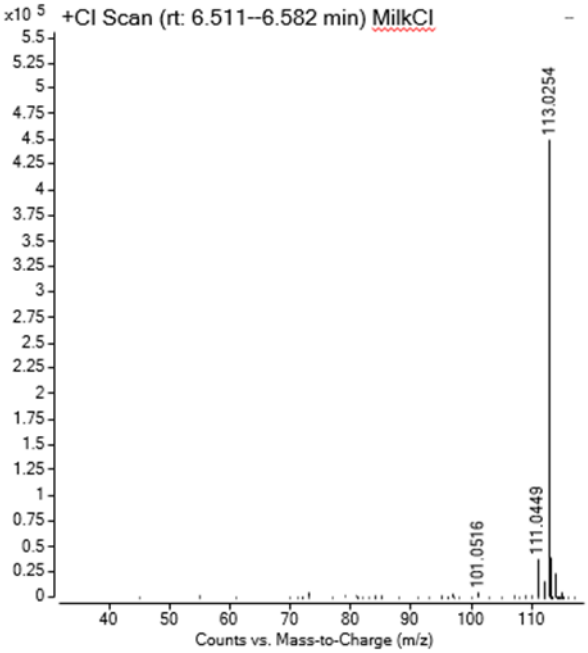




2H-Pyran-2,6(3H)-dione

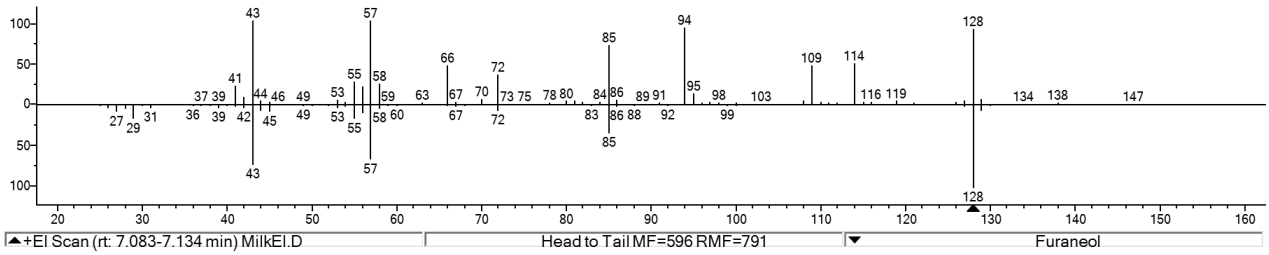


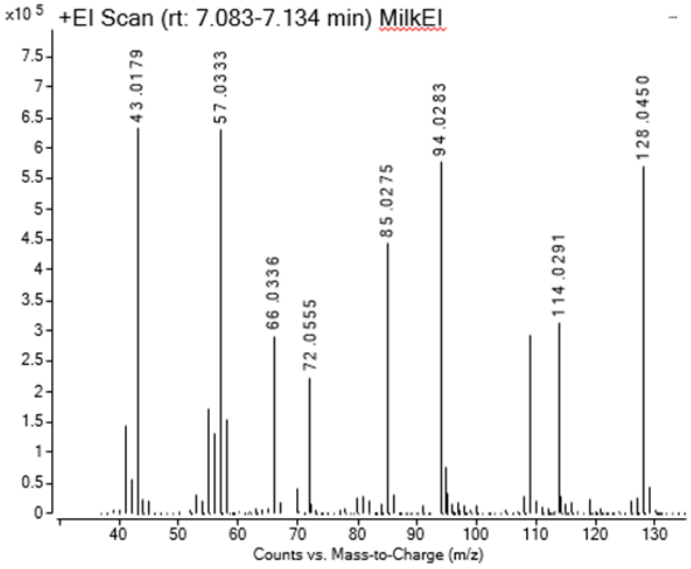


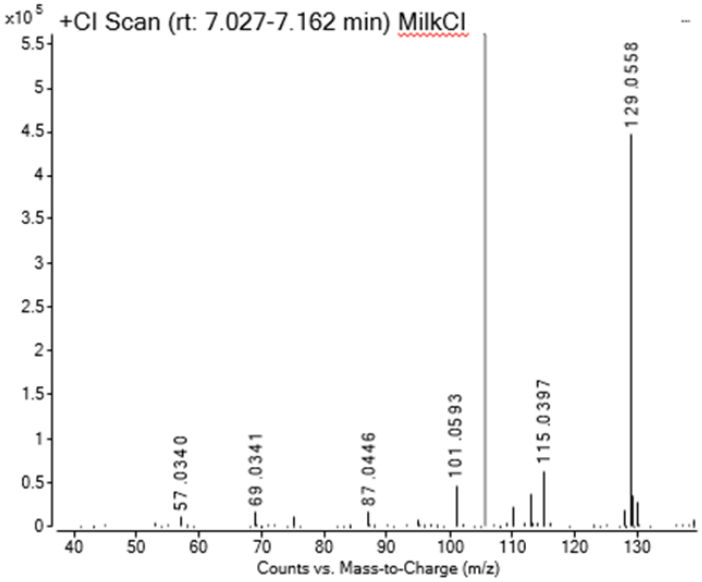


Furaneol

Mass: 128.047344

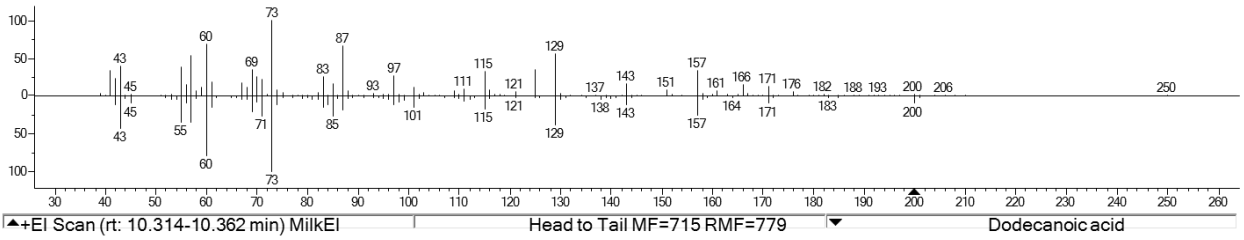


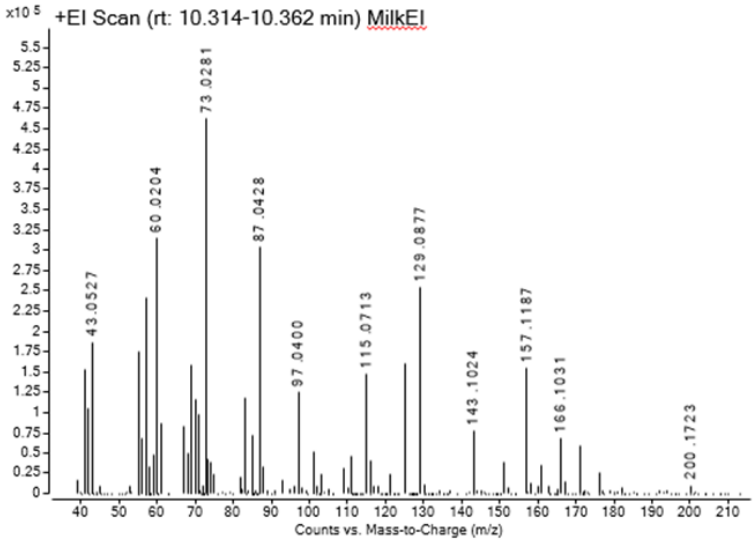


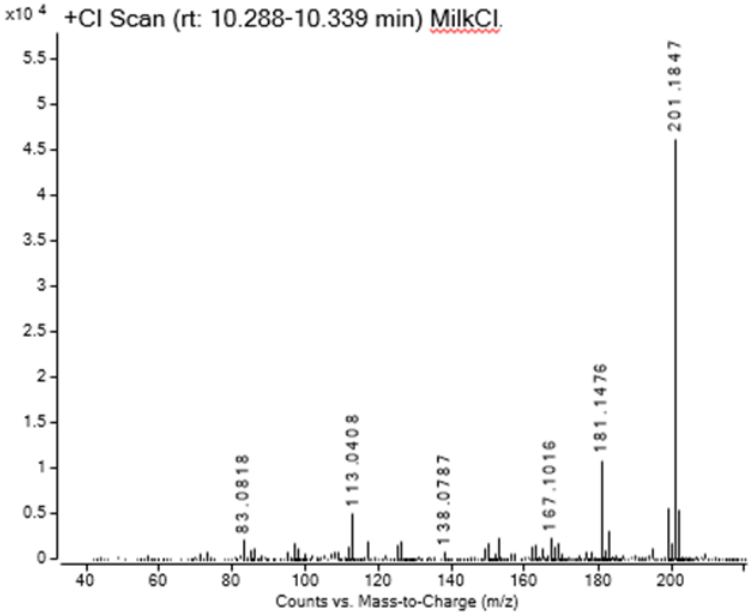


Dodecanoic acid

Mass: 200.17763

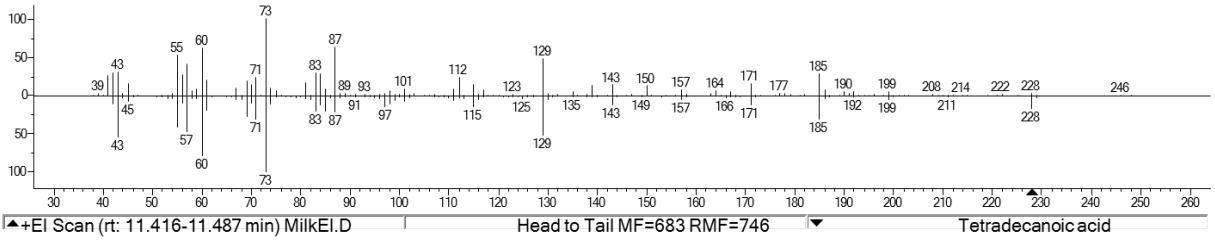


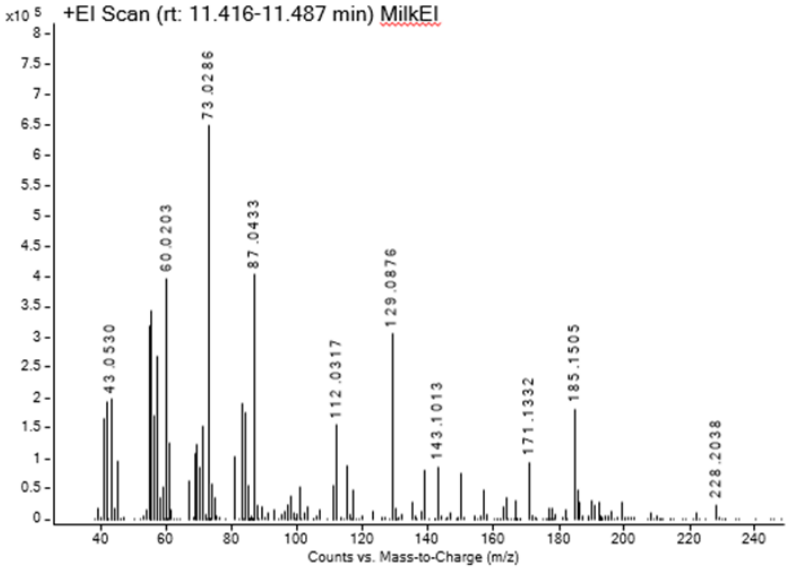


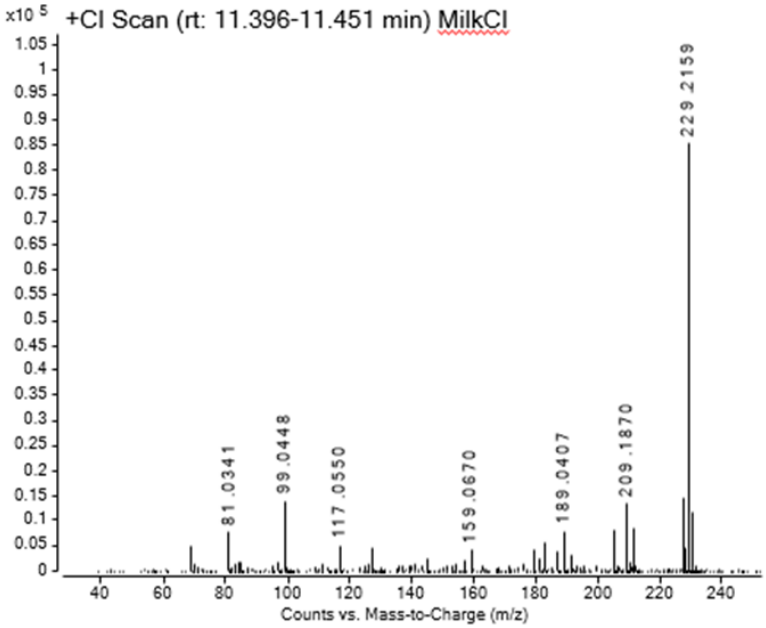


Tetradecanoic acid

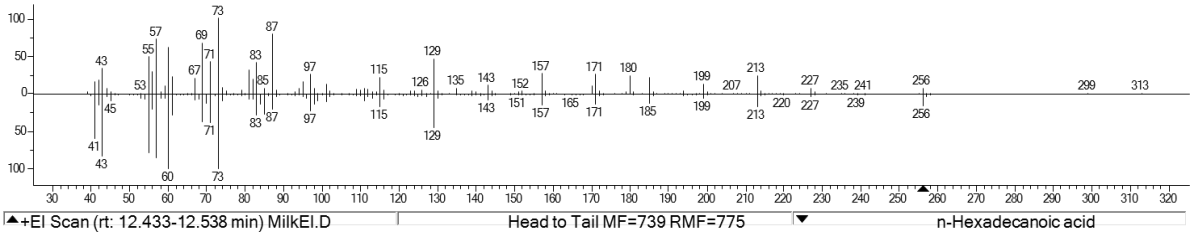
Mass: 228.20893

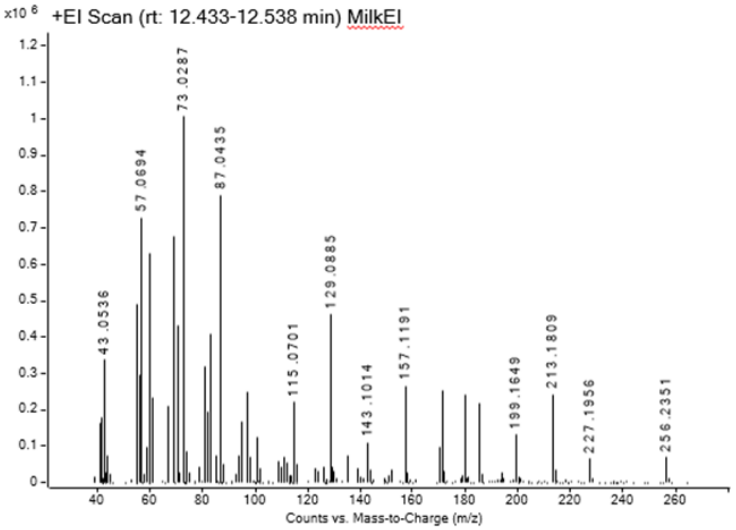


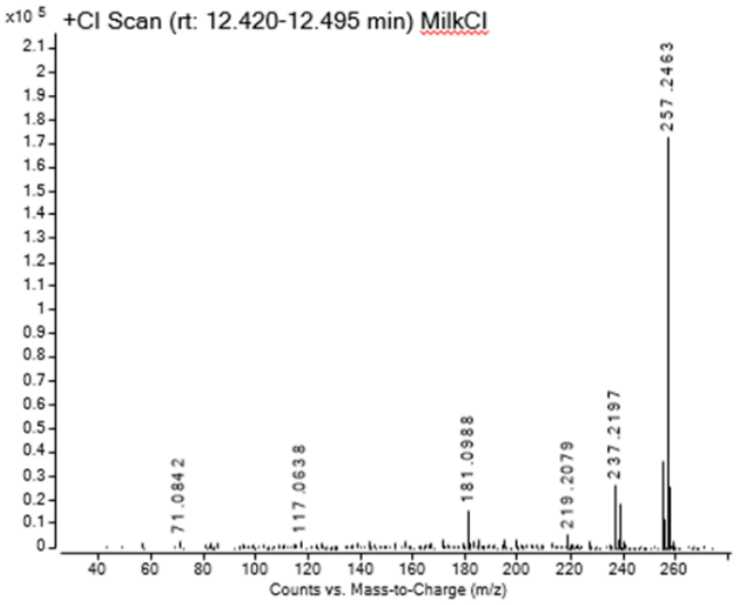




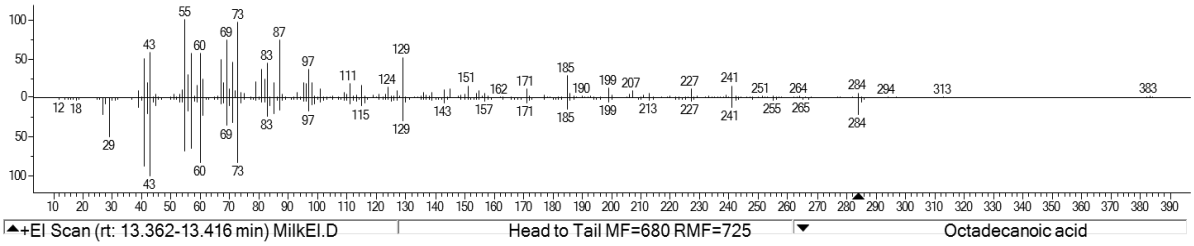
n-Hexadecanoic acid

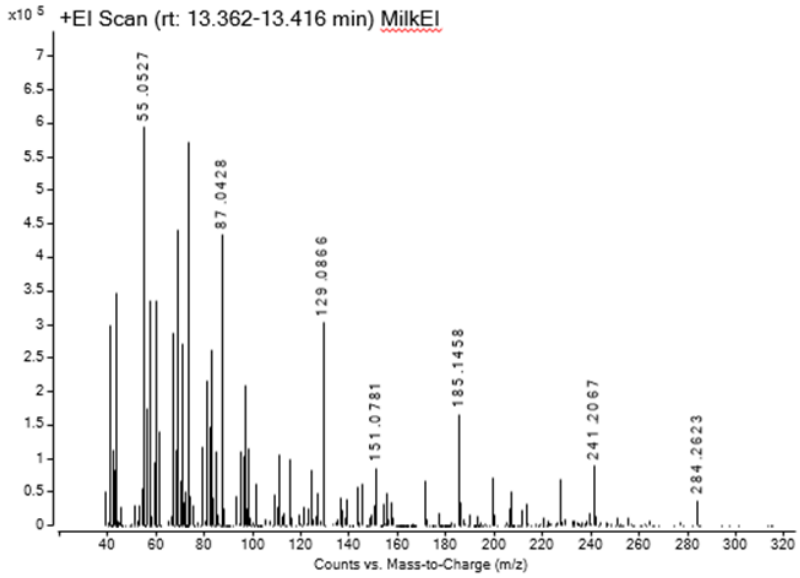


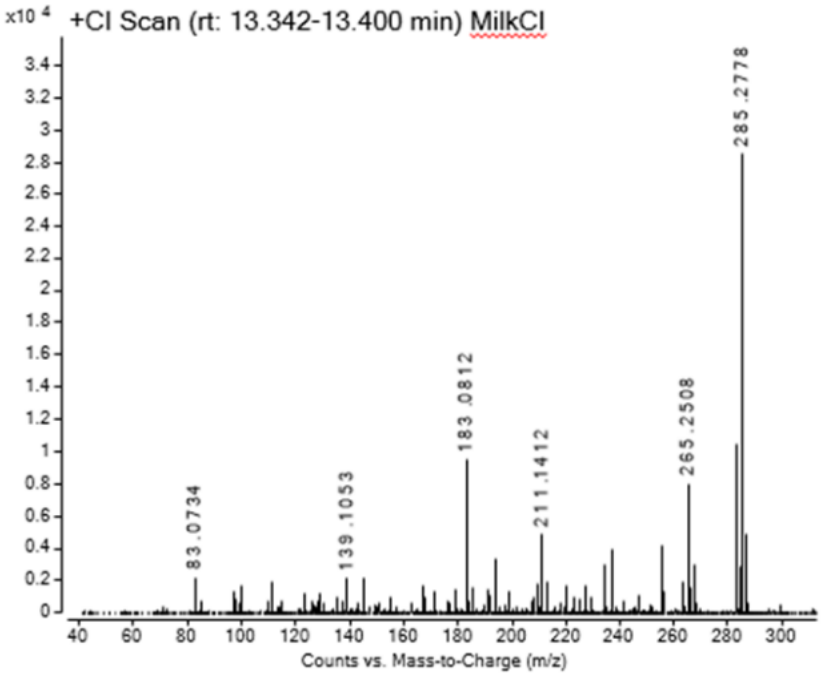




Octadecanoic acid

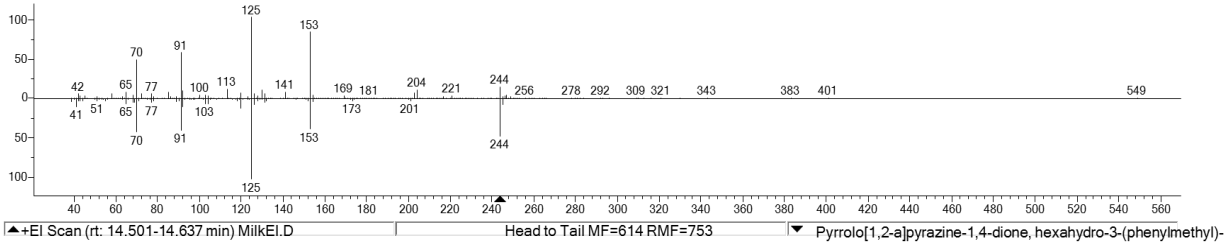


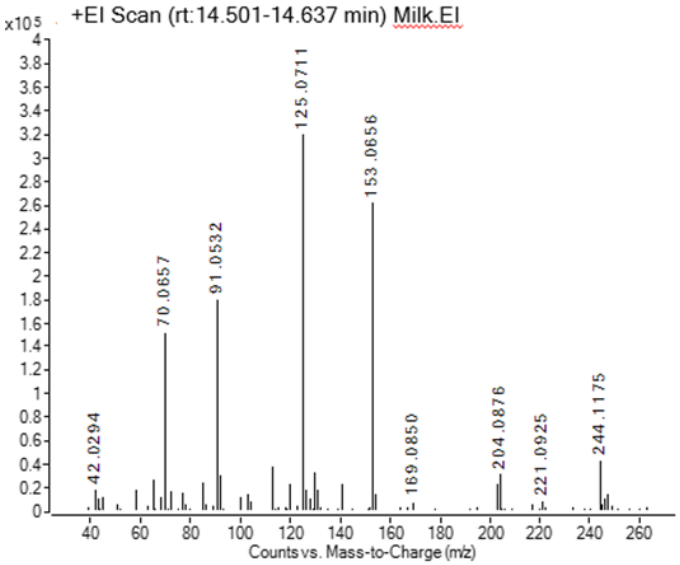


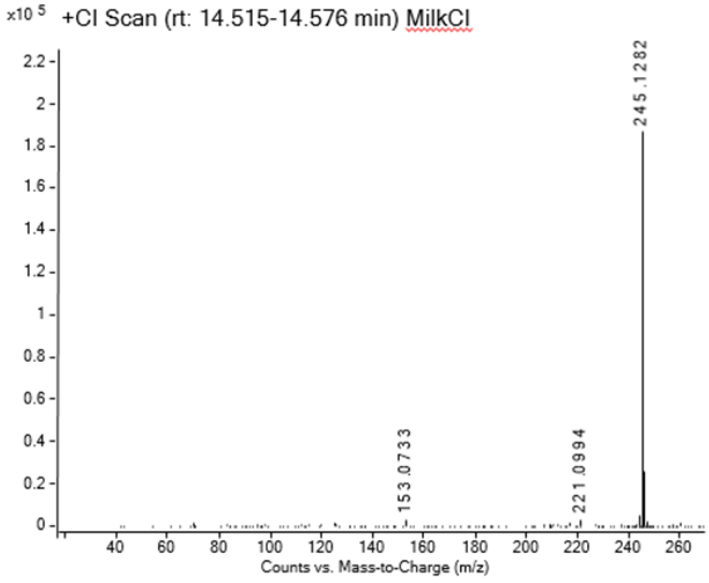


Pyrrolo[1,2-a]pyrazine-1,4-dione, hexahydro-3-(phenylmethyl)-

Mass: 244.121178

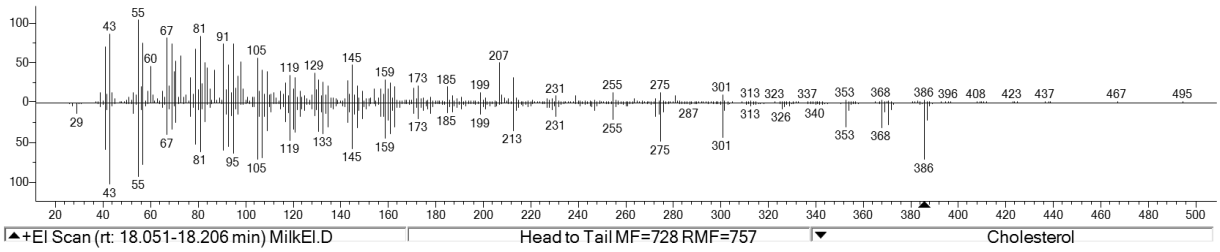


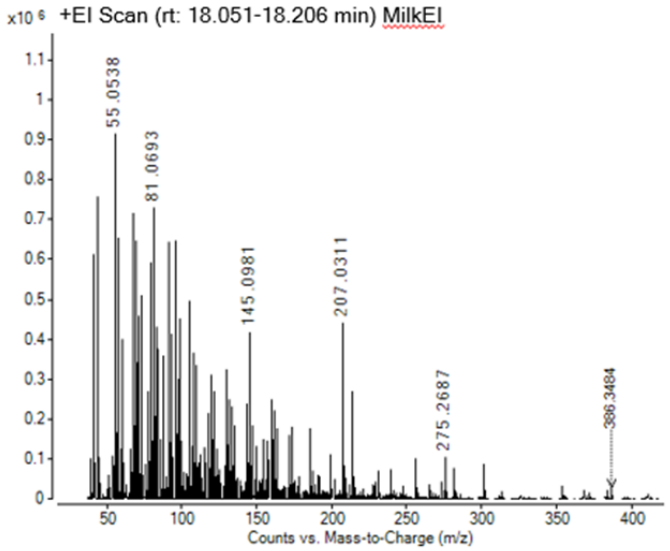


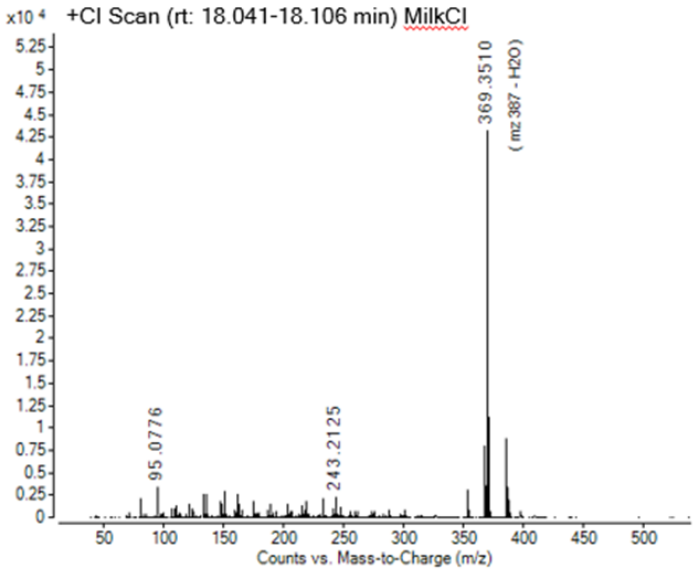


Cholesterol

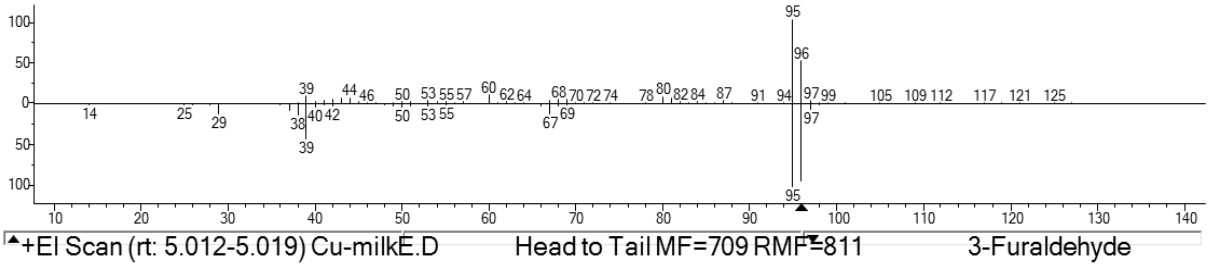
Mass: 386.354866

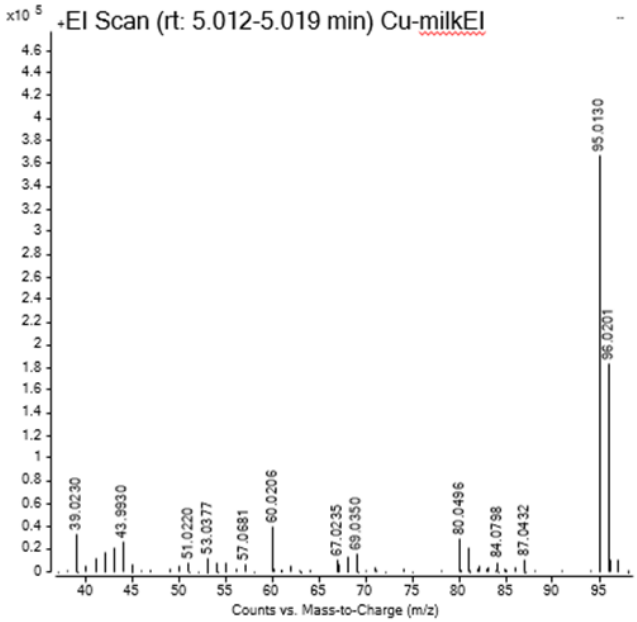


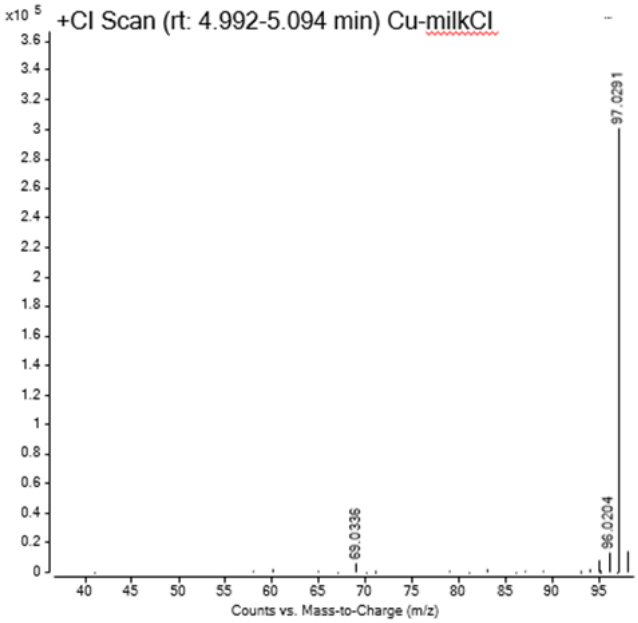




3-Furaldehyde

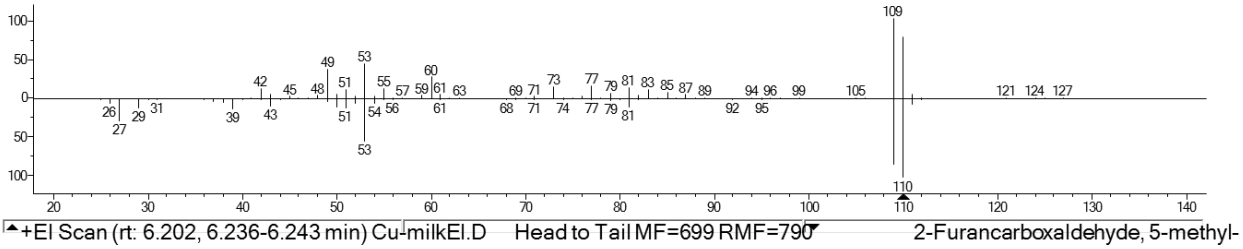


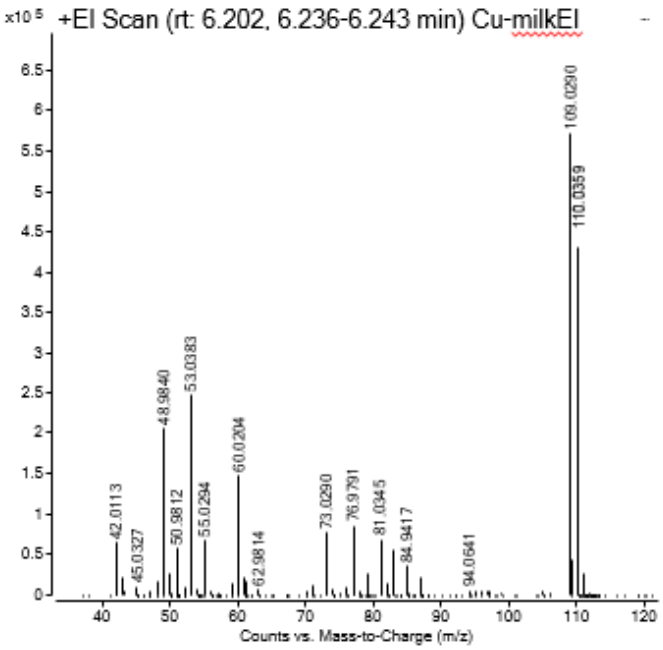


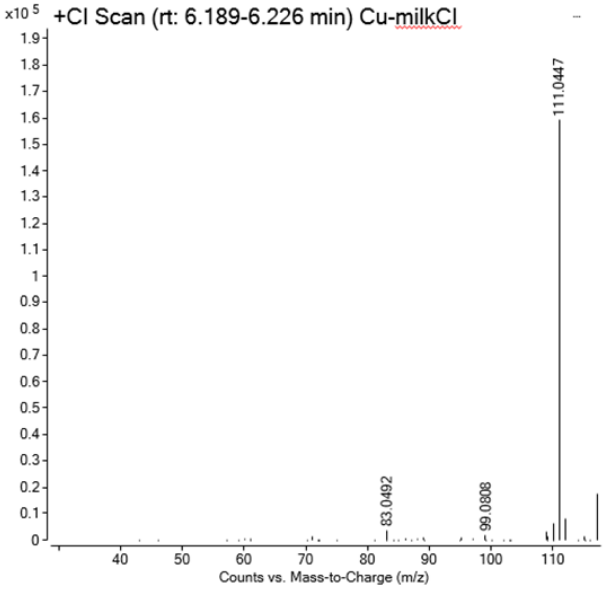


2-Furancarboxaldehyde, 5-methyl-

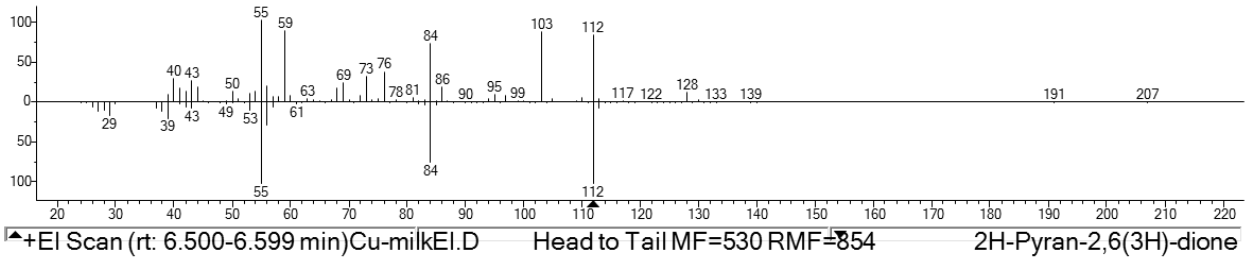
Mass: 110.0367794

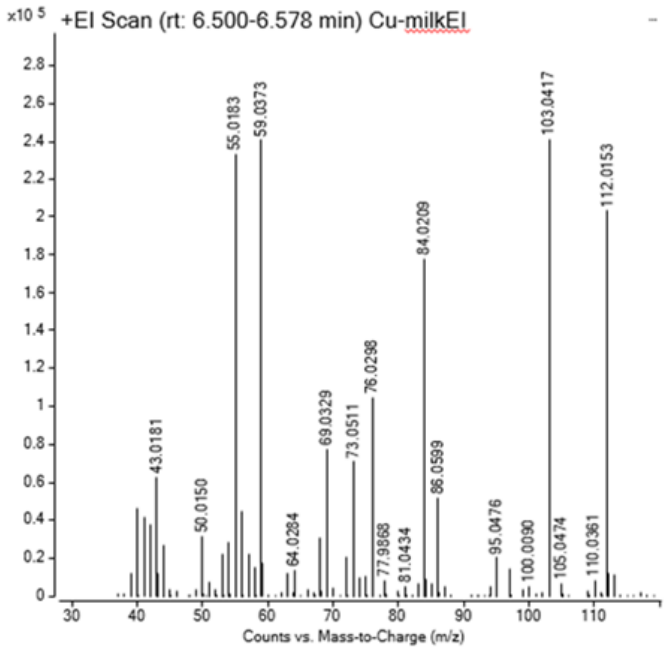


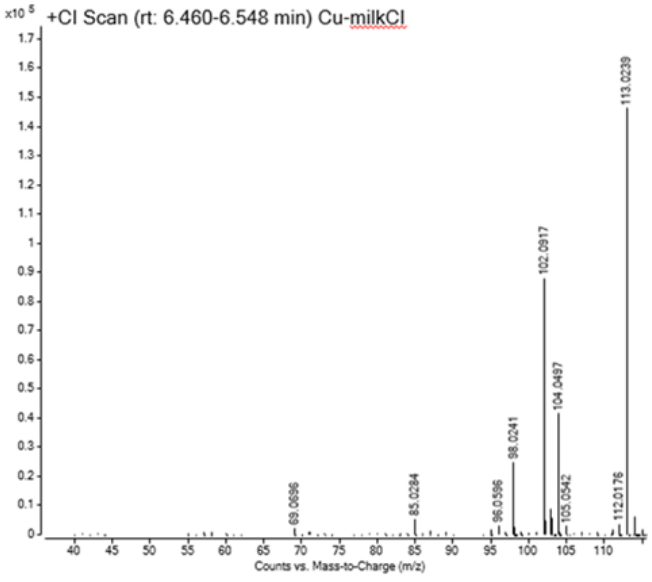




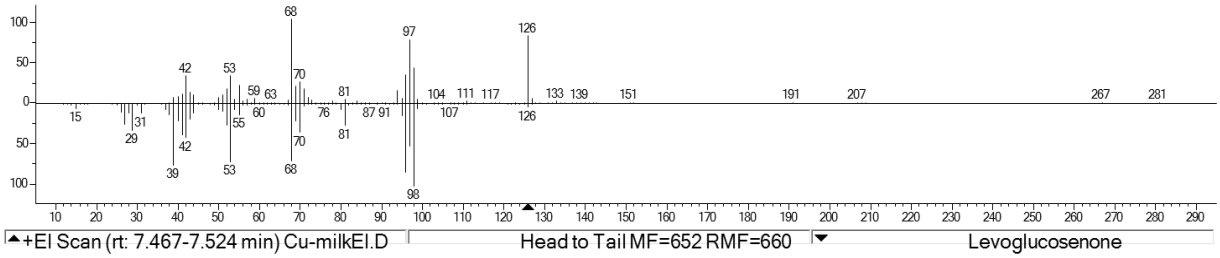
2H-Pyran-2,6(3H)-dione

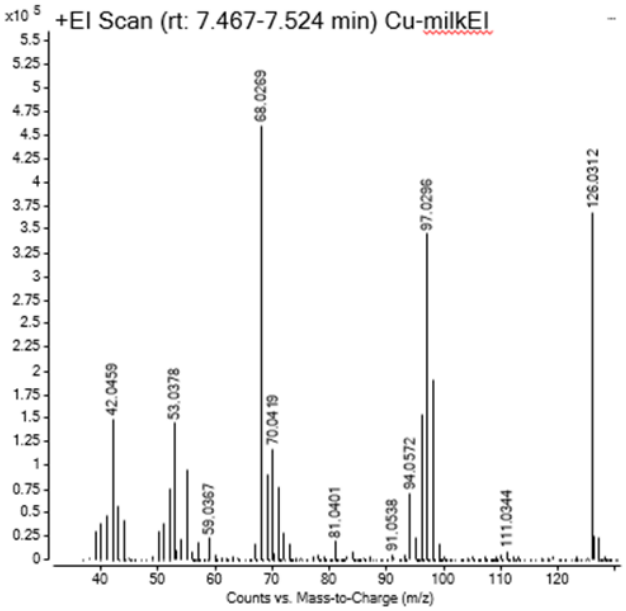


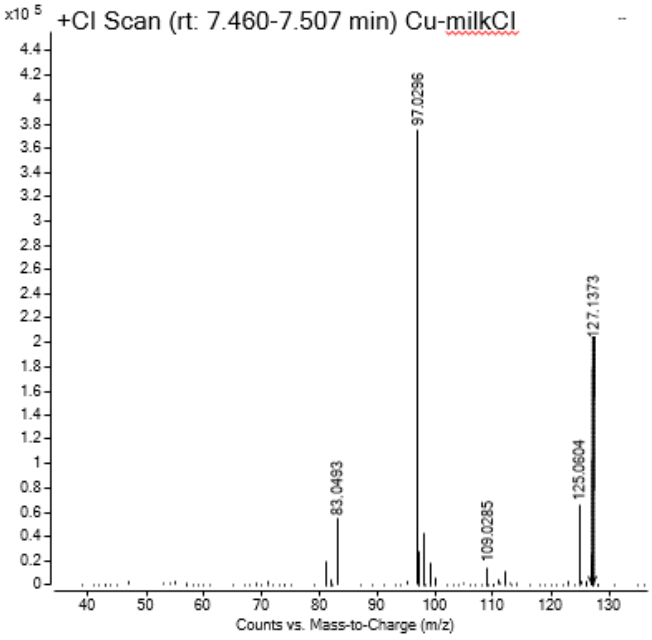




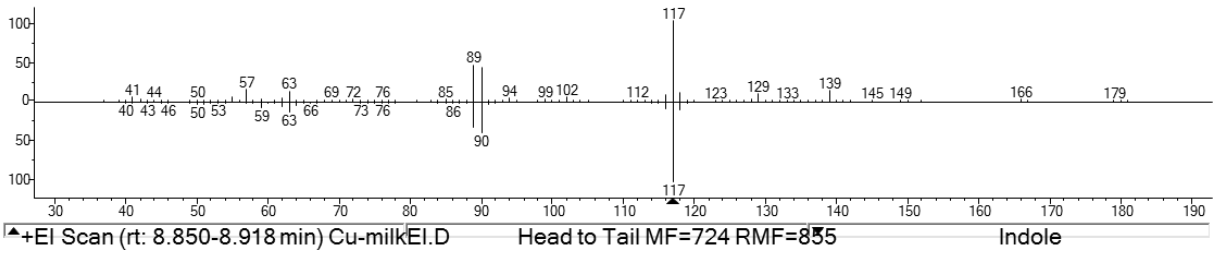
Levoglucosenone

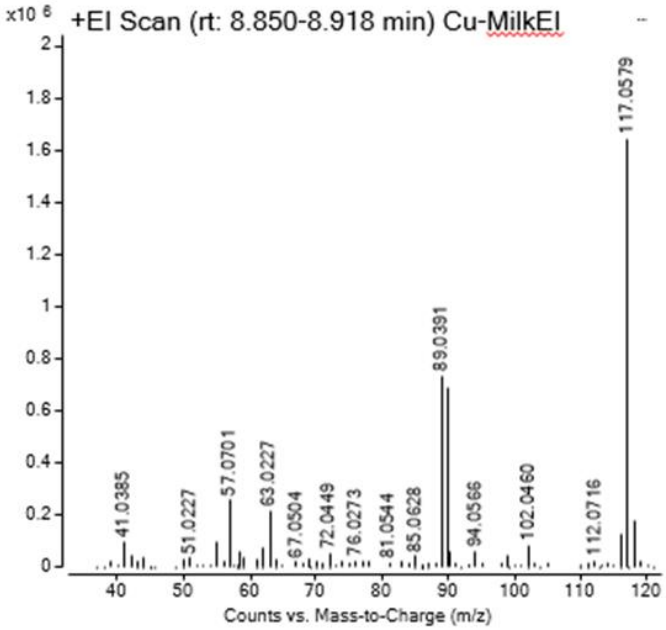


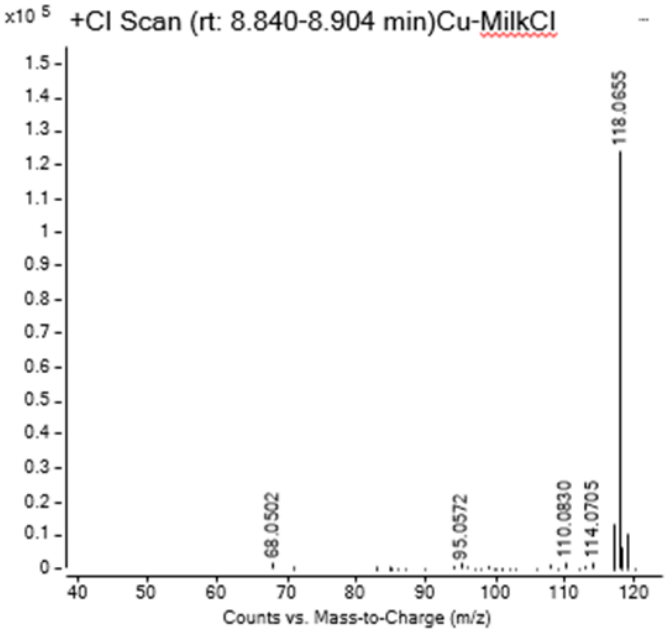




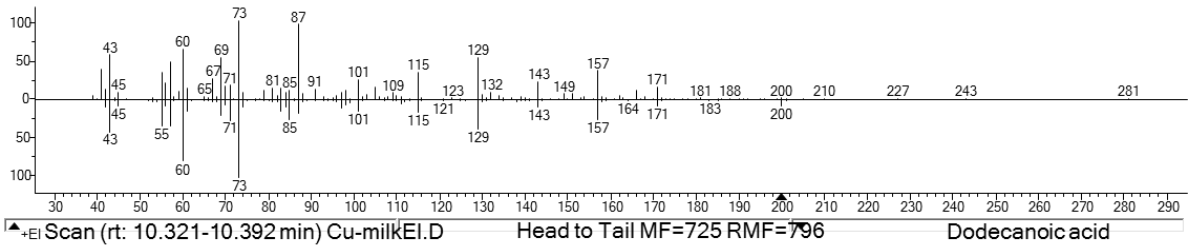
Indole

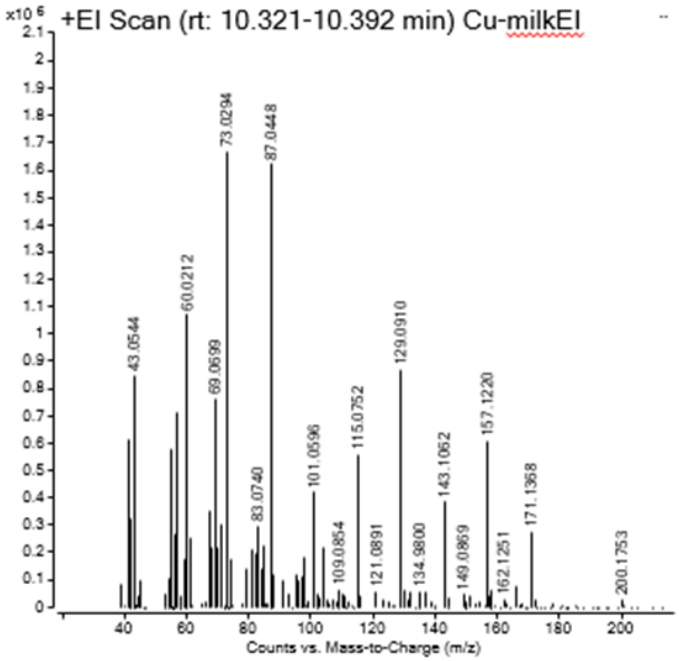

+EI Scan (rt: 8.850-8.918 min) Cu-milkEI.D
Head to Tail MF=724 RMF=855
Indole

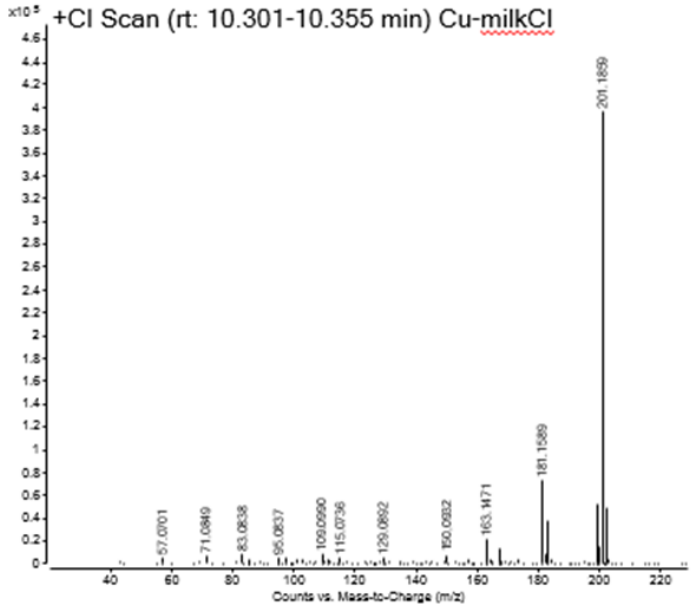

x10 6
+EI Scan (rt: 8.850-8.918 min) Cu-MilkEI
117.0579
89.0391
41.0385
51.0227
57.0701
63.0227
67.0504
72.0449
76.0273
81.0544
85.0628
94.0566
102.0460
112.0716
Counts vs. Mass-to-Charge (m/z)


x10 5
+CI Scan (rt: 8.840-8.904 min)Cu-MilkCI
118.0655
68.0502
95.0572
110.0830
114.0705
Counts vs. Mass-to-Charge (m/z)

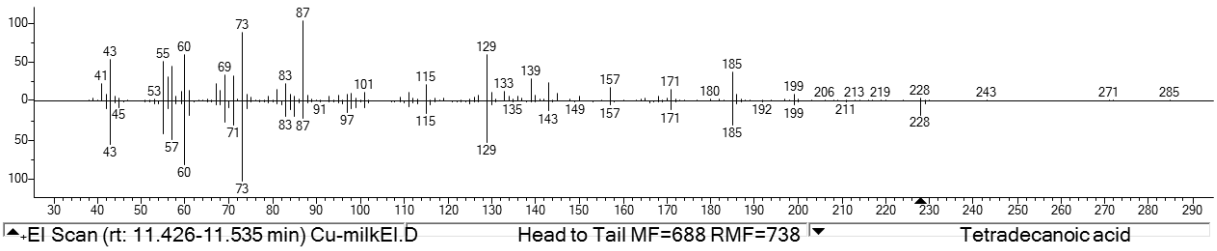
Dodecanoic acid

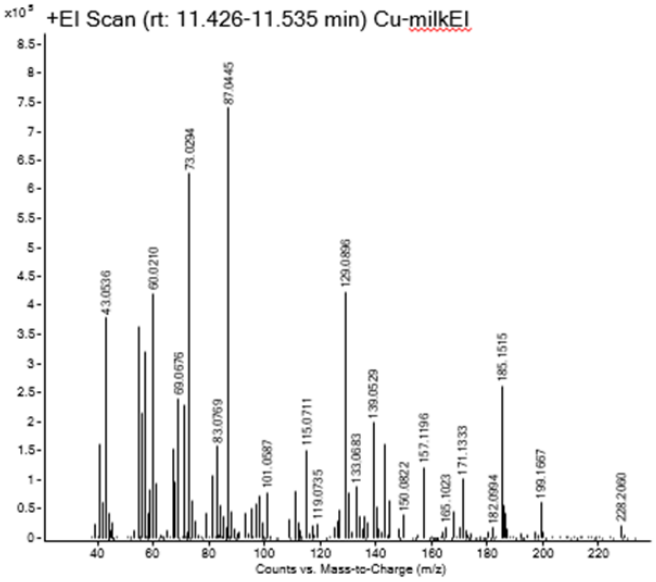


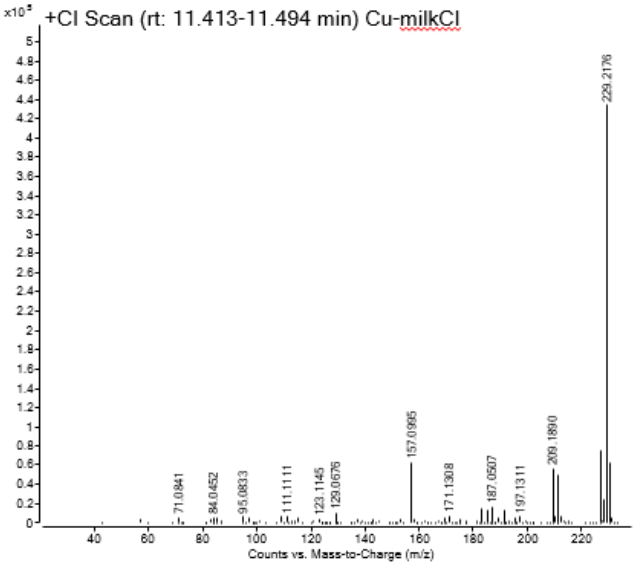




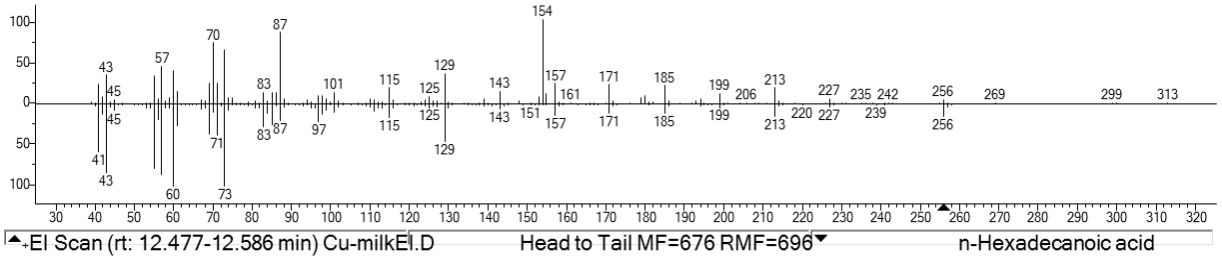
Tetradecanoic acid

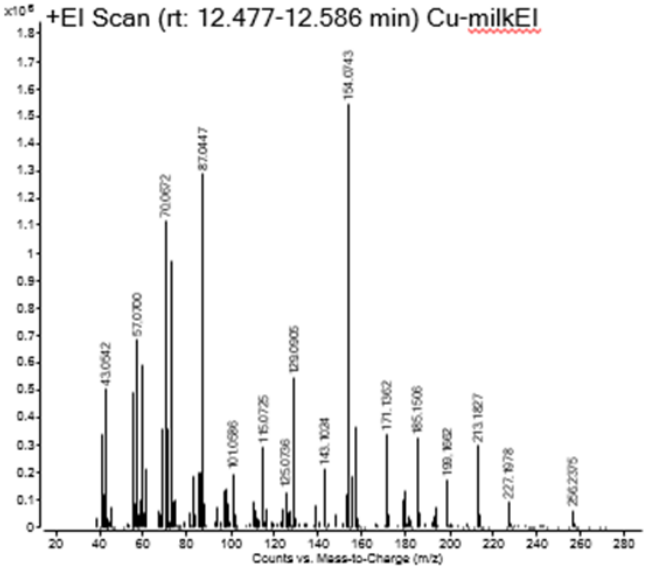


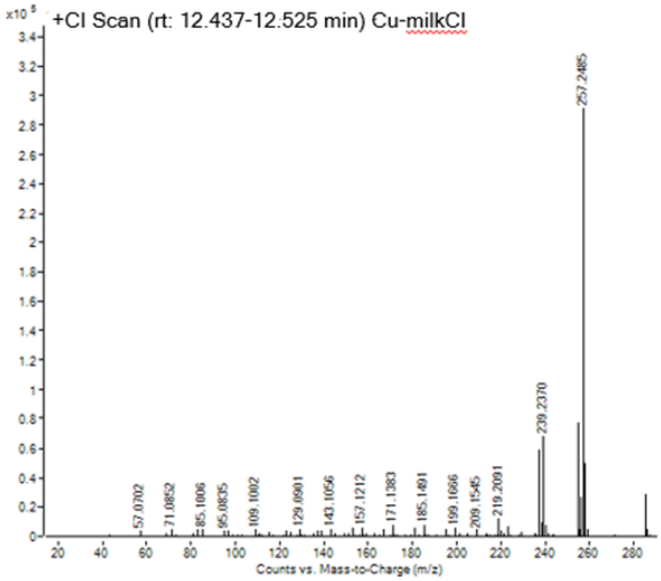




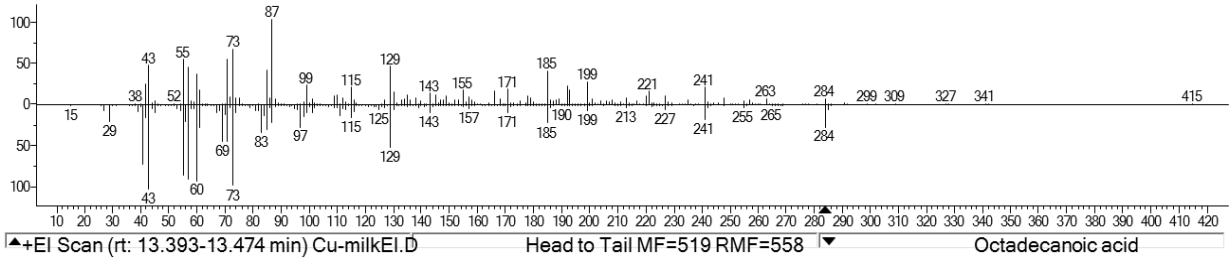
n-Hexadecanoic acid

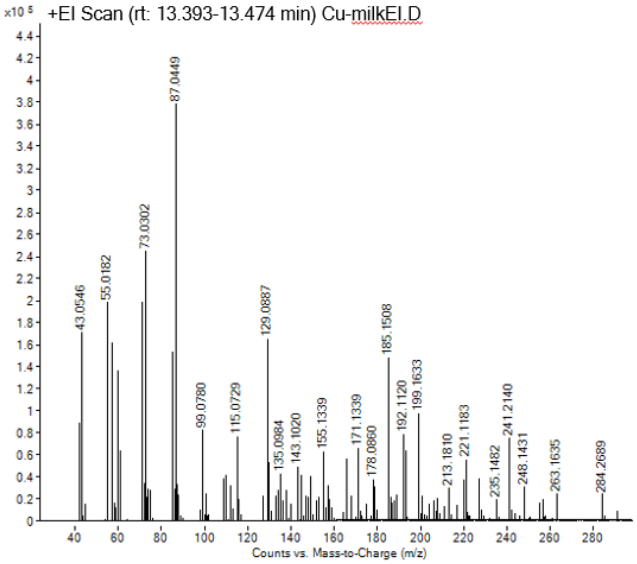


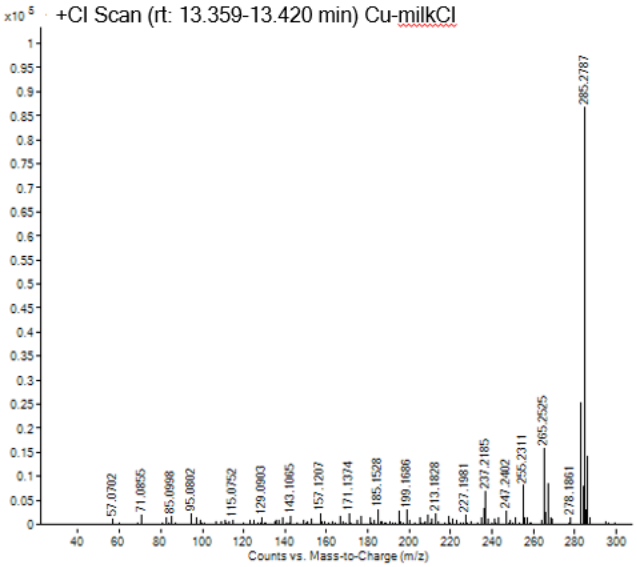




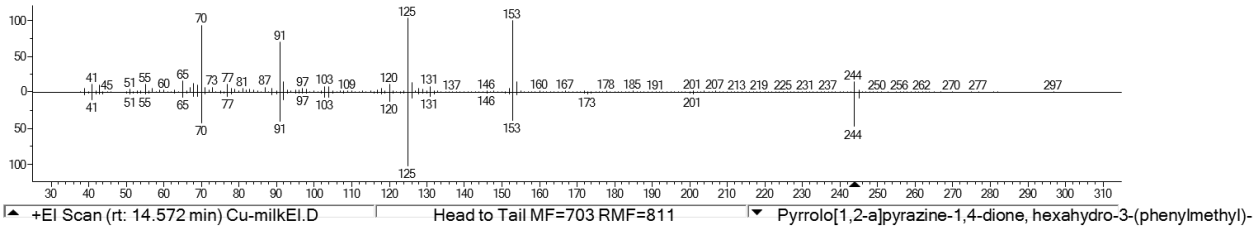
Octadecanoic acid

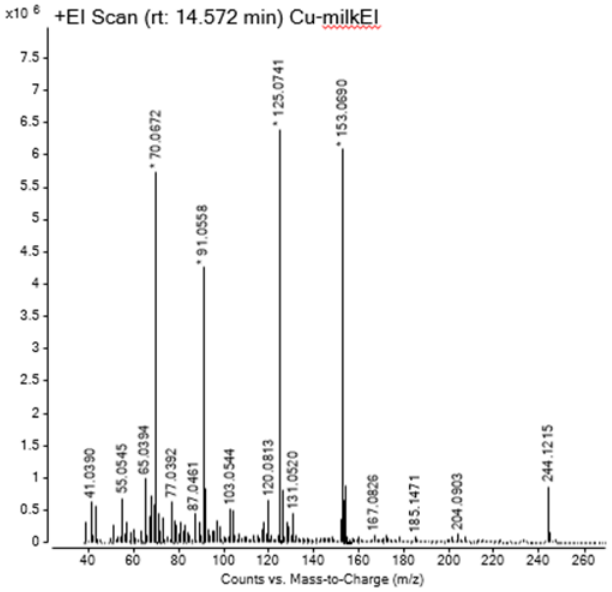


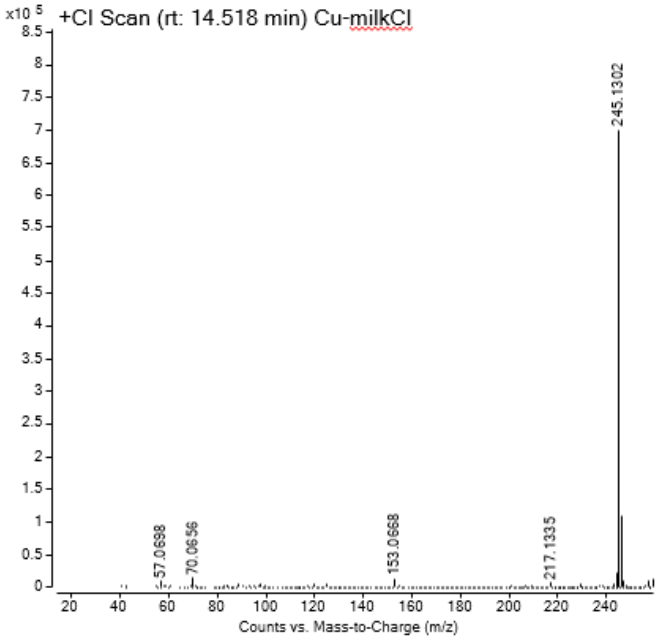




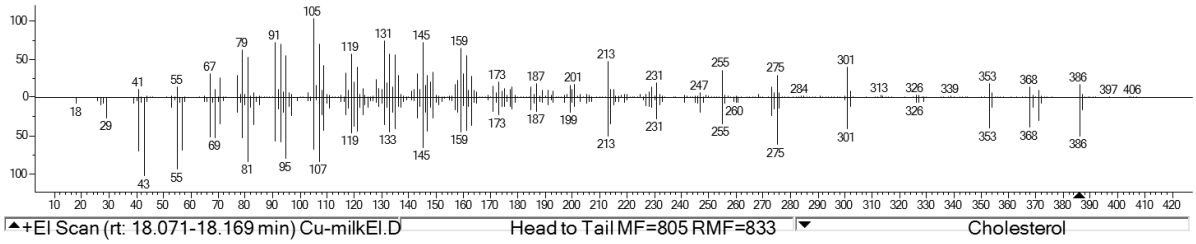
Pyrrolo[1,2-a]pyrazine-1,4-dione, hexahydro-3-(phenylmethyl)-

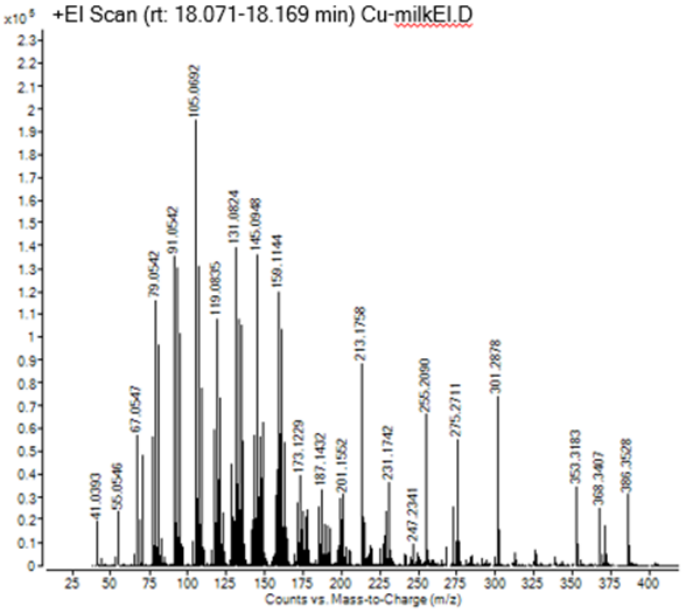


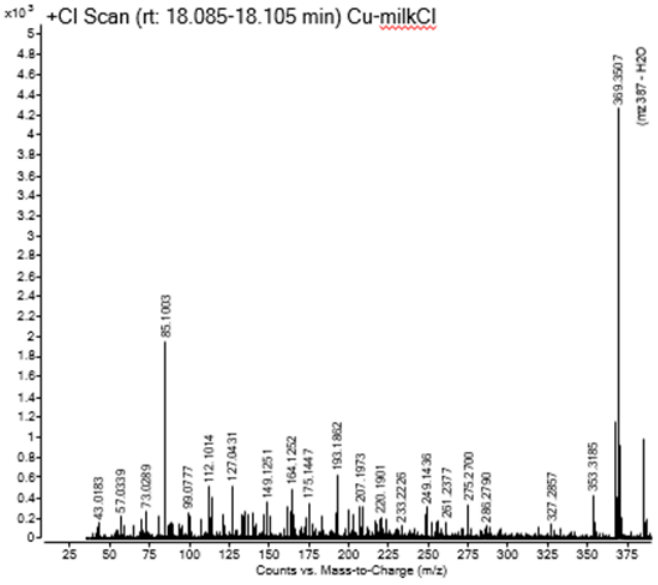




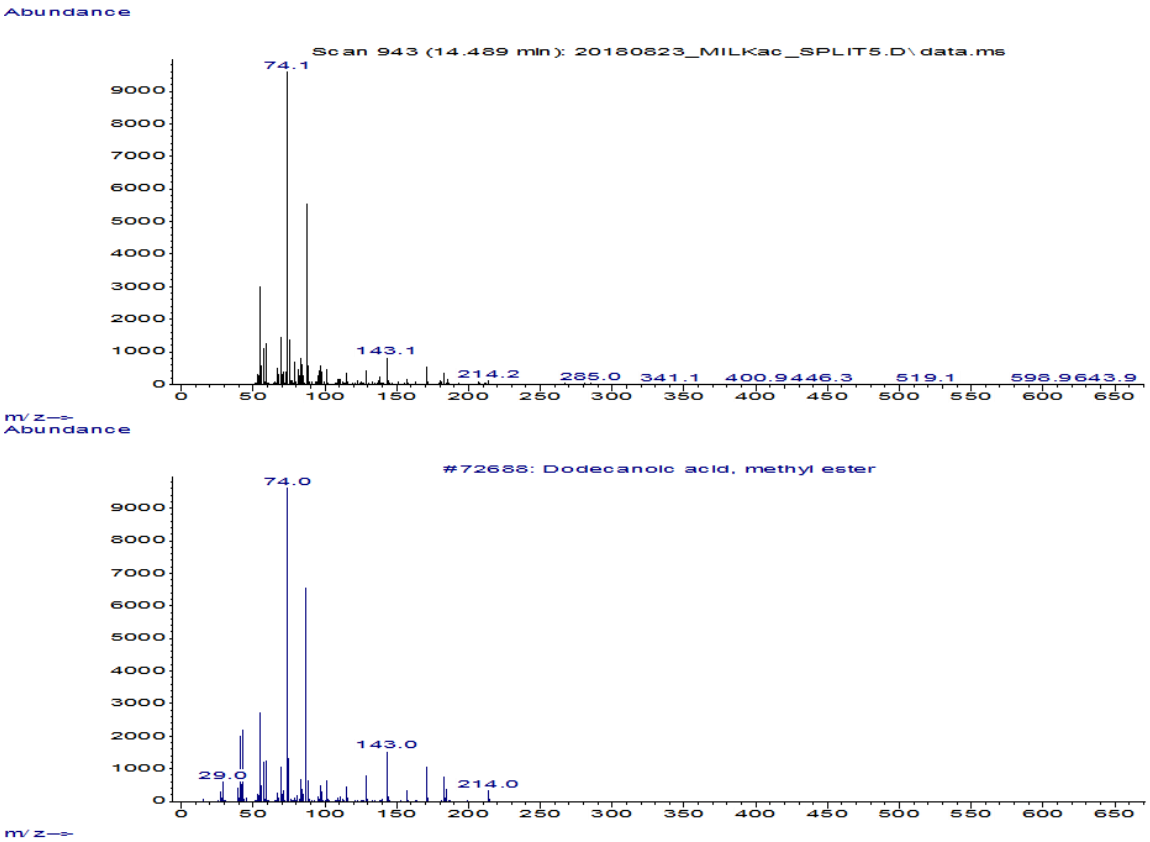
Cholesterol



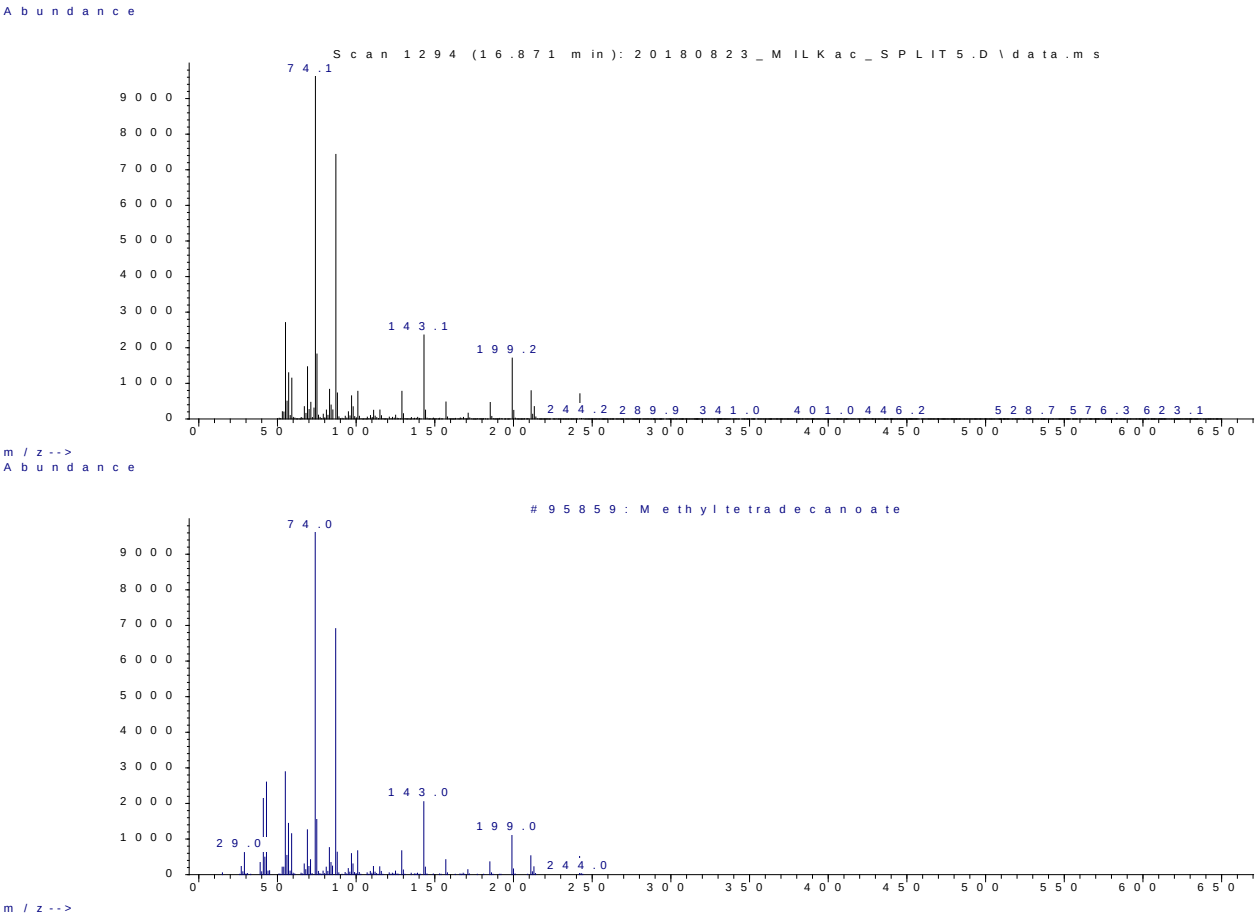




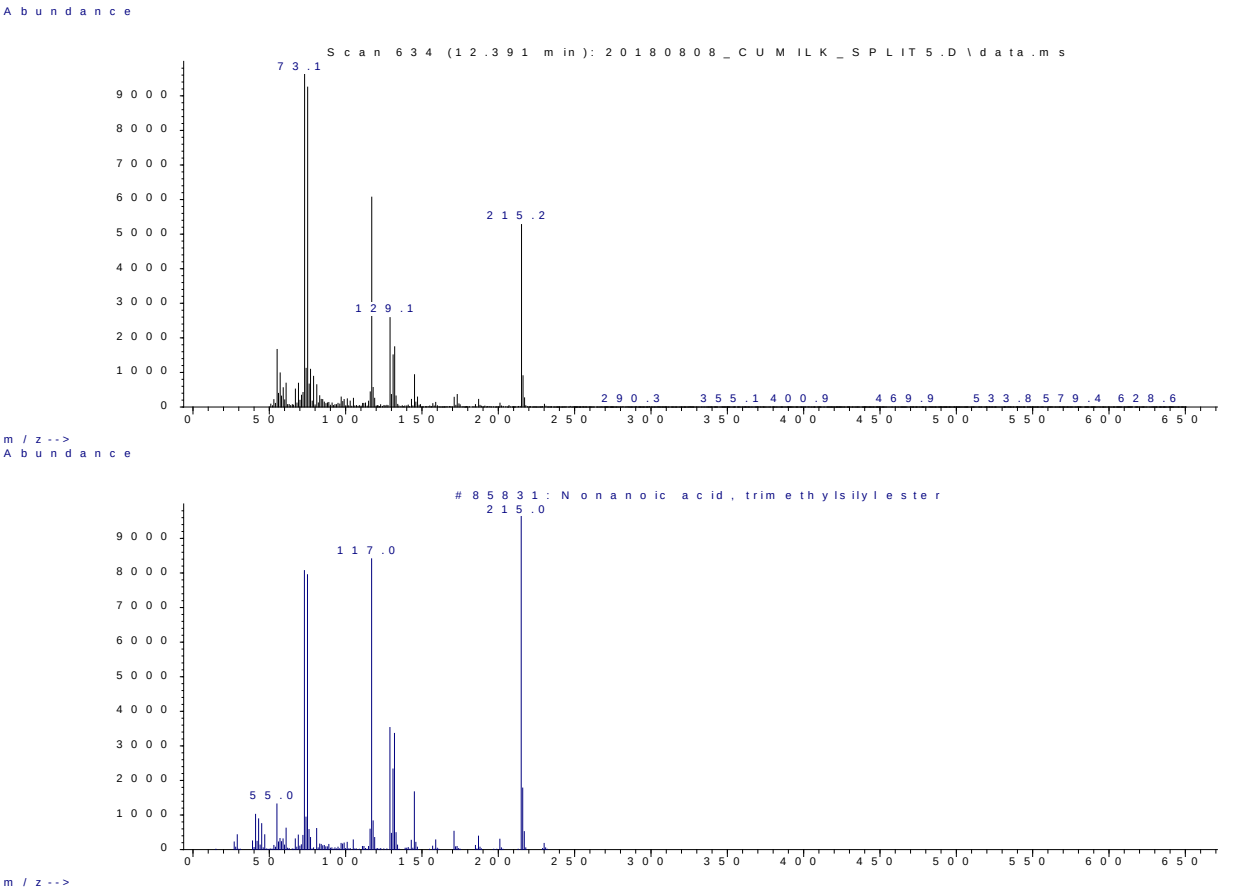
Dodecanoic acid (as methyl ester)



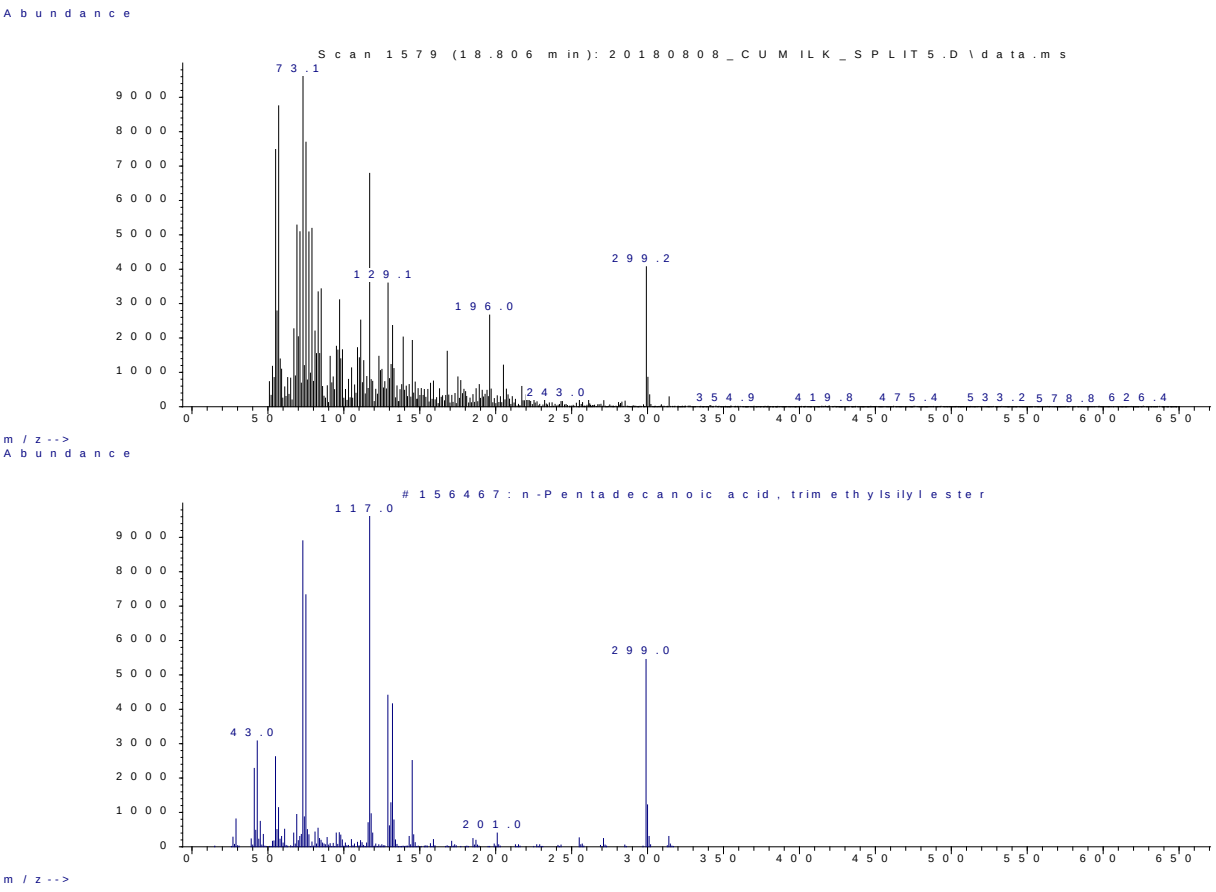
Tetradecanoic acid (as methyl ester)



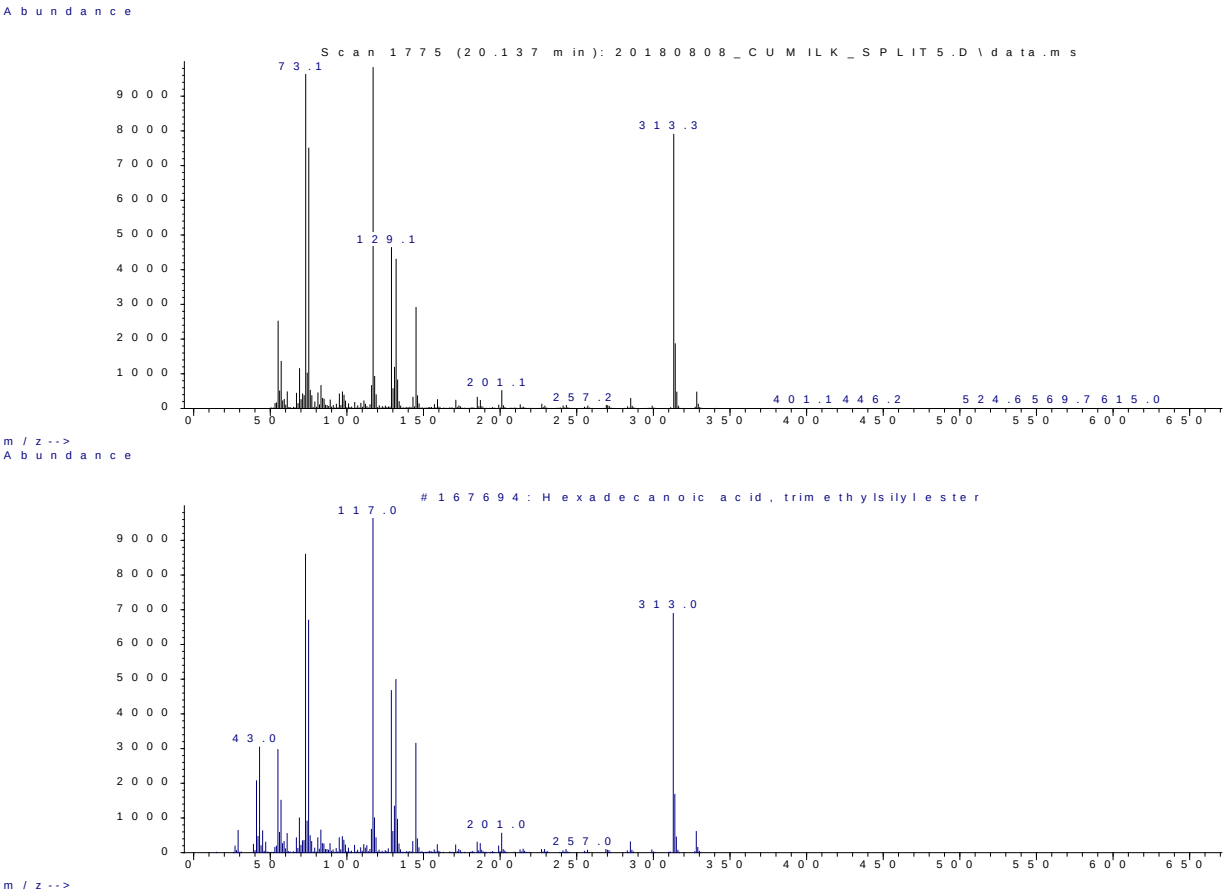
Nonanoic Acid (as a trimethylsilyl ester)



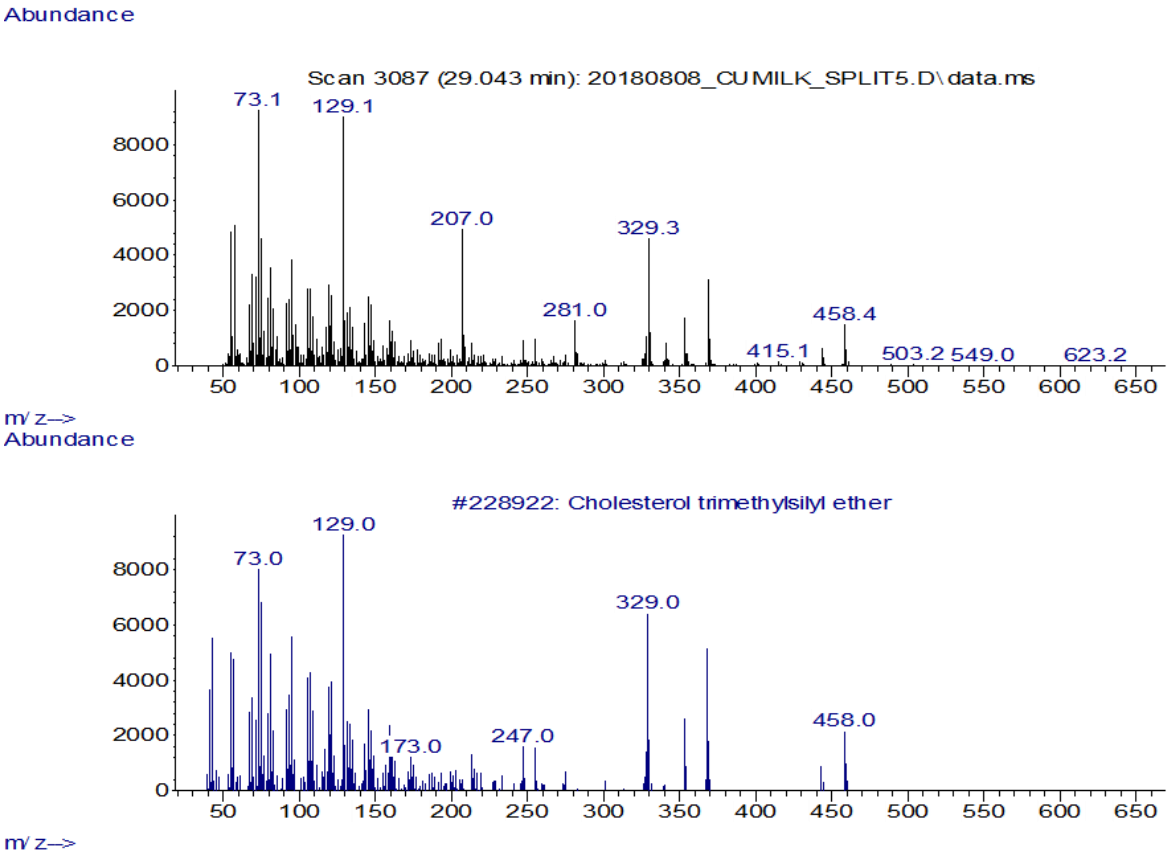
n-Pentadecanoic acid (as a trimethylsilyl ester)



n-Hexadecanoic acid (as a trimethylsilyl ester)



Cholesterol (as a trimethylsilyl ester)



P02662 Peptides	-10lgP	m/z	Peptide intensity	PTM/Score
R.FFVAPFPEVF.G	34.97	600.3105	4.63E+04	
H.QGLPQEVLNEN.L	17.65	620.812	4.79E+04	
L.PQEVLNENLLR.F	26.04	662.8644	7.59E+04	
Y.LGYLEQLLR.L	35.88	552.8245	9.64E+04	
K.VN(+.98)ELSK.D	20.01	345.6868	1.07E+05	N2:Deamidation (NQ):1000.00
N.PIGSENSEK.T	29.31	480.735	1.28E+05	
R.LHSMK.E	19.64	308.1677	1.43E+05	
G.LPQEVLNENLLR.F	39.92	719.4072	1.51E+05	
K.EGIHAQ.Q	19.7	327.6638	1.54E+05	
Q.LDAYPSGAWYYVPLGTQYTDAPSFSDIPNPIGSENSEK.T	32.83	1383.9812	1.70E+05	
F.SDIPNPIGSENSEK.T	54.38	743.854	1.77E+05	
K.HQGLPQEVLNENLL.R	41.32	802.4265	2.61E+05	
W.YYVPLGTQYTDAPSFSDIPNPIGSEN(+.98)SEK.T	51.22	1064.1633	2.72E+05	N26:Deamidation (NQ):33.66
W.YYVPLGTQYTDAPSF.S	31.77	861.4061	2.78E+05	
K.EGIHAQQ.K	22.66	391.6933	2.93E+05	
K.EPMIGVNQELAYFYPELFR.Q	68.37	1158.5737	4.15E+05	
K.EDVPSERYLGYLEQLLR.L	40.79	694.0286	4.18E+05	
K.EPM(+15.99)IGVNQELAYFYPEL.F	38.51	1014.9856	4.18E+05	M3:Oxidation (M):1000.00
Y.QLDAYPSGAW.Y	26.16	554.2587	4.41E+05	
Y.TDAPSFSDIPNPIGSENSEK.T	75.48	1052.9862	5.50E+05	
R.FFVAPFPEVFGKEK.V	34.37	547.9604	5.52E+05	
K.HIQKEDVPSER.Y	42.11	446.5652	5.61E+05	
K.HQ(+.98)GLPQEVLNENLLR.F	52.14	880.9677	6.15E+05	Q2:Deamidation (NQ):28.71
R.QFYQLDAYPSGAWY.Y	18.86	854.8867	6.32E+05	
T.DAPSFSDIPNPIGSENSEK.T	74.96	1002.4637	6.86E+05	
K.HQGLPQEVLNEN.L	50.56	689.3414	7.42E+05	
V.LNENLLR.F	21.54	436.2533	7.65E+05	
F.VAPFPEVFGK.E	18.01	545.7995	7.87E+05	
K.YKVPQLEIVPN.S	43.02	650.369	8.89E+05	
M.IGVNQELAYFYPEL.F	20.7	828.4199	9.73E+05	
K.EKVNELSK.D	33.95	473.7632	1.16E+06	
D.IPNPIGSENSEK.T	58.82	642.8255	1.29E+06	
H.SM(+15.99)KEGIHAQQ(+.98)KEPM(+15.99)IGVNQELAYFYPELFR.Q	15.74	1196.2432	1.29E+06	M2:Oxidation (M):1000.00;Q10:Deamidation (NQ):8.69;M14:Oxidation (M):1000.00
Y.QLDAYPSGAWYYVPLGTQYTDAPSFSDIPNPIGSENSEK.T	21.09	1070.2488	1.30E+06	
Y.FYPELFR.Q	18.94	486.2534	1.46E+06	
R.QFYQLDAYPSGAW.Y	25.92	773.3541	1.64E+06	
L.GTQYTDAPSFSDIPNPIGSENSEK.T	72.77	1277.5836	1.91E+06	
Q.GLPQEVLNENLLR.F	48.54	747.9175	1.94E+06	
E.GIHAQQK.E	22.77	391.2192	1.95E+06	
I.HAQQK.E	15.56	306.1671	2.24E+06	
A.YFYPELFR.Q	30.95	567.7846	2.34E+06	
Q.YTDAPSFSDIPNPIGSENSEK.T	81.06	1134.5183	2.87E+06	
D.APSFSDIPNPIGSENSEK.T	61.37	944.9503	3.82E+06	
K.YKVPQLEIVPNSAEER.L	62.47	936.4971	4.43E+06	
F.FVAPFPEVFGK.E	43.43	619.3343	4.44E+06	
L.AYFYPELFR.Q	37.16	603.303	6.50E+06	
K.VPQLEIVPNSAEER.L	57.22	790.9176	7.84E+06	
L.DAYPSGAWYYVPLGTQYTDAPSFSDIPNPIGSENSEK.T	43.99	1009.9672	1.19E+07	
K.EGIHAQQK.E	38.57	455.7403	1.22E+07	
R.QFYQLDAYPSGAWYYVPLGTQYTDAPSFSDIPNPIGSENSEK.T	38.96	1179.8	1.34E+07	

P02662 Peptides	-10lgP	m/z	Peptide intensity	PTM/Score
H.QGLPQEVLNENLLR.F	59.93	811.9465	1.70E+07	
Y.YVPLGTQYTDAPSFSDIPNPIGSENSEK.T	57.25	1009.4813	2.43E+07	
K.VNELSK.D	35.71	345.1949	4.85E+07	
K.EPM(+15.99)IGVNQELAYFYPELFR.Q	61.84	1166.5708	5.05E+07	M3:Oxidation (M):1000.00
W.YYVPLGTQYTDAPSFSDIPNPIGSENSEK.T	60.91	1063.8369	1.30E+08	
K.EDVPSER.Y	25.04	416.1958	1.47E+08	
M.IGVNQELAYFYPELFR.Q	54.9	980.0049	2.02E+08	
R.FFVAPFPEVFGK.E	47.75	692.8689	2.62E+08	
K.HQGLPQEVLNENLLR.F	74.61	880.4767	2.75E+08	
R.YLGYLEQLLR.L	46.68	634.3559	2.75E+08	

P02663 Peptides	-10lgP	m/z	Peptide intensity	PTM/Score
N.LC(+57.02)STFC(+57.02)K.E	18.88	458.2065	4.18E+04	C2:Carbamidomethylation:1000.00;C 6:Carbamidomethylation:1000.00
T.KLTEEEK.N	20.62	438.7371	5.39E+04	
K.NRLNFLKK.I	26.28	344.8813	8.51E+04	
N.M(+15.99)AINPSK.E	20.9	388.7021	9.03E+04	M1:Oxidation (M):1000.00
M.KPWIQPK.T	26.24	448.7712	9.69E+04	
K.TVYQHQ.K	16.11	388.1903	1.07E+05	
K.NMAINPSK.E	22.35	437.7266	1.30E+05	
K.NRLNFLK.K	24.85	452.7718	1.31E+05	
E.VATEEVK.I	20.55	388.2133	1.42E+05	
L.NEINQFYQK.F	31.18	592.2908	1.50E+05	
K.TKLTEEEK.N	40.05	489.2612	1.54E+05	
L.C(+57.02)STFC(+57.02)K.E	27.5	401.6646	1.59E+05	C1:Carbamidomethylation:1000.00;C 5:Carbamidomethylation:1000.00
Y.QGPIVLNPWDQVK.R	50.78	747.4099	2.08E+05	
K.FPQYLQYL.Y	20.91	536.2791	2.08E+05	
N.EINQFYQK.F	23.29	535.2687	2.16E+05	
R.EQLSTSEENSK.K	33.04	626.2887	2.39E+05	
K.FPQYLQY.L	20.57	479.7373	2.91E+05	
V.PITPTLNR.E	17.99	456.2692	3.10E+05	
K.ALNEIN(+.98)QFYQK.F	53.35	684.8431	3.55E+05	N6:Deamidation (NQ):12.28
Q.YLQYLYQGPIVLNPWDQVK.R	46.69	1169.1157	5.72E+05	
K.ITVDDKHYQK.A	43.11	623.8244	7.37E+05	
L.PQYLK.T	25.98	324.6894	7.38E+05	
K.TVYQH.Q	22.82	324.1611	9.17E+05	
K.LTEEEKNR.L	28.18	509.7616	1.32E+06	
K.VIPYVR.Y	15	373.7314	1.68E+06	
V.YQHQK.A	26.48	352.1798	1.82E+06	
F.ALPQYLK.T	22.75	416.7501	3.11E+06	
Q.YLYQGPIVLNPWDQVK.R	63.65	967.0133	5.58E+06	
K.RNAVPITPTLNR.E	44.06	676.3936	6.10E+06	
K.PWIQPK.T	30.98	384.7236	6.94E+06	
K.AM(+15.99)KPWIQPK.T	41.74	557.8079	8.75E+06	M2:Oxidation (M):1000.00
K.NM(+15.99)AINPSK.E	37.78	445.7239	9.72E+06	M2:Oxidation (M):1000.00
Y.LYQGPIVLNPWDQVK.R	61.33	885.483	1.17E+07	
K.TVYQHQK.A	43.76	452.2379	1.70E+07	
R.N(+.98)AVPITPTLNR.E	26.4	598.8353	1.76E+07	N1:Deamidation (NQ):140.79
K.LTEEEK.N	31.23	374.6897	2.08E+07	
L.YQGPIVLNPWDQVK.R	58.08	828.9417	2.10E+07	
K.FPQYLQYLYQGPIVLNPWDQVK.R	73.65	1355.2081	2.22E+07	
K.ITVDDK.H	31.79	345.6871	2.92E+07	
K.ENLC(+57.02)STFC(+57.02)K.E	44.57	579.7493	2.99E+07	C4:Carbamidomethylation:1000.00;C 8:Carbamidomethylation:1000.00

P02663 Peptides	-10lgP	m/z	Peptide intensity	PTM/Score
K.FALPQYLK.T	40.06	490.284	7.00E+07	
K.ALNEINQFYQK.F	61.79	684.3513	1.19E+08	
N.LC(+57.02)STFC(+57.02)K.E	48.99	667.12022	3.34E+07	C2:Carbamidomethylation:1000.00;C 6:Carbamidomethylation:1000.01

P02666 Peptides	-10lgP	m/z	Peptide intensity	PTM/Score
K.IHPFAQTQS.L	23.01	514.7617	3.67E+04	
E.EQQQTEDELQDK.I	46.52	745.8336	4.98E+04	
K.YPVEPFTESQSLTLTDVEN(+.98)LHLPLPLLQSWMHQ(+.98)PHQPLPPTVM(+15.99)FPPQSVLSLSQSK.V	18.83	1276.2606	5.76E+04	N19:Deamidation (NQ):0.00;Q33:Deamidation (NQ):0.00;M43:Oxidation (M):8.44
N.LHLPLPLLQSW.M	15.96	658.8892	7.36E+04	
L.LYQ(+.98)EPVLGPVRGPFPIIV	26.59	998.0566	9.23E+04	Q3:Deamidation (NQ):1000.00
S.QSLTLTDVENLHLPLPLLQ.S	32.89	1072.6017	1.22E+05	
Q.RDMPIQ(+.98)AFLLYQEPVLGPVR.G	27.1	781.7435	1.46E+05	Q6:Deamidation (NQ):113.99
V.LSLSQSK.V	18.14	381.7215	1.57E+05	
N.SLPQNIPPLTQTPVVVPPF.L	24.04	1022.5768	1.62E+05	
Q.AFLLYQEPVLGPVRG.P	20.97	829.9667	2.01E+05	
K.YPVEPFTESQ.S	16.74	598.7771	2.18E+05	
K.IHPFAQTQSL.V	35.39	571.3033	2.34E+05	
K.IHPFAQT.Q	18.23	407.2159	2.63E+05	
S.QSLTLTDVENLHLPLPL.L	56.3	952.0312	2.72E+05	
Q.KAVPYPQR.D	19.17	479.777	4.03E+05	
N.SLPQNIPPLTQTPVVVPPFLQPE.V	42.48	837.8005	4.13E+05	
R.DMPIQAFLL.Y	23.29	524.2805	5.12E+05	
A.VPYPQR.D	17.39	380.2112	5.13E+05	
K.HKEM(+15.99)PFPK.Y	26.91	515.2632	5.24E+05	M4:Oxidation (M):1000.00
K.YPVEPFTESQSLTLTDVEN(+.98)LHLPLPLL.Q	16.74	1533.7902	5.33E+05	N19:Deamidation (NQ):64.02
S.VLSLSQSK.V	27.9	431.2554	5.66E+05	
R.DMPIQAFLLYQEPVLGPVRG.P	35.36	1122.0995	6.54E+05	
L.TLTDVENLHLPLPL.L	37.6	787.9433	6.84E+05	
K.YPVEPFTESQSLTLTDVENLHLPLPLLQ.S	34.9	1597.34	6.97E+05	
Q.SLTLTDVENLHLPLPL.L	56.09	888.0014	8.32E+05	
P.NSLPQNIPPLTQTPVVVPPFLQPEVM(+15.99)GVSK.V	18.27	1081.5865	8.42E+05	M26:Oxidation (M):1000.00
F.LLYQEPVLGPVRGPFPIIV	46.81	1054.1195	8.46E+05	
L.VYPFPGPIPN.S	39.08	550.7924	8.77E+05	
K.YPVEPFTESQSL.T	37.84	698.8346	9.73E+05	
K.IHPFAQ.T	20.76	356.6925	1.33E+06	
R.GPFPIIV	18.35	371.7285	1.54E+06	
K.YPVEPFTESQSLTLTDVENLHLPLPLLQSW.M	57.19	1156.2653	2.03E+06	
M.PIQAFLLYQEPVLGPVRG.P	37.15	999.0641	2.05E+06	
K.VLPVPQKAVPYPQR.D	44.58	796.4692	2.10E+06	
Q.SLVYPFPGPIPN.S	43.42	650.8506	2.28E+06	
Q.AFLLYQEPVLGPVR.G	53.94	801.4566	2.72E+06	
Y.QEPVLGPVR.G	26.22	497.7874	2.96E+06	
K.YPVEPFTESQSLTLTDVENLHLPLPLLQSWM(+15.99)HQPHQPLPPTVMFPPQSVLSLSQSK.V	27.73	1275.855	3.09E+06	M31:Oxidation (M):20.93
N.SLPQNIPPLTQTPVVVPPFLQ(+.98)PEVMGVSKV.K	21.91	1606.8774	3.18E+06	Q21:Deamidation (NQ):100.45
F.TESQSLTLTDVENLHLPLPL.L	54.05	1110.5919	3.49E+06	
M.FPPQSVLSLSQSK.V	46.06	709.3872	3.69E+06	
Q.TQSLVYPFPGPIPN.S	43.33	765.4036	3.87E+06	
K.FQSEEQQQTEDELQDK.I	71.96	991.4354	4.44E+06	
L.YQEPVLGPVRGPFPIIV	55.78	941.0349	7.21E+06	
K.IHPFAQTQ.S	30.4	471.2455	9.82E+06	
R.DMPIQAFLLYQEPVLGPVR.G	59.44	1093.5875	1.06E+07	

P02668 Peptides	-10lgP	m/z	Peptide intensity	PTM/Score
Y.YAKPAAVR.S	19.34	292.5083	2.18E+04	
R.HPHPHLS.F	16.37	412.7112	7.24E+04	
R.FFSDKIAK.Y	28.51	478.2658	8.47E+04	
E.QNQEQPIR.C	15.71	506.7621	9.50E+04	
K.YIPIQYVL.S	28.18	504.7919	1.03E+05	
L.NYYQQK.P	19.52	422.2034	1.21E+05	
R.SPAQILQWQVLSN(+.98)TVPAK.S	73.65	991.0401	1.24E+05	N13:Deamidation (NQ):111.84
S.C(+57.02)QAQPTTM(+15.99)AR.H	21.07	590.2659	1.37E+05	C1:Carbamidomethylation:1000.00;M 8:Oxidation (M):1000.00
K.DERFFSDK.I	16.82	522.2431	1.64E+05	
P.SYGLNYYQQK.P	52.99	632.304	2.20E+05	
L.QWQVLSNTVPAK.S	37.24	685.8752	3.21E+05	
K.PVALIN(+.98)NQFLPYPYYAK.P	51.35	1006.53	3.29E+05	N6:Deamidation (NQ):30.46
Q.WQVLSNTVPAK.S	21.49	621.8457	3.36E+05	
N.QFLPYPYYAK.P	24.31	645.3318	3.44E+05	
F.M(+15.99)AIPPK.K	19.11	336.691	3.72E+05	M1:Oxidation (M):1000.00
A.QEQNQEQPIR.C	30.32	635.3125	4.79E+05	
A.LINNQFLPYPYYAK.P	50.92	872.4594	4.95E+05	
N.YYQQKPVALINNQFLPYPY.Y	41.27	1180.1075	5.70E+05	
N.YYQQKPVAL.I	24.1	555.3027	5.83E+05	
R.YPSYGLNY.Y	30.34	488.7243	6.13E+05	
Q.VLSNTVPAK.S	35.9	464.7766	6.14E+05	
R.YPSYGLNYY.Q	33.45	570.2557	7.45E+05	
Q.NQEQPIR.C	24.69	442.7326	7.72E+05	
L.INNQFLPYPY.Y	23.34	634.8193	9.51E+05	
R.HPHPHLSFMAIPPK.K	46.83	536.9542	1.26E+06	
H.LSFM(+15.99)AIPPK.K	35	510.2832	1.26E+06	M4:Oxidation (M):1000.00
V.ALINNQFLPYPY.Y	28.4	726.8803	1.26E+06	
K.YIPIQY.V	24.63	398.7156	1.37E+06	
C.QAQPTTM(+15.99)AR.H	19.12	510.2507	1.40E+06	M7:Oxidation (M):1000.00
R.YPSYGLNYYQQKPV.A	57.6	860.4228	1.42E+06	
L.SNTVPAK.S	34.99	358.7004	1.45E+06	
Q.ILQWQVLSNTVPAK.S	58.09	798.9588	1.46E+06	
Y.YQQKPVAL.I	23.32	473.7716	1.49E+06	
S.YGLNYYQQKPVALINNQFLPYPY.Y	29.96	1403.7164	1.53E+06	
R.SPAQILQW.Q	17.25	471.756	1.57E+06	
N.YYQQK.P	19.24	365.1816	1.62E+06	
N.YYQQKPVALINNQFLPYPYYAK.P	51.86	907.8071	1.90E+06	
R.YPSYGLNYYQQKPVALINNQFLPYPY.Y	48.25	1051.865	2.14E+06	
R.HPHPHLSFM(+15.99)AIPPK.K	44.22	542.2852	2.35E+06	M9:Oxidation (M):1000.00
K.SC(+57.02)QAQPTTMAR.H	52.71	625.7845	2.40E+06	C2:Carbamidomethylation:1000.00
R.SPAQILQWQVLSN.T	29.64	742.3992	2.53E+06	
Y.QQKPVALINNQFLPYPY.Y	37.58	1017.047	3.05E+06	
R.SPAQILQWQVL.S	28.14	641.8619	3.25E+06	
S.YGLNYYQQK.P	55.14	588.7879	3.82E+06	
Y.YQQKPVALINNQFLPYPY.Y	41.9	1098.5789	4.71E+06	
A.QILQWQVLSNTVPAK.S	63.32	862.9888	6.07E+06	
V.ALINNQFLPYPYYAK.P	65.71	907.978	6.28E+06	
R.YPSYGLNYYQQKPVAL.I	52.36	952.4835	6.37E+06	
R.HPHPHLSF.M	28.16	486.2458	7.93E+06	
R.YPSYGLNYYQQKPVALINNQFLPYPYYAK.P	47.17	1172.5939	1.08E+07	
K.PVALINNQFLPYPY.Y	50.04	824.9409	1.14E+07	
W.QVLSNTVPAK.S	34.92	528.8059	1.18E+07	
S.YGLNYYQQKPVALINNQFLPYPYYAK.P	44.36	1056.8777	1.54E+07	
Y.QQKPVALINNQFLPYPYYAK.P	47.28	1198.1442	1.76E+07	
Y.YQQKPVALINNQFLPYPYYAK.P	59.5	1279.6766	1.98E+07	
L.INNQFLPYPYYAK.P	50.15	815.9167	2.49E+07	
K.PVALINNQFLPYPYYAK.P	70.08	1006.0389	2.82E+07	

P02668 Peptides	-10lgP	m/z	Peptide intensity	PTM/Score
R.FFSDK.I	20.13	322.158	2.88E+07	
K.YIPIQYVLSR.Y	43.68	626.3589	3.49E+07	
R.YPSYGLNYYQQK.P	55.86	762.3621	3.75E+07	
K.SC(+57.02)QAQPTTM(+15.99)AR.H	48.11	633.7822	7.80E+07	C2:Carbamidomethylation:1000.00;M 9:Oxidation (M):1000.00
R.SPAQILQWQVLSNTVPAK.S	75.99	990.5496	1.82E+08	

P02662 Peptides	-10lgP	m/z	Peptide intensity	PTM/Score
K.KYKVPQLEIVPNSAEER.L	19.6	667.3655	3.57E+03	
I.KHQGLPQEVLNENLLR.F	27.86	630.0189	1.01E+04	
P.SFSDIPNPIGSENSEK.T	34.27	860.9064	1.08E+04	
K.EGIHAQ(+.98)QK.E	24.7	456.2332	1.32E+04	Q6:Deamidation (NQ):12.79
P.NPIGSENSEK.T	33.37	537.7574	1.44E+04	
I.PNPIGSENSEK.T	27.84	586.2831	1.76E+04	
A.YFYPELFR.Q	24.36	567.785	2.15E+04	
V.APFPEVFGK.E	33.66	496.2665	2.52E+04	
M.KEGIHAQQK.E	16.45	346.8612	2.65E+04	
K.YKVPQLEIVPN.S	19.54	650.3694	2.70E+04	
W.YYVPLGTQYTDAPSF.S	15.78	861.406	3.65E+04	
L.GTQYTDAPSFSDIPNPIGSENSEK.T	43.21	1277.585	4.08E+04	
H.IQKEDVPSER.Y	24.35	600.8151	5.35E+04	
K.HIQ(+.98)KEDVPSER.Y	32.29	669.8364	5.37E+04	Q3:Deamidation (NQ):1000.00
D.IPNPIGSENSEK.T	30.42	642.826	5.94E+04	
Q.KEDVPSER.Y	15.16	480.2432	7.22E+04	
T.DAPSFSDIPNPIGSENSEK.T	73.46	1002.4623	7.68E+04	
F.VAPFPEVFGK.E	25.26	545.8005	7.91E+04	
Y.TDAPSFSDIPNPIGSENSEK.T	45.26	1052.988	8.18E+04	
K.VPQLEIVPNSAEER.L	44.5	949.1118	8.61E+04	
P.KHPIK.H	18.17	790.9175	9.60E+04	
G.LPQEVLNENLLR.F	36.52	311.7057	1.08E+05	
K.VN(+.98)ELSK.D	20.42	719.4069	1.11E+05	
K.YKVPQLEIVPNSAEER.L	44.3	345.6872	1.35E+05	N2:Deamidation (NQ):1000.00
H.AQQKEPM(+15.99)IGVNQELAYFYPELFR.Q	25.58	624.6675	1.36E+05	
D.APSFSDIPNPIGSENSEK.T	42.82	929.7996	1.59E+05	M7:Oxidation (M):1000.00
L.AYFYPELFR.Q	28.89	944.9513	1.82E+05	
R.PKHPIK.H	17.82	603.3034	2.06E+05	
K.HQGLPQEVLNEN.L	52.27	240.4907	2.40E+05	
L.GYLEQLLR.L	21.9	689.3415	2.73E+05	
L.PQEVLNENLLR.F	30.06	496.2825	2.77E+05	
E.GIHAQQKEPM(+15.99)IGVNQELAYFYPELFR.Q	15.46	662.8648	2.91E+05	
K.EGIHAQQKEPM(+15.99)IGVNQELAYFYPELFR.Q	23.75	774.3928	3.14E+05	M10:Oxidation (M):1000.00
K.HQGLPQEVLNENLL.R	42.69	806.653	3.27E+05	M11:Oxidation (M):1000.00
Y.LGYLEQLLR.L	29.57	802.4261	3.35E+05	
H.QGLPQEVLNENLLR.F	57.07	552.8246	4.47E+05	
R.QFYQLDAYPSGAW.Y	20.56	811.9474	4.85E+05	
Q.YTDAPSFSDIPNPIGSENSEK.T	47.58	773.3543	6.10E+05	
K.EPM(+15.99)IGVNQELAYFYPELFR.Q	45.72	1134.5208	7.65E+05	
F.FVAPFPEVFGK.E	37.01	1166.5701	8.74E+05	M3:Oxidation (M):1000.00
E.GIHAQQK.E	17.95	619.3346	9.65E+05	
Q.GLPQEVLNENLLR.F	49.64	391.2193	1.02E+06	
Y.YVPLGTQYTDAPSFSDIPNPIGSENSEK.T	55.1	747.918	1.18E+06	
K.HQGLPQEVLNEN(+.98)LLR.F	46.32	1009.481	1.27E+06	
K.EKVNELSK.D	33.14	880.9686	1.33E+06	N12:Deamidation (NQ):51.51
K.HIQKEDVPSER.Y	46.05	473.7638	1.46E+06	
K.EGIHAQQK.E	41.69	446.5652	1.69E+06	
K.HQGLPQEVLN(+.98)ENLLR.F	16.98	455.7404	1.79E+06	
A.RPKHPIK.H	22.09	587.6479	2.41E+06	N10:Deamidation (NQ):0.00
K.VNELSK.D	35.69	292.5244	3.82E+06	
R.YLGYLEQLLR.L	47.04	345.195	1.02E+07	
K.EDVPSER.Y	17.99	634.3561	1.11E+07	
W.YYVPLGTQYTDAPSFSDIPNPIGSENSEK.T	40.59	416.1959	1.15E+07	
R.FFVAPFPEVFGK.E	39.65	1063.8356	1.38E+07	
K.HQGLPQEVLNENLLR.F	77.99	692.8677	1.75E+07	

P02663 Peptides	-10lgP	m/z	Peptide intensity	PTM/Score
T.KLTEEEK.N	16.06	438.7378	5.74E+03	
K.LTEEEKN(+.98)R.L	20.39	510.2547	8.25E+03	N7:Deamidation (NQ):1000.00
K.FALPQ(+.98)YLK.T	20.01	490.7764	1.66E+04	Q5:Deamidation (NQ):1000.00
R.YQKFALPQYLK.T	18.71	466.931	1.85E+04	
K.ENLC(+57.02)STFC(+57.02)K.E	36.45	579.7497	1.86E+04	C4:Carbamidomethylation:1000.00;C8:Carbamidomethylation:1000.00
K.TKLTEEEKNR.L	34.33	624.3332	1.86E+04	
Y.LYQGPIVLNPWDQVK.R	40.25	885.4843	2.46E+04	
V.PITPTLNR.E	15.56	456.2694	3.15E+04	
N.AVPITPTLNR.E	16.44	541.3222	3.52E+04	
L.PQYLK.T	18.3	324.6897	3.79E+04	
E.VATEEVK.I	20.17	388.2137	4.95E+04	
K.ITVDDKHYQ(+.98)K.A	25.43	624.317	5.02E+04	Q9:Deamidation (NQ):1000.00
K.LTEEEKNR.L	26.97	509.7617	1.01E+05	
K.ISQRYQK.F	26.93	461.7592	1.17E+05	
K.ALNEINQFYQ(+.98)K.F	56.4	684.8428	1.31E+05	Q10:Deamidation (NQ):91.37
K.ALNEIN(+.98)QFYQK.F	29.1	684.8432	1.46E+05	N6:Deamidation (NQ):14.02
K.NRLNFLKK.I	24.17	344.8822	2.77E+05	
L.YQGPIVLNPWDQVK.R	39.72	828.9408	4.32E+05	
K.AM(+15.99)KPWIQPK.T	31.33	557.8079	5.18E+05	M2:Oxidation (M):1000.00
K.NM(+15.99)AINPSK.E	37.86	445.7237	5.59E+05	M2:Oxidation (M):1000.00
K.ITVDDK.H	34.55	345.6871	8.36E+05	
K.TKLTEEEK.N	34.18	489.2613	1.56E+06	
R.NAVPITPTLNR.E	21.01	598.3436	1.69E+06	
K.ALNEINQFYQK.F	62.1	684.3516	2.85E+06	
K.FALPQYLK.T	42.29	490.2844	2.89E+06	
K.TVYQHQK.A	30.05	452.238	4.45E+06	
K.ITVDDKHYQK.A	50.11	623.8254	5.35E+06	
K.LTEEEK.N	32.63	374.6898	6.49E+06	

P02666 Peptides	-10lgP	m/z	Peptide intensity	PTM/Score
Q.PEVM(+15.99)GVSK.V	26.64	431.7211	1.71E+03	M4:Oxidation (M):1000.00
R.GPFPIIV	15.8	371.7286	4.69E+03	
E.QQQTEDELQDK.I	19.02	681.313	1.51E+04	
K.IHPFAQTQSLVYPFPGPIPNSLPQNIPPLTQTPVVVPPFLQPEVM(+15.99)GVSK.V	33.99	1778.2906	1.52E+04	M45:Oxidation (M):1000.00
F.AQTQSLVYPFPGPIPN.S	15	864.9522	2.40E+04	
K.EAM(+15.99)APKHK.E	27.59	464.2399	2.73E+04	M3:Oxidation (M):1000.00
P.IQAFLLYQEPVLGPVR.G	41.96	922.0283	2.79E+04	
N.SLPQNIPPLTQTPVVVPPFLQPEVMGVSK.V	30.83	1556.8618	2.90E+04	
Q.TEDELQDK.I	23.69	489.2246	3.28E+04	
K.VKEAMAPK.H	28.22	437.247	3.57E+04	
Q.SVLSLSQSK.V	30.38	474.772	4.72E+04	
L.LYQEPVLGPVR.G	39.1	635.8616	5.03E+04	
K.YPVEPFTESQSLTLTDVENL.H	43.98	1141.5575	6.97E+04	
K.IHPFAQTQSL.V	34.2	571.3036	6.98E+04	
K.IHPFAQ.T	22.58	356.6923	8.22E+04	
S.VLSLSQSK.V	29.89	431.2554	8.39E+04	
Q.AFLLYQEPVLGPVR.G	34.56	801.4569	9.99E+04	
K.IHPFAQTQ(+.98)SLVYPFPGPIPN.S	39.37	1112.578	1.00E+05	Q8:Deamidation (NQ):27.83
K.FQSEEQQQTEDELQDK.I	46.48	991.4359	1.08E+05	
K.YPVEPFTESQSL.T	30.57	698.8354	1.10E+05	
K.YPVEPFTESQ.S	41.73	598.7773	1.15E+05	
K.IHPFAQ(+.98)TQSLVYPFPGPIPN.S	38.56	1112.5782	1.15E+05	Q6:Deamidation (NQ):48.87
K.VLPVPQK.A	22.37	390.7524	1.32E+05	
M.PIQAFLLYQEPVLGPVRG.P	49.42	999.0647	1.42E+05	

P02666 Peptides	-10lgP	m/z	Peptide intensity	PTM/Score
K.IHPFAQTQSLVYPFPG.P	31.31	901.4684	1.60E+05	
A.RELEELNVPGEIVE.S	30.65	813.4228	1.76E+05	
R.DMPIQAFLLYQEPVLGPVR.G	40.88	1093.5879	2.05E+05	
K.IHPFAQTQSLVYPFPGPI.P	36.48	1006.5367	2.18E+05	
K.AVPYPQR.D	16.35	415.7295	2.24E+05	
P.HQPLPPTVM(+15.99)FPPQSVLSLSQSK.V	21.93	812.0979	3.77E+05	M9:Oxidation (M):1000.00
K.IHPFAQTQ.S	34.32	471.2453	3.79E+05	
R.DM(+15.99)PIQAFLLYQEPVLGPVRG.P	60.62	1130.0955	5.18E+05	M2:Oxidation (M):1000.00
Q.PHQPLPPTVM(+15.99)FPPQSVLSLSQSK.V	36.31	844.4502	5.24E+05	M10:Oxidation (M):1000.00
L.YQEPVLGPVRGPFPIIV	61.04	941.0372	6.89E+05	
W.M(+15.99)HQPHQPLPPTVM(+15.99)FPPQSVLSLSQSK.V	29.89	736.6268	7.52E+05	M1:Oxidation (M):1000.00;M13:Oxidation (M):1000.00
N.SLPQNIPPLTQTPVVVPPFLQ(+.98)PEVM(+15.99)GVSK.V	24.31	1043.9008	1.11E+06	Q21:Deamidation (NQ):0.00;M25:Oxidation (M):1000.00
A.FLLYQEPVLGPVR.G	37.97	765.9384	1.20E+06	
N.SLPQNIPPLTQTPVVVPPFLQPEVM(+15.99)GVSK.V	36.94	1564.8522	1.38E+06	M25:Oxidation (M):1000.00
D.M(+15.99)PIQAFLLYQEPVLGPVR.G	42.91	1044.0726	1.41E+06	M1:Oxidation (M):1000.00
L.YQEPVLGPVR.G	43.06	579.3193	1.49E+06	
K.EM(+15.99)PFPK.Y	25.08	382.6859	1.78E+06	M2:Oxidation (M):1000.00
K.VKEAM(+15.99)APK.H	31.82	297.1653	1.90E+06	M5:Oxidation (M):1000.00
M.PIQAFLLYQEPVLGPVR.G	63.27	970.5527	2.35E+06	
F.LLYQEPVLGPVR.G	52.73	692.4039	4.63E+06	
K.HKEM(+15.99)PFPK.Y	32.42	515.2634	6.74E+06	M4:Oxidation (M):1000.00
R.DM(+15.99)PIQAFLLYQEPVLGPVR.G	59.76	1101.5844	1.03E+07	M2:Oxidation (M):1000.00
K.IHPFAQTQSLVYPFPGPIPN.S	61.89	1112.0823	1.08E+07	M4:Oxidation (M):1000.00

P02668 Peptides	-10lgP	m/z	Peptide intensity	PTM/Score
K.YIPIQY.V	19.48	398.7161	1.45E+04	
A.QEQNQEQPIR.C	16.24	635.3138	1.65E+04	
K.PVALINNQFLPYPY.Y	25.04	824.9406	1.84E+04	
R.SPAQILQWQVLSN(+.98)TVPAK.S	46.51	991.0415	2.19E+04	N13:Deamidation (NQ):109.97
R.SPAQILQWQVLSNTV.P	18.35	842.458	2.29E+04	
R.YPSYGLNYYQQKPV.A	53.58	860.4225	2.35E+04	
V.ALINNQFLPYPYYAK.P	67.64	907.9788	3.13E+04	
L.SNTVPAK.S	15.95	358.7005	7.60E+04	
K.PVALINNQFLPYPYYAKPAAVR.S	36.8	835.7941	8.67E+04	
K.TEIPTINTIASGEPTSTPTTEAVESTVATLED.S	40.23	1092.536	9.78E+04	
W.QVLSNTVPAK.S	32.1	528.8058	1.03E+05	
A.QILQWQVLSNTVPAK.S	44.62	862.9892	1.13E+05	
R.FFSDK.I	15.68	322.1579	1.28E+05	
P.AQILQWQVLSNTVPAK.S	44.35	898.5081	1.29E+05	
R.YPSYGLNYYQQKPVAL.I	55.65	952.4845	1.36E+05	
Y.IPIQYVLSR.Y	24.22	544.8273	1.51E+05	
I.PIQYVLSR.Y	19.92	488.2855	1.78E+05	
R.SPAQILQWQVLSN.T	22.97	742.3986	1.90E+05	
R.YPSYGLNYYQQK.P	68.59	762.3619	2.92E+05	
Y.QQKPVALINNQFLPYPYYAK.P	38.58	799.0991	4.64E+05	
R.SPAQILQ(+.98)WQVLSNTVPAK.S	26.79	661.0304	4.72E+05	Q7:Deamidation (NQ):0.00
K.SC(+57.02)QAQPTTM(+15.99)AR.H	48.92	633.7825	5.02E+05	C2:Carbamidomethylation:1000.00;M9: Oxidation (M):1000.00
R.SPAQ(+.98)ILQWQVLSNTVPAK.S	45.68	991.0432	5.69E+05	Q4:Deamidation (NQ):101.94
L.INNQFLPYPYYAK.P	49.15	815.9174	5.92E+05	
S.YGLNYYQQKPVALINNQFLPYPYYAK.P	38.08	1056.8789	6.22E+05	
Y.YQQKPVALINNQFLPYPYYAK.P	49.7	853.4535	7.49E+05	
K.DERFFSDK.I	41.71	522.2432	9.19E+05	

P02668 Peptides	-10lgP	m/z	Peptide intensity	PTM/Score
K.PVALINNQFLPYPYYAK.P	74.44	1006.0393	1.61E+06	
R.YPSYGLNYYQQKPVALINNQFLPYPYYAK.P	32.55	1172.5955	5.77E+06	
K.YIPIQYVLSR.Y	36.39	626.3589	6.75E+06	
R.SPAQILQWQVLSNTVPAK.S	80.11	990.5509	3.04E+07	

Cauldron Rim Interior

Name	Formula	PDF Number	FOM	%
Si O2	O2 Si	00-153-6389	0.847	100.00

Peak List Serial	2theta [°]	d [Å]	I/I0		Peak List Serial	2theta [°]	d [Å]	I/I0
1	16.41	5.3963	0.438		19	63.92	1.4551	0.620
2	20.84	4.2586	10.005		20	65.71	1.4198	0.280
3	26.57	3.3516	58.477		21	67.72	1.3826	4.178
4	27.43	3.2493	1.159		22	68.10	1.3757	2.282
5	30.45	2.9331	1.173		23	68.28	1.3724	0.416
6	33.16	2.6996	0.302		24	69.59	1.3499	0.134
7	36.42	2.4651	2.381		25	73.42	1.2887	1.974
8	36.53	2.4575	5.769		26	75.65	1.2560	1.546
9	39.41	2.2846	2.640		27	77.63	1.2289	2.313
10	40.24	2.2391	1.318		28	79.80	1.2009	2.049
11	42.40	2.1301	4.739		29	79.95	1.1990	0.752
12	45.77	1.9806	5.015		30	80.10	1.1971	0.492
13	50.07	1.8203	3.610		31	81.14	1.1844	1.134
14	50.55	1.8039	0.174		32	81.47	1.1804	1.301
15	54.80	1.6738	6.139		33	83.74	1.1540	1.212
16	55.27	1.6608	0.505		34	84.90	1.1413	0.064
17	57.05	1.6129	0.217		35	87.03	1.1187	0.113
18	59.91	1.5426	6.585		36	87.47	1.1142	0.262

Vessel A Interior

Name	Formula	PDF Number	FOM	%
Plumbonacrite	C3 H2 O12 Pb5	00-900-9518	0.554	**25.171**
Hydrocerussite	C H O4 Pb1.5	00-901-1388	0.683	**74.829**

Peak List Serial	2theta [°]	d [Å]	I/I0		Peak List Serial	2theta [°]	d [Å]	I/I0
1	11.24	7.8646	8.643		55	43.78	2.0661	74.521
2	13.36	6.6200	7.649		56	44.08	2.0527	37.280
3	14.22	6.2250	1.905		57	44.21	2.0468	42.689
4	19.53	4.5415	7.944		58	44.33	2.0417	29.626
5	19.91	4.4547	71.470		59	44.91	2.0165	10.784
6	20.08	4.4180	124.782		60	45.87	1.9768	33.639
7	20.23	4.3855	72.478		61	45.98	1.9720	38.918
8	20.40	4.3500	47.678		62	46.23	1.9619	57.542
9	20.60	4.3081	50.014		63	46.49	1.9519	67.879
10	20.75	4.2772	55.374		64	46.57	1.9486	83.519
11	20.87	4.2535	77.529		65	46.74	1.9420	106.944
12	21.45	4.1388	7.429		66	46.89	1.9362	144.510
13	21.60	4.1103	6.309		67	47.10	1.9277	57.644
14	22.25	3.9914	9.767		68	48.27	1.8837	9.707
15	24.79	3.5879	1000.000		69	49.01	1.8572	247.811
16	25.23	3.5271	324.764		70	50.16	1.8171	23.475
17	26.45	3.3671	25.515		71	50.88	1.7931	26.678
18	26.77	3.3279	33.070		72	51.30	1.7795	4.696
19	26.92	3.3097	42.459		73	51.78	1.7640	0.000
20	27.12	3.2856	96.153		74	52.05	1.7556	6.923
21	27.18	3.2777	106.318		75	53.54	1.7102	3.355
22	27.40	3.2522	45.282		76	53.92	1.6990	44.797
23	28.64	3.1145	4.108		77	54.07	1.6946	32.307
24	28.84	3.0933	74.250		78	54.76	1.6750	2.495
25	28.97	3.0794	312.880		79	55.24	1.6614	17.695
26	29.76	2.9998	37.903		80	55.71	1.6486	5.517
27	29.91	2.9851	61.682		81	55.98	1.6413	4.777
28	30.07	2.9689	89.411		82	56.86	1.6179	22.777
29	30.19	2.9576	100.648		83	56.96	1.6153	28.426
30	30.34	2.9433	71.730		84	57.10	1.6118	20.757
31	30.64	2.9151	36.030		85	58.07	1.5872	36.731
32	31.09	2.8738	23.446		86	58.17	1.5847	36.183
33	31.83	2.8091	5.476		87	58.30	1.5814	38.663
34	33.00	2.7122	18.483		88	58.68	1.5719	23.155
35	34.00	2.6344	34.214		89	59.09	1.5622	18.953
36	34.12	2.6257	145.818		90	60.12	1.5377	30.758
37	34.70	2.5827	19.420		91	60.46	1.5300	4.985
38	35.39	2.5343	97.086		92	61.26	1.5119	22.845
39	35.56	2.5228	251.739		93	61.59	1.5045	32.146
40	35.76	2.5091	192.573		94	61.74	1.5012	30.789
41	35.87	2.5012	193.682		95	62.36	1.4878	9.317
42	36.01	2.4922	199.393		96	62.58	1.4831	10.681
43	36.24	2.4766	48.476		97	63.03	1.4736	24.602
44	38.10	2.3602	4.880		98	64.10	1.4516	35.260
45	39.43	2.2832	1.446		99	64.28	1.4479	32.340
46	39.70	2.2684	8.618		100	65.50	1.4238	3.735
47	40.42	2.2297	65.614		101	65.94	1.4155	4.809
48	40.79	2.2105	58.926		102	66.41	1.4066	6.260
49	40.89	2.2053	50.925		103	67.21	1.3918	3.434
50	41.09	2.1950	25.217		104	67.63	1.3842	13.363
51	41.29	2.1848	21.136		105	68.14	1.3749	23.610

Peak List Serial	2theta [°]	d [Å]	I/I0		Peak List Serial	2theta [°]	d [Å]	I/I0
52	42.58	2.1217	21.219		106	69.06	1.3589	14.312
53	43.16	2.0943	10.309		107	69.28	1.3551	5.088
54	43.48	2.0797	203.257		108	69.91	1.3444	11.394

Vessel A Exterior

Name	Formula	PDF Number	FOM	%
Chalcocite	Cu2 S	00-901-5068	0.594	15.12
Silicon Oxide (Quartz)	Si O2	00-500-0035	0.681	84.88

Peak List Serial	2theta [°]	d [Å]	I/I0		Peak List Serial	2theta [°]	d [Å]	I/I0
1	6.36	13.8820	5.225		110	36.58	2.4548	60.196
2	6.78	13.0275	4.525		111	36.78	2.4418	6.221
3	7.43	11.8863	6.846		112	37.04	2.4248	6.590
4	8.63	10.2325	7.658		113	37.11	2.4206	6.697
5	8.75	10.0959	5.418		114	37.28	2.4101	8.571
6	8.89	9.9443	6.160		115	37.39	2.4029	8.034
7	9.40	9.3976	7.307		116	37.73	2.3823	9.294
8	10.49	8.4267	5.464		117	37.95	2.3692	11.416
9	12.83	6.8947	6.073		118	38.66	2.3268	6.588
10	13.11	6.7460	7.711		119	38.98	2.3086	6.292
11	13.20	6.7035	8.245		120	39.18	2.2972	7.830
12	13.81	6.4048	5.638		121	39.50	2.2795	57.646
13	14.07	6.2912	8.650		122	39.72	2.2675	10.783
14	15.10	5.8618	7.728		123	39.92	2.2566	11.004
15	15.45	5.7295	8.811		124	40.20	2.2413	8.256
16	16.17	5.4765	6.863		125	40.29	2.2368	28.723
17	16.56	5.3502	5.412		126	40.45	2.2280	8.943
18	16.97	5.2194	8.342		127	40.87	2.2062	5.614
19	17.24	5.1391	6.073		128	41.51	2.1739	8.471
20	17.37	5.0998	11.447		129	42.11	2.1442	10.890
21	17.59	5.0373	8.232		130	42.34	2.1329	16.219
22	17.81	4.9764	7.439		131	42.46	2.1273	119.330
23	17.93	4.9442	4.087		132	42.58	2.1217	12.686
24	18.08	4.9034	3.388		133	43.09	2.0974	6.127
25	18.24	4.8588	8.056		134	43.18	2.0935	8.654
26	18.56	4.7764	6.936		135	43.79	2.0654	7.058
27	19.41	4.5686	6.827		136	45.03	2.0115	8.168
28	19.55	4.5377	18.847		137	45.38	1.9968	6.577
29	19.66	4.5109	22.160		138	45.52	1.9912	9.465
30	19.78	4.4845	15.580		139	45.72	1.9829	8.536
31	19.88	4.4621	12.993		140	45.80	1.9795	21.563
32	20.05	4.4253	8.674		141	46.39	1.9559	8.448
33	20.12	4.4108	10.852		142	46.54	1.9499	7.152
34	20.23	4.3855	7.862		143	47.17	1.9252	16.020
35	20.30	4.3712	11.588		144	47.27	1.9213	11.151
36	20.65	4.2977	5.507		145	47.54	1.9111	15.146
37	20.87	4.2535	207.831		146	48.16	1.8880	7.121
38	20.98	4.2300	16.262		147	48.39	1.8794	9.098
39	21.52	4.1261	8.484		148	48.56	1.8734	9.086
40	21.64	4.1040	5.614		149	49.23	1.8495	6.916
41	21.77	4.0791	8.204		150	49.39	1.8436	8.031
42	21.84	4.0668	5.423		151	50.20	1.8160	136.248
43	22.09	4.0212	7.622		152	50.35	1.8109	7.318
44	22.50	3.9475	7.072		153	50.41	1.8087	10.740
45	22.81	3.8961	9.266		154	50.60	1.8025	11.288
46	22.92	3.8765	9.442		155	51.06	1.7871	6.847
47	23.06	3.8543	6.902		156	51.25	1.7811	7.070
48	23.27	3.8188	4.789		157	51.48	1.7736	10.134
49	23.89	3.7214	9.299		158	51.78	1.7640	8.759
50	23.98	3.7086	9.055		159	52.08	1.7545	8.167
51	24.16	3.6808	9.949		160	52.53	1.7405	6.673
52	24.53	3.6264	10.442		161	52.79	1.7328	7.286
53	24.88	3.5761	7.027		162	53.07	1.7242	10.347
54	25.10	3.5456	7.450		163	53.25	1.7187	7.469

Peak List Serial	2theta [°]	d [Å]	I/I0		Peak List Serial	2theta [°]	d [Å]	I/I0
55	25.21	3.5294	7.467		164	53.52	1.7107	8.941
56	25.31	3.5157	9.585		165	53.59	1.7088	8.613
57	25.63	3.4728	14.229		166	53.79	1.7029	7.612
58	25.68	3.4662	10.688		167	54.42	1.6845	8.346
59	25.80	3.4507	8.456		168	54.62	1.6788	6.743
60	26.10	3.4116	13.738		169	54.89	1.6712	49.325
61	26.23	3.3945	9.374		170	55.34	1.6587	15.475
62	26.33	3.3818	17.396		171	55.59	1.6518	9.486
63	26.67	3.3402	784.968		172	56.13	1.6373	6.901
64	26.88	3.3137	17.461		173	56.93	1.6161	6.225
65	26.92	3.3097	15.229		174	57.05	1.6131	6.112
66	27.08	3.2896	6.893		175	57.23	1.6083	9.785
67	27.45	3.2464	16.633		176	57.40	1.6041	7.166
68	27.72	3.2157	7.331		177	57.46	1.6023	7.427
69	27.94	3.1912	17.444		178	57.72	1.5960	7.978
70	28.09	3.1744	7.203		179	57.90	1.5914	7.183
71	28.86	3.0916	4.756		180	58.00	1.5888	6.680
72	29.42	3.0331	38.432		181	58.20	1.5838	10.340
73	29.52	3.0231	13.571		182	58.70	1.5715	7.101
74	29.66	3.0098	7.080		183	59.27	1.5578	6.011
75	29.81	2.9949	8.616		184	59.54	1.5514	5.663
76	29.94	2.9818	14.528		185	59.65	1.5487	5.758
77	30.48	2.9307	10.299		186	59.79	1.5455	7.963
78	31.06	2.8769	12.574		187	60.00	1.5404	50.891
79	31.19	2.8648	12.137		188	60.31	1.5335	5.665
80	31.33	2.8529	16.613		189	60.84	1.5213	5.298
81	31.65	2.8250	8.628		190	61.11	1.5153	9.365
82	31.73	2.8178	12.942		191	61.19	1.5134	9.000
83	31.86	2.8062	16.483		192	61.29	1.5112	11.081
84	32.20	2.7779	11.109		193	61.51	1.5063	8.297
85	32.26	2.7723	9.736		194	61.59	1.5045	10.539
86	32.70	2.7364	7.653		195	61.81	1.4997	7.291
87	32.75	2.7323	6.983		196	61.94	1.4968	7.504
88	32.88	2.7215	10.109		197	62.01	1.4954	6.782
89	33.02	2.7108	10.268		198	62.28	1.4896	6.965
90	33.07	2.7068	7.204		199	62.83	1.4778	6.605
91	33.20	2.6962	8.502		200	63.65	1.4608	5.733
92	33.33	2.6857	6.360		201	64.07	1.4522	19.264
93	33.80	2.6496	7.754		202	64.17	1.4502	8.848
94	33.92	2.6407	7.347		203	64.60	1.4415	7.690
95	34.24	2.6170	12.009		204	64.98	1.4339	6.589
96	34.39	2.6059	16.321		205	65.55	1.4229	6.709
97	34.44	2.6022	16.681		206	65.84	1.4174	9.052
98	34.57	2.5924	20.117		207	66.07	1.4129	7.792
99	34.72	2.5815	24.704		208	66.22	1.4101	5.976
100	34.84	2.5731	16.904		209	66.62	1.4026	7.258
101	34.90	2.5684	16.395		210	67.47	1.3869	8.705
102	35.07	2.5565	13.216		211	67.63	1.3842	5.444
103	35.21	2.5471	6.217		212	67.78	1.3815	32.930
104	35.37	2.5355	12.970		213	68.11	1.3755	20.335
105	35.57	2.5216	5.919		214	68.16	1.3746	35.649
106	35.71	2.5125	6.722		215	68.33	1.3717	29.412
107	35.87	2.5012	8.266		216	68.61	1.3667	10.503
108	36.11	2.4855	7.080		217	69.48	1.3517	10.569
109	36.27	2.4744	7.700					

Vessel B Interior Body

Name	Formula	PDF Number	FOM	%
Quartz	O2 Si	00-900-9666	0.856	100.00

Peak List Serial	2theta [°]	d [Å]	I/I0		Peak List Serial	2theta [°]	d [Å]	I/I0
1	19.55	4.5377	5.790		21	45.88	1.9761	26.029
2	20.83	4.2602	301.088		22	48.99	1.8577	9.820
3	22.05	4.0272	1.427		23	50.11	1.8188	119.356
4	23.46	3.7893	7.091		24	50.25	1.8143	60.904
5	23.99	3.7060	2.687		25	51.58	1.7704	4.130
6	26.62	3.3464	1000.000		26	54.84	1.6726	36.280
7	29.69	3.0064	6.106		27	54.99	1.6684	20.382
8	30.46	2.9323	8.033		28	55.29	1.6601	21.495
9	33.82	2.6483	6.349		29	57.23	1.6083	2.937
10	34.60	2.5900	5.525		30	59.94	1.5420	82.394
11	35.02	2.5600	5.000		31	60.11	1.5381	41.678
12	36.51	2.4591	61.268		32	64.02	1.4533	25.204
13	36.59	2.4537	31.849		33	64.18	1.4499	12.602
14	39.43	2.2832	78.487		34	65.90	1.4161	2.874
15	39.53	2.2776	37.616		35	67.73	1.3824	52.135
16	40.25	2.2386	46.274		36	67.91	1.3791	26.631
17	40.35	2.2333	21.478		37	68.11	1.3755	28.494
18	42.42	2.1289	108.872		38	68.29	1.3723	54.202
19	42.52	2.1241	56.388		39	68.49	1.3687	20.831
20	45.77	1.9809	49.620					

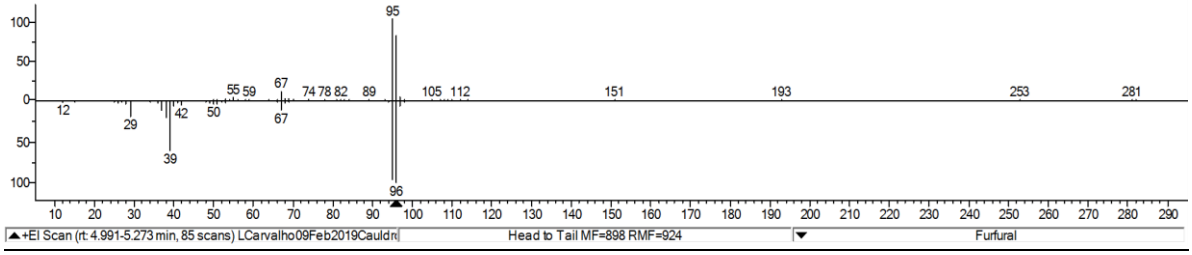
Vessel B Interior Base

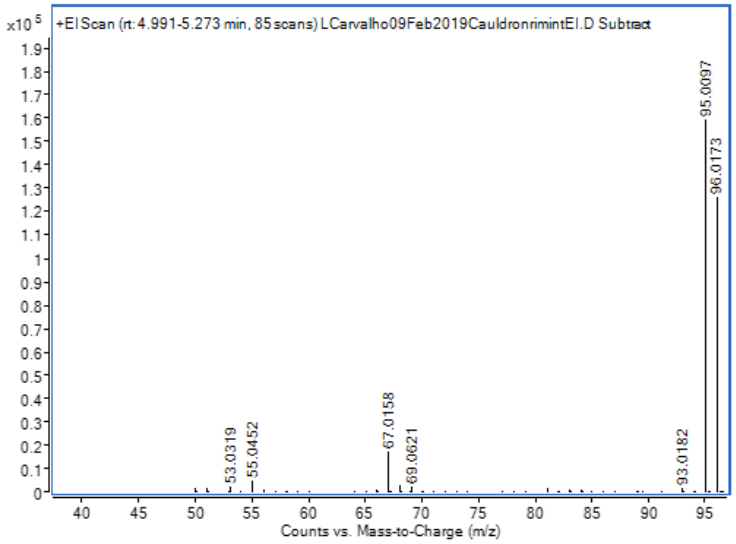
Name	Formula	PDF Number	FOM	%
Quartz	O2 Si	00-901-0145	0.752	100.00

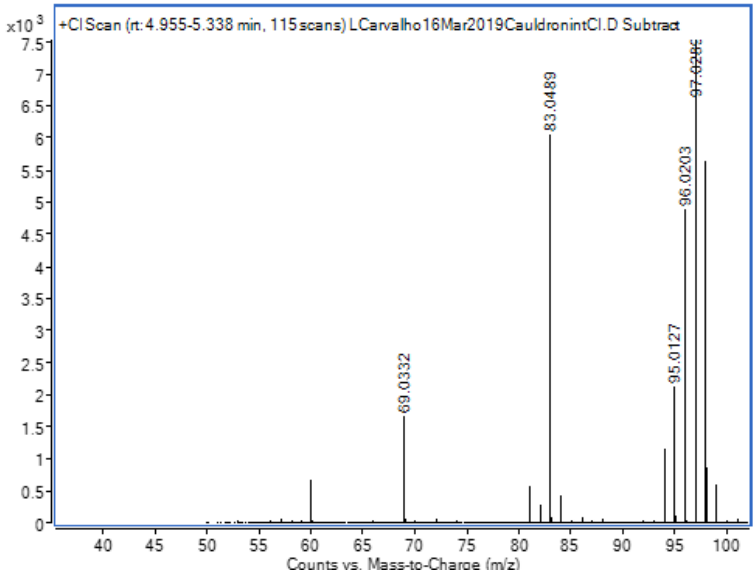
Peak List Serial	2theta [°]	d [Å]	I/I0		Peak List Serial	2theta [°]	d [Å]	I/I0
1	6.75	13.0919	32.586		42	40.24	2.2395	61.541
2	7.85	11.2545	33.417		43	42.46	2.1273	62.458
3	8.65	10.2127	28.997		44	43.21	2.0920	42.887
4	10.19	8.6748	29.533		45	44.25	2.0454	41.094
5	10.72	8.2434	21.786		46	44.76	2.0229	37.052
6	11.88	7.4455	29.496		47	45.75	1.9816	46.335
7	12.21	7.2425	33.941		48	46.82	1.9388	82.958
8	12.58	7.0316	28.126		49	47.91	1.8973	32.215
9	14.07	6.2912	68.024		50	48.64	1.8703	86.297
10	15.42	5.7418	29.927		51	49.14	1.8524	38.557
11	16.14	5.4877	34.863		52	49.59	1.8366	49.846
12	17.86	4.9625	38.886		53	50.10	1.8194	112.163
13	18.66	4.7510	28.288		54	50.56	1.8037	52.161
14	19.03	4.6600	27.590		55	51.15	1.7844	34.339
15	19.70	4.5034	44.004		56	51.72	1.7661	33.331
16	20.83	4.2602	142.736		57	52.57	1.7395	53.250
17	21.22	4.1839	45.723		58	52.94	1.7283	61.241
18	21.67	4.0978	28.495		59	54.12	1.6931	40.838
19	22.79	3.8989	37.809		60	55.43	1.6564	39.821
20	23.74	3.7446	67.571		61	55.96	1.6418	39.267
21	24.38	3.6485	34.310		62	56.53	1.6266	37.588
22	24.83	3.5832	30.031		63	57.38	1.6045	40.694
23	26.58	3.3505	1000.000		64	57.67	1.5973	33.892
24	26.98	3.3016	92.741		65	58.47	1.5772	40.507
25	27.62	3.2271	36.079		66	58.89	1.5670	43.526
26	29.01	3.0759	38.158		67	59.49	1.5526	38.421
27	29.29	3.0467	54.005		68	59.94	1.5420	98.426
28	29.79	2.9965	49.211		69	60.82	1.5217	53.076
29	30.14	2.9625	33.680		70	61.27	1.5115	54.908
30	30.79	2.9012	50.992		71	61.46	1.5074	46.235
31	31.31	2.8544	37.124		72	62.14	1.4925	35.668
32	32.20	2.7779	42.511		73	63.08	1.4726	42.614
33	32.72	2.7351	37.514		74	63.88	1.4560	45.476
34	33.08	2.7055	65.562		75	64.03	1.4529	36.543
35	34.02	2.6332	33.756		76	65.00	1.4336	54.791
36	34.69	2.5839	60.607		77	66.07	1.4129	32.835
37	35.22	2.5459	70.826		78	67.26	1.3909	39.188
38	36.49	2.4602	143.166		79	67.76	1.3818	39.069
39	37.91	2.3712	35.801		80	68.06	1.3764	70.803
40	39.42	2.2841	130.423		81	68.36	1.3711	57.758
41	39.88	2.2584	44.938		82	69.26	1.3554	31.421

[1] Furfural Mass: 96.021129

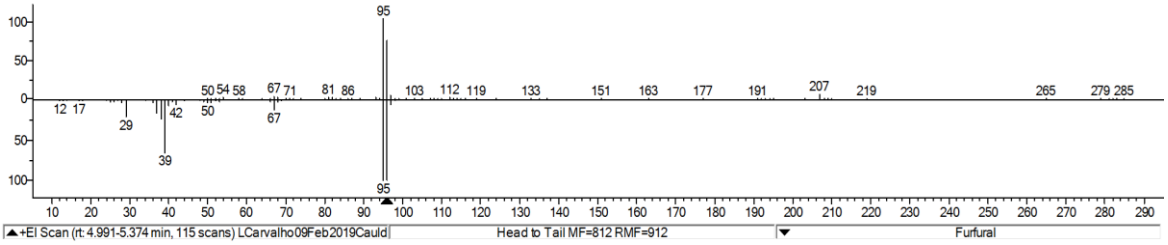
Interior

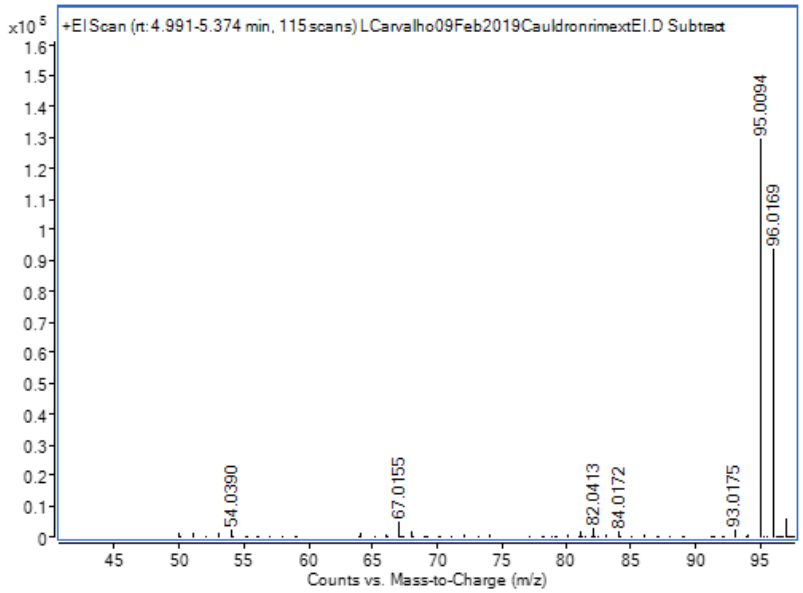


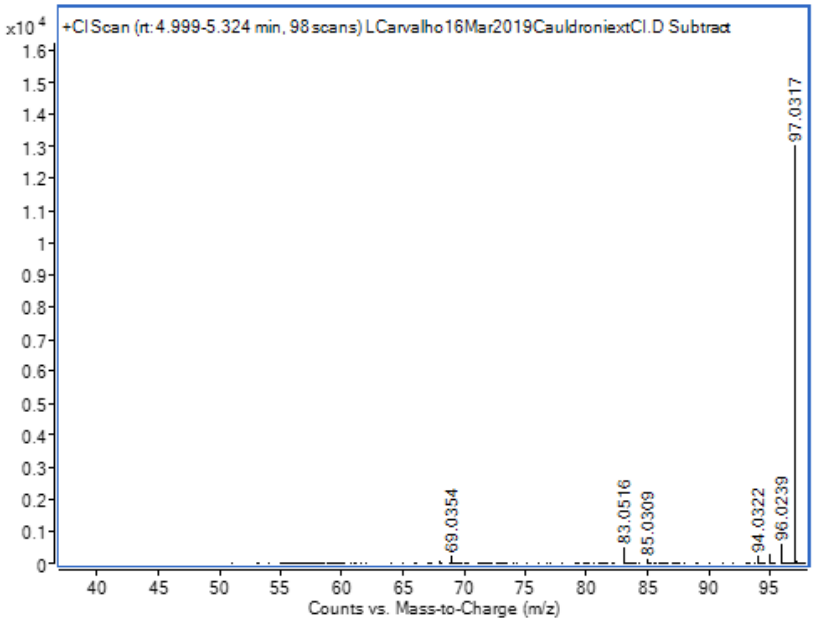




Exterior

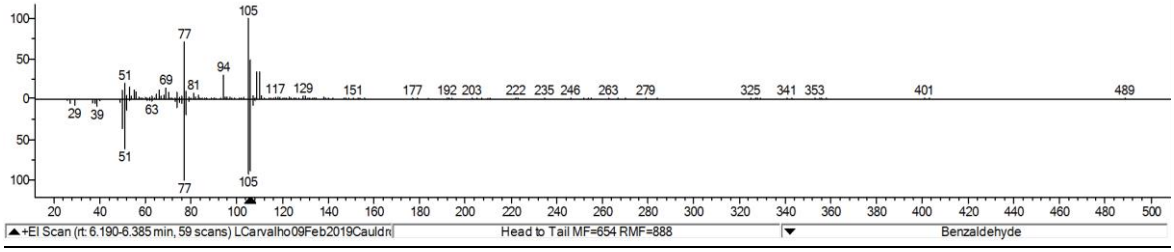


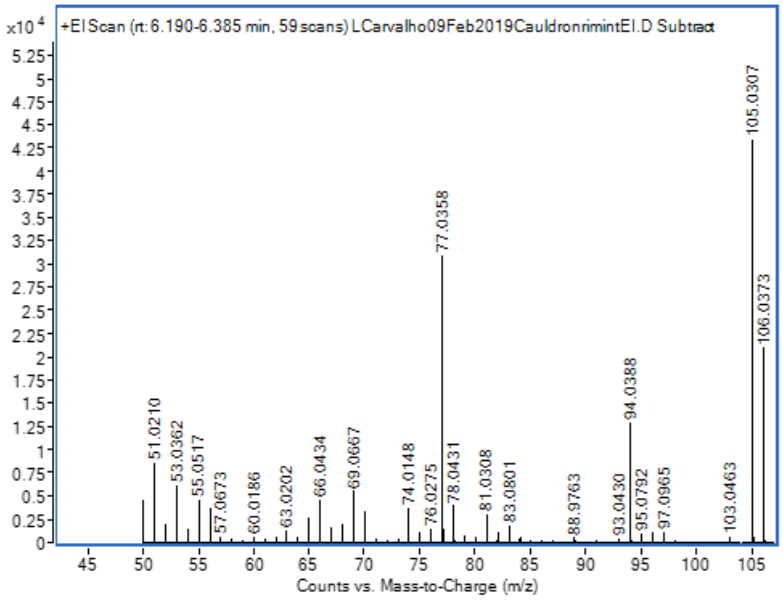


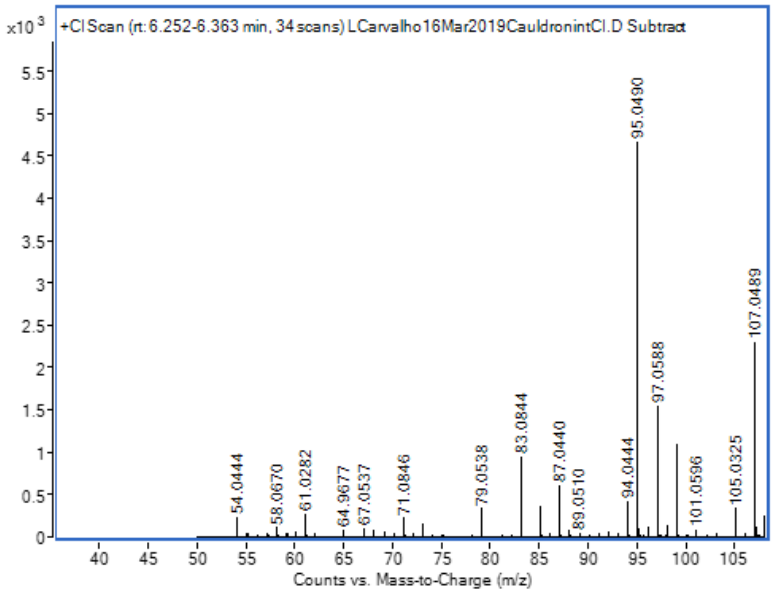


[2] Benzaldehyde Mass: 106.041865

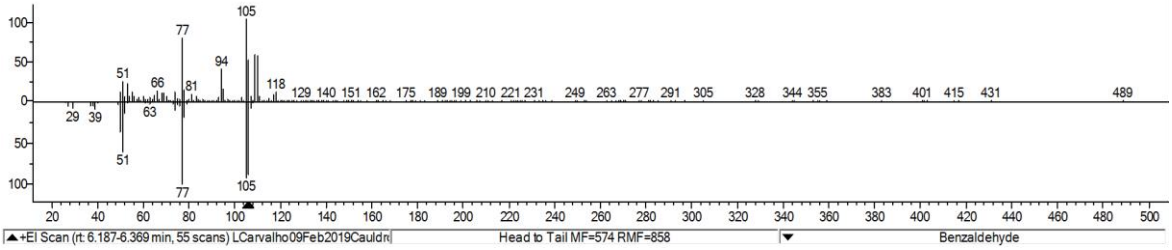
Interior

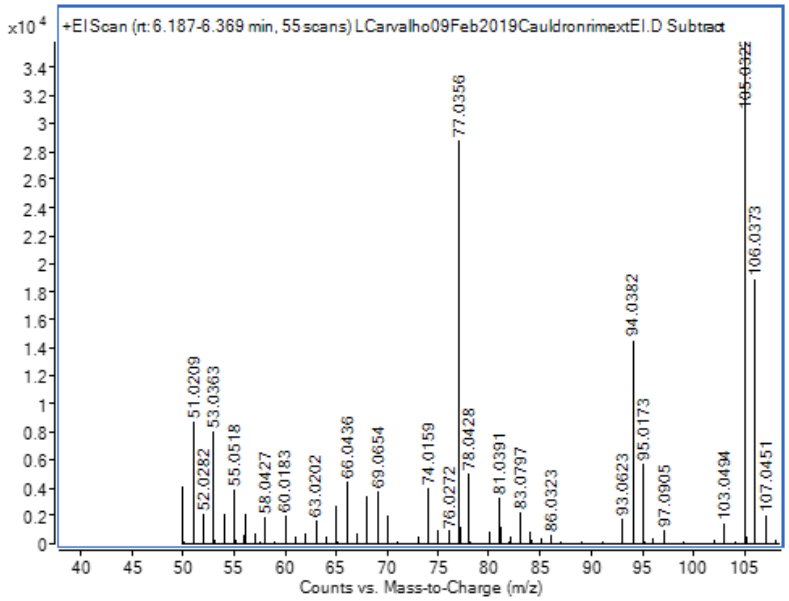


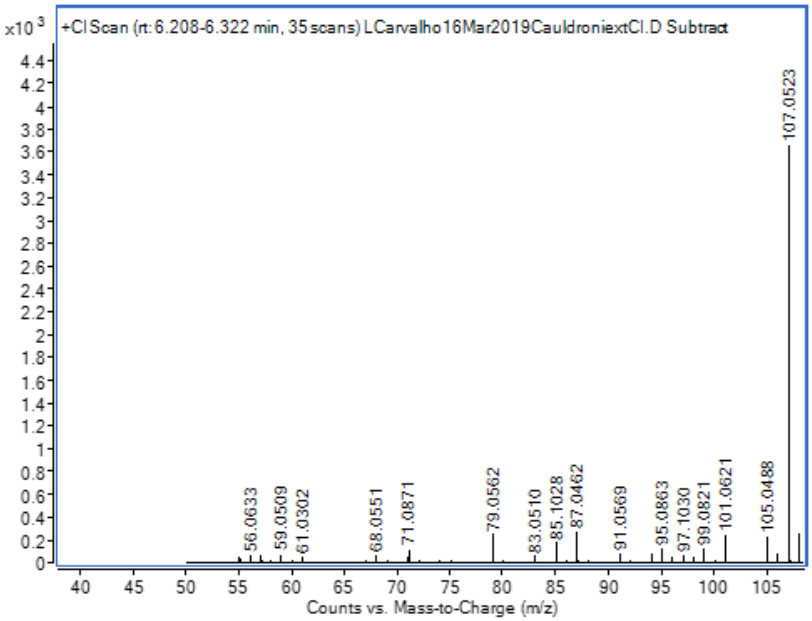




Exterior

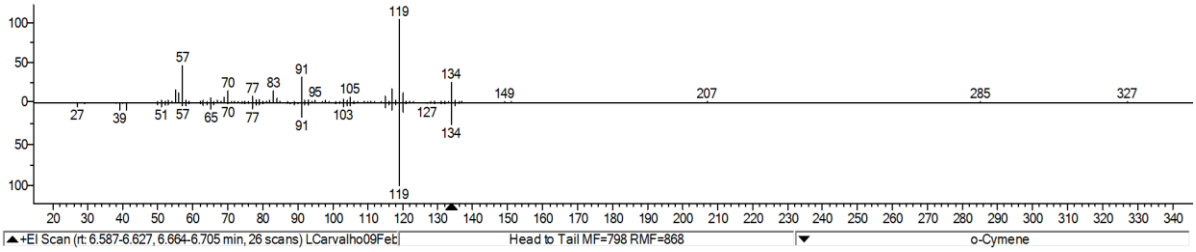


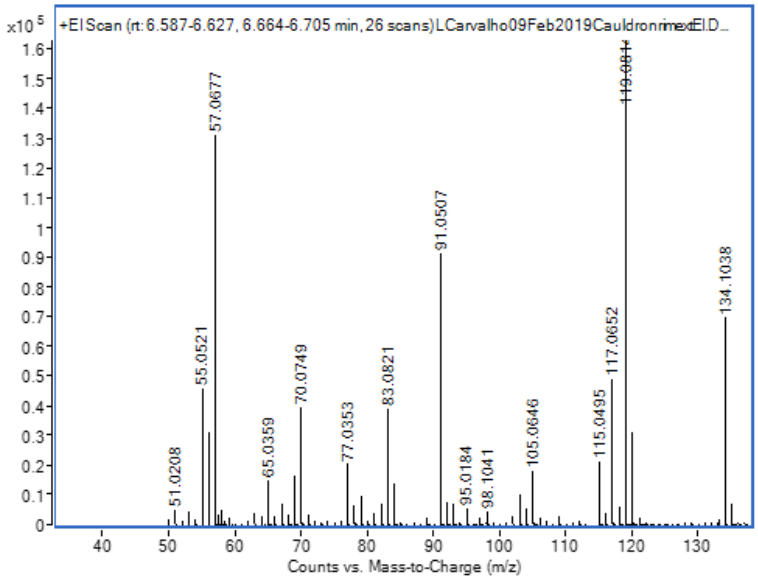


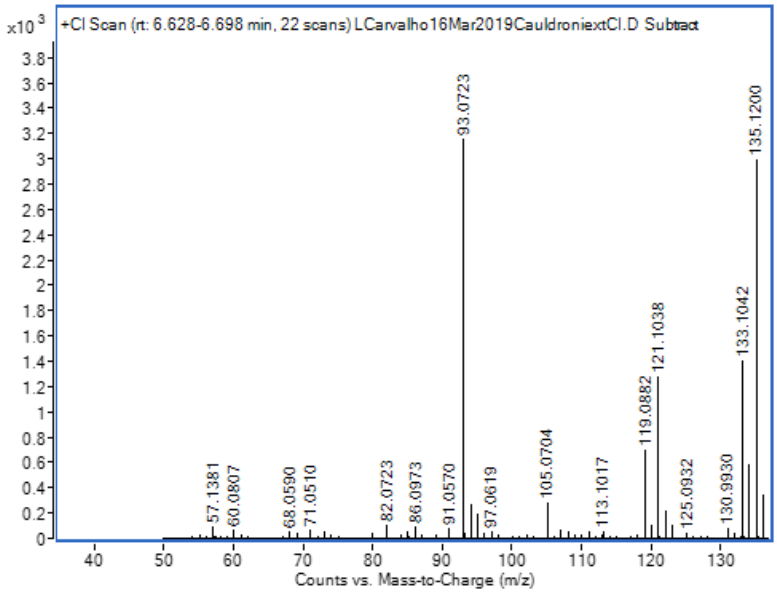


[3] o-Cymene Mass: 134.10955

Exterior

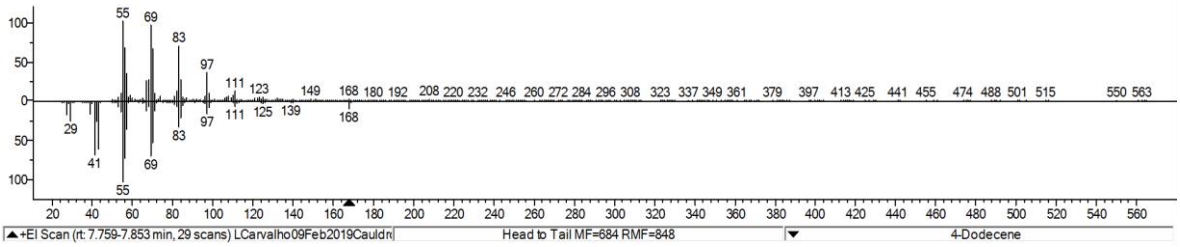


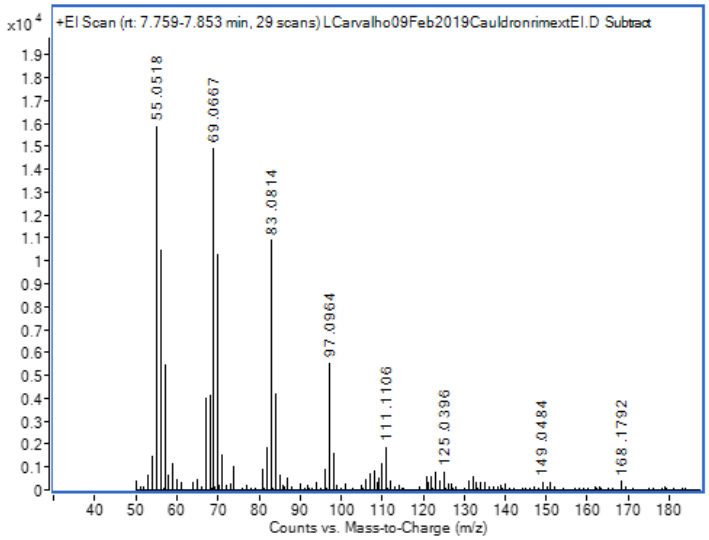


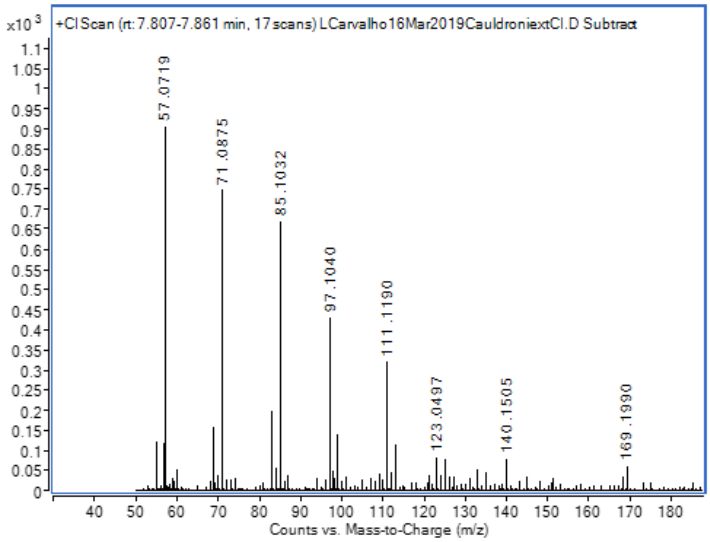


[4] 4-Dodecene Mass: 168.1878

Exterior

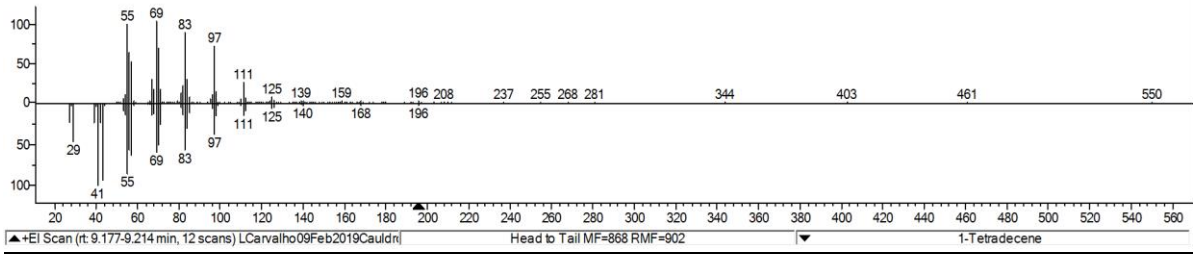

+EI Scan (rt: 7.759-7.853 min, 29 scans) LCarvalho09Feb2019Cauldr
Head to Tail MF=684 RMF=848
4-Dodecene

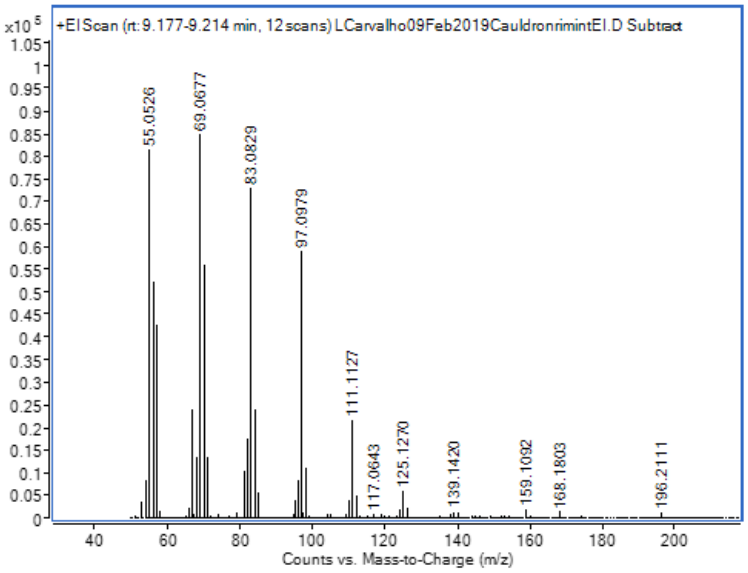

+EI Scan (rt: 7.759-7.853 min, 29 scans) LCarvalho09Feb2019CauldronrimextEI.D Subtract
55.0518
69.0667
83.0814
97.0964
111.1106
125.0396
149.0484
168.1792
Counts vs. Mass-to-Charge (m/z)

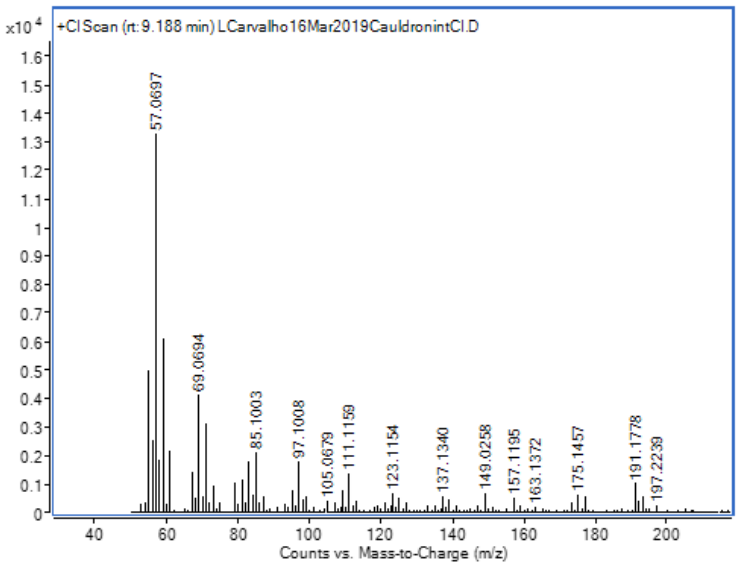

+CI Scan (rt: 7.807-7.861 min, 17 scans) LCarvalho16Mar2019CauldroniextCI.D Subtract
57.0719
71.0875
85.1032
97.1040
111.1190
123.0497
140.1505
169.1990
Counts vs. Mass-to-Charge (m/z)

[5] 1-Tridecene Mass: 182.203451

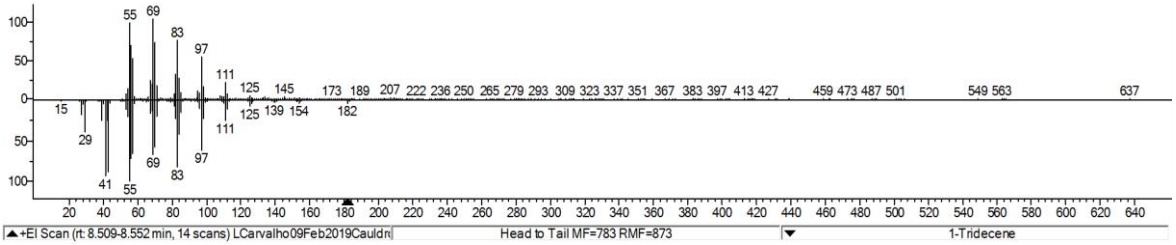
Interior

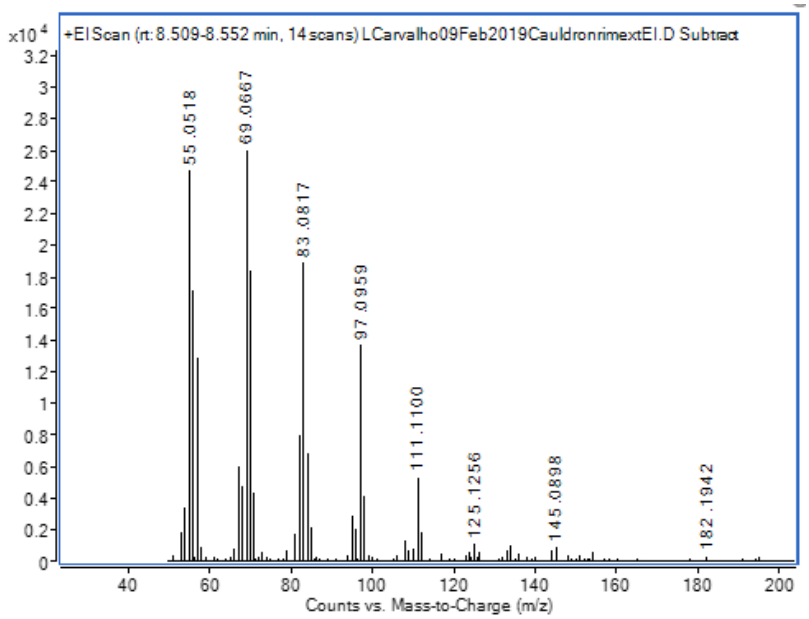


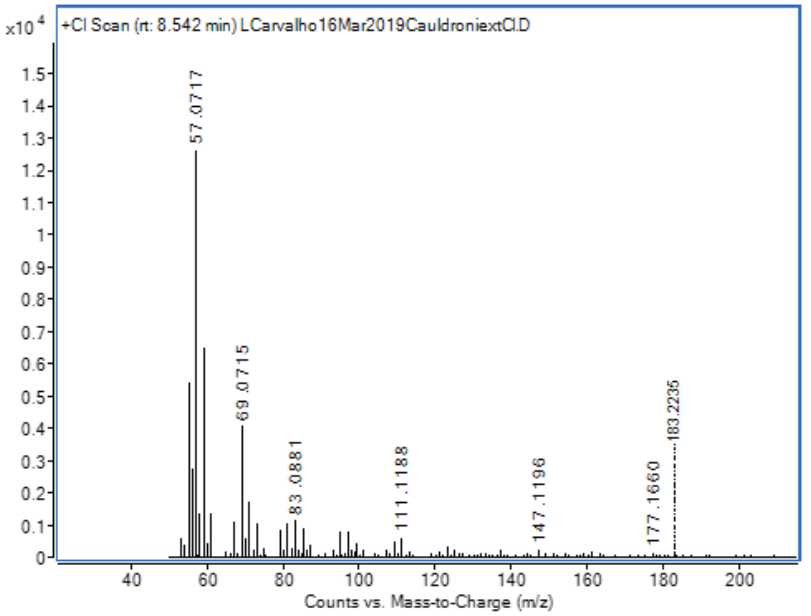




Exterior

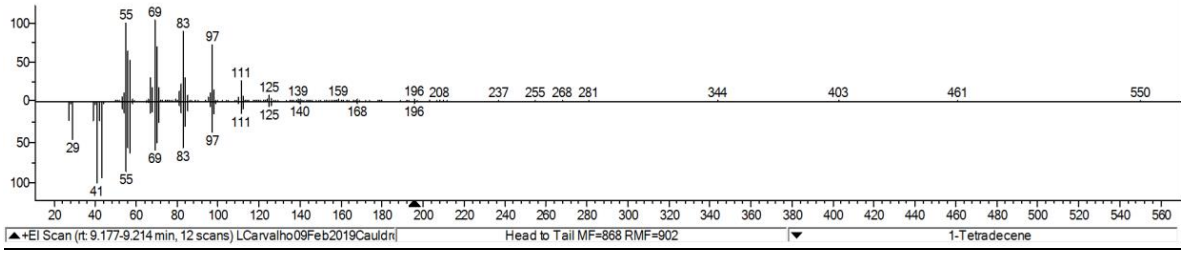


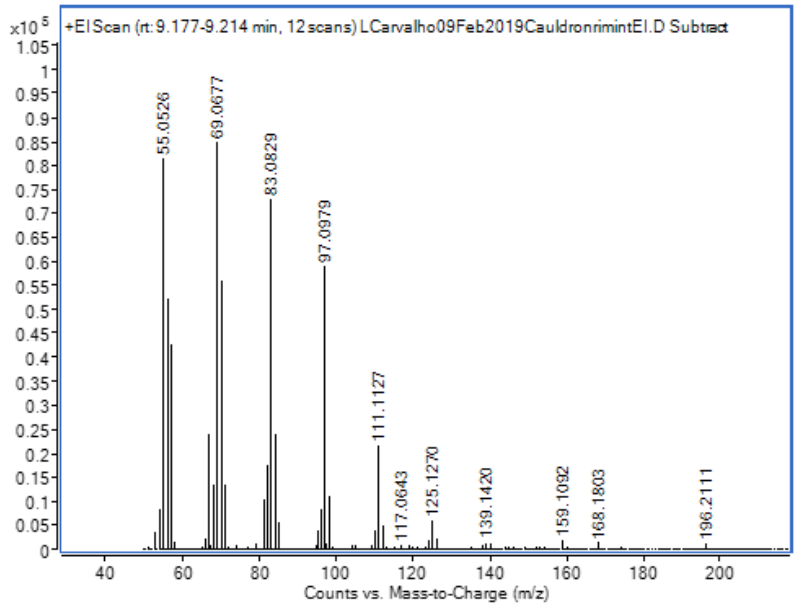


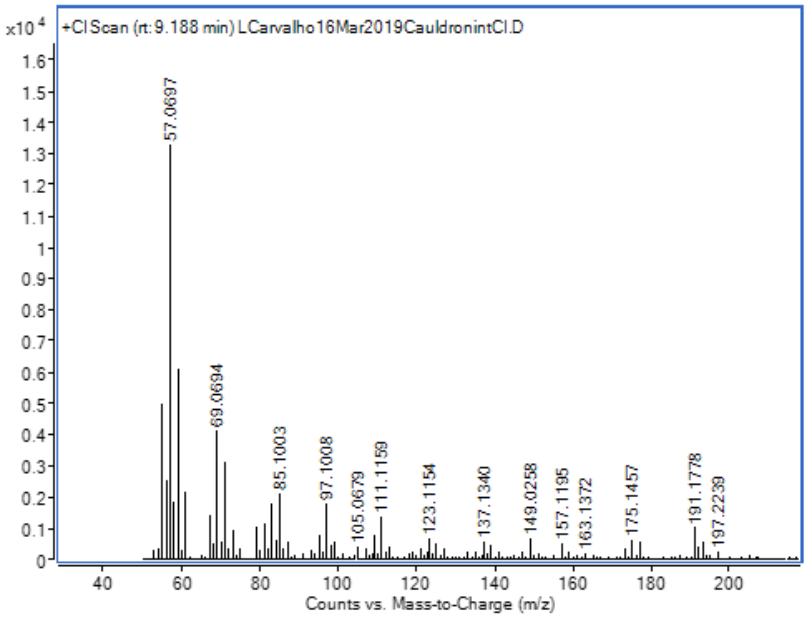


[6] 1-Tetradecene Mass: 196.219101

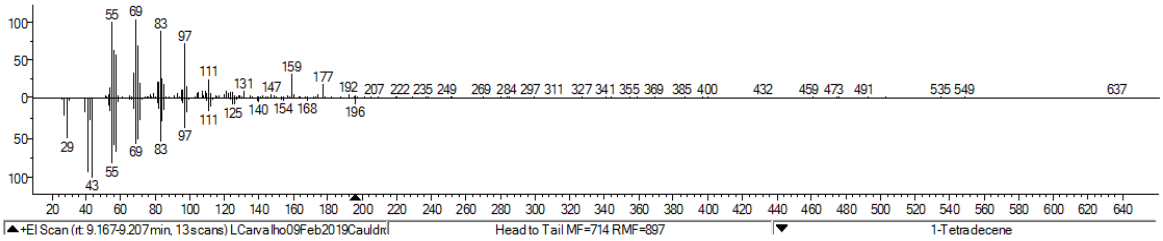
Interior

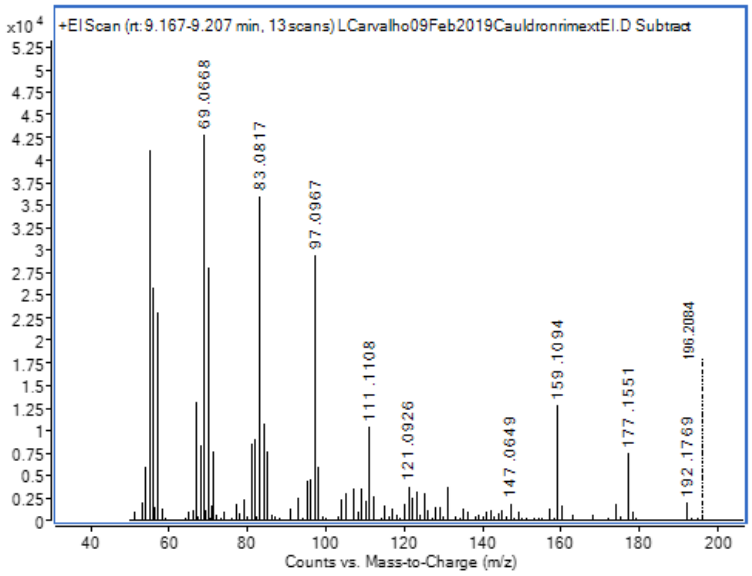


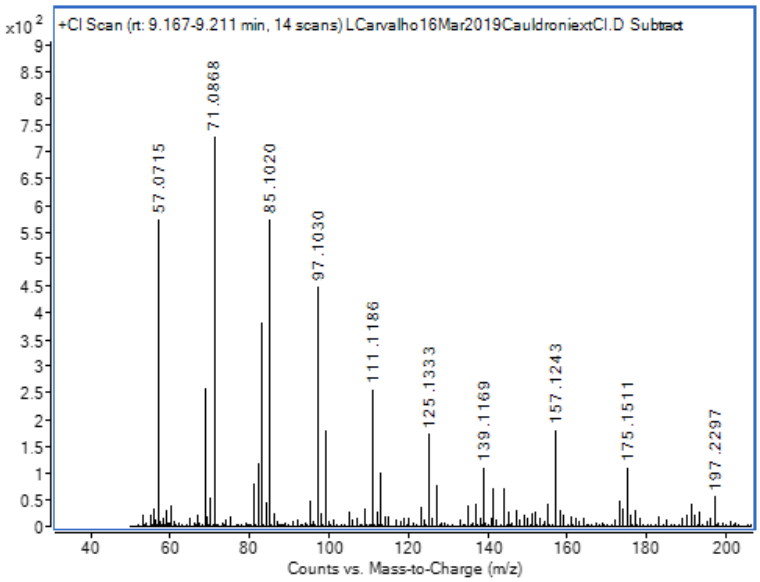




Exterior

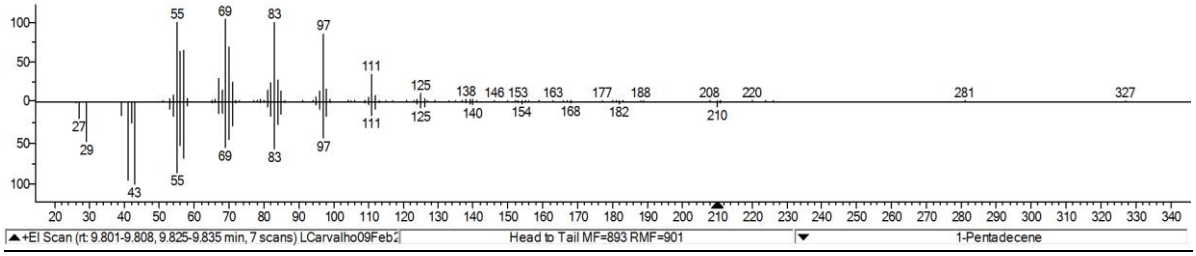

+EI Scan (rt: 9.167-9.207 min, 13 scans) LCarvalho09Feb2019Cauldr
Head to Tail MF=714 RMF=897
1-Tetradecene

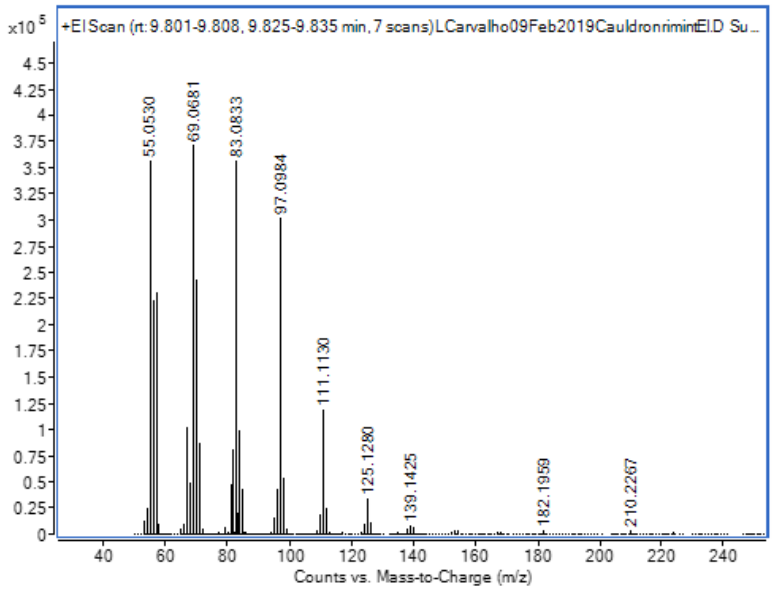

x10 4
+EI Scan (rt: 9.167-9.207 min, 13 scans) LCarvalho09Feb2019CauldronrimextEI.D Subtract
69.0668
83.0817
97.0967
111.1108
121.0926
147.0649
159.1094
177.1551
192.1769
196.2084
Counts vs. Mass-to-Charge (m/z)

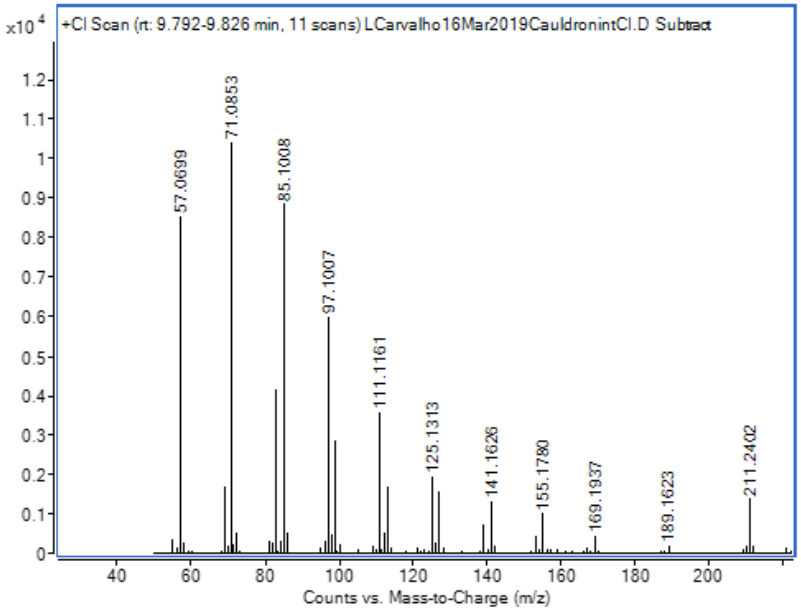

x10 2
+CI Scan (rt: 9.167-9.211 min, 14 scans) LCarvalho16Mar2019CauldroniextCI.D Subtract
57.0715
71.0868
85.1020
97.1030
111.1186
125.1333
139.1169
157.1243
175.1511
197.2297
Counts vs. Mass-to-Charge (m/z)

[7] 1-Pentadecene Mass: 210.234751

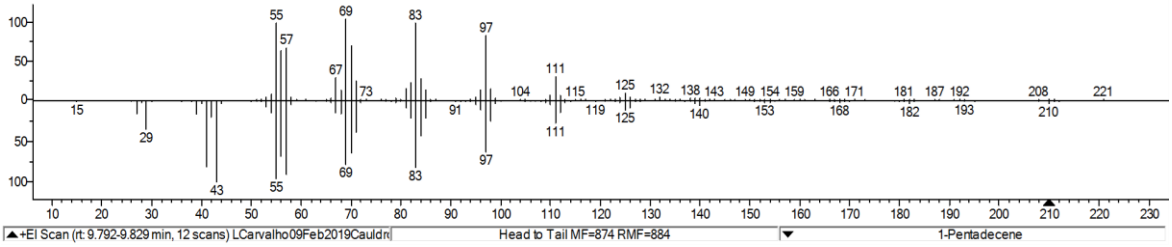
Interior

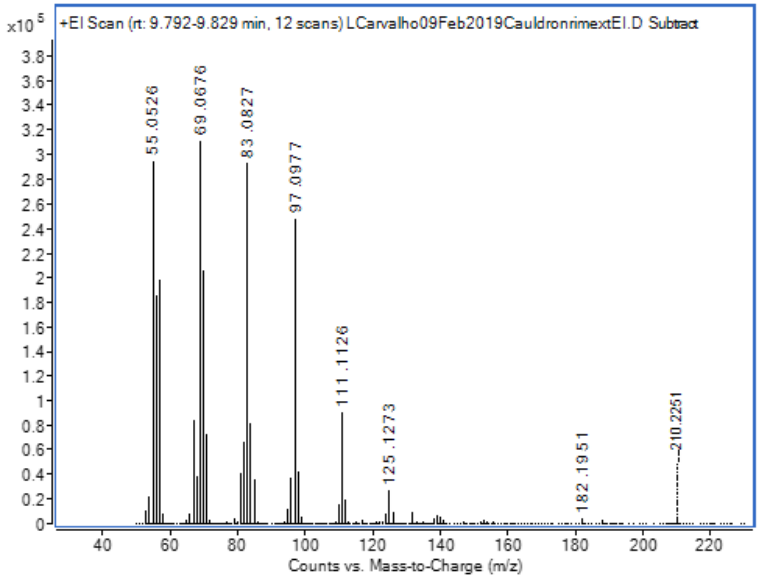


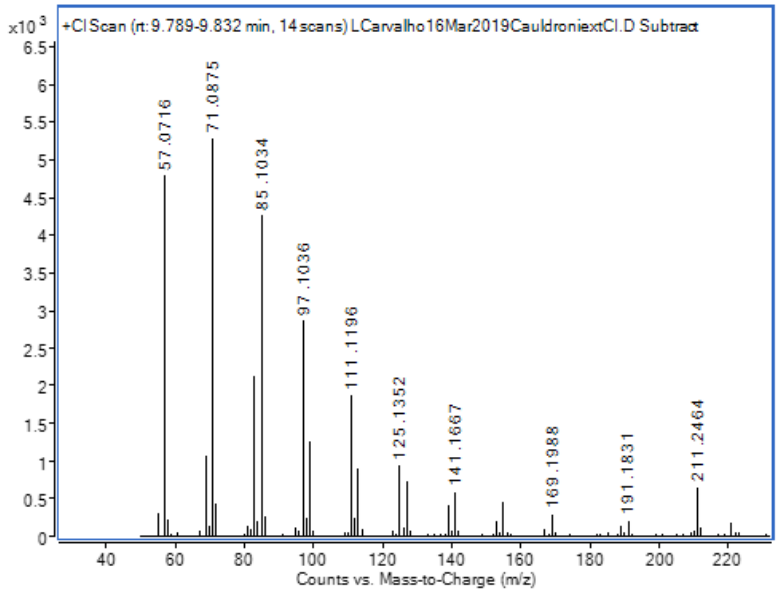




Exterior



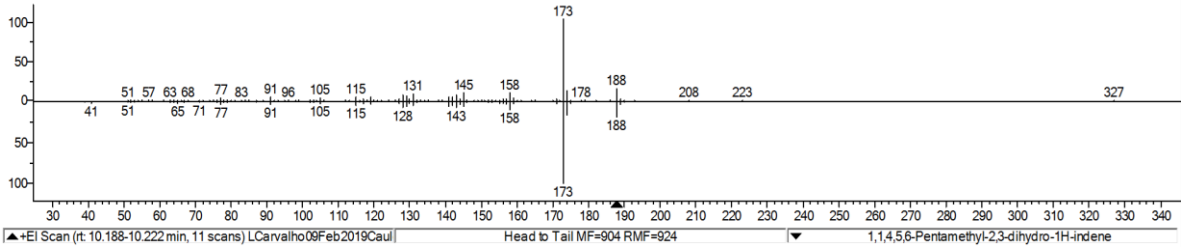


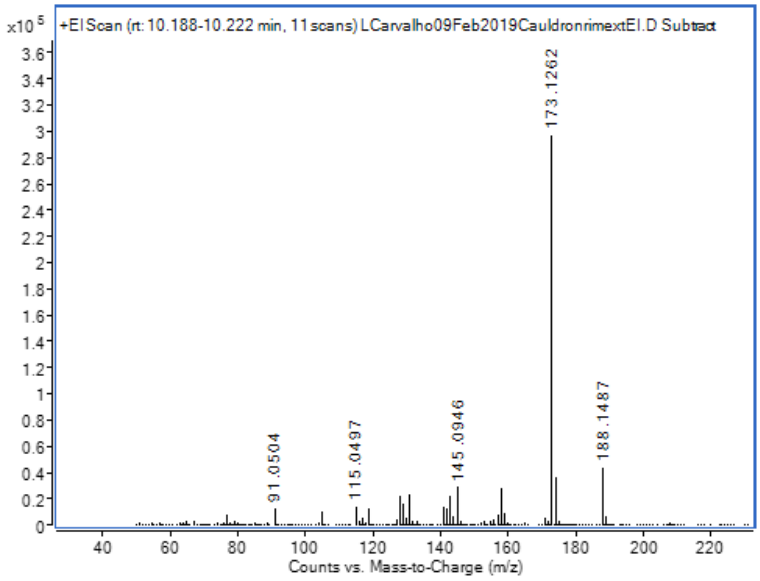


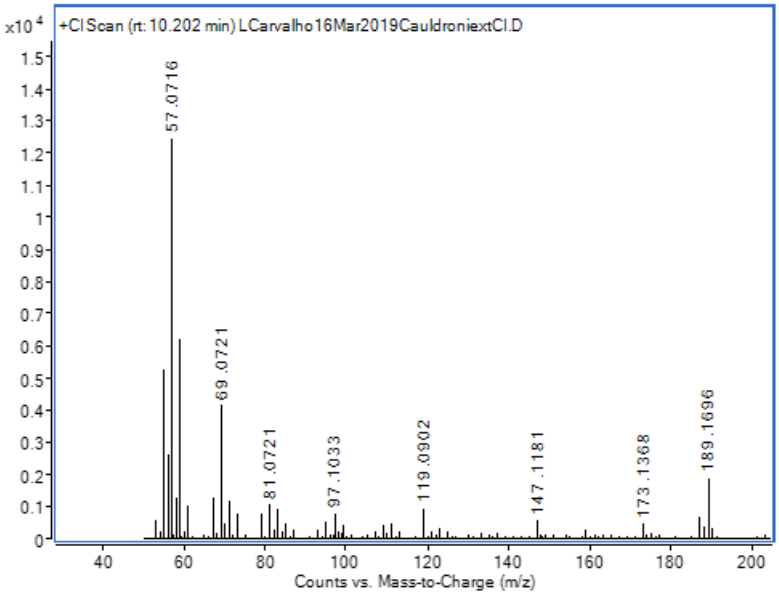
[8] 1,1,4,5,6-Pentamethyl-2, 3-dihydro=1H-indene

Mass:188.156501

Exterior

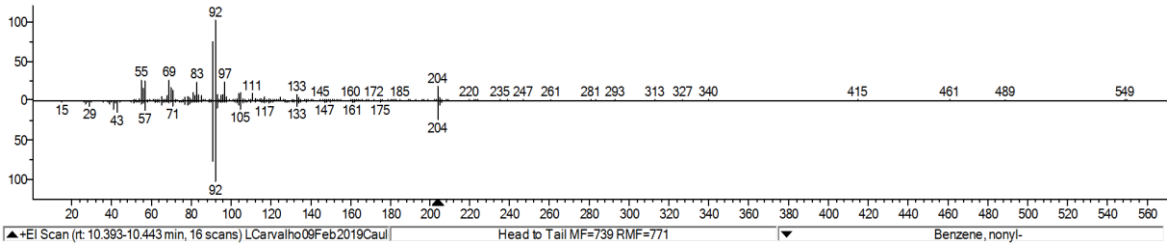


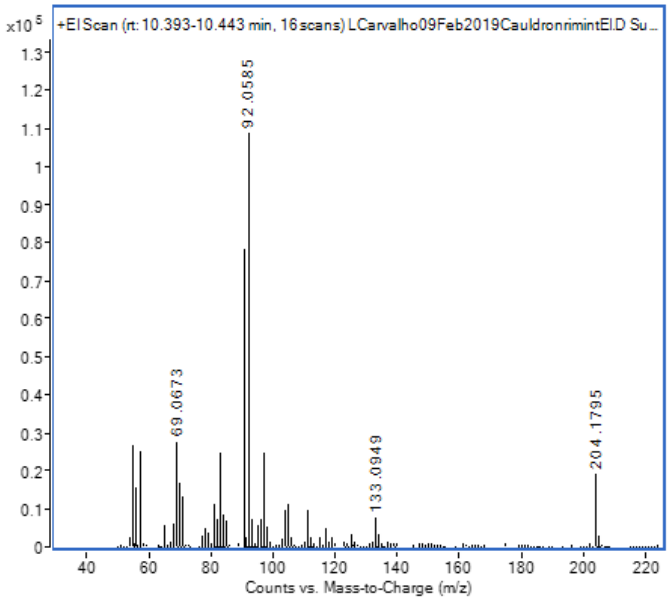


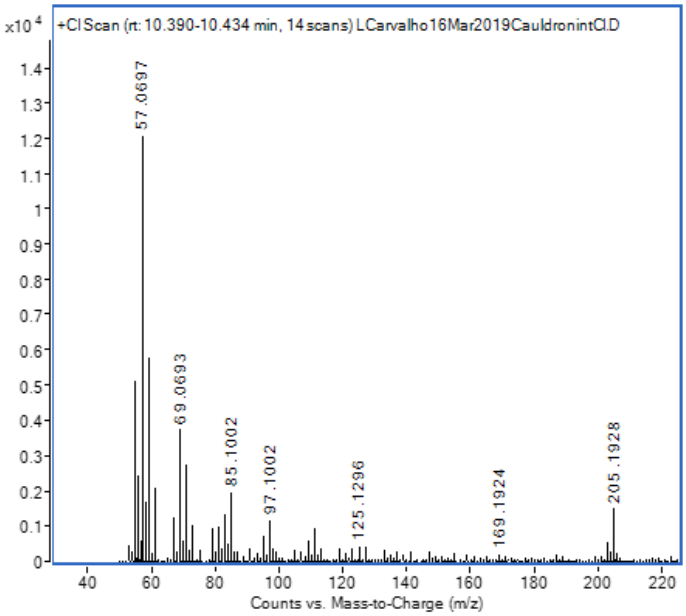


[9] Benzene, nonyl Mass: 204.1878

Interior

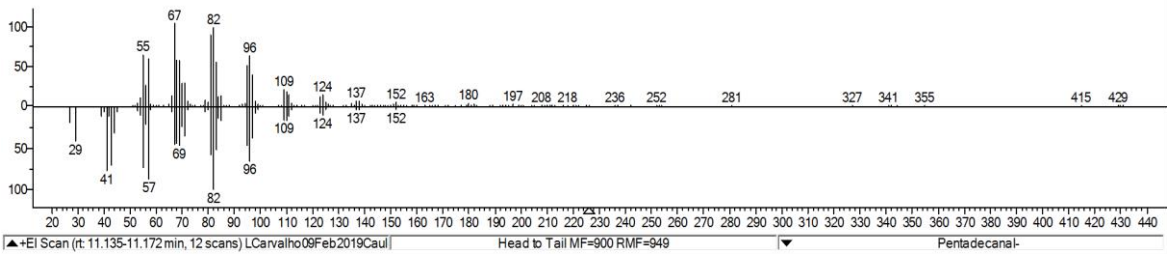


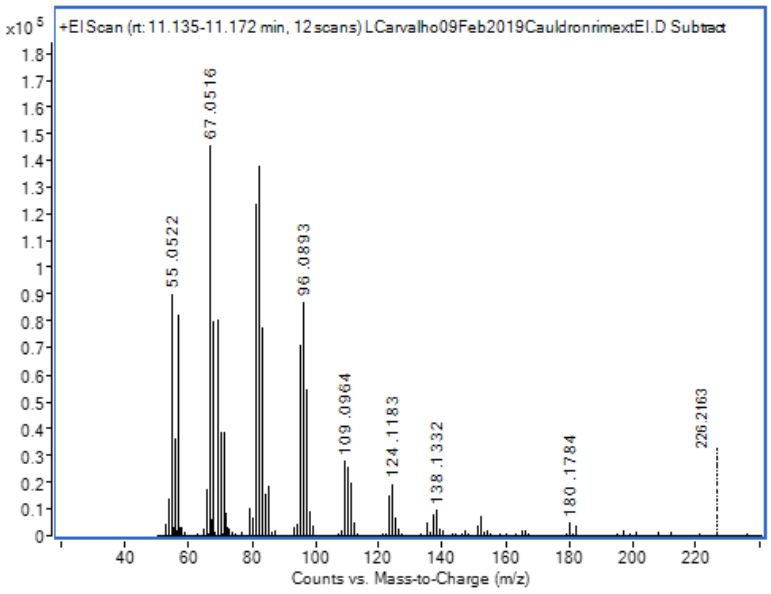


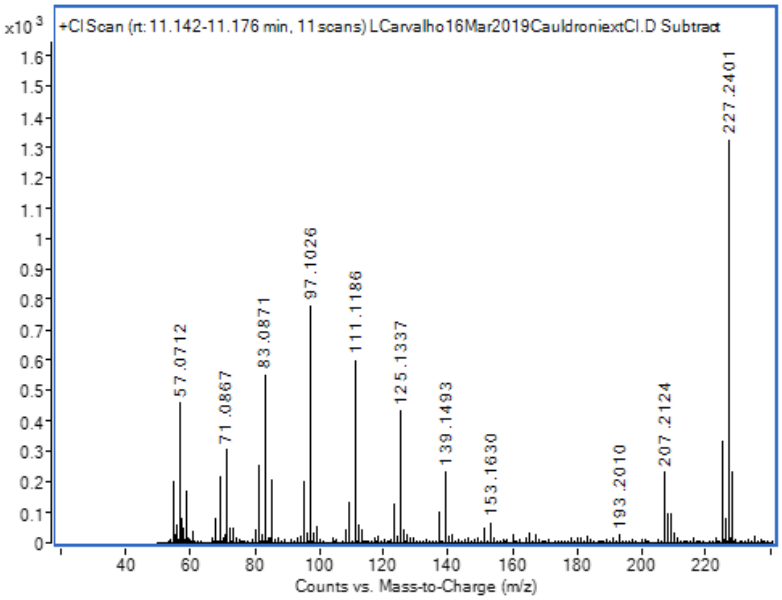


[10] Pentadecanal Mass: 226.229666

Exterior

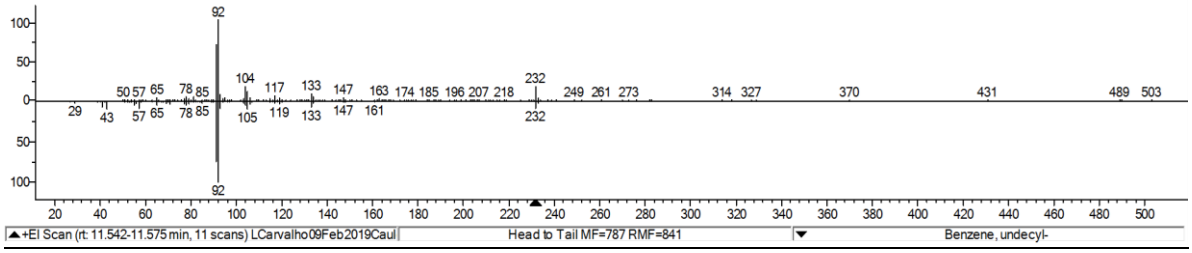


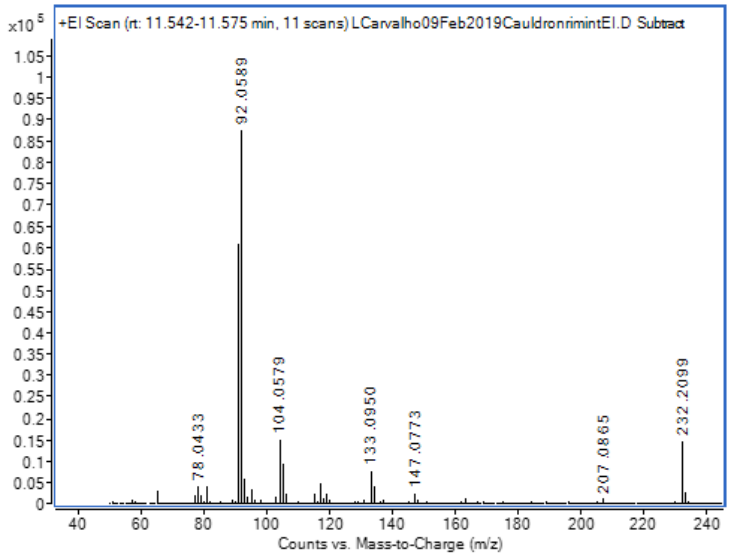


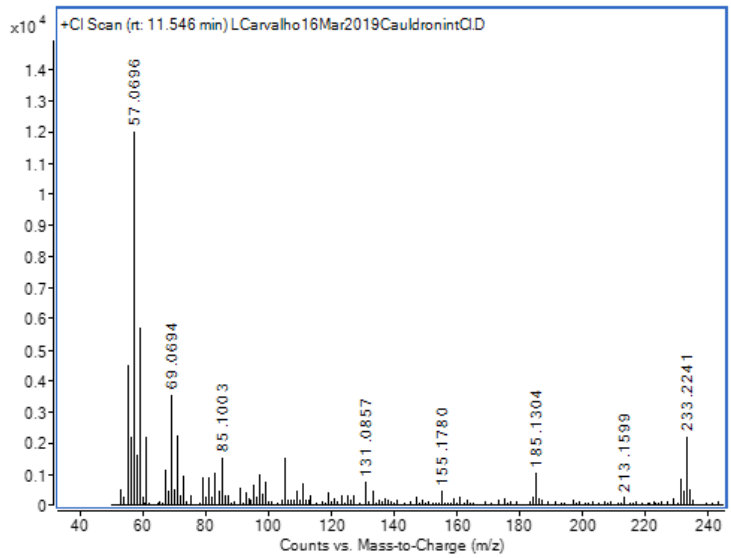


[11] Benzene, undecyl Mass: 232.219101

Interior

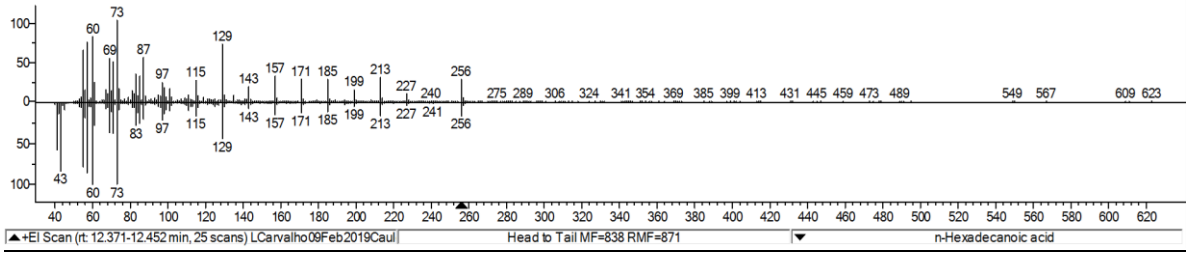


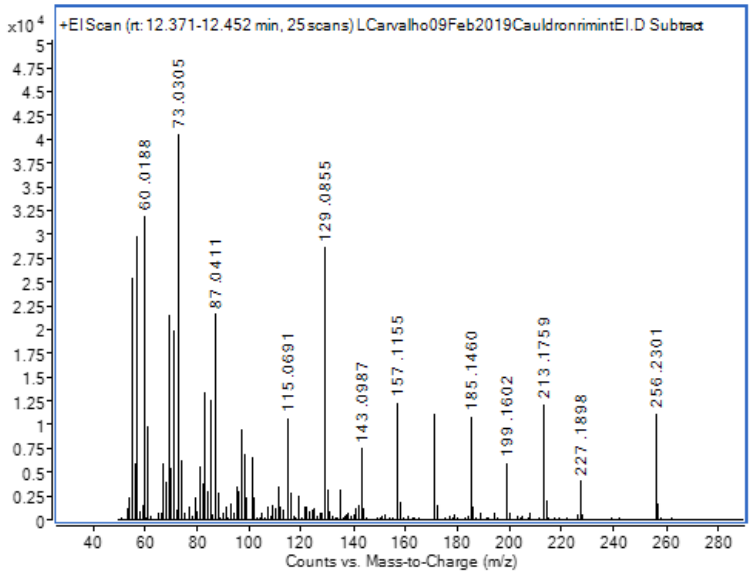


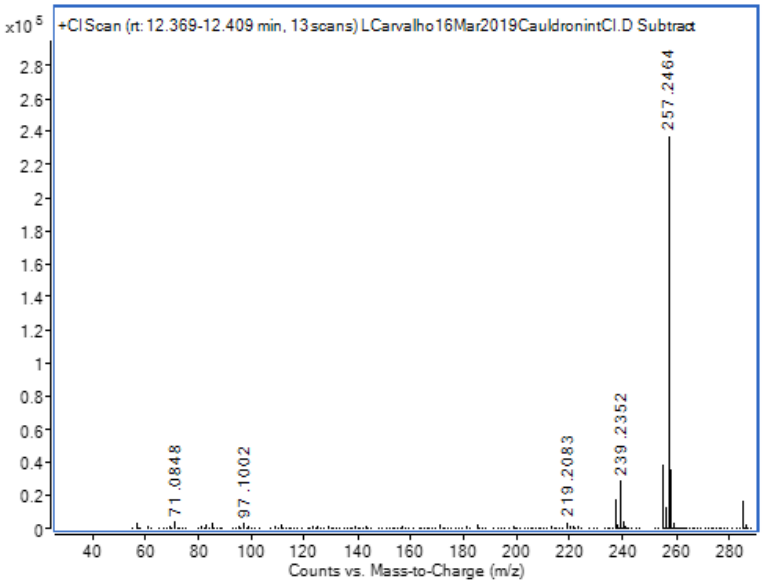


[12] n-Hexadecanoic acid

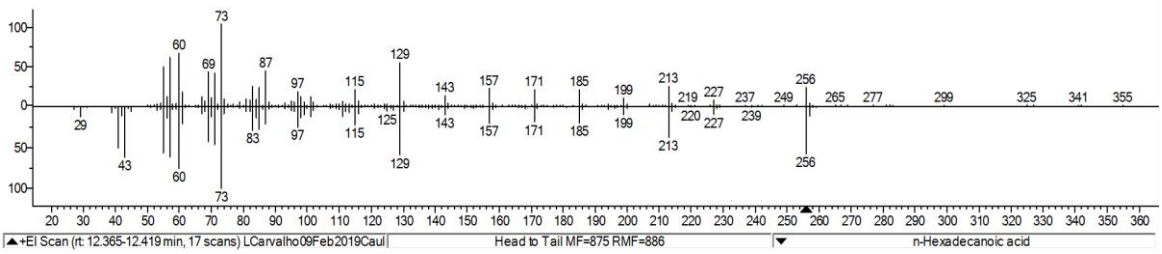
Interior

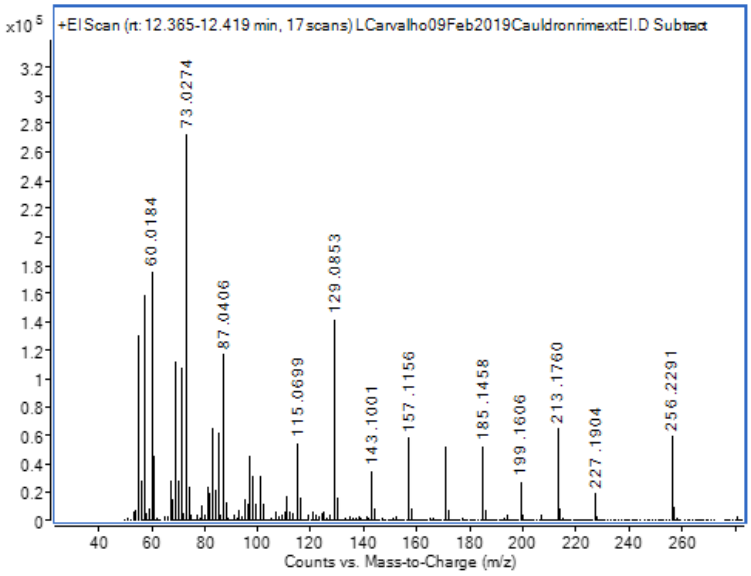


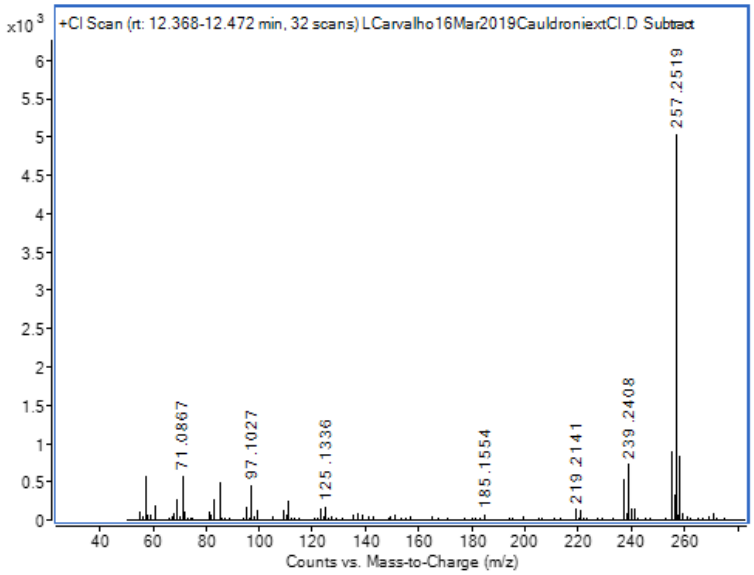




Exterior

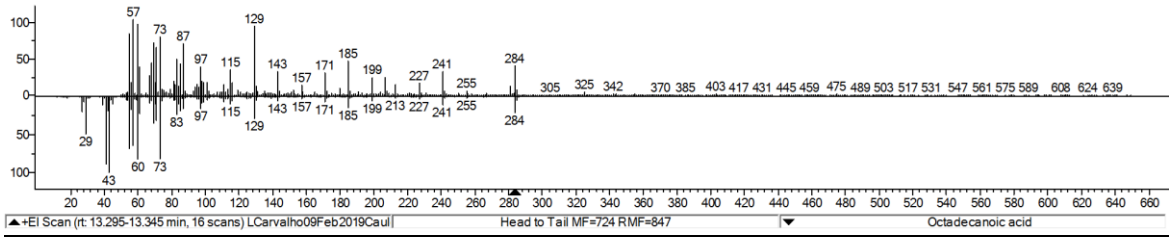

+EI Scan (rt: 12.365-12.419 min, 17 scans) LCarvalho09Feb2019Caul
Head to Tail MF=875 RMF=886
n-Hexadecanoic acid

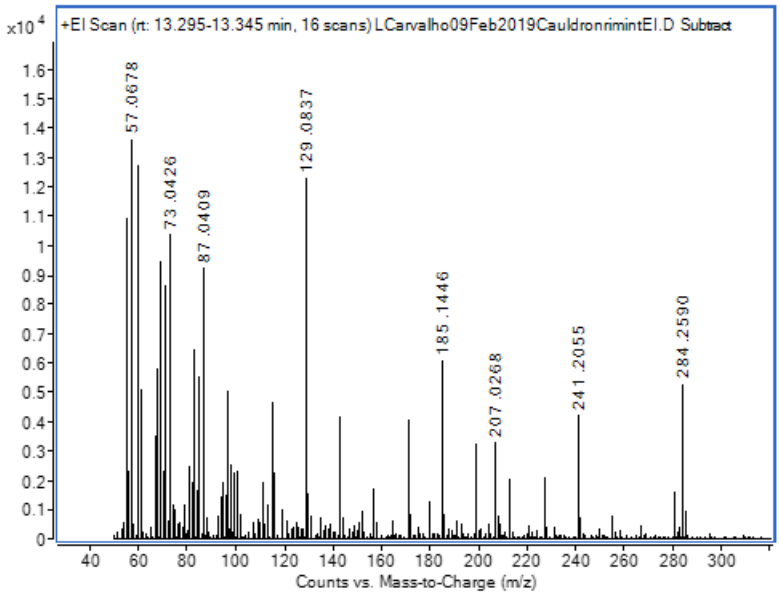

x10 5
+EI Scan (rt: 12.365-12.419 min, 17 scans) LCarvalho09Feb2019CauldronrimextEI.D Subtract
73.0274
60.0184
87.0406
129.0853
115.0699
143.1001
157.1156
185.1458
199.1606
213.1760
227.1904
256.2291
Counts vs. Mass-to-Charge (m/z)

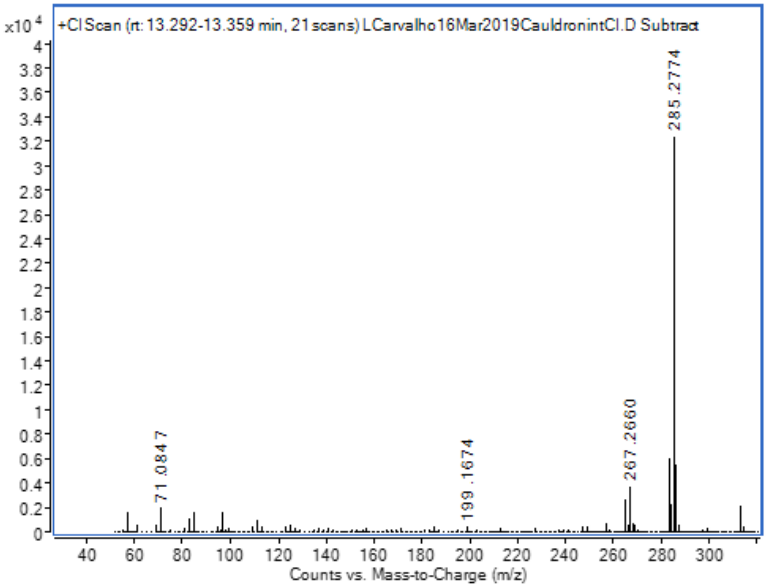

x10 3
+CI Scan (rt: 12.368-12.472 min, 32 scans) LCarvalho16Mar2019CauldroniextCI.D Subtract
257.2519
71.0867
97.1027
125.1336
185.1554
219.2141
239.2408
Counts vs. Mass-to-Charge (m/z)

[13] Octadecanoic acid

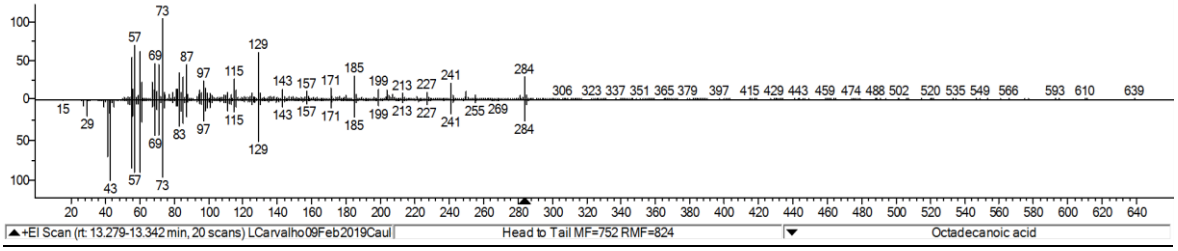
Interior

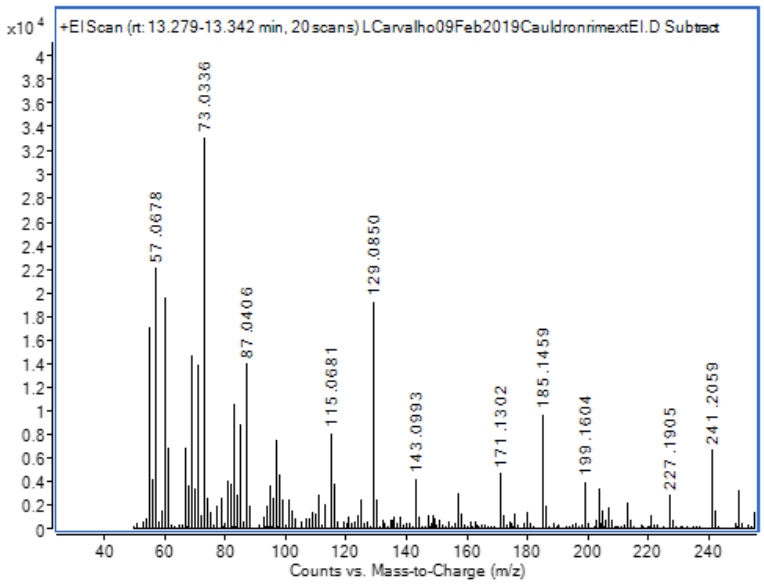


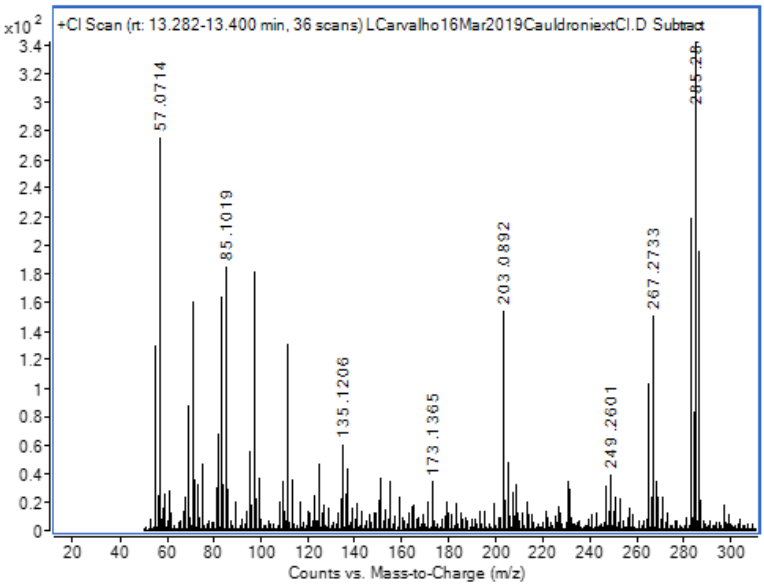




Exterior

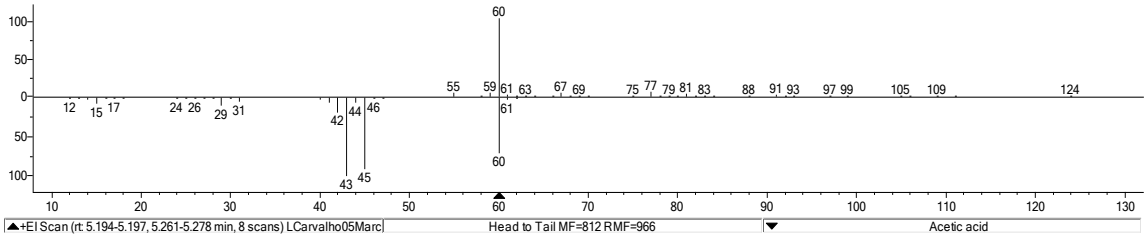

+EI Scan (rt: 13.279-13.342 min, 20 scans) LCarvalho09Feb2019Caul
Head to Tail MF=752 RMF=824
Octadecanoic acid

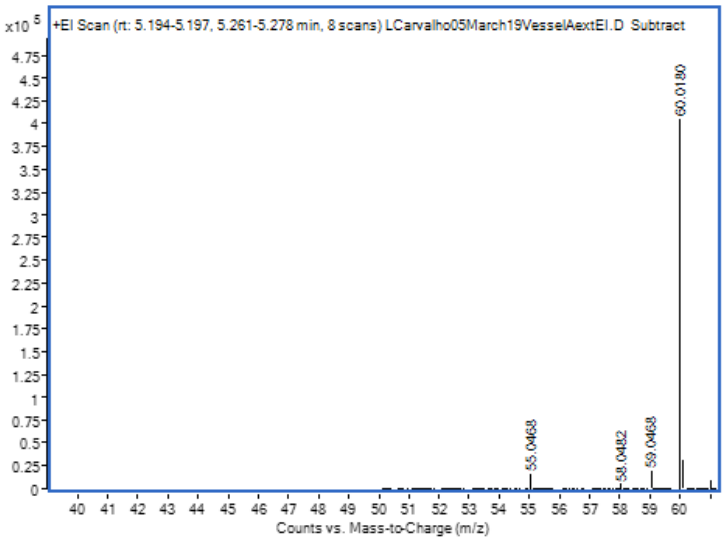

x10 4
+EI Scan (rt: 13.279-13.342 min, 20 scans) LCarvalho09Feb2019CauldronrimextEI.D Subtract
73.0336
57.0678
87.0406
129.0850
115.0681
143.0993
171.1302
185.1459
199.1604
227.1905
241.2059
Counts vs. Mass-to-Charge (m/z)

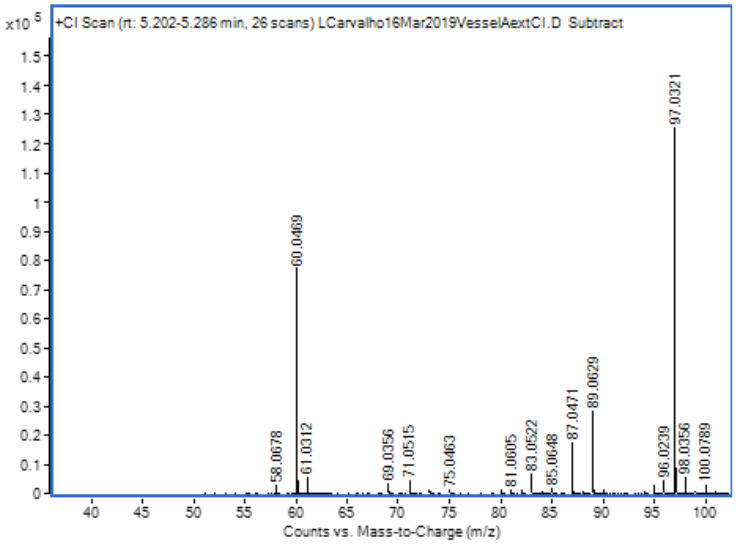

x10 2
+CI Scan (rt: 13.282-13.400 min, 36 scans) LCarvalho16Mar2019CauldroniextCI.D Subtract
57.0714
85.1019
135.1206
173.1365
203.0892
249.2601
267.2733
285.28
Counts vs. Mass-to-Charge (m/z)

[1] Acetic Acid Mass: 60.0211294

Exterior Sample

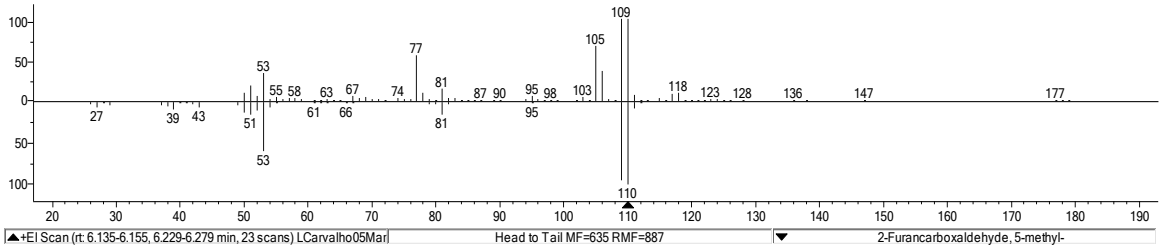


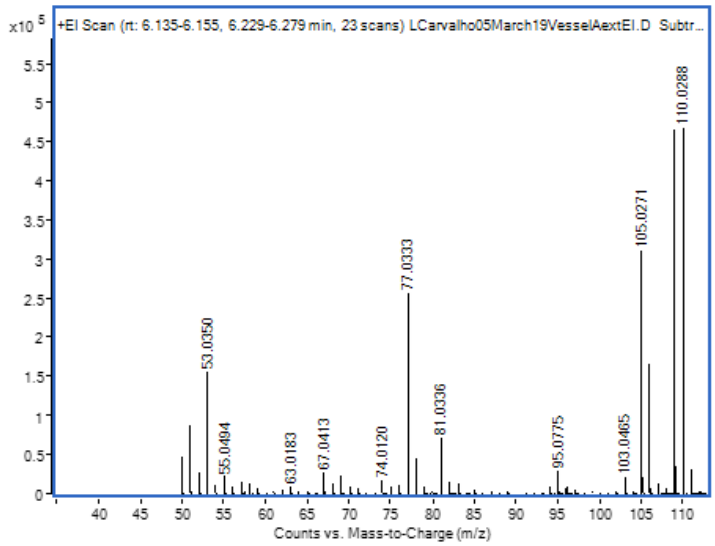


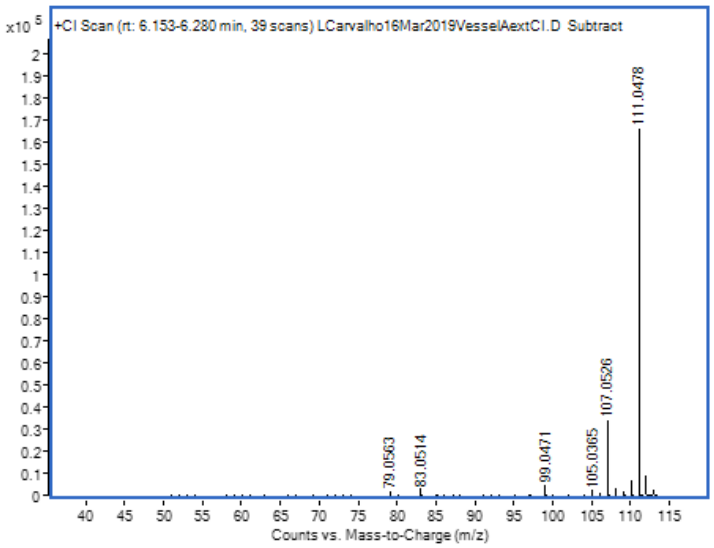


[2] 5-methyl Furfural Mass: 110.0367794

Exterior

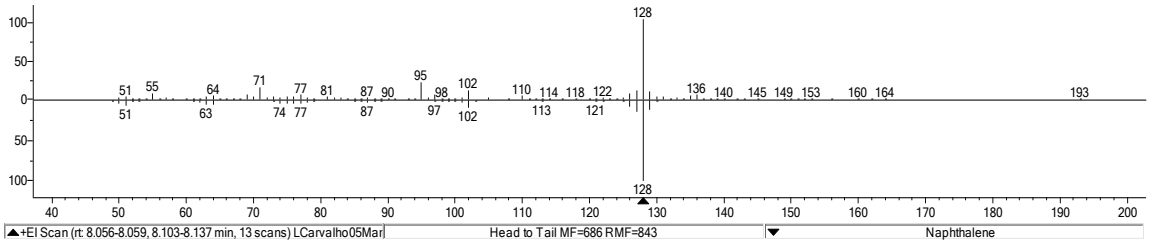


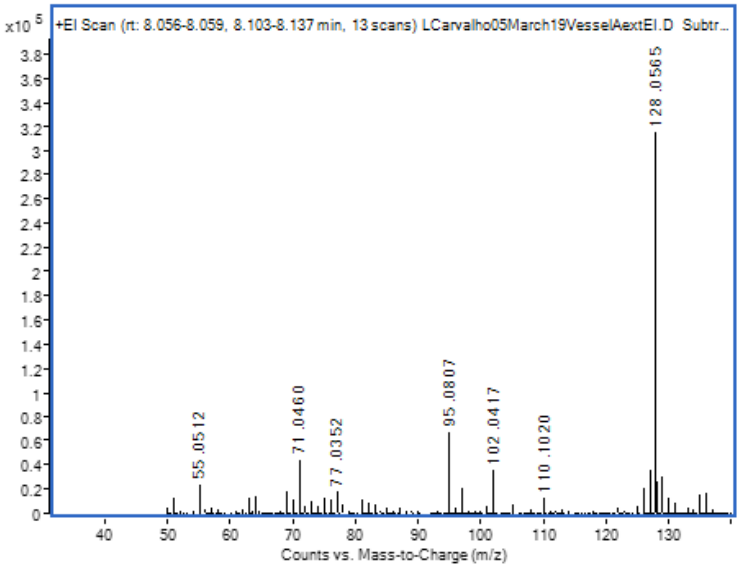


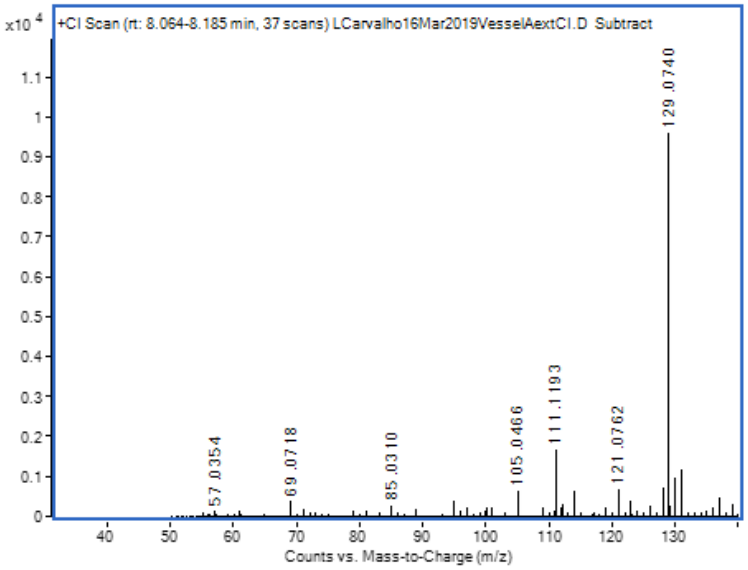


[3] Naphthalene Mass: 128.0626

Exterior

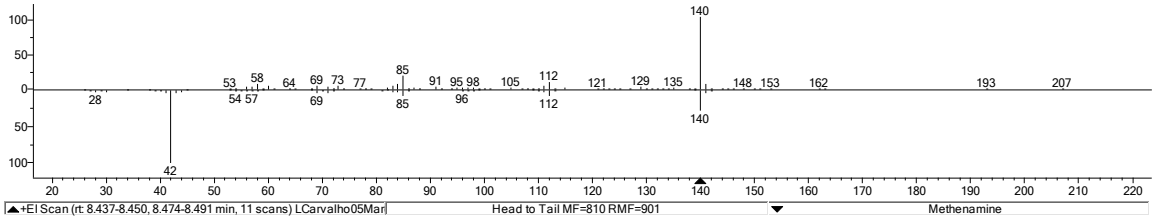

+EI Scan (rt: 8.056-8.059, 8.103-8.137 min, 13 scans) LCarvalho05Mar
Head to Tail MF=686 RMF=843
Naphthalene

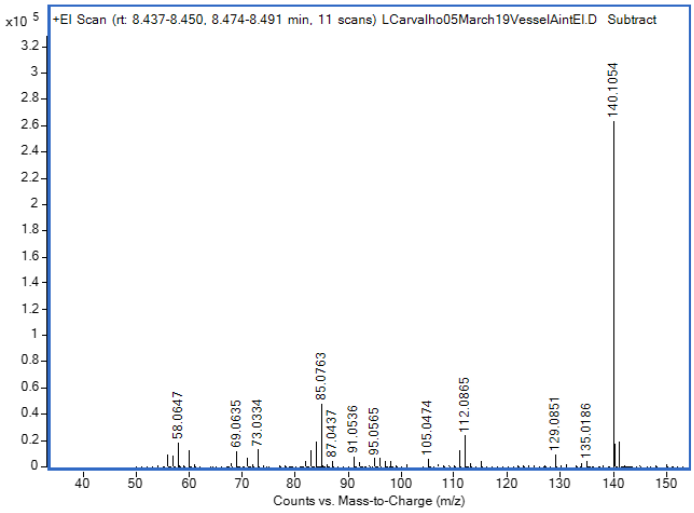

+EI Scan (rt: 8.056-8.059, 8.103-8.137 min, 13 scans) LCarvalho05March19VesselAextEI.D Subtr...
128.0565
95.0807
71.0460
102.0417
55.0512
77.0352
110.1020
Counts vs. Mass-to-Charge (m/z)

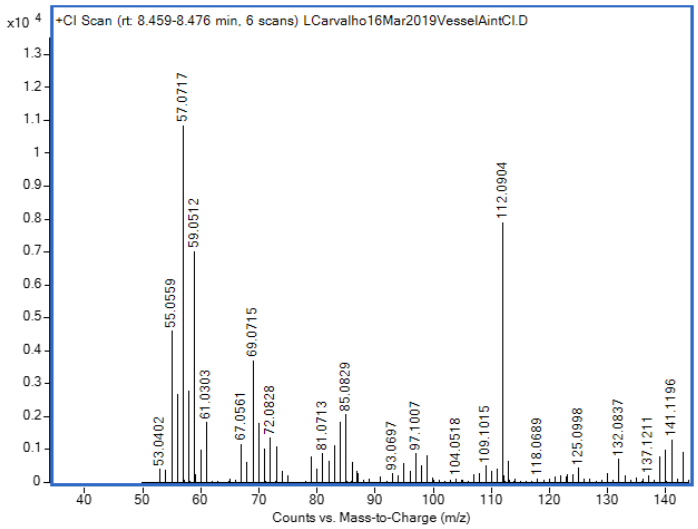

+CI Scan (rt: 8.064-8.185 min, 37 scans) LCarvalho16Mar2019VesselAextCI.D Subtract
129.0740
111.1193
105.0466
121.0762
69.0718
85.0310
57.0354
Counts vs. Mass-to-Charge (m/z)

[4] Methenamine Mass: 140.106196

Interior

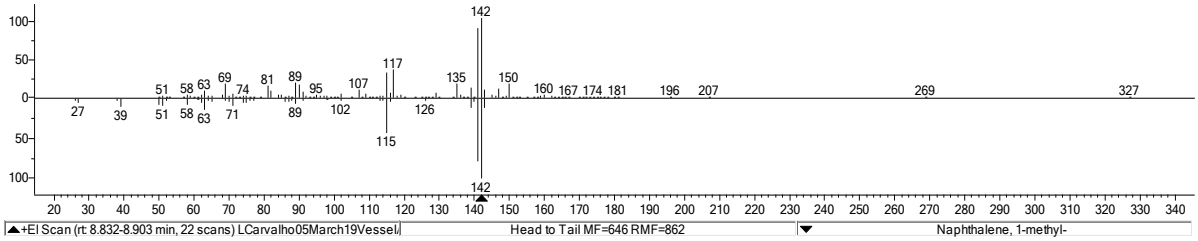


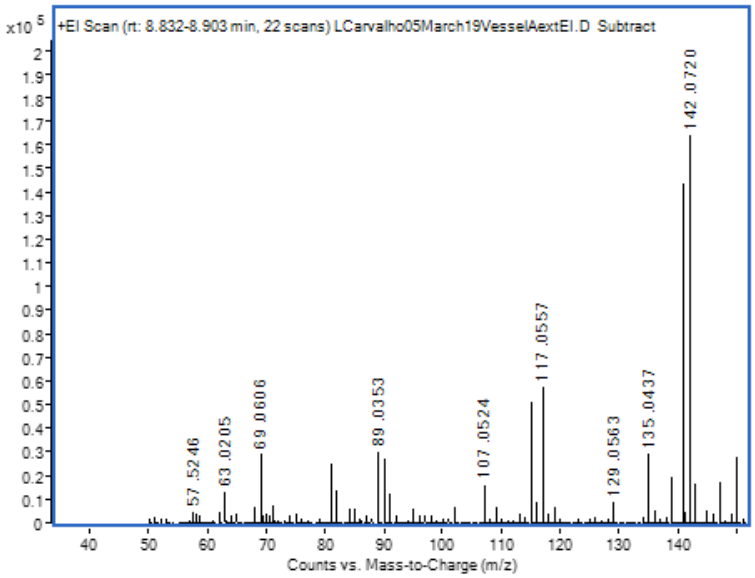


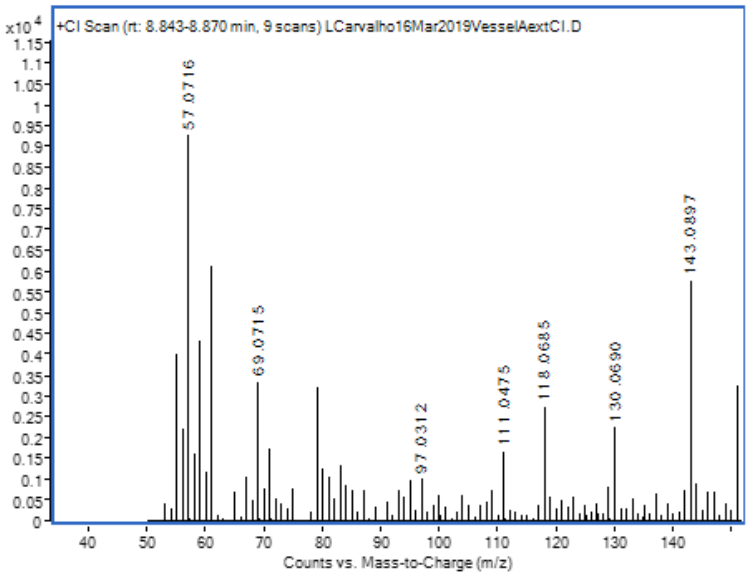


[5] 1-methyl Naphthalene Mass: 142.07825

Exterior

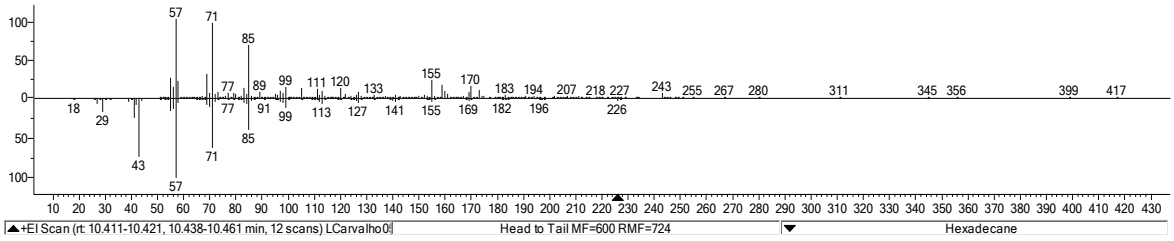


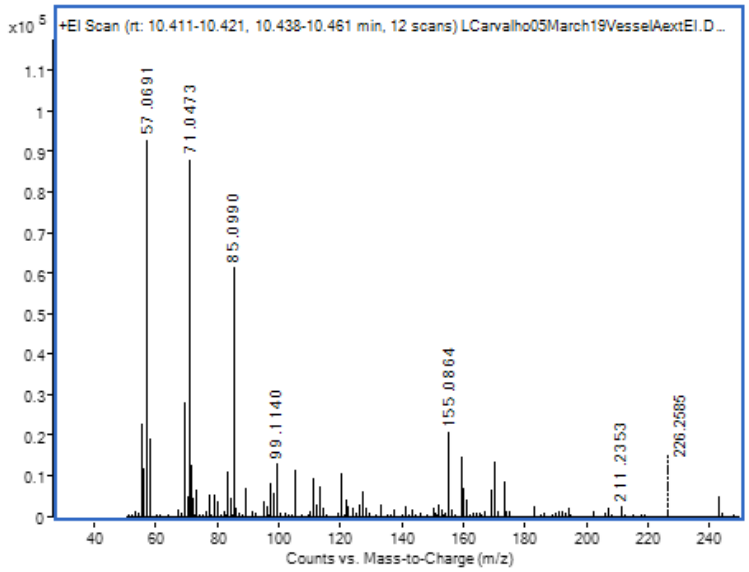


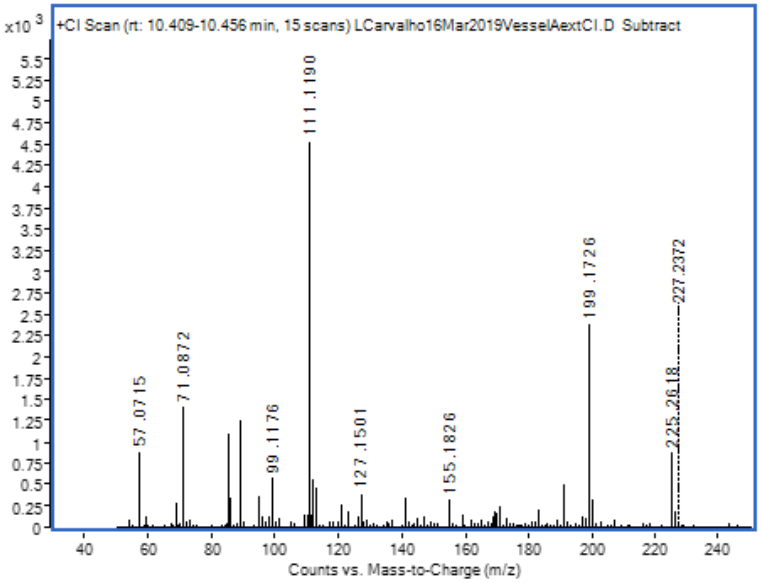


[6] Hexadecane Mass: 226.266051 NIST#: 228773

Exterior

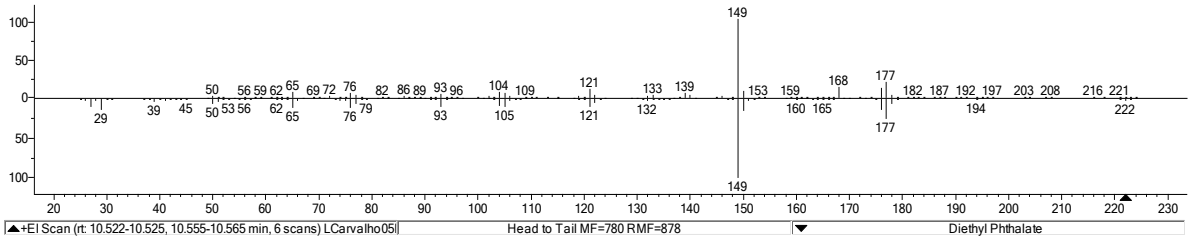


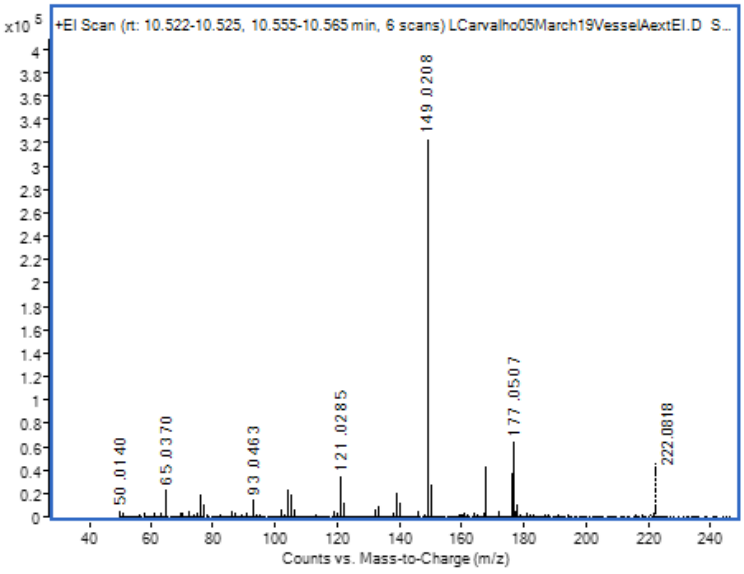


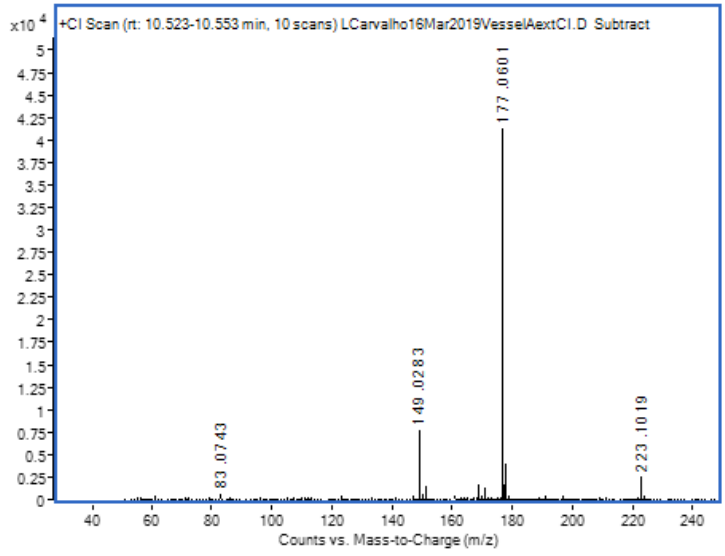


[7] Diethyl Phthalate Mass: 222.089209 NIST#: 155450

Exterior

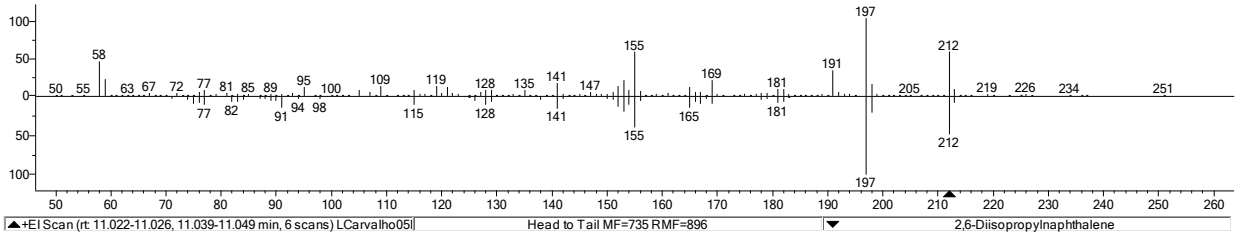


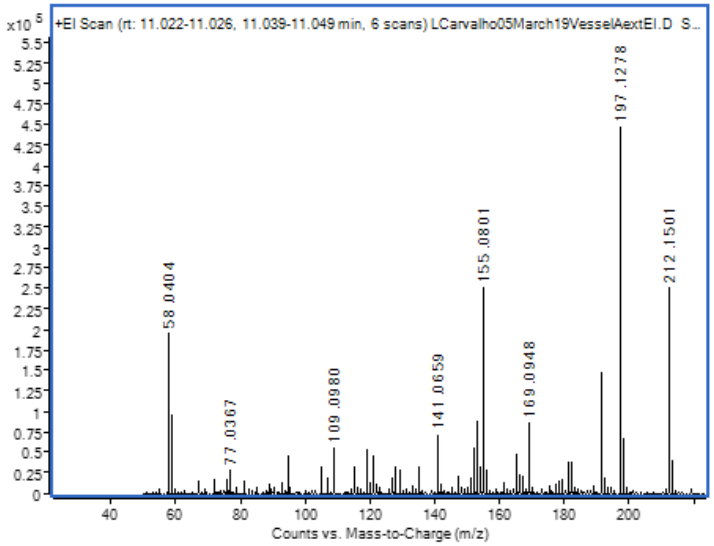


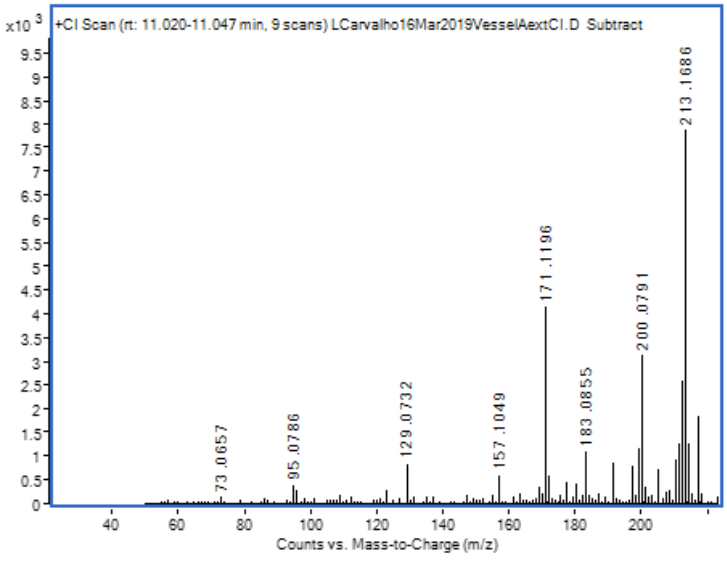


[8] 2,6-Diisopropylnaphthalene Mass: 212.156501

Exterior

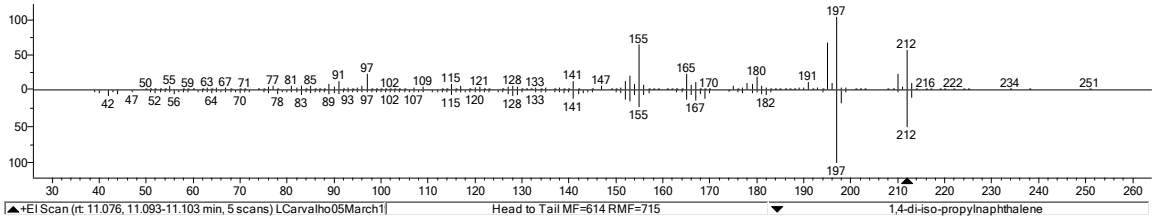


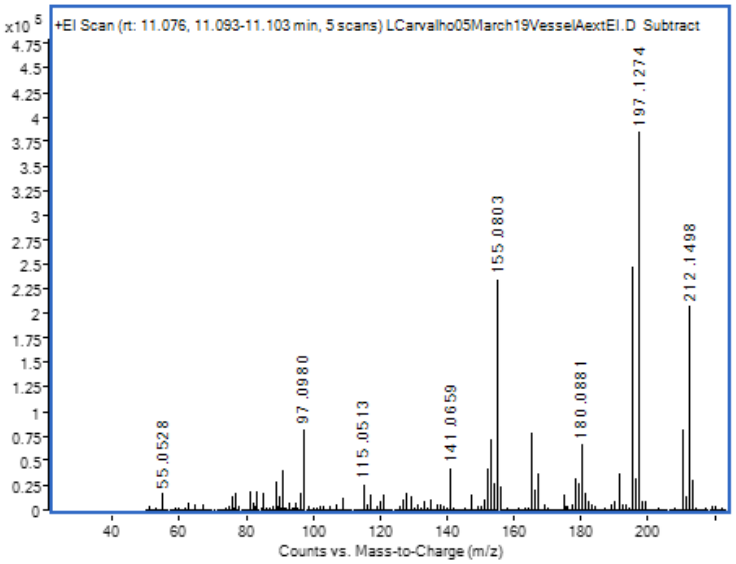


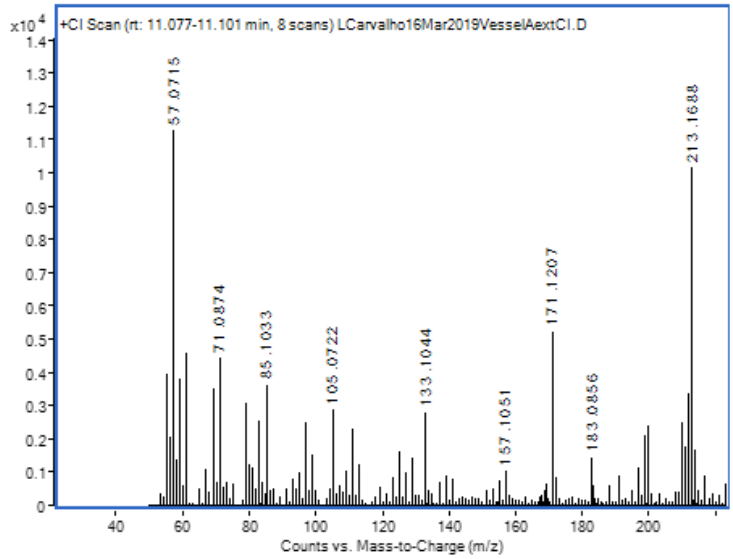


[9] 1,4-di-iso-propylnaphthalene Mass: 212.156501

Exterior

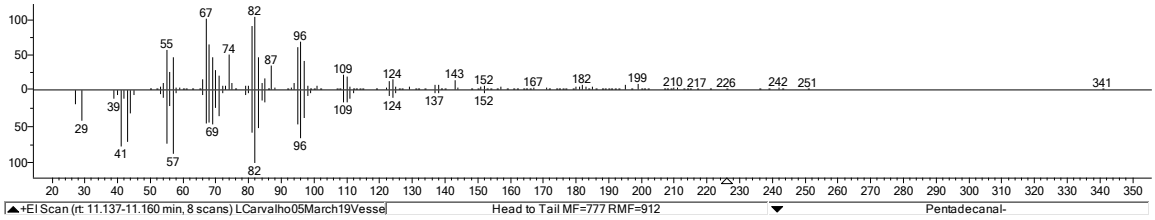


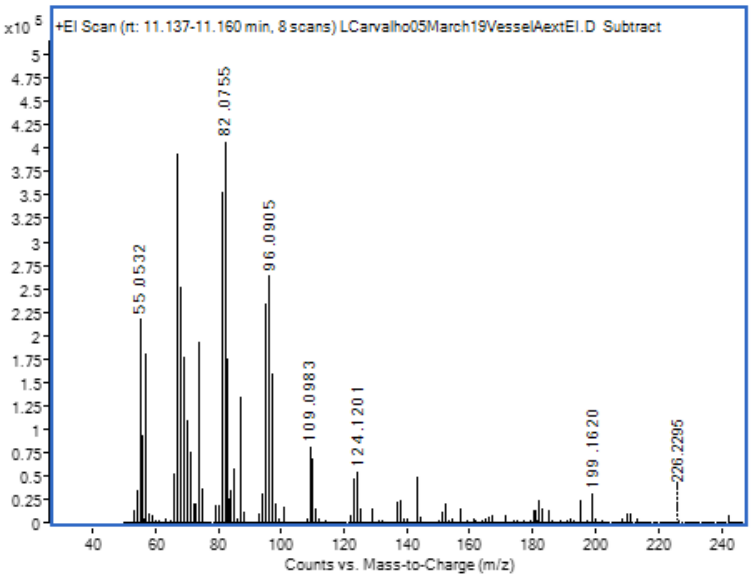


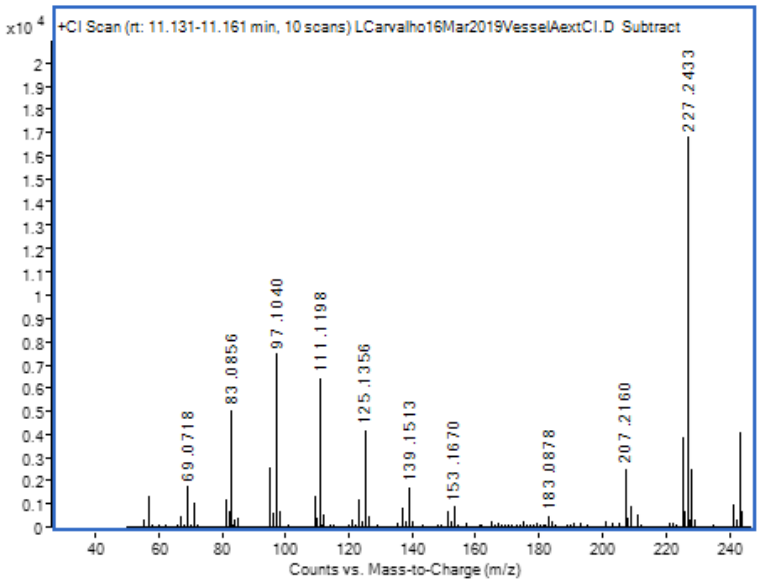


[10] Pentadecanal Mass: 226.229666

Exterior

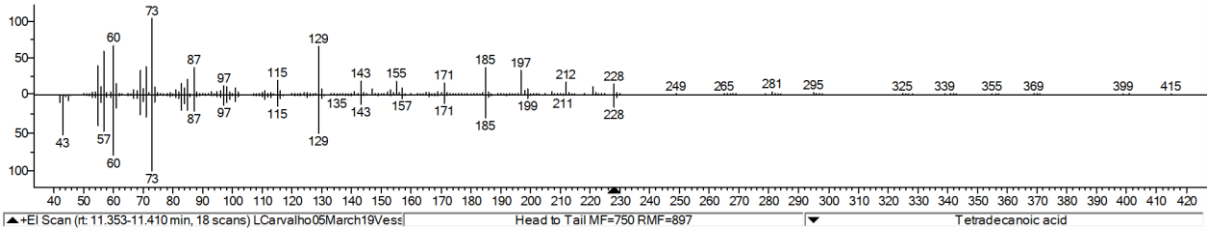


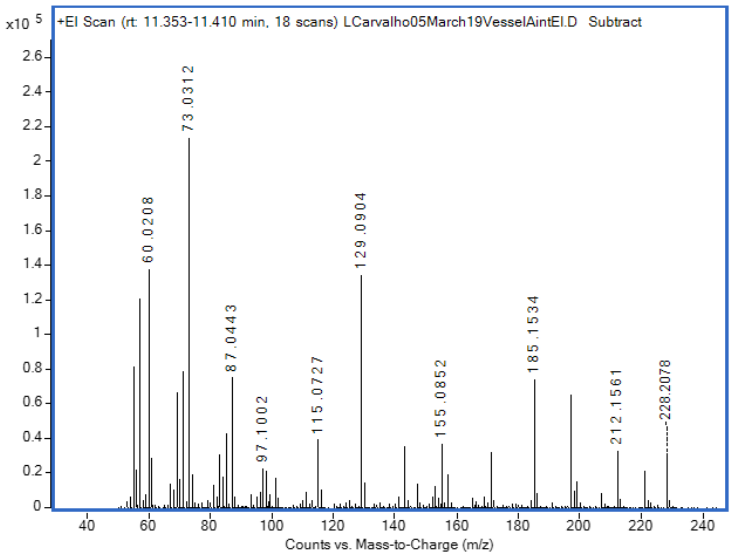


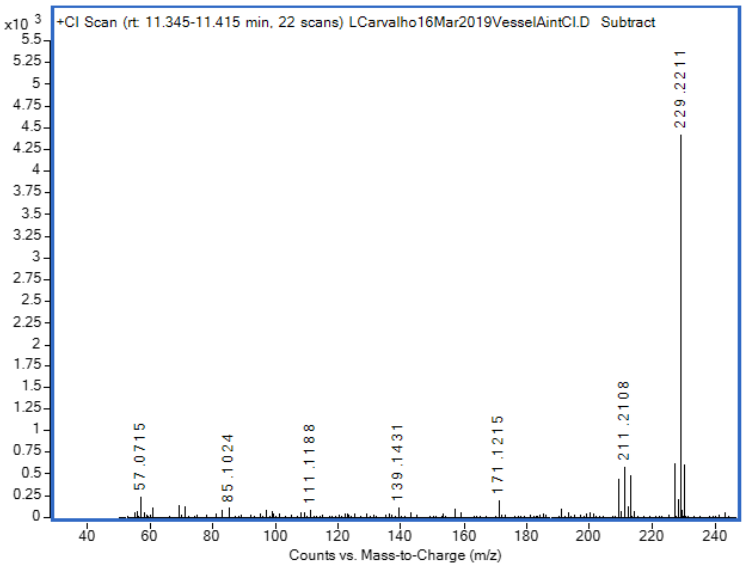


[11] Tetradecanoic acid Mass: 228.20893

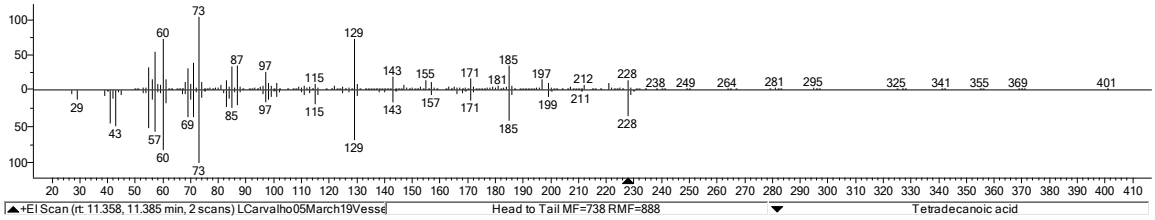
Interior

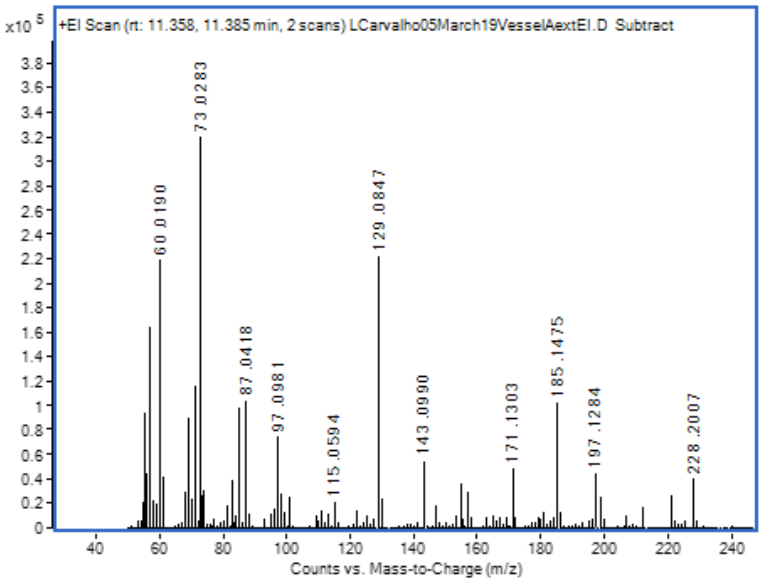


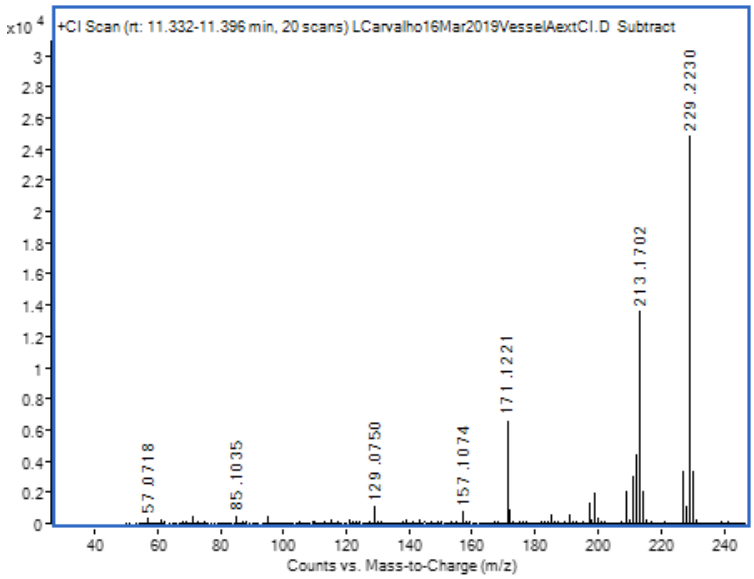




Exterior

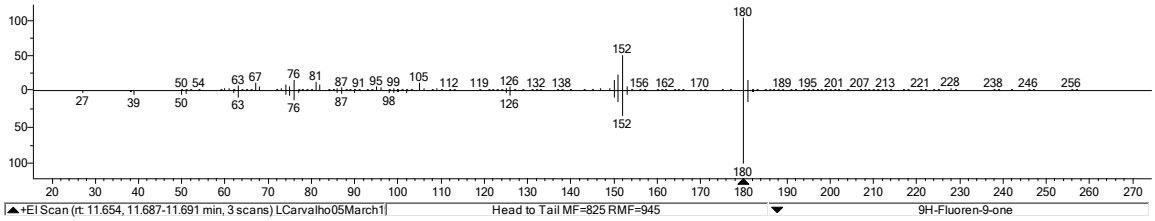

+EI Scan (rt: 11.358, 11.385 min, 2 scans) LCarvalho05March19Vesse
Head to Tail MF=738 RMF=888
Tetradecanoic acid

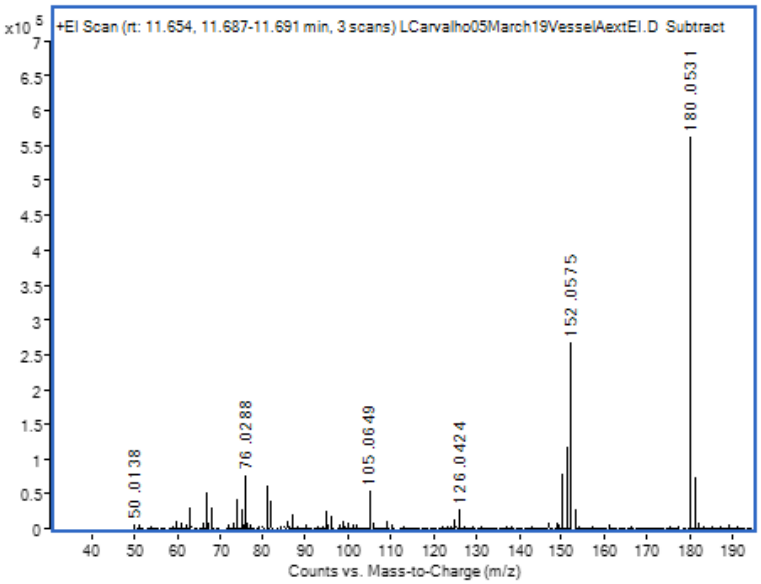

x10 5
+EI Scan (rt: 11.358, 11.385 min, 2 scans) LCarvalho05March19VesselAextEI.D Subtract
73.0283
60.0190
129.0847
87.0418
97.0981
115.0594
143.0990
171.1303
185.1475
197.1284
228.2007
Counts vs. Mass-to-Charge (m/z)

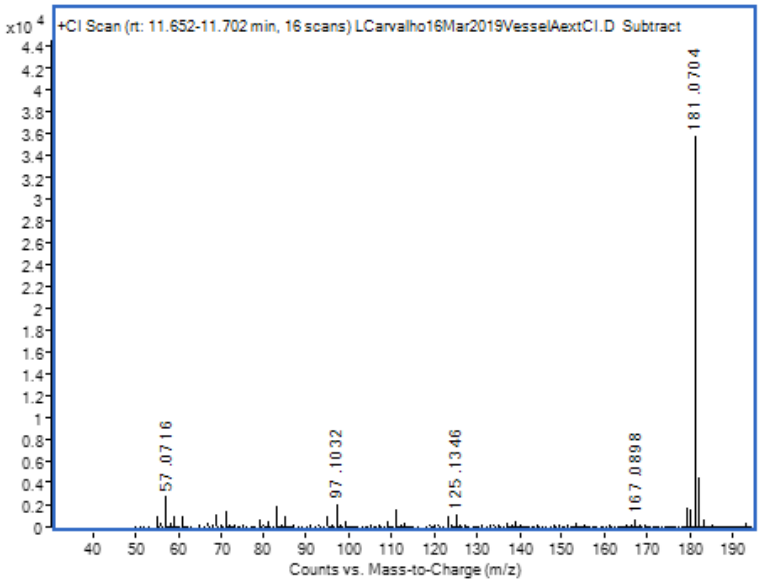

x10 4
+CI Scan (rt: 11.332-11.396 min, 20 scans) LCarvalho16Mar2019VesselAextCI.D Subtract
229.2230
213.1702
171.1221
157.1074
129.0750
85.1035
57.0718
Counts vs. Mass-to-Charge (m/z)

[12] 9H-Fluoren-9-one Mass: 180.057515

Exterior

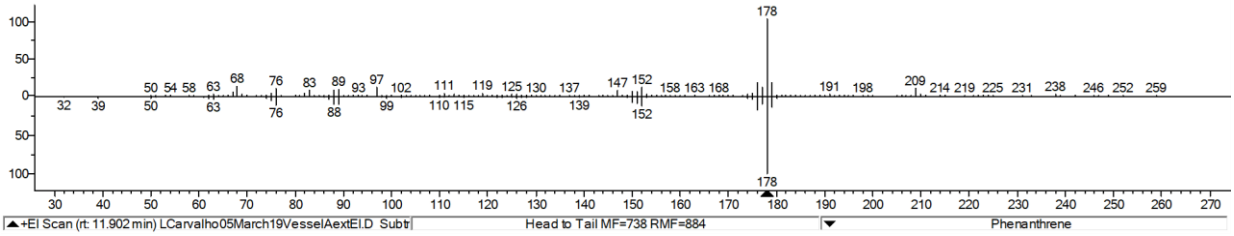


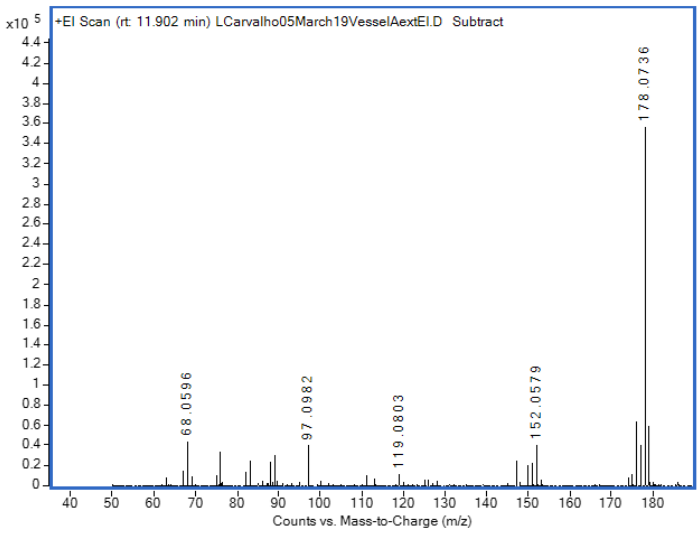


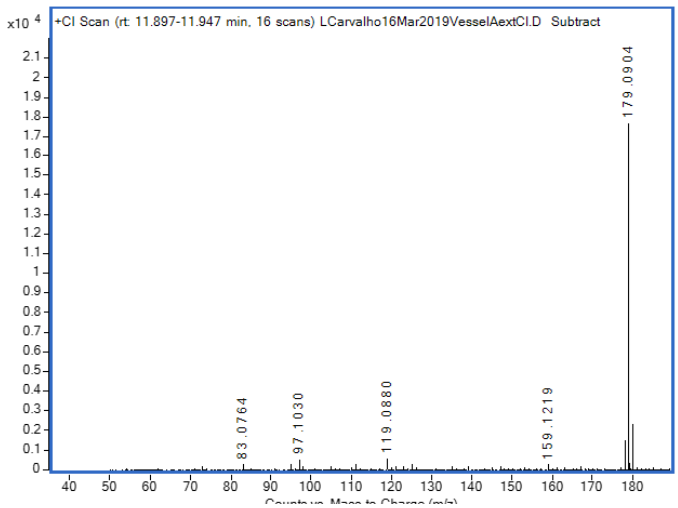


[13] Phenanthrene Mass: 178.07825

Exterior

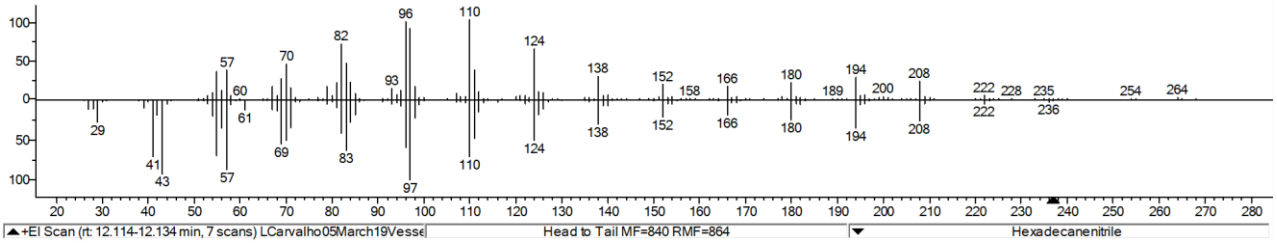


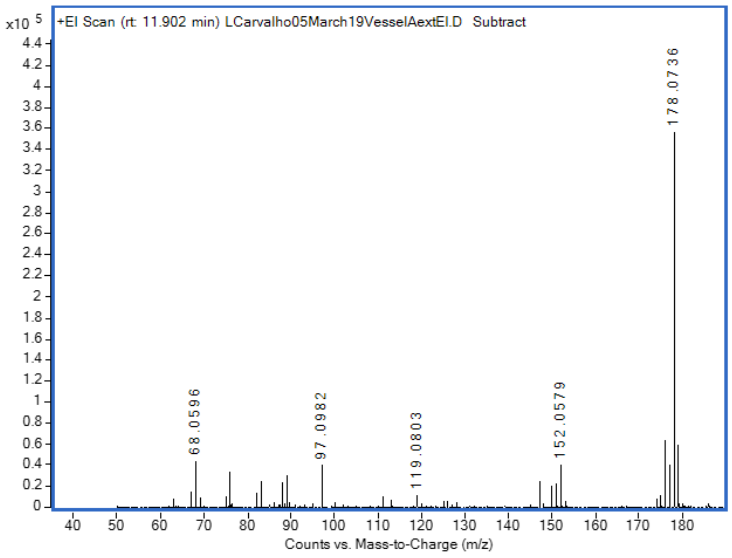


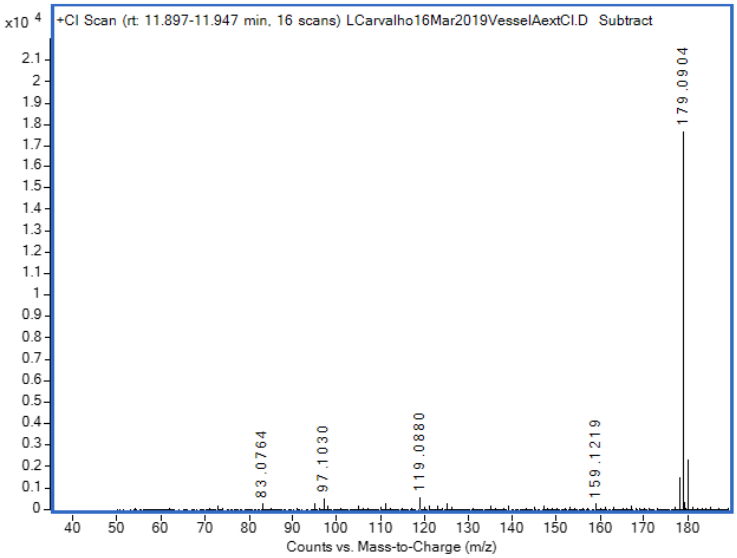


[14] Hexadecanenitrile Mass: 237.24565

Exterior

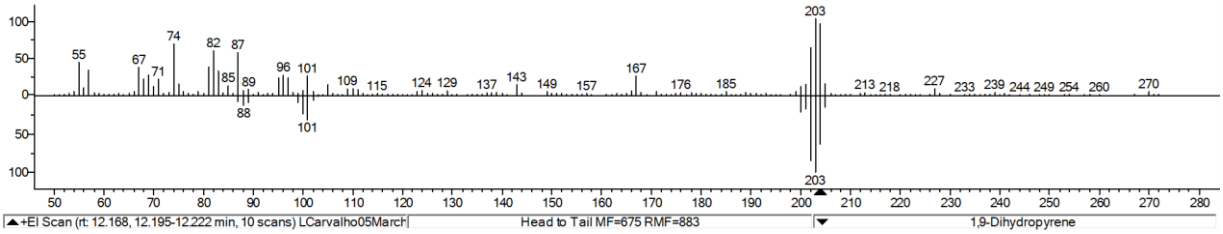


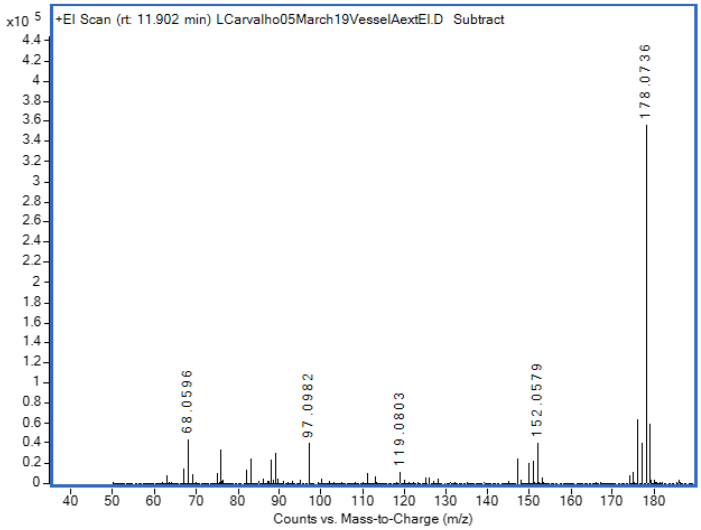


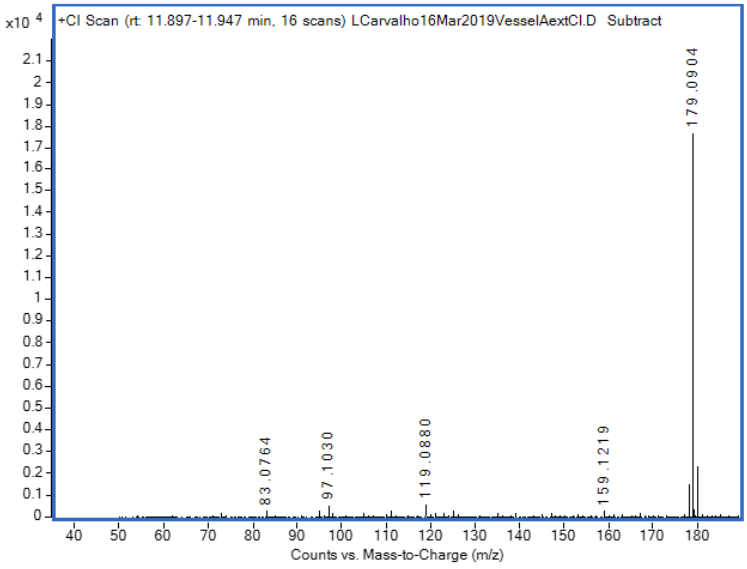


[15] 1,9-Dihydropyrene Mass: 204.093901

Exterior

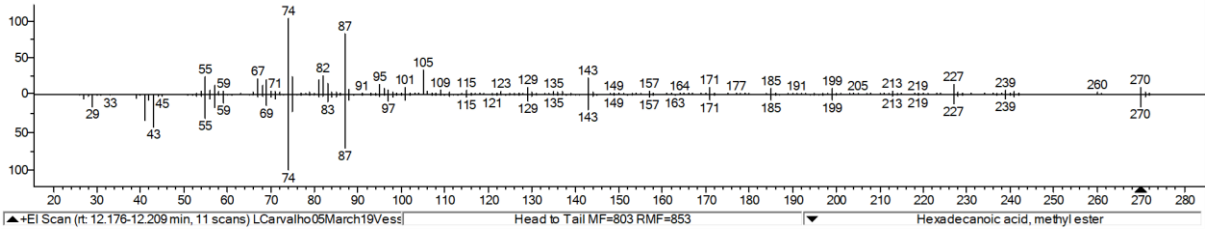


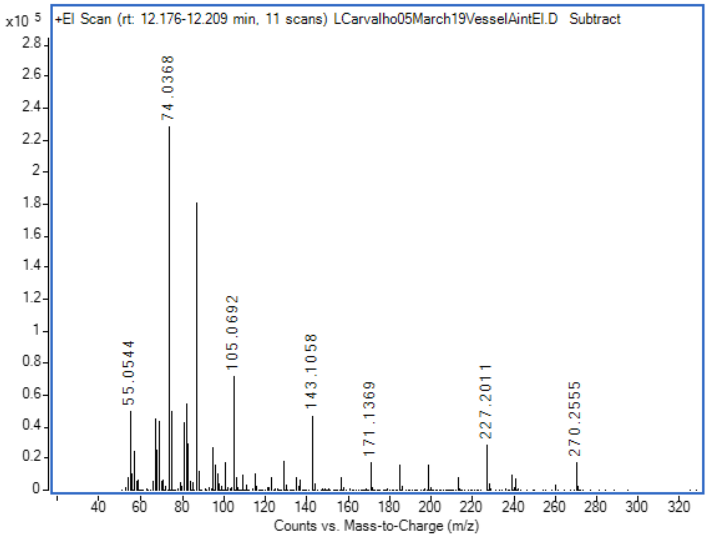


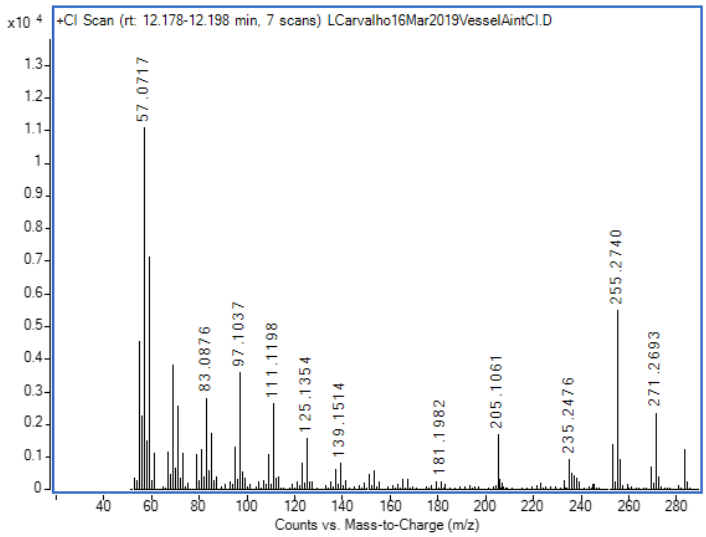


[16] Hexadecanoid acid methyl ester Mass: 270.25588

Interior

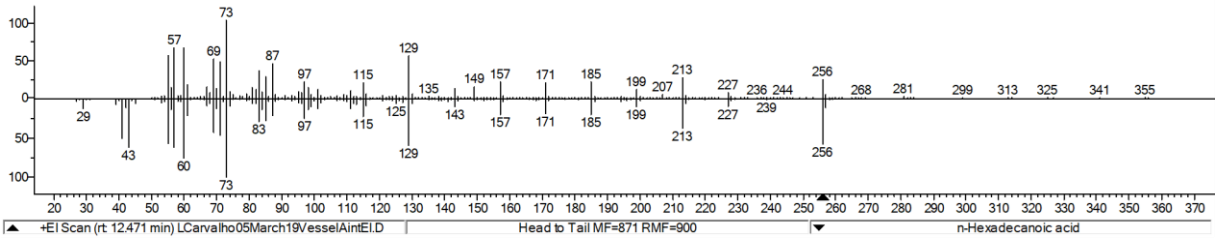


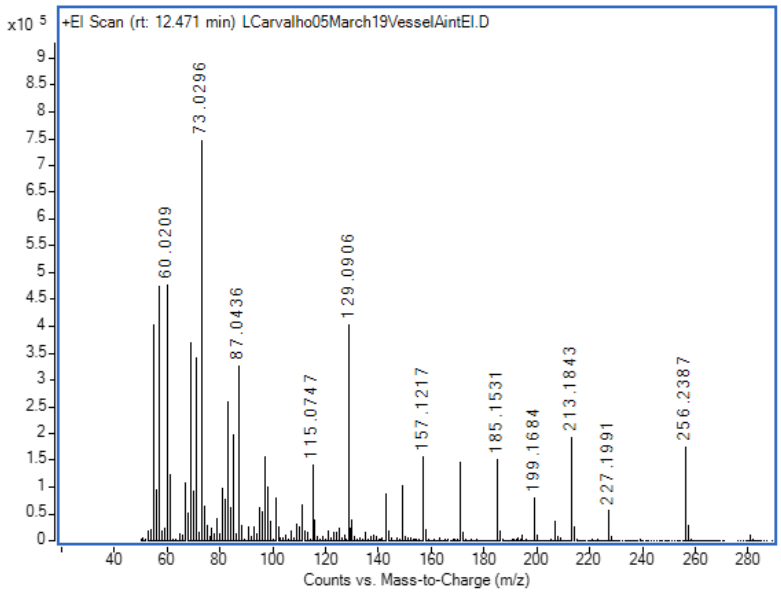


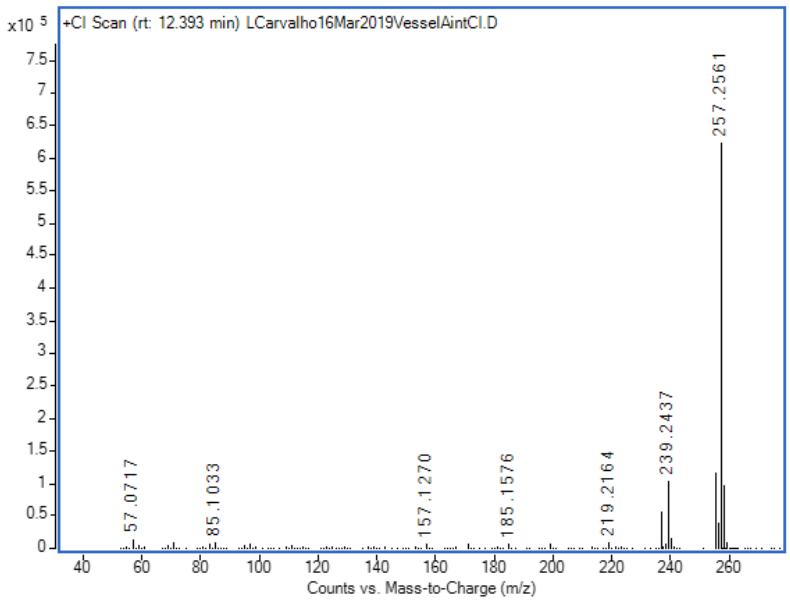


[17] n-Hexadecanoic acid

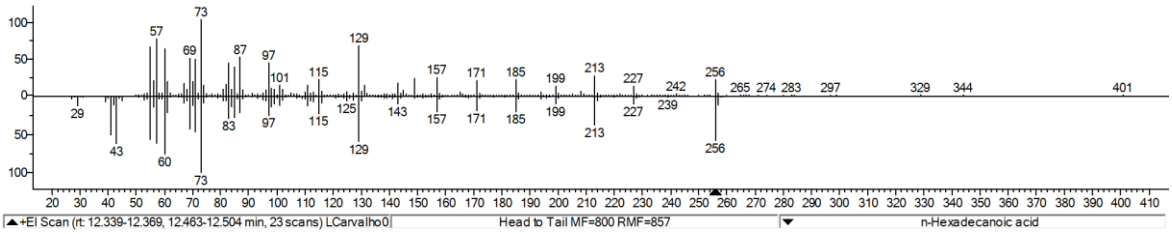
Interior

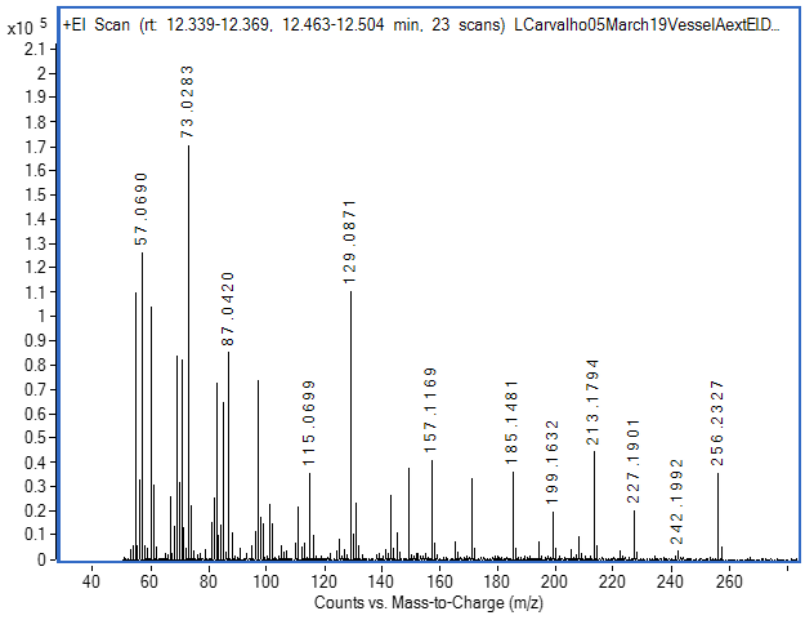


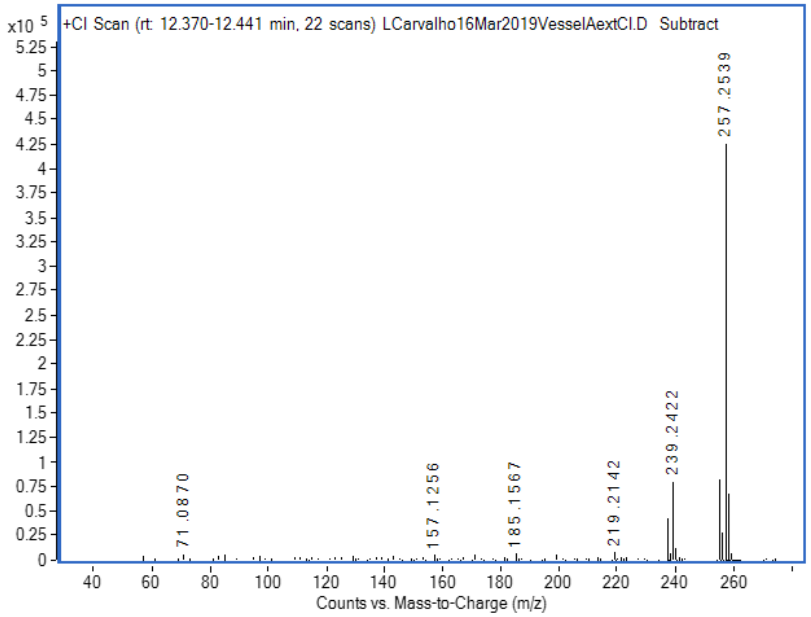




Exterior

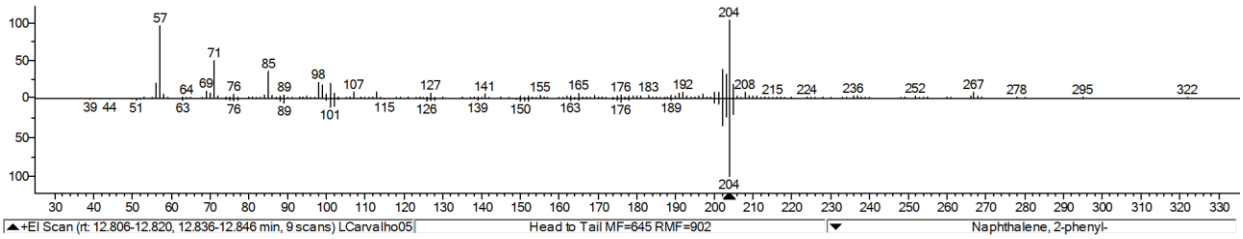

+EI Scan (rt: 12.339-12.369, 12.463-12.504 min, 23 scans) LCarvalho0
Head to Tail MF=800 RMF=857
n-Hexadecanoic acid

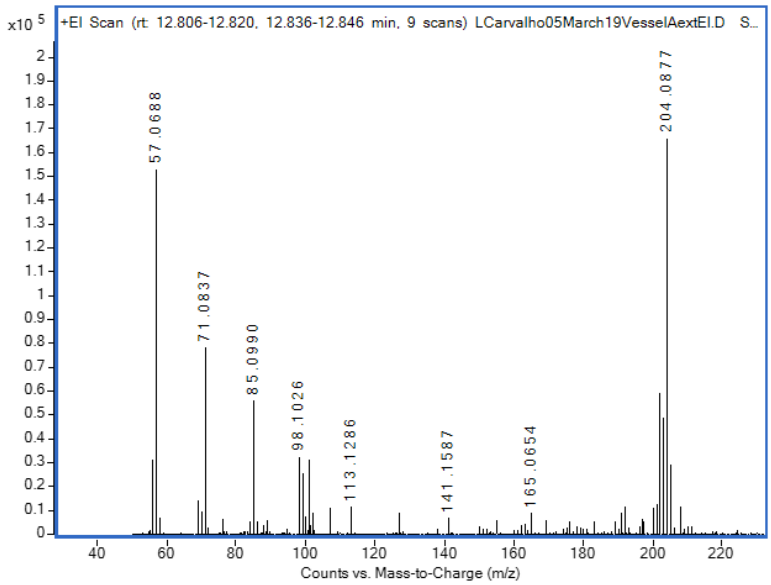

x10 5
+EI Scan (rt: 12.339-12.369, 12.463-12.504 min, 23 scans) LCarvalho05March19VesselAextEID...
73.0283
57.0690
87.0420
129.0871
115.0699
157.1169
185.1481
199.1632
213.1794
227.1901
242.1992
256.2327
Counts vs. Mass-to-Charge (m/z)

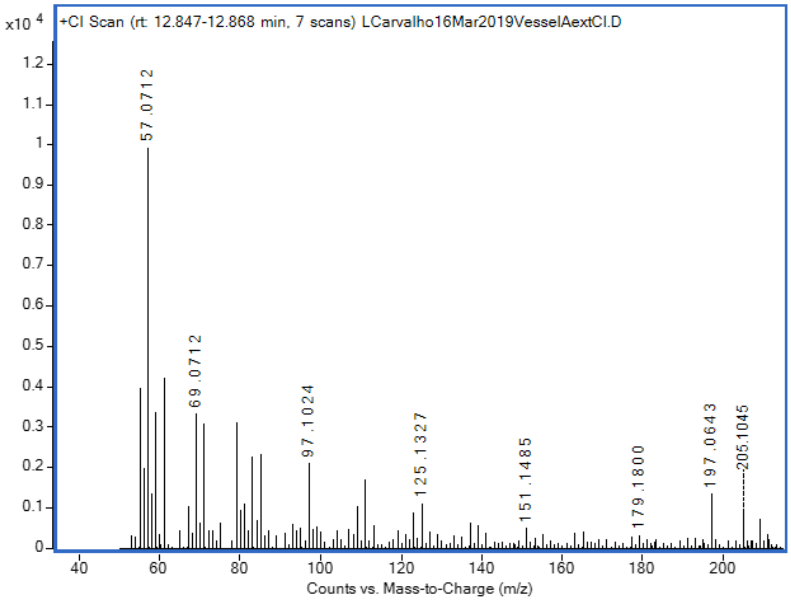

x10 5
+CI Scan (rt: 12.370-12.441 min, 22 scans) LCarvalho16Mar2019VesselAextCI.D Subtract
257.2539
239.2422
71.0870
157.1256
185.1567
219.2142
Counts vs. Mass-to-Charge (m/z)

[18] 2-phenyl Naphthalene Mass: 204.093901

Exterior

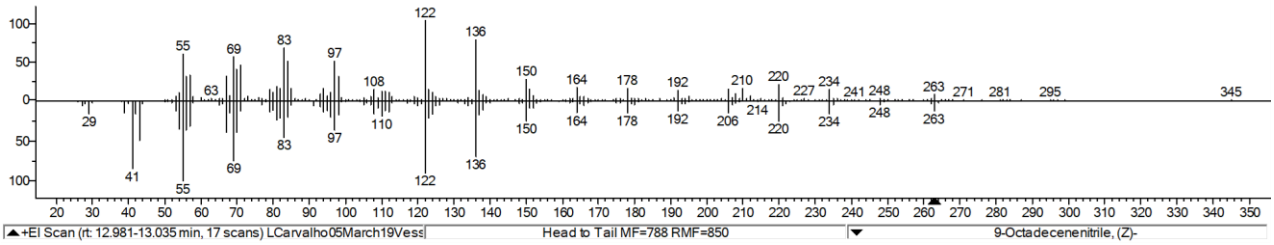


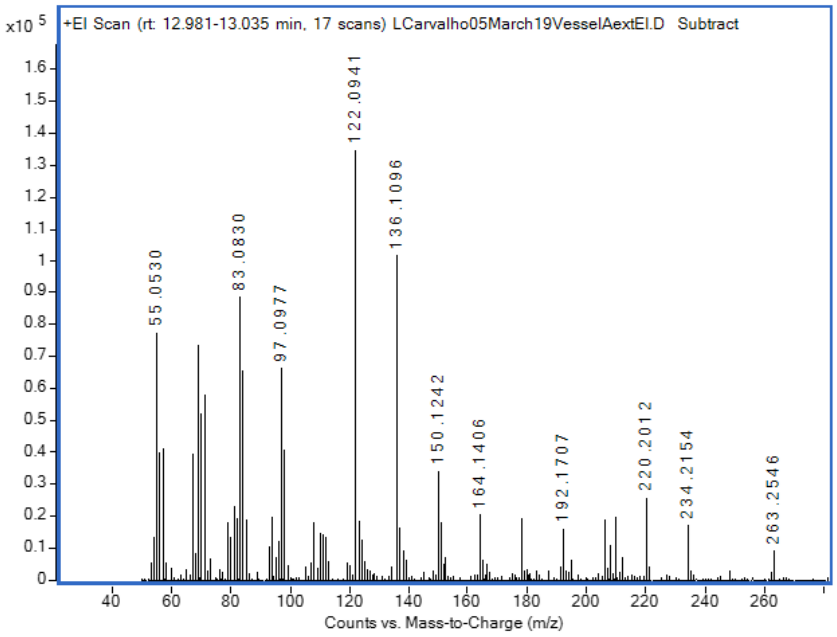


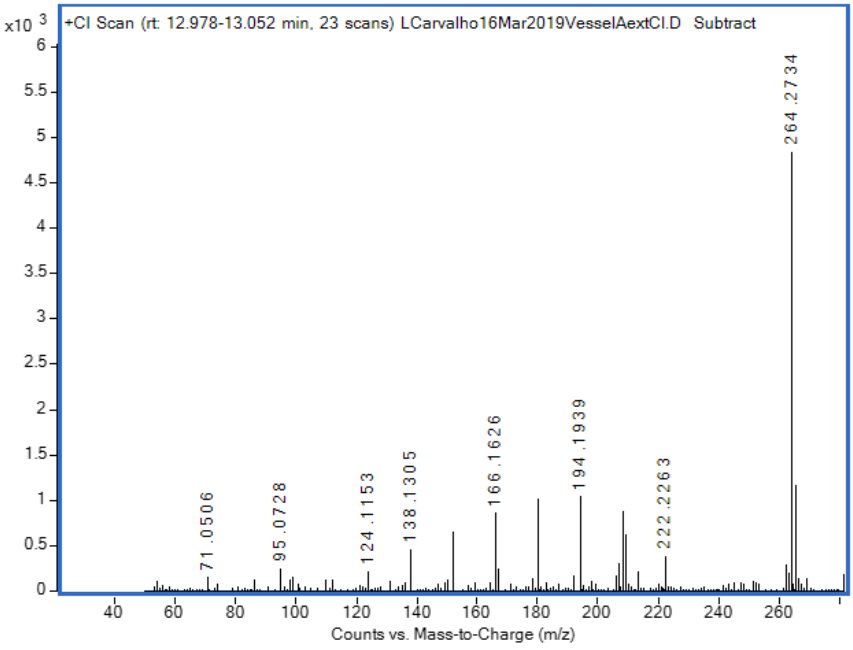


[19] 9-Octadecenitrile Mass: 263.2613

Exterior

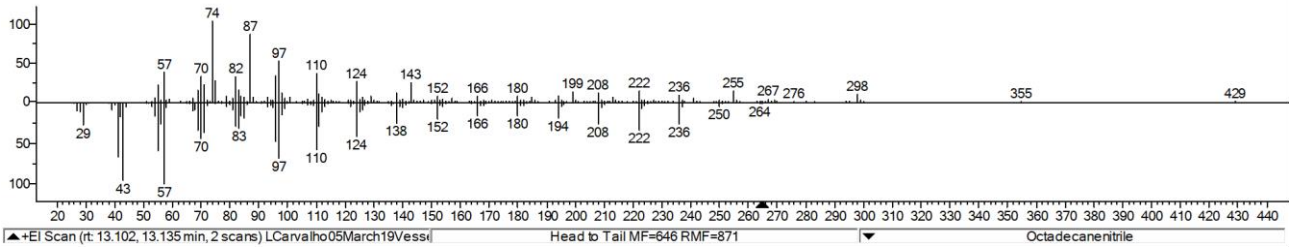


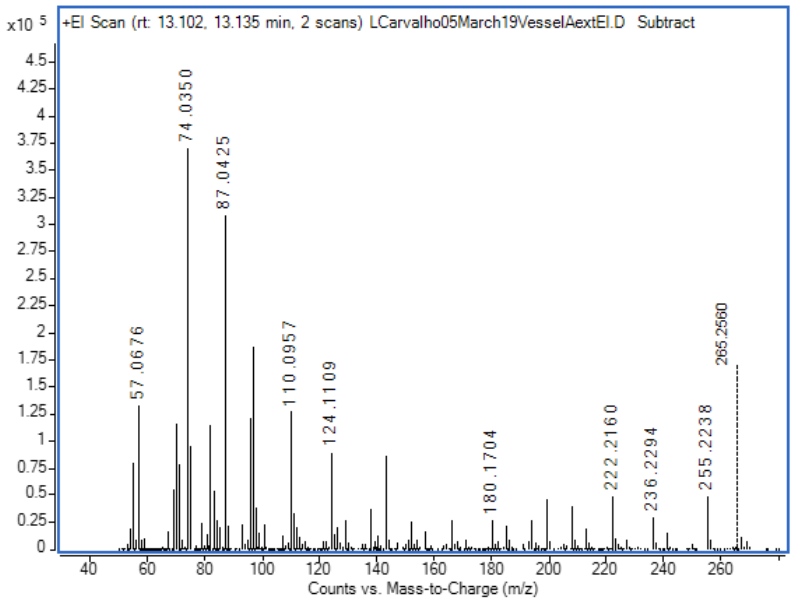


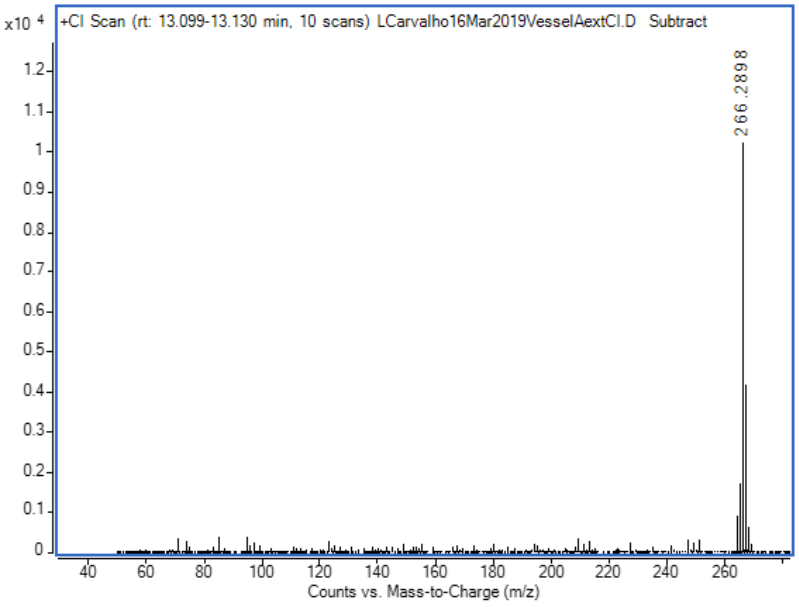


[20] Octadecanenitrile Mass: 265.27695

Exterior

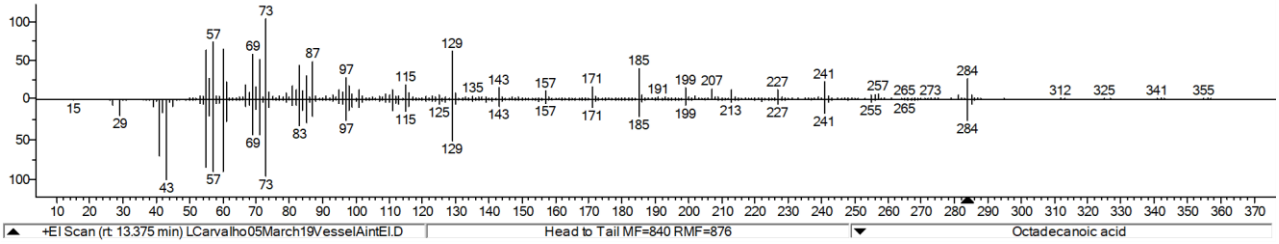


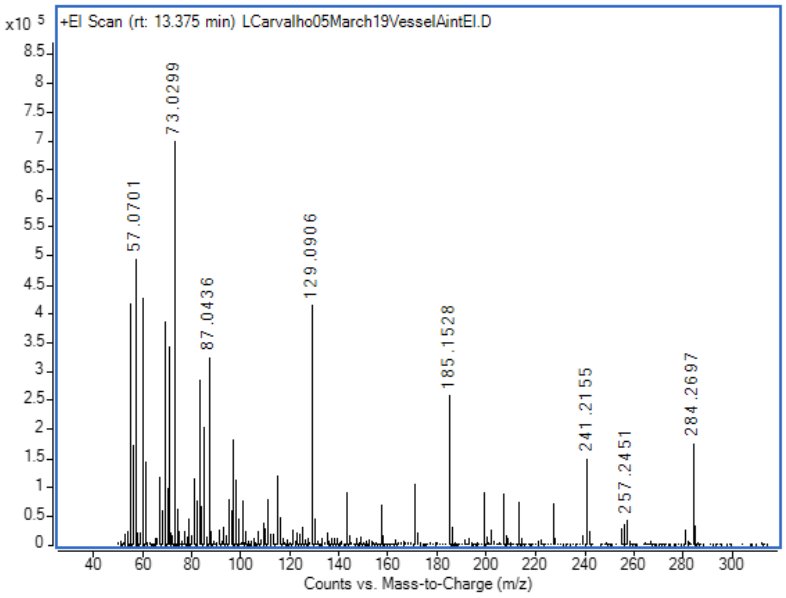


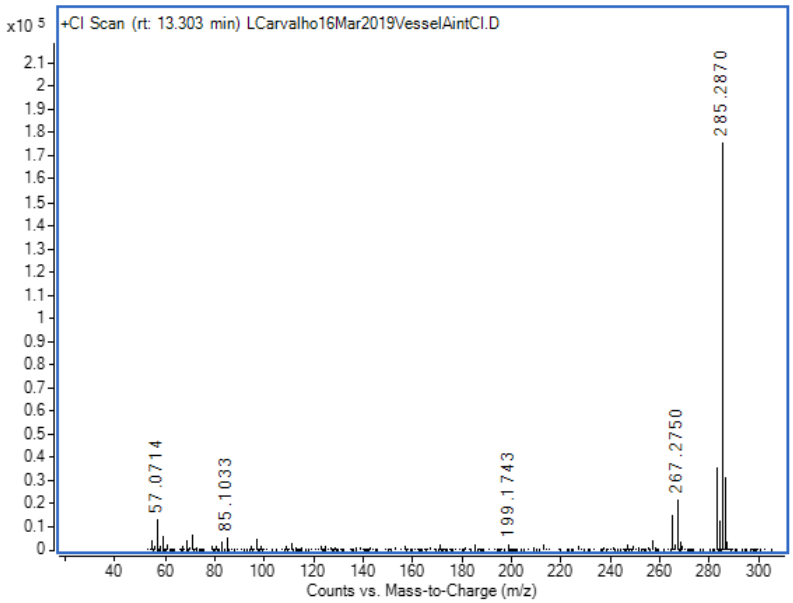


[21] Octadecanoic acid

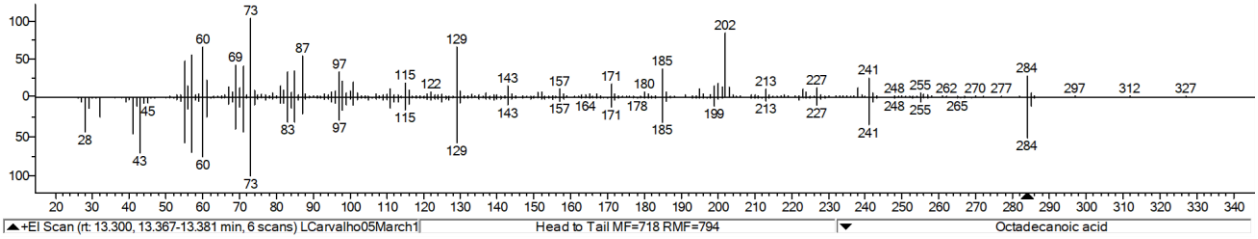
Interior

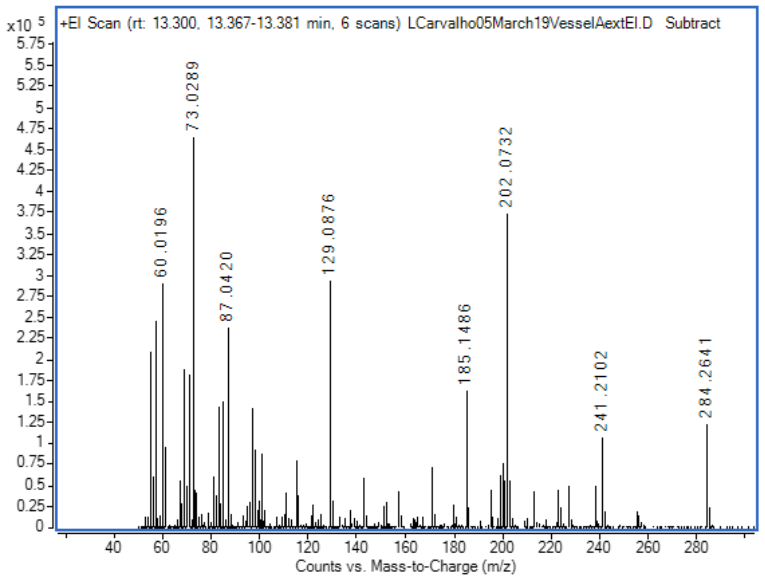


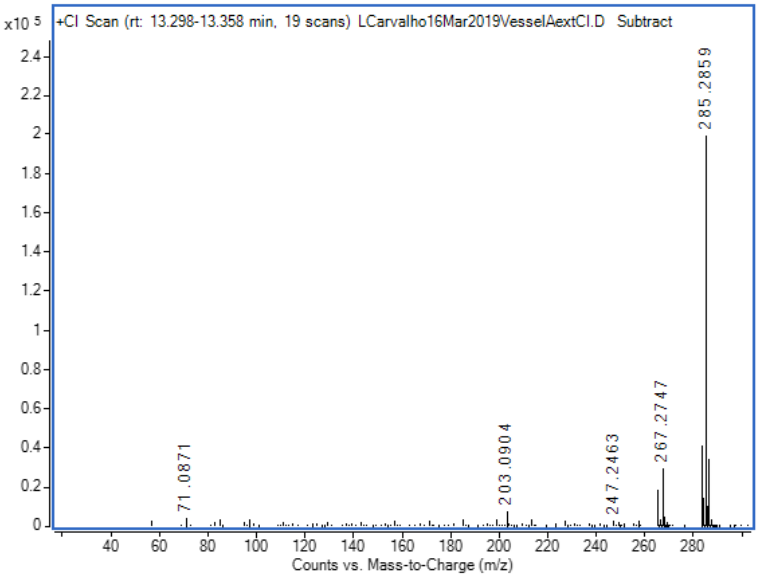




Exterior

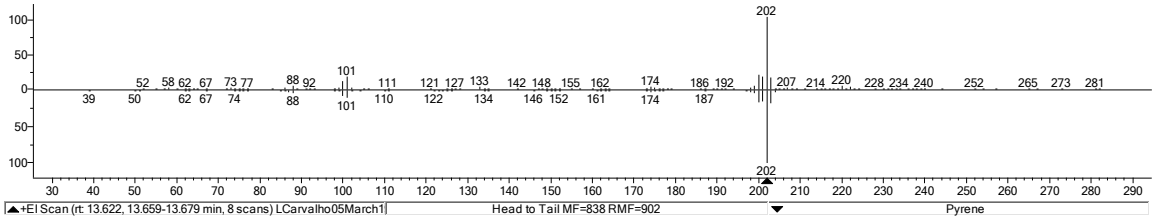

+EI Scan (rt: 13.300, 13.367-13.381 min, 6 scans) LCarvalho05March1
Head to Tail MF=718 RMF=794
Octadecanoic acid

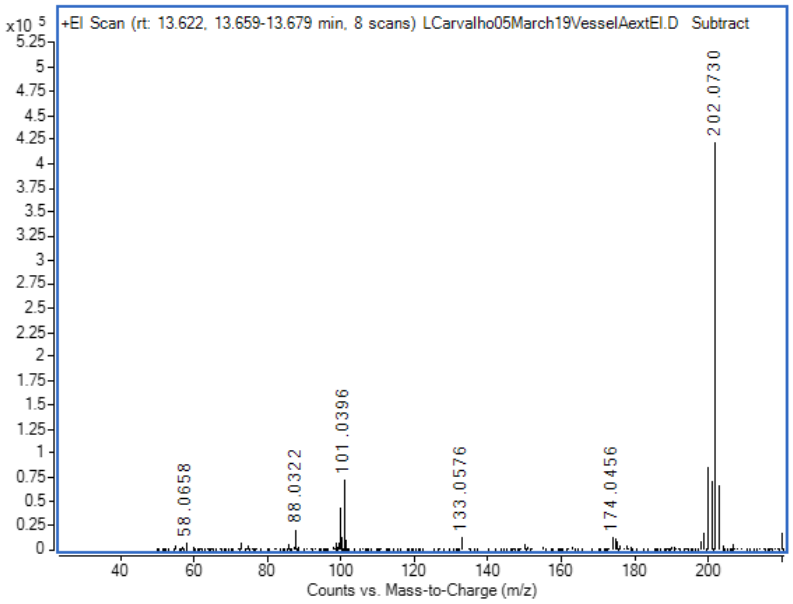

+EI Scan (rt: 13.300, 13.367-13.381 min, 6 scans) LCarvalho05March19VesselAextEI.D Subtract
x10 5
73.0289
60.0196
87.0420
129.0876
202.0732
185.1486
241.2102
284.2641
Counts vs. Mass-to-Charge (m/z)

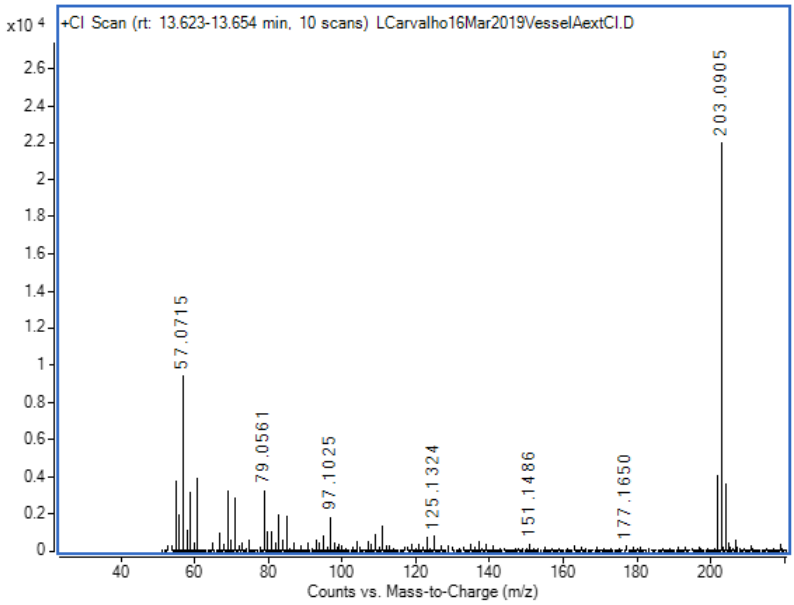

+CI Scan (rt: 13.298-13.358 min, 19 scans) LCarvalho16Mar2019VesselAextCI.D Subtract
x10 5
285.2859
71.0871
203.0904
247.2463
267.2747
Counts vs. Mass-to-Charge (m/z)

[22] Pyrene Mass: 202.07825

Exterior

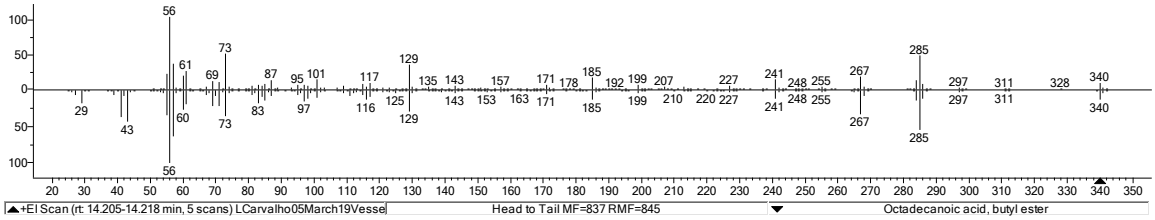


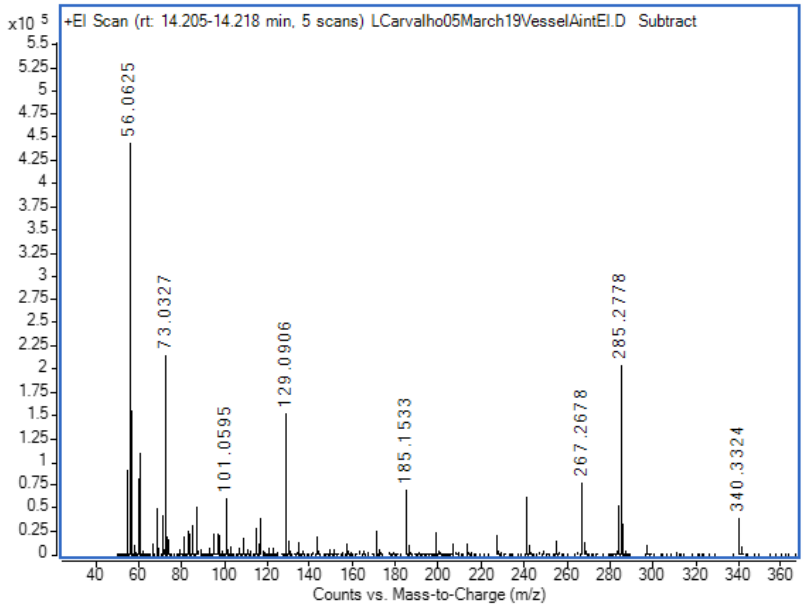


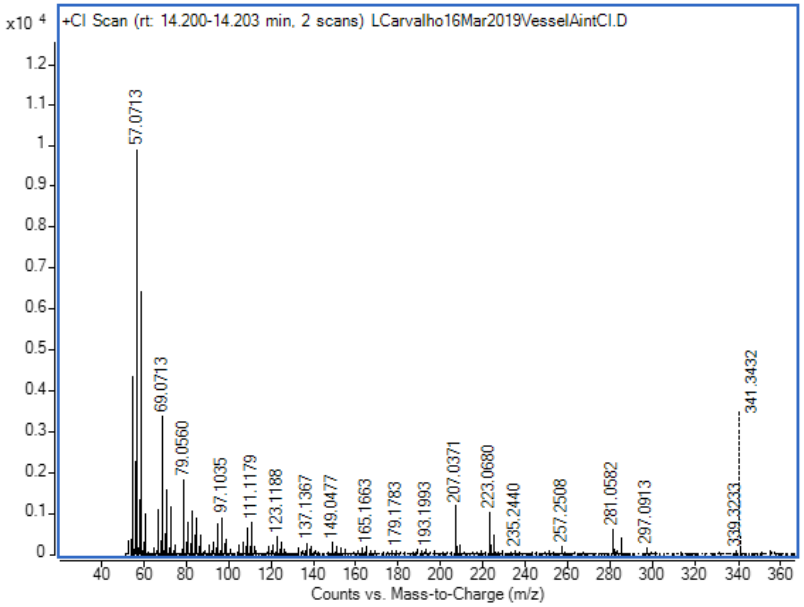


[23] Octadecanoic acid, butyl ester Mass: 340.334131

Interior

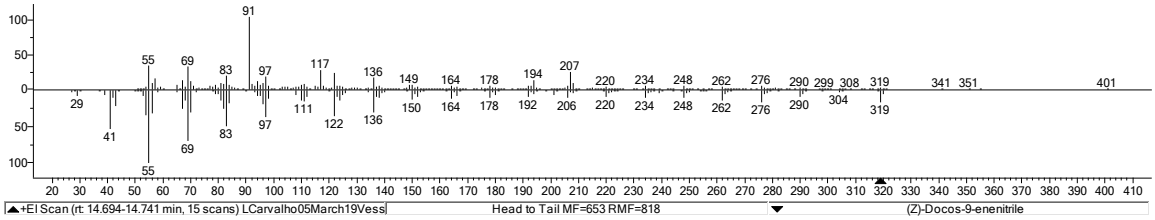


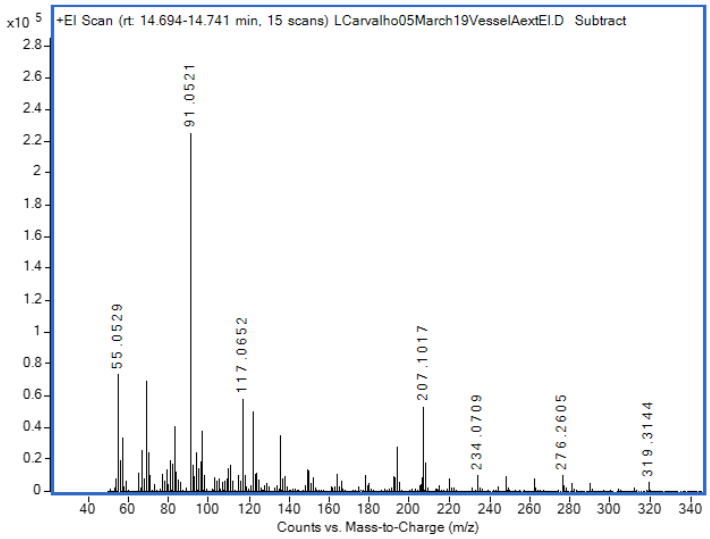


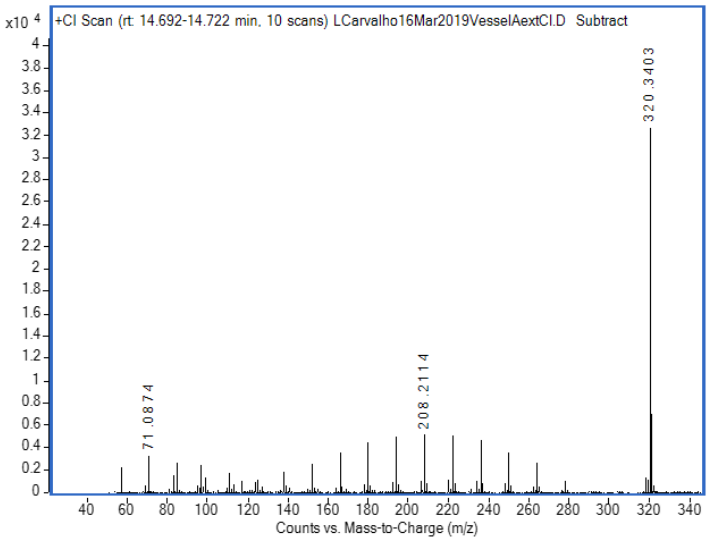


[24] (Z)-docos-9-enenitrile Mass: 319.3239

Exterior

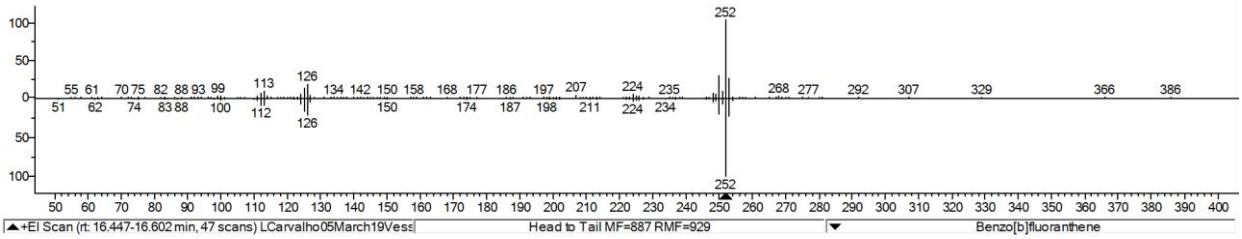


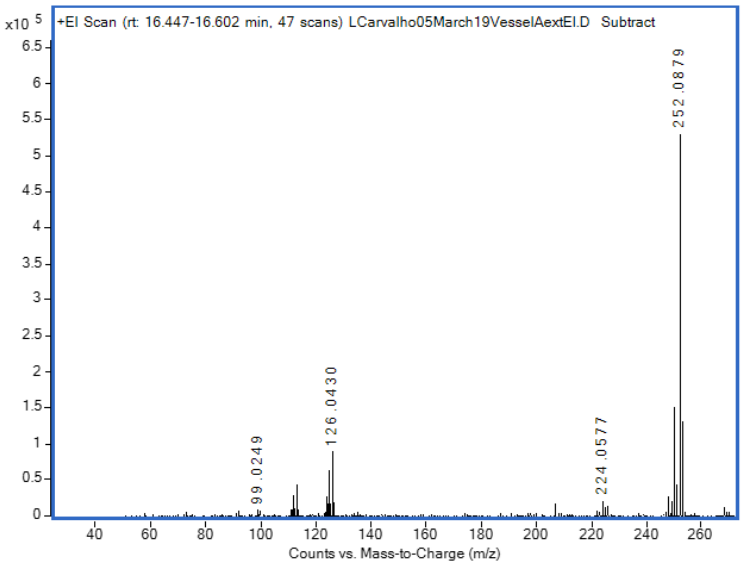


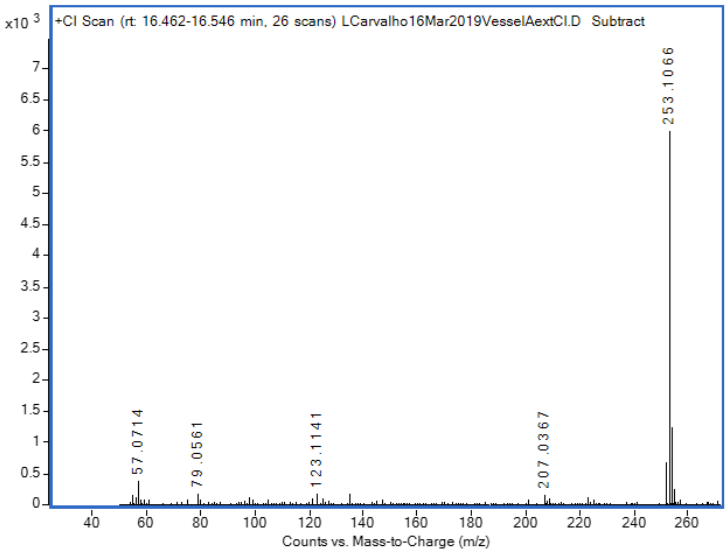


[25] Benzo[b]fluoranthene Mass: 252.093901

Exterior



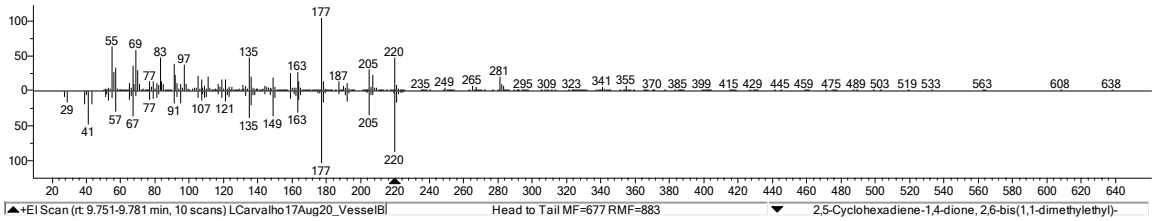


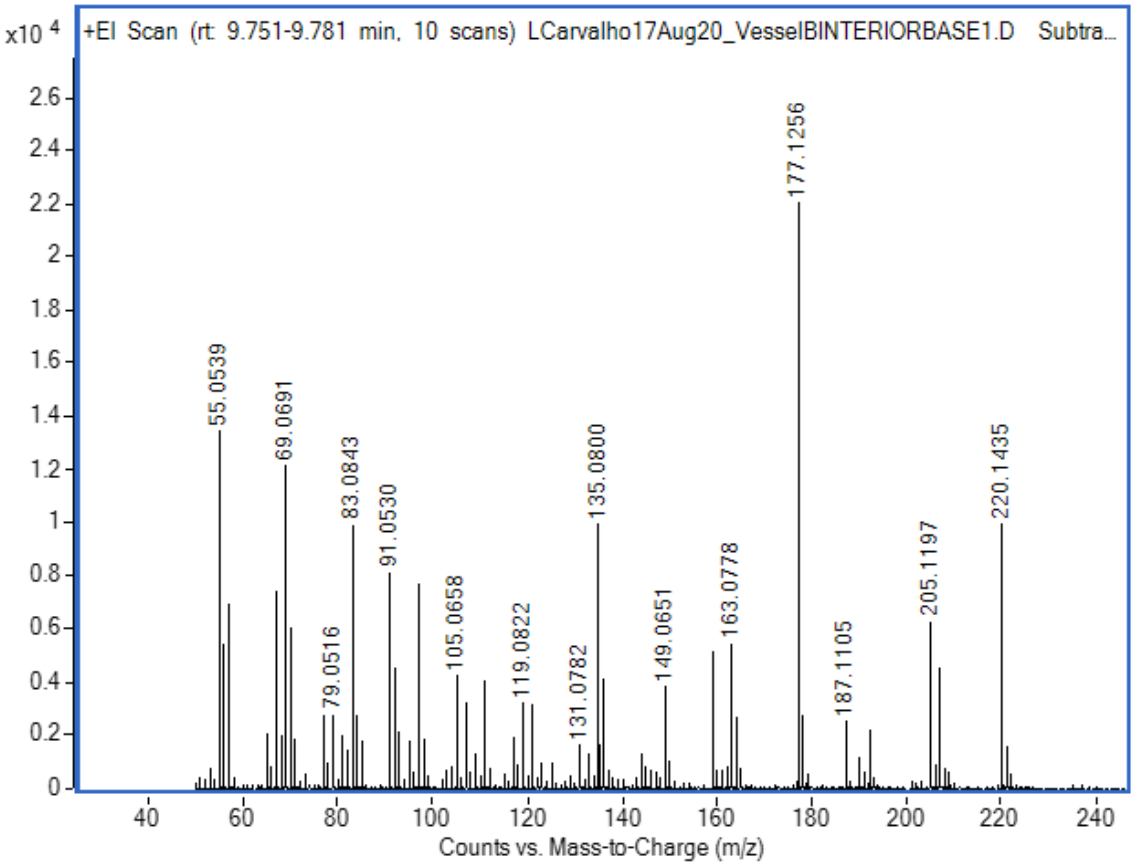


[1] 2,5-Cyclohexadiene-1,4-dione, 2,6-bis(1,1-dimethylethyl)-

Mass: 220.14633

Base

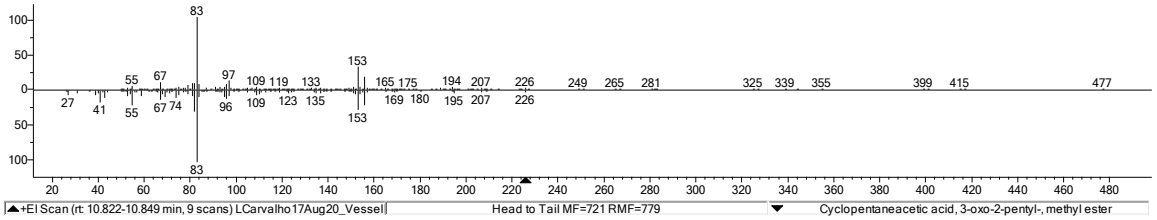


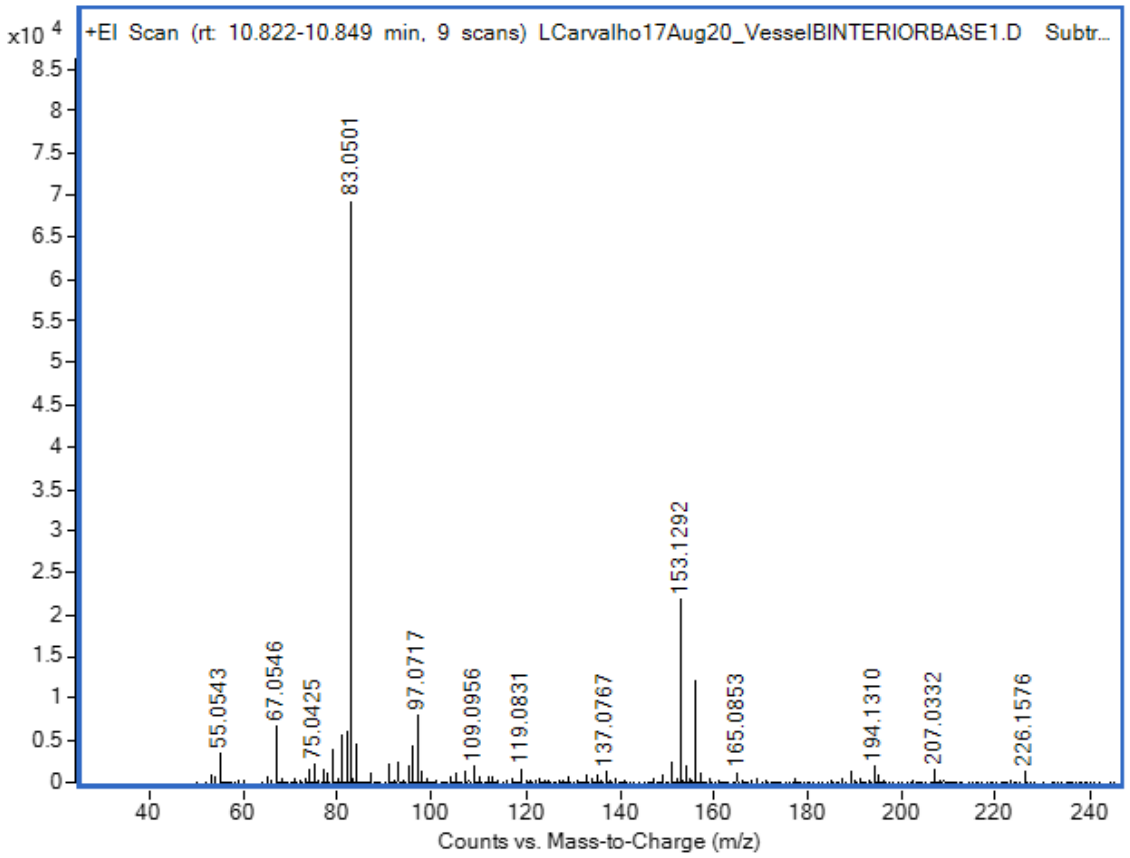


[2] Cyclopentaneacetic acid, 3-oxo-2-pentyl-, methyl ester

Mass: 226.156895

Base

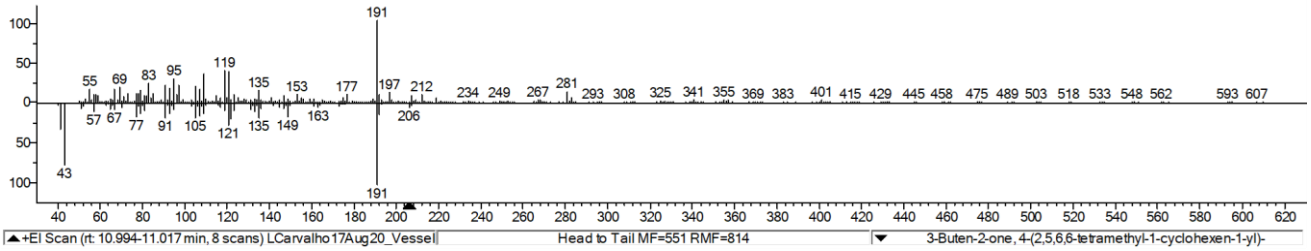


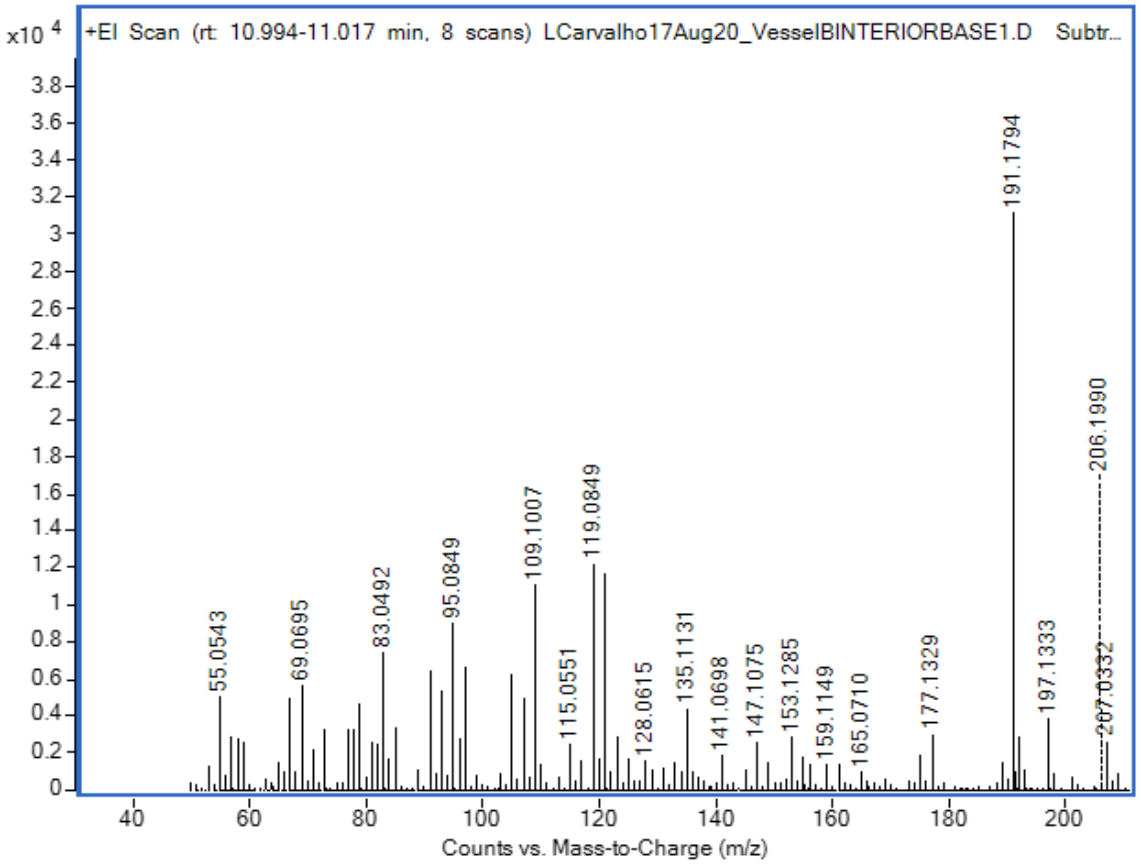


[3] Cyclopentaneacetic acid, 3-oxo-2-pentyl-, methyl ester

Mass: 226.156895

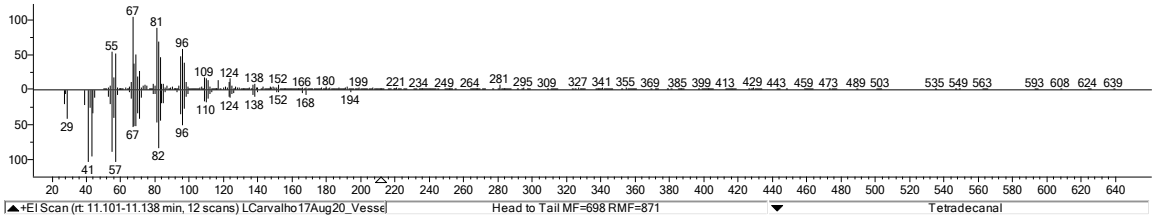
Base

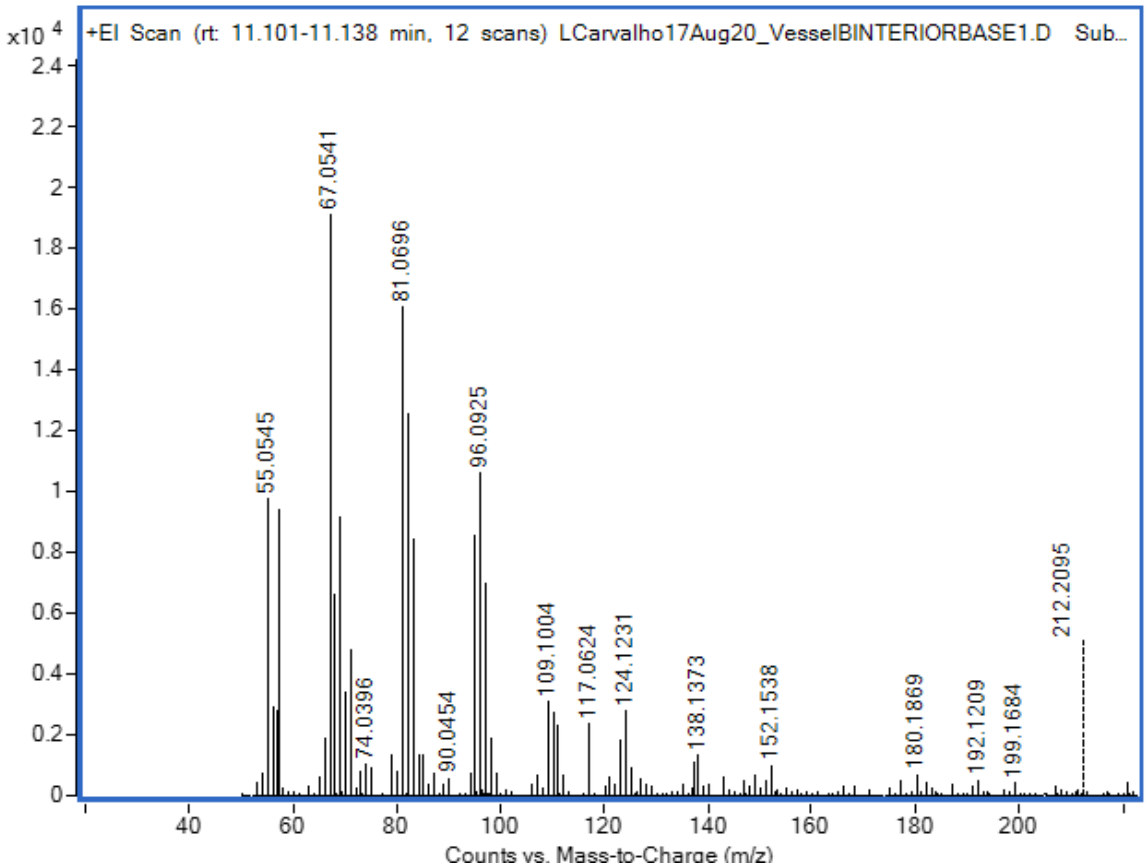




[4] Tetradecanal Mass: 212.214016

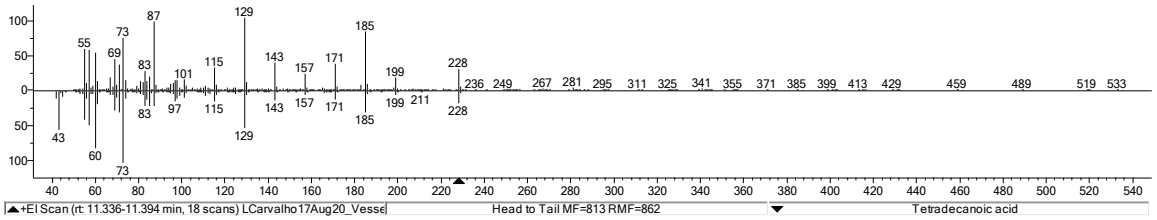
Base

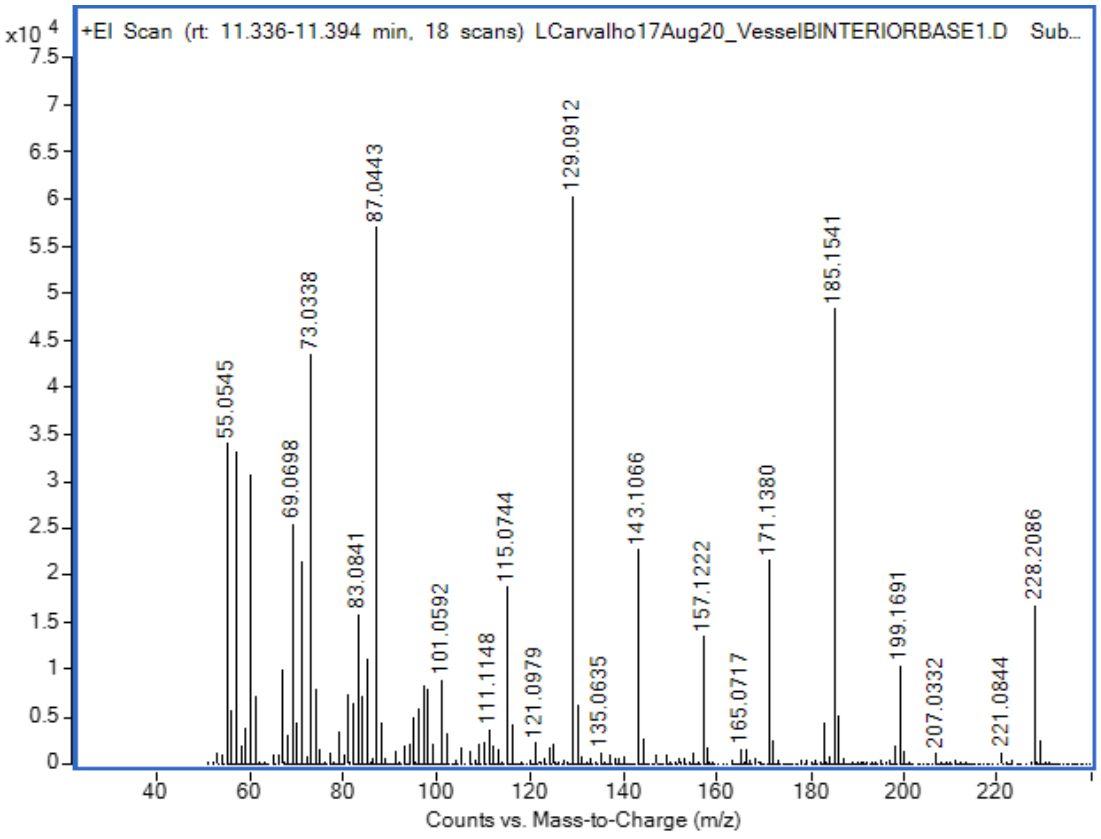




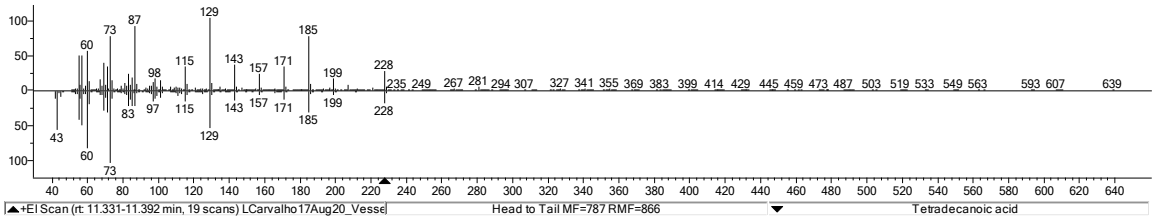
[5] Tetradecanoic acid

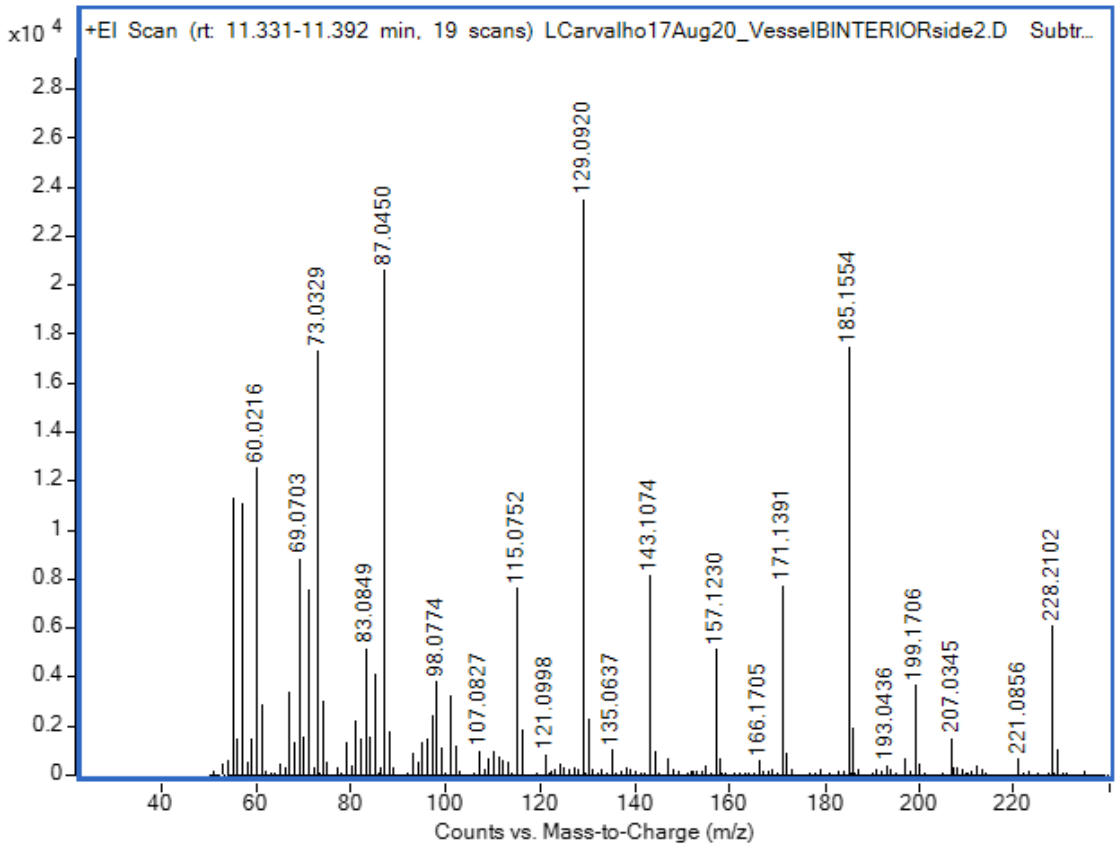
Base





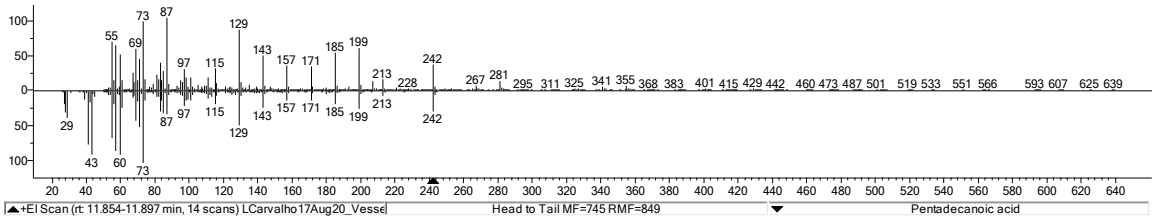
Body

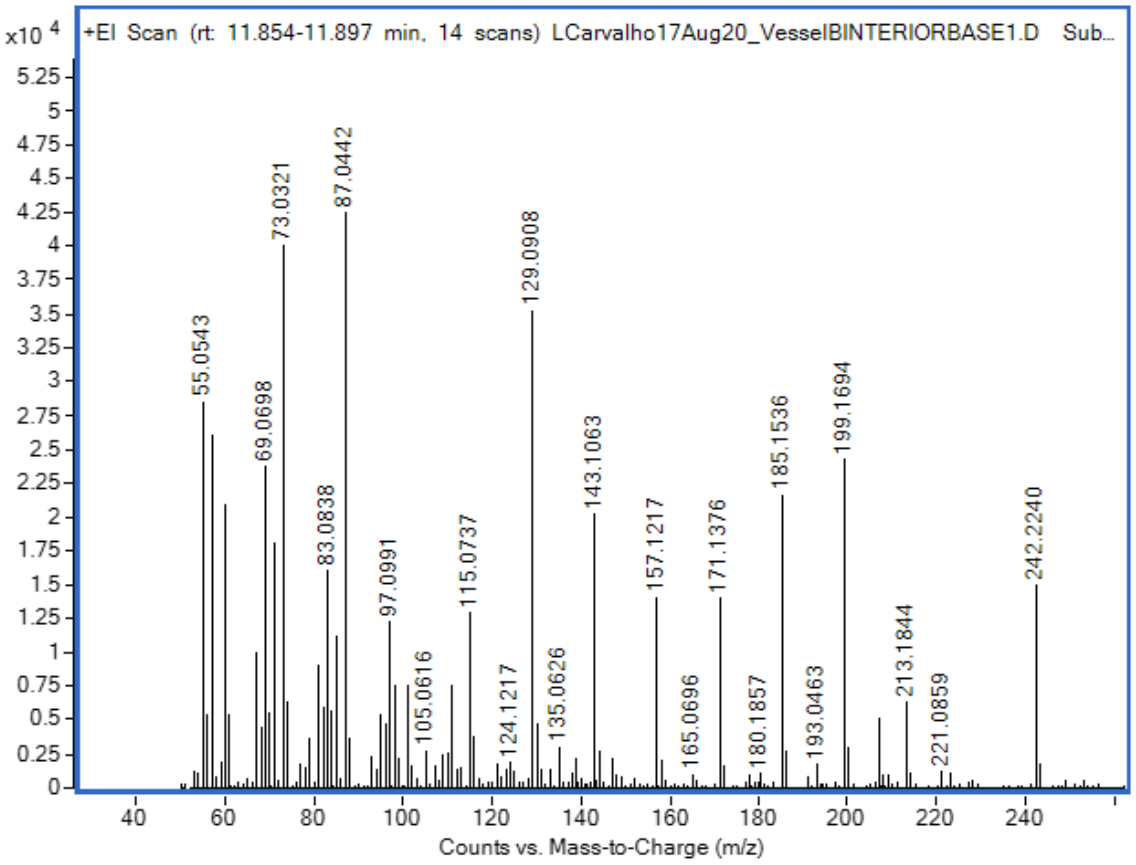

+EI Scan (rt: 11.331-11.392 min, 19 scans) LCarvalho17Aug20_Vesse
Head to Tail MF=787 RMF=866
Tetradecanoic acid


x10 4
+EI Scan (rt: 11.331-11.392 min, 19 scans) LCarvalho17Aug20_VesselBINTERIORside2.D Subtr...
129.0920
87.0450
73.0329
185.1554
60.0216
69.0703
143.1074
115.0752
171.1391
157.1230
83.0849
98.0774
228.2102
107.0827
121.0998
135.0637
199.1706
207.0345
193.0436
166.1705
221.0856
Counts vs. Mass-to-Charge (m/z)

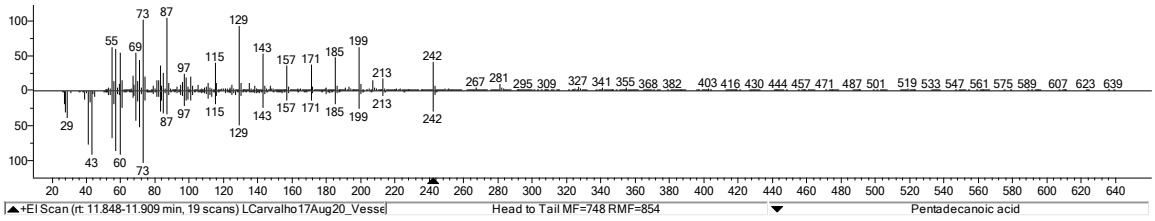
[6] Pentadecanoic acid Mass: 242.22458

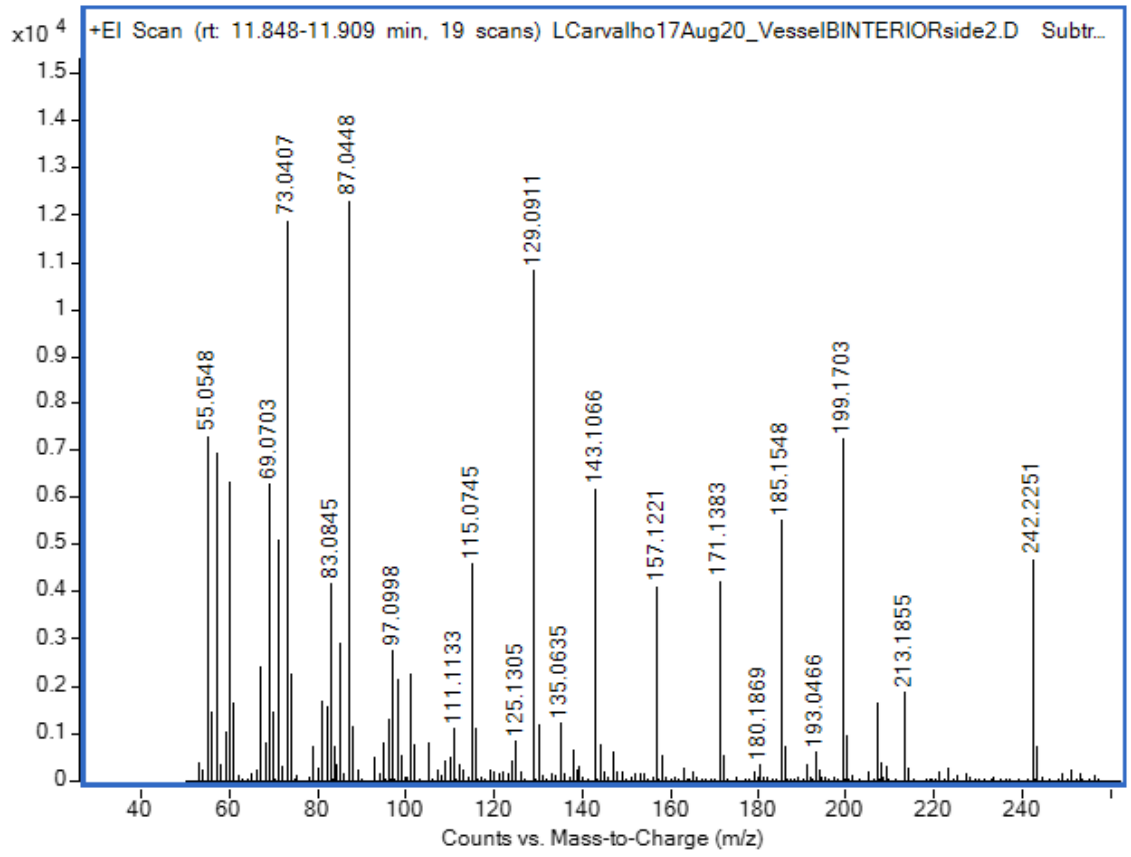
Base





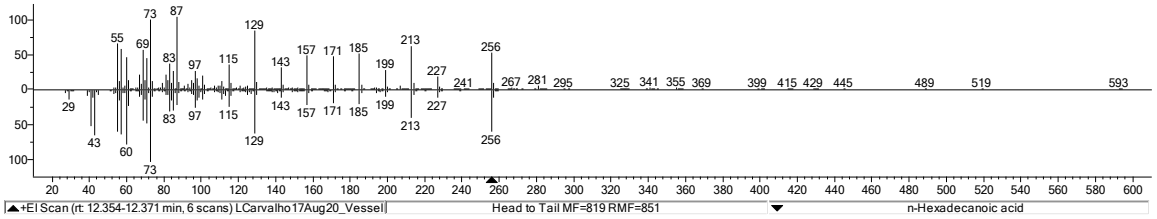
Body

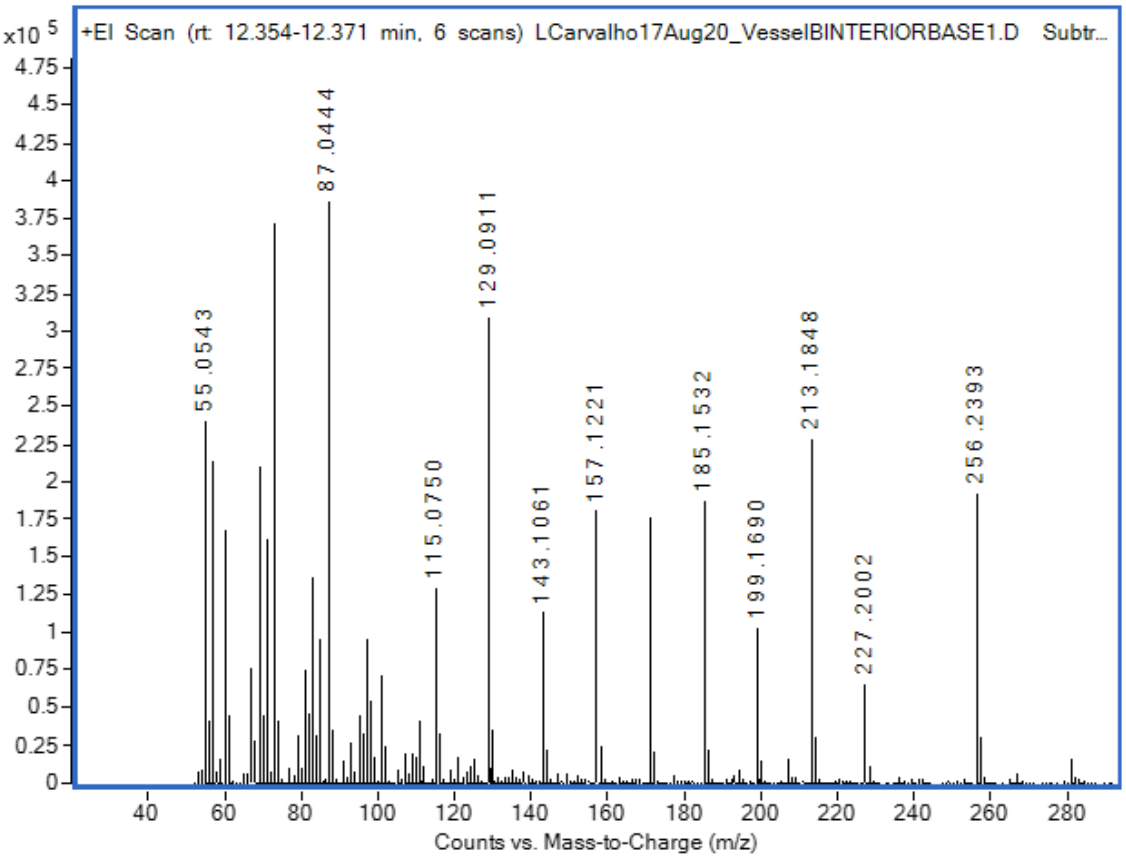

+EI Scan (rt: 11.848-11.909 min, 19 scans) LCarvalho17Aug20_Vesse
Head to Tail MF=748 RMF=854
Pentadecanoic acid


x10 4
+EI Scan (rt: 11.848-11.909 min, 19 scans) LCarvalho17Aug20_VesselBINTERIORside2.D Subtr...
55.0548
69.0703
73.0407
83.0845
87.0448
97.0998
111.1133
115.0745
125.1305
129.0911
135.0635
143.1066
157.1221
171.1383
180.1869
185.1548
193.0466
199.1703
213.1855
242.2251
Counts vs. Mass-to-Charge (m/z)

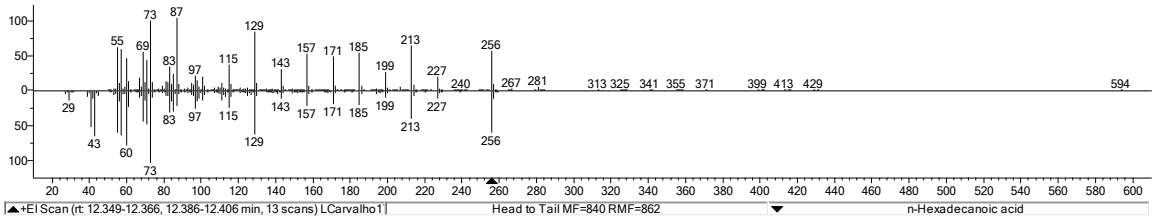
[7] n-Hexadecanoic acid

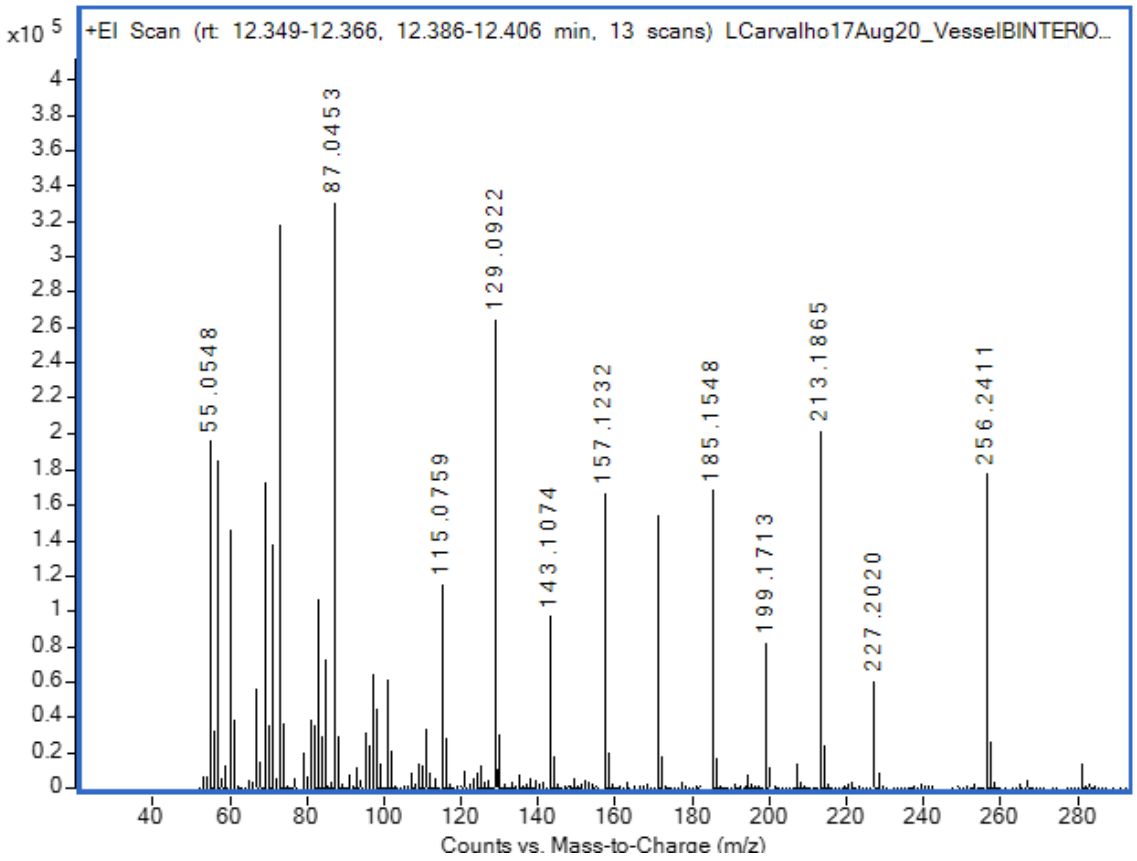
Base





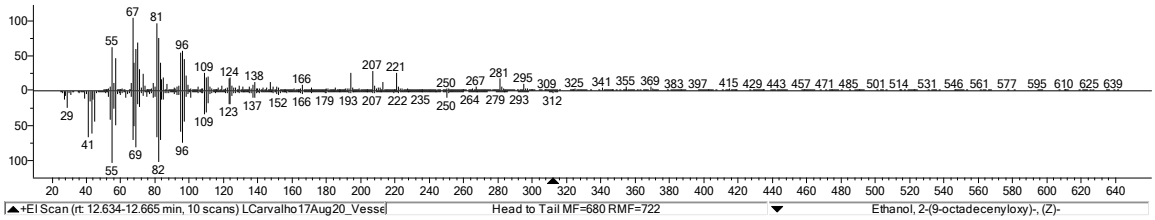
Body

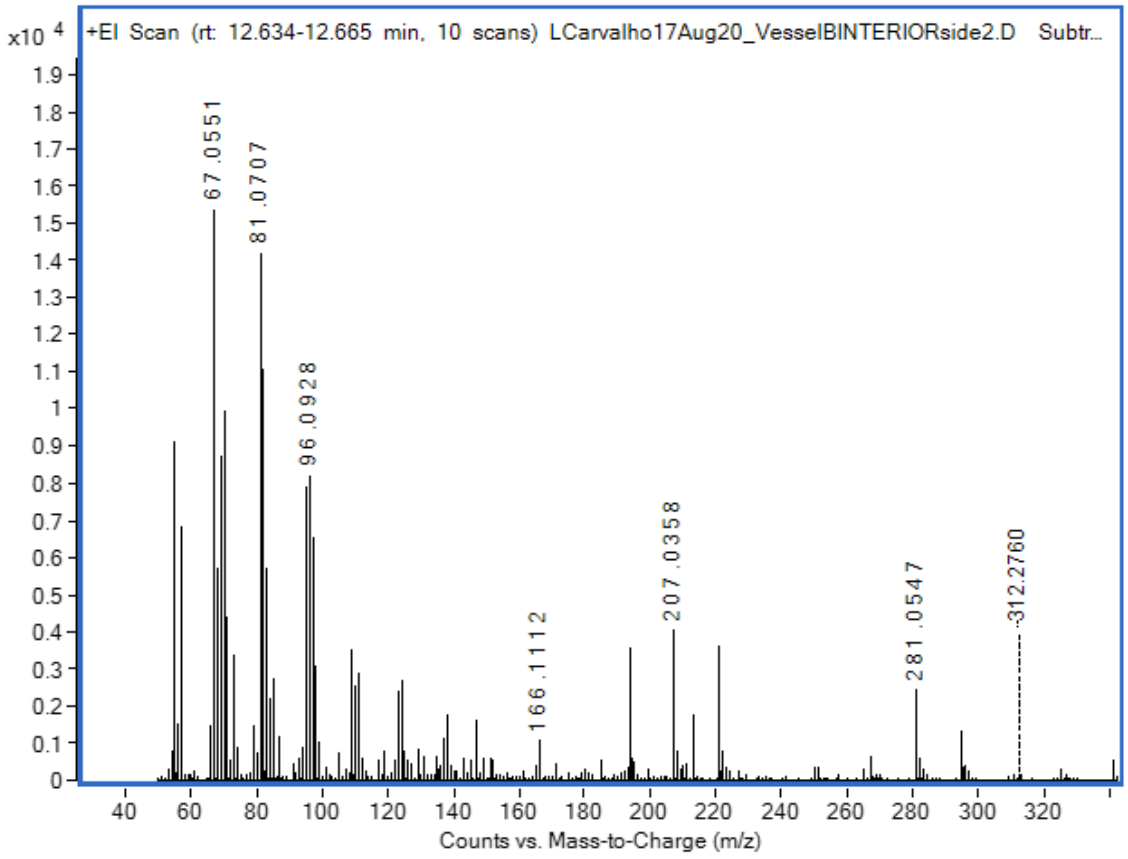

+EI Scan (rt: 12.349-12.366, 12.386-12.406 min, 13 scans) LCarvalho1
Head to Tail MF=840 RMF=862
n-Hexadecanoic acid


+EI Scan (rt: 12.349-12.366, 12.386-12.406 min, 13 scans) LCarvalho17Aug20_VesselBINTERIO...
x10 5
87.0453
129.0922
55.0548
115.0759
143.1074
157.1232
185.1548
213.1865
199.1713
227.2020
256.2411
Counts vs. Mass-to-Charge (m/z)

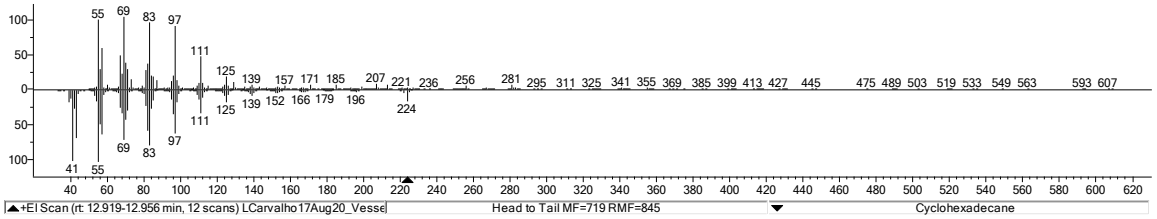
[8] Ethanol, 2-(9-octadecenyloxy)-, (Z)- Mass: 312.30283

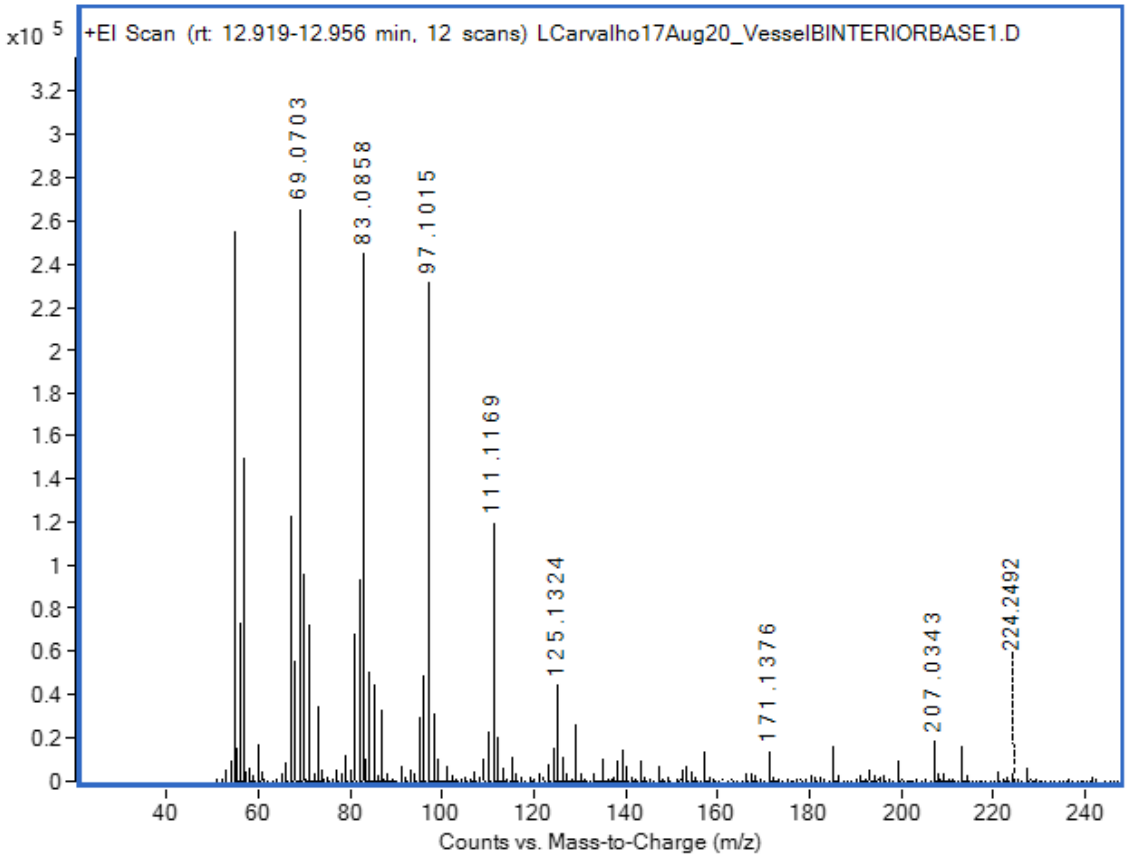
Body



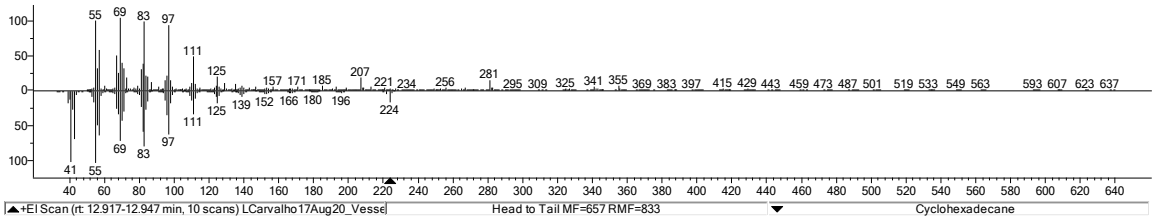


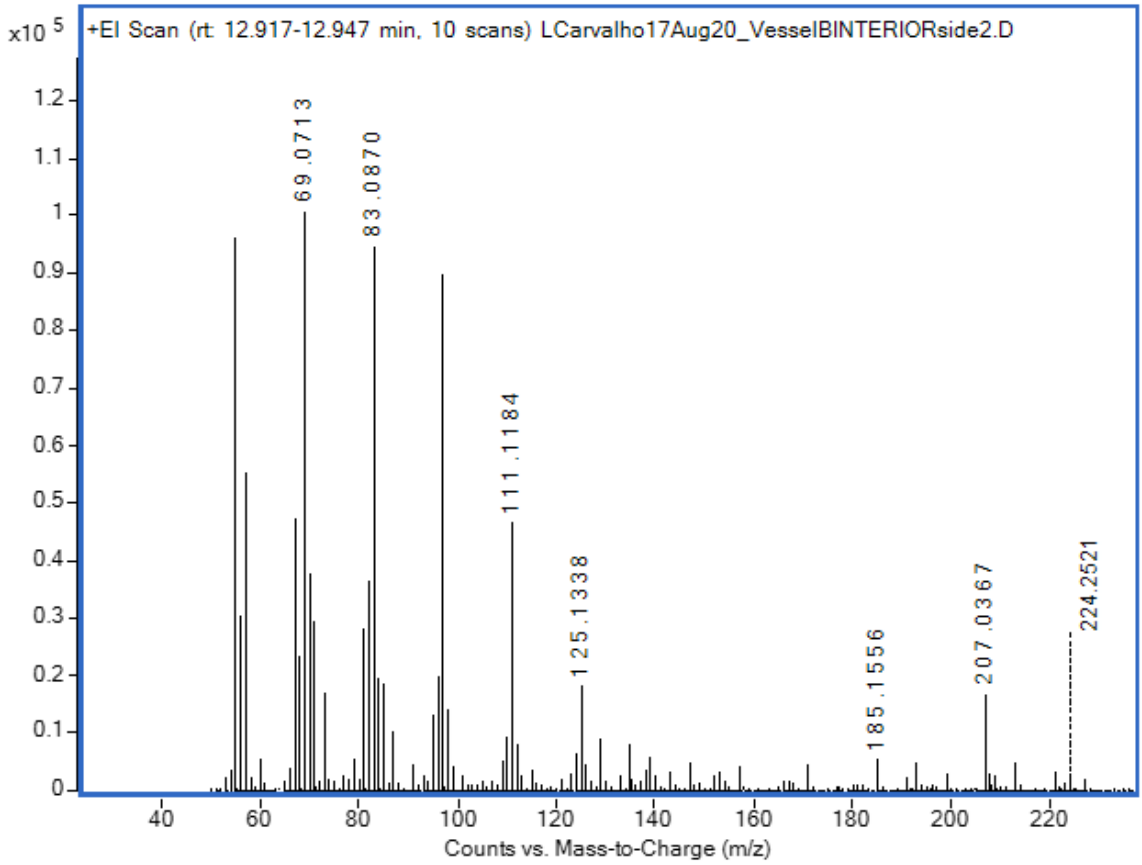
[9] Cyclohexadecane Mass: 224.2504015





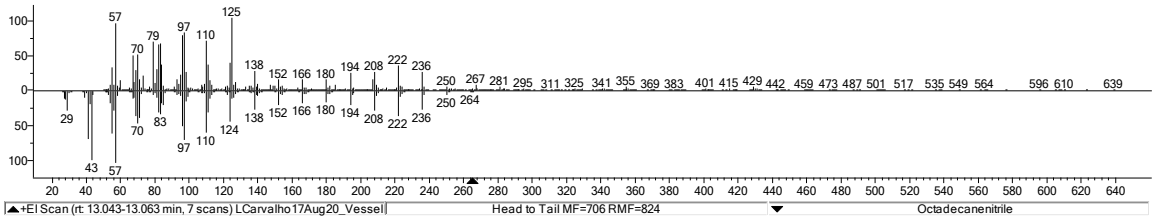
Body

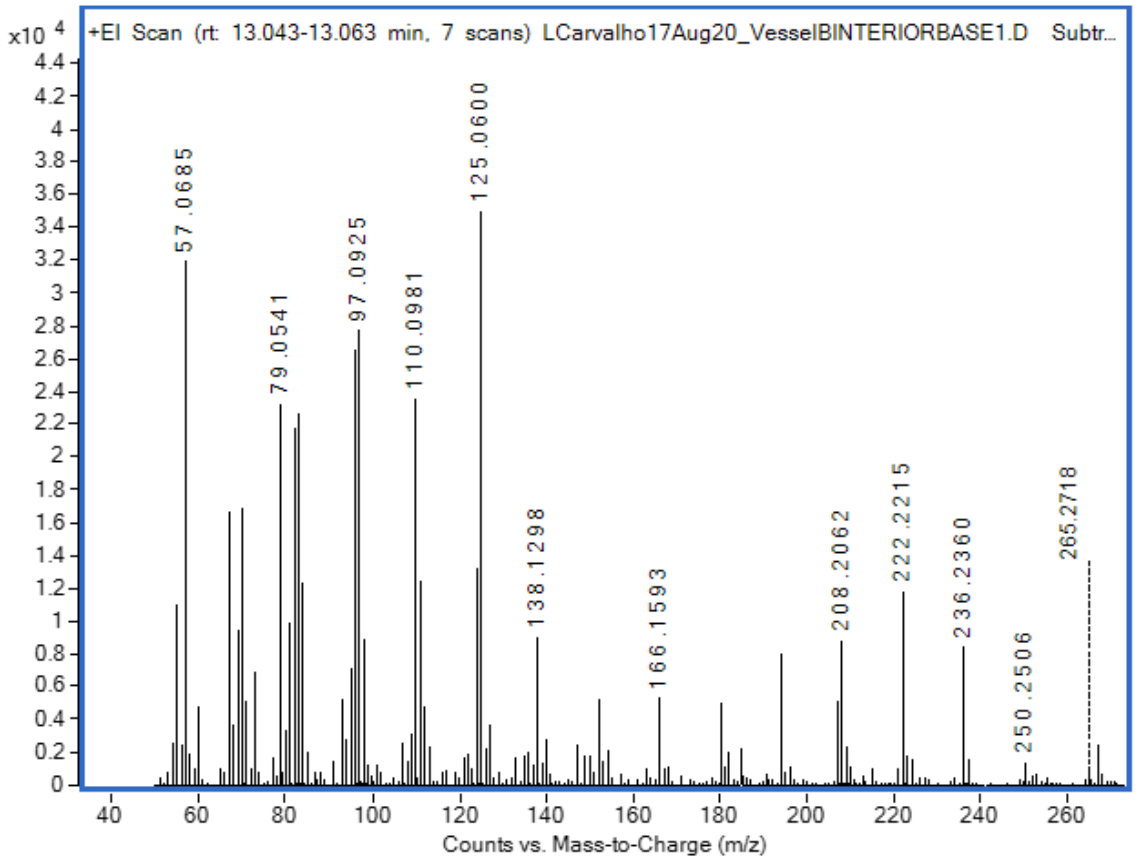

+EI Scan (rt: 12.917-12.947 min, 10 scans) LCarvalho17Aug20_Vesse
Head to Tail MF=657 RMF=833
Cyclohexadecane


x10 5
+EI Scan (rt: 12.917-12.947 min, 10 scans) LCarvalho17Aug20_VesselBINTERIORside2.D
69.0713
83.0870
111.1184
125.1338
185.1556
207.0367
224.2521
Counts vs. Mass-to-Charge (m/z)

[10] Octadecanenitrile Mass: 265.27695

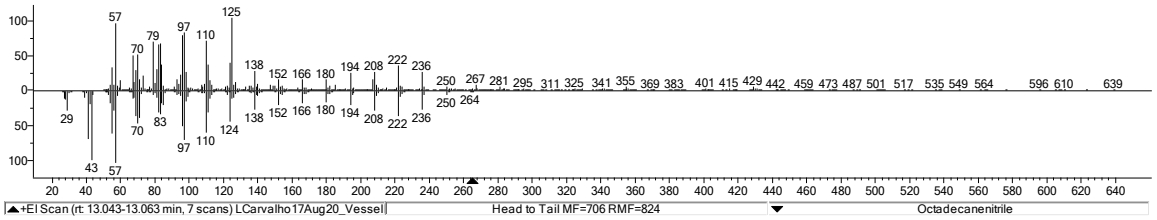
Base

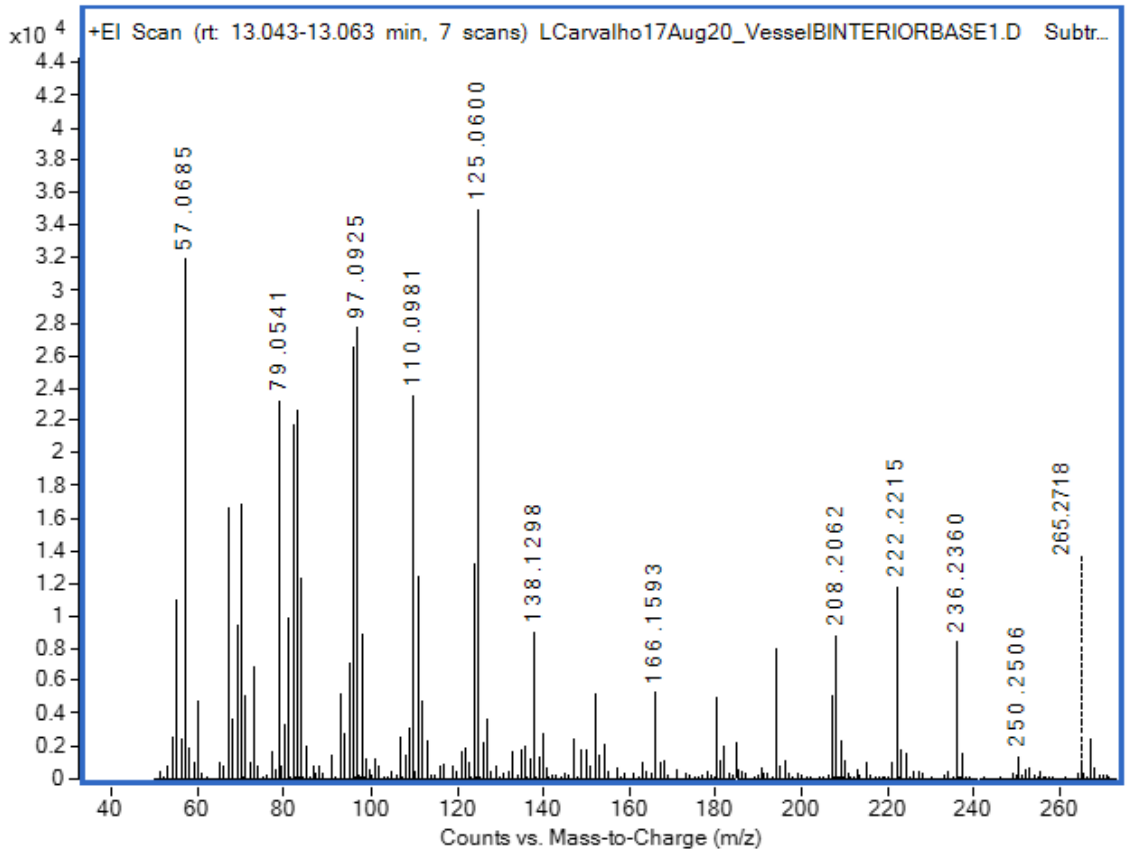




[11] 6-Octadecenoic acid Mass: 282.25588

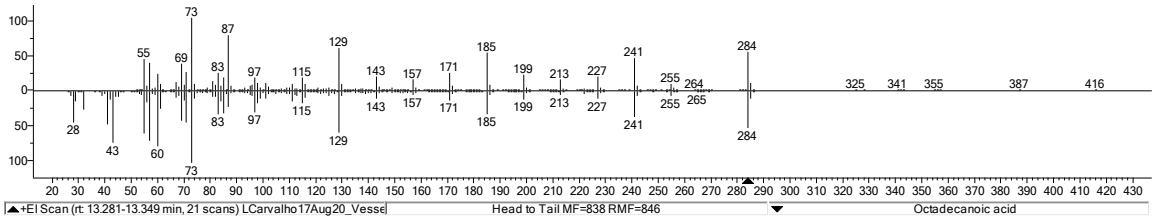
Base

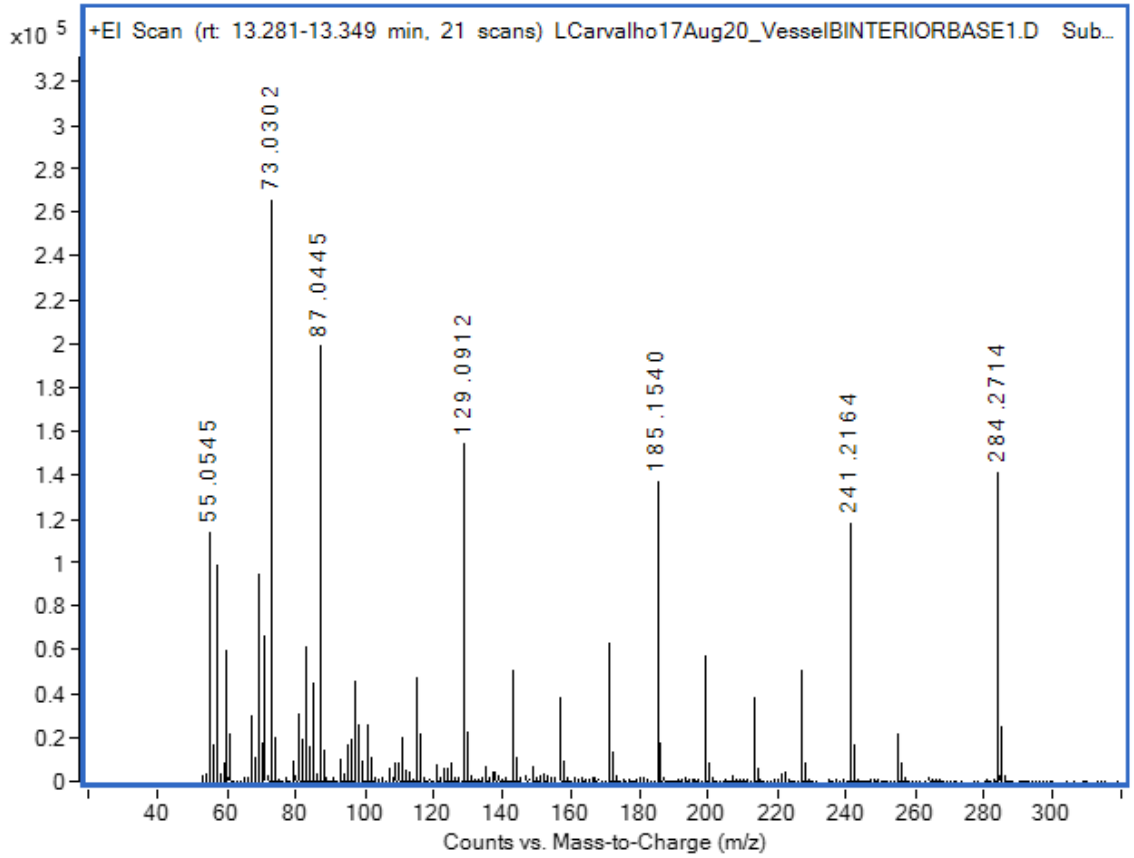




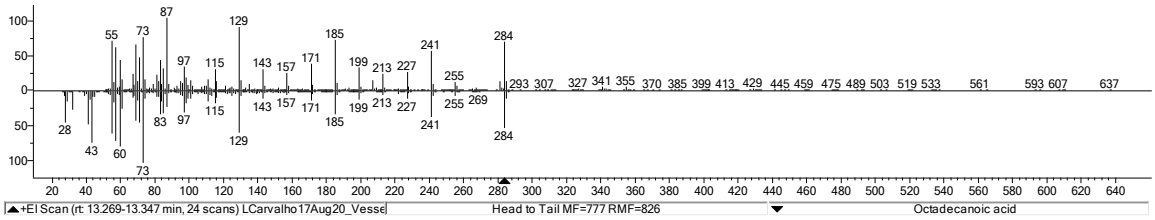
[12] Octadecanoic acid

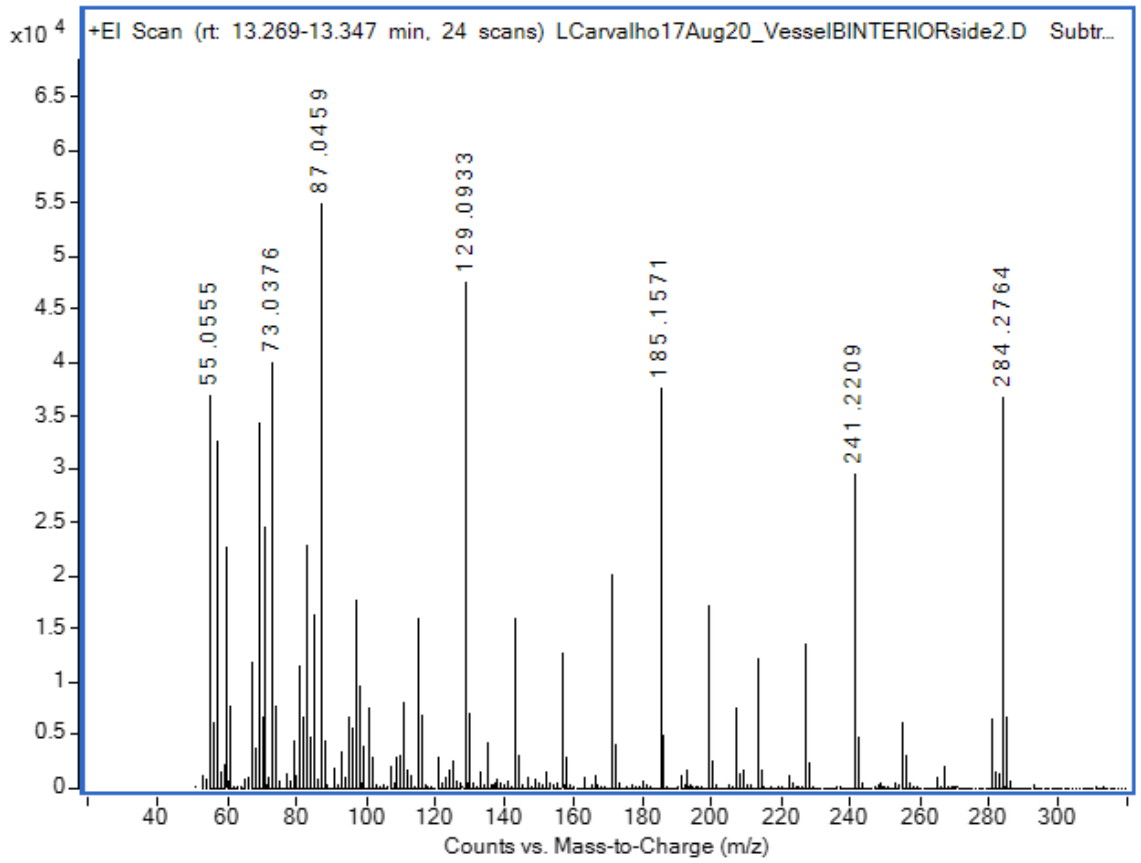
Base





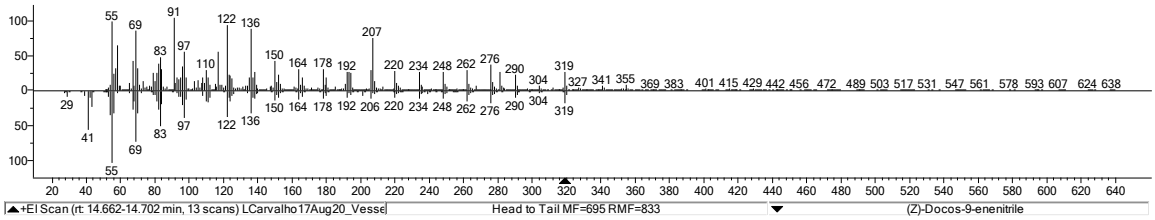
Body

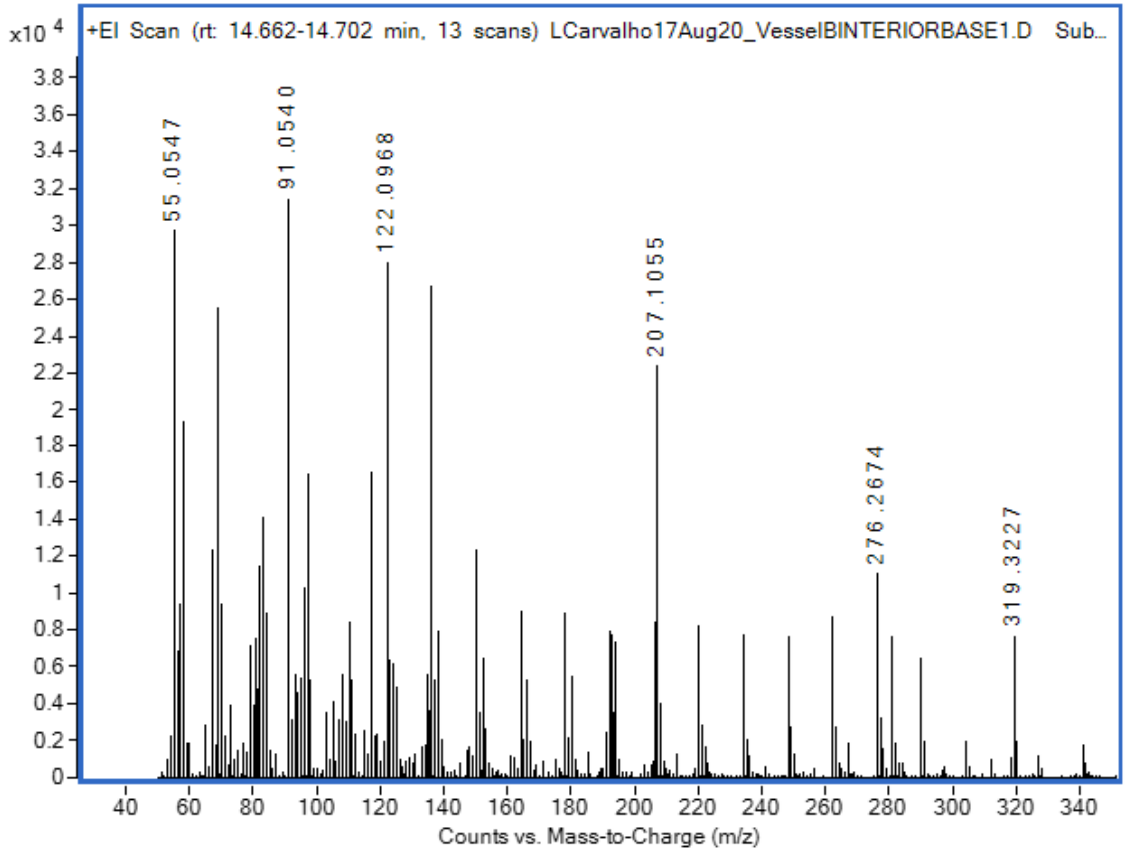

+EI Scan (rt: 13.269-13.347 min, 24 scans) LCarvalho17Aug20_Vesse
Head to Tail MF=777 RMF=826
Octadecanoic acid


x10 4
+EI Scan (rt: 13.269-13.347 min, 24 scans) LCarvalho17Aug20_VesselBINTERIORside2.D Subtr...
55.0555
73.0376
87.0459
129.0933
185.1571
241.2209
284.2764
Counts vs. Mass-to-Charge (m/z)

[13] (Z)-Docos-9-enenitrile

Base

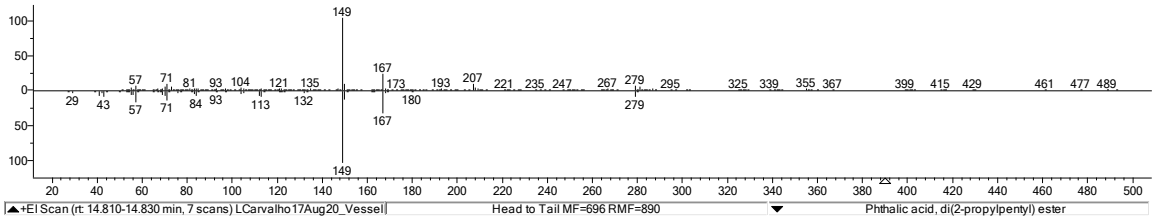


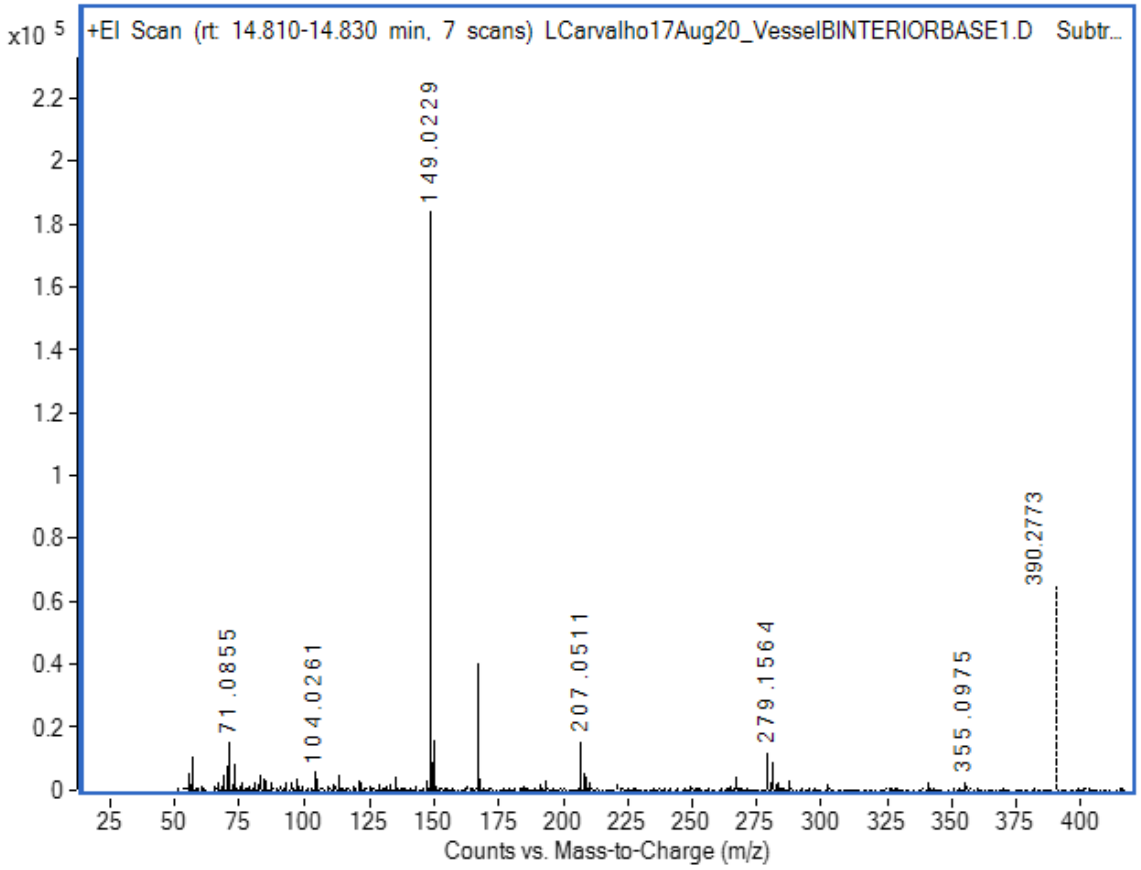


[14] Phthalic acid, di(2-propylpentyl) ester

Mass: 390.27701

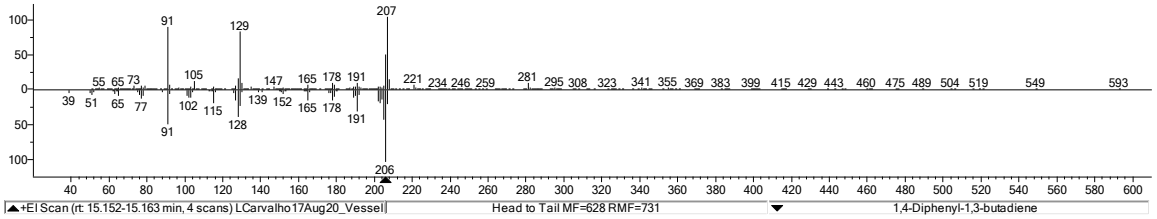
Base

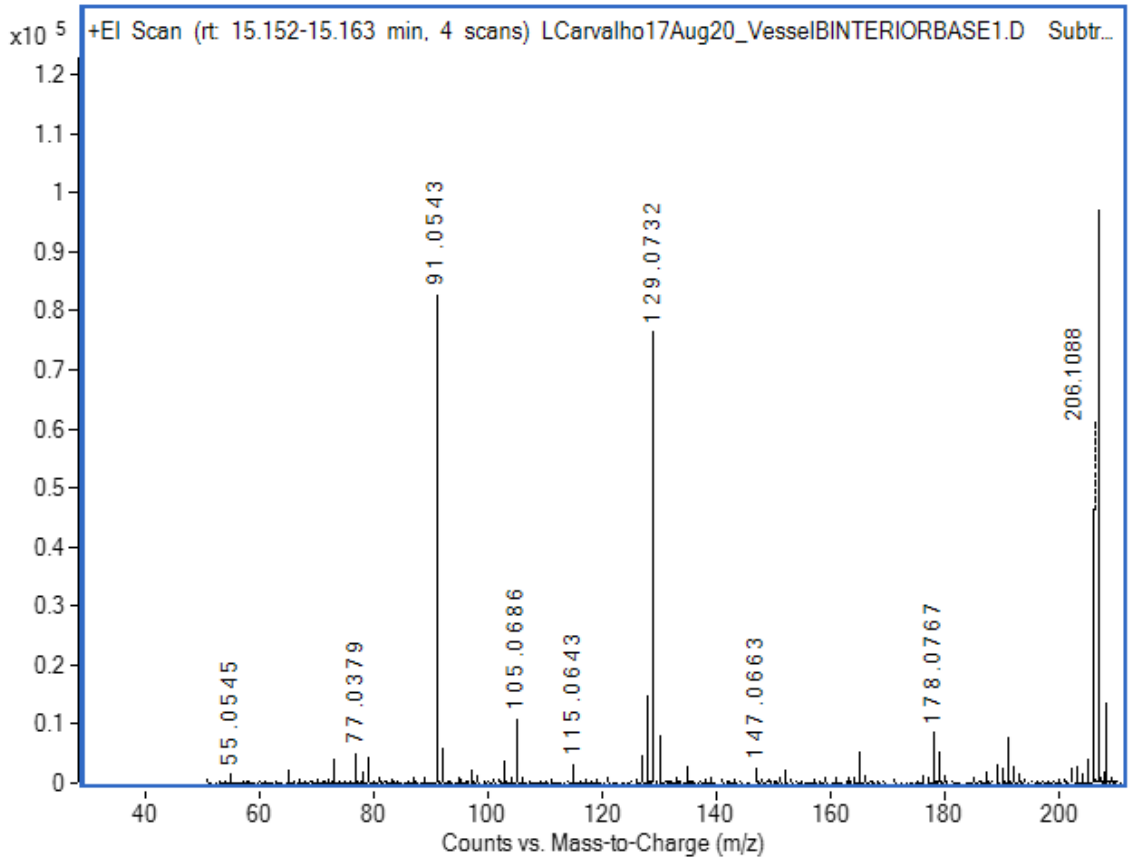




[15] 1,4-Diphenyl-1,3-butadiene Mass: 206.10955

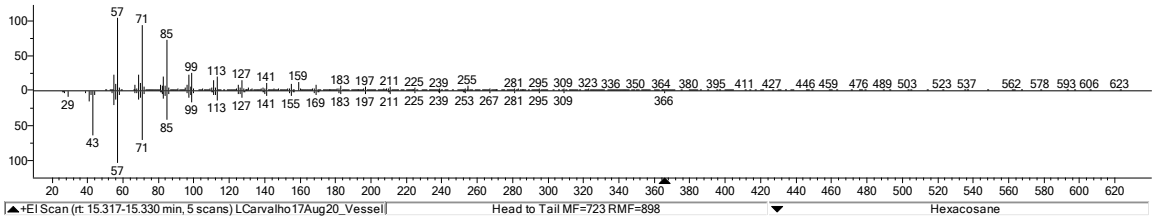
Base

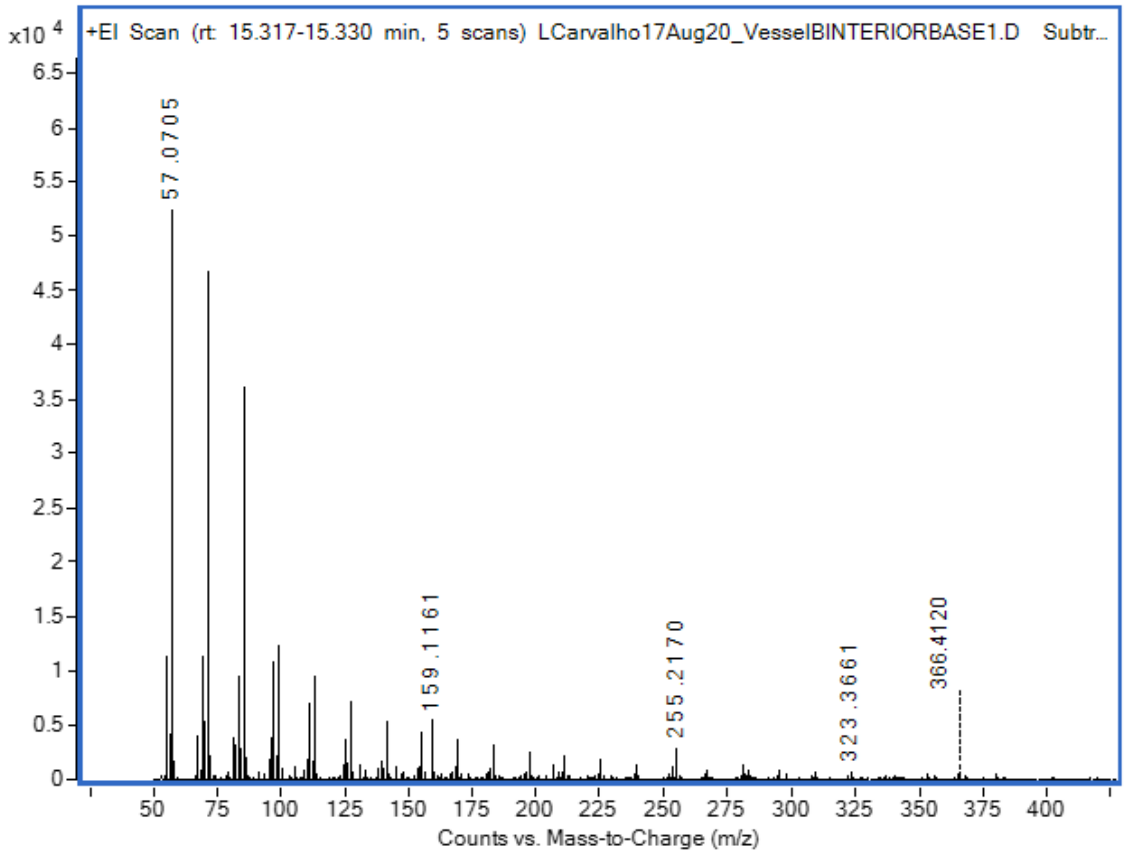




[16] Hexacosane Mass: 366.422552

Base

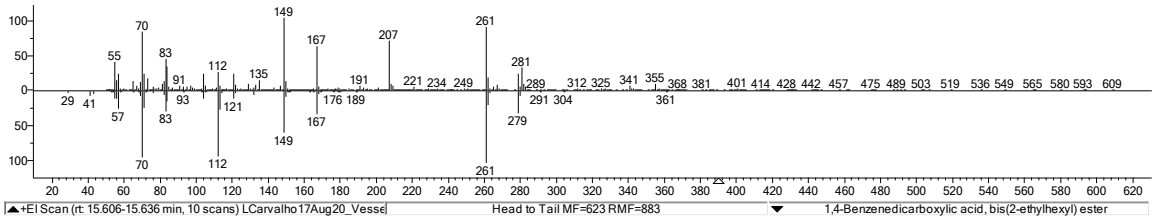


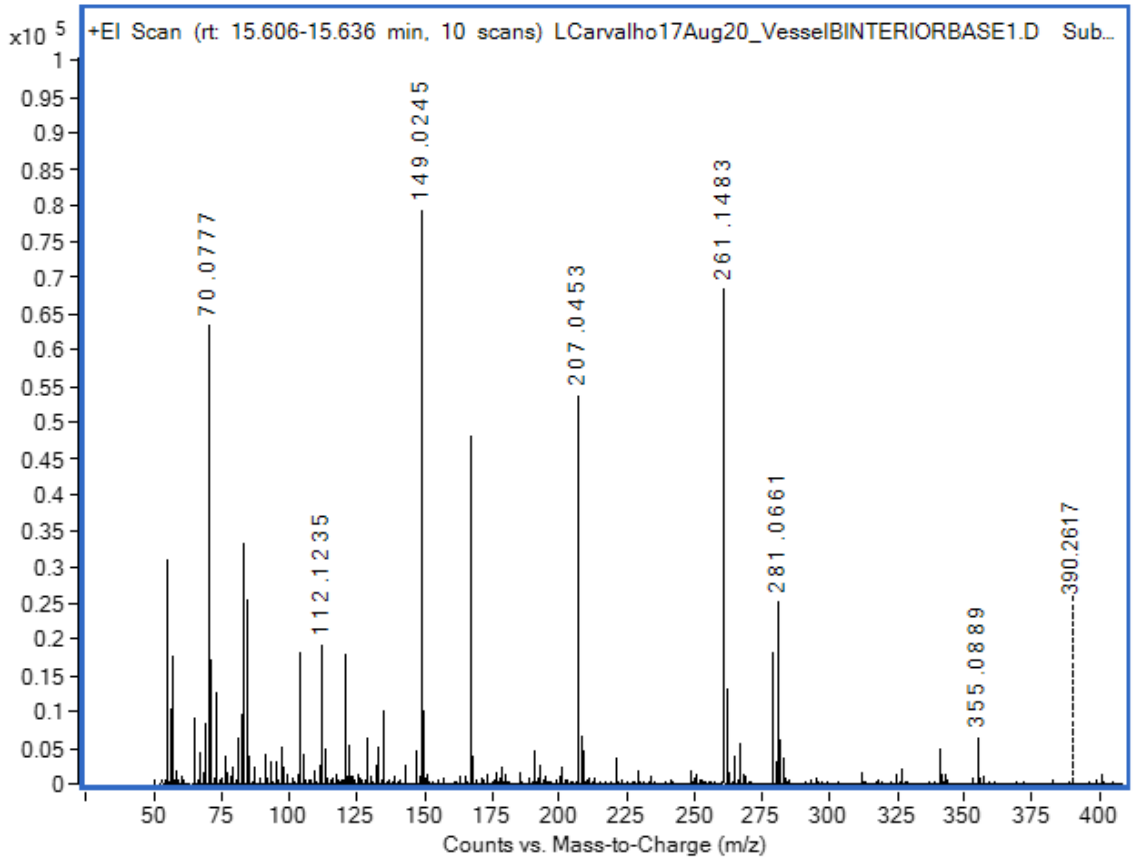


[17] 1,4-Benzenedicarboxylic acid, bis(2-ethylhexyl) ester

Mass: 390.27701

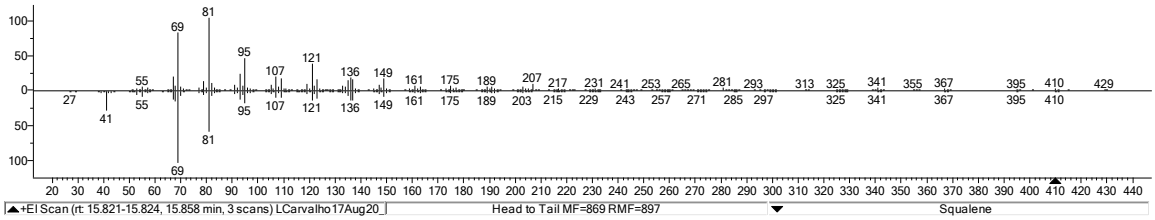
Base

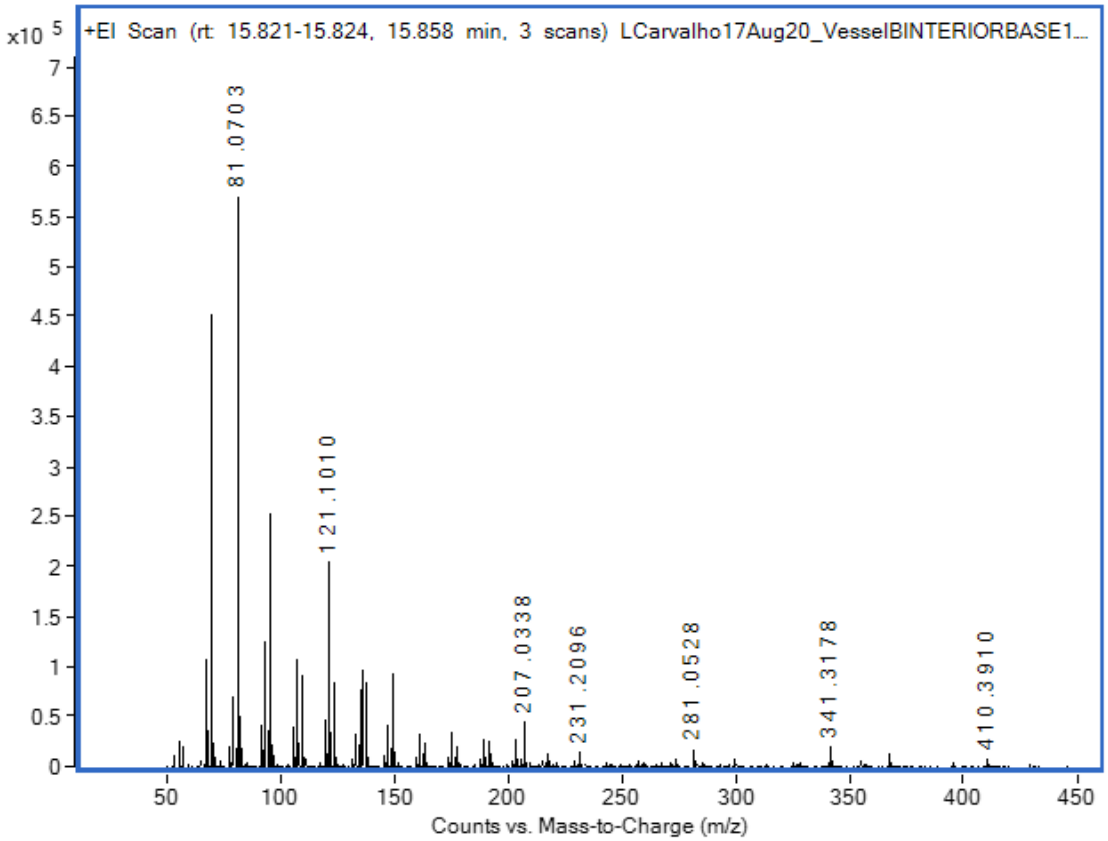




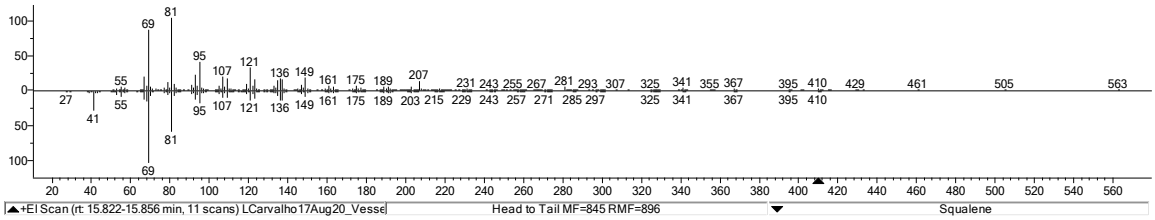
[18] Squalene Mass: 410.391253

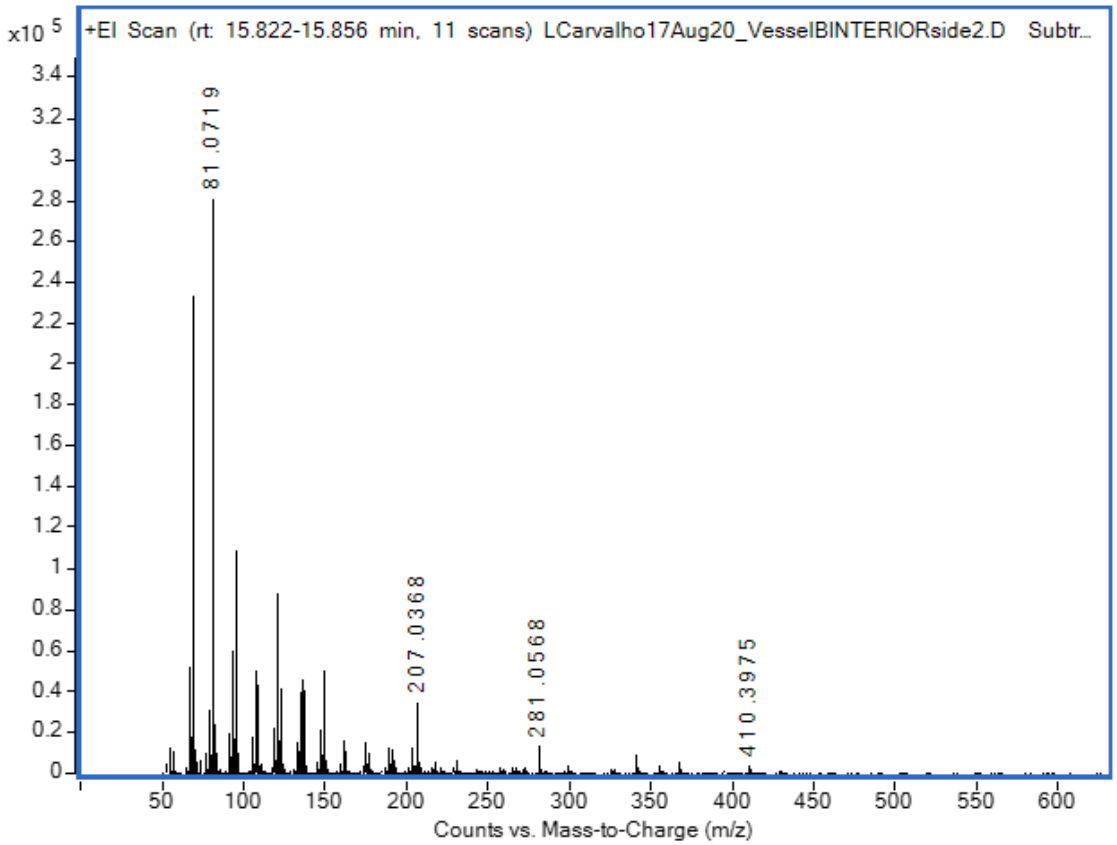
Base





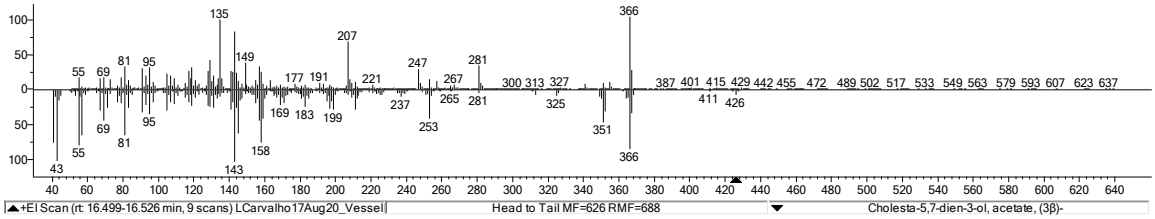
Body

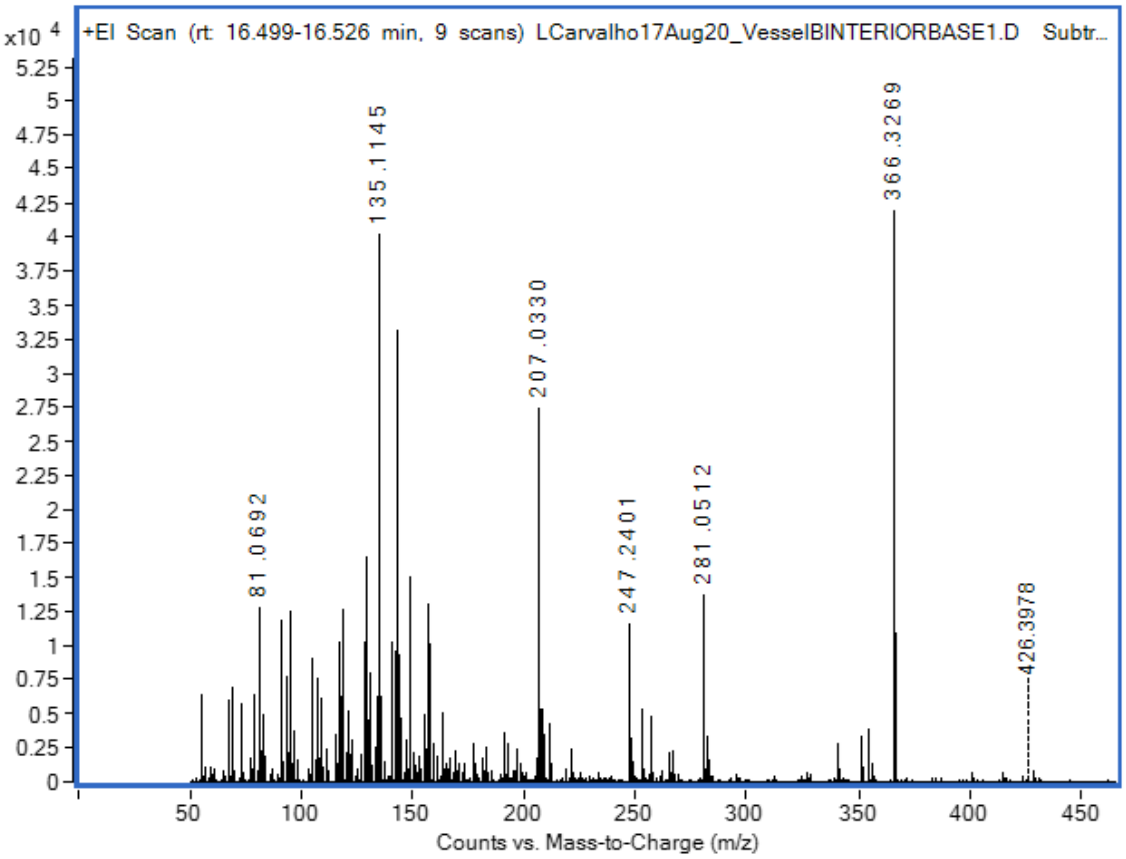

+EI Scan (rt: 15.822-15.856 min, 11 scans) LCarvalho17Aug20_Vesse
Head to Tail MF=845 RMF=896
Squalene


x10 5
+EI Scan (rt: 15.822-15.856 min, 11 scans) LCarvalho17Aug20_VesselBINTERIORside2.D Subtr...
81.0719
207.0368
281.0568
410.3975
Counts vs. Mass-to-Charge (m/z)

[19] Cholesta-5,7-dien-3-ol, acetate, (3β)- Mass: 426.349781

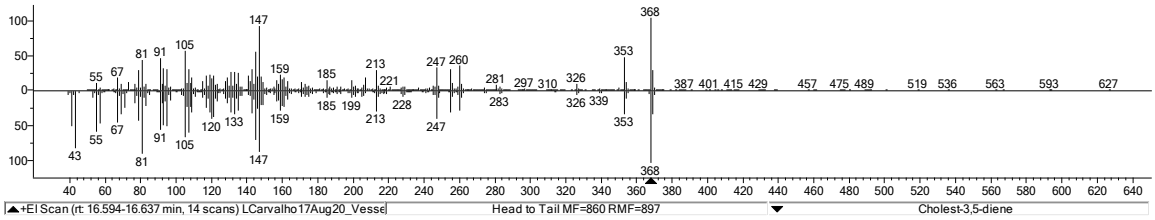
Base

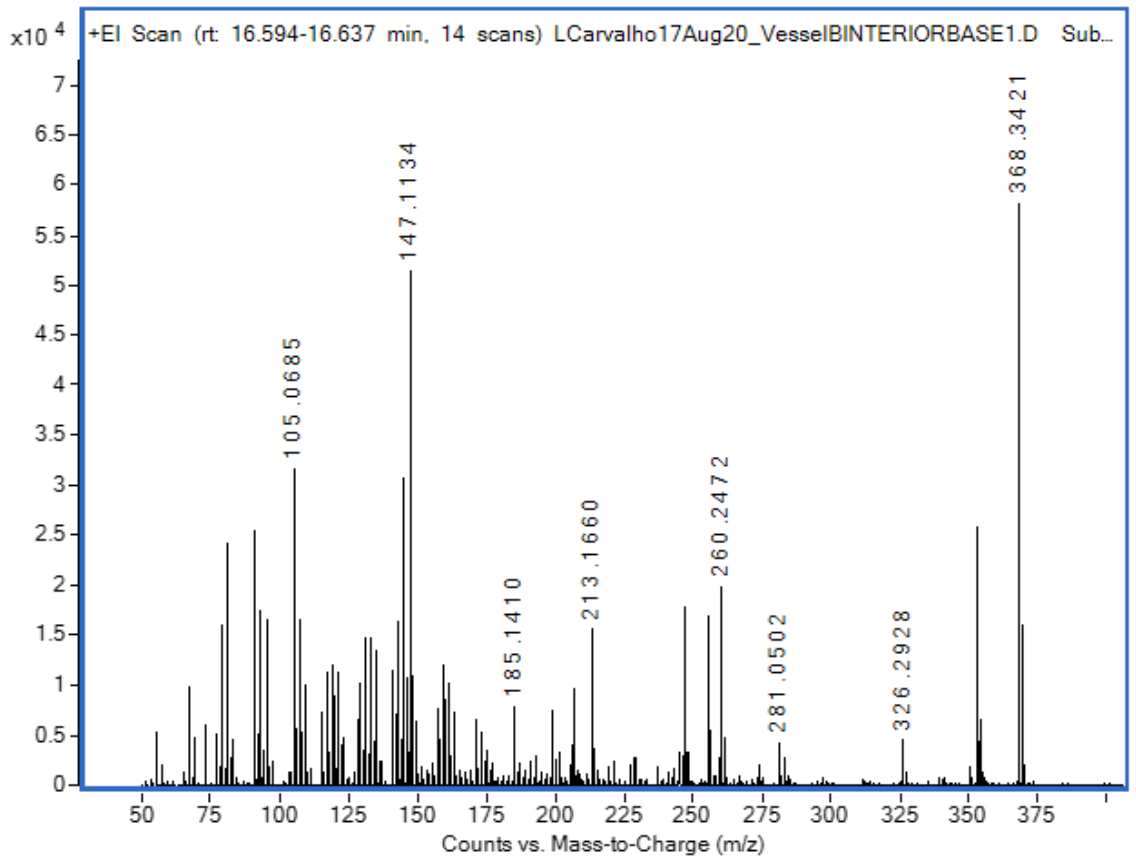




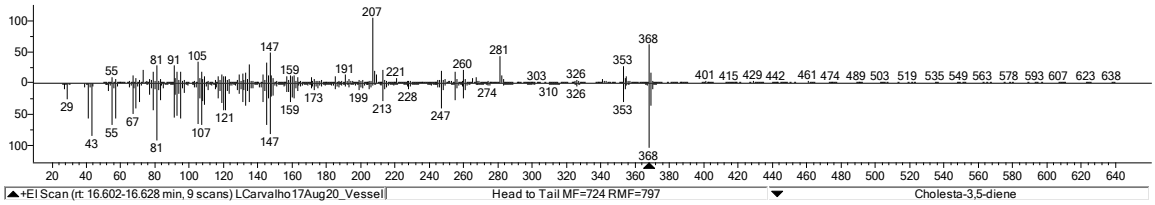
[20] Cholest-3,5-diene C27H44 Mass: 368.344301

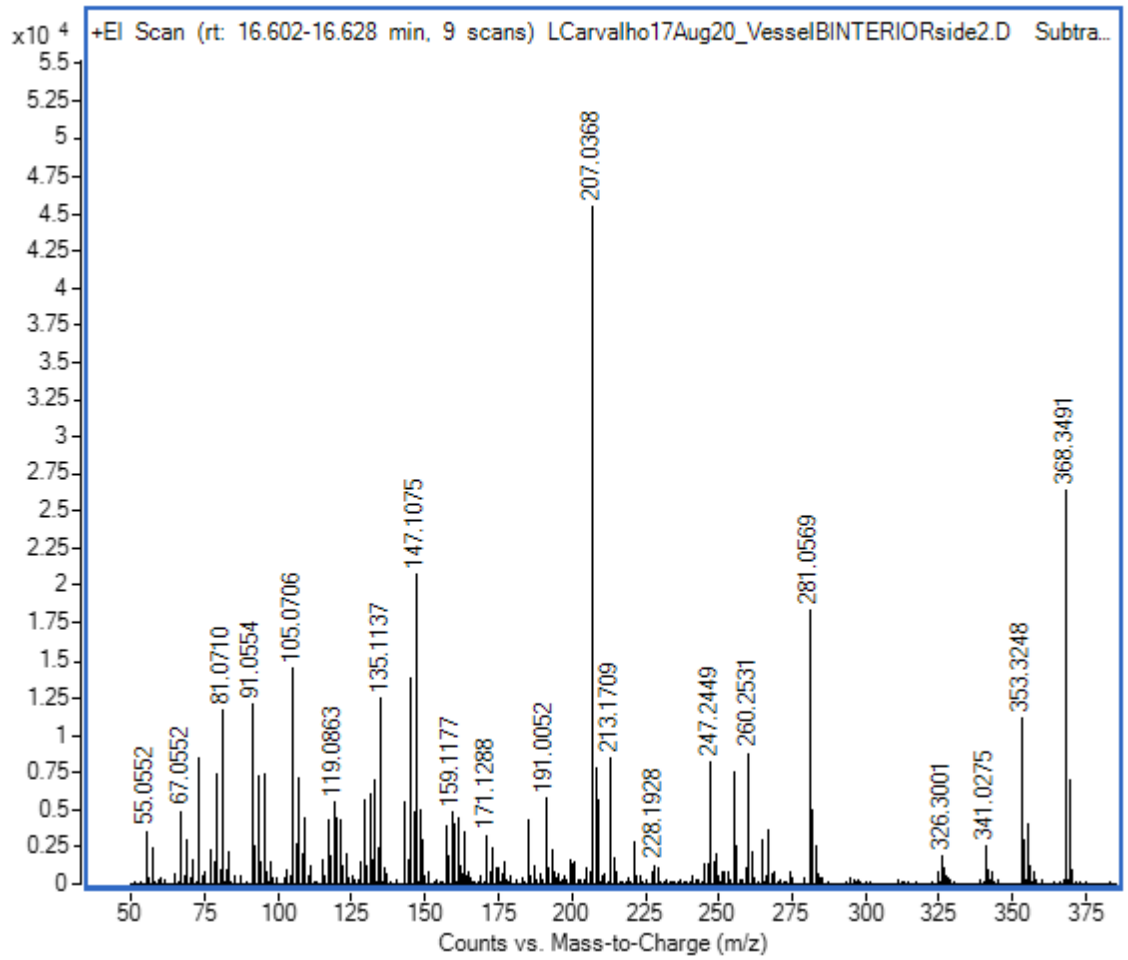
Base





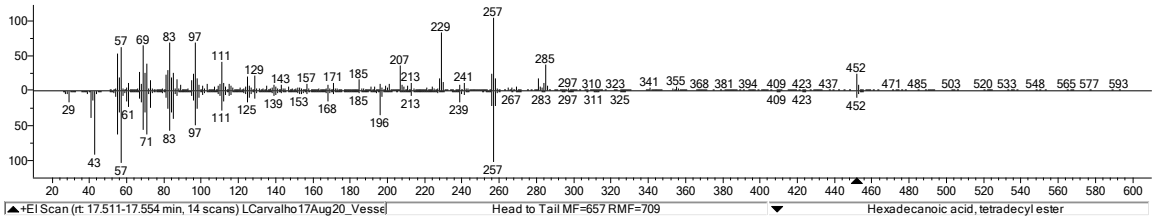
Body

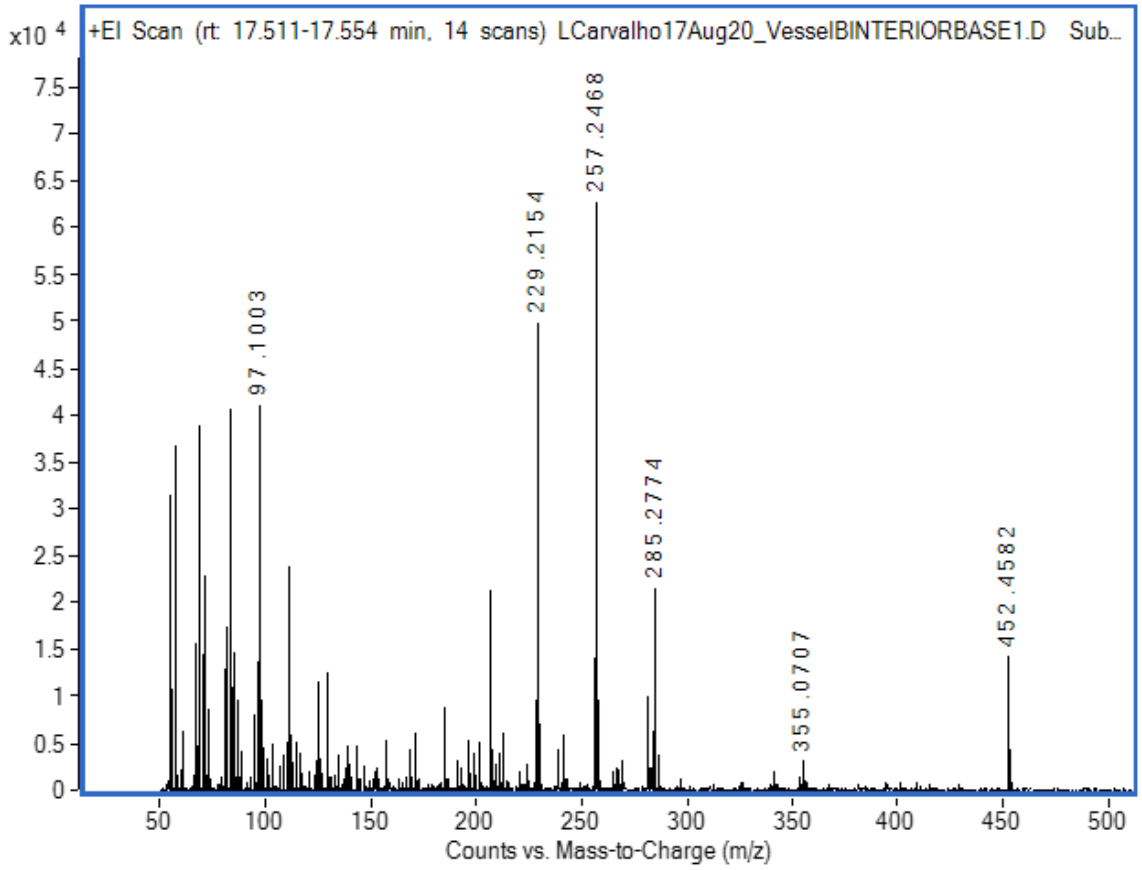

+EI Scan (rt: 16.602-16.628 min, 9 scans) LCarvalho17Aug20_VesselI
Head to Tail MF=724 RMF=797
Cholesta-3,5-diene


x10 4
+EI Scan (rt: 16.602-16.628 min, 9 scans) LCarvalho17Aug20_VesselBINTERIORside2.D Subtra...
55.0552
67.0552
81.0710
91.0554
105.0706
119.0863
135.1137
147.1075
159.1177
171.1288
191.0052
207.0368
213.1709
228.1928
247.2449
260.2531
281.0569
326.3001
341.0275
353.3248
368.3491
Counts vs. Mass-to-Charge (m/z)

[21] Hexadecanoic acid, tetradecyl ester Mass: 452.459332

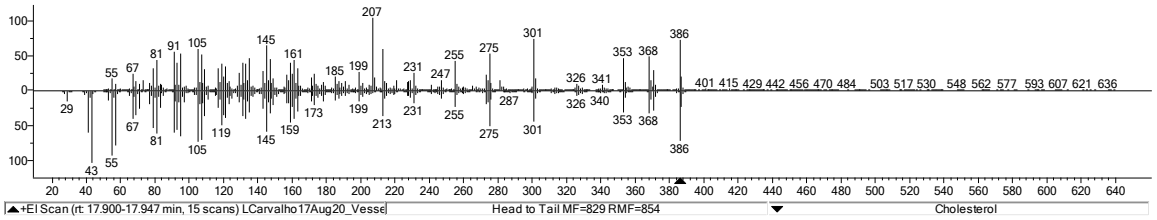
Base

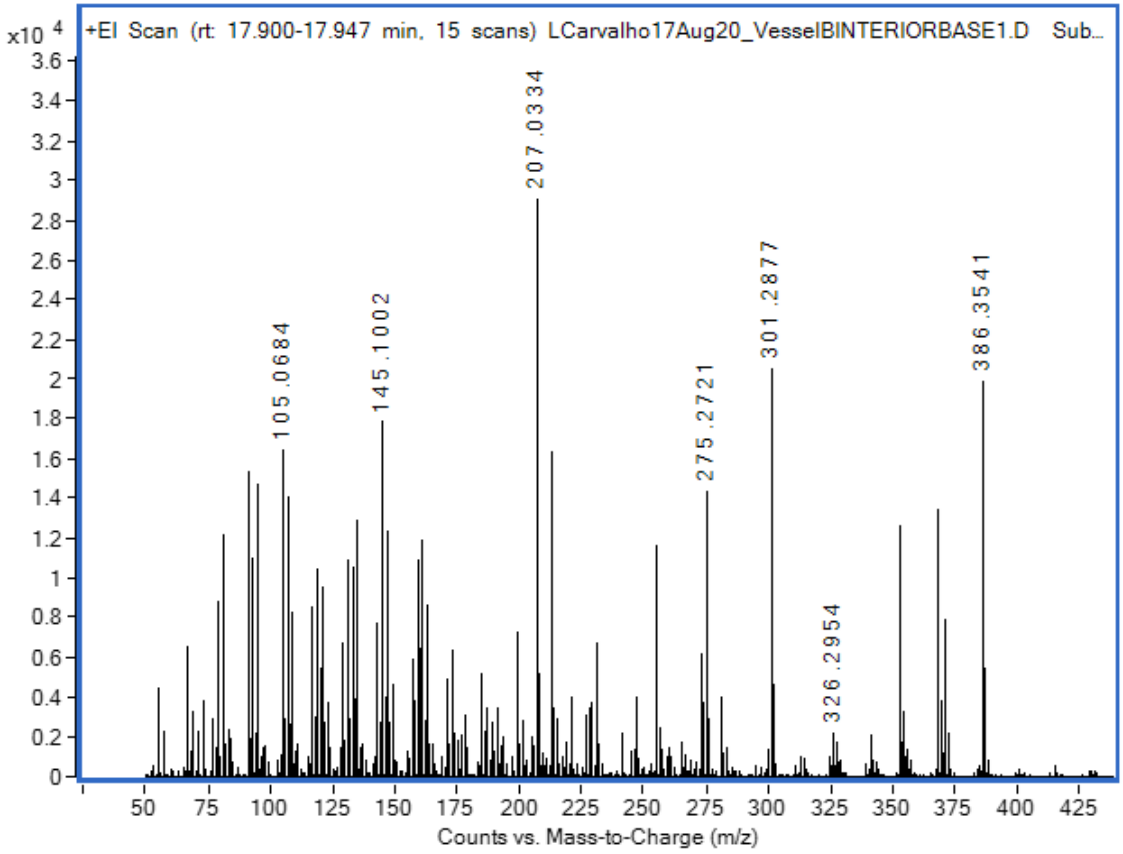




[22] Cholesterol Mass: 386.354866

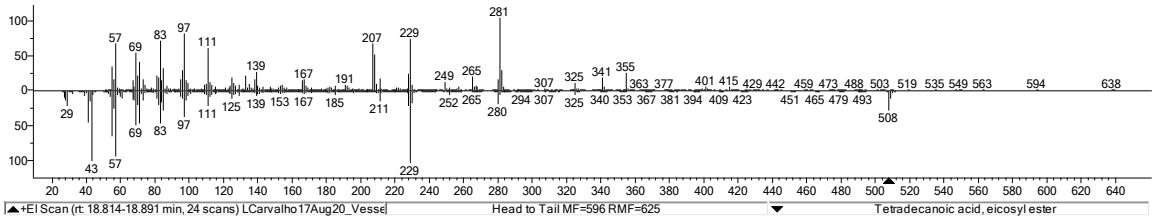
Base

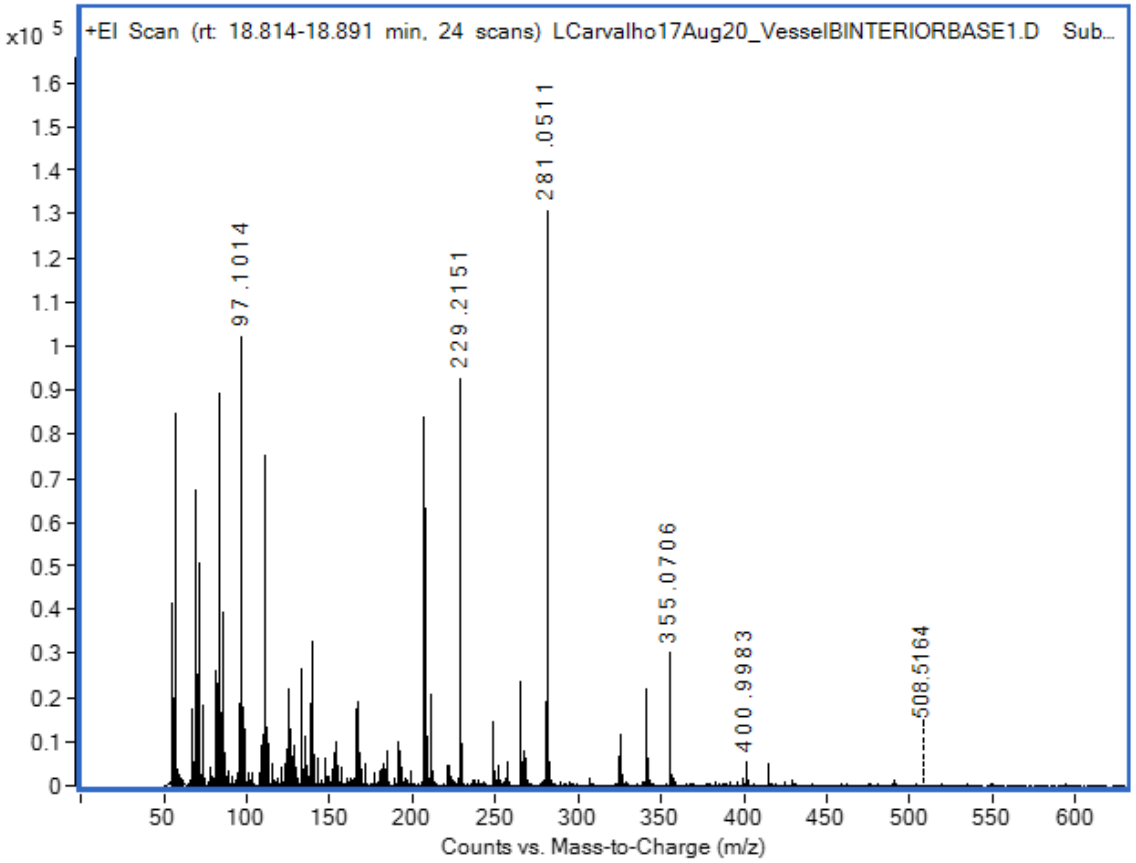




[23] Tetradecanoic acid, eicosyl ester Mass: 508.52193

Base

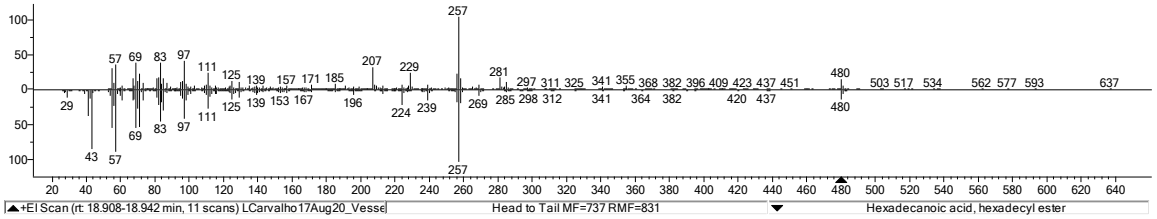


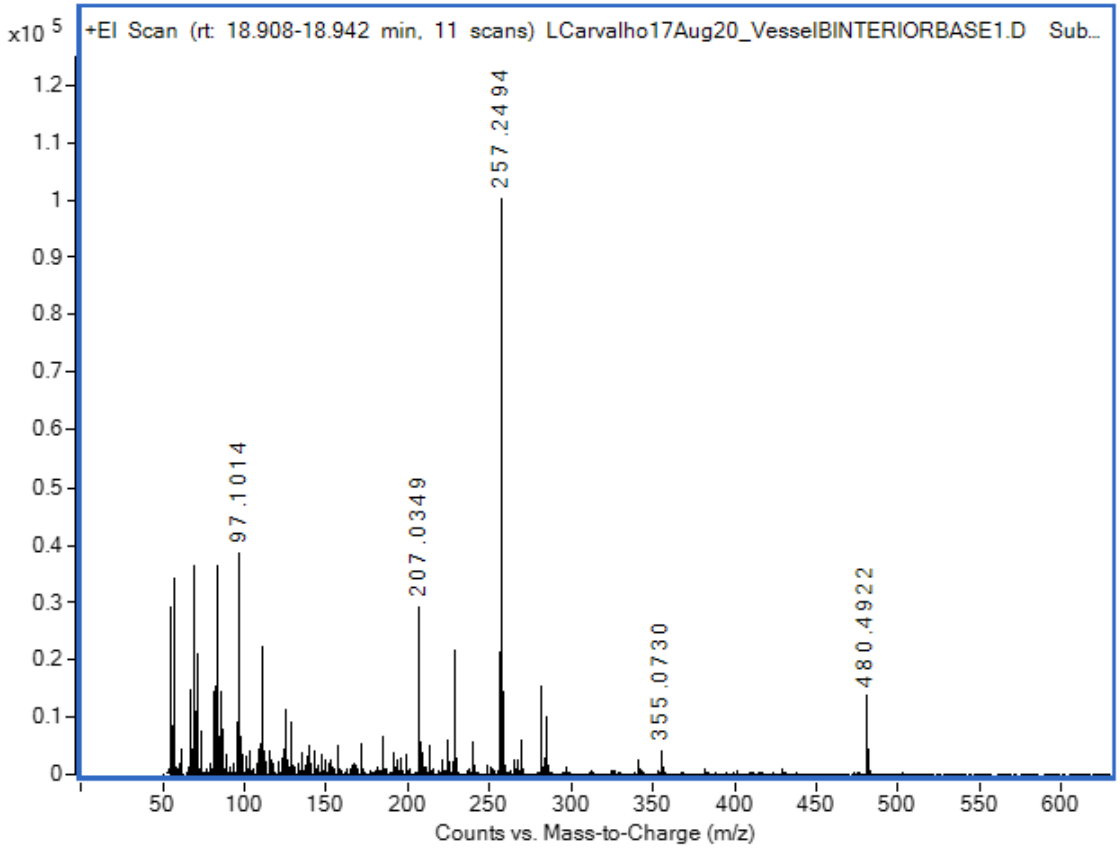


[24] Hexadecanoic acid, hexadecyl ester

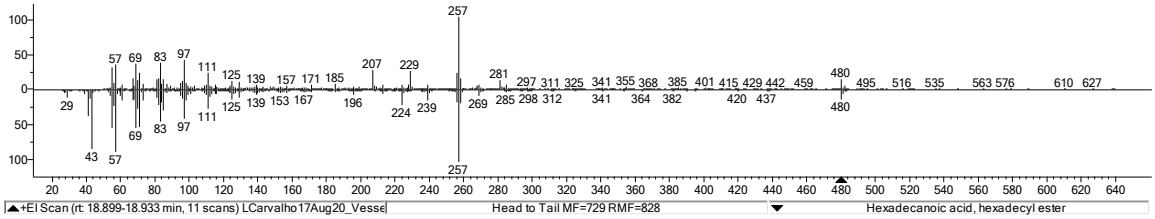
Mass: 480.490631

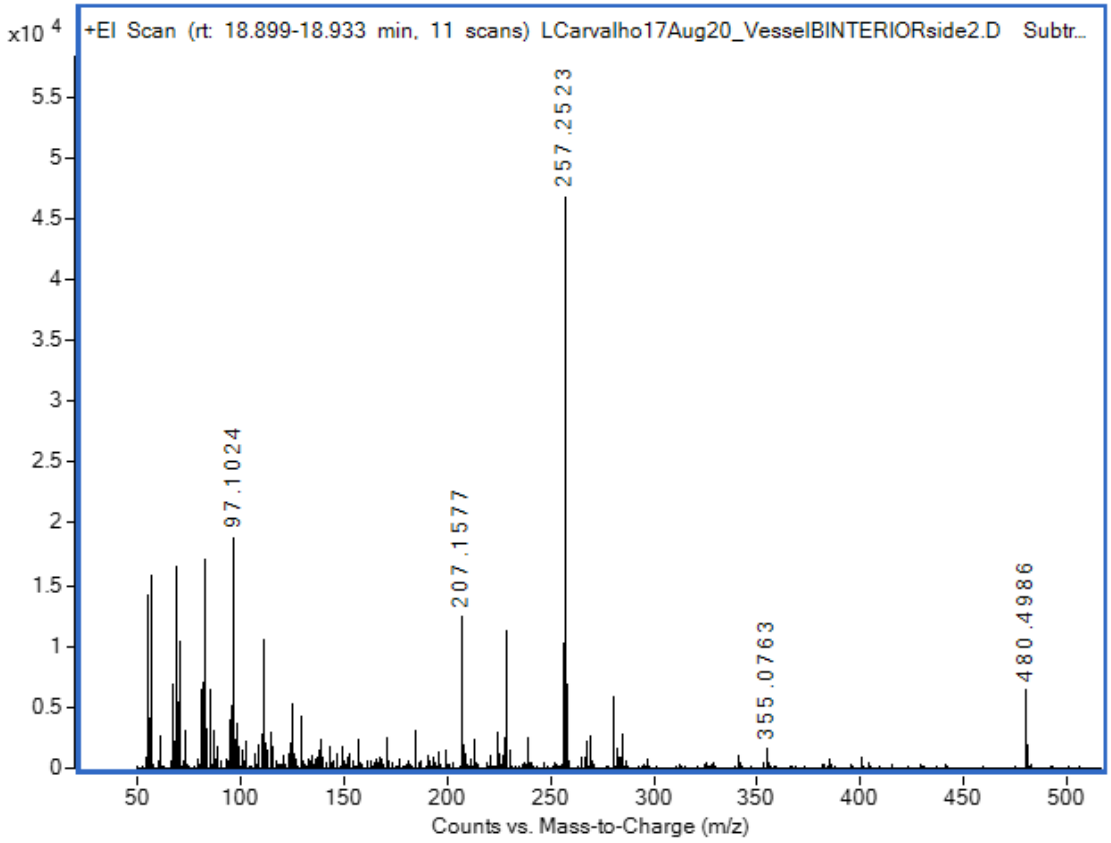
Base



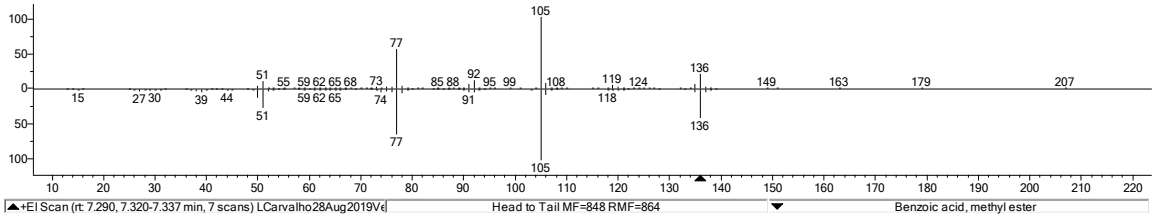


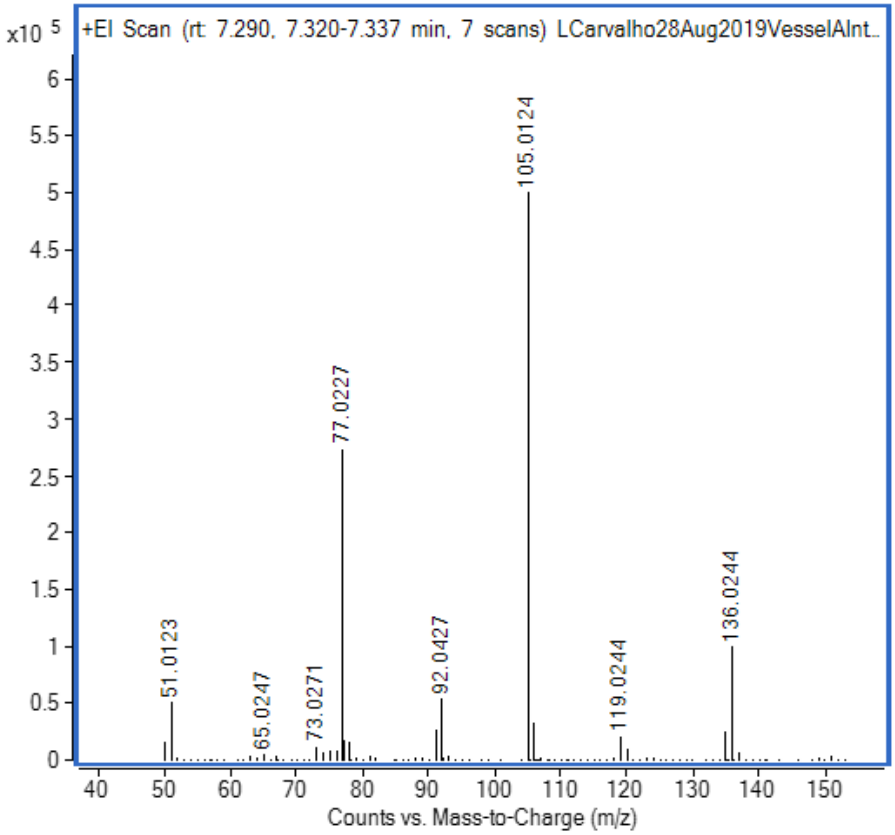
Body


+EI Scan (rt: 18.899-18.933 min, 11 scans) LCarvalho17Aug20_Vesse
Head to Tail MF=729 RMF=828
Hexadecanoic acid, hexadecyl ester

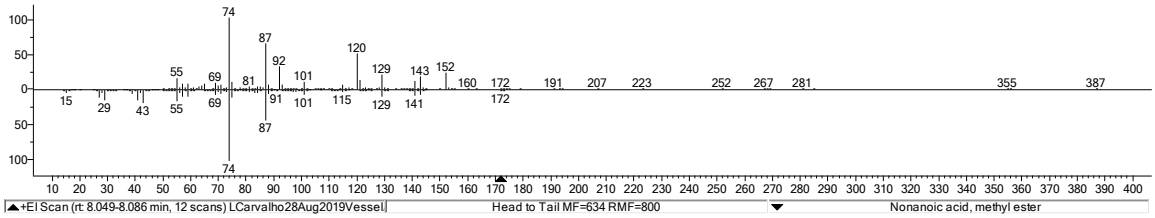

x10 4
+EI Scan (rt: 18.899-18.933 min, 11 scans) LCarvalho17Aug20_VesselBINTERIORside2.D Subtr...
257.2523
97.1024
207.1577
355.0763
480.4986
Counts vs. Mass-to-Charge (m/z)

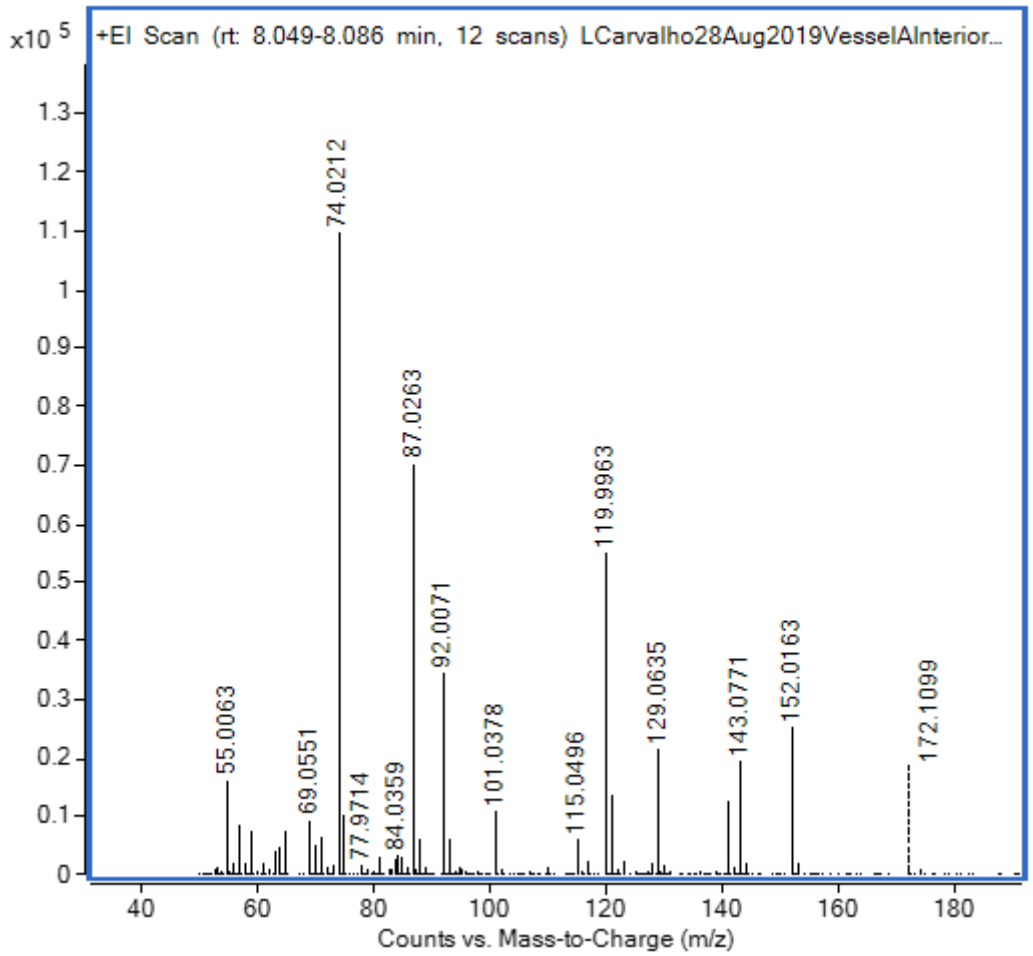
Benzoic acid, methyl ester Mass: 136.05242



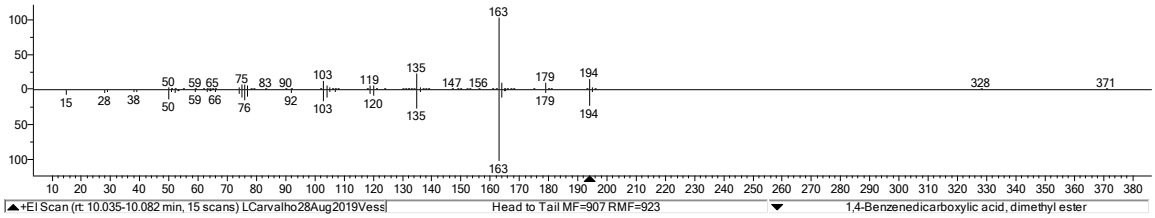


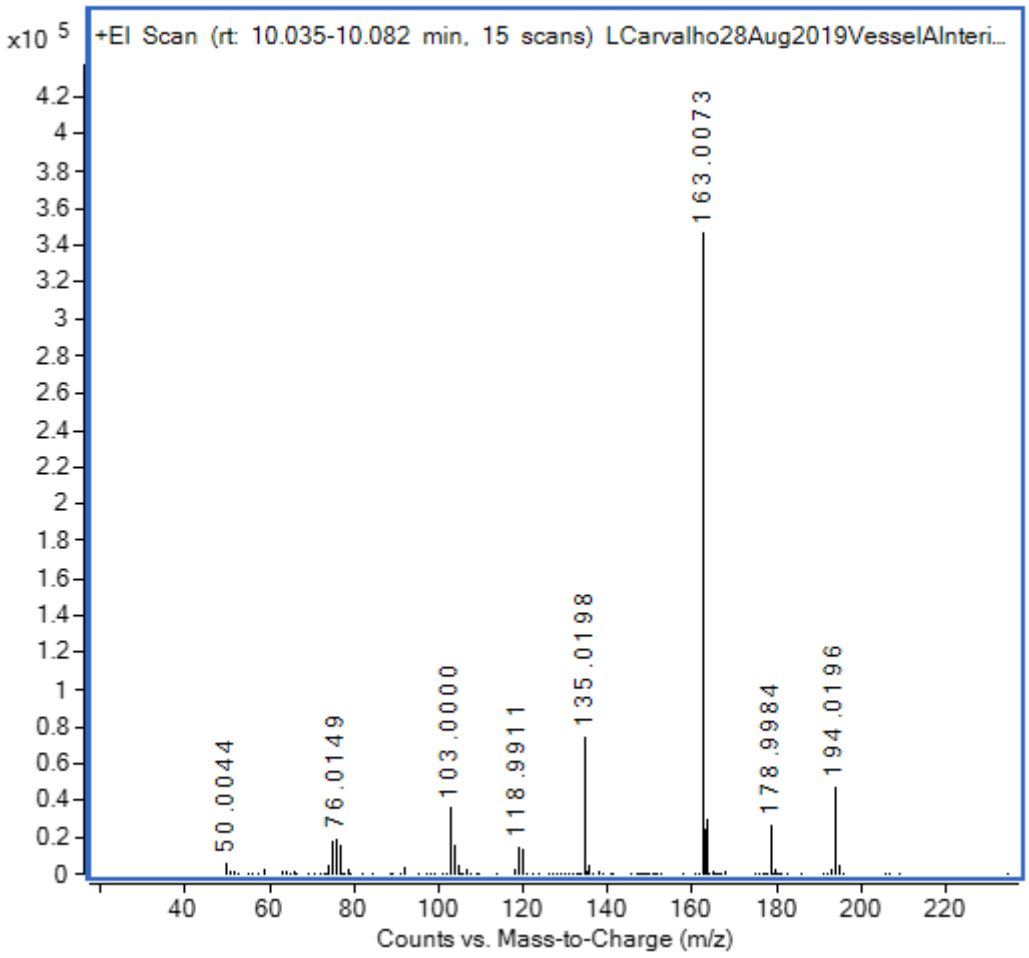
Nonanoic acid, methyl ester Mass: 172.14633



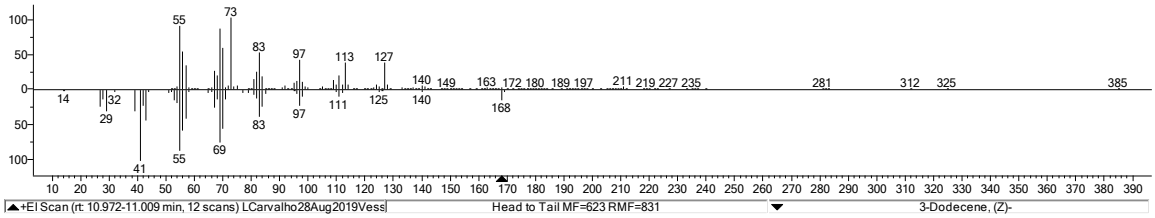


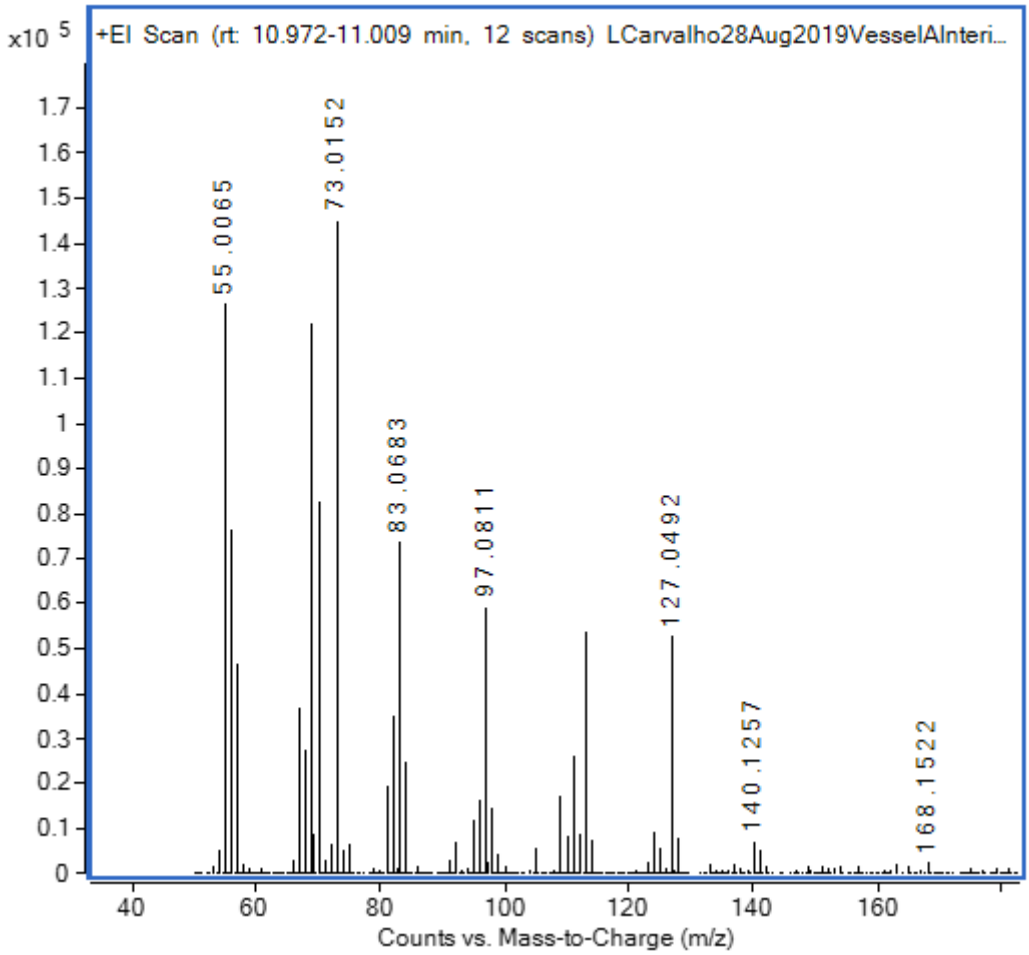
1,4-Benzenedicarboxylic acid, dimethyl ester Mass: 194.057909



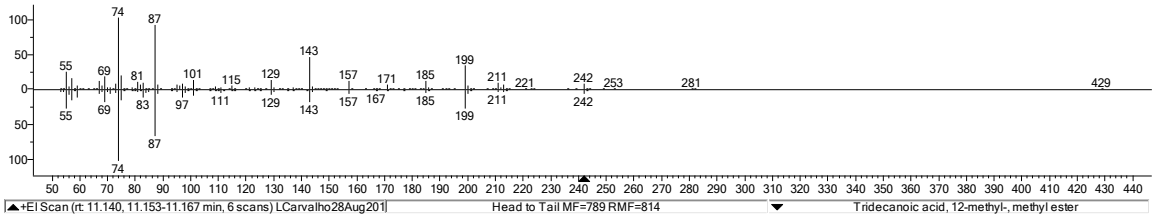


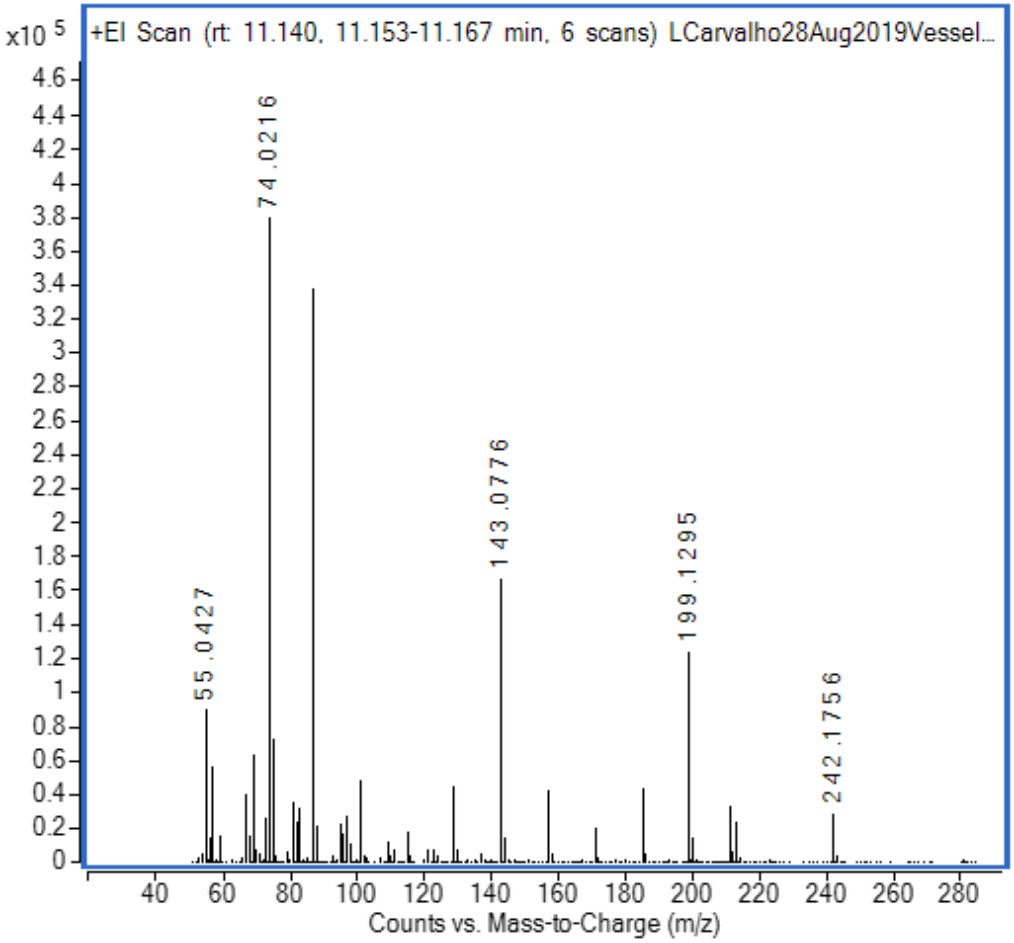
3-Dodecene, (Z)- Mass: 168.1878



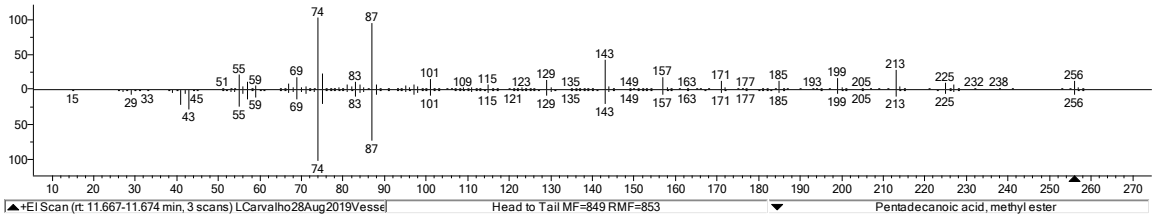


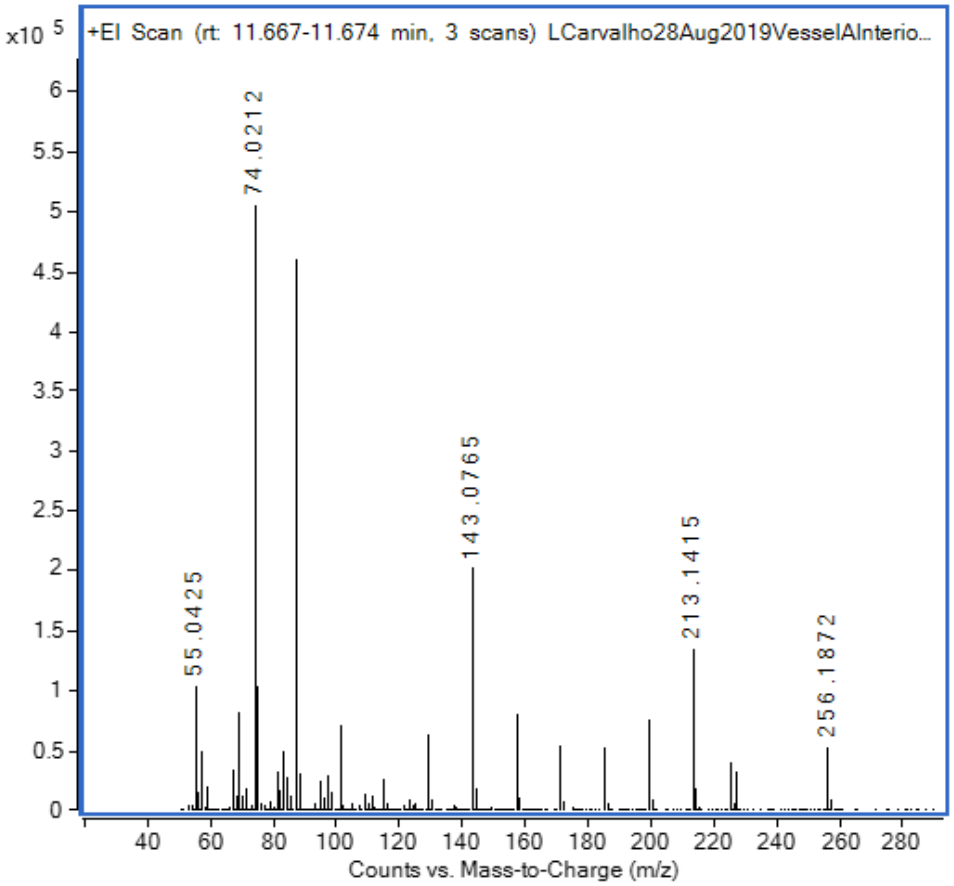
Tridecanoic acid, 12-methyl-, methyl ester Mass: 242.22458



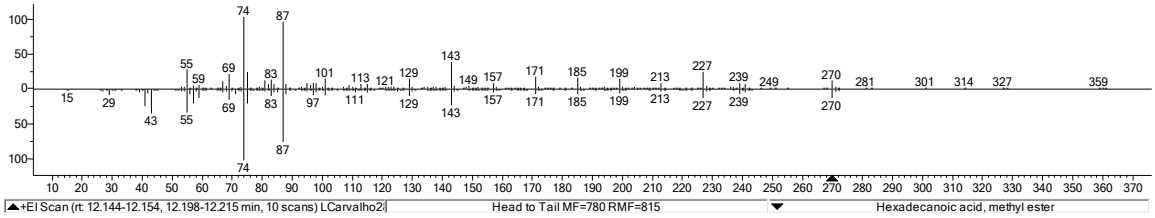


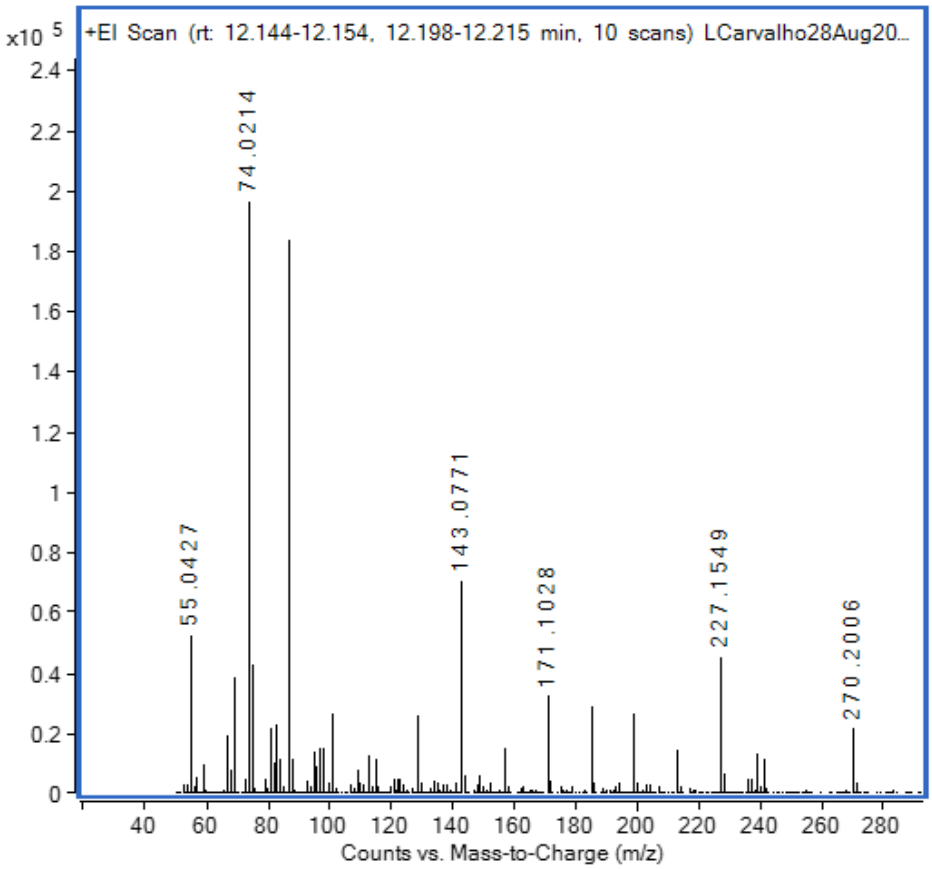
Pentadecanoic acid, methyl ester Mass: 256.24023



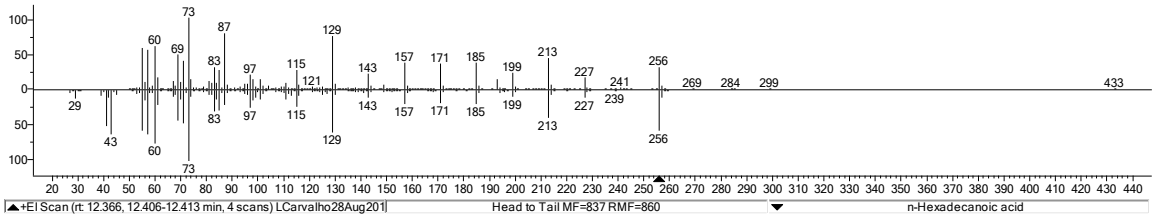


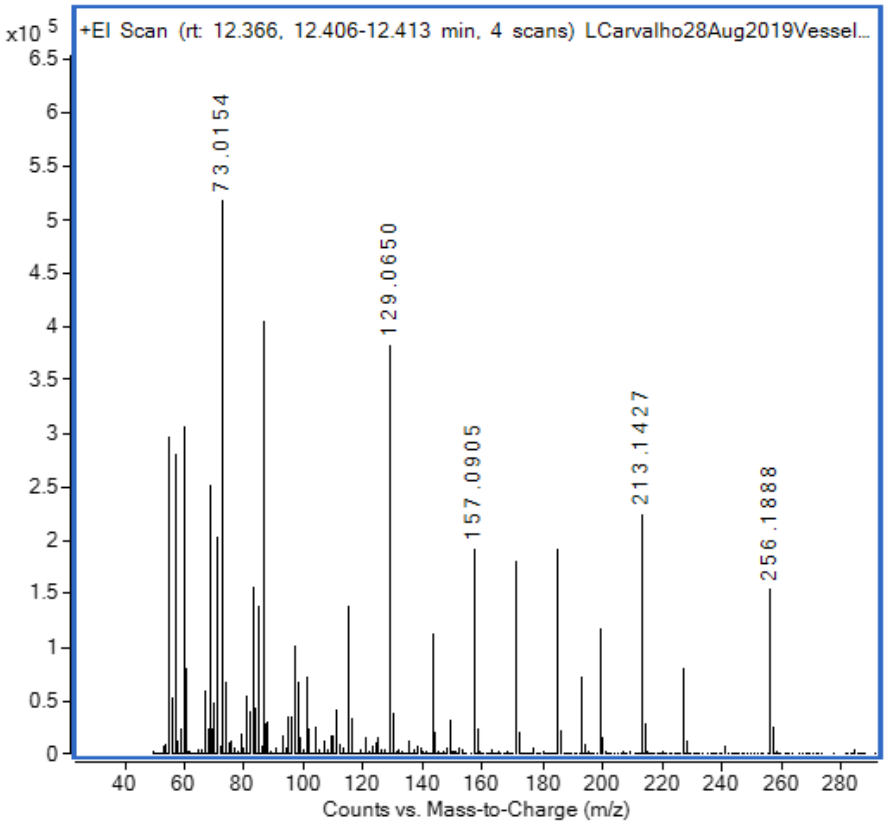
Hexadecanoic acid, methyl ester **Mass: 270.25588**



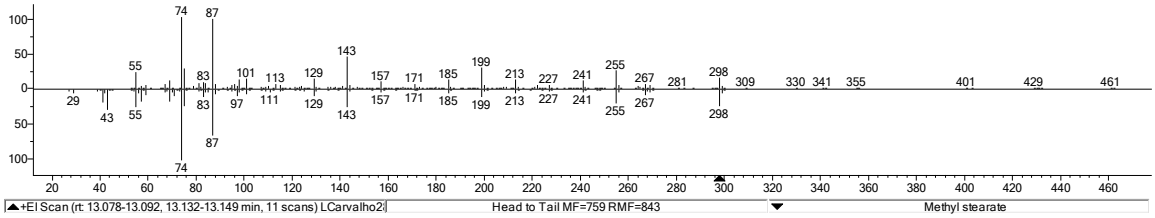


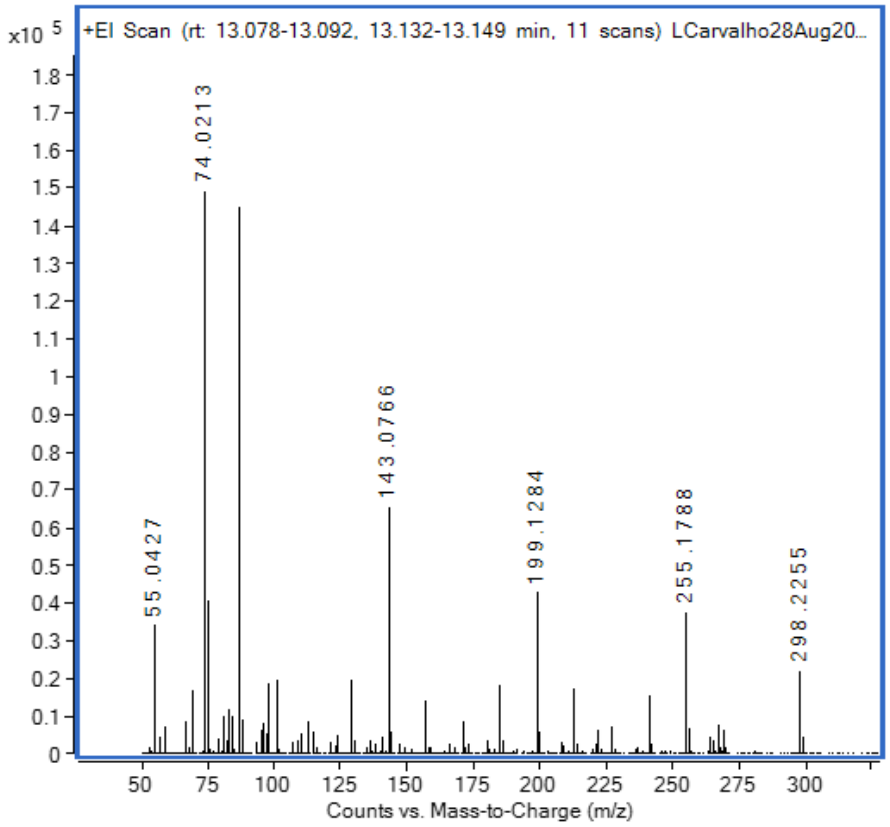
n-Hexadecanoic acid



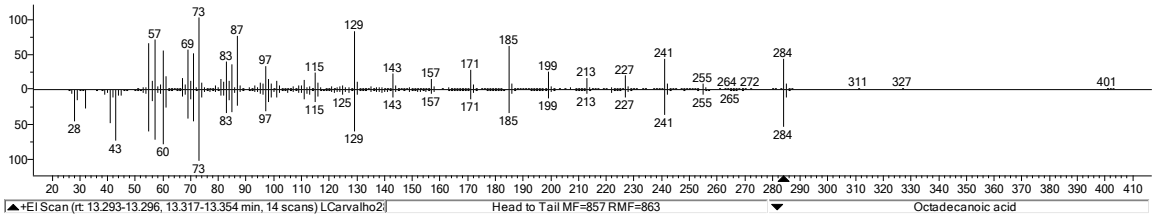


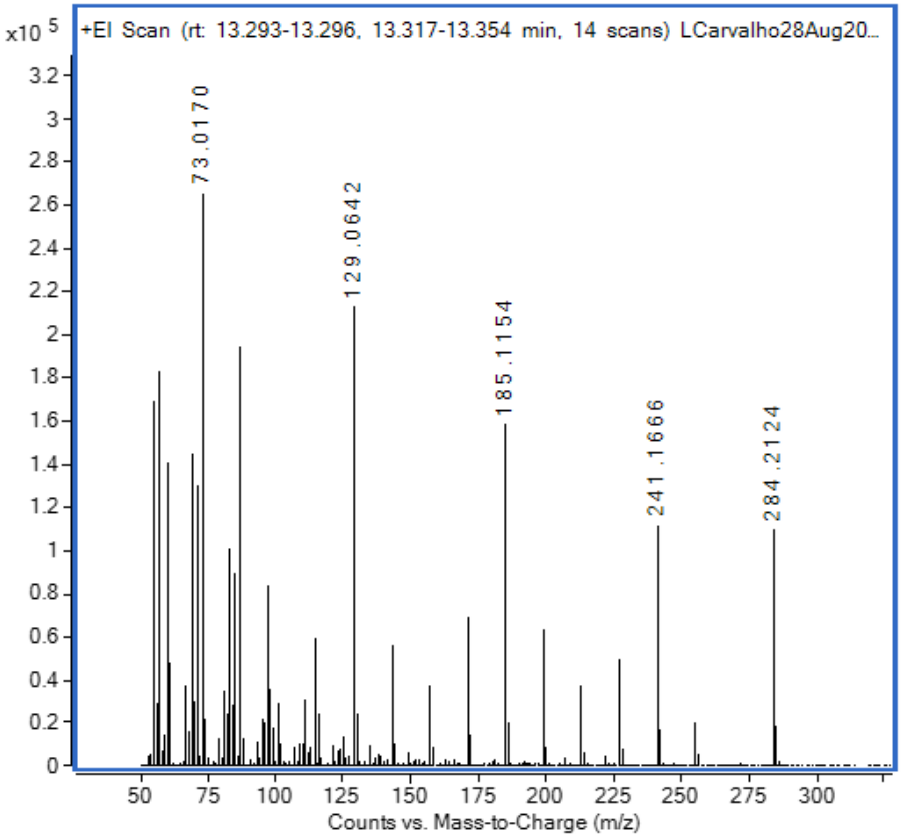
Methyl stearate Mass: 298.28718



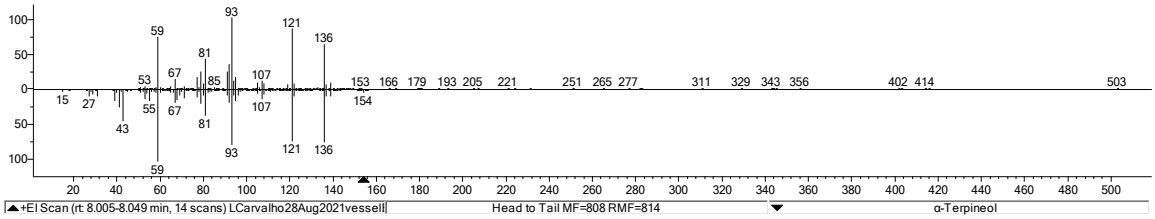


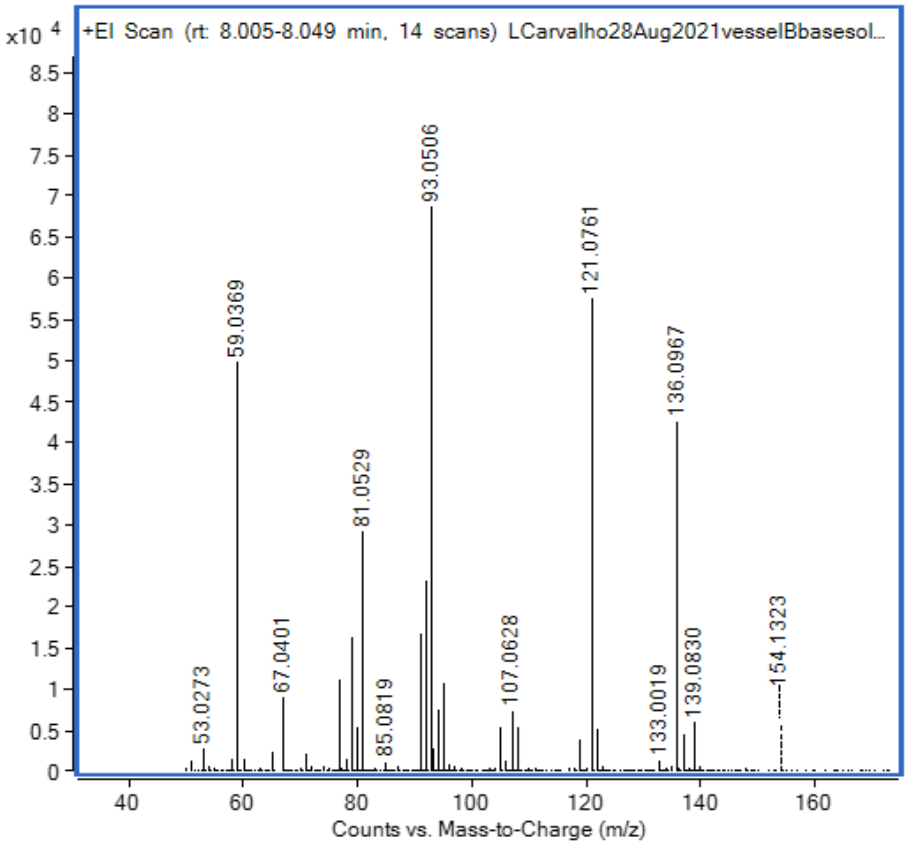
Octadecanoic acid



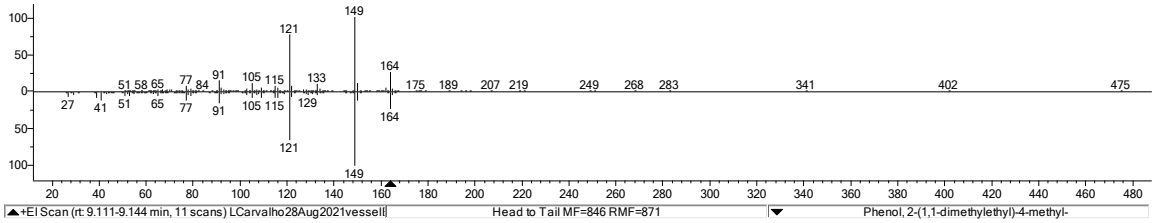


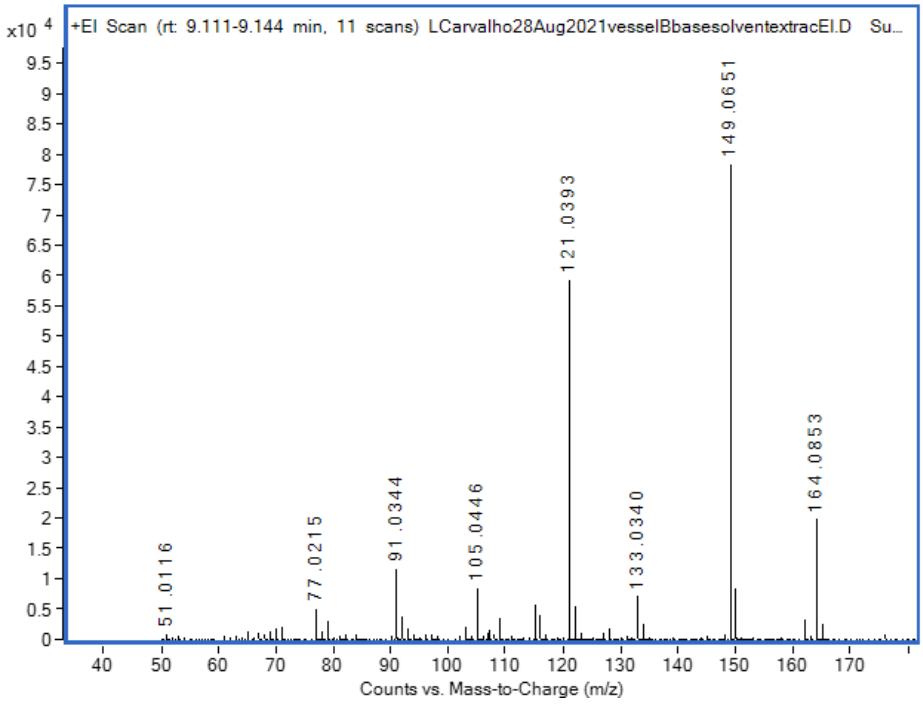
α-Terpineol Mass: 154.135765



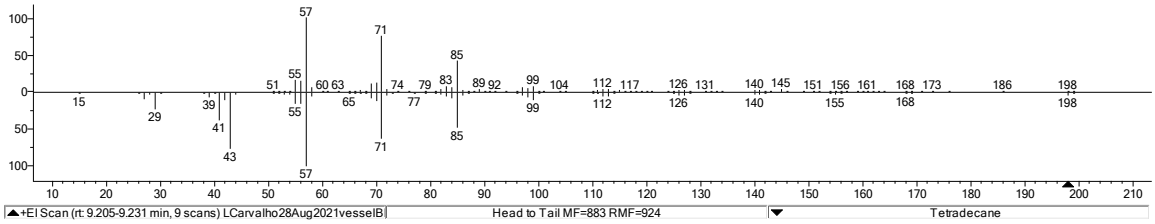


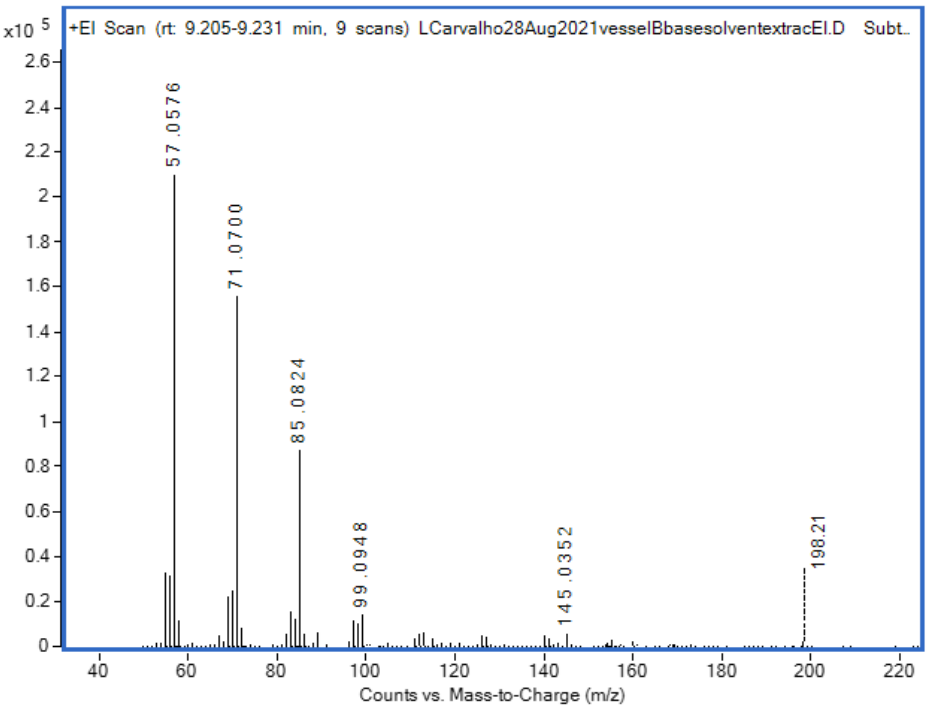
Phenol, 2-(1,1-dimethylethyl)-4-methyl- Mass: 164.120115



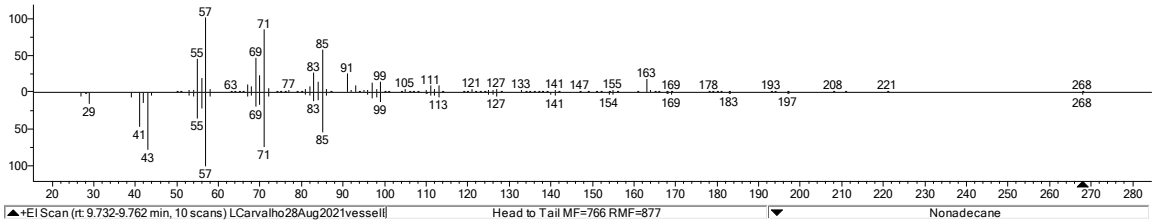


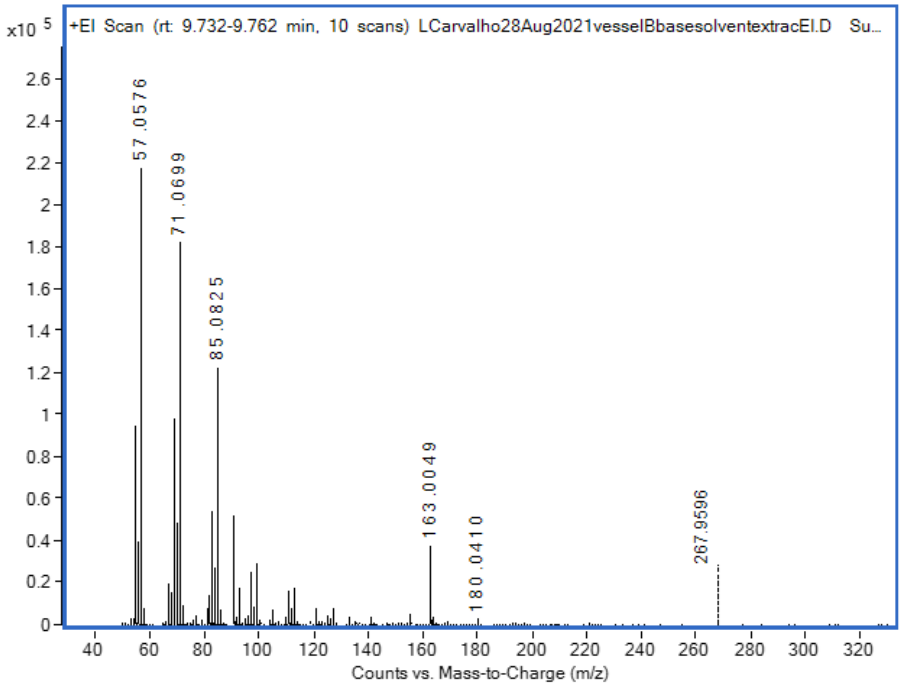
Tetradecane **Mass: 198.234751**



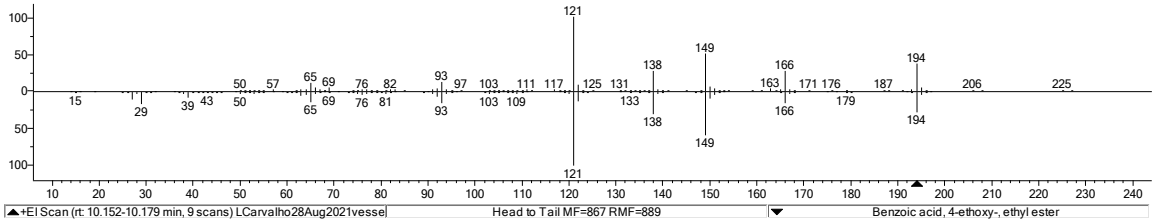


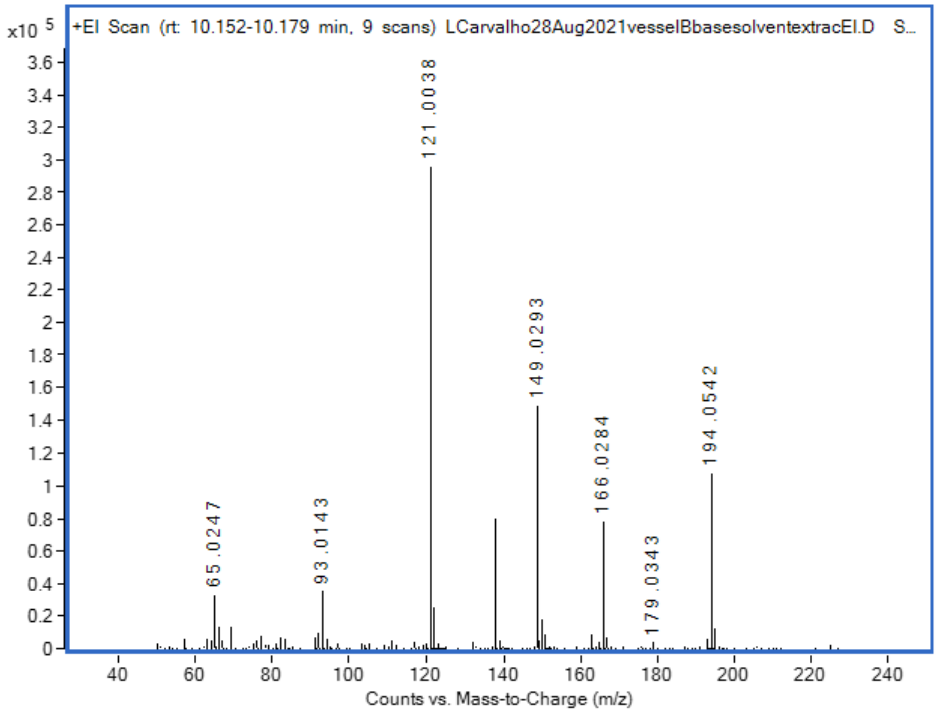
Nonadecane **Mass: 268.313002**



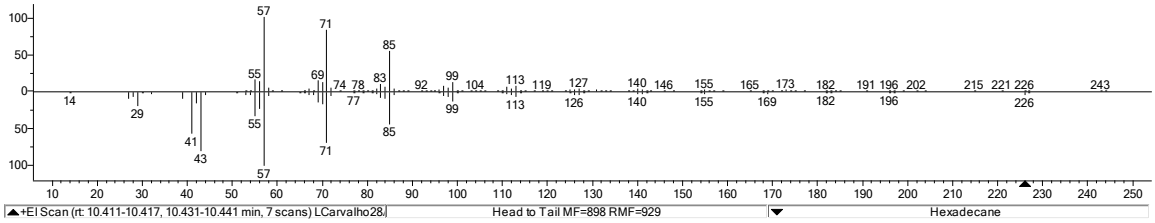


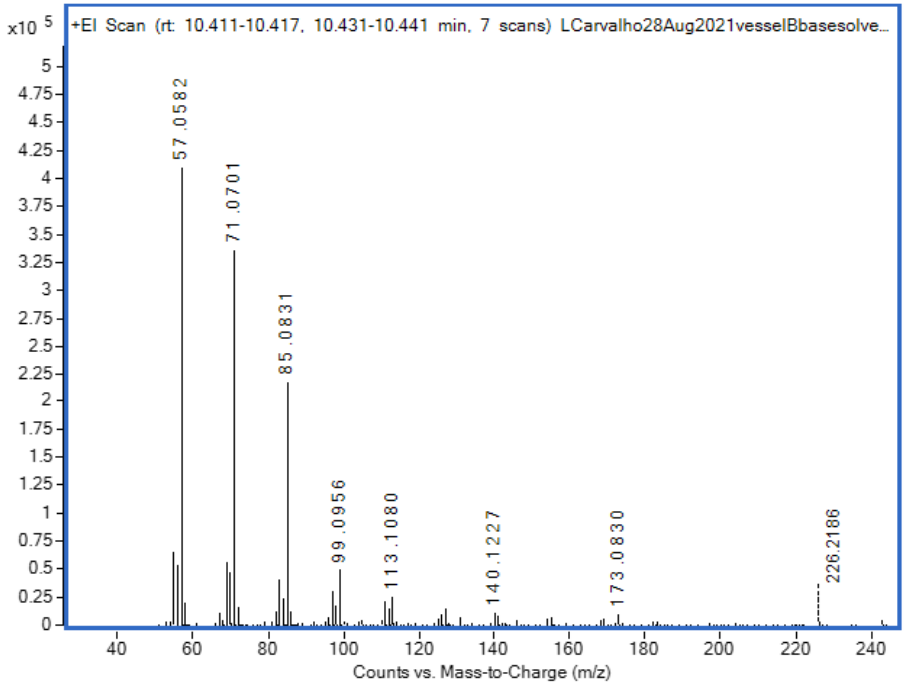
Benzoic acid, 4-ethoxy-, ethyl ester Mass: 194.094295



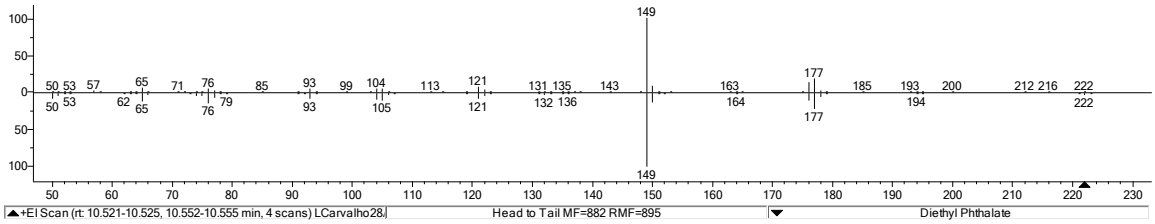


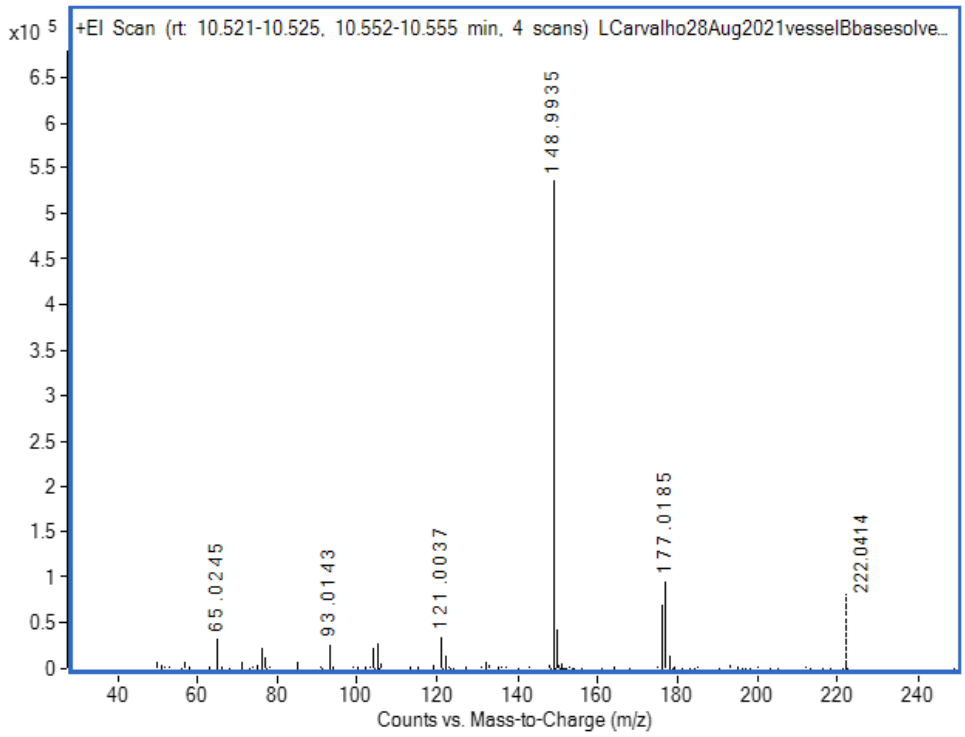
Hexadecane **Mass: 226.266051**



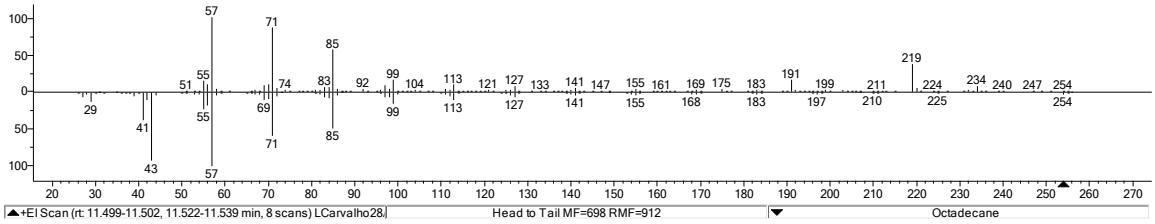


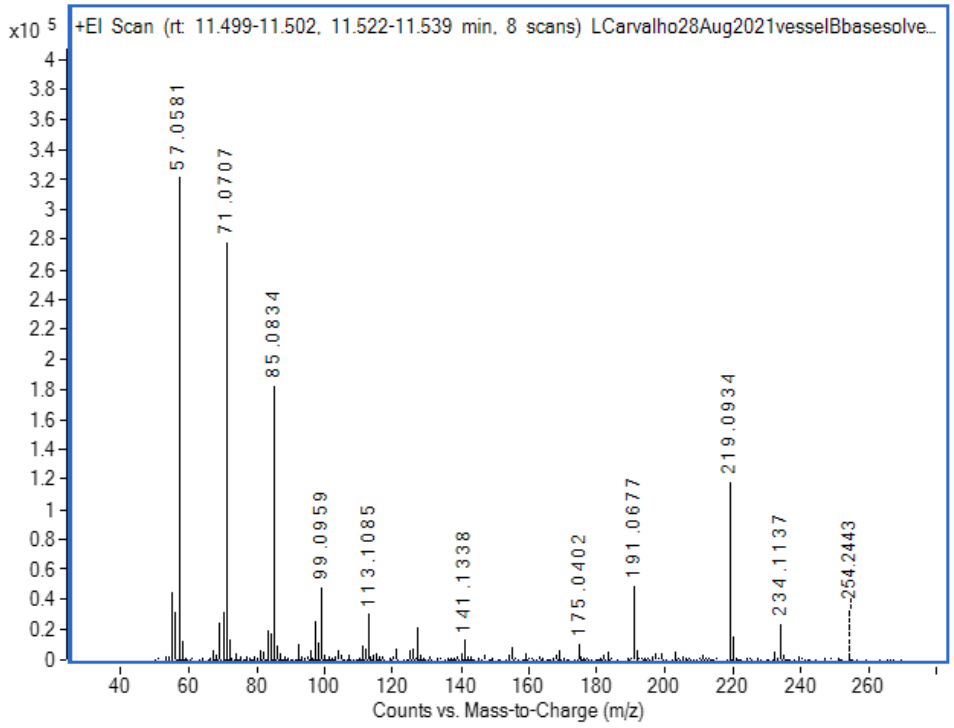
Diethyl Phthalate Mass: 222.089209



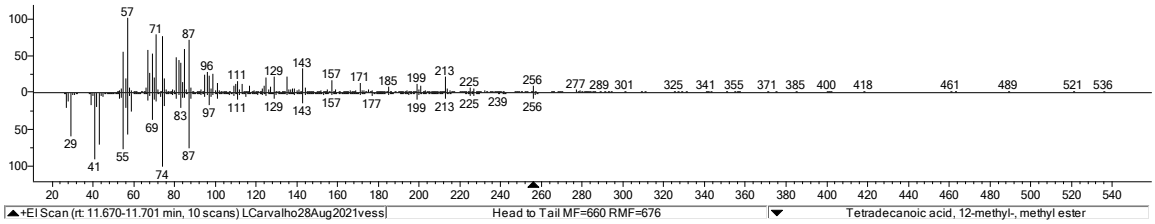


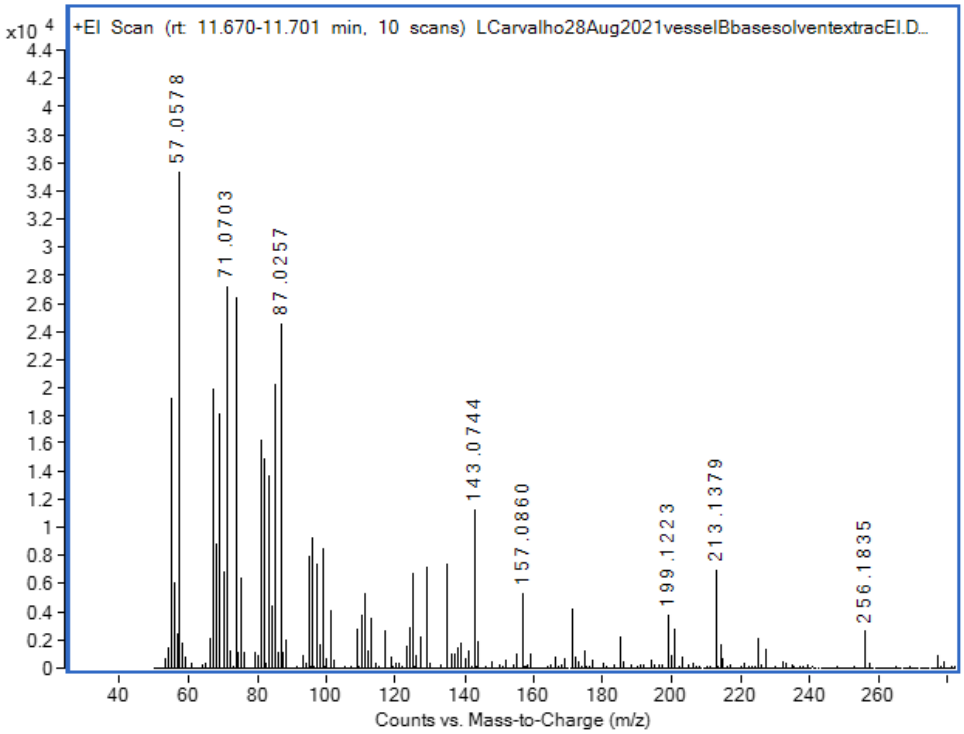
Octadecane **Mass: 254.297351**



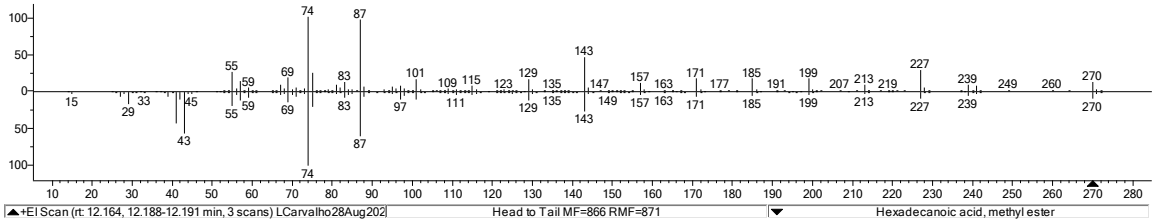


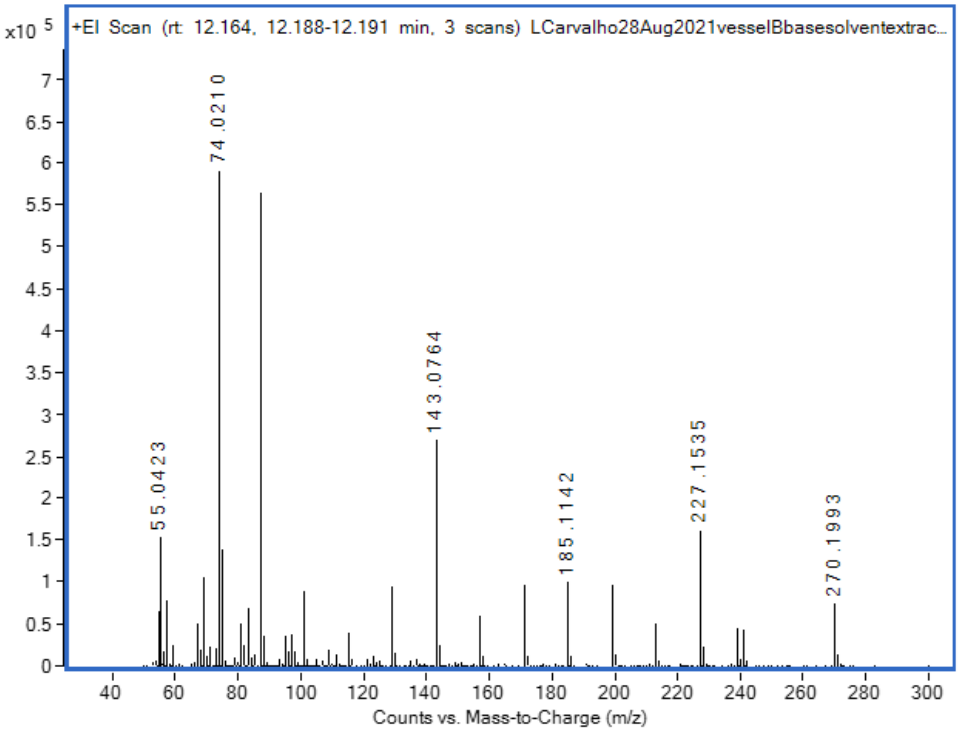
Tetradecanoic acid, 12-methyl-, methyl ester Mass: 256.24023



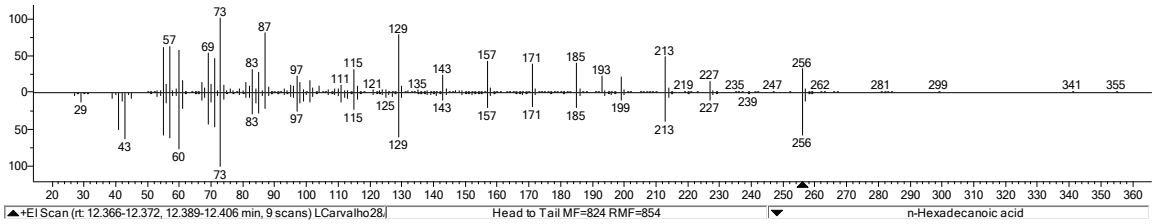


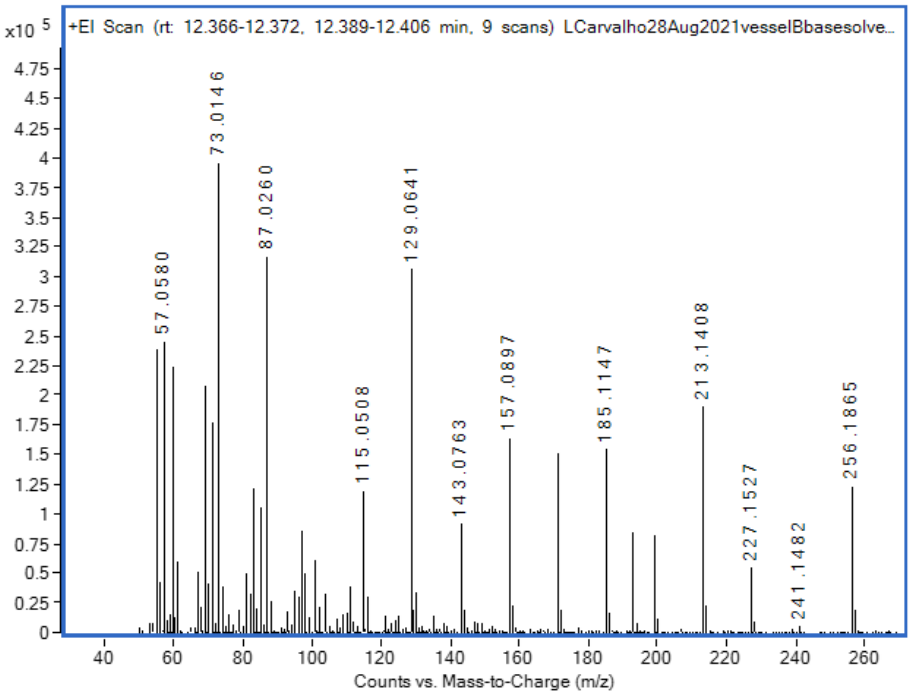
Hexadecanoic acid, methyl ester



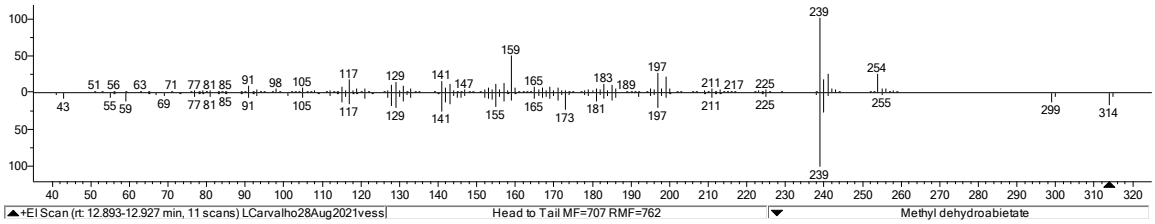


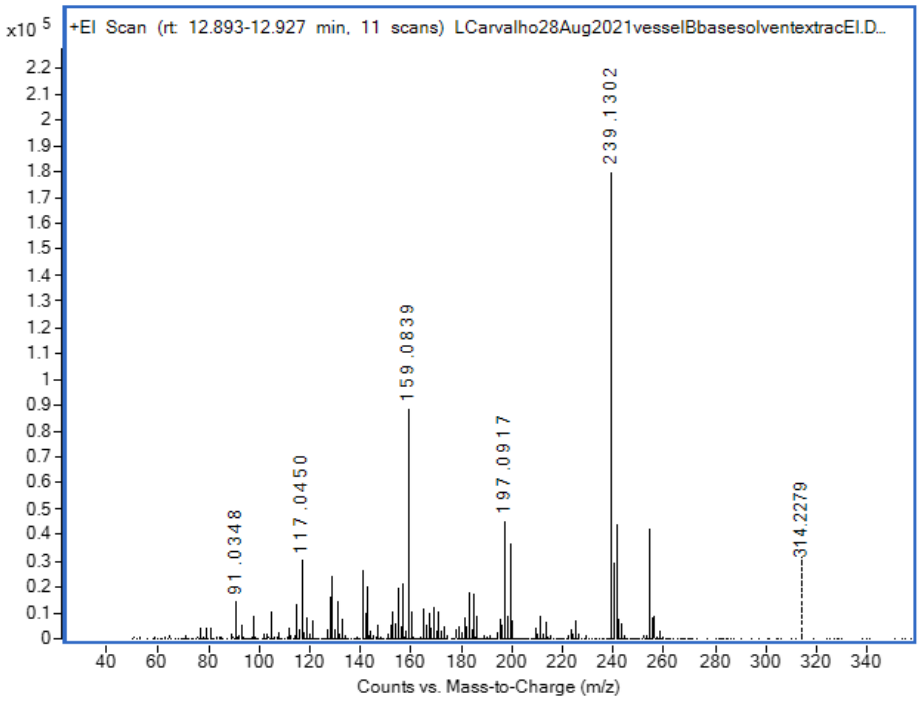
n-Hexadecanoic acid



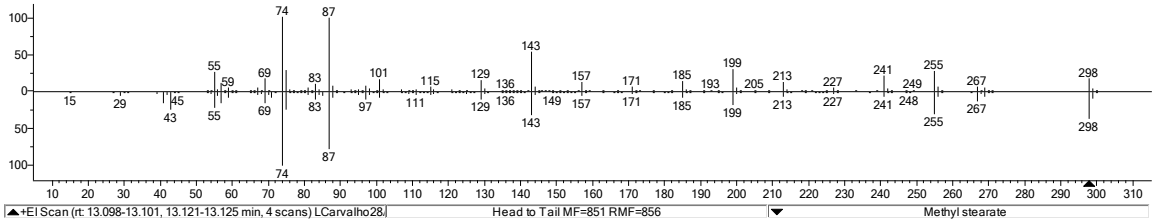


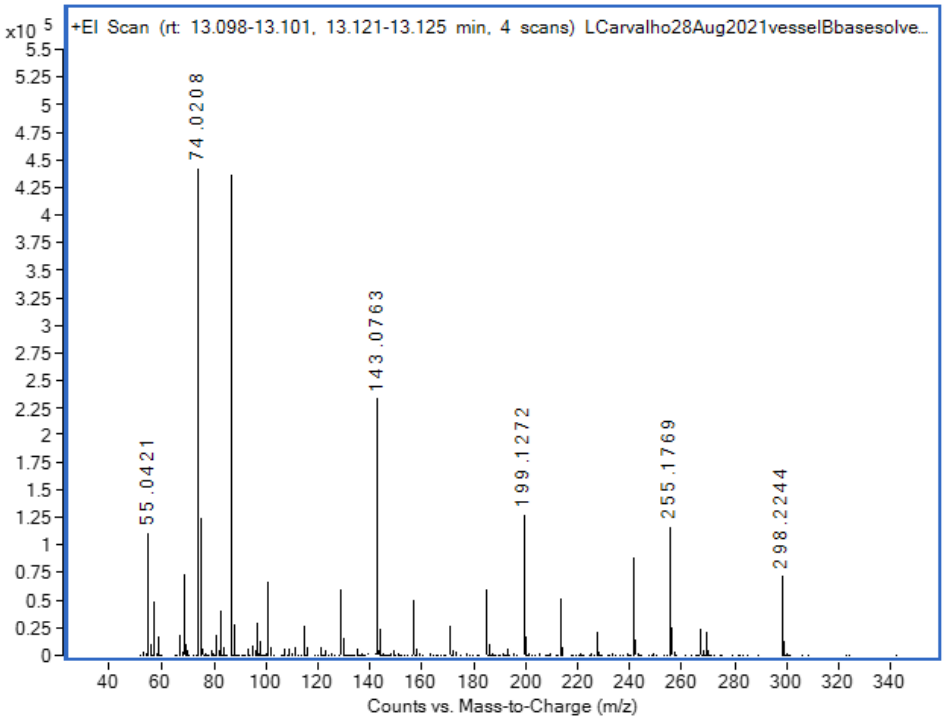
Methyl dehydroabietate **Mass: 314.22458**



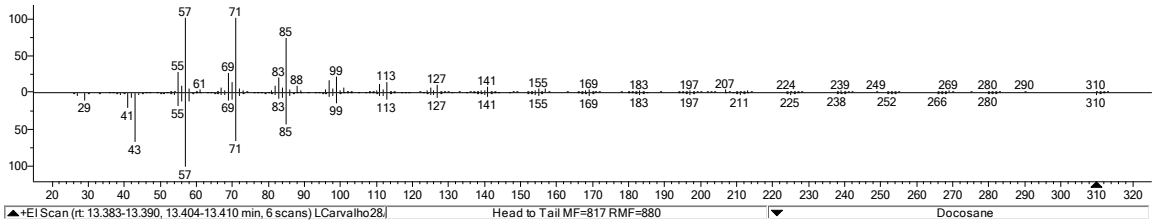


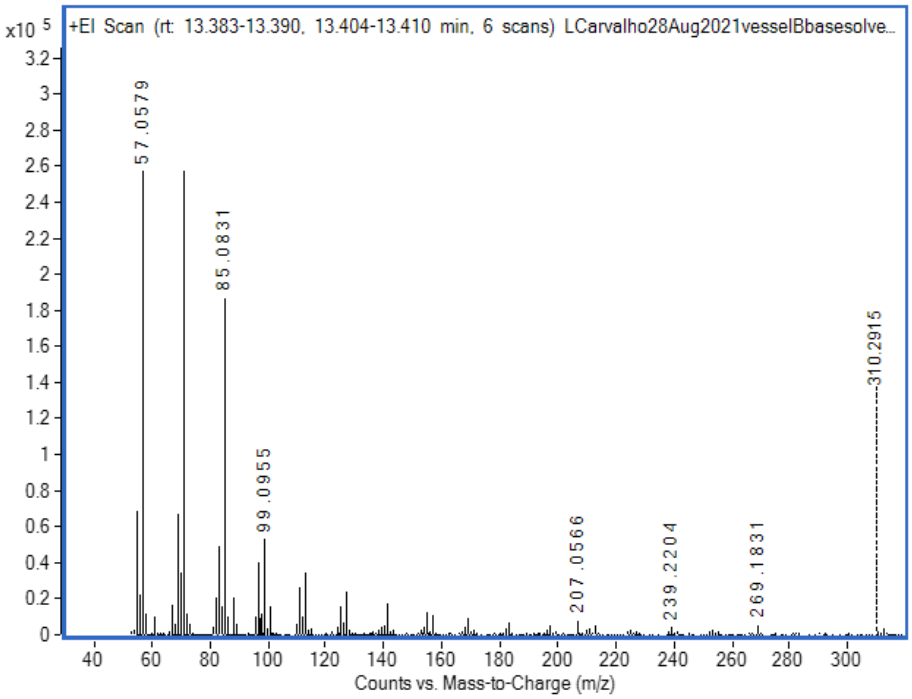
Methyl stearate





Docosane **Mass: 310.359951**





Compound	Name	Formula	m/z	Score	Mass Error (ppm)	RT Error (min)	Isotope Similarity (ppm)	Maximum Fold Change	Isotope Distribution	Normalised abundance CRIn	VAExt	VAInt	VBBASE	VBBODY
2.57_181.0715m/z	Mannitol	C6H14O6	181.0715	40.1	-1.4694	-0.19	96.86	11.70	100 - 4.33 - 0.581	1149.79	3707.47	2898.65	13456.89	3938.41
4.37_89.0244m/z	Dihydroxyacetone	C3H6O3	89.0244	40.6	-0.2441	-0.37	98.50	5.85	100 - 2.41 - 0.116	1254.94	4151.74	5742.92	7335.72	5846.90
10.39_133.0143m/z	Malic acid	C4H6O5	133.0143	40.8	0.1075	-0.75	98.41	45.90	100 - 3.45 - 0.565	174.04	136.68	255.89	6272.93	287.38
10.09_147.0299m/z	Citramalic acid	C5H8O5	147.0299	40.9	0.1929	-0.66	98.51	Infinity	100 - 4.59 - 0.666	0.00	0.00	42.61	4482.52	71.30
4.11_128.0353m/z	1-Pyrroline hydroxycarboxylic acid	C5H7NO3	128.0353	39.7	0.1813	-0.37	93.81	Infinity	100 - 0.127	0.00	0.00	0.00	4248.76	1318.99
10.39_117.0193m/z	Succinic acid	C4H6O4	117.0193	40.9	0.0712	-0.72	98.51	6.00	100 - 3.32 - 0.556	807.26	582.58	1664.06	3493.63	2076.81
11.59_259.0224m/z	Fructose 6-phosphate	C6H13O9P	259.0224	41.9	-0.2616	-0.29	95.82	161.96	100 - 4.61	20.40	1084.63	268.77	3304.37	401.08
12.58_129.0107m/z	Fluorouracil	C4H3FN2O2	129.0107	40	0.9455	-0.99	95.70	226.34	100 - 1.14	44.76	20.24	11.36	2572.09	117.98
8.97_259.0224m/z	Galactose 1-phosphate	C6H13O9P	259.0224	40.7	-0.1441	-0.42	95.08	Infinity	100 - 3.8	0.00	0.00	198.97	2409.08	324.11
10.69_159.0662m/z	3,3 Dimethyl glutarate	C7H12O4	159.0662	41	-0.2341	-0.72	99.08	55.62	100 - 7.26 - 0.682	41.90	166.39	838.31	2330.50	1892.84
16.34_191.0197m/z	Citric acid	C6H8O7	191.0197	41.9	-0.1904	-0.57	98.84	38.90	100 - 6.61 - 0.715	1685.02	57.25	78.00	2226.98	78.61
15.25_205.0354m/z	Methylisocitric acid	C7H10O7	205.0354	41.8	0.0822	-0.56	98.66	Infinity	100 - 7.28 - 1.03	1142.77	0.00	0.00	1984.94	0.00
9.48_174.0408m/z	N-Acetyl-aspartate	C6H9NO5	174.0408	40.4	-0.2443	-0.55	95.40	Infinity	100 - 3.41	0.00	0.00	53.13	1640.83	130.09
8.25_206.0823m/z	N-Acetyl-L-phenylalanine	C11H13NO3	206.0823	39.9	0.1457	-0.64	94.17	Infinity	100 - 7.32	0.00	58.24	779.82	1488.04	1514.35
19.16_143.1077m/z	Octanoic acid	C8H16O2	143.1077	41.5	-0.0281	-0.79	98.29	6.41	100 - 7.61 - 0.195	210.72	835.27	708.38	1351.01	941.13
15.65_154.9752m/z	Phosphoglycolic acid	C2H5O6P	154.9752	41.3	0.8300	-0.67	98.52	Infinity	100 - 2.17	0.00	0.00	0.00	1304.29	12.76
2.67_341.1093m/z	Lactose	C12H22O11	341.1093	39.9	-0.6462	-0.37	97.25	41.37	100 - 12.3 - 1.55	31.05	1284.44	132.03	101.59	233.54
10.29_209.0304m/z	Galactaric acid (mucic acid)	C6H10O8	209.0304	40.4	0.3017	-0.65	96.08	Infinity	100 - 4.6	0.00	0.00	0.00	1162.00	0.00
12.68_115.0037m/z	Fumarate	C4H4O4	115.0037	40.8	-0.0242	-0.95	98.58	2.45	100 - 3.46 - 0.469	1102.82	451.03	465.00	553.01	828.80
10.19_145.0507m/z	Methylglutaric acid	C6H10O4	145.0507	41	0.3144	-0.54	98.01	2.72	100 - 5.15 - 0.481	399.29	810.74	1037.32	1084.28	736.83
12.48_88.9880m/z	Oxalic acid	C2H2O4	88.9880	40.7	-0.0875	-0.92	97.97	8.32	100 - 0.904 - 0.181	128.42	192.24	129.57	1068.28	140.89
4.37_158.0823m/z	N-Acetylvaline	C7H13NO3	158.0823	40	-0.0933	-0.46	96.20	Infinity	100 - 4.97	0.00	0.00	13.28	986.14	41.14
10.99_165.0557m/z	3-methoxyphenylacetic acid	C9H10O3	165.0557	39.5	-0.1985	0.95	93.71	Infinity	100 - 4.04	0.00	0.00	12.14	750.15	0.00
4.86_103.0401m/z	3-Hydroxyisobutyric acid	C4H8O3	103.0401	41.5	-0.1444	-0.18	97.48	17.40	100 - 2.57	37.89	53.05	96.25	659.30	210.02
16.64_167.0350m/z	Homogentisic acid	C8H8O4	167.0350	40.5	-0.0145	-0.85	94.93	Infinity	100 - 4.49	649.97	27.16	25.61	172.66	0.00
10.19_129.0194m/z	Gamma-delta-Dioxovaleric acid	C5H6O4	129.0194	41.2	0.5396	-0.46	97.95	Infinity	100 - 4.4	88.42	0.00	24.96	644.14	62.75
4.28_165.0405m/z	Arabinonic acid	C5H10O6	165.0405	40.2	-0.0237	-0.62	97.83	19.05	100 - 4.45 - 0.349	29.68	187.46	489.74	565.47	263.71
4.56_75.0087m/z	Glycolic acid	C2H4O3	75.0087	40.1	-0.6941	-0.68	98.35	Infinity	100 - 1.05 - 0.202	0.00	0.00	117.47	465.60	513.47
2.77_503.1615m/z	Raffinose	C18H32O16	503.1615	44.8	-0.5682	-0.03	95.54	Infinity	100 - 19.1 - 1.9	0.00	0.00	0.00	436.66	9.13
11.99_101.0244m/z	Succinic acid semialdehyde	C4H6O3	101.0244	40.3	-0.5677	-0.71	95.58	8.84	100 - 0.557	85.04	87.52	45.88	405.47	65.00
7.54_176.0386m/z	N-Formyl-methionine	C6H11NO3S	176.0386	37	-0.2651	0.81	82.07	Infinity	100 - 25.7	0.00	327.42	0.00	16.39	11.36
5.68_101.0243m/z	Acetoacetate	C4H6O3	101.0243	39.8	-0.6959	0.54	96.18	11.98	100 - 1.19	20.52	28.17	66.02	245.91	81.56
9.98_161.0455m/z	3-Hydroxymethylglutarate	C6H10O5	161.0455	40.6	-0.1574	-0.78	97.68	Infinity	100 - 5.16 - 0.353	11.27	0.00	25.44	240.59	21.77
17.90_201.1133m/z	Sebacic acid	C10H18O4	201.1133	42.7	0.1141	-0.40	97.58	Infinity	100 - 9.51 - 0.43	0.00	229.54	222.75	32.41	93.39
9.07_193.0353m/z	Glucuronic acid	C6H10O7	193.0353	40.3	-0.5895	0.80	98.36	Infinity	100 - 5.77 - 1.07	0.00	82.42	0.00	13.48	217.74
10.09_131.0350m/z	Glutaric acid	C5H8O4	131.0350	40.8	-0.0702	-0.78	98.57	5.57	100 - 4.56 - 0.514	33.96	39.19	151.93	189.05	93.64
4.01_179.0560m/z	Glucose	C6H12O6	179.0560	40	-0.6096	0.58	98.43	2.34	100 - 5.83 - 0.752	76.17	85.59	139.29	79.46	178.29
10.89_103.0037m/z	Hydroxypyruvic acid	C3H4O4	103.0037	40.3	-0.2145	-0.75	95.87	Infinity	100	0.00	0.00	0.00	141.16	0.00
4.47_218.1035m/z	Pantothenic acid	C9H17NO5	218.1035	39.9	0.3485	-0.53	96.35	Infinity	100 - 8.04	0.00	0.00	0.00	128.79	0.00
13.68_303.0838m/z	N-Acetylaspartylglutamic acid	C11H16N2O8	303.0838	40.4	1.2661	-0.72	95.91	Infinity	100 - 9.73 - 1.34	0.00	0.00	0.00	7261.65	0.00

Vessel A Interior Oxidation (M); Deamidation (NQ) Carbamidomethylation (CAM)

Data base	Protein Number	-10lgP	Coverage (%)	Peptide intensity	#Peptides	PTM Score	Mass	
PINUS	A0A1B9I2X0	37.21	12	2.63E+03	2(2)	(M)	14737	Ubiquitin OS=Kwoniella pini CBS 10737
	A0A4U0NM48	34.28	2	1.74E+04	2(1)		57127	Glucose-6-phosphate 1-dehydrogenase OS=Streptomyces piniterrae
	A0A1B9I6P3	33.68	1	9.43E+03	1(1)		103499	Uncharacterized protein OS=Kwoniella pini CBS 10737
	A9NQT3	33.45	15	1.12E+05	2(2)		15898	RRM domain-containing protein OS=Picea sitchensis
	A0A1B9HS90	32.03	1	4.84E+03	1(1)		209976	Uncharacterized protein OS=Kwoniella pini CBS 10737
	A9NQ94	28.91	4	6.72E+04	1(1)		19456	U6 snRNA-associated Sm-like protein LSm1 OS=Picea sitchensis
	A0A1B9IBP8	28.88	2	2.05E+03	1(1)		55139	Peptidyl-prolyl cis-trans isomerase OS=Kwoniella pini CBS 10737
	I4N2E4	27.46	2	5.72E+03	1(1)	(NQ)	75394	Putative carbohydrate translocase OS=Pseudomonas sp. M47T1
	A0A1B9I3T0	22.96	2	1.62E+04	1(1)		39443	Uncharacterized protein OS=Kwoniella pini CBS 10737
	I4N0Z9	22.48	2	1.70E+04	1(1)		59708	Peptide chain release factor 3 OS=Pseudomonas sp. M47T1
	P84720	21.64	100	9.73E+05	1(1)		870	Putative LRR disease resistance protein/transmembrane receptor kinase PS4 (Fragment) OS=Pinus strobus
	P84732	21.64	100	9.73E+05	1(1)		870	Putative LRR disease resistance protein/transmembrane receptor kinase PS16 (Fragment) OS=Pinus strobus
	P84735	21.64	100	9.73E+05	1(1)		870	Putative LRR disease resistance protein/transmembrane receptor kinase PS19 (Fragment) OS=Pinus strobus
	A0A4U0MXV4	20.93	2	8.02E+03	1(1)	(NQ)	86331	Lon protease OS=Streptomyces piniterrae
	A9NMF5	20.51	2	1.22E+04	1(1)		39615	Fe2OG dioxygenase domain-containing protein OS=Picea sitchensis
	I4N4Z1	20.51	1	1.22E+04	1(1)		60817	Response regulator receiver modulated diguanylate cyclase OS=Pseudomonas sp. M47T1
	W8EH69	20.51	3	1.22E+04	1(1)		19225	Actin (Fragment) OS=Pinus massoniana
	A0A4U0NBD5	20.5	5	1.45E+04	1(1)	(CAM)(NQ)	35488	SDR family NAD(P)-dependent oxidoreductase OS=Streptomyces piniterrae
	A0A4U0NRF8	20.29	1	2.66E+03	1(1)		58630	Carbohydrate kinase OS=Streptomyces piniterrae
	A0A6G9W3F8	20.11	2	4.88E+03	1(1)	(NQ)	44579	Pectinesterase OS=Cunninghamia lanceolata
RESIN	A0A077D6G6	51.09	22	1.47E+05	6(6)	(CAM)(M)	79459	NADPH--cytochrome P450 reductase OS=Pinus contorta
	A7LA02	47.52	6	3.81E+03	2(2)	(NQ)	80047	1-deoxy-D-xylulose-5-phosphate synthase OS=Picea abies
	M4HY05	45.12	7	4.39E+03	5(2)	(CAM)(NQ)	98445	Bifunctional levopimaradiene synthase chloroplastic OS=Pinus contorta
	E5FA65	23.98	9	1.87E+05	2(2)	(NQ)	55409	CYP720B15 OS=Picea sitchensis
FLOWER	O22040	26.55	1	1.22E+04	1(1)		73470	Mitogen-activated protein kinase kinase kinase ANP1 OS=Arabidopsis thaliana
	O22042	26.55	1	1.22E+04	1(1)		71655	Mitogen-activated protein kinase kinase kinase 3 OS=Arabidopsis thaliana
	Q8H0V4	26.55	1	1.22E+04	1(1)		80740	DUF724 domain-containing protein 7 OS=Arabidopsis thaliana
	Q9FKE9	26.55	1	1.22E+04	1(1)		93570	Protein ROOT HAIR DEFECTIVE 3 homolog 2 OS=Arabidopsis thaliana
	Q9FZ36	26.55	1	1.22E+04	1(1)		71849	Mitogen-activated protein kinase kinase kinase 2 OS=Arabidopsis thaliana
	A0A1E8GRR9	26.24	1	4.32E+04	1(1)		54312	Uncharacterized protein OS=Floricoccus tropicus
	Q069K2	26.24	1	4.32E+04	1(1)		84828	5-methyltetrahydropteroyltriglutamate--homocysteine S-methyltransferase OS=Nicotiana suaveolens
	Q9LTP5	25.43	22	7.37E+03	2(2)		13718	Glycine-rich protein 5 OS=Arabidopsis thaliana

Data base	Protein Number	-10lgP	Coverage (%)	Peptide intensity	#Peptides	PTM Score	Mass	
	Q6UFU7	24.19	2	2.04E+03	1(1)		68570	Rad21-4 protein OS=Oryza sativa subsp. japonica
	O22040	26.55	1	1.22E+04	1(1)		73470	Mitogen-activated protein kinase kinase kinase ANP1 OS=Arabidopsis thaliana
BACTERIA	Q02SZ7	236.58	35	6.02E+06	17(17)	(M)(NQ)	48178	Lysyl endopeptidase OS=Pseudomonas aeruginosa (strain UCBPP-PA14)
	Q8E6F5	39.66	2	1.65E+05	1(1)	(M)	50993	Uncharacterized RNA methyltransferase gbs0613 OS=Streptococcus agalactiae serotype III (strain NEM316)
	C4LIF4	34.25	4	2.13E+04	3(2)		60931	CTP synthase OS=Corynebacterium kroppenstedtii (strain DSM 44385 / JCM 11950 / CIP 105744 / CCUG 35717)
	O33406	29.8	2	4.80E+03	1(1)		67144	Uptake hydrogenase large subunit OS=Oligotropha carboxidovorans (strain ATCC 49405 / DSM 1227 / KCTC 32145 / OM5)
	A1IRQ3	29.22	3	1.80E+03	1(1)		35551	Fructose-1 6-bisphosphatase class 1 OS=Neisseria meningitidis serogroup A / serotype 4A (strain DSM 15465 / Z2491)
	P23878	25.82	3	4.45E+04	1(1)		29784	Ferric enterobactin transport ATP-binding protein FepC OS=Escherichia coli (strain K12)
	A1VZC8	22.66	1	2.19E+04	1(1)	(NQ)	104771	Periplasmic nitrate reductase OS=Campylobacter jejuni subsp. jejuni serotype O:23/36 (strain 81-176)
	Q04GN0	22.32	1	1.81E+05	1(1)	(NQ)	90524	Translation initiation factor IF-2 OS=Oenococcus oeni (strain ATCC BAA-331 / PSU-1)
	Q6F0Y1	22.07	2	6.72E+04	1(1)		34594	tRNA N6-adenosine threonylcarbamoyltransferase OS=Mesoplasma florum (strain ATCC 33453 / NBRC 100688 / NCTC 11704 / L1)

Vessel A Exterior

Data base	Protein Number	-10lgP	Coverage (%)	Peptide intensity	#Peptides (# Unique)	PTM Score	Mass	
PINUS	A0A4U0NN06	32.82	2	4.74E+04	1(1)	(NQ)	35643	Aldo/keto reductase OS=Streptomyces piniterrae OX=2571125 GN=FCH28_10505 PE=4 SV=1
	A0A1B9I3V5	32.14	1	5.12E+03	1(1)		74968	Photolyase/cryptochrome alpha/beta domain-containing protein OS=Kwoniella pini CBS 10737 OX=1296096 GN=I206_03522 PE=3 SV=1
	A0A1B9IDS6	32.14	1	5.12E+03	1(1)		55329	Kynurenine 3-monooxygenase OS=Kwoniella pini CBS 10737 OX=1296096 GN=BNA4 PE=3 SV=1
	A0A3G6JCL0	32.14	2	5.12E+03	1(1)		40765	NAC domain-containing protein 53 OS=Pinus taeda OX=3352 GN=NAC27 PE=2 SV=1
	A9NMF5	32.14	2	5.12E+03	1(1)		39615	Fe2OG dioxygenase domain-containing protein OS=Picea sitchensis OX=3332 PE=2 SV=1
	I4N4Z1	32.14	1	5.12E+03	1(1)		60817	Response regulator receiver modulated diguanylate cyclase OS=Pseudomonas sp. M47T1 OX=1179778 GN=PMM47T1_11407 PE=4 SV=1
	W8EH69	32.14	3	5.12E+03	1(1)		19225	Actin (Fragment) OS=Pinus massoniana OX=88730 PE=3 SV=1
	A0A4U0NM48	31.82	2	1.54E+05	2(2)		57127	Glucose-6-phosphate 1-dehydrogenase OS=Streptomyces piniterrae OX=2571125 GN=zwf PE=3 SV=1
	A0A1B9I946	31.68	1	2.14E+04	2(2)		192995	JmjC domain-containing protein OS=Kwoniella pini CBS 10737 OX=1296096 GN=I206_01319 PE=4 SV=1
	A0A1B9HT30	29.34	1	4.60E+03	1(1)	(NQ)	318061	AGC protein kinase OS=Kwoniella pini CBS 10737 OX=1296096 GN=I206_07662 PE=4 SV=1
	A0A0G7ZP00	27.48	1	9.88E+03	1(1)		99199	Putative terpene synthase PgTPS2 OS=Picea glauca OX=3330 GN=PgTPS2 PE=4 SV=1
	A0A1B9HSW7	27.48	2	9.88E+03	1(1)		38446	Uncharacterized protein OS=Kwoniella pini CBS 10737 OX=1296096 GN=I206_07584 PE=4 SV=1
	A0A1B9IBW0	27.48	1	9.88E+03	1(1)		47001	Rho-GAP domain-containing protein OS=Kwoniella pini CBS 10737 OX=1296096 GN=I206_00436 PE=4 SV=1
	A0A1B9IE68	27.48	1	9.88E+03	1(1)		63035	Gamma-glutamyltransferase OS=Kwoniella pini CBS 10737 OX=1296096 GN=I206_01182 PE=4 SV=1
	A9NTX6	27.48	2	9.88E+03	1(1)		26026	DLH domain-containing protein OS=Picea sitchensis OX=3332 PE=2 SV=1
	A9NVS5	27.48	2	9.88E+03	1(1)		38901	SAM domain-containing protein OS=Picea sitchensis OX=3332 PE=2 SV=1
	A9P2I9	27.48	4	9.88E+03	1(1)		15026	Uncharacterized protein OS=Picea sitchensis OX=3332 PE=2 SV=1
	B8LLZ3	27.48	2	9.88E+03	1(1)		40624	V-type proton ATPase subunit OS=Picea sitchensis OX=3332 PE=2 SV=1
	C0PSQ9	27.48	1	9.88E+03	1(1)		99361	Uncharacterized protein OS=Picea sitchensis OX=3332 PE=2 SV=1
	D5AB33	27.48	2	9.88E+03	1(1)		26664	DLH domain-containing protein OS=Picea sitchensis OX=3332 PE=2 SV=1
	F2XFB2	27.48	1	9.88E+03	1(1)		98563	Levopimaradiene/abietadiene synthase OS=Picea sitchensis OX=3332 PE=2 SV=1
	I4MYI6	27.48	1	9.88E+03	1(1)		59097	Sulfatase OS=Pseudomonas sp. M47T1 OX=1179778 GN=PMM47T1_22847 PE=4 SV=1
	I4MZ08	27.48	3	9.88E+03	1(1)		19670	NTP_transf_3 domain-containing protein OS=Pseudomonas sp. M47T1 OX=1179778 GN=PMM47T1_22128 PE=4 SV=1
	K7NMS5	27.48	5	9.88E+03	1(1)		12536	Gb3_synth domain-containing protein (Fragment) OS=Pinus taeda OX=3352 GN=2_6009_01 PE=4 SV=1
	A0A4U0NVD6	26.46	2	2.42E+04	1(1)		110810	DEAD/DEAH box helicase OS=Streptomyces piniterrae OX=2571125 GN=FCH28_00550 PE=4 SV=1
	A0A117NIX9	25.96	27	1.65E+04	1(1)	(M)(NQ)	7173	Uncharacterized protein OS=Picea glauca OX=3330 GN=ABT39_MTgene517 PE=4 SV=1
	A0A1B9I374	25.44	3	2.94E+03	2(2)	(NQ)	147752	Uncharacterized protein OS=Kwoniella pini CBS 10737 OX=1296096 GN=I206_04520 PE=4 SV=1
RESIN	Q7BRJ6	59.44	28	5.41E+03	4(4)	(CAM)(M)(NQ)	31675	3-hydroxyacyl-CoA dehydrogenase OS=Pseudomonas abietaniphila OX=89065 GN=ditN PE=4 SV=1
	M4HYC6	43.52	3	2.39E+04	3(3)	(NQ)	97780	Bifunctional levopimaradiene synthase chloroplastic OS=Pinus contorta OX=3339 GN=TPS-LAS2 PE=1 SV=1
	M4HY05	43.52	3	2.39E+04	3(3)	(NQ)	98445	Bifunctional levopimaradiene synthase chloroplastic OS=Pinus contorta OX=3339 GN=TPS-LAS1 PE=1 SV=1
	M4HXU6	43.52	3	2.39E+04	3(3)	(NQ)	98479	Bifunctional levopimaradiene synthase chloroplastic OS=Pinus banksiana OX=3353 GN=TPS-LAS1 PE=1 SV=1
	Q9X4X7	31.37	11	4.74E+04	3(3)	(M)	26315	DitB OS=Pseudomonas abietaniphila OX=89065 GN=ditB PE=4 SV=1

Data base	Protein Number	-10lgP	Coverage (%)	Peptide intensity	#Peptides (# Unique)	PTM Score	Mass	
	M4HYC8	36.26	6	9.52E+04	3(3)	(CAM)(NQ)	100104	Monofunctional pimaradiene synthase OS=Pinus contorta OX=3339 GN=TPS-mPim1 PE=1 SV=1
	M4HYP3	37.83	7	2.78E+05	5(5)	(M)(NQ)	100687	Monofunctional isopimaradiene synthase chloroplastic OS=Pinus contorta OX=3339 GN=TPS-mISO1 PE=1 SV=1
FLOWER	A0A0A0KU04	39.23	2	5.12E+03	2(2)	(NQ)	151925	Uncharacterized protein OS=Cucumis sativus OX=3659 GN=Csa_5G492330 PE=4 SV=1
	A0A072VYY2	24.35	1	9.88E+03	1(1)		70925	Receptor-like kinase in in flowers protein OS=Medicago truncatula OX=3880 GN=25484795 PE=4 SV=1
	A0A0A0L3I8	24.35	1	9.88E+03	1(1)		103226	Uncharacterized protein OS=Cucumis sativus OX=3659 GN=Csa_4G430880 PE=3 SV=1
	A0A0A0LG26	24.35	2	9.88E+03	1(1)		41733	V-type proton ATPase subunit OS=Cucumis sativus OX=3659 GN=Csa_3G827290 PE=3 SV=1
	A0A0A0LKP2	24.35	1	9.88E+03	1(1)		113170	Uncharacterized protein OS=Cucumis sativus OX=3659 GN=Csa_2G000590 PE=3 SV=1
	A0A0A0LUR5	24.35	0	9.88E+03	1(1)		137113	Uncharacterized protein OS=Cucumis sativus OX=3659 GN=Csa_1G015650 PE=4 SV=1
	A0A1E8GH01	24.35	3	9.88E+03	1(1)		26686	Uncharacterized protein OS=Floricoccus penangensis OX=1859475 GN=BG262_09300 PE=4 SV=1
	A0A1E8GL26	24.35	1	9.88E+03	1(1)		64477	Alpha-amylase OS=Floricoccus tropicus OX=1859473 GN=BG261_04680 PE=3 SV=1
	A0A1E8GLQ4	24.35	3	9.88E+03	1(1)		26789	Uncharacterized protein OS=Floricoccus tropicus OX=1859473 GN=BG261_03680 PE=4 SV=1
	A0A1E8GM23	24.35	2	9.88E+03	1(1)		31416	ABC2_membrane domain-containing protein OS=Floricoccus tropicus OX=1859473 GN=BG261_01610 PE=4 SV=1
	A0A2U1PES0	24.35	1	9.88E+03	1(1)		72864	Receptor-like kinase in in flowers 3 OS=Artemisia annua OX=35608 GN=CTI12_AA160710 PE=4 SV=1
	A0A0A0L2W2	23.76	1	1.43E+04	1(1)		100303	DNA topoisomerase I OS=Cucumis sativus OX=3659 GN=Csa_3G063680 PE=3 SV=1
	A0A1E8GRR9	23.76	1	1.43E+04	1(1)		54312	Uncharacterized protein OS=Floricoccus tropicus OX=1859473 GN=BG261_00040 PE=3 SV=1
	A0A1X9ISN9	23.76	1	1.43E+04	1(1)		76698	Ent-copalyl diphosphate synthase 5 (Fragment) OS=Isodon rubescens OX=587669 GN=CPS5 PE=1 SV=2
	A0A0A0KR86	20.95	1	2.85E+06	1(1)		78294	Protein kinase domain-containing protein OS=Cucumis sativus OX=3659 GN=Csa_5G610420 PE=4 SV=1
	A0A0A0KRR9	20.63	3	5.60E+03	1(1)		25891	GRAM domain-containing protein OS=Cucumis sativus OX=3659 GN=Csa_5G579020 PE=3 SV=1
	A0A1E8GGV6	20.63	2	5.60E+03	1(1)		30251	Histidinol-phosphatase OS=Floricoccus penangensis OX=1859475 GN=BG262_10035 PE=3 SV=1
	A0A1E8GQ36	20.63	2	5.60E+03	1(1)		30233	Histidinol-phosphatase OS=Floricoccus tropicus OX=1859473 GN=BG261_09260 PE=3 SV=1
BACTERIA	Q02SZ7	192.98	29	4.77E+06	11(11)	(M)	48178	Lysyl endopeptidase OS=Pseudomonas aeruginosa (strain UCBPP-PA14) OX=208963 GN=prpL PE=1 SV=1
	P0A854	34.01	2	7.24E+03	1(1)	(M)	52773	Tryptophanase OS=Shigella flexneri OX=623 GN=tnaA PE=3 SV=1
	Q8E6F5	31.8	2	9.14E+04	1(1)	(M)	50993	Uncharacterized RNA methyltransferase gbs0613 OS=Streptococcus agalactiae serotype III (strain NEM316) OX=211110 GN=gbs0613 PE=3 SV=1
	Q8E0T7	31.8	2	9.14E+04	1(1)	(M)	50993	Uncharacterized RNA methyltransferase SAG0633 OS=Streptococcus agalactiae serotype V (strain ATCC BAA-611 / 2603 V/R) OX=208435 GN=SAG0633 PE=3 SV=1
	C0QHJ8	31.52	2	1.10E+05	1(1)		46621	ATP-dependent Clp protease ATP-binding subunit ClpX OS=Desulfobacterium autotrophicum (strain ATCC 43914 / DSM 3382 / HRM2) OX=177437 GN=clpX PE=3 SV=1
	P23878	26.84	3	2.96E+04	1(1)		29784	Ferric enterobactin transport ATP-binding protein FepC OS=Escherichia coli (strain K12) OX=83333 GN=fepC PE=2 SV=2
	A4VZG6	26.77	2	1.68E+04	1(1)		53184	Aspartyl/glutamyl-tRNA(Asn/Gln) amidotransferase subunit B OS=Streptococcus suis (strain 98HAH33) OX=391296 GN=gatB PE=3 SV=1
	Q8E3P5	26.77	2	1.68E+04	1(1)		53716	Aspartyl/glutamyl-tRNA(Asn/Gln) amidotransferase subunit B OS=Streptococcus agalactiae serotype III (strain NEM316) OX=211110 GN=gatB PE=3 SV=1
	B8ZLK0	26.77	2	1.68E+04	1(1)		53716	Aspartyl/glutamyl-tRNA(Asn/Gln) amidotransferase subunit B OS=Streptococcus pneumoniae (strain ATCC 700669 / Spain 23F-1) OX=561276 GN=gatB PE=3 SV=1

Data base	Protein Number	-10lgP	Coverage (%)	Peptide intensity	#Peptides (# Unique)	PTM Score	Mass	
	B1I9M7	26.77	2	1.68E+04	1(1)		53689	Aspartyl/glutamyl-tRNA(Asn/Gln) amidotransferase subunit B OS=Streptococcus pneumoniae (strain Hungary19A-6) OX=487214 GN=gatB PE=3 SV=1
	Q04M42	26.77	2	1.68E+04	1(1)		53659	Aspartyl/glutamyl-tRNA(Asn/Gln) amidotransferase subunit B OS=Streptococcus pneumoniae serotype 2 (strain D39 / NCTC 7466) OX=373153 GN=gatB PE=3 SV=1
	B2ILX7	26.77	2	1.68E+04	1(1)		53689	Aspartyl/glutamyl-tRNA(Asn/Gln) amidotransferase subunit B OS=Streptococcus pneumoniae (strain CGSP14) OX=516950 GN=gatB PE=3 SV=1
	P12255	25.45	1	6.79E+03	2(1)	(M)(NQ)	367523	Filamentous hemagglutinin OS=Bordetella pertussis (strain Tohama I / ATCC BAA-589 / NCTC 13251) OX=257313 GN=fhaB PE=1 SV=4
	A8F866	25.38	1	1.01E+04	1(1)		97052	Alanine--tRNA ligase OS=Pseudothermotoga lettingae (strain ATCC BAA-301 / DSM 14385 / NBRC 107922 / TMO) OX=416591 GN=alaS PE=3 SV=1
	Q92RM6	24.08	5	2.28E+04	1(1)		21038	ATP synthase subunit b 2 OS=Rhizobium meliloti (strain 1021) OX=266834 GN=atpF2 PE=3 SV=1
	P12410	24.08	6	2.28E+04	1(1)		17973	ATP synthase subunit b' OS=Nostoc sp. (strain PCC 7120 / SAG 25.82 / UTEX 2576) OX=103690 GN=atpG PE=3 SV=1
	Q3M9V7	24.08	6	2.28E+04	1(1)		17960	ATP synthase subunit b' OS=Trichormus variabilis (strain ATCC 29413 / PCC 7937) OX=240292 GN=atpG PE=3 SV=1
	A6U6M6	24.08	5	2.28E+04	1(1)		21174	ATP synthase subunit b 2 OS=Sinorhizobium medicae (strain WSM419) OX=366394 GN=atpF2 PE=3 SV=1
	Q492D5	23.61	6	5.60E+03	2(2)		46392	Serine hydroxymethyltransferase OS=Blochmannia pennsylvanicus (strain BPEN) OX=291272 GN=glyA PE=3 SV=1
	P66385	23.05	7	1.77E+03	1(1)	(CAM)	13360	30S ribosomal protein S13 OS=Neisseria meningitidis serogroup A / serotype 4A (strain DSM 15465 / Z2491) OX=122587 GN=rpsM PE=3 SV=1
	Q7UR95	22.55	2	3.26E+03	1(1)		81118	Polyribonucleotide nucleotidyltransferase OS=Rhodopirellula baltica (strain DSM 10527 / NCIMB 13988 / SH1) OX=243090 GN=pnp PE=3 SV=2
	Q7NXR0	20.87	3	8.08E+03	1(1)	(CAM)	39916	Cobalt-precorrin-5B C(1)-methyltransferase OS=Chromobacterium violaceum (strain ATCC 12472 / DSM 30191 / JCM 1249 / NBRC 12614 / NCIMB 9131 / NCTC 9757) OX=243365 GN=cbiD PE=3 SV=1
	A4TCS1	20.73	2	4.59E+06	1(1)		37531	Uroporphyrinogen decarboxylase OS=Mycolicibacterium gilvum (strain PYR-GCK) OX=350054 GN=hemE PE=3 SV=1
	Q8YSL0	20.37	4	3.56E+03	1(1)	(NQ)	37431	UDP-3-O-acylglucosamine N-acyltransferase OS=Nostoc sp. (strain PCC 7120 / SAG 25.82 / UTEX 2576) OX=103690 GN=lpxD PE=3 SV=1
	Q73IE9	20.37	2	5.12E+03	1(1)		27949	DNA repair protein RecO OS=Wolbachia pipientis wMel OX=163164 GN=recO PE=3 SV=1
	C0R5J8	20.37	2	5.12E+03	1(1)		27947	DNA repair protein RecO OS=Wolbachia sp. subsp. Drosophila simulans (strain wRi) OX=66084 GN=recO PE=3 SV=1
	B3CPG9	20.37	2	5.12E+03	1(1)		28233	DNA repair protein RecO OS=Wolbachia pipientis subsp. Culex pipiens (strain wPip) OX=570417 GN=recO PE=3 SV=1
	A3PJ80	20.33	5	1.01E+03	1(1)	(M)	48424	Methylenetetrahydrofolate--tRNA-(uracil-5-)-methyltransferase TrmFO OS=Rhodobacter sphaeroides (strain ATCC 17029 / ATH 2.4.9) OX=349101 GN=trmFO PE=3 SV=1
	C5CC70	20.02	0	9.88E+03	1(1)	(NQ)	142417	DNA-directed RNA polymerase subunit beta' OS=Micrococcus luteus (strain ATCC 4698 / DSM 20030 / JCM 1464 / NBRC 3333 / NCIMB 9278 / NCTC 2665 / VKM Ac-2230) OX=465515 GN=rpoC PE=3 SV=1
	B2GIK0	20.02	0	9.88E+03	1(1)	(NQ)	143320	DNA-directed RNA polymerase subunit beta' OS=Kocuria rhizophila (strain ATCC 9341 / DSM 348 / NBRC 103217 / DC2201) OX=378753 GN=rpoC PE=3 SV=1
	B8HD15	20.02	0	9.88E+03	1(1)	(NQ)	143389	DNA-directed RNA polymerase subunit beta' OS=Pseudarthrobacter chlorophenolicus (strain ATCC 700700 / DSM 12829 / CIP 107037 / JCM 12360 / KCTC 9906 / NCIMB 13794 / A6) OX=452863 GN=rpoC PE=3 SV=1

Vessel B Base

Data base	Protein Number	-10lgP	Coverage (%)	Peptide intensity	#Peptides (#unique)	PTM Score	Mass	
PINUS	P84720	32.08	100	5.69E+05	1		870	Putative LRR disease resistance protein/transmembrane receptor kinase PS4 (Fragment) OS=Pinus strobus
	A9NQ94	28.6	4	1.14E+04	1		19456	U6 snRNA-associated Sm-like protein LSm1 OS=Picea sitchensis
	A0A1B9HX87	21.11	1	6.33E+03	1		115153	MMS19 nucleotide excision repair protein OS=Kwoniella pini CBS 10737
	K7NQA8	21.08	11	1.30E+03	1		9350	Uncharacterized protein (Fragment) OS=Pinus taeda
RESIN	M4HXU7	59.67	8	8.59E+03	5(5)	(CAM)(NQ)	97712	Putative monofunctional diterpene synthase OS=Pinus banksiana
	B9U4U6	52.12	15	5.02E+03	9(7)	(CAM)(M)(NQ)	76095	1-deoxy-D-xylulose-5-phosphate synthase OS=Pinus densiflora
	I1V0B8	44.58	7	1.67E+04	5(5)	(NQ)	61918	Tetrahydrocannabinolic acid synthase (Fragment) OS=Cannabis sativa
	I1V0C1	44.58	7	1.67E+04	5(5)	(NQ)	61946	Tetrahydrocannabinolic acid synthase (Fragment) OS=Cannabis sativa
	I1V0C2	44.58	7	1.67E+04	5(5)	(NQ)	61974	Tetrahydrocannabinolic acid synthase (Fragment) OS=Cannabis sativa
FLOWER	A0A0A0LN01	43.96	64	2.70E+04	4(4)	(NQ)	16875	Uncharacterized protein OS=Cucumis sativus
	A0A0A0KR86	27.3	1	5.69E+05	1(1)		78294	Protein kinase domain-containing protein OS=Cucumis sativus
	A0A1E8GRR9	25.3	1	2.73E+04	1(1)		54312	Uncharacterized protein OS=Floricoccus tropicus
	A0A1X9ISN9	25.3	1	2.73E+04	1(1)		76698	Ent-copalyl diphosphate synthase 5 (Fragment) OS=Isodon rubescens
	A0A072VYY2	22.43	1	4.39E+03	1(1)		70925	Receptor-like kinase in in flowers protein OS=Medicago truncatula
	A0A0A0LUR5	22.43	0	4.39E+03	1(1)		137113	Uncharacterized protein OS=Cucumis sativus
	A0A1E8GH01	22.43	3	4.39E+03	1(1)		26686	Uncharacterized protein OS=Floricoccus penangensis
	A0A1E8GL26	22.43	1	4.39E+03	1(1)		64477	Alpha-amylase OS=Floricoccus tropicus
	A0A1E8GLQ4	22.43	3	4.39E+03	1(1)		26789	Uncharacterized protein OS=Floricoccus tropicus
	A0A1E8GM23	22.43	2	4.39E+03	1(1)		31416	ABC2_membrane domain-containing protein OS=Floricoccus tropicus
	A0A0A0LUE3	21.53	1	3.08E+03	1(1)		83813	DDT domain-containing protein OS=Cucumis sativus
BACTERIA	Q02SZ7	177.15	19	1.54E+06	6(6)	(NQ)	48178	Lysyl endopeptidase OS=Pseudomonas aeruginosa (strain UCBPP-PA14)
	Q9HWK6	177.15	19	1.54E+06	6(6)	(NQ)	48213	Lysyl endopeptidase OS=Pseudomonas aeruginosa (strain ATCC 15692 / DSM 22644 / CIP 104116 / JCM 14847 / LMG 12228 / 1C / PRS 101 / PAO1)
	C0QHJ8	37.03	2	2.28E+04	1(1)		46621	ATP-dependent Clp protease ATP-binding subunit ClpX OS=Desulfobacterium autotrophicum (strain ATCC 43914 / DSM 3382 / HRM2)
	A7GJ81	30.67	1	4.01E+04	2(2)		131692	DNA-directed RNA polymerase subunit beta' OS=Clostridium botulinum (strain Langeland / NCTC 10281 / Type F)
	B4TR97	26.12	4	1.04E+05	2(2)		43512	Dual-specificity RNA methyltransferase RlmN OS=Salmonella schwarzengrund (strain CVM19633)
	Q493H3	25.39	3	1.04E+05	1(1)	(M)	41983	Queuine tRNA-ribosyltransferase OS=Blochmannia pennsylvanicus (strain BPEN)

Interior Green Corrosion

Name	Formula	PDF Number	FOM	%
Atacamite	Cl Cu2 H3 O3	00-900-7718	0.625	74.84
Quartz	O2 Si	00-900-5020	0.543	25.16

Peak List Serial	2theta [°]	d [Å]	I/I0		Peak List Serial	2theta [°]	d [Å]	I/I0
1	14.79	5.9827	0.464		56	45.99	1.9716	0.996
2	16.03	5.5239	7.368		57	46.70	1.9436	0.621
3	17.49	5.0677	2.924		58	47.48	1.9132	0.749
4	18.77	4.7231	1.584		59	47.72	1.9044	1.204
5	19.42	4.5661	0.401		60	48.13	1.8889	0.350
6	20.61	4.3059	0.332		61	48.35	1.8809	0.327
7	20.73	4.2818	0.559		62	49.96	1.8242	3.051
8	21.73	4.0865	0.498		63	50.21	1.8156	1.811
9	23.94	3.7146	0.893		64	50.89	1.7928	0.518
10	23.97	3.7095	1.067		65	51.89	1.7605	0.680
11	24.12	3.6867	0.673		66	52.11	1.7537	0.600
12	25.77	3.4537	0.486		67	52.38	1.7453	0.721
13	25.96	3.4297	1.076		68	53.18	1.7209	0.945
14	26.28	3.3889	0.495		69	53.25	1.7189	1.214
15	26.44	3.3679	1.216		70	53.55	1.7099	3.377
16	26.54	3.3554	3.553		71	53.83	1.7016	0.429
17	27.63	3.2259	0.551		72	54.75	1.6752	0.454
18	27.86	3.1993	0.363		73	55.00	1.6681	0.344
19	29.23	3.0524	0.672		74	55.37	1.6579	0.373
20	29.48	3.0270	0.665		75	56.21	1.6352	0.501
21	30.74	2.9064	2.719		76	56.34	1.6317	0.637
22	31.05	2.8774	0.663		77	56.42	1.6294	1.019
23	31.21	2.8639	1.174		78	57.12	1.6111	1.097
24	31.37	2.8490	2.803		79	57.74	1.5953	0.443
25	31.52	2.8357	0.639		80	58.04	1.5877	0.307
26	32.11	2.7854	7.976		81	58.90	1.5668	0.499
27	32.34	2.7658	7.079		82	59.28	1.5575	0.577
28	32.46	2.7561	5.270		83	60.82	1.5218	0.462
29	32.83	2.7261	1.292		84	61.09	1.5158	0.604
30	33.75	2.6539	0.638		85	61.27	1.5117	1.308
31	35.38	2.5347	0.765		86	61.30	1.5109	1.150
32	35.52	2.5255	1.670		87	61.49	1.5068	1.031
33	35.68	2.5140	0.520		88	61.57	1.5050	0.610
34	35.85	2.5027	0.390		89	62.15	1.4922	0.749
35	35.98	2.4937	0.523		90	62.24	1.4904	0.774
36	36.30	2.4726	3.703		91	62.79	1.4787	0.493
37	37.57	2.3919	0.400		92	64.13	1.4510	0.673
38	38.16	2.3566	0.847		93	64.24	1.4487	0.913
39	38.27	2.3496	1.314		94	64.39	1.4456	0.555
40	39.38	2.2863	3.734		95	65.23	1.4291	0.509
41	39.58	2.2752	9.191		96	65.46	1.4246	0.647
42	39.85	2.2605	2.889		97	65.60	1.4220	0.842
43	40.81	2.2091	0.665		98	65.73	1.4194	0.568
44	40.86	2.2065	0.558		99	65.86	1.4169	0.432
45	42.22	2.1388	1.487		100	67.23	1.3913	0.742

Peak List Serial	2theta [°]	d [Å]	I/I0		Peak List Serial	2theta [°]	d [Å]	I/I0
46	42.37	2.1316	1.013		101	67.35	1.3892	0.699
47	42.42	2.1292	0.669		102	67.64	1.3840	0.771
48	42.94	2.1047	0.412		103	67.77	1.3816	0.773
49	43.54	2.0770	0.366		104	67.89	1.3795	0.624
50	43.84	2.0634	0.630		105	68.09	1.3759	1.021
51	44.01	2.0560	0.765		106	68.22	1.3736	1.559
52	44.24	2.0456	0.703		107	68.87	1.3621	0.619
53	44.37	2.0398	0.930		108	69.01	1.3598	0.938
54	44.51	2.0340	1.193		109	69.39	1.3532	0.681
55	45.86	1.9770	0.523					

Exterior Green Corrosion

Name	Formula	PDF Number	FOM	%
Atacamite	Cl Cu2 H3 O3	00-900-7718	0.736	68.27
Cuprite	Cu2 O	00-900-5769	0.621	31.73

Peak List Serial	2theta [°]	d [Å]	I/I0		Peak List Serial	2theta [°]	d [Å]	I/I0
1	5.89	14.9831	17.807		60	44.11	2.0513	31.570
2	7.87	11.2307	13.528		61	44.30	2.0432	32.905
3	9.94	8.8931	14.964		62	44.60	2.0301	44.232
4	10.89	8.1173	18.085		63	45.52	1.9912	11.852
5	12.56	7.0409	14.499		64	45.78	1.9802	21.526
6	12.75	6.9398	11.716		65	46.02	1.9707	36.304
7	14.85	5.9602	22.869		66	46.17	1.9646	40.747
8	15.85	5.5854	19.525		67	46.37	1.9566	17.796
9	16.15	5.4821	454.140		68	46.82	1.9388	15.765
10	16.29	5.4374	221.048		69	47.07	1.9290	18.451
11	17.59	5.0373	156.538		70	47.87	1.8986	49.116
12	17.83	4.9718	20.122		71	50.15	1.8177	142.651
13	18.91	4.6886	56.013		72	50.31	1.8121	69.421
14	20.87	4.2535	20.781		73	50.61	1.8020	19.220
15	21.27	4.1742	17.108		74	51.05	1.7877	27.601
16	21.87	4.0607	22.303		75	51.98	1.7577	28.945
17	22.61	3.9302	15.992		76	52.15	1.7524	27.131
18	24.06	3.6959	54.662		77	52.35	1.7462	38.656
19	24.28	3.6633	25.224		78	53.30	1.7172	57.803
20	24.41	3.6436	18.670		79	53.65	1.7068	135.297
21	25.18	3.5340	15.716		80	54.19	1.6912	14.705
22	25.93	3.4332	28.956		81	56.45	1.6288	31.902
23	26.10	3.4116	45.057		82	56.56	1.6258	24.347
24	26.26	3.3903	14.917		83	57.28	1.6071	74.368
25	26.62	3.3464	75.042		84	57.73	1.5956	16.991
26	26.75	3.3300	18.737		85	57.90	1.5914	17.793
27	27.48	3.2425	15.171		86	58.92	1.5662	25.113
28	27.72	3.2157	23.316		87	59.20	1.5594	32.690
29	29.39	3.0365	18.657		88	59.37	1.5554	19.774
30	29.56	3.0197	52.936		89	60.00	1.5404	15.928

Peak List Serial	2theta [°]	d [Å]	I/I0		Peak List Serial	2theta [°]	d [Å]	I/I0
31	29.97	2.9786	17.954		90	60.92	1.5194	26.449
32	30.86	2.8951	104.447		91	61.34	1.5100	210.233
33	31.51	2.8367	154.979		92	61.56	1.5052	57.116
34	32.18	2.7793	323.881		93	61.68	1.5027	30.504
35	32.45	2.7570	257.582		94	61.91	1.4975	16.617
36	32.56	2.7473	197.845		95	62.14	1.4925	19.821
37	32.78	2.7296	40.407		96	62.31	1.4889	25.570
38	32.95	2.7162	65.592		97	62.34	1.4881	26.447
39	33.90	2.6420	39.212		98	62.95	1.4754	28.089
40	34.35	2.6083	15.753		99	63.13	1.4715	39.275
41	34.62	2.5888	11.388		100	63.40	1.4659	19.982
42	35.67	2.5148	58.050		101	64.18	1.4499	23.133
43	35.89	2.5000	24.944		102	64.28	1.4479	34.909
44	36.07	2.4877	18.884		103	64.38	1.4459	21.239
45	36.41	2.4656	838.944		104	65.14	1.4310	15.931
46	38.21	2.3532	22.412		105	65.42	1.4254	30.214
47	38.36	2.3444	57.069		106	65.80	1.4180	38.486
48	39.37	2.2869	45.778		107	66.27	1.4092	13.893
49	39.52	2.2786	197.975		108	67.34	1.3894	41.073
50	39.70	2.2684	404.027		109	67.46	1.3872	33.589
51	39.88	2.2584	114.745		110	67.76	1.3818	24.075
52	40.05	2.2494	110.263		111	67.84	1.3803	21.106
53	40.90	2.2044	33.192		112	68.09	1.3758	21.238
54	41.07	2.1959	26.371		113	68.34	1.3714	51.786
55	41.20	2.1890	19.441		114	68.48	1.3690	27.463
56	42.27	2.1361	260.034		115	69.11	1.3580	36.126
57	42.56	2.1225	35.154		116	69.35	1.3540	22.949
58	42.76	2.1130	15.318		117	69.50	1.3514	33.032
59	43.95	2.0587	20.247					

Interior Brown Corrosion

Name	Formula	PDF Number	FOM	%
Quartz	O2 Si	00-900-1493	0.894	100.00

Peak List Serial	2theta [°]	d [Å]	I/I0		Peak List Serial	2theta [°]	d [Å]	I/I0
1	20.78	4.2716	10.610		11	45.71	1.9832	6.080
2	26.54	3.3554	80.938		12	50.06	1.8207	11.827
3	27.48	3.2432	1.661		13	54.80	1.6737	3.540
4	28.23	3.1585	2.903		14	55.25	1.6611	1.541
5	29.33	3.0422	1.850		15	59.87	1.5437	9.088
6	34.15	2.6236	1.916		16	63.96	1.4544	1.841
7	36.45	2.4628	7.084		17	67.69	1.3831	5.706
8	39.39	2.2854	5.414		18	68.07	1.3762	3.761
9	40.23	2.2398	3.357		19	68.22	1.3736	4.918
10	42.37	2.1316	4.206					

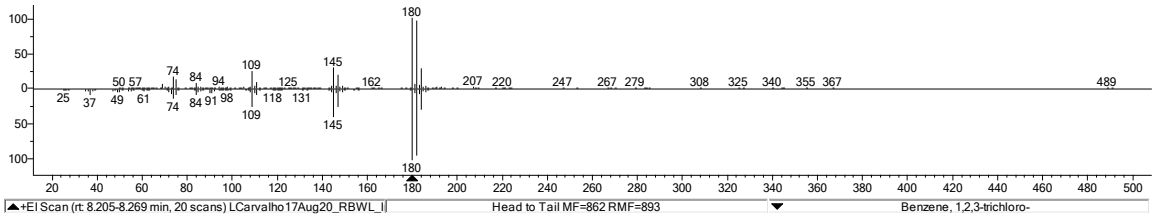
Exterior Brown Corrosion

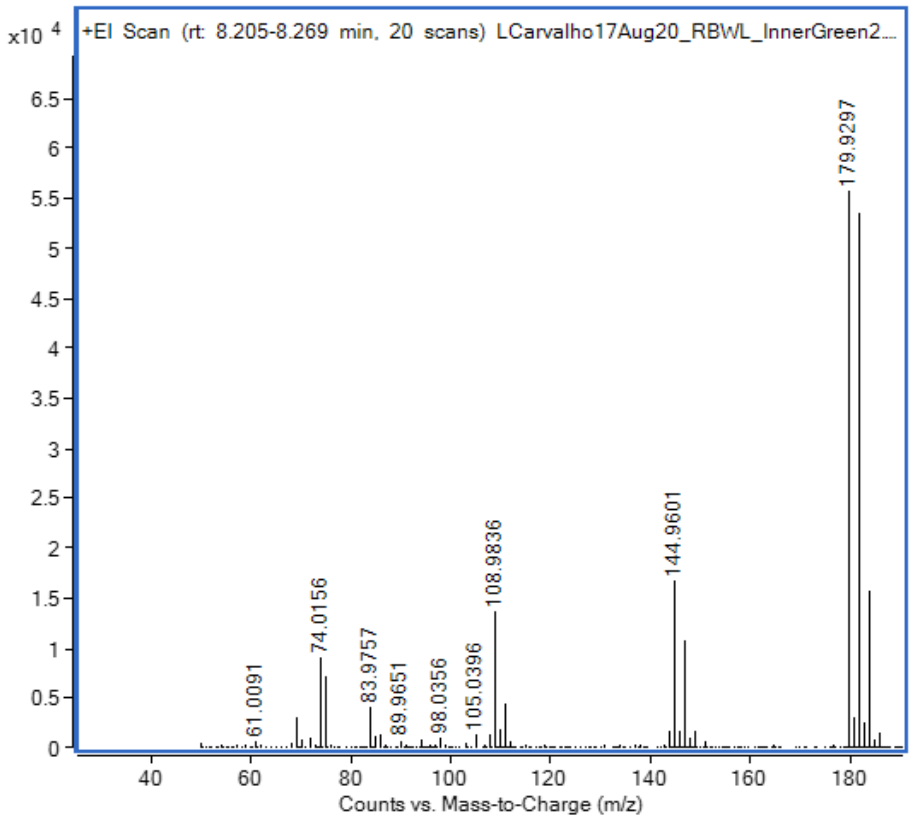
Name	Formula	PDF Number	FOM	%
Quartz	O2 Si	00-901-3321	0.889	100.00

Peak List Serial	2theta [°]	d [Å]	I/I0		Peak List Serial	2theta [°]	d [Å]	I/I0
1	1.91	46.2039	35.520		13	45.79	1.9798	3.112
2	19.67	4.5085	1.030		14	48.48	1.8760	0.512
3	20.86	4.2547	10.079		15	50.16	1.8173	7.879
4	25.69	3.4647	0.534		16	50.62	1.8016	0.821
5	26.66	3.3409	54.008		17	54.89	1.6714	2.072
6	29.43	3.0321	1.445		18	55.30	1.6598	1.103
7	34.80	2.5760	0.997		19	59.97	1.5414	5.536
8	34.98	2.5628	0.959		20	64.04	1.4527	1.618
9	36.55	2.4562	5.389		21	67.75	1.3819	4.269
10	39.48	2.2807	4.606		22	68.15	1.3747	4.642
11	40.31	2.2354	2.119		23	68.30	1.3721	1.878
12	42.45	2.1276	3.993					

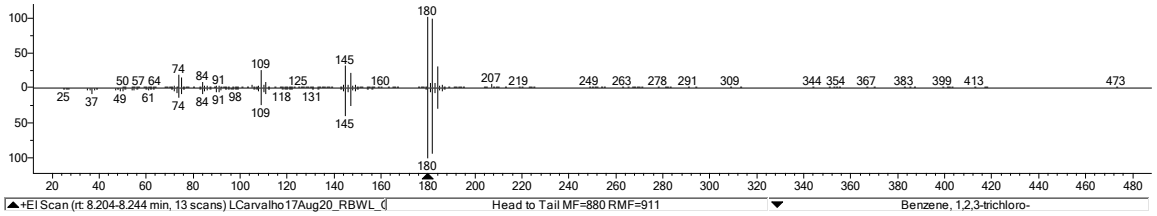
[1] Benzene, 1,2,3-trichloro- Mass: 179.930033

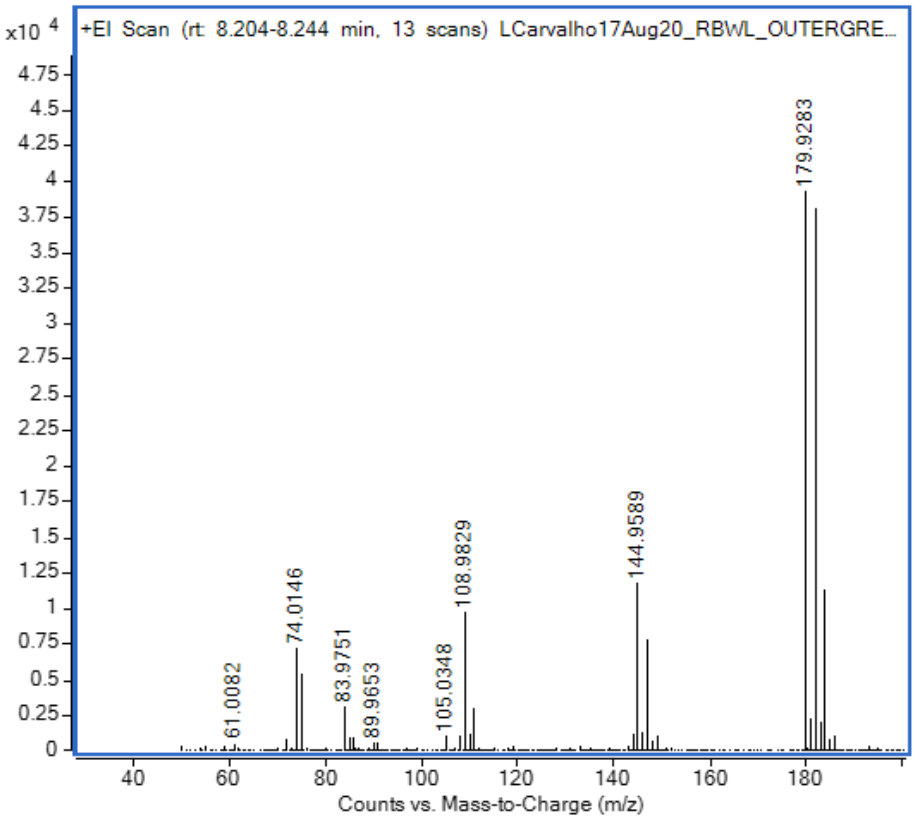
Interior





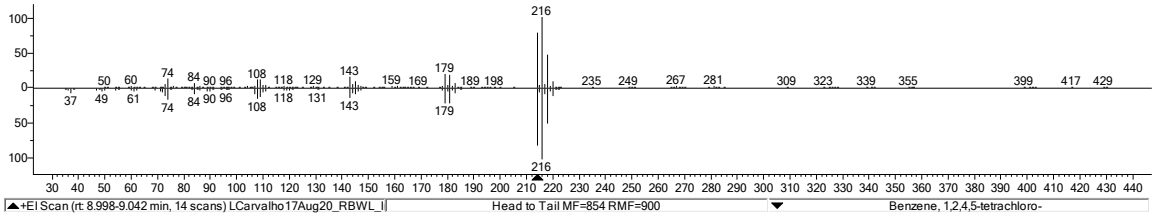
Exterior

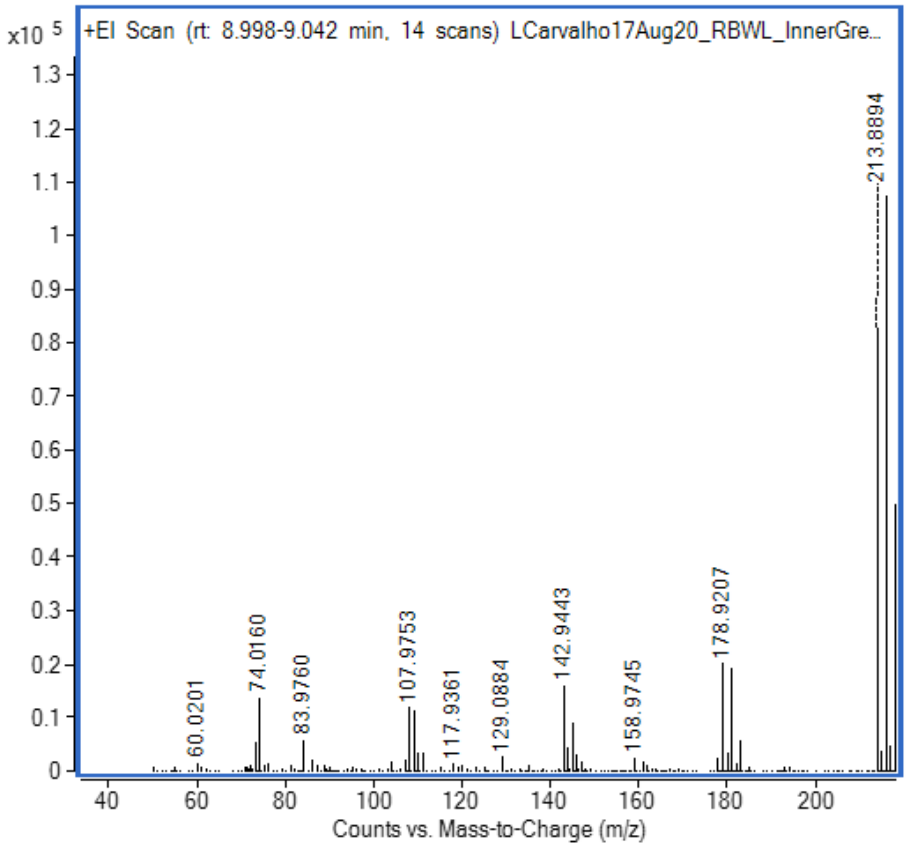

+EI Scan (rt: 8.204-8.244 min, 13 scans) LCarvalho17Aug20_RBWL_O
Head to Tail MF=880 RMF=911
Benzene, 1,2,3-trichloro-


x10 4
+EI Scan (rt: 8.204-8.244 min, 13 scans) LCarvalho17Aug20_RBWL_OUTERGRE...
179.9283
144.9589
108.9829
105.0348
89.9653
83.9751
74.0146
61.0082
Counts vs. Mass-to-Charge (m/z)

[2] Benzene, 1,2,4,5-tetrachloro- Mass: 213.891061 NIST#: 221324

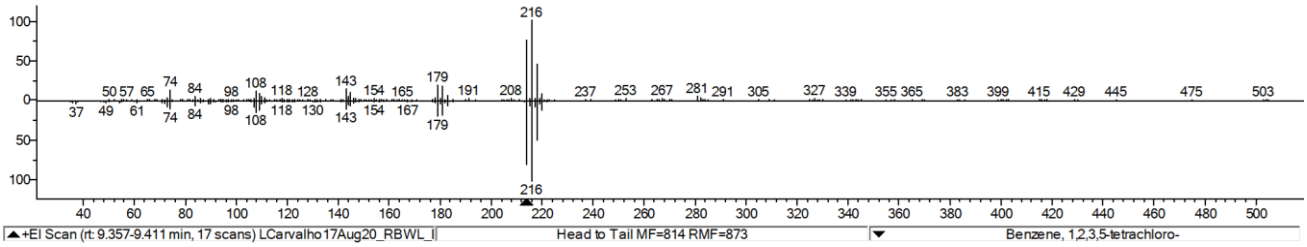
Interior

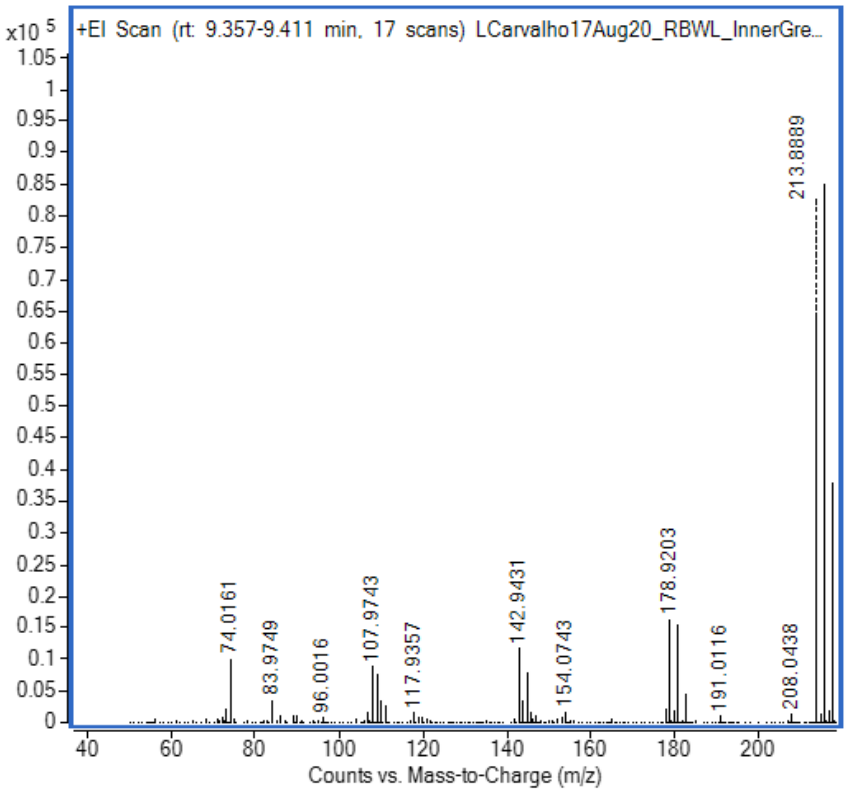




[3] Benzene, 1,2,3,5-tetrachloro- Mass: 213.891061

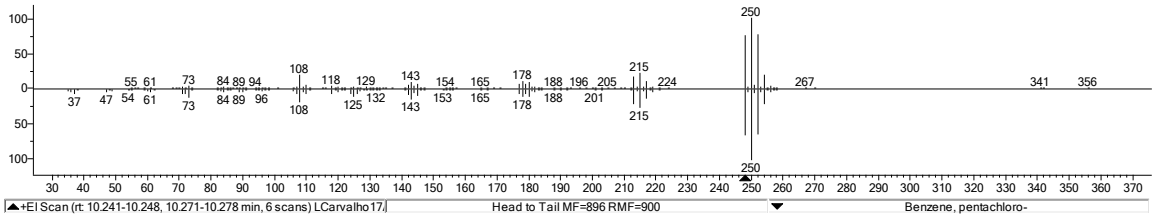
Interior

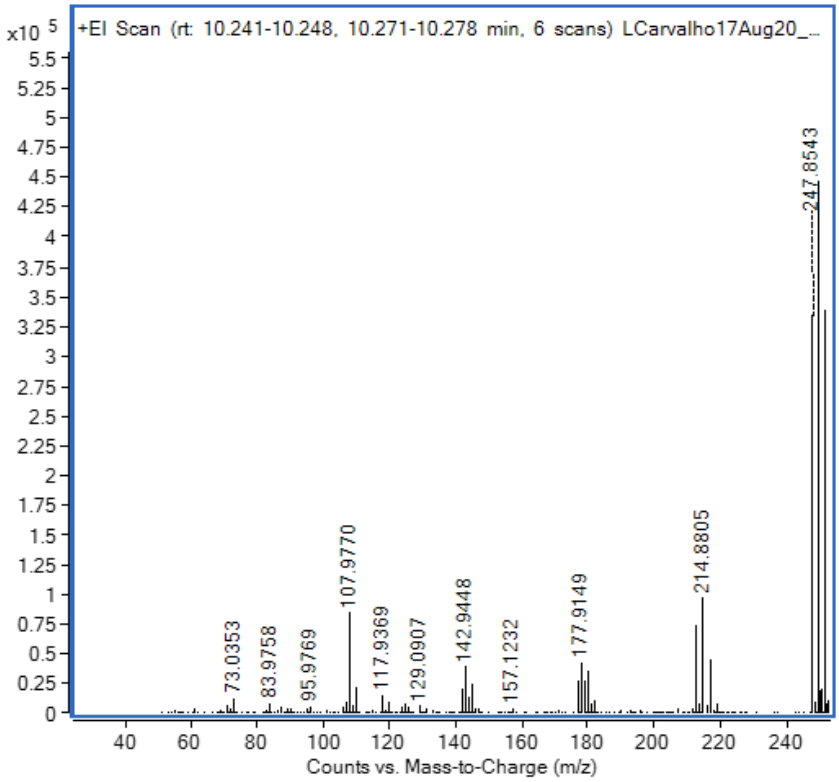




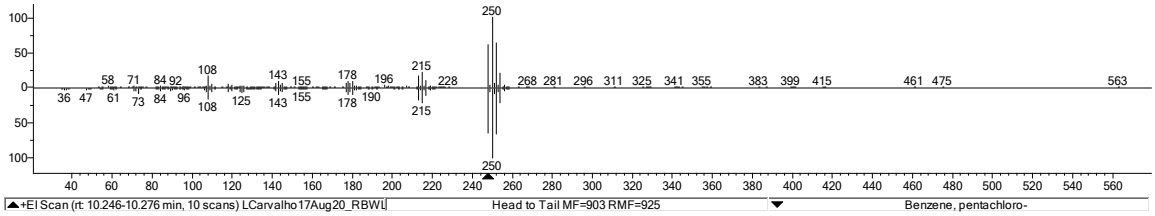
[4] Benzene, pentachloro- Mass: 247.852088

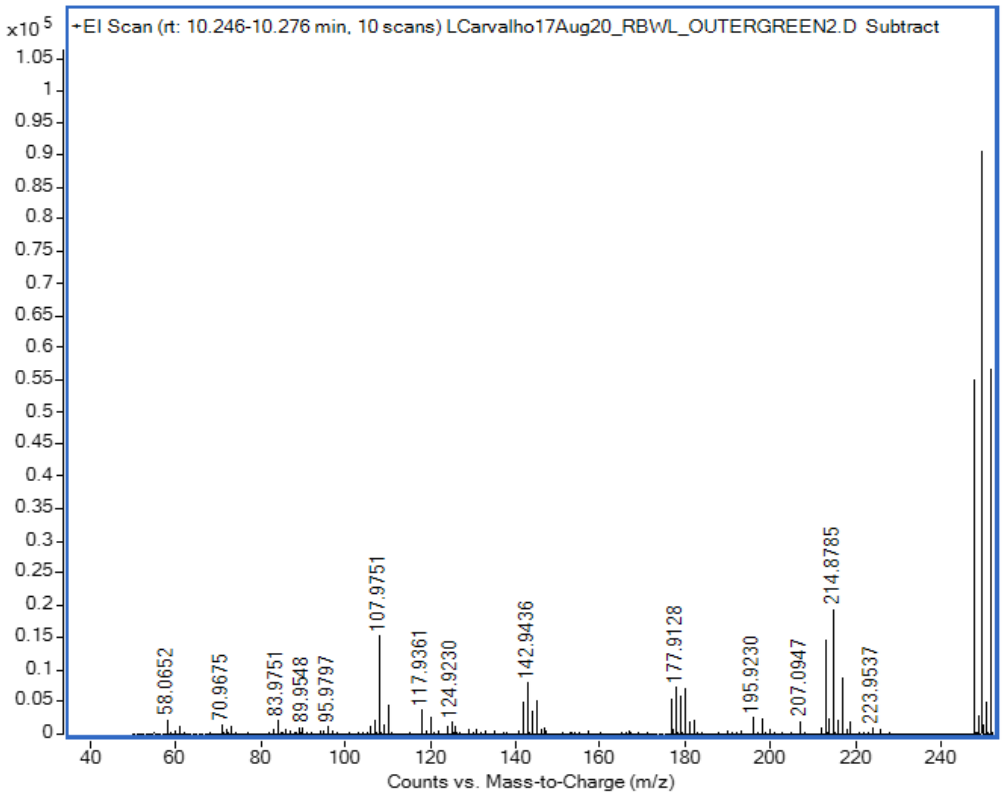
Interior





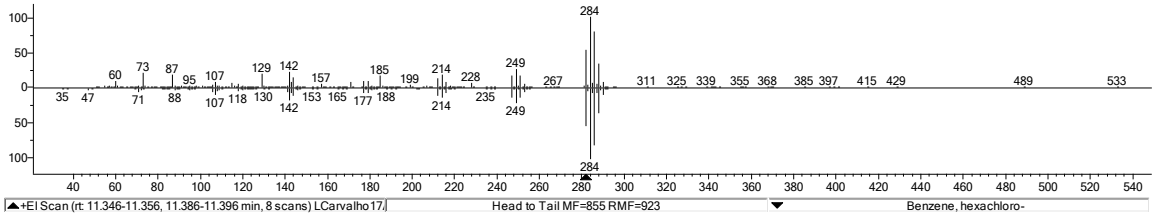
Exterior

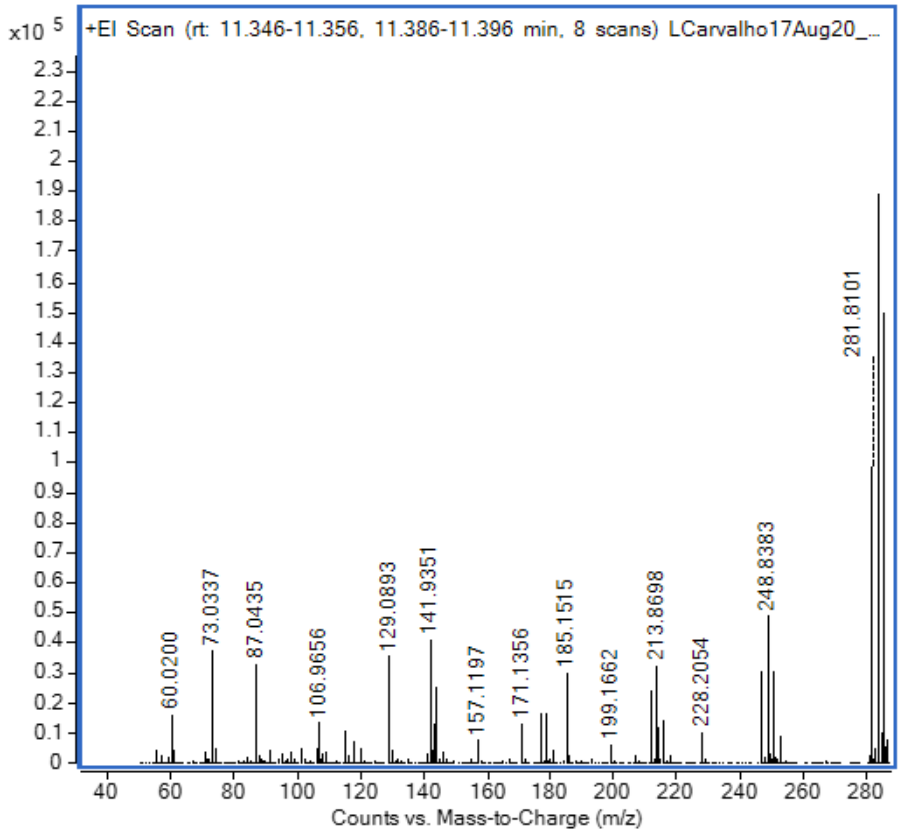

+EI Scan (rt: 10.246-10.276 min, 10 scans) LCarvalho17Aug20_RBWL
Head to Tail MF=903 RMF=925
Benzene, pentachloro-


x10 5
+EI Scan (rt: 10.246-10.276 min, 10 scans) LCarvalho17Aug20_RBWL_OUTERGREEN2.D Subtract
58.0652
70.9675
83.9751
89.9548
95.9797
107.9751
117.9361
124.9230
142.9436
177.9128
195.9230
207.0947
214.8785
223.9537
Counts vs. Mass-to-Charge (m/z)

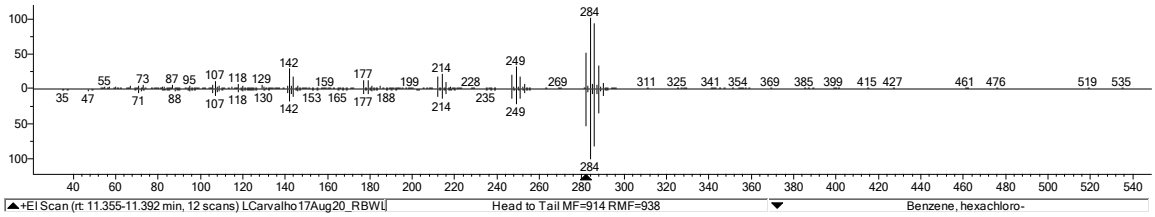
[5] Benzene, hexachloro- Mass: 281.813116

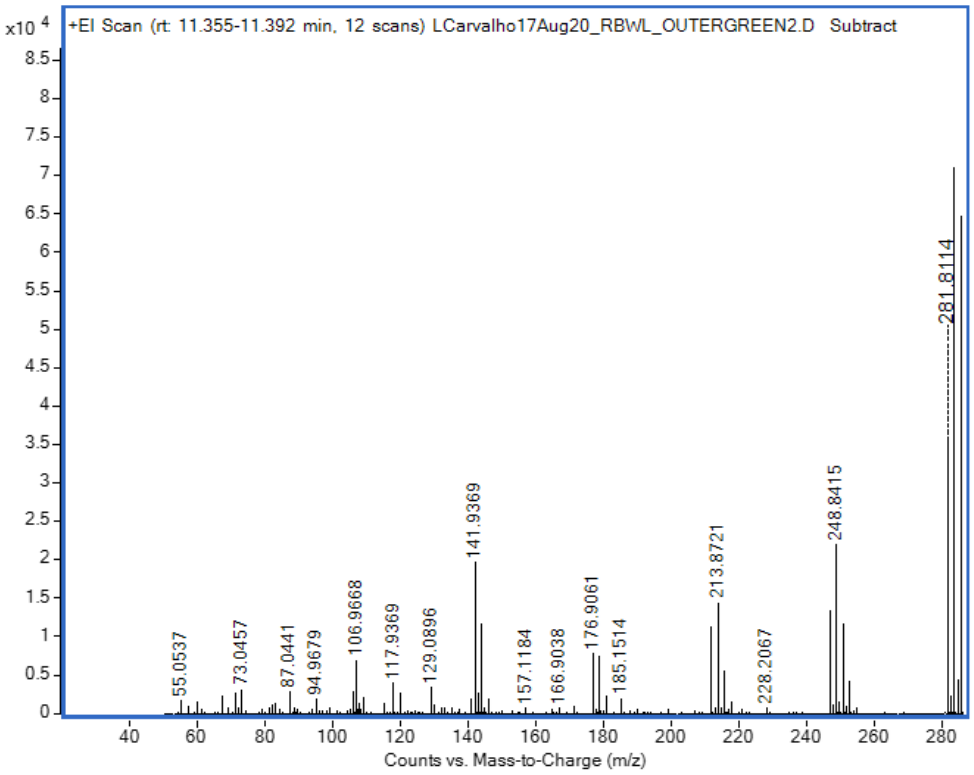
Interior





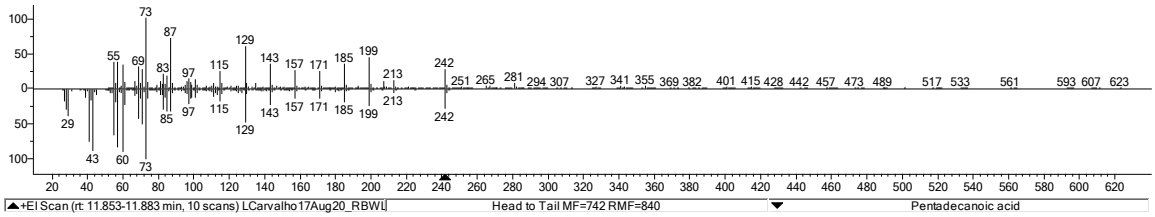
Exterior

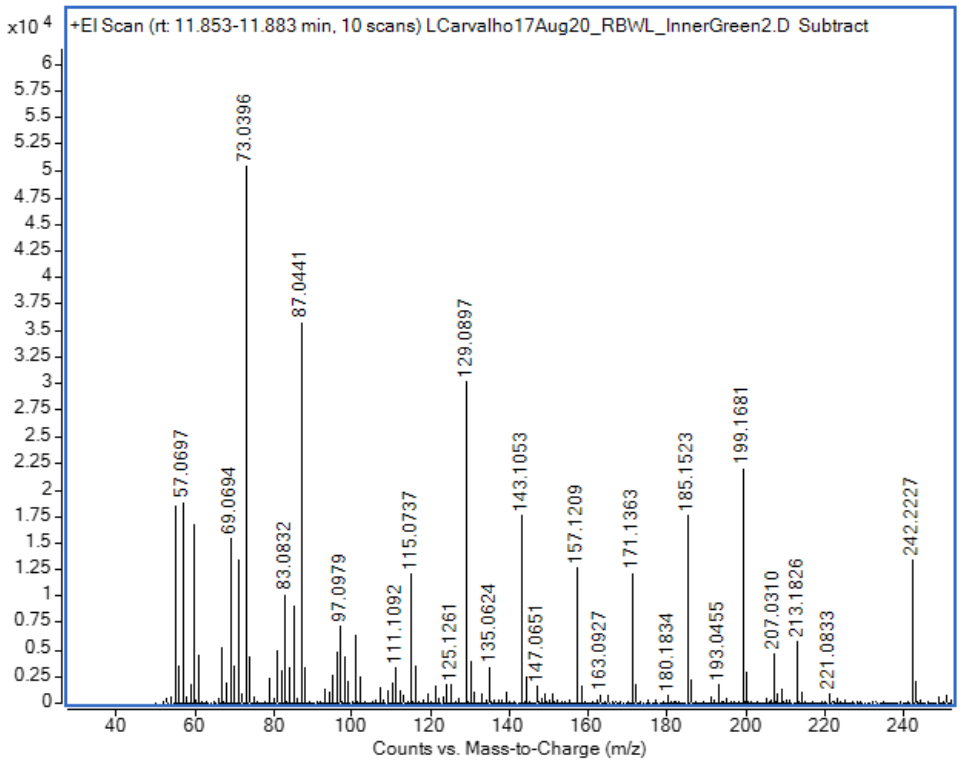

+EI Scan (rt: 11.355-11.392 min, 12 scans) LCarvalho17Aug20_RBWL
Head to Tail MF=914 RMF=938
Benzene, hexachloro-


x10 4
+EI Scan (rt: 11.355-11.392 min, 12 scans) LCarvalho17Aug20_RBWL_OUTERGREEN2.D Subtract
281.8114
248.8415
213.8721
176.9061
185.1514
141.9369
106.9668
117.9369
129.0896
55.0537
73.0457
87.0441
94.9679
157.1184
166.9038
228.2067
Counts vs. Mass-to-Charge (m/z)

[6] Pentadecanoic acid

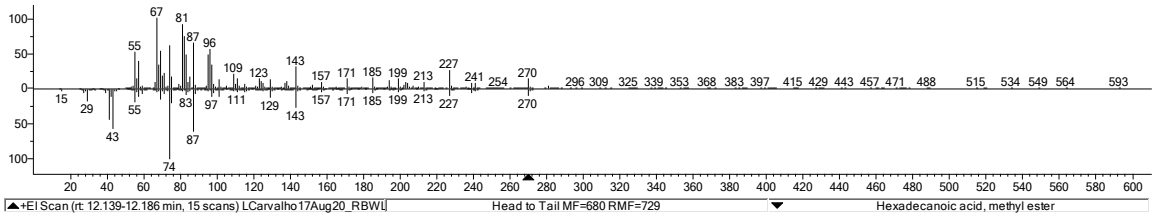
Interior

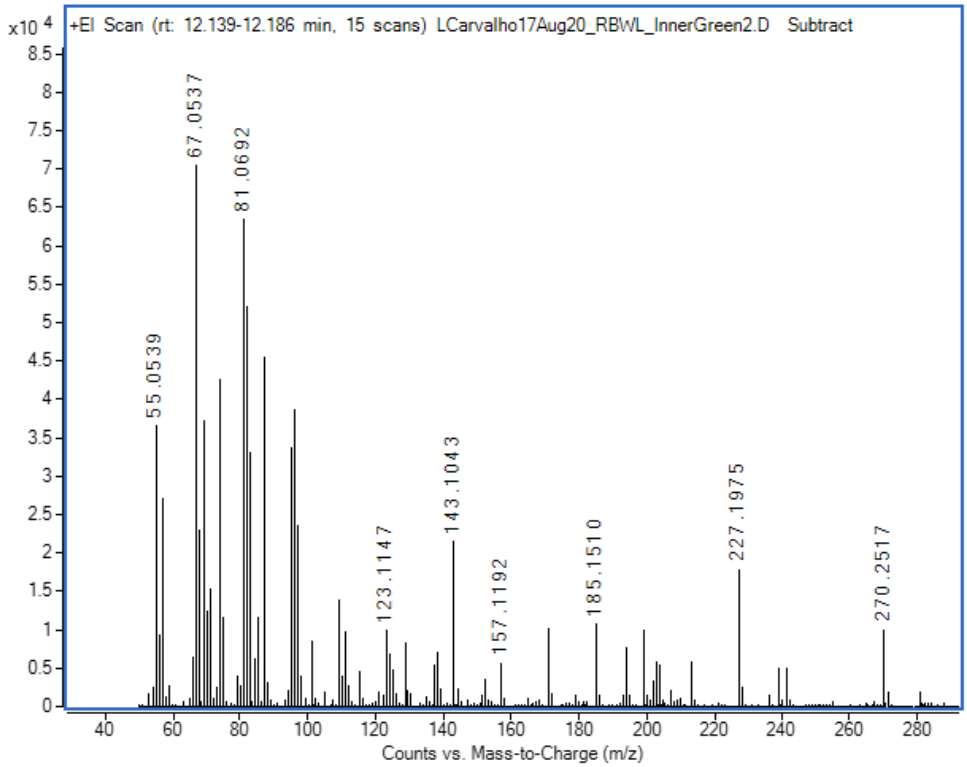




[7] Hexadecanoic acid, methyl ester

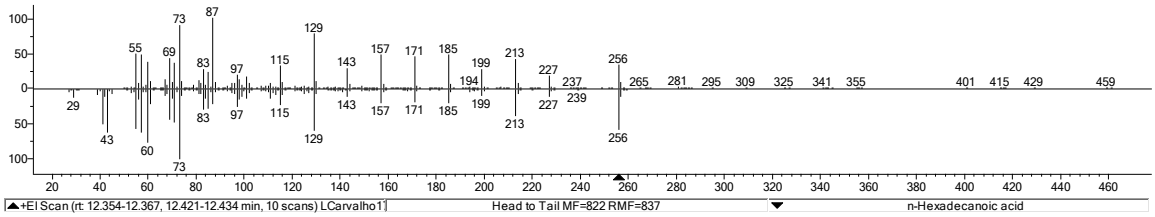
Interior

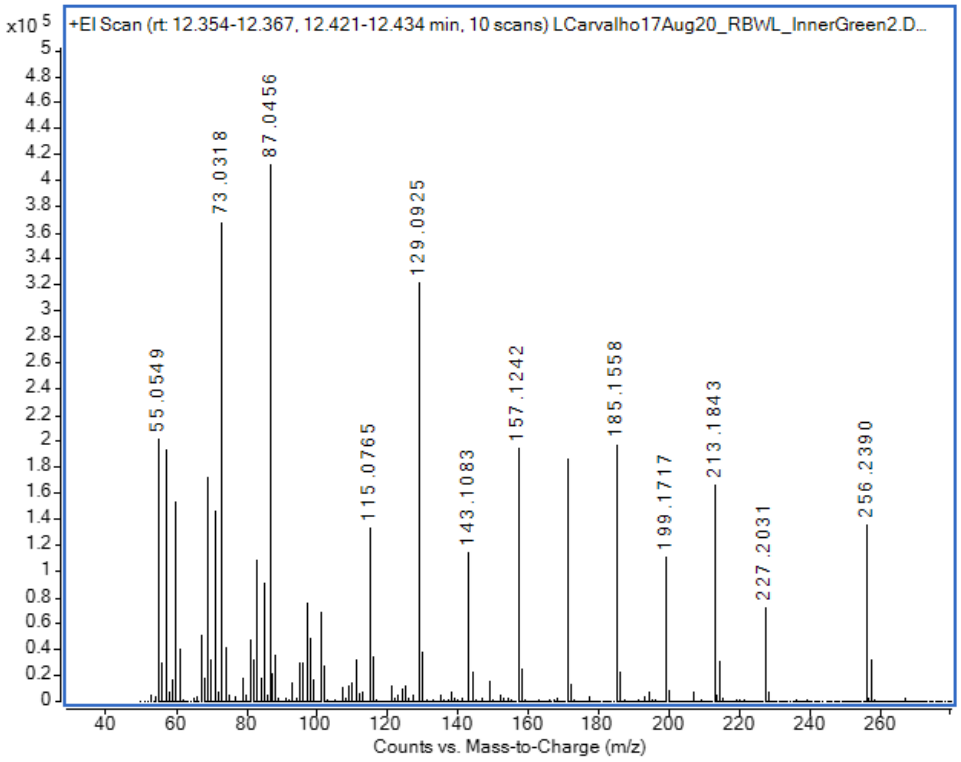




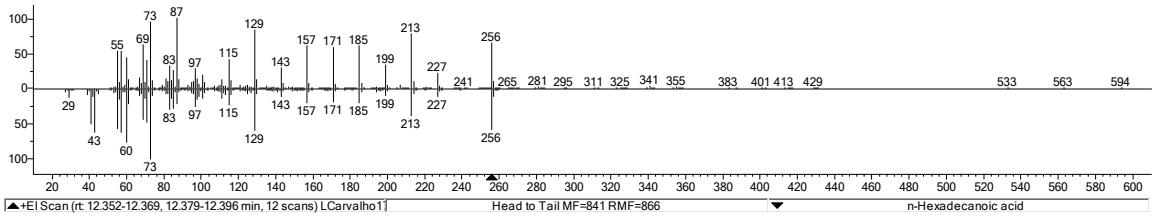
[8] n-hexadecanoic acid

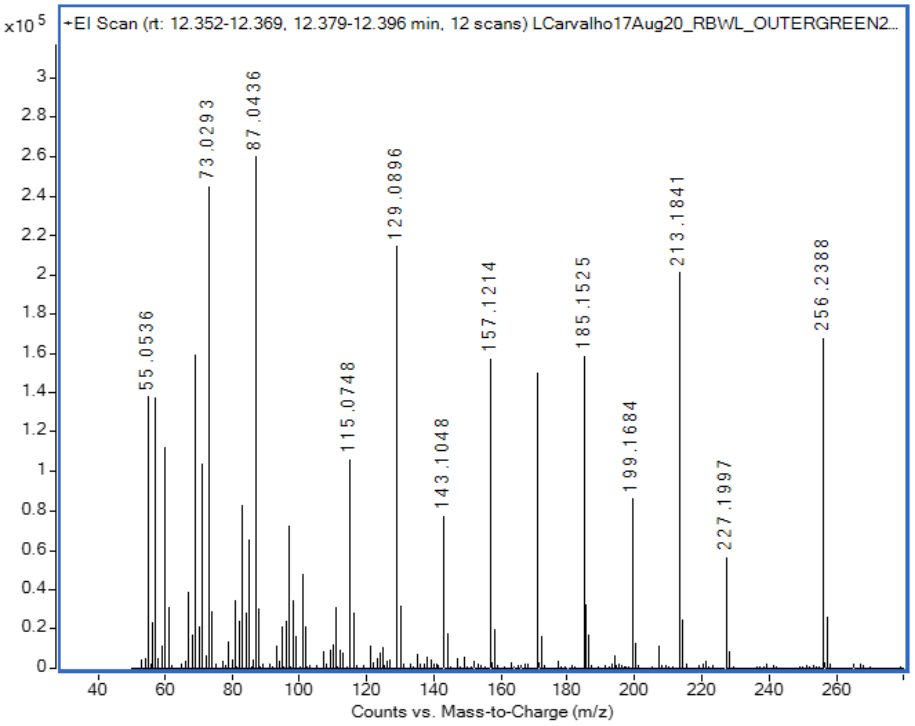
Interior





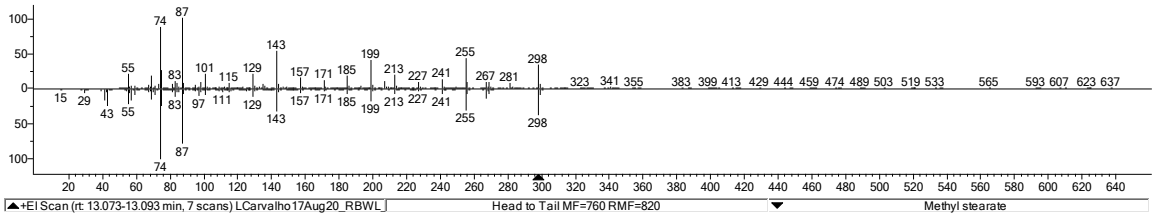
Exterior

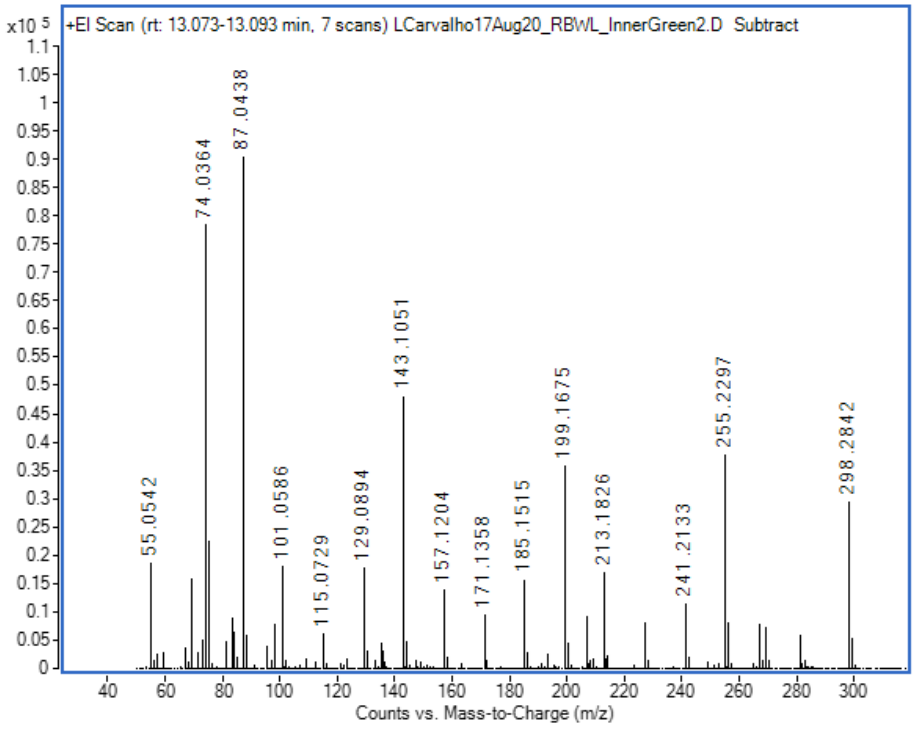

+EI Scan (rt: 12.352-12.369, 12.379-12.396 min, 12 scans) LCarvalho1]
Head to Tail MF=841 RMF=866
n-Hexadecanoic acid


x10 5
+EI Scan (rt: 12.352-12.369, 12.379-12.396 min, 12 scans) LCarvalho17Aug20_RBWL_OUTERGREEN2...
55.0536
73.0293
87.0436
115.0748
129.0896
143.1048
157.1214
185.1525
199.1684
213.1841
227.1997
256.2388
Counts vs. Mass-to-Charge (m/z)

[9] Methyl stearate

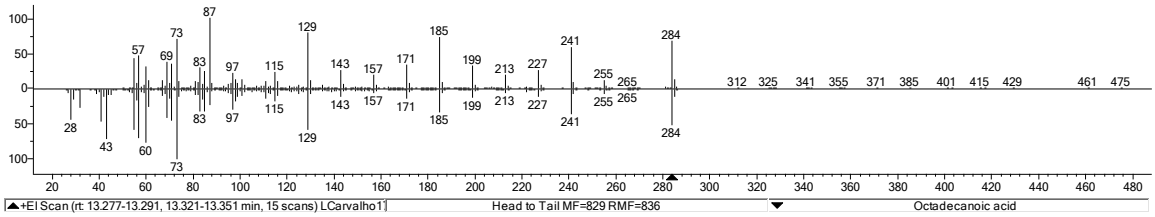
Interior

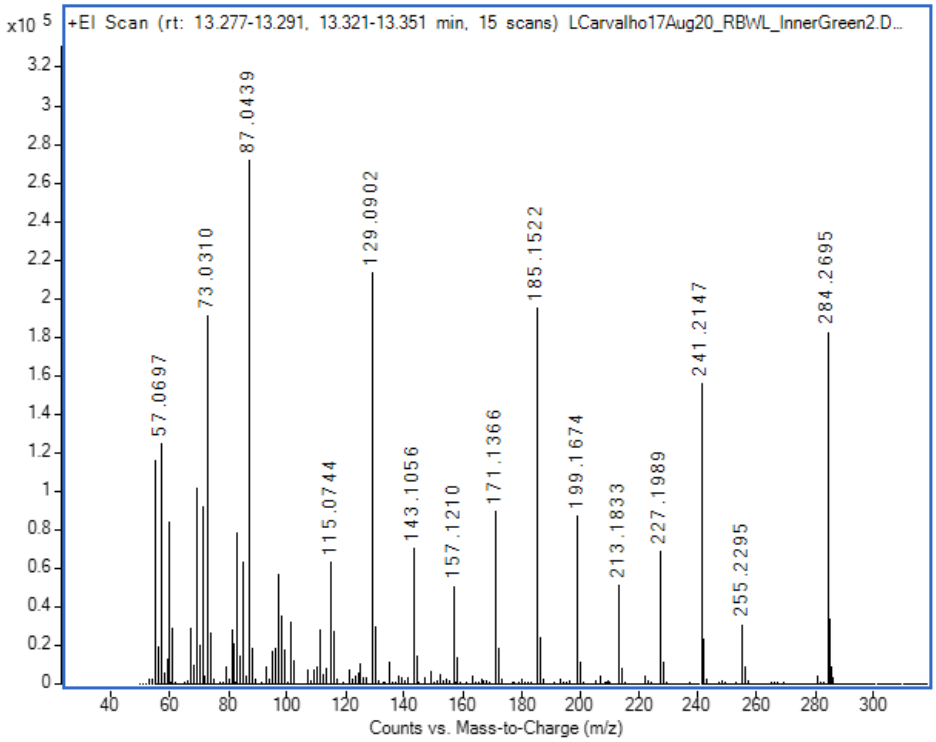




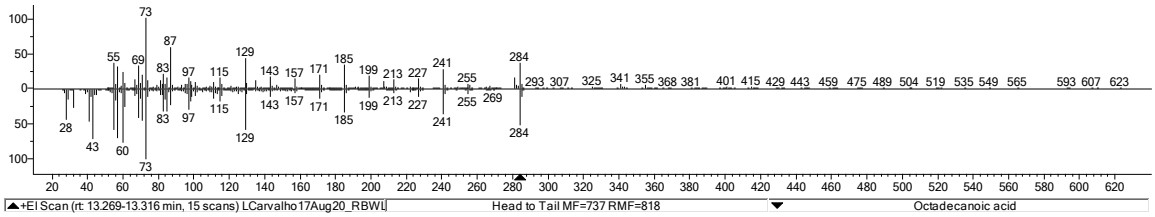
[10] Octanoic acid

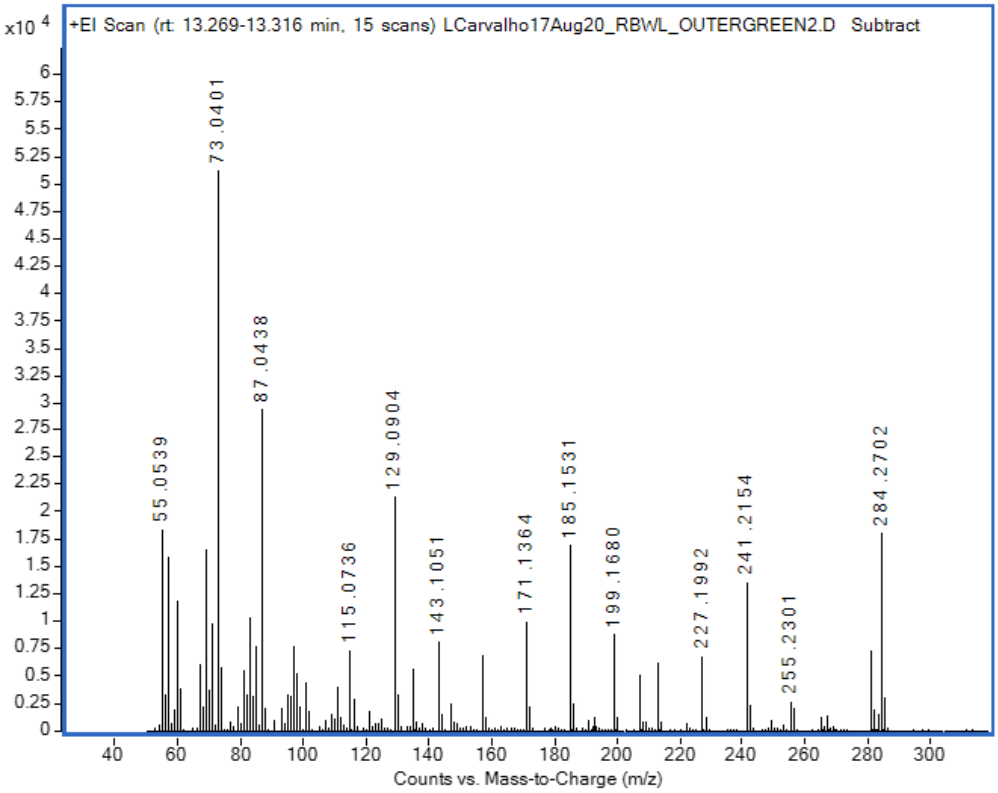
Interior





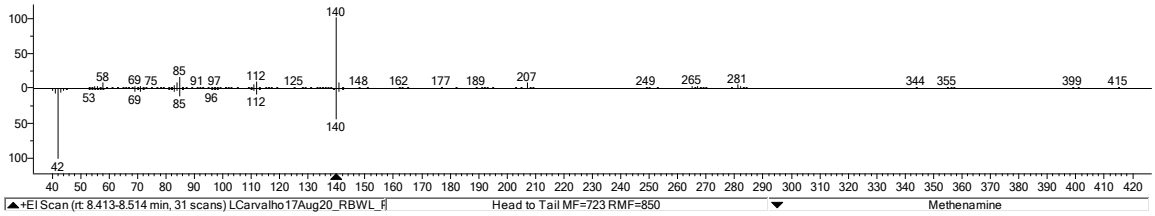
Exterior

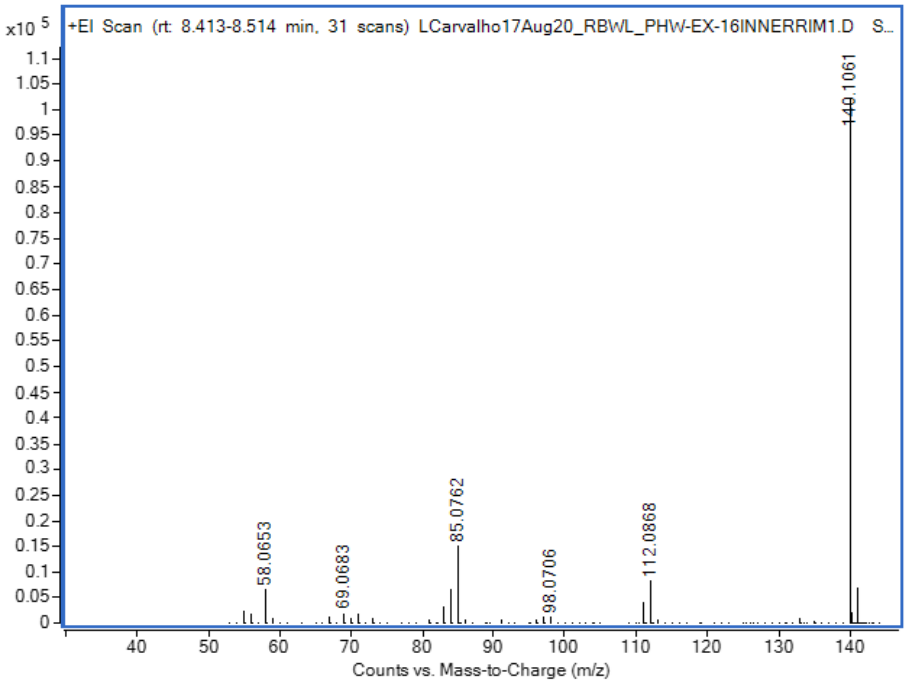

+EI Scan (rt: 13.269-13.316 min, 15 scans) LCarvalho17Aug20_RBWL
Head to Tail MF=737 RMF=818
Octadecanoic acid


x10 4
+EI Scan (rt: 13.269-13.316 min, 15 scans) LCarvalho17Aug20_RBWL_OUTERGREEN2.D Subtract
73.0401
87.0438
55.0539
129.0904
115.0736
143.1051
171.1364
185.1531
199.1680
227.1992
241.2154
255.2301
284.2702
Counts vs. Mass-to-Charge (m/z)

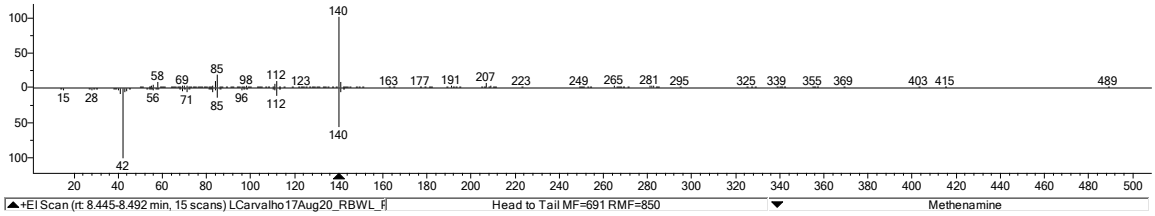
[1] Methenamine

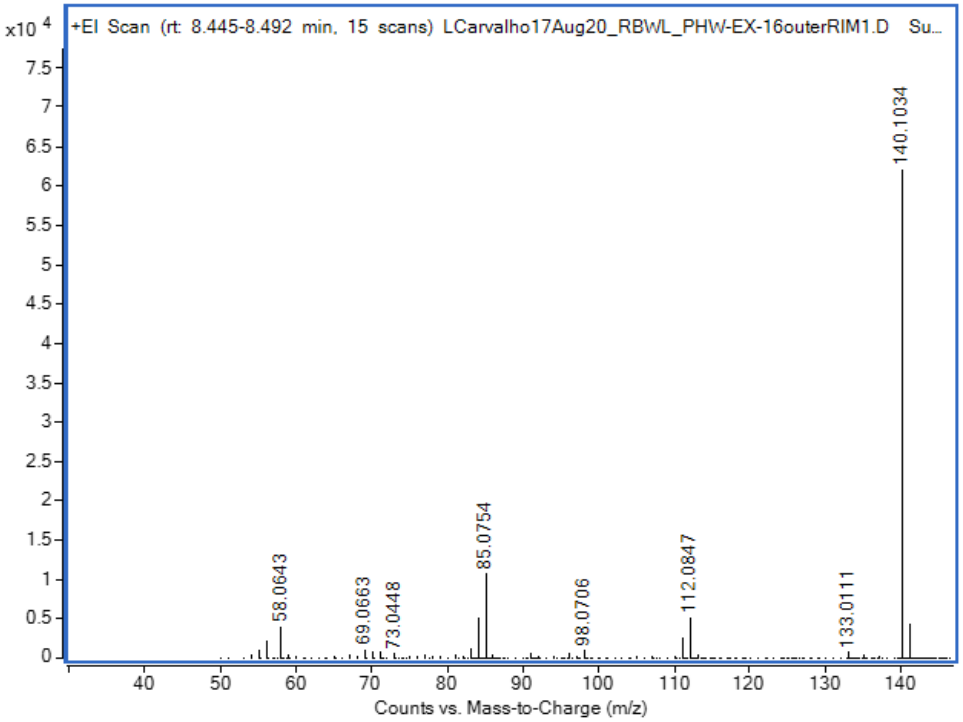
Interior





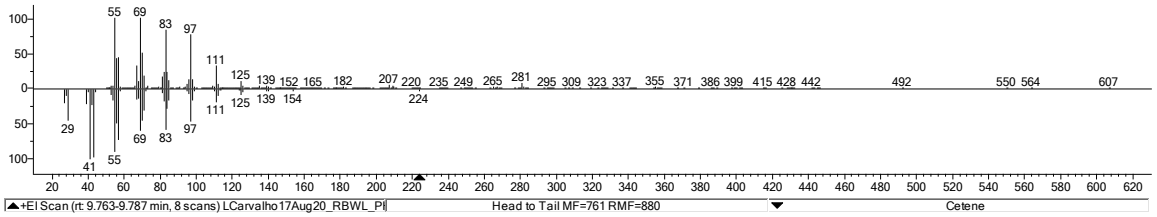
Exterior

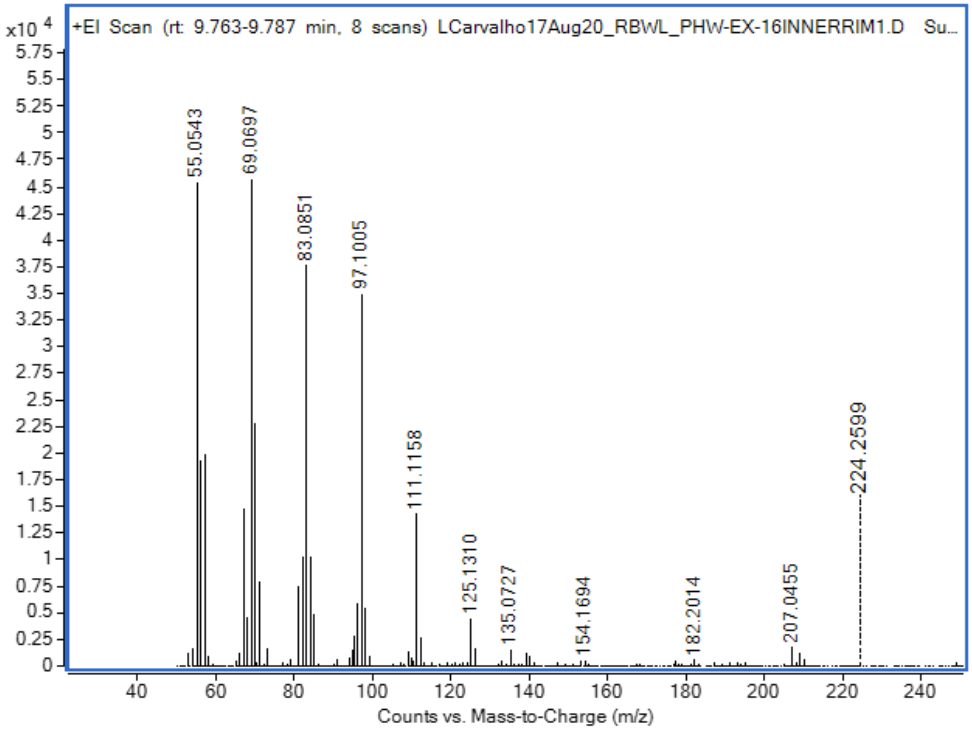

+EI Scan (rt: 8.445-8.492 min, 15 scans) LCarvalho17Aug20_RBWL_F
Head to Tail MF=691 RMF=850
Methenamine


x10 4
+EI Scan (rt: 8.445-8.492 min, 15 scans) LCarvalho17Aug20_RBWL_PHW-EX-16outerRIM1.D Su...
140.1034
85.0754
58.0643
69.0663
73.0448
98.0706
112.0847
133.0111
Counts vs. Mass-to-Charge (m/z)

[2] Cetene Mass: 224.2504015

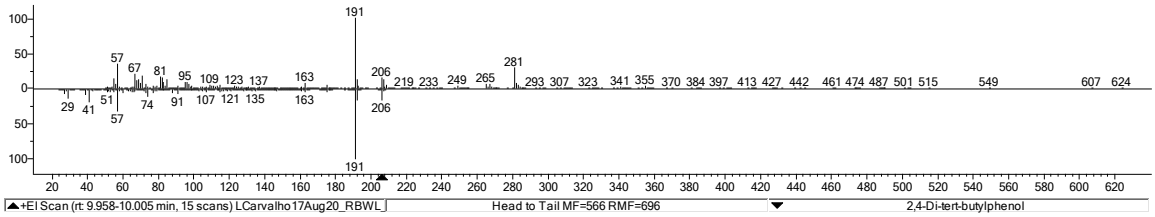
Interior

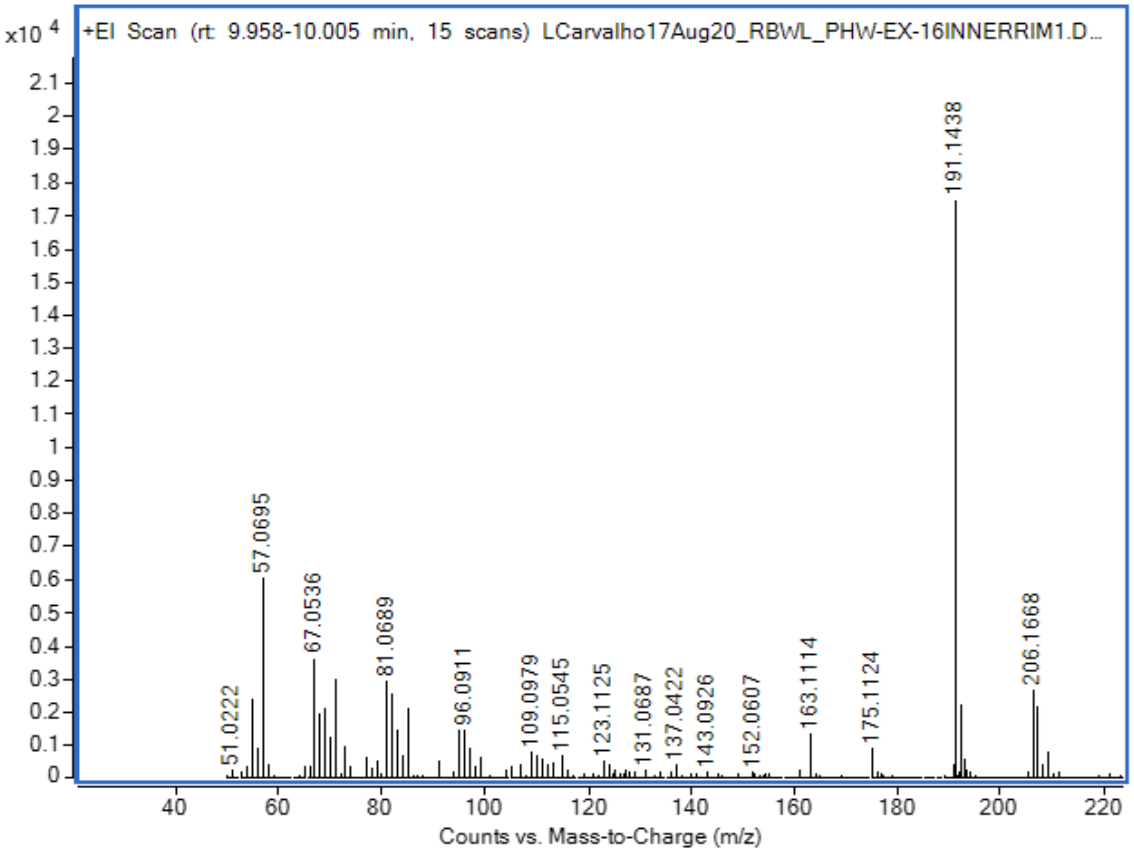




[3] 2,4-Di-tert-butylphenol Mass: 206.167066

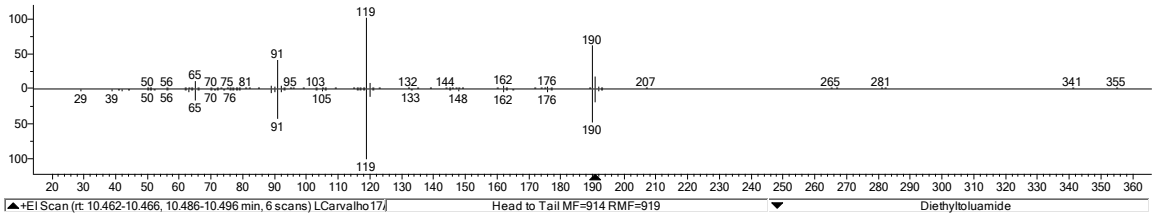
Interior

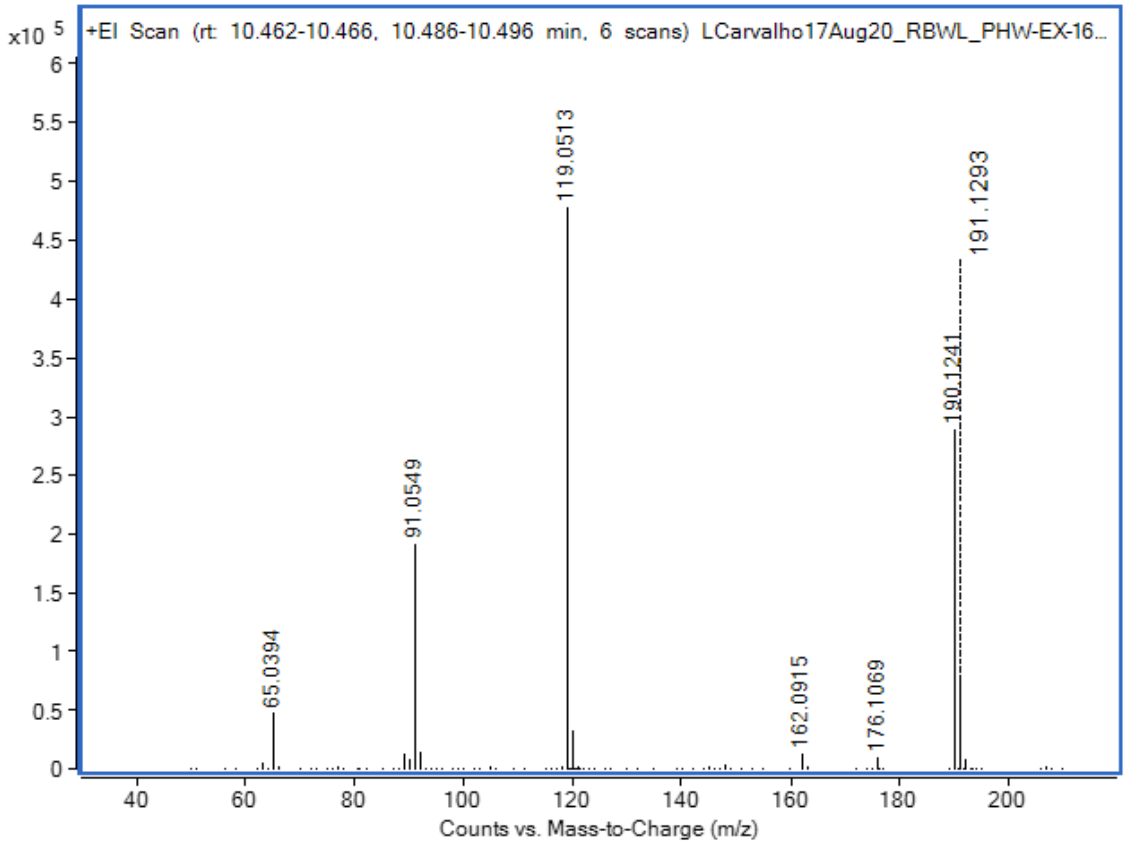




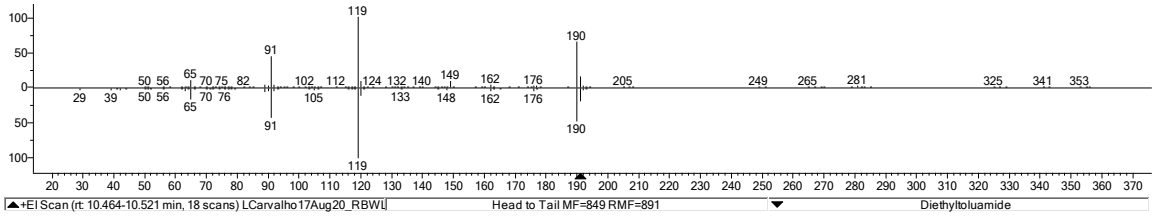
[4] Diethyltoluamide Mass: 191.131014

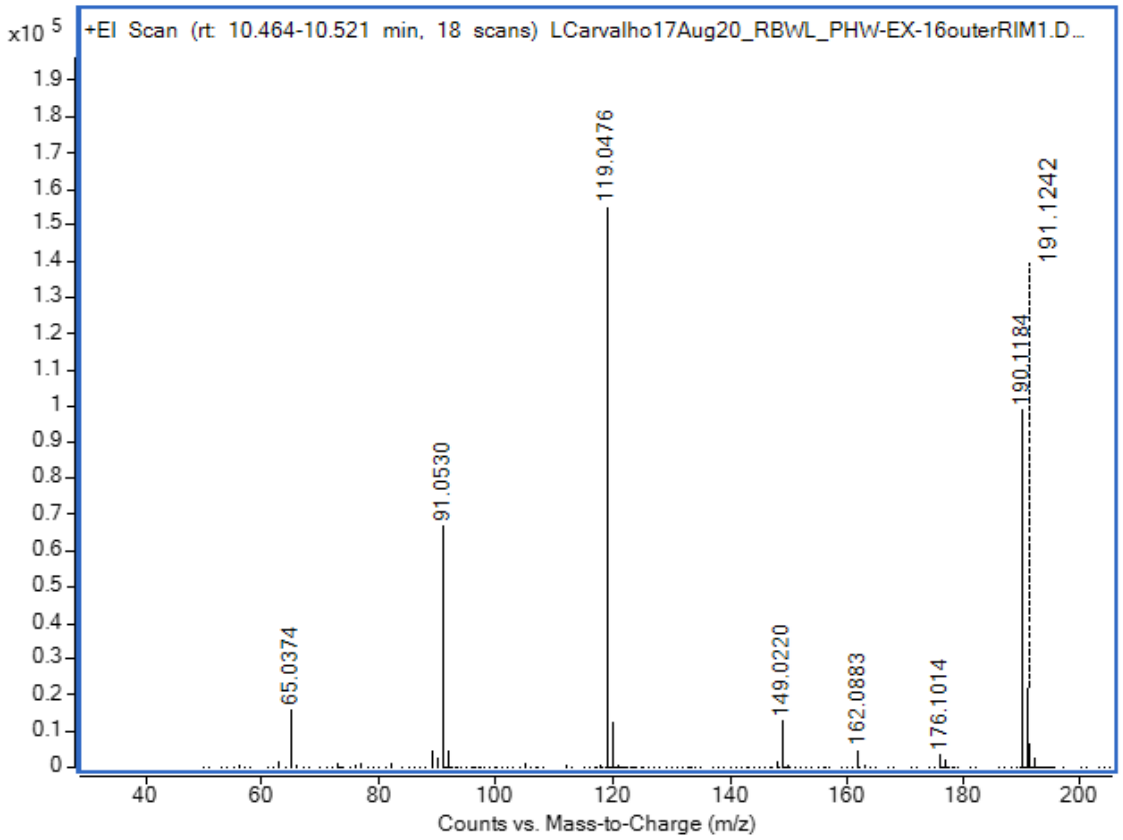
Interior





Exterior

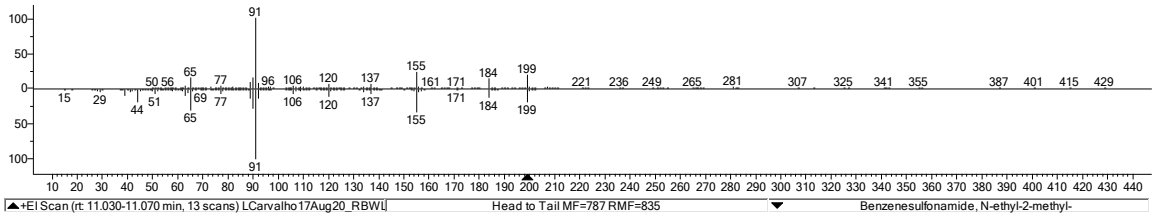

+EI Scan (rt: 10.464-10.521 min, 18 scans) LCarvalho17Aug20_RBWL
Head to Tail MF=849 RMF=891
Diethyltoluamide

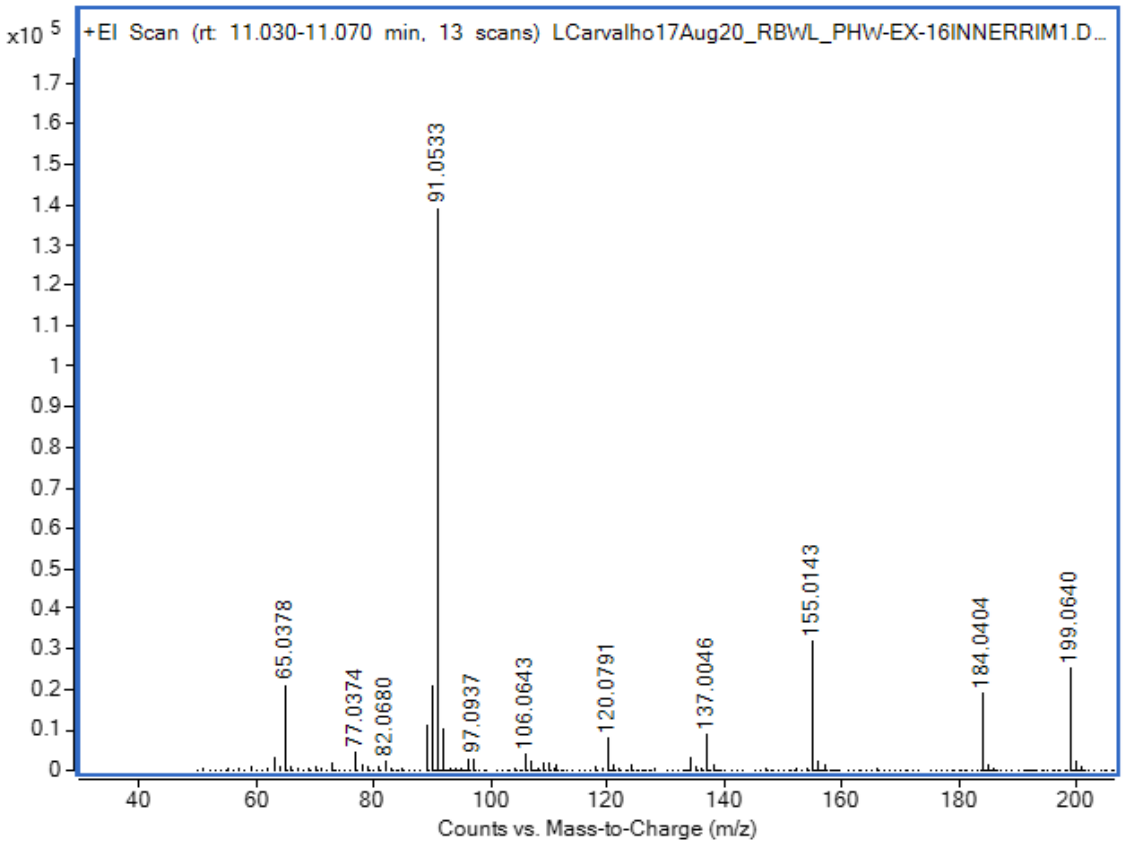

x10 5
+EI Scan (rt: 10.464-10.521 min, 18 scans) LCarvalho17Aug20_RBWL_PHW-EX-16outerRIM1.D...
119.0476
191.1242
190.1184
91.0530
65.0374
149.0220
162.0883
176.1014
Counts vs. Mass-to-Charge (m/z)

[5] Benzenesulfonamide, N-ethyl-2-methyl-

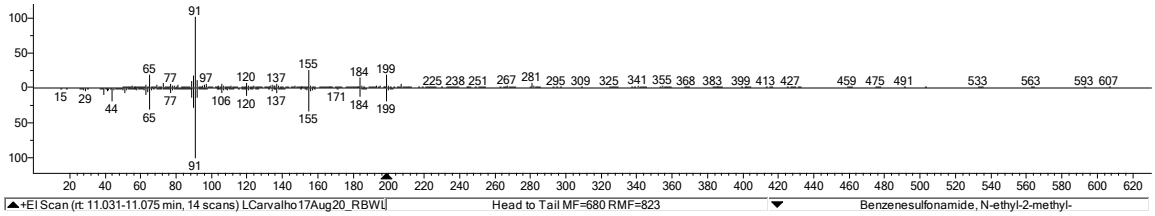
Mass: 199.0667 NIST#: 290603

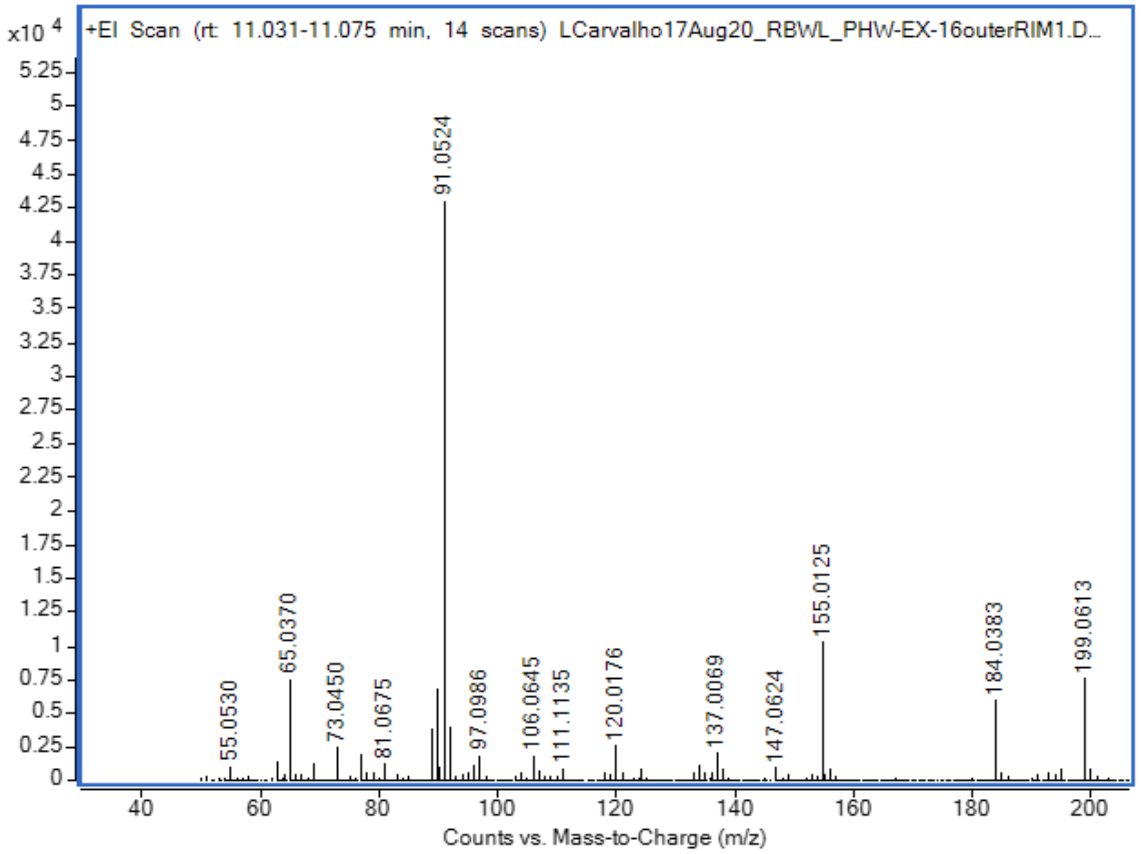
Interior





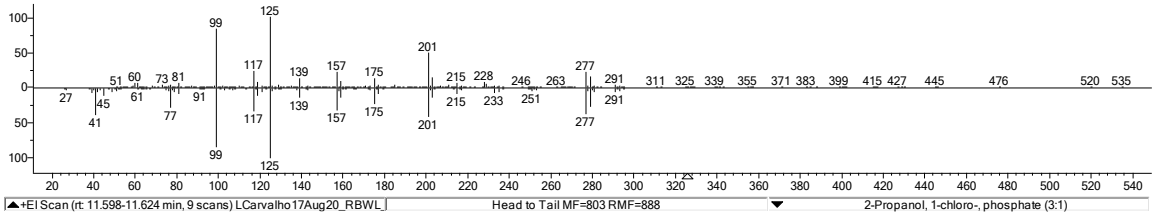
Exterior

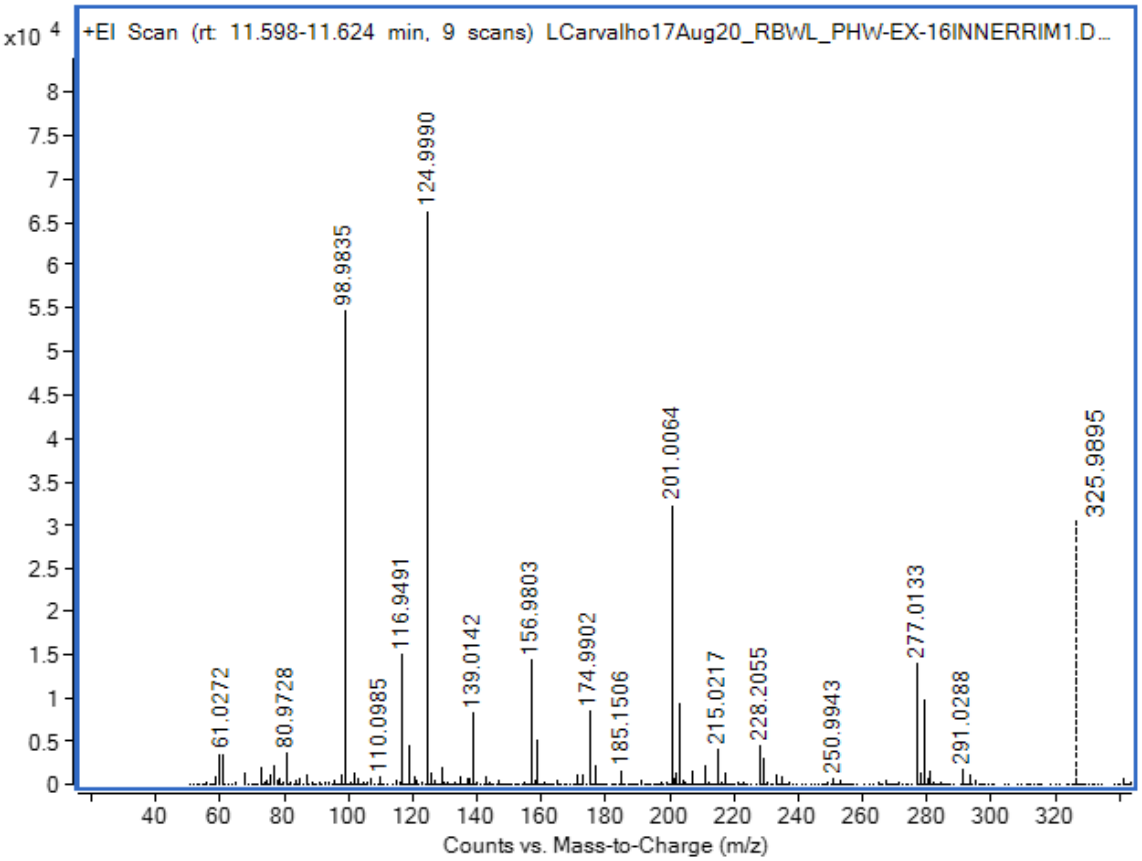

+EI Scan (rt: 11.031-11.075 min, 14 scans) LCarvalho17Aug20_RBWL
Head to Tail MF=680 RMF=823
Benzenesulfonamide, N-ethyl-2-methyl-


x10 4
+EI Scan (rt: 11.031-11.075 min, 14 scans) LCarvalho17Aug20_RBWL_PHW-EX-16outerRIM1.D...
91.0524
65.0370
73.0450
81.0675
55.0530
97.0986
106.0645
111.1135
120.0176
137.0069
147.0624
155.0125
184.0383
199.0613
Counts vs. Mass-to-Charge (m/z)

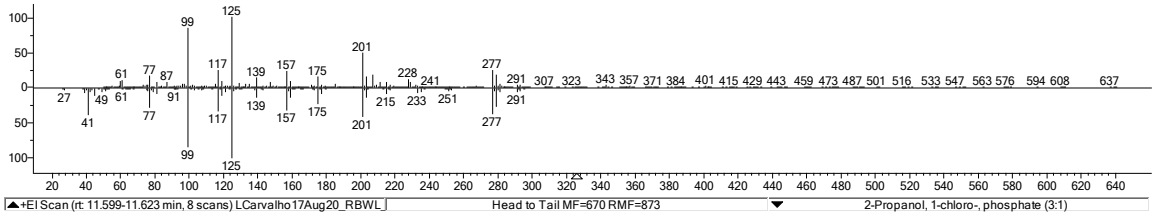
[6] 2-Propanol, 1-chloro-, phosphate (3:1) Mass: 326.000828

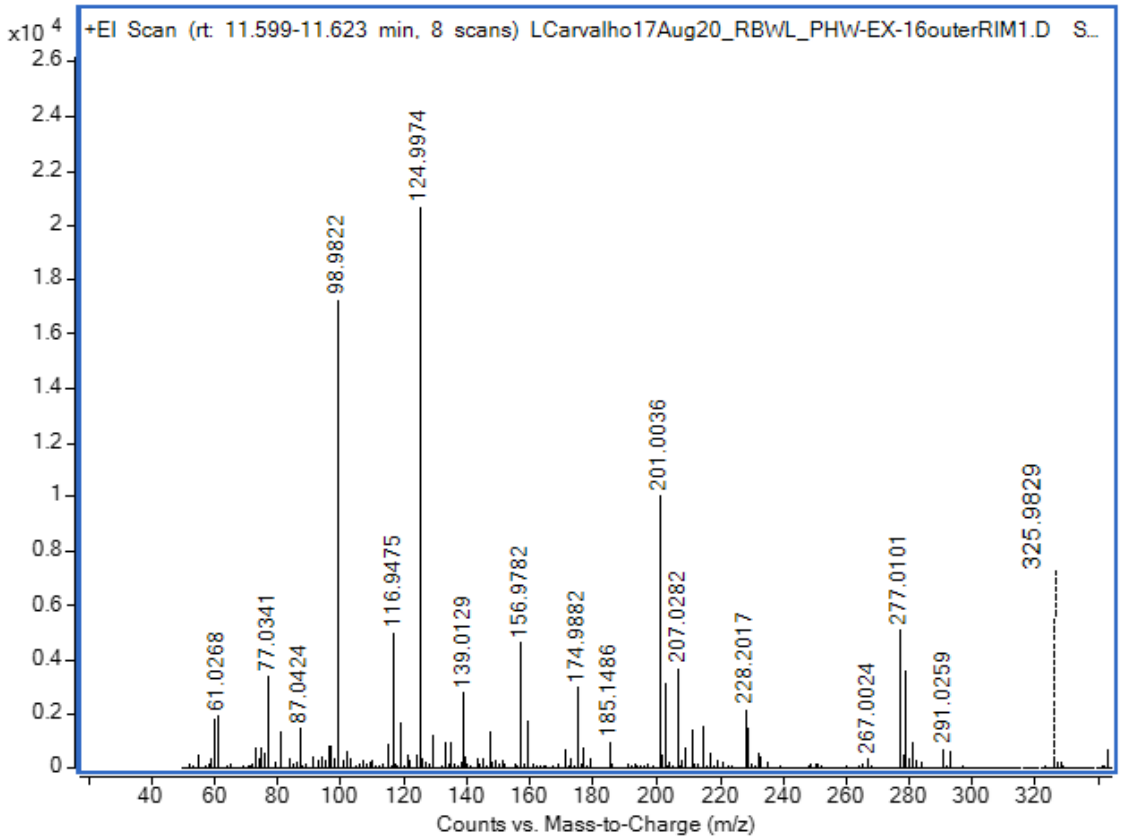
Interior





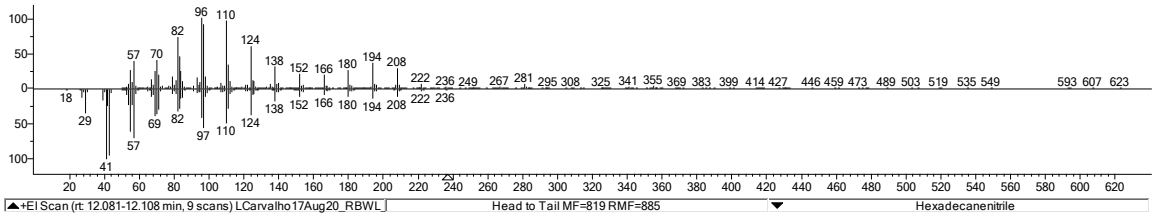
Exterior

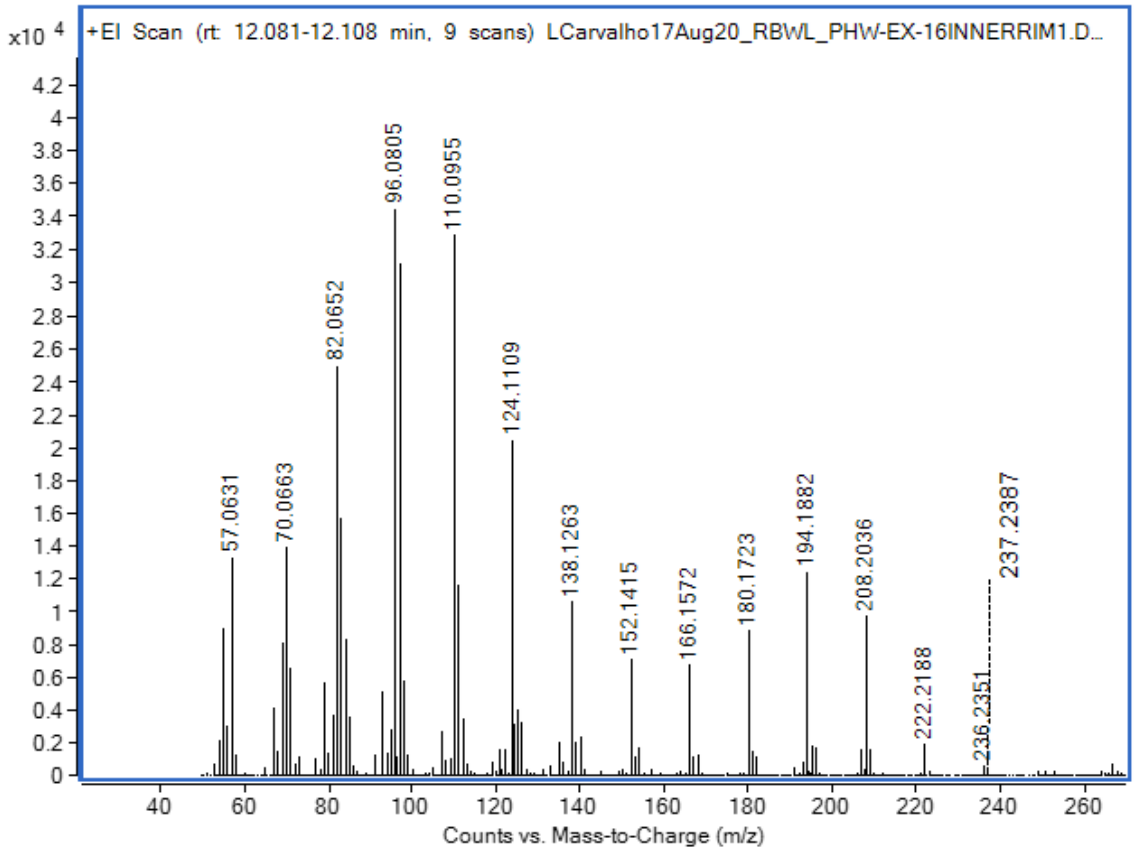

+EI Scan (rt: 11.599-11.623 min, 8 scans) LCarvalho17Aug20_RBWL_
Head to Tail MF=670 RMF=873
2-Propanol, 1-chloro-, phosphate (3:1)


x10 4
+EI Scan (rt: 11.599-11.623 min, 8 scans) LCarvalho17Aug20_RBWL_PHW-EX-16outerRIM1.D S...
61.0268
77.0341
87.0424
98.9822
116.9475
124.9974
139.0129
156.9782
174.9882
185.1486
201.0036
207.0282
228.2017
267.0024
277.0101
291.0259
325.9829
Counts vs. Mass-to-Charge (m/z)

[7] Hexadecanenitrile Mass: 237.24565

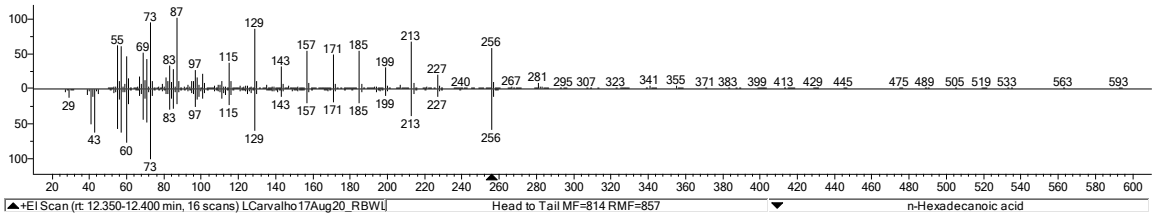
Interior

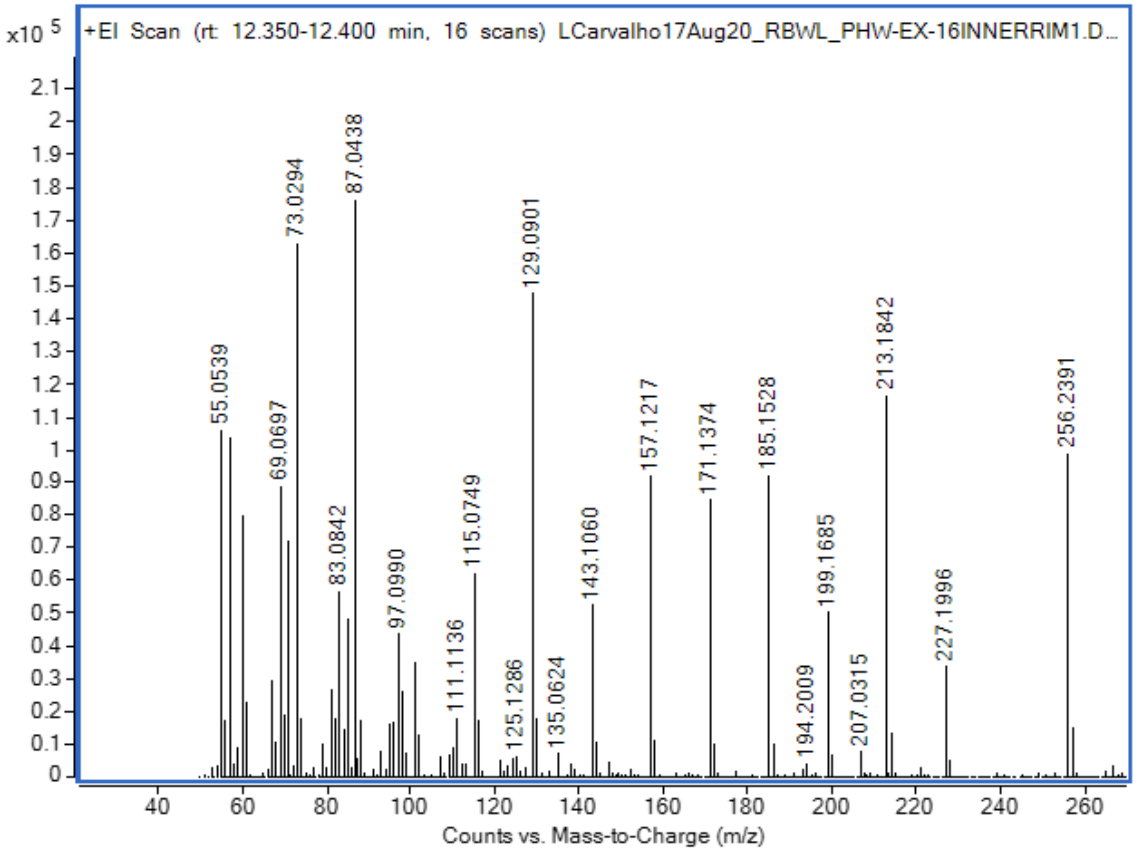




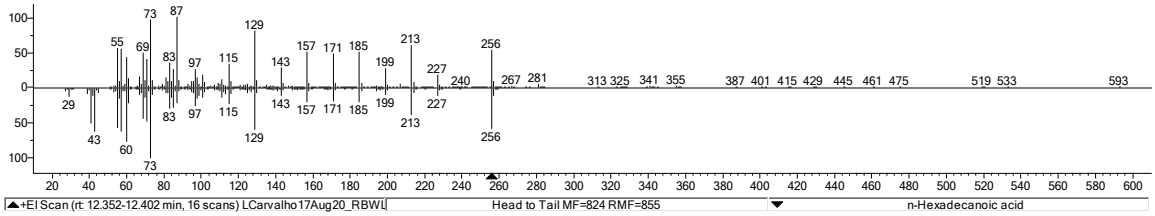
[8] n-hexadecanoic acid

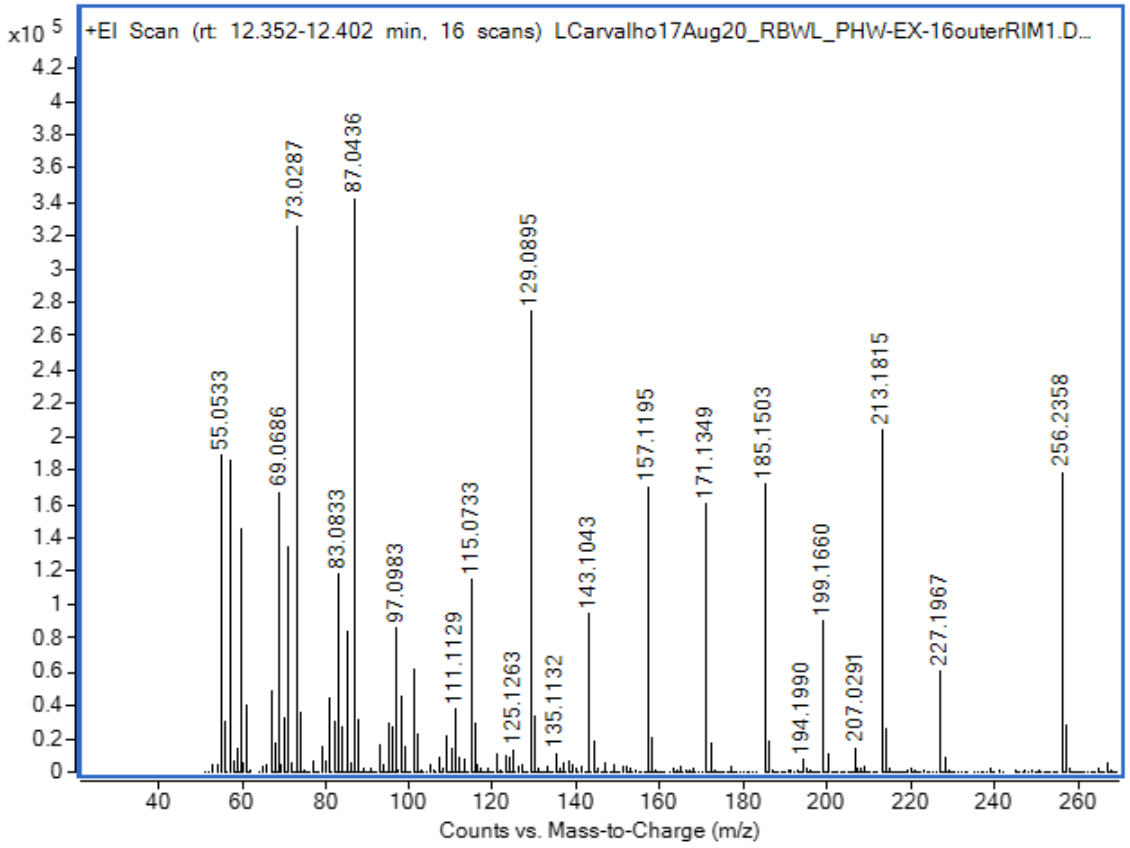
Interior





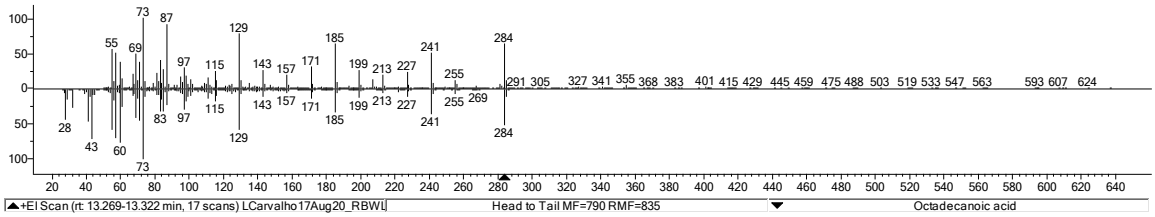
Exterior

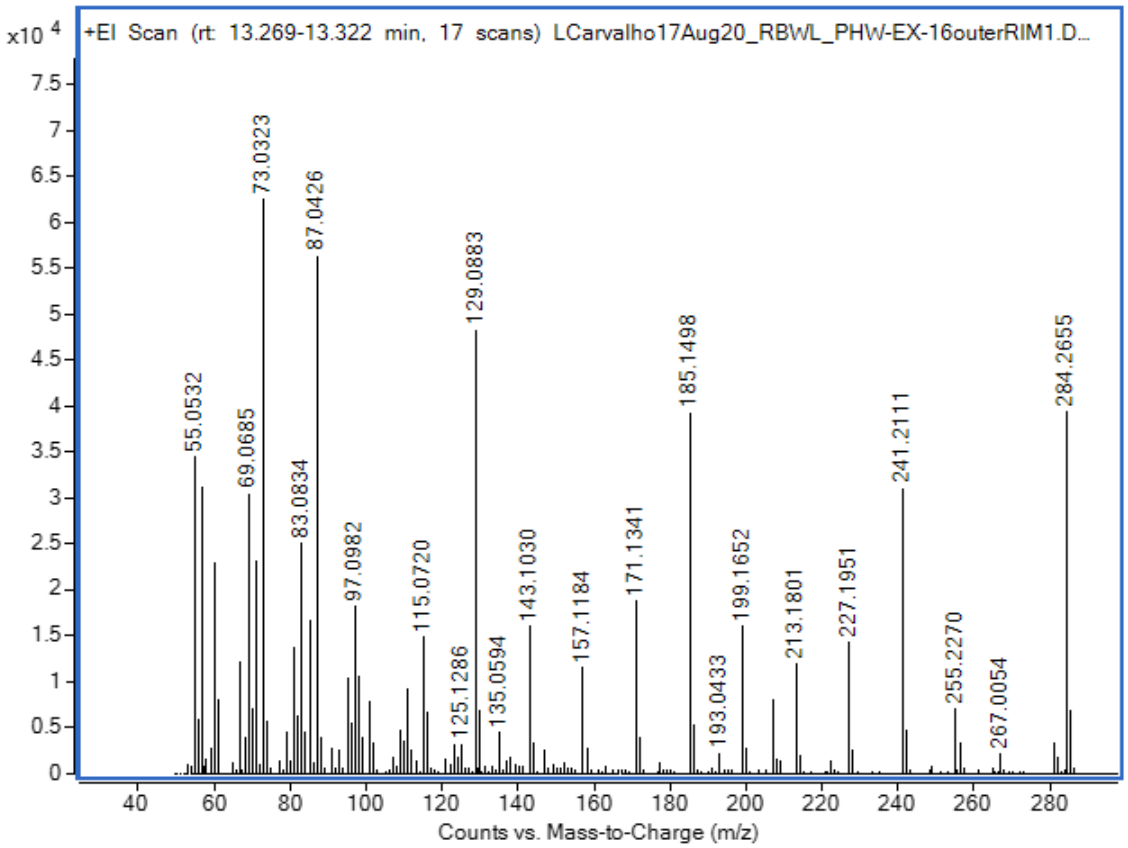

+EI Scan (rt: 12.352-12.402 min, 16 scans) LCarvalho17Aug20_RBWL
Head to Tail MF=824 RMF=855
n-Hexadecanoic acid


x10 5
+EI Scan (rt: 12.352-12.402 min, 16 scans) LCarvalho17Aug20_RBWL_PHW-EX-16outerRIM1.D...
55.0533
69.0686
73.0287
83.0833
87.0436
97.0983
111.1129
115.0733
125.1263
129.0895
135.1132
143.1043
157.1195
171.1349
185.1503
194.1990
199.1660
207.0291
213.1815
227.1967
256.2358
Counts vs. Mass-to-Charge (m/z)

[9] octadecanoic acid

Exterior





Roman Bowl IC-MS Results

Compound	Name	Formula	m/z	Score	Mass Error (ppm)	RT Error (min)	Isotope Similarity (ppm)	Maximum Fold Change	Isotope Distribution	Normalised abundance RBGInt	RBRExt	RBRInt	RBGExt
16.34_191.0197m/z	Citric acid	C6H8O7	191.0197	41.9	-0.1904	-0.57	98.84	1.34	100 - 6.61 - 0.715	665.3634	674.8070	517.0679	502.6804
4.37_89.0244m/z	Dihydroxyacetone	C3H6O3	89.0244	40.6	-0.2441	-0.37	98.50	1.41	100 - 2.41 - 0.116	3436.7413	2476.1955	3128.8694	3497.8854
2.57_181.0715m/z	Mannitol	C6H14O6	181.0715	40.1	-1.4694	-0.19	96.86	1.51	100 - 4.33 - 0.581	5569.2108	3977.8938	5987.3408	4745.7771
17.51_137.0244m/z	4-Hydroxybenzoic acid	C7H6O3	137.0244	40.3	0.0817	-1.35	96.23	1.56	100 - 4.48 - 0.0571	10068.2731	6448.5132	7596.3010	8528.0035
13.88_187.0975m/z	Nonate	C9H16O4	187.0975	52.5	-3.2775	0.03	98.98	1.70	100 - 9.61 - 0.602	2896.9783	2797.7339	1708.4167	2104.0099
15.25_205.0354m/z	Methylisocitric acid	C7H10O7	205.0354	41.8	0.0822	-0.56	98.66	1.73	100 - 7.28 - 1.03	305.2934	225.3179	201.8619	348.6615
12.68_115.0037m/z	Fumarate	C4H4O4	115.0037	40.8	-0.0242	-0.95	98.58	2.59	100 - 3.46 - 0.469	437.2714	482.9511	186.1087	234.6852
11.99_101.0244m/z	Succinic acid semialdehyde	C4H6O3	101.0244	40.3	-0.5677	-0.71	95.58	3.04	100 - 0.557	58.0655	118.8485	145.8196	176.4018
24.23_153.0194m/z	Protocatechuic acid	C7H6O4	153.0194	40.4	0.3477	-1.06	93.38	3.06	100 - 1.67	365.1629	277.3960	644.5763	848.2702
10.19_145.0507m/z	Methylglutaric acid	C6H10O4	145.0507	41	0.3144	-0.54	98.01	4.23	100 - 5.15 - 0.481	1481.0424	349.8569	1139.9761	1472.2163
10.39_117.0193m/z	Succinic acid	C4H6O4	117.0193	40.9	0.0712	-0.72	98.51	4.52	100 - 3.32 - 0.556	1534.4015	384.1115	1517.8144	1737.0178
12.48_88.9880m/z	Oxalic acid	C2H2O4	88.9880	40.7	-0.0875	-0.92	97.97	6.66	100 - 0.904 - 0.181	126.9044	192.7951	819.9288	845.8178
2.67_341.1093m/z	Lactose	C12H22O11	341.1093	39.9	-0.6462	-0.37	97.25	7.01	100 - 12.3 - 1.55	99.2549	290.3419	696.2076	272.8722
19.16_143.1077m/z	Octanoic acid	C8H16O2	143.1077	41.5	-0.0281	-0.79	98.29	10.74	100 - 7.61 - 0.195	433.6845	536.0176	653.4660	4658.4818
7.43_131.0714m/z	Leucic acid	C6H12O3	131.0714	44.4	-4.1365	-0.08	98.11	11.18	100 - 5.16 - 0.36	873.2002	187.2387	772.2362	2093.7045
10.19_129.0194m/z	Gamma-delta-Dioxovaleric acid	C5H6O4	129.0194	41.2	0.5396	-0.46	97.95	27.51	100 - 4.4	23.3527	5.8676	85.5585	161.4399
16.64_167.0350m/z	Homogentisic acid	C8H8O4	167.0350	40.5	-0.0145	-0.85	94.93	30.71	100 - 4.49	264.8391	30.5273	8.6234	41.0245
16.93_245.0933m/z	N-Acetyltryptophan	C13H14N2O3	245.0933	39.6	0.3453	-1.48	93.40	35.16	100 - 9.16	29.8625	50.4486	535.9337	1050.0270
10.69_159.0662m/z	3,3 Dimethyl glutarate	C7H12O4	159.0662	41	-0.2341	-0.72	99.08	65.37	100 - 7.26 - 0.682	456.8286	8.4834	354.5466	554.5848
9.27_115.0764m/z	Caproic acid/Hexanoic acid	C6H12O2	115.0764	39.5	-4.8475	0.69	98.25	Infinity	100 - 5.34 - 0.0939	31.8326	0.0000	242.6640	4597.9761
4.28_165.0405m/z	Arabinonic acid	C5H10O6	165.0405	40.2	-0.0237	-0.62	97.83	Infinity	100 - 4.45 - 0.349	322.1810	0.0000	757.6121	2016.4993
10.39_133.0143m/z	Malic acid	C4H6O5	133.0143	40.8	0.1075	-0.75	98.41	Infinity	100 - 3.45 - 0.565	178.8492	0.0000	1158.6807	1925.6385
13.68_303.0838m/z	N-Acetylaspartylglutamic acid	C11H16N2O8	303.0838	40.4	1.2661	-0.72	95.91	Infinity	100 - 9.73 - 1.34	1350.8245	0.0000	42.3124	1669.5926
9.38_188.0565m/z	N-Acetylglutamate	C7H11NO5	188.0565	39.2	-2.7353	-0.46	91.26	Infinity	100	777.4857	0.0000	561.4609	1148.7842
12.99_346.0563m/z	3'-AMP	C10H14N5O7	346.0563	40.2	2.9943	-0.44	93.41	Infinity	100 - 7.91	0.0000	0.0000	575.2172	1016.9781
10.09_147.0299m/z	Citramalic acid	C5H8O5	147.0299	40.9	0.1929	-0.66	98.51	Infinity	100 - 4.59 - 0.666	7.2921	0.0000	676.7164	1015.6648
4.11_128.0353m/z	1-Pyrroline hydroxycarboxylic acid	C5H7NO3	128.0353	39.7	0.1813	-0.37	93.81	Infinity	100 - 0.127	240.8542	0.0000	553.5983	823.4444
12.58_129.0107m/z	Fluorouracil	C4H3FN2O2	129.0107	40	0.9455	-0.99	95.70	Infinity	100 - 1.14	0.0000	0.0000	478.6606	688.7588
16.34_173.0090m/z	cis-Aconitic acid	C6H6O6	173.0090	40.4	-0.8681	-1.78	98.94	Infinity	100 - 6.16 - 0.909	602.5406	358.5241	28.8839	0.0000
8.25_206.0823m/z	N-Acetyl-L-phenylalanine	C11H13NO3	206.0823	39.9	0.1457	-0.64	94.17	Infinity	100 - 7.32	411.0924	0.0000	202.7673	550.4816
11.59_259.0224m/z	Fructose 6-phosphate	C6H13O9P	259.0224	41.9	-0.2616	-0.29	95.82	Infinity	100 - 4.61	78.5250	0.0000	263.9428	523.4949
9.48_174.0408m/z	N-Acetyl-aspartate	C6H9NO5	174.0408	40.4	-0.2443	-0.55	95.40	Infinity	100 - 3.41	0.0000	0.0000	246.1352	501.0551
4.86_103.0401m/z	3-Hydroxyisobutyric acid	C4H8O3	103.0401	41.5	-0.1444	-0.18	97.48	Infinity	100 - 2.57	81.7828	0.0000	175.1854	487.6334
14.18_259.0225m/z	Mannose 6-phosphate	C6H13O9P	259.0225	39.8	0.1025	1.45	95.42	Infinity	100 - 2.2 - 2.15	466.6049	76.8919	0.0000	20.2257
4.56_75.0087m/z	Glycolic acid	C2H4O3	75.0087	40.1	-0.6941	-0.68	98.35	Infinity	100 - 1.05 - 0.202	199.1426	0.0000	393.1581	456.8072
19.36_338.9894m/z	Fructose 2,6 diphosphate	C6H14O12P2	338.9894	38.5	1.9820	1.84	90.93	Infinity	100	0.0000	272.0581	225.2918	455.3749
8.97_259.0224m/z	Galactose 1-phosphate	C6H13O9P	259.0224	40.7	-0.1441	-0.42	95.08	Infinity	100 - 3.8	31.4569	0.0000	383.2889	221.2667
16.93_166.9752m/z	Phosphoenolpyruvic acid	C3H5O6P	166.9752	40.3	0.3162	-1.03	95.41	Infinity	100	0.0000	0.0000	0.0000	297.1804
10.29_209.0304m/z	Galactaric acid (mucic acid)	C6H10O8	209.0304	40.4	0.3017	-0.65	96.08	Infinity	100 - 4.6	0.0000	0.0000	185.4861	288.4710
10.09_131.0350m/z	Glutaric acid	C5H8O4	131.0350	40.8	-0.0702	-0.78	98.57	Infinity	100 - 4.56 - 0.514	141.4625	0.0000	155.4678	285.3380
4.37_158.0823m/z	N-Acetylvaline	C7H13NO3	158.0823	40	-0.0933	-0.46	96.20	Infinity	100 - 4.97	0.0000	0.0000	112.7476	259.6049
4.20_195.0509m/z	Gluconate	C6H12O7	195.0509	20.6	-0.5238	-0.47		Infinity	100 - 6.62 - 1.41	0.0000	0.0000	164.7435	231.2022
2.77_503.1615m/z	Raffinose	C18H32O16	503.1615	44.8	-0.5682	-0.03	95.54	Infinity	100 - 19.1 - 1.9	158.4936	0.0000	198.7729	188.3138
10.99_165.0557m/z	3-methoxyphenylacetic acid	C9H10O3	165.0557	39.5	-0.1985	0.95	93.71	Infinity	100 - 4.04	0.0000	0.0000	102.6425	192.3086
5.68_101.0243m/z	Acetoacetate	C4H6O3	101.0243	39.8	-0.6959	0.54	96.18	Infinity	100 - 1.19	26.1521	0.0000	94.0819	182.4125
15.65_154.9752m/z	Phosphoglycolic acid	C2H5O6P	154.9752	41.3	0.8300	-0.67	98.52	Infinity	100 - 2.17	0.0000	0.0000	145.7035	61.0106

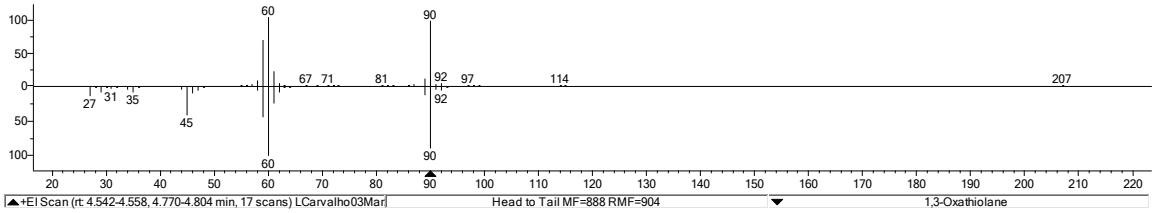
Pompeii INV10653 Interior

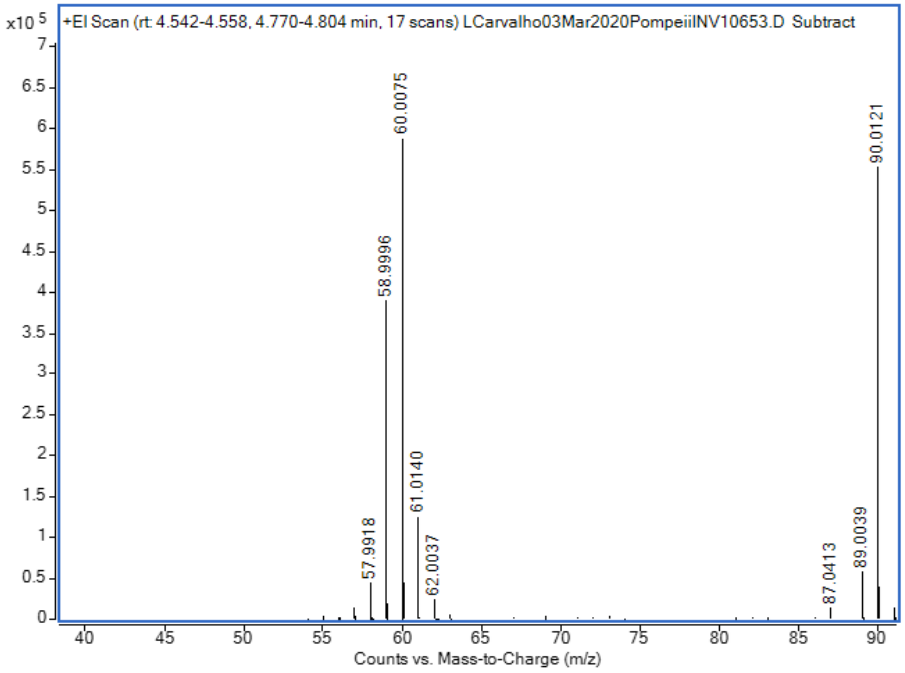
Name	Formula	PDF Number	FOM	%
Azurite	C2 H2 Cu3 O8	00-900-7013	0.709	100.00

Peak List Serial	2theta [°]	d [Å]	I/I0		Peak List Serial	2theta [°]	d [Å]	I/I0
1	7.10	12.4453	28.991		72	47.92	1.8967	95.853
2	7.56	11.6765	35.591		73	48.11	1.8899	30.557
3	8.33	10.6011	27.074		74	48.46	1.8770	56.587
4	8.58	10.2921	31.964		75	49.53	1.8389	103.859
5	12.06	7.3324	28.209		76	49.73	1.8320	95.796
6	14.03	6.3061	26.140		77	49.94	1.8245	253.816
7	14.80	5.9803	55.298		78	50.04	1.8211	173.169
8	14.90	5.9403	61.040		79	50.71	1.7987	36.743
9	17.04	5.1991	106.882		80	50.96	1.7904	135.912
10	17.21	5.1490	534.415		81	51.11	1.7855	165.322
11	17.46	5.0756	336.579		82	51.83	1.7624	14.980
12	17.68	5.0137	187.166		83	51.88	1.7608	23.438
13	17.96	4.9350	41.914		84	52.08	1.7545	6.954
14	18.84	4.7051	26.204		85	52.60	1.7384	38.597
15	18.98	4.6722	35.804		86	52.74	1.7344	40.852
16	20.05	4.4253	30.073		87	53.24	1.7192	45.902
17	20.82	4.2636	30.234		88	53.54	1.7102	27.263
18	20.98	4.2300	24.676		89	53.74	1.7043	38.485
19	21.57	4.1166	23.506		90	54.04	1.6956	84.943
20	22.02	4.0333	29.324		91	54.27	1.6888	47.267
21	23.04	3.8571	32.102		92	54.57	1.6802	46.291
22	23.41	3.7973	73.906		93	54.72	1.6759	53.003
23	24.21	3.6733	600.352		94	55.04	1.6670	19.101
24	25.25	3.5248	1000.000		95	55.63	1.6509	17.946
25	26.05	3.4181	21.954		96	55.86	1.6445	41.206
26	27.22	3.2738	49.325		97	56.29	1.6328	41.731
27	27.67	3.2214	54.972		98	57.03	1.6135	37.332
28	28.39	3.1415	37.849		99	57.15	1.6105	45.797
29	28.69	3.1092	138.872		100	57.23	1.6083	57.375
30	29.49	3.0264	36.725		101	57.43	1.6032	67.752
31	29.61	3.0147	31.648		102	57.77	1.5947	343.579
32	30.11	2.9657	43.222		103	57.88	1.5918	208.523
33	30.61	2.9182	131.842		104	58.13	1.5855	33.554
34	30.89	2.8920	54.473		105	58.45	1.5776	31.796
35	31.09	2.8738	132.321		106	58.85	1.5678	97.284
36	31.19	2.8648	140.369		107	58.95	1.5654	55.578
37	31.31	2.8544	165.423		108	59.22	1.5590	52.714
38	31.38	2.8485	133.649		109	59.37	1.5554	53.546
39	31.60	2.8294	113.516		110	59.50	1.5522	59.169
40	31.83	2.8091	131.154		111	60.41	1.5312	48.737
41	32.31	2.7681	52.437		112	60.66	1.5254	99.410
42	32.50	2.7528	42.895		113	60.81	1.5220	65.552
43	34.55	2.5936	129.145		114	60.97	1.5183	65.125
44	35.29	2.5413	346.324		115	61.14	1.5145	196.832
45	35.76	2.5091	529.460		116	61.29	1.5112	164.664
46	36.22	2.4777	68.578		117	61.43	1.5082	193.005
47	36.44	2.4635	402.049		118	61.56	1.5052	103.437
48	37.36	2.4049	26.510		119	62.33	1.4885	33.405

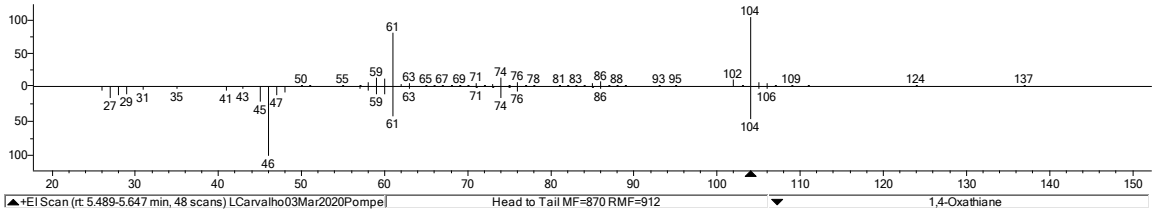
Peak List Serial	2theta [°]	d [Å]	I/I0		Peak List Serial	2theta [°]	d [Å]	I/I0
49	38.53	2.3346	249.890		120	62.56	1.4835	42.622
50	39.13	2.3001	87.863		121	62.81	1.4782	144.583
51	39.38	2.2860	321.424		122	63.60	1.4618	59.999
52	39.78	2.2639	241.906		123	63.90	1.4556	39.436
53	40.10	2.2467	115.249		124	64.33	1.4469	36.402
54	40.47	2.2271	366.597		125	64.85	1.4365	38.117
55	41.59	2.1697	111.068		126	65.15	1.4306	132.177
56	42.34	2.1329	105.448		127	65.27	1.4284	93.258
57	42.94	2.1044	68.049		128	65.65	1.4209	40.257
58	43.08	2.0982	59.091		129	65.85	1.4171	92.560
59	43.28	2.0889	80.796		130	66.04	1.4136	54.811
60	43.61	2.0737	20.640		131	66.46	1.4057	53.284
61	44.11	2.0513	31.760		132	67.14	1.3930	66.009
62	44.50	2.0344	33.776		133	67.29	1.3903	85.404
63	45.03	2.0115	56.521		134	67.44	1.3875	88.898
64	45.35	1.9982	28.023		135	67.78	1.3815	76.826
65	45.68	1.9843	30.997		136	67.98	1.3779	46.917
66	45.98	1.9720	30.048		137	68.16	1.3746	66.126
67	46.62	1.9466	385.511		138	68.38	1.3708	45.443
68	46.72	1.9427	272.651		139	69.10	1.3583	87.947
69	47.04	1.9303	37.656		140	69.41	1.3529	94.170
70	47.59	1.9092	37.930		141	69.56	1.3503	56.253
71	47.86	1.8992	86.200					

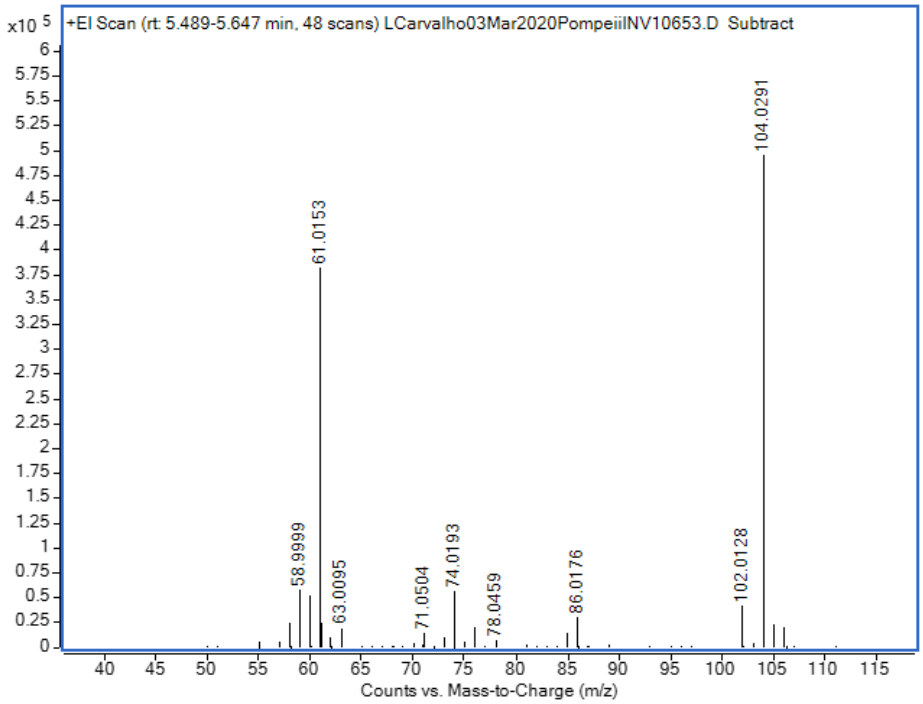
[1] 1,3-Oxathiolane Mass: 90.013936



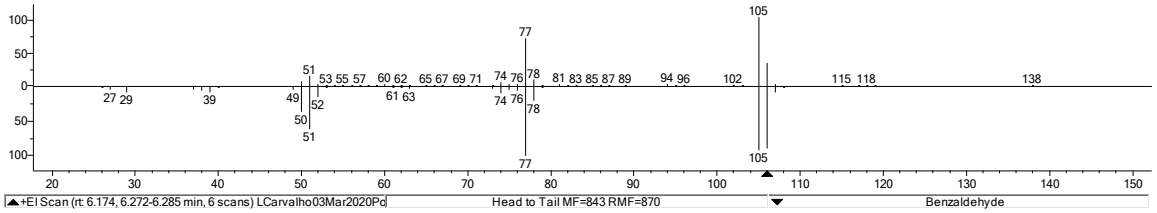


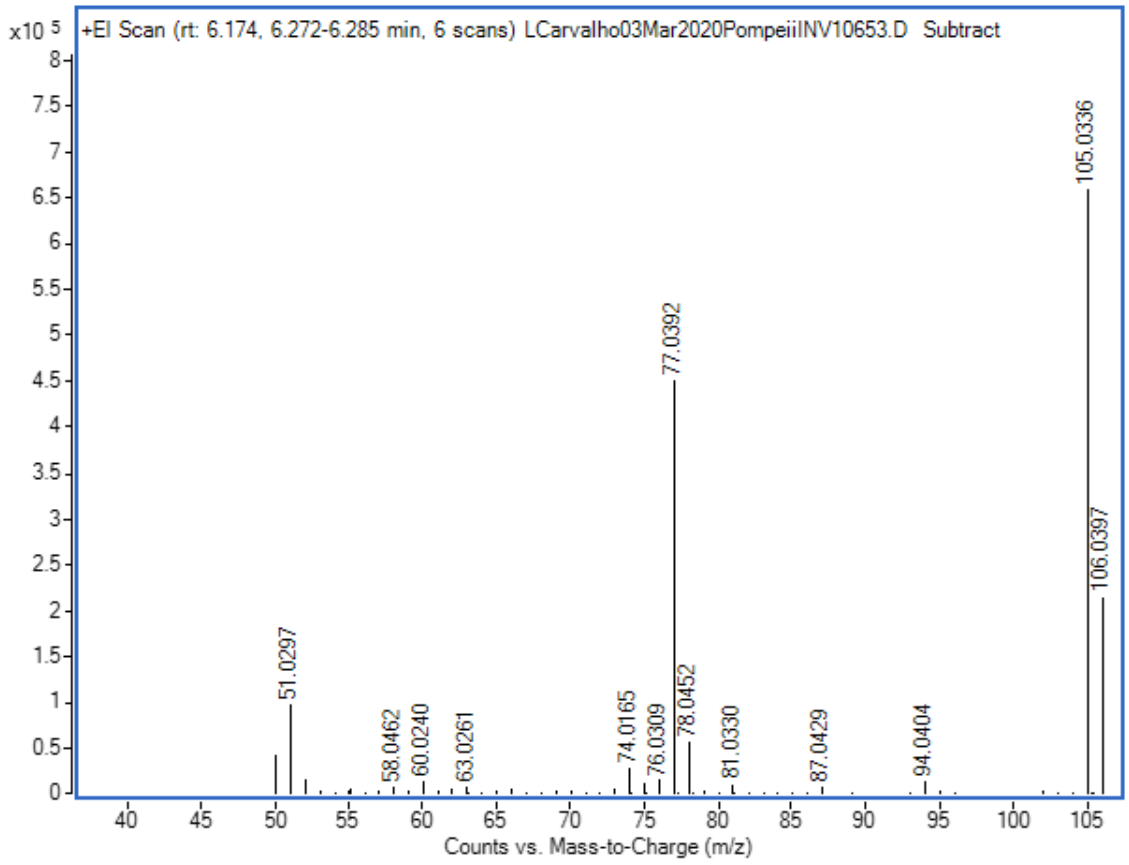
[2] 1,4-Oxathiane Mass: 104.029586





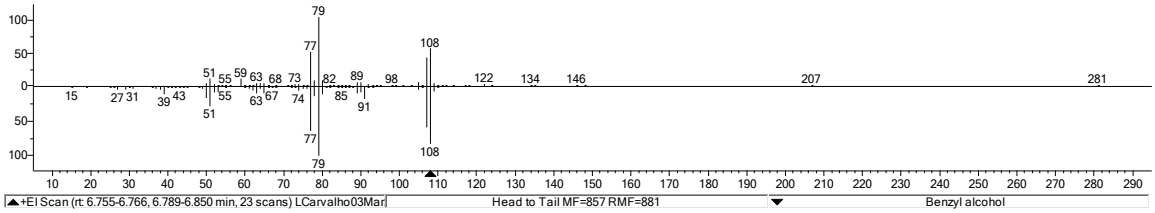
[3] Benzaldehyde Mass: 106.041865

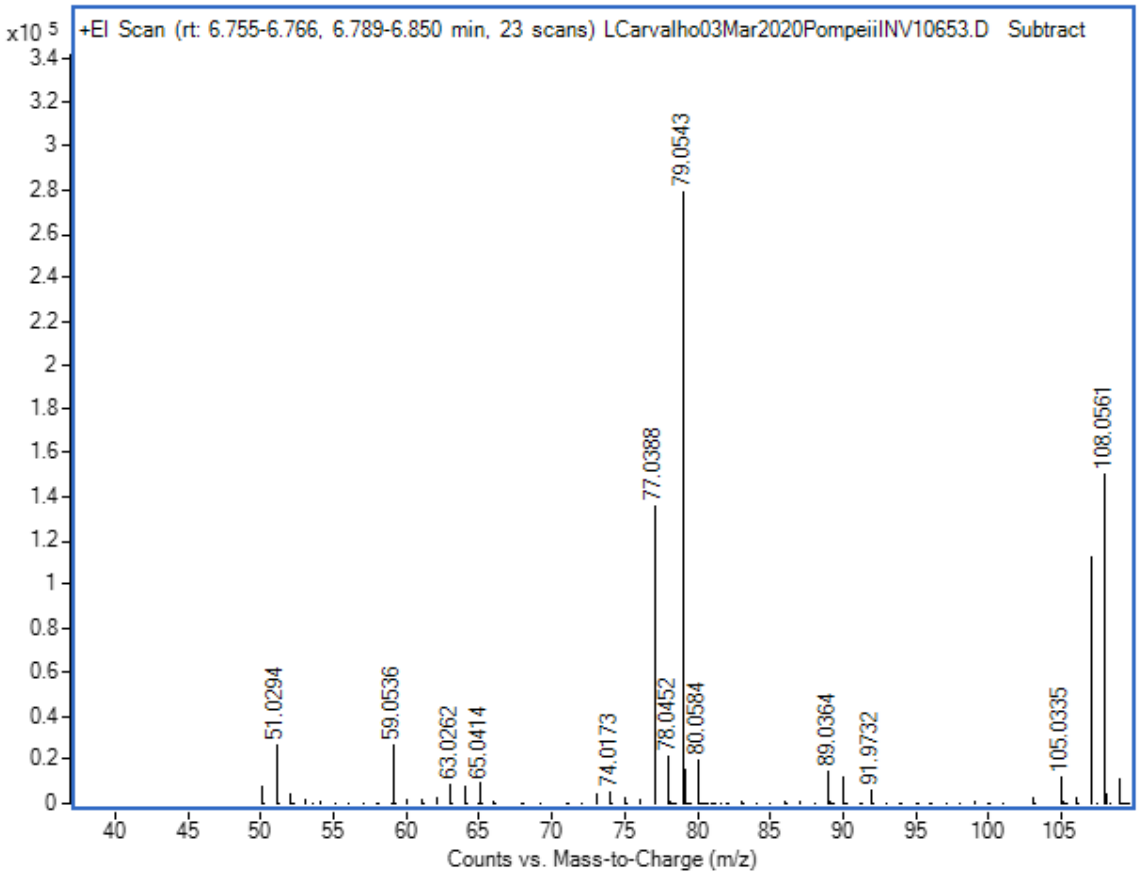




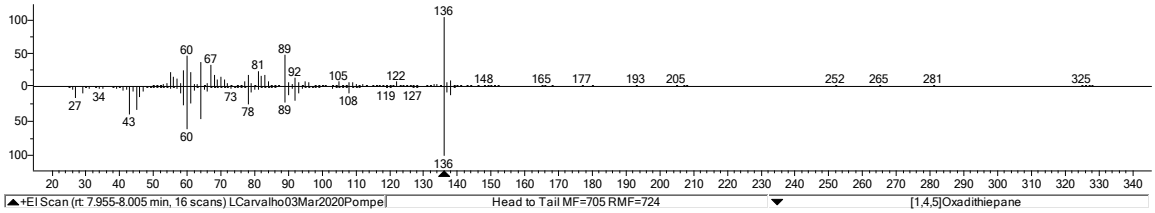
[

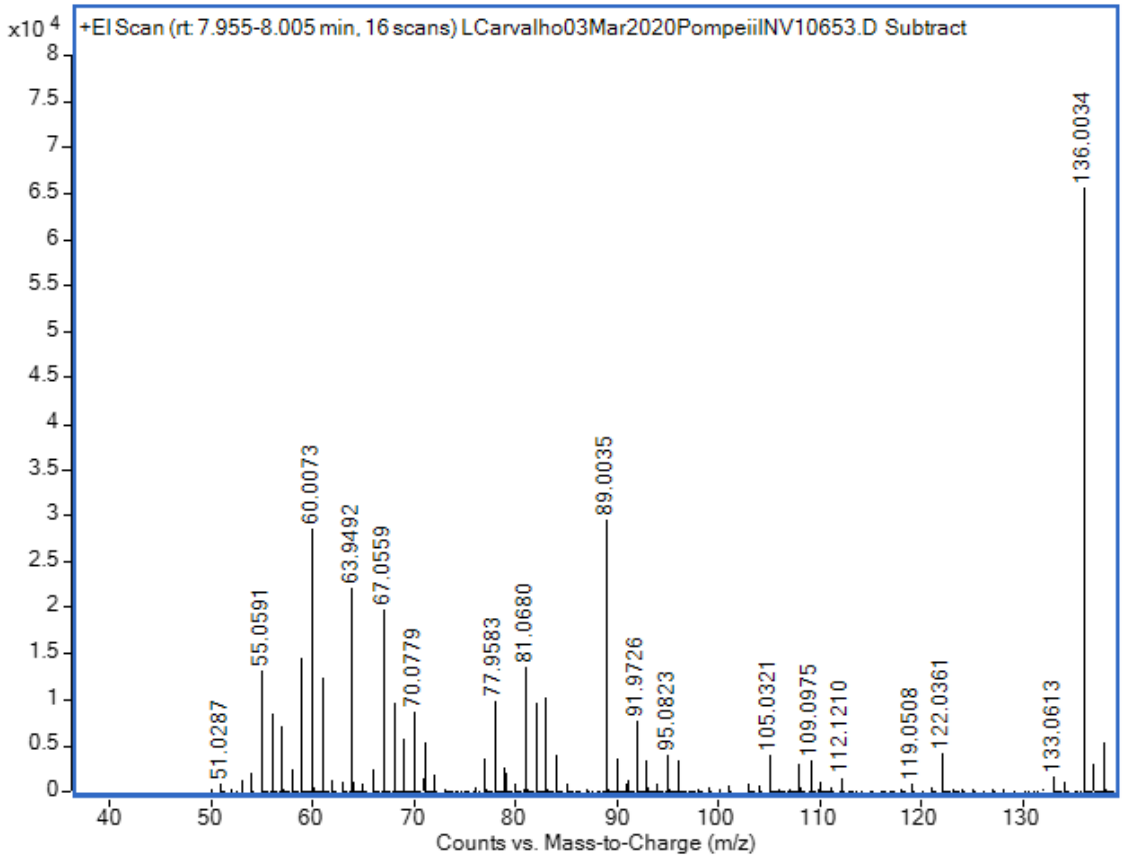
4] Benzyl alcohol Mass: 108.0575147



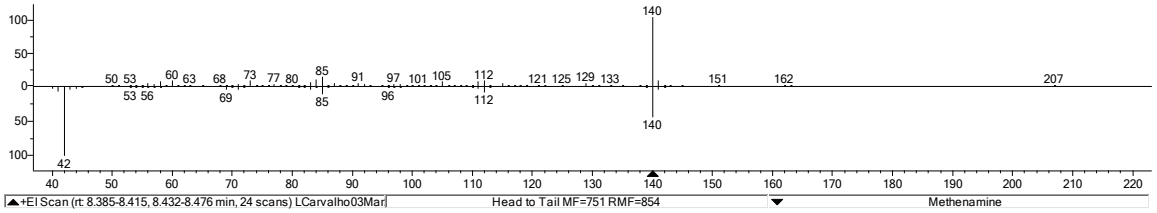


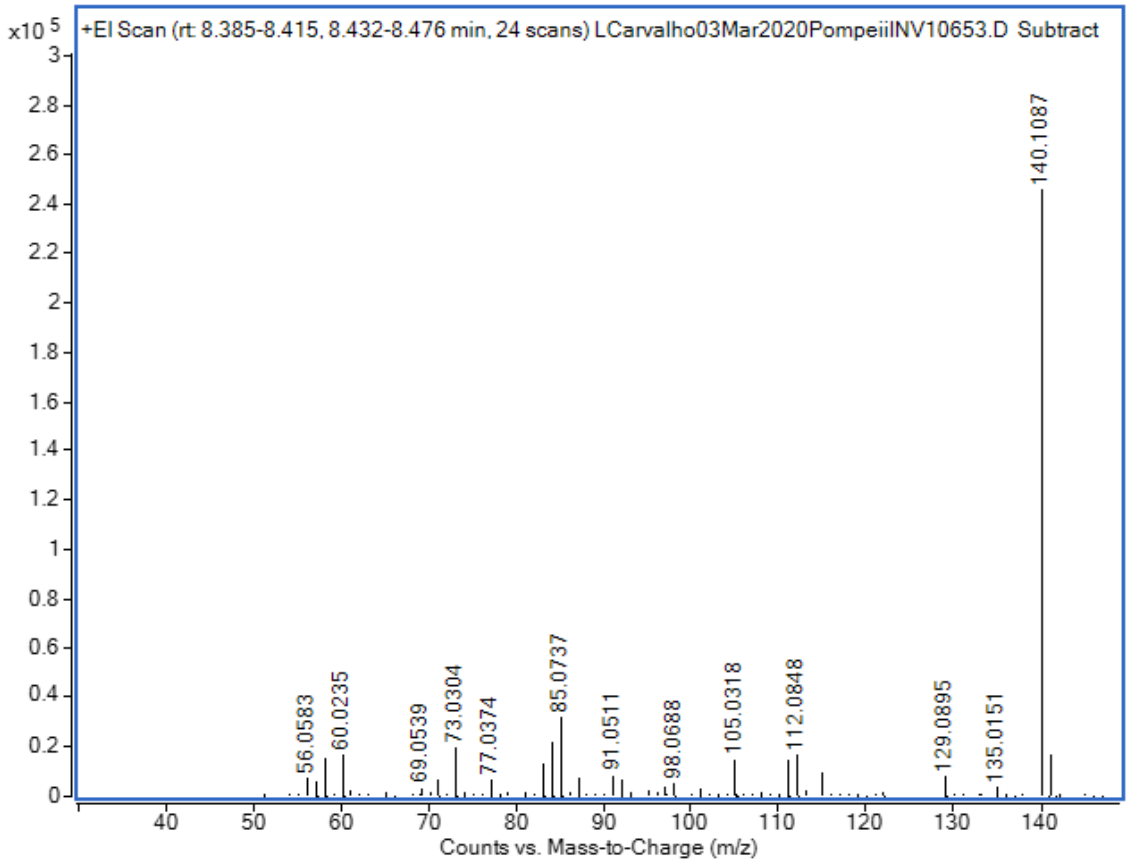
[5] 1,4,5 Oxadithiepane Mass: 136.001657



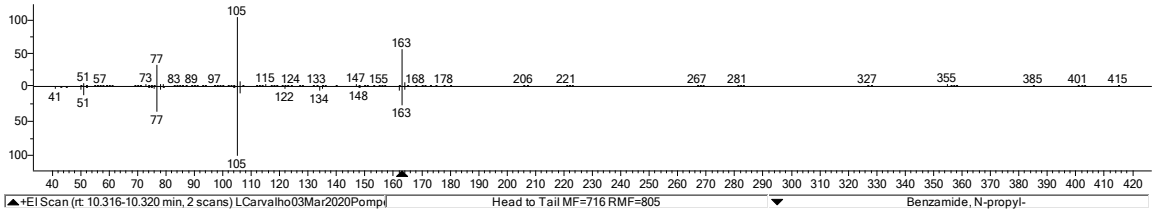


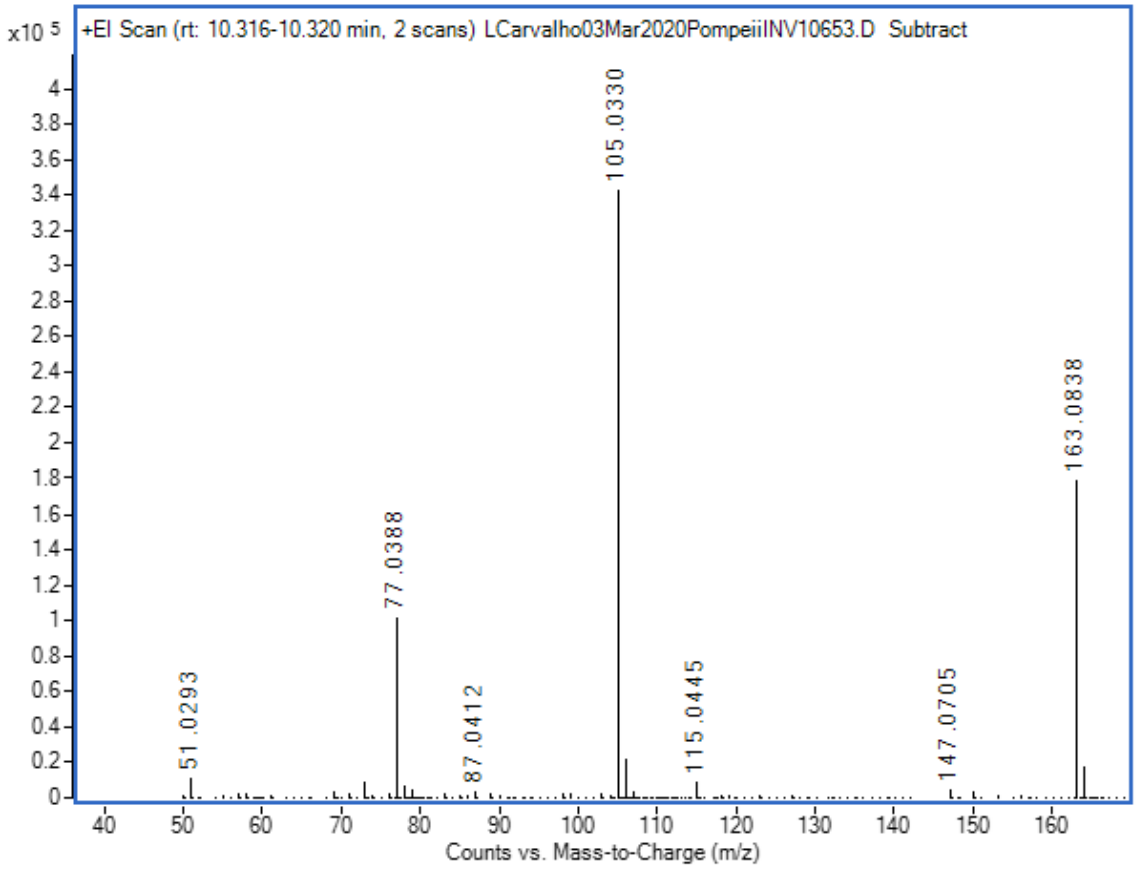
[6] Methenamine Mass: 140.106196



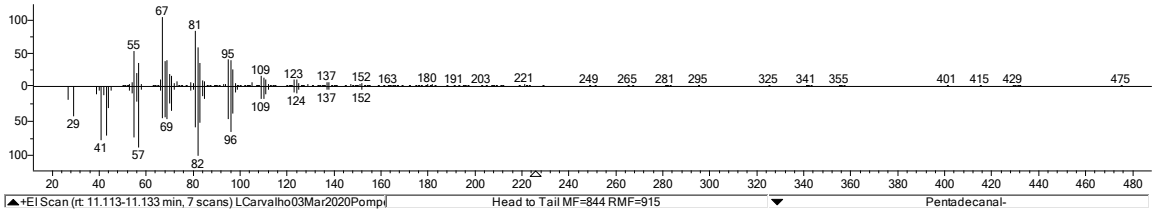


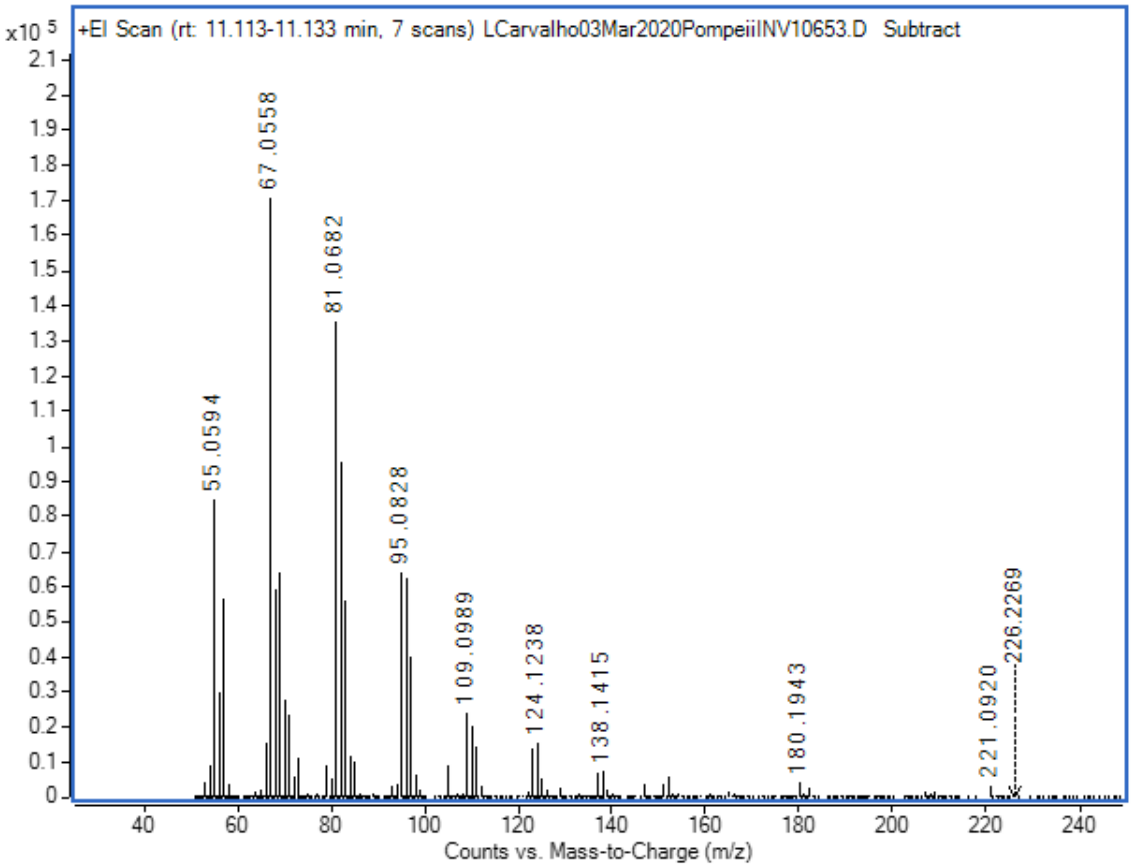
[7] Benzamide, N-propyl- Mass: 163.099714



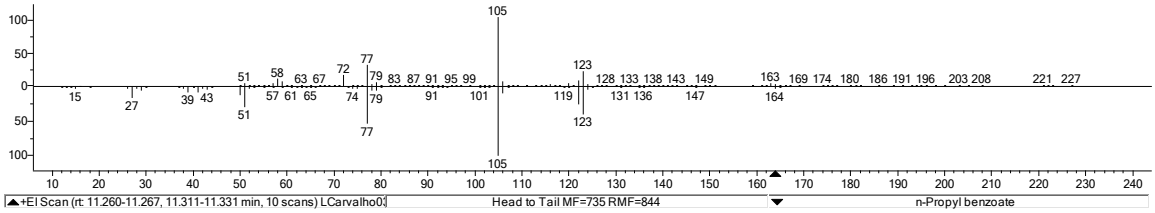


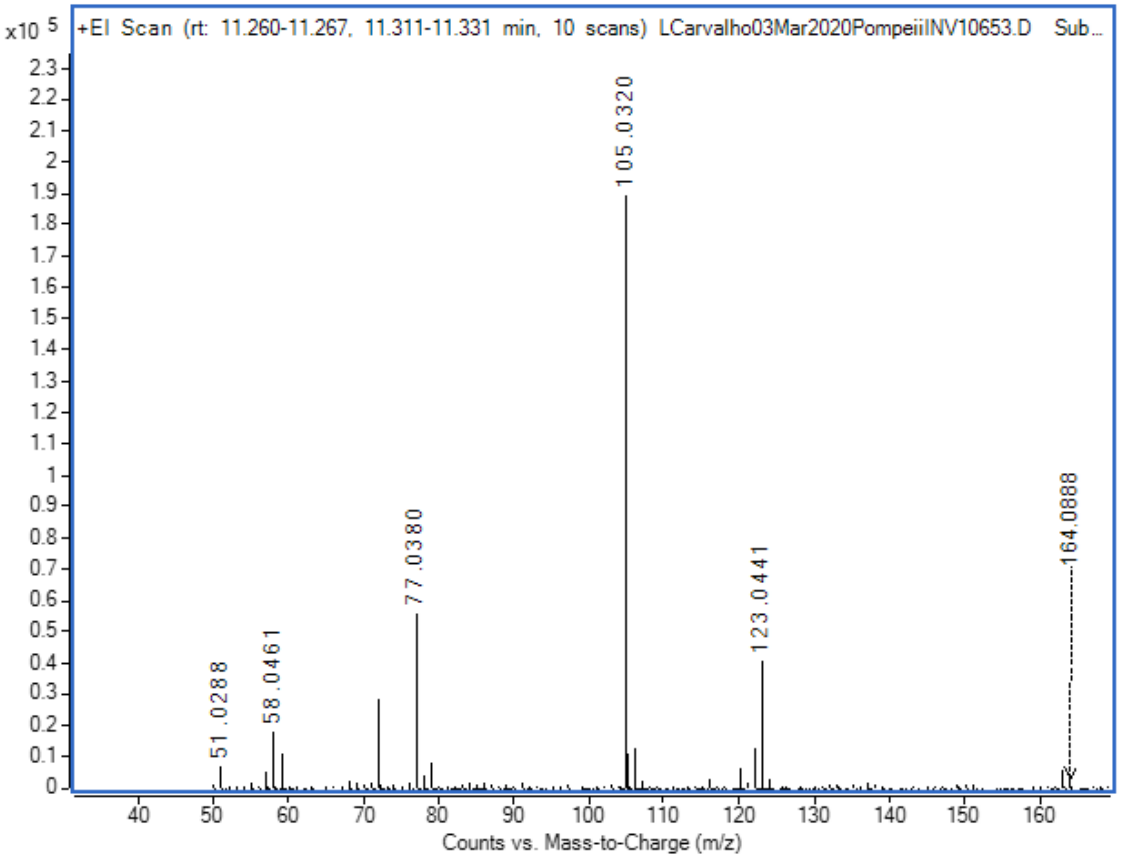
[8] Pentadecanal-



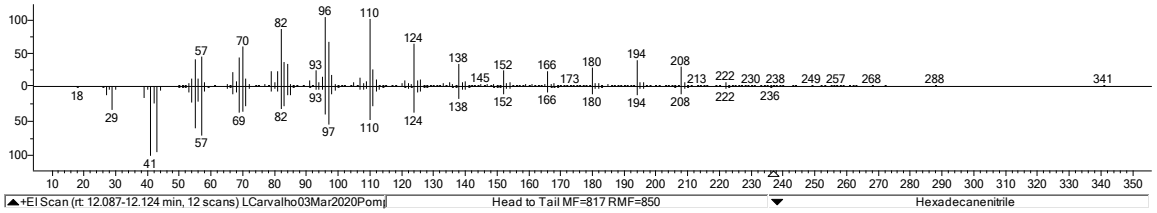


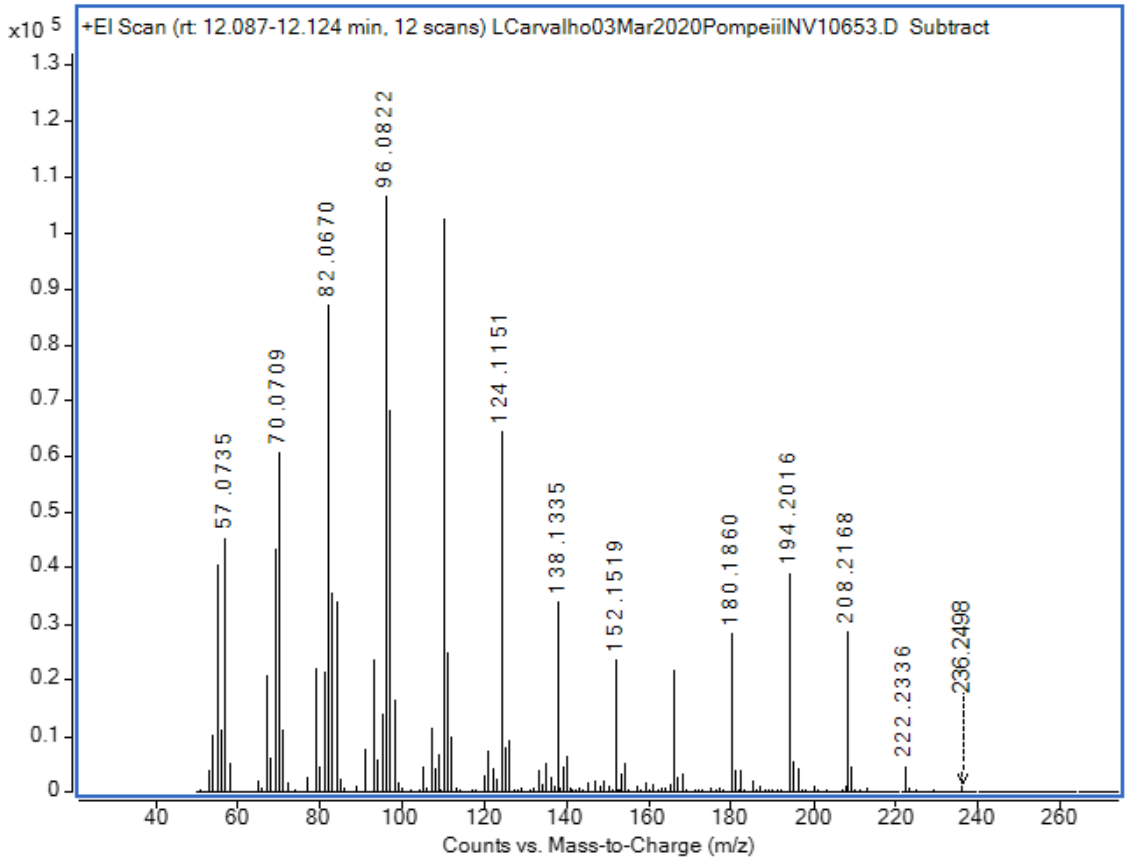
[9] n-Propyl benzoate Mass: 164.08373 NIST#: 342339



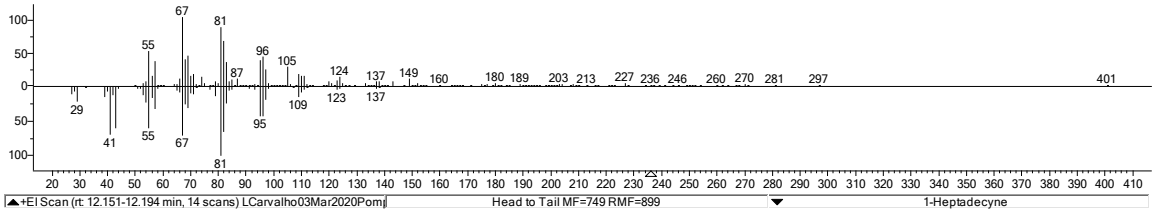


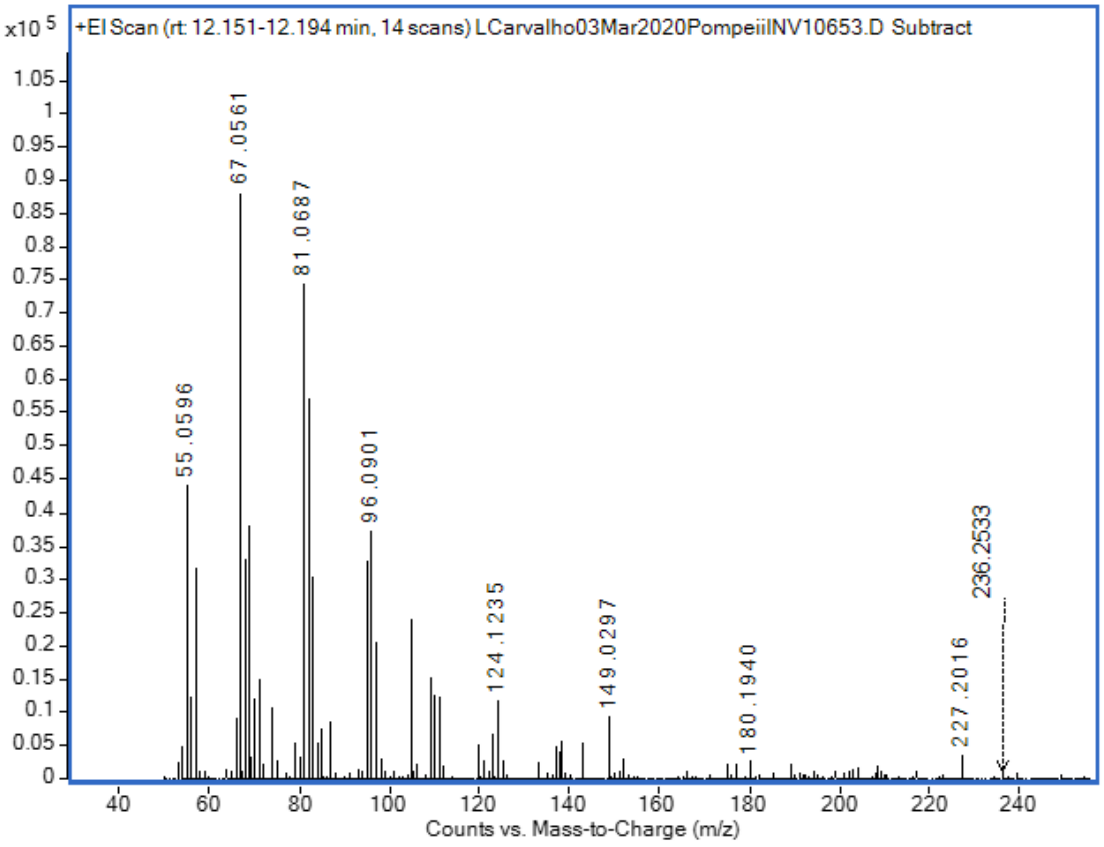
[10] Hexadecanenitrile Mass: 237.24565



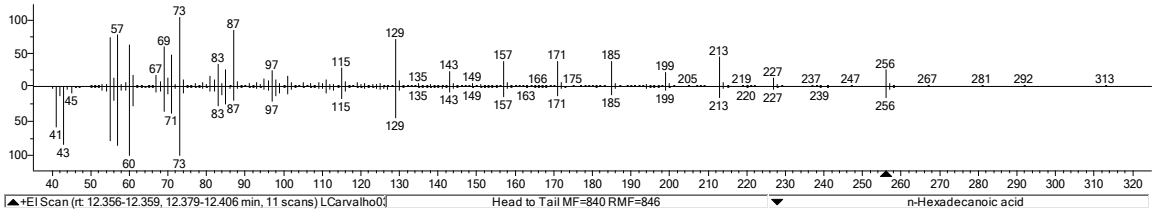


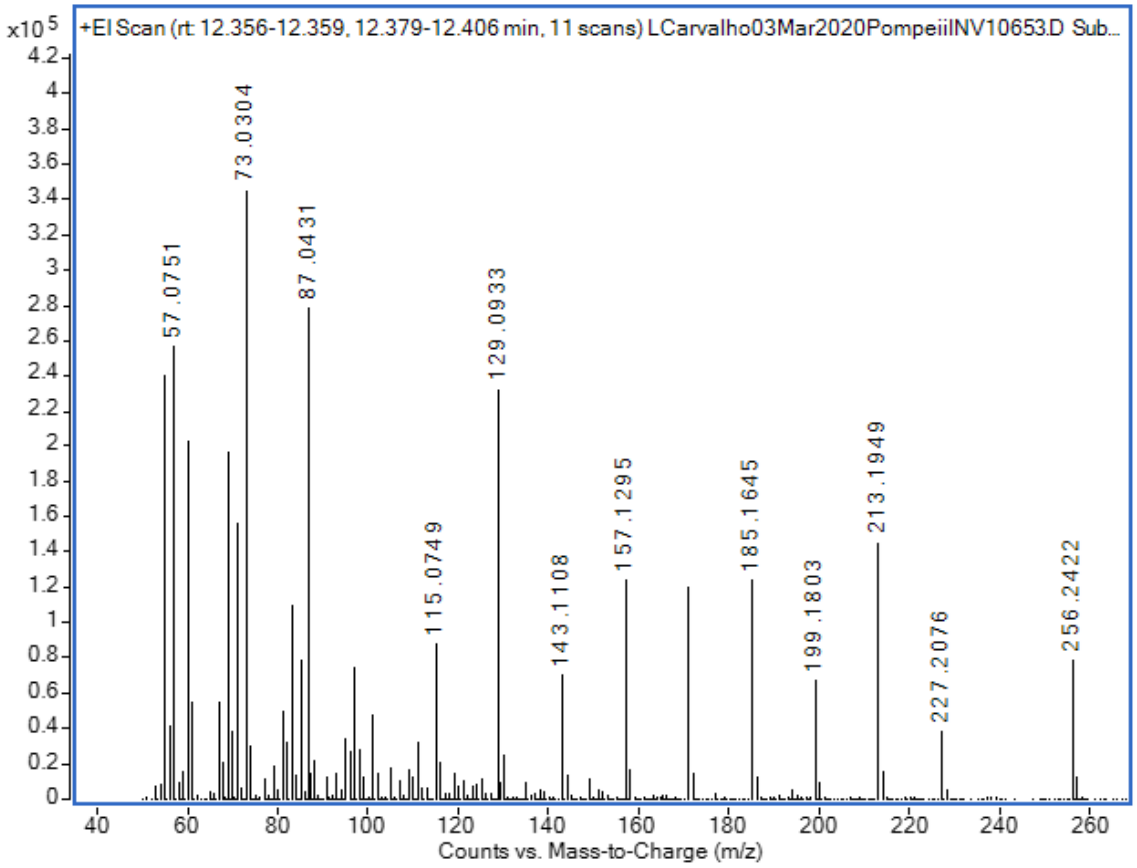
[11] 1-Heptadecyne Mass: 236.2504015



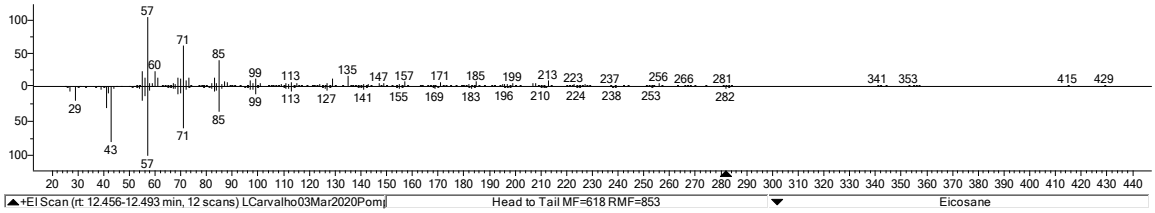


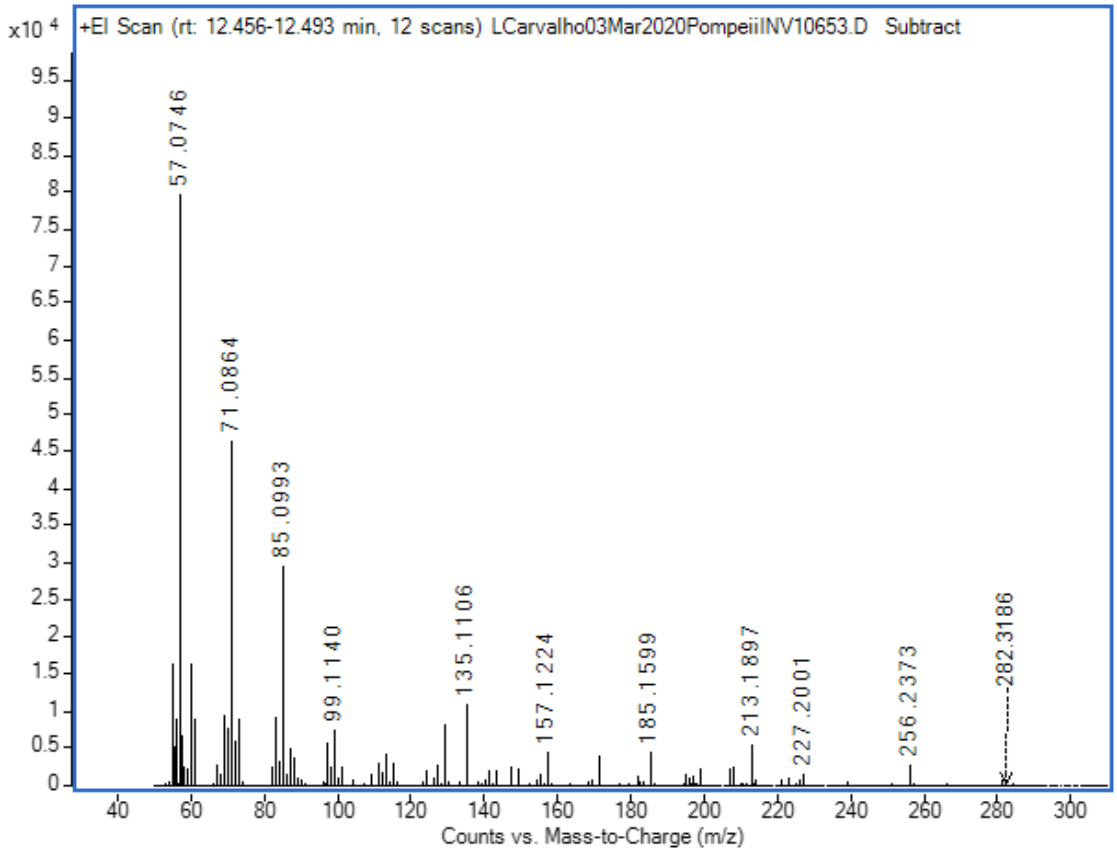
[12] n-Hexadecanoic acid



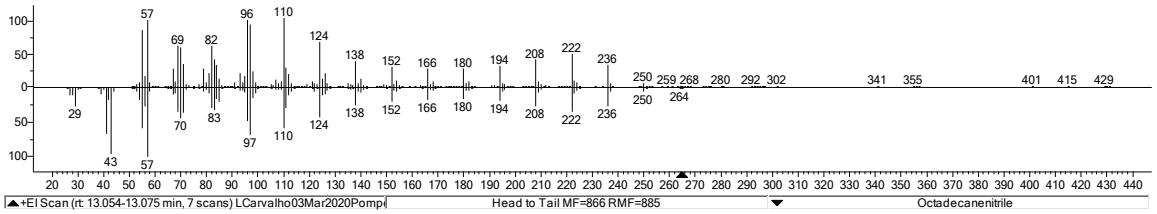


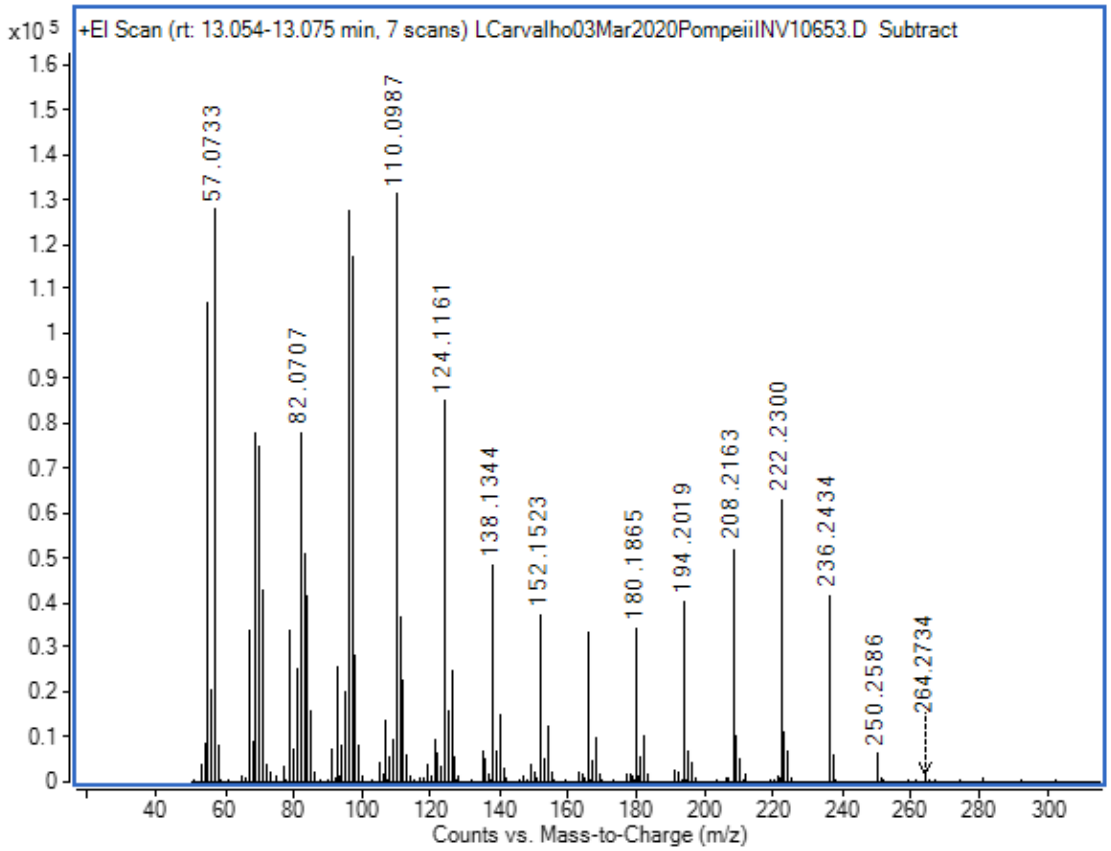
[13] Eicosane Mass: 282.328651



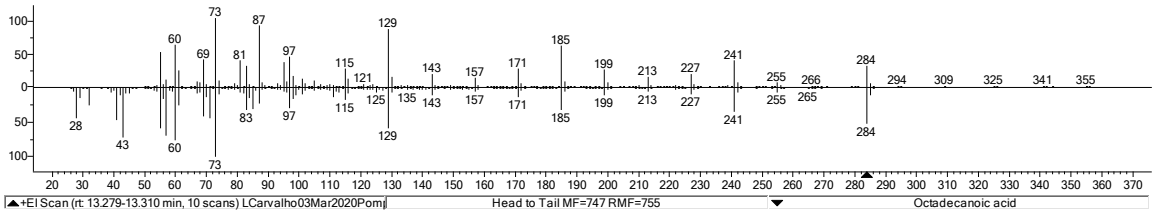


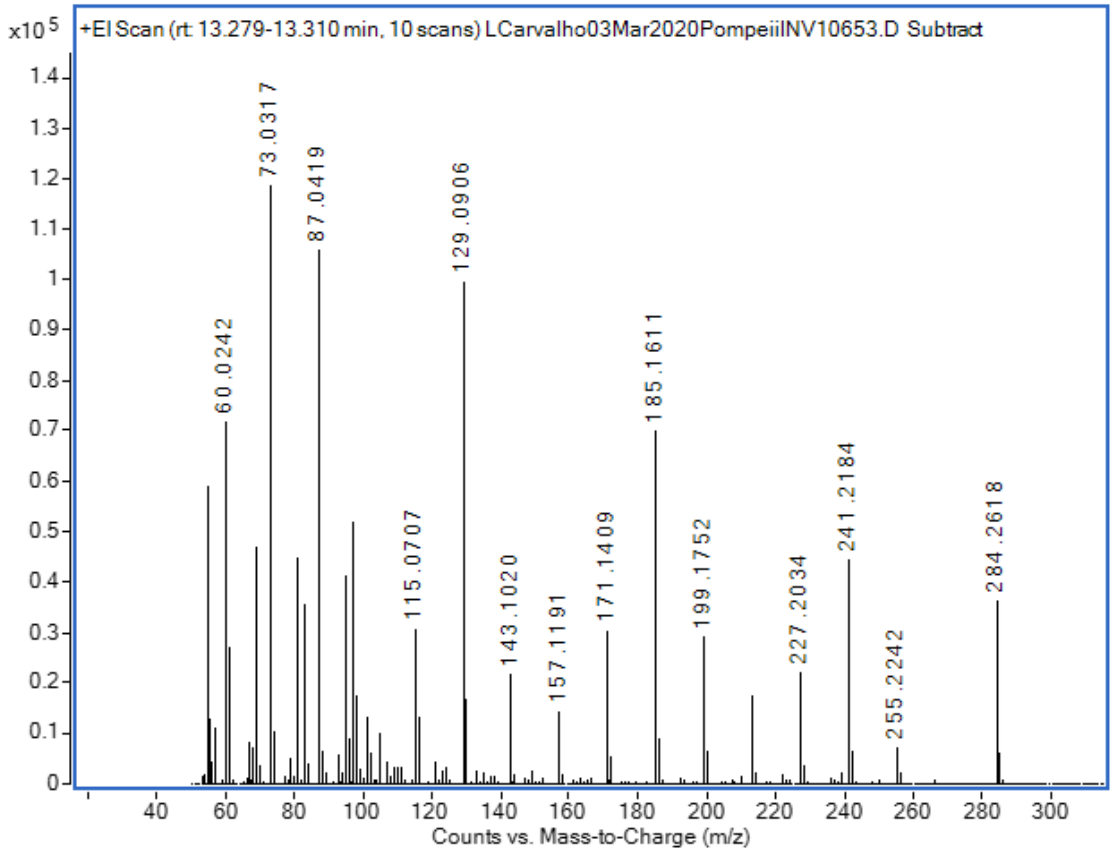
[14] Octadecanenitrile Mass: 265.27695



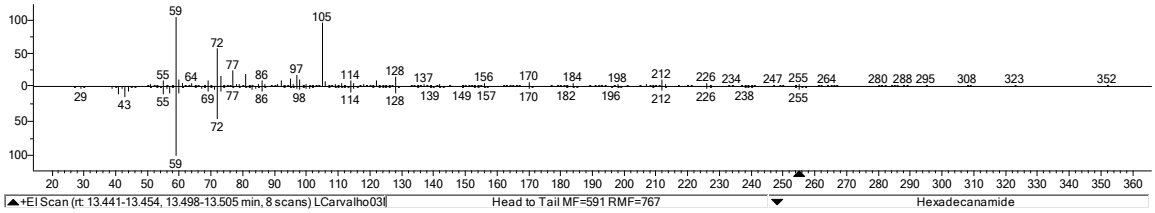


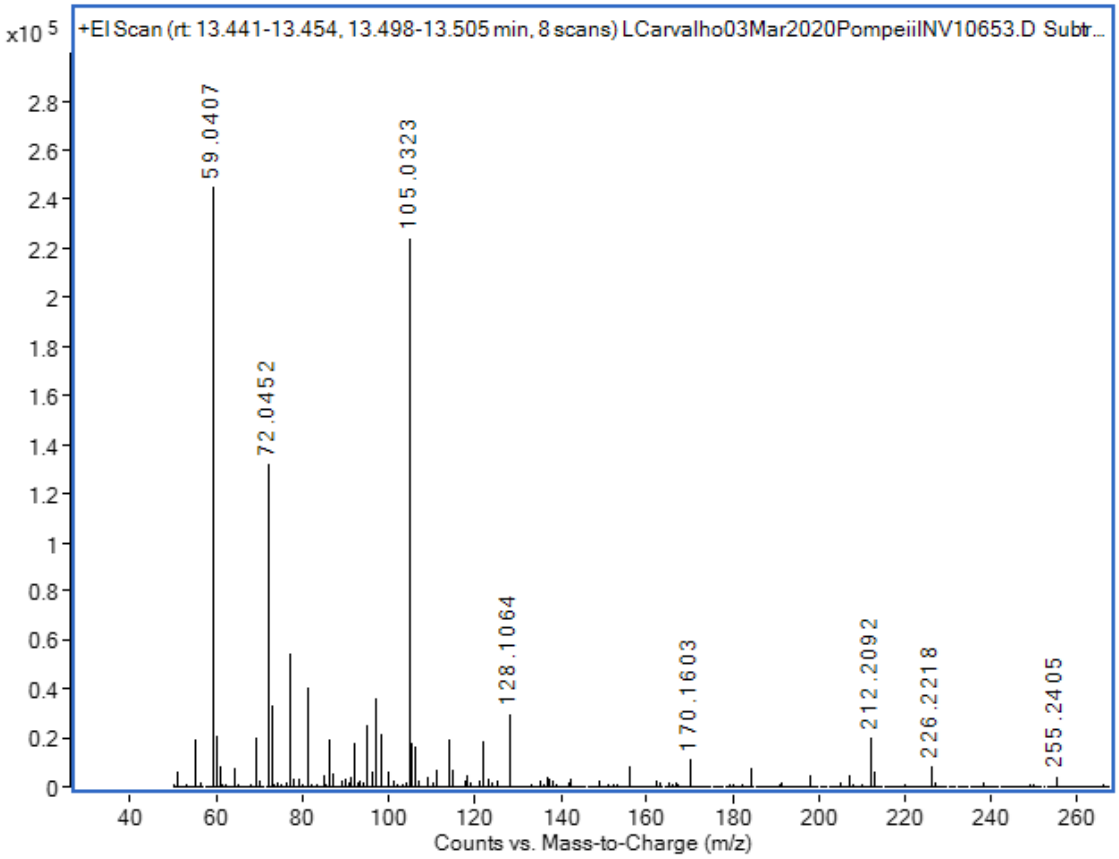
[15] Octadecanoic acid



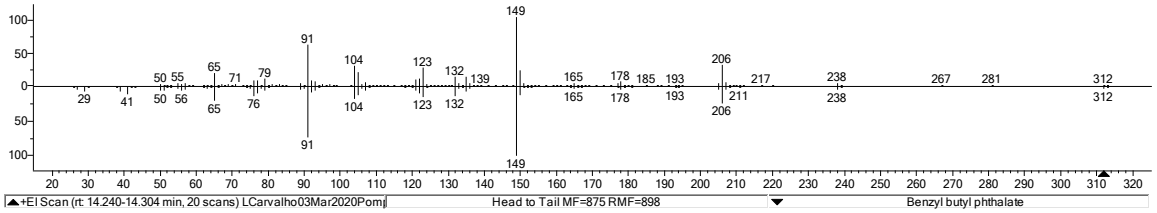


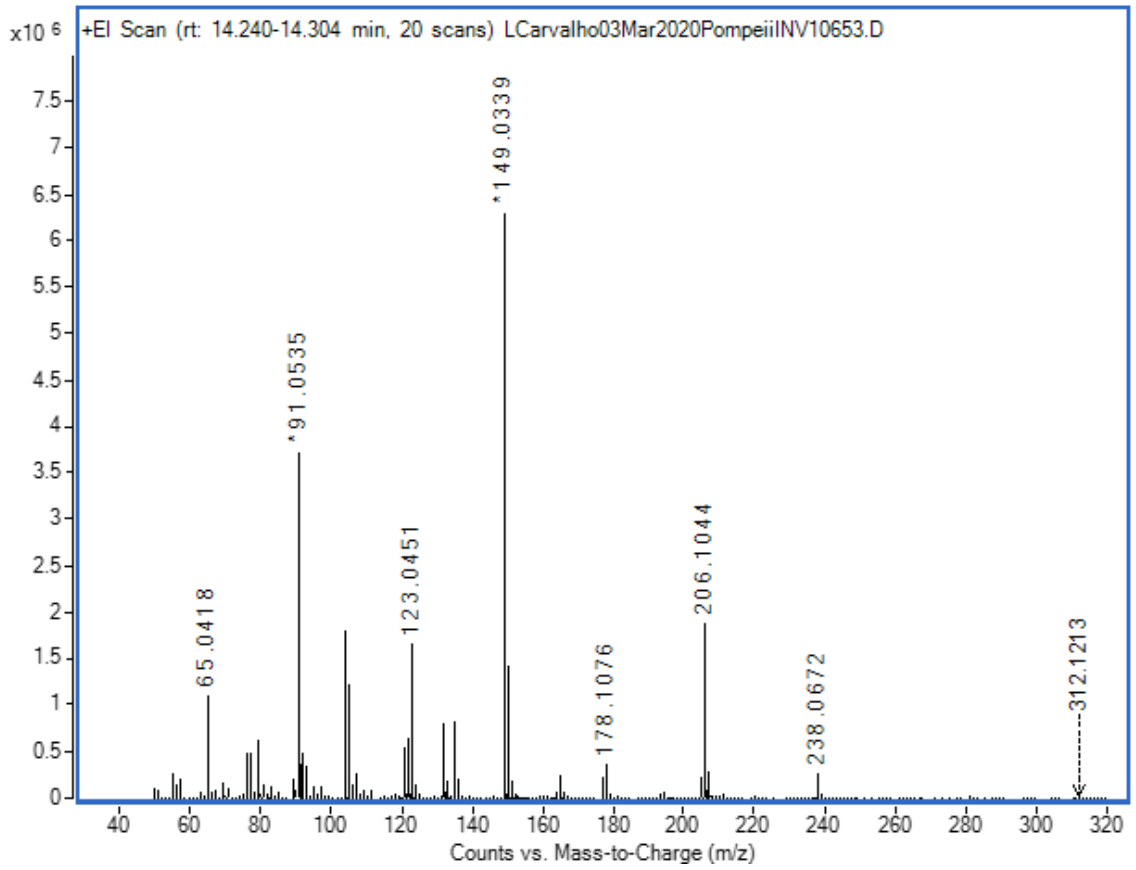
[16] Hexadecanamide Mass: 255.256215





[17] Benzyl butyl phthalate Mass: 312.13616





Compound	Name	Formula	m/z	Score	Mass Error (ppm)	RT Error (min)	Isotope Similarity (ppm)	Maximum Fold Change	Isotope Distribution	Normalised abundance 10653.00	6515.00	6515s	10268s
8.24_71.0138m/z	Malondialdehyde	C3H4O2	71.0138	40.4	-1.4256	-0.62	98.45	35.87	100 - 2.21	535.64	32.63	39.20	14.93
10.78_165.0557m/z	3-methoxyphenylacetic acid	C9H10O3	165.0557	39	-0.253	0.74	90.07	7.68	100	345.04	57.86	134.06	44.94
12.61_115.0037m/z	Maleic acid	C4H4O4	115.0037	47.8	0.3322	0.18	94.85	5.6	100	264.16	76.90	66.71	47.18
10.00_161.0456m/z	3-Hydroxymethylglutarate	C6H10O5	161.0456	39.6	0.1826	-0.76	92.58	4.71	100	793.10	636.48	740.12	168.42
5.56_101.0244m/z	Acetoacetate	C4H6O3	101.0244	39.9	-0.2894	0.42	95.05	4.68	100	1143.95	267.88	260.58	244.37
3.67_100.0404m/z	4-Hydroxypyrrolidinone	C4H7NO2	100.0404	39.3	0.2214	0.73	94.92	4.42	100	131.96	81.90	57.66	29.86
13.96_115.0037m/z	Fumarate	C4H4O4	115.0037	41.8	0.318	0.33	94.85	3.14	100	103.74	33.01	48.35	43.45
12.70_129.0107m/z	Fluorouracil	C4H3FN2O2	129.0107	39.9	0.9451	-0.87	94.62	2.83	100	250.55	134.04	107.33	88.44
9.61_101.0244m/z	2-Ketobutyric acid	C4H6O3	101.0244	39.3	-0.3377	1.75	95.05	2.54	100	227.28	107.15	130.39	89.50
12.51_88.9880m/z	Oxalic acid	C2H2O4	88.988	40.7	0.1356	-0.89	97.72	2.44	100 - 0.828	1998.27	1216.28	1475.43	817.79
19.02_143.1078m/z	Octanoic acid	C8H16O2	143.1078	40.9	0.276	-0.93	96.82	2.17	100 - 6.18	5606.16	3284.40	5515.04	2583.32
10.20_129.0194m/z	Gamma-delta-Dioxovaleric acic	C5H6O4	129.0194	40.4	0.7848	-0.44	93.83	2.16	100	140.06	64.88	88.33	68.85

Appendix 25Pompeii INV10653: IC-MS Results

Sample 4

Name	Formula	PDF Number	FOM	%
Azurite	C2 H2 Cu3 O8	00-900-7013	0.792	100.00

Peak List Serial	2theta [°]	d [Å]	I/I0		Peak List Serial	2theta [°]	d [Å]	I/I0
1	6.09	14.4905	28.053		53	46.60	1.9473	256.743
2	10.82	8.1673	36.135		54	46.97	1.9329	55.412
3	12.04	7.3426	32.543		55	47.61	1.9086	48.795
4	14.60	6.0620	43.268		56	47.81	1.9011	76.292
5	14.85	5.9602	108.413		57	48.37	1.8800	37.453
6	17.14	5.1689	334.393		58	49.04	1.8560	8.106
7	17.42	5.0853	298.583		59	49.58	1.8372	63.010
8	17.59	5.0373	229.124		60	49.93	1.8251	178.805
9	18.90	4.6927	41.636		61	50.93	1.7915	110.155
10	19.73	4.4958	28.012		62	51.15	1.7844	93.876
11	20.25	4.3819	40.975		63	51.63	1.7688	6.956
12	20.80	4.2670	24.406		64	51.85	1.7619	8.536
13	21.28	4.1709	11.259		65	52.17	1.7519	9.747
14	21.92	4.0515	13.354		66	53.19	1.7207	34.345
15	22.82	3.8933	19.502		67	53.44	1.7132	10.071
16	23.39	3.8000	61.274		68	53.64	1.7073	13.467
17	24.14	3.6833	457.919		69	54.11	1.6936	59.198
18	25.20	3.5317	735.486		70	54.41	1.6850	70.839
19	26.47	3.3651	7.983		71	54.59	1.6797	67.583
20	27.79	3.2081	19.360		72	54.89	1.6712	54.317
21	28.70	3.1074	82.792		73	55.14	1.6642	34.589
22	29.52	3.0231	50.461		74	55.78	1.6468	34.636
23	29.94	2.9818	46.611		75	56.55	1.6262	29.734
24	30.56	2.9229	137.684		76	56.83	1.6187	66.969
25	31.08	2.8753	140.903		77	57.18	1.6096	58.832
26	31.29	2.8559	383.947		78	57.75	1.5951	228.955
27	31.61	2.8279	121.467		79	57.95	1.5901	90.641
28	31.80	2.8120	124.133		80	58.73	1.5707	77.164
29	32.20	2.7779	104.169		81	59.30	1.5570	38.122
30	34.45	2.6010	69.480		82	59.89	1.5432	2.573
31	35.24	2.5448	297.429		83	60.67	1.5251	87.420
32	35.66	2.5159	428.278		84	61.14	1.5145	143.386
33	36.19	2.4799	76.874		85	61.41	1.5086	82.602
34	36.39	2.4667	268.233		86	61.63	1.5038	24.579
35	36.89	2.4344	15.868		87	61.78	1.5005	31.723
36	38.48	2.3375	121.023		88	62.21	1.4910	16.425
37	39.08	2.3029	65.714		89	62.80	1.4785	96.781
38	39.32	2.2897	236.262		90	63.08	1.4726	41.775
39	39.72	2.2675	134.564		91	63.63	1.4611	60.845
40	40.07	2.2485	125.188		92	64.58	1.4418	-0.654
41	40.42	2.2297	201.449		93	65.00	1.4336	63.166
42	41.32	2.1831	60.351		94	65.15	1.4306	73.406
43	41.56	2.1714	76.491		95	65.52	1.4235	44.687
44	42.29	2.1353	120.386		96	65.84	1.4174	67.742
45	42.49	2.1257	86.064		97	66.47	1.4054	37.244
46	42.96	2.1036	41.504		98	67.27	1.3906	76.966
47	43.61	2.0737	45.859		99	67.74	1.3821	83.791
48	43.93	2.0594	61.180		100	68.13	1.3752	34.026
49	44.66	2.0272	13.715		101	68.54	1.3679	-1.063
50	44.81	2.0207	5.347		102	69.21	1.3563	76.122

Peak List Serial	2theta [°]	d [Å]	I/I0		Peak List Serial	2theta [°]	d [Å]	I/I0
51	44.95	2.0150	64.829		103	69.50	1.3514	64.374
52	45.93	1.9741	37.954					

Sample 6

Name	Formula	PDF Number	FOM	%
Malachite	Cu2 (OH)2 (CO3)	00-500-0043	0.751	100.00

Peak List Serial	2theta [°]	d [Å]	I/I0		Peak List Serial	2theta [°]	d [Å]	I/I0
1	8.80	10.0385	13.552		78	46.64	1.9460	84.994
2	8.92	9.9071	18.414		79	46.82	1.9388	64.094
3	11.44	7.7272	17.743		80	47.49	1.9130	37.400
4	11.73	7.5407	20.785		81	47.52	1.9118	28.335
5	11.93	7.4143	31.828		82	47.92	1.8967	93.874
6	12.03	7.3527	39.948		83	48.27	1.8837	15.389
7	14.85	5.9602	290.837		84	48.89	1.8613	28.029
8	17.32	5.1145	44.976		85	49.79	1.8297	40.655
9	17.61	5.0326	534.630		86	49.89	1.8262	42.294
10	18.11	4.8944	16.050		87	50.11	1.8188	20.679
11	18.83	4.7092	59.720		88	50.73	1.7981	77.429
12	19.48	4.5531	14.495		89	50.91	1.7920	66.801
13	19.81	4.4770	12.599		90	51.13	1.7849	23.846
14	20.43	4.3429	15.464		91	51.95	1.7587	17.842
15	21.15	4.1970	13.946		92	52.23	1.7498	12.141
16	21.33	4.1612	17.902		93	53.24	1.7192	3.092
17	21.55	4.1198	12.647		94	53.84	1.7014	31.647
18	22.50	3.9475	15.852		95	54.01	1.6965	43.487
19	22.72	3.9102	9.368		96	54.11	1.6936	63.065
20	24.08	3.6934	708.998		97	54.39	1.6854	54.888
21	25.20	3.5317	16.872		98	54.66	1.6778	102.070
22	25.28	3.5202	18.315		99	54.89	1.6712	59.345
23	26.55	3.3546	16.258		100	55.98	1.6413	7.596
24	26.92	3.3097	42.365		101	56.06	1.6391	19.368
25	27.13	3.2836	13.847		102	56.33	1.6319	19.138
26	27.69	3.2195	18.943		103	56.68	1.6227	12.548
27	27.89	3.1968	17.373		104	56.93	1.6161	65.687
28	28.65	3.1127	14.260		105	57.57	1.5998	23.578
29	28.86	3.0916	14.731		106	58.00	1.5888	75.058
30	29.39	3.0365	108.530		107	58.33	1.5805	17.011
31	29.94	2.9818	109.942		108	58.68	1.5719	56.123
32	30.88	2.8936	63.051		109	59.75	1.5463	15.519
33	31.03	2.8799	148.759		110	60.04	1.5397	19.261
34	31.28	2.8574	360.395		111	60.86	1.5209	39.025
35	31.43	2.8440	182.892		112	60.92	1.5194	39.374
36	31.58	2.8308	99.901		113	61.07	1.5160	37.027
37	31.73	2.8178	81.020		114	61.21	1.5130	37.513
38	31.93	2.8005	45.701		115	61.36	1.5097	36.225
39	32.21	2.7765	153.640		116	61.46	1.5074	35.663
40	34.24	2.6170	15.252		117	61.88	1.4983	45.419
41	34.62	2.5888	3.429		118	61.96	1.4964	50.869
42	35.64	2.5170	534.742		119	62.08	1.4939	30.913
43	36.01	2.4922	32.311		120	62.73	1.4799	68.719
44	36.27	2.4744	92.725		121	62.85	1.4775	133.090
45	36.39	2.4667	122.753		122	62.95	1.4754	105.714
46	36.51	2.4591	102.747		123	63.10	1.4722	61.716
47	37.09	2.4217	49.822		124	63.16	1.4708	56.350
48	37.16	2.4175	28.449		125	63.31	1.4677	28.738
49	37.68	2.3854	16.324		126	63.51	1.4635	19.778

Peak List Serial	2theta [°]	d [Å]	I/I0		Peak List Serial	2theta [°]	d [Å]	I/I0
50	38.13	2.3582	75.888		127	63.93	1.4550	13.670
51	38.25	2.3513	62.888		128	64.18	1.4499	4.658
52	38.88	2.3143	107.011		129	64.60	1.4415	2.039
53	39.03	2.3057	61.372		130	64.75	1.4385	7.604
54	39.10	2.3019	51.446		131	64.97	1.4342	8.055
55	39.35	2.2879	51.353		132	65.57	1.4225	63.003
56	39.63	2.2721	14.007		133	65.65	1.4209	67.963
57	39.93	2.2557	19.982		134	65.79	1.4184	45.879
58	41.19	2.1899	101.503		135	66.12	1.4120	10.093
59	41.25	2.1865	91.635		136	66.29	1.4088	7.944
60	41.56	2.1714	21.148		137	66.44	1.4060	14.896
61	41.76	2.1614	42.252		138	66.66	1.4020	9.598
62	41.91	2.1540	21.329		139	66.71	1.4010	16.092
63	42.49	2.1257	185.819		140	67.37	1.3887	71.172
64	42.86	2.1083	17.337		141	67.54	1.3857	52.885
65	43.24	2.0904	20.316		142	67.78	1.3815	23.865
66	43.46	2.0805	30.665		143	68.44	1.3696	4.856
67	43.63	2.0729	42.117		144	68.54	1.3679	4.595
68	43.95	2.0587	44.416		145	68.85	1.3626	18.798
69	44.01	2.0557	45.647		146	68.86	1.3623	17.535
70	44.08	2.0527	47.449		147	69.01	1.3597	10.790
71	44.13	2.0505	46.611		148	69.26	1.3554	29.503
72	44.75	2.0236	17.694		149	69.46	1.3520	28.352
73	44.76	2.0229	7.002		150	69.53	1.3509	33.837
74	45.58	1.9884	61.047		151	69.60	1.3497	26.448
75	46.02	1.9707	44.512		152	69.85	1.3455	16.246
76	46.07	1.9686	55.192		153	70.00	1.3430	7.632
77	46.32	1.9586	10.958					

Sample 10

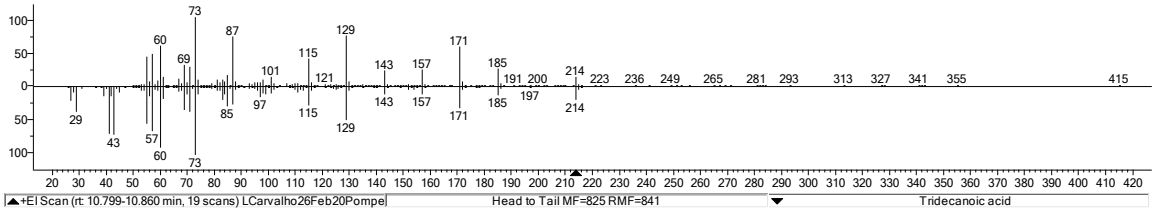
Name	Formula	PDF Number	FOM	%
Malachite	Cu2 (OH)2 (CO3)	00-900-7490	0.781	75.28
Azurite	C2 H2 Cu3 O8	00-900-7013	0.700	24.72

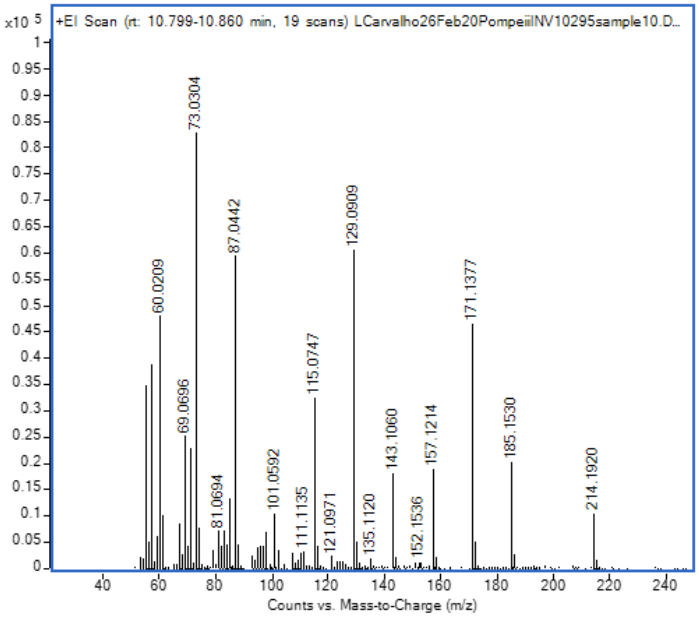
Peak List Serial	2theta [°]	d [Å]	I/I0		Peak List Serial	2theta [°]	d [Å]	I/I0
1	5.39	16.3748	21.769		57	44.03	2.0550	74.892
2	5.99	14.7326	22.185		58	44.90	2.0172	31.626
3	7.23	12.2155	22.224		59	45.58	1.9884	63.950
4	8.77	10.0767	103.837		60	46.05	1.9693	82.360
5	11.12	7.9471	36.577		61	46.55	1.9493	152.045
6	11.48	7.7048	23.344		62	46.82	1.9388	51.340
7	11.96	7.3937	52.716		63	47.55	1.9105	60.695
8	14.57	6.0758	50.708		64	47.84	1.8998	110.380
9	14.82	5.9736	378.028		65	48.04	1.8923	37.017
10	16.59	5.3395	30.962		66	48.51	1.8752	29.631
11	17.12	5.1739	99.783		67	49.21	1.8501	24.623
12	17.57	5.0421	631.521		68	49.73	1.8320	53.742
13	18.51	4.7892	29.546		69	49.89	1.8262	66.573
14	18.90	4.6927	57.411		70	50.15	1.8177	45.908
15	19.31	4.5921	26.948		71	50.65	1.8009	44.584
16	19.56	4.5338	29.436		72	50.91	1.7920	91.707
17	20.60	4.3081	27.164		73	51.13	1.7849	45.634
18	20.77	4.2738	43.563		74	52.28	1.7483	43.158
19	21.69	4.0947	31.920		75	52.52	1.7410	25.773
20	23.77	3.7394	51.920		76	53.07	1.7242	31.725
21	24.06	3.6959	735.928		77	53.34	1.7162	27.059
22	25.15	3.5387	155.299		78	54.02	1.6960	71.136
23	25.88	3.4398	34.722		79	54.31	1.6878	63.220
24	26.13	3.4073	26.742		80	54.66	1.6778	117.610
25	26.48	3.3630	117.341		81	54.96	1.6694	46.578
26	27.17	3.2797	42.209		82	55.93	1.6427	39.203
27	27.57	3.2329	69.622		83	56.33	1.6319	19.787
28	27.97	3.1874	135.445		84	57.00	1.6144	89.799
29	28.55	3.1234	28.951		85	57.16	1.6101	47.909
30	29.39	3.0365	142.478		86	57.73	1.5956	66.395
31	29.87	2.9884	162.415		87	57.95	1.5901	105.408
32	30.89	2.8920	123.210		88	58.38	1.5793	25.738
33	31.23	2.8618	426.661		89	58.68	1.5719	64.269
34	31.66	2.8236	119.828		90	60.00	1.5404	41.512
35	32.18	2.7793	194.112		91	60.47	1.5296	43.377
36	33.85	2.6458	41.065		92	60.66	1.5254	37.059
37	34.19	2.6207	44.646		93	61.06	1.5164	48.207
38	34.49	2.5985	27.319		94	61.43	1.5082	45.784
39	35.24	2.5448	105.571		95	61.89	1.4979	54.384
40	35.59	2.5205	595.757		96	62.96	1.4750	91.014
41	35.82	2.5045	80.330		97	63.23	1.4694	40.198
42	36.24	2.4766	110.024		98	63.65	1.4608	28.284
43	36.43	2.4645	130.503		99	63.95	1.4546	28.705
44	37.01	2.4269	96.109		100	65.10	1.4316	39.114
45	38.33	2.3463	75.310		101	65.60	1.4219	82.995
46	38.85	2.3162	118.914		102	65.89	1.4164	42.878
47	39.35	2.2879	126.336		103	66.42	1.4063	47.594
48	39.77	2.2648	57.776		104	67.01	1.3955	31.033
49	40.03	2.2503	47.651		105	67.36	1.3890	55.363
50	40.44	2.2289	50.855		106	67.47	1.3869	62.805
51	41.27	2.1857	110.945		107	67.71	1.3827	38.945

Peak List Serial	2theta [°]	d [Å]	I/I0		Peak List Serial	2theta [°]	d [Å]	I/I0
52	41.69	2.1647	33.336		108	67.98	1.3779	52.364
53	42.41	2.1297	186.243		109	68.38	1.3708	25.916
54	42.88	2.1075	20.989		110	68.86	1.3623	37.315
55	43.43	2.0820	49.462		111	69.18	1.3569	54.429
56	43.76	2.0669	47.043		112	69.58	1.3500	29.863

[1] Tridecanoic acid Mass: 214.19328

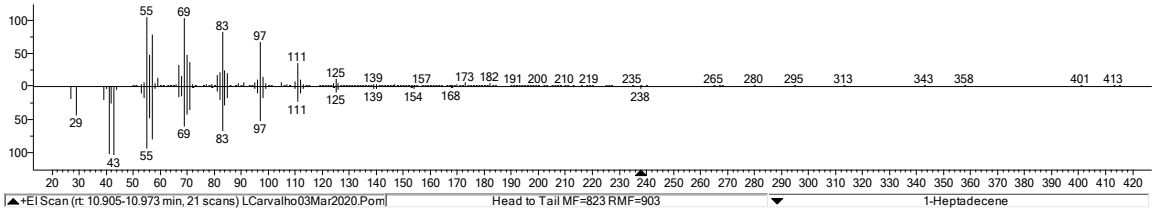
Sample 10

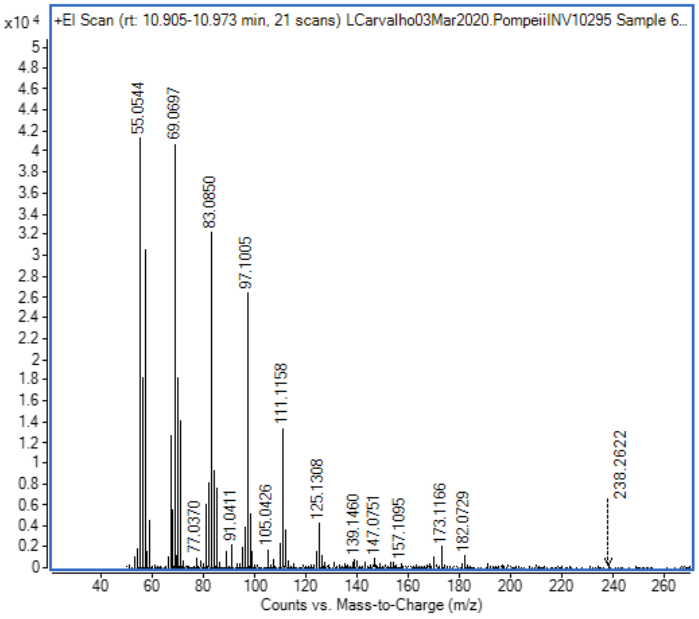




[2] 1-Heptadecene Mass: 238.266051

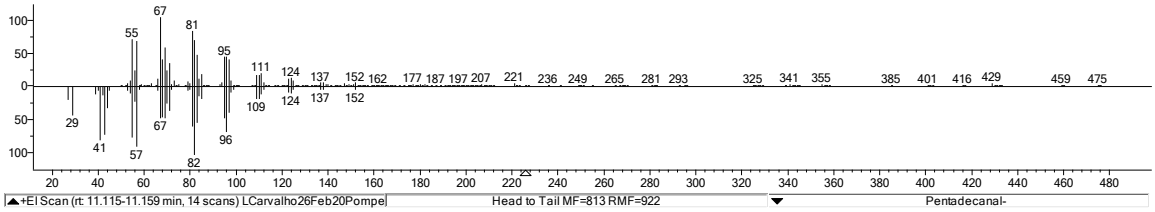
Sample 6

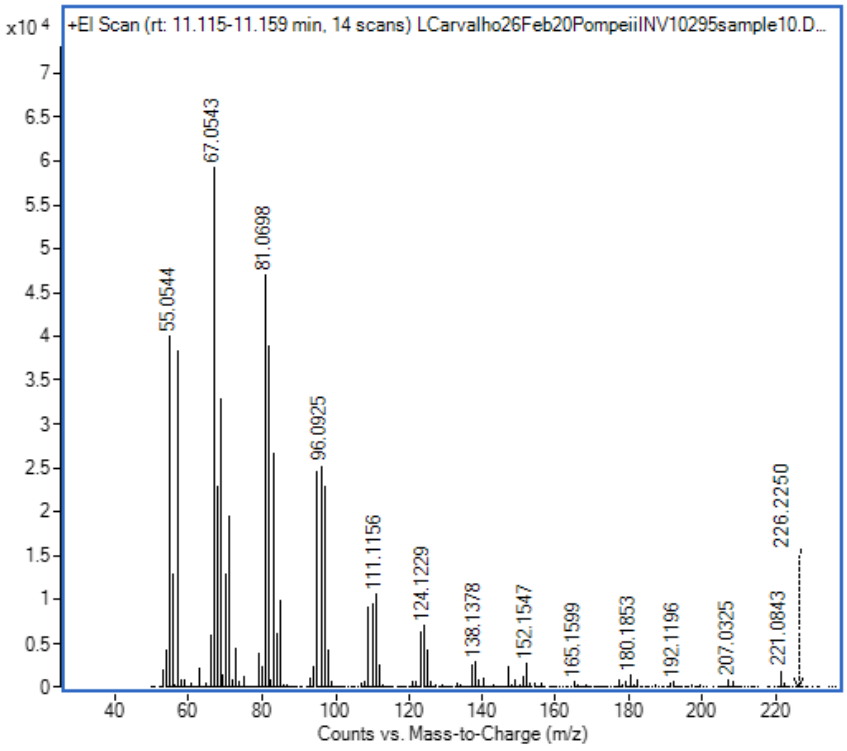




[3] Pentadecanal

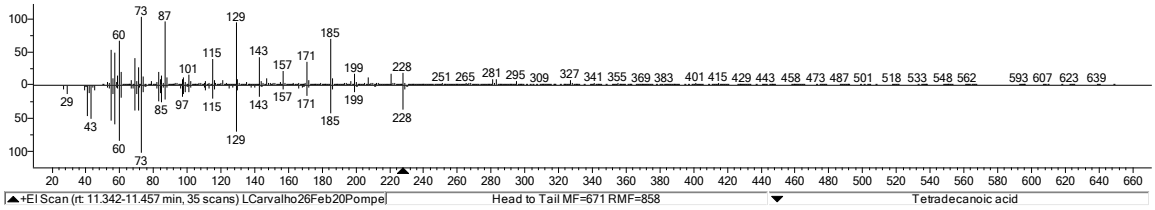
Sample 10

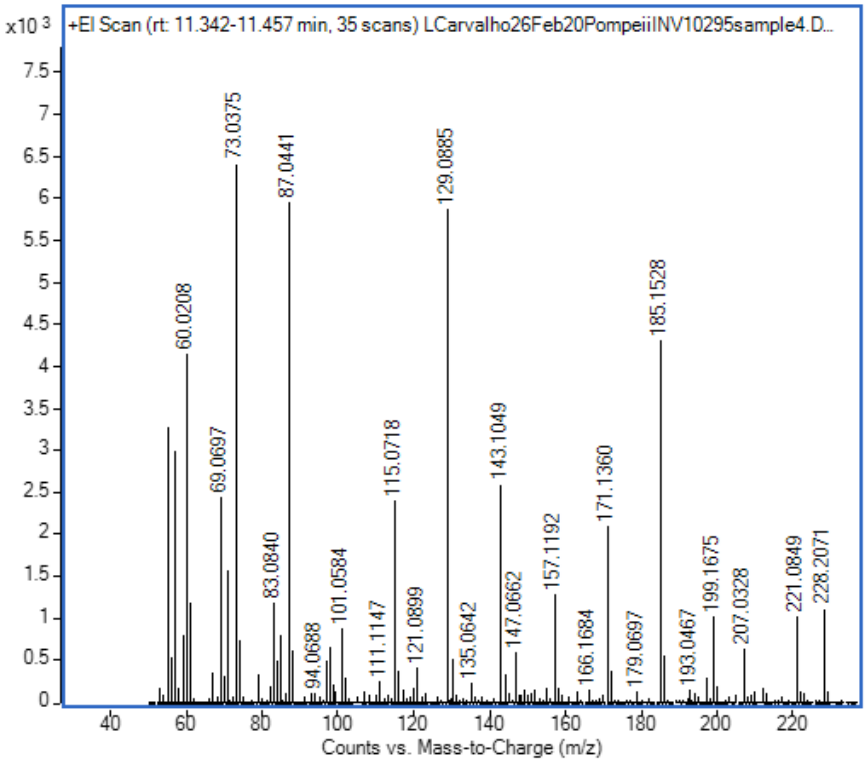




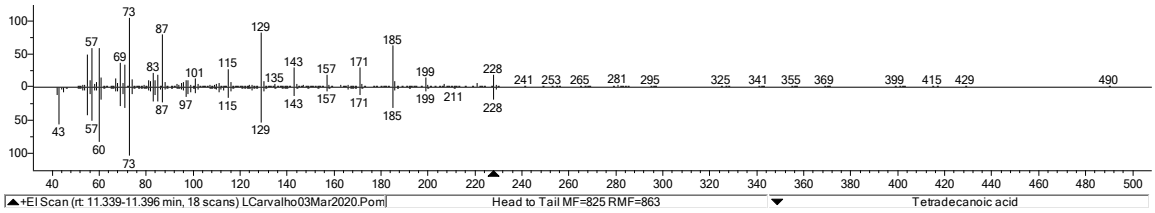
[4] Tetradecanoic acid

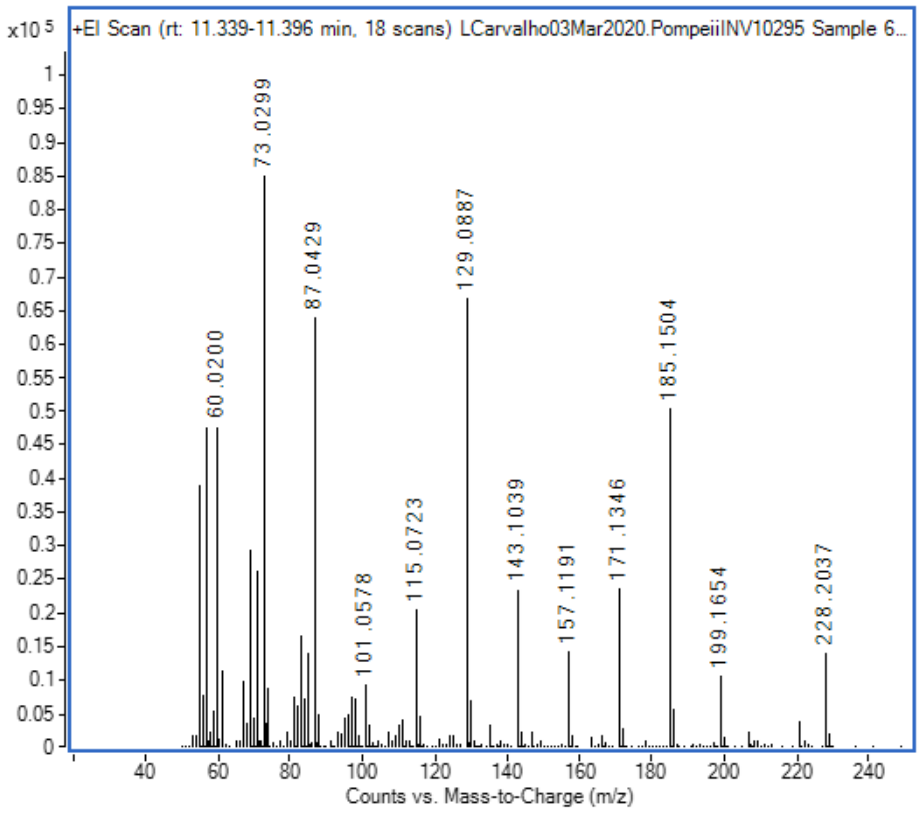
Sample 4



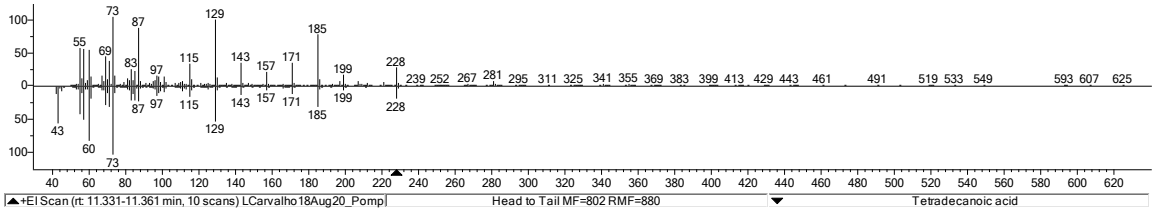


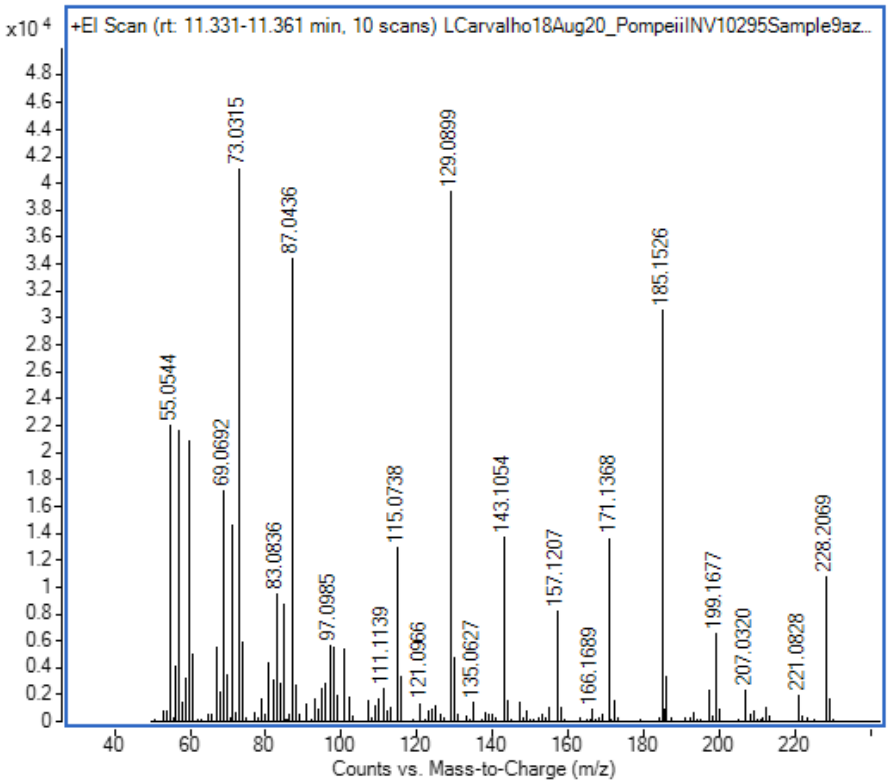
Sample 6


+EI Scan (rt: 11.339-11.396 min, 18 scans) LCarvalho03Mar2020.Pom
Head to Tail MF=825 RMF=863
Tetradecanoic acid

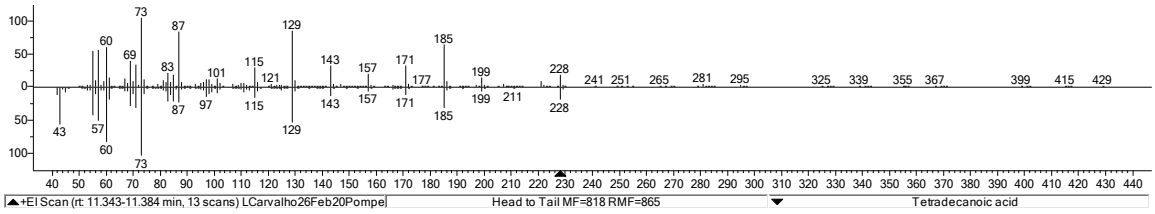

x10 5
+EI Scan (rt: 11.339-11.396 min, 18 scans) LCarvalho03Mar2020.PompeiiINV10295 Sample 6...
60.0200
73.0299
87.0429
101.0578
115.0723
129.0887
143.1039
157.1191
171.1346
185.1504
199.1654
228.2037
Counts vs. Mass-to-Charge (m/z)

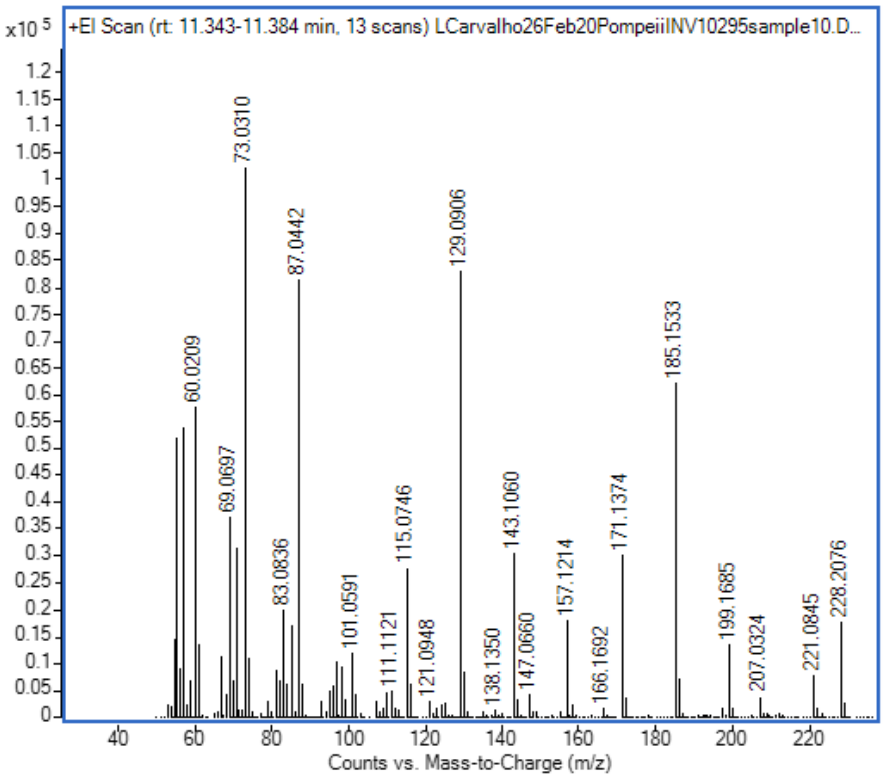
Sample 9


+EI Scan (rt: 11.331-11.361 min, 10 scans) LCarvalho18Aug20_Pomp
Head to Tail MF=802 RMF=880
Tetradecanoic acid


x10 4
+EI Scan (rt: 11.331-11.361 min, 10 scans) LCarvalho18Aug20_PompeiiINV10295Sample9az...
55.0544
69.0692
73.0315
83.0836
87.0436
97.0985
111.1139
115.0738
121.0966
129.0899
135.0627
143.1054
157.1207
166.1689
171.1368
185.1526
199.1677
207.0320
221.0828
228.2069
Counts vs. Mass-to-Charge (m/z)

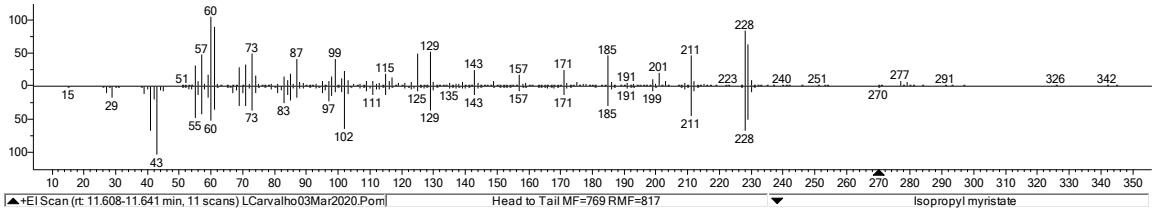
Sample 10

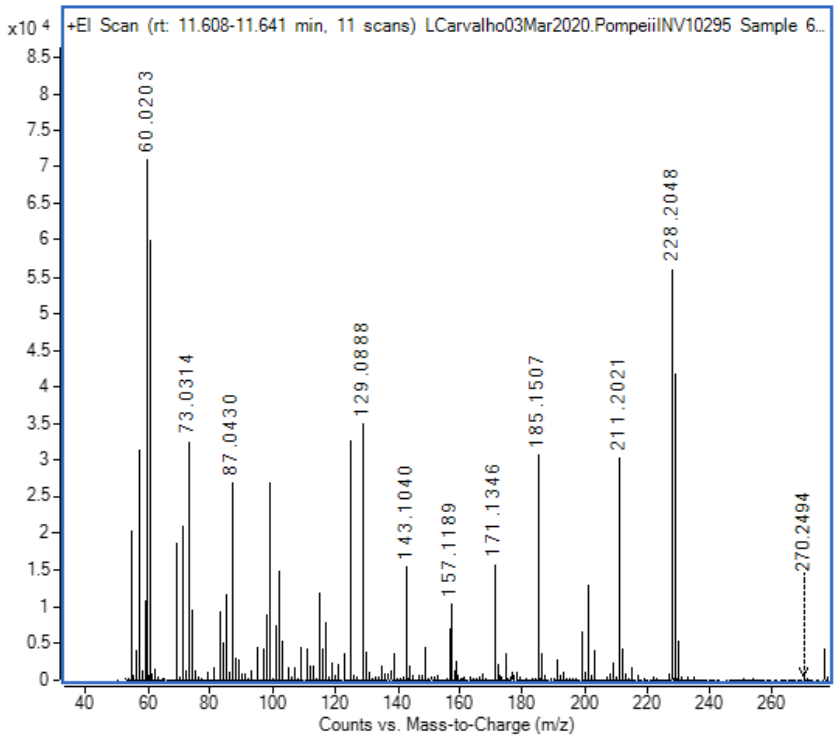

+EI Scan (rt: 11.343-11.384 min, 13 scans) LCarvalho26Feb20Pompe
Head to Tail MF=818 RMF=865
Tetradecanoic acid


x10 5
+EI Scan (rt: 11.343-11.384 min, 13 scans) LCarvalho26Feb20PompeiiINV10295sample10.D...
73.0310
87.0442
129.0906
60.0209
185.1533
69.0697
143.1060
171.1374
83.0836
115.0746
157.1214
101.0591
199.1685
111.1121
121.0948
207.0324
138.1350
147.0660
221.0845
166.1692
228.2076
Counts vs. Mass-to-Charge (m/z)

[5] Isopropyl myristate Mass: 270.25588

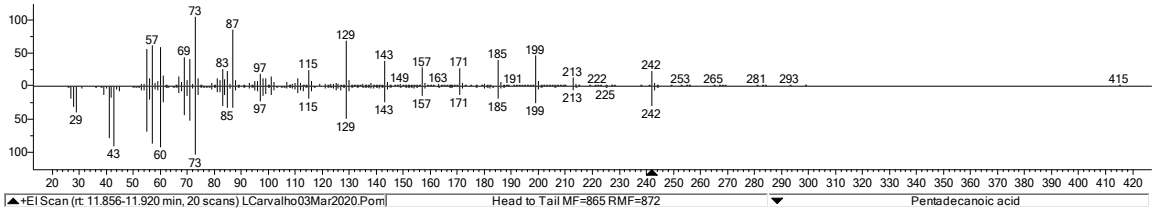
Sample 6

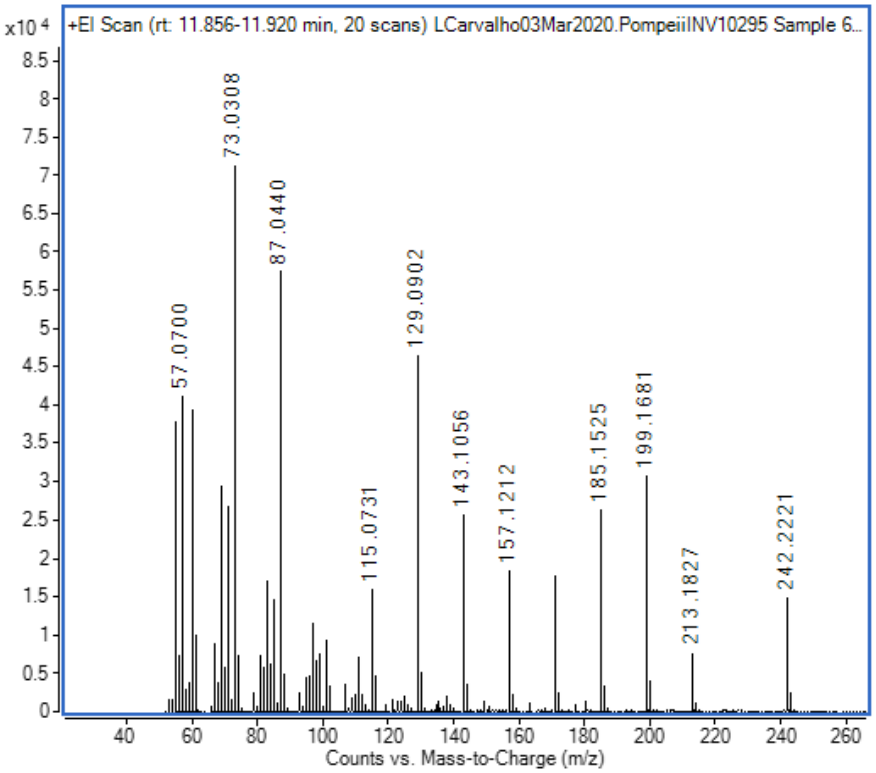




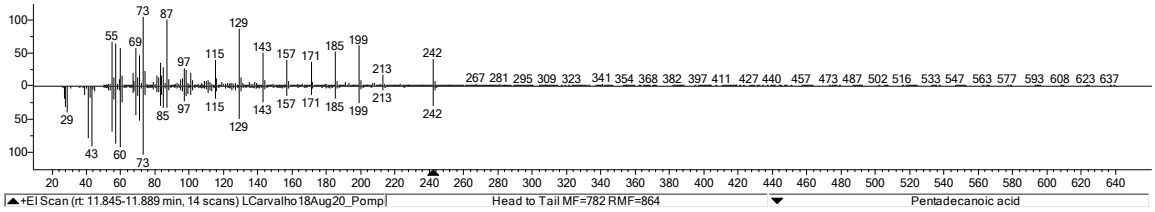
[6] Pentadecanoic acid

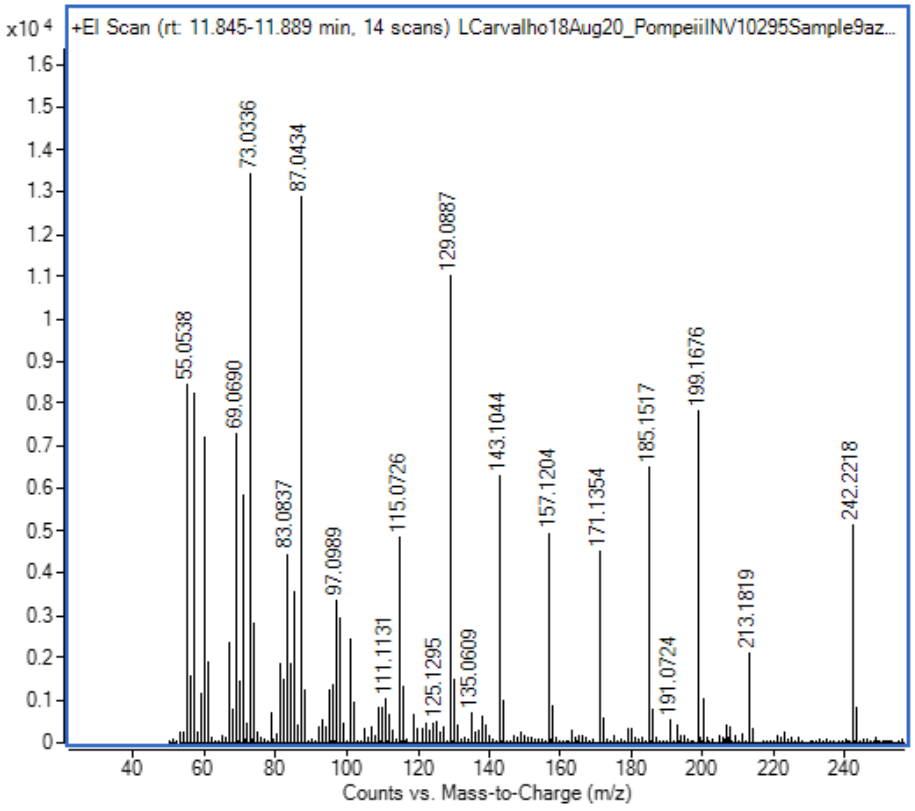
Sample 6



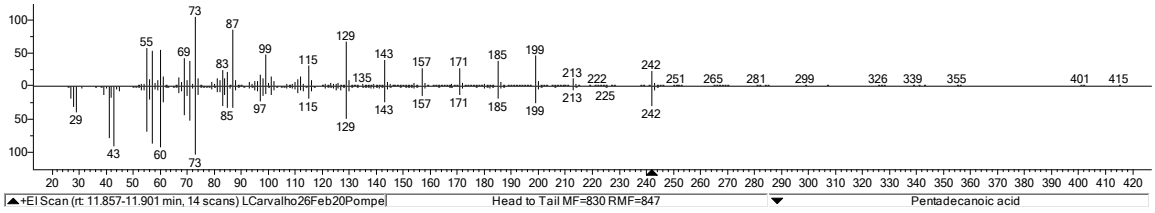


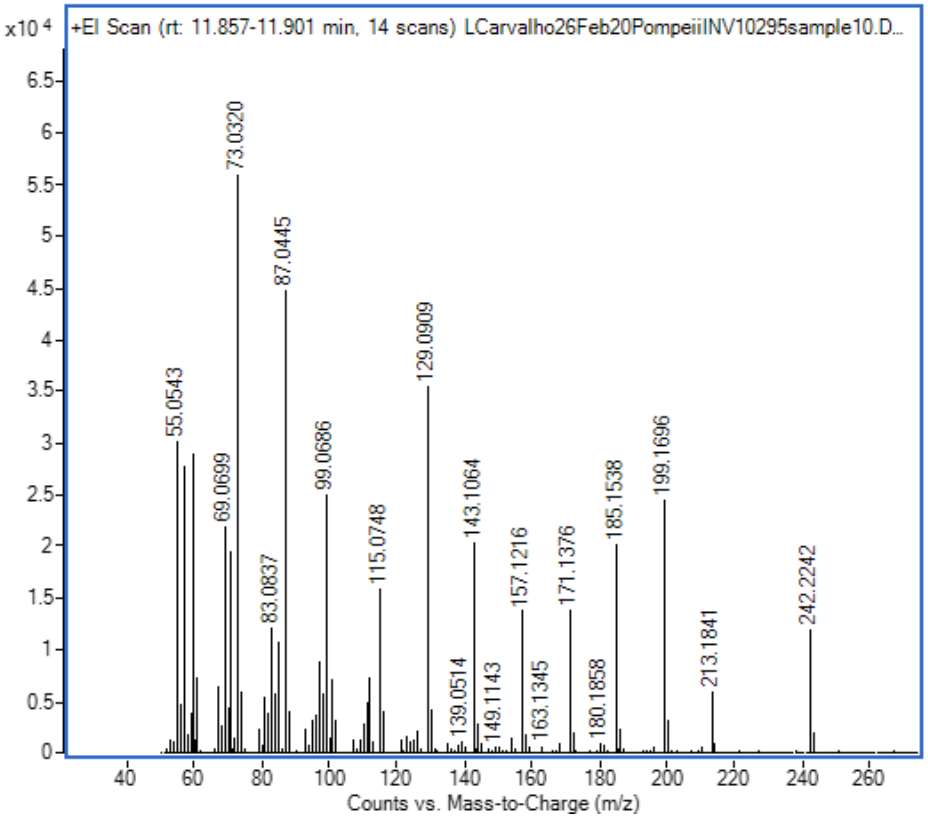
Sample 9


+EI Scan (rt: 11.845-11.889 min, 14 scans) LCarvalho18Aug20_Pomp
Head to Tail MF=782 RMF=864
Pentadecanoic acid


x10 4
+EI Scan (rt: 11.845-11.889 min, 14 scans) LCarvalho18Aug20_PompeiiINV10295Sample9az...
55.0538
69.0690
73.0336
83.0837
87.0434
97.0989
111.1131
115.0726
125.1295
129.0887
135.0609
143.1044
157.1204
171.1354
185.1517
191.0724
199.1676
213.1819
242.2218
Counts vs. Mass-to-Charge (m/z)

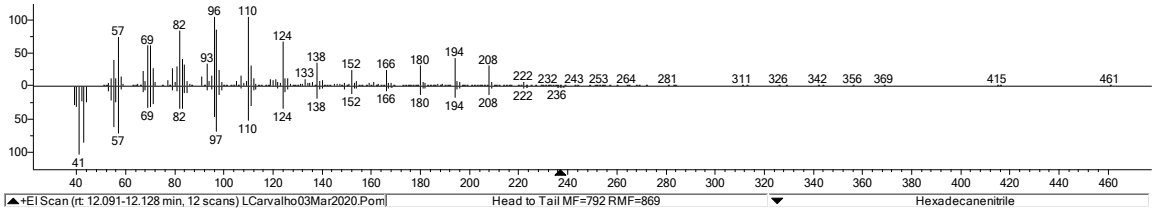
Sample 10

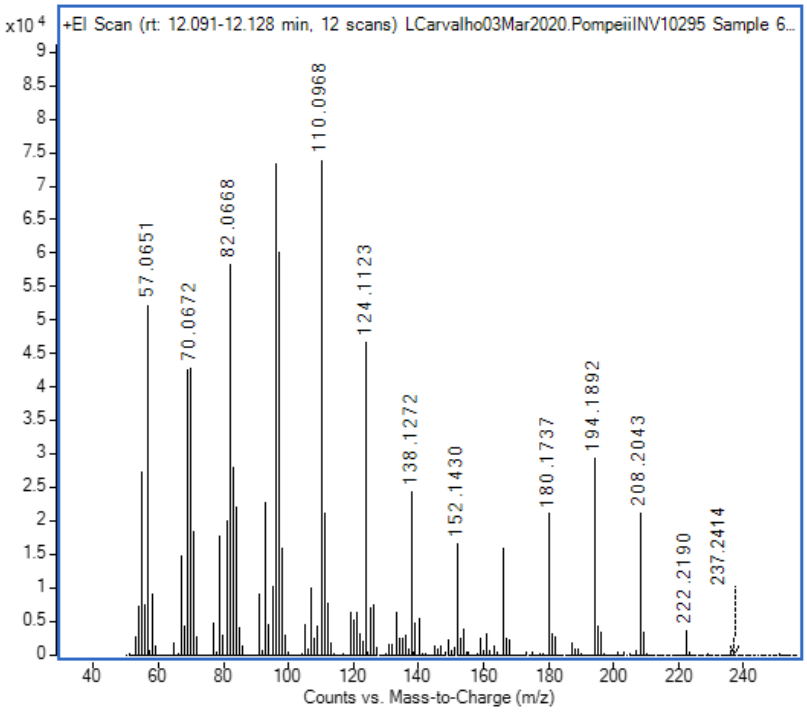

+EI Scan (rt: 11.857-11.901 min, 14 scans) LCarvalho26Feb20Pompe
Head to Tail MF=830 RMF=847
Pentadecanoic acid


x10 4
+EI Scan (rt: 11.857-11.901 min, 14 scans) LCarvalho26Feb20PompeiiINV10295sample10.D...
73.0320
87.0445
55.0543
129.0909
69.0699
99.0686
143.1064
115.0748
157.1216
83.0837
171.1376
185.1538
199.1696
242.2242
213.1841
139.0514
149.1143
163.1345
180.1858
Counts vs. Mass-to-Charge (m/z)

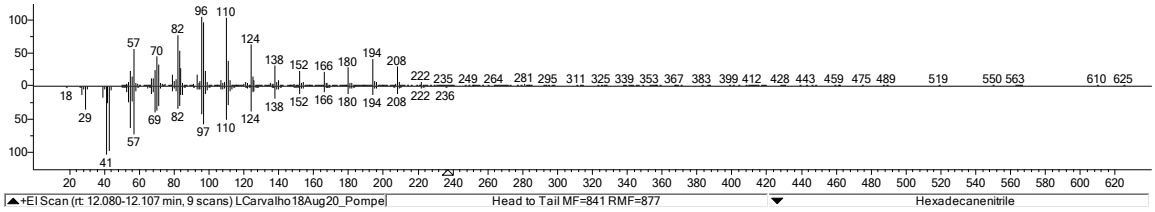
[7] Hexadecanenitrile Mass: 237.24565

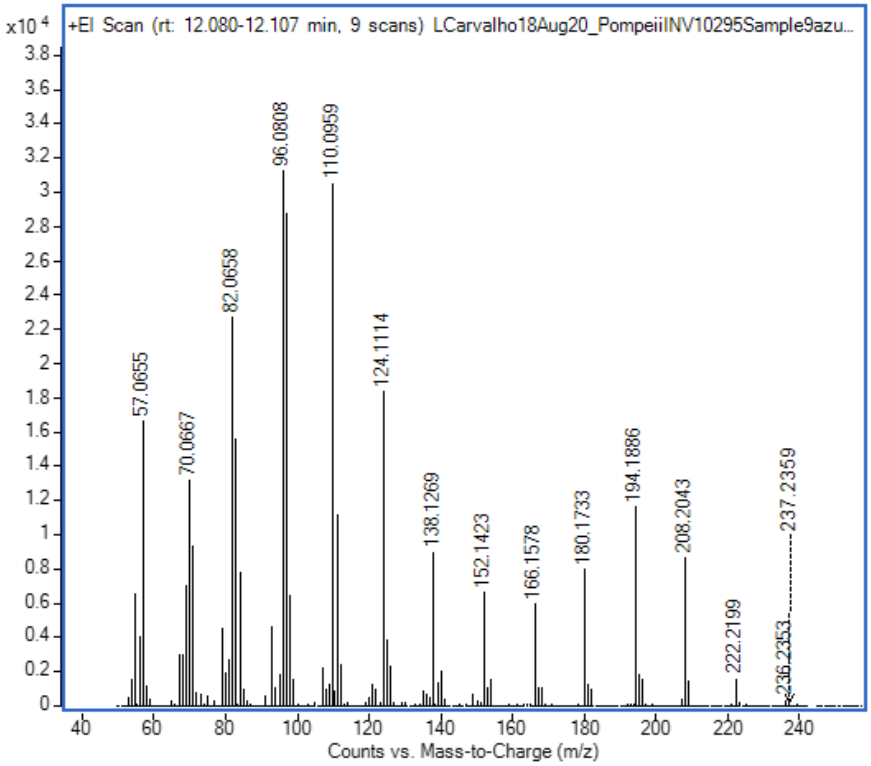
Sample 6





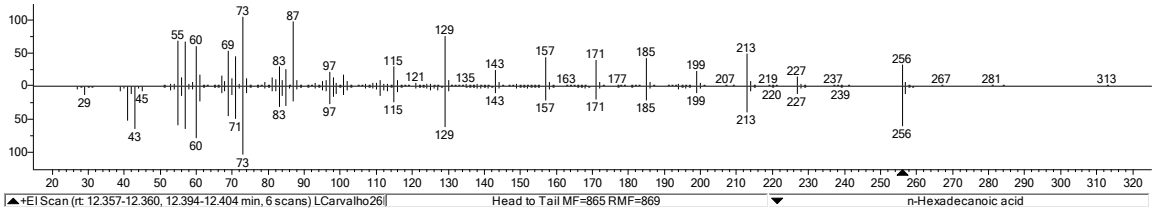
Sample 9

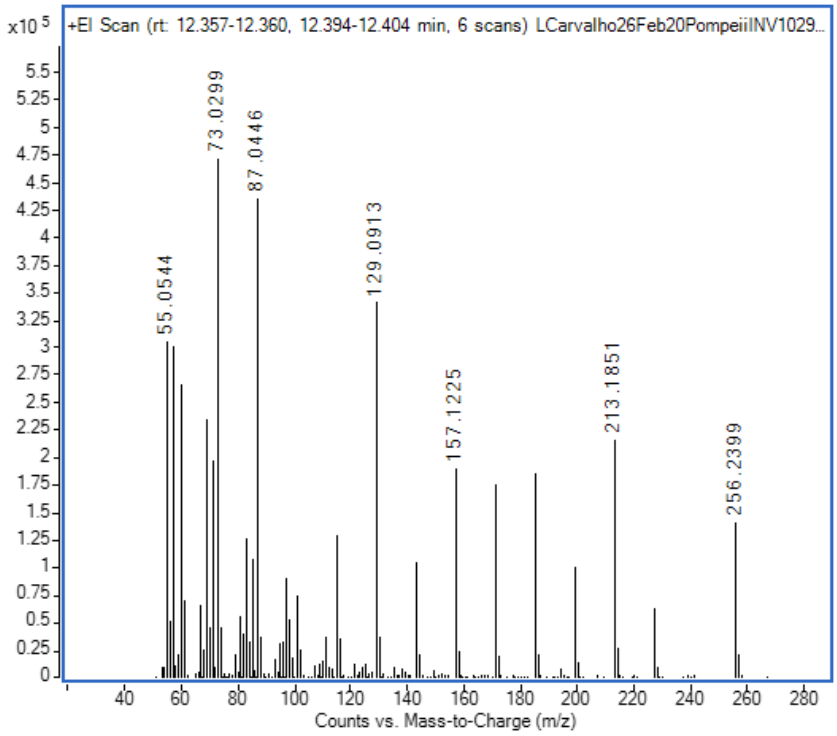

+EI Scan (rt: 12.080-12.107 min, 9 scans) LCarvalho18Aug20_Pompe
Head to Tail MF=841 RMF=877
Hexadecanenitrile


x10 4
+EI Scan (rt: 12.080-12.107 min, 9 scans) LCarvalho18Aug20_PompeiiINV10295Sample9azu...
96.0808
110.0959
82.0658
57.0655
124.1114
70.0667
138.1269
152.1423
166.1578
180.1733
194.1886
208.2043
237.2359
222.2199
236.2353
Counts vs. Mass-to-Charge (m/z)

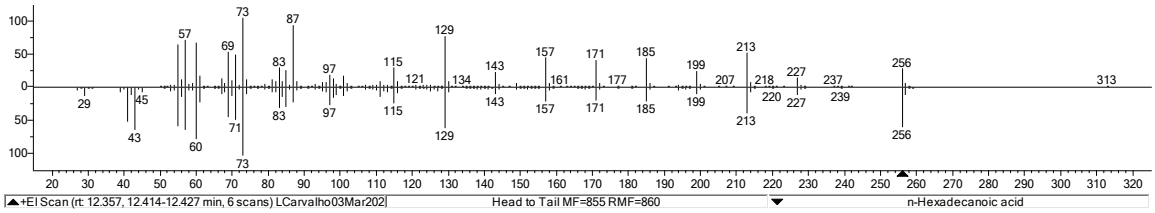
[8] n-Hexadecanoic acid

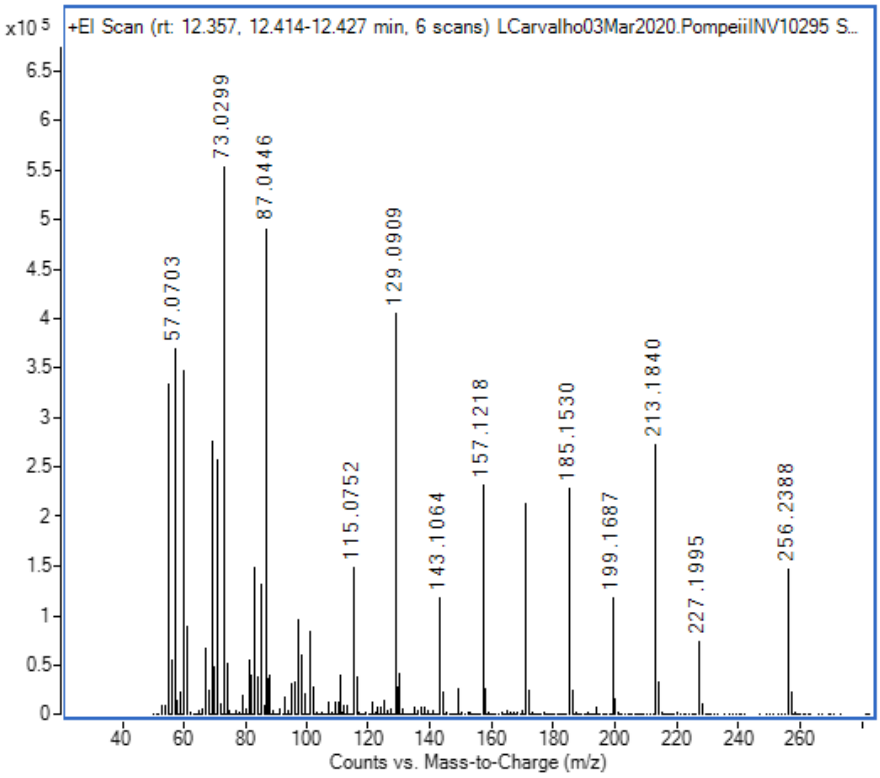
Sample 4



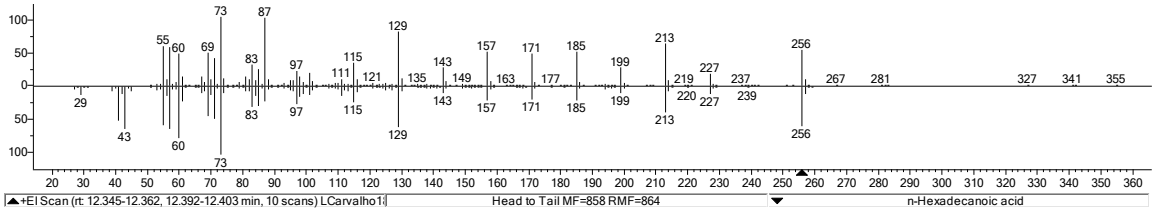


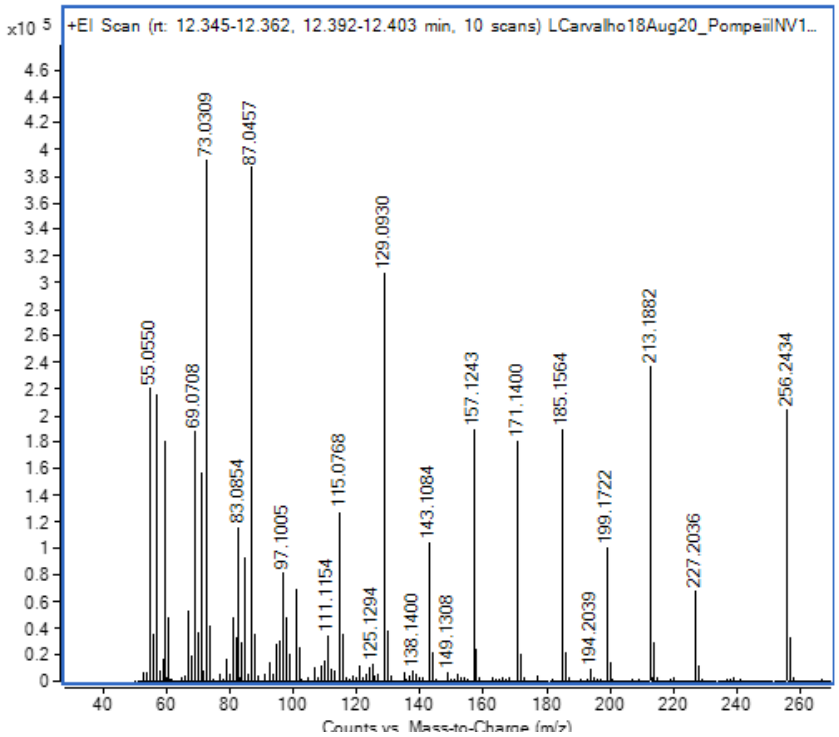
Sample 6


+EI Scan (rt: 12.357, 12.414-12.427 min, 6 scans) LCarvalho03Mar202
Head to Tail MF=855 RMF=860
n-Hexadecanoic acid

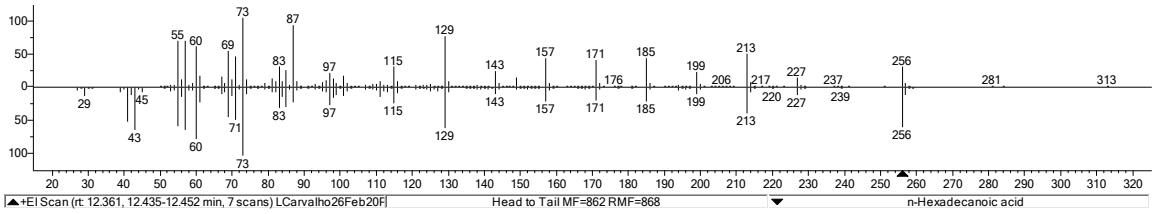

x10 5
+EI Scan (rt: 12.357, 12.414-12.427 min, 6 scans) LCarvalho03Mar2020.PompeiiINV10295 S...
57.0703
73.0299
87.0446
115.0752
129.0909
143.1064
157.1218
185.1530
199.1687
213.1840
227.1995
256.2388
Counts vs. Mass-to-Charge (m/z)

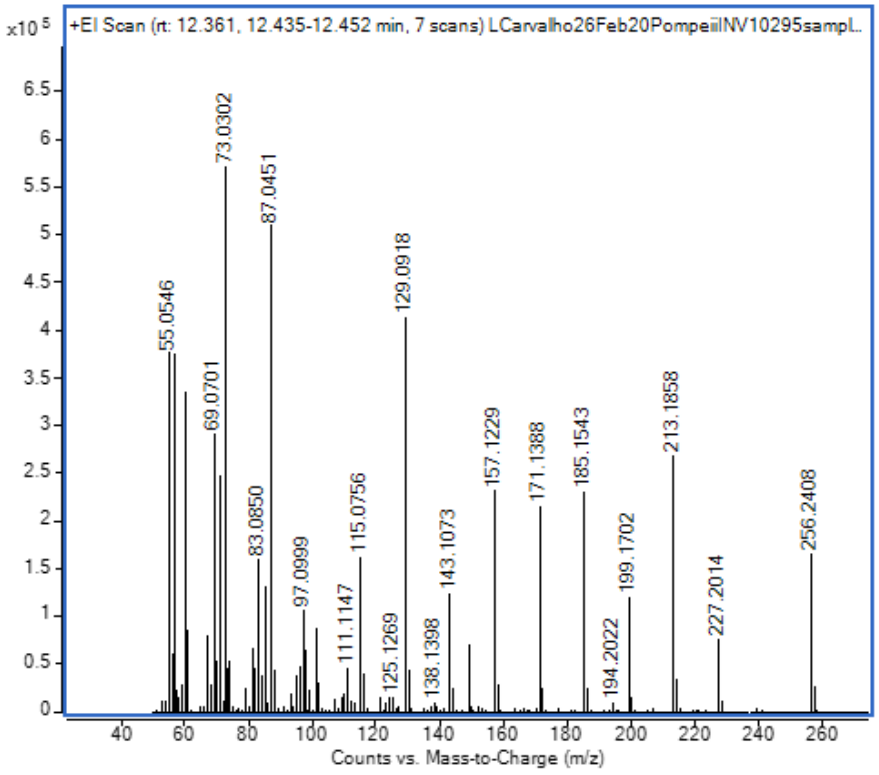
Sample 9


+EI Scan (rt: 12.345-12.362, 12.392-12.403 min, 10 scans) LCarvalho1
Head to Tail MF=858 RMF=864
n-Hexadecanoic acid


x10 5
+EI Scan (rt: 12.345-12.362, 12.392-12.403 min, 10 scans) LCarvalho18Aug20_PompeiiINV1...
73.0309
87.0457
129.0930
55.0550
69.0708
213.1882
256.2434
83.0854
157.1243
171.1400
185.1564
115.0768
97.1005
143.1084
199.1722
111.1154
227.2036
125.1294
138.1400
149.1308
194.2039
Counts vs. Mass-to-Charge (m/z)

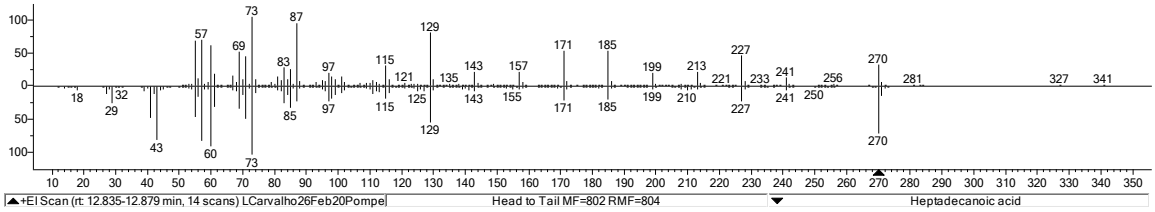
Sample 10

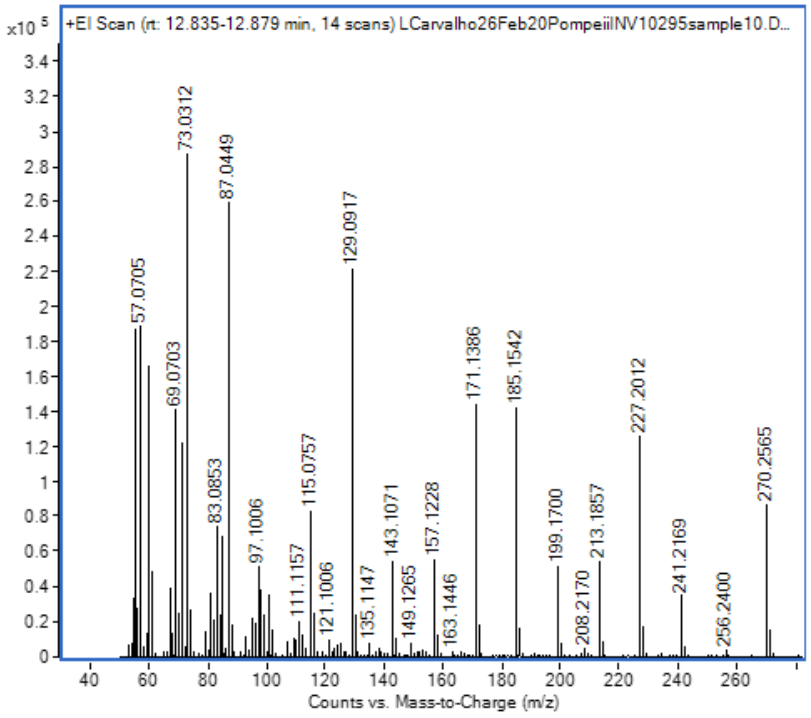

+EI Scan (rt: 12.361, 12.435-12.452 min, 7 scans) LCarvalho26Feb20F
Head to Tail MF=862 RMF=868
n-Hexadecanoic acid


x10 5
+EI Scan (rt: 12.361, 12.435-12.452 min, 7 scans) LCarvalho26Feb20PompeiiINV10295sampl..
73.0302
87.0451
55.0546
129.0918
69.0701
83.0850
97.0999
115.0756
111.1147
125.1269
138.1398
143.1073
157.1229
171.1388
185.1543
213.1858
199.1702
194.2022
227.2014
256.2408
Counts vs. Mass-to-Charge (m/z)

[9] Heptadecanoic acid Mass: 270.25588

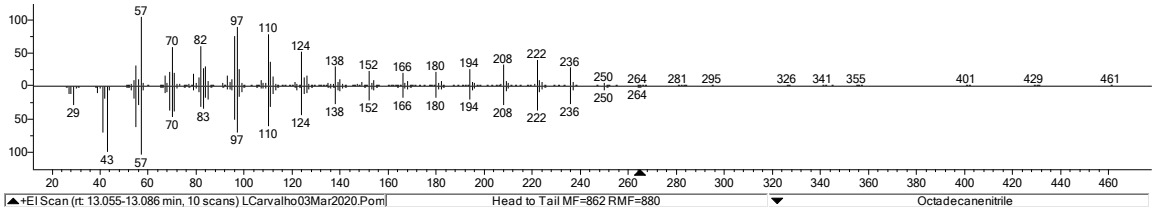
Sample 10

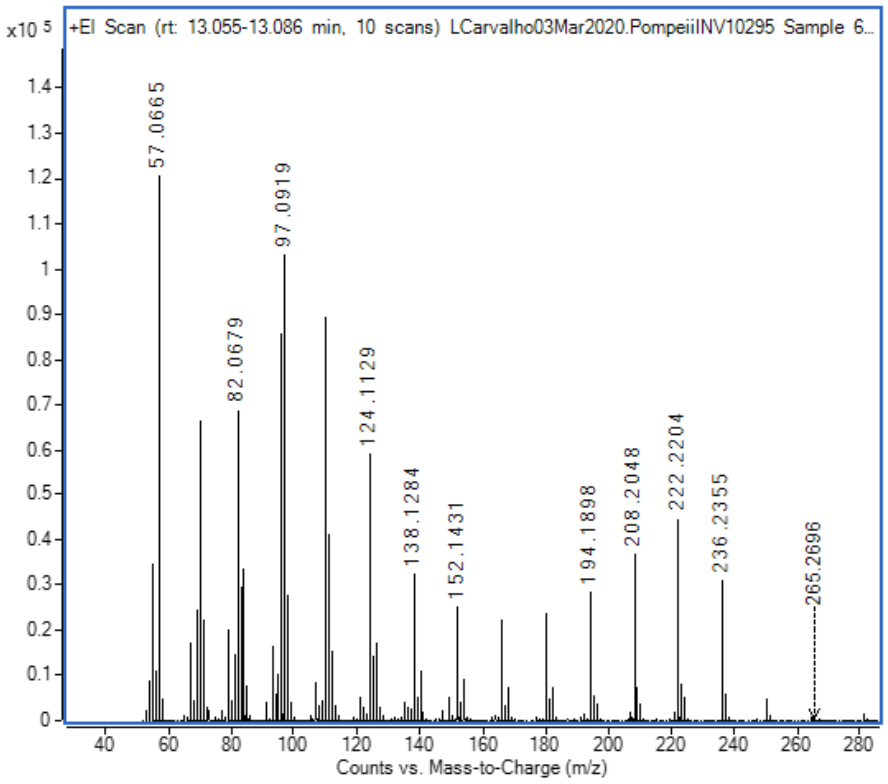




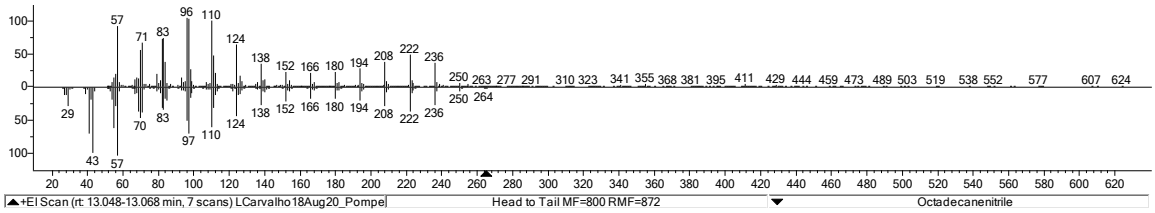
[10] Octadecanenitrile Mass: 265.27695

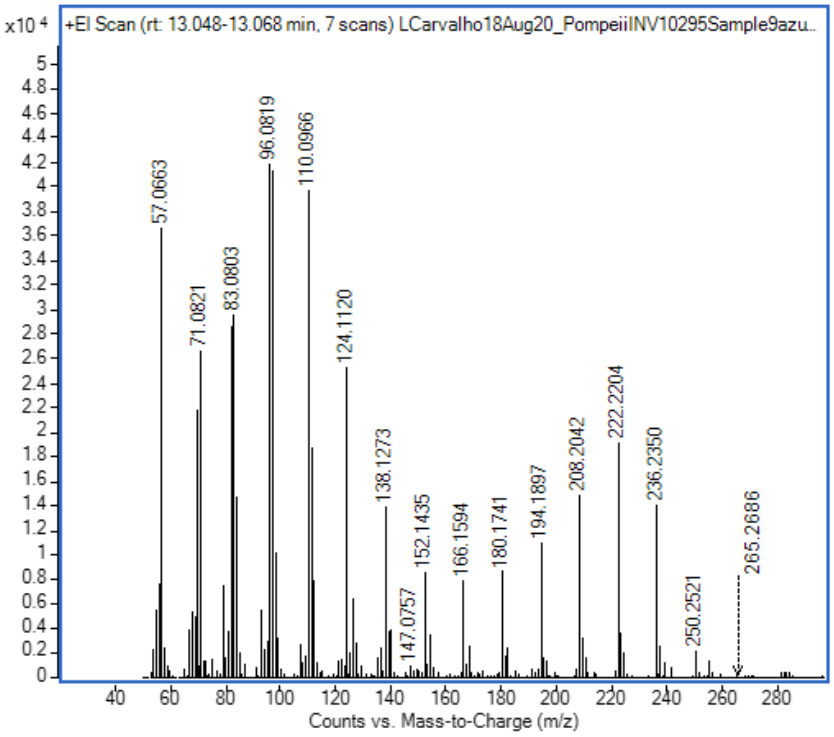
Sample 6



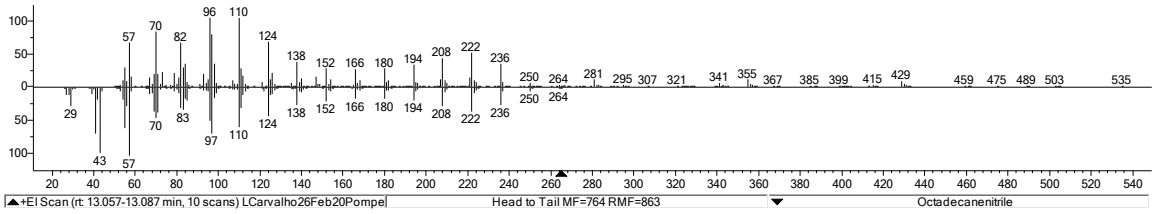


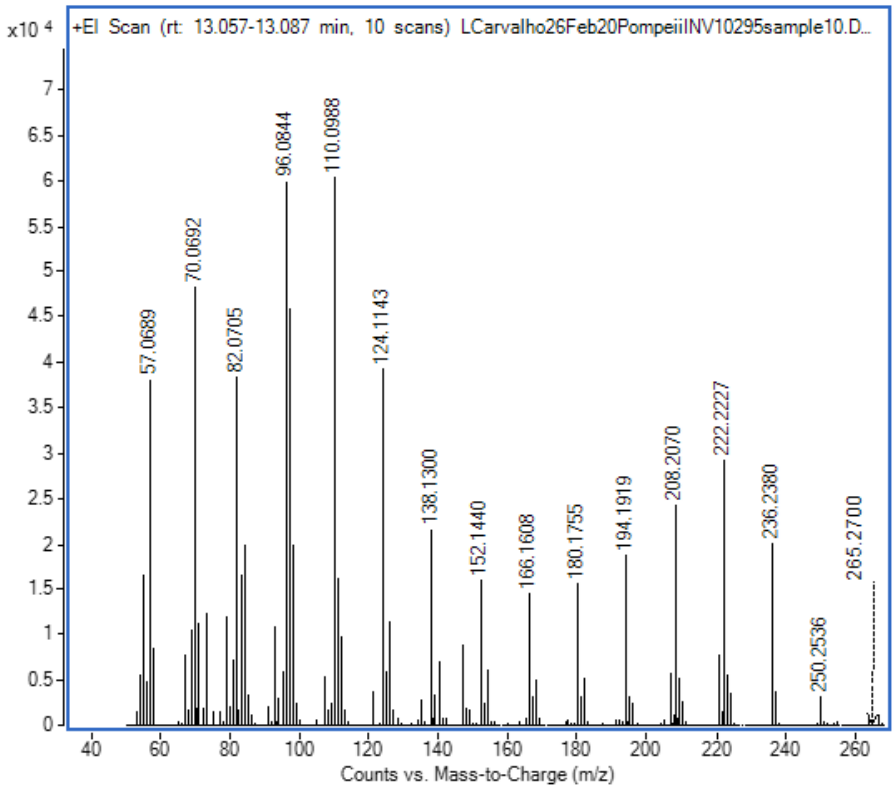
Sample 9


+EI Scan (rt: 13.048-13.068 min, 7 scans) LCarvalho18Aug20_Pompe
Head to Tail MF=800 RMF=872
Octadecanenitrile


x10 4
+EI Scan (rt: 13.048-13.068 min, 7 scans) LCarvalho18Aug20_PompeiiINV10295Sample9azu..
57.0663
71.0821
83.0803
96.0819
110.0966
124.1120
138.1273
147.0757
152.1435
166.1594
180.1741
194.1897
208.2042
222.2204
236.2350
250.2521
265.2686
Counts vs. Mass-to-Charge (m/z)

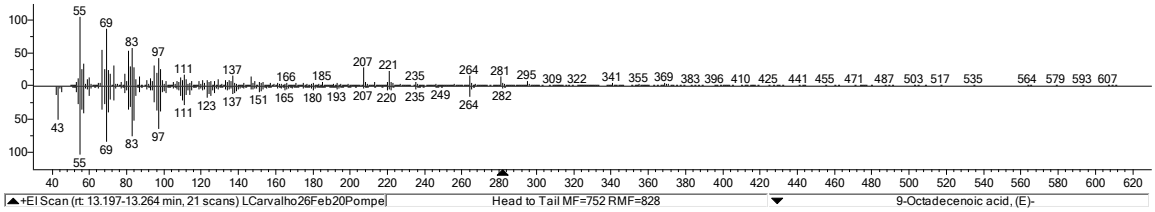
Sample 10

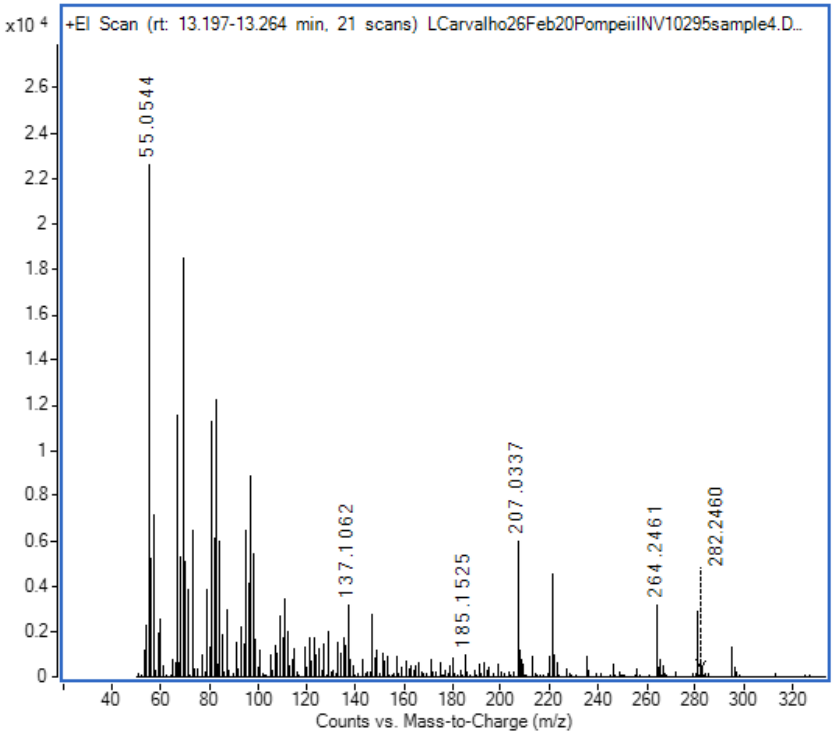

+El Scan (rt: 13.057-13.087 min, 10 scans) LCarvalho26Feb20Pompe
Head to Tail MF=764 RMF=863
Octadecanenitrile


x10 4
+El Scan (rt: 13.057-13.087 min, 10 scans) LCarvalho26Feb20PompeiiINV10295sample10.D...
57.0689
70.0692
82.0705
96.0844
110.0988
124.1143
138.1300
152.1440
166.1608
180.1755
194.1919
208.2070
222.2227
236.2380
250.2536
265.2700
Counts vs. Mass-to-Charge (m/z)

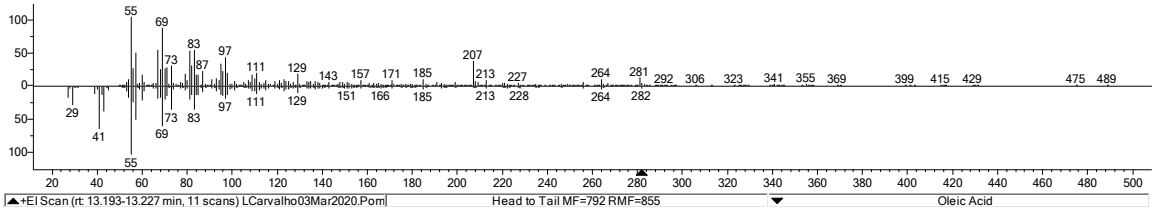
[11] 9-Octadecenoic acid (Oleic Acid) Mass: 282.25588 NIST#: 379356

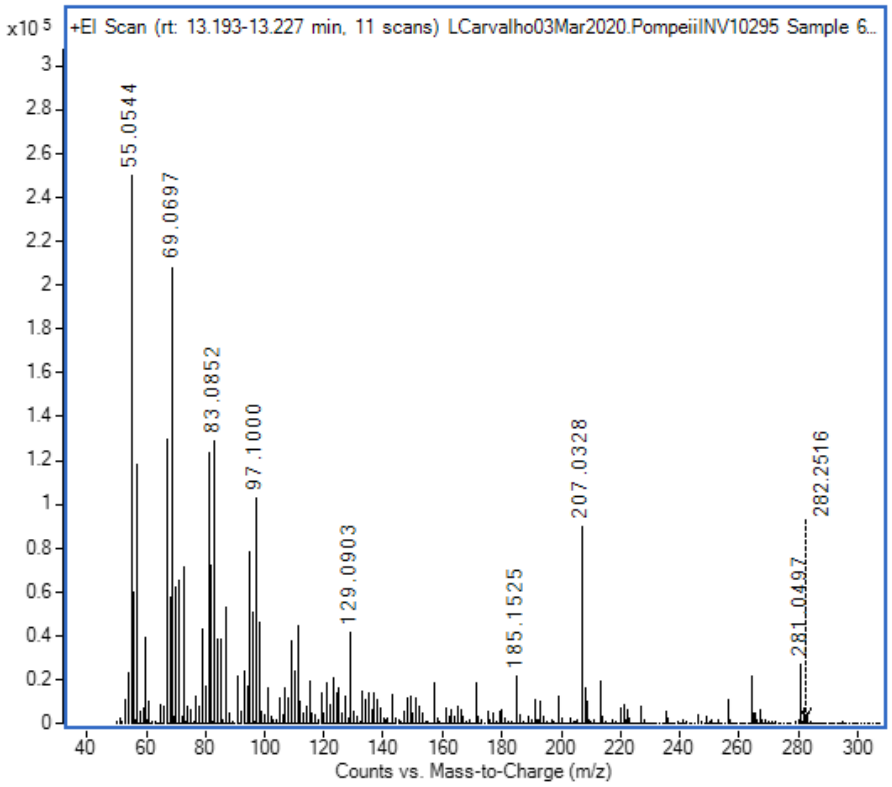
Sample 4



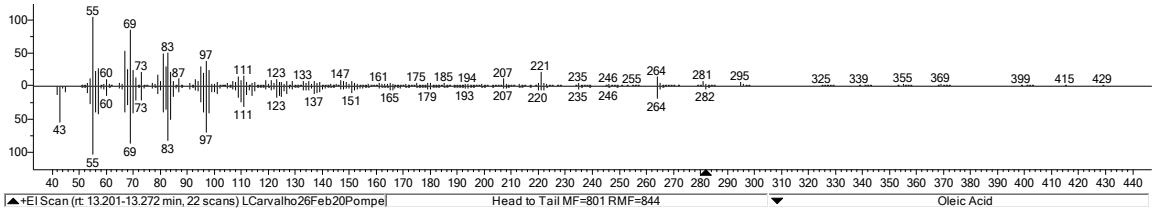


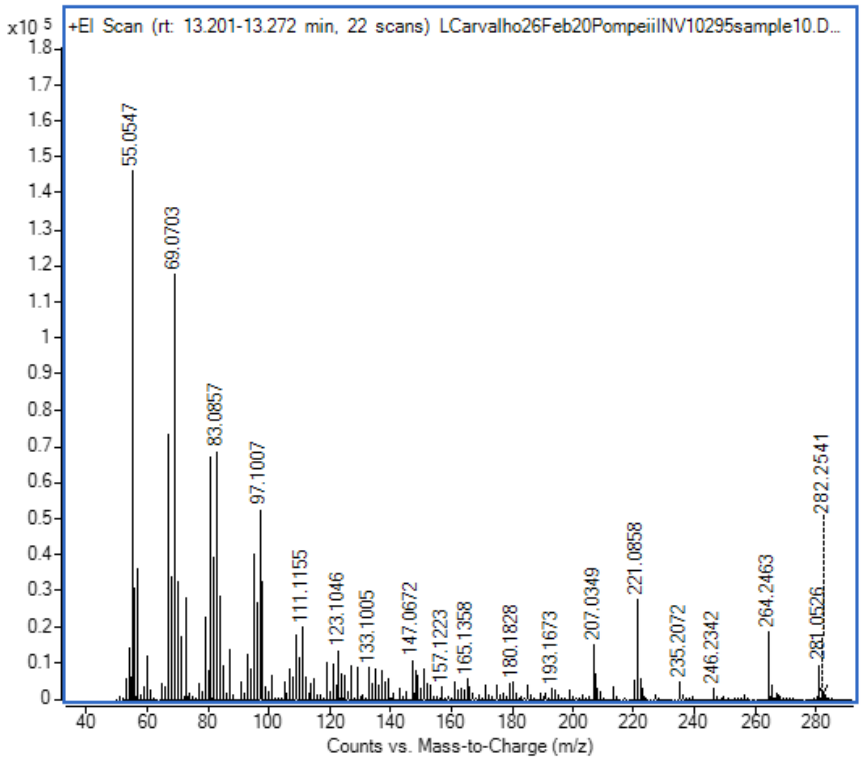
Sample 6


+El Scan (rt: 13.193-13.227 min, 11 scans) LCarvalho03Mar2020.Pom
Head to Tail MF=792 RMF=855
Oleic Acid


x10 5
+El Scan (rt: 13.193-13.227 min, 11 scans) LCarvalho03Mar2020.PompeiiINV10295 Sample 6...
55.0544
69.0697
83.0852
97.1000
129.0903
185.1525
207.0328
281.0497
282.2516
Counts vs. Mass-to-Charge (m/z)

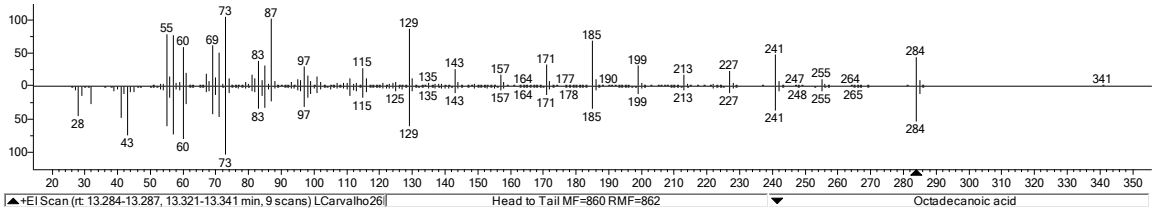
Sample 10

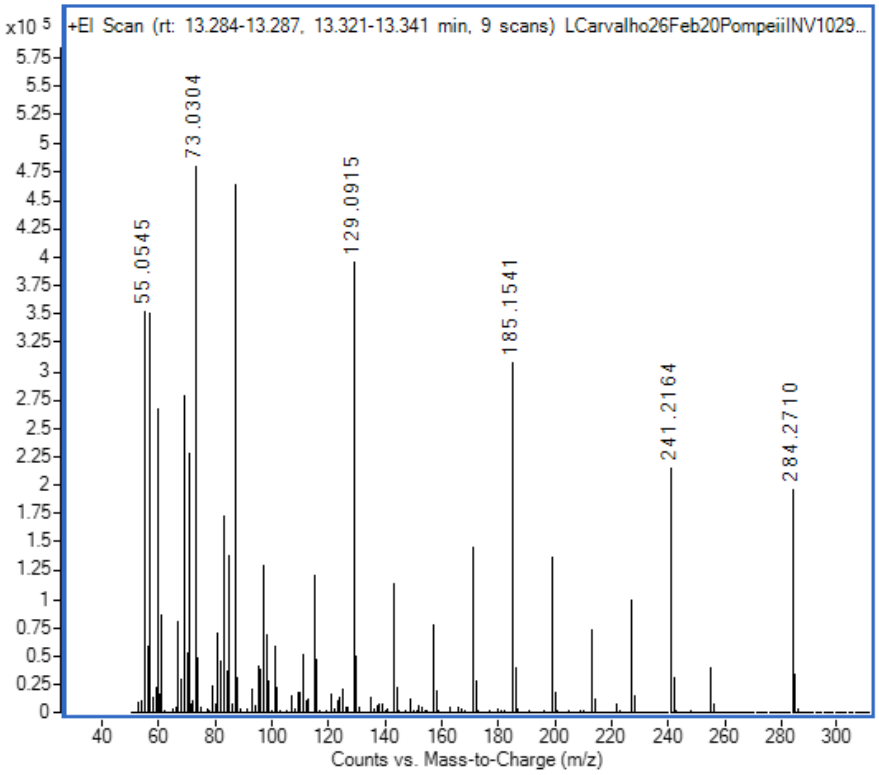

+EI Scan (rt: 13.201-13.272 min, 22 scans) LCarvalho26Feb20Pompe
Head to Tail MF=801 RMF=844
Oleic Acid


x10 5
+EI Scan (rt: 13.201-13.272 min, 22 scans) LCarvalho26Feb20PompeiiINV10295sample10.D...
55.0547
69.0703
83.0857
97.1007
111.1155
123.1046
133.1005
147.0672
157.1223
165.1358
180.1828
193.1673
207.0349
221.0858
235.2072
246.2342
264.2463
281.0526
282.2541
Counts vs. Mass-to-Charge (m/z)

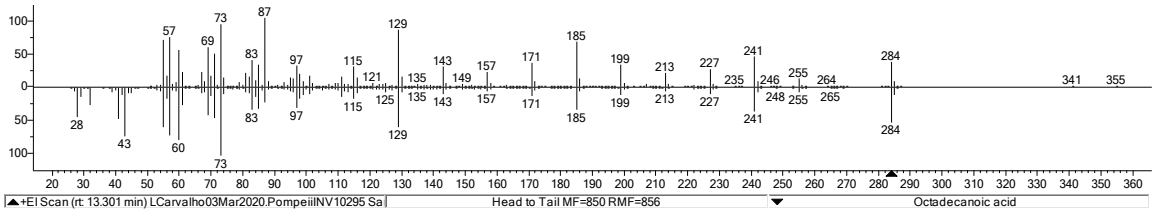
[12] Octadecanoic acid

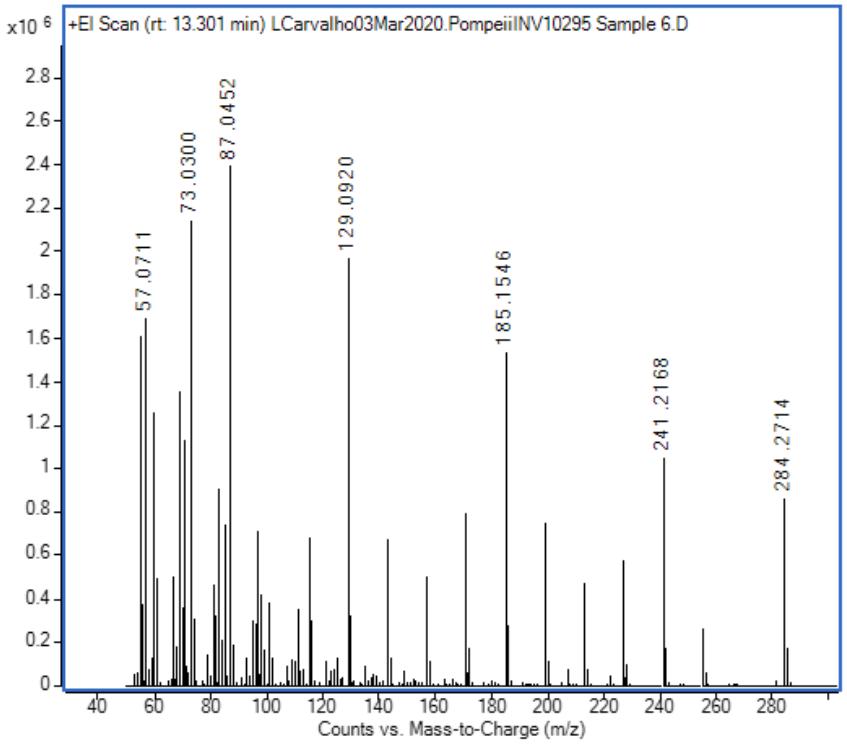
Sample 4



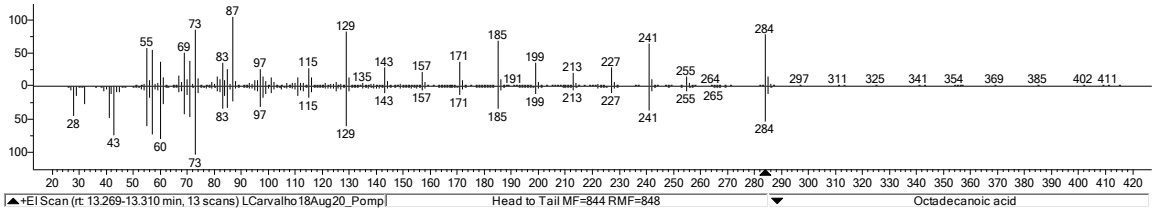


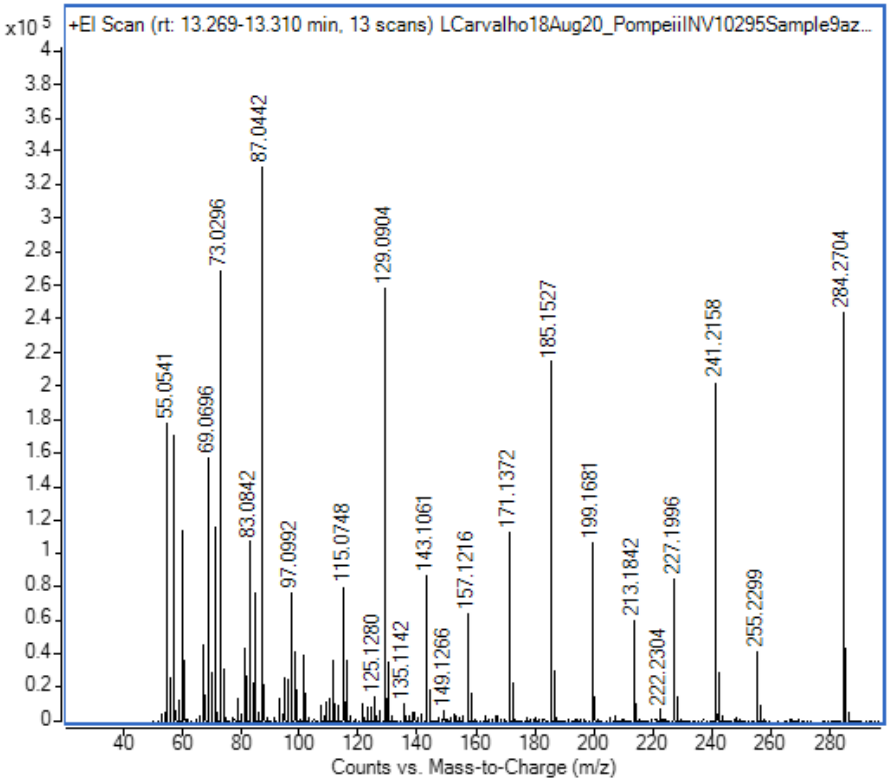
Sample 6


+El Scan (rt: 13.301 min) LCarvalho03Mar2020.PompeiiINV10295 Sa
Head to Tail MF=850 RMF=856
Octadecanoic acid

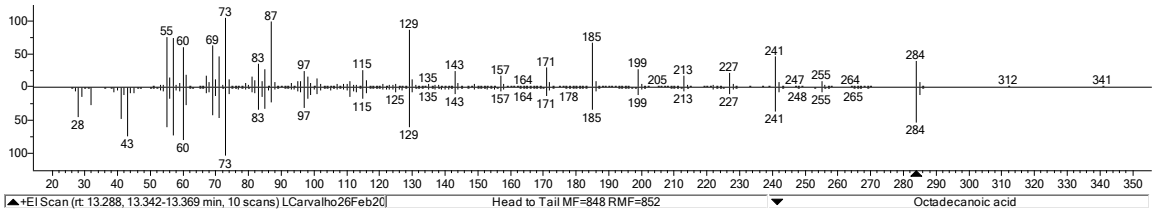

x10 6
+El Scan (rt: 13.301 min) LCarvalho03Mar2020.PompeiiINV10295 Sample 6.D
57.0711
73.0300
87.0452
129.0920
185.1546
241.2168
284.2714
Counts vs. Mass-to-Charge (m/z)

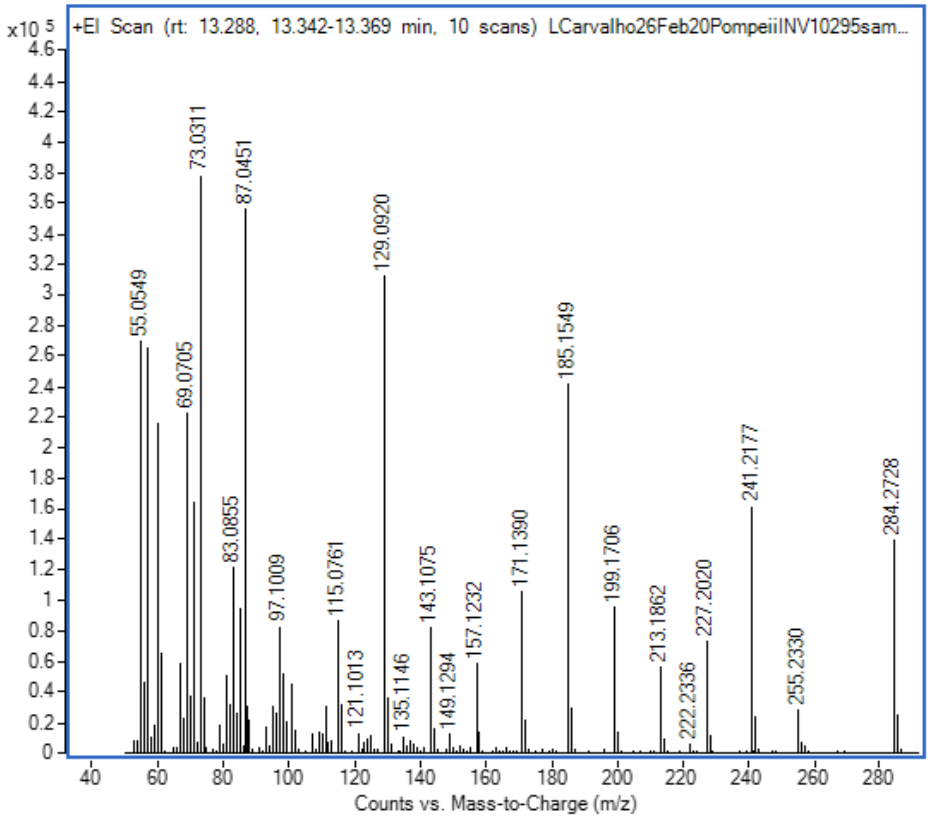
Sample 9


+El Scan (rt: 13.269-13.310 min, 13 scans) LCarvalho18Aug20_Pomp
Head to Tail MF=844 RMF=848
Octadecanoic acid


x10 5
+El Scan (rt: 13.269-13.310 min, 13 scans) LCarvalho18Aug20_PompeiiINV10295Sample9az...
55.0541
69.0696
73.0296
83.0842
87.0442
97.0992
115.0748
125.1280
129.0904
135.1142
143.1061
149.1266
157.1216
171.1372
185.1527
199.1681
213.1842
222.2304
227.1996
241.2158
255.2299
284.2704
Counts vs. Mass-to-Charge (m/z)

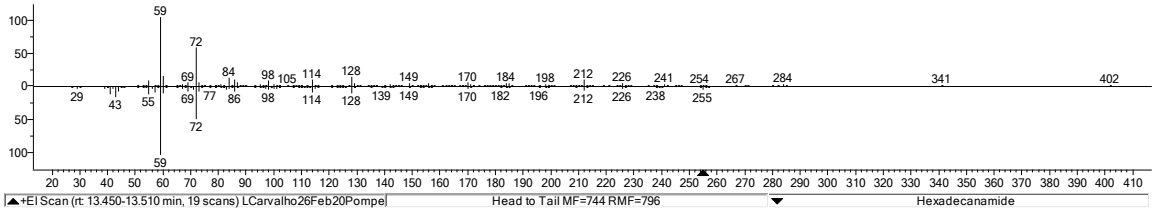
Sample 10

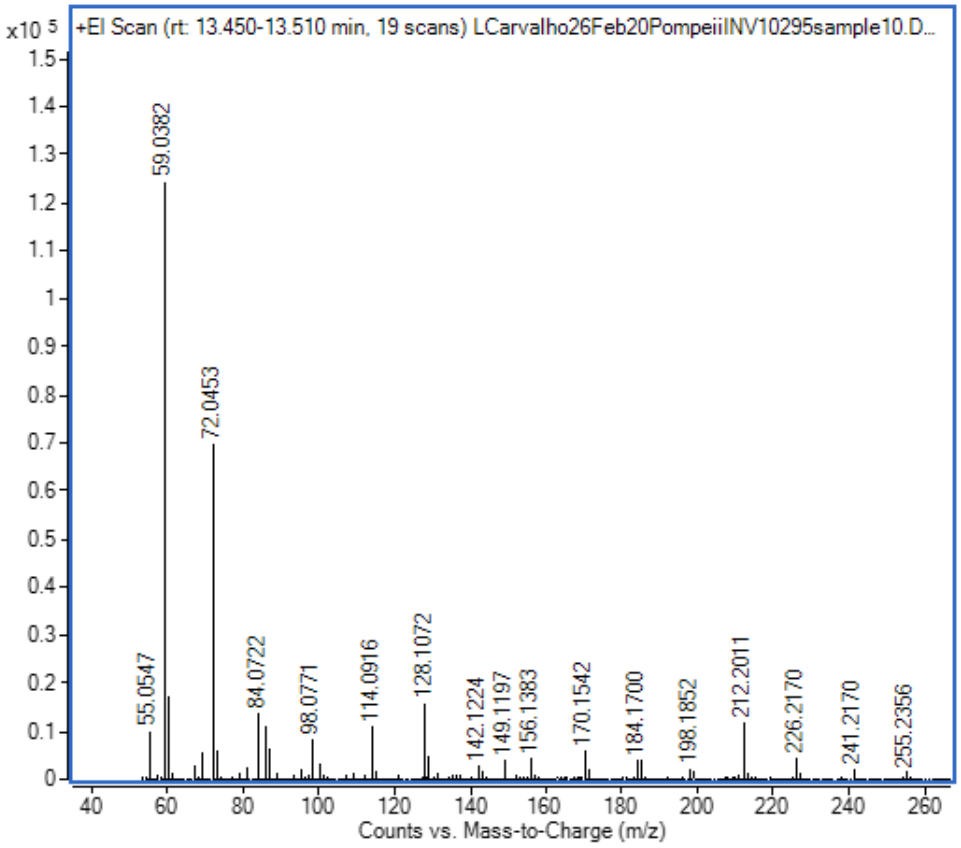

+EI Scan (rt: 13.288, 13.342-13.369 min, 10 scans) LCarvalho26Feb20
Head to Tail MF=848 RMF=852
Octadecanoic acid


x10 5
+EI Scan (rt: 13.288, 13.342-13.369 min, 10 scans) LCarvalho26Feb20PompeiiINV10295sam...
55.0549
69.0705
73.0311
83.0855
87.0451
97.1009
115.0761
121.1013
129.0920
135.1146
143.1075
149.1294
157.1232
171.1390
185.1549
199.1706
213.1862
222.2336
227.2020
241.2177
255.2330
284.2728
Counts vs. Mass-to-Charge (m/z)

[13] Hexadecanamide Mass: 255.256215

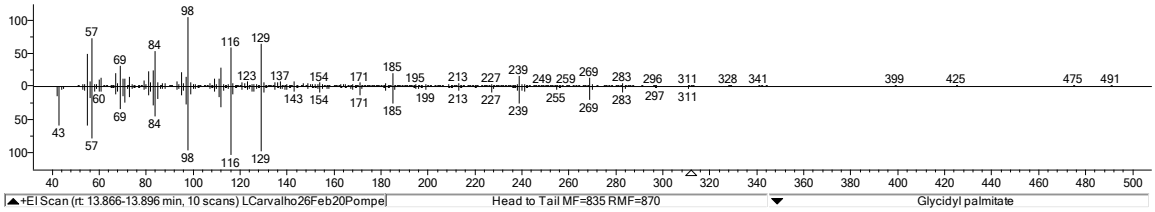
Sample 10

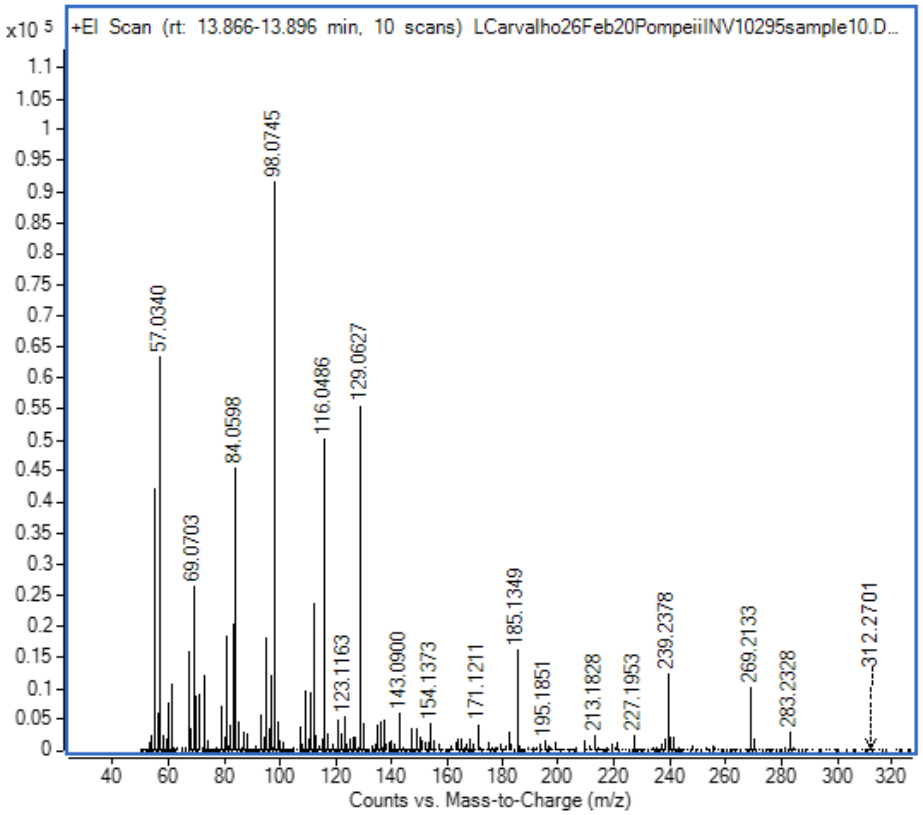




[14] Glycidyl palmitate Mass: 312.266445

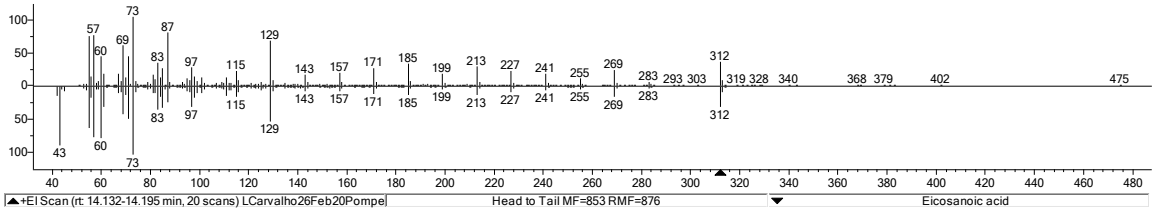
Sample 10

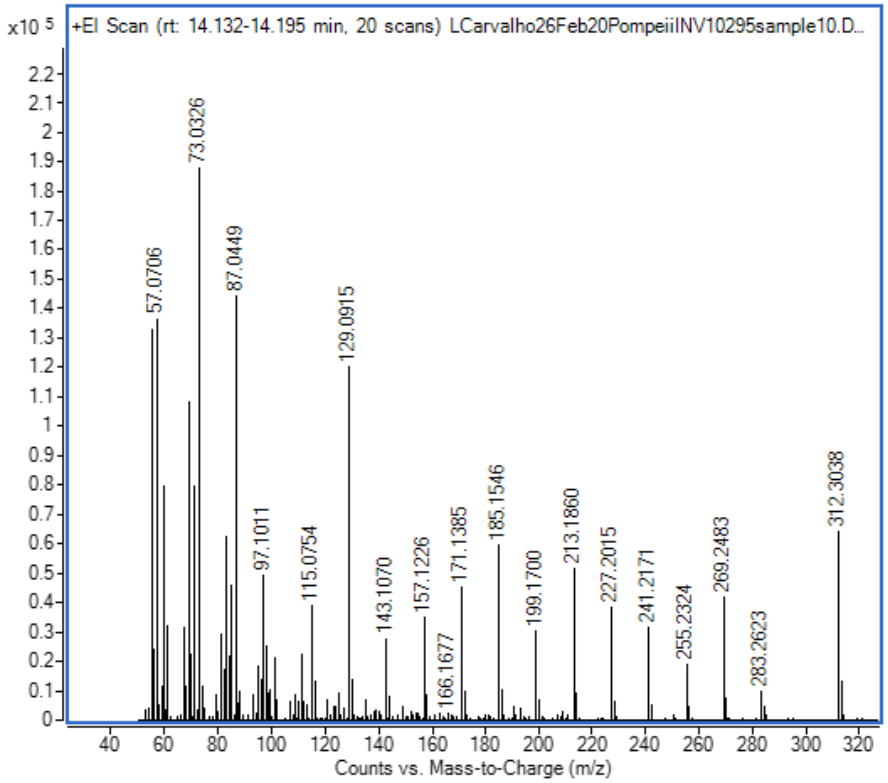




[15] Eicosanoic acid Mass: 312.30283

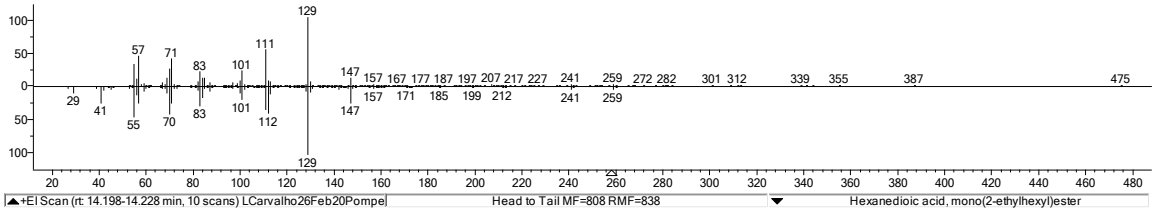
Sample 10

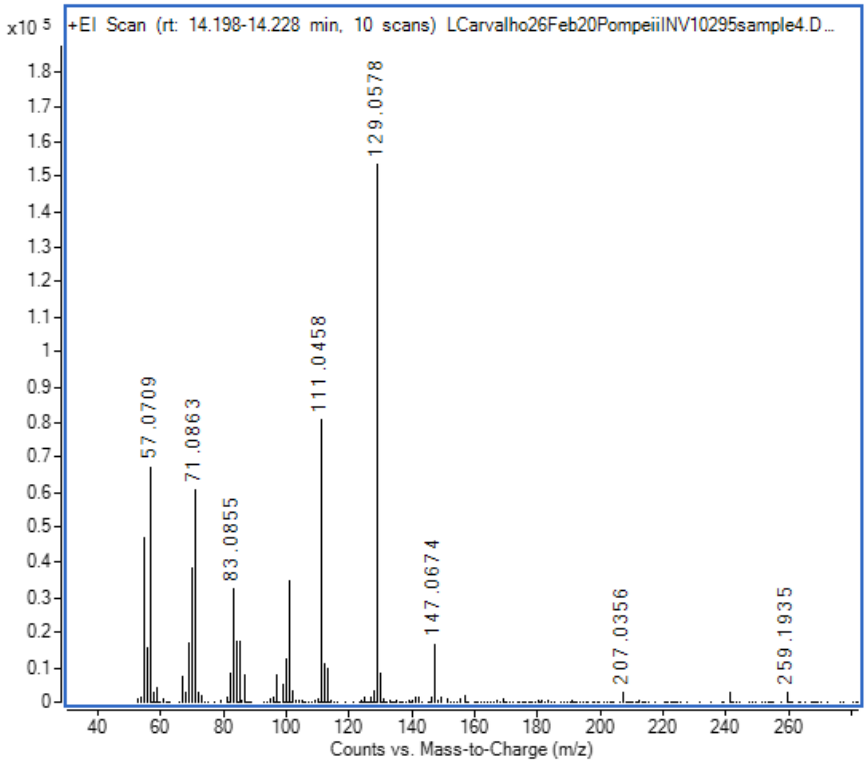




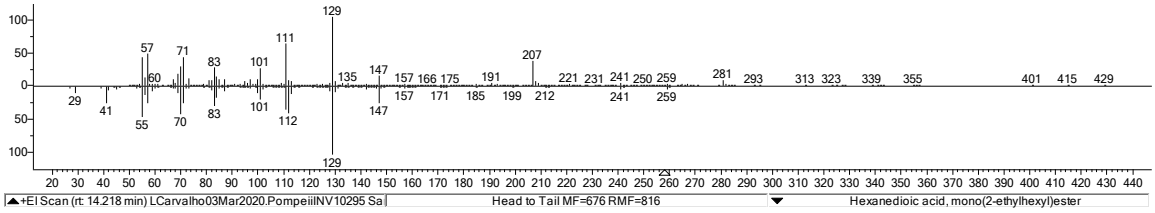
[16] Hexanedioic acid, mono(2-ethylhexyl)ester (Mono-2-ethylhezyl adipate)
Mass: 258.18311

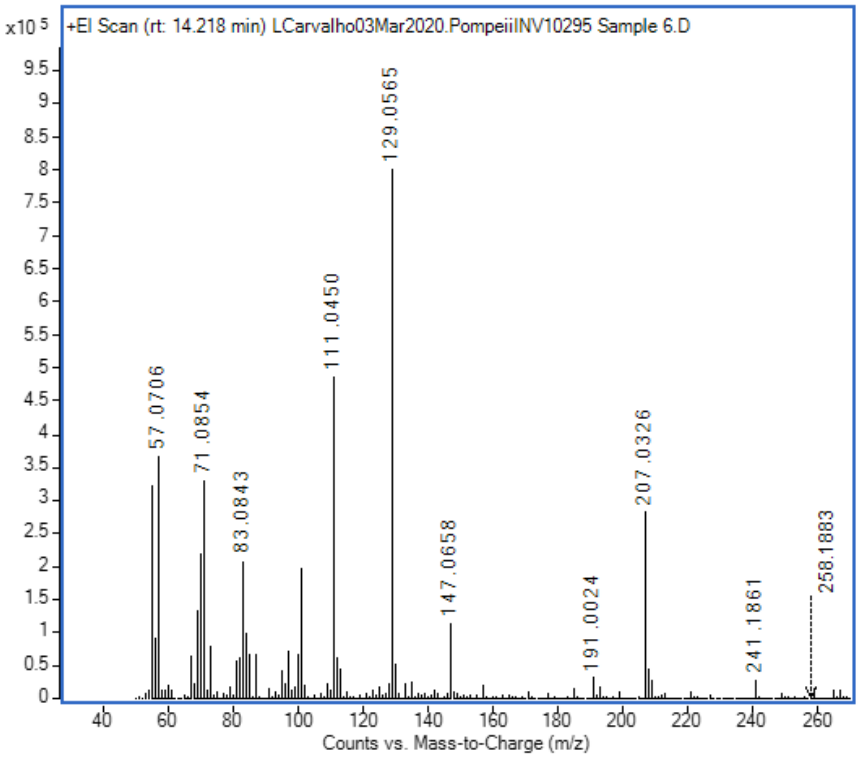
Sample 4



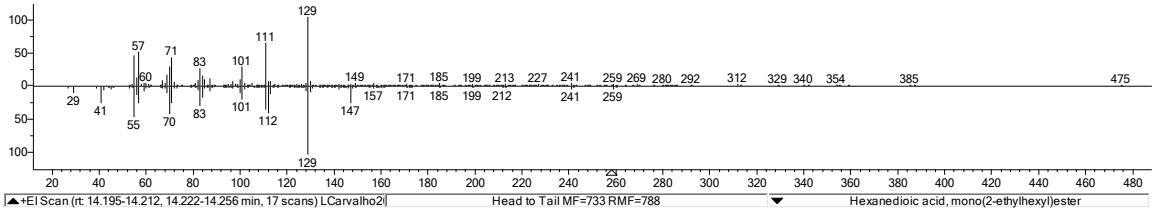


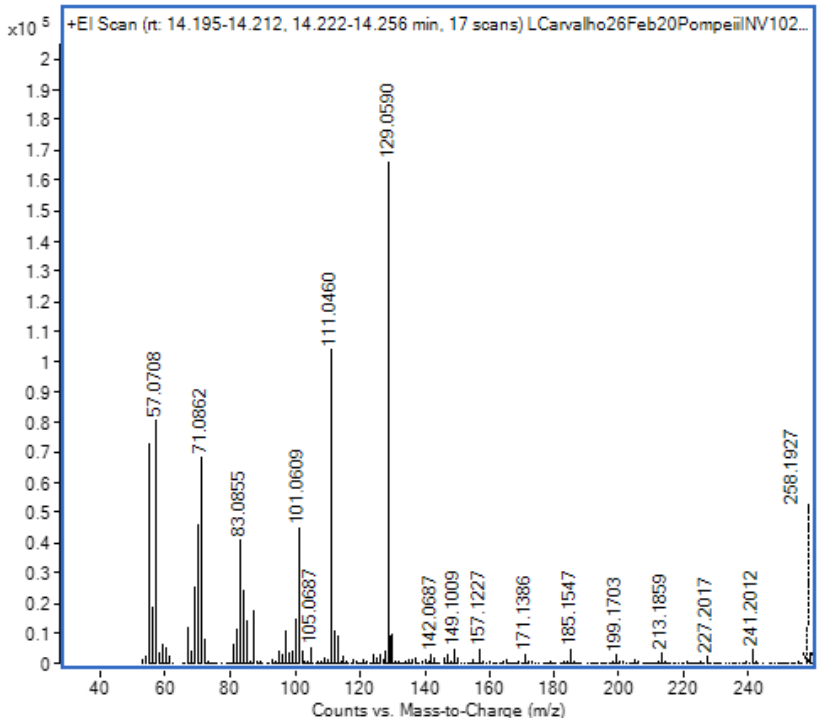
Sample 6


+El Scan (rt: 14.218 min) LCarvalho03Mar2020.PompeiiINV10295 Sa
Head to Tail MF=676 RMF=816
Hexanedioic acid, mono(2-ethylhexyl)ester


x10 5
+El Scan (rt: 14.218 min) LCarvalho03Mar2020.PompeiiINV10295 Sample 6.D
129.0565
111.0450
57.0706
71.0854
83.0843
147.0658
207.0326
191.0024
241.1861
258.1883
Counts vs. Mass-to-Charge (m/z)

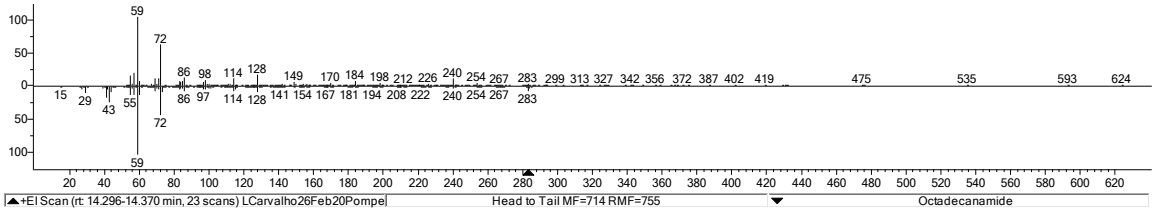
Sample 10

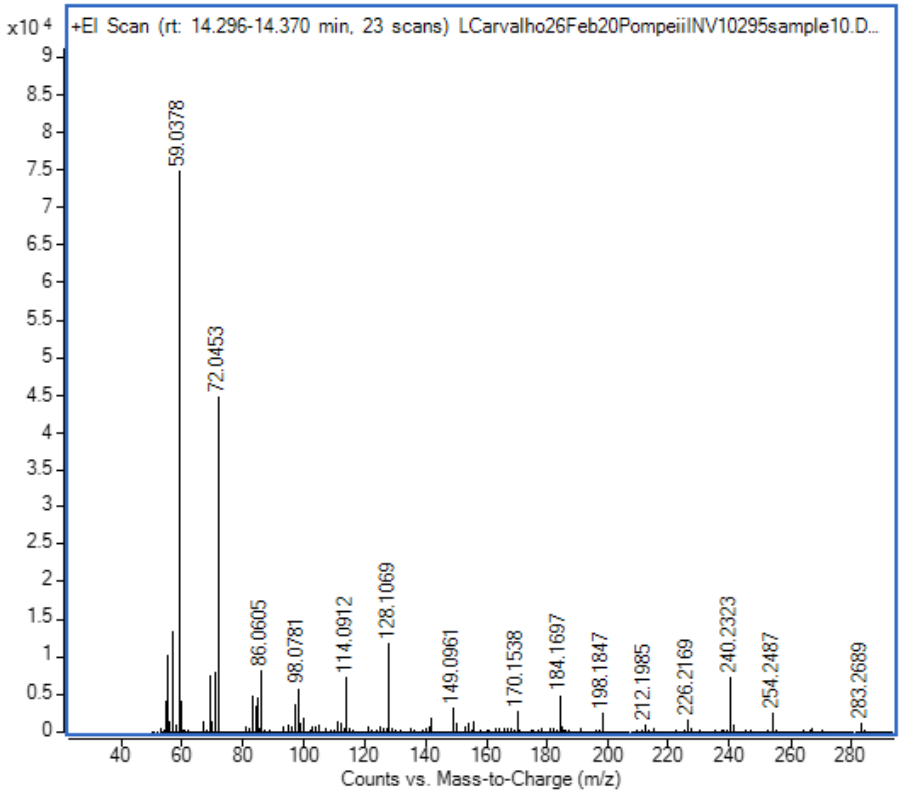

+EI Scan (rt: 14.195-14.212, 14.222-14.256 min, 17 scans) LCarvalho2(
Head to Tail MF=733 RMF=788
Hexanedioic acid, mono(2-ethylhexyl)ester


+EI Scan (rt: 14.195-14.212, 14.222-14.256 min, 17 scans) LCarvalho26Feb20PompeiiINV102...
x10 5
129.0590
111.0460
57.0708
71.0862
83.0855
101.0609
105.0687
142.0687
149.1009
157.1227
171.1386
185.1547
199.1703
213.1859
227.2017
241.2012
258.1927
Counts vs. Mass-to-Charge (m/z)

[17] Octadecanamide Mass: 283.287516

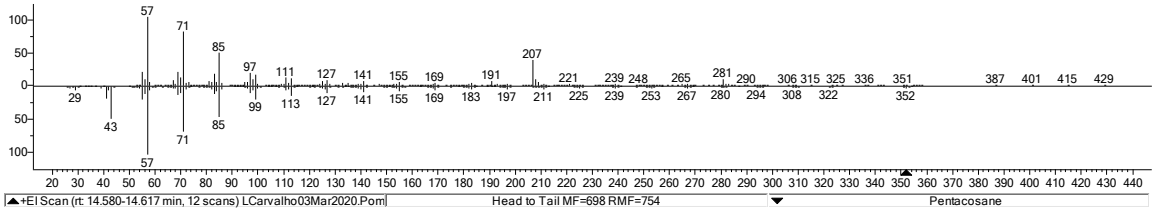
Sample 10

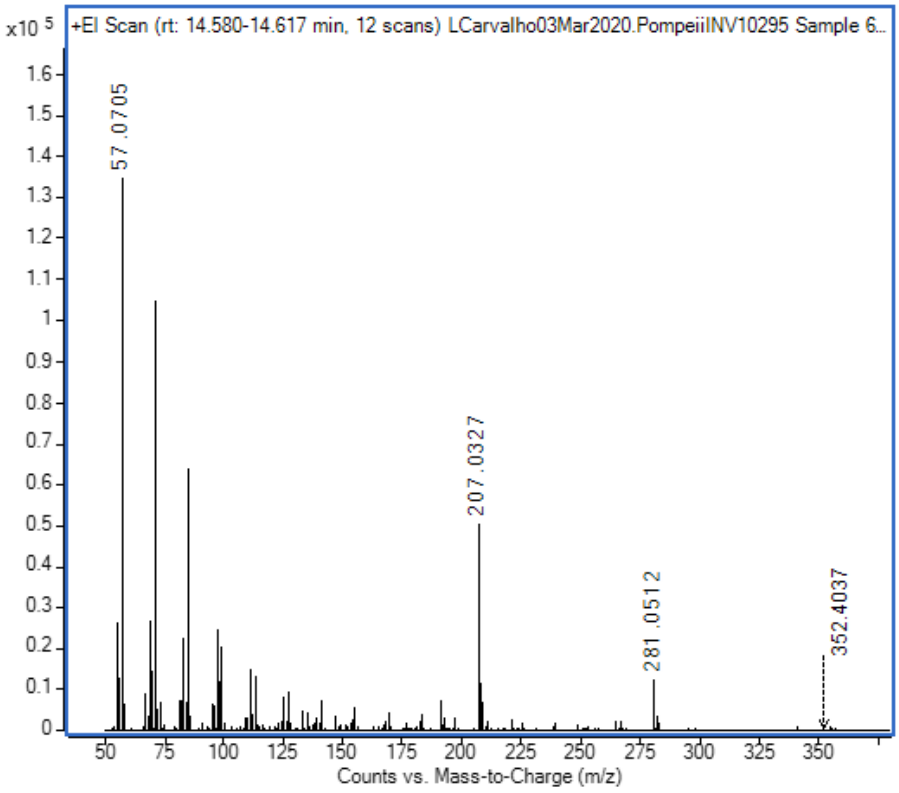




[18] Pentacosane Mass: 352.406902

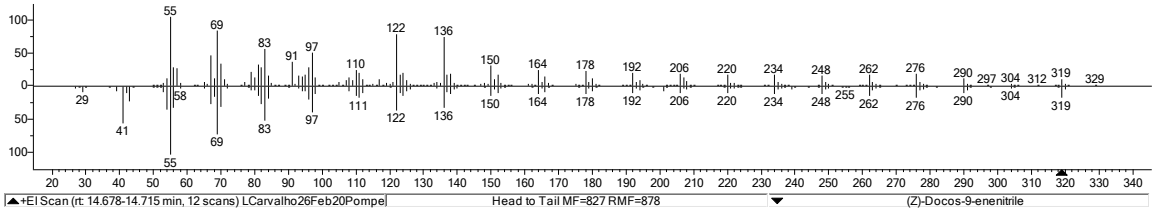
Sample 6

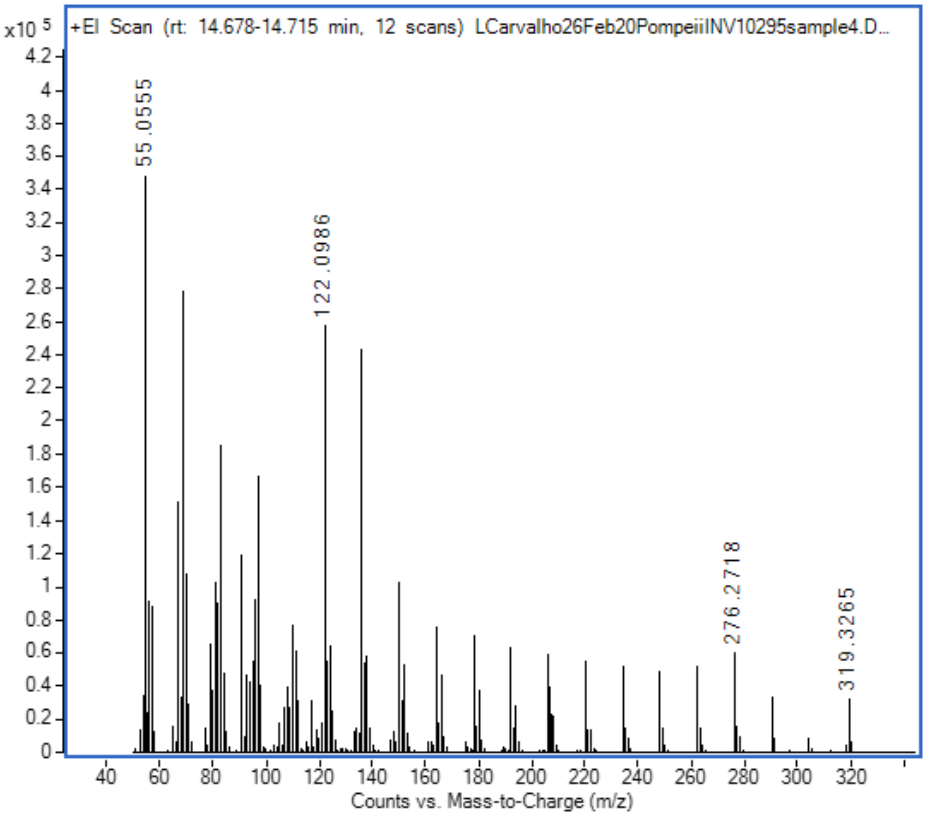




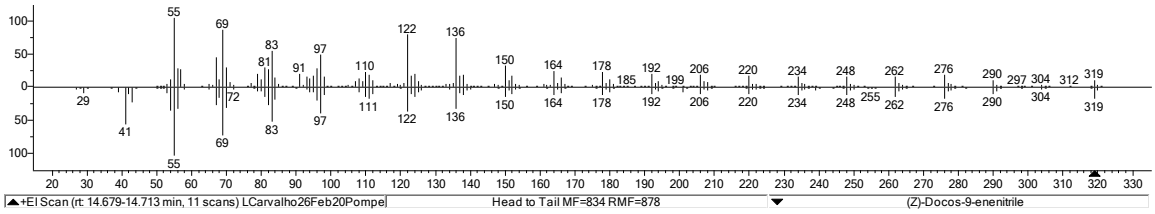
[19] (Z)-Docos-9-enenitrile

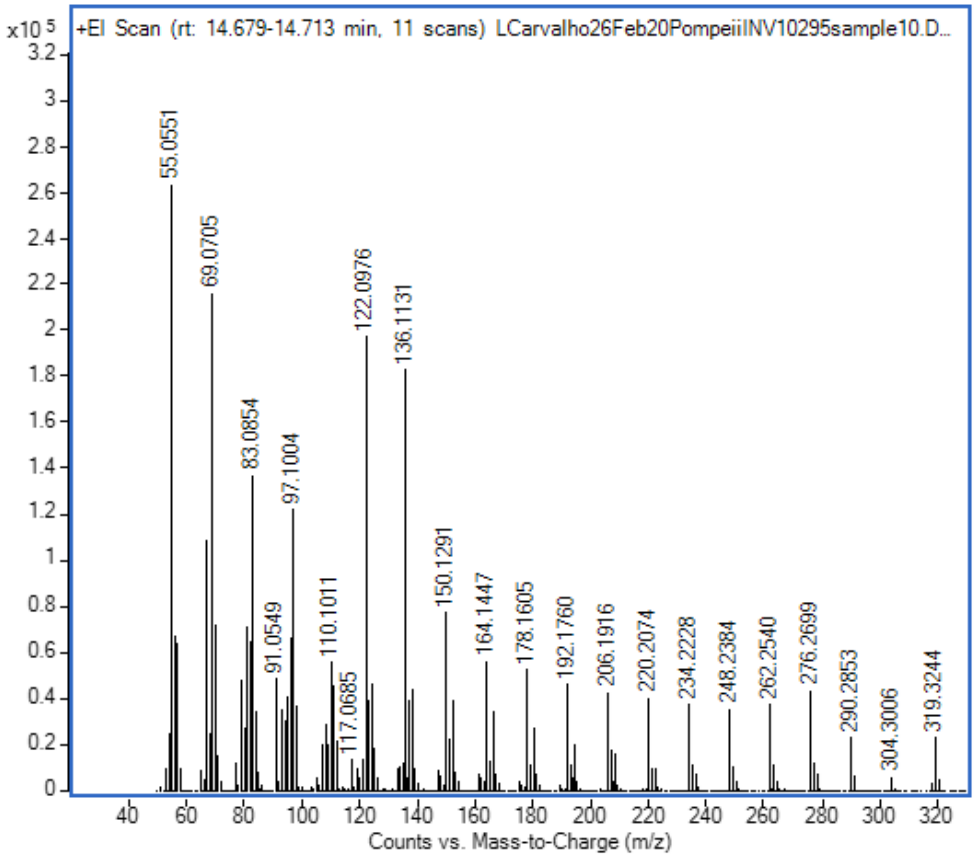
Sample 4





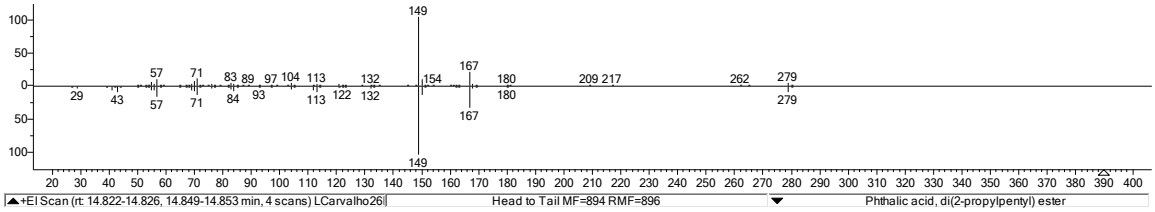
Sample 10

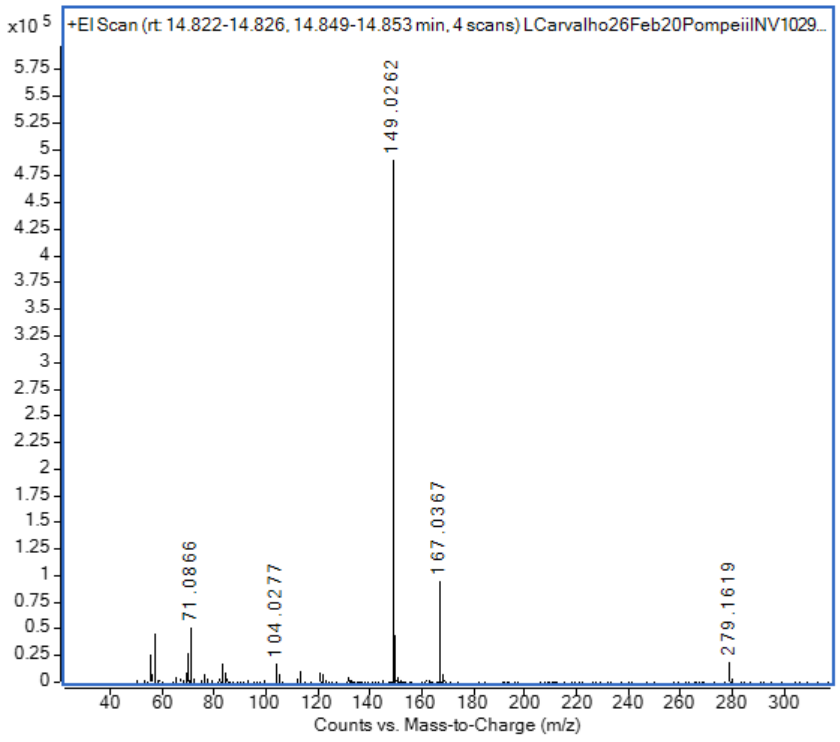

+EI Scan (rt: 14.679-14.713 min, 11 scans) LCarvalho26Feb20Pompe
Head to Tail MF=834 RMF=878
(Z)-Docos-9-enenitrile


x10 5
+EI Scan (rt: 14.679-14.713 min, 11 scans) LCarvalho26Feb20PompeiiINV10295sample10.D...
55.0551
69.0705
83.0854
97.1004
91.0549
110.1011
117.0685
122.0976
136.1131
150.1291
164.1447
178.1605
192.1760
206.1916
220.2074
234.2228
248.2384
262.2540
276.2699
290.2853
304.3006
319.3244
Counts vs. Mass-to-Charge (m/z)

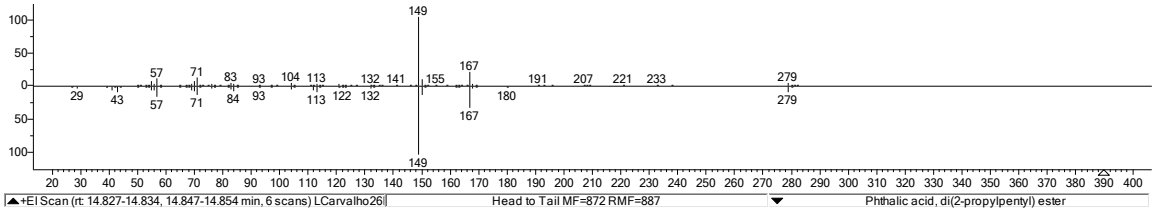
[20] Phthalic acid, di(2-propylpentyl) ester Mass: 390.27701

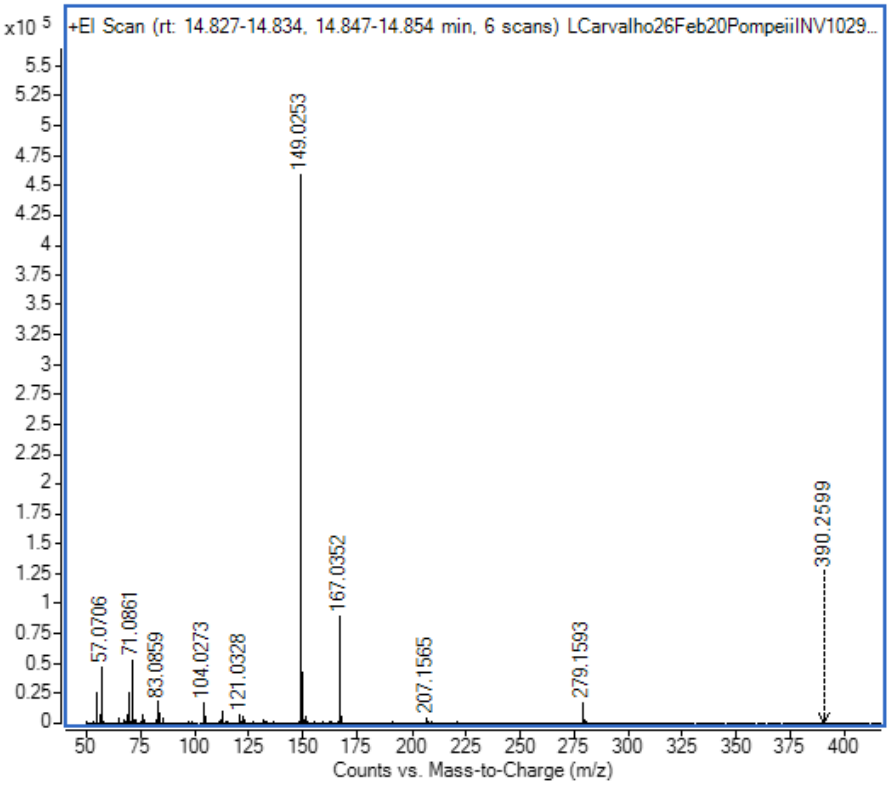
Sample 4





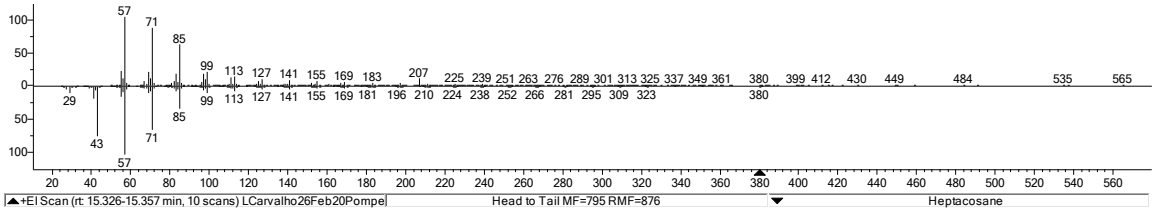
Sample 10

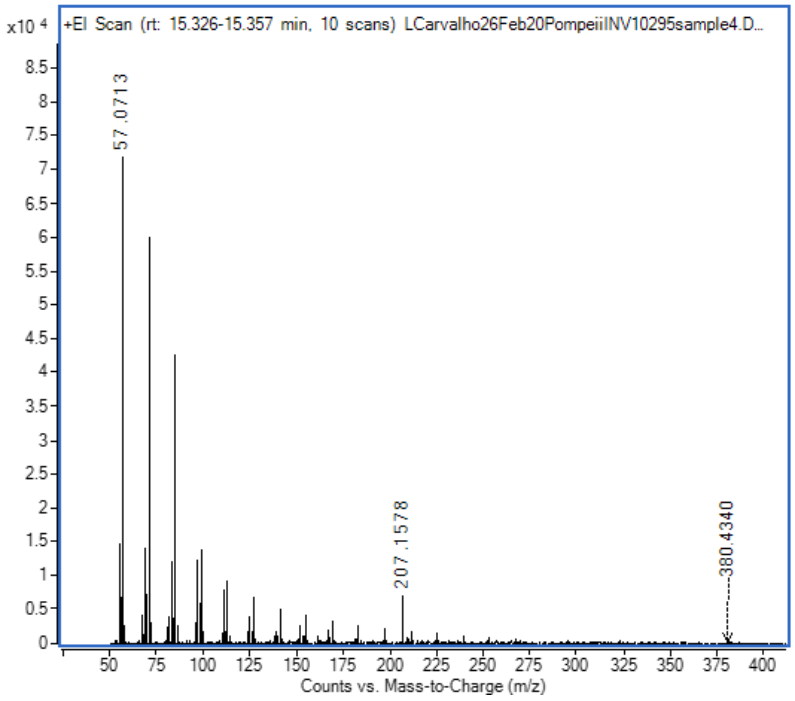

+EI Scan (rt: 14.827-14.834, 14.847-14.854 min, 6 scans) LCarvalho26
Head to Tail MF=872 RMF=887
Phthalic acid, di(2-propylpentyl) ester


x10 5
+EI Scan (rt: 14.827-14.834, 14.847-14.854 min, 6 scans) LCarvalho26Feb20PompeiiINV1029...
149.0253
167.0352
390.2599
57.0706
71.0861
83.0859
104.0273
121.0328
207.1565
279.1593
Counts vs. Mass-to-Charge (m/z)

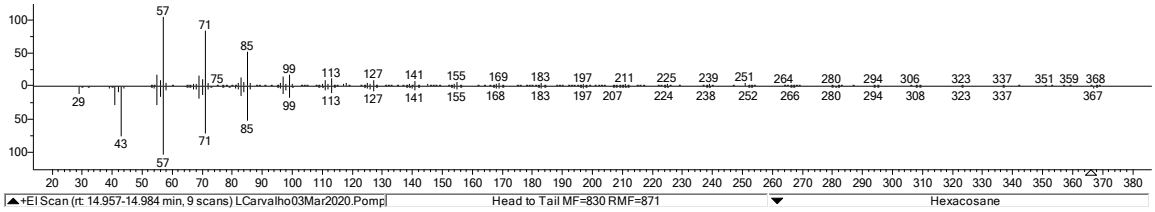
[21] Hexacosane Mass: 380.438202

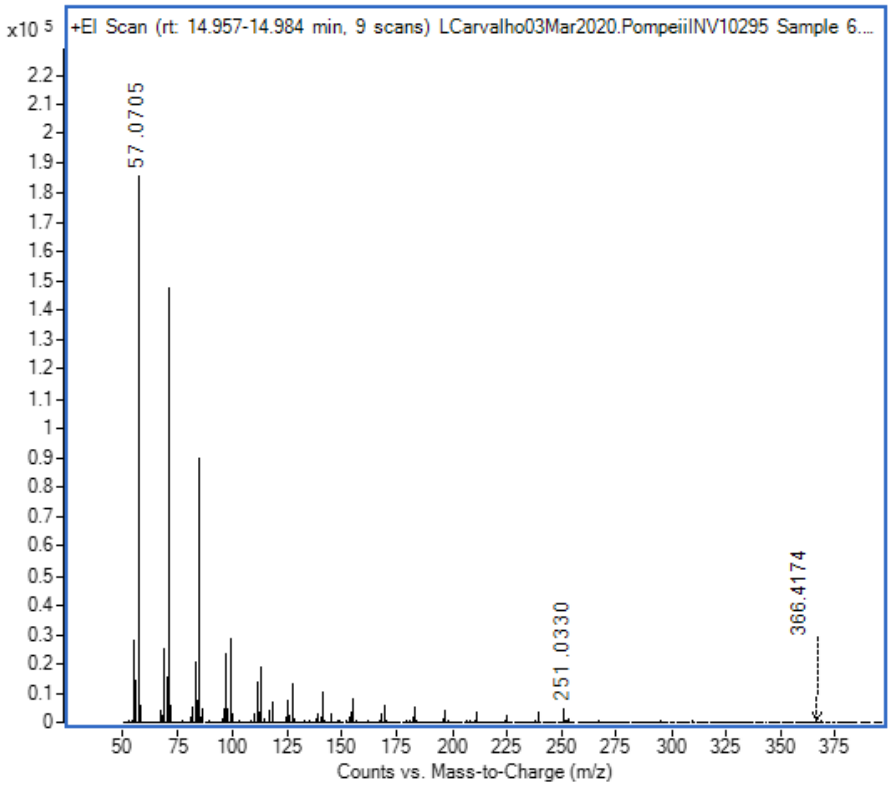
Sample 4





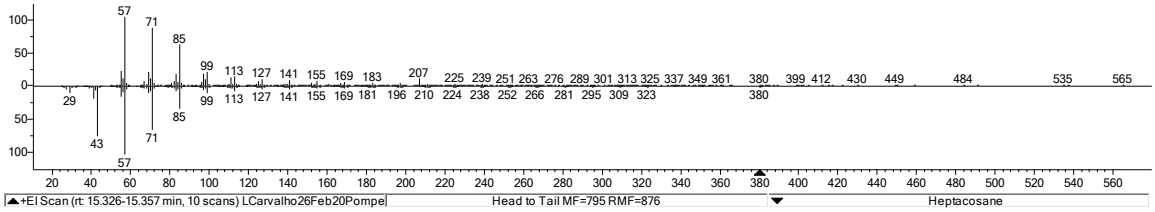
Sample 6

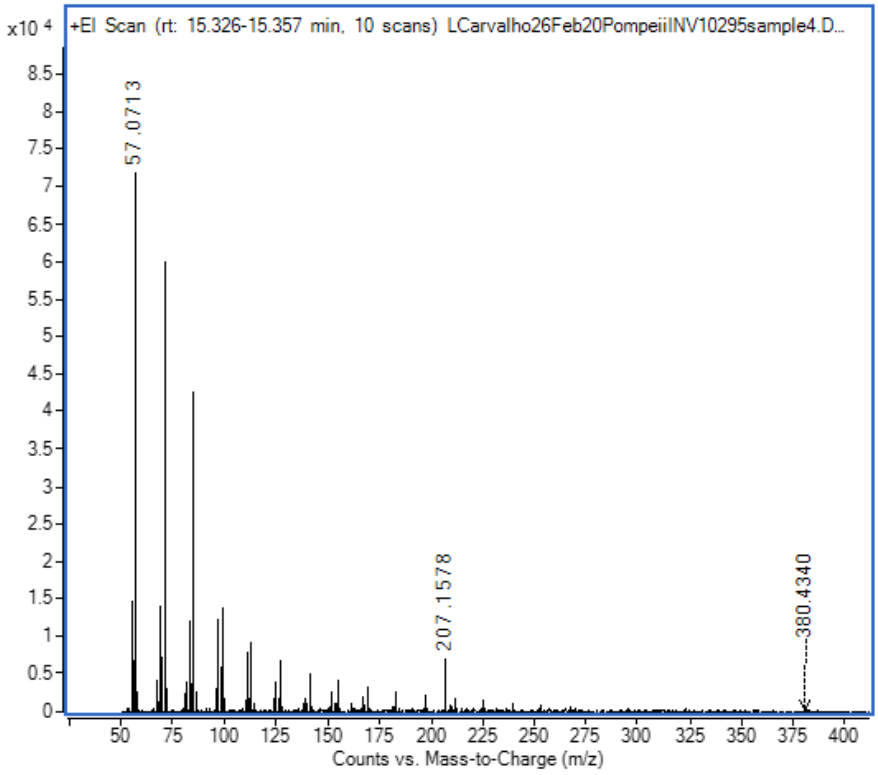

+EI Scan (rt: 14.957-14.984 min, 9 scans) LCarvalho03Mar2020.Pomp
Head to Tail MF=830 RMF=871
Hexacosane


x10 5
+EI Scan (rt: 14.957-14.984 min, 9 scans) LCarvalho03Mar2020.PompeiiINV10295 Sample 6...
57.0705
251.0330
366.4174
Counts vs. Mass-to-Charge (m/z)

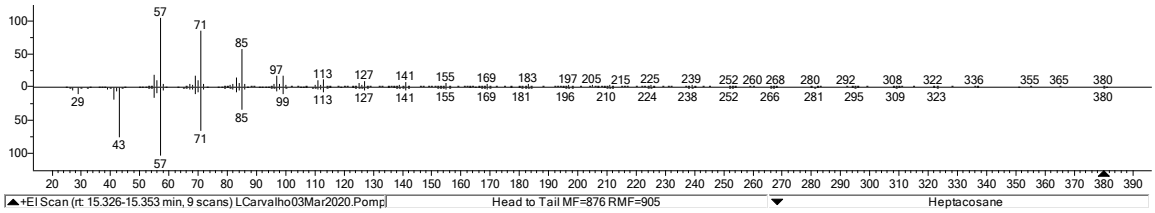
[22] Heptacosane Mass: 380.438202

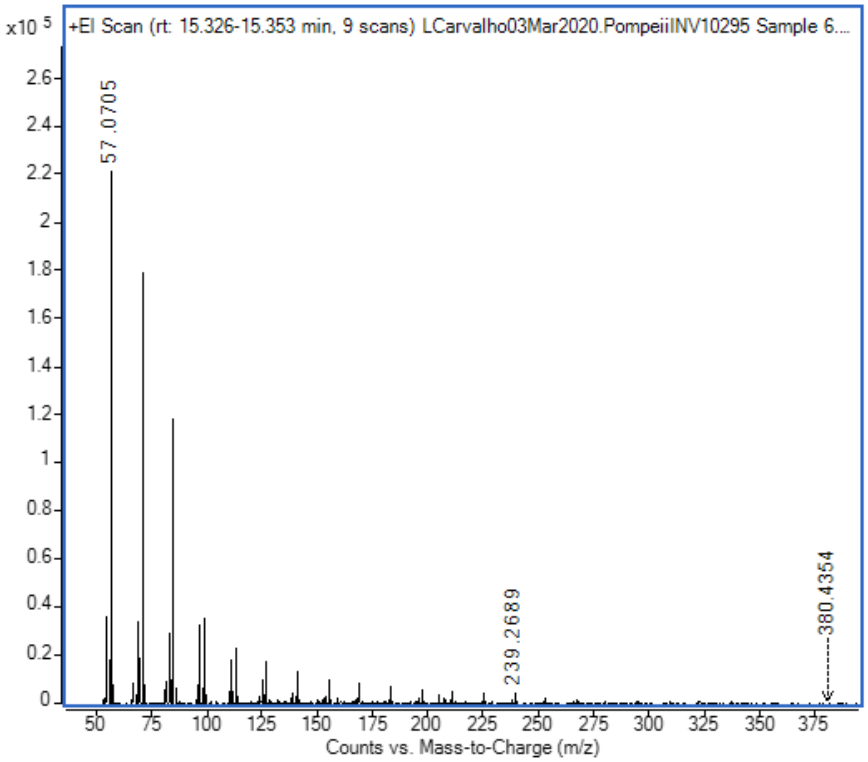
Sample 4





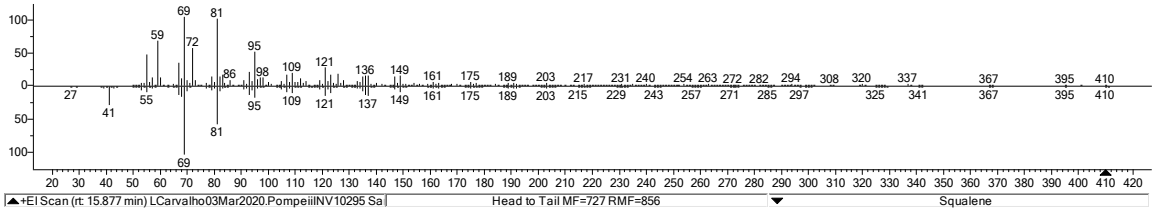
Sample 6

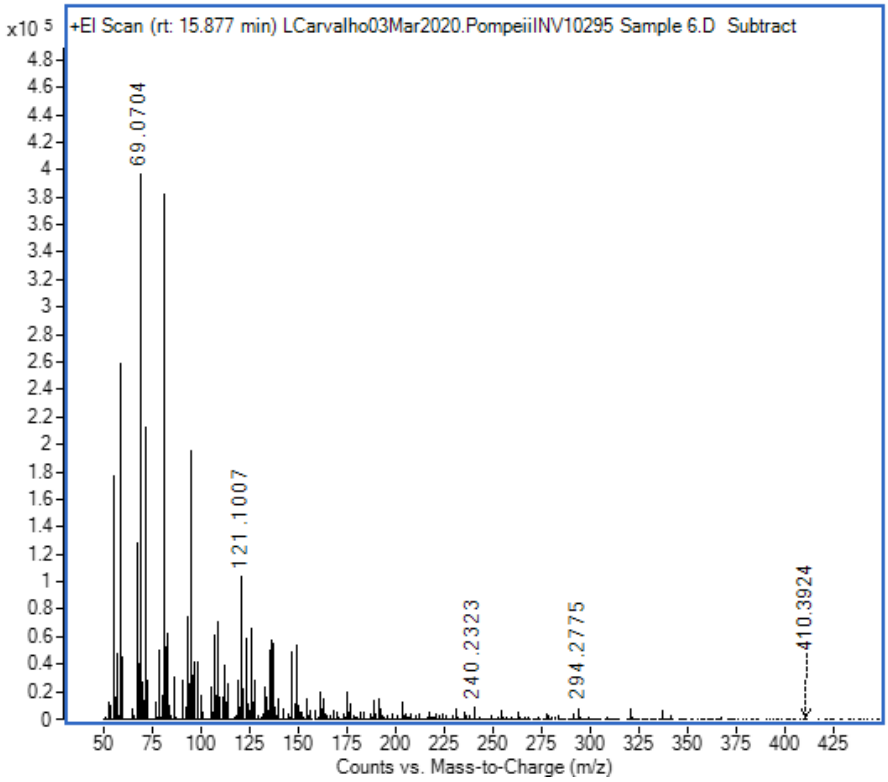

+EI Scan (rt: 15.326-15.353 min, 9 scans) LCarvalho03Mar2020.Pomp
Head to Tail MF=876 RMF=905
Heptacosane


x10 5
+EI Scan (rt: 15.326-15.353 min, 9 scans) LCarvalho03Mar2020.PompeiiINV10295 Sample 6....
57.0705
239.2689
380.4354
Counts vs. Mass-to-Charge (m/z)

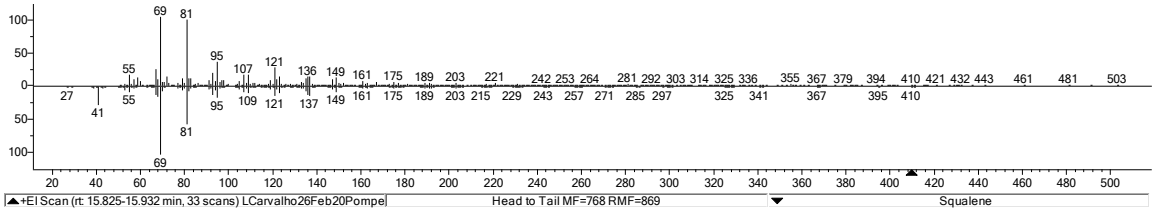
[23] Squalene

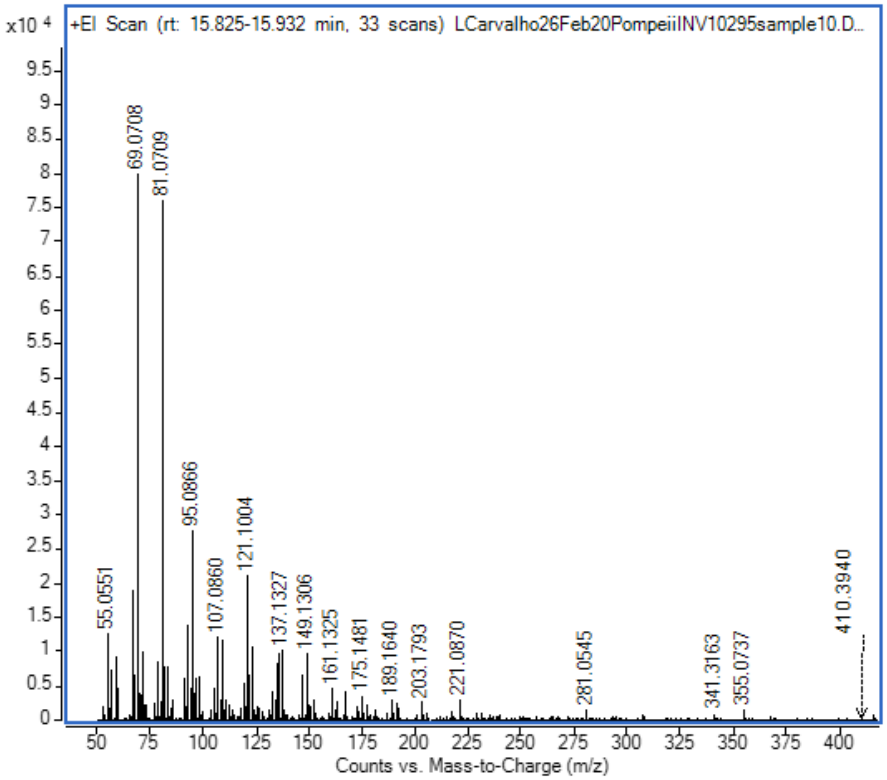
Sample 6





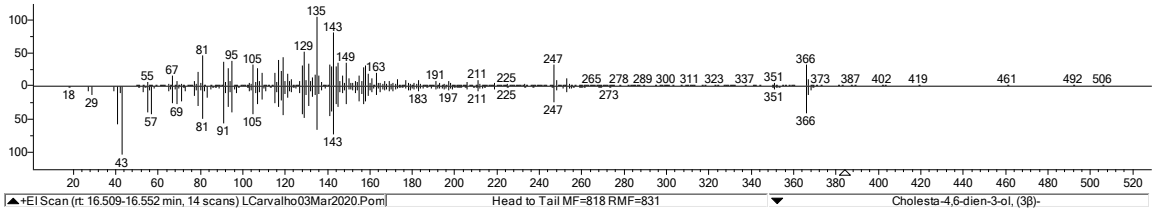
Sample 10

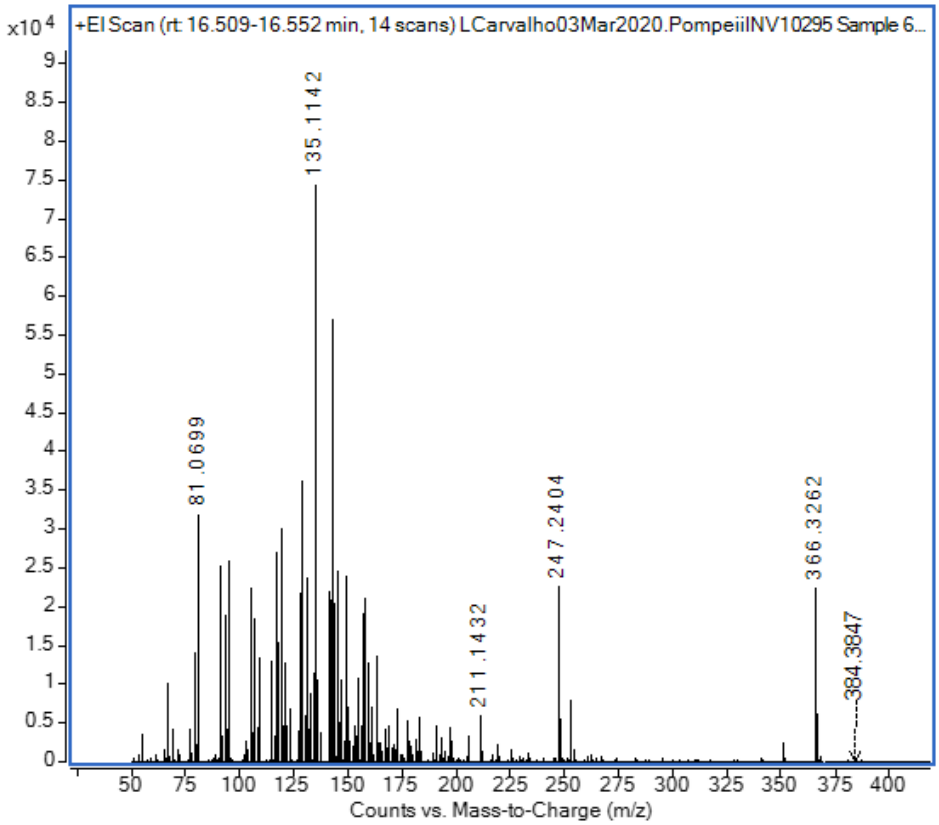

+EI Scan (rt: 15.825-15.932 min, 33 scans) LCarvalho26Feb20Pompe
Head to Tail MF=768 RMF=869
Squalene


x10 4
+EI Scan (rt: 15.825-15.932 min, 33 scans) LCarvalho26Feb20PompeiiINV10295sample10.D...
69.0708
81.0709
95.0866
121.1004
55.0551
107.0860
137.1327
149.1306
161.1325
175.1481
189.1640
203.1793
221.0870
281.0545
341.3163
355.0737
410.3940
Counts vs. Mass-to-Charge (m/z)

[24] Cholesta-4,6-dien-3-ol, (3β)- Mass: 384.339216

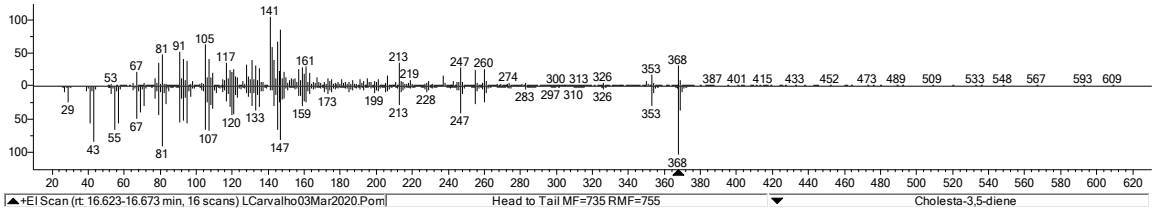
Sample 6

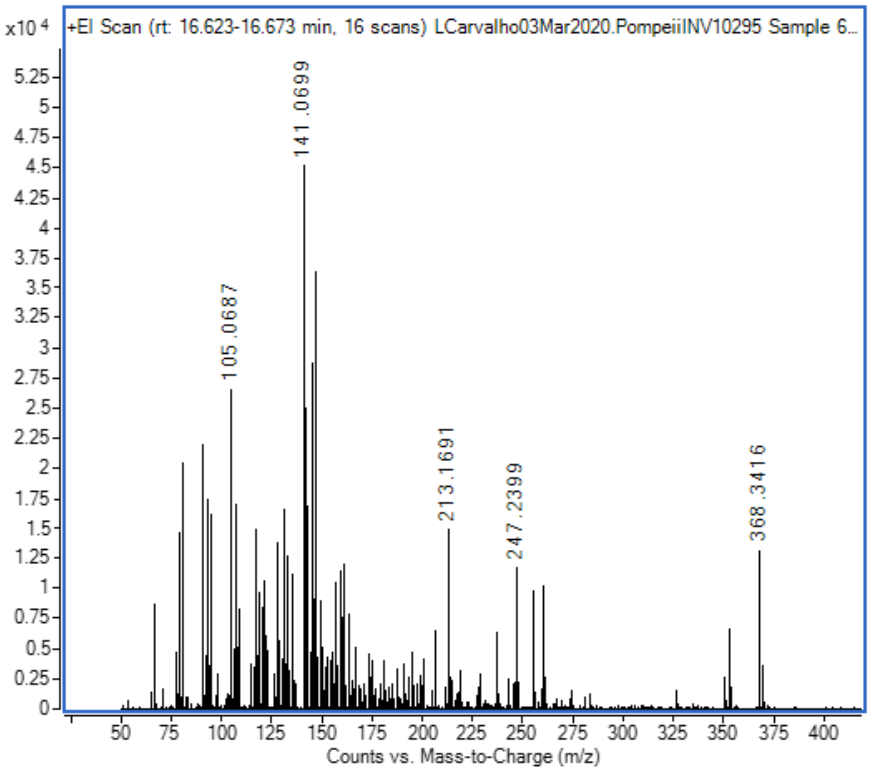




[25] Cholesta-3,5-diene Mass: 368.344301

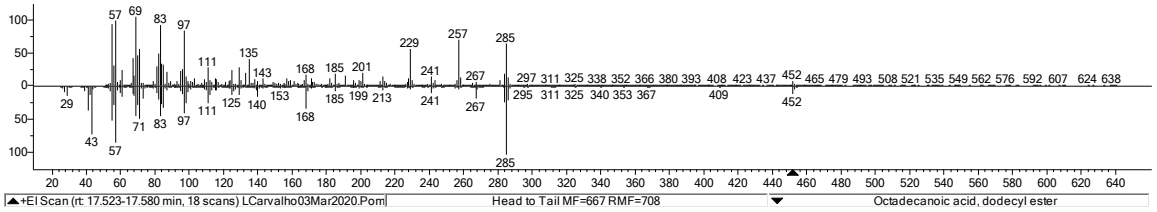
Sample 6

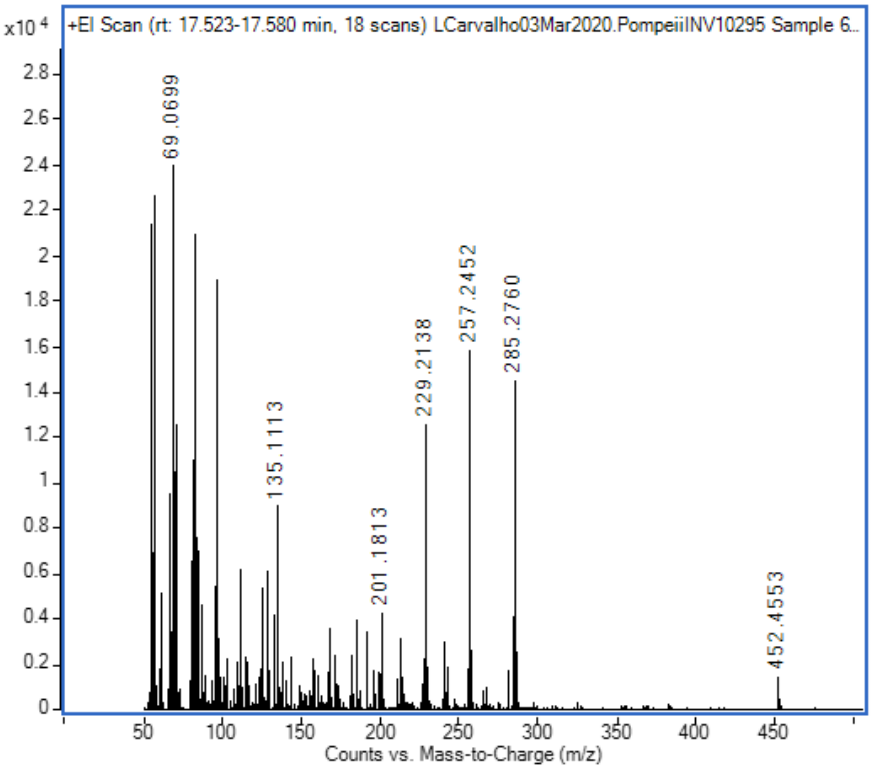




[26] Octadecanoic acid, dodecyl ester Mass: 452.459332

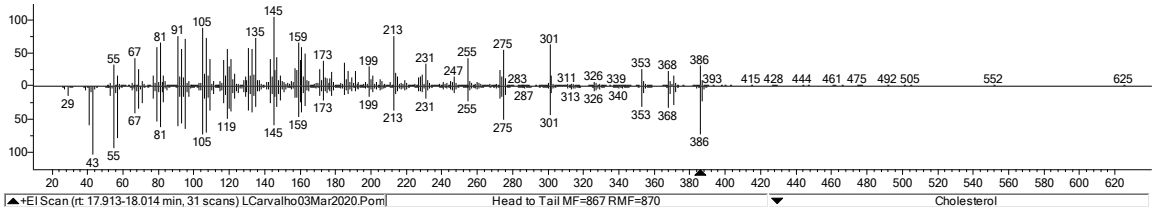
Sample 6

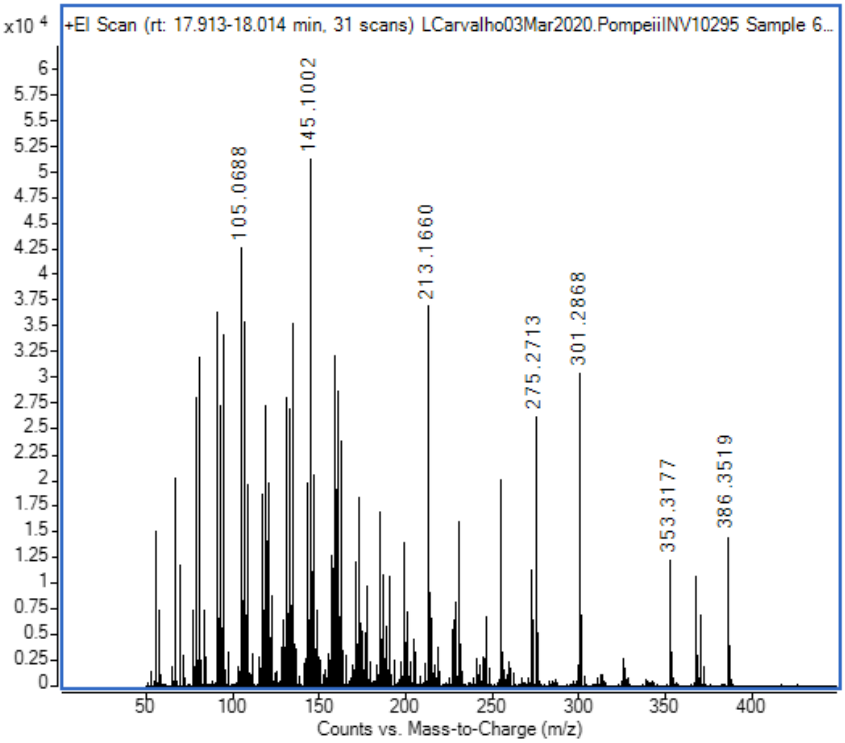




[27] Cholesterol

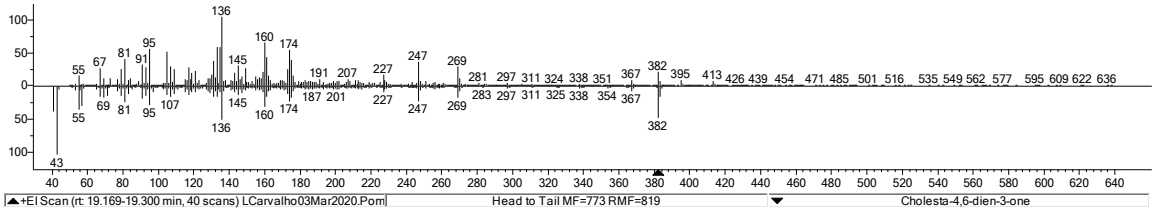
Sample 6

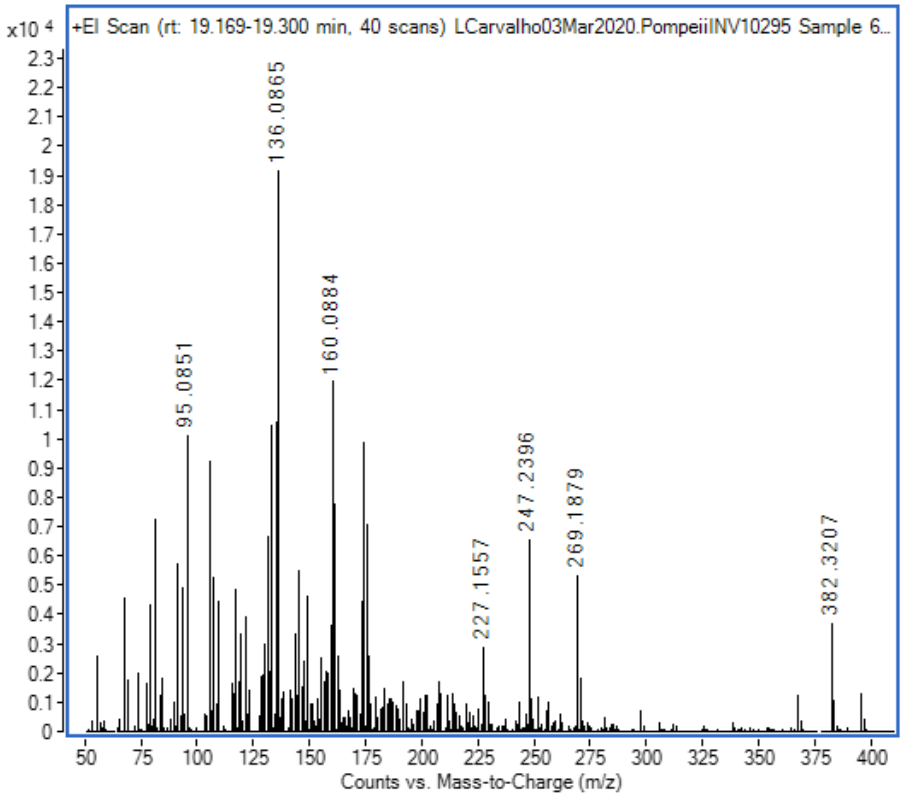




[18] Cholesta-4,6-dien-3-one Mass: 382.323566

Sample 6





Compound	Name	Formula	m/z	Score	Mass Error (ppm)	RT Error (min)	Isotope Similarity (ppm)	Maximum Fold Change	Isotope Distribution	Normalised abundance P10295_1	P10295_2A	P10295_2B	P10295_4	P10295_5	P10295_6	P10295_10
13.88_187.0975m/z	Nonate	C9H16O4	187.0975	52.5	-3.2775	0.03	98.98	11.13	100 - 9.61 - 0.602	33095.96	30545.03	31653.21	29679.63	32946.55	30014.95	2972.71
4.37_89.0244m/z	Dihydroxyacetone	C3H6O3	89.0244	40.6	-0.2441	-0.37	98.50	7.23	100 - 2.41 - 0.116	10647.59	7535.30	31422.33	4346.15	6472.12	8458.89	9051.04
19.16_143.1077m/z	Octanoic acid	C8H16O2	143.1077	41.5	-0.0281	-0.79	98.29	3.60	100 - 7.61 - 0.195	6773.67	3085.94	4325.89	1879.23	3313.70	2592.08	2831.93
17.90_201.1133m/z	Sebacic acid	C10H18O4	201.1133	42.7	0.1141	-0.40	97.58	2.32	100 - 9.51 - 0.43	2620.02	2233.02	2129.76	2375.72	2618.27	2290.89	4932.59
10.19_145.0507m/z	Methylglutaric acid	C6H10O4	145.0507	41	0.3144	-0.54	98.01	2.15	100 - 5.15 - 0.481	3565.28	2352.73	3947.96	2062.21	2815.53	2372.20	1836.58
2.67_341.1093m/z	Lactose	C12H22O11	341.1093	39.9	-0.6462	-0.37	97.25	14.66	100 - 12.3 - 1.55	966.23	1078.20	3199.23	305.22	218.30	468.48	1845.40
9.27_115.0764m/z	Caproic acid	C6H12O2	115.0764	39.5	-4.8475	0.69	98.25	128.51	100 - 5.34 - 0.0939	2919.08	1010.01	1677.09	379.76	546.93	925.29	22.71
7.43_131.0714m/z	Leucic acid	C6H12O3	131.0714	44.4	-4.1365	-0.08	98.11	4.59	100 - 5.16 - 0.36	2763.78	1723.48	2843.97	686.39	619.03	1056.50	1080.80
10.69_159.0662m/z	3,3 Dimethyl glutarate	C7H12O4	159.0662	41	-0.2341	-0.72	99.08	7.77	100 - 7.26 - 0.682	2704.62	2236.57	2402.10	2159.32	2414.13	2302.47	348.10
10.39_117.0193m/z	Succinic acid	C4H6O4	117.0193	40.9	0.0712	-0.72	98.51	1.51	100 - 3.32 - 0.556	1694.54	1898.58	1761.00	1257.29	1678.47	1645.70	1606.86
10.39_133.0143m/z	Malic acid	C4H6O5	133.0143	40.8	0.1075	-0.75	98.41	37.38	100 - 3.45 - 0.565	797.33	1442.62	790.57	474.34	607.14	547.26	38.59
9.79_145.0870m/z	Hydroxyisoheptanoic acid	C7H14O3	145.0870	48.3	-3.8191	0.05	99.32	2.50	100 - 7.36 - 0.637	1250.07	666.62	945.65	499.27	611.32	628.16	647.85
12.48_88.9880m/z	Oxalic acid	C2H2O4	88.9880	40.7	-0.0875	-0.92	97.97	13.11	100 - 0.904 - 0.181	1134.56	808.62	997.88	699.81	947.20	867.62	86.53
16.34_191.0197m/z	Citric acid	C6H8O7	191.0197	41.9	-0.1904	-0.57	98.84	34.63	100 - 6.61 - 0.715	1038.35	672.25	730.98	571.68	816.44	761.66	29.98
10.09_147.0299m/z	Citramalic acid	C5H8O5	147.0299	40.9	0.1929	-0.66	98.51	94.51	100 - 4.59 - 0.666	263.84	853.93	352.69	261.68	220.51	264.28	9.04
2.77_503.1615m/z	Raffinose	C18H32O16	503.1615	44.8	-0.5682	-0.03	95.54	Infinity	100 - 19.1 - 1.9	810.53	201.58	236.84	178.65	662.34	229.80	0.00
10.09_131.0350m/z	Glutaric acid	C5H8O4	131.0350	40.8	-0.0702	-0.78	98.57	1.83	100 - 4.56 - 0.514	786.56	669.76	593.04	429.18	585.50	467.86	441.56
4.86_103.0401m/z	3-Hydroxyisobutyric acid	C4H8O3	103.0401	41.5	-0.1444	-0.18	97.48	Infinity	100 - 2.57	728.39	344.63	529.94	176.39	189.53	269.65	0.00
9.98_161.0455m/z	3-Hydroxymethylglutarate	C6H10O5	161.0455	40.6	-0.1574	-0.78	97.68	7.36	100 - 5.16 - 0.353	289.06	725.04	294.48	189.40	205.25	147.02	98.57
4.56_75.0087m/z	Glycolic acid	C2H4O3	75.0087	40.1	-0.6941	-0.68	98.35	10.00	100 - 1.05 - 0.202	576.77	522.48	590.25	518.95	589.20	611.34	61.15
5.68_101.0243m/z	Acetoacetate	C4H6O3	101.0243	39.8	-0.6959	0.54	96.18	36.60	100 - 1.19	178.83	545.77	180.39	148.97	119.86	114.26	14.91
4.28_165.0405m/z	Arabinonic acid	C5H10O6	165.0405	40.2	-0.0237	-0.62	97.83	Infinity	100 - 4.45 - 0.349	336.17	316.23	295.89	525.68	155.34	218.12	0.00
12.68_115.0037m/z	Fumarate	C4H4O4	115.0037	40.8	-0.0242	-0.95	98.58	1.79	100 - 3.46 - 0.469	459.25	353.78	256.33	258.73	295.07	281.29	403.92
6.30_87.0451m/z	Butyric acid	C4H8O2	87.0451	51.9	-0.3756	-0.02	98.36	13.99	100 - 3.27	124.96	138.40	215.37	58.33	46.48	108.04	15.40
4.01_179.0560m/z	Glucose	C6H12O6	179.0560	40	-0.6096	0.58	98.43	10.02	100 - 5.83 - 0.752	54.18	37.18	128.48	15.74	13.94	29.59	139.62

Appendix 28 - Pompeii INV10295: IC-MS Results

Interior Sample 3

Name	Formula	PDF Number	FOM	%
Malachite	C H2 Cu2 O5	00-900-7490	0.686	63.03
Azurite	C2 H2 Cu3 O8	00-900-7013	0.730	36.97

Peak List Serial	2theta [°]	d [Å]	I/I0		Peak List Serial	2theta [°]	d [Å]	I/I0
1	8.78	10.0576	145.006		59	47.61	1.9086	149.588
2	9.44	9.3644	139.415		60	48.24	1.8849	186.498
3	10.79	8.1925	127.559		61	49.01	1.8572	40.411
4	11.86	7.4560	96.680		62	49.81	1.8291	89.030
5	12.96	6.8239	119.404		63	50.21	1.8154	36.808
6	13.50	6.5548	36.790		64	50.76	1.7970	158.510
7	14.97	5.9139	232.785		65	51.11	1.7855	116.774
8	15.80	5.6030	110.276		66	51.62	1.7693	103.822
9	17.19	5.1540	263.705		67	51.82	1.7629	19.541
10	17.57	5.0421	592.103		68	52.02	1.7566	26.096
11	18.98	4.6722	74.987		69	52.43	1.7436	-9.540
12	20.30	4.3712	66.812		70	53.07	1.7242	152.340
13	20.72	4.2840	125.703		71	53.45	1.7127	191.756
14	21.72	4.0884	52.013		72	54.14	1.6927	53.020
15	22.42	3.9620	53.255		73	54.34	1.6869	97.631
16	22.81	3.8961	98.405		74	54.74	1.6755	262.396
17	23.41	3.7973	57.289		75	55.23	1.6619	194.995
18	24.06	3.6959	686.473		76	55.86	1.6445	119.156
19	24.43	3.6411	391.076		77	56.33	1.6319	36.843
20	25.11	3.5433	49.411		78	56.95	1.6157	84.780
21	25.16	3.5363	158.632		79	57.30	1.6066	166.769
22	25.95	3.4310	78.415		80	57.57	1.5998	183.197
23	26.48	3.3630	130.056		81	57.73	1.5956	201.399
24	27.42	3.2503	72.802		82	58.07	1.5872	224.457
25	27.58	3.2310	143.816		83	58.25	1.5826	108.361
26	28.62	3.1163	70.396		84	58.37	1.5797	65.274
27	29.42	3.0331	230.844		85	58.73	1.5707	79.369
28	29.79	2.9965	331.294		86	58.78	1.5695	96.149
29	30.48	2.9307	95.769		87	59.15	1.5606	8.990
30	31.26	2.8589	673.675		88	59.45	1.5534	17.192
31	31.81	2.8105	233.524		89	59.65	1.5487	55.813
32	32.30	2.7695	116.815		90	60.36	1.5323	58.501
33	33.47	2.6753	97.871		91	60.72	1.5239	184.865
34	34.35	2.6083	80.838		92	61.17	1.5138	189.277
35	34.75	2.5791	44.479		93	61.58	1.5049	156.788
36	35.66	2.5159	573.272		94	61.89	1.4979	210.027
37	36.29	2.4733	315.745		95	62.33	1.4885	261.644
38	36.73	2.4450	107.924		96	62.71	1.4803	235.885
39	37.06	2.4238	116.835		97	63.16	1.4708	106.389
40	37.83	2.3763	189.073		98	63.46	1.4646	69.951
41	38.50	2.3365	146.355		99	63.87	1.4563	96.138
42	39.32	2.2897	145.531		100	64.35	1.4465	60.584
43	39.47	2.2813	116.357		101	64.77	1.4382	114.732
44	40.27	2.2377	32.235		102	65.09	1.4319	109.826
45	40.77	2.2114	18.576		103	65.27	1.4284	140.300
46	41.37	2.1806	26.460		104	65.62	1.4216	221.886
47	41.64	2.1672	84.050		105	65.92	1.4158	173.320
48	42.44	2.1281	227.223		106	66.49	1.4051	139.884
49	42.98	2.1028	122.719		107	67.27	1.3906	91.932
50	43.23	2.0912	193.523		108	67.31	1.3900	197.289
51	43.69	2.0699	123.786		109	67.69	1.3830	76.768
52	43.90	2.0609	174.946		110	68.09	1.3758	21.122

Peak List Serial	2theta [°]	d [Å]	I/I0		Peak List Serial	2theta [°]	d [Å]	I/I0
53	44.26	2.0446	80.840		111	68.29	1.3723	75.505
54	44.85	2.0193	190.377		112	68.49	1.3687	34.294
55	45.40	1.9961	35.616		113	69.10	1.3583	83.093
56	46.10	1.9673	55.476		114	69.18	1.3569	172.707
57	46.65	1.9453	181.640		115	69.78	1.3466	79.401
58	47.35	1.9181	119.816		116	69.80	1.3463	99.989

Interior Sample 4

Name	Formula	PDF Number	FOM	%
Malachite	C H2 Cu2 O5	00-900-7490	0.685	100.0

Peak List Serial	2theta [°]	d [Å]	I/I0		Peak List Serial	2theta [°]	d [Å]	I/I0
1	9.45	9.3479	32.566		86	46.30	1.9592	48.187
2	10.67	8.2820	29.247		87	46.69	1.9440	107.036
3	11.99	7.3731	48.092		88	46.94	1.9342	56.854
4	12.09	7.3122	45.542		89	47.14	1.9264	31.936
5	14.48	6.1107	37.803		90	47.61	1.9086	56.723
6	14.67	6.0345	63.175		91	47.71	1.9048	52.956
7	14.85	5.9602	332.902		92	47.86	1.8992	122.387
8	16.42	5.3934	43.189		93	48.26	1.8843	39.229
9	16.52	5.3609	68.226		94	49.16	1.8518	42.977
10	17.63	5.0279	567.617		95	49.46	1.8413	29.220
11	17.81	4.9764	94.572		96	49.58	1.8372	56.953
12	17.94	4.9396	40.743		97	49.69	1.8331	84.432
13	18.84	4.7051	72.464		98	49.79	1.8297	76.037
14	18.96	4.6763	78.746		99	49.94	1.8245	44.260
15	20.27	4.3784	17.736		100	50.15	1.8177	36.114
16	20.83	4.2602	33.006		101	50.76	1.7970	107.614
17	21.37	4.1548	48.196		102	50.98	1.7899	111.006
18	22.00	4.0363	23.716		103	51.35	1.7779	50.718
19	22.79	3.8989	18.976		104	51.52	1.7725	34.333
20	23.66	3.7576	78.648		105	51.68	1.7672	27.403
21	24.13	3.6858	697.482		106	52.20	1.7509	45.474
22	24.33	3.6559	245.820		107	52.47	1.7426	40.690
23	24.44	3.6387	126.836		108	52.84	1.7313	39.617
24	25.28	3.5202	46.789		109	53.00	1.7262	51.298
25	25.66	3.4684	30.916		110	53.27	1.7182	27.421
26	25.95	3.4310	110.109		111	53.55	1.7098	37.887
27	26.50	3.3609	35.992		112	53.86	1.7009	38.823
28	27.32	3.2620	196.102		113	54.04	1.6956	95.651
29	27.48	3.2425	92.158		114	54.34	1.6869	92.321
30	27.67	3.2214	183.270		115	54.61	1.6793	145.188
31	27.79	3.2081	138.253		116	54.72	1.6759	134.911
32	28.02	3.1818	123.567		117	54.84	1.6726	116.281
33	29.04	3.0724	16.082		118	54.97	1.6689	62.959
34	29.42	3.0331	89.462		119	56.04	1.6395	51.478
35	29.52	3.0231	98.220		120	56.33	1.6319	49.076
36	29.81	2.9949	98.099		121	56.51	1.6271	43.312
37	29.97	2.9786	122.293		122	56.90	1.6170	90.618
38	30.88	2.8936	58.499		123	57.20	1.6092	51.566
39	31.01	2.8814	161.310		124	57.41	1.6036	33.465
40	31.19	2.8648	339.351		125	57.88	1.5918	81.282
41	31.26	2.8589	455.077		126	57.98	1.5893	107.718
42	31.46	2.8411	321.427		127	58.17	1.5847	85.573
43	31.65	2.8250	145.610		128	58.28	1.5818	53.872
44	31.83	2.8091	123.751		129	58.68	1.5719	83.029
45	31.93	2.8005	101.260		130	59.07	1.5626	44.783
46	32.15	2.7821	137.333		131	59.42	1.5542	15.970
47	32.20	2.7779	201.047		132	60.00	1.5404	37.427
48	33.48	2.6740	33.483		133	60.05	1.5393	49.294
49	34.39	2.6059	50.906		134	60.27	1.5343	40.281
50	35.00	2.5612	42.924		135	60.57	1.5274	58.399
51	35.42	2.5320	84.122		136	60.67	1.5251	52.311
52	35.66	2.5159	614.476		137	60.92	1.5194	56.388
53	36.17	2.4810	96.560		138	61.12	1.5149	37.618

Peak List Serial	2theta [°]	d [Å]	I/I0		Peak List Serial	2theta [°]	d [Å]	I/I0
54	36.27	2.4744	130.268		139	61.34	1.5100	60.260
55	36.44	2.4635	129.541		140	61.68	1.5027	39.564
56	37.08	2.4227	81.080		141	61.91	1.4975	56.099
57	37.78	2.3793	17.128		142	62.01	1.4954	64.203
58	37.98	2.3672	47.750		143	62.06	1.4943	77.007
59	38.16	2.3562	73.212		144	62.14	1.4925	45.828
60	38.25	2.3513	77.061		145	62.44	1.4860	38.305
61	38.31	2.3473	71.559		146	62.58	1.4831	45.087
62	38.81	2.3181	50.079		147	62.78	1.4789	101.265
63	38.93	2.3114	123.167		148	62.96	1.4750	136.459
64	39.10	2.3019	90.720		149	63.13	1.4715	108.948
65	39.30	2.2907	85.769		150	63.76	1.4584	13.248
66	39.43	2.2832	65.141		151	64.12	1.4512	16.949
67	39.92	2.2566	34.894		152	64.45	1.4445	28.295
68	40.59	2.2210	22.783		153	64.83	1.4369	9.360
69	41.25	2.1865	134.483		154	65.35	1.4267	40.689
70	41.32	2.1831	97.125		155	65.54	1.4232	110.785
71	41.79	2.1597	51.719		156	65.64	1.4212	96.491
72	41.99	2.1499	61.895		157	65.92	1.4158	64.822
73	42.46	2.1273	211.196		158	66.17	1.4110	42.180
74	42.98	2.1028	42.528		159	67.07	1.3942	43.148
75	43.59	2.0744	49.674		160	67.29	1.3903	80.881
76	43.71	2.0691	62.526		161	67.42	1.3878	76.551
77	43.85	2.0631	59.642		162	67.58	1.3851	119.529
78	44.05	2.0542	94.335		163	67.66	1.3836	66.921
79	44.26	2.0446	41.432		164	67.96	1.3782	37.833
80	44.40	2.0388	41.550		165	68.14	1.3749	40.380
81	44.90	2.0172	29.636		166	68.69	1.3652	39.838
82	45.57	1.9891	58.141		167	69.06	1.3589	75.592
83	45.68	1.9843	45.988		168	69.30	1.3548	46.320
84	45.85	1.9775	55.179		169	69.45	1.3523	66.288
85	46.08	1.9680	95.394		170	69.58	1.3500	56.692

Exterior Sample 5

Name	Formula	PDF Number	FOM	%
Azurite	C2 H2 Cu3 O8	00-900-7013	0.785	77.23
Malachite	C H2 Cu2 O5	00-900-7490	0.667	22.77

Peak List Serial	2theta [°]	d [Å]	I/I0		Peak List Serial	2theta [°]	d [Å]	I/I0
1	12.11	7.3022	47.432		53	46.62	1.9466	352.489
2	14.80	5.9803	81.848		54	46.84	1.9381	45.494
3	17.19	5.1540	377.718		55	47.54	1.9111	76.013
4	17.42	5.0853	273.615		56	47.77	1.9023	95.314
5	17.61	5.0326	300.465		57	48.34	1.8813	40.984
6	18.01	4.9214	58.252		58	48.54	1.8740	59.333
7	18.81	4.7133	54.813		59	49.53	1.8389	99.461
8	20.35	4.3606	12.620		60	49.91	1.8257	212.126
9	22.82	3.8933	6.480		61	50.73	1.7981	65.544
10	23.37	3.8027	51.457		62	50.95	1.7909	121.888
11	24.18	3.6783	539.647		63	51.13	1.7849	96.645
12	25.21	3.5294	755.689		64	51.87	1.7614	47.081
13	25.65	3.4706	45.099		65	52.12	1.7535	41.406
14	26.68	3.3381	59.094		66	53.09	1.7237	39.193
15	27.28	3.2659	91.043		67	53.37	1.7152	41.932
16	27.69	3.2195	40.452		68	53.55	1.7098	43.937
17	28.62	3.1163	84.935		69	54.06	1.6951	69.676
18	29.42	3.0331	218.811		70	54.37	1.6859	69.025
19	30.06	2.9705	55.310		71	54.56	1.6807	70.669
20	30.58	2.9213	158.386		72	54.86	1.6722	67.460
21	30.96	2.8859	210.530		73	55.23	1.6619	45.661
22	31.13	2.8708	259.156		74	55.68	1.6495	43.623
23	31.16	2.8678	273.373		75	56.38	1.6306	37.535
24	31.33	2.8529	196.738		76	56.93	1.6161	51.310
25	31.56	2.8323	141.903		77	57.40	1.6041	79.806
26	31.78	2.8134	130.501		78	57.75	1.5951	277.879
27	32.20	2.7779	84.537		79	58.07	1.5872	91.530
28	34.54	2.5949	112.600		80	58.80	1.5691	66.990
29	35.26	2.5436	263.320		81	59.34	1.5562	54.825
30	35.52	2.5251	303.189		82	59.69	1.5479	52.022
31	35.71	2.5125	550.617		83	60.66	1.5254	99.077
32	35.97	2.4944	95.493		84	61.12	1.5149	161.530
33	36.34	2.4700	109.719		85	61.39	1.5089	109.846
34	37.60	2.3905	29.504		86	61.74	1.5012	64.051
35	38.48	2.3375	173.156		87	62.36	1.4878	73.318
36	39.08	2.3029	70.640		88	62.78	1.4789	119.001
37	39.37	2.2869	276.789		89	63.01	1.4740	57.187
38	39.72	2.2675	217.239		90	63.36	1.4666	50.032
39	40.05	2.2494	93.730		91	63.66	1.4604	85.844
40	40.44	2.2289	285.477		92	64.65	1.4405	42.013
41	41.22	2.1882	36.081		93	65.15	1.4306	119.753
42	41.54	2.1722	104.854		94	65.52	1.4235	47.513
43	41.77	2.1606	56.939		95	65.80	1.4180	96.396
44	42.46	2.1273	107.991		96	66.41	1.4066	59.058
45	42.98	2.1028	61.431		97	66.82	1.3989	26.372
46	43.19	2.0928	61.944		98	67.29	1.3903	84.456
47	43.48	2.0797	47.101		99	67.76	1.3818	56.297
48	44.01	2.0557	47.673		100	67.96	1.3782	56.192
49	45.03	2.0115	49.264		101	68.13	1.3752	56.767
50	45.33	1.9989	34.171		102	69.06	1.3589	71.876
51	45.62	1.9871	42.429		103	69.31	1.3546	87.286
52	45.92	1.9747	46.398					

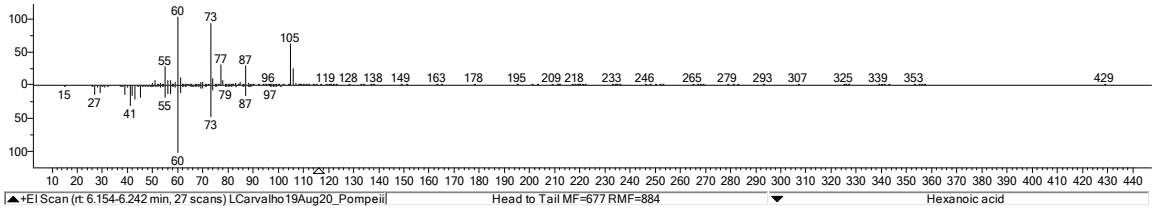
Exterior Sample 6

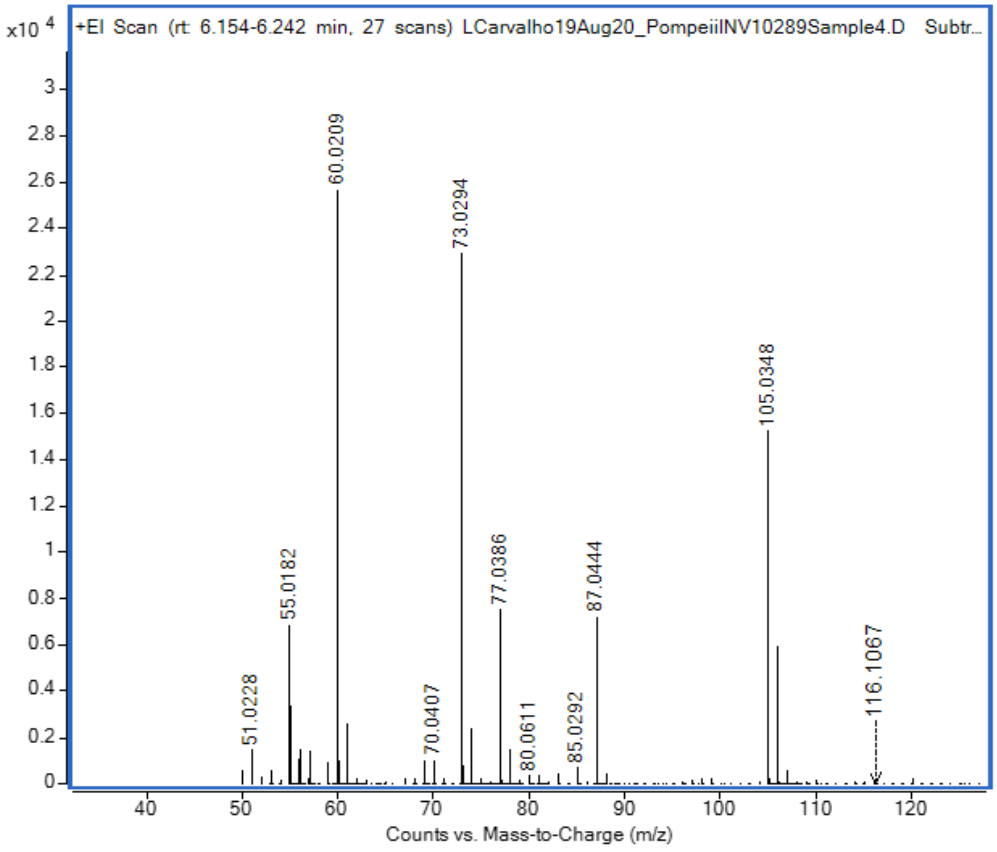
Name	Formula	PDF Number	FOM	%
Azurite	C2 H2 Cu3 O8	00-900-7013	0.761	100.00

Peak List Serial	2theta [°]	d [Å]	I/I0		Peak List Serial	2theta [°]	d [Å]	I/I0
1	5.54	15.9309	78.339		50	45.68	1.9843	100.020
2	6.01	14.6917	57.202		51	46.59	1.9480	301.772
3	7.10	12.4453	99.118		52	47.17	1.9252	68.110
4	11.96	7.3937	80.084		53	47.77	1.9023	132.483
5	14.48	6.1107	88.141		54	48.44	1.8776	142.439
6	15.75	5.6208	58.695		55	49.41	1.8430	123.905
7	17.14	5.1689	420.699		56	49.89	1.8262	183.615
8	17.39	5.0950	208.846		57	50.90	1.7926	117.078
9	17.74	4.9950	151.901		58	51.16	1.7839	136.469
10	18.11	4.8944	90.764		59	51.80	1.7635	103.020
11	19.08	4.6479	76.938		60	52.18	1.7514	74.950
12	21.92	4.0515	94.967		61	52.45	1.7431	87.195
13	22.59	3.9331	75.846		62	52.74	1.7344	83.848
14	22.96	3.8709	95.606		63	53.02	1.7257	70.424
15	23.31	3.8134	100.878		64	53.74	1.7043	68.100
16	24.18	3.6783	350.296		65	54.06	1.6951	79.823
17	24.46	3.6362	80.765		66	54.84	1.6726	65.320
18	25.20	3.5317	732.563		67	55.44	1.6559	69.646
19	25.88	3.4398	186.078		68	55.81	1.6459	86.798
20	26.92	3.3097	95.732		69	56.16	1.6364	73.397
21	27.28	3.2659	358.886		70	57.05	1.6131	45.623
22	27.64	3.2252	127.179		71	57.75	1.5951	179.080
23	28.69	3.1092	124.844		72	58.13	1.5855	71.759
24	29.41	3.0348	235.233		73	58.90	1.5666	91.557
25	29.86	2.9900	90.560		74	59.12	1.5614	98.918
26	30.56	2.9229	130.472		75	59.42	1.5542	76.495
27	31.13	2.8708	118.255		76	59.84	1.5443	72.752
28	31.78	2.8134	150.500		77	60.41	1.5312	142.954
29	32.10	2.7863	124.520		78	60.67	1.5251	107.738
30	32.95	2.7162	126.104		79	61.09	1.5156	125.288
31	34.50	2.5973	131.391		80	61.36	1.5097	87.141
32	35.22	2.5459	229.801		81	62.06	1.4943	30.574
33	35.71	2.5125	423.895		82	62.46	1.4856	91.520
34	36.56	2.4558	40.023		83	62.85	1.4775	136.480
35	36.86	2.4365	33.110		84	63.73	1.4591	86.023
36	37.48	2.3977	83.631		85	64.08	1.4519	83.829
37	38.46	2.3385	180.668		86	64.48	1.4438	80.815
38	39.00	2.3076	113.124		87	64.85	1.4365	99.193
39	39.32	2.2897	211.002		88	65.29	1.4280	98.774
40	39.68	2.2694	176.089		89	65.75	1.4190	73.339
41	40.09	2.2476	123.036		90	66.12	1.4120	75.428
42	40.42	2.2297	260.168		91	66.47	1.4054	79.364
43	41.57	2.1705	126.991		92	67.27	1.3906	97.906
44	42.94	2.1044	111.099		93	67.73	1.3824	71.094
45	43.16	2.0943	146.427		94	68.08	1.3761	90.760
46	43.49	2.0790	24.622		95	68.41	1.3702	64.554
47	44.00	2.0564	37.531		96	68.85	1.3626	97.614
48	44.78	2.0222	90.843		97	69.08	1.3586	81.737
49	45.42	1.9954	87.811		98	69.43	1.3526	80.602

[1] Hexanoic acid Mass: 116.0837297

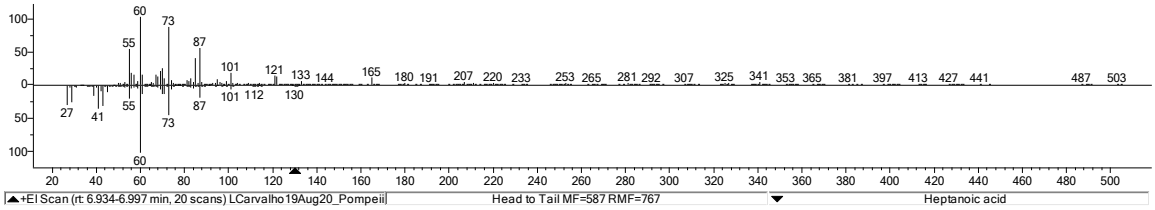
Sample 4

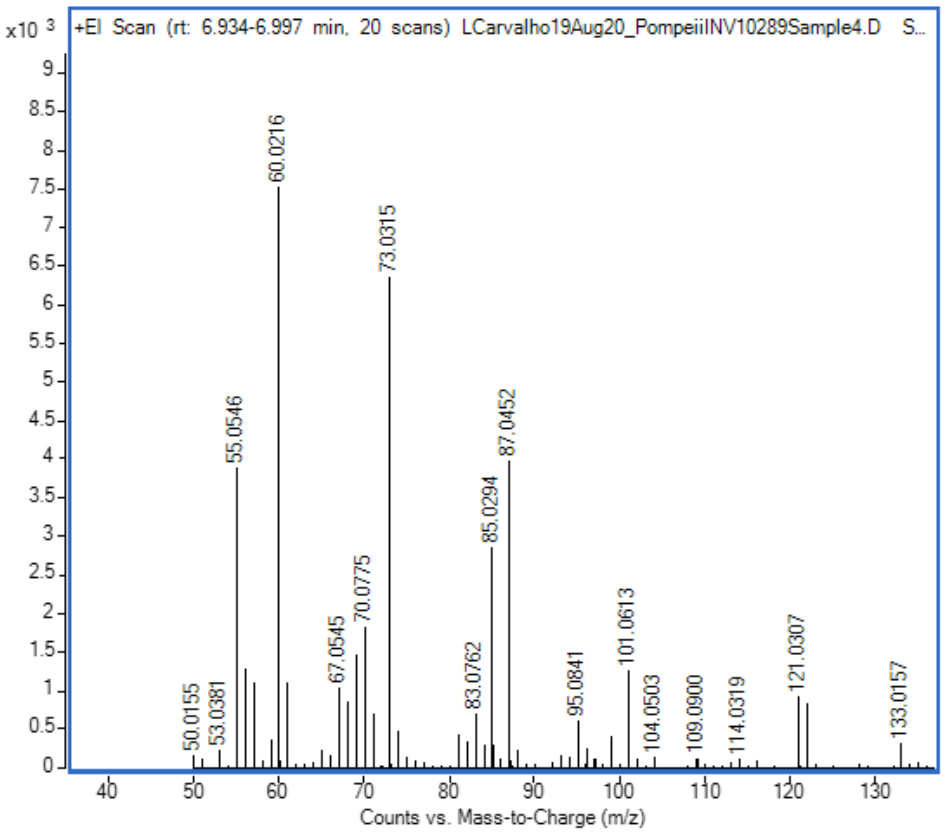




[2] Heptanoic acid Mass: 130.09938

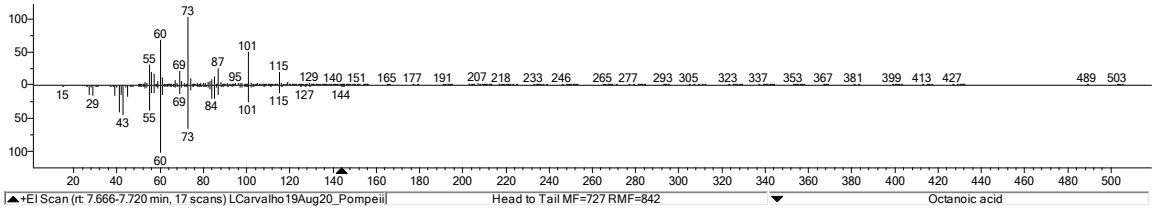
Sample 4

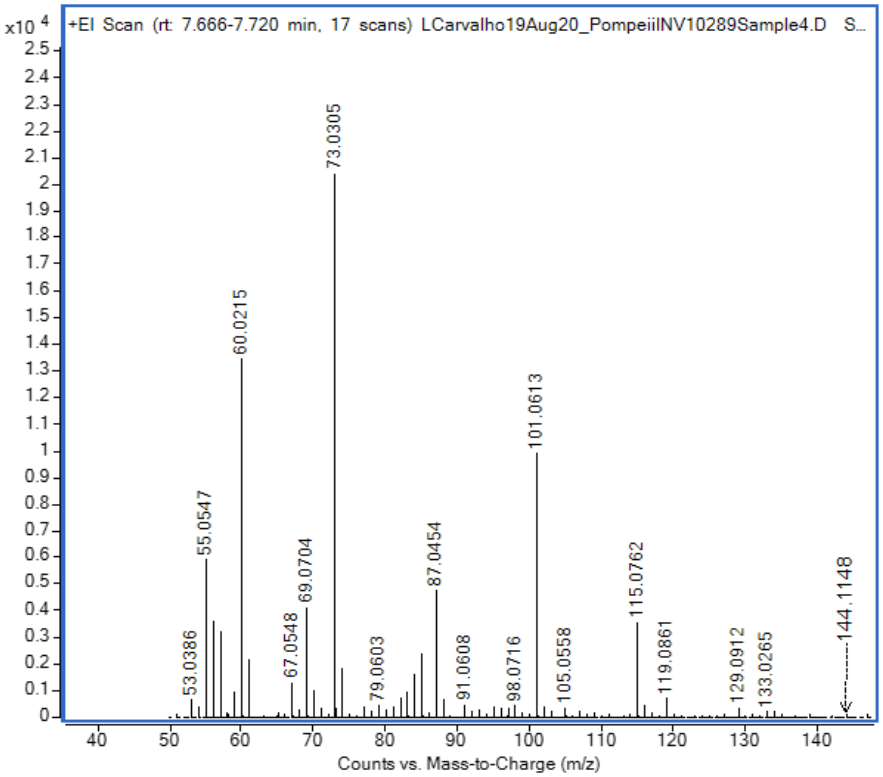




[3] Octanoic acid Mass: 144.115029

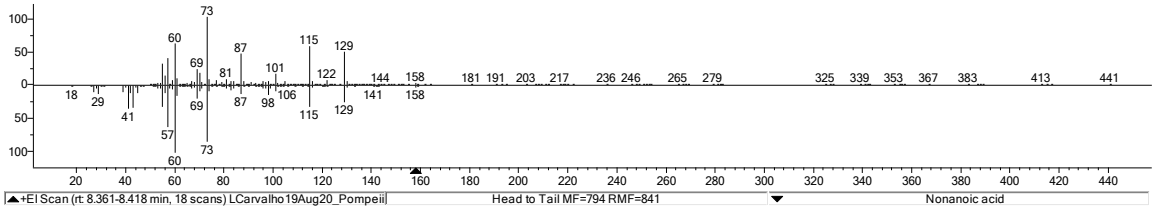
Sample 4

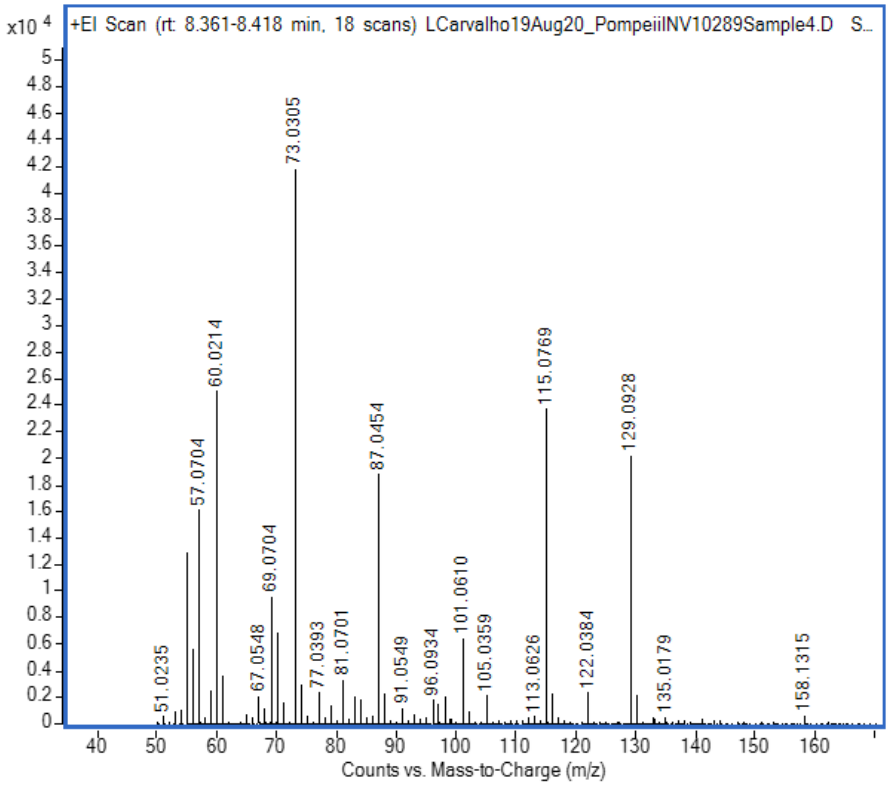




[4] Nonanoic acid ss: 158.13068

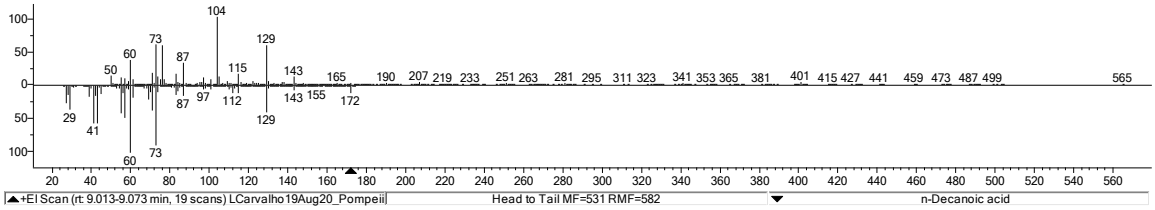
Sample 4

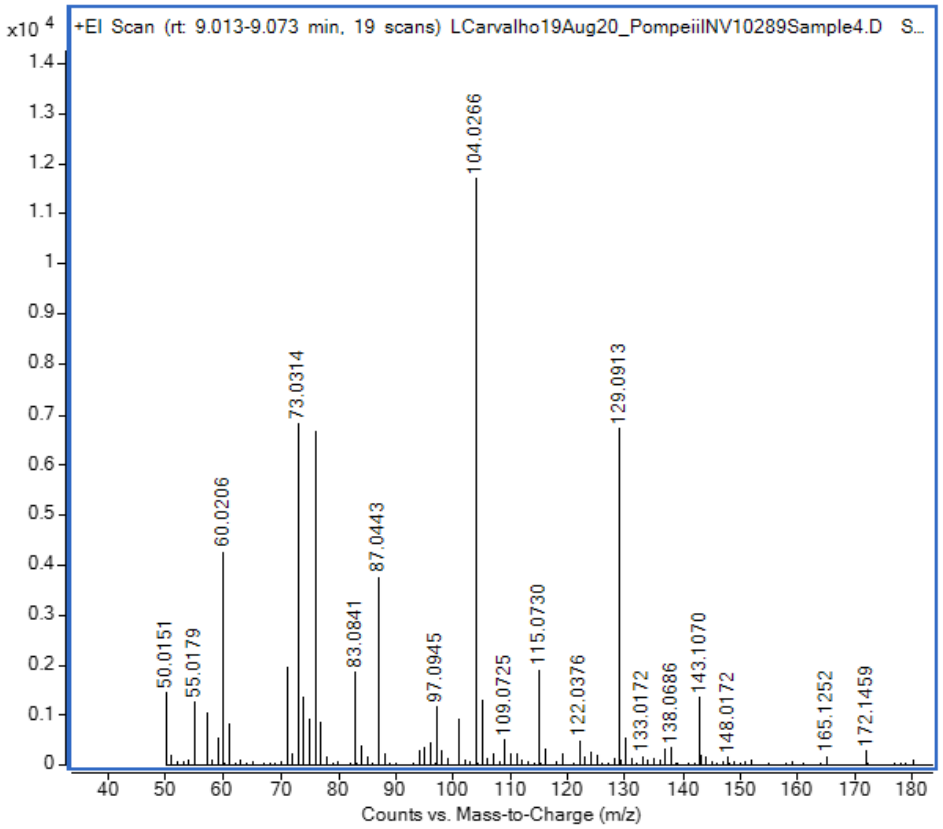




[5] n-Decanoic acid Mass: 172.14633

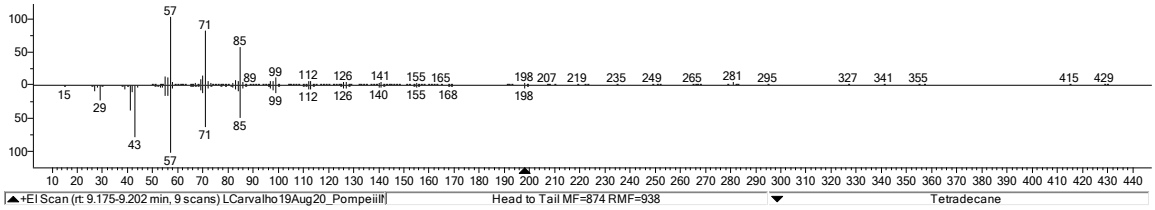
Sample 4

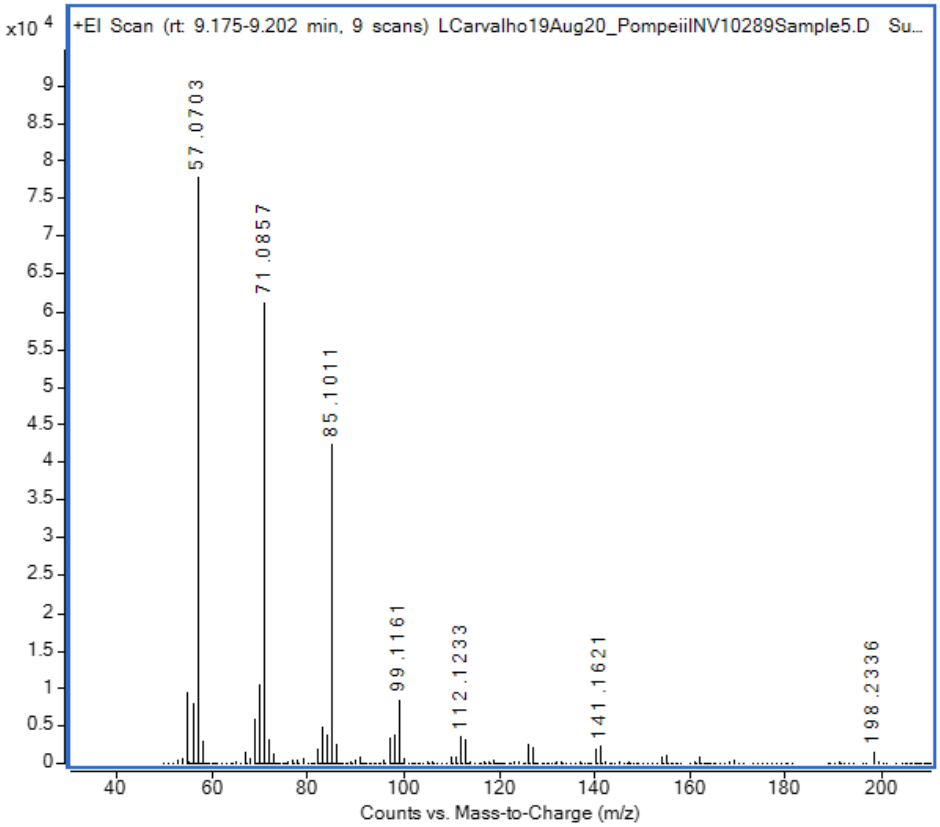




[6] Tetradecane Mass: 198.234751

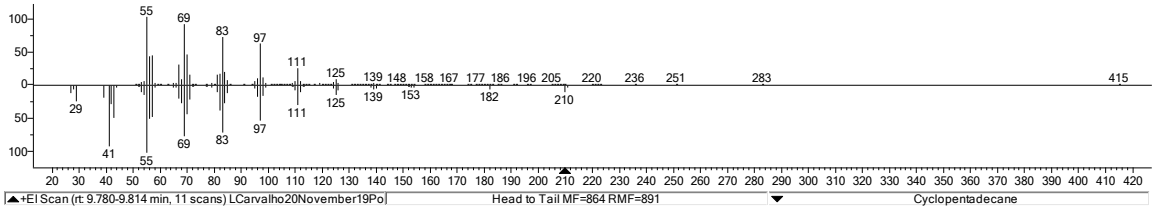
Sample 5

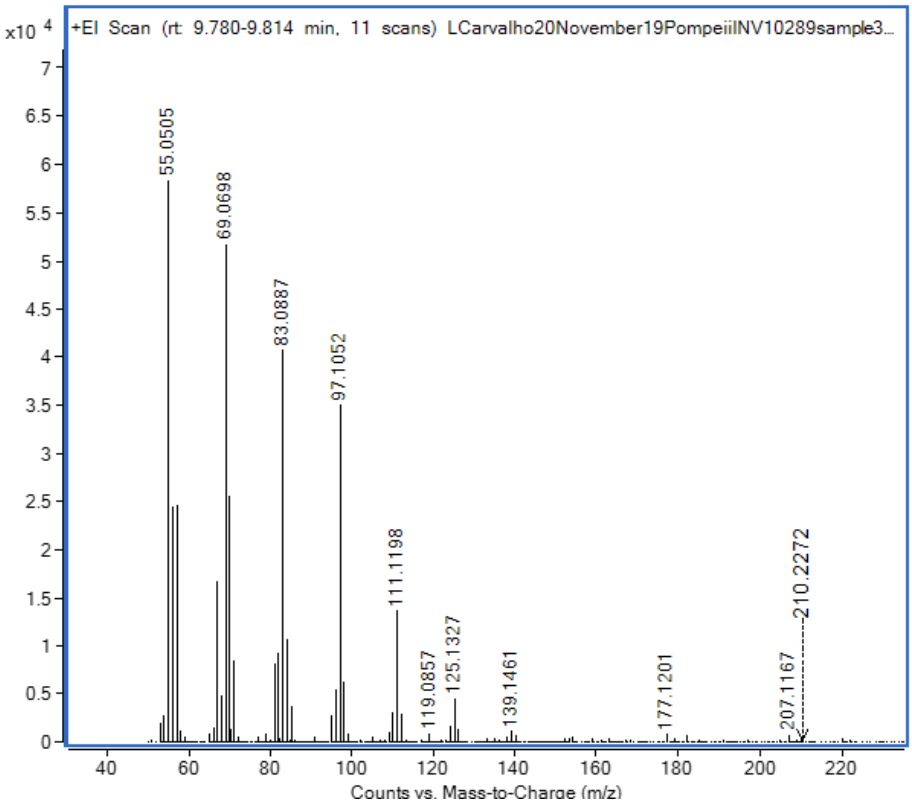




[7] Cyclopentadecane Mass: 210.234751

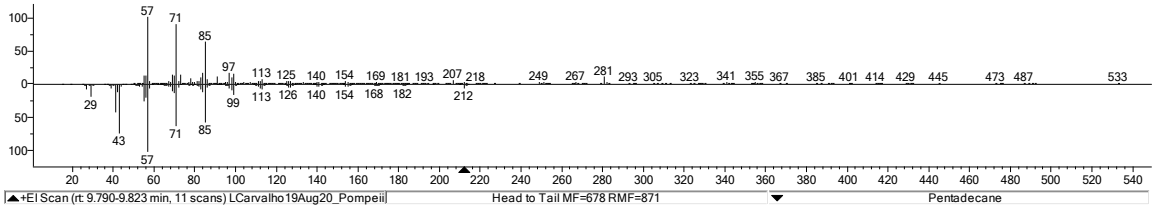
Sample 3

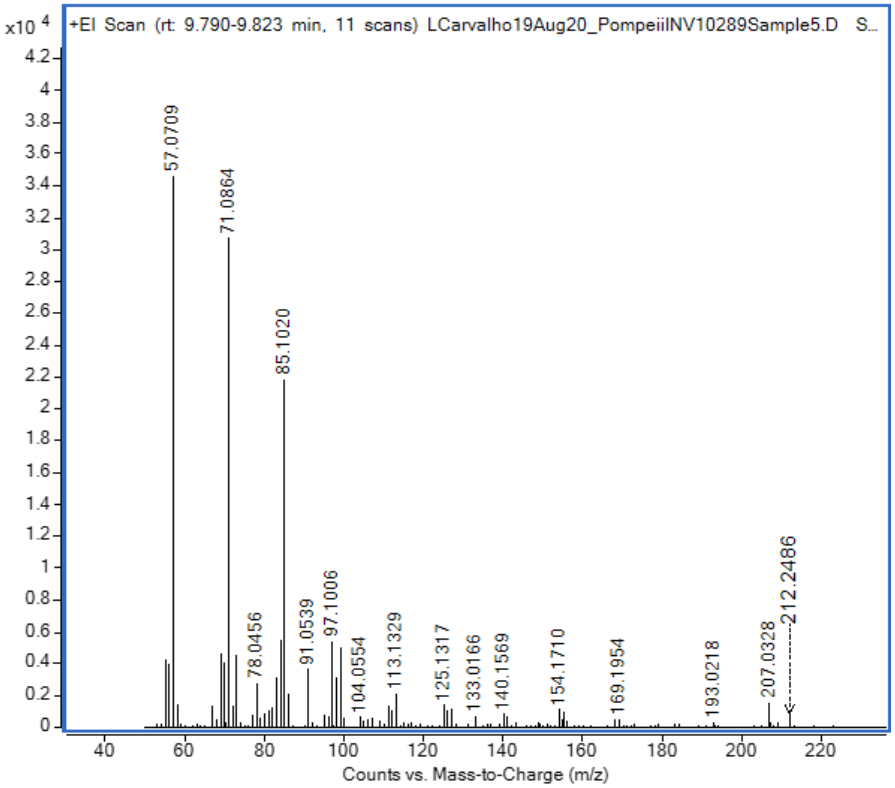




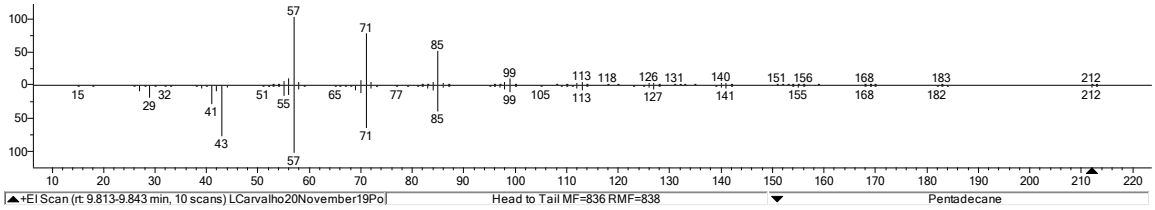
[8] Pentadecane Mass: 212.2504015

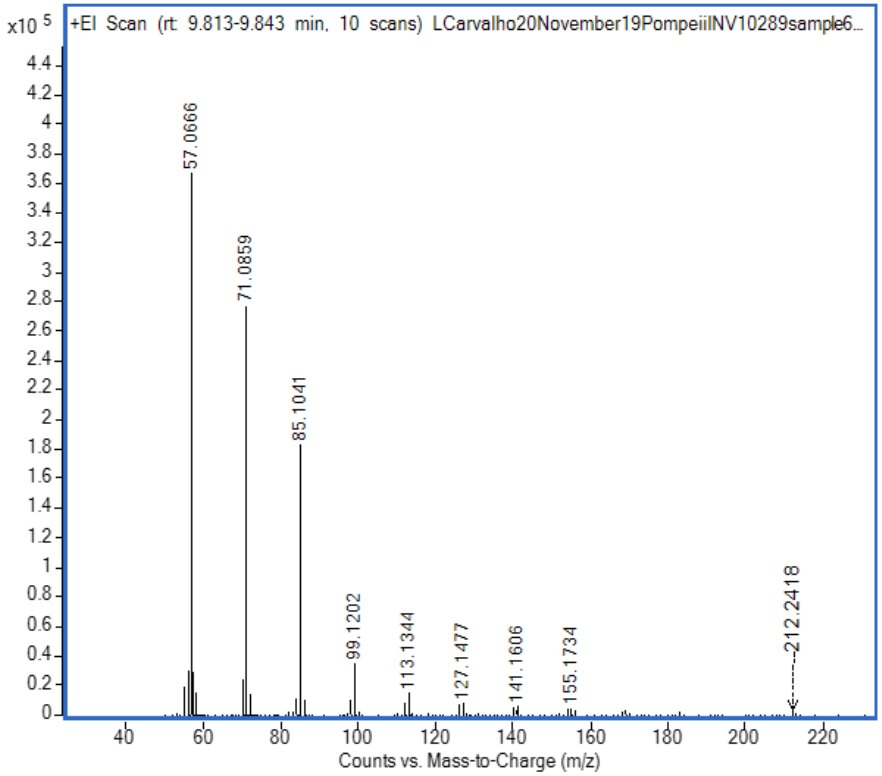
Sample 5





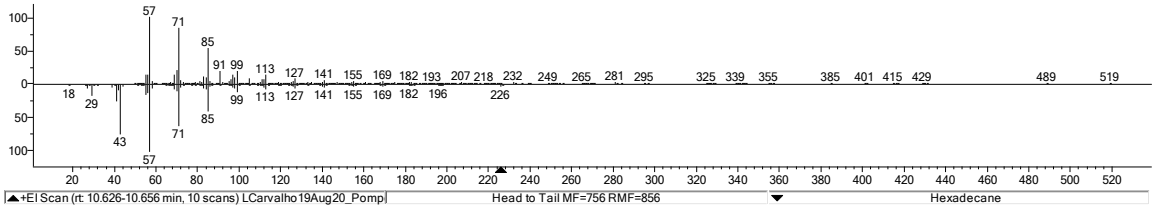
Sample 6

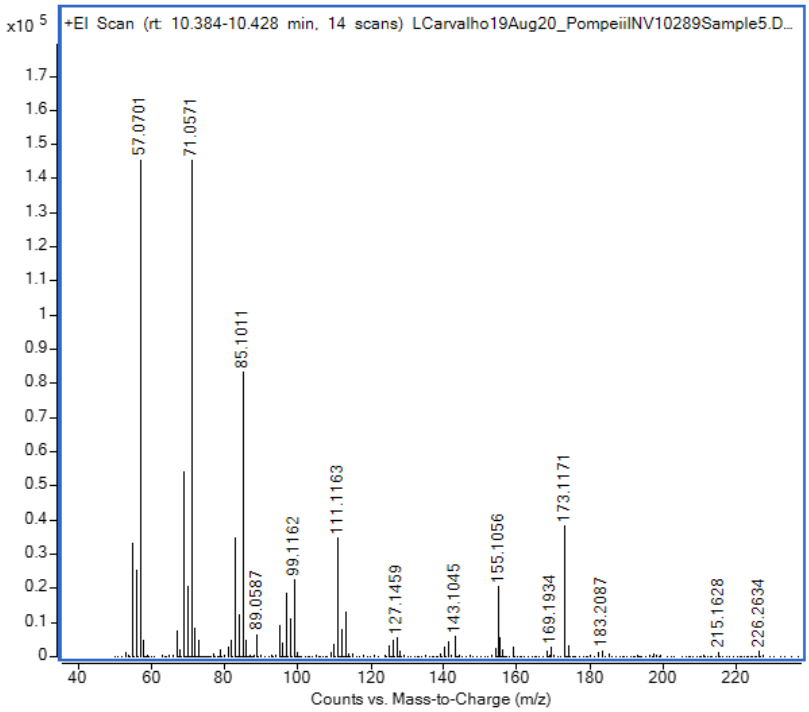

+EI Scan (rt: 9.813-9.843 min, 10 scans) LCarvalho20November19Po
Head to Tail MF=836 RMF=838
Pentadecane


x10 5
+EI Scan (rt: 9.813-9.843 min, 10 scans) LCarvalho20November19PompeiiINV10289sample6...
57.0666
71.0859
85.1041
99.1202
113.1344
127.1477
141.1606
155.1734
212.2418
Counts vs. Mass-to-Charge (m/z)

[9] Hexadecane Mass: 226.266051 NIST#: 228773

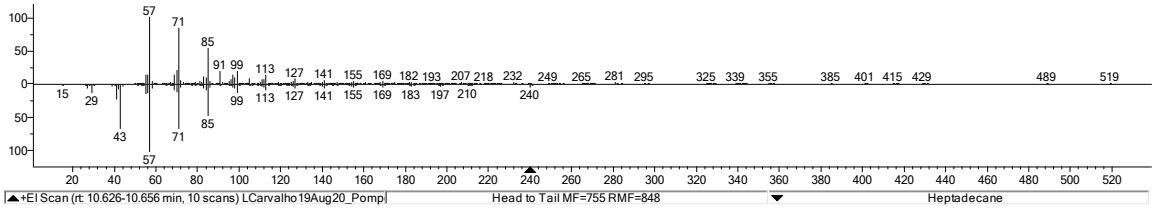
Sample 5

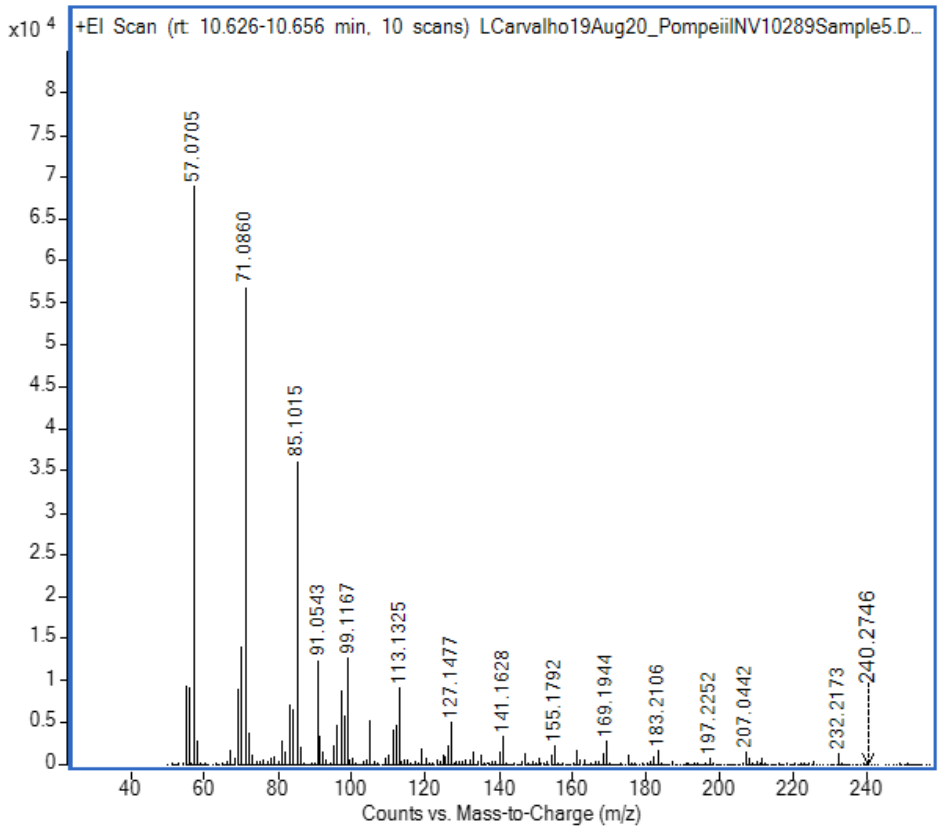




[10] Heptadecane Mass: 240.281701

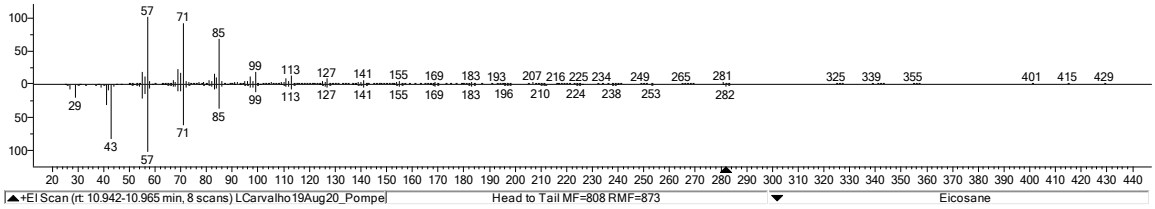
Sample 5

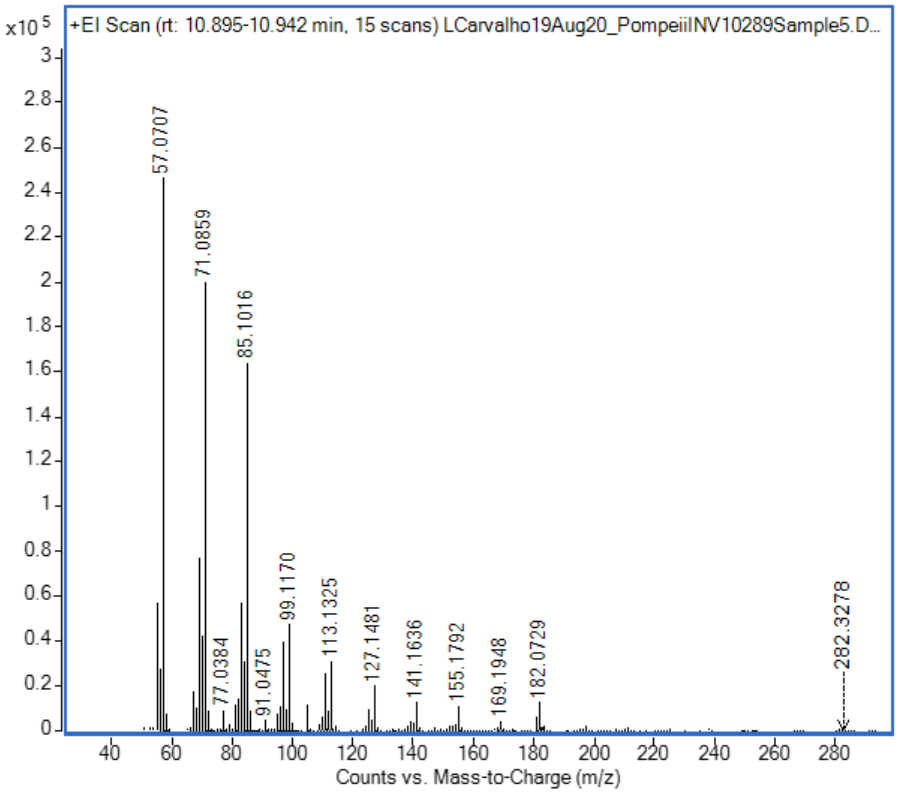




[11] Eicosane Mass: 282.328651

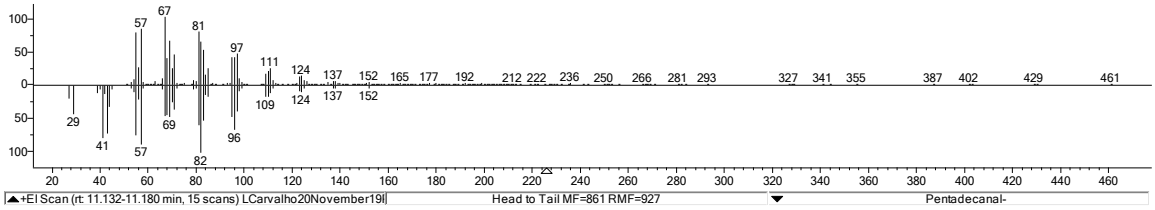
Sample 5

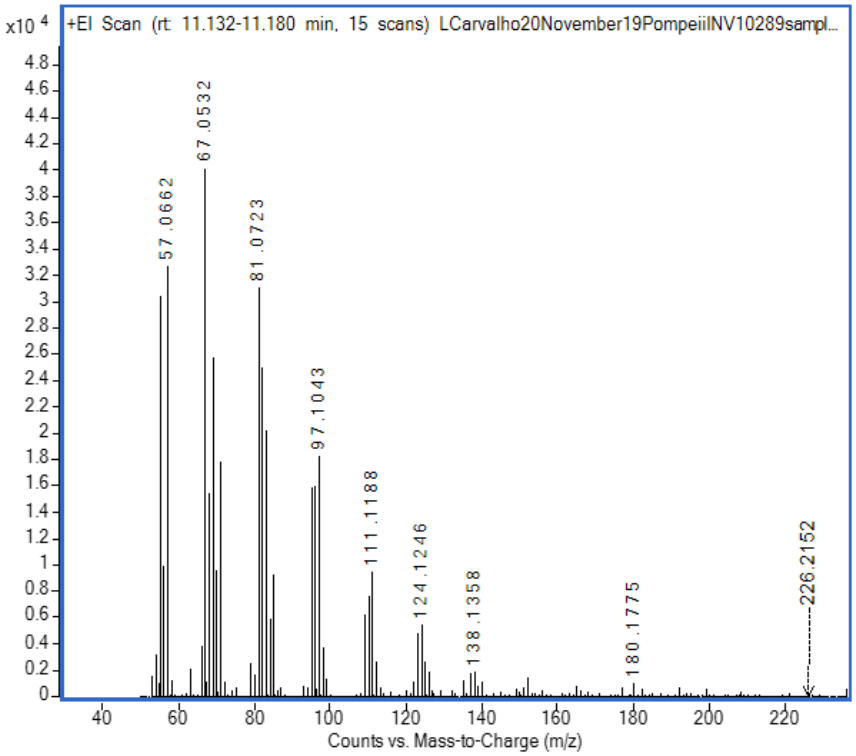




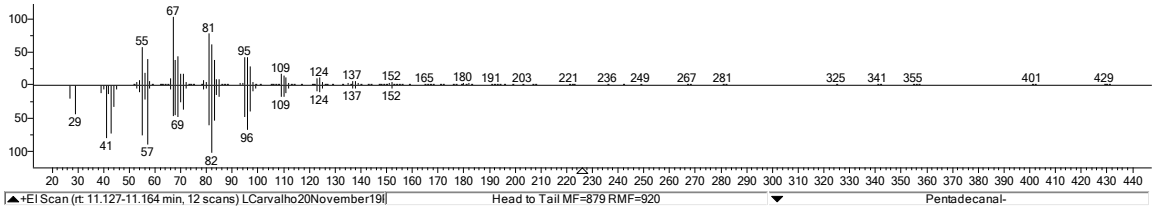
[12] Pentadecanal

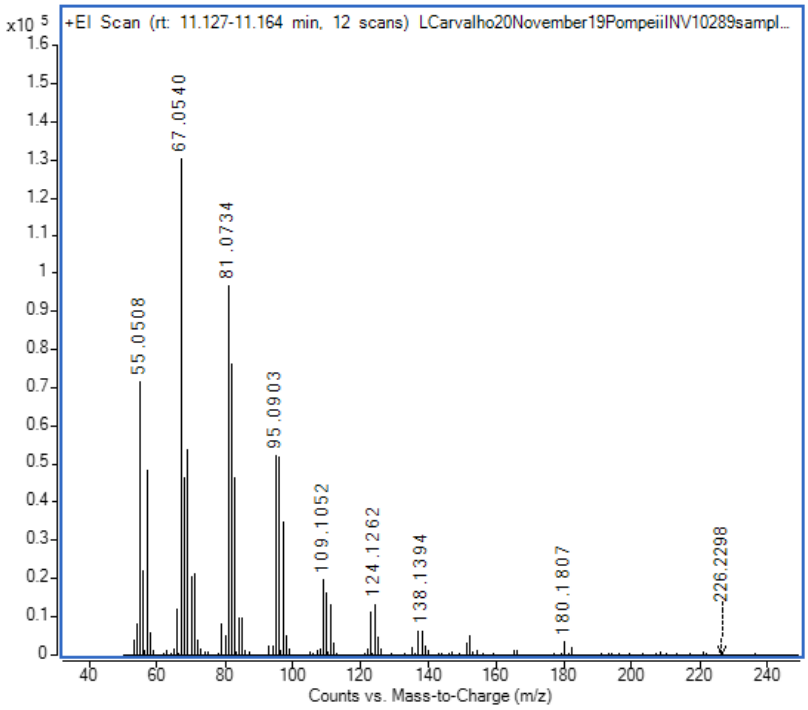
Sample 2





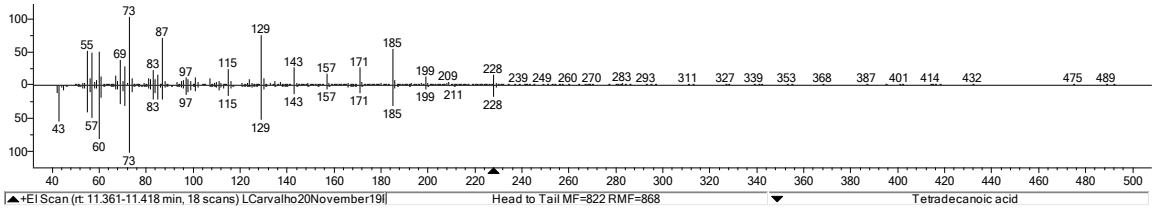
Sample 3

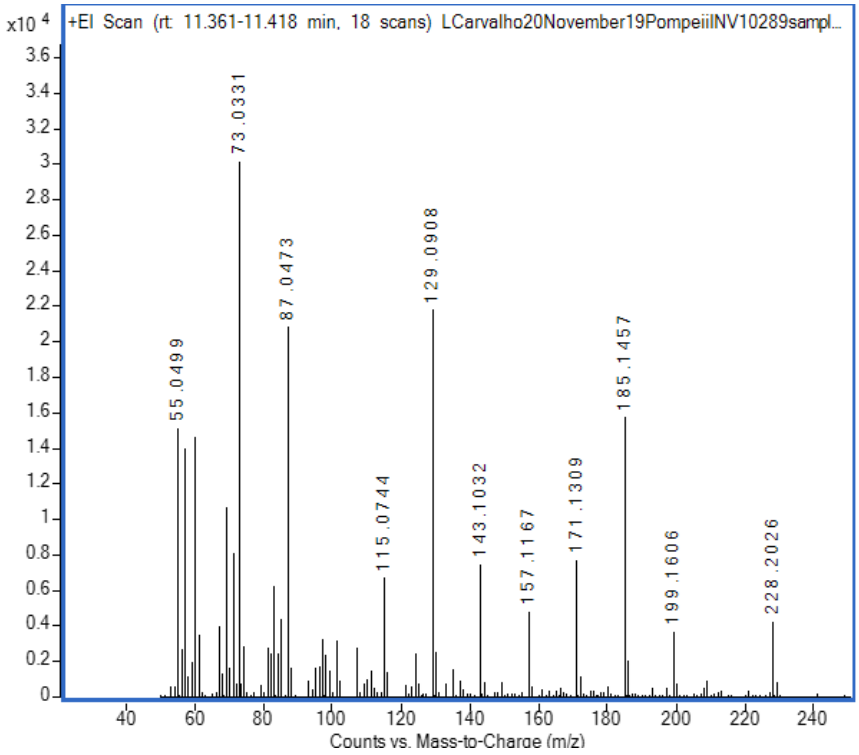

+EI Scan (rt: 11.127-11.164 min, 12 scans) LCarvalho20November19II
Head to Tail MF=879 RMF=920
Pentadecanal-


x10 5
+EI Scan (rt: 11.127-11.164 min, 12 scans) LCarvalho20November19PompeiiINV10289sampl...
67.0540
81.0734
55.0508
95.0903
109.1052
124.1262
138.1394
180.1807
226.2298
Counts vs. Mass-to-Charge (m/z)

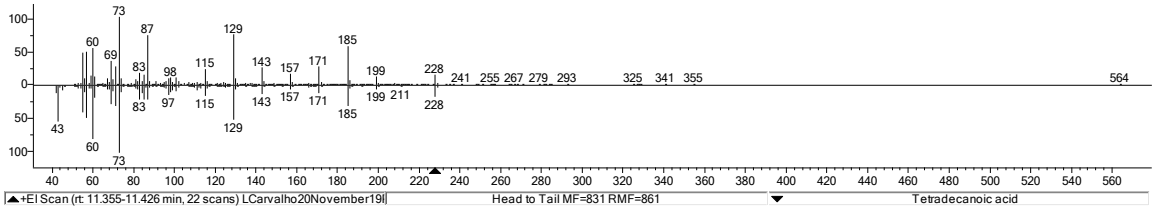
[13] Tetradecanoic acid

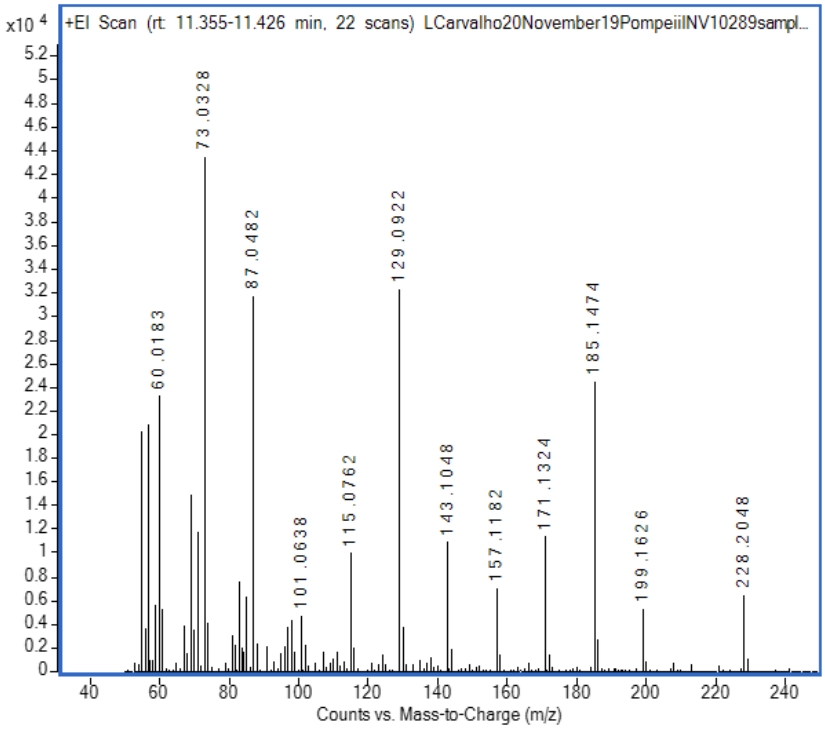
Sample 2



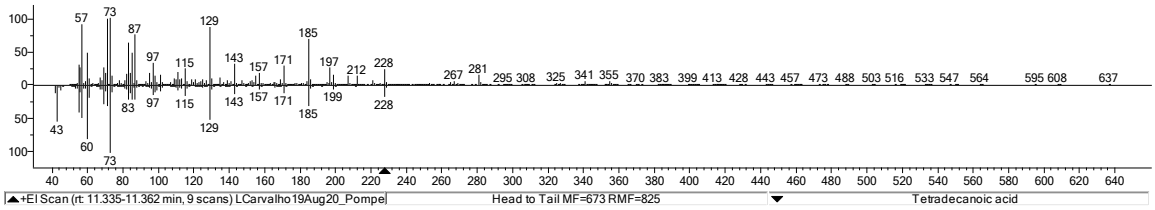


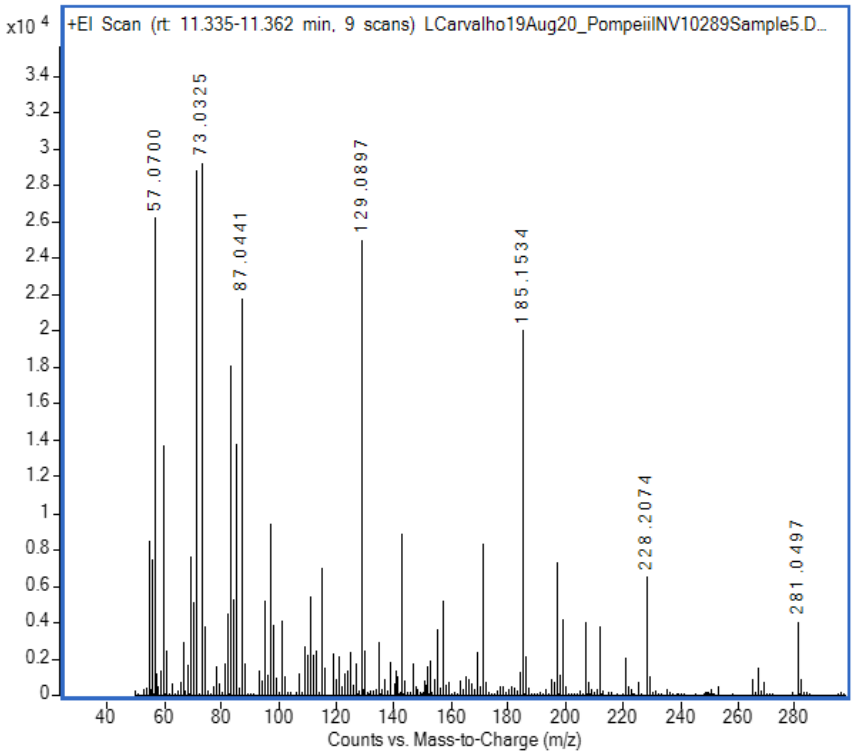
Sample 3


+EI Scan (rt: 11.355-11.426 min, 22 scans) LCarvalho20November19II
Head to Tail MF=831 RMF=861
Tetradecanoic acid

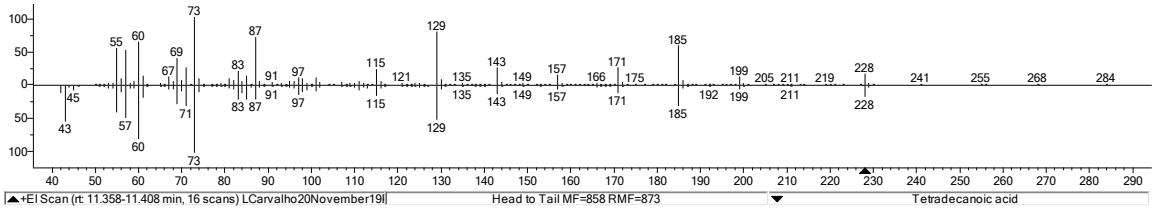

x10 4
+EI Scan (rt: 11.355-11.426 min, 22 scans) LCarvalho20November19PompeiiINV10289sampl...
73.0328
87.0482
129.0922
60.0183
185.1474
101.0638
115.0762
143.1048
157.1182
171.1324
199.1626
228.2048
Counts vs. Mass-to-Charge (m/z)

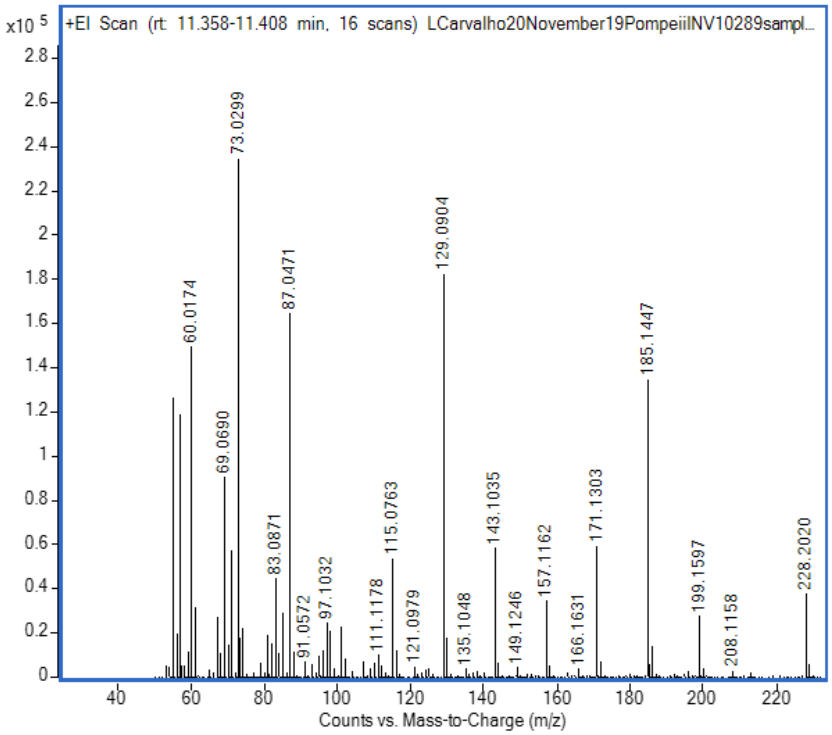
Sample 5


+EI Scan (rt: 11.335-11.362 min, 9 scans) LCarvalho19Aug20_Pompe
Head to Tail MF=673 RMF=825
Tetradecanoic acid


x10 4
+EI Scan (rt: 11.335-11.362 min, 9 scans) LCarvalho19Aug20_PompeiiINV10289Sample5.D...
57.0700
73.0325
87.0441
129.0897
185.1534
228.2074
281.0497
Counts vs. Mass-to-Charge (m/z)

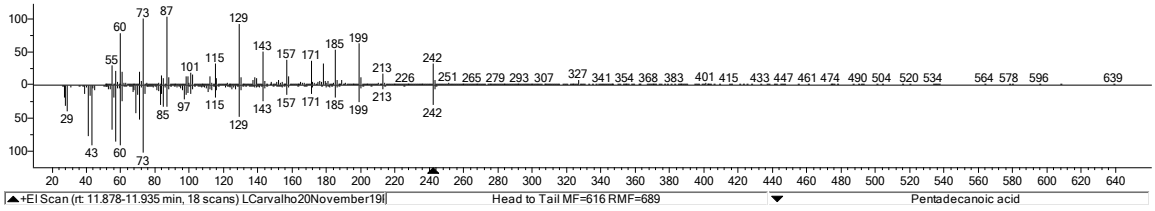
Sample 6

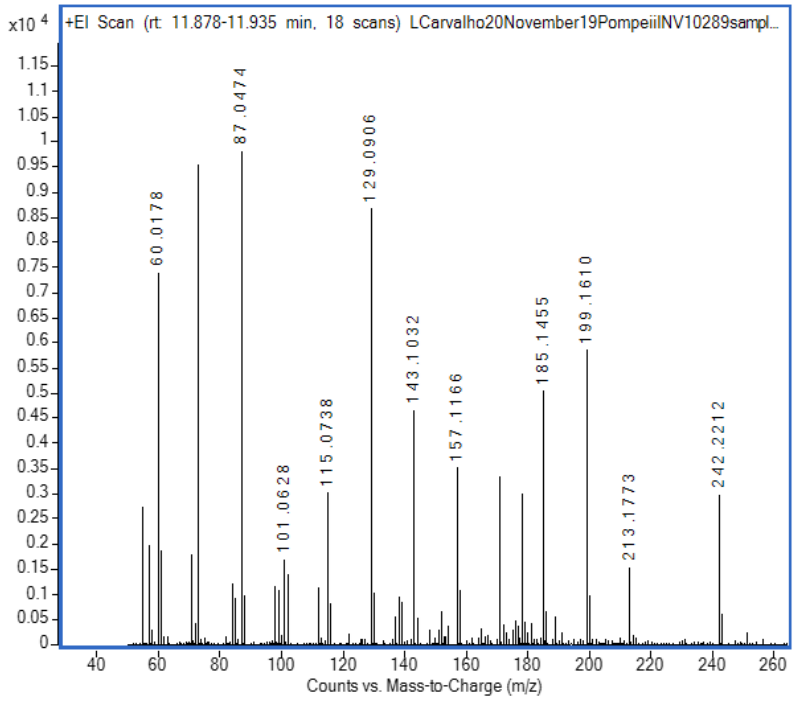

+EI Scan (rt: 11.358-11.408 min, 16 scans) LCarvalho20November19II
Head to Tail MF=858 RMF=873
Tetradecanoic acid


x10 5
+EI Scan (rt: 11.358-11.408 min, 16 scans) LCarvalho20November19PompeiiINV10289sampl...
73.0299
60.0174
87.0471
129.0904
185.1447
69.0690
83.0871
115.0763
143.1035
171.1303
97.1032
157.1162
199.1597
228.2020
91.0572
111.1178
121.0979
135.1048
149.1246
166.1631
208.1158
Counts vs. Mass-to-Charge (m/z)

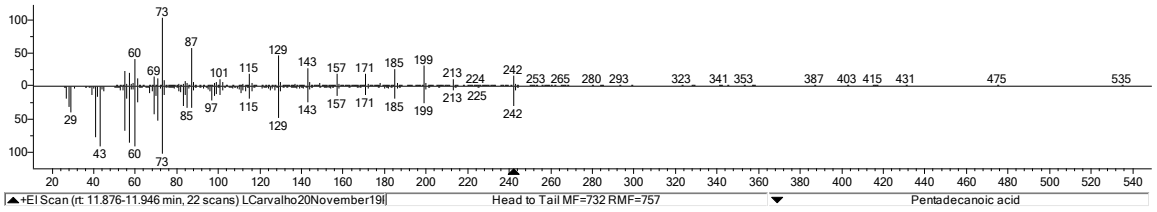
[14] Pentadecanoic acid

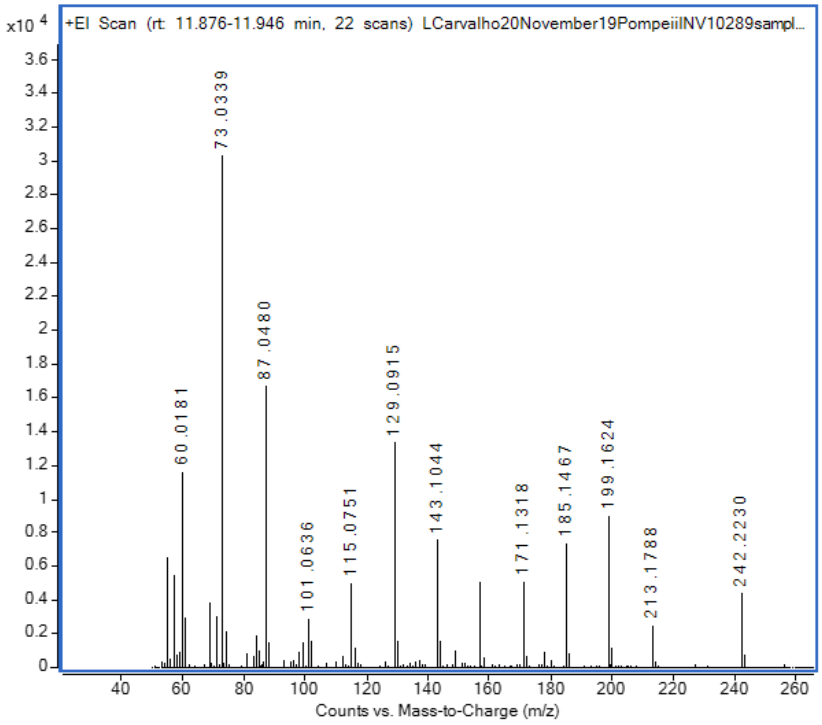
Sample 2



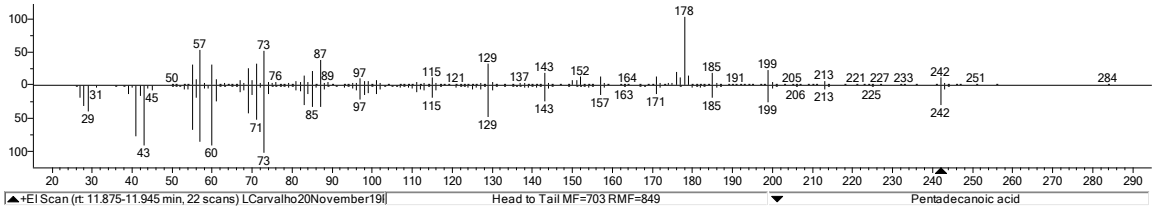


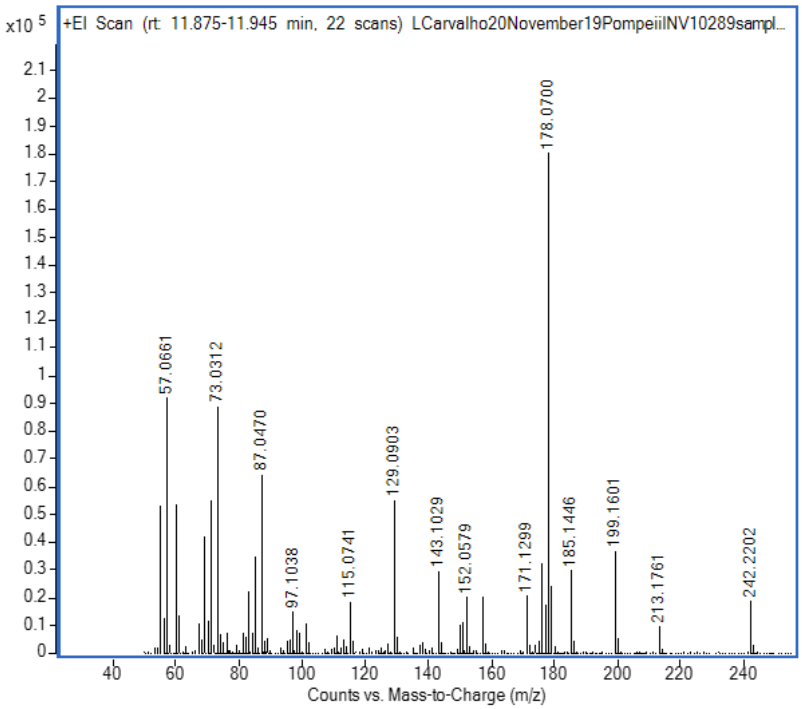
Sample 3


+EI Scan (rt: 11.876-11.946 min, 22 scans) LCarvalho20November19I
Head to Tail MF=732 RMF=757
Pentadecanoic acid


x10 4
+EI Scan (rt: 11.876-11.946 min, 22 scans) LCarvalho20November19PompeiiINV10289sampl...
73.0339
87.0480
60.0181
101.0636
115.0751
129.0915
143.1044
171.1318
185.1467
199.1624
213.1788
242.2230
Counts vs. Mass-to-Charge (m/z)

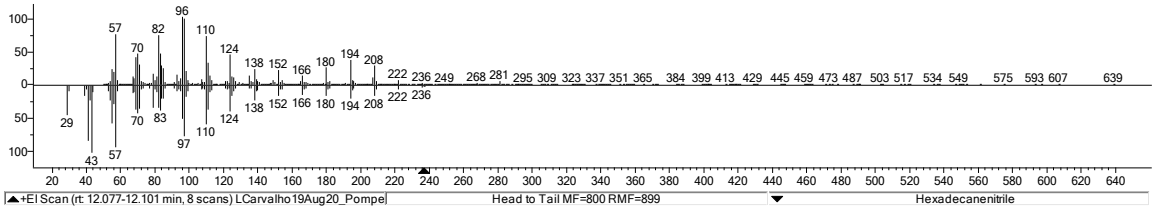
Sample 6

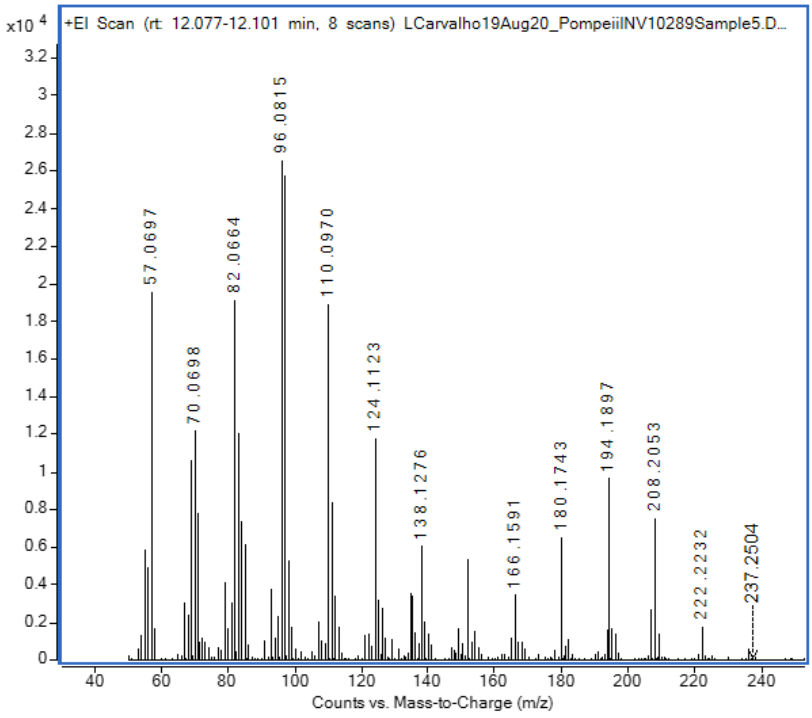

+EI Scan (rt: 11.875-11.945 min, 22 scans) LCarvalho20November19I
Head to Tail MF=703 RMF=849
Pentadecanoic acid


x10 5
+EI Scan (rt: 11.875-11.945 min, 22 scans) LCarvalho20November19PompeiiINV10289sampl...
178.0700
57.0661
73.0312
87.0470
129.0903
143.1029
152.0579
171.1299
185.1446
199.1601
97.1038
115.0741
213.1761
242.2202
Counts vs. Mass-to-Charge (m/z)

[15] Hexadecanenitrile

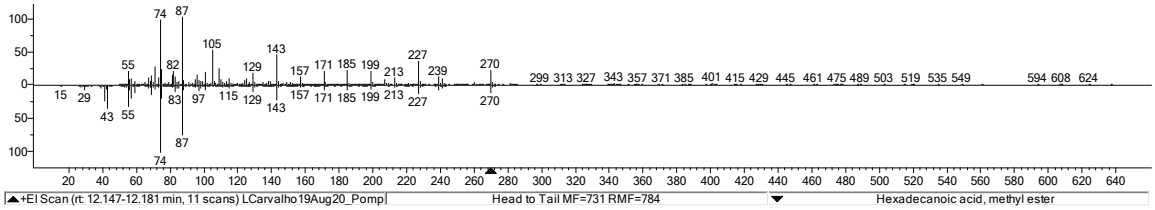
Sample 5

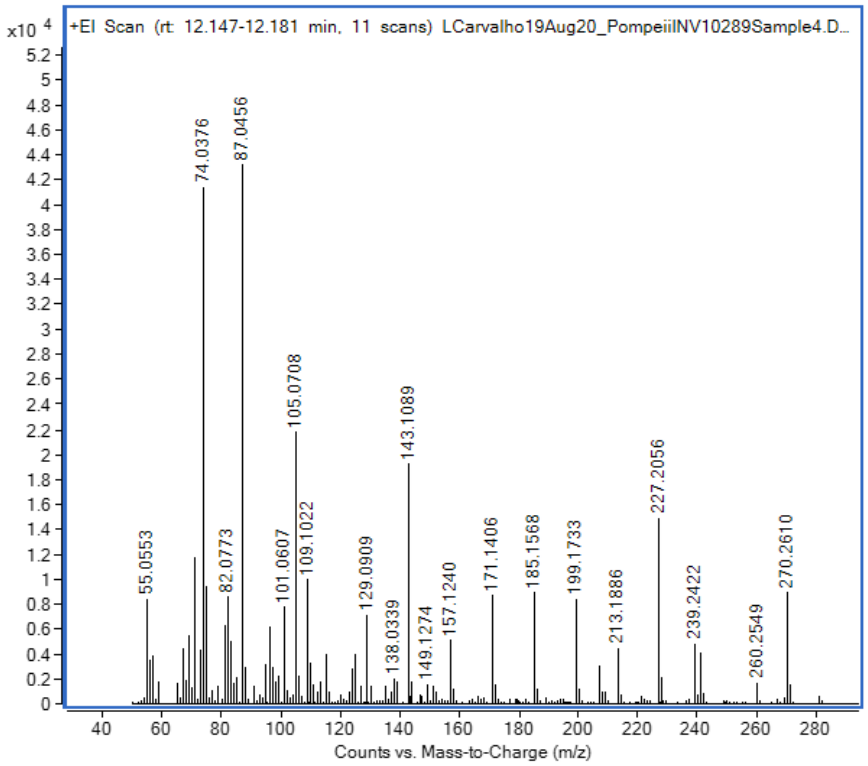




[16] Hexadecanoic acid methyl ester Mass: 270.25588

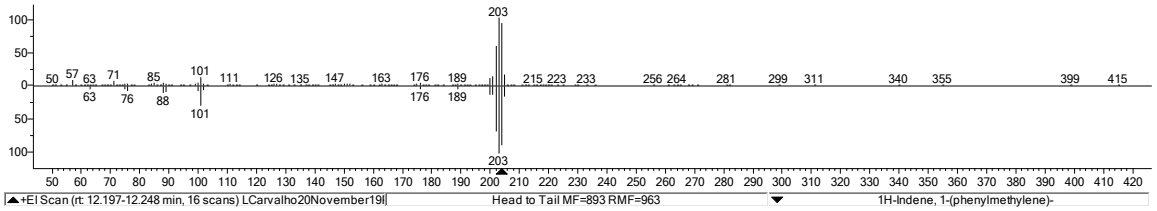
Sample 4

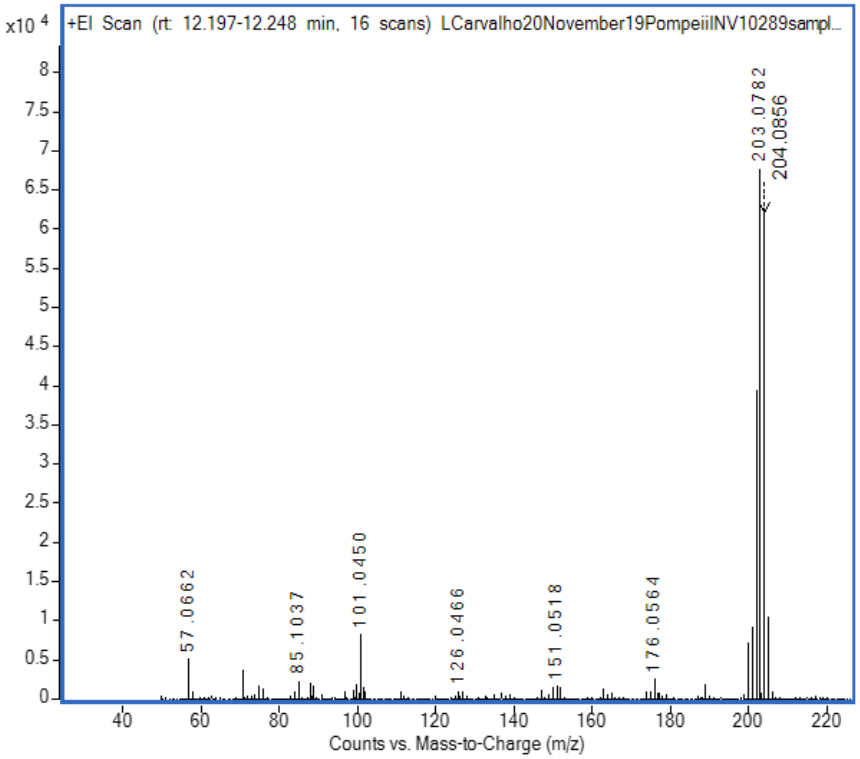




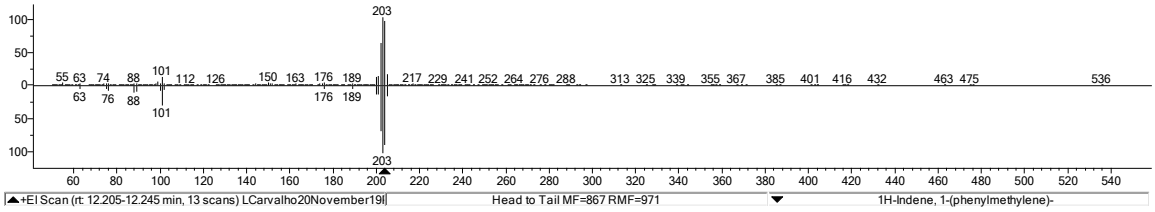
[17] 1H-Indene, 1-(phenylmethylene)- Mass: 204.093901

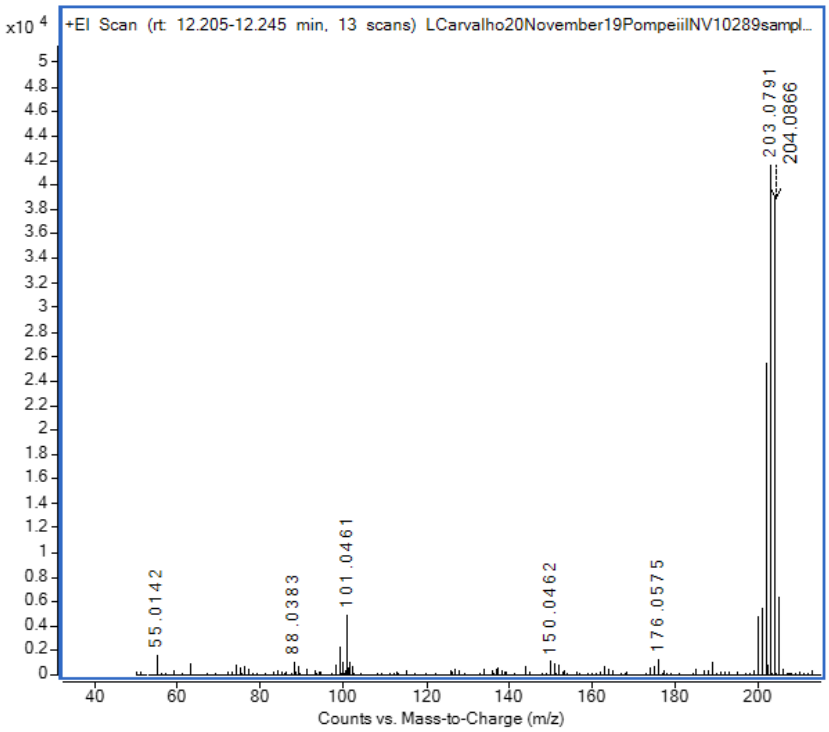
Sample 2



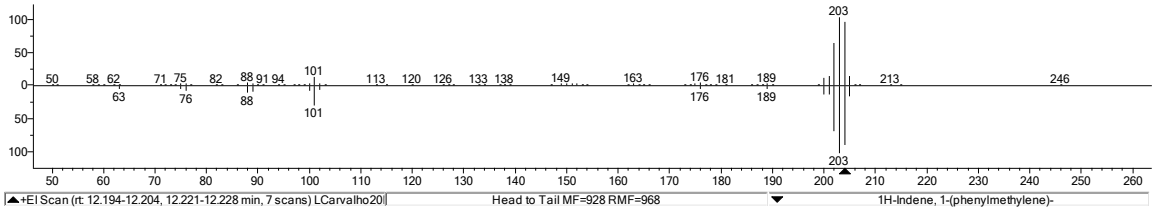


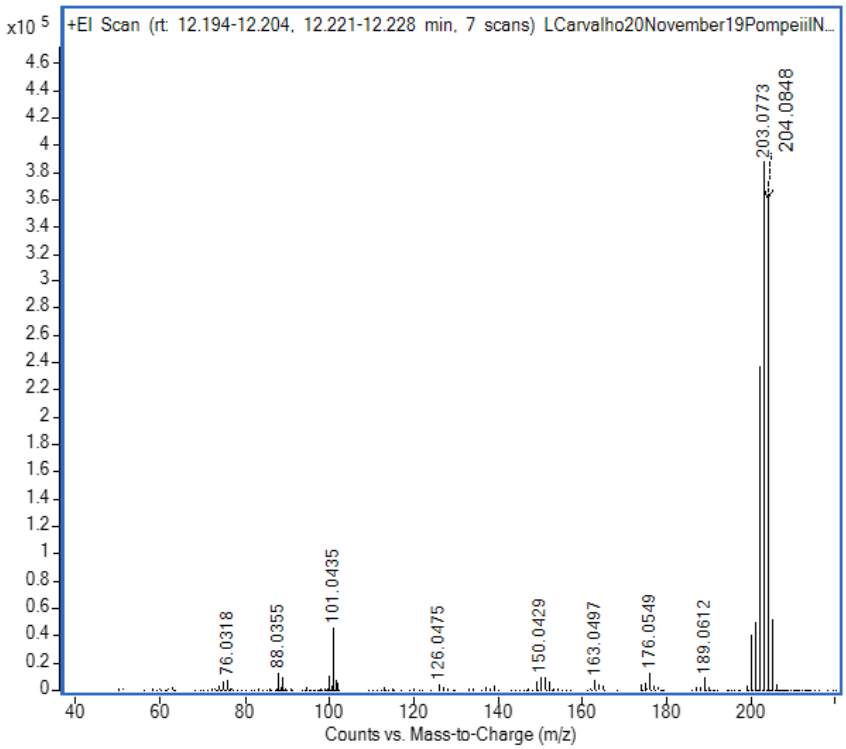
Sample 3


+EI Scan (rt: 12.205-12.245 min, 13 scans) LCarvalho20November19I
Head to Tail MF=867 RMF=971
1H-Indene, 1-(phenylmethylene)-


+EI Scan (rt: 12.205-12.245 min, 13 scans) LCarvalho20November19PompeiiINV10289sampl...
x10 4
55.0142
88.0383
101.0461
150.0462
176.0575
203.0791
204.0866
Counts vs. Mass-to-Charge (m/z)

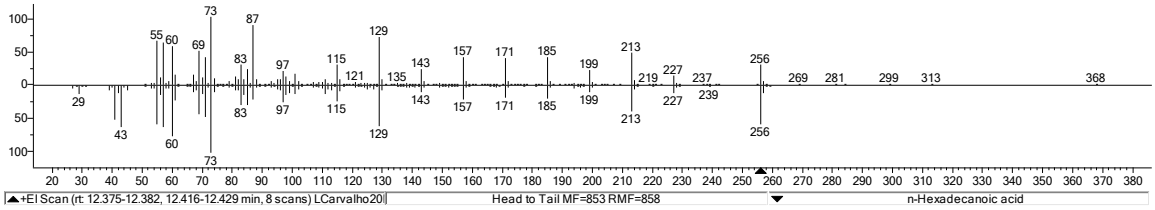
Sample 6

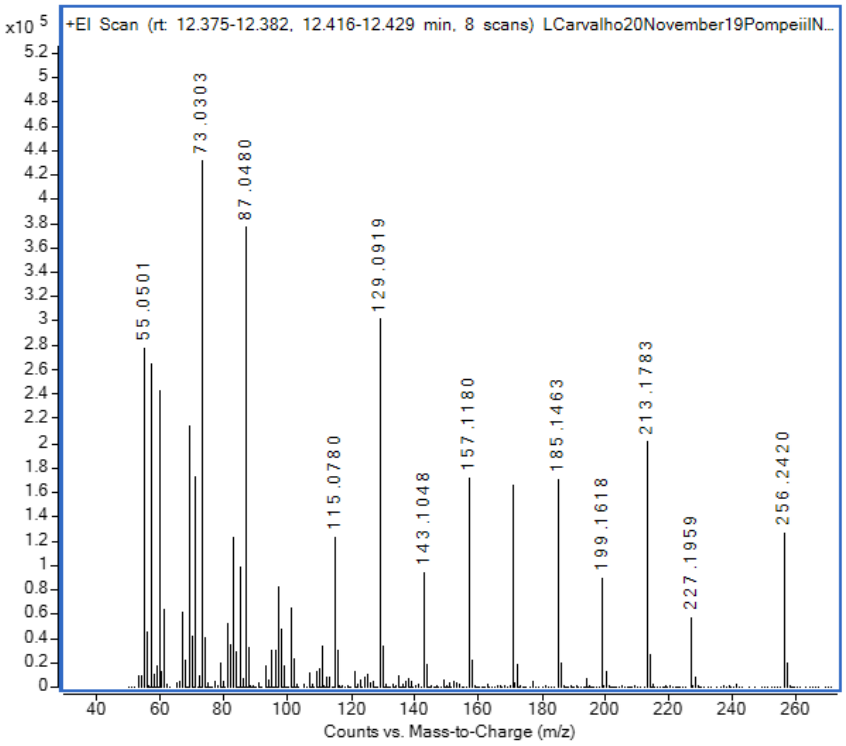

+EI Scan (rt: 12.194-12.204, 12.221-12.228 min, 7 scans) LCarvalho20
Head to Tail MF=928 RMF=968
1H-Indene, 1-(phenylmethylene)-


x10 5
+EI Scan (rt: 12.194-12.204, 12.221-12.228 min, 7 scans) LCarvalho20November19PompeiiIN...
203.0773
204.0848
76.0318
88.0355
101.0435
126.0475
150.0429
163.0497
176.0549
189.0612
Counts vs. Mass-to-Charge (m/z)

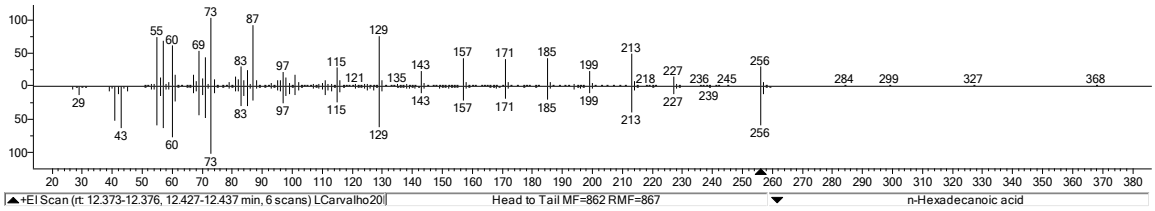
[18] n-Hexadecanoic acid

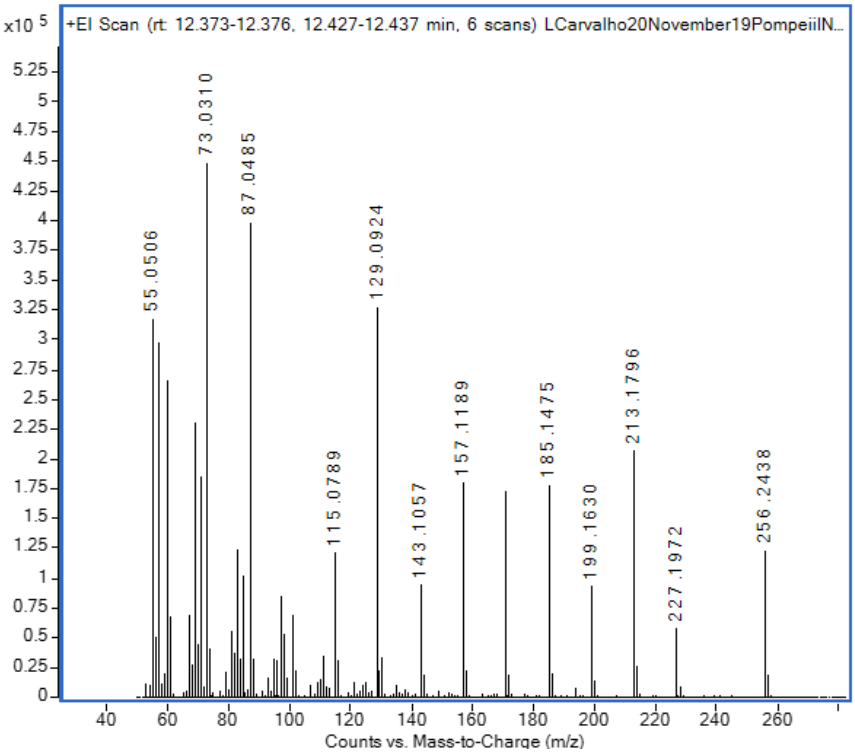
Sample 2



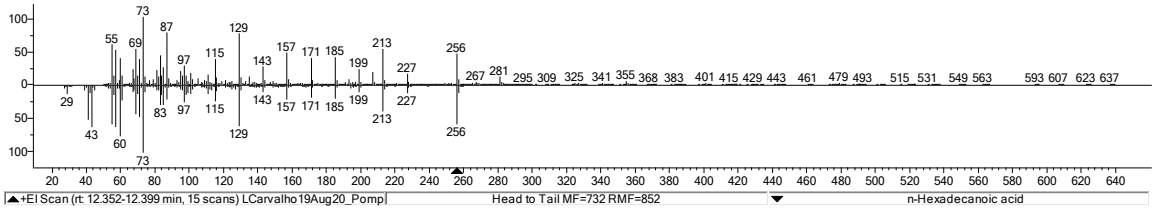


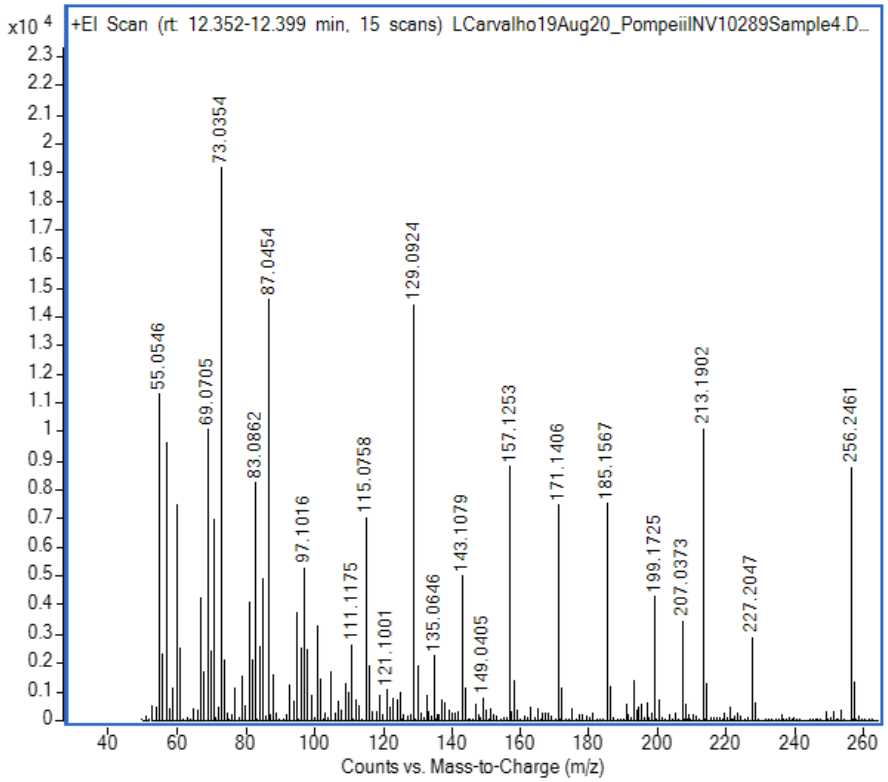
Sample 3


+EI Scan (rt: 12.373-12.376, 12.427-12.437 min, 6 scans) LCarvalho20
Head to Tail MF=862 RMF=867
n-Hexadecanoic acid

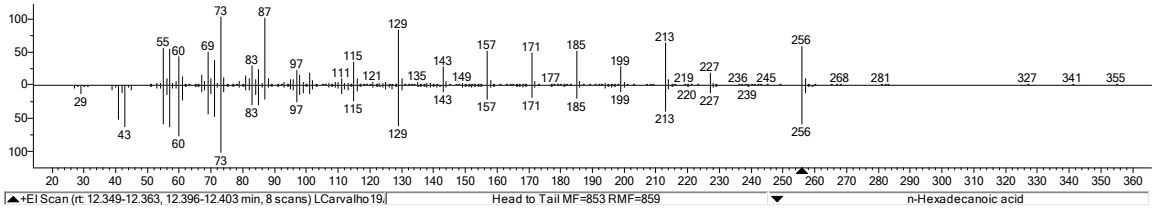

x10 5
+EI Scan (rt: 12.373-12.376, 12.427-12.437 min, 6 scans) LCarvalho20November19PompeiilN...
73.0310
87.0485
55.0506
129.0924
115.0789
143.1057
157.1189
185.1475
199.1630
213.1796
227.1972
256.2438
Counts vs. Mass-to-Charge (m/z)

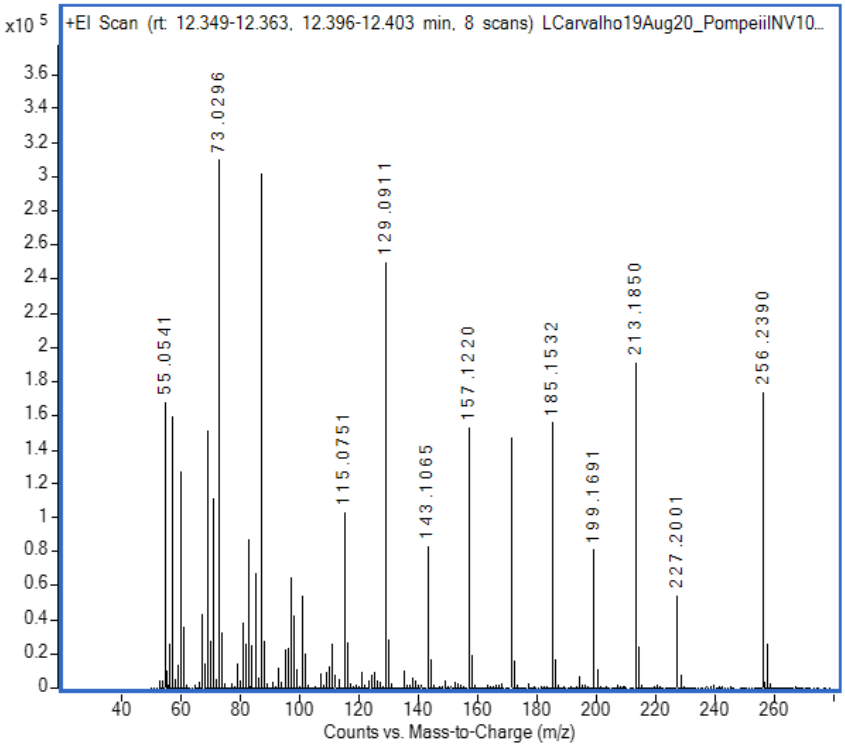
Sample 4


+EI Scan (rt: 12.352-12.399 min, 15 scans) LCarvalho19Aug20_Pomp
Head to Tail MF=732 RMF=852
n-Hexadecanoic acid

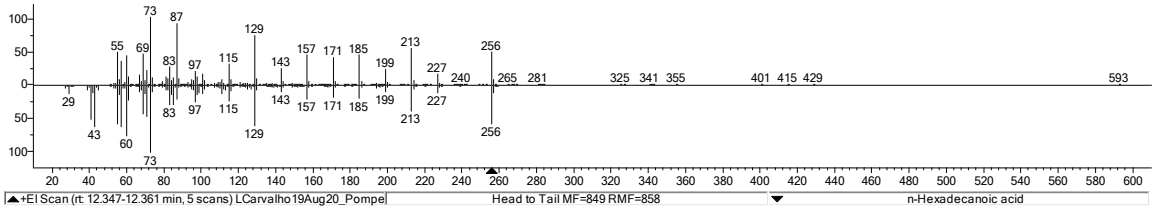

x10 4
+EI Scan (rt: 12.352-12.399 min, 15 scans) LCarvalho19Aug20_PompeiiINV10289Sample4.D...
73.0354
87.0454
129.0924
55.0546
69.0705
83.0862
97.1016
115.0758
111.1175
121.1001
135.0646
143.1079
149.0405
157.1253
171.1406
185.1567
199.1725
207.0373
213.1902
227.2047
256.2461
Counts vs. Mass-to-Charge (m/z)

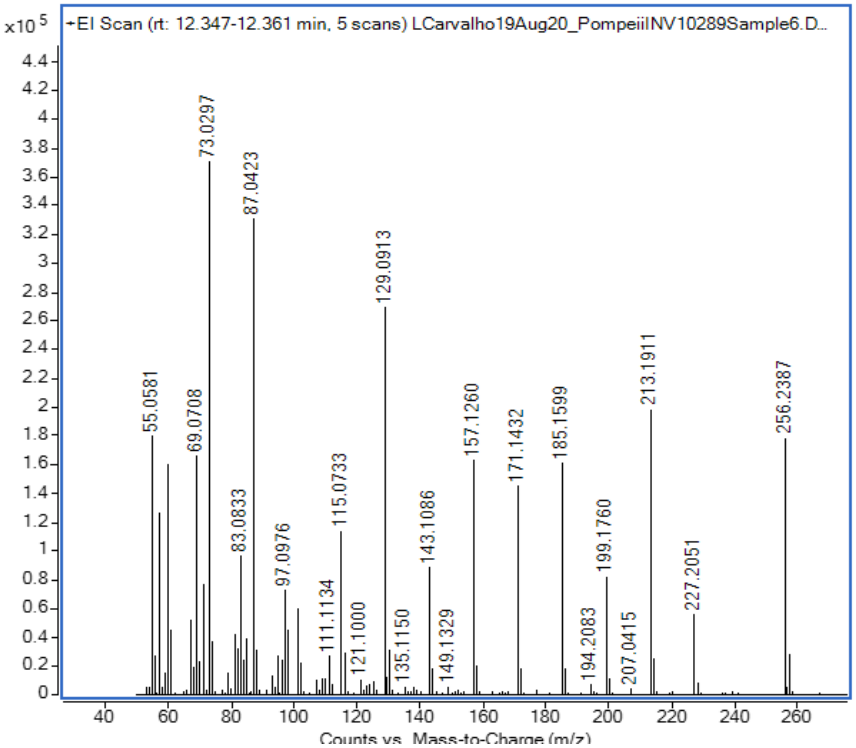
Sample 5


+EI Scan (rt: 12.349-12.363, 12.396-12.403 min, 8 scans) LCarvalho19
Head to Tail MF=853 RMF=859
n-Hexadecanoic acid


x10 5
+EI Scan (rt: 12.349-12.363, 12.396-12.403 min, 8 scans) LCarvalho19Aug20_PompeiiINV10...
55.0541
73.0296
115.0751
129.0911
143.1065
157.1220
185.1532
199.1691
213.1850
227.2001
256.2390
Counts vs. Mass-to-Charge (m/z)

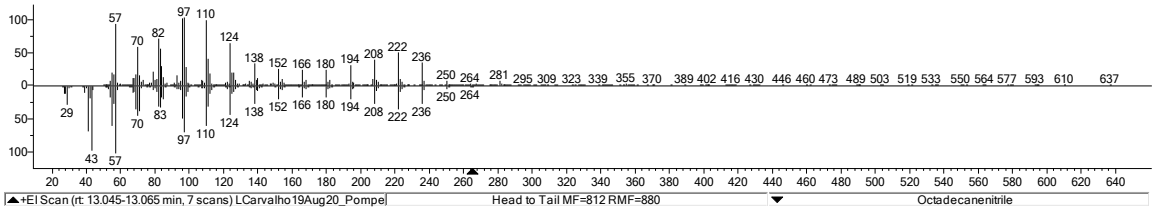
Sample 6

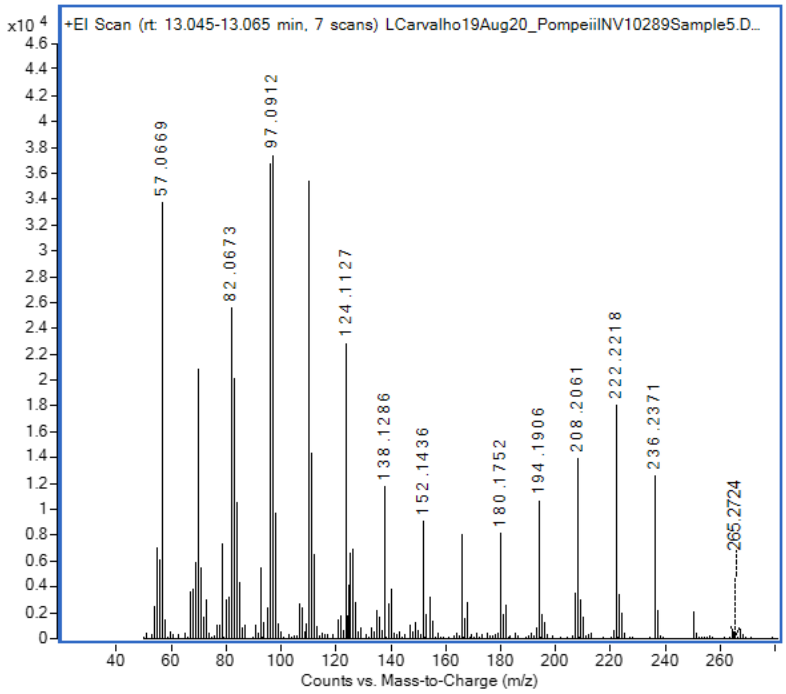

+EI Scan (rt: 12.347-12.361 min, 5 scans) LCarvalho19Aug20_Pompe
Head to Tail MF=849 RMF=858
n-Hexadecanoic acid


x10 5
+EI Scan (rt: 12.347-12.361 min, 5 scans) LCarvalho19Aug20_PompeiiINV10289Sample6.D...
55.0581
69.0708
73.0297
83.0833
87.0423
97.0976
111.1134
115.0733
121.1000
129.0913
135.1150
143.1086
149.1329
157.1260
171.1432
185.1599
194.2083
199.1760
207.0415
213.1911
227.2051
256.2387
Counts vs. Mass-to-Charge (m/z)

[19] Octadecanenitrile

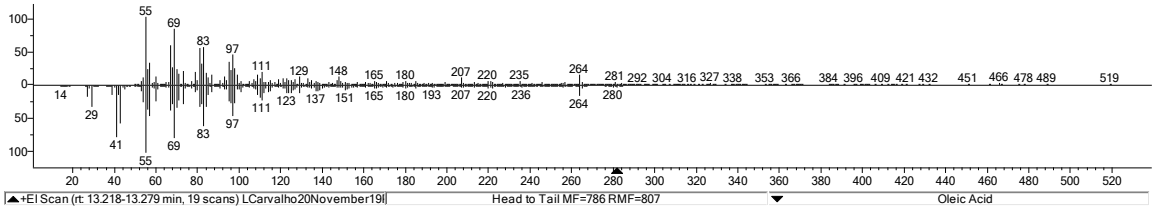
Sample 5

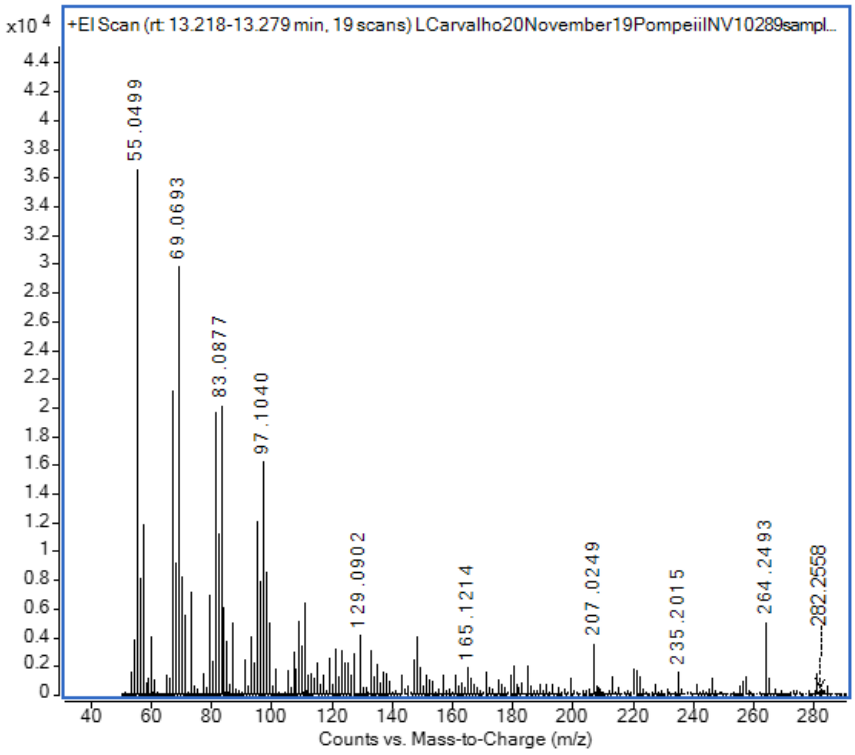




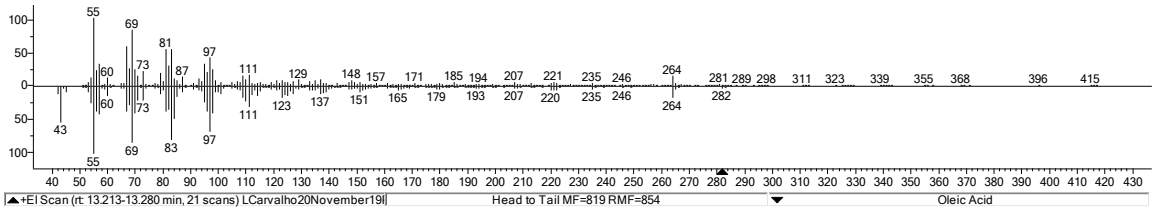
[20] 9-Octadecenoic acid (Oleic acid)

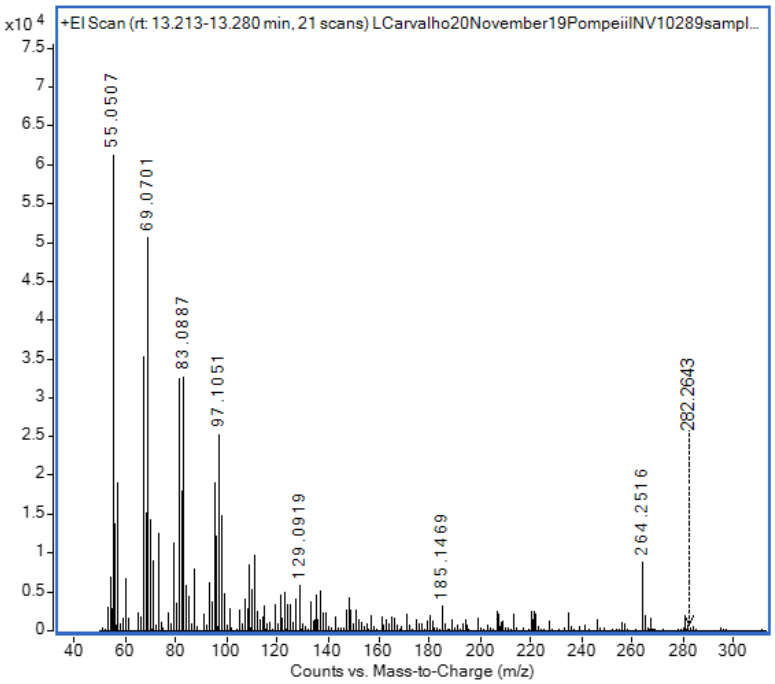
Sample 2



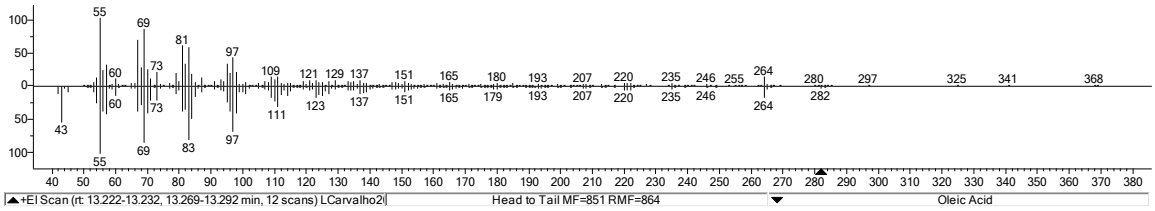


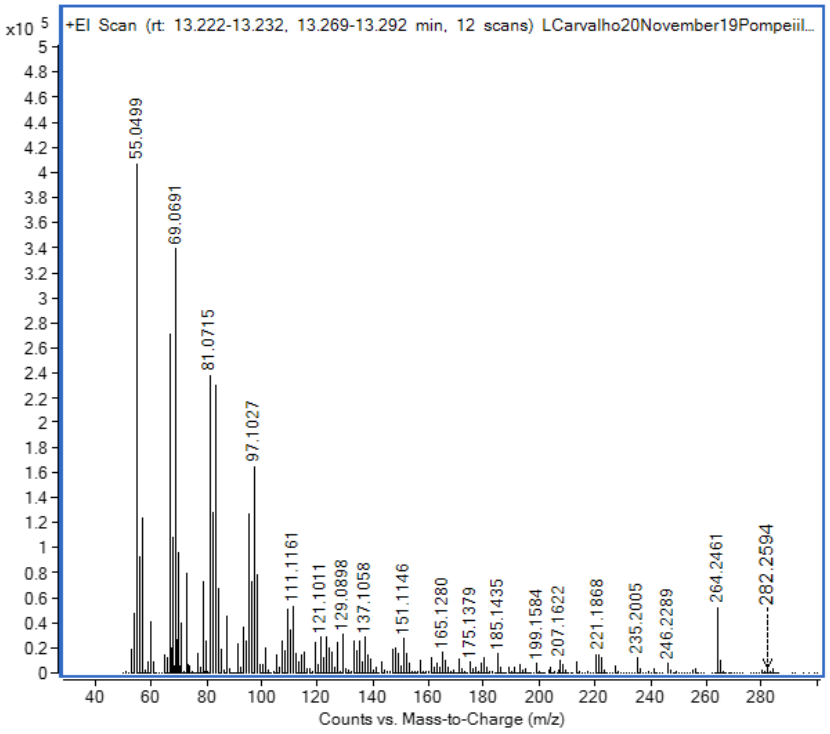
Sample 3


+EI Scan (rt: 13.213-13.280 min, 21 scans) LCarvalho20November19II
Head to Tail MF=819 RMF=854
Oleic Acid


x10 4
+EI Scan (rt: 13.213-13.280 min, 21 scans) LCarvalho20November19PompeiiINV10289sampl...
55.0507
69.0701
83.0887
97.1051
129.0919
185.1469
264.2516
282.2643
Counts vs. Mass-to-Charge (m/z)

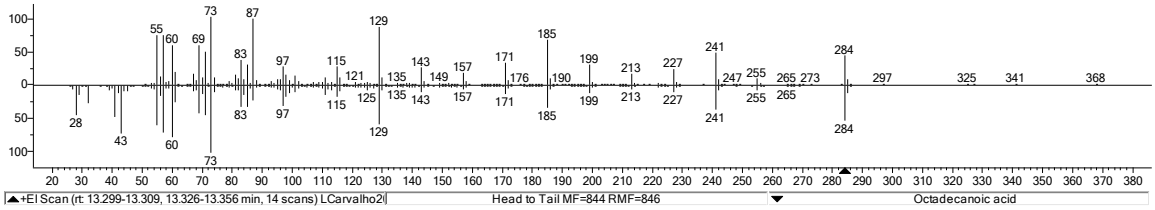
Sample 6

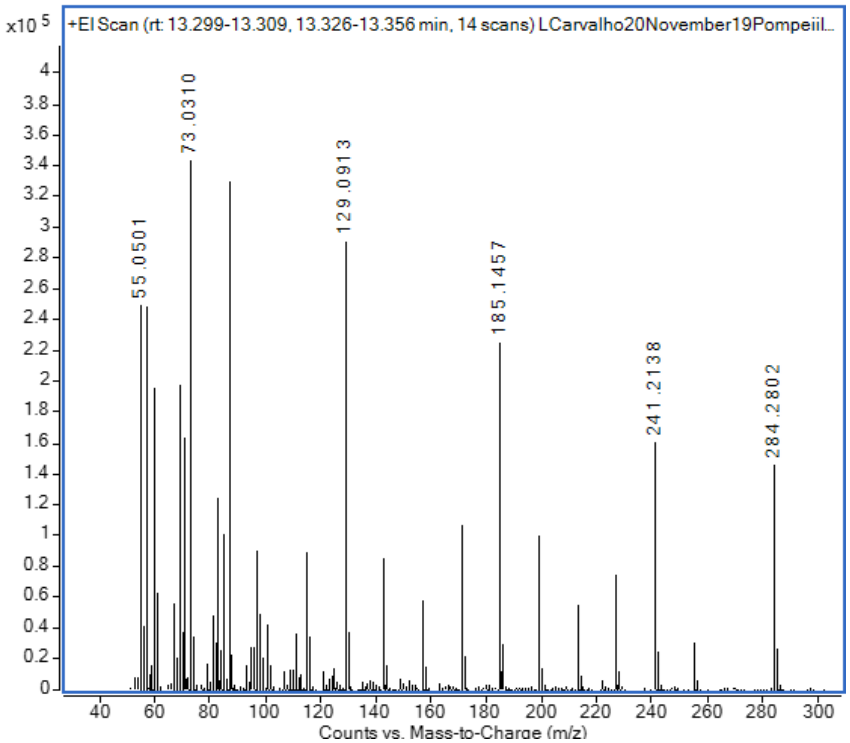

+EI Scan (rt: 13.222-13.232, 13.269-13.292 min, 12 scans) LCarvalho2(
Head to Tail MF=851 RMF=864
Oleic Acid


+EI Scan (rt: 13.222-13.232, 13.269-13.292 min, 12 scans) LCarvalho20November19Pompeiil...
x10 5
55.0499
69.0691
81.0715
97.1027
111.1161
121.1011
129.0898
137.1058
151.1146
165.1280
175.1379
185.1435
199.1584
207.1622
221.1868
235.2005
246.2289
264.2461
282.2594
Counts vs. Mass-to-Charge (m/z)

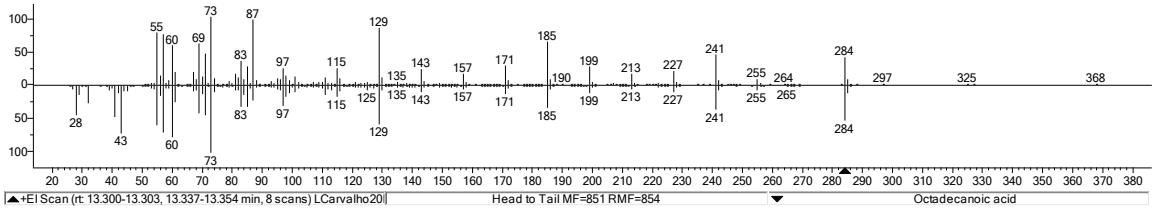
[21] Octadecanoic acid

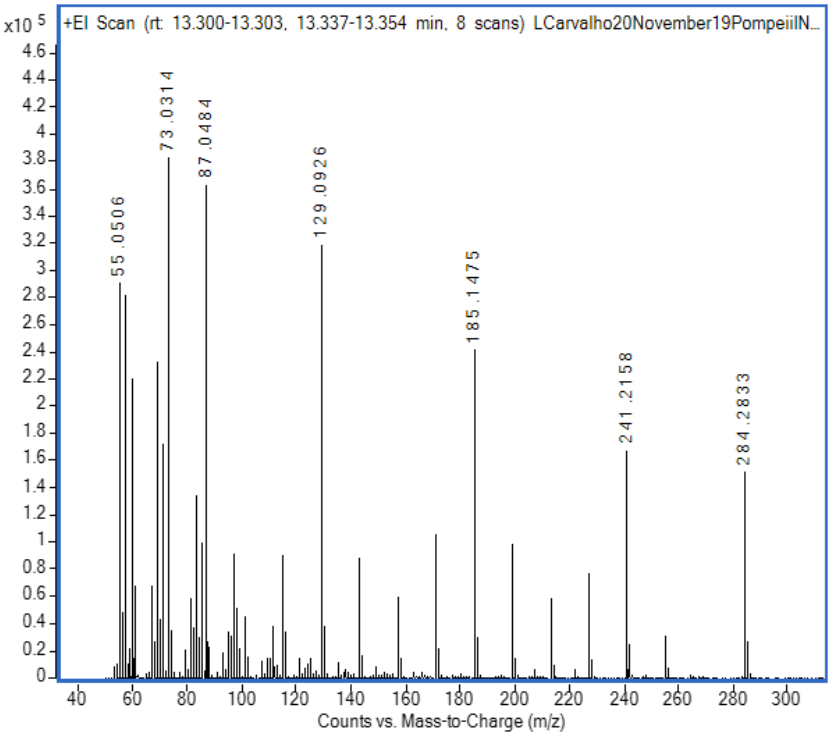
Sample 2



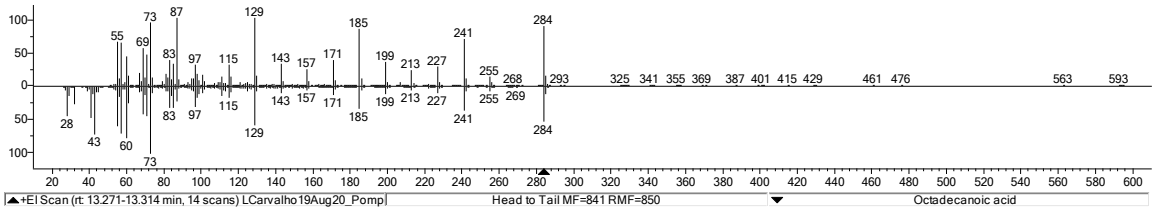


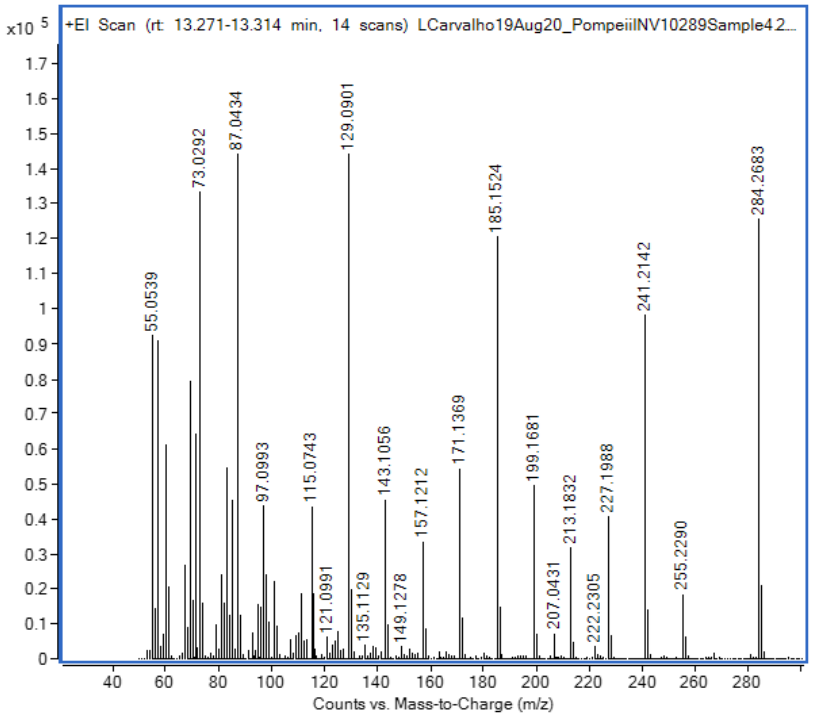
Sample 3


+EI Scan (rt: 13.300-13.303, 13.337-13.354 min, 8 scans) LCarvalho20
Head to Tail MF=851 RMF=854
Octadecanoic acid

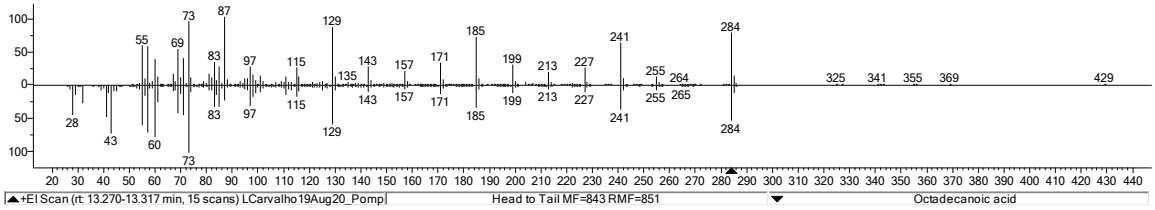

x10 5
+EI Scan (rt: 13.300-13.303, 13.337-13.354 min, 8 scans) LCarvalho20November19PompeiiIN...
55.0506
73.0314
87.0484
129.0926
185.1475
241.2158
284.2833
Counts vs. Mass-to-Charge (m/z)

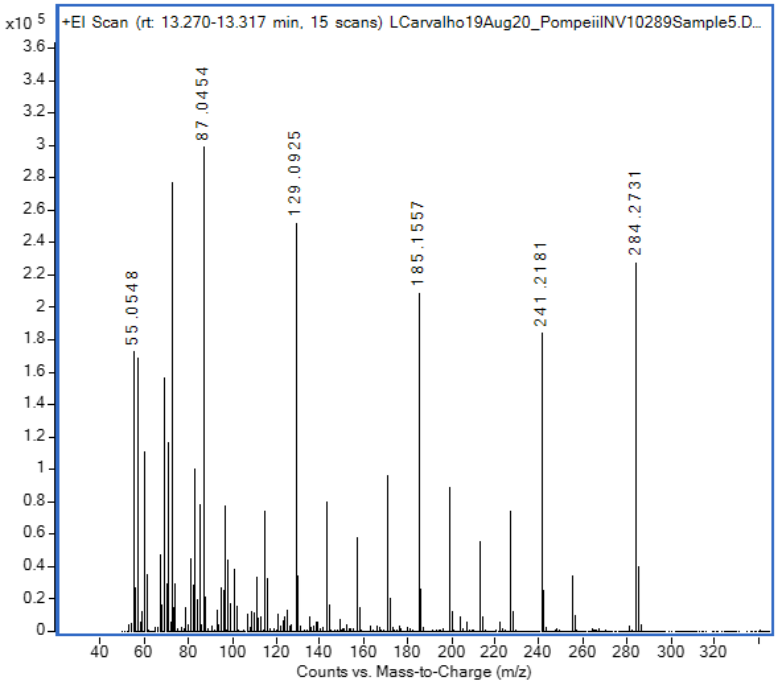
Sample 4


+EI Scan (rt: 13.271-13.314 min, 14 scans) LCarvalho19Aug20_Pomp
Head to Tail MF=841 RMF=850
Octadecanoic acid

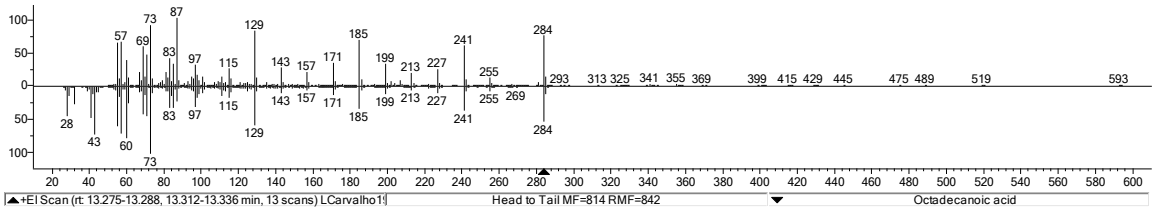

x10 5
+EI Scan (rt: 13.271-13.314 min, 14 scans) LCarvalho19Aug20_PompeiiINV10289Sample4.2...
55.0539
73.0292
87.0434
97.0993
115.0743
121.0991
129.0901
135.1129
143.1056
149.1278
157.1212
171.1369
185.1524
199.1681
207.0431
213.1832
222.2305
227.1988
241.2142
255.2290
284.2683
Counts vs. Mass-to-Charge (m/z)

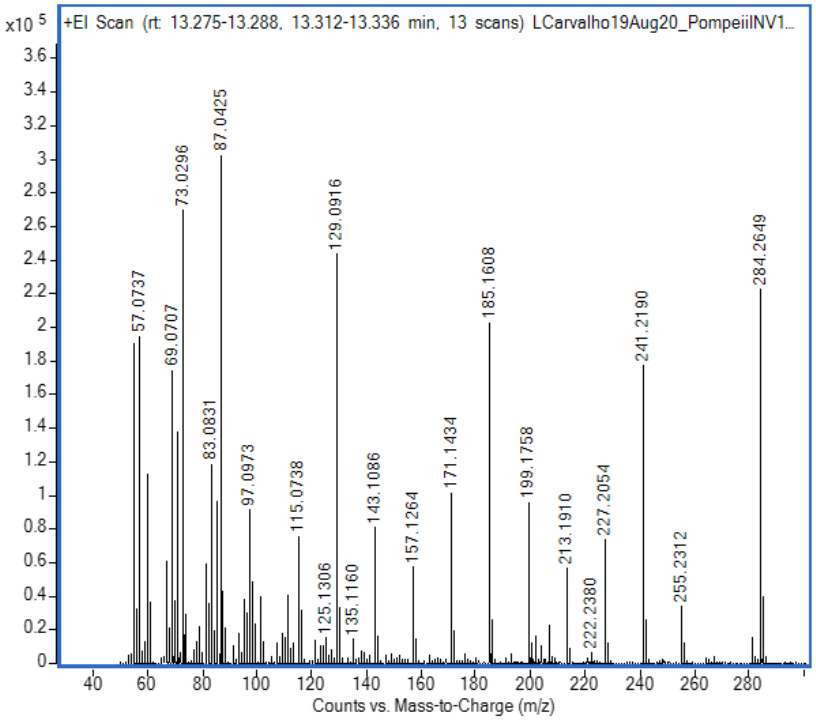
Sample 5


+EI Scan (rt: 13.270-13.317 min, 15 scans) LCarvalho19Aug20_Pompl
Head to Tail MF=843 RMF=851
Octadecanoic acid


x10 5
+EI Scan (rt: 13.270-13.317 min, 15 scans) LCarvalho19Aug20_PompeiiINV10289Sample5.D...
55.0548
87.0454
129.0925
185.1557
241.2181
284.2731
Counts vs. Mass-to-Charge (m/z)

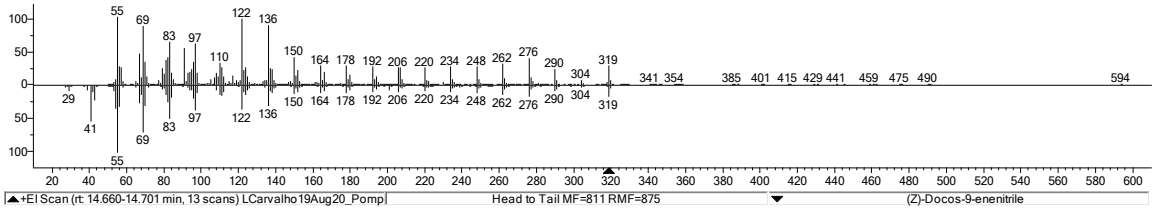
Sample 6

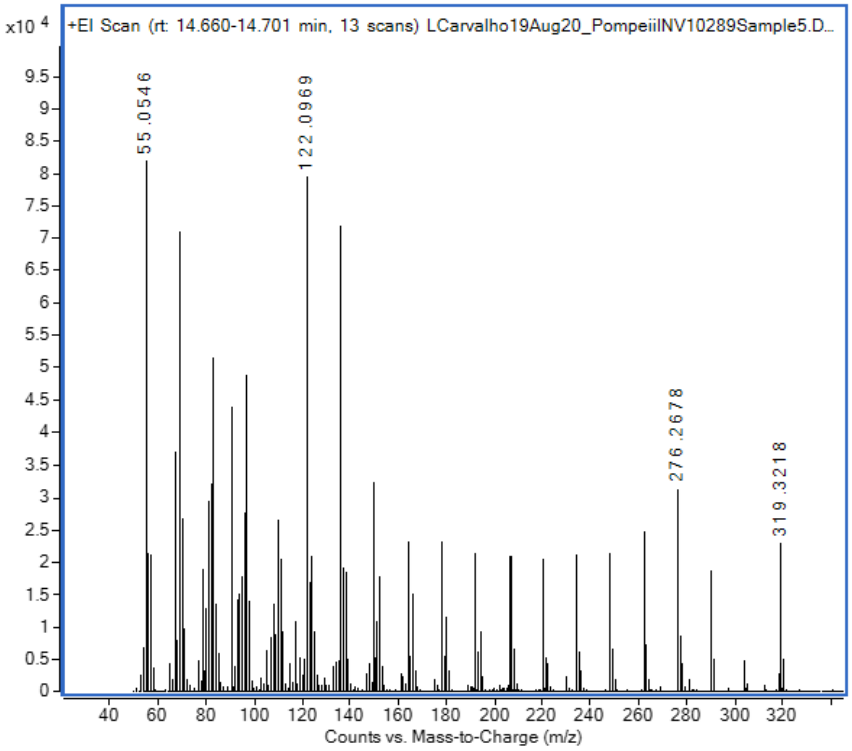

+EI Scan (rt: 13.275-13.288, 13.312-13.336 min, 13 scans) LCarvalho1
Head to Tail MF=814 RMF=842
Octadecanoic acid


x10 5
+EI Scan (rt: 13.275-13.288, 13.312-13.336 min, 13 scans) LCarvalho19Aug20_PompeiiINV1...
57.0737
69.0707
73.0296
83.0831
87.0425
97.0973
115.0738
125.1306
129.0916
135.1160
143.1086
157.1264
171.1434
185.1608
199.1758
213.1910
222.2380
227.2054
241.2190
255.2312
284.2649
Counts vs. Mass-to-Charge (m/z)

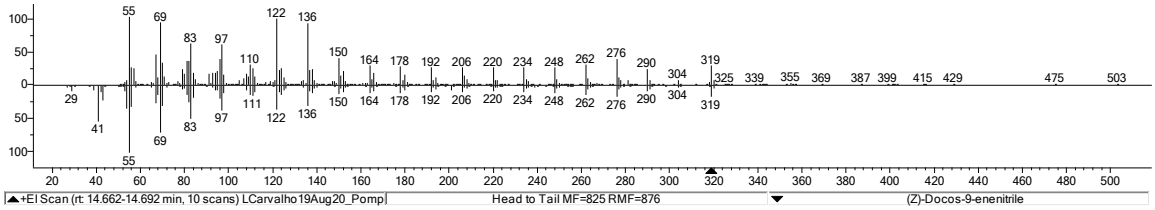
[22] (Z)-Docos-9-enenitrile

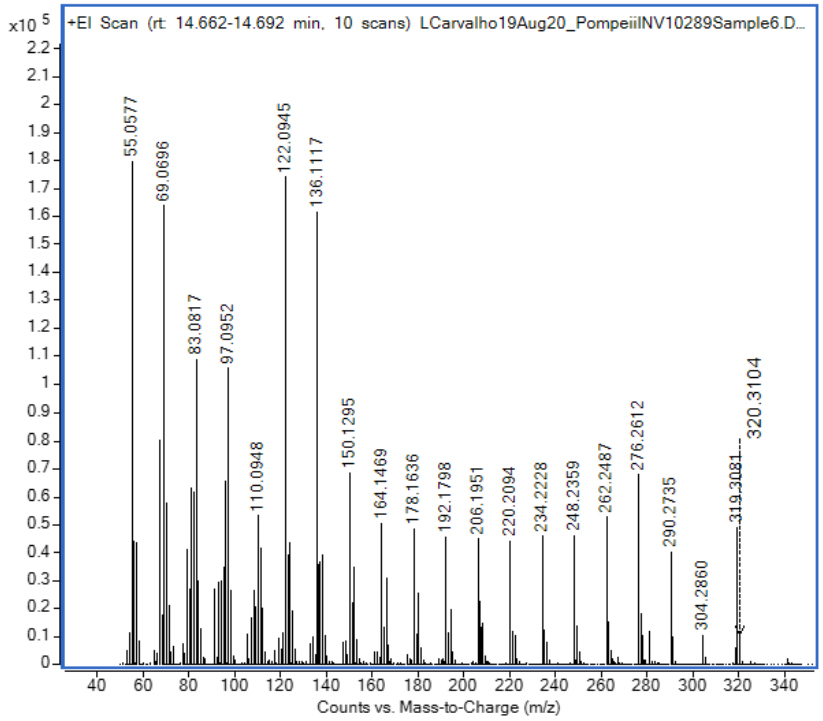
Sample 5





Sample 6


+EI Scan (rt: 14.662-14.692 min, 10 scans) LCarvalho19Aug20_Pompl
Head to Tail MF=825 RMF=876
(Z)-Docos-9-enenitrile


+EI Scan (rt: 14.662-14.692 min, 10 scans) LCarvalho19Aug20_PompeiiINV10289Sample6.D...
x10 5
55.0577
69.0696
83.0817
97.0952
110.0948
122.0945
136.1117
150.1295
164.1469
178.1636
192.1798
206.1951
220.2094
234.2228
248.2359
262.2487
276.2612
290.2735
304.2860
319.3081
320.3104
Counts vs. Mass-to-Charge (m/z)

Compound	Name	Formula	m/z	Score	Mass Error (ppm)	RT Error (min)	Isotope Similarity (ppm)	Maximum Fold Change	Isotope Distribution	Normalised abundance P10289_2	P10289_3	P10289_4	P10289_5	P10289_6
2.57_343.1249m/z	Malitol	C12H24O11	343.1249	39.3	0.8011	-0.51	94.94	Infinity	100 - 11.2	2601.28	0.00	0.00	0.00	0.00
4.86_103.0401m/z	3-Hydroxyisobutyric acid	C4H8O3	103.0401	41.5	-0.1444	-0.18	97.48	Infinity	100 - 2.57	83.27	0.00	125.47	283.95	67.03
4.28_165.0405m/z	Arabinonic acid	C5H10O6	165.0405	40.2	-0.0237	-0.62	97.83	Infinity	100 - 4.45 - 0.349	246.39	0.00	174.23	139.88	272.55
10.09_147.0299m/z	Citramalic acid	C5H8O5	147.0299	40.9	0.1929	-0.66	98.51	27.89	100 - 4.59 - 0.666	209.79	8.62	204.98	240.51	218.25
4.11_128.0353m/z	1-Pyrroline hydroxycarboxylic acid	C5H7NO3	128.0353	39.7	0.1813	-0.37	93.81	16.09	100 - 0.127	393.25	84.94	1113.61	361.46	1366.33
16.34_191.0197m/z	Citric acid	C6H8O7	191.0197	41.9	-0.1904	-0.57	98.84	15.89	100 - 6.61 - 0.715	981.05	69.74	773.44	751.01	1108.12
2.77_503.1615m/z	Raffinose	C18H32O16	503.1615	44.8	-0.5682	-0.03	95.54	14.25	100 - 19.1 - 1.9	247.41	168.57	19.60	238.98	279.30
4.56_75.0087m/z	Glycolic acid	C2H4O3	75.0087	40.1	-0.6941	-0.68	98.35	6.76	100 - 1.05 - 0.202	459.39	81.88	412.08	475.82	553.55
6.30_87.0451m/z	Butyric acid	C4H8O2	87.0451	51.9	-0.3756	-0.02	98.36	6.76	100 - 3.27	42.99	15.68	106.00	98.88	50.38
12.48_88.9880m/z	Oxalic acid	C2H2O4	88.9880	40.7	-0.0875	-0.92	97.97	5.23	100 - 0.904 - 0.181	685.12	202.86	701.46	1061.83	855.78
12.68_115.0037m/z	Fumaric Acid	C4H4O4	115.0037	40.8	-0.0242	-0.95	98.58	5.06	100 - 3.46 - 0.469	2197.51	977.67	683.15	560.43	433.95
9.98_161.0455m/z	3-Hydroxymethylglutarate	C6H10O5	161.0455	40.6	-0.1574	-0.78	97.68	4.82	100 - 5.16 - 0.353	155.11	43.67	146.18	210.32	187.26
4.37_89.0244m/z	Dihydroxyacetone	C3H6O3	89.0244	40.6	-0.2441	-0.37	98.50	4.54	100 - 2.41 - 0.116	5834.04	3401.30	10955.24	3857.01	15446.16
5.68_101.0243m/z	Acetoacetate	C4H6O3	101.0243	39.8	-0.6959	0.54	96.18	4.00	100 - 1.19	144.81	42.37	99.17	169.40	145.52
2.67_341.1093m/z	Lactose	C12H22O11	341.1093	39.9	-0.6462	-0.37	97.25	3.15	100 - 12.3 - 1.55	618.87	579.27	1766.51	706.17	560.25
4.01_179.0560m/z	Glucose	C6H12O6	179.0560	40	-0.6096	0.58	98.43	2.67	100 - 5.83 - 0.752	162.96	90.08	70.36	84.13	61.10
19.16_143.1077m/z	Octanoic acid	C8H16O2	143.1077	41.5	-0.0281	-0.79	98.29	2.60	100 - 7.61 - 0.195	1649.40	4289.12	1896.33	4070.63	1835.09
17.90_201.1133m/z	Sebacic acid	C10H18O4	201.1133	42.7	0.1141	-0.40	97.58	2.54	100 - 9.51 - 0.43	3220.68	6573.27	2812.04	2587.37	2673.63
10.39_133.0143m/z	Malic acid	C4H6O5	133.0143	40.8	0.1075	-0.75	98.41	1.87	100 - 3.45 - 0.565	774.30	491.34	619.74	920.79	795.30
10.69_159.0662m/z	3,3 Dimethyl glutarate	C7H12O4	159.0662	41	-0.2341	-0.72	99.08	1.84	100 - 7.26 - 0.682	2917.18	1581.47	2728.35	2746.87	2825.16
10.39_117.0193m/z	Succinic acid	C4H6O4	117.0193	40.9	0.0712	-0.72	98.51	1.52	100 - 3.32 - 0.556	1505.07	1224.02	1458.29	1466.21	1864.89
10.09_131.0350m/z	Glutaric acid	C5H8O4	131.0350	40.8	-0.0702	-0.78	98.57	1.19	100 - 4.56 - 0.514	525.03	500.83	592.66	570.20	596.04
10.19_145.0507m/z	Methylglutaric acid	C6H10O4	145.0507	41	0.3144	-0.54	98.01	1.10	100 - 5.15 - 0.481	2231.14	2121.84	2189.63	2199.98	2343.23

Appendix 31 - Pompeii INV10289: IC-MS Results

Appendix 32 –

S3 interior

Data base	Protein Number	-10lgP	Coverage (%)	Peptide intensity	#Peptides (#unique)	Mass	
MEAT	O62654	87.16	6	2.83E+04	4(4)	53532	Desmin OS=Bos taurus
	P13135	55.51	28	3.00E+05	8(8)	27931	Calpain small subunit 1 OS=Bos taurus
	B9DKW3	38.48	3	8.53E+03	2(2)	53847	Cysteine--tRNA ligase OS=Staphylococcus carnosus (strain TM300)
	Q38W81	31.58	4	5.48E+04	2(2)	103215	Translation initiation factor IF-2 OS=Lactobacillus sakei subsp. sakei (strain 23K)
	Q38WS5	21.11	2	8.11E+05	1(1)	67808	UvrABC system protein C OS=Lactobacillus sakei subsp. sakei (strain 23K)
	B9DN20	21.01	2	3.16E+03	1(1)	59336	Phosphoenolpyruvate carboxykinase (ATP) OS=Staphylococcus carnosus (strain TM300)
MILK	Q6B411	145.85	48	3.68E+05	5(5)	16783	Lysozyme C milk isozyme OS=Bos taurus
	Q95L76	66.89	65	5.24E+05	6(4)	24992	Beta-casein OS=Capra hircus
	I6WY32	48.84	28	2.49E+04	4(3)	24177	Alpha-S1-casein OS=Capra hircus
	P85295	46.51	20	3.35E+04	2(2)	10078	Serum albumin (Fragments) OS=Capra hircus
	P80457	40.85	2	1.42E+04	4(4)	146790	Xanthine dehydrogenase/oxidase OS=Bos taurus
	Q865B7	38.61	4	9.38E+04	3(3)	90309	Peroxisome proliferator-activated receptor gamma coactivator 1-alpha OS=Bos taurus
	Q9TUM6	33.4	4	2.36E+04	2(2)	49368	Perilipin-2 OS=Bos taurus
	Q6VLX2	31.73	13	4.32E+05	1(1)	11256	Prolactin (Fragment) OS=Bos taurus
	Q95115	31.52	3	2.52E+04	2(2)	90700	Signal transducer and activator of transcription 5A OS=Bos taurus
	Q8MIH3	25.61	17	1.13E+03	2(1)	12999	Alpha s1 casein OS=Capra hircus
CEREAL	A0A2S4VGG4	28.53	1	2.00E+06	1(1)	118765	Suf domain-containing protein OS=Puccinia striiformis
	K3VT46	26.16	1	8.86E+04	1(1)	73085	Uncharacterized protein OS=Fusarium pseudograminearum (strain CS3096)
	L7HIN7	25.67	5	5.36E+04	1(1)	15809	Uncharacterized protein OS=Pseudomonas fluorescens BRIP34879
	A0A2S4U9Z8	24.93	1	2.71E+03	1(1)	80646	Uncharacterized protein OS=Puccinia striiformis
	K3UK62	23.63	1	3.51E+04	1(1)	106239	Uncharacterized protein OS=Fusarium pseudograminearum (strain CS3096)
	K3VR96	23.5	1	7.34E+04	1(1)	70251	Phosphoinositide phospholipase C OS=Fusarium pseudograminearum (strain CS3096)
	A0A0F4HAU3	22.16	4	7.43E+03	1(1)	20586	16S rRNA (Guanine(966)-N(2))-methyltransferase RsmD OS=Limosilactobacillus fermentum
	K3V550	22.13	0	4.19E+03	1(1)	232996	Uncharacterized protein OS=Fusarium pseudograminearum (strain CS3096)
	A0A481S1Y3	21.65	6	2.33E+05	1(1)	27743	Beta-sesquiphellandrene synthase (Fragment) OS=Triticum aestivum
	A0A352AEQ9	21.48	2	4.78E+04	1(1)	64466	Endoglucanase OS=Cyanobacteria bacterium UBA9273
	K3VCI1	20.37	1	1.46E+04	1(1)	168592	Sec3-PIP2_bind domain-containing protein OS=Fusarium pseudograminearum (strain CS3096)
	B8I2K6	20.14	1	8.53E+04	1(1)	105918	Cellulase OS=Ruminiclostridium cellulolyticum (strain ATCC 35319 / DSM 5812 / JCM 6584 / H10)
YEAST	B3LNV9	28.22	3	1.44E+04	1(1)	26976	MICOS complex subunit MIC27 OS=Saccharomyces cerevisiae (strain RM11-1a)
	B5RSM1	28.22	7	1.44E+04	1(1)	10282	Transcription and mRNA export factor SUS1 OS=Yarrowia lipolytica (strain CLIB 122 / E 150)
	B5VQU2	28.22	3	1.44E+04	1(1)	26976	MICOS complex subunit MIC27 OS=Saccharomyces cerevisiae (strain AWRI1631)
	B9WFC9	28.22	1	1.44E+04	1(1)	48087	Maintenance of mitochondrial morphology protein 1 OS=Candida dubliniensis (strain CD36 / ATCC MYA-646 / CBS 7987 / NCPF 3949 / NRRL Y-17841)

Data base	Protein Number	-10lgP	Coverage (%)	Peptide intensity	#Peptides (#unique)	Mass	
	C4YI11	28.22	1	1.44E+04	1(1)	49026	Maintenance of mitochondrial morphology protein 1 OS=Candida albicans (strain WO-1)
	C7GR78	28.22	3	1.44E+04	1(1)	26960	MICOS complex subunit MIC27 OS=Saccharomyces cerevisiae (strain JAY291)
	O74778	28.22	2	1.44E+04	1(1)	31776	BTB/POZ domain-containing protein 2 OS=Schizosaccharomyces pombe (strain 972 / ATCC 24843
	P50945	28.22	3	1.44E+04	1(1)	26960	MICOS complex subunit MIC27 OS=Saccharomyces cerevisiae (strain ATCC 204508 / S288c)
	Q08412	28.22	1	1.44E+04	1(1)	46870	Ubiquitin-binding protein CUE5 OS=Saccharomyces cerevisiae (strain ATCC 204508 / S288c)
	Q12361	28.22	1	1.44E+04	1(1)	110709	G protein-coupled receptor GPR1 OS=Saccharomyces cerevisiae (strain ATCC 204508 / S288c)
	Q59SI5	28.22	1	1.44E+04	1(1)	49014	Maintenance of mitochondrial morphology protein 1 OS=Candida albicans (strain SC5314 / ATCC MYA-2876)
	Q6BZE1	28.22	1	1.44E+04	1(1)	72009	Autophagy-related protein 20 OS=Debaryomyces hansenii (strain ATCC 36239 / CBS 767 / JCM 1990 / NBRC 0083 / IGC 2968)
	P87052	25.46	2	2.71E+03	1(1)	39121	Meiotically up-regulated gene 10 protein OS=Schizosaccharomyces pombe (strain 972 / ATCC 24843)
	H6TB12	23.81	1	7.40E+04	1(1)	142459	Sophorolipid transporter OS=Starmerella bombicola
	P46678	22.53	1	1.23E+05	1(1)	67688	Transcription factor TFIIIB component B" OS=Saccharomyces cerevisiae (strain ATCC 204508 / S288c)
	Q6CWJ6	22.53	2	1.23E+05	1(1)	39248	Cytochrome b-c1 complex subunit 2 mitochondrial OS=Kluyveromyces lactis (strain ATCC 8585 / CBS 2359 / DSM 70799 / NBRC 1267 / NRRL Y-1140 / WM37)
	Q6FUD8	22.53	2	1.23E+05	1(1)	38915	Heterogeneous nuclear rnp K-like protein 2 OS=Candida glabrata (strain ATCC 2001 / CBS 138 / JCM 3761 / NBRC 0622 / NRRL Y-65)
	P39526	20.44	1	6.83E+03	1(1)	229898	AP-1 accessory protein LAA1 OS=Saccharomyces cerevisiae (strain ATCC 204508 / S288c)

S5 exterior

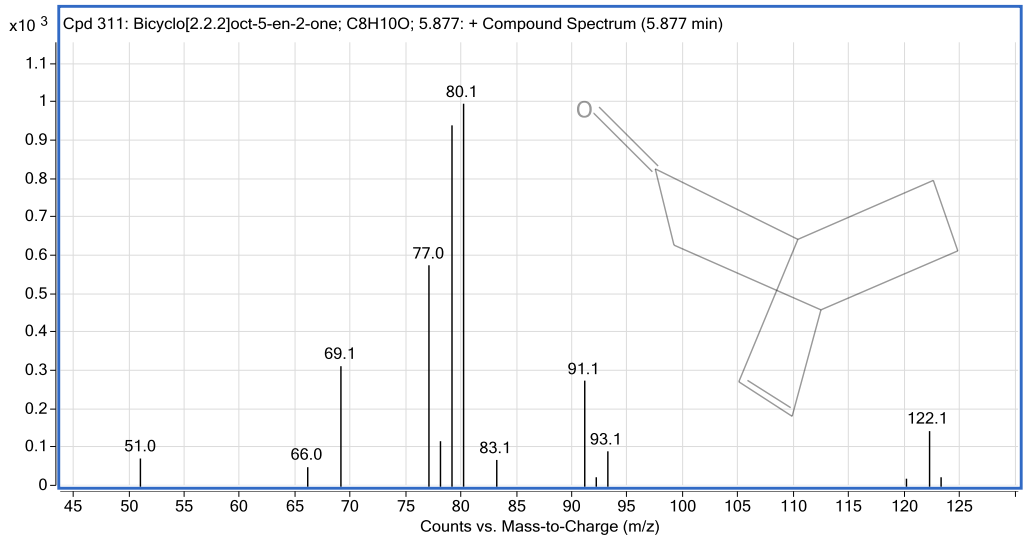
Data base	Protein Number	-10lgP	Coverage (%)	Peptide intensity	#Peptides (#unique)	Mass	
MEAT	P04776	121.2	5	1.26E+04	2(2)	55706	Glycinin G1 OS=Glycine max
	O62654	64.99	6	4.56E+04	3(3)	53532	Desmin OS=Bos taurus
	Q9BE40	58.02	6	1.84E+04	8(8)	222988	Myosin-1 OS=Bos taurus
	B9DIJ2	48.62	12	1.16E+06	2(2)	32991	N-acetylneuraminate lyase OS=Staphylococcus carnosus (strain TM300)
	Q9BE39	47.53	4	1.02E+05	5(5)	223227	Myosin-7 OS=Bos taurus
	Q38YN3	31.78	1	4.69E+05	1(1)	87609	Endonuclease MutS2 OS=Lactobacillus sakei subsp. sakei (strain 23K)
	Q93MM1	29.27	2	9.61E+03	1(1)	56295	Galactose-1-phosphate uridylyltransferase OS=Lactobacillus sakei subsp. sakei (strain 23K)
	B9DPG7	25.44	3	4.23E+03	1(1)	28625	GTP-sensing transcriptional pleiotropic repressor CodY OS=Staphylococcus carnosus (strain TM300)
	B9DPM7	21.43	2	4.47E+03	1(1)	42157	Probable dual-specificity RNA methyltransferase RlmN OS=Staphylococcus carnosus (strain TM300)
	B9DNK1	20.2	3	1.66E+05	1(1)	22998	Protein GrpE OS=Staphylococcus carnosus (strain TM300)
MILK	Q712N8	48.03	15	1.20E+06	3(2)	24865	Beta-casein OS=Capra hircus
	Q95115	43.19	5	1.47E+04	3(3)	90700	Signal transducer and activator of transcription 5A OS=Bos taurus
	Q9TUM6	43.08	16	1.04E+05	5(5)	49368	Perilipin-2 OS=Bos taurus
	A0A452DHW7	37.46	16	7.95E+03	4(3)	29221	Beta-casein OS=Bos taurus
	E1BBG2	30.18	4	1.82E+05	2(2)	92095	MICAL-like protein 1 OS=Bos taurus
	A9XTK4	28.93	3	6.33E+04	2(2)	37659	3-keto-steroid reductase OS=Bos taurus
	Q6VLX2	26.37	13	4.63E+05	1(1)	11256	Prolactin (Fragment) OS=Bos taurus
CEREAL	L7HKY3	36.64	5	1.25E+04	1(1)	17686	30S ribosomal protein S5 OS=Pseudomonas fluorescens BRIP34879
	K3VR96	33.83	2	1.77E+05	2(2)	70251	Phosphoinositide phospholipase C OS=Fusarium pseudograminearum (strain CS3096)
	K3VT46	32	1	2.04E+04	1(1)	73085	Uncharacterized protein OS=Fusarium pseudograminearum (strain CS3096)
	A0A2S4UDD1	29.64	1	1.76E+05	1(1)	119309	Rho-GAP domain-containing protein OS=Puccinia striiformis
	K3VUT6	28.94	1	1.79E+06	1(1)	69353	SWR1-complex protein 4 OS=Fusarium pseudograminearum (strain CS3096)
	K3VSQ8	27.46	2	9.12E+04	2(2)	96053	Uncharacterized protein OS=Fusarium pseudograminearum (strain CS3096)
	K3UH53	27.39	1	3.36E+03	2(1)	273540	JAB_MPN domain-containing protein OS=Fusarium pseudograminearum (strain CS3096)
	K3VGT9	22.49	3	2.12E+05	1(1)	38979	Uncharacterized protein OS=Fusarium pseudograminearum (strain CS3096)
	A0A2S4VUT3	22.23	1	1.13E+04	1(1)	173211	DNA polymerase OS=Puccinia striiformis
	K3W1R7	22.12	2	8.01E+04	1(1)	41045	Zn(2)-C6 fungal-type domain-containing protein OS=Fusarium pseudograminearum (strain CS3096)
	A0A2S4VVE2	21.24	3	7.14E+03	1(1)	35459	DUF2040 domain-containing protein OS=Puccinia striiformis
	A0A2S4VDB9	20.91	1	1.25E+05	1(1)	120686	Uncharacterized protein OS=Puccinia striiformis
	K3VWV1	20.27	2	4.41E+05	1(1)	53923	Uncharacterized protein OS=Fusarium pseudograminearum (strain CS3096)
YEAST	A0A1B2JIM9	31.68	1	5.17E+04	2(1)	117861	BA75_04357T0 OS=Komagataella pastoris
	A0A1B2JAW5	31.51	3	5.19E+03	3(2)	123408	BA75_02279T0 OS=Komagataella pastoris
	A0A1B2J655	30.91	1	2.04E+04	1(1)	69695	BA75_00387T0 OS=Komagataella pastoris
	A0A1B2JAA3	25.67	3	1.13E+04	1(1)	70877	BA75_03049T0 OS=Komagataella pastoris
	I6LAC7	25.41	1	1.76E+05	1(1)	58317	Snx41 OS=Komagataella pastoris

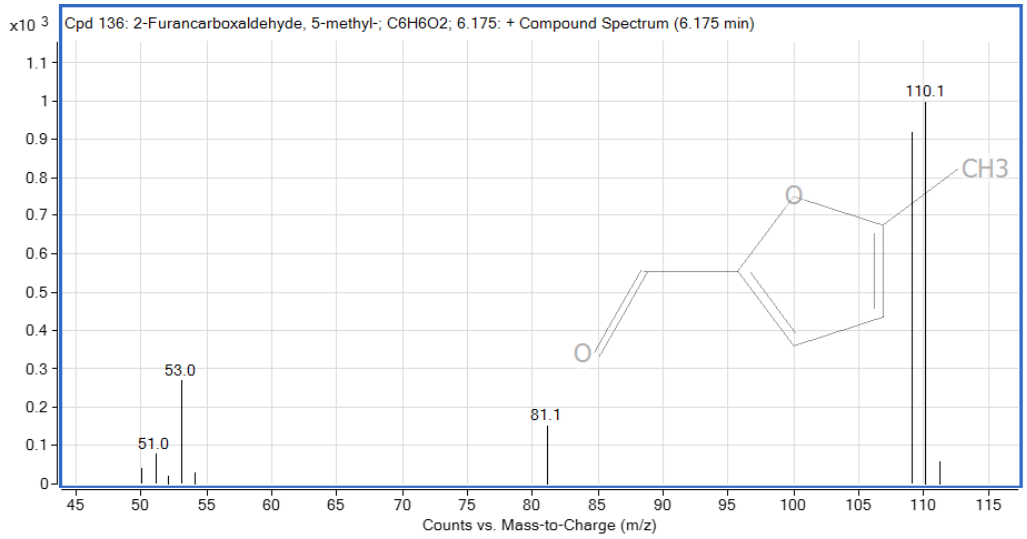
Data base	Protein Number	-10lgP	Coverage (%)	Peptide intensity	#Peptides (#unique)	Mass	
	A0A1B2JA71	22.62	0	1.66E+05	1(1)	155560	BA75_02507T0 OS=Komagataella pastoris
	A0A1B2J6V1	21.3	4	3.98E+03	1(1)	32899	BA75_01346T0 OS=Komagataella pastoris
	A0A1B2JE13	21.3	2	1.79E+06	1(1)	44557	BA75_04021T0 OS=Komagataella pastoris
	A0A1B2JCZ3	20.75	3	8.53E+03	1(1)	40959	tRNA-dihydrouridine synthase OS=Komagataella pastoris
	A0A1B2JH05	20.36	3	4.56E+04	1(1)	40789	Protein phosphatase OS=Komagataella pastoris

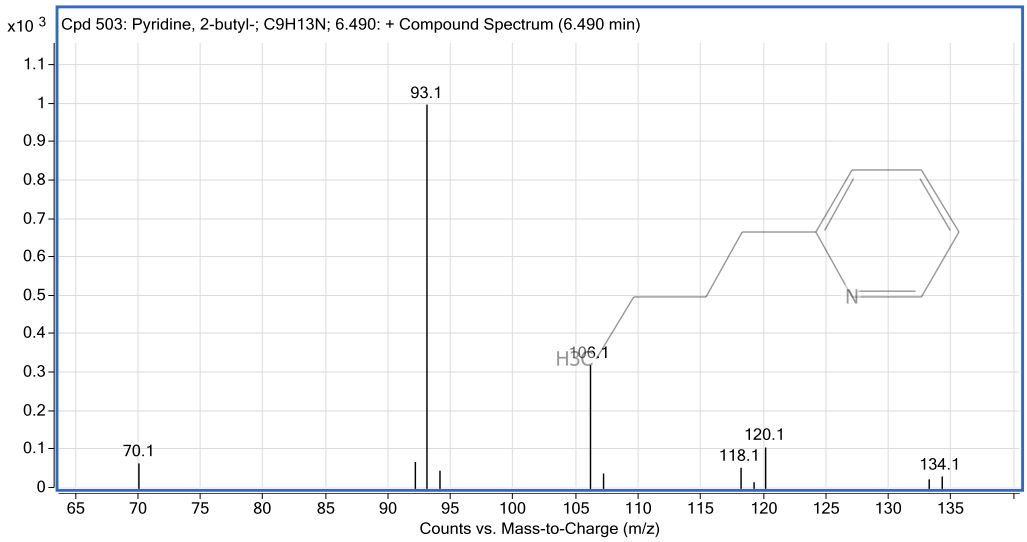
S6 exterior

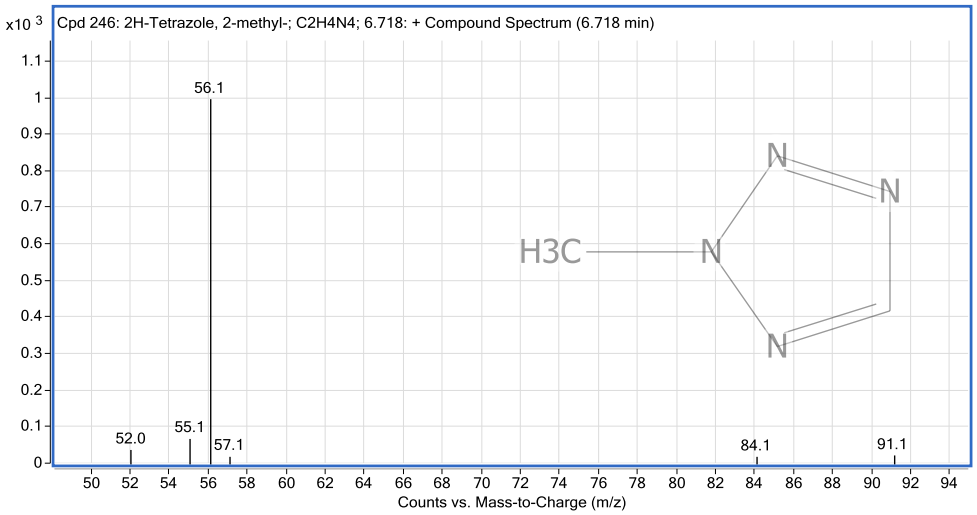
Data base	Protein Number	-10lgP	Coverage (%)	Peptide intensity	#Peptides (#unique)	PTM Score	Mass	
MEAT	Q38YA4	50.3	2	9.46E+05	3(2)		76402	UvrABC system protein B OS=Lactobacillus sakei subsp. sakei (strain 23K)
	Q38X70	43.77	2	2.53E+04	3(2)	(NQ)	136081	ATP-dependent helicase/deoxyribonuclease subunit B OS=Lactobacillus sakei subsp. sakei (strain 23K)
	B9DK35	39.82	7	1.09E+03	2(1)	(NQ)	26235	Iron-sulfur cluster repair protein ScdA OS=Staphylococcus carnosus (strain TM300)
	Q38YR4	39.38	2	1.20E+04	2(2)	(NQ)	96749	DNA mismatch repair protein MutS OS=Lactobacillus sakei subsp. sakei (strain 23K)
	B9DKV0	32.33	3	4.00E+03	2(2)	(NQ)	133212	DNA-directed RNA polymerase subunit beta OS=Staphylococcus carnosus (strain TM300)
	Q38ZS1	21.69	2	6.51E+03	1(1)		43246	DNA replication and repair protein RecF OS=Lactobacillus sakei subsp. sakei (strain 23K)
MILK	Q95115	45.57	5	6.57E+03	4(4)	(NQ)	90700	Signal transducer and activator of transcription 5A OS=Bos taurus
	Q865B7	42.11	4	4.57E+04	3(3)	(NQ)	90309	Peroxisome proliferator-activated receptor gamma coactivator 1-alpha OS=Bos taurus
	P80457	40.62	1	2.25E+03	2(2)	(NQ)	146790	Xanthine dehydrogenase/oxidase OS=Bos taurus
	Q8HYJ9	32.59	4	2.51E+04	2(2)		60093	Dimethylaniline monooxygenase [N-oxide-forming] 3 OS=Bos taurus
	Q6VLX2	30.67	13	1.96E+05	1(1)		11256	Prolactin (Fragment) OS=Bos taurus
CEREAL	K3W1C1	61.3	3	1.73E+03	1(1)		41608	Uncharacterized protein OS=Fusarium pseudograminearum (strain CS3096)
	M4GR03	61.3	3	1.73E+03	1(1)		39219	Actin 2 OS=Heterodera avenae
	K3W2K5	32.81	1	1.00E+04	1(1)		57488	Uncharacterized protein OS=Fusarium pseudograminearum (strain CS3096)
	K3W2Z8	32.81	1	1.00E+04	1(1)		99546	Uncharacterized protein OS=Fusarium pseudograminearum (strain CS3096)
	A0A2S4W2Z5	28.32	1	6.88E+04	1(1)	(NQ)	180991	Uncharacterized protein (Fragment) OS=Puccinia striiformis
	K3VCD2	24.82	3	1.32E+04	1(1)		21961	S4 RNA-binding domain-containing protein OS=Fusarium pseudograminearum (strain CS3096)
	K3VPM9	24.82	1	1.32E+04	1(1)		76186	Fungal_trans domain-containing protein OS=Fusarium pseudograminearum (strain CS3096)
	K3VZS3	24.82	1	1.32E+04	1(1)		100882	Uncharacterized protein OS=Fusarium pseudograminearum (strain CS3096)
	A0A2S4WDT7	24.5	1	9.00E+03	1(1)		246130	DNA polymerase epsilon catalytic subunit OS=Puccinia striiformis
	K3V807	24.26	1	1.27E+03	1(1)	(NQ)	138546	Uncharacterized protein OS=Fusarium pseudograminearum (strain CS3096)
	A0A6A6UW72	22.31	3	4.70E+03	1(1)		48113	Cellulase OS=Sporormia fimetaria CBS 119925
	K3VR96	21.57	1	4.25E+04	1(1)		70251	Phosphoinositide phospholipase C OS=Fusarium pseudograminearum (strain CS3096)
	K3V776	21.02	1	8.68E+03	1(1)	(NQ)	64293	Uncharacterized protein OS=Fusarium pseudograminearum (strain CS3096)
YEAST	A0A1B2JEH8	41.43	2	7.73E+03	2(2)	(NQ)	69361	BA75_02906T0 OS=Komagataella pastoris
	A0A1B2J5M9	33.31	1	5.08E+03	2(2)		59865	Amidophosphoribosyltransferase OS=Komagataella pastoris
	A0A1B2JAT9	31.44	3	6.42E+04	1(1)		28310	BA75_02178T0 OS=Komagataella pastoris
	I6LAC7	25.83	1	8.68E+03	1(1)		58317	Snx41 OS=Komagataella pastoris
	A0A1B2JFT3	25.83	1	8.68E+03	1(1)		58294	BA75_03354T0 OS=Komagataella pastoris
	A0A1B2J9K8	24.34	1	1.27E+03	1(1)		129051	BA75_01193T0 OS=Komagataella pastoris
	A0A1B2JG11	23.64	6	3.44E+03	1(1)		17185	BA75_03821T0 OS=Komagataella pastoris
	A0A1B2JAS9	23.64	7	3.44E+03	1(1)		14568	Ubiquitin OS=Komagataella pastoris
	A0A1B2JIZ2	23.64	3	3.44E+03	1(1)		34399	BA75_04552T0 OS=Komagataella pastoris
	A0A1B2JI74	21.62	1	6.18E+03	1(1)		65857	Kinesin-like protein OS=Komagataella pastoris
	A0A1B2JFQ0	21.62	1	6.18E+03	1(1)		69500	BA75_03685T0 OS=Komagataella pastoris

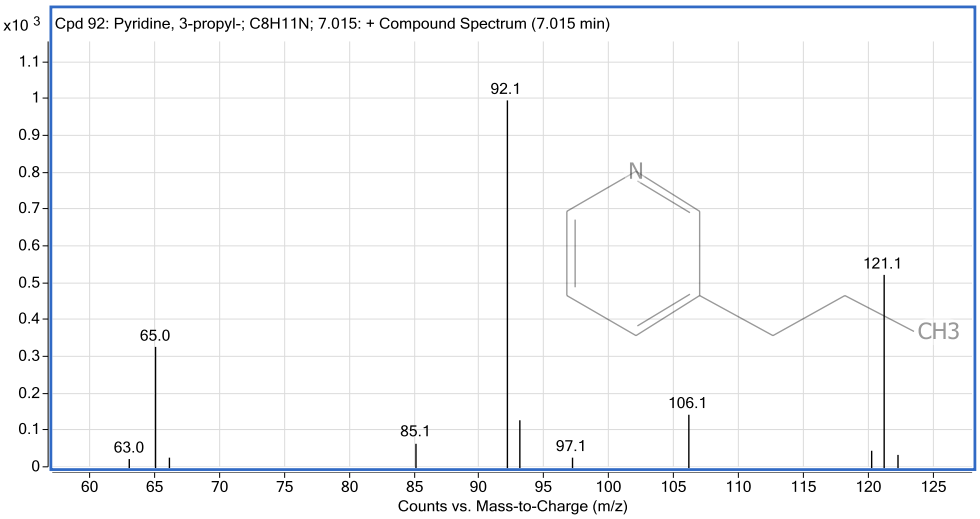
Data base	Protein Number	-10lgP	Coverage (%)	Peptide intensity	#Peptides (#unique)	PTM Score	Mass	
	A0A1B2JEZ0	21.62	1	6.18E+03	1(1)		88149	BA75_03752T0 OS=Komagataella pastoris
	A0A1B2JDA8	21.57	3	7.04E+03	1(1)	(NQ)	42316	BA75_02700T0 OS=Komagataella pastoris
	A0A1B2JF59	21.4	1	1.16E+04	1(1)		181333	BA75_03888T0 OS=Komagataella pastoris
	A0A1B2JE12	21.08	1	1.00E+04	1(1)		125817	BA75_03733T0 OS=Komagataella pastoris
	A0A1B2JA53	21.08	1	1.00E+04	1(1)		45418	BA75_01650T0 OS=Komagataella pastoris
	A0A1B2JAB9	21.08	1	1.00E+04	1(1)		110268	Chitin synthase OS=Komagataella pastoris
	A0A1B2JIM9	21.08	1	1.00E+04	1(1)		117861	BA75_04357T0 OS=Komagataella pastoris
	A0A1B2JHF5	21.08	1	1.00E+04	1(1)		118203	BA75_04425T0 OS=Komagataella pastoris
	A0A1B2JF65	21.08	0	1.00E+04	1(1)		149120	BA75_03781T0 OS=Komagataella pastoris

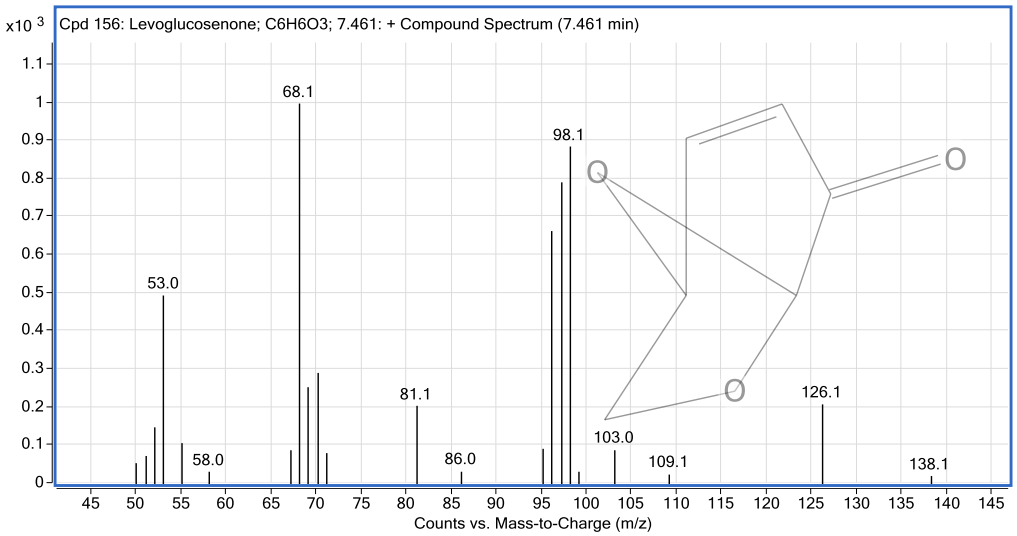

Cpd 311: Bicyclo[2.2.2]oct-5-en-2-one; C8H10O; 5.877: + Compound Spectrum (5.877 min)
x10 3
80.1
77.0
69.1
91.1
122.1
51.0
66.0
83.1
93.1
O
Counts vs. Mass-to-Charge (m/z)

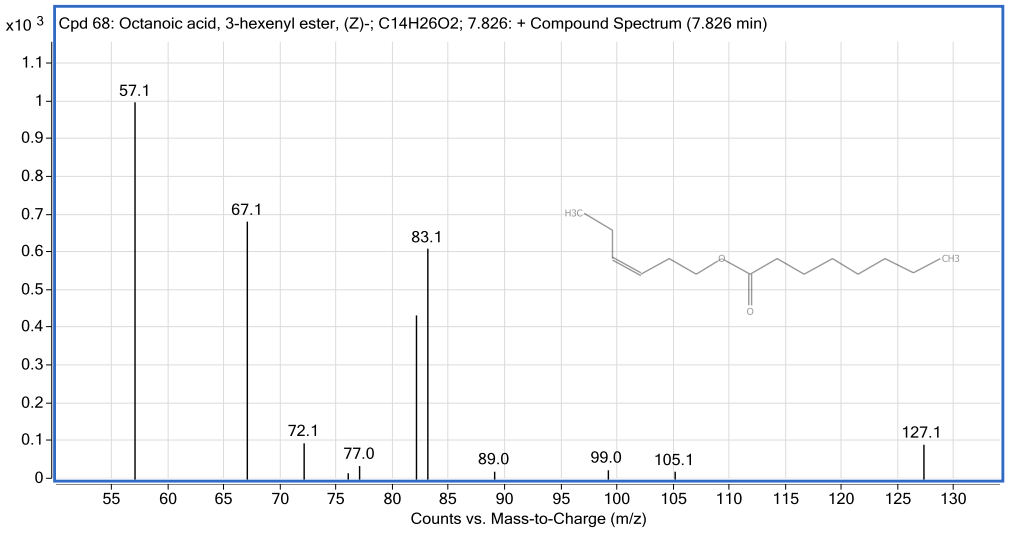

Cpd 136: 2-Furancarboxaldehyde, 5-methyl-; C6H6O2; 6.175: + Compound Spectrum (6.175 min)
x10 3
110.1
CH3
O
O
53.0
81.1
51.0
Counts vs. Mass-to-Charge (m/z)

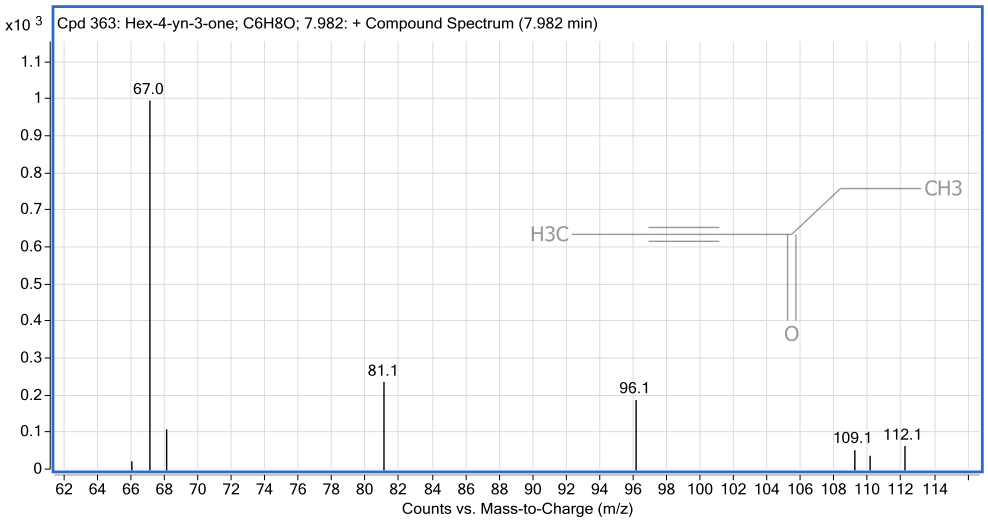

Cpd 503: Pyridine, 2-butyl-; C9H13N; 6.490: + Compound Spectrum (6.490 min)
x10 3
93.1
106.1
H3C
N
70.1
120.1
118.1
134.1
Counts vs. Mass-to-Charge (m/z)

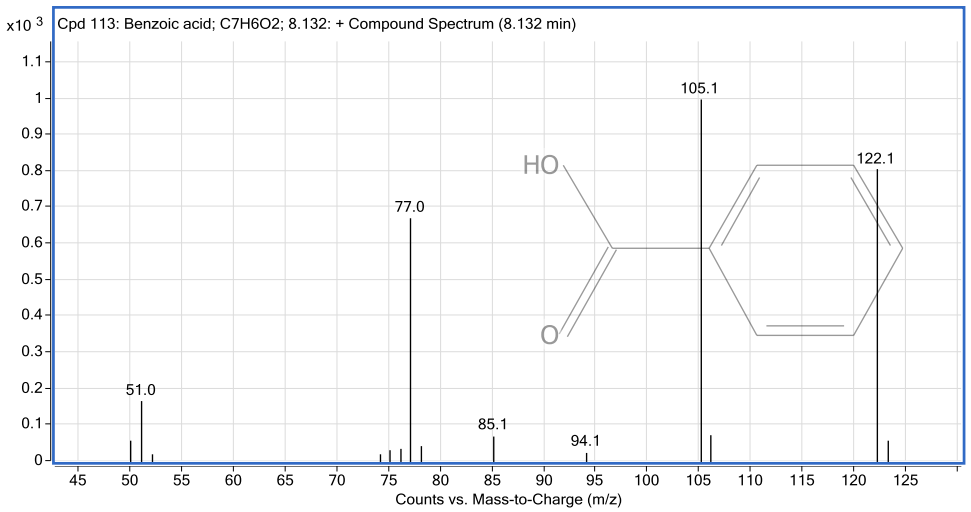

Cpd 246: 2H-Tetrazole, 2-methyl-; C2H4N4; 6.718: + Compound Spectrum (6.718 min)
x10 3
56.1
52.0
55.1
57.1
84.1
91.1
H3C
N
Counts vs. Mass-to-Charge (m/z)

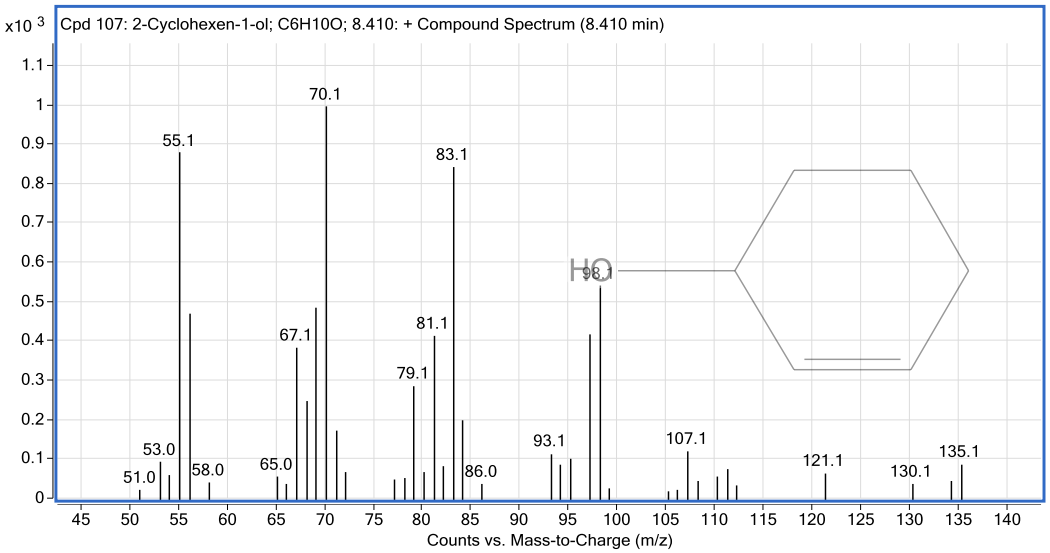

Cpd 92: Pyridine, 3-propyl-; C8H11N; 7.015: + Compound Spectrum (7.015 min)
x10 3
92.1
65.0
63.0
85.1
97.1
106.1
121.1
CH3
N
Counts vs. Mass-to-Charge (m/z)

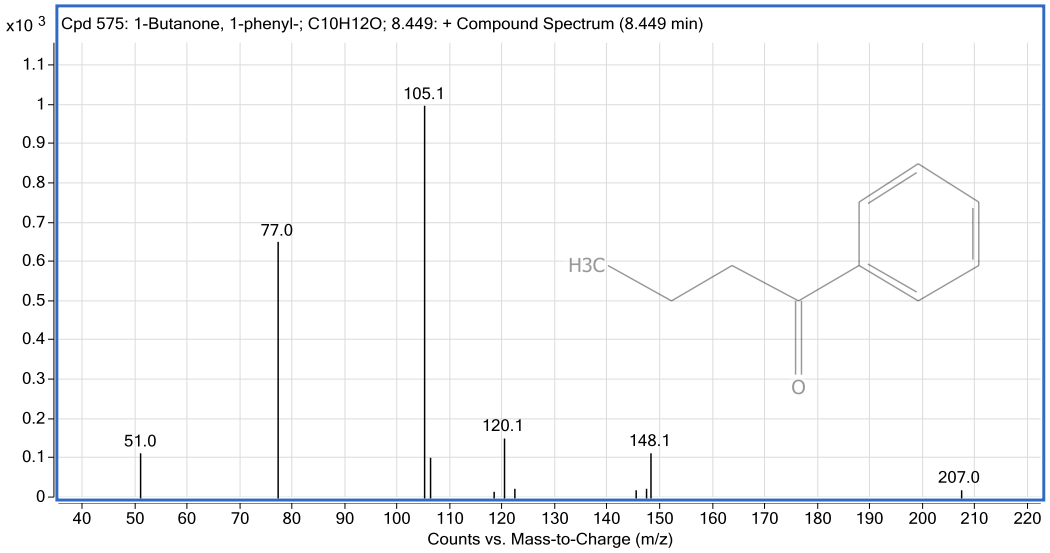

Cpd 156: Levoglucosenone; C6H6O3; 7.461: + Compound Spectrum (7.461 min)
x10 3
68.1
98.1
53.0
58.0
81.1
86.0
103.0
109.1
126.1
138.1
O
Counts vs. Mass-to-Charge (m/z)

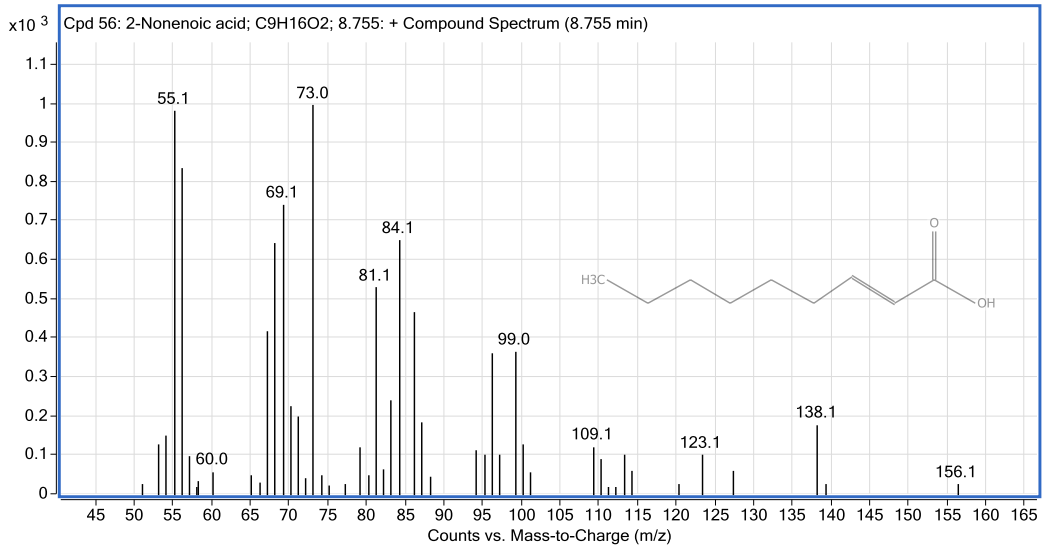

x10 3
Cpd 68: Octanoic acid, 3-hexenyl ester, (Z)-; C14H26O2; 7.826: + Compound Spectrum (7.826 min)
57.1
67.1
83.1
72.1
77.0
89.0
99.0
105.1
127.1
H3C
O
O
CH3
Counts vs. Mass-to-Charge (m/z)

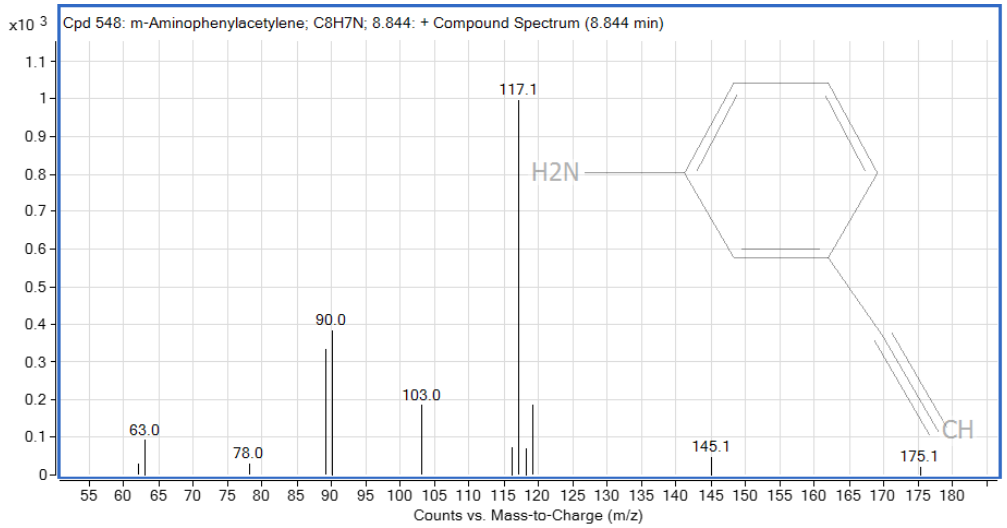

x10 3
Cpd 363: Hex-4-yn-3-one; C6H8O; 7.982: + Compound Spectrum (7.982 min)
67.0
81.1
96.1
109.1
112.1
H3C
CH3
O
Counts vs. Mass-to-Charge (m/z)

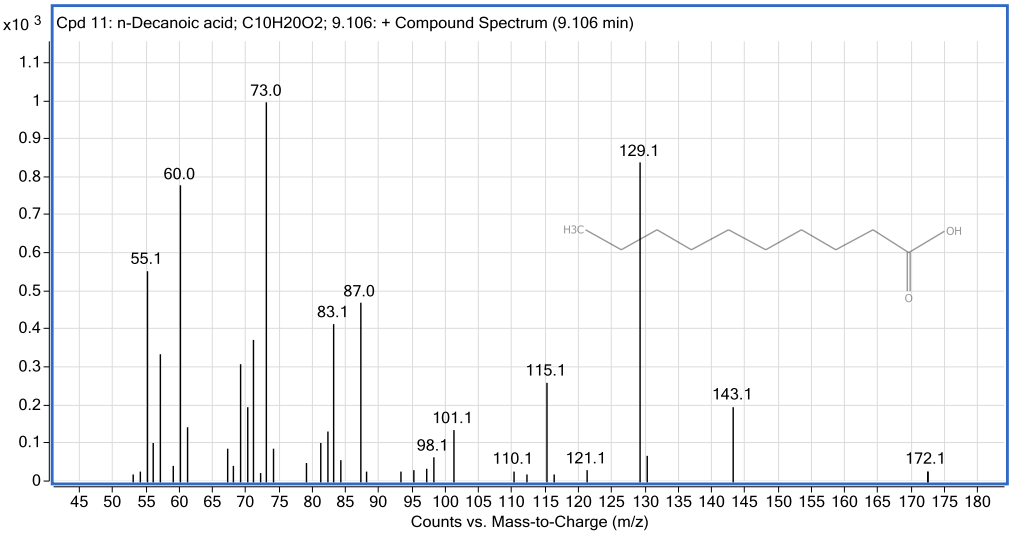

x10 3
Cpd 113: Benzoic acid; C7H6O2; 8.132: + Compound Spectrum (8.132 min)
105.1
122.1
77.0
51.0
85.1
94.1
HO
O
Counts vs. Mass-to-Charge (m/z)

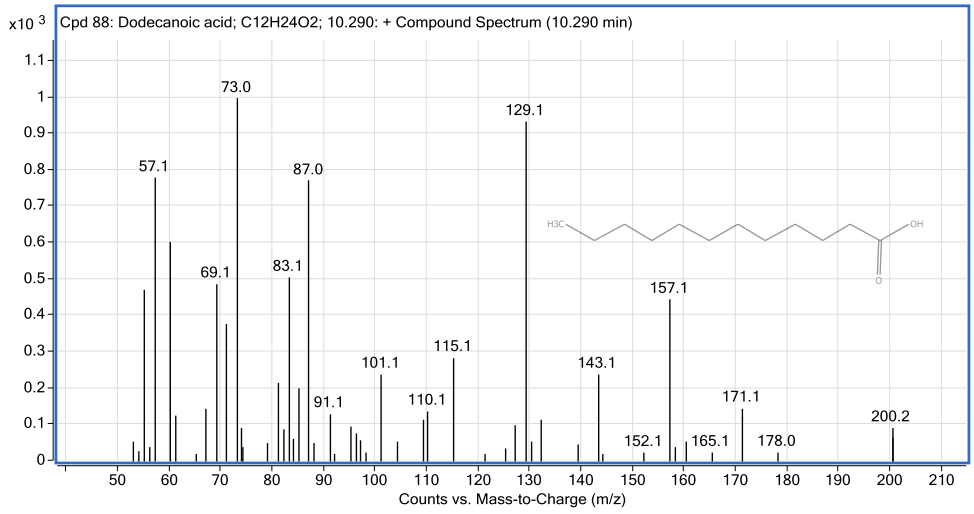

Cpd 107: 2-Cyclohexen-1-ol; C6H10O; 8.410: + Compound Spectrum (8.410 min)
x10 3
70.1
55.1
83.1
98.1
67.1
81.1
79.1
53.0
51.0
58.0
65.0
86.0
93.1
107.1
121.1
130.1
135.1
HO
Counts vs. Mass-to-Charge (m/z)

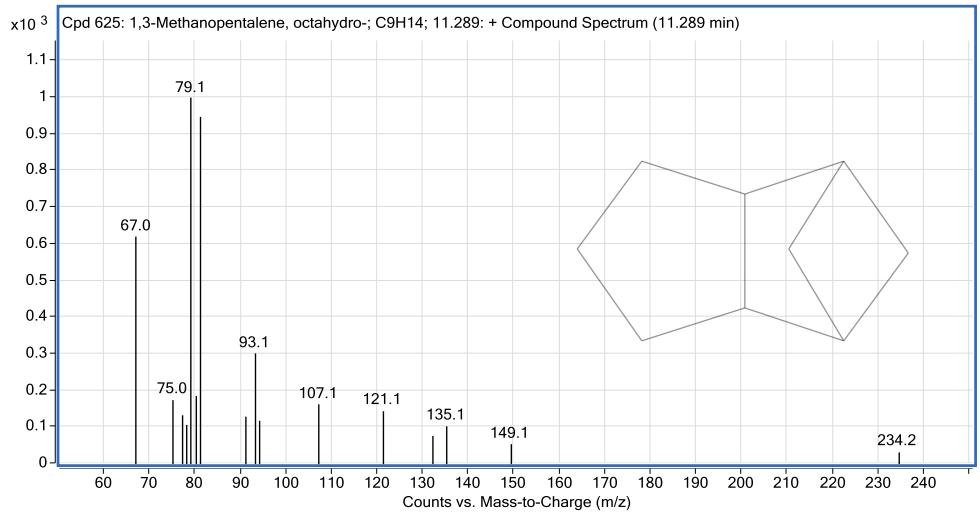

Cpd 575: 1-Butanone, 1-phenyl-; C10H12O; 8.449: + Compound Spectrum (8.449 min)
x10 3
105.1
77.0
51.0
120.1
148.1
207.0
H3C
O
Counts vs. Mass-to-Charge (m/z)

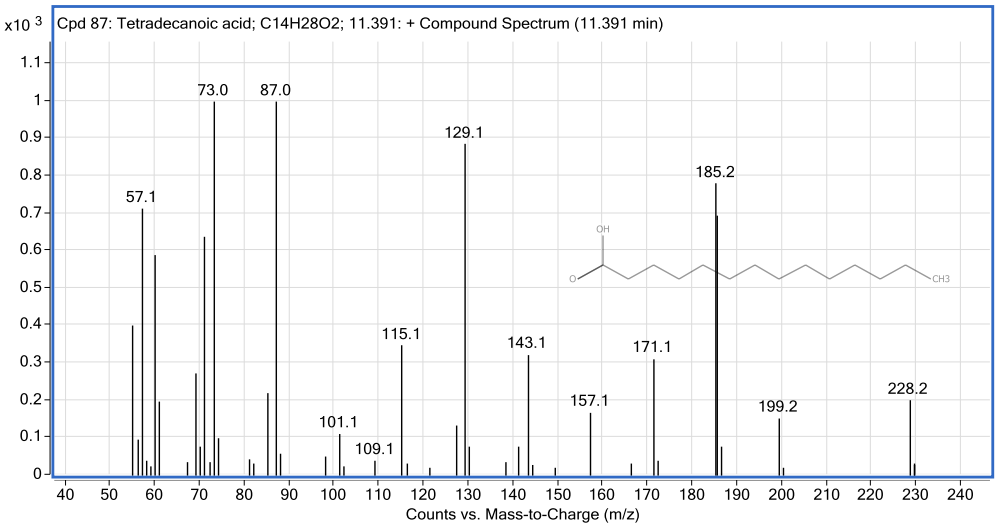

Cpd 56: 2-Nonenoic acid; C9H16O2; 8.755: + Compound Spectrum (8.755 min)
x10 3
55.1
73.0
69.1
84.1
81.1
99.0
60.0
109.1
123.1
138.1
156.1
H3C
O
OH
Counts vs. Mass-to-Charge (m/z)

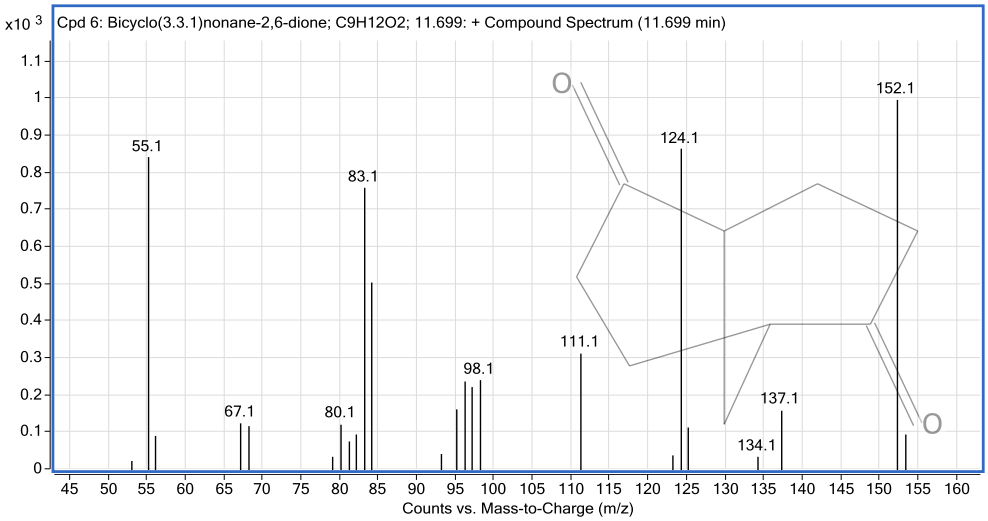

Cpd 548: m-Aminophenylacetylene; C8H7N; 8.844: + Compound Spectrum (8.844 min)
x10 3
117.1
90.0
103.0
63.0
78.0
145.1
175.1
H2N
CH
Counts vs. Mass-to-Charge (m/z)

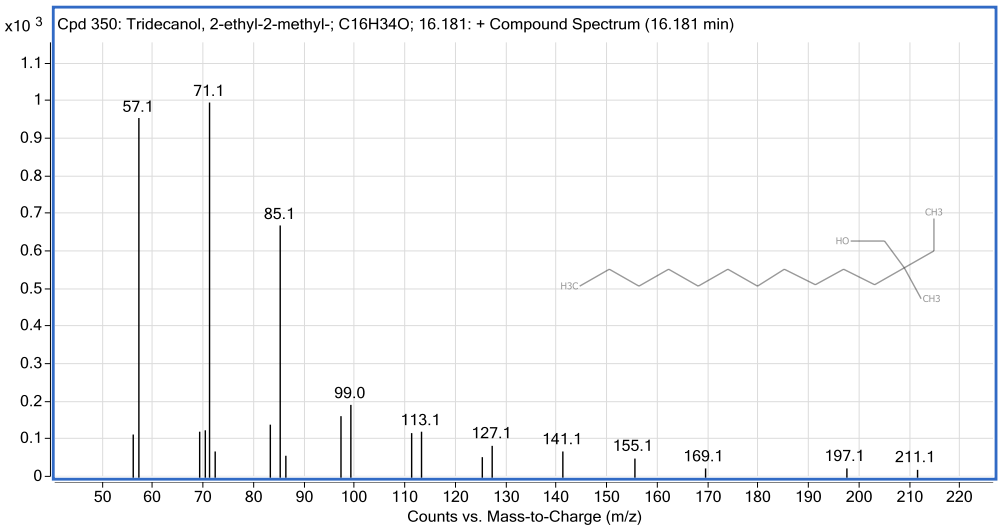

Cpd 11: n-Decanoic acid; C10H20O2; 9.106: + Compound Spectrum (9.106 min)
x10 3
73.0
129.1
60.0
55.1
87.0
83.1
115.1
143.1
101.1
98.1
110.1
121.1
172.1
H3C
OH
O
Counts vs. Mass-to-Charge (m/z)


Cpd 88: Dodecanoic acid; C12H24O2; 10.290: + Compound Spectrum (10.290 min)
x10 3
73.0
129.1
57.1
87.0
69.1
83.1
157.1
115.1
101.1
143.1
91.1
110.1
171.1
200.2
152.1
165.1
178.0
H3C
OH
O
Counts vs. Mass-to-Charge (m/z)

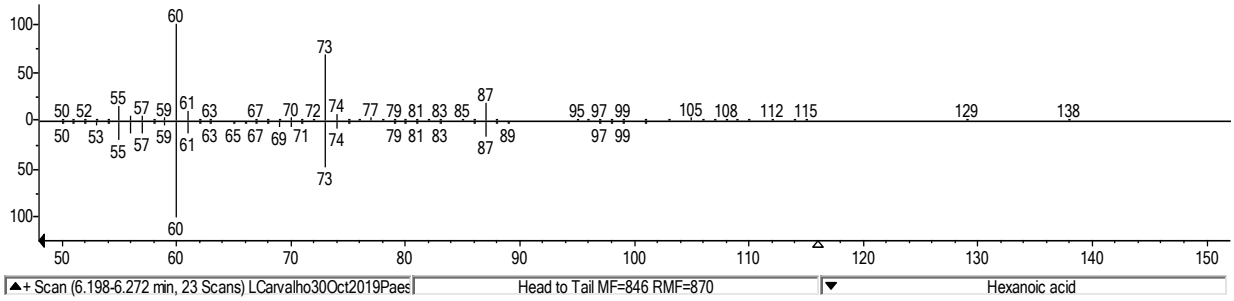

x10 3
Cpd 625: 1,3-Methanopentalene, octahydro-; C9H14; 11.289: + Compound Spectrum (11.289 min)
79.1
67.0
93.1
75.0
107.1
121.1
135.1
149.1
234.2
Counts vs. Mass-to-Charge (m/z)

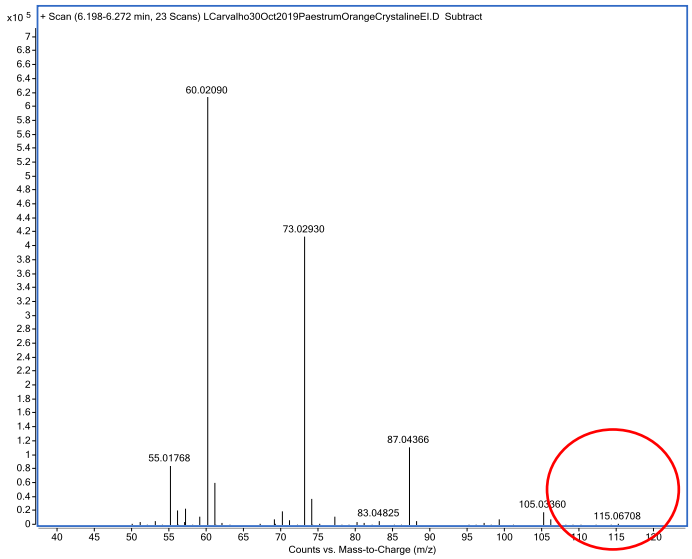

x10 3
Cpd 87: Tetradecanoic acid; C14H28O2; 11.391: + Compound Spectrum (11.391 min)
73.0
87.0
129.1
185.2
57.1
115.1
143.1
171.1
157.1
199.2
228.2
101.1
109.1
OH
O
CH3
Counts vs. Mass-to-Charge (m/z)

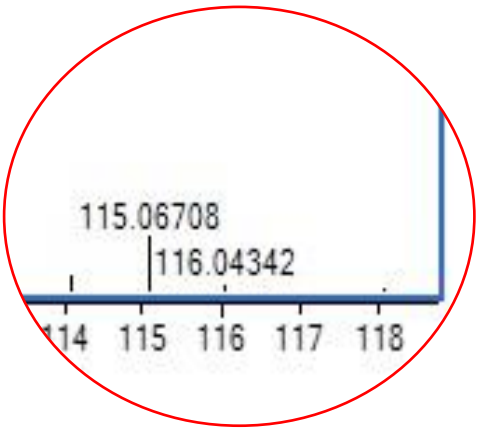

x10 3
Cpd 6: Bicyclo(3.3.1)nonane-2,6-dione; C9H12O2; 11.699: + Compound Spectrum (11.699 min)
O
152.1
124.1
55.1
83.1
111.1
98.1
137.1
67.1
80.1
134.1
O
Counts vs. Mass-to-Charge (m/z)


x10 3
Cpd 350: Tridecanol, 2-ethyl-2-methyl-; C16H34O; 16.181: + Compound Spectrum (16.181 min)
1.1
1
0.9
0.8
0.7
0.6
0.5
0.4
0.3
0.2
0.1
0
57.1
71.1
85.1
99.0
113.1
127.1
141.1
155.1
169.1
197.1
211.1
50 60 70 80 90 100 110 120 130 140 150 160 170 180 190 200 210 220
Counts vs. Mass-to-Charge (m/z)
CH3
HO
H3C
CH3

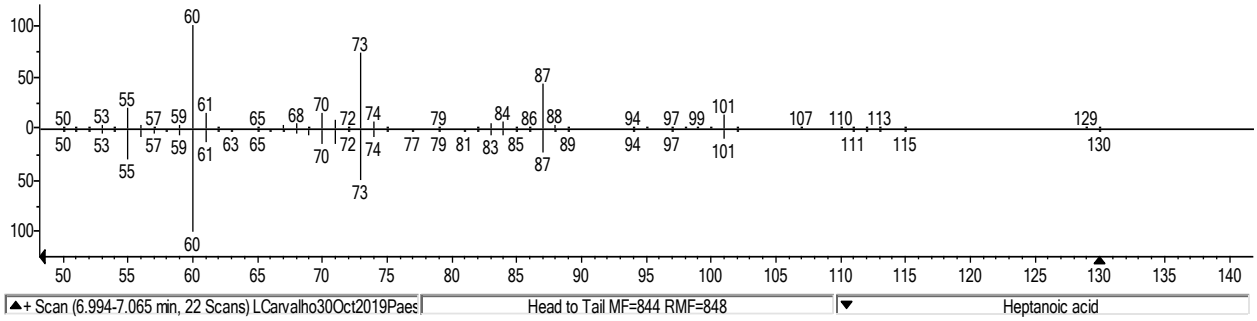
Hexanoic acid

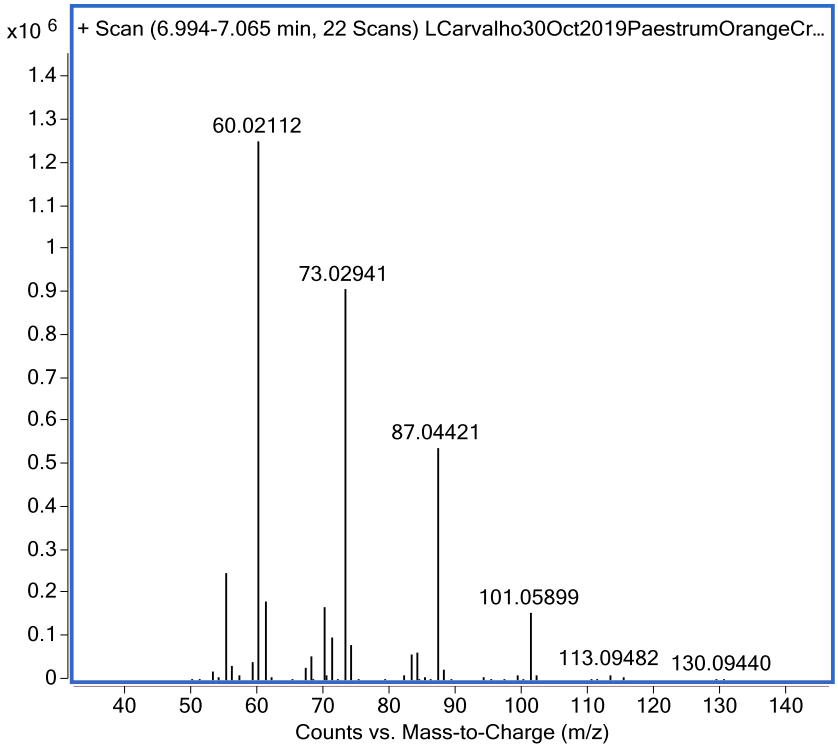




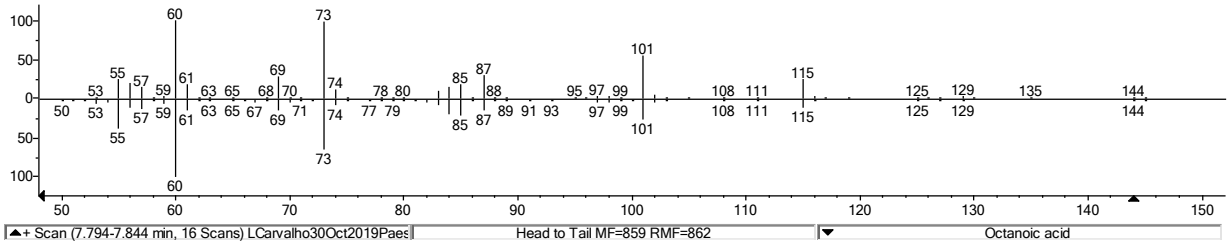


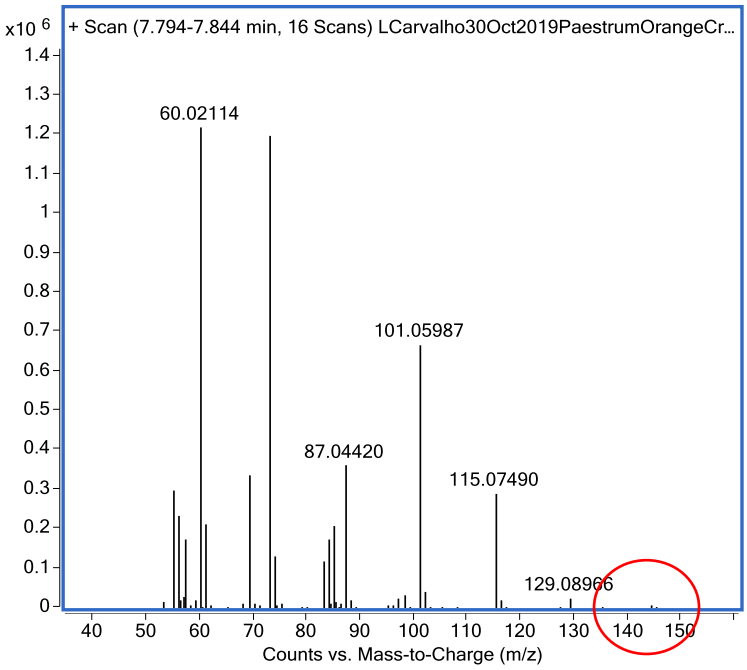
Heptanoic acid

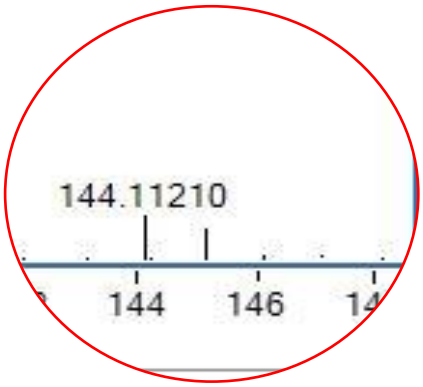




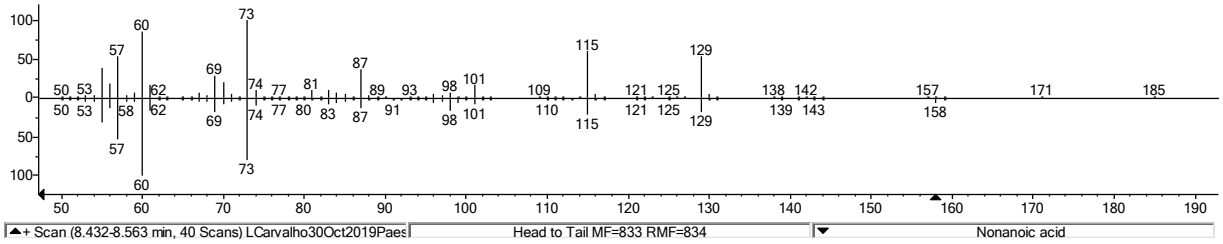
Octanoic acid

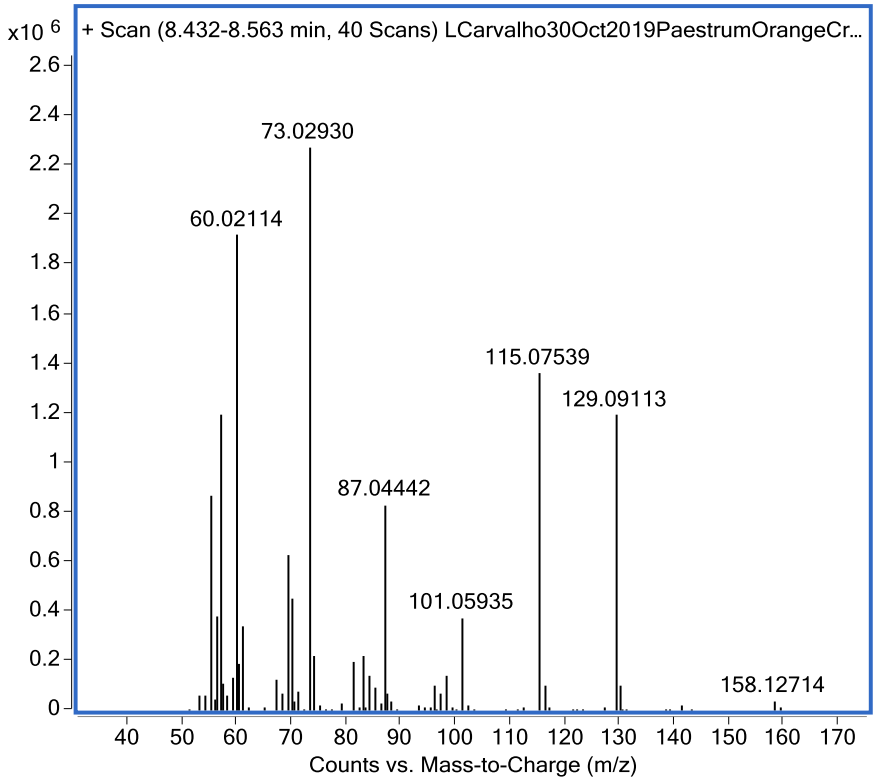




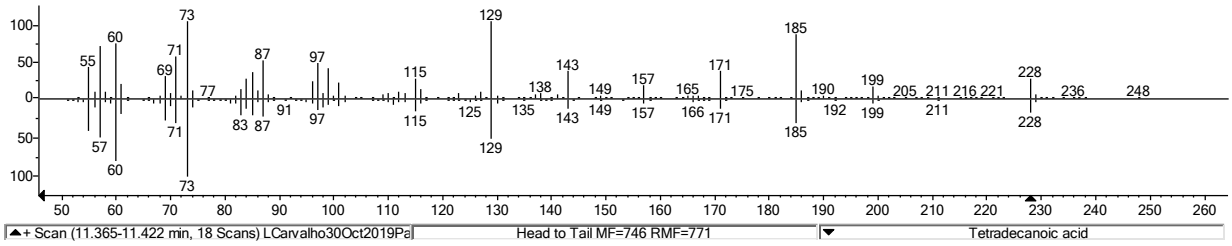


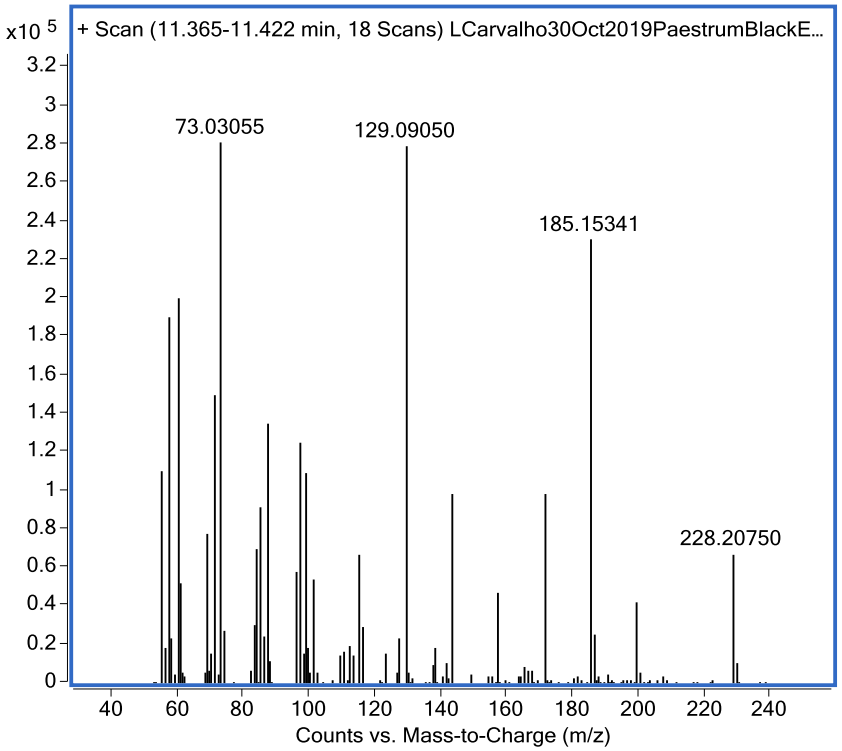
Nonanoic acid



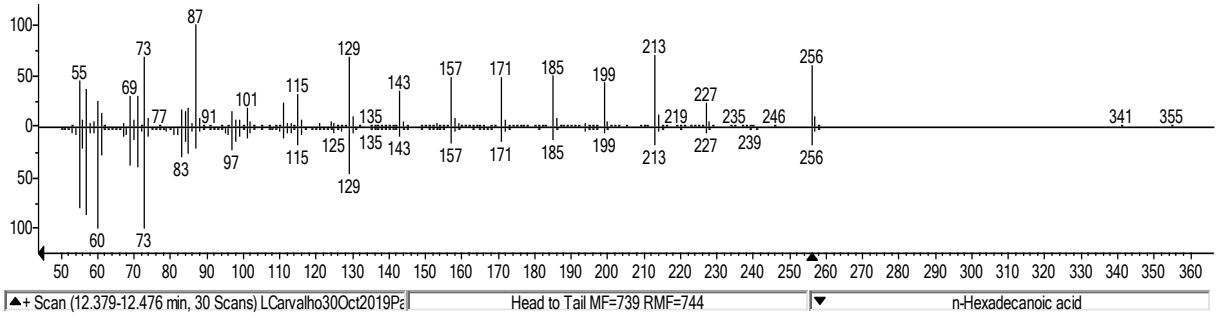


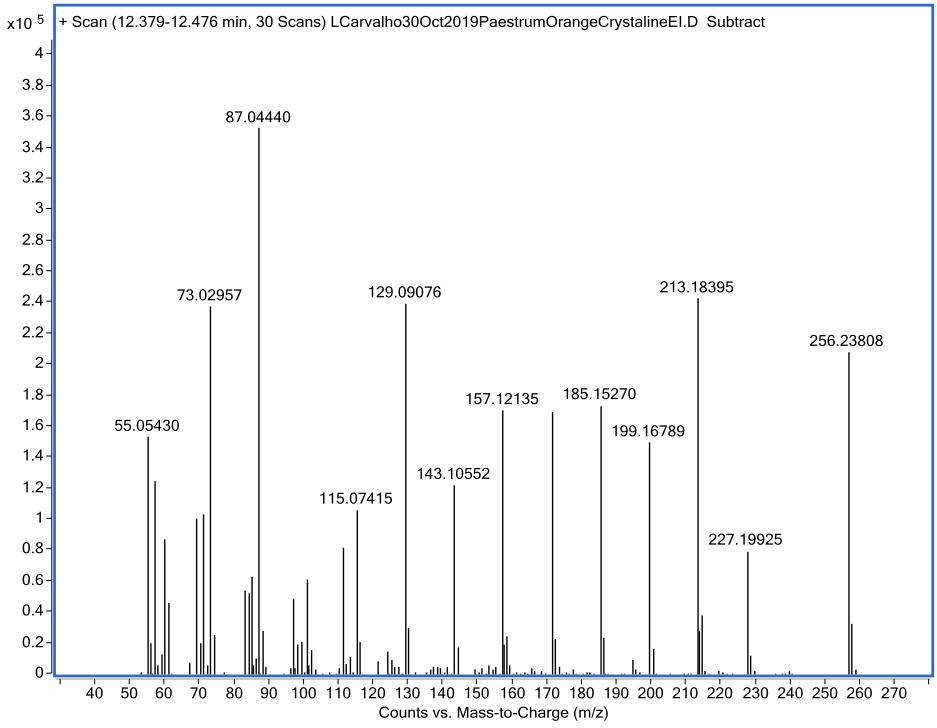
Tetradecanoic acid





n-Hexadecanoic acid





IC-MS Honey x Beeswax

M-H adduct m/z	RT (min)	Peak width (min)	IDs	Max Fold Change	Highest Mean	Lowest Mean	Isotope Distribution	Maximum Abundance	HONEY	BEESWAX	Accepted Compound ID	Accepted Description	Formula	Score	Mass Error (ppm)	Isotope Similarity(%)	RT error (mins)
124.0072	4.46	1.0323	1	7.9010	HONEY	BEESWAX	100	104.5535	104.55	13.23	HMDB0000251	Taurine	C2H7NO3S	38.5	-1.3731	91.8689	-1.07
117.0190	10.50	36.9468	1	1.0043	BEESWAX	HONEY	100	25101.0738	24992.51	25101.07	HMDB0000254	Succinic acid	C4H6O4	39.1	-3.2256	94.8320	-0.98
163.0400	29.37	0.5682	2	Infinity	BEESWAX	HONEY	100	59.4145	0.00	59.41	HMDB0002035	p-Coumaric acid	C9H8O3	45.2	-0.4730	90.0914	0.21
179.0559	2.89	1.9571	9	122.8732	HONEY	BEESWAX	100 - 4.54 - 0.566	4924.3835	4924.38	40.08	HMDB0000660	Fructose	C6H12O6	39.6	-1.3533	97.0578	-0.54
143.0348	11.27	3.8835	1	1.1482	HONEY	BEESWAX	100	359.3998	359.40	313.01	HMDB0031257	Dimethyl fumarate	C6H8O4	38.8	-1.3433	92.8097	-1.89
191.0196	16.13	0.8815	2	1.5234	HONEY	BEESWAX	100 - 2.31	957.9213	957.92	628.80	HMDB0000094	Citric acid	C6H8O7	39.9	-0.5134	94.2153	-1.15
165.0405	4.34	1.8345	1	1.2627	BEESWAX	HONEY	100	530.6257	420.25	530.63	HMDB0000539	Arabinonic acid	C5H10O6	39.3	0.3587	93.3528	-0.56
159.0661	10.82	36.9468	1	1.0352	BEESWAX	HONEY	100	6036.2288	5831.16	6036.23	HMDB0002441	3,3-Dimethylglutaric ac	C7H12O4	39.7	-1.2500	91.7840	0.47

Honey x Paestum

M-H adduct m/z	RT (min)	Peak width (min)	IDs	Max Fold Change	Highest Mean	Lowest Mean	Isotope Distribution	Maximum Abundance	HONEY	PAESTRUM	Accepted Compound ID	Accepted Description	Formula	Score	Mass Error (ppm)	Isotope Similarity(%)	RT error (mins)
163.0400	29.37	0.5682	2	Infinity	PAESTUM	HONEY	100	26.9119	0.00	26.91	HMDB0002035	p-Coumaric acid	C9H8O3	45.2	-0.4730	90.0914	0.21
124.0072	4.46	1.0323	1	14.2143	PAESTUM	HONEY	100	1486.1581	104.55	1486.16	HMDB0000251	Taurine	C2H7NO3S	38.5	-1.3731	91.8689	-1.07
179.0559	2.89	1.9571	9	11.5530	HONEY	PAESTUM	100 - 4.54 - 0.566	4924.3835	4924.38	426.24	HMDB0000660	Fructose	C6H12O6	39.6	-1.3533	97.0578	-0.54
191.0196	16.13	0.8815	2	1.3481	PAESTUM	HONEY	100 - 2.31	1291.3855	957.92	1291.39	HMDB0000094	Citric acid	C6H8O7	39.9	-0.5134	94.2153	-1.15
143.0348	11.27	3.8835	1	1.2304	HONEY	PAESTUM	100	359.3998	359.40	292.11	HMDB0031257	Dimethyl fumarate	C6H8O4	38.8	-1.3433	92.8097	-1.89
165.0405	4.34	1.8345	1	1.2267	PAESTUM	HONEY	100	515.5126	420.25	515.51	HMDB0000539	Arabinonic acid	C5H10O6	39.3	0.3587	93.3528	-0.56
159.0661	10.82	36.9468	1	1.1204	PAESTUM	HONEY	100	6533.1648	5831.16	6533.16	HMDB0002441	3,3-Dimethylglutaric acid	C7H12O4	39.7	-1.2500	91.7840	0.47
117.0190	10.50	36.9468	1	1.0232	HONEY	PAESTUM	100	24992.5106	24992.51	24425.91	HMDB0000254	Succinic acid	C4H6O4	39.1	-3.2256	94.8320	-0.98

Paestum x Beeswax

M-H adduct m/z	RT (min)	Peak width (min)	IDs	Max Fold Change	Highest Mean	Lowest Mean	Isotope Distribution	Maximum Abundance	BEESWAX	PAESTRUM	Accepted Compound ID	Accepted Description	Formula	Score	Mass Error (ppm)	Isotope Similarity(%)	RT error (mins)
163.0400	29.37	0.5682	2	2.2077	BEESWAX	PAESTUM	100	59.4145	26.91	59.41	HMDB0002035	p-Coumaric acid	C9H8O3	45.2	-0.4730	90.0914	0.21
191.0196	16.13	0.8815	2	2.0537	PAESTUM	BEESWAX	100 - 2.31	1291.3855	1291.39	628.80	HMDB0000094	Citric acid	C6H8O7	39.9	-0.5134	94.2153	-1.15
143.0348	11.27	3.8835	1	1.0715	BEESWAX	PAESTUM	100	313.0071	292.11	313.01	HMDB0031257	Dimethyl fumarate	C6H8O4	38.8	-1.3433	92.8097	-1.89
124.0072	4.46	1.0323	1	112.3076	PAESTUM	BEESWAX	100	1486.1581	1486.16	13.23	HMDB0000251	Taurine	C2H7NO3S	38.5	-1.3731	91.8689	-1.07
165.0405	4.34	1.8345	1	1.0293	BEESWAX	PAESTUM	100	530.6257	515.51	530.63	HMDB0000539	Arabinonic acid	C5H10O6	39.3	0.3587	93.3528	-0.56
159.0661	10.82	36.9468	1	1.0823	PAESTUM	BEESWAX	100	6533.1648	6533.16	6036.23	HMDB0002441	3,3-Dimethylglutaric acid	C7H12O4	39.7	-1.2500	91.7840	0.47
117.0190	10.50	36.9468	1	1.0276	BEESWAX	PAESTUM	100	25101.0738	24425.91	25101.07	HMDB0000254	Succinic acid	C4H6O4	39.1	-3.2256	94.8320	-0.98

M-H Adduct m/z	Retention time (min)	Compound ID	Description	Formula	Score	Mass Error (ppm)	Isotope Similarity	Max Fold Change
205.0718	9.39	CSID227875	4,6-O-Ethylidenehexopyranose	C8H14O6	39.4	0.1244	97.38	Infinity
217.0716	9.85	CSID13835706	Triacetin	C9H14O6	40.5	-0.6061	96.84	Infinity
203.0926	9.95	CSID225666	Methyl 2,3-O-isopropylidenepentofuranoside	C9H16O5	44.7	0.4059	98.1	Infinity
219.0874	10.53	CSID190653	1,2-O-Isopropylidenehexofuranose	C9H16O6	39.6	-0.1549	98.09	Infinity
159.0662	11	CSID376	Pimelic acid	C7H12O4	54.8	-0.4779	99.67	1620.5027
203.0925	11.14	CSID225666	Methyl 2,3-O-isopropylidenepentofuranoside	C9H16O5	49.3	0.1748	98.22	Infinity
173.0818	12.36	CSID10025	Suberic acid	C8H14O4	49.5	-0.527	99.55	2097.3439
203.0926	12.61	CSID225666	Methyl 2,3-O-isopropylidenepentofuranoside	C9H16O5	42.4	0.313	98.27	Infinity
275.1503	13.57	CSID4444279	p-coumaroylagmatine	C14H20N4O2	44.4	-3.7385	96.79	Infinity
229.108	13.99	CSID4576376	Diethyl 2-(2-oxopropyl)succinate	C11H18O5	39.5	-0.4573	97.26	Infinity
187.0975	14.28	CSID2179	Azelaic acid	C9H16O4	54.2	-0.3385	99.29	3743.7475
203.0563	15.58	CSID19071365	2-O-Ethyl Ascorbic Acid	C8H12O6	46.8	0.796	97.76	Infinity
201.1133	17.64	CSID5004	Sebacic acid	C10H18O4	48.8	0.3477	98.6	495.53557
259.1188	18.96	CSID200654	6-(2,2-Dimethyl-1,3-dioxolan-4-yl)-2,2-dimethyltetrahydrofuro[3,4-d][1,3]dioxol-4-ol	C12H20O6	51.5	0.2786	97.32	Infinity
187.1339	24.35	CSID66903	10-Hydroxydecanoic acid	C10H20O3	43.8	-0.3704	97.72	Infinity
213.1132	24.74	CSID2018394	Camphoric acid monomethyl ester	C11H18O4	41.1	-0.1815	98.19	Infinity
301.1655	25.91	CSID13849665	Butyrin	C15H26O6	39	-0.5201	95.5	Infinity

Appendix 36 - ICMS Paestum water extract

	RT	Peak width	Max	Isotope	Maximum	PAESTUM RESIDUE			GREEK HONEYCOMB			ITALIAN HONEYCOMB			Accepted		Mass	Isotope	RT Error
m/z	(Min)	(min)	Fold Change	Distribution	Abundance	Green	Black	Orange	Fresh	Aged	Aged Cu	Fresh	Aged	Aged Cu	Description	Score	Error (ppm)	Similarity (%)	(min)
191.0197	16.34	3.65	3942.85	100 - 6.67 - 1.35	3728465.82	945.63	3728465.82	6947.86	11375.46	2355.53	6972.53	26146.84	10580.11	4853.17	Citric acid	42	-0.234	99.48	-0.57
187.0975	13.88	3.06	120.71	100 - 9.82 - 0.698	2937341.19	1662463.18	2107688.58	2937341.19	177661.59	24334.61	120894.37	221256.87	144128.00	101414.30	Nonate	52.5	-3.549	99.26	0.03
145.0870	9.79	4.91	5744.28	100 - 7.67 - 0.676	501094.86	501094.86	25202.27	30786.03	4559.12	87.23	1227.67	5552.19	4138.60	3115.79	Hydroxyisoheptanoic acid	48.4	-3.783	99.65	0.05
201.1132	17.90	2.52	214.44	100 - 10.4 - 0.538	411637.68	31272.52	28489.95	411637.68	12450.37	1919.62	3592.12	18488.75	11129.56	5764.47	Sebacic acid	42.9	0.067	98.50	-0.40
159.0662	10.69	1.70	Infinity	100 - 7.7 - 0.819	332251.52	168070.63	259175.80	332251.52	15372.30	1476.77	0.00	19565.75	12742.03	400.76	3,3 Dimethyl glutarate	41.1	-0.322	99.60	-0.72
173.0090	16.34	2.17	Infinity	100 - 6.19 - 0.924	235089.34	0.00	235089.34	222.70	449.17	25.05	126.82	1257.39	414.98	125.95	cis-Aconitic acid	40.4	-0.769	98.98	-1.78
143.1077	19.16	5.21	135.44	100 - 8.76 - 0.259	215333.36	215333.36	86445.12	103570.21	6242.65	1589.92	1624.40	7921.20	5589.33	3683.20	Octanoic acid	41.7	-0.077	99.40	-0.79
179.0560	4.01	7.82	2331.72	100 - 5.83 - 0.684	185557.92	79.58	3817.41	104.15	111888.62	185557.92	43449.87	85833.43	124581.69	19838.42	Glucose	40	-0.730	98.36	0.58
181.0717	2.57	7.21	125.10	100 - 5.75 - 0.81	138036.01	6307.68	138036.01	5204.47	2095.33	1103.40	1390.28	2755.46	2763.33	2275.88	Mannitol	40.8	-0.133	98.38	-0.19
145.0506	10.19	1.81	1365.21	100 - 6.4 - 0.723	108194.41	65675.60	102627.24	108194.41	5575.22	1574.58	79.25	7219.86	5581.70	595.35	Methylglutaric acid	41.4	0.073	99.40	-0.54
117.0193	10.39	2.73	332.60	100 - 4.17 - 0.785	105158.92	26547.68	105158.92	47150.03	5343.05	4602.76	1352.89	7364.66	5474.93	316.17	Succinic acid	41.1	-0.111	99.53	-0.72
341.1092	2.67	1.84	Infinity	100 - 12.2 - 2.35	97663.46	506.26	2278.90	50.91	97663.46	93951.10	0.00	67474.68	78233.09	20808.95	Lactose	40	-0.755	97.80	-0.37
131.0350	10.09	1.31	649.25	100 - 5.03 - 0.667	91572.70	36492.45	91572.70	58002.05	2920.65	1052.57	384.51	4076.92	2738.29	141.04	Glutaric acid	40.8	-0.216	99.15	-0.78
205.0354	15.25	2.17	Infinity	100 - 7.49 - 1.04	89697.88	1988.75	89697.88	3287.95	322.44	78.10	0.00	935.86	455.81	172.53	Methylisocitric acid	41.8	0.001	98.86	-0.56
131.0714	7.43	1.43	1156.74	100 - 6.4 - 0.587	63769.48	63769.48	3218.35	4846.83	364.19	249.76	55.13	510.23	379.25	1463.39	Leucic acid	44.7	-4.189	99.48	-0.08
147.0299	10.09	1.82	561.90	100 - 5 - 0.797	59408.10	34625.75	59408.10	14789.92	1470.31	3870.90	185.94	2293.17	3770.29	105.73	Citramalic acid	41	0.020	99.01	-0.66
503.1614	2.77	1.93	Infinity	100 - 16.4 - 1.48	48243.02	223.29	1100.44	117.32	32006.06	48243.02	0.00	13291.28	27349.22	4684.35	Raffinose	44.3	-0.623	93.12	-0.03
161.0455	9.68	3.04	120.02	100 - 5.57 - 0.389	35827.36	15992.55	35827.36	16003.74	5278.81	5228.67	9550.78	5270.60	2721.32	298.51	3-Hydroxymethylglutarate	40.3	-0.250	98.09	-1.08
165.0404	4.28	2.28	6309.83	100 - 4.77 - 0.365	30846.52	128.96	15930.73	333.89	8341.58	30846.52	4.89	17045.15	24512.54	2031.07	Arabinonic acid	40.1	-0.507	98.15	-0.62
89.0244	4.37	5.47	8.44	100 - 2.78 - 0.0553	30414.04	30414.04	3603.70	4017.69	14139.24	22662.69	8299.98	12555.26	19021.27	6084.30	Lactic acid	40.3	-0.392	98.80	-0.68
133.0142	10.39	1.00	3596.32	100 - 3.9 - 0.866	28231.08	5008.42	28231.08	6515.49	3594.34	2573.82	7.85	13374.73	4745.08	43.98	Malic acid	41	-0.042	99.12	-0.75
149.0455	4.01	2.19	Infinity	100 - 4.42 - 0.539	17957.02	204.98	1967.21	9.68	2461.42	14218.18	0.00	2246.34	17957.02	437.94	Arabinose	39.8	-0.498	98.20	0.95
128.0353	4.11	1.26	Infinity	100 - 4.91 - 0.399	16385.21	16385.21	1221.77	69.99	2090.66	1082.73	0.00	378.25	455.68	102.85	1-Pyrroline hydroxycarboxylic acid	40.6	0.116	98.67	-0.37
177.0403	4.20	0.95	Infinity	100 - 0.262	15237.44	0.00	315.32	0.00	8094.27	6475.70	0.00	15237.44	5035.92	0.00	Gluconolactone	39	-0.943	92.61	-0.51
117.0558	5.89	0.72	Infinity	100 - 5.52	14144.06	14144.06	915.16	211.03	13.36	21.20	0.00	65.23	25.65	44.45	3-Hydroxyisovaleric acid	39.6	-4.346	99.19	0.55
193.0352	7.02	0.52	Infinity	100 - 6.06	10129.00	0.00	50.69	0.00	10129.00	6516.09	0.00	1870.18	1983.61	25.24	Glucuronic acid	39.9	-0.689	97.65	-1.25

Appendix 37 - ICMS Paestum and Honeycombs methanol extract

Appendix 38

Residue – Honey Database

Protein accession	-10lgP	Coverage (%)	Peptides intensity	#Peptides (Unique)	PTM	Avg. Mass	Protein Name
O18330	156.2	26	8.46E+05	10 (10)	Carbamidomethylation; Oxidation (M); Mutation	48886	Major royal jelly protein 1 OS=**Apis mellifera**
O77061	147.7	13	7.96E+04	5 (4)	Oxidation (M); Mutation	51074	Major royal jelly protein 2 OS=**Apis mellifera**
Q17060	130.74	18	3.93E+05	10 (7)	Oxidation (M); Mutation	61662	Major royal jelly protein 3 OS=**Apis mellifera**
A0A2A3EM69	127.07	17	3.33E+05	5 (4)		41806	Actin-5C OS=**Apis cerana cerana**
A0A2A3EG18	74.11	12	6.17E+04	5 (5)	Deamidation (NQ); Oxidation (M)	71086	Heat shock OS=**Apis cerana cerana**
A0A2A3ECX5	47.43	11	1.97E+05	2 (2)	Carbamidomethylation	29815	Trypsin-2 OS=**Apis cerana cerana**
A0A2H3EAA9	69.38	13	7.17E+04	3 (2)	Deamidation (NQ); Oxidation (M)	41855	Actin 2 OS=**Armillaria gallica**
A0A1V9XJI7	48.38	11	3.30E+05	3 (3)		60119	SWI/SNF-related matrix-associated actin-dependent regulator of chromatin subfamily D member 1-like OS=**Tropilaelaps mercedesae**
A0A1V9XCK9	41.78	34	1.21E+04	4 (4)	Deamidation (NQ)	9408	UPF0480 protein C15orf24-like OS=**Tropilaelaps mercedesae**
A0A1V9XNM0	38.71	29	2.79E+05	3 (3)	Deamidation (NQ)	17125	Uncharacterized protein OS=**Tropilaelaps mercedesae**
A0A347SQJ1	25.09	15	2.07E+05	1 (1)	Deamidation (NQ); Oxidation (M)	8622	Uncharacterized protein OS=**Lactobacillus bombi**
A0A0F4LK07	20.41	11	6.37E+05	1 (1)	Carbamidomethylation; Oxidation (M); Mutation	11332	Cytosolic protein YlxR OS=**Lactobacillus kimbladii**

Residue Resin Database

Protein accession	-10lgP	Coverage (%)	Peptides intensity	#Peptides (Unique)	PTM	Avg. Mass	Protein Name
A7LA02	144.97	63	6.66E+06	97 (82)	Carbamidomethylation; Deamidation (NQ); Oxidation (M)	80047	1-deoxy-D-xylulose-5-phosphate synthase OS=**Picea abies**
A7LA01	113.12	43	3.38E+06	43 (29)	Carbamidomethylation; Deamidation (NQ); Oxidation (M)	79697	1-deoxy-D-xylulose-5-phosphate synthase OS=**Picea abies**
A7LA00	85.34	21	4.88E+05	14 (8)	Deamidation (NQ); Oxidation (M)	77327	1-deoxy-D-xylulose-5-phosphate synthase OS=**Picea abies**
Q1HK32	55.89	27	9.50E+05	9 (8)	Carbamidomethylation; Deamidation (NQ)	36525	ACC oxidase OS=**Picea glauca**
E5FA64	79.5	31	5.60E+04	18 (2)	Carbamidomethylation; Deamidation (NQ); Oxidation (M)	56414	CYP720B12 OS=**Picea sitchensis**
E5FA69	78.66	34	3.15E+05	17 (2)	Carbamidomethylation; Deamidation (NQ); Oxidation (M)	56199	CYP720B2 OS=**Picea sitchensis**
E5FA65	69.66	30	6.20E+05	15 (4)	Carbamidomethylation; Deamidation (NQ); Oxidation (M)	55409	CYP720B15 OS=**Picea sitchensis**
E5FA77	65.56	23	1.01E+06	11 (10)	Deamidation (NQ); Oxidation (M)	55300	CYP720B9 OS=**Picea sitchensis**
E5FA70	65.52	28	8.37E+04	12 (4)	Carbamidomethylation; Deamidation (NQ); Oxidation (M)	55433	CYP720B4 OS=**Picea sitchensis**
E5FA67	58.42	22	1.25E+04	10 (1)	Carbamidomethylation; Deamidation (NQ); Oxidation (M)	55624	CYP720B17v1 OS=**Picea sitchensis**
E5FA73	55.97	18	3.84E+05	9 (4)	Carbamidomethylation; Deamidation (NQ); Oxidation (M)	55559	CYP720B7 (Fragment) OS=**Picea sitchensis**

Fresh Greek Honeycomb Honey Database

Protein accession	-10lgP	Coverage (%)	Peptides intensity	#Peptides (Unique)	PTM	Avg. Mass	Protein Name
O18330	204.77	43	1.19E+07	17 (16)	Carbamidomethylation; Oxidation (M); Deamidation (NQ)	48886	Major royal jelly protein 1 OS=**Apis mellifera**
Q17060	189.59	23	2.02E+06	13 (10)	Carbamidomethylation; Oxidation (M); Deamidation (NQ)	61662	Major royal jelly protein 3 OS=**Apis mellifera**
O77061	167.25	27	9.52E+05	9 (5)	Carbamidomethylation; Oxidation (M); Deamidation (NQ)	51074	Major royal jelly protein 2 OS=**Apis mellifera**
O97432	98.36	12	2.91E+05	6 (4)	Oxidation (M)	70236	Major royal jelly protein 5 OS=**Apis mellifera**
A0A2H3E6M2	77.91	10	2.02E+05	3 (3)		41678	Actin 1 OS=**Armillaria gallica**
A0A2A3ECX5	36.37	11	2.74E+05	2 (2)	Carbamidomethylation	29815	Trypsin-2 OS=**Apis cerana cerana**

Aged Greek Honeycomb

Protein accession	-10lgP	Coverage (%)	Peptides intensity	#Peptides (Unique)	PTM	Avg. Mass	Protein Name
O18330	241.85	64	2.03E+07	32 (28)	Carbamidomethylation; Oxidation (M); Deamidation (NQ)	48886	Major royal jelly protein 1 OS=**Apis mellifera**
Q17060	221.3	45	4.37E+06	25 (15)	Carbamidomethylation; Oxidation (M); Deamidation (NQ)	61662	Major royal jelly protein 3 OS=**Apis mellifera**
O77061	178.21	35	4.06E+06	14 (8)	Carbamidomethylation; Oxidation (M); Deamidation (NQ)	51074	Major royal jelly protein 2 OS=**Apis mellifera**
O97432	163.73	25	1.65E+06	13 (10)	Oxidation (M)	70236	Major royal jelly protein 5 OS=**Apis mellifera**
B6V6A2	122.66	15	1.78E+05	4 (4)		33530	Silk fibroin 3 OS=**Apis mellifera**
Q17061	114.64	14	2.19E+05	6 (4)	Oxidation (M)	52916	Major royal jelly protein 4 OS=**Apis mellifera**
A0A2A3EHI0	142.63	32	2.91E+03	11 (1)	Carbamidomethylation; Oxidation (M); Deamidation (NQ)	34111	Bee-milk protein OS=**Apis cerana cerana**
A0A2A3E8C9	131.73	12	5.71E+05	8 (8)	Carbamidomethylation; Oxidation (M)	66292	Alpha-glucosidase OS=**Apis cerana cerana**
A0A1V9XCK9	22.7	19	4.80E+03	1 (1)		9408	UPF0480 protein C15orf24-like OS=**Tropilaelaps mercedesae**
A0A083XUW8	20.05	10	5.66E+05	1 (1)	Deamidation (NQ)	13220	50S ribosomal protein L7/L12 OS=**Bifidobacterium longum subsp. infantis EK3**

Fresh Greek Honeycomb Resin Database

Protein accession	-10lgP	Coverage (%)	Peptides intensity	#Peptides (Unique)	PTM	Avg. Mass	Protein Name
A7LA01	122.46	37	3.93E+05	29 (12)	Oxidation (M); Deamidation (NQ); Sodium adduct; Dehydration; Phosphorylation (STY); 5 more	79697	1-deoxy-D-xylulose-5-phosphate synthase OS=**Picea abies**
A7LA02	93.85	36	4.35E+06	24 (18)	Carbamidomethylation; Oxidation (M); Deamidation (NQ); Sodium adduct; Dehydration; 7 more	80047	1-deoxy-D-xylulose-5-phosphate synthase OS=**Picea abies**
A7LA00	70.14	18	2.91E+05	8 (6)	Oxidation (M); Deamidation (NQ); Phosphorylation (STY); Dihydroxy	77327	1-deoxy-D-xylulose-5-phosphate synthase OS=**Picea abies**
M4HXU6	123	33	7.29E+05	35 (3)	Carbamidomethylation; Oxidation (M); Deamidation (NQ); Methylation(others); Dehydration; 12 more	98479	Bifunctional levopimaradiene synthase chloroplastic OS=**Pinus banksiana**
A0A076U7E2	72.33	28	5.95E+05	14 (12)	Carbamidomethylation; Deamidation (NQ); Amidation; Sodium adduct; Phosphorylation (STY); 5 more	56274	CYP720PB12 OS=**Pinus banksiana**
A0A076U5D6	47.8	14	5.08E+05	6 (5)	Carbamidomethylation; Oxidation (M); Deamidation (NQ); Mutation	56459	CYP720B10 OS=**Pinus banksiana**
M4HYC6	109.45	32	1.86E+04	28 (1)	Carbamidomethylation; Oxidation (M); Deamidation (NQ); Methylation(others); Dehydration; 7 more	97780	Bifunctional levopimaradiene synthase chloroplastic OS=**Pinus contorta**
M4HYP3	84.76	18	1.42E+06	15 (9)	Carbamidomethylation; Oxidation (M); Deamidation (NQ); Sodium adduct; Phosphorylation (STY); 8 more	100687	Monofunctional isopimaradiene synthase chloroplastic OS=**Pinus contorta**
M4HYC8	78.64	17	1.77E+03	13 (1)	Carbamidomethylation; Oxidation (M); Deamidation (NQ); Sodium adduct; Dehydration; 9 more	100104	Monofunctional pimaradiene synthase OS=**Pinus contorta**
A0A076U5L5	71.85	25	7.99E+05	13 (12)	Carbamidomethylation; Oxidation (M); Deamidation (NQ); Amidation; Sodium adduct; 4 more	56346	CYP720B12 OS=**Pinus contorta** OX=3339 GN=CYP720B12 PE=2 SV=1
A0A076U5E1	45.07	12	4.50E+05	5 (4)	Carbamidomethylation; Oxidation (M); Deamidation (NQ)	56444	CYP720B10v1 OS=**Pinus contorta**
A0A076U7E6	33.97	13	3.62E+04	3 (2)	Oxidation (M); Deamidation (NQ)	56580	CYP720B11 OS=**Pinus contorta**

Protein accession	-10lgP	Coverage (%)	Peptides intensity	#Peptides (Unique)	PTM	Avg. Mass	Protein Name
B9U4U0	99.01	38	4.72E+05	25 (9)	Oxidation (M); Deamidation (NQ); Sodium adduct; Methylation(others); Dehydration; 6 more	79288	1-deoxy-D-xylulose-5-phosphate synthase OS=**Pinus densiflora** OX=77912 GN=DXS PE=2 SV=1
A0A2S0DDS3	68.51	23	8.54E+05	11 (11)	Carbamidomethylation; Oxidation (M); Dehydration; Phosphorylation (STY); Dihydroxy; Methylphosphonylation	73781	Cycle OS=**Plodia interpunctella**
B3IUN8	40.48	14	7.50E+04	5 (5)	Carbamidomethylation; Oxidation (M); Deamidation (NQ)	52754	Cis-aconitate decarboxylase OS=**Aspergillus terreus**
B7TWW5	76.07	36	2.85E+06	16 (16)	Carbamidomethylation; Oxidation (M); Deamidation (NQ); Sodium adduct; Methylation(others); 7 more	60209	Squalene monooxygenase SE2 OS=**Panax ginseng**
I1V0B8	41.25	11	6.06E+05	4 (4)	Deamidation (NQ)	61918	Tetrahydrocannabinolic acid synthase (Fragment) OS=**Cannabis sativa**
I1V0C1	41.25	11	6.06E+05	4 (4)	Deamidation (NQ)	61946	Tetrahydrocannabinolic acid synthase (Fragment) OS=**Cannabis sativa**
I1V0C2	41.25	11	6.06E+05	4 (4)	Deamidation (NQ)	61974	Tetrahydrocannabinolic acid synthase (Fragment) OS=**Cannabis sativa**
Q38710	108.71	25	2.55E+06	27 (12)	Carbamidomethylation; Oxidation (M); Deamidation (NQ); Sodium adduct; Methylation(others); 12 more	99536	Bifunctional abietadiene synthase chloroplastic OS=**Abies grandis**
Q7BRJ3	115.22	39	3.08E+06	32 (32)	Deamidation (NQ); Sodium adduct; Dehydration; Phosphorylation (STY); Biotinylation; 16 more	27558	DitK OS=**Pseudomonas abietaniphila**
Q9X4X6	57.31	10	9.31E+04	3 (3)	Phosphorylation (STY)	35473	2 3-dihydroxybiphenyl 1 2-dioxygenase OS=**Pseudomonas abietaniphila**
Q7BRJ7	33.04	12	1.82E+05	3 (3)	Deamidation (NQ)	41412	Acetyl-CoA acetyltransferases OS=**Pseudomonas abietaniphila**
Q947C4	88.88	18	6.39E+06	20 (17)	Carbamidomethylation; Oxidation (M); Deamidation (NQ); Methylation(others); Phosphorylation (STY); 4 more	100290	Bifunctional levopimaradiene synthase chloroplastic OS=**Ginkgo biloba**

Aged Greek Honeycomb

Protein accession	-10lgP	Coverage (%)	Peptides intensity	#Peptides (Unique)	PTM	Avg. Mass	Protein Name
A7LA01	96.95	49	1.78E+06	34 (9)	Carbamidomethylation; Oxidation (M); Deamidation (NQ); Acetylation (K); Acetylation (N-term); 11 more	79697	1-deoxy-D-xylulose-5-phosphate synthase OS=**Picea abies**
A7LA02	75.93	26	7.50E+05	19 (12)	Carbamidomethylation; Oxidation (M); Deamidation (NQ); Acetylation (K); Acetylation (N-term); 7 more	80047	1-deoxy-D-xylulose-5-phosphate synthase OS=**Picea abies**
M4HXW5	124.55	46	3.19E+05	58 (4)	Carbamidomethylation; Oxidation (M); Deamidation (NQ); Acetylation (K); Acetylation (N-term); 18 more	100632	Monofunctional isopimaradiene synthase chloroplastic OS=**Pinus banksiana**
M4HY08	79.3	22	5.93E+04	16 (2)	Carbamidomethylation; Oxidation (M); Deamidation (NQ); Acetylation (N-term); Dehydration; 7 more	100159	Monofunctional pimaradiene synthase OS=**Pinus banksiana**
A0A076U7E2	59.41	22	3.59E+04	12 (1)	Carbamidomethylation; Oxidation (M); Deamidation (NQ); Carbamylation; Hexose (NSY); 2 more	56274	CYP720PB12 OS=**Pinus banksiana**
M4HYC8	78.15	18	1.23E+03	15 (1)	Carbamidomethylation; Oxidation (M); Deamidation (NQ); Acetylation (N-term); Dehydration; 7 more	100104	Monofunctional pimaradiene synthase OS=**Pinus contorta**
M4HY12	72.03	20	1.35E+05	14 (4)	Carbamidomethylation; Deamidation (NQ); Acetylation (N-term); Carboxylation (E); Methylation(KR); Phosphorylation (STY)	97917	Putative monofunctional diterpene synthase OS=**Pinus contorta**
M4HXW7	68.15	13	2.41E+05	11 (1)	Carbamidomethylation; Deamidation (NQ); Acetylation (N-term); Carboxylation (E); Methylation(KR); Phosphorylation (STY)	97893	Putative monofunctional diterpene synthase OS=**Pinus contorta**
A0A076UAC7	45.47	11	9.59E+03	5 (2)	Carbamidomethylation; Oxidation (M); Deamidation (NQ)	55853	CYP720B2 OS=**Pinus contorta**
B9U4U0	118.46	48	2.61E+06	50 (26)	Carbamidomethylation; Oxidation (M); Deamidation (NQ); Acetylation (K); Acetylation (N-term); 15 more	79288	1-deoxy-D-xylulose-5-phosphate synthase OS=**Pinus densiflora**
B9U4U7	77.44	30	9.37E+05	14 (14)	Carbamidomethylation; Oxidation (M); Deamidation (NQ); Acetylation (N-term); Carbamylation; 6 more	51955	1-deoxy-D-xylulose-5-phosphate reductoisomerase OS=**Pinus densiflora**

Protein accession	-10lgP	Coverage (%)	Peptides intensity	#Peptides (Unique)	PTM	Avg. Mass	Protein Name
Q1HK32	40.91	15	1.96E+05	3 (2)	Oxidation (M); Deamidation (NQ)	36525	ACC oxidase OS=**Picea glauca**
E5FA69	45.2	10	3.34E+05	5 (1)	Carbamidomethylation; Oxidation (M); Deamidation (NQ)	56199	CYP720B2 OS=**Picea sitchensis**
Q1HK33	40.91	15	1.96E+05	3 (2)	Oxidation (M); Deamidation (NQ)	36525	ACC oxidase OS=**Picea sitchensis**
I1V0B8	38.37	14	7.68E+04	5 (5)	Deamidation (NQ)	61918	Tetrahydrocannabinolic acid synthase (Fragment) OS=**Cannabis sativ**a
I1V0C1	38.37	14	7.68E+04	5 (5)	Deamidation (NQ)	61946	Tetrahydrocannabinolic acid synthase (Fragment) OS=**Cannabis sativa**
Q1HK31	40.76	23	1.49E+05	4 (3)	Carbamidomethylation; Oxidation (M); Deamidation (NQ)	35849	ACC oxidase (Fragment) OS=**Pseudotsuga menziesii**
Q38710	87.83	18	5.45E+05	21 (12)	Carbamidomethylation; Oxidation (M); Deamidation (NQ); Acetylation (K); Acetylation (N-term); 9 more	99536	Bifunctional abietadiene synthase chloroplastic OS=**Abies grandis**
Q7BRJ3	120.87	29	2.81E+06	40 (40)	Oxidation (M); Deamidation (NQ); Acetylation (K); Acetylation (Protein N-term); Acetylation (N-term); 29 more	27558	DitK OS=**Pseudomonas abietaniphila**
Q9X4X7	68.38	35	1.58E+06	10 (10)	Carbamidomethylation; Oxidation (M); Deamidation (NQ); Acetylation (K); Carbamylation; 3 more	26315	DitB OS=**Pseudomonas abietaniphila**

Fresh Italian Honeycomb Honey Database

Protein accession	-10lgP	Coverage (%)	Peptides intensity	#Peptides (Unique)	PTM	Avg. Mass	Protein Name
O18330	268.05	67	1.30E+08	43 (37)	Carbamidomethylation; Deamidation (NQ); Oxidation (M)	48886	Major royal jelly protein 1 OS=**Apis mellifera**
Q17060	257.37	58	3.90E+07	41 (34)	Carbamidomethylation; Deamidation (NQ); Oxidation (M)	61662	Major royal jelly protein 3 OS=**Apis mellifera**
O77061	242.75	52	1.58E+07	33 (21)	Carbamidomethylation; Deamidation (NQ); Oxidation (M)	51074	Major royal jelly protein 2 OS=**Apis mellifera**
O97432	176.49	25	3.01E+06	12 (9)	Oxidation (M)	70236	Major royal jelly protein 5 OS=**Apis mellifera**
Q17061	116.86	20	8.64E+05	12 (5)	Carbamidomethylation; Oxidation (M)	52916	Major royal jelly protein 4 OS=**Apis mellifera**
A0A2A3E8C9	157.99	16	2.31E+06	10 (10)	Carbamidomethylation; Oxidation (M)	66292	Alpha-glucosidase OS=**Apis cerana cerana**
A0A2A3EG07	80.56	13	1.10E+05	8 (1)	Carbamidomethylation; Oxidation (M)	54971	Bee-milk protein OS=**Apis cerana cerana**
A0A2A3ECX5	71.87	11	6.19E+05	6 (6)	Carbamidomethylation	29815	Trypsin-2 OS=**Apis cerana cerana**
A0A2A3EPA8	31.4	11	1.96E+03	1 (1)	Carbamidomethylation	7942	Trypsin inhibitor isl-1 OS=**Apis cerana cerana**
A0A2S8AEU0	23.67	10	2.14E+03	1 (1)	Carbamidomethylation	25326	Peptide methionine sulfoxide reductase MsrA OS=**Apibacter adventoris**

Aged Italian Honeycomb

Protein accession	-10lgP	Coverage (%)	Peptides intensity	#Peptides (Unique)	PTM	Avg. Mass	Protein Name
O18330	158.74	29	1.56E+06	11 (11)	Oxidation (M)	48886	Major royal jelly protein 1 OS=**Apis mellifera**
A0A2A3EM69	98.71	10	8.30E+04	3 (3)		41806	Actin-5C OS=**Apis cerana cerana**
A0A2A3ECX5	41.73	11	6.43E+04	2 (2)	Carbamidomethylation	29815	Trypsin-2 OS=**Apis cerana cerana**
A0A1V9XCK9	57.66	35	3.35E+04	6 (6)	Deamidation (NQ)	9408	UPF0480 protein C15orf24-like OS=**Tropilaelaps mercedesae** O
A0A6H9Y183	24.01	13	3.66E+04	1 (1)		8135	GNAT family N-acetyltransferase OS=**Bifidobacterium longum subsp. infantis**
A0A1V9XJD9	21.77	10	7.43E+04	1 (1)		11001	Uncharacterized protein OS=**Tropilaelaps mercedesae**

Fresh Italian Honeycomb Resin Database

Protein accession	-10lgP	Coverage (%)	Peptides intensity	#Peptides (Unique)	PTM	Avg. Mass	Protein Name
A7LA01	85.27	31	1.89E+06	21 (18)	Carbamidomethylation; Oxidation (M); Deamidation (NQ)	79697	1-deoxy-D-xylulose-5-phosphate synthase OS=**Picea abies**
A7LA02	81.16	27	1.32E+06	15 (11)	Carbamidomethylation; Oxidation (M); Deamidation (NQ)	80047	1-deoxy-D-xylulose-5-phosphate synthase OS=**Picea abies**
M4HXU7	56.94	15	1.98E+04	11 (3)	Carbamidomethylation; Oxidation (M); Deamidation (NQ)	97712	Putative monofunctional diterpene synthase OS=**Pinus banksiana**
A0A076U5L5	68.23	32	1.36E+05	13 (7)	Carbamidomethylation; Oxidation (M); Deamidation (NQ)	56346	CYP720B12 OS=**Pinus contorta**
A0A076UAC7	65.59	12	2.10E+04	8 (1)	Carbamidomethylation; Oxidation (M); Deamidation (NQ)	55853	CYP720B2 OS=**Pinus contorta**
M4HYC8	59.53	15	3.66E+05	9 (8)	Carbamidomethylation; Oxidation (M); Deamidation (NQ)	100104	Monofunctional pimaradiene synthase OS=**Pinus contorta**
M4HXW7	51.6	15	3.19E+05	9 (1)	Carbamidomethylation; Oxidation (M); Deamidation (NQ)	97893	Putative monofunctional diterpene synthase OS=**Pinus contorta**
M4HY12	50.28	13	5.30E+04	9 (2)	Carbamidomethylation; Oxidation (M); Deamidation (NQ)	97917	Putative monofunctional diterpene synthase OS=**Pinus contorta** O
B9U4U6	65.48	30	2.80E+05	12 (8)	Carbamidomethylation; Oxidation (M); Deamidation (NQ)	76095	1-deoxy-D-xylulose-5-phosphate synthase OS=**Pinus densiflora**
E5FA69	69.78	14	2.55E+05	9 (1)	Carbamidomethylation; Oxidation (M); Deamidation (NQ)	56199	CYP720B2 OS=**Picea sitchensis** OX=3332 PE=2 SV=1
E5FA77	64.95	25	6.95E+05	11 (10)	Oxidation (M); Deamidation (NQ)	55300	CYP720B9 OS=**Picea sitchensis**
E5FA64	63.62	15	5.47E+03	9 (1)	Carbamidomethylation; Oxidation (M); Deamidation (NQ)	56414	CYP720B12 OS=**Picea sitchensis**
E5FA65	54.45	14	6.32E+04	7 (2)	Carbamidomethylation; Oxidation (M); Deamidation (NQ)	55409	CYP720B15 OS=**Picea sitchensis**
E5FA66	50.42	14	2.23E+04	6 (1)	Carbamidomethylation; Oxidation (M); Deamidation (NQ)	55843	CYP720B16 (Fragment) OS=**Picea sitchensis**

Protein accession	-10lgP	Coverage (%)	Peptides intensity	#Peptides (Unique)	PTM	Avg. Mass	Protein Name
Q38710	59.74	11	1.03E+05	7 (6)	Carbamidomethylation; Oxidation (M); Deamidation (NQ)	99536	Bifunctional abietadiene synthase chloroplastic OS=**Abies grandis**
B7TWW5	65.29	23	1.42E+06	8 (7)	Carbamidomethylation; Oxidation (M); Deamidation (NQ)	60209	Squalene monooxygenase SE2 OS=**Panax ginseng**
O48651	52.5	10	2.87E+04	5 (4)	Oxidation (M); Deamidation (NQ)	59375	Squalene monooxygenase SE1 OS=**Panax ginseng**
Q7BRJ3	57.6	20	2.60E+04	6 (6)	Deamidation (NQ)	27558	DitK OS=**Pseudomonas abietaniphila**
Q7BRJ6	28.1	22	2.71E+04	2 (2)	Oxidation (M); Deamidation (NQ)	31675	3-hydroxyacyl-CoA dehydrogenase OS=**Pseudomonas abietaniphila**
Q7BRJ7	32.93	18	1.80E+05	3 (3)	Carbamidomethylation; Deamidation (NQ)	41412	Acetyl-CoA acetyltransferases OS=**Pseudomonas abietaniphila**
Q9X4W6	59.51	11	4.32E+05	5 (5)	Carbamidomethylation; Oxidation (M); Deamidation (NQ)	60018	Crotonobetaine/carnitine-CoA ligase OS=**Pseudomonas abietaniphila**
Q9X4W9	43.58	13	1.74E+05	4 (4)	Oxidation (M); Deamidation (NQ)	52537	Dioxygenase DitA oxygenase component large subunit OS=**Pseudomonas abietaniphila**
Q9XCB5	34.14	10	9.84E+04	2 (2)	Carbamidomethylation; Oxidation (M); Deamidation (NQ)	34682	Putative DitA1 homolog (Fragment) OS=**beta proteobacterium DhA-73**
Q9XCB6	34.14	10	9.84E+04	2 (2)	Carbamidomethylation; Oxidation (M); Deamidation (NQ)	34698	Putative DitA1 homolog (Fragment) OS=**beta proteobacterium DhA-71**

Aged Italian Honeycomb

Protein accession	-10lgP	Coverage (%)	Peptides intensity	#Peptides (Unique)	PTM	Avg. Mass	Protein Name
Q7BRJ3	91.77	20	1.03E+06	9 (9)	Deamidation (NQ)	27558	DitK OS=**Pseudomonas abietaniphila**
Q7BRJ7	71.21	13	5.75E+05	5 (5)	Carbamidomethylation; Oxidation (M); Deamidation (NQ)	41412	Acetyl-CoA acetyltransferases OS=**Pseudomonas abietaniphila**

Protein accession	-10lgP	Coverage (%)	Peptides intensity	#Peptides (Unique)	PTM	Avg. Mass	Protein Name
Q9X4W9	49.61	15	1.04E+06	5 (3)	Oxidation (M); Deamidation (NQ)	52537	Dioxygenase DitA oxygenase component large subunit OS=**Pseudomonas abietaniphila**
Q9X4X2	43.39	12	1.09E+05	4 (4)	Oxidation (M); Deamidation (NQ)	42776	DitF OS=**Pseudomonas abietaniphila**
Q9X4X6	38.82	6	2.22E+04	2 (2)	Oxidation (M)	35473	2 3-dihydroxybiphenyl 1 2-dioxygenase OS=**Pseudomonas abietaniphila**
Q7BRJ6	38.53	10	1.30E+04	2 (2)	Oxidation (M)	31675	3-hydroxyacyl-CoA dehydrogenase OS=**Pseudomonas abietaniphila**
Q9X4W7	34.87	19	1.56E+05	3 (3)	Oxidation (M); Deamidation (NQ)	30303	DitI OS=**Pseudomonas abietaniphila**
A7LA01	89.72	21	8.91E+04	18 (6)	Carbamidomethylation; Deamidation (NQ)	79697	1-deoxy-D-xylulose-5-phosphate synthase OS=**Picea abies**
A7LA02	81.41	27	1.49E+06	13 (9)	Carbamidomethylation; Oxidation (M); Deamidation (NQ)	80047	1-deoxy-D-xylulose-5-phosphate synthase **OS=Picea abies**
B7TWW5	71.56	10	3.92E+05	7 (7)	Deamidation (NQ)	60209	Squalene monooxygenase SE2 OS=**Panax ginseng**
A0A076U7E2	63.74	18	7.30E+04	11 (5)	Carbamidomethylation; Oxidation (M); Deamidation (NQ)	56274	CYP720PB12 OS=**Pinus banksiana**
M4HXU7	62.68	10	4.95E+04	8 (1)	Carbamidomethylation; Oxidation (M); Deamidation (NQ)	97712	Putative monofunctional diterpene synthase OS=**Pinus banksiana**
M4HXU6	61.74	8	1.95E+06	6 (3)	Oxidation (M); Deamidation (NQ)	98479	Bifunctional levopimaradiene synthase chloroplastic OS=**Pinus banksiana**
A0A076U5D6	55.48	12	1.65E+06	4 (4)	Carbamidomethylation; Oxidation (M); Deamidation (NQ)	56459	CYP720B10 OS=**Pinus banksiana**
A0A076U5K7	50.29	9	2.76E+05	6 (6)	Oxidation (M); Deamidation (NQ)	55663	CYP720B1v2 OS=**Pinus banksiana**

Protein accession	-10lgP	Coverage (%)	Peptides intensity	#Peptides (Unique)	PTM	Avg. Mass	Protein Name
Q38710	61.18	10	2.83E+05	7 (2)	Carbamidomethylation; Oxidation (M); Deamidation (NQ)	99536	Bifunctional abietadiene synthase chloroplastic OS=**Abies grandis**
Q947C4	58.15	5	2.78E+05	6 (5)	Deamidation (NQ)	100290	Bifunctional levopimaradiene synthase chloroplastic OS=**Ginkgo biloba**
E5FA64	56.01	15	1.67E+03	7 (1)	Carbamidomethylation; Oxidation (M); Deamidation (NQ)	56414	CYP720B12 OS=**Picea sitchensis**
E5FA77	39.17	6	1.30E+05	4 (4)	Deamidation (NQ)	55300	CYP720B9 OS=**Picea sitchensis**
Q1HK33	32.85	5	4.61E+04	2		36525	ACC oxidase OS=**Picea sitchensis**
E5FA65	30.96	9	2.13E+05	3	Carbamidomethylation; Oxidation (M); Deamidation (NQ)	55409	CYP720B15 OS=**Picea sitchensis**
E5FA72	25.49	8	1.32E+04	2	Carbamidomethylation; Deamidation (NQ)	55084	CYP720B5v2 (Fragment) OS=**Picea sitchensis**
E5FA74	22.64	7	3.29E+04	2	Deamidation (NQ)	54922	CYP720B8 OS=**Picea sitchensis**
B9U4U7	67.08	18	7.40E+05	9 (9)	Carbamidomethylation; Oxidation (M)	51955	1-deoxy-D-xylulose-5-phosphate reductoisomerase OS=**Pinus densiflora**
B9U4U6	53.46	22	3.80E+05	9 (7)	Oxidation (M); Deamidation (NQ)	76095	1-deoxy-D-xylulose-5-phosphate synthase OS=**Pinus densiflora**
M4HYP3	45.62	3	3.61E+05	3 (2)	Deamidation (NQ)	100687	Monofunctional isopimaradiene synthase chloroplastic OS=**Pinus contorta**
Q9XCB8	42.18	20	4.95E+05	4 (2)	Deamidation (NQ)	34972	Putative DitA1 homolog (Fragment) OS=**Burkholderia sp. IpA-51**
Q9XCB7	41.17	17	5.35E+04	5 (5)	Oxidation (M); Deamidation (NQ)	34511	Putative DitA1 homolog (Fragment) OS=**Mycobacterium sp. DhA-55**
A0A2S0DDS3	38.18	8	1.36E+05	3 (3)	Carbamidomethylation; Deamidation (NQ)	73781	Cycle OS=**Plodia interpunctella**

Protein accession	-10lgP	Coverage (%)	Peptides intensity	#Peptides (Unique)	PTM	Avg. Mass	Protein Name
Q9XCB5	36.16	16	1.80E+05	4 (4)	Deamidation (NQ)	34682	Putative DitA1 homolog (Fragment) OS=**beta proteobacterium DhA-73** 1
A0A455XAL6	34.61	10	6.02E+06	3 (3)	Oxidation (M); Deamidation (NQ)	31609	Maturase K (Fragment) OS=**Aquilaria crassna**
A0A140F3N4	28.03	11	4.11E+05	2	Oxidation (M); Deamidation (NQ)	20469	Arginine kinase (Fragment) OS=**Curculionidae sp. CB-2016**
A0A060GPB5	27.02	14	8.01E+03	2	Oxidation (M)	12456	Translation elongation factor 1-alpha (Fragment) OS=**Fusarium oxysporum**

Residue Bacteria Database

Protein accession	-10lgP	Coverage (%)	Peptides intensity	#Peptides (Unique)	PTM	Avg. Mass	Protein Name
Q02SZ7	277.43	51	3.62E+07	39 (39)	Carbamidomethylation; Deamidation (NQ); Acetylation (N-term); Formylation; Carbamylation; 8 more	48178	Lysyl endopeptidase OS=**Pseudomonas aeruginosa** (strain UCBPP-PA14)
P0AEY0	237.03	51	2.77E+06	30 (8)	Deamidation (NQ); Oxidation (M); Carbamylation; Biotinylation; Sodium adduct; Replacement of proton with ammonium ion	43388	Maltose/maltodextrin-binding periplasmic protein OS=**Escherichia coli O157:H7**
B1LMA4	100.04	11	6.79E+05	2 (2)		18695	DNA protection during starvation protein OS=**Escherichia coli (strain SMS-3-5 / SECEC)**
Q0TCC0	96.97	20	1.39E+05	6 (6)	Acetylation (N-term); Formylation; Phosphorylation (STY); Carbamylation; Dimethylation(KR); Aminoethylcysteine	43284	Elongation factor Tu 1 OS=**Escherichia coli O6:K15:H31** (strain 536 / UPEC)
Q0TA81	73.83	10	1.53E+04	1 (1)	Deamidation (NQ); Oxidation (M); Carbamylation	24730	50S ribosomal protein L1 OS=**Escherichia coli O6:K15:H31** (strain 536 / UPEC)
B7NRR4	41.74	10	1.24E+07	1 (1)	Mutation	12295	50S ribosomal protein L7/L12 OS=**Escherichia coli O7:K1 (strain IAI39 / ExPEC)**
O53553	125	48	1.53E+07	81 (81)	Deamidation (NQ); Oxidation (M); Myristoylation; Acetylation (N-term); Formylation; 23 more	147625	Uncharacterized PE-PGRS family protein PE_PGRS54 OS=**Mycobacterium tuberculosis** (strain ATCC 25618 / H37Rv)
P9WIG5	81.87	27	3.39E+05	15 (15)	Deamidation (NQ); Oxidation (M); Myristoylation; Formylation; Phosphorylation (STY); 3 more	74354	WAG22 antigen OS=**Mycobacterium tuberculosis** (strain ATCC 25618 / H37Rv)
P9WIF9	39.88	18	5.68E+03	3 (3)	Deamidation (NQ)	39305	Uncharacterized PE-PGRS family protein PE_PGRS20 OS=**Mycobacterium tuberculosis** (strain ATCC 25618 / H37Rv)
B4RLD4	105.2	11	2.04E+07	8 (8)	Deamidation (NQ); Oxidation (M); Acetylation (N-term); Formylation; Carbamylation; 3 more	35474	Fructose-1 6-bisphosphatase class 1 OS=**Neisseria gonorrhoeae** (strain NCCP11945**)**
P0A9L2	94.85	13	1.88E+05	2 (2)	Oxidation (M)	20853	FKBP-type peptidyl-prolyl cis-trans isomerase SlyD OS=**Shigella flexneri**
A1KV69	47.72	16	2.25E+05	2 (2)	Mutation	7500	DNA-directed RNA polymerase subunit omega OS=**Neisseria meningitidis serogroup C / serotype 2a** (strain ATCC 700532 / DSM 15464 / FAM18)

Protein accession	-10lgP	Coverage (%)	Peptides intensity	#Peptides (Unique)	PTM	Avg. Mass	Protein Name
Q07J67	37.48	10	9.51E+03	1 (1)		11050	30S ribosomal protein S21 OS=**Rhodopseudomonas palustris** (strain BisA53)
A5VBQ5	34.43	11	1.85E+06	1 (1)		10128	10 kDa chaperonin OS=**Sphingomonas wittichii** (strain RW1 / DSM 6014 / JCM 10273)
B4RBP5	32.89	12	4.92E+05	2 (2)	Carbamidomethylation; Oxidation (M)	35754	Biotin synthase OS=**Phenylobacterium zucineum** (strain HLK1)
A8LNY7	22.06	10	2.31E+06	1 (1)	Oxidation (M)	23216	Probable transaldolase OS=**Dinoroseobacter shibae** (strain DSM 16493 / NCIMB 14021 / DFL 12)
Q92ST6	21.73	10	2.62E+05	1 (1)		20936	Elongation factor P OS=**Rhizobium meliloti** (strain 1021)